physics and chemistry of fission

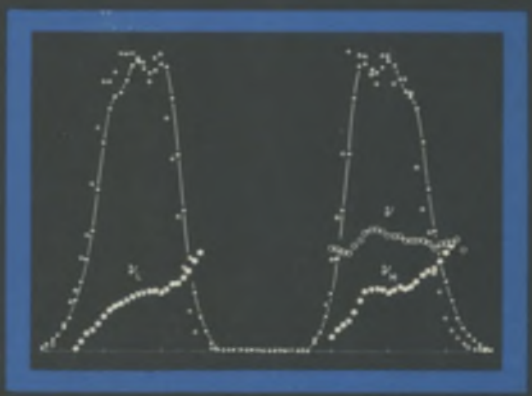

PROCEEDINGS
OF A SYMPOSIUM,
SALZBURG,
22-26 MARCH 1965

vol. I

IPS 101

INTERNATIONAL ATOMIC ENERGY AGENCY, VIENNA, 1965

PHYSICS AND CHEMISTRY OF FISSION

VOL. I

The following States are Members of the International Atomic Energy Agency:

AFGHANISTAN
ALBANIA
ALGERIA
ARGENTINA
AUSTRALIA
AUSTRIA
BELGIUM
BOLIVIA
BRAZIL
BULGARIA
BURMA
BYELORUSSIAN SOVIET SOCIALIST REPUBLIC
CAMBODIA
CAMEROON
CANADA
CEYLON
CHILE
CHINA
COLOMBIA
CONGO, DEMOCRATIC REPUBLIC OF
COSTA RICA
CUBA
CYPRUS
CZECHOSLOVAK SOCIALIST REPUBLIC
DENMARK
DOMINICAN REPUBLIC
ECUADOR
EL SALVADOR
ETHIOPIA
FINLAND
FRANCE
FEDERAL REPUBLIC OF GERMANY
GABON
GHANA
GREECE
GUATEMALA
HAITI
HOLY SEE
HONDURAS
HUNGARY
ICELAND
INDIA
INDONESIA
IRAN
IRAQ
ISRAEL
ITALY
IVORY COAST
JAPAN
REPUBLIC OF KOREA
KUWAIT
LEBANON
LIBERIA
LIBYA
LUXEMBOURG
MADAGASCAR
MALI
MEXICO
MONACO
MOROCCO
NETHERLANDS
NEW ZEALAND
NICARAGUA
NIGERIA
NORWAY
PAKISTAN
PARAGUAY
PERU
PHILIPPINES
POLAND
PORTUGAL
ROMANIA
SAUDI ARABIA
SENEGAL
SOUTH AFRICA
SPAIN
SUDAN
SWEDEN
SWITZERLAND
SYRIA
THAILAND
TUNISIA
TURKEY
UKRAINIAN SOVIET SOCIALIST REPUBLIC
UNION OF SOVIET SOCIALIST REPUBLICS
UNITED ARAB REPUBLIC
UNITED KINGDOM OF GREAT BRITAIN AND NORTHERN IRELAND
UNITED STATES OF AMERICA
URUGUAY
VENEZUELA
VIET-NAM
YUGOSLAVIA

The Agency's Statute was approved on 23 October 1956 by the Conference on the Statute of the IAEA held at United Nations Headquarters, New York; it entered into force on 29 July 1957. The Headquarters of the Agency are situated in Vienna. Its principal objective is "to accelerate and enlarge the contribution of atomic energy to peace, health and prosperity throughout the world".

© IAEA, 1965

Permission to reproduce or translate the information contained in this publication may be obtained by writing to the International Atomic Energy Agency, Kärntner Ring 11, Vienna I, Austria.

Printed by the IAEA in Austria
July 1965

PROCEEDINGS SERIES

PHYSICS AND CHEMISTRY OF FISSION

PROCEEDINGS OF THE SYMPOSIUM ON
PHYSICS AND CHEMISTRY OF FISSION
HELD BY THE
INTERNATIONAL ATOMIC ENERGY AGENCY
IN SALZBURG, 22 - 26 MARCH 1965

In two volumes

VOL.I

INTERNATIONAL ATOMIC ENERGY AGENCY
VIENNA, 1965

Symposium on Physics and Chemistry of Fission,
Salzburg, 22 - 26 March 1965.
Proceedings . . . held by the International Atomic
Energy Agency . . . Vienna, the Agency, 1965.
2 vols. (IAEA Proceedings series)

539.173
541.28

PHYSICS AND CHEMISTRY OF FISSION
IAEA, VIENNA, 1965
STI/PUB/101

FOREWORD

In recognition of recent significant developments in nuclear fission, the International Atomic Energy Agency convened this first International Symposium on the Physics and Chemistry of Fission at Salzburg, Austria, from 22 to 26 March, 1965. Nearly 200 delegates from 29 countries and 5 international organizations participated in the Symposium in which all aspects of the fission process and its products were considered.

Each of the nine technical sessions of the Symposium was opened with a survey paper intended to provide an up-to-date picture of the current status of the session topic. Contributed original papers were then presented during the remainder of each session. The first two sessions were concerned with dynamics in the neighbourhood of the saddle point and the descent from saddle point to scission point, and the interpretation of angular distribution and fission cross-section data. The remaining seven sessions were concerned largely with experimental studies of post-scission phenomena. These sessions were marked by reports of truly impressive advances in new experimental techniques such as solid-state detectors in conjunction with ultra-fast time-of-flight and coincidence methods, on-line mass separators, detailed studies of nuclear gamma rays, X-rays and conversion electrons, and the increasing use of big computers for ever more elaborate (and, it is to be hoped, more accurate) data processing and analysis.

It was clear at the Salzburg Symposium that the long-standing gap between empirical knowledge and theoretical understanding of fission is still widening. The fission theorists nevertheless have welcomed this flood of new information as additional material for a systematic approach that must ultimately lead to fuller theoretical understanding of the process of nuclear fission.

EDITORIAL NOTE

The papers and discussions incorporated in the proceedings published by the International Atomic Energy Agency are edited by the Agency's editorial staff to the extent considered necessary for the reader's assistance. The views expressed and the general style adopted remain, however, the responsibility of the named authors or participants.

For the sake of speed of publication the present Proceedings have been printed by composition typing and photo-offset lithography. Within the limitations imposed by this method, every effort has been made to maintain a high editorial standard; in particular, the units and symbols employed are to the fullest practicable extent those standardized or recommended by the competent international scientific bodies.

The affiliations of authors are those given at the time of nomination.

The use in these Proceedings of particular designations of countries or territories does not imply any judgement by the Agency as to the legal status of such countries or territories, of their authorities and institutions or of the delimitation of their boundaries.

The mention of specific companies or of their products or brand-names does not imply any endorsement or recommendation on the part of the International Atomic Energy Agency.

CONTENTS

LOW-ENERGY FISSION - THEORY AND RELATED EXPERIMENTS
(Sessions I and II)

Review of fission theory (SM-60/1) (Review paper) 3
W.J. Swiatecki (United States of America)
On the role of the transition state nucleus in fission (SM-60/3) 11
J.R. Huizenga, J.P. Unik and B.D. Wilkins (United States of America)
Transition states at the fission barrier (SM-60/4)..... 23
J.J. Griffin (United States of America)
Discussion 37
Saddle-point rotational states from resonance fission of oriented nuclei (SM-60/5) 39
J.W.T. Dabbs, F.J. Walter and G.W. Parker (United States of America)
Effects of orbital angular momentum and target spin on fission anisotropy (SM-60/6) 51
R.B. Leachman and J. Gursky (United States of America)
Discussion 61
Channel analysis of neutron-induced fission of even-even isotopes near threshold (SM-60/7)..... 63
R.W. Lamphere (United States of America)
Discussion 76
A study of fission following (d, p) and (t, p) reactions in uranium isotopes (SM-60/21) 77
D. Eccleshall and M.J.L. Yates (United Kingdom)
Discussion 84
Nuclear fission as a Markov process (SM-60/9) (Abstract only)..... 85
R. Ramanna, R. Subramanian and R.N. Aiyer (India)
Discussion 86
Channel effects in the kinetic energy of fragments of fission induced by low-energy resonance neutrons (SM-60/10) 87
M.S. Moore and L.G. Miller (United States of America)
Discussion 101
Dependence of fission-fragment primary charge on nuclear structure (SM-60/11)..... 103
P. Armbruster (Federal Republic of Germany)
Discussion 119
Об оболочечных эффектах при делении ядер (SM-60/85) 121
Б.Т. Гейликман (СССР)
Об эффектах спаривания при делении четно-четного составного ядра вблизи порога (SM-60/90) 127
В.М. Струтинский и В.А. Павлинчук (СССР)

Фотоделение четно-четных ядер вблизи порога (SM-60/81) 135
Н.С.Работнов, Г.Н. Смиренкин, А.С. Солдатов и Л.Н. Усачев (ФЭИ), С.П. Капица и Ю.М. Ципенюк (ИФП, СССР)
Угловые распределения осколков деления Th^{230}, Pu^{238} и Am^{241} нейтронами (SM-60/88) 157
П.Е. Воротников, С.М. Дубровина, В.А. Шигин и Г.А. Отрощенко (СССР)
О делении деформированных ядер (SM-60/89) 171
В.М. Струтинский (СССР)

FISSION CROSS-SECTIONS, THRESHOLDS, RESONANCES
(Sessions II and III)

Cross-sections for low-energy neutron-induced fission (SM-60/12) (Review Paper) 187
E.R. Rae (United Kingdom)
Mesure et analyse de la section efficace de fission du plutonium-239 de O à 5 keV (SM-60/13) 205
G. de Saussure, J. Blons, C. Jousseaume, A. Michaudon et Y. Pranal (France)
Discussion 217
Measurement of fission cross-sections for neutrons of energies in the range 40-500 keV (SM-60/14) 219
P.H. White, J.C. Hodgkinson and G.C. Wall (United Kingdom)
Fission cross-section measurements on Pu^{239}, Pu^{241}, U^{232}, and a search for fission components in Pu^{238} resonances (SM-60/15) 235
G.D. James (United Kingdom)
Analyse de la section efficace de fission de l'uranium-233 pour des neutrons d'énergie comprise entre 1,7 eV et 30 eV (SM-60/16) 245
H. Nifenecker et G. Perrin (France)
Discussion 253
Fission cross-section measurement of U^{235} and Pu^{239} for low-energy neutrons (SM-60/17) 255
G. Fraysse and A. Prosdocimi (EURATOM)
Discussion 279
The fission cross-section of Pu^{240} for 0.03 - 2.0 MeV neutrons (SM-60/19) 281
M. De Vroey, A.T. Ferguson and N. Starfelt (United Kingdom)
Взаимодействие нейтронов с ядрами урана-235 в области энергий 0,002 ÷ 30 кэв (SM-60/86) 287
Ван Ши-ди, Ван Юн-чан, Е. Дерменджиев и Ю.В. Рябов (СССР)
Discussion 304
The excitation function and the isomeric yield ratio for the 14-ms fissioning isomer from deuteron irradiation of plutonium (SM-60/96) 307
G.N. Flerov, A.A. Pleve, S.M. Polikanov, E. Ivanov, N. Martalogu, D. Poenaru and N. Vîlcov (Romania)
Discussion 314

DISTRIBUTION OF MASS AND CHARGE IN FISSION (Sessions III and IV)

Mass and charge distribution in low-energy fission (SM-60/22) (Review Paper) 317
A. C. Wahl (United States of America)
Fission mass yield studies (SM-60/24) 333
G. P. Ford and R. B. Leachman (United States of America)
Symmetry of neutron-induced Pu^{239} fission in resonance region (SM-60/26) 347
G. Cowan, B. P. Bayhurst, R. J. Prestwood, J. S. Gilmore and G. W. Knobeloch (United States of America)
Some yields in the thermal- and epi-cadmium-neutron fission Pu^{239} (SM-60/27) 355
I. F. Croall and H. H. Willis (United Kingdom)
Discussion 367
General Discussion 368
Determination of the primary nuclear charge of fission fragments from their characteristics K-X-ray emission in spontaneous fission of Cf^{252} (SM-60/31) 369
L. E. Glendenin, J. P. Unik and H. C. Griffin (United States of America)
X-rays emitted in coincidence with the fission of Cf^{252} (SM-60/57) ... 385
T. D. Thomas, R. A. Atneosen, W. M. Gibson and M. L. Perlman (United States of America)
Discussion 399
Primary distribution of nuclear charge for fission-fragment masses 132, 134, 136 and 137 from thermal fission of U^{235} (SM-60/33) 401
E. Konecny, H. Opower, H. Gunther and H. Göbel (Federal Republic of Germany)
Fission yields of some isotopes in the fission of Th^{232} by reactor neutrons (SM-60/28) 415
A. Wyttenbach and H. R. von Gunten (Switzerland)
Mass and cumulative yields in near-symmetric fission of U^{235} with thermal neutrons. Part I. The 121-mass chain (SM-60/29) 423
H. V. Weiss and N. E. Ballou (United States of America)
Neutron-induced fission of actinium-227, protactinium-231 and neptunium-237: mass distribution (SM-60/30) 439
R. S. Iyer, H. C. Jain, M. N. Namboodiri, M. Rajagopalan Rajkishore, M. V. Ramaniah, C. L. Rao, N. Ravindran and H. D. Sharma (India)

DISTRIBUTION OF ENERGY IN FISSION (Sessions IV and V)

The energy release in low-energy fission (SM-60/34) (Review Paper) 451
J. S. Fraser (Canada)
Discussion 465
Thermal-neutron-induced fission of U^{235}, U^{233} and Pu^{239} (SM-60/36) .. 467
T. D. Thomas, W. M. Gibson and G. J. Safford (United States of America)
Discussion 479

Simultaneous measurements of flight times and energies of fission fragments (SM-60/35) 481
G. Andritsopoulos, T. Cornell and A.L. Rodgers (United Kingdom)
Discussion 489
Simultaneous velocity and energy measurement of fission fragments (SM-60/37) 491
W.E. Stein (United States of America)
Experiments with mass-spectroscopically separated fission product ions (SM-60/38) 505
H. Ewald, E. Konecny and H. Opower (Federal Republic of Germany)
Correlated fragment energy measurements and mass-versus-angle correlations in Ra^{226}+p fission (SM-60/39) 517
H.W. Schmitt, J.W.T. Dabbs and P.D. Miller (United States of America)
Discussion 528
Absolute energy calibration of solid-state detectors for fission fragments and heavy ions (SM-60/40) 531
H.W. Schmitt, W.M. Gibson, J.H. Neiler, F.J. Walter and T.D. Thomas (United States of America)
Discussion 545
Fission-fragment angular, energy, and mass division correlations for the U^{234} (d, pf) reaction (SM-60/25) 547
R. Vandenbosch, J.P. Unik and J.R. Huizenga (United States of America)
Discussion 558
Étude des spectres en masse des fragments de fission après émission neutronique prompte (SM-60/23) 561
C. Signarbieux et M. Ribrag (France)
Range and range dispersion of some fission products formed by the $Pu^{239}(n_{th}, f)$ reaction (SM-60/41) 573
H. Münzel, M. Hollstein and T. Ishimori (Federal Republic of Germany)
Discussion 584
Нейтроны и кинетическая энергия осколков при делении тяжелых ядер (SM-60/92) 587
В.Ф. Апалин, Ю.Н. Грицюк, И.Е. Кутиков, В.Е. Лебедев и Л.А. Микаэлян (СССР)
Discussion 598
Многопараметровые исследования осколков при делении ядер быстрыми нейтронами (SM-60/79) 601
П.П. Дьяченко и Б.Д. Кузьминов (СССР)
Discussion 609
Угловая анизотропия и ассиметрия масс осколков при делении Th^{232} нейтронами (SM-60/80) 611
Б.Д. Кузьминов и А.И. Сергачев (СССР)

APPLICATIONS OF NEW FISSION DATA TO NUCLEAR TECHNOLOGY
(Session V)

Fission data and nuclear technology (SM-60/50) (Review Paper)..... 621
G. C. Hanna (Canada)
Discussion 632

LOW-ENERGY FISSION – THEORY AND RELATED EXPERIMENTS

(Sessions I and II)

Review Paper

REVIEW OF FISSION THEORY

W.J. SWIATECKI
LAWRENCE RADIATION LABORATORY, UNIVERSITY OF CALIFORNIA,
BERKELEY, CALIF., UNITED STATES OF AMERICA

Abstract — Résumé — Аннотация — Resumen

REVIEW OF FISSION THEORY. A survey of the present state of fission theory is attempted. The basic requirements of a theory of a physical process are outlined and against this background the state of fission theory is summarized, with special emphasis on developments in the past few years. An attempt is made to bring out the most important outstanding problems to be settled by future experiments and theory.

ÉTUDE D'ENSEMBLE DE LA THÉORIE DE LA FISSION. Ce mémoire est une étude d'ensemble qui fait le point des travaux sur la théorie de la fission. L'auteur rappelle brièvement les conditions essentielles de toute théorie relative à un phénomène physique et fait un résumé de la théorie de la fission, en insistant spécialement sur les découvertes des dernières années. Il cherche à dégager les problèmes les plus importants qu'il faudrait résoudre par l'expérimentation et la théorie.

ОБЗОР ТЕОРИИ ДЕЛЕНИЯ ЧАСТИЦАМИ МАЛОЙ ЭНЕРГИИ. Предпринимается попытка составить обзор положения в области теории деления в настоящее время. Намечаются основные требования теории физического процесса, и на этой основе обобщается положение в области теории деления с особым упором на достижениях последних нескольких лет. Делается попытка наметить наиболее важные основные проблемы, которые предстоит решить в будущем теоретически и экспериментально.

ESTUDIO PANORAMICO DE LA TEORIA DE LA FISION. El author se propone estudiar panorámicamente el estado actual de la teoría de la fisión. Enuncia los requisitos fundamentales que ha de cumplir la teoría de un proceso físico y, sobre este fondo, expone brevemente la teoría de la fisión en su grado actual de desarrollo, destacando las novedades registradas en los últimos años. Procura señalar los principales problemas que ha de resolver la investigación experimental y teórica en el futuro.

I would like to review the dozen or so contributions to fission theory that have appeared in the past few years. The review will be based on the following scheme of fission models:

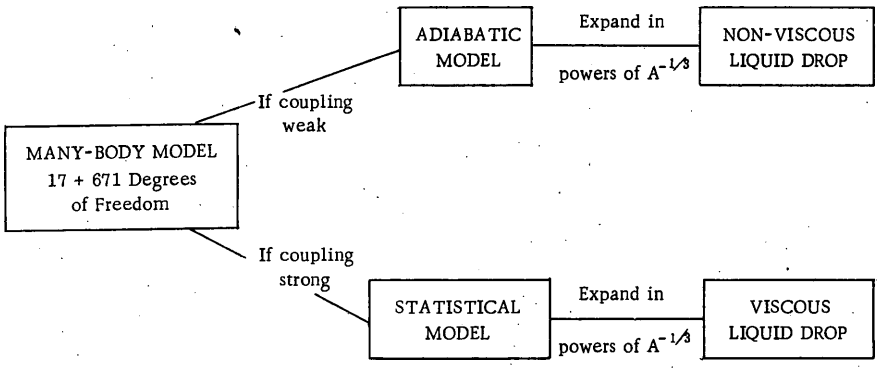

On the left is the many-body model. A complete description of all aspects of fission could be obtained, in principle, from this model, specified by the complete nuclear many-body Hamiltonian. The degrees of freedom in this model are those of the 236 particles constituting the uranium nucleus, say. This model is excellent in principle but useless in practice. It is uneconomical, for in discussing fission we are not interested in what all the 236 particles are doing, ($3 \times 236 = 708$ degrees of freedom) but only in the over-all collective deformation of the nucleus and the separation of the vibrating and rotating fragments. Counting up the number of degrees of freedom required to describe the separation of n rotating and vibrating fragments we find, in an elementary way, about (9n-1) as the required number. (Each fragment has 9 degrees of freedom: 3 translational, 3 rotational and 3 for a rough description of its extension in 3 dimensions. The "minus one" conserves the total volume of the n fragments.) For binary fission ($n = 2$) we thus find 17 as the number of collective degrees of freedom necessary for a description of fission.

Thus in constructing a practicable yet adequate model of fission we would select about 17 suitable collective degrees of freedom out of the 708 and treat them separately from the remaining 691 ($= 708-17$) "internal" degrees of freedom.

Two extreme assumptions have been made about the relation of the collective and internal degrees of freedom, namely that the coupling between them is weak or is strong. These two assumptions give rise to the two principal branches of fission models, the adiabatic models and the statistical models.

If further assumptions are introduced in either branch, of which the principal assumption is the smallness of the surface thickness compared to the nuclear radius (i.e. an expansion in powers of $A^{-1/3}$), we obtain the non-viscous and the viscous versions of the liquid drop model. (This classification of fission models brings out the fact that the liquid drop model is not to be regarded as opposed to either the statistical or adiabatic models, but, on the contrary, that it is a particularly simple version of these models and could be – I would say should be – used as a starting point for either.)

I would like to use this scheme of models as a background for discussing recent theoretical contributions to fission theory.

Let me begin by mentioning some contributions on the fundamental question whether, from first principles, one would expect the strong or weak coupling approximations to be more nearly correct. WILETS has discussed this in various publications [1, 2, 3]. It is a difficult problem and the conclusions are not clear-cut. At high excitation energies the strong-coupling, statistical approximation may be valid, but at low energies, partly because of the superfluidity of nuclear matter, the situation may be rather different. On superfluidity, the work of GRIFFIN [4] and GRIN [5] on the interpretation of angular distributions of fission fragments in low energy fission indeed points to the super-fluid nature of the saddle-point configuration for energies up to several MeV. In a recent note FONG has presented arguments for the statistical treatment [6].

Obviously the question is far from settled, and both the statistical and the adiabatic assumptions will probably continue to be explored in the future.

What has been done in a systematic way with either assumption? The most unambiguous progress is being made with the simplest version of these

models, the liquid drop model. Compared to a few years ago we are in the fortunate position of being clear about the essentials of the static deformation energy of a charged liquid drop. This has come about through the work of STRUTINSKIĬ, LYASHCHENKO and POPOV [7, 8] on the one hand, and COHEN and myself [9] on the other.

These calculations have also been extended in recent years by PIK-PICHAK [10], HISKES [11], CARLSON and PAO LU [12], SPERBER [13], MOLLENAUER and WHEELER [14], and COHEN, PLASIL and myself [15] to the case of a rotating drop. A fascinating aspect of these extensions is the direct connection that can be established between the nuclear equilibrium shapes and the classic astronomical shapes of rotating, gravitating masses studied in the past 300 years by NEWTON, JACOBI, POINCARÉ, LIAPOUNOFF, DARWIN, JEANS and many others [16]. Recently CHANDRASEKHAR [17] has come to the rescue of nuclear physicists and with his powerful methods of analysis has helped to clarify some of the intricate problems concerning the stability of rotating liquid systems.

The liquid drop model is now developing beyond the static stage. In the important work of NIX [18] a simplified version of the model has been developed to the point where the dynamics, statistical mechanics and certain aspects of quantum mechanics have been worked out from first principles and without adjustable constants. So far the theory has been worked out fairly completely only for the lighter fissionable elements, below about radium. It has been strikingly successful in accounting for the main features of the fission of these elements and for some, but not all, of the finer details.

The reason why corresponding progress has not been made for the heavier nuclei is that this involves the difficult problem of calculating the dynamics of the descent from saddle to scission (which for lighter nuclei is short and may be disregarded). Progress in this fundamental problem has been made since the early work of HILL and WHEELER [19], BUSINARO and GALLONE [20], and INGLIS [21]. Recently KELSON [22] and MIYATAKE [23] have studied the dynamics of the pinch-off of the neck in scission, but so far the results are fragmentary. A more limited but more systematic study is being made by Nix, who is working out the dynamics of the small oscillations of a liquid drop around its saddle-point shape for all values of the fissionability parameter.

Before leaving the subject of the pure liquid drop model I might mention that, although personally I am convinced that the statics of the deformation energy of a charged drop is now clear, it is my duty as reviewer to report that there are still some disagreements on the subject of the stability of the symmetric saddle-point shapes against asymmetry. A recent note by GALLONE, GARRIBBA and GHILARDOTTI [24] adds fuel to the controversy. Perhaps this conference will give us the chance to arrive at the truth (decribed in the 1963 paper of COHEN and myself [9]). Turning now to the group of calculations relying principally on the statistical assumption, there have been several recent calculations along the lines of Fong's original work in the 1950s. PIK-PICHAK and STRUTINSKIĬ have made several applications to the calculation of mass, charge and kinetic energy distributions in fission [25]. ERBA, FACCHINI, SAETTA-MENICHELLA, TONOLINI and TONOLINI-SEVERINI [26] have used this approach and believe they have explained the asymmetry of heavy element fission. ABDELMALEK and

STAVINSKIĬ [27] have also considered mass distributions, making use of an improved prescription for estimating the effect of shells on nuclear level densities.

I feel that the difficulty plaguing all these attempts is the ill-defined nature of the scission configuration, which plays a central role in the present formulations of the statistical model. The root of the trouble is that a scission configuration, unlike a saddle configuration, cannot be found from the potential energy alone (by making it stationary), but must be calculated by following in time the history of the descent from saddle to scission, and this is never done in the statistical treatments. The reason why it is never done is, I think, not because it is a difficult problem, but because it is apparently not realized that there is a problem at all. There appears to be a feeling that the statistical assumption makes it unnecessary to go through the saddle-to-scission calculation. I think this is wrong. On the contrary, I believe one of the outstanding problems in fission theory today is the working out of the saddle-to-scission stage both in the adiabatic and the statistical approximations. In the liquid drop idealization the former corresponds to the dynamical descent from saddle of a non-viscous drop and the latter to the descent of a viscous drop, i.e. the slow, creeping division of a honey-like drop.

The first step in a discussion of the dynamics of the saddle-to-scission stage is a discussion of the small normal modes of motion in the neighbourhood of the saddle. This really central problem is in the so-called channel analysis of fission described in several of the papers in this Session. The channel analysis may be regarded as the determination by experiment of the (quantized) normal modes of motion of the fissioning nucleus in the vicinity of the saddle. An example of a calculation of such normal modes from first principles is the determination of the small oscillations of a liquid drop around the saddle shape. Some of these modes, like the rotational modes and the stretching, bending, wriggling modes, may be found to correspond to some of the experimentally determined channels. Others, characterized by single-particle degrees of freedom, will require the working out of a more refined model than the liquid drop model. The clarification of the experimental information on the observed channels and the working out of the theory of the normal modes around the saddle shape seems to me to be a very central problem in fission theory, and a first step in the working out of the saddle-to-scission dynamics.

Let me now mention several recent considerations that do not qualify as well-defined fission models but that have been useful to a greater or lesser extent.

The series of papers by BRUNNER and PAUL [28] centre on certain correlations between fragment excitations, kinetic energies and mass yields. In the work of WILDERMUTH and FAISSNER [29] the empirical mass distributions are analysed into a number of components, some of them associated with magic numbers. The dumb-bell picture of Whetstone and Vladimirskii, discussed in Ref. [30], is a compact way of summarizing qualitatively certain experimental features associated with fragment excitations, kinetic energies and mass yields. It is partly equivalent to a similar summary based on imagining the fragments to be a pair of variously deformed tangent spheroids,

as discussed, for example, by VANDENBOSCH [31] and also by MILTON[32]. Such summaries are more or less direct experimental deductions of the sizes, shapes and separations of the fragments at scission, and we learn that there appears to be at least a qualitative correlation between these shapes and the magic numbers $Z = 50$, $N = 82$. The outstanding problem here is to make these considerations more quantitative. In the meantime an interesting confirmation of the correctness of the fragment shapes summarized in the dumbbell or two-spheroid pictures has come from the work of FRAENKEL and THOMPSON [33] on the long-range alpha particles in fission, especially the unexpected zig-zag behaviour of the angular distributions, paralleling the saw-tooth in the plot of the frequency of neutron emission versus fragment mass.

As regards the formulation of a theory of the long-range alpha particles some exploratory work has been done by HALPERN [34] and by GEILIKMAN and KHLEBNIKOV [35], especially on the motion of the alpha particle in the field of the fragments after it has been formed. But no theory of the formation of the alpha particles exists.

Let me now mention some theoretical work that has an indirect bearing on fission. The foundations of the liquid drop model have been discussed by STRUTINSKIĬ and TYAPIN [36], who also discuss corrections, in particular the curvature correction to the surface energy and the compressibility correction. (Quite recently STRUTINSKIĬ [37] has argued that the introduction of the curvature correction helps to interpret angular distribution experiments.) Other corrections to the liquid drop model, namely the surface symmetry correction and the correction for the diffuseness of the charge distribution [38] can, it turns out, be included without any extra labour by a trivial redefinition of the fissionability parameter x.

An understanding of the nature of the nuclear surface tension is essential for fission theory, and the recent thesis of HILF [39] is an important contribution in this direction.

Finally, a group of indirect contributions to fission theory are the several "new generation" mass formulae that are now appearing. They have in common their concern with the oscillations in the masses associated with shell effects. The mass formula of MYERS and myself [38, 40] claims to be, in fact, a semi-empirical theory of the nuclear deformability, and as such is of particular interest for fission. The formula may be used to predict fission barriers and the most startling application so far has been the estimate that if the magic numbers $Z = 126$, $N = 184$ exist then nuclei in that neighbourhood might have fission barriers as high as 10 MeV. This could make them sufficiently stable to be produced and studied, perhaps even by chemical methods.

Let me end my talk with a few reflections on the state of fission theory. My general impression is that our efforts are much too fragmented and unsystematic, and thoroughly inefficient. Figure 1 illustrates our way of doing fission theory. I believe that this is an historical anachronism, a legacy from the early days of nuclear physics when practically nothing was known about nuclear structure and no well-defined direction could be mapped out in advance. Today we have a broad understanding of nuclear physics and, I believe, a more direct and systematic approach is possible. I think we should produce today fewer ill-defined and rough estimates and suggestions

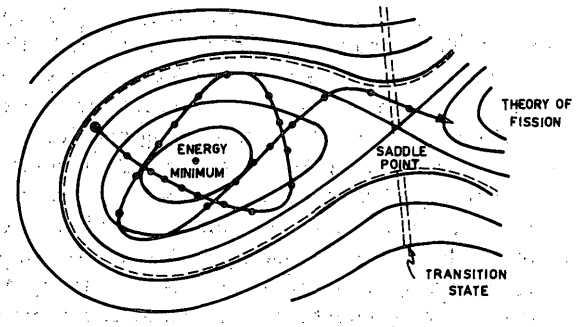

Fig. 1

Theory of fission

and settle down to working things out from first principles, in a thorough and definitive manner. We should also aim at a degree of uniformity between different workers in the field, so that different contributions can be more easily integrated into a single theoretical structure, and progress made step by step in well-defined stages.

On the question of what these steps should be I hope we shall find some answers in the discussions in this Symposium. I have given some thought to this question and my prescription centres on half a dozen stages, the first being the isolation of the relevant degrees of freedom and the writing down of the Hamiltonian function defining a model. This would then be followed by the working out of the potential and kinetic energy maps, the solution of the equations of motion and a discussion of the statistical mechanics. The final stage would be a comparison with experiment and an evaluation and modification of the model, followed by a re-cycling of the above steps. A more detailed description of these ideas would be outside the scope of this review talk, but I hope some of these points will be raised in our discussions.

To conclude, I would like to make an analogy between the development of fission theory and geographical exploration. I would say that in both cases there is a time for blazing trails in the wilderness and a time for building highways. I think we are at the stage in fission theory where we should be building a highway.

REFERENCES

[1] WILETS, L., Phys. Rev. 115 (1959) 372.

[2] WILETS, L., Proc. Int. Conf. on Nuclear Physics with Reactor Neutrons (THROW, F. E., Ed.), Argonne National Lab. (1963).

[3] WILETS, L., Theories of Nuclear Fission, Clarendon Press, Oxford, (1964).

[4] GRIFFIN, J.J., Phys. Rev. 132 (1963) 2204.

[5] GRIN, Yu. T., Ž. eksp. teor. Fiz. 43 (1962) 1880.

[6] FONG, P., Phys. Rev. 135 (1964) B1338.

[7] STRUTINSKIĬ, V.M., LYASHCHENKO, N. Ya. and POPOV, N. A. Ž. eksp. teor. Fiz. 43 (1962) 584; Nucl. Phys. 46 (1962) 639.

[8] STRUTINSKIĬ, V.M., Ž. eksp. teor. Fiz. 45 (1963) 1891; ibid. 45 (1963) 1900.
[9] COHEN, S. and SWIATECKI, W.J., Ann. Phys. 22 (1963) 406.
[10] PIK-PICHAK, G.A., Ž. eksp. teor. Fiz. 34 (1958) 341; ibid. 43 (1962) 1701.
[11] HISKES, J.R., The Liquid Drop Model of Fission: Equilibrium Configurations and Energetics of Uniform Rotating Charged Drops, Lawrence Radiation Lab. Report UCRL-9275 (1960) (unpublished).
[12] CARLSON, B.C. and PAO LU, Proc. Rutherford Jubilee Int. Conf. (BIRKS, J.B., Ed.) (1962) 291.
[13] SPERBER, D., Phys. Rev. 130 (1963) 468.
[14] MOLLENAUER, J. and WHEELER, J.A., private communication.
[15] COHEN, S., PLASIL, F. and SWIATECKI, W.J., Proc. Third Int. Conf. on Reactions between Complex Nuclei, (GHIRSO, A., DIAMOND, R.M. and CONZETT, H.E., Eds.) University of California Press, Berkeley (1963); also unpublished work.
[16] LYTTELTON, R.A., The Stability of Rotating Liquid Masses, Cambridge University Press, Cambridge, (1953).
[17] CHANDRASEKHAR, S., Astrophys. J. 136 (1963) 1048; also preprint, The Stability of a Rotating Liquid Drop (1964); Chandrasekhar and Rosenkilde, private communication, 1964.
[18] NIX, J.R., Studies in the Liquid Drop Theory of Nuclear Fission, Lawrence Radiation Lab. Report UCRL-11338 (1964). Also Nix, J.R. and Swiatecki, W.J., paper submitted to Nucl. Phys.
[19] HILL, D.L. and WHEELER, J.A., Phys. Rev. 89 (1953) 1102.
[20] BUSINARO, U.L. and GALLONE, S., Nuovo Cim. 1 (1955) 629.
[21] INGLIS, D.R., Ann. Phys. 5 (1958) 106.
[22] KELSON, I., Phys. Rev. 136 (1964) B1667.
[23] MIYATAKE, O., Mathematica jap. 9 (1964) 49.
[24] GALLONE, S., GARRIBBA, S. and GHILARDOTTI, G., unpublished manuscript (1965) to appear in Nuovo Cim.
[25] PIK-PICHAK, G.A. and STRUTINSKIĬ, V.M., "Statistical Theory of Fission", Fizika Deleniya Atomnykh Yader (PERFILOV, N.A. and EISMONT, V.P. Eds.) Moscow (1962).
[26] ERBA, E., FACCHINI, U., SAETTA-MENICHELLA, E., TONOLINI, F. and TONOLINI-SEVERINI, L., Phys. Lett. 6 (1963) 294.
[27] ABDELMALEK, N.N. and STAVINSKIĬ, V.S., Nucl. Phys. 58 (1964) 601.
[28] BRUNNER, W. and PAUL, H., Z. Naturf. 150 (1960) 1018, 1109; Ann. Phys.; Lpz. 6 (1960) 267; ibid. 7 (1961) 326; ibid 7 (1961) 333, 146.
[29] FAISSNER, H. and WILDERMUTH, K., Nucl. Phys. 58 (1964) 177.
[30] HALPERN, I., Ann. Rev. nucl. Sci. 9 (1959) 245.
[31] VANDENBOSCH, R., Nucl. Phys. 46 (1963) 129.
[32] MILTON, J.C.D., unpublished work.
[33] FRAENKEL, Z. and THOMPSON, S.G., Phys. Rev. Lett. 13 (1964) 438.
[34] HALPERN, I., CERN preprint, Geneva (1963).
[35] GEILIKMAN, B.T. and KHLEBNIKOV, G.I., preprint, Moscow (1964) (Nucl. Sci. Abstr. 18 (1964) 42652).
[36] STRUTINSKIĬ, V.M. and TYAPIN, A.S., Ž. eksp. teor. Fiz. 45 (1963) 960.
[37] STRUTINSKIĬ, V.M., preprint, Moscow (1964).
[38] SWIATECKI, W.J., Proc. Second Int. Conf. on Nuclidic Masses (JOHNSON, W.H., Ed.) Vienna (1963).
[39] HILF, E. (Thesis), Institute for Theoretical Physics, Frankfurt/Main (1963).
[40] MYERS, W.D. and SWIATECKI, W.J., Nuclear Masses and Deformations, Lawrence Radiation Laboratory Report UCRL-11980 (1965, in press).

ON THE ROLE OF THE TRANSITION STATE NUCLEUS IN FISSION*

J. R. HUIZENGA**, J. P. UNIK AND B. D. WILKINS
ARGONNE NATIONAL LABORATORY, ARGONNE, ILL.,
UNITED STATES OF AMERICA

Abstract — Résumé — Аннотация — Resumen

ON THE ROLE OF THE TRANSITION STATE NUCLEUS IN FISSION. Although it is well-known that heavy nuclei decay by spontaneous fission, the lifetime for this process is very long compared to nuclear decay times. In order for fission to compete favourably with gamma-ray and neutron emission, a fixed amount of energy, equivalent to an activation energy in a chemical reaction, must be supplied to the heavy nucleus. This energy (often referred to as the fission threshold) is approximately 5 to 6 MeV for U^{238}, and is the minimum energy required to produce the deformed transition state nucleus (zero internal excitation energy). In the process of stretching the original nucleus into the transition state nucleus (whose distortion is sometimes described as the saddle-point deformation), the increase in energy due to the short-range nuclear forces (surface tension) is greater than the decrease in energy due to the long-range Coulomb forces. However, as the particular distortion defining the transition state nucleus is approached, the decrease in Coulomb energy becomes equal to the increase in surface energy. The degree of distortion needed to produce the transition state nucleus is a function of several nuclear parameters and, hence, the saddle shape and threshold energy for fission change markedly for different nuclei. Since a large fraction of the excitation energy of the initial compound nucleus is consumed in deformation energy in passing to the fission saddle point, the transition state nucleus is thermodynamically "cold". Hence, for low excitation energies where the non-fission degrees of freedom favour the passage of the barrier with only a small kinetic energy, it seems reasonable to postulate that the traversal time of the saddle or the lifetime of the transition state nucleus is many orders of magnitude longer than the characteristic nuclear time. This leads to the prediction that the highly deformed transition state nucleus will have properties, including a spectrum of excited states, analogous to those of normal nuclei. Information on highly deformed transition state nuclei obtained by fission-fragment angular distribution studies will be discussed. The $(\alpha, \alpha' f)$ reaction, which is very important for the study of even-even transition state nuclei, will be stressed.

RÔLE DU NOYAU CRITIQUE DANS LA FISSION. On sait que des noyaux lourds se désintègrent par fission spontanée; cependant, la durée de ce processus est très longue si on la compare à celles des processus de désintégration nucléaire. Si l'on veut que la fission ait des effets comparables à ceux des émissions de photons et de neutrons, il faut fournir au noyau lourd une quantité d'énergie déterminée équivalant à l'énergie d'activation d'une réaction chimique. Cette énergie (souvent désignée par l'expression «seuil de fission», est d'environ 5 à 6 MeV pour ^{238}U; elle représente le minimum d'énergie nécessaire pour produire le noyau critique déformé (énergie d'excitation interne nulle). Lors de l'allongement du noyau primitif et de la formation du noyau critique (dont la déformation est quelquefois décrite comme un étranglement), l'accroissement d'énergie dû aux forces nucléaires de faible portée (tension superficielle) est plus grand que la diminution d'énergie due aux forces coulombiennes de grande portée. Cependant, à mesure que se produit la déformation qui définit le noyau critique, la diminution de l'énergie coulombienne devient égale à l'accroissement de l'énergie superficielle. Le degré de déformation nécessaire pour produire le noyau critique est fonction de plusieurs paramètres du noyau; de ce fait, la forme de l'étranglement et le seuil de fission varient considérablement d'un noyau à l'autre. Etant donné qu'une grande partie de l'énergie d'excitation du noyau composé initial est consommée sous forme d'énergie de déformation lorsque l'étranglement se produit, le noyau critique est «froid» du point de vue thermodynamique. En conséquence, dans les cas de faibles énergies d'excitation où les degrés de liberté de la «non-fission» favorisent le passage de la barrière avec une faible énergie

* Based on work performed under the auspices of the United States Atomic Energy Commission.

** Currently a Guggenheim Fellow at the Laboratoire Joliot-Curie, Université de Paris, Orsay (S.& O.), France.

cinétique seulement, il semble raisonnable d'admettre que la durée de l'étranglement - ou la durée de vie du noyau critique - est plus longue de plusieurs ordres de grandeur que le temps de transit nucléaire. Ce fait permet de prévoir que le noyau critique fortement déformé aura des propriétés - notamment un spectre des états excités - analogues à celles des noyaux normaux. Les auteurs étudient des données sur les noyaux critiques fortement déformés qui ont été obtenues dans des études sur la distribution angulaire des fragments de fission. Ils insistent particulièrement sur la réaction $(\alpha, \alpha' f)$, qui est très importante pour l'étude des noyaux critiques pairs-pairs.

О РОЛИ ЯДРА В ПЕРЕХОДНОМ СОСТОЯНИИ ПРИ ДЕЛЕНИИ. Хотя хорошо известно, что тяжелые ядра распадаются в результате спонтанного деления, продолжительность этого процесса очень велика по сравнению со временем ядерного распада. Для того, чтобы процесс деления благоприятно конкурировал с процессом испускания гамма-лучей и нейтронов, необходимо сообщить тяжелым ядрам определенное количество энергии, эквивалентное энергии активации при химической реакции. Величина такой энергии (часто именуемая порогом деления) составляет приблизительно 5—6 Мэв для урана-238 и является минимально необходимой для образования деформированного ядра в переходном состоянии (с нулевой энергией внутреннего возбуждения). В процессе вытягивания первоначального ядра в ядро переходного состояния (деформация которого иногда описывается как деформация в седловой точке) увеличение энергии под действием ядерных сил с небольшим диапазоном действия (поверхностное напряжение) больше, чем уменьшение энергии благодаря кулоновским силам с большим радиусом действия. Однако по мере приближения к определенной деформации, характеризующей ядро в переходном состоянии, уменьшение кулоновской энергии становится равным увеличению поверхностной энергии. Степень деформации, необходимой для образования ядра в переходном состоянии, представляет собой функцию нескольких ядерных параметров, и, таким образом, у различных ядер форма седловины и пороговая энергия деления значительно изменяются. Поскольку большая доля энергии возбуждения первоначального составного ядра переходит в энергию деформации при прохождении к седловой точке деления, ядро в переходном состоянии является термодинамически "холодным". Таким образом, при низких значениях энергии возбуждения, когда степени свободы в условиях отсутствия деления благоприятствуют прохождению барьера только при небольшой кинетической энергии, представляется разумным утверждать, что время прохождения через седловину или период жизни ядра в переходном состоянии составляет величину на много порядков больше, чем характеристическое ядерное время. Это приводит к предположению о том, что сильно деформированное ядро в переходном состоянии будет обладать свойствами, аналогичными свойствам обычных ядер, в том числе в отношении спектра возбужденных состояний. Будет обсуждена информация относительно сильно деформированных ядер в переходном состоянии, полученная при исследовании углового распределения осколков деления. Упор будет сделан на реакцию $(\alpha, \alpha' f)$, которая имеет очень важное значение для изучения четно-четных ядер в переходном состоянии.

ACERCA DE LA FUNCION DEL NUCLEO DE TRANSICION EN LA FISION. Si bien es sabido que los núcleos pesados pueden desintegrarse por fisión espontánea, la duración de este proceso es muy larga en comparación con los tiempos de desintegración nuclear. Para que la fisión pueda competir favorablemente con la emisión de rayos gamma y de neutrones, es preciso suministrar al núcleo pesado una cantidad fija de energía, equivalente a la energía de activación de una reacción química. Esta energía (que se suele denominar umbral de fisión) es de unos 5 ó 6 MeV en el caso del ^{238}U, y constituye la energía mínima requerida para producir el núcleo de transición deformado (energía nula de excitación interna). En el proceso de estiramiento del núcleo original para formar el núcleo de transición (cuya distorsión se denomina a veces deformación de estrangulación), el aumento de energía debido a las fuerzas nucleares de corto alcance (tensión superficial) es mayor que la disminución de energía debida a las fuerzas coulombianas de largo alcance. Sin embargo, a medida que nos vamos aproximando a la distorsión particular que define el núcleo de transición, la disminución de la energía coulombiana se hace igual al aumento de la energía superficial. El grado de distorsión necesario para producir el núcleo de transición es función de varios parámetros nucleares y, por consiguiente, la configuración de estrangulación y la energía umbral de fisión varían sensiblemente de un núcleo a otro. Como gran parte de la energía de excitación del núcleo inicial compuesto se consume como energía de deformación al pasar a la estrangulación de fisión, el núcleo de transición es termodinámicamente "frío". Por consiguiente, en el caso de las bajas energías de excitación, en que los grados de libertad sin fisión favorecen el paso de la barrera con una energía cinética reducida, parece razonable postular que el tiempo de transición de la estrangulación o la duración del núcleo de transición supera en muchos órdenes de magnitud al tiempo nuclear caracte-

rístico. Esto permite predecir que el núcleo de transición fuertemente deformado poseerá propiedades, inclusive un espectro de estados excitados, análogas a las de los núcleos normales. Se examinan datos sobre núcleos de transición fuertemente deformados, obtenidos por análisis de la distribución angular de fragmentos de fisión. Se considera en particular la reacción $(\alpha,\alpha'f)$, tan importante para el estudio de los núcleos de transición.

INTRODUCTION

The mechanism of nuclear fission was first described in detail in a classic paper by BOHR and WHEELER [1]. On the basis of a liquid drop model of the nucleus they developed a fission theory that gives a satisfactory picture of many aspects of nuclear fission. For the heaviest group of nuclei the repulsion of the long-range electrical Coulombic forces cancels to a large extent the short-range nuclear forces that act in a manner analogous to a surface tension. However, in order for fission to compete favourably with gamma-ray and neutron emission, a fixed amount of energy, equivalent to an activation energy in a chemical reaction, must be supplied to a heavy nucleus. This energy (often referred to as the fission threshold) is approximately 5 to 6 MeV for U^{238}, and is the minimum energy required to produce the deformed transition state nucleus (zero interval excitation energy). As the particular distortion defining the transition state nucleus is approached, the decrease in Coulomb energy becomes equal to the increase in surface energy. The degree of distortion needed to produce the transition state nucleus is a function of several nuclear parameters and, hence, the saddle shape and threshold energy for fission change markedly for different nuclei. A nucleus possessing an excitation energy that only slightly exceeds the fission barrier will result in a transition state nucleus that is thermodynamically "cold" [2]. This highly deformed transition state nucleus is expected to have properties including a spectrum of excited states analogous to those of a normal nucleus.

Information on the nuclear states at the stretched saddle configuration can be derived from fission-fragment angular distributions. From the excitation energy dependence of the angular distributions it is possible to characterize the saddle states in terms of their energies and quantum numbers I and K. A number of such states have been identified experimentally in (n, f) [3] and (d, pf) [4, 5] reactions. Both of these reactions can be used to produce transition state nuclei at excitation energies that are precisely known. However, for studies of even-even transition state nuclei, these reactions have the shortcoming of smearing out the angular momentum direction due to the finite spin of the odd-A target nucleus. In addition, most of the even-even nuclei produced by neutron capture have an excitation energy that far exceeds the fission threshold and eliminates the possibility of studying the low-lying saddle states. In this report we wish to stress that the $(\alpha,\alpha'f)$ reaction is an important method for investigating the saddle or transition states in an even-even nucleus since for this case both the projectile and target have spin zero [6]. Preliminary results obtained for the U^{238} $(\alpha,\alpha'f)$ reaction will be described and their interpretation discussed briefly.

EXPERIMENTAL METHOD AND RESULTS

The present experiment was carried out with a depleted U^{238} target bombarded with an external beam of 43-MeV helium ions accelerated in the Argonne 60-in fixed frequency cyclotron. The angular correlation between the coincident scattered alpha particles and fission fragments was measured for two fixed angles of the α' detector, 45° and 60° to the beam direction. A schematic diagram of the experimental arrangement is shown in Fig. 1. An Argonne multiparameter analyser [7] was used to record three bits of information for each coincident event: (1) the scattered alpha-particle (α') energy, (2) the fission-fragment energy and (3) the time delay between the coincident α' and fission fragment.

Gold-surface barrier semi-conductor detectors were used for both the α' and fission-fragment detectors. The α' detector was shielded from fission fragments by a thin absorber foil. The circular α' and fission-fragment detectors subtended angles of 13° and 16° respectively. The experimental resolution (including beam-energy resolution, gain stability and kinetic energy dispersion introduced by the large counter angles) observed for elastically scattered alpha particles was 350 keV. By recording the time spectrum obtained with a time-to-pulse-height converter, pulses from different RF cycles could be discerned, enabling one to unfold the true events from the chance events.

From the measured α' energy and the reaction kinematics, the nuclear excitation energy, E*, is readily calculated. With the α' detector fixed at either 45° or 60°, the maximum coincidence rate for an α' energy bin corresponding to an excitation energy of 5.6 to 6.2 MeV in the excited U^{238} nucleus coincided in angle, to within ±2°, with the inelastic recoil axis, θ_R. The angular distribution of fission events in this energy bin is shown in Fig. 2a where θ_{sym} is equal to the recoil direction θ_R. The experimental points, shown as circles with statistical errors, have been corrected for the finite solid angle of the detectors. The differential cross-section decreases very rapidly as the fission counter is moved away from the recoil direction. The experimental 0° to 90° anisotropy is 7. The fission-fragment angular distribution is symmetric around the angle $(\theta - \theta_R) = 90°$ in the centre of mass system.

The fission-fragment angular distribution for an α' energy bin corresponding to an excitation energy of 6.2 to 7.1 MeV in the excited U^{238} nucleus is shown in Fig. 2b. This distribution is very different from that shown in Fig. 2a, and shows a general filling-in of the intensity for intermediate angles around 45°.

The coincident inelastic alpha-particle spectra taken concurrently with the α' detector at 45°, and the fission fragment detectors parallel and perpendicular to θ_R, are shown in Fig. 3a. A value of 5.6 ± 0.2 MeV was obtained for the fission threshold, E_f, as defined by NORTHROP et al. [8]. The 0° to 90° anisotropy with respect to the recoil axis is shown as a function of the α' energy in Fig. 3b. In this figure the two points with an anisotropy of 7 are associated with an excitation energy bin 5.6 to 6.2 MeV, the same energy bin for which the full angular distribution was given in Fig. 2a. With increasing excitation energy (or decreasing α' energy) the anisotropy decreases rapidly with a small amount of structure appearing.

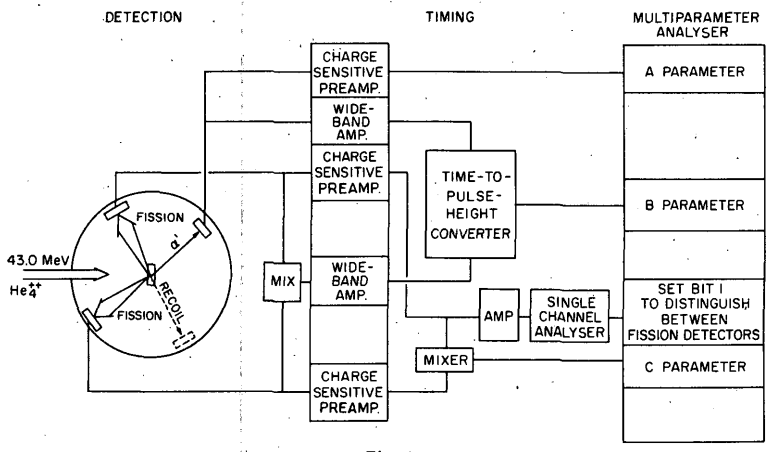

Fig. 1

Schematic diagram of counter arrangement and electronics used in the U^{238} $(\alpha, \alpha' f)$ experiment.

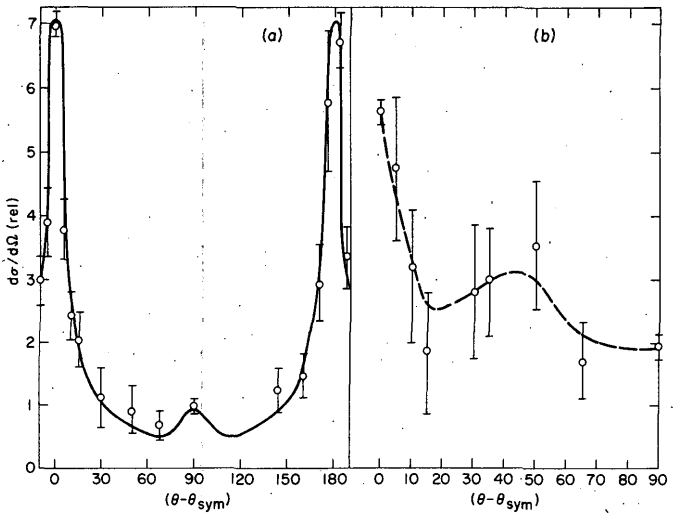

Fig. 2a

Angular distribution of fission events passing through channels within 600 keV of fission threshold. The solid curve represents an empirical fit to the data using Eq. (3) as discussed in text.

Fig. 2b

Angular distribution of fission events with $(E^* - E_f)$ from 600 to 1500 keV. The dashed curve is drawn only to emphasize the trend of the data.

THEORETICAL PREDICTIONS ABOUT THE LOW-LYING STATES OF AN EVEN-EVEN TRANSITION NUCLEUS

According to the BOHR [2] postulate, the lowest energy state of the highly deformed transition state nucleus is expected to have quantum numbers

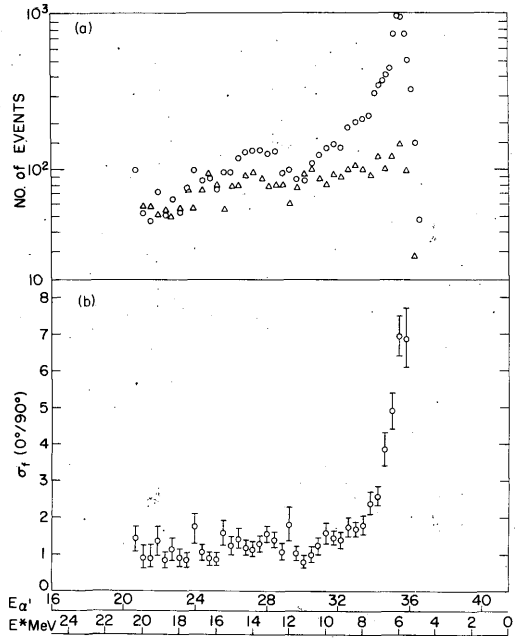

Fig. 3a

Coincident alpha-particles spectrum at 45° with the fission-fragment detector parallel (open circles) and perpendicular (triangles) to θ_R

Fig. 3b

The 0° to 90° anisotropy with respect to θ_R shown as a function of excitation energy

I = 0+, K = 0 analogous to the less deformed ground state. It is this state that defines the amount of energy required to produce the transition state nucleus. Built upon this state one expects to observe collective rotational states with energy,

$$E_R(I) = \hbar^2 I(I+1)/2\mathcal{I}_{\perp,\text{saddle}} \quad (I = 0, 2, 4, 6---), \qquad (I)$$

where $h^2/2\mathcal{I}_{\perp,\text{saddle}}$ is calculated for a rigid body from liquid drop theory [9] to be approximately 2 keV for U^{238}. Hence, the rotational levels in the transition state nucleus are predicted to be more closely spaced than the comparable ground state band that has a value of $h^2/2\mathcal{I}_{\perp}$ of about 7 keV.

Although the energies of other bands of collective levels of the transition state nucleus in the first one or two MeV of the excitation spectrum are not known, qualitative predictions can be made from analogy to less deformed nuclei. The K = 0, I = 1−, 3−, 5−.... band is expected to lie in the first MeV of the excitation spectrum. These odd parity states with K = 0 have been observed for a number of heavy nuclei in their equilibrium deformation at energies of less than 1 MeV. These odd parity states have been assigned to a pear-shaped vibration in which material sloshes back and forth from one end of the extended form to the other. The difference in vibrational energy

between this odd parity band and the lowest lying K = 0, even parity band at the saddle deformation is unknown but presumably lies somewhere within a few hundred keV [10].

The elongated transition state spectrum is also expected to have low-lying levels built on a bending vibration $\hbar\omega_{bending}$ like the bending vibration of a linear molecule. The bending vibration channel will couple with collective rotation to give a band of states with K = 1 and spins and parities of 1−, 2−, 3−, 4− etc. The energy of the bending vibration (above the threshold) is again unknown but the frequency of this mode can be expected [10] to have dropped considerably for the stretched saddle configuration and must be considered a likely contributor to the low-lying excitation energy spectrum of the transition state nucleus.

The energy spectra of normal even-even heavy nuclei contain a level designated as a "γ-vibration" at an excitation energy of $\hbar\omega_\gamma \approx 1$ MeV. It describes a collective rotation with K = 2 units of angular momentum about the axis of extension. Collective rotations can be superimposed on a γ-vibration giving a band with K = 2 and I = 2+, 3+, 4+.... The energy of this band at the saddle configuration is expected to be higher than observed for normal nuclei [10]. The circumference of a circle perpendicular to the elongated axis is less, reducing the average wavelength of waves of rotatory vibration, and the moment of inertia defined by the two short axes is less for the saddle deformation. Both of these factors lead to an increase in energy of the γ-vibrational level in the transition state nucleus.

Hence, the expected low-lying channels [10] of an even-even nucleus at the saddle deformation are the K = 0, I = 0+, 2+, 4+.....band, and several bands with one quantum of vibration, namely, the K = 0, I = 1−, 3−, 5− .... sloshing mode band, the K = 1, I = 1−, 2−, 3−, 4− ... bending mode band, and the K = 2, I = 2+, 3+, 4+ ... gamma band (see Fig. 4). Note should be made of the fact that the band built on the beta vibrational level, well-known for normal heavy even-even nuclei, is missing from the above list of saddle excitations. At the saddle configuration the restoring force constant associated with the beta vibrational mode is no longer positive, but negative. This is therefore the fission mode and does not contribute to the count of channels.

In the preceding discussion we have assumed a macroscopic description of the beta vibrational levels, and one should not on this basis completely rule out all possibility of any excited K = 0 band at the saddle. Since the presence or absence of such levels at the saddle have interesting implications about nuclear structure, one should be on the lookout for them. In a similar spirit, a nuclear model with pairing correlations may not necessarily predict the K = 2 band to lie at a higher energy for the highly deformed saddle configuration. Again, an experimental measurement of this energy is needed. It should also be mentioned that the low-lying levels above the threshold for an odd-A transition state nucleus will be radically different from those in an even-even nucleus. In the odd-A nucleus, intrinsic excitations with collective rotational bands built upon them are expected to play a major role in fission immediately above the threshold. In the heavy element (transuranic) region, single-particle (or hole) states are observed to have an average spacing of about 250 keV for the normal equilibrium shape nuclei

[11]. Therefore, if one assumes a comparable spacing between intrinsic states in the transition state nucleus, one expects a new band of levels with a particular K value to appear on the average with every additional 250 keV of excitation energy.

DISCUSSION OF EXPERIMENTAL RESULTS

With our present α' energy resolution, rotational members of the same K band are unresolvable. However, it may be possible to resolve different K bands. With this in mind the present experimental results were analysed in terms of excitation energy, and particular emphasis is given to an energy bin 0 to 600 keV above the fission threshold. With the α' detector fixed at either 45° or 60°, the maximum coincidence rate for an energy bin corresponding to 5.6–6.2 MeV of excitation energy in the originally excited U^{238} nucleus (or an excitation energy of 0 to 60 keV in the transition state nucleus) coincided in angle, to within ±2°, with the theoretical inelastic recoil axis θ_R. This result is interpreted to mean that the angular momentum symmetry axis is identical to the theoretical inelastic recoil axis for α' angles studied in this work. Throughout this report the two angles, θ_{sym} and θ_R, are assumed identical. The theoretical inelastic recoil axis (plane-wave Born approximation) for the above α' energy bin differs from the elastic (adiabatic) recoil axis by 4 to 5 degrees.

The population of various fissioning channels with different I and K, and the orientation of the I values with respect to the symmetry axis θ_R, are dependent on the nuclear reaction mechanism. In addition to these complexities, barrier penetration may affect the relative weights of different channels near threshold. To date, the details of the reaction mechanism and the barrier penetrability are not completely understood. However, various features of the angular distribution can be interpreted in a qualitative manner.

The differential fission cross-section at a given angle θ is given in general by [10]

$$W_{KM}^{I}(\theta) \propto |D_{MK}^{I}(\varphi, \theta, \gamma)|^2, \tag{2}$$

where $D_{MK}^{I}(\varphi, \theta, \gamma)$ are the symmetrical top wave functions. For the case M and K = 0 the differential cross-section reduces to

$$W(\theta) \propto \sum_{I} (2I+1) b_I |P_I(\theta)|^2, \tag{3}$$

where b_I is the relative probability of fissioning through a specific I state.

The angular distribution of fission events passing through channels within 600 keV of threshold is shown in Fig. 2a. The large experimental 0° to 90° anisotropy of 7 is characteristic of fission through levels where K = 0 and $M \ll I$. Since the exact form of b_I for this $(\alpha, \alpha' f)$ reaction is not known, we have attempted to fit empirically the data using various functional forms for b_I. The solid curve in Fig. 2a shows one of these empirical fits to the data using Eq. (3) with $b_I = e^{-(I/7)^2}$ and summing over only even values of I.

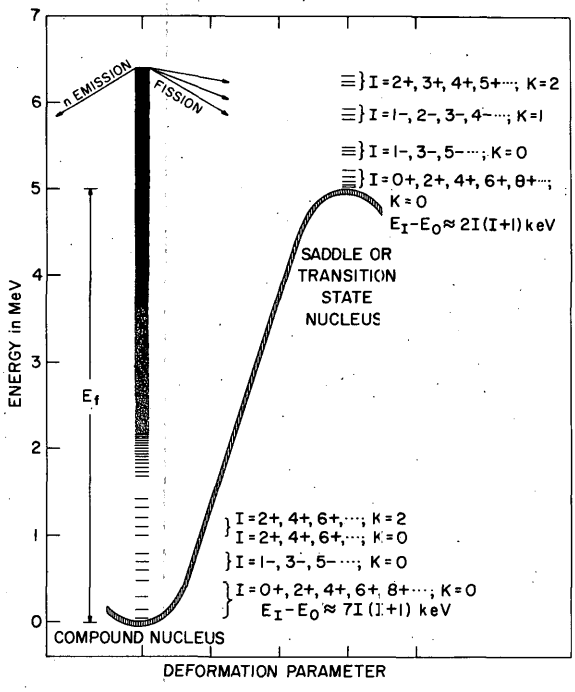

Fig. 4

Schematic representation of the levels of an even-even compound nucleus and transition state nucleus.
The low energy levels illustrated in the transition state nucleus are collective excitations.
At an energy approximately $2\theta_0$ (where $2\theta_0$ is the pairing energy) above threshold, quasiparticle excitations become possible.
At excitation energies producing fission the levels in the compound nucleus are very closely spaced (~1 eV) whereas the levels in the transition state nucleus more nearly compare to the levels in the compound nucleus with energy only slightly exceeding the ground state.

Here we have implicitly assumed M = 0. The theoretical values of $W(\theta)$ (given in Fig. 5 as W(K, I) where $b_I = 1$) for M = K = 0 and various values of I are shown in Fig. 5. Zero degrees on the abscissa corresponds to the direction of the angular momentum symmetry axis, which in the present experiment is identical to the inelastic recoil axis, θ_R. Each curve is normalized such that $\int_{-1}^{1} W(K, I)d(\cos\theta) = 1$, hence the independent angular contributions of several fissioning states can be combined if the factor b_I in Eq. (3) is known.

In Figs. 6 and 7, plots similar to those in Fig. 5 are shown with M = 0. However, in Fig. 6, K = 1, and in Fig. 7, K = 2. The striking feature of all these plots is the sharp reduction of cross-section for small angles, and the large enhancement of cross-section for intermediate angles. Since these figures are symmetric in M and K, the same curves result for K = 0, M = 1, and K = 0, M = 2.

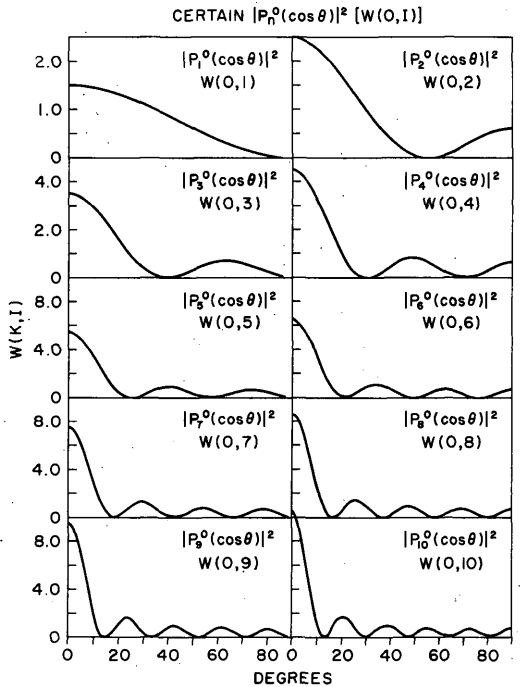

Fig. 5

Square of Legendre polynomials normalized such that $\int_{-1}^{1} W_I^K d(\cos\theta) = 1$.

If the angular momentum I lies with equal probability in all directions in the plane perpendicular to the axis of quantization (M = 0), and fission is occurring through states with K = 0 only, the curves in this figure give the fission-fragment angular distributions measured relative to the axis of quantization for various values of I.

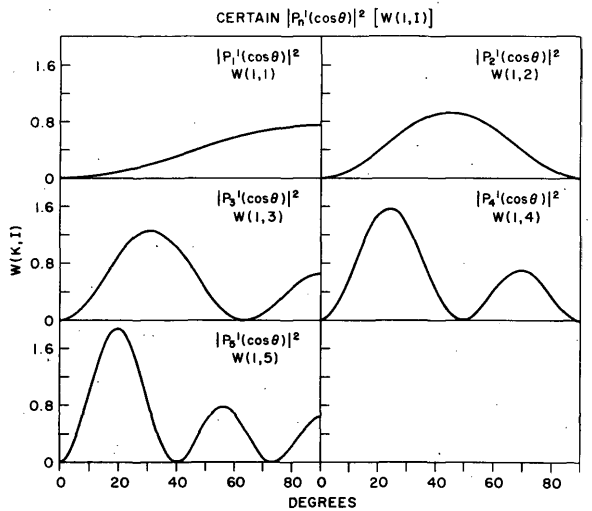

Fig. 6

Square of Legendre polynomials normalized such that $\int_{-1}^{1} W_I^K d(\cos\theta) = 1$.

If the angular momentum I lies with equal probability in all directions in the plane perpendicular to the axis of quantization (M = 0), and fission is occurring through states with K = 1 only, the curves in this figure give the fission-fragment angular distributions measured relative to the axis of quantization for various values of I.

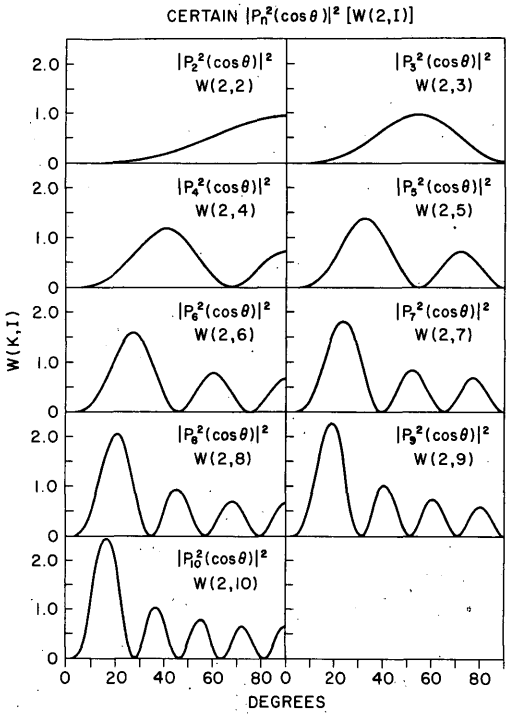

Fig. 7

Square of Legendre polynomials normalized such that $\int_{-1}^{1} W_I^K \, d(\cos\theta) = 1$.
If the angular momentum I lies with equal probability in all directions
in the plane perpendicular to the axis of quantization (M = 0),
and fission is occurring through states with K = 2 only,
the curves in this figure give the fission-fragment angular distributions
measured relative to the axis of quantization for various values of I.

The experimental fission-fragment angular distribution for fission events within 600 keV of the U^{238} transition state nucleus indicates that these saddle states have K = 0, and, in addition, that the nuclear reaction mechanism leaves the excited U^{238} recoil nucleus (which eventually fissions) with an aligned angular momentum symmetry axis θ_R on which the projection $M \ll I$. Hence, this type of experiment may be significant not only for fission studies but also for reaction mechanism studies.

Although the opening of the neutron channels may slightly fractionate the angular momentum distribution, the large reduction in anisotropy at $(E^* - E_f)$ of approximately 600 keV (see Fig. 3b) is most probably associated with the opening of one or more new K channels. The fission-fragment angular distribution of events with $(E^* - E_f)$ from 600 to 1500 keV is plotted in Fig. 2b. This curve differs from the angular distribution near threshold in that there is a general filling-in of the intermediate angles around 45°. If one considers channel analysis of fission, this filling-in is entirely consistent with the opening of one or more $K \neq 0$ bands.

The general increase in the anisotropy around E* of 13 MeV, seen in Fig. 3b, corresponds to the opening of the $(\alpha, \alpha' nf)$ channel. The fissioning nucleus is now of odd-A type and the forward peaking may indicate the presence of a $K = 1/2$ band.

Great interest exists in the identification of the quasi-particle threshold at the saddle deformation. While such information can be obtained from experiments of this type, the statistical uncertainties of the data reported here are too large for a significant measure of this quantity.

REFERENCES

[1] BOHR, N. and WHEELER, J. A., Phys. Rev. 56 (1939) 426.
[2] BOHR, A., Proc. UN Int. Conf. PUAE 2 (1956) 151.
[3] LAMPHERE, R. W., Nucl. Phys. 38 (1962) 561.
[4] BRITT, H. C., STOKES, R. C., GIBBS, W. R. and GRIFFIN, J. J., Phys. Rev. Lett. 11 (1963) 343.
[5] VANDENBOSCH, R., UNIK, J. P., HUIZENGA, J. R. and WILKINS, B. D., Bull. Amer. phys. Soc. 9 (1964) 422.
[6] WILKINS, B. D., UNIK, J. P. and HUIZENGA, J. R., Phys. Lett. 12 (1964) 243.
[7] ROCKWOOD, C. and STRAUSS, M., Rev. sci. Instrum. 32 (1961) 1211.
[8] NORTHROP, J. A., STOKES, R. H. and BOYER, K., Phys. Rev. 115 (1959) 1277.
[9] COHEN, S. and SWIATECKI, W. J., University of California Radiation Laboratory Report, UCRL 10450 (1962).
[10] WHEELER, A., Fast Neutron Physics, Part II. (MARION, J. B. and FOWLER, J. L., Eds.) Interscience Publishers, New York - London (1963) 2051.
[11] STEPENS, S., ASARO, F. and PERLMAN, I., Phys. Rev. 113 (1959) 212.

TRANSITION STATES AT THE FISSION BARRIER*

J. J. GRIFFIN
UNIVERSITY OF CALIFORNIA, LOS ALAMOS SCIENTIFIC LABORATORY,
LOS ALAMOS, N. MEX., UNITED STATES OF AMERICA

Abstract — Résumé — Аннотация — Resumen

TRANSITION STATES AT THE FISSION BARRIER. The current knowledge of the transition states that a nucleus traverses en route to fission is reviewed, together with the relevant theory of fission-fragment anisotropy. Theoretical progress in understanding this kind of data in terms of nuclear superfluidity is summarized. The evidence indicates that nuclear pairing effects play an important role in determining the transition state spectrum. Recent (d,pf) experimental data are noted, and their statistical analysis in terms of a pairing Hamiltonian considered in the fixed-energy ensemble appropriate for finite nuclei is presented. The results indicate that such pairing effects lead in Pu^{240} to an energy gap in the transition spectrum nearly twice that which occurs at the ground state shape of the same nucleus. Such a result is quite significant from the point of view of nuclear many-body physics, suggesting that the nuclear surface plays an important role in the pairing of nucleons in the finite nuclei. The significance for nuclear fission is also broad. Such a large energy gap forces reassessment of certain detailed conjectures that have been put forward concerning fission widths and mass asymmetry associated with capture resonances of specific spin and parity. The new situation suggests that the even-even and odd-odd spin-parity correlation that rules in the low energy spectra of deformed even-even nuclei does not prevail in the transition state spectrum. A possible explanation in terms of low energy mass-asymmetric and bending vibrations of the fissioning nucleus is discussed. Possible experimental studies that could support or negate the validity of this viewpoint are mentioned.

ÉTATS DE TRANSITION A LA BARRIÈRE DE FISSION. L'auteur fait le point des connaissances actuelles relatives aux états de transition qu'un noyau subit sur la voie de la fission, et à la théorie de l'anisotropie des fragments de fission. Il rappelle les progrès accomplis dans les théories permettant d'expliquer ces données par la superfluidité du noyau. Les faits prouvent que les effets d'appariage jouent un rôle important dans la détermination du spectre à l'état de transition. L'auteur mentionne des données expérimentales récentes relatives à la réaction (d,pf) et en présente une analyse statistique en fonction d'un hamiltonien d'appariage, considéré dans l'ensemble d'énergie fixe approprié pour des noyaux finis. Les résultats indiquent que ces effets d'appariage entraînent pour ^{240}Pu une lacune d'énergie dans le spectre de transition presque double de celle qui se produit pour la forme du même noyau à l'état fondamental. Ce résultat, qui est très important du point de vue de la physique du noyau à plusieurs corps, donne à penser que la surface du noyau joue un rôle important dans l'appariage des nucléons à l'intérieur des noyaux finis. Du point de vue de la fission nucléaire, il a aussi une grande importance. Etant donné cette importante lacune, il faut réévaluer certaines hypothèses détaillées qui ont été mises en avant en ce qui concerne les largeurs de fission et l'asymétrie des masses associées aux résonances de capture d'un spin et d'une parité déterminés. La nouvelle situation donne à penser que la corrélation spin-parité pair-pair et impair-impair qui est de règle dans les spectres de faible énergie de noyaux pairs-pairs déformés ne l'est pas dans le spectre de l'état de transition. L'auteur étudie la possibilité d'une explication en fonction des vibrations de basse énergie, asymétriques par rapport à la masse, et de flexion du noyau qui subit la fission. Il indique quelles expériences pourraient éventuellement confirmer ou infirmer le bien-fondé de cette explication.

ПЕРЕХОДНЫЕ СОСТОЯНИЯ ПРИ БАРЬЕРЕ ДЕЛЕНИЯ. Дается обзор современных знаний о переходных состояниях, которые проходит ядро на пути к делению, вместе с соответствующей теорией анизотропии осколков деления. Обобщается прогресс в теории с целью достижения понимания такого рода данных в рамках ядерной сверхтекучести. Данные показывают, что эффекты ядерного спаривания играют важную роль при определении спектра переходного состояния. Отмечаются последние экспериментальные данные (d, pf), и приводится их статистический анализ в рамках гамильтониана спаривания, рассматриваемого в

* Work done under the auspices of the United States Atomic Energy Commission.

ансамбле фиксированной энергии, подходящей для конечных ядер. Результаты показывают, что такие эффекты спаривания приводят в плутонии-240 к разрыву в энергетической кривой в переходном спектре почти в два раза большему, чем при основном состоянии того же ядра. Такой результат весьма показателен с точки зрения ядерной физики многих тел и приводит к предположению о том, что ядерная поверхность играет важную роль в спаривании нуклонов в конечных ядрах. Ядерное деление также имеет большое значение. Такой большой разрыв энергетической кривой вынуждает провести переоценку некоторых выдвинутых подробных предположений относительно ширины деления и асимметрии массы, связанных с резонансами захвата при определенном спине и парности. В новых условиях предполагается, что (четно-четная) и (нечетно-нечетная) (спин-парность) корреляция, которая господствует в спектрах низкой энергии деформированных четно-четных ядер, не превалирует в спектре переходного состояния. Обсуждается возможное объяснение в рамках масс-асимметрических и искривляющих колебаний низкой энергии делящегося ядра. Упоминаются возможные экспериментальные исследования, которые могли бы подтвердить или отрицать правомерность этой точки зрения.

ESTADOS DE TRANSICION EN LA BARRERA DE FISION. El autor pasa revista a los conocimientos actuales sobre los estados de transición por los que un núcleo pasa hasta llegar a la fisión, así como a la teoría conexa de la anisotropía de los fragmentos de fisión. Resume los progresos de carácter teórico realizados con miras a explicar esta clase de datos en función de la superfluidez nuclear. Hay indicios de que los efectos de apareamiento nuclear desempeñan un papel importante en la determinación del espectro de estados de transición. El autor cita datos experimentales relativos a la reacción (d, pf), recientemente obtenidos, y expone su análisis estadístico en función de un Hamiltoniano de apareamiento, considerado en el conjunto de energía constante correspondiente a núcleos finitos. Los resultados indican que esos efectos de apareamiento originan en el ^{240}Pu una discontinuidad de la energía en el espectro de transición aproximadamente igual al doble de la que existe en la configuración correspondiente al estado fundamental del mismo núcleo. Este resultado es sumamente significativo desde el punto de vista de la física nuclear de los cuerpos múltiples, y sugiere que la superficie nuclear juega un papel importante en el apareamiento de nucleones en los núcleos finitos. Su significación en cuanto a la fisión nuclear es también considerable. Una discontinuidad tan apreciable de la energía impone la revisión de ciertas hipótesis detalladas que se formularon con el propósito de explicar las amplitudes de fisión y la asimetría de masas asociadas a las resonancias en la captura para spins y paridades determinadas. La nueva situación indica que la correlación spin-paridad (par-par) e (impar-impar), que rige para bajas energías en los espectros de núcleos par-par deformados no prevalece en el espectro de los estados de transición. El autor examina una posible explicación basada en vibraciones de baja energía, asimétricas respecto de la masa, y de flexión, del núcleo a punto de sufrir la fisión. Por último, menciona estudios experimentales que tienden a confirmar o a impugnar la validez de esta teoría.

THE DEVELOPMENT OF THE TRANSITION STATE CONCEPT

BOHR [1] first suggested that a nucleus with only slightly more excitation energy than its fission threshold must pass over the fission potential energy barrier in an almost "cold" state of internal excitation, and that at the fission barrier the spectrum of "transition states" of the highly deformed nucleus ought to resemble the spectra near the ground states of stably deformed nuclei. Such a picture is in Fig. 1. This proposal led immediately to a qualitative understanding of the photon-induced and neutron-induced fission-fragment anisotropy. Later, it provided the basis for a detailed explanation of the (Th^{232} + n) fragment angular distribution [2], and for the statistical treatment that explained the detailed energy dependence of the neutron-induced fission angular distributions [3, 4, 5], and the tendency in high energy fission for symmetric mass fragments associated with early-chance fissions from

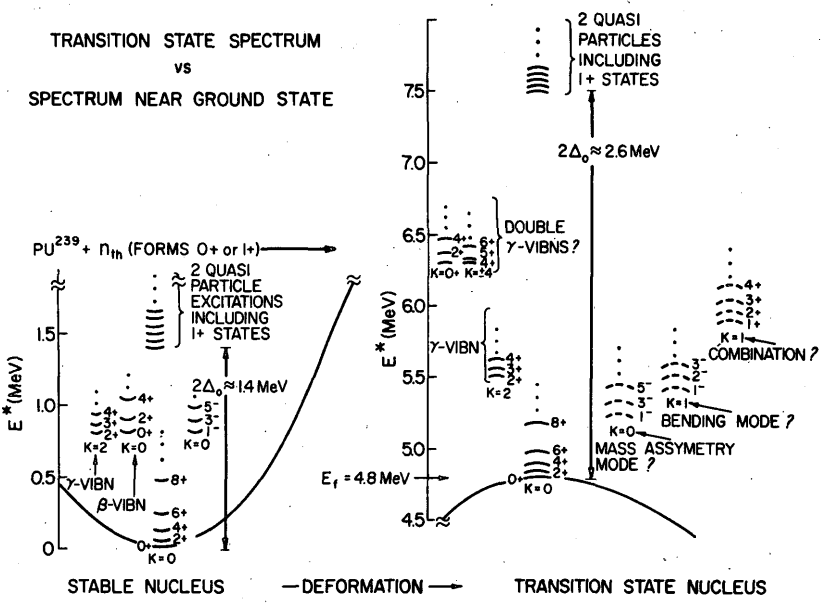

Fig. 1

The transition states at the fission barrier
are compared with the low-lying spectrum of a heavy deformed nucleus.
Various energies indicated are specifically appropriate to Pu^{240}.
The gamma and double gamma vibrations in the transition spectrum
have been suggested [24] by the data of Ref. [23].
The mass-asymmetry and bending modes are hypothesized here
in order to place a 1^+ state low in the transition spectrum,
as present (fragmentary) data seem to require.

highly excited nuclei to be more isotropic than the mass asymmetric events [6]. During this evolution improved data supported the assumption that the fission threshold energy and not, for example, the energy of the scission configuration was the relevant zero of excitation energy for the transition state spectrum.

For slow neutron fission, the transition state concept explained the fact, established from fission width fluctuations [7], that at most a few channels were determining the statistical properties of fission width distributions. It led also to certain conjectures [8] concerning possible correlations between the spin of a slow neutron fission resonance, its fission width and the mass asymmetry of the resonance fission.

Under the stimulus of a successful theory, data concerning the fission transition states improved qualitatively and quantitatively [9]. During this period the relevance of the superfluid model of BARDEEN, COOPER and SCHRIEFFER [10] to nuclei was first suggested [11] and established by a variety of theoretical successes[1]. The fission-fragment angular distribution data had meanwhile become sufficiently detailed to substantiate clear-cut

[1] e.g. The resolution of the problem of nuclear moments of inertia and various detailed features of nuclear spectra. See References [12] to [18].

deviation from the behaviour of a Fermi gas or independent particle model of the heavy nucleus. It is this matter, and the new implications for fission that the experimental data obtained in studying it, which are the concern of this talk.

FISSION FRAGMENT ANGULAR DISTRIBUTIONS AND THE TRANSITION STATES AT THE FISSION BARRIER

A few qualitative notions about fission-fragment anisotropy will be helpful in the following discussion. We digress to present them here[2]. The basic elements of the theoretical description are (a) the assumption that orientation of the highly deformed nucleus passing over the fission barrier is described by the wave functions of the symmetric top, $\mathcal{D}^{I}_{MK}$, which form the basis for the rotational model of deformed nuclei, and (b) that fission occurs rapidly enough afterwards so that the fragments are emitted along the direction of the nuclear axis. For a nucleus with angular momentum (I, M) passing through a transition state with projection K of angular momentum on the nuclear axis the angular distribution of the fragments is then given by

$$W^{I}_{MK}(\theta) \propto |\mathcal{D}^{I}_{MK}|^2. \tag{1}$$

If $M \ll I$, then these wave functions are peaked forwards and backwards for small K and sidewards for $K \approx I$. If all K-values were equally available in the transition state spectrum then the sum over various terms (1) would yield an isotropic distribution of fragments. It is in fact the preponderance of low K-values in the transition spectrum just above threshold that causes the forwards–backwards peaking of fragments from fission induced by energetic projectiles. Also, the increase in the average K-value of the transition states as more excitation energy becomes available explains the decrease in anisotropy with increasing energy above threshold. When many different transition states are available one assumes a statistical distribution of K-values and takes an angular distribution of the form [3]

$$W^{I}_{M}(\theta) \propto \sum_{K=-I}^{+I} |\mathcal{D}^{I}_{MK}(\theta)|^2 \exp - \frac{K^2}{2K_0^2} \tag{2}$$

for each (I, M) value of the compound nucleus. It is then possible to extract from adequate data the dependence of K_0^2 on the excitation energy, E^*-E_f. In this way the transition state spectrum can be studied and subjected to comparison with theoretical expectations.

CONFLICT BETWEEN THE DATA AND THE INDEPENDENT PARTICLE MODEL

The Gaussian weighting in Eq. (2) is essentially a statistical Boltzmann factor. From this point of view one expects that $\hbar^2 K_0^2 = \mathcal{I}_{eff} \cdot T$. Then, if the

[2] References [1] to [4] and [23] supply further technical details.

nucleus were composed of independent particles in a potential well exhibiting a uniform single particle spacing, $\mathcal{I}_{eff}$ could be estimated from the rigid body moments of the nucleus, and T would be proportional to $(E^*-E_f)^{\frac{1}{2}}$. Such a dependence is shown by the dotted curve of Fig. 2. A careful experimental study of Pu^{239} + n angular distributions was carried out to check this dependence [19]. The results indicated that K_0^2 increases very nearly as (E^*-E_f) and not as $(E^*-E_f)^{\frac{1}{2}}$. The BCS model of nuclear pairing gives just such a dependence[3] for K_0^2 (solid line, Fig. 2). It predicts also that above some critical excitation energy E_c^*, the pairing effects should disappear and the nucleus should behave according to the independent particle model. Moreover, the value of E_c^*, is, according to BCS, related quite simply to the magnitude of the ground state energy gap, $2\Delta_0$.

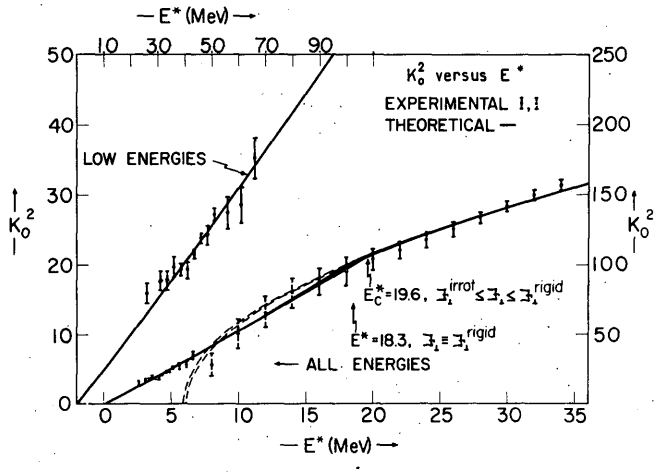

Fig. 2

The implications for K_0^2 of the independent particle model (parabola) and the superfluid model of nuclear pairing (linear at low energy, parabolic above E_c^*) are compared with the data.
The energy difference between zero excitation energy and the energy where the parabola goes to zero is the energy gain due to nuclear pairing.
From the best fit (solid line) to the data the gap is estimated to be $2\Delta_0 \approx 2.3$ MeV.

By utilizing the high energy data of VANDENBOSCH et al. [21], and choosing E_c^* and $(K_0^2)_c$ to fit both those and the low energy data optimally [22], it was possible to estimate that $2\Delta_0$ for the Pu^{240} transition state spectrum is about 2.3 MeV, nearly twice the value appropriate for the low energy spectrum of stable Pu^{240} [14].

VERIFICATION IN (d, pf) DATA

More recently, the large pairing gap in the transition state spectrum of Pu^{240} has been observed directly by measuring the fragment angular

[3] This qualitative feature was first pointed out by GRIN [20].

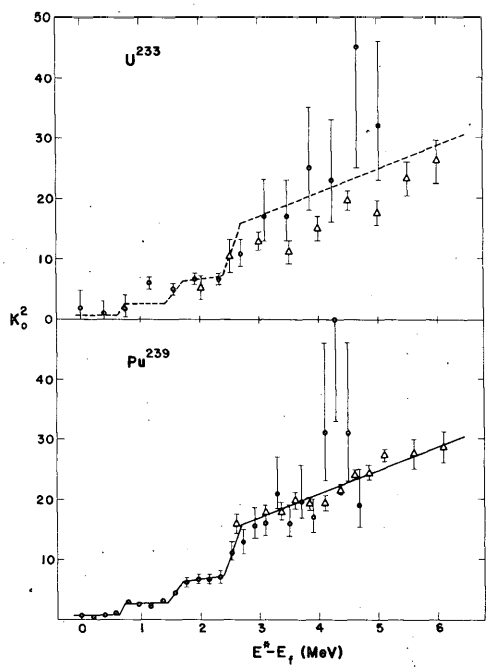

Fig. 3

The (d, pf) experimental results for K_0^2 versus E^*-E_f in Pu^{240}
and (of lower statistical quality) U^{234} are presented.
Near threshold $K_0^2 \approx 0$, as is expected for an even-even nucleus.
At ~2.6 MeV, K_0^2 jumps to a value appropriate for an average over two quasi-particle states.
The smaller jumps at 0.7 MeV and 1.5 MeV
may correspond to low-lying collective excitations in the transition state spectrum [24].
At higher excitation energies, the results agree well with
comparable results from neutron work [10], indicated by triangles.

distributions from (d, pf) on Pu^{239} [23]. This reaction allows one to explore excitation energies below the neutron binding energy all the way down to the threshold, and provides enough angular momentum to guarantee strong anisotropies.

Figure 3 shows a summary of these results. One sees that $K_0^2 = 0$ is observed near threshold and that K_0^2 jumps from ~8 to ~16 at $E^*-E_c = 2.6$ MeV $K_0^2 = 16$ is consistent with the expectation for two quasi-particle-states in a heavy nucleus, whereas $K_0^2 = 8$ is rather too small for this average. This experiment therefore corroborates directly the estimate based on the smooth BCS dependence.

STATISTICAL DESCRIPTION OF DISCONTINUITIES IN K_0^2

The smooth BCS description of K_0^2 in Fig. 2 is an inevitable result of the use of the macro-ensemble, $\exp -\kappa/T$, to describe the statistical mechanical system. It is possible, however, to treat the BCS Hamiltonian in

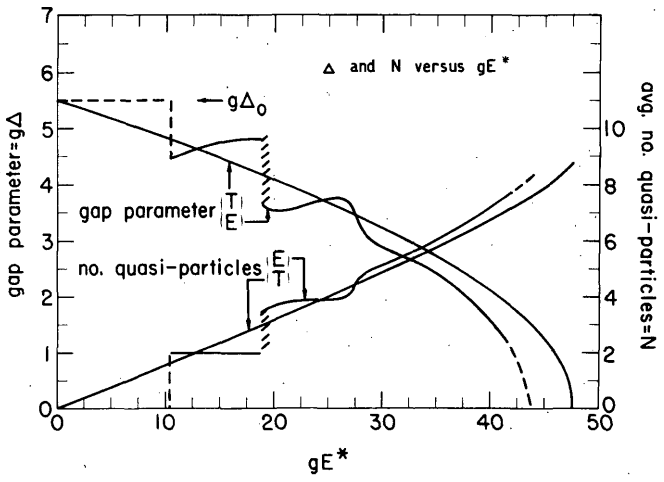

Fig. 4

The results of optimizing the choice of independent quasi-particles for a BCS (pairing) Hamiltonian are compared for (a) the fixed temperature ensemble and (b) the fixed energy ensemble. The latter replaces the smooth dependence on energy by one that exhibits appropriate discontinuities in the various energy dependent functions of the system. The energy gap and the average number of quasi-particles are shown here as examples.

a (approximately) fixed energy ensemble [25], $\delta(E-\kappa)$. Then the minimization of the Free Energy (U-TS) is replaced by the maximization of the entropy as the condition for the optimal pairing solution. In such a treatment the discontinuities associated with the two (and four) quasi-particle excitations become evident, and the BCS formulas are seen as averages in which such discontinuities are smoothed out.

The results of such a calculation for the gap parameter Δ, and the average number of quasi-particles excited, are shown in Fig. 4. It could also be noted that the decrease in the gap in such a treatment is fully analogous to the phenomenon of "blocking" that has been considered in some detail for the low-lying spectra of stable nuclei [26].

IMPLICATIONS OF THE LARGE GAP FOR NUCLEAR MANY-BODY THEORY

The problem of nuclear pairing has been studied for infinite nuclear matter [27]. The results indicate that nuclear matter should exhibit a gap of nearly zero energy. This result arises from the repulsive nuclear core that nearly cancels out the nuclear attraction for particles near the top of the Fermi sea in heavy nuclei.

It has been suggested, therefore, that the pairing effects observed in nuclei are essentially connected with the finite size of nuclei and, in particular, with the influence of the nuclear surface. Calculations [28] based on a slab model, finite in one of three dimensions, show a gap that is very sensitive

to the thickness of the slab, diminishing towards zero as the slab becomes thicker.

The relevance of the present result – that the gap in highly deformed Pu^{240} is rather larger than the gap in the same nucleus at its stable shape – is obvious. In the process of deformation, the surface area of the nucleus is increased noticeably, so that one should expect a surface-sensitive gap also to be affected. In analogy to W. Swiatecki's proposal that nuclei deformed to the fission barrier ought to fit into an adequate semi-empirical mass formula, one can suggest that such highly deformed nuclei also warrant consideration in theories designed to describe nuclear many-body phenomena.

IMPLICATIONS OF THE LARGE PAIRING GAP FOR NUCLEAR FISSION

Conjectures[4] concerning the correlation between the spin of a resonance and its fission properties have been mentioned above. We discuss here in particular the suggestion that the regular (e-e or o-o) spin-parity resonances ought to have greater average fission widths than the irregular combinations. This idea followed quite simply from the assumption that for even-even nuclei the transition state spectrum would exhibit in its low-lying states the correlation between spin and parity that dominates the spectra of stable deformed nuclei, and that odd-even or even-odd spin-parity combinations could arise only from two quasi-particle excitations. It has survived for several years because (a) of the difficulty in determining certainly the spins of given resonances and (b) of the fact that thermal neutrons commonly provide excitation energies about 1 MeV above the fission threshold, an amount not very different from the lowest two-quasi-particle energy in stable spectra.

With the new information from (d, pf) about the transition state pairing gap, the possibility that any two particle transition state is available at thermal neutron energies appears to be excludable, at least for Pu^{239} + n. On the other hand, measurements of spins for eight resonances [31] reveals five of spin 1+ and three of spin 0+ states, thereby precluding the possibility that all the observed resonances have the same spin, 0+. Moreover, the average fission widths among these measured-spin resonances show no significant tendency for 0+ states to fission more easily than 1+ states.

One is therefore forced to take seriously the possibility that irregular spin-parity combinations lie low in the transition state spectrum. Although the lowest lying collective states are all expected to exhibit regular spin-parity, one could build irregular spin parity states by combinations of collective states. These would occur at energies no less than the sum of the two component energies. Thus for example a gamma vibration, $K = 2^+$, $I = 2, 3, 4 \ldots$, plus a mass asymmetry vibration, $K = 0^-$, $I = 1^-, 3^- \ldots$, could provide states $K = 2^-$, $I = 2^-, 3^-, \ldots$, beginning at an energy $E_{2^-} \approx \hbar\omega_\gamma + \hbar\omega_{MA}$.

Plutonium is a somewhat fortunate choice for detailed study in this respect, since its irregular combination is 1+, the least easily constructed from the well-known collective states. No 1+ state, for example, could be

---

[4] For a summary of these conjectures and their confrontation with the data available at the time, see Ref. [29]. Earlier discussions occur in Refs. [9] and [30].

constructed in the manner noted above. In fact, the simplest 1+ combination of collective states is that formed from the mass-asymmetry and bending vibrations[5]. It would provide a transition state at energy $E_{1^+} \approx \hbar\omega_{MA} + \hbar\omega_B$, which might be less than the 1.6 MeV available from thermal-neutron capture, if only these odd parity vibrations in the transition state spectrum have low enough excitation energy.

To check this possibility, we have investigated the trend of these modes' frequencies as a function of the nuclear elongation in a pure liquid drop model[6]. The calculation is outlined in the Appendix and the results are given in Fig. 5. The results indicate that as deformation increases the energy of these modes decreases. These calculations are by no means a complete treatment, even within the liquid drop model, since only relatively simple shapes are included. Still, they offer qualitative support to the conjecture that these excitations will be found to lie low in the transition state spectrum, and provide thereby a reasonable basis for understanding the various features of Pu^{239} fission now evident in the experimental data.

Another implication of the large gap at the fission barrier is that spontaneous fission will be retarded in odd nuclei by an increase in their fission barrier in an amount $\Delta E_f = \Delta_0^{barrier} - \Delta_0^{stable}$. This difference is about 0.600 MeV in this case, and may be adequate[7] to explain the entire retardation ($\sim 4 \times 10^4$) factor from Pu^{240} to Pu^{239}, without recourse to the assumption that K remains a good quantum number en route to the fission barrier [35].

FURTHER EXPERIMENTAL STUDY

In order to study further the "spectroscopy" of highly deformed nuclei, more certain information on resonance spins is essential. Fragment anisotropy measurements for specific fission resonances [36], which require aligned or polarized targets, could provide a solid basis for such spin assignments, and provide as well an indication of the K-values relevant to the different spin states.

(D, pf) evidence of the kind now available for plutonium is required for other nuclides to preclude the possibility that the large pairing gap in plutonium is a quirk of this element alone, and not to be extrapolated to neighbouring isotopes. The $(\alpha, \alpha' f)$ reaction also promises to be useful in such studies [37, 38].

Angular studies of photon-induced fission of even-even isotopes also offer a possible tool for studying the transition states, especially if the pre-

---

[5] The mass asymmetry mode corresponds to a Y_3^0 deformation of the deformed nucleus, the bending mode to a Y_3^1. In classical terms, the mass asymmetry mode is the oscillation of a pear shape into its mirror image, or the running of a bulb about the greatest perimeter of the deformed nucleus. Bending (Y_3^1) corresponds to a wave running about the surface at an angle, $\theta = \cos^{-1} 1/(3.4)^{\frac{1}{2}}$ with the symmetry axis. Higher excitations of order three can exist with $K = \pm 2, \pm 3$, but presumably, at higher excitation energies than the motions considered here. cf. Ref. [32].

[6] Note that in Ref. [33], similar calculations are made for saddle point shapes in the two-spheroid model. However in that model, the mass asymmetry mode exhibits infinite inertia, and therefore, zero frequency.

[7] This statement is based on the assumption that each increase of one MeV in the barrier energy corresponds to a factor 10^{-8} in lifetime [34].

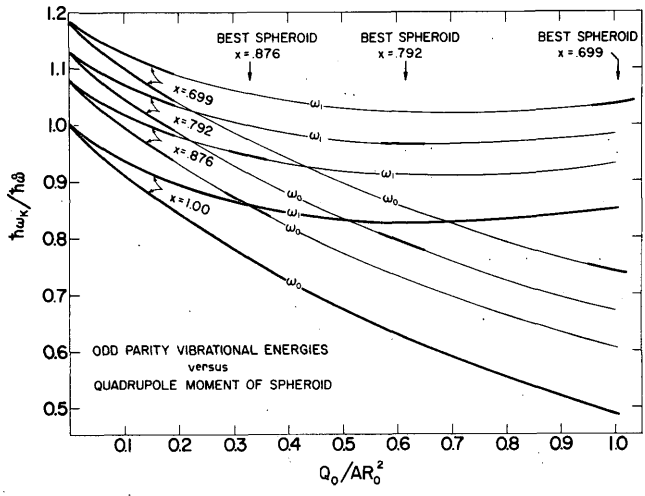

Fig. 5

The liquid-drop energy is plotted against the quadrupole moment of the spheroidal equilibrium shape for several values of X. Also indicated are the optimal spheroidal approximations to the fission barrier shapes, as obtained in Ref. [46] for the particular X-values considered here.

cision of the process could be increased. The picture discussed above implies that a $K = 1, 1^-$ state lies not too far above the lowest $(K = 0)1^-$ state. The observed rate of decrease in an isotropy from photon-induced fission [39], which has been interpreted to imply a $K = 1$ state at ≈ 0.230 MeV above the $K = 0, 1^-$ state is not inconsistent with this picture[8]. Sufficient precision to specify or to put bounds on the energy difference between the lowest 1^- transition state and the fission threshold (0+) energy would be a valuable advance. Quadrupole transition states might also be studied in detail by this process [40].

Properties associated with specific neutron resonances other than the angular distributions will also be useful in constructing a solidly interlocked picture of the transition state spectrum. Studies, for example, of fragment mass asymmetry [41], of the probabilities of α-emission in fission [42], and, indeed, of the basic partial widths for each resonance, will, it is hoped, find a place in such a picture. Regarding the latter, due cognizance must be taken of the recent work of LYNN [43], which suggests firmly for U^{233} and U^{235}, and less definitely for Pu^{239}, that resonances come within a width of one another often enough to deceive the naive one-level student into accepting a warped picture of the underlying resonance properties.

To summarize, the transition state spectra have grown in recent years into a fruitful object for study, and there is every promise that the range and interest of such studies will continue to grow.

---

[8] This estimate would be decreased by at least a factor of two if the assumed barrier curvature were chosen as small as the data of Ref. [23] requires.

APPENDIX

LIQUID DROP CALCULATIONS

Calculations are described of odd parity vibrational frequencies of a spheroidal liquid drop with quantum numbers (K, π) equal to $(0, -)$ and $(1, -)$, corresponding respectively to the "mass asymmetry" and "bending" modes of Ref. [33].

An incompressible, irrotational liquid drop is considered, specified in prolate spheroidal co-ordinates (ξ, μ, φ) by the equation $\xi = \xi_0$. Computations are made of kinetic and potential energies associated with small deviations from the spheroidal shape, of the form

$$\xi = \xi_0 + \zeta(\mu, \varphi), \tag{3}$$

where

$$\zeta = \xi_0 \left[a_0 \cdot \left(\frac{\xi_0^2 - d^2}{\xi_0^2 - d^2\mu^2} \right) P_{30}(\mu) + a_1 \left(\frac{\xi_0^2 - d^2}{\xi_0^2 - d^2\mu^2} \right) P_{31}(\mu) \cos \varphi \right]. \tag{4}$$

Since the spheroidal liquid drop is stable against deformations of this type, the potential energy is of the form

$$V = V_0 + \tfrac{1}{2} \kappa_K a_K^2 \quad (K = 0,1). \tag{5}$$

The kinetic energy of irrotational motion is given by

$$R = \tfrac{1}{2} \mathscr{M}_K (\dot{a}_K)^2 \tag{6}$$

and, in first approximation, the quantized vibrations have energy

$$\hbar\omega_K = \hbar(\kappa_K / \mathscr{M}_K)^{\frac{1}{2}}. \tag{7}$$

The quantities κ_K have been computed as second derivatives of the potential (surface and Coulomb) energy:

$$\kappa_K = \frac{d^2[B_S + 2X B_C]}{da_K^2}\Bigg|_{a_K = 0}, \tag{8}$$

where B_S and B_C are in units of the spherical surface energy and Coulomb energies, E_S^0 and E_C^0 respectively, and $X = E_C^0 / 2E_s^0$ is the usual fissionability parameter. For a perturbed spheroid,

$$B_S = \frac{1}{4\pi[\xi_0(\xi_0^2 - 1)]^{\frac{2}{3}}} \int d\mu \int d\varphi \left\{ [\xi^2 - d^2\mu^2][\xi^2 - d^2] \left[1 + \frac{(1-\mu^2)}{(\xi^2 - d^2)} \left(\frac{\partial \xi}{\partial \mu} \right)^2 + \frac{(\xi^2 - d^2\mu^2)}{(\xi^2 - 1)^2 (1 - \mu^2)} \left(\frac{\partial \xi}{\partial \varphi} \right)^2 \right] \right\}^{\frac{1}{2}} \tag{9}$$

and

$$B_C = \frac{15}{32\pi^2[\xi_0(\xi_0^2 - d^2)]^{\frac{5}{3}}} \int d\mu_1 \int d\varphi_1 \int d\mu_2 \int d\varphi_2$$

$$\int_d^{\xi} d\xi_1 \int_d^{\xi} d\xi_2 \cdot [\xi_1^2 - d^2\mu_1^2][\xi_2^2 - d^2\mu_2^2] \frac{1}{r_{12}} \tag{10}$$

The appropriate expansion of $1/r_{12}$ in spheroidal co-ordinates is given e.g. by HOBSON [44].

To obtain the inertia coefficients, $\mathscr{M}_K$, the velocity potential φ is expanded in prolate spheroidal harmonics and the coefficients determined from the boundary condition [45]

$$\frac{\partial f}{\partial t} + \nabla\varphi \cdot \nabla f = 0, \tag{11}$$

where $f = \xi - \xi_0 = 0$ describes the surface of the drop at the (spheroidal) equilibrium shape.

The results of this calculation are presented in Fig. 5 for several values of X for which the fission barrier shapes have been shown by SWIATECKI [46] to correspond to optimal spheroids with distortion $\xi_0/d = 1.1$, 1.2, 1.4 and ∞ (the X = 1, spherical, saddle point shape). In Fig. 6, the difference, Δ, in energy between the K = 1 and K = 0 vibrations is plotted against X and compared with the results of BAERG et al. [39] as inferred from photofission fragment anisotropy data for Th^{232}, U^{238}, U^{236}, U^{234} and Pu^{240} (ordered in ascending X-values).

One sees in Fig. 5 a general tendency for these odd parity vibrational energies to decrease with increasing spheroidal deformation, a trend consistent with the conjecture that such vibrations may lie lower in energy at the fission saddle shape than at stable nuclear deformations. The appropriate energy scale for such vibrations is not expected to be given by the liquid drop model, since low-lying collective vibrations generally lie much lower in energy than the liquid drop model predicts.

Figure 6 shows that the dependence of the liquid drop Δ is consistent only very qualitatively with the photofission data. If one insists, nonetheless, on estimating from Fig. 6 an energy scale factor between the liquid drop and the actual nucleus, then that factor is about five. With such a factor Fig. 5 implies actual vibrational energies for Pu^{240} of $\hbar\omega_0 \approx 0.5$ MeV and $\hbar\omega_1 \approx 0.6$ MeV. Then a 1+ state could have an energy as low as 1.1 MeV in the transition state spectrum of Pu^{240}, well below the 1.6 MeV available in thermal-neutron fission.

To summarize, one concludes that the odd-parity vibrational states might well lie sufficiently low at the fission barrier shape to resolve the apparent conflict between the occurrence in thermal-neutron fission of easily fissionable spin 1+ states [31] and the implication of (d, pf) studies [23] that two-particle states, including 1+ states, lie about 1 MeV above the energy available to thermal neutrons. An interesting corollary to this conclusion is the suggestion that the photofission studies actually provide a measure of

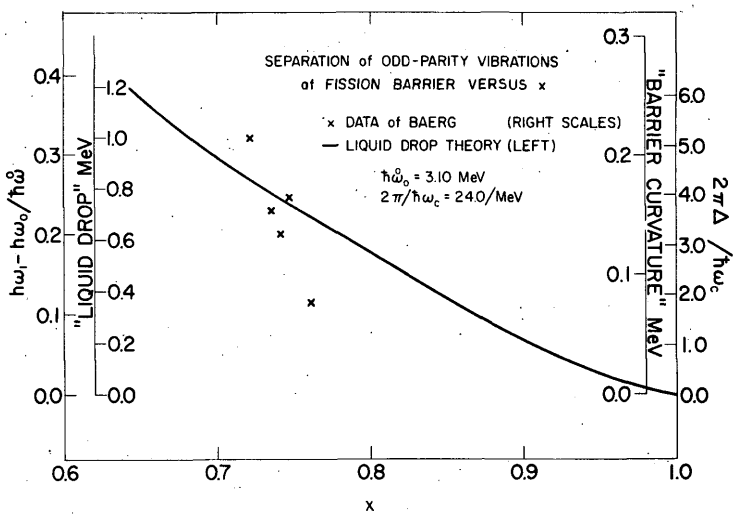

Fig. 6

The computed difference between the K = 1 and K = 0 odd parity vibrational energies (smooth curve) is plotted against $X = (Z^2/A)/(48.4)$ [47], together with the photofission results (crosses), $(2\pi\Delta)/\hbar\omega_C$, for the several nuclei studied in Ref. [39]. The "Liquid-Drop" energy scale (left) corresponds to the semi-empirical surface energy of Green, 17.80 $A^{\frac{2}{3}}$ MeV. The "Barrier Curvature" energy scale (right) corresponds to the assumption $2\pi/\hbar\omega_C = 24.0\ (\mathrm{MeV})^{-1}$, suggested by recent (d, pf) experiments [23]. There appears to be (roughly) a factor of five between the two scales.

the energy difference between the K = 0, K = 1 vibrational states at the fission barrier rather than of the difference between the two particle $(I K\pi) = (1, 1, -)$ state and the collective $(I K\pi) = (1, 0, -)$ state, as had previously been supposed [39].

REFERENCES

[1] BOHR, A., Proc. UN Int. Conf. PUAE 2 (1956) 151.

[2] WILETS, L. and CHASE, D., Phys. Rev. 103 (1956) 1296.

[3] HALPERN, I. and STRUTINSKII, V., Proc. 2nd UN Int. Conf. PUAE 15 (1958).

[4] GRIFFIN, J., Proc. Int. Conf. on Nuclear Structure, Paris (1958); Phys. Rev. 116 (1959) 107; Phys. Rev. 127 (1962) 1248; with GIBBS, W. R., Phys. Rev. (in press).

[5] BROLLEY, J., DICKINSON, W. and HENKEL, R., Phys. Rev. 99 (1955) 193; Phys. Rev. 103 (1956) 1292.

[6] COHEN, B. L. et al., Phys. Rev. 94 (1954) 625; 98 (1955) 685; FAIRHALL, A. et al., Phys. Rev. 94 (1954) 733.

[7] PORTER, C. E. and THOMAS, R. G., Phys. Rev. 104 (1956) 483.

[8] WHEELER, J. A., Int. Conf. on Nuclear Reactions, Amsterdam, Physica XXII (1956) 1103.

[9] SIMMONS, J and HENKEL, R., Phys. Rev. 120 (1960) 198; BLUMBERG, L. and LEACHMAN, R., Phys. Rev. 116 (1959) 102.

[10] BARDEEN, J., COOPER, L. and SCHREIFFER, J., Phys. Rev. 108 (1957) 1175, referred to as BCS.

[11] BOHR, A., MOTTELSON, B. and PINES, D., Phys. Rev. 110 (1958) 936.

[12] BELYAEV, S. T., Mat.-fys. Meddr 31 No. 11 (1959).
[13] GRIFFIN, J. and RICH, M., Phys. Rev. Lett. 3 (1959) B516; Phys. Rev. 118 (1960) 850.
[14] NILSSON, S. G. and PRIOR, O., Mat.-fys. Meddr 32, No. 16 (1960).
[15] KISSLINGER, L. and SORENSEN, R., Mat.-fys. Skr. 32, No. 9 (1960).
[16] SOLOVIEV, V., Mat.-fys. Skr. 1, No. 11 (1961).
[17] BES, D. R. and SZYMANSKI, Z., Nucl. Phys. 28 (1961) 42.
[18] GALLAGHER, C. and SOLOVIEV, V., Mat.-fys. Meddr 32, No. 16 (1960).
[19] SIMMONS, J. E., Unpublished; see Ref. [22] for the results of this experiment.
[20] GRIN, YU. T., Z. eksp. teor. Fiz. 43 (1962) 1880.
[21] VANDENBOSCH, R., WARHANECK, H. and HUIZENGA, J., Phys. Rev. 124 (1961) 846.
[22] GRIFFIN, J., Phys. Rev. 132 (1963) 2204.
[23] BRITT, H. C., STOKES, R., GIBBS, W. and GRIFFIN, J., Phys. Rev. Lett. 11 (1963) R502 and to be published.
[24] GRIFFIN, J. and RICH, M., Bull. Amer. phys. Soc. II 18 (1963) 526.
[25] RICH, M. and GRIFFIN, J., Phys. Rev. Lett. 11 (1963) L518, and to be published.
[26] WAHLBORN, S., Nucl. Phys. 37 (1962) 554.
[27] EMORY, V. and SESSLER, A., Phys. Rev. 119 (1960) 248.
[28] HENLEY, E. and WILETS, L., Phys. Rev. Lett. 11 (1963) 326; KENNEDY, R., WILETS, L., and HENLEY, E., Phys. Rev. Lett. 12 (1964) 36.
[29] GRIFFIN, J., Int. Conf. on Nuclear Structure, Kingston, Ont., Canada, University of Toronto Press (1960).
[30] WILETS, L., Proc. Int. Conf. on Nuclear Structure, Rehovota, Israel, North-Holland Publishers, Amsterdam (1957).
[31] FRASER, J. and SCHWARTZ, R., Nucl. Phys. 30 (1962) 296.
[32] WHEELER, J. A., in Fast Neutron Physics, Part II (MARION, J. and FOWLER, J., Eds.) Interscience, New York (1963).
[33] NIX, J. R., Lawrence Radiation Laboratory Report, UCRL 11338 (1964), unpublished.
[34] SWIATECKI, W. J., private communication.
[35] WHEELER, J. A., Proc. UN Int. Conf. PUAE 2 (1956) 155.
[36] DABBS, J., private communication; such experiments are in progress at the Oak Ridge National Laboratories.
[37] WILKINS, B. D. et al., Phys. Lett. 12 (1964) 243.
[38] BRITT, H. C., private communication.
[39] BAERG, A. P. et al., Canad. J. Phys. 37 (1959) 1418.
[40] FORKMAN, B. and JOHANSSON, S. A. E., Nucl. Phys. 20 (1960) 136.
[41] FALER, K. T. and TROMP, R. L., Phys. Rev. 131 (1963) 1746, and references cited therein; COWAN, G. A. et al., Phys. Rev. 130 (1963) 2380, and references cited therein.
[42] MELKONIAN, E., Columbia University Progress Report, CU (PNPL) 212 (1961), unpublished.
[43] LYNN, J. E., Phys. Rev. Lett. 13 (1964) 412.
[44] HOBSON, E. W., The Theory of Spherical and Ellipsoidal Harmonics, Chelsea Publishing Co., New York (1955).
[45] LAMB, H., Hydrodynamics, Dover Publications, New York (1945) 7.
[46] SWIATECKI, W. J., Phys. Rev. 104 (1956) 993.
[47] BURNETT, D. S., GATTI, R. C. et al., University of California, Lawrence Radiation Laboratory Report, UCRL 11079 (1963), unpublished.

DISCUSSION[1]
(on the foregoing three papers)

R. JOLY: I should like to ask Dr. Huizenga what is the threshold energy of the $(\alpha, \alpha' f)$ reaction mentioned in his paper and if, at 43 MeV for the incident α-particle energy, he can eliminate the possibility of a 3-step process such as $(\alpha, \alpha' nf)$ taking place.

J. R. HUIZENGA: The $U^{238}(\alpha, \alpha' nf)$ reaction has a threshold that is larger than that of the $U^{238}(\alpha, \alpha' f)$ reaction by approximately the neutron-binding energy of U^{238}. Since our energy resolution is 350 keV, these two processes are very well separated.

S. S. KAPOOR: It should be possible to see whether only M = 0 states are involved by determining angular distributions in the azimuthal direction.

J. R. HUIZENGA: That is correct. Angular distribution measurements will be made out of the reaction plane to investigate the M distributions.

E. R. RAE: With regard to the paper presented by Dr. Griffin I should like to make two comments concerning the relative fission widths of the 0+ and 1+ states excited in the slow neutron fission of Pu^{239}. Firstly, I think that it may be misleading to infer from the work of Schwartz and Fraser that there is a rough equality of these fission widths because the scattering measurement from which they determined the spins of a selection of levels would tend to favour the observation of narrow levels and the omission of the broad 0+ levels. It is also possible that strong interference effects may lead to some doubt regarding one or two of their spin assignments.

Secondly, recent unpublished work on the Pu^{239} levels up to a few hundreds of electron volts reveal the presence of many very wide levels with fission widths of a few eV. These wide levels are almost certainly 0+ levels, so that a difference of as much as a factor of 10 may yet exist between the mean fission widths of the 0+ and 1+ levels.

J.J. GRIFFIN: Dr. Rae's comments are quite relevant and stress the need for reliable knowledge of resonance spins. I should like to note, however, that if the Pu^{240} (1+) states had to fission through a two quasi-particle state, then they would be expected to have average fission probabilities reduced by an amount corresponding to about 1 MeV of barrier penetration, i.e. perhaps a reduction of 10^5 to 10^8. Then the fact that one sees any fission at all from spin 1+ resonances seems to indicate a 1+ transition state with a threshold at least somewhat lower than the lowest two quasi-particle transition state.

R. VANDENBOSCH: In your paper, Dr. Griffin, you indicated that the lowest band, apart from the even-even K = 0+ band, might be an odd parity K = 0 band. In the paper presented by Dr. Huizenga one notices that there is a characteristic difference in the angular distribution patterns for fission through even spin, even parity transition states and those for odd spin, odd parity states - namely that for K = 0 and M = 0 the yield at 90°

---

[1] For further discussion of GRIFFIN, J.J., "Transition states at the fission barrier", see also: RAE, E.R., "Cross-sections for low-energy neutron-induced fission"; and DE SAUSSURE, G., BLONS, J., JOUSSEAUME, C., MICHAUDON, A. et PRANAL, Y., "Mesure et analyse de la section efficace de fission du plutonium-239 de 0 à 5 keV".

vanishes for odd spin states. I would like to ask Dr. Huizenga if, from his data, he can set an upper limit to the amount of fission occurring through the odd parity band.

J. R. HUIZENGA: For the case M = K = 0, Dr. Vandenbosch observed correctly that the even and odd I values give slightly different angular distributions. Hence, one can in principle use observed angular distributions to measure the contributions of even and odd spin transition states. However, the absence of contributions from odd spin transition states in the angular distributions does not necessarily mean that no such states exist in the transition state nucleus. This is due to the fact that we do not at present understand the (α, α') reaction mechanism. It may be that the direct reaction mechanism discriminates against odd spin values and, if this is true, odd spin values will made little contribution to the angular distribution even if they are present in the transition state nucleus.

SADDLE-POINT ROTATIONAL STATES FROM RESONANCE FISSION OF ORIENTED NUCLEI*

J.W.T. DABBS, F.J. WALTER** AND G.W. PARKER
OAK RIDGE NATIONAL LABORATORY, OAK RIDGE, TENN., UNITED STATES OF AMERICA

Abstract — Résumé — Аннотация — Resumen

SADDLE-POINT ROTATIONAL STATES FROM RESONANCE FISSION OF ORIENTED NUCLEI. Nuclei of the actinide elements uranium, neptunium and plutonium can be aligned in the compounds $XO_2Rb(NO_3)_3$ through the interaction of the quadrupole moment of the nucleus with the gradient of the crystalline electric field simply by cooling the appropriate single crystal. A nuclear alignment of this type corresponds to a non-uniform angular distribution of the symmetry axis of the compound nucleus in space, which reflects primarily the value of K. If the assumption is made that the fragments also have this distribution, a method for establishing the K quantum number at the saddle point is obtained. Experiments on aligned U^{233} and U^{235} nuclei at 1.2°K and using thermal neutrons have been performed at Oak Ridge National Laboratory and reported previously.

These experiments have now been extended to resonance neutron energies and to temperatures of 0.5°K. When taken together with direct determinations (using polarized neutrons and polarized nuclei) of the J-values associated with each resonance, this extension permits a much more detailed understanding of the number and nature of the fission channels available; these are questions of long standing in fission. In U^{235}, an anisotropy of the fission fragments approaching the maximum possible was found for the 1.14- and 8.8-eV resonances, with a sign opposite to that previously found for alpha particles. In addition, a substantial decrease in the anisotropy was found for neutron energies in the neighbourhood of the well-known 0.3-eV resonance. In the absence of direct information on the J-values in U^{235}, resort was made to a multi-level fit to σ_f similar to that of Kirpichnikov et al., in which it was assumed that $J(0.3\ eV) \neq J(1.14\ eV)$, in contrast to earlier multi-level fits. These preliminary data are consistent with an anisotropy proportional to the calculated contribution to σ_f of the two possible J-values. The shape of the curve is, however, not consistent with other data such as the variation of peak-to-valley ratio of Faler and Tromp; thus the rather strong indication that $J(0.3\ eV) \neq J(1.14\ eV)$ should not yet be accepted as conclusive. Further measurements are in progress.

ÉTATS ROTATIONNELS A L'ETRANGLEMENT RESULTANT DE LA FISSION, PAR NEUTRONS DE RÉSONANCE, DE NOYAUX ORIENTÉS. Il est possible d'aligner des noyaux des actinides U, Np et Pu dans les composés $XO_2Rb(NO_3)_3$ par interaction du moment quadrupolaire du noyau avec le gradient du champ électrique du cristal, en refroidissant tout simplement le monocristal intéressant. Un alignement de ce genre correspond à une distribution angulaire non uniforme, dans l'espace, de l'axe de symétrie du noyau composé, qui reflète en premier lieu la valeur de K. Si l'on suppose que les fragments présentent cette même distribution, on arrive à une méthode qui permet d'établir le nombre quantique K à l'étranglement. Des expériences faites à Oak Ridge sur des noyaux alignés de ^{233}U et de ^{235}U à 1,2°K et avec des neutrons thermiques ont déjà fait l'objet d'articles dans des revues.

Depuis, ces expériences ont été étendues aux énergies des neutrons de résonance et à des températures de l'ordre de 0,5°K. Faite conjointement avec des déterminations directes (à l'aide de neutrons polarisés et de noyaux polarisés) des valeurs de J associées à chaque résonance, la nouvelle série d'expériences permet de se faire une idée beaucoup plus exacte du nombre et de la nature des voies de fission disponibles; il s'agit là de questions qui se posent depuis longtemps en matière de fission. Dans ^{235}U, une anisotropie des fragments de fission approchant le maximum possible a été relevée pour les résonances de 1,14 et 8,8 eV, avec le signe contraire de celui qui avait été trouvé antérieurement pour les particules alpha. En outre, une diminution considérable de l'anisotropie a été observée pour les énergies neutroniques dans le voisinage de la résonance

* Research sponsored by the United States Atomic Energy Commission under contract with the Union Carbide Corporation.

** Now with Radiation Instrument Development Laboratory, Oak Ridge, Tenn.

bien connue de 0,3 eV. En l'absence de renseignements directs sur les valeurs de J dans ^{235}U, on a procédé à un ajustement à σ_f analogue à celui de Kirpichnikov et al., pour lequel il avait été admis que J(0,3 eV) était différent de J (1,14 eV), contrairement à ce qui avait été fait pour des ajustements à plusieurs niveaux antérieurs. Ces données préliminaires sont compatibles avec une anisotropie proportionnelle à la contribution à σ_f des deux valeurs de J possibles, qui a été calculée. Toutefois, la forme de la courbe n'est pas en accord avec d'autres données, telles que la variation du rapport «sommet-vallée» de Faler et Tromp; en conséquence, bien qu'elle paraisse extrêmement plausible, l'hypothèse selon laquelle J (0,3 eV) est différent de J (1,14 eV) ne doit pas encore être considérée comme démontrée. On procède actuellement à de nouvelles mesures.

ВРАЩАТЕЛЬНЫЕ СОСТОЯНИЯ СЕДЛОВОЙ ТОЧКИ В РЕЗУЛЬТАТЕ РЕЗОНАНСНОГО ДЕЛЕНИЯ ОРИЕНТИРОВАННЫХ ЯДЕР. Ядра актинидных элементов урана, нептуния и плутония можно выстроить в соединениях $XO_2Rb(NO_3)_3$ путем взаимодействия квадрупольного момента ядра с градиентом кристаллического электрического поля просто в результате охлаждения соответствующего единичного кристалла. Выстраивание ядер этого типа соответствует неравномерному угловому распределению оси симметрии составного ядра в пространстве, что отражает в первую очередь величину K. Если предположить, что таково же и распределение осколков, то получим метод для установления числа квантов K в седловой точке. В Окридже были выполнены эксперименты с выстроенными ядрами урана-233 и урана-235 при температуре 1,2° K с помощью тепловых нейтронов, о чем сообщалось ранее.

Эти эксперименты теперь расширены с включением резонансных энергий нейтронов и при температуре 0,5° K. При использовании вместе с непосредственным определением (с помощью поляризованных нейтронов и поляризованных ядер) значений J, связанных с каждым резонансом, такое расширение дает возможность значительно полнее понять число и характер имеющихся каналов деления. Эти вопросы давно стоят в области деления. Для урана-235 было установлено, что анизотропия осколков деления приближается к вероятному максимуму при резонансах с энергиями 1,14 и 8,8 эв, со знаком, противоположным установленному ранее для альфа-частиц. Кроме того, было установлено значительное уменьшение в анизотропии при энергии нейтронов в районе хорошо известного резонанса 0,3 эв. При отсутствии непосредственной информации относительно значений J в уране-235 была сделана ссылка на многоуровневую апроксимацию к σ_f, подобную апроксимации Кирпичникова и др., в которой предполагалось, что J(0,3 эв) ≠ J(1,14 эв) в противоположность предыдущим многоуровневым апроксимациям. Эти предварительные данные совместимы с данными относительно анизотропии, пропорциональной расчетному вкладу в σ_f двух возможных значений J. Форма кривой, однако, не совместима с другими данными, например, с данными относительно изменения соотношения пик-впадина Фалера и Тромпа, что, таким образом, довольно категорически указывает на то, что J(0,3 эв) ≠ J(1,14 эв) не следует принимать как исчерпывающее. Проводятся новые измерения.

ESTADOS ROTACIONALES EN EL PUNTO DE ESTRANGULACION DEBIDOS A LA FISION POR RESONANCIA DE NUCLEOS ORIENTADOS. Los núcleos de los elementos actínidos uranio, neptunio y plutonio pueden alinearse en los compuestos del tipo $XO_2Rb(NO_3)_3$, en virtud de la interacción del momento cuadripolar del núcleo con el gradiente del campo eléctrico cristalino, por simple enfriamiento del monocristal correspondiente. Una alineación nuclear de este tipo corresponde a una distribución angular no uniforme del eje de simetría del núcleo compuesto en el espacio, que refleja principalmente el valor de K. Si se supone que los fragmentos presentan también la misma distribución, se obtiene un método para determinar el número cuántico K en el punto de estrangulación. Como se menciona en trabajos anteriores, en el Oak Ridge National Laboratory se han realizado experimentos con núcleos alineados de ^{233}U y de ^{235}U a 1,2°K utilizando neutrones térmicos.

Dichos experimentos se han ampliado ahora a energías neutrónicas de resonancia y a temperaturas de 0,5°K. Si se considera juntamente con la determinación directa (mediante neutrones y núcleos polarizados) de los valores J asociados a cada resonancia, esa ampliación permite llegar a un conocimiento mucho más preciso del número y naturaleza de los canales de fisión disponibles, cuestiones ambas que el fenómeno de la fisión suscita desde hace mucho tiempo. En el ^{235}U se observó, para las resonancias de 1,14 y 8,8 eV, una anisotropía de los fragmentos de fisión próxima al máximo posible, y de signo contrario al de la observada previamente en el caso de los heliones. Asimismo, se comprobó una marcada disminución de la anisotropía para energías neutrónicas próximas a la conocida resonancia de 0,3 eV. Como se carecía de información directa sobre los valores J del ^{235}U, se recurrió a un ajuste de niveles múltiples a σ_f, análogo al de Kirpichnikov y col., para el que se supuso que J(0,3 eV) ≠ J(1,14 eV), a diferencia de ajustes anteriores de carácter análogo.

Estos datos iniciales son compatibles con una anisotropía proporcional a la contribución que se ha calculado aportan a σ_f los dos valores posibles de J. Sin embargo, la forma de la curva no concuerda con otros datos tales como la variación de la razón cresta a valle de Faler y Tromp; por consiguiente, no deben aceptarse aún como concluyentes los fuertes indicios de que $J(0,3\ eV) \neq J(1,14\ eV)$. Los autores están efectuando mediciones complementarias para aclarar este concepto.

INTRODUCTION

The process of low energy neutron-induced fission can be considered to take place in three regimes. These are (a) capture and subsequent redistribution of excitation energy, corresponding to approach to the fission barrier; (b) passage over the saddle point (or tunnelling through the barrier); and (c) scission or breakup. Of these, only (b) represents a relatively simple situation, because (a) and (c) involve large numbers of states and many possible paths. As BOHR [1] has pointed out, the situation is considerably simplified during passage through or over the barrier; here the number of states available to the compound nucleus can be small, and these states are thought to be analogous to the collective states near the ground state of a deformed heavy nucleus. The simplification given by this picture provides a basis for understanding of the present experiments.

A number of experiments [2, 3, 4] have demonstrated that nuclei of the actinide elements uranium, neptunium and plutonium can be aligned in the compounds $XO_2Rb(NO_3)_3$, simply by cooling a single crystal of the compound. Although there was for some time a question about the direction of the nuclear orientation, this now appears to have been satisfactorily resolved [4, 5]. Both U^{233} and U^{235} are known to have positive nuclear electric quadrupole moments [6] ($Q > 0$), and both are believed to align with the major nuclear axis in the plane perpendicular to the c-axis of the (pseudo-hexagonal) $UO_2Rb(NO_3)_3$ crystal. In both cases, α-particles were found to be preferentially emitted in the plane perpendicular to the c-axis, with an anisotropy given by

$$W(\beta) = 1 + (A/T)\, P_2(\cos\beta), \qquad (1)$$

where A had the value -0.073 ± 0.013 for U^{235}, and the value -0.064 ± 0.004 for U^{233} [2].

One set of measurements has also been made on the anisotropy of fission fragments from U^{233} and U^{235} oriented in this fashion, using unfiltered reactor neutrons from the graphite reactor at the Oak Ridge National Laboratory [7]. The results showed an anisotropy of the type (1), but with $A = +0.035 \pm 0.009$ for U^{235} and $A \approx 0$ for U^{233}.

The present work is an extension of these experiments to selected neutron energies in the resonance range, and to lower temperatures where the coefficient of $P_2(\cos\beta)$ in (1) is larger, and thus easier to determine. We shall first discuss certain theoretical aspects of the problem, then describe the experimental apparatus and the (interim) results, and finally give the conclusions that may now be drawn.

THEORY

For present purposes, the compound nucleus during passage over the barrier may be considered to be represented by a suitable sum (over magnetic substates M) of symmetric top wave functions $\mathfrak{D}^J_{MK}$ $(\alpha\beta\gamma)$ where α, β, γ are the Eulerian angles. The three quantum number indices J, M, and K are those associated with the compound system at the saddle point, K being the projection of the total angular momentum J along the symmetry axis; and M being the projection of J along the spatial axis, i.e. along the c-axis of the crystal in the present case.

In his 1955 paper [1] BOHR suggested that small values of K should predominate in low-excitation fission. This argument is based on energetic considerations; i.e. those nuclei that have "used up" the least energy in preserving angular momentum and parity have more energy that can go into producing deformation. Nuclei in rotational states with low values of K have the largest moments of inertia and thus the smallest energy of rotation for a given J. These nuclei should therefore have a higher probability for fission.

In the aligned compound state system the angular distribution $W(\alpha, \beta, \gamma)$ of the symmetry axis is then given for each K by [8]

$$W_K(\beta) \propto \sum_M |\mathfrak{D}^J_{MK}|^2 P(M). \tag{2}$$

The populations P(M) are determined by the initial nuclear orientation. If the target nucleus has angular momentum quantum numbers j, m, and captures a neutron with spin projection μ, Eq. (2) may be written [8]

$$W_K(\beta) \propto \sum_{m,\mu} |\mathfrak{D}^J_{MK}|^2 \left(C\left(j\,\tfrac{1}{2}\,J;\ m\mu M\right)\right)^2 P(m), \tag{3}$$

where C is a Clebsch-Gordan coefficient. BOHR [1] identifies the angular distribution of the fragments after scission with the angular distribution of the symmetry axis at the saddle point. Within this identification, Eqs. (2) and (3) give an expression for the fragment angular distributions. These expressions may be shown to lead to the following for both the $J = j + \frac{1}{2}$ and $J = j - \frac{1}{2}$ cases of slow neutron fission:

$$W_K(\beta) = 1 + \frac{3K^2 - J(J+1)}{J(J+1)} \left[\frac{5(2j-1)(2j+1)(2j+3)}{4\,(2j)(2j+2)}\right]^{\frac{1}{2}} S_2 P_2(\cos\beta), \tag{4}$$

where S_2 is essentially the alignment parameter G_2 of ROSE [9][1]. In the present case, the nuclear alignments come from electric quadrupole coupling

[1] The second terms of Eq. (17) of Ref. [8] should be multiplied by the factor $-(2j+1)/(2j+2)$ to conform to Eq. (4) above; the second terms of the second equation in Ref. [6] and of Eq. (21b) in Ref. [3] contain a numerical error and should be multiplied by a factor 2/3.

with a spin Hamiltonian

$$\mathcal{H} = P\left[j_z^2 - \tfrac{1}{3}\, j(j+1)\right], \tag{5}$$

where P is the quadrupole coupling constant in cm^{-1}. The alignment parameter S_2 is then given in good approximation [10] by

$$S_2 = G_2 = \frac{1}{2j+1}\left[\frac{(2j+3)!}{180\,(2j-2)!}\right]^{\frac{1}{2}}\left(-\frac{Phc}{kT}\right), \tag{6}$$

where k is the Boltzmann constant and T is the absolute temperature. Thus in the Bohr approximation this formulation leads to an angular distribution that indeed has the form of Eq. (1).

For rather general types of nuclear alignment, including both the Pound (electric quadrupole coupling) and Bleaney (anisotropic magnetic hfs coupling) types, it has been shown [11] that in the angular distributions expected, i.e. in a more general form of Eq. (1)

$$W(B) = \sum_{\nu \text{ even}} A_\nu G_\nu P_\nu\ (\cos\beta), \tag{7}$$

an expansion of the alignment parameter G_4 in powers of $1/T$ cannot have terms of lower order than $(1/T)^2$. This point is important for demonstrating the absence of $P_4(\cos\beta)$ terms in the present experiment, where strict linearity of the anisotropy with $1/T$ is found within experimental error.

The coefficient of $P_2(\cos\beta)$ in Eq. (4) contains the parameter $[3K^2 - J(J+1)]$, and thus reverses sign in going from small K-values to values $K = J$. Table I gives values of A for each of the K-values that may occur for s-wave neutron-induced fission of U^{233} and U^{235}. Wheeler in a recent discussion [12] has suggested that certain K-values should be important. These values are starred in Table I [13].

Table I shows that the sign and magnitude of the anisotropy primarily reflects the value of K and is relatively insensitive to the value of J. Thus measurements of the angular distribution of fission from aligned nuclei should be quite useful in determining at least the average, or effective, value of K associated with rotational states at the saddle point of fission. As is now well known, it is also possible to determine J values associated with the compound nucleus (and thus with these same saddle point states) by using the interaction of polarized neutrons and polarized nuclei [14]. The existence of these two complementary methods thus gives promise of providing means for resonance-by-resonance studies of the saddle-point states in favourable cases.

The values in Table I include as a factor the degree of orientation that occurs in $U^{235}O_2Rb(NO_3)_3$, Eq. (6). There are three estimates of the coupling constant (Phc/k) at present available. The first is 0.0216°K and was obtained from low-temperature specific heat measurements on a related compound $U^{235}O_2F_2$ [2]. The second was obtained by CHASMAN and RASMUSSEN

TABLE I

CALCULATED A VALUES IN EQ. (1) (IN °K) CORRESPONDING TO VARIOUS J, K VALUES

The assumed values of the quadrupole coupling constant of Eq. (6) are given in each case

J / K	U^{233} (Phc/k = 0.0277°K)		U^{235} (Phc/k = 0.0154°K)	
	2^+	3^+	3^-	4^-
0	+0.074*	Parity forbidden	+0.077**	Parity forbidden
± 1	+0.037	+0.055	+0.058*	+0.065*
± 2	-0.037*	0*	0**	+0.031**
± 3		-0.092	-0.96	-0.027
± 4				-0.108

* Ref. [12]
** Refs. [12 and 13]

[15], using our results on U^{233} alpha particle anisotropy and a correctly phased partial wave analysis [3]. This gave a value of 0.0277°K for $U^{233}O_2 Rb(NO_3)_3$. Since the ratio of the quadrupole moments Q(235)/Q(233) is known approximately [16], a value of 0.0154 ± 0.0027°K can be derived for $U^{235}O_2Rb(NO_3)_3$. This value can also be considered as a minimum value of Phc/k, since the alpha anisotropy for the particular choice of partial wave amplitudes is very near the maximum for given Phc/k. A similar analysis has recently been made possible by a calculation of SALUSTI [17], who has given another derivation of the partial wave amplitudes in the alpha decay of U^{233}. This calculation in a similar way lowers the possible minimum value of Phc/k for U^{235} to 0.0123 ± 0.0022°K. The Chasman-Rasmussen values have been used in Table I to indicate the size of the expected anisotropies. These estimates emphasize the importance of an independent measurement of Phc/k [18].

APPARATUS

The apparatus for measurement of the fission-fragment anisotropy as a function of neutron energy and 1/T is in theory simple but somewhat more difficult in practice. A single crystal of $U^{238}O_2 Rb(NO_3)_3$, grown with a surface layer of the same material where U^{235} was substituted for U^{238}, was mounted in a variable energy neutron beam in such a way that its c-axis could be rotated with respect to a fission-fragment detector. The apparatus permitted cooling the crystal to temperatures as low as 0.45°K.

Figure 1 is a schematic diagram of the lower end of the cryostat in which the experiment was carried out. The dewar had an outside diameter

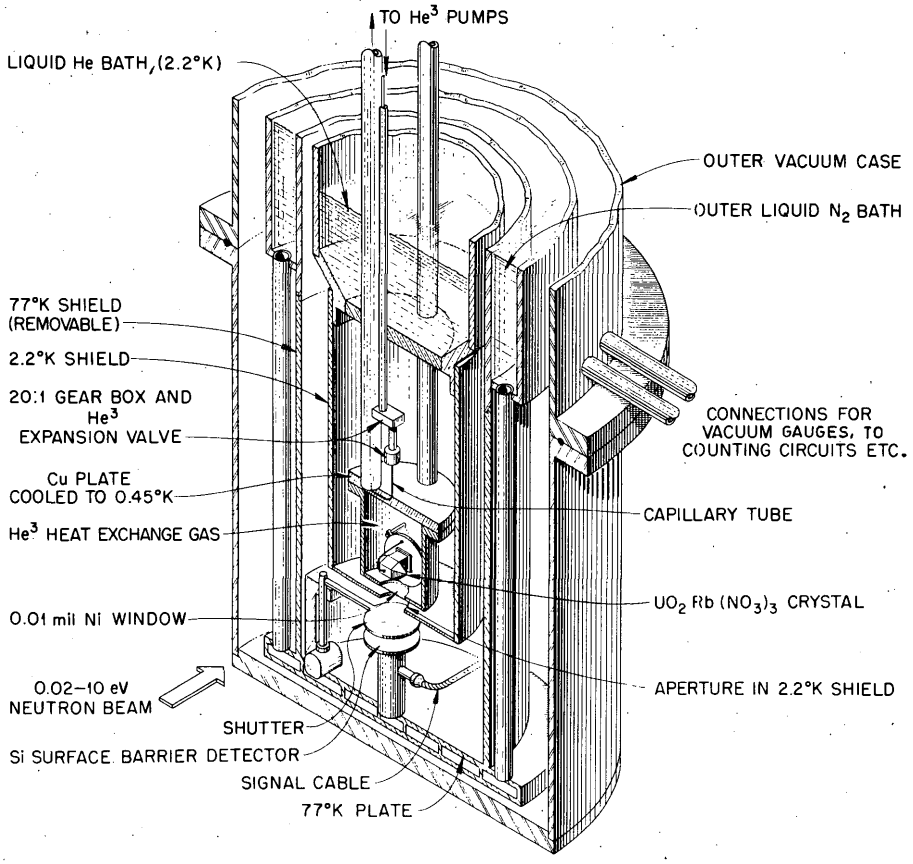

Fig. 1

Nuclear alignment apparatus

of 25 cm and contained two liquid nitrogen baths, a He^4 bath, and a section (the sample chamber) cooled by a continuously operating He^3 refrigerator. The temperature of the sample chamber was monitored by a carbon resistance thermometer and recorded continuously. A heater on the sample chamber was controlled so that the inverse temperature of the chamber is held within 1% of the desired 1/T value.

He^3 gas surrounded the sample, and provided adequate and reliable heat contact to the walls; the pressure of He^3 was $\sim 25 \times 10^{-3}$ mm Hg. The density was thus sufficiently low that (n, p) reactions in the He^3 were not important. This technique of gas cooling necessitated development of a thin gas-tight window. Nickel foil 2.5×10^{-5} cm thick (from Chromium Corp. of America) was used, and a dilute coating of 1% VYNS resin in cyclohexanone covered the small pinholes in the foil. A mesh support improved the ability of the foil to support a pressure differential, although great care had to be taken. Fission fragments passing through the foil lose $\lesssim 30\%$ in energy, and were detected by a silicon or germanium surface barrier detector at 77°K.

The He^3 refrigerator was unusual because it operated with a condenser temperature of 2.20°K rather than the usual 1.2°K.

The monochromator was a beryllium single crystal and the $12\bar{3}1$ reflection was used except at the lowest energies. Soller slits determined the entrance and exit collimations. The energy spread of the monochromator was 2.6% at 1 eV and 8.5% at 10 eV. The apparatus was at the Oak Ridge Research Reactor (30 MW). Even the high flux afforded by this reactor, however, gave counting rates that were quite small in the 1 - 10 eV energy range, and it was necessary to operate the experiment continuously for periods up to several weeks per resonance, an automated counting system being developed for this purpose. The low counting-rates also dictated the use of the He^3 refrigerator; an increase in the size of effect (by increasing $1/T$) of a factor n, for example, permits a reduction in counting time of a factor n^2 for a given accuracy.

Counts were taken in each of two sample positions (c-axis at 0° or 90° with respect to the detector direction). The counting periods were determined by the integrated neutron flux through the dewar as seen by a parallel plate fission chamber containing U^{235} (for measurements on U^{235}).

RESULTS

The results below represent approximately 7 months' operation of the experiment. The dependence of the anisotropies (both α and fission) on $1/T$ have been measured rather extensively at 0.28 eV. A graph of these values is shown in Fig. 2. The slope of the upper curve of Fig. 2 is a measure of the coefficient A in Eq. (1). It is the variation in this slope with energy which is interesting here. The linear dependence of both the alpha and fission effects on $1/T$ in Fig. 2 is a strong indication that the angular distributions are indeed of the form given by Eq. (1); additional confirmation of the absence of P_4 terms was found in the behaviour of the absolute counting-rates at 0° and 90°, although these indications are less accurate. The alpha particle anisotropy serves as an excellent monitor of the degree of orientation actually obtained, and thus can serve as a basis for normalizing measurements made under various conditions.

At neutron energies above 1 eV, low counting-rates have restricted the measurements to energies where large resonance appears in the U^{235} cross-section. Some analyses [19] have indicated that the resonance near 2 eV has a different J-value from the bound state and the 0.28 eV resonance. However, this resonance is quite small and probably cannot be studied without very prolonged measurements. Accordingly, the resonance at 1.14 eV was chosen for the initial measurements, followed by the large resonance at 8.8 eV. Measurements were then carried out from 0.28 eV down to 0.14 eV, the lowest energy available from beryllium in our monochromator arrangement. There was a sharp change in the anisotropy between 0.14 eV and 0.28 eV. An examination of the fission cross-section of U^{235} in this region shows that this sharp change corresponds roughly to the change from a very small contribution to the cross-section from the 0.28 eV resonance at 0.14 eV to the maximum contribution that occurs near 0.28 eV. The measured points are plotted in Fig. 3 (use right-hand scale).

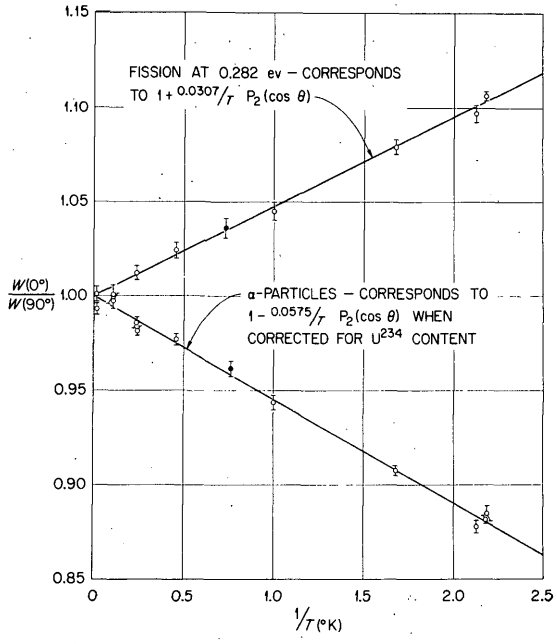

Fig. 2

U^{235} in $UO_2Rb(NO_3)_3$ using carbon resistance thermometer for 1/T values

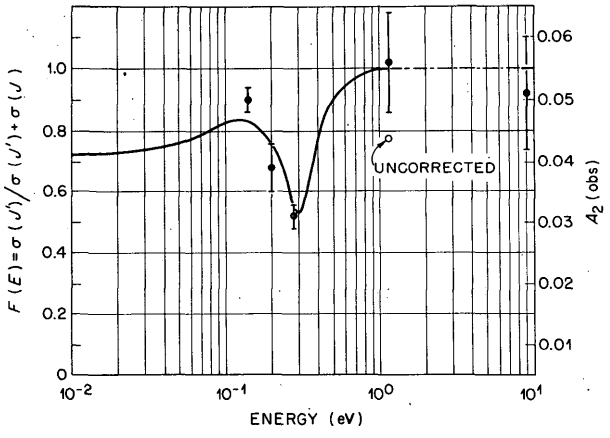

Fig. 3

Comparison of fission anisotropy with the cross-section contribution from spin J' as a function of neutron energy. The curve is derived from multilevel fit (see text).

PRELIMINARY ANALYSIS AND DISCUSSION

Since the observed anisotropy in the neighbourhood of the 0.28 eV resonance varied strongly and in a manner suggesting that the variation

might be proportional to the contribution (above "background") to the cross-section, a trial analysis was made on this basis. In the absence of direct measurements of J, resort was made to a multilevel fit to σ_f using parameters recently obtained by KIRPICHNIKOV et al. for the 0.28 and 1.14 eV levels [20], and estimates of the parameters for two assumed bound levels. The bound level nearest E = 0 was assumed to have the same J as the 0.28 eV level, while the other bound level and the level at 1.14 eV were assumed to have spin $J' = J \pm 1$, in accord with KIRPICHNIKOV et al. This choice was made in contradiction to other multilevel fits [19] because of the presence of the observed variation in A.

The quantity $F(E) = \sigma_f(J', E)/[\sigma_f(J', E) + \sigma_f(J, E)]$ was then calculated, and is shown as the smooth curve of Fig. 3. The scale for the observed anisotropies was adjusted to give an approximate fit of these points to the F(E) curve. Such a comparison makes the tacit assumption that only one channel/spin value is operative, i.e. for each spin J there is one particular K-value (or more properly, one set of K's). It is doubtful that such a relation actually holds, however. The apparent agreement in Fig. 3 may well be illusory. Two other pieces of evidence may be adduced to suggest this. Firstly, the radiochemical studies of FALER and TROMP give an asymmetric/symmetric fission ratio that clearly does not follow the F(E) curve of Fig. 3. The variation in their ratio bears little relation to the cross-section curve and is particularly flat in the region just below 0.3 eV [21]. Secondly, the same remark may be applied to the results of MOORE and MILLER, whose result [22] shows yet another variation with energy. It would appear that while results such as the above [21, 22] may give strong indications regarding the channels (saddle-point states) associated with thermal fission, the approaches outlined here provide the best hope for actual determination of the angular momentum character of such states.

ACKNOWLEDGEMENTS

We wish to thank L. D. Roberts for his many contributions to the initial conception of the alignment experiment and for the design of the neutron monochromator. J. O. Thomson made several contributions to the cryostat design. We particularly wish to thank C. T. Hall who constructed the cryostat.

REFERENCES

[1] BOHR, A., Proc. UN Int. Conf. PUAE (2) (1956) 151.
[2] DABBS, J.W.T., ROBERTS, L.D. and PARKER, G.W., Physica XXIV (1958) 569.
[3] ROBERTS, L.D., DABBS, J.W.T. and PARKER, G.W., Proc. 2nd Int. Conf. PUAE (15) (1958) 322.
[4] ROBERTS, L.D. and DABBS, J.W.T., Annu. Rev. nucl. Sci. 11 (1961) 175.
[5] HANAUER, S.H., DABBS, J.W.T., ROBERTS, L.D. and PARKER, G.W., Phys. Rev. 124 (1961) 1512.
[6] HILL, D.L., Handbuch der Physik 39 (1957) 178.
[7] ROBERTS, L.D., WALTER, F.J., DABBS, J.W.T., PARKER, G.W. and THOMSON, J.O., Proc. Int. Conf. Nucl. Structure, Kingston, 1960, University of Toronto Press, Toronto (1960) 884.
[8] Oak Ridge National Laboratory Rpt. 2430 (1957) 51.
[9] ROSE, M.E., Elementary Theory of Angular Momentum, John Wiley and Sons, New York (1957) 179.

[10] ROBERTS, L.D. and DABBS, J.W.T., Annu. Rev. nucl. Sci. 11 (1961) 175, where a more general form is given in Eq.(18).

[11] ROSE, M.E., ROBERTS, L.D., DABBS, J.W.T., Bull. Am. Phys. Soc. 1 (1956) 207.

[12] WHEELER, J.A., chapter on fission in Fast Neutron Physics, Part II, (MARION, J.B. and FOWLER, J.L., Eds) Interscience, New York (1963).

[13] MOORE, M.S. and MILLER, L.G., "Channel effects in the kinetic energy of fragments of fission induced by low-energy resonance neutrons", these Proceedings I.

[14] ROSE, M.E., Phys. Rev. 75 (1949) 213; recent works illustrating the power of the method can be found in, e.g. STOLOVY, A., Phys. Rev. 134 (1964) 68B, and SHORE, REYNOLDS, SAILOR and BRUNHART, Phys. Rev. (to be published, preprint available as Brookhaven National Laboratory Report 8788). It should be noted that no successful experiments on polarizing either U^{233} or U^{235} have been reported; this may be attributed to the very small nuclear magnetic moments of these isotopes.

[15] CHASMAN, R. and RASMUSSEN, J.O., Phys. Rev. 115 (1959) 1257.

[16] DORAIN, P.B., HUTCHISON, C.A. and WONG, E., Phys. Rev. 105 (1957) 1307; HUTCHISON, C.A., private communication.

[17] SALUSTI, E., Nuovo Cim. 30 (1963) 171, and private communication.

[18] HUTCHISON, C.A., Jr., private communication (attempts to find the quadrupole resonance); NEWMAN, J.B., private communication (attempts planned).

[19] SHORE, F.J. and SAILOR, V.L., Phys. Rev. 112 (1958) 191; VOGT, E., Phys. Rev. 112 (1958) 203; Phys. Rev. 118 (1960) 724.

[20] KIRPICHNIKOV, I.V., IGNAT'EV, K.G., and SUKHORUVHKIN, S.I., Atomnaja energija 16 (1964) 211.

[21] FALER, K.T. and TROMP, R.L., Phys. Rev. 131 (1963) 1736; cf. Fig.6 of Ref.13.

[22] MOORE, M.S. and MILLER, L.G., "Channel effects in the kinetic energy of fragments of fission induced by low-energy resonance neutrons", these Proceedings I, Fig.5.

EFFECTS OF ORBITAL ANGULAR MOMENTUM AND TARGET SPIN ON FISSION ANISOTROPY*

R. B. LEACHMAN AND JUDITH GURSKY
LOS ALAMOS SCIENTIFIC LABORATORY, LOS ALAMOS, N. MEX., UNITED STATES OF AMERICA

Abstract — Résumé — Аннотация — Resumen

EFFECTS OF ORBITAL ANGULAR MOMENTUM AND TARGET SPIN ON FISSION ANISOTROPY. Measurements of improved accuracy are reported for the anisotropy of fragments from fission induced by 17-MeV alpha-particle bombardment of Th^{230}, Th^{232}, U^{236}, and U^{238}. To investigate the effects of target spins on fission anisotropy, the relative anisotropy of these cases, which involve spinless particles and targets, is compared with the relative anisotropy of fragments from neutron-induced fission of the same compound nuclei. The comparison gives strong indication that the target spin effect is small, as expected from theory, and that the relative changes of anisotropy are due to the different elongations of the saddle-point nuclei. The absolute values of fission anisotropy for these alpha-particle-induced cases and for the neutron-induced equivalents allow determinations of the orbital angular momenta imparted to the nuclei for bombardment at this energy, which is far below the Coulomb barrier energy. The results grossly disagree with anisotropies calculated with transmission coefficients, and this is interpreted as resulting from errors in the transmission coefficients usually available at this energy. The agreement with anisotropies calculated from transmission coefficients derived from the square-well model is satisfactory only if an unrealistically small radius is used.

EFFETS DU MOMENT CINÉTIQUE ORBITAL DU PROJECTILE ET DU SPIN DE LA CIBLE SUR L'ANISOTROPIE DE LA FISSION. Les auteurs présentent des mesures d'une précision améliorée de l'anisotropie de fragments de la fission provoquée par le bombardement de ^{230}Th, ^{232}Th, ^{236}U et ^{238}U par des particules alpha de 17 MeV. Ils ont étudié les effets des spins de la cible sur l'anisotropie de la fission en comparant l'anisotropie relative de ces cas de fission, qui mettent en jeu des cibles et des particules sans spin, à l'anisotropie relative de fragments résultant de la fission par neutrons des mêmes noyaux composés. La comparaison donne fortement à penser que l'effet du spin de la cible est peu important, comme le laissait prévoir la théorie, et que les variations relatives de l'anisotropie sont dues aux différentes élongations des noyaux subissant l'étranglement. Les valeurs absolues de l'anisotropie de la fission pour ces cas de fission par particules alpha et pour les cas équivalents de fission par neutrons permettent de déterminer les moments cinétiques orbitaux communiqués aux noyaux pour des projectiles de cette énergie, qui est très inférieure à la barrière coulombienne. Les résultats diffèrent considérablement des anisotropies calculées à l'aide de coefficients de transmission, ce qui est expliqué par le fait que les valeurs des coefficients de transmission habituellement disponibles pour cette énergie sont erronées. Les résultats ne concordent de manière satisfaisante avec les anisotropies calculées à partir de coefficients de transmission dérivés du modèle du puits carré que si l'on utilise un rayon si faible qu'il ne correspond pas à la réalité.

ВЛИЯНИЕ ОРБИТАЛЬНОГО МОМЕНТА КОЛИЧЕСТВА ДВИЖЕНИЯ И СПИНА МИШЕНИ НА АНИЗОТРОПИЮ ДЕЛЕНИЯ. Сообщается о более точных измерениях для анизотропии осколков деления, вызванного бомбардировкой альфа-частиц тория-230, тория-232, урана-236 и урана-238 с энергией 17 Мэв. Для изучения влияния спинов мишеней на анизотропию деления относительная анизотропия этих случаев, которые включают частицы и мишени без спинов, сравнивается с относительной анизотропией осколков деления, вызванного нейтронами тех же самых ядер соединения. Сравнение ясно указывает на то, что влияние спина мишени является небольшим, как предполагалось теоретически, и что относительные изменения анизотропии вызываются различными удлинениями седловой точки ядра. Абсолютные величины анизотропии деления для этих случаев, вызванных альфа-частицами, и для эквивалентов, вызванных нейтронами, позволяют определить орбитальные моменты количества движения, сообщенного ядру для бомбардировки при этой энергии, которая значительно ниже кулоновско-

* Work performed under the auspices of the United States Atomic Energy Commission.

го энергетического барьера. Результаты в общем не согласуются с анизотропиями, вычисленными с помощью коэффициентов пропускания, и это интерпретируется как результат ошибок в обычно имеющихся коэффициентах пропускания при этой энергии. Соответствие с анизотропиями, вычисленными из коэффициентов пропускания, выведенных из модели "квадратного колодца", является удовлетворительным, если применяется лишь нереально малый радиус.

EFECTOS DEL MOMENTO ANGULAR ORBITAL DEL PROYECTIL Y DEL SPIN DEL BLANCO EN LA ANISOTROPIA DE LA FISION. Se describen mediciones, cuya precisión se ha mejorado, relativas a la anisotropía de los fragmentos de la fisión inducida por bombardeo de ^{230}Th, ^{232}Th, ^{236}U y ^{238}U con heliones de 17 MeV. A fin de investigar los efectos del spin del blanco en la anisotropía de la fisión, se compara la anisotropía relativa de estos casos, en los que intervienen partículas y blancos carentes de spin, con la anisotropía relativa de los fragmentos de fisión inducida por neutrones de los mismos núcleos compuestos. Esta comparación sugiere netamente que el efecto del spin del blanco es reducido, como permitía prever la teoría, y que las variaciones relativas de la anisotropía se deben al diferente alargamiento de los núcleos en el punto de estrangulación. Los valores absolutos de la anisotropía en fisiones inducidas por heliones y en las equivalentes inducidas por neutrones permiten determinar los momentos angulares orbitales comunicados a los núclidos al bombardearlos a esta energía, que es muy inferior a la de la barrera de Coulomb. Los resultados discrepan sensiblemente de las anisotropías calculadas mediante los coeficientes de transmisión, lo que se atribuye a los errores inherentes a los coeficientes de trasmisión habitualmente utilizados a esta energía. La concordancia con las anisotropías calculadas a partir de los coeficientes de transmisión deducidos del modelo de pozo cuadrado, es satisfactoria únicamente si se aplica un radio de valor inferior al corrientemente admitido.

INTRODUCTION

The fission process is distinctive in its liberation of much greater energy into particles of much greater mass than other nuclear reactions. In the measurements being reported, these characteristics are used to measure the angular momentum properties of low-energy alpha-particle-induced fission. The measurements are used to analyse two angular momentum properties of fission: (1) the effects of target spin and the saddle-point elongation on fission anisotropy; and (2) the orbital angular momentum imparted to the target nuclei by incident alpha particles whose energy is far below the Coulomb barrier.

Experimentally, the difficulty of measuring properties of low-energy charged-particle-induced fission is the low cross-section, which decreases exponentially with decreasing energy of the incident particle. FORD and LEACHMAN [1] have used radiochemical techniques to measure fission cross-sections for alpha particles as low as 19 MeV. These measurements showed that optical-model calculations [2] of cross-section were plainly inadequate at these lowest energies, but the square-well calculations [3] made by Gursky[1] gave improved agreement.

Fission anisotropy provides a different critical test of the adequacy of these calculations of low-energy charged-particle reactions. However, measurements of fission anisotropy involve additional experimental difficulties. Fission anisotropy is the ratio $W(0)/W(90)$ of fragment yields at 0° (or 180°) and 90° with respect to the incident beam, and is thus a convenient measure of the angular distribution $W(\theta)$ of fragments from fission.

[1] M. L. GURSKY, private communication (1963); calculations based on the infinite square-well model of BLATT and WEISSKOPF [3]. We are grateful to Dr. Gursky for these calculations.

To observe the anisotropy, a limited solid angle of acceptance is required. Also, for simplicity in the interpretations of data, a still lower incident energy, namely $E_\alpha \lesssim 17$ MeV, is required so that all fissions are the (α, f) process and that none are the more complicated (α, nf), etc., processes. The solid angle and the reduced energy each lower the yield by orders of magnitude, and so a pulse technique recording each fragment is desired. Particular care is required to distinguish the rare fission fragments from cumulative effects of the prolific yield of scattered alpha particles.

EXPERIMENT

New techniques with semiconductor detectors were used to discriminate fission fragments from pile-up of alpha particles. As is shown in Fig. 1, this involved a stack of two detectors at each angle. The first was a 60-μm-thick transmission counter facing the fission source. This counter absorbed all

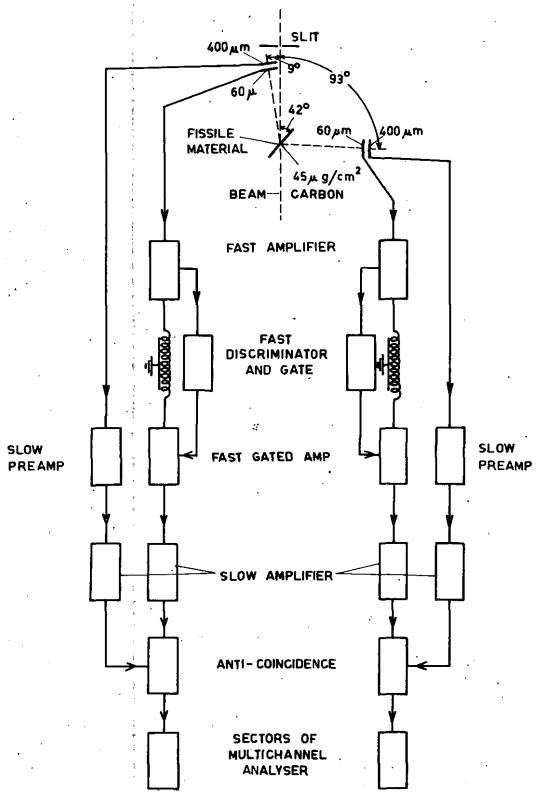

Fig. 1

Schematic diagram of the experimental arrangement.
Nanosecond electronics are labelled fast; microsecond electronics are labelled slow.
The delays before the gated amplifier were to compensate for the times required to activate the discriminator and gate circuits.
Other details are provided in the text.

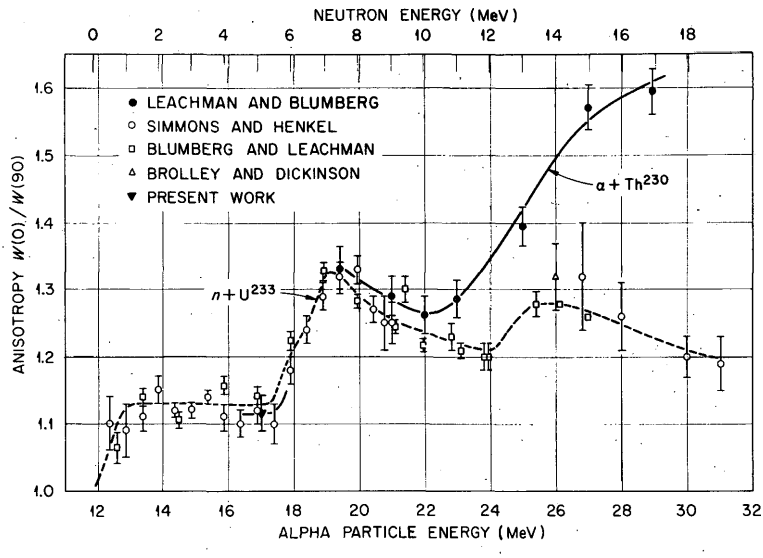

Fig. 2

Anisotropy data of fragments from the compound nucleus U^{234}. Curves are intended only as a guide for consolidating points. The angles for the present data were actually 171° and 90°. See Ref. [5] for earlier data.

$\mathcal{I}_0$ for the nucleus formed by neutron emission, $\mathcal{I}_\perp$ for the saddle-point nucleus about an axis perpendicular to the nuclear symmetry axis, and $\mathcal{I}_{||}$ for the saddle-point nucleus about this symmetry axis. The distribution in K is assumed to be Gaussian with a standard deviation K_0, where $K_0^2 = \mathcal{I}_{\text{eff}}\, T/\hbar^2$, $\mathcal{I}_{\text{eff}}^{-1} = \mathcal{I}_{||}^{-1} - \mathcal{I}_\perp^{-1}$, and T is the nuclear temperature. It is seen from Eq. (1) that the fission anisotropy should decrease slightly with increasing target spin I_0 and should decrease with increasing fissionability (increasing Z^2/A of the compound nucleus). The latter decrease is due to the smaller elongation required for fission of nuclei with large Z^2/A and the consequently large value of the dominant $\mathcal{I}_\perp$ in the K_0^2 expression.

The semiclassical anisotropy expression of Eq. (1) has been used by LEACHMAN and BLUMBERG [5] qualitatively to show that K_0^2 is independent of whether the compound nucleus is formed by alpha particles or neutrons. SIMMONS et al. [9] have used Eq. (1) with data of neutron-induced fission to show that the rate at which K_0^2 increases with Z^2/A is the same for compound nuclei with both odd and even A. Since these data for the even-A compound nuclei correspond to targets with considerably different target spins I_0, this result conforms to Eq. (1) by showing the target spin effects to be negligible. However, the argument is based on the expectation that the rate of K_0^2 increase with Z^2/A is the same for even and odd nuclei. This is a plausible, but unproven, assumption.

In the present investigation, least squares fits of the data were made to the exact expression for the angular distribution [10]

$$W(\theta) = \sum_I \sum_M \sum_K G(I,M) F(K_0;I,K) \mid D^I_{MK}(\theta) \mid^2 , \qquad (3)$$

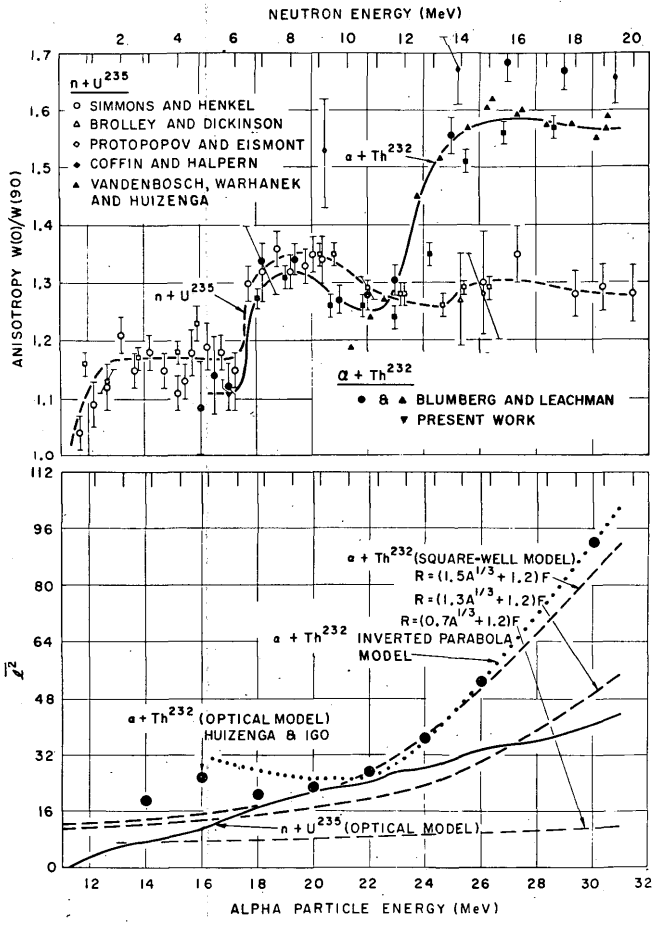

Fig. 3

Anisotropy data of fragments from the compound nucleus U^{236} and, below, orbital angular momentum calculations.
The calculations in the lower figure were based on:
the square-well method of footnote 1 and Ref. [3];
the alpha-particle optical model from Ref. [2] (also see footnote 6);
the neutron optical model with parameters extrapolated from Ref. [11];
and the inverted parabola model from Ref. [12] (also see footnote 7).
See the caption of Fig. 2 for other details.

where

$$G(I,M) = \frac{\sum_{\ell}\sum_{j} (2\ell + 1)T_{\ell}(E_n) \mid C^{j\ell I}_{MOM} \mid^2}{(2S + 1)(2I_o + 1)\sum_{\ell}(2\ell + 1)T_{\ell}(E_n)} \qquad (4)$$

and

$$F(K_o;I,K) = \frac{\exp(-K^2/2K_o^2)}{\sum_{K=-I}^{I} \exp(-K^2/2K_o^2)}, \qquad (5)$$

in the energy region of exclusively (n, f) fissions. The lines in the figure are least squares fits of a linear [6] relation between K_0^2 and energy.

The open points in Fig. 6 are the K_0^2 values from the equivalent alpha-particle-induced anisotropy of the present work. Here, the transmission coefficients were calculated from the use of a radius $R = (0.7\ A^{\frac{1}{3}} + 1.2)F$ in the square-well model. It is clearly seen from Fig. 3 that this radius is far too small properly to calculate anisotropy at higher energies, but nevertheless these calculations provide a consistent set to give the small differences between the transmission coefficients for these thorium and uranium isotopes. The K_0^2 comparison in Fig. 6 shows that change of K_0^2 with Z^2/A of the compound nuclei is just as large for the spinless case of alpha-particle-induced fission as for neutron-induced fission (with spins). This shows that the change of neutron-induced fission anisotropy with target spin is neither anomalously large nor of the wrong sign, and that the change instead is adequately explained by the variation of K_0^2 with Z^2/A. This is summarized in Table I.

TABLE I

FISSION ANISOTROPY PARAMETERS AND RESULTS

Compound nucleus	Z^2/A	Spin and parity of neutron target	Neutron-induced K_0^2	Alpha particle-induced K_0^2
Pu^{240}	36.82	1/2(+)	34.46	42.74
Pu^{242}	36.51	5/2(+)	30.11	43.86
U^{234}	36.17	5/2(+)	26.48	21.44
U^{236}	35.86	7/2(-)	20.85	23.50

Note: The target spins and parities for neutron irradiations are given. The K_0^2 for neutron-induced fission are from the least squares fits in Fig. 6 at the excitation energies corresponding to 17-MeV alpha-particle bombardments. The K_0^2 values are calculated from Eq. (3) for 17-MeV alpha-particle-induced fission data. Transmission coefficients from the square-well calculation [radius $R = (0.7\ A^{\frac{1}{3}} + 1.2)F$] were used.

Orbital angular momenta calculations

The results of ℓ^2 calculations shown in the lower part of Fig. 3 can be compared [5] with the anisotropy data in the upper part of the figure by means of the simplification

$$\frac{\left[\frac{W(0)}{W(90)} - 1\right]_\alpha}{\left[\frac{W(0)}{W(90)} - 1\right]_n} = \frac{\overline{\ell_\alpha^2}}{\overline{\ell_n^2}} \qquad (6)$$

to Eq.(1), where the subscript α denotes alpha particles and n denotes neutrons. (The $\overline{l^2}$ calculated values for the other nuclei in Figs. 2, 4, and 6 are essentially the same.) Comparison at 17-MeV alpha-particle energy shows the $\overline{l_\alpha^2}$ from the square-well calculations with the usual $R = (1.5\ A^{\frac{1}{3}} + 1.2)F$ radius, from the optical model calculation of HUIZENGA and IGO[6] [2], and from the inverted parabola model[7] [12] to be progressively too large. Table I shows that the use of $R = (0.7\ A^{\frac{1}{3}} + 1.2)F$ radius in the square-well calculation gives agreement with these low-energy data, but, as noted above, disagreement at higher energies. Apparently, the use of an unrealistically sharp nuclear surface causes this disagreement in the square-well model calculation.

REFERENCES

[1] FORD, G. P. and LEACHMAN, R. B., Phys. Rev. 137 (1965) B826. Also see earlier work cited in this reference.

[2] HUIZENGA, J. R. and IGO, G., Nucl. Phys. 29 (1962) 462; and Argonne National Laboratory Report 6373 (1961) (unpublished).

[3] BLATT, J. M. and WEISSKOPF, V. F., in Theoretical Nuclear Physics, John Wiley & Sons, New York (1952) 360.

[4] BARNA, A. and MARSHALL, J. H., Rev. Sci. Instrum. 35 (1964) 881.

[5] LEACHMAN, R. B. and BLUMBERG, L., Phys. Rev. 137 (1965) B814.

[6] GRIFFIN, J. J., Phys. Rev. 132 (1963) 2204.

[7] BOHR, A., in Proc. UN Int. Conf. PUAE 2 (1956) 151.

[8] LEACHMAN, R. B. and SANMANN, E. E., Ann. Phys. 18 (1962) 274.

[9] SIMMONS, J. E., PERKINS, R. B. and HENKEL, R. L., Phys. Rev. 137 (1965) B809.

[10] BLUMBERG, L. N., thesis, Columbia University (1962) (unpublished). See also Ref. [6].

[11] BEYSTER, J. R., SCHRANDT, R. G., WALT, M. and SALMI, E. W., Los Alamos Scientific Laboratory Report LA-2099 (1956) (unpublished).

[12] HILL, D. L., and WHEELER, J. A., Phys. Rev. 89 (1953) 1102.

DISCUSSION

J. R. HUIZENGA: Have you extracted from your experimental data the total fission cross-sections with helium-ion-projectiles of 14-18 MeV energy and compared these values with the theoretical optical model reaction cross-sections?

R. LEACHMAN: No, only relative yields for the two angles were measured. The data of Ford and Leachman* give the absolute cross-sections for 19-MeV α-particle-induced fission and higher. Here also, the transmission coefficients obtained from calculations are not in good agreement with data.

---

[6] In a private communication (1962), Huizenga suspects the calculated values in Ref. [2] to be in error below 18 MeV.

[7] Kindly made with the Bunthorne code [T. D. THOMAS, Phys. Rev. 116 (1959) 703] by J. O. Rasmussen and R. Kiefer (1964).

* FORD, G. P. and LEACHMAN, R. B., "Fission mass yield studies", these Proceedings I.

CHANNEL ANALYSIS OF NEUTRON-INDUCED FISSION OF EVEN-EVEN ISOTOPES NEAR THRESHOLD*

R. W. LAMPHERE
OAK RIDGE NATIONAL LABORATORY,
OAK RIDGE, TENN., UNITED STATES OF AMERICA

Abstract — Résumé — Аннотация — Resumen

CHANNEL ANALYSIS OF NEUTRON-INDUCED FISSION OF EVEN-EVEN ISOTOPES NEAR THRESHOLD. A well-known theory by A. Bohr postulates that fission occurs via bands of channels akin to the K-bands observed by radioactive decay spectra or Coulomb excitation of heavy nuclei. Each of these channels would cause a unique angular distribution of the fragments from fission. Therefore measurements of fragment angular distribution as function of bombarding energy of the projectile should in principle permit identification of K-bands through which fission is taking place. In practice, limitations of energy and angular resolution as well as intensity preclude recognition of more than the first two or three K-bands above threshold.

One of the simplest situations, bombardment of even-even target nuclei with neutrons, has been analysed theoretically and measurements carried out near threshold for Th^{230}, Th^{232}, U^{234}, U^{236} and U^{238}. The first four of these show great similarity but U^{238} is strikingly different. In all cases experimental limitations rule out the possibility of identifying individual levels within a band. Since, however, these levels are quite close together one can make a reasonable estimate of their relative strengths and so arrive at an over-all predicted fragment angular distribution for any given K-band. The greatest uncertainty in such a calculation arises from the effects of competition of compound nucleus decay by neutron emission.

Bands for which K is equal to $\frac{1}{2}$ (either parity) will give rise to fragment distributions strongly peaked in intensity at zero and 180° to the incident beam. All bands of higher K produce peaking normal to the beam. Although the angular distribution is independent of parity, the parity of contributing bands can often be found from the fact that cross-sections for formation of a compound nucleus with negative parity are substantially higher than for positive parity over the ranges of mass, spin and energy of interest near the thresholds for fission.

It is possible to make reasonable estimates for the first three K bands for Th^{230}, Th^{232} and U^{234}, and with perhaps a bit more uncertainty for U^{236} as well. For U^{238} one can say with certainty that the first band has K equal to $\frac{1}{2}$, and further, that if bands with K greater than $\frac{1}{2}$ are present then they are weak. Further calculations are in progress.

ANALYSE DES VOIES DE LA FISSION DE NOYAUX PAIRS-PAIRS PAR NEUTRONS, AU VOISINAGE DU SEUIL. D'après une théorie bien connue de A. Bohr, la fission s'opère par des bandes de voies analogues aux bandes K que l'on observe par des spectres de désintégration radioactive ou par une excitation coulombienne de noyaux lourds. Chacune de ces voies donnerait lieu à une distribution angulaire unique des fragments de fission. C'est pourquoi les valeurs mesurées de la distribution angulaire des fragments en fonction de l'énergie du projectile devraient en principe permettre d'identifier les bandes K par lesquelles la fission se produit. Dans la pratique, les limitations du pouvoir de résolution en énergie et en valeur d'angle et celles de l'intensité empêchent de reconnaître des bandes plus nombreuses que les deux ou trois premières bandes K au-delà du seuil.

Une des situations les plus simples, savoir le bombardement de noyaux pairs-pairs avec des neutrons, a fait l'objet d'une analyse théorique et de mesures à proximité du seuil pour ^{230}Th, ^{232}Th, ^{234}U, ^{236}U et ^{238}U. Les quatre premiers de ces éléments présentent une forte analogie entre eux, mais ^{238}U est extrêmement différent. Dans tous les cas, les limitations expérimentales excluent la possibilité d'identifier des niveaux distincts à l'intérieur d'une bande. Cependant, étant donné que ces niveaux sont très proches les uns des autres, il est possible de formuler une estimation raisonnable de leurs intensités relatives pour arriver ainsi à prévoir en gros la distribution angulaire des fragments pour une bande K donnée. La plus grande incertitude

* Research sponsored by the United States Atomic Energy Commission under contract with the Union Carbide Corporation.

dans un calcul de ce genre résulte des effets de la concurrence de la désintégration du noyau composé par émission de neutrons.

Des bandes pour lesquelles K est égal à $\frac{1}{2}$ (quelle que soit la parité) donneront lieu à des distributions de fragments dont l'intensité présentera un pic très marqué pour 0° et 180° par rapport au faisceau incident. Toutes les bandes de K plus élevé présentent des pics pour une direction normale au faisceau. Bien que la distribution angulaire soit indépendante de la parité, on peut souvent trouver la parité des bandes contribuantes en se fondant sur le fait que les sections efficaces de formation d'un noyau composé à parité négative sont sensiblement plus élevées que pour la parité positive dans les gammes de masses, spins et énergies intéressantes au voisinage des seuils de fission.

Il est possible de formuler des estimations raisonnables pour les trois premières bandes K en ce qui concerne ^{230}Th, ^{232}Th et ^{232}U, *ainsi que* - *peut-être avec un peu plus d'incertitude* - ^{236}U. Pour ce qui est de ^{238}U, on peut dire avec certitude que, pour la première bande, K est égal à $\frac{1}{2}$ et en outre que, si des bandes à K plus grand que $\frac{1}{2}$ sont présentes, elles sont nécessairement faibles. De nouveaux calculs sont en cours.

КАНАЛЬНЫЙ АНАЛИЗ ВЫЗВАННОГО НЕЙТРОНАМИ ДЕЛЕНИЯ ЧЕТНО-ЧЕТНЫХ ИЗОТОПОВ ОКОЛО ПОРОГОВОГО ЗНАЧЕНИЯ. В хорошо известной теории Бора утверждается, что деление возникает при прохождении частиц через полосы каналов к полосам K, отмеченным в спектрах радиоактивного распада или при кулоновском возбуждении тяжелых ядер. Каждый из этих каналов вызывает уникальное угловое распределение осколков деления. Поэтому измерения углового распределения осколков как функции бомбардирующей энергии налетающей частицы должны в принципе дать возможность различать полосы K, при прохождении через которые происходит деление. На практике ограничения энергии и углового разрешения, а также интенсивности мешают различать больше чем первые две-три полосы K выше порогового значения.

В одном из простейших положений бомбардировка четно-четных ядер мишени нейтронами анализировалась теоретически и проводились измерения тория-230, тория-232, урана-234, урана-236 и урана-238 около порогового значения. Результаты для первых четырех элементов имеют большое сходство, однако, для урана-238 резко отличаются. Во всех случаях ограничения эксперимента исключают возможность различать отдельные уровни в полосе. Поскольку, однако, эти уровни очень близки друг другу, можно сделать разумную оценку их относительной силы и тем самым придти к общему предсказанному угловому распределению осколков для любой данной полосы K. Наибольшая неопределенность при таком расчете возникает в связи с эффектами конкуренции со стороны распада составных ядер при испускании нейтронов.

Полосы, в которых K равно 1/2 (любой четности), будут давать распределение осколков с большим пиком интенсивности при 0 и 180° к падающему пучку. Во всех полосах с большими значениями K пики образуются в направлении нормали к пучку. Хотя угловое распределение не зависит от четности, четность делающих вклад полос часто может быть установлена из того факта, что сечения образования составного ядра с отрицательной четностью значительно выше, чем с положительной четностью в диапазонах масс, спина и энергии, представляющих интерес для процесса деления около пороговых значений.

Можно дать разумные оценки для первых трех полос K для тория-230, тория-232 и урана-234 и, вероятно, с несколько большей неопределенностью также для урана-236. В отношении урана-238 можно сказать определенно, что первая полоса имеет K, равное 1/2, а если присутствуют полосы с K выше 1/2, то они являются слабыми. Проводятся дальнейшие расчеты.

ANALISIS POR CANALES DE LA FISION DE ISOTOPES PAR-PAR INDUCIDA POR NEUTRONES EN LAS PROXIMIDADES DEL UMBRAL. Una conocida teoría de A. Bohr afirma que la fisión tiene lugar según bandas de canales afines a las bandas K que ponen de manifiesto los espectros de desintegración radiactiva o la excitación coulombiana de los núcleos pesados. Cada uno de esos canales originaría una sola distribución angular de los fragmentos de fisión. Por consiguiente la identificación de las bandas K por conducto de las cuales tiene lugar la fisión debería en principio poder hacerse midiendo la distribución angular de esos fragmentos en función de la energía de impacto del proyectil. En la práctica, las limitaciones del poder de resolución en cuanto a la energía y a la distribución angular, así como la intensidad, impiden identificar más de dos o tres bandas K situadas por encima del umbral.

Se ha analizado *teóricamente uno de los casos más simples*, a saber, el bombardeo neutrónico de los núcleos blanco par-par y se han efectuado mediciones, en las proximidades del umbral, relativas al ^{230}Th, ^{232}Th, ^{234}U, ^{236}U y ^{238}U. Los cuatro primeros de estos isótopos muestran considerables analogías, pero el ^{238}U

difiere muy sensiblemente. En todos los casos, las limitaciones inherentes a la experimentación excluyen la posibilidad de identificar los diferentes niveles de una banda. Pero como estos niveles se hallan muy próximos unos a otros, es posible calcular con razonable aproximación su intensidad relativa y deducir una distribución angular teórica de los fragmentos para cualquier banda K. En este cálculo, el mayor factor de indeterminación se debe a los efectos competitivos de la desintegración por emisión neutrónica de núcleos compuestos.

Las bandas para las que K es igual a $\frac{1}{2}$ (de una u otra paridad) darán lugar a distribuciones de fragmentos cuya intensidad presenta un máximo acusado a ángulos de 0 y 180 grados respecto del haz incidente. Todas las bandas para las que K es superior producen picos normales al haz. Si bien la distribución angular es independiente de la paridad, la de las bandas contribuyentes puede determinarse en muchos casos basándose en el hecho de que las secciones eficaces de formación de un núcleo compuesto con paridad negativa son considerablemente mayores que las de uno con paridad positiva, en los intervalos de masa, spin y energía de interés en las proximidades de los umbrales de fisión.

Es posible calcular con una aproximación razonable las tres primeras bandas K correspondientes al ^{230}Th, ^{232}Th y ^{234}U y también, quizá con un margen de indeterminación ligeramente mayor, la correspondiente al ^{236}U. En cuanto al ^{238}U, se puede afirmar con seguridad que, en la primera banda, K es igual a $\frac{1}{2}$, mientras que las posibles bandas de K superior a $\frac{1}{2}$, han de ser débiles. Los autores están efectuando cálculos complementarios.

INTRODUCTION

Since the discovery of fission-fragment anisotropy by WINHOLD, DEMOS and HALPERN in 1952 [1] many measurements have been made of the angular distribution of fragments from fission induced by various means. By far the majority of these have been at high energies, well above the thresholds for fission, so that many channels contribute and statistical methods need to be used to analyse the results. The reason for this is, of course, that close to threshold it takes a much longer time to acquire a meaningful quantity of data.

Very close to threshold where only a few channels are open to fission one can hope to identify these in terms of I, K, and parity from measurements of the fragment angular distribution as function of projectile energy, using the theory proposed by BOHR [2] in 1955. According to this theory the nucleus as it passes the saddle point is greatly elongated (the major axis is roughly twice that of the minor) to the extent that nearly all the energy brought in by the projectile is concentrated in potential energy of deformation. Under such conditions a structure of K bands will exist based on collective motions, similar to those of the heavy deformed nuclei in and near the ground state. Therefore fission offers perhaps the only means of studying such levels in very highly deformed nuclei. Following the lead of NILSSON [3] one might hope to develop a theory accurate enough to relate the positions of levels at saddle point to levels near ground state of the same nucleus, thus depicting how the levels shift with deformation.

This paper is concerned with bombardment of even-even target nuclei of masses from 230 to 240 with mono-energetic neutrons over the energy range close to threshold for fission in each case. The first work of this kind was done at Los Alamos by BROLLEY and DICKINSON [4] on Th^{232}. The results were later analysed by WILETS and CHASE [5] who showed that fission was occurring largely through a K band with K equal to 3/2. Measure-

ments have been made at Oak Ridge in more detail, on this and other isotopes. For example, in the case of Th^{232} one can now say that the K-band sequence is 1/2 plus, $3/2^-$, $1/2^-$, the bands being separated by a few hundred kilovolts. These measurements have of necessity taken many years to complete because of lack of accelerator time for the project. Results have been analysed, as in the case of U^{234} reported in 1962 [6]. Only the highlights can be presented here. A more complete report will follow when more experimental data have been collected.

METHOD

Mono-energetic neutrons from either the Li(p, n) or T(p, n) reaction were directed onto a collimated fission counter as shown in Fig. 1. In this case the neutrons originate in a tritium gas target. Figure 2 shows the counter

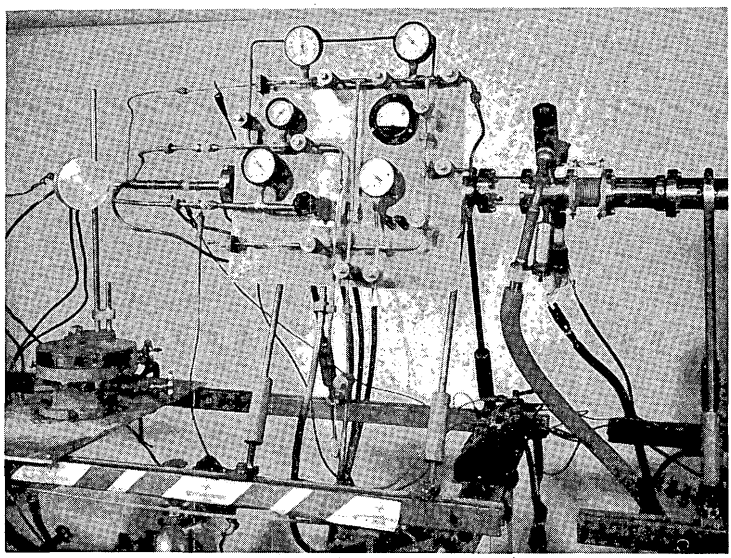

Fig. 1

Gas target and collimated fission detector set-up

in more detail, and Fig. 3 shows one of two identical collimators that are the heart of the apparatus. Fission foils are placed back to back in the counter with a collimator in front of each. A collimator consists of an aluminium disc with a grid of 0.020-in diam. holes drilled at 45° to the surface. The collimator has a transmission factor of 1/275. By use of two foils and collimators one measures the relative fragment intensity at two angles, usually 0 and 90° to the beam. A neutron monitor enables intensities at other angles to be measured by suitable rotations of the counter. The monitor took the form of a long counter placed at 90° to the beam axis. As expected, symmetry was found about 90°. However in all experiments it was customary

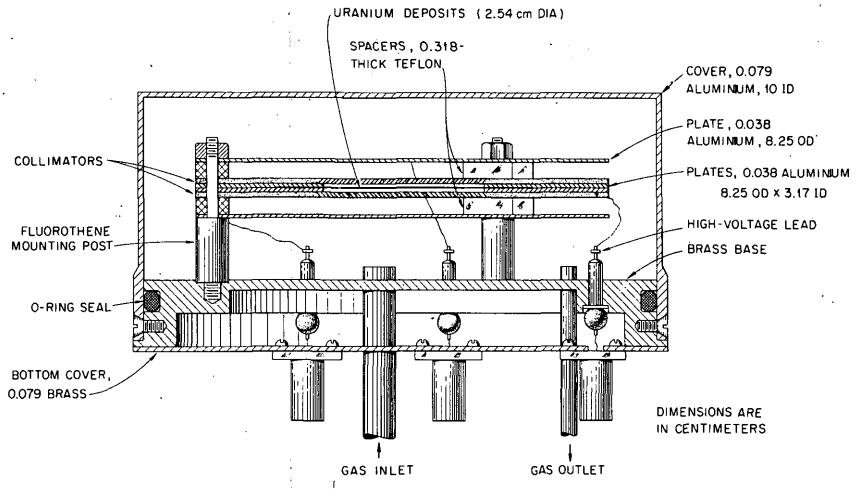

Fig. 2

Collimated fission detector

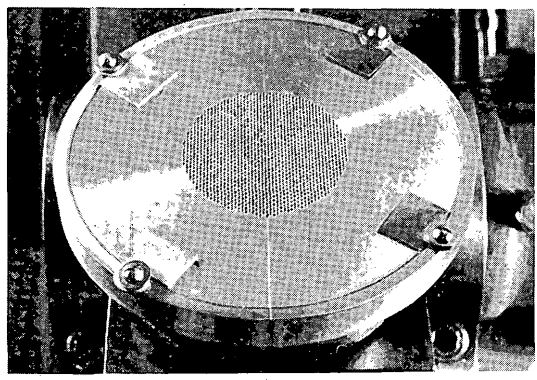

Fig. 3

Collimator surface after completion of drilling

to take readings at 0, 90, 180 and 270° as a check on equipment. Data were found always to be self-consistent and were combined to yield the angular anisotropy, α, defined as $\sigma_f(0°/90°)$. As previously reported [6], in the case of U^{234} measurements were made at other angles, but were not considered worth the time required to obtain them with this type of apparatus. Solid state detectors are a good means to obtain simultaneous data at many angles and have been used by SIMMONS and HENKEL [7] in an extensive work on angular anisotropy from neutron-induced fission. Most of their data was taken at energies too far above threshold to yield to channel analyses, and instead was interpreted by use of statistical methods. However, in some cases it does overlap slightly the work reported here.

The target nuclei studied consisted of Th^{230}, Th^{232}, U^{234}, U^{236}, U^{238} and Pu^{240}. In each case a measure of the angular anisotropy, a, was obtained as a function of neutron energy starting at an energy as low as one could expect to get significant statistics in a reasonable time, and continuing to energies several hundred kilovolts above the fission threshold. Suitable theoretical expressions were then used to ascertain the order in which the various K bands contributed to fission. The levels within the K bands lie very close together, a few kilovolts or in some cases a few tens of kilovolts apart, so that they could not be distinguished individually. Predictions from the optical model indicate that strengths of the first two or three levels within any given band will overshadow the effects of all others together in determining the angular anisotropy.

Probable errors are primarily statistical as there is no background except that Pu^{240} gave a small background from spontaneous fission. Such fragments are distributed isotropically in angle. All results have been corrected for this effect. Although chamber components were made as light as possible, there will be a correction of about 5 to 10% due to neutrons scattered elastically and inelastically from these components. The uncertainty in this correction is estimated to be not greater than 20%. Scattering from objects outside the chamber produce negligible effects. Scattered neutrons are essentially isotropic and so tend to reduce measured departures from isotropy in the fragment distribution. All results have been corrected for this effect, which introduces an additional 1 to 2%, to be compounded with the counting statistical error. As far as could be ascertained, other sources of error were negligible.

METHODS OF ANALYSIS

A compound nucleus formed by capture of a fast neutron will decay either by neutron emission or by fission, neutron emission being much more probable, at least for the cases considered here. The theory relating to this is far from exact, particularly for such levels of collective vibration as the so-called beta or gamma types. Also level structures for the residual nuclei are never known completely. This complicates interpretation of angular distribution data in terms of channels in that formulae for partial cross-sections can only serve as rough guides. The simplest assumption, which may be quite crude, is that Γ_n/Γ_f is independent of K and I of the compound nucleus. Here I is the total angular momentum and remains constant from capture to scission. K is the component of I along the axis of deformation of the nucleus, and is generally presumed not to be constant, except that during the final oscillation prior to scission K will not change, while the nucleus elongates more and more and finally passes over the saddle point. Neutron emission will be expected to occur with highest probability when least energy is concentrated in potential energy of deformation, hence when deformation is small and K not a good quantum number. For compound nuclei with large I a considerable fraction of the momentum may be carried off as intrinsic spin of the individual fragments. There is some evidence of this from studies of fission induced with charged particles of several MeV

energy. However, since the extent to which this occurs is not known, no allowance is made for it in the formulae to be presented. In fact for studies near threshold it is not thought to be a serious obstacle to analysis, but should be borne in mind, especially for such target nuclei as Th^{232} and where one is attempting to estimate the effects of the K bands on fragment angular distribution well above its rather high fission threshold.

The following relations have been discussed in detail elsewhere [6]. The angular distributions of fragments relative to the neutron beam are symmetric about 90° and independent of parity. They depend on K, I, and θ as follows:

$$W(K,I,\theta) = \tfrac{1}{2}(-1)^K + \tfrac{1}{2}\sum_x C^{IIx}_{-KK0}\,\bar{Z}(\ell I \ell I, \tfrac{1}{2}x)P_x(\cos\theta). \qquad (1)$$

From the independence of parity it follows that either of the two allowed values of ℓ for a given I may be taken, and the function will be the same. These functions have been plotted and are shown in Fig. 4. Note that for K and I equal to 1/2 the distribution is isotropic, and this is the only level that gives this. Also note that for K equal to 1/2 and all possible values of I greater than 1/2 the distribution is forward and backward peaked, and that for all higher values of K the peaking is sidewise regardless of I. These are very important factors in recognizing channels near threshold. For an entire K band the resultant angular distribution is

$$\sigma_K(\theta) = \frac{\lambda\!\!\!^{-2}}{4}\sum_{\ell I}(2I+1)\,T_\ell^{\,I}\,W(KI), \qquad (2)$$

where the T_ℓ^I are neutron transmission functions, and for this work those of PEREY and BUCK [8] based on a non-local optical potential have been used.

Relative strengths of the various K bands may be estimated roughly from the following relations that give the maximum possible strengths:

$$\begin{aligned}
\sigma_{1/2-} &= \pi\lambda\!\!\!^{-2}\,[T_1^{\,1/2} + 2\,T_1^{\,3/2} + 3\,T_3^{\,5/2} + 4\,T_3^{\,7/2} + \ldots]\\
\sigma_{1/2+} &= \pi\lambda\!\!\!^{-2}\,[T_0 + 2\,T_2^{\,3/2} + 3\,T_2^{\,5/2} + 4\,T_4^{\,7/2} + \ldots]\\
\sigma_{3/2-} &= \pi\lambda\!\!\!^{-2}\,[\quad 2\,T_1^{\,3/2} + 3\,T_3^{\,5/2} + 4\,T_3^{\,7/2} + \ldots]\\
\sigma_{3/2+} &= \pi\lambda\!\!\!^{-2}\,[\quad 2\,T_2^{\,3/2} + 3\,T_2^{\,5/2} + 4\,T_4^{\,7/2} + \ldots]\\
&\text{etc.}
\end{aligned} \qquad (3)$$

In the hypothetical situation where all compound nuclear decay occurs via fission through one K band the various terms give the strengths of the levels in that band directly. This is still true if fission occurs via two bands of

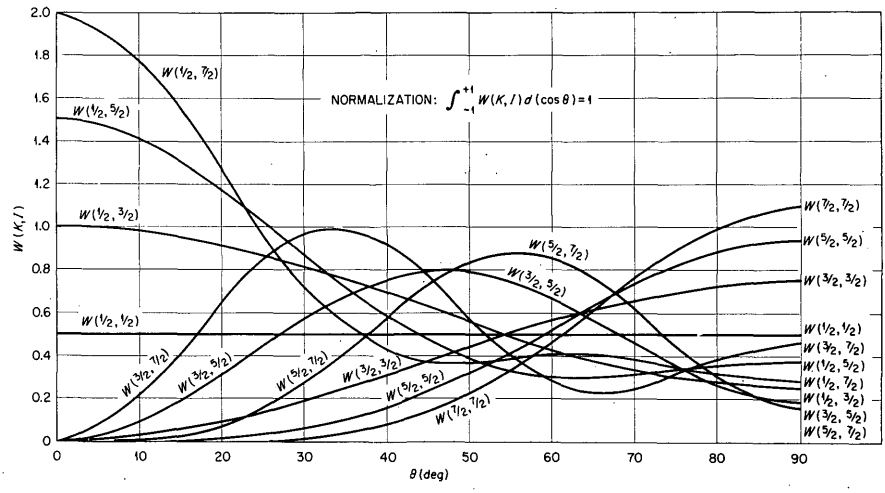

Fig. 4

Theoretical fission fragment angular distributions for fission through pure rotational states, W(K, I)

opposite parity. Where like parity bands are competing the common terms represent the sum of the strengths of the various levels of these two bands. The following experimental results are discussed in the light of the foregoing relations.

EXPERIMENTAL RESULTS

Thorium-230

Figure 5 shows the fission cross-section and angular anisotropy for Th^{230}. The cross-section curve is preliminary as there still remains a 10% disagreement between two methods of measuring the quantity of Th^{230} on the foils used. The curve is either as shown or 10% higher throughout. The cross-section was measured relative to U^{235} and values for U^{235} were taken from Ref. [9]. The procedure followed was similar to that described in Ref. [10]. Reasons for the rather wide disagreement between the various laboratories in the angular anisotropy measurements at low energy is not known [7, 11].

The forward peaking at the lowest energies is clear indication of a K = 1/2 band. The subsequent sidewise peaking shows a higher lying band with K greater than 1/2 and stronger than the first band. The partial cross-sections indicate that the only combination that fits is a K = 1/2+ band followed by a K = 3/2- band. The forward peaking at still greater energies can then be explained only by a third band with K = 1/2-. Thus the K band sequence at saddle-point deformation of the compound nucleus Th^{231} is believed to be 1/2+, 3/2-, 1/2-. As both parity 1/2 bands are already present the forward peaking would be expected to remain at all higher energies, as indeed it does.

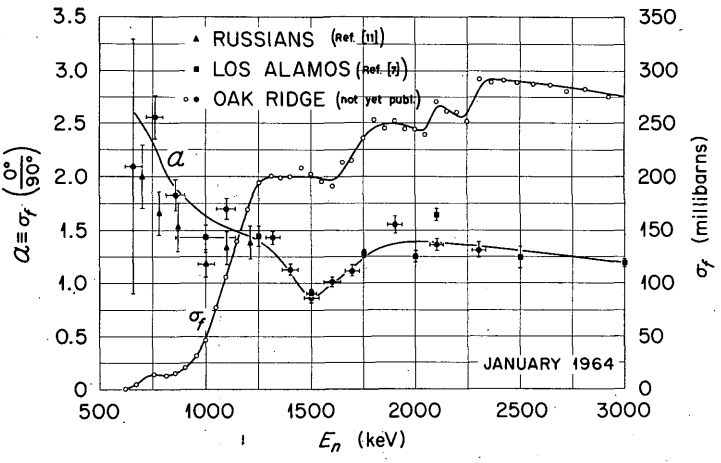

Fig. 5

Fission cross-section and fragment anisotropy for neutron-induced fission of Th^{230}

Thorium-232

Figure 6 shows the angular anisotropy for Th^{232}; the fission cross-section is taken from the Los Alamos work given in Ref. [9]. The coincidence of energy in the extrema should be noted, leading one to suspect that Γ_n/Γ_f may

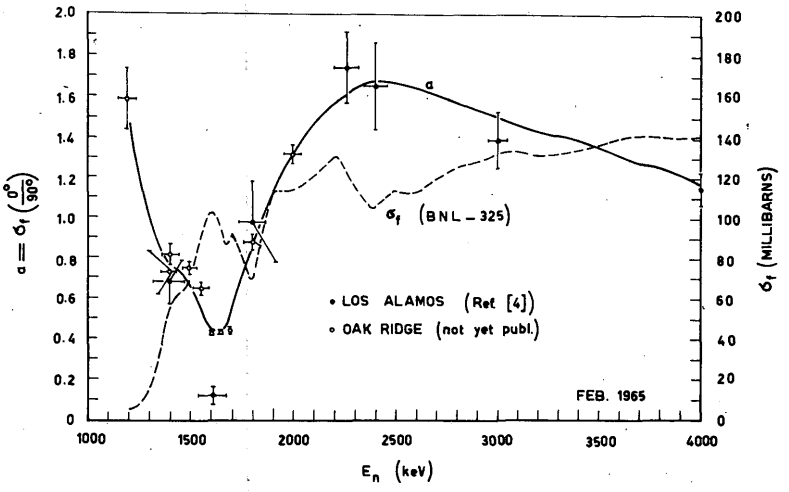

Fig. 6

Fission cross-section and fragment anisotropy for neutron-induced fission of Th^{232}

vary quite widely in some cases at least from level to level. Despite this, however, the variations in a are so marked that one can make K band assignments on the same basis as for Th^{230}, and the same sequence is found. Thus

for the compound nucleus Th^{233} at saddle-point deformation the K band sequence is believed to be 1/2+, 3/2-, 1/2-.

There remains an unsolved question in regard to this nucleus, however, It should be noted that at 1600-keV neutron energy, Los Alamos [12] finds an anisotropy of 0.12 to very good statistics. The Oak Ridge data do not confirm this. However, if the Los Alamos point is correct it cannot be explained by any of the theory given here. It can only be said that there must be some extraordinary selection rules at work regarding inelastic neutron scattering that inhibit formation of the K = 1/2+ states at saddle point once the bombarding neutron energy approaches 1600 keV.

Uranium-234

Since the fairly comprehensive report [6] published on this nucleus in 1962 additional data on α at lower energies were taken in 1963. The total of all data are shown in Fig. 7. The additional data merely serves to strengthen

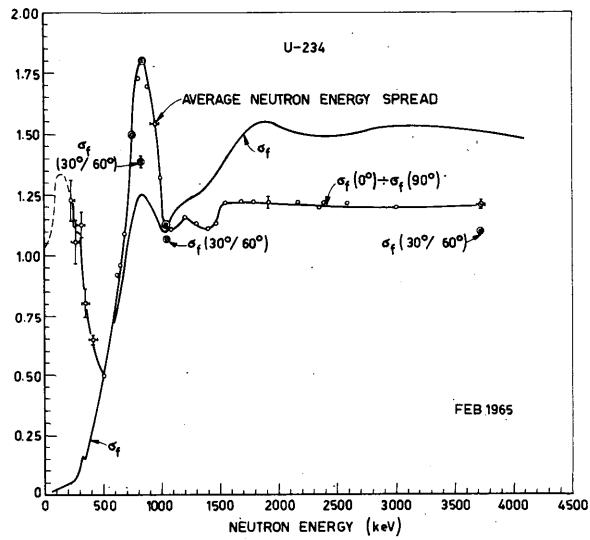

Fig. 7

Fission cross-section and fragment anisotropy for neutron-induced fission of U^{234}

the arguments for the K band sequence given in the 1962 paper. Based on the same reasoning as above, the K band sequence for the compound nucleus U^{235} at saddle-point deformation is believed to be the same as the two preceding; namely, 1/2+, 3/2-, 1/2-. Above about 1100-keV neutron energy the picture becomes clouded by the addition of other channels and the overriding effect of the very strong 1/2- band so that predictions of higher bands cannot be made.

However, it is interesting to note that the reaction, d(p, f), on U^{234} by VANDENBOSCH [13] shows additional structure as indicated in Fig. 8. Energy resolution was about the same for both sets of data, but statistics were con-

siderably better for the Oak Ridge points. The agreement over the rest of the curve is quite good. The discrepancy may be due to the fact that the deuterons introduce considerably more angular momentum into the compound nucleus, and so may excite more of the available states. Dr. Vandenbosch will discuss this in more detail later in the Symposium[1].

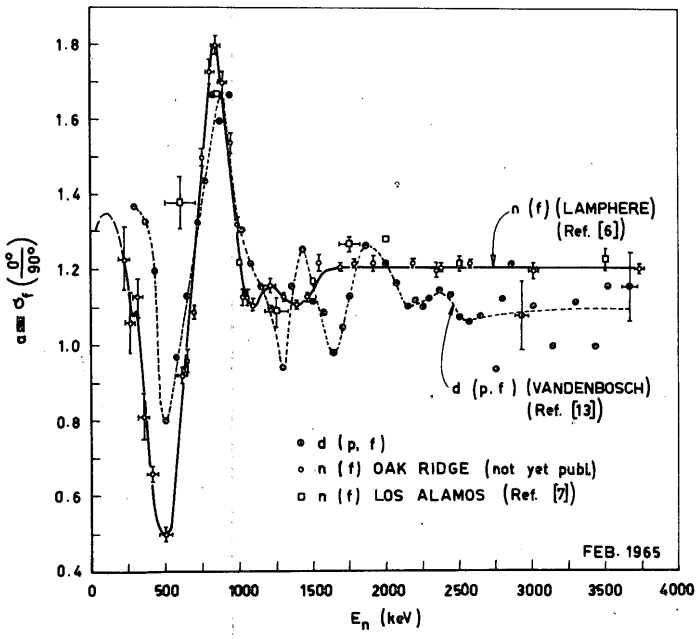

Fig. 8

Fragment angular anisotropy for neutron-induced and deuteron-induced fission of U^{234}

Uranium-236

The low-energy angular anisotropy data for this nucleus is shown in Fig. 9. This is another case where more data are needed. To obtain these data better U^{236} is required. The U^{236} used had about 1% U^{235} in it, and the background counts from this at the lowest energies amounted to a substantial fraction of the total. Material is needed having, say, not more than 0.2% U^{235}. A request for a few milligrams of such material was made about a year ago. On the basis of present data it is difficult to make a firm assignment of the first three K bands. A K band sequence of 3/2+, 1/2+, 3/2-, 1/2- will explain the curve as it is shown, and is consistent with the partial cross-sections and angular anisotropies given by the appropriate formulae. However, 5/2+ or 5/2- may be alternate possibilities for the first level. More careful calculations concerning this first level are scarcely justified until better data can be obtained between 600- and 400-keV neutron energy. It

[1] VANDENBOSCH, R., UNIK, J. P. and HUIZENGA, J. R., "Fission-fragment angular, energy, and mass division correlations for the U^{234} (d, pf) reaction", these Proceedings I.

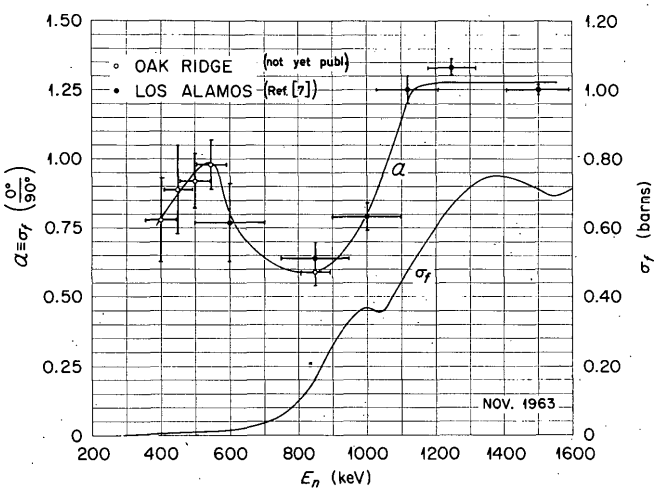

Fig. 9

Fragment angular anisotropy and fission cross-section for neutron-induced fission of U^{236}

is quite possible that additional data will show that the curve does not dip in this region, in which case the level sequence might be the same as for the preceding mass numbers.

Uranium-238

Figure 10 shows the low-energy angular anisotropy data for this target nucleus. The striking difference compared to lower mass numbers should be noted. It is clear that here fission is predominantly through channels of K = 1/2 at all energies. As the angular anisotropy is not as large as would be predicted by 1/2 bands alone others of larger K must be present, but so

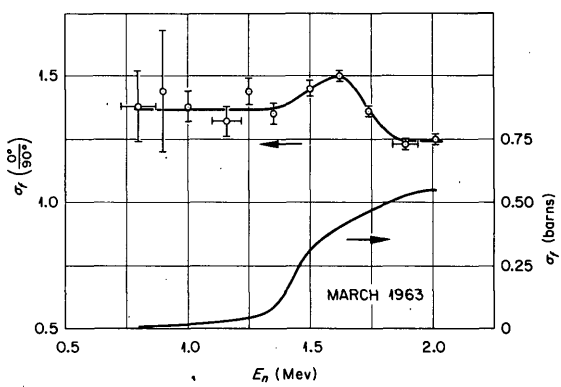

Fig. 10

Fission cross-section and fragment anisotropy for neutron-induced fission of U^{238}

close to the 1/2 band or bands that no level sequence can be predicted. Thus the compound nucleus U^{239} at saddle-point deformation has low lying K = 1/2 band or bands intermingled with one or more of higher K. The relatively small hump in the curve could be explained by additional strength from a K = 1/2 band in this region or by preferential decay of certain states by neutron emission.

Plutonium-240

Figure 11 shows results obtained so far for Pu^{240}, the last nucleus so far studied. Even after a full two weeks' accelerator time results are scanty

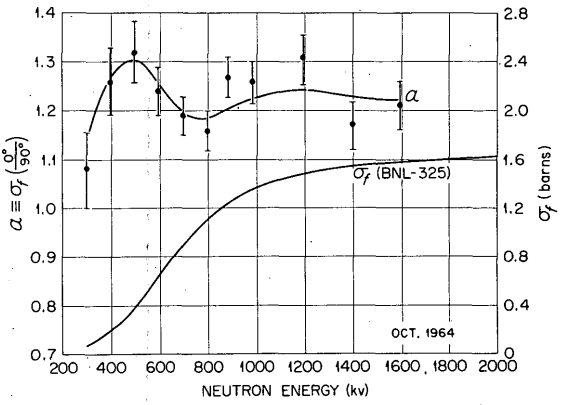

Fig. 11

Fragment angular anisotropy and fission cross-section for neutron-induced fission of Pu^{240}

because only extremely poor quality foils were available. More data are needed in the lowest energy region. At the lowest energy point the background from spontaneous fission was a substantial fraction of the total count rate. The similarity to U^{238} should be noted. Clearly K = 1/2 bands are dominant, although if the curve is correct as shown then the first K band will be one of K greater than 1/2, and the second will be a K equal to 1/2 band.

ACKNOWLEDGEMENTS

It is a pleasure to acknowledge the help of George Petit, of the Oak Ridge Gaseous Diffusion Plant, who developed a method for the quantitative deposition of thorium and who plated all the thorium foils, as also the special thickly coated foils of U^{236} and U^{238}. The U^{234} and U^{235} foils were plated by Ralph Greene of the same laboratory [10]. Thanks are also due to A. J. Wyrick and to Dick Robinson who ran the accelerator and took data on most of the evening shifts.

REFERENCES

[1] WINHOLD, E.J., DEMOS, P.T. and HALPERN, I., Phys. Rev. 87 (1952) 1139.
[2] BOHR, A., Proc. UN Int. Conf. PUAE 2 (1956) 151.
[3] NILSSON, S.G., Mat.-fys. Meddr. 29, No. 16 (1955).
[4] BROLLEY, Jr., J.E. and DICKINSON, W.C., Phys. Rev. 94 (1954) 640.
[5] WILETS, L. and CHASE, D.M., Phys. Rev. 103 (1956) 1296.
[6] LAMPHERE, R.W., Nucl. Phys. 38 (1962) 561.
[7] SIMMONS, J.E. and HENKEL, R.L., Phys. Rev. 120 (1960) 198.
[8] AUERBACH, E.H. and PEREY, F.G.J., Brookhaven National Laboratory Report No. 765 (1962).
[9] HUGHES, D.J. and SCHWARTZ, R.B., Brookhaven National Laboratory Report No. 325.
[10] LAMPHERE, R.W. and GREENE, R.E., Phys. Rev. 100 (1955) 763.
[11] GOKHBERG, B.M., OTROSHCHENKO, G.A. and SHIGIN, V.A., Dokl. Akad. Nauk SSSR 128 (1959) 1157. Trans: Soviet Phys.-Dokl. 4 (1960) 1074.
[12] HENKEL, R.L. and BROLLEY, Jr., J.E., Phys. Rev. 103 (1956) 1292.
[13] VANDENBOSCH, R., private communication (1964).

DISCUSSION

V.I. LEBEDEV: I should like to comment on the data on Th^{230} given in Dr. Lamphere's interesting paper. In the work carried out in the I.V. Kurchatov Institute, Moscow [1], an unusual cross-section curve for Th^{230} was observed near the threshold. An analysis of this cross-section and of the angular distributions of fission fragments shows that this is the first case in which a sequence of bands for the odd-even fissionable nucleus deviates from $1/2^+$, $3/2^-$, $1/2^-$. The cross-section curve for this isotope at energies of 600-1000 keV can be attributed to the effect of the band with $K = 1/2$, $\pi = (-)$; a $3/2^-$ channel then comes into play, as can be seen from the disappearance of anisotropy in the angular distributions, but at energies of 1100-1200 keV the effect of the $1/2^-$ band is again evident.

J.J. GRIFFIN: Could Dr. Lamphere comment on the limitations imposed by the angular momentum available from the neutron beam at the energies mentioned?

R. LAMPHERE: In general, K-bands, if present with $K > 7/2$, will be only very weakly excited. In this connection it should be noted that, despite the greater angular momentum brought in by the d(pf) reaction compared with the n(f) reaction, the results of the angular anisotropy measurements of these two reactions on U^{234} do not differ widely.

[1] Воротников, П.Е., Дубровина, С.М., Шигин, В.А. и Отрощенко, Г.А., "Угловые распределения осколков деления Th^{230}, Pu^{238}, Am^{241} нейтронами", these Proceedings I.

A STUDY OF FISSION FOLLOWING (d, p) AND (t, p) REACTIONS IN URANIUM ISOTOPES

D. ECCLESHALL AND M.J.L. YATES
ATOMIC WEAPONS RESEARCH ESTABLISHMENT, ALDERMASTON, BERKS., UNITED KINGDOM

Abstract — Résumé — Аннотация — Resumen

A STUDY OF FISSION FOLLOWING (d, p) AND (t, p) REACTIONS IN URANIUM ISOTOPES. The fission of U^{233}, U^{234}, U^{235}, U^{236} and U^{238} induced by (d, p) and (t, p) reactions has been studied, at a bombarding energy of 13 MeV. The protons were detected in an annular counter system situated at about 170° to the beam, and the proton spectrum in coincidence with fission fragments was recorded. The annular counter system consisted of an E-ΔE telescope with a thin (0.002-in) surface barrier semiconductor counter in front of a thick surface barrier counter in which the protons were stopped. The particles were identified using a conventional pulse multiplier.

The fission fragments were detected in other surface barrier counters at 90°, 135° and 170°. For this latter angle the annular ΔE counter was used to detect the fission fragments, since it was found that of the various particles emerging from the target only the protons were in coincidence with fission fragments.

Differences in the fission thresholds deduced from the U^{234} (t, pf) and U^{235} (d, pf) reactions were observed, indicating that the (t, p) reaction feeds fissioning states of lower excitation in the compound nucleus. A difference in the behaviour of the fission-fragment angular distributions for these two reactions was also observed at energies close to the fission threshold. Both effects provide evidence for a detailed structure consistent with the existence of the low-lying collective excitations at the saddle point of fission, analogous to those observed at the stable shape, which has been described by A. Bohr.

ÉTUDE DE LA FISSION CONSÉCUTIVE AUX REACTIONS (d, p) ET (t, p) DANS LES ISOTOPES DE L'URANIUM. Les auteurs ont étudié la fission de ^{233}U, ^{234}U, ^{235}U, ^{236}U et ^{238}U consécutive aux réactions (d, p) et (t, p), les projectiles ayant une énergie de 13 MeV. Ils ont décelé les protons dans un dispositif de comptage annulaire placé à 170° environ par rapport au faisceau, et ils ont noté le spectre des protons en coïncidence avec des fragments de fission. Le dispositif de comptage annulaire était formé d'un appareil E-ΔE muni d'un compteur à semi-conducteur à barrière de surface mince (0,002 pouce), placé devant un compteur à barrière de surface épaisse dans lequel les protons étaient arrêtés. Les auteurs ont identifié les particules au moyen d'un multiplicateur d'impulsions classique.

Ils ont décelé les fragments de fission dans d'autres compteurs à barrière de surface, à 90°, 135° et 170°. Pour ce dernier angle, ils ont utilisé le compteur annulaire ΔE pour déceler les fragments de fission, car ils ont établi que, des diverses particules émises par la cible, seuls les protons étaient en coïncidence avec les fragments de fission.

Ils ont observé des différences entre les seuils de fission pour les réactions ^{234}U(t, pf) et ^{235}U(d, pf), ce qui indique que la réaction (t, p) provoque des états de fission de basse excitation dans le noyau composé. Ils ont également observé une différence dans le comportement des distributions angulaires de fragments de fission pour ces deux réactions à des énergies proches du seuil de fission. Ces deux effets démontrent la présence d'une structure détaillée compatible avec l'existence d'excitations collectives de basse énergie au point d'étranglement, analogues à celles qui ont été observées pour la forme stable décrite par A. Bohr.

ИЗУЧЕНИЕ ДЕЛЕНИЯ ПОСЛЕ РЕАКЦИЙ (d, p) и (t, p) В ИЗОТОПАХ УРАНА. Изучалось деление урана-233, 234, 235, 236 и 238, вызванное реакциями (d, p) и (t, p) при энергии бомбардировки 13 мэв. Протоны детектировались в системе кольцевых счетчиков, расположенных приблизительно под углом 170° к пучку, и спектр протонов регистрировался в совпадении с осколками деления. Система кольцевых счетчиков состояла из телескопа E−ΔE с полупроводниковым счетчиком с тонким (0,002 дюйма) поверхностным барьером перед счетчиком

с толстым поверхностным барьером, в котором протоны задерживались. Частицы распознавались с помощью обычного импульсного фотоумножителя.

Осколки деления детектировались в других счетчиках с поверхностным барьером под углом 90, 135 и 170°. Для последнего угла кольцевой ΔE счетчик применялся для детектирования осколков деления, поскольку было установлено, что из различных частиц, вылетающих из мишени, только протоны совпадают с осколками деления.

Различия в порогах деления выводились из реакций урана-234 (t, pf) и урана-235 (d, pf), что свидетельствовало о том, что реакция (t, p) способствует поддержанию состояний деления при низком возбуждении в составном ядре. При энергиях около порога деления отмечалось также различие в характеристике угловых распределений осколков деления для этих двух реакций. Оба эффекта свидетельствуют о том, что детальная структура совместима с существованием низко лежащих коллективных возбуждений в седловой точке деления, аналогично эффектам, отмеченным при устойчивой форме, которая описана Бором.

ESTUDIO DE LA FISION CONSECUTIVA A REACCIONES (d,p) Y (t,p) EN ISOTOPES DEL URANIO. Se ha estudiado, para energías de bombardeo de 13 MeV, la fisión de ^{233}U, ^{234}U, ^{235}U, ^{236}U y ^{238}U inducidas por reacciones (d,p) y (t,p). Los protones se detectaron en un contador anular colocado en ángulo de unos 170° con respecto al haz, y se registró el espectro de los protones en coincidencia con los fragmentos de fisión. El contador anular consistía en un telescopio E-ΔE provisto de un contador de semiconductor con barrera superficial delgada (0,002 pulg) situado frente a un contador de barrera superficial gruesa en el que los neutrones quedaban detenidos. La identificación de la partículas se realizó mediante un multiplicador de impulsos de tipo usual.

Los fragmentos de fisión se detectaron mediante otros contadores de barrera superficial dispuestos en ángulos de 90°, 135° y 170°. Para esta última posición, se empleó el contador anular ΔE en la detección de los fragmentos de fisión, ya que se comprobó que de las diversas partículas procedentes del blanco, sólo los protones se hallaban en coincidencia con los fragmentos de fisión.

Las diferencias observadas entre los umbrales de fisión deducidos de las reacciones $^{234}U(t,pf)$ y $^{235}U(d,pf)$, indican que la reacción (t,p) alimenta en el núcleo compuesto estados de fisión de excitación más baja. También se observó, a energías próximas al umbral de fisión, un comportamiento distinto de las distribuciones angulares de los fragmentos de fisión correspondientes a esas dos reacciones. Ambos efectos facilitan pruebas de una estructura fina compatible con la existencia de excitaciones colectivas bajas en el punto de estrangulación, análogas a las observadas y descritas por A. Bohr para la forma estable.

INTRODUCTION

NORTHROP et al. [1] showed that fissioning states could be excited by (d, p) reactions in uranium and plutonium isotopes using 14-MeV deuterons. These authors observed structure in the proton energy spectra in coincidence with fission fragments consistent with the existence of low-lying collective states at the fission saddle points, analogous to those observed in stable nuclei. BRITT et al. [2] have studied the angular distribution of fission fragments in the U^{233} (d, pf) and Pu^{239} (d, pf) experiments, from which they derived values of K_0, the rms value of the quantum member K representing the projection of the total angular momentum on the symmetry axis of the fissioning nucleus. More recently WILKINS et al. [3] have obtained similar information for the fission of U^{238} by studying the $U^{238}(\alpha, \alpha'f)$ reaction.

In a series of experiments at the Atomic Weapons Research Establishment the fission of several uranium isotopes has been induced by (d, p) and (t, p) reaction at a bombarding energy of 13 MeV. In contrast to the earlier experiments protons were detected in a counter system situated near 180° to the incident beam direction. At this angle in heavy target nuclei and for bombarding energies close to the Coulomb barrier, the differential cross-

sections for the direct (d,p) and (t,p) reactions are near the maximum value for all angular momentum transfers (see e.g. Ref. [4]). Furthermore, the final nuclei can be highly oriented with this particular geometry, and a less detailed knowledge of the reaction mechanism leading to the fissioning nucleus is required. In the case of the (t,p) reaction this is especially so because, if the reaction proceeds by the direct stripping process, then the two neutrons are captured with S = 0. Hence in the reaction the magnetic substate population is unchanged, $\Delta M = 0$, and for an even target nucleus the fissioning states will have only M = 0 (the axis of quantization is the beam axis).

A preliminary survey of the (t,pf) and some of the (d,pf) reactions on U^{233}, U^{234}, U^{235}, U^{236} and U^{238} has been made, looking at fission thresholds and yields as a function of bombarding energy. The reactions U^{233}(d,pf) and U^{234}(t,pf) were selected for a more detailed study of the fragment angular distributions. These are the reactions leading to the even fissioning nuclei that have the highest fission probabilities. In this paper we discuss mainly the results of the U^{234}(t,pf) reaction.

THE EXPERIMENTAL ARRANGEMENT

Beams of deuterons and tritons at an energy of 13 MeV were used to bombard thin ($300\,\mu g/cm^2$) targets, with currents up to 0.1 μA. After passing through the target the beam was collected in a large Faraday cup about 2 m away. Targets of U^{235} and U^{238} were made by evaporating uranium dioxide onto a thin carbon backing, but for all other targets a painting technique was used. The isotope was painted onto a thin aluminium sheet, covered with a thin plastic film, and the aluminium then dissolved away with caustic soda. Targets produced by this method tended to contain a larger number of impurities than those made by evaporation, and consequently it was not possible to obtain straight proton spectra from the uranium isotope itself.

The counter assembly consisted of an annular E - ΔE system close to 180° from the beam direction, and a movable circular fission counter, and is shown in Fig. 1. All the counters were gold-silicon surface barrier semiconductor counters. The E counter was made from a 2-mm slice of 20 000 Ω cm material, and was used with a bias of between 250 and 1000 V. The ΔE counter was 0.05-mm thick corresponding to an absorption of about 0.5 MeV from 13 MeV protons. A 0.012-mm nickel absorber was placed in front of the E-ΔE system to absorb fission fragments. The angular spreads and solid angle of the system were 172.3° - 176°, and 0.040 sr respectively. The fission counter, made from 300 Ω cm material, subtended a half angle of 10°, which corresponds to a solid angle of 0.096 sr.

The electronics consisted of three charge-sensitive amplifiers feeding a conventional fast-slow coincidence system, used with coincidence resolving times of 5 - 10 ns. Particle identification was made with an E-ΔE pulse multiplier, and spectra were accumulated using a 4096 channel analyser, which was routed when certain coincidence conditions were satisfied. For example, in one arrangement different memory blocks were used to display proton, deuteron and triton spectra simultaneously.

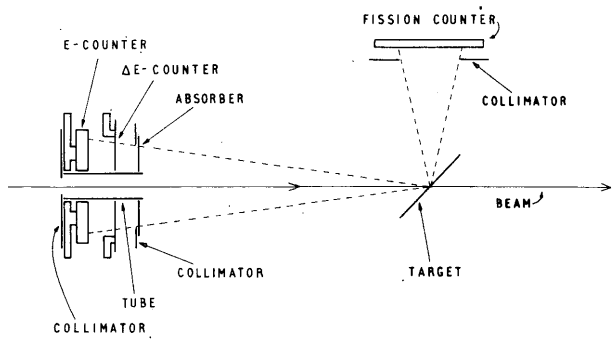

Fig. 1

The counter geometry. Protons emerging from the thin target near 180° to the beam direction are detected in the E-ΔE system, and fission fragments are counted by the movable counter.

THE RESULTS

Some preliminary measurements were made of the proton-fission coincidence yield from the U^{238}(t, pf) reaction with the fission counter of 90° to the beam and at bombarding energies of 12.0, 12.5, 13.0 and 14 MeV. The yield increased with energy although not significantly in going from 13 MeV to 14 MeV. The energy of 13 MeV was chosen for the later experiments because it was considered to be the highest at which the accelerator could be run reliably for long periods.

At the bombarding energy of 13 MeV it was found that, for several target isotopes and for comparable ranges of excitation energy in the final nuclei, $d\sigma(t, pf)/d\sigma(d, pf) \approx 0.1$. It was also shown that charged particles other than protons were not associated with fission fragments. In particular there was a negligible number of fission events following (d, d'), (t, t') and (t, d) reactions. In the latter case the chief factor was presumably that deuterons feeding fissioning states would be about 4.5 MeV lower in energy than the protons.

The fact that only protons were associated with fission fragments made it possible to dispense with the particle identification system and use the ΔE counter, after removal of the nickel foil, to count fission fragments at angles close to 180°. In the U^{233}(d, pf) and the U^{234}(t, pf) experiments proton spectra in coincidence with fission fragments at 90° and 174° were recorded simultaneously with the direct proton spectrum. The direct spectrum contained identifiable peaks from reactions with carbon and oxygen in the target, from which a proton energy calibration was constructed. In the case of U^{234}(t, pf) a measurement was also made with the movable fission counter at 135° to the beam.

The U^{233}(d, pf) angular distribution results were similar to those obtained by BRITT et al. [2]. The anisotropy, $d\sigma(174°)/d\sigma(90°)$, increased as the excitation of the fissioning nucleus decreased but, within the errors, there was no detailed structure observed.

The result of the anisotropy measurement in U^{234}(t, pf) is shown in Fig. 2. In the figure each of the points plotted in the upper curves is the sum of two kicksorter channels. The resulting over-all energy resolution is about 170 keV, somewhat worse than that which could be achieved in

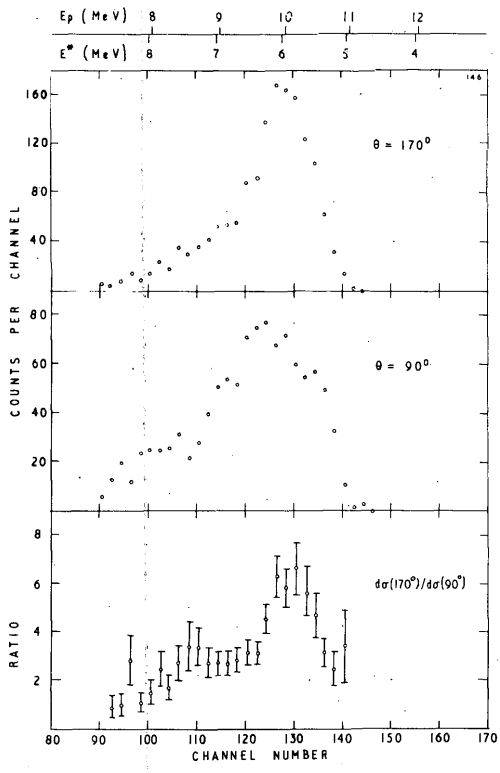

Fig. 2

Proton spectra in coincidence with fission fragments from the U^{234} (t, pf) reaction at 13 MeV, measured at two different angles of emission for the fission fragments. The two scales at the top of the figure indicate the energy of the proton (in the lab. system) and the corresponding excitation energy in the final fissioning nucleus. This latter scale was derived assuming a Q value of 3.28(±0.1)MeV for the U^{234} (t, p)U^{236} reaction. The lowest curve shows the ratio of the average differential cross-sections observed by the two fission counters.

principle. A small (≈ 5%) contribution from the U^{235} (t, pf) reaction due to an isotopic impurity in the target has been subtracted. The lower graph shows the ratio of the two spectra corrected for the ratio of the solid angles of the two fission counters. It therefore represents the ratio of the cross-sections for fragments emitted at 174° and 90° averaged over the finite size of the counters.

In Table I the ratio of the yields of the fission fragments emitted at 90° and 135° to the 174° yield is shown for three intervals, each about 0.5 MeV wide and centred at about 5 MeV (≈ channel 138), 6 MeV (≈ channel 130) and 7 MeV (≈ channel 114) excitation energy. These intervals correspond to the three regions of interest in the lower curve of Fig. 2.

The fission threshold for the U^{235} (n, f) reaction, T_{nf} (half height of the fission probability curve [1]), may be derived from the various U^{234} (t, pf) reaction data. Taking Q = 3.08 MeV for the U^{234} (d, p)U^{235} reaction[1] we ob-

[1] The Q values quoted in this paper are derived from the experiments of MIDDLETON and MARCHANT [4] using, in some cases, known four-neutron binding energies.

TABLE I

THE RATIO OF THE NUMBER OF FISSION FRAGMENTS EMITTED AT 90° AND 135° TO THE NUMBER EMITTED AT 174° FOR THREE DIFFERENT ENERGY INTERVALS IN EXCITATION ENERGY FOR THE U^{234} (t, pf) REACTION

	Excitation energy (MeV)		
	5.00 ± 0.25	6.00 ± 0.25	7.00 ± 0.25
$\frac{d\sigma(90°)}{d\sigma(174°)}$	0.36 ± 0.05	0.135 ± 0.015	0.39 ± 0.05
$\frac{d\sigma(135°)}{d\sigma(174°)}$	0.180 ± 0.025	0.24 ± 0.03	0.48 ± 0.06

tain $T_{nf} = -1.00 \pm 0.15$ MeV. The result obtained both here and by NORTHROP et al. from the U^{235} (d, pf) reaction is $T_{nf} = -0.60 \pm 0.10$ MeV.

DISCUSSION

The general form of the fission fragment angular distributions from oriented nuclei has been given by WHEELER [5]. For the U^{233}(d, pf) experiment the increase in the anisotropy as the excitation energy decreases is consistent with the conclusions drawn from the experiments of BRITT et al. [2]. These were that, at extreme threshold, fission proceeds through barrier states with K = 0 and that at higher energies rotational bands with successively higher values of K occur.

In the U^{234} (t, pf) experiment we have M = 0 and the angular distribution for a state with a given spin, I, and K is given by

$$W(\theta) \propto \left[P_I^K (\theta) \right]^2$$

when $P_I^K(\theta)$ is the associated Legendre polynomial. In the analysis of the U^{238} $(\alpha, \alpha' f)$ experiment WILKINS et al. [3] assumed that M = 0 relative to the symmetry axis of their angular distributions. In this experiment the anisotropy was a maximum at threshold although their energy resolution of 0.35 MeV may not have enabled them to determine precisely what was happening at extreme threshold. These authors calculated that their angular distribution was consistent with a rotational band having K = 0 extending from extreme threshold for about 0.600 MeV in excitation energy.

The results shown in Fig. 2 contrast sharply with previous work in showing the maximum anisotropy at a slightly higher excitation energy of the fissioning nucleus. The maximum anisotropy of about 6 is, however, very similar to that observed by WILKINS et al. [3].

Discounting the possibility that the fissioning nucleus studied here, U^{236}, is fundamentally different from U^{234} and U^{238} studied in previous experiments [2,3], the difference might be accounted for by assuming that the (t,p) reaction emphasizes different saddle-point states. This is also suggested by the threshold measurements since the threshold deduced from U^{234} (t,pf) appears to be at a lower excitation energy in the final nucleus than that deduced from U^{235}(d,pf). It is possible that the (t,pf) reaction enhances the lowest 0+ saddle-point state as happens, for example, in the U^{238} (t,p)U^{240} reaction [4] and many other (t,p) reactions in medium mass nuclei. On the other hand the evidence in Table I, which shows that at the lowest excitation energy the 90° yield is higher than the 45° yield, suggests that perhaps the explanation is that K = 0 states with fairly low angular momentum are involved at this excitation, or possibly that there is a contribution from odd values of K. (These could give rise to angular distributions that have maximum at 90°.) A much more detailed angular distribution would be needed to settle the above points.

The step in the anisotropy at about 6 MeV excitation may correspond to the onset of higher K bands, but it also happens to be close to the neutron binding energy in U^{236} (B_n = 6.45 MeV) where neutron emission becomes possible.

The decrease in anisotropy about 2.5 MeV above threshold is similar to that observed by UNIK et al. [2] in the U^{239} (d,pf) experiment, which they attributed to the onset of unpaired nucleon states.

CONCLUSIONS

The behaviour of the angular anisotropy of the fission fragments following the U^{234} (t,pf) experiment was found to be markedly different in its behaviour near threshold from that observed in the U^{233} (d,pf) and U^{238} (α, α'f) experiments. Possible causes of the difference have been discussed. A more detailed study of the angular distributions would probably explain the difference, and would certainly throw as much light on the (t,p) reaction as the fission mechanism.

ACKNOWLEDGEMENTS

We are indebted to A. H. Muggleton for supplying the targets and counters. Our thanks go also to P. J. Nind and R. A. Brown for their assistance with the experiments, and to Miss H. Jewel who carried out some of the data analysis.

REFERENCES

[1] NORTHROP, J.A., STOKES, R.H. and BOYER, K., Phys. Rev. 115 (1959) 1277.
[2] BRITT, H.C., STOKES, R.H., GIBBS, W.R. and GRIFFIN, J.J., Phys. Rev. Lett. 11 (1963) 343.
[3] WILKINS, B.D., UNIK, J.P. and HUIZENGA, J.R., Phys. Lett. 12 (1964) 243.
[4] MIDDLETON, R. and MARCHANT, H., in Proc. of Second Conf. on Nuclidic Masses (JOHNSON, W.H., Ed.) Springer-Verlag, Vienna (1964) 329.

[5] WHEELER, J.A., in Fast Neutron Physics Pt. II (MARION, J.B. and FOWLER, J.L., Eds.) John Wiley & Sons, London (1963) 2051.

DISCUSSION

M. PETRASCU: I should like to draw attention to a fission mechanism based on low-energy excitation, caused by a particle produced with the aid of high energy accelerators. This mechanism occurs in μ mesic atoms. The last transition, i.e. the 2p-1s transition of the mesic atom, can be a radiationless transition in which the nucleus is excited directly by an energy of about 6 MeV. Previous work done at Dubna and at the Lawrence Radiation Laboratory has shown that in uranium and thorium the contribution of this mechanism is less than 10% of the total number of fissions produced by μ mesons. Last autumn we started a study of the fission of Pu^{239} by negative μ mesons and the preliminary results show a total probability of fission that is about ten times higher than in uranium, and this may indicate a much higher contribution of the radiationless mechanism.

NUCLEAR FISSION AS A MARKOV PROCESS*

R. RAMANNA, R. SUBRAMANIAN AND R. N. AIYER
ATOMIC ENERGY ESTABLISHMENT TROMBAY, BOMBAY, INDIA

Abstract — Résumé — Аннотация — Resumen

NUCLEAR FISSION AS A MARKOV PROCESS. Starting from the assumption of a random transfer of nucleons between the two sides of a fissioning nucleus, during the time from saddle point to scission, it is shown that the mass distribution data in low, intermediate and high energy fission can be given a reasonable explanation based on the ground state properties of nuclei. The theory is extended to explain the shape of the deformation energy mass curves. These relations follow as a direct consequence of the equilibrium conditions that determine the mass distributions while the gap in the "zig-zag" curves is essentially due to the proton transfers. The time of fission is shown to be about 500 nucleonic times in thermal fission and this results from the properties of the transition matrix. The theory is also able to explain the small range of the threshold energies of fission, and the formation of a symmetry axis early in the process.

APPLICATION DE LA THÉORIE DE MARKOV A LA FISSION NUCLÉAIRE. En partant de l'hypothèse qu'un transfert stochastique de nucléons se produit entre les deux parties d'un noyau qui subit le processus de fission, au cours de l'intervalle de temps compris entre la formation de l'étranglement (saddle point) et la scission proprement dite, les auteurs montrent que les données relatives à la répartition de la masse dans la fission à basse, moyenne et haute énergie peuvent recevoir une explication rationnelle fondée sur les propriétés des noyaux à l'état fondamental. Par extension, ils expliquent à l'aide de cette théorie la forme des courbes de l'énergie de déformation en fonction de la masse. Ces relations résultent directement des conditions d'équilibre, qui déterminent la répartition de la masse, alors que la vallée des courbes en zigzag est due essentiellement aux transferts de protons. Les auteurs montrent que dans la fission thermique le temps de fission est d'environ 500 fois le temps de transit nucléaire, ce qui résulte des propriétés de la matrice de la transition. La théorie peut également expliquer la faible étendue des seuils de fission, ainsi que la formation d'un axe de symétrie au début du processus.

ЯДЕРНОЕ ДЕЛЕНИЕ КАК ПРОЦЕСС МАРКОВА. На основе предположения относительно беспорядочного переноса нуклонов между двумя сторонами делящегося ядра в течение времени от седловой точки до деления показывается, что данные относительно распределения массы в процессе деления, вызванного частицами низкой, промежуточной и высокой энергии, могут быть разумно объяснены на основе свойств ядер в основном состоянии. Эта теория распространяется для объяснения формы кривых энергии деформации массы. Эти связи следуют в качестве прямого следствия условий равновесия, которые определяют распределения массы, в то время как разрыв в "зигзаговых" кривых по существу объясняется переносом протонов. Показывается, что время деления составляет приблизительно 500 нуклоновых периодов при делении под действием тепловых нейтронов, это вытекает из свойств матрицы перехода. Теория может также объяснить небольшой диапазон пороговых энергий деления и образование оси симметрии в начале процесса.

LA FISION NUCLEAR CONSIDERADA COMO PROCESO DE MARKOV. Partiendo de la hipótesis de una transferencia aleatoria de nucleones entre las dos partes de un núcleo en fisión, durante el tiempo que media entre la estrangulación y la escisión, se demuestra que los datos sobre la distribución de masa en la fisión de energía baja, media y elevada, pueden explicarse satisfactoriamente sobre la base de las propiedades de los núcleos en estado fundamental. Se amplía la teoría para explicar la forma de las curvas que representan la energía de deformación en función de la masa. Estas relaciones son consecuencia directa de las condiciones de equilibrio que determinan las distribuciones de masa, mientras que la solución de continuidad de las curvas

* Abstract only; paper to be published in J. nucl. Phys.

en forma de zig-zag se debe esencialmente a las transferencias protónicas. Se demuestra que, en la fisión térmica, el tiempo de fisión es equivalente a unos 500 tiempos de tránsito nuclear, lo que se deduce de las propiedades de la matriz de transición. La teoría permite asimismo explicar el corto alcance de las energías umbral de fisión, así como la formación de un eje de simetría en las fases iniciales del proceso.

DISCUSSION

H. NIFENECKER: When one studies the fragment mass distributions as a function of the total kinetic energy of the fission induced by slow neutrons one finds that, firstly, the higher the kinetic energy, the sharper the peaks, secondly, the lower the kinetic energy, the more widely separated the peaks and, thirdly, the higher the kinetic energy, the less symmetric the fission. Figure 4 in Dr. Ramanna's paper shows the same trend as a function of N, except for the last feature. It may be possible to correlate the number N with the total kinetic energy.

R. RAMANNA: I should like to thank you very much for your very interesting comment.

CHANNEL EFFECTS IN THE KINETIC ENERGY OF FRAGMENTS OF FISSION INDUCED BY LOW-ENERGY RESONANCE NEUTRONS

M. S. MOORE AND L. G. MILLER
PHILLIPS PETROLEUM COMPANY, ATOMIC ENERGY DIVISION,
IDAHO FALLS, IDAHO, UNITED STATES OF AMERICA

Abstract — Résumé — Аннотация — Resumen

CHANNEL EFFECTS IN THE KINETIC ENERGY OF FRAGMENTS OF FISSION INDUCED BY LOW-ENERGY RESONANCE NEUTRONS. Recently, Blyumkina et al. have noted the existence of fission channel effects in the total kinetic energy of fragments of fission induced by s- and p-wave neutrons. Effects of this nature can also be expected in the variation of the fragment kinetic energies from resonance to resonance in low-energy (s-wave) neutron-induced fission. A fission-fragment detector whose efficiency is dependent on the kinetic energy of the fragments was used in the study of the slow-neutron-induced fission of U^{235}. Comparing the counting-rate of this detector with a conventional fission detector, whose efficiency is independent of the fragment kinetic energy, shows that there exists a variation in the kinetic energy of certain fragments with neutron energy in the neutron energy region from 0.025 to 1 eV. In order to determine the response of the kinetic-energy-sensitive detector, it was necessary to measure the range-energy relations of fission fragments in various media, including noble gases and metallic foils. It was estimated from these data that the variation in the fragment kinetic energy release is ~500 keV, for those fission events that give the lightest and most energetic of the heavy fragments. The variation in fragment kinetic energy is strongly asymmetric about the 0.28-eV resonance in U^{235}, and suggests that the fragment kinetic energy sensitively reflects the presence of interference effects among resonances in fission. A multi-level multi-channel analysis of the data has been made, based on the parameters of Vogt and under the assumption that different fission channels lead to different configurations at scission, such that the kinetic energy release is also different. Previously a major objection to multi-level multi-channel analysis in fission has been that the parameters obtained are not unique. However, the possibility of observing partial fission cross-sections (fission occurring by way of one channel only) removes one of the ambiguities inherent in the multi-level approach. Studies of this type can not only be expected to give information on the nature of the constraints that exist during the transition from the saddle point to the scission point in the fission process, but may also be of interest in inferring the existence of small variations from resonance to resonance in $\bar{\nu}$, the average number of neutrons emitted per fission.

VARIATIONS, SELON LA VOIE DE FISSION, DE L'ÉNERGIE CINÉTIQUE DES FRAGMENTS RÉSULTANT DE LA FISSION PAR NEUTRONS DE RÉSONANCE DE FAIBLE ÉNERGIE. Blyumkina et al. ont constaté récemment l'existence de variations, selon la voie de fission, dans l'énergie cinétique totale des fragments résultant de la fission par neutrons d'ondes-s et -p. On peut également prévoir des variations de cette nature, d'une résonance à l'autre, des énergies cinétiques des fragments dans la fission produite par des neutrons de faible énergie (onde-s). Les auteurs ont utilisé un détecteur de fragments de fission dont l'efficacité est fonction de l'énergie cinétique des fragments pour étudier la fission de ^{235}U par neutrons lents. En comparant le taux de comptage de ce détecteur à celui d'un détecteur de fission classique dont l'efficacité ne dépend pas de l'énergie cinétique des fragments, ils ont constaté que l'énergie cinétique de certains fragments varie avec l'énergie des neutrons dans la région des énergies de neutrons comprise entre 0,025 et 1 eV. Pour déterminer la réponse du détecteur sensible à l'énergie cinétique, il leur a fallu mesurer les relations parcours-énergie des fragments de fission pour différents milieux, en particulier les gaz rares et les feuilles métalliques. D'après ces données, ils ont estimé que la variation de l'énergie cinétique des fragments libérés est d'environ 500 keV pour les fissions qui produisent les plus légers et les plus énergétiques des fragments lourds. La variation de l'énergie cinétique des fragments est fortement asymétrique au voisinage de la résonance 0,28 eV dans ^{235}U, ce qui donne à penser que l'énergie cinétique des fragments est sensiblement influencée par l'existence d'effets d'interférence entre les résonances lors de la fission. Les auteurs ont procédé à une analyse à plusieurs niveaux et plusieurs

voies de fission, sur la base des paramètres de Vogt et en supposant que des voies de fission différentes aboutissent à des configurations différentes au moment de la scission, de sorte que l'énergie cinétique libérée est également différente. Jusqu'alors, l'une des principales objections élevées contre l'utilisation de l'analyse à plusieurs niveaux et à plusieurs voies de fission était que les paramètres obtenus ne sont pas uniques. Toutefois, la possibilité d'observer la section efficace de fission partielle - fission se produisant par une seule voie - supprime l'une des ambiguïtés inhérentes à l'analyse à plusieurs niveaux. Des études de cette nature pourraient non seulement fournir des indications sur la nature des contraintes qui existent pendant la transition entre le point d'étranglement et le point de scission lors du processus de fission, mais également aider à établir, par déduction, l'existence d'une résonance à l'autre de petites variations de $\bar{\nu}$, nombre moyen des neutrons émis par fission.

КАНАЛЬНЫЕ ЭФФЕКТЫ ПРИ КИНЕТИЧЕСКОЙ ЭНЕРГИИ ОСКОЛКОВ ДЕЛЕНИЯ, ВЫЗВАННОГО РЕЗОНАНСНЫМИ НЕЙТРОНАМИ НИЗКОЙ ЭНЕРГИИ. Недавно Блюмкина и другие заметили существование канальных эффектов деления при полной кинетической энергии осколков деления, вызванного s-волновыми и p-волновыми нейтронами. Эффекты такого рода можно также ожидать при изменении кинетической энергии осколков от резонанса к резонансу при делении, вызываемом (s-волновыми) нейтронами низкой энергии. Детектор осколков деления, эффективность которого зависит от кинетической энергии осколков, применялся для изучения деления урана-235, вызванного медленными нейтронами. Сравнение скорости счета этого детектора с обычным детектором деления, эффективность которого не зависит от кинетической энергии осколков, показывает, что имеет место изменение в кинетической энергии некоторых осколков с энергией нейтронов в диапазоне от 0,025 до 1 эв. В целях определения характеристики чувствительного к кинетической энергии детектора необходимо было провести измерения отношений диапазонов энергии осколков деления в различных средах, в том числе в благородных газах и металлических фольгах. Из этих данных было выведено, что изменение в высвобождении кинетической энергии осколков составляет приблизительно 500 кэв в тех случаях деления, при которых образуются самые легкие и самые тяжелые осколки большой энергии. Изменение в кинетической энергии осколков является сильно асимметричным около резонанса 0,28 эв в уране-235, и предполагается, что кинетическая энергия осколков чувствительно отражает наличие эффектов интерференции среди резонансов в процессе деления. Многоуровневый-многоканальный анализ этих данных был проведен с учетом параметров Фогта и в предположении, что различные каналы деления приводят к различным конфигурациям при делении, так что разным также является высвобождение кинетической энергии. Ранее основным возражением против проведения многоуровневого-многоканального анализа в процессе деления было то, что полученные параметры не являются одинаковыми. Однако возможность наблюдения парциального сечения деления (деления, возникающего путем только одного канала) устраняет одну из неопределенностей, свойственных многоуровневому подходу. Можно предполагать, что в результате таких исследований будет получена информация не только относительно характера ограничений, которые существуют во время перехода от седловой точки к точке деления в процессе деления, но это может также представлять интерес при предположении наличия небольших вариаций от резонанса к резонансу в $\bar{\nu}$ среднем количестве нейтронов, испускаемых на деление.

EFECTOS DE CANAL EN LA ENERGIA CINETICA DE LOS FRAGMENTOS DE LA FISION INDUCIDA POR NEUTRONES DE RESONANCIA DE BAJA ENERGIA. Blyumkina y col. han observado recientemente la existencia de efectos de canal en la energía cinética total de los fragmentos resultantes de la fisión inducida por neutrones de onda s y p. También son de esperar efectos de esta índole en la variación de la energía cinética de los fragmentos, al pasar de un nivel de resonancia a otro, en la fisión inducida por neutrones de baja energía (onda s). Se ha utilizado un detector de fragmentos de fisión cuyo rendimiento depende de la energía cinética de éstos para estudiar la fisión del ^{235}U inducida por neutrones lentos. La comparación de la velocidad de recuento de este detector con la de un detector de fisión clásico, cuyo rendimiento es independiente de la energía cinética de los fragmentos, muestra que, en el intervalo de energía neutrónica comprendido entre 0,025 y 1 eV, la energía cinética de determinados fragmentos varía en función de la energía de los neutrones. A fin de determinar la respuesta del detector sensible a la energía cinética, fue preciso establecer las relaciones entre el alcance y la energía de los fragmentos de fisión en varios medios, entre ellos gases nobles y láminas metálicas. Basándose en estos datos, se ha calculado que la variación de la energía cinética liberada por los fragmentos es del orden de los 500 keV, para los sucesos de fisión que producen los fragmentos más pequeños y energéticos dentro del grupo de los pesados. La variación de la energía cinética de los fragmentos es fuertemente asimétrica en las proximidades del nivel de resonancia de 0,28 eV del ^{235}U, lo que sugiere que dicha

energía es un índice sensible de la existencia de efectos de interferencia entre los diferentes niveles de resonancia en la fisión. Se ha efectuado un análisis de los datos, en niveles y canales múltiples, basado en los parámetros de Vogt y en la hipótesis de que los distintos canales de fisión originan configuraciones de escisión diferentes, de forma que la energía cinética liberada es también distinta. Una objeción importante que se formulaba anteriormente a los análisis de fisión según niveles y canales múltiples era la falta de unicidad de los parámetros obtenidos. Ahora bien, la posibilidad de observar las secciones eficaces parciales de fisión (fisión que se produce por un solo canal) elimina una de las ambigüedades inherentes a ese enfoque del problema. Es de esperar que los estudios de este tipo no sólo proporcionen información sobre la naturaleza de las restricciones impuestas durante la transición del punto de estrangulación al de escisión en el proceso de fisión, sino que también pueden ser interesantes para determinar la existencia de ligeras variaciones de $\bar{\nu}$, esto es, el número medio de neutrones emitidos por fisión, de un nivel de resonancia a otro.

INTRODUCTION

It has recently been noted by MELKONIAN and MEHTA [1, 2, 3] that the relative yield of fragments of U^{235} fission induced by neutrons below 100 eV appears to vary according to the thickness of the target of fissile material. From resonance to resonance, the relative yield of fragments from thick targets (targets that are so thick that fragments from only those events near the surface can escape) differs from the yield from thin targets from which all the fragments can escape. This behaviour was interpreted by Melkonian and Mehta as evidence that the kinetic energy of U^{235} fission fragments varies from resonance to resonance.

A variation of fragment kinetic energies at higher neutron energies has been reported for U^{233} and U^{235} fission by BLYUMKINA et al. [4, 5, 6]. In these experiments, an anomalous variation was observed at neutron energies of approximately 500–700 keV. It was suggested by Blyumkina et al. that these effects can be attributed to the opening of p-wave fission channels, for which the energy release is different from that characteristic of s-wave channels. It was also noted that the fragment kinetic energy variation was accompanied by characteristic variations in the fragment angular distributions and particularly in $\bar{\nu}$, the number of neutrons emitted per fission. These variations in $\bar{\nu}$ are in accord with recent models of fission discussed by VANDENBOSCH [7] and by TERRELL [8, 9], in which the number of neutrons emitted is correlated with the nuclear structure and the excitation energy of the nascent fragments.

Channel effects similar to those reported by Blyumkina et al. can also be expected for purely s-wave neutron-induced fission. According to the Bohr model of fission [10] the fissioning nucleus at the saddle point in the potential barrier is not highly excited. Most of the available energy is in the form of potential energy of deformation, with very little left over for excitation. At the saddle point the number of degrees of freedom is small, and there are expected to be only a few modes of motion or open channels that can lead to fission. Data that have been obtained on the low-energy neutron cross-sections of fissile isotopes show effects such as strong interference in fission and a large variation in the sizes of fission widths, which are consistent with the view of fission as a few-channel process. In particular, for U^{235}, multilevel analyses of the low-energy neutron cross-section data, carried out by SHORE and SAILOR [11], by VOGT [12, 13] and

by KIRPICHNIKOV et al. [14], indicate that there are one or two open fission channels that dominate in one or both of the possible resonance spin states.

A variation with neutron energy of the U^{235} fission product mass distribution has also been noted. COWAN et al. [15, 16] observed a variation in the relative yield of symmetric and asymmetric U^{235} fission products, over the neutron energy region of 8 to 60 eV, by radiochemical techniques. FALER and TROMP [17] observed similar variations below 1 eV, and CUNINGHAME et al. [18] have measured the ratio of symmetric to asymmetric fission at neutron energies above 60 keV. A correlation of the symmetric fission yield and the variation of fragment kinetic energy might be expected on the basis of energy balance in fission. In comparing the kinetic-energy studies of MELKONIAN and MEHTA [1, 2, 3] with the mass yield data of COWAN et al. [15, 16], the expected correlation appears to be established only for certain resonances. A comparison of the results of BLYUMKINA et al. [4, 5, 6] and CUNINGHAME et al. [18] is less conclusive.

The present experiment was performed for the purpose of investigating the existence of a variation in the fragment kinetic energies in the region of the lowest neutron energy resonances in U^{235}, and to compare such a variation with the mass distribution data of FALER and TROMP [17].

EXPERIMENTAL ARRANGEMENT

The Materials Testing Reactor (MTR) crystal spectrometer was used as a source of monochromatic neutrons, whose energy was varied from 0.02 to 10 eV. Primary emphasis was given to the energy region below 1 eV, to permit a comparison with the mass distribution data of FALER and TROMP [17].

The experiment consisted of the simultaneous measurement of the following quantities as a function of incident neutron energy: (1) the U^{235} fission-fragment yield with a detector whose efficiency is independent of the fragment kinetic energy; (2) the U^{235} fission-fragment yield with a detector whose efficiency depends on the fragment kinetic energy; and (3) the neutron beam flux with a detector whose efficiency varies inversely as the neutron velocity. The fission-fragment detectors were argon gas scintillation counters, which used in the initial stages of the work RCA 6342A photomultiplier tubes with p-quaterphenyl wavelength shifter, and in the later stages 56 UVP tubes without a wavelength shifter. The neutron beam monitor consisted of a single 1-in diam. proportional tube, containing BF_3 gas, at 67-cm pressure, depleted to 11% B^{10}.

A schematic drawing of the fission chamber is shown in Fig. 1. The detector whose efficiency is dependent upon fragment energy (thick foil detector) consisted of a layer of U^{235} approximately 600 $\mu g/cm^2$ thick, sandwiched between two copper foils of thickness 0.0025 mm. Each copper foil was thick enough to stop about 60% of the heavier of the two fragments emitted isotropically from the U^{235} layer. Coincidence was required between the two fission fragments, and the number of coincidences per unit time was recorded as a function of neutron energy. The detector whose efficiency was independent of fragment energy (thin foil detector) consisted of a layer of U^{235} approximately 200 $\mu g/cm^2$ in thickness, deposited on a

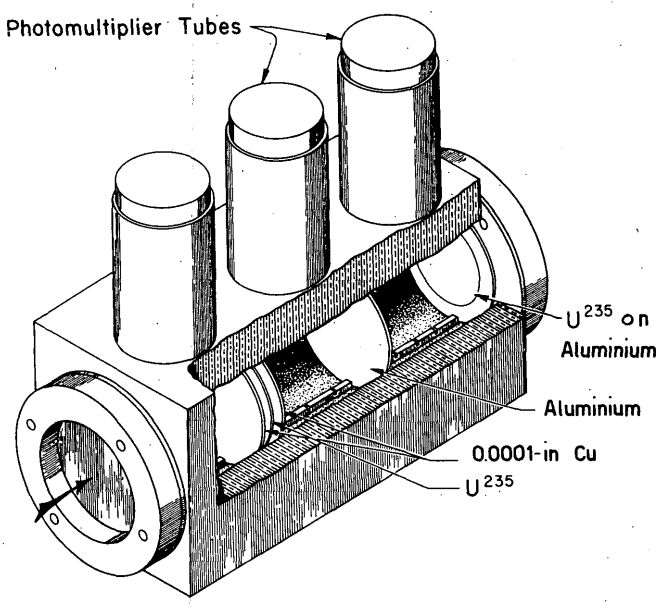

Fig. 1

Fission chamber in which the variation of fission-fragment kinetic energies with neutron energy was detected. The neutron beam, entering from the left, first traverses the "thick-foil" detector, which consists of a thick deposit of U^{235} between two absorber foils. This array of U^{235} and absorber foils is shown as separated; in fact there was no separation between them, since the U^{235} was deposited upon the absorber foils as a backing. The neutron beam then traverses the "thin-foil" detector, which is a conventional single-sided gas scintillation detector. The detector was operated not only as shown but also in a reversed configuration, allowing the beam to pass first through the "thin-foil" detector and then through the "thick-foil" detector, to eliminate possible effects due to neutron-beam attenuation by the foils.

thick aluminium backing, and viewed in the conventional way by a single photomultiplier tube.

The pulse-height resolution that can be obtained with gas scintillation fission-fragment detectors, as shown in Fig. 2, is typical of the present thin foil detector, when viewing a U^{235} layer of 10–15 $\mu g/cm^2$ in thickness. With thicker U^{235} layers, the double-humped distribution is obscured, but the fission-fragment pulses can still be clearly resolved from the lower-level alpha-particle and noise pulses.

The pulse-height distribution observed with the thick-foil detectors is shown in Fig. 3. The bias conditions that were established by requiring a coincidence between both fragments are somewhat complex, and a supplementary set of experiments was undertaken in order to understand them. These experiments, described in detail elsewhere [19], consisted of a high resolution measurement of range-energy relations of coincident fission fragments slowed in noble gases and in metallic foils. In Fig. 4 are shown a

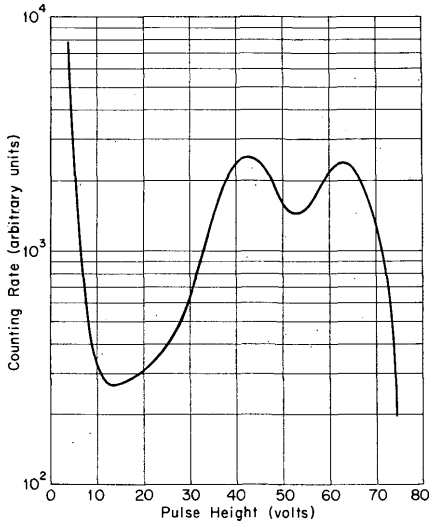

Fig. 2

Typical fission-fragment pulse-height distribution
taken with a conventional single-sided argon gas scintillation fission chamber,
similar to the "thin-foil" detector shown in Fig. 1,
and a thin (10-15 $\mu g/cm^2$) deposit of U^{235} on a thick backing.

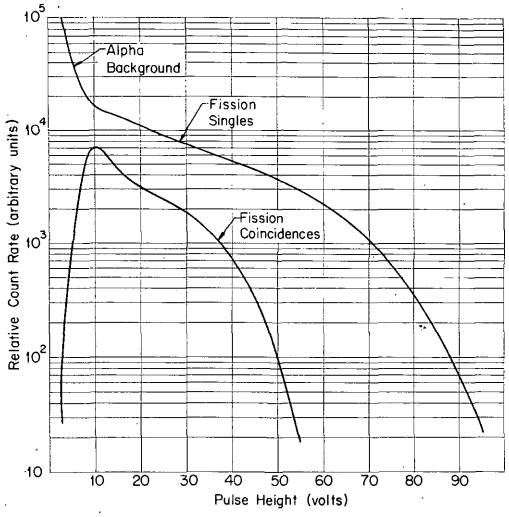

Fig. 3

Fission pulse-height distribution obtained from the "thick-foil" U^{235} detector shown in Fig. 1,
consisting of a thick (600 $\mu g/cm^2$) U^{235} layer covered on both sides with 0.025 mm of copper foil.
Upper curve is that of the singles spectrum from either side of the covered foil,
showing the alpha background below 10 V and the single fission pulses.
Lower curve shows the pulse height of the fragments
on one side in coincidence with fragments on the opposite side.

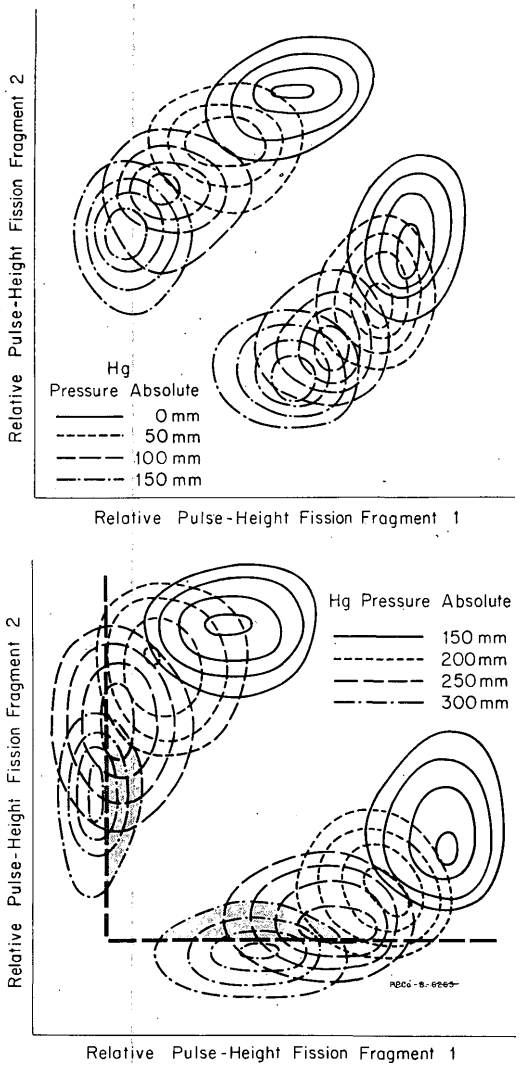

Fig. 4

A series of contour plots showing pulse-height distributions
of coincident fission fragments from reactor neutron-induced fission of U^{235},
as a function of varying amounts of argon gas as an absorber.
These distributions were taken with high-resolution surface-barrier solid-state detectors.
A scale change of a factor of 2 is to be noted between Figs. 4a and 4b.
The bias condition established by the 0.0025-mm copper foil absorber,
shown in Fig. 1, corresponds on the average to the dashed line in Fig. 4b,
applied to the contour plot for a pressure of 30 cm of argon absolute.
On the average, only those fragments lying above and to the right of the dashed line
are recorded in our experimental arrangement by the "thick-foil" detector.
As can be seen by following the various distributions,
this corresponds to those fission events
that involve the lightest and most energetic of the heavy binary fragments.

series of two-dimensional distributions of residual pulse-heights of coincident fission fragments slowed in argon. These distributions have been found [19] to be representative of those in copper and nickel foils, and in krypton and xenon gas as well, if one uses the dimensionless range-energy parameters developed by LINDHARD et al. [20, 21]. The bias condition established by the thick foil detector can be represented very approximately by the dashed line applied to the lowest contour plot in Fig. 4b. Following the curve upward to the highest contour plot in Fig. 4a (that for unslowed fragments), one sees that the bias condition corresponds to detection of the relative yield of those fission events in which the most energetic of the heavier of the two fragments is emitted. It should be noted that these are the fission events in which fine structure has been observed in both the unslowed energy distributions [22, 23, 24] and in the slowed velocity distributions [25] of U^{235} fission fragments.

The experimental data obtained consist of the ratio of the relative yield from the thick foil detector to that from the thin foil detector, as a function of neutron energy. The data obtained for U^{235} below 1.0 eV are shown in Fig. 5. In Fig. 6 are shown the results of the mass distribution studies of FALER and TROMP [17] on U^{235}, which show the relative yield of selected fission products representative of symmetric fission to that of asymmetric fission, over the same neutron energy region. Shown also in Fig. 6 is the variation of the fission cross-section relative to a detector whose efficiency varies inversely as the square root of the neutron energy. The curves showing the fragment kinetic energy variation (Fig. 5) and the mass asymmetry ratio (Fig. 6) are similar between 0.02 and 0.3 eV. Above 0.3 eV there is some evidence for a discrepancy, based on a single point at 0.5 eV in the mass asymmetry ratio studies of FALER and TROMP [17].

CHANNEL ANALYSIS OF THE KINETIC ENERGY DATA

It can readily be seen from a comparison of the curve showing the variation of fragment kinetic energy (Fig. 5) and the curve showing the fission cross-section variation in Fig. 6 that the fragment kinetic energy does not vary symmetrically about the 0.28-eV resonance. This behaviour suggests strong interference among the fission resonances, of a type not previously observed.

The low-energy cross-sections of U^{235} have been analysed by SHORE and SAILOR [11], and VOGT [12, 13], using multilevel techniques [12, 13, 26]. Vogt found that a two-fission channel representation gave an adequate fit to the data, whereas Shore and Sailor were able to obtain an adequate fit by using a single-fission channel in one of the two spin states. The results of these analyses are most conveniently compared by using Vogt's technique [12, 13] of plotting the fission-width vector parameters in a two-dimensional channel space, as is done in Fig. 7. The similarity between Fig. 7a (the Vogt parameters) and Fig. 7b (the Shore and Sailor parameters),

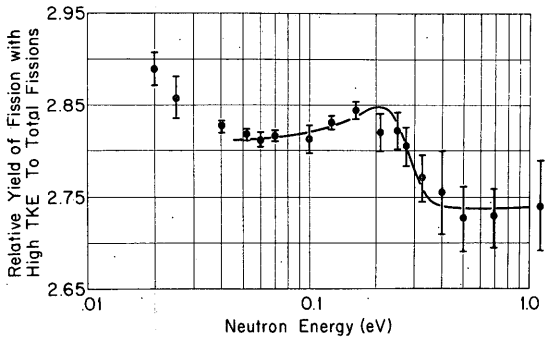

Fig. 5

Relative yield of fission fragments observed by the "thick-foil" detector to that observed by the "thin-foil" detector, as a function of incident neutron energy.
It should be noted that the two data points shown at lowest energies are in error. Later data have shown that the theoretical curve is followed even at the lowest neutron energies.

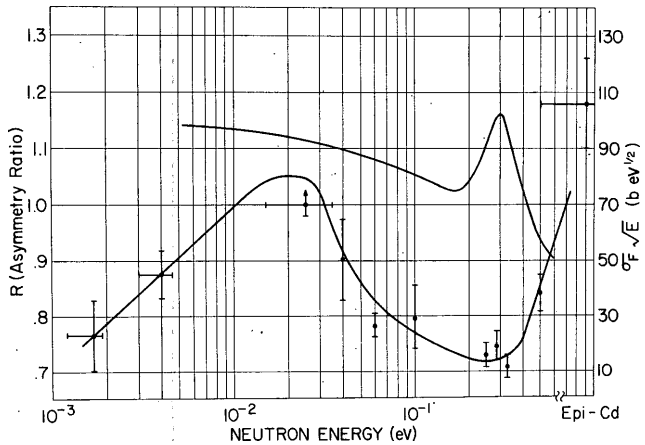

Fig. 6

The relative asymmetry ratio, or peak-to-valley mass distribution ratio, for U^{235} as a function of neutron energy.
Shown also is the variation of the fission cross-section in this energy region, relative to a neutron detector whose efficiency varies as 1/v where v is the neutron velocity.
The mass distribution data are those of FALER and TROMP [17].

shows why either set of parameters is adequate to represent the low energy data above 0.1 eV[1].

It should be noted that, in fitting the fission cross-section with a two-fission-channel formula, only the relative orientation of the fission-width

[1] Below 0.1 eV an additional small resonance appears to be required [27, 28] ; the parameters for this resonance were included by Shore and Sailor in their analysis. If the fission-width vector for this resonance had been included in Fig. 7b, it would appear as orthogonal to both of the co-ordinates shown. It is presumably this resonance that is responsible for the high thermal peak-to-valley mass ratio.

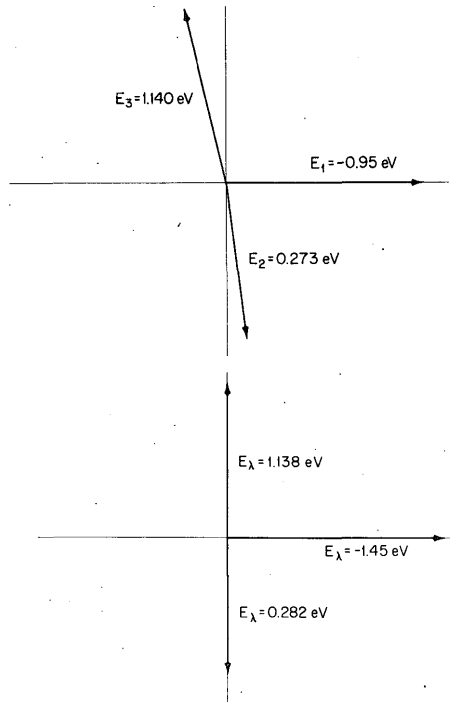

Fig. 7

Comparison of the fission-width vector parameters for the negative-energy and first two strong positive-energy resonances in U^{235}, as determined by SHORE and SAILOR [11] (Fig. 7b) and by VOGT [13] (Fig. 7a). The fission-width vector for a given resonance has a magnitude equal to the square root of the fission width. These vectors are shown in a two-channel co-ordinate system as described by VOGT [12, 13]. Both sets of parameters have been found to give an adequate fit to the fission and total cross-section data between 0.1 and 1.5 eV.

vectors to one another is important. The fission cross-section is the sum of the contributions in all channels, and this sum is invariant to a rotation of the channel co-ordinate system with respect to the set of fission-width vectors. If, however, one has a technique by which one can observe partial fission cross-sections (fission proceeding through only one of two channels, for example), then it is possible to fix the channel co-ordinate system with respect to the set of fission-width vectors.

The analysis of the data shown in Fig. 5 has been carried out under the assumption that the fragment kinetic energy release is slightly different for different s-wave neutron-fission channels. Under this assumption, if the counting-rate F from the thin detector is given by $F = F_1 + F_2$, where F_1 and F_2 are the number of fission events per unit time at a given neutron energy from the two assumed fission channels, the counting-rate F' from the thick detector at the same neutron energy is given by $F' = AF_1 + BF_2$, where A and B are assumed to be unequal constants. The ratio F'/F (the quantity plotted in Fig. 5) can then be written as

$$\frac{F'}{F} = C + \frac{DF_1}{F_1 + F_2} = C + DF_1/F,$$

where C and D are non-zero constants.

In Fig. 8 are plotted the ratio F_1/F, calculated on the basis of Vogt's parameters for the low-energy cross-sections of U^{235}, for various orientations of the fission channel co-ordinate system with respect to the set of fission-width vectors (Fig. 7a). An adequate fit to the data is given by the solid curve in Fig. 5, which corresponds to the orientation of the channel co-ordinate system with Vogt's set of fission-width vectors as shown in Fig. 9.

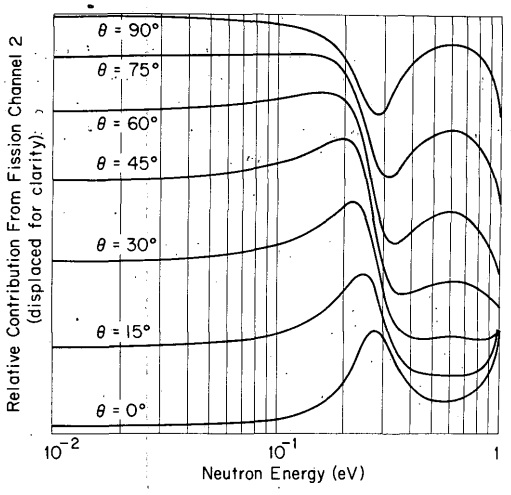

Fig. 8

Ratio of the fission yield from one of the two assumed fission channels to that from both channels as a function of neutron energy, calculated from the parameters of VOGT [13] as shown in Fig. 7a, for various orientations of the fission-channel co-ordinate system and the set of fission vectors. The angle θ gives the angle between the horizontal axis (channel 1) and the fission-width vector for the -0.95-eV resonance. The fission cross-section predicted from these parameters is insensitive to a rotation of this nature.

DISCUSSION OF THE ANALYSIS

The expected correlation of the fission product mass distribution studies as a function of neutron energy with the fragment kinetic energy variation is based on a consideration of the nuclear structure of the fragments at the scission point as suggested by VANDENBOSCH [7]. BRUNNER and PAUL [29, 30, 31, 32] have discussed the importance of the shell structure of the nascent fragments in determining the fission product mass distribution, and TERRELL [8] has noted the effects of fragment shell structure on prompt neutron emission probabilities. It has been reasonably well established [22, 23] that in symmetric fission the kinetic energy release is anomalously

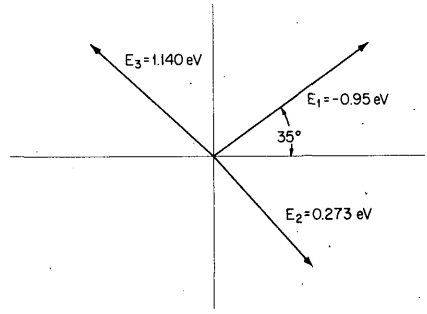

Fig. 9

Fission-width vector diagram showing the relative orientation between the fission-width vectors of VOGT [13] and the fission-channel co-ordinate system from which the fit to the data in Fig. 5 was calculated. The assumptions used in obtaining this fit, shown by the solid curve in Fig. 5, are described in the text.

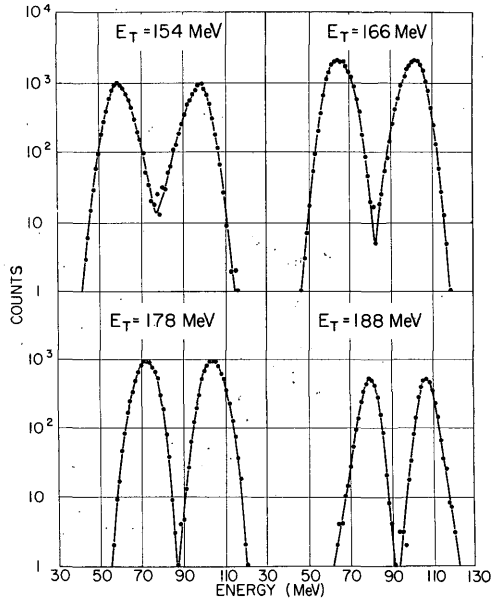

Fig. 10

Relative fission probability as a function of the kinetic energy of one of the fragments, for various values of the total kinetic energy release. These data are those of SAFFORD [33].

low. This is illustrated, for example, by data taken by SAFFORD [33] as shown in Fig. 10; symmetric fission is found to occur only for relatively low total kinetic energy release. The energy that does not appear as kinetic energy in symmetric fission can be accounted for by a larger number of prompt neutrons emitted by the symmetric fragments.

According to VANDENBOSCH [7], the variation in the kinetic energy release with fragment mass number can be attributed to the fragment deformation probability. If both fragments are relatively soft to deformation, scission would be expected to occur for larger effective separations of the fragment charge centres, resulting in the lower kinetic energy (the case at symmetric fission). If one of the fragments has a nearly closed-shell configuration, then it will be more nearly spherical; the effective separation distance at scission will be relatively lower, the total kinetic energy release will be high, and the number of prompt neutrons emitted, as the fragment reaches its final equilibrium shape, will be low.

If it is assumed that there is some neutron-energy dependent parameter, related to the compound-nucleus resonance spin or to the saddle-point fission channel involved, which can affect the scission configuration, then arguments such as those given above lead one to expect that a lowered average total kinetic energy release should be accompanied by an increased symmetric fission yield, as well as by an increased number of neutrons emitted per fission. The data reported here are generally consistent with the expected behaviour, even though there is some indication that the mechanisms responsible for a variation in fragment kinetic energy may be different.

It is of interest to consider the possible nature of such mechanisms. According to the BOHR model of fission [10], the channel structure at the saddle point of a fissioning deformed even-even compound nucleus should resemble the low-lying nuclear level structure of such a nucleus in its ground state. Following this argument for the compound system (U^{235} + n) formed by s-wave neutrons, where the channel spins are 3^- and 4^-, one expects the predominant modes of motion that lead to fission (the fission channels) to correspond to octupole vibrations with K, the angular momentum projection on the nuclear symmetry axis, equal to 0 and 2. These are the so-called b- and g-vibrational bands discussed by LIPAS and DAVIDSON [34] and by LEPER [35]. The b-vibrational band contains levels with spin sequence 1^-, 3^-, 5^-, ..., and the g-vibrational band levels of spin 2^-, 3^-, 4^-, ... Thus for the low-energy resonance structure of U^{235} one might expect that 3^- resonances would be characterized by fission channels having K = 0 and 2, whereas 4^- resonances would be characterized by only a K = 2 channel. This argument is, of course, too much simplified, since the effects of higher octupole bands and quadrupole band structure based on negative parity intrinsic states cannot be dismissed so lightly. Nevertheless, the above discussion is consistent with the view of fission as a few-channel process.

There is evidence that K is conserved in the transition from the saddle point to the scission point, and that it does show a variation with neutron energy. DABBS et al. [36, 37] have measured the angular distribution of fragments from low-energy neutron-induced fission of aligned U^{235} nuclei, from which the variation of K can be determined. They have found that K varies in a manner that is not inconsistent with the data on the fragment kinetic energy variation shown in Fig. 5, although neither their data nor ours are yet complete enough to permit a detailed comparison to be made.

The present series of measurements is being extended to 10 eV, to permit a comparison with the higher energy work of DABBS et al. [36, 37], and with that of MELKONIAN and MEHTA [1, 2, 3]. Although these measure-

ments are not yet complete there is evidence that there are even more pronounced variations in the fragment kinetic energy over the resonances between 1 and 10 eV.

Of considerable interest is the implication that a variation in the fragment kinetic energy should be accompanied by a variation in $\bar{\nu}$. A crude estimate of the magnitude of the maximum variation shown in Fig. 5 has been made, utilizing the results of our range-energy studies [19]. If this variation, which amounts to ~500 keV in the total kinetic energy release, occurs for the entire fission distribution instead of for just certain high-energy fragments, a variation of perhaps 2% might be expected in $\bar{\nu}$, based on the size of the effects observed by BLYUMKINA et al. [4, 5, 6]. An experiment to measure $\bar{\nu}$ for U^{235} as a function of neutron energy is being planned.

ACKNOWLEDGEMENTS

The authors wish to acknowledge many helpful discussions with Drs. R.G. Fluharty, K.T. Faler, J.W.T. Dabbs, H.W. Schmitt, R.B. Leachman J. Terrell, E. Melkonian, and G.K. Mehta, during the course of this experiment. Dr. G.J. Safford has kindly granted permission for us to use his unpublished data. The authors would also like to express their thanks to Drs. K.T. Faler and J.R. Berreth for fabricating the fission foils used in this series of measurements.

REFERENCES

[1] MELKONIAN, E. and MEHTA, G. K., Trans. Amer. nucl. Soc. 6 (1963) 262.
[2] MEHTA, G. K. and MELKONIAN, E., Bull. Amer. phys. Soc. 8 (1963) 368.
[3] MEHTA, G. K., Doctoral dissertation, Columbia University (1963) (unpublished).
[4] BLYUMKINA, Yu.A., BONDARENKO, I. I., KUZNETSOV, V.F., NESTEROV, V.G., OKOLOVITCH, V. N., SMIRENKIN, G. N. and USACHEV, L. N., Nucl. Phys. 52 (1964) 648.
[5] OKOLOVITCH, V. N. and SMIRENKIN, G. N., Atomnaja energija 15 (1963) 250.
[6] BLYUMKINA, Yu. A., BONDARENKO, I. I., KUZNETSOV, V. F., NESTEROV, V. G., OKOLOVITCH, V.N. and SMIRENKIN, G. N., Atomnaja energija 15 (1963) 64.
[7] VANDENBOSCH, R., Nucl. Phys. 46 (1963) 129.
[8] TERRELL, J., Phys. Rev. 127 (1962) 880.
[9] TERRELL, J., "Prompt neutrons from fission", these Proceedings II.
[10] BOHR, A., Proc. UN Int. Conf. PUAE 2 (1956) 151.
[11] SHORE, F.J. and SAILOR, V.F., Phys. Rev. 112 (1958) 191.
[12] VOGT, E., Phys. Rev. 112 (1958) 203.
[13] VOGT, E., Phys. Rev. 118 (1960) 724.
[14] KIRPICHNIKOV, I. V., IGNATYEV, K. G. and SUKHORUCHKIN, S. I., Atomnaja energija 16 (1964) 211.
[15] COWAN, G. A., TURKEVICH, A., BROWNE, C. I. and Los Alamos Radiochemistry Group, Phys. Rev. 122 (1961) 1286.
[16] COWAN, G. A., BAYHURST, B. P. and PRESTWOOD, R. J., Phys. Rev. 130 (1963) 2380.
[17] FALER, K. T. and TROMP, R. L., Phys. Rev. 131 (1963) 1746.
[18] CUNINGHAME, J. G., KITT, G. P. and RAE, E. R., Nucl. Phys. 27 (1961) 154.
[19] MILLER, L. G. and MOORE, M. S., (to be published).
[20] LINDHARD, J., SCHARFF, M. and SCHITT, H. E., Mat.-fys. Meddr. 33, No. 14 (1963).
[21] LINDHARD, J., NIELSEN, V., SCHARFF, M. and THOMSEN, P. V., Mat.-fys. Meddr. 33, No. 10 (1963).
[22] GIBSON, W. M., THOMAS, T. D. and MILLER, G. L., Phys. Rev. Lett. 7 (1961) 65.
[23] MILTON, J. C. D. and FRASER, J. S., Phys. Rev. Lett. 7 (1961) 67.
[24] THOMAS, T. D. and VANDENBOSCH, R., Phys. Rev. 133 (1964) B976.

[25] SCHMITT, H. W. and LEACHMAN, R. B., Phys. Rev. 102 (1956) 183.
[26] REICH, C. W. and MOORE, M. S., Phys. Rev. 111 (1958) 929.
[27] HARVEY, J. A. and SANDERS, J. E., in Progress in Nuclear Energy I, McGraw-Hill, New York (1956) 1.
[28] DERUYTTER, A. J., J. nucl. Energy, Parts A and B, 15 (1961) 165.
[29] BRUNNER, W. and PAUL, H., Ann. Phys. (7) 6 (1960) 267.
[30] BRUNNER, W. and PAUL, H., Ann. Phys. (7) 7 (1961) 326.
[31] BRUNNER, W. and PAUL, H., Ann. Phys. (7) 7 (1961) 333.
[32] BRUNNER, W. and PAUL, H., Ann. Phys. (7) 8 (1961) 146.
[33] SAFFORD, G. J., private communication (1960).
[34] LIPAS, P. O. and DAVIDSON, J. P., Nucl. Phys. 26 (1961) 80.
[35] LEPER, D. P., Nucl. Phys. 50 (1964) 234.
[36] DABBS, J. W. T., WALTER, F. J. and PARKER, G. W., Bull. Am. Phys. Soc. 9 (1964) 421.
[37] DABBS, J. W. T., WALTER, F. J. and PARKER, G. W., "Saddle-point rotational states from resonance fission of oriented nuclei", these Proceedings I.

DISCUSSION

M. NÈVE de MEVERGNIES: In your experiment, Dr. Moore, when the neutron energy changes the cross-section also changes, especially in the vicinity of the 0.3-eV resonance. Hence, the distribution of the fissioning nuclei within the target foil is likewise modified. I wonder how large is the correction for this effect compared with the total net effect you have measured.

M. S. MOORE: I think that would be important only in the case of relatively thick foils. All our foils were extremely thin - only 500 $\mu g/cm^2$.

DEPENDENCE OF FISSION-FRAGMENT PRIMARY CHARGE ON NUCLEAR STRUCTURE

P. ARMBRUSTER
KERNFORSCHUNGSANLAGE JÜLICH, JÜLICH,
FEDERAL REPUBLIC OF GERMANY

Abstract — Résumé — Аннотация — Resumen

DEPENDENCE OF FISSION-FRAGMENT PRIMARY CHARGE ON NUCLEAR STRUCTURE. Assuming a quasi-static scission configuration the potential energy of this configuration has been calculated. The energy release between saddle point and scission point has been maximized using the liquid drop model and taking into account the mass dependence of the deformability of the fission fragments.

The leading terms that determine the charge distribution depend on the Coulomb and the asymmetry energy of the scission configuration.

The deformability of the fragments shows dependence from nuclear structure. A term proportional to the difference of the deformation energies of the two fragments gives rise to a strong influence from this nuclear structure effect. In the region of closed shells the difference in the deformation energies is much the same as the total deformation energy. A term comparable to the Coulomb energy term has to be taken into account in these mass regions.

The calculated Z_p-values have been compared to experimental results for U^{235}. Calculated Z_p-values for Cf^{252} are given.

VARIATIONS DE LA CHARGE PRIMAIRE DES FRAGMENTS DE FISSION SELON LA STRUCTURE DU NOYAU. L'auteur a calculé l'énergie potentielle d'une configuration de scission supposée quasi statique. Il a maximisé l'énergie libérée entre l'étranglement (saddle point) et la scission, en utilisant le modèle de la goutte liquide et en tenant compte des variations de la déformabilité des fragments de fission suivant la masse.

Les principaux termes qui déterminent la répartition selon la charge dépendent de l'énergie coulombienne et de l'énergie d'asymétrie de la configuration de scission.

Il s'avère que la déformabilité des fragments dépend étroitement de la stricture du noyau. Un terme proportionnel à la différence entre les énergies de déformation des deux fragments traduit une influence importante de cet effet de structure nucléaire. Dans la région des couches saturées, la différence entre les énergies de déformation est de l'ordre de l'énergie totale de déformation. Dans ces régions de la masse, il faut faire intervenir un terme comparable à celui de l'énergie coulombienne.

L'auteur compare les valeurs calculées de Z_p aux résultats expérimentaux pour ^{235}U. Il indique les valeurs calculées de Z_p pour ^{252}Cf.

ЗАВИСИМОСТЬ ВЕЛИЧИНЫ ПЕРВИЧНОГО ЗАРЯДА ОСКОЛКОВ ДЕЛЕНИЯ ОТ ЯДЕРНОЙ СТРУКТУРЫ. В предположении, что конфигурация деления является квазистатической, рассчитана потенциальная энергия этой конфигурации. Высвобождение энергии между седловой точкой и точкой деления увеличено до максимума в результате использования модели "жидкой капли" и учета зависимости массы от способности осколков к деформации.

Основные члены, которые определяют распределение заряда, зависят от кулоновской и асимметричной энергии конфигурации деления.

Способность осколков к деформации свидетельствует о наличии сильной зависимости от ядерной структуры. Член, пропорциональный различию между энергиями деформации двух осколков, является причиной большого влияния эффекта ядерной структуры. В области закрытых оболочек различие между энергиями деформации составляет величину порядка общей энергии деформации. В этих диапазонах масс необходимо учитывать член, сравнимый с членом кулоновской энергии.

Расчетные значения Z_p сравниваются с результатами экспериментов для U^{235}. Приводятся расчетные значения Z_p для Cf^{252}.

RELACION ENTRE LA CARGA PRIMARIA DE LOS FRAGMENTOS DE FISION Y LA ESTRUCTURA NUCLEAR. Se ha calculado la energía potencial de la configuración de escisión suponiendo que esta configuración es cuasiestática. Se ha asignado a la energía liberada entre el punto de estrangulación y el punto de escisión un valor máximo empleando el modelo de la gota y teniendo en cuenta la influencia de la masa de los fragmentos de fisión sobre la deformabilidad de éstos.

Los términos principales, que determinan la distribución de la carga, dependen de la energía coulombiana y de la energía de asimetría de la configuración de escisión.

La deformabilidad de los fragmentos revela una acentuada dependencia con respecto a la estructura nuclear. Un término proporcional a la diferencia entre las energías de deformación de los dos fragmentos expresa la fuerte influencia de este efecto de la estructura nuclear. En la región de las capas completas, la diferencia entre las energías de deformación es del orden de la energía total de deformación. En estas regiones másicas, es preciso introducir un término comparable al de la energía coulombiana.

Se comparan los valores calculados de Z_p con los resultados experimentales correspondientes al ^{235}U. Se presentan los valores de Z_p calculado para el ^{252}Cf.

INTRODUCTION

The mean primary nuclear charge Z_p of fission fragments may easily be calculated in two cases, making use of extreme assumptions on the time scale of nuclear fission.

If the time taken by the breaking of the nucleus is comparable to the average collision time of nucleons in nuclear matter ($t \sim 2 \times 10^{-22}$ s), no deviations of the charge density of the fission fragments from the charge density of the fissioning nucleus are to be expected. In this case Eq. (1) with $\rho = Z/A$ holds.

$$Z_{po} = \rho A_p \tag{1}$$

For long breaking times ($t \sim 10^{-18}$ s) the process may be considered as quasistatic. The potential energy in all deformation stages has to be a minimum. The last stage where nuclear forces are effective, and that finally determines the properties of the fragments, is the scission stage. The minimum of the potential energy of a properly chosen scission configuration, that is the maximum energy release between saddle-point configuration and scission configuration, will determine the final properties of the fragments [1], e.g. the primary nuclear charge [2].

The distance between saddle point and scission point may be estimated from calculated saddle-point configurations [3, 4], and the breaking distances determined from kinetic energy data. For thermal-neutron fissioners it amounts to $\Delta R \sim 10^{-12}$ cm. The uncertainty principle connects this uncertainty in distance with an uncertainty in momentum, to which there corresponds an uncertainty in time $\Delta t \sim 10^{-21}$ s. Whenever the breaking time is shorter than this time, the scission stage will not be defined. The charge values to be expected are between the values given by Eq. (1) and the values calculated from the maximum energy release. If the breaking time is longer than 10^{-21} s a scission configuration is defined. The potential energy of such a quasistatic configuration may be calculated, and the energy release E between saddle point and scission point may be maximized.

The actual breaking time of the nucleus has been estimated to be greater than 10^{-21} s [5]. The potential energy of the scission configuration is included in the quasistatic liquid drop model calculations of VANDENBOSCH [1] as well as in the calculations of FONG [6] based on the statistical theory. The following calculations should be valid as long as these theories hold, i.e. for breaking times greater than 10^{-21} s. They are independent of the specific theory.

Even if the breaking time in fission is shorter than the time required to establish statistical equilibrium, the calculation would give an upper limit of the deviations of Z_p from Z_{po}.

CALCULATIONS

The difference between the value of the primary charge Z_p and the value given by Eq. (1) may be introduced as a quantity Δ:

$$Z_p = Z_{po} + \Delta \,. \tag{2}$$

The values of Δ for a pair of complementary fission fragments have to be equal in amount, but different in sign, as charge has to be conserved.

The energy release between saddle point and scission point E has to be maximized only according to one parameter $\Delta = \Delta_1 = -\Delta_h$, which characterizes the two charge values of a pair of complementary fragments.

$$\frac{dE}{d\Delta} = \frac{d(Q + E_F - P_{sc})}{d\Delta} = 0 \tag{3}$$

with $E = Q + E_F - P_{sc}$.

Figure 1 demonstrates the distribution of the total energy $(Q + E_F)$ available for the reaction in different stages of the fission process. It is assumed that the excitation energy of the saddle point is negligible, which will be fulfilled for fission energies near the fission threshold E_F. In the scission con-

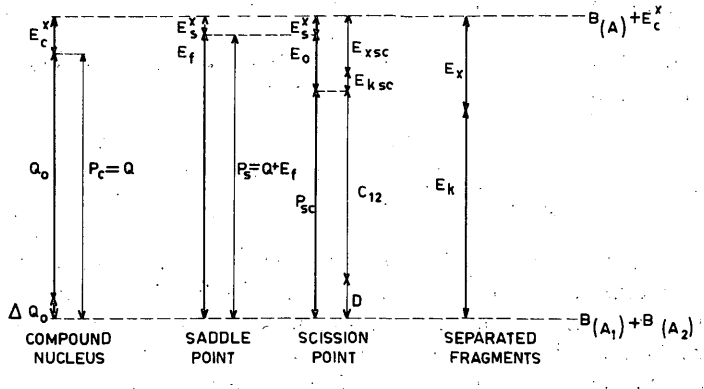

Fig. 1

The assumed distribution of the total reaction energy Q in the different stages of the fission process

figuration the energy is distributed between potential energy P_{sc}, mutual kinetic energy E_{ksc} and excitation energy E_{xcc}. The potential energy P_{sc} is made up from the mutual Coulomb energy and the deformation energy of the fragments.

$$P_{sc} = C_{12} + (D_1 + D_2) \tag{4}$$

Calculation of Q

The total energy released in fission with all $\Delta = 0$, no shell effects and pairing effects may be Q_0. Equation (5) gives the dependence of Q on the small quantity Δ, if all linear and square terms in Δ are taken into account.

$$Q = Q_0 + 2a_c \rho (A_2^{2/3} - A_1^{2/3})\,\Delta - \left[\frac{4 \times A \times a_a}{A_1 A_2} + a_c (A_1^{-1/3} + A_2^{-1/3})\right]\Delta^2 + Q_p + Q_s \tag{5}$$

a_a = asymmetry constant = 23.5 MeV
a_c = Coulomb constant = 0.71 MeV
Q_p = pairing energy $(+2\delta)$ (even-even)
$(\ 0\ )$ for (odd -even) nuclei
(-2δ) (odd - odd)
Q_s = additional binding energy for closed shells
ρ = charge density of the fissioning nucleus

A's are mass numbers of nuclei: the indices 1 and 2 refer to the light and the heavy fragment respectively.

The linear term in Eq. (5) arises from the dependence of the total energy on the Coulomb energy, and the leading quadratic term arises from the dependence on the asymmetry energy. The latter is always negative. The asymmetry energy tends to make Q always smaller than Q_0. The linear term increases Q over Q_0 for small positive values of Δ. A small positive value of Δ exists, which increases Q to a maximum.

Calculation of the potential energy P_{sc}

The scission configuration may be described by two tangent deformed nuclei, the surfaces of which are given by

$$R_i = R_{oi} \sum_{\lambda=2}^{\lambda=5} [1 + \alpha_{\lambda i}\, P_\lambda(\cos\theta)]. \tag{6}$$

The nuclei described by Eq. (6) are rotational symmetric to the deformation axis. Physical arguments restrict λ to values smaller than 5 [7].

The deformation of the fragments changes the potential energy for different reasons. The surface energy and Coulomb energy of the two fragments are changed. These energies depend quadratically on the deformation parameters α_λ. The mutual Coulomb energy is changed by shifting the distance of the centres of charge for the two fragments, and by changing the

interaction energy of the λ-th multipole field with a point charge in the centre of mass of its complementary fragment. These terms are linear in α_λ. Equation (7) gives the leading linear and square terms in $\alpha\lambda$ that contribute to the potential energy. This equation is quoted in Ref. [7] and is linearized in α_λ.

$$P_{sc} = C + \sum_{i=1}^{i=\lambda} \sum_{\lambda=2}^{\lambda=5} \left\{ a_{si} A_i^{2/3} \frac{(\lambda-1)(\lambda+2)}{2(2\lambda+1)} \alpha_{\lambda i}^2 - C \left[\frac{A_i^{1/3}}{A_1^{1/3}+A_2^{1/3}} - 3 \frac{A_i^{\lambda/3}}{(2\lambda+1)(A_1^{1/3}+A_2^{1/3})^\lambda} \alpha_{\lambda i} \right] \right\} \tag{7}$$

with

a_{si} = surface energy parameter

$$C = \frac{5}{3} a_c \frac{Z_{10} \times Z_{20}}{A_1^{1/3}+A_2^{1/3}} \left(1+\frac{\Delta}{Z_{10}}\right)\left(1-\frac{\Delta}{Z_{20}}\right) = C_0\left(1+\frac{\Delta}{Z_{10}}\right)\left(1-\frac{\Delta}{Z_{20}}\right).$$

P is minimized by variation of $\alpha_{\lambda i}$.

$$P_{sc} = C - \sum_{i=1}^{i=2} \sum_{\lambda=2}^{\lambda=5} \frac{C^2}{a_{si}(A_1^{2/3}+A_2^{2/3})} \frac{9}{800} K_\lambda \tag{8}$$

with

$$K_\lambda = \frac{100 \times (2\lambda+1)}{9 \times (\lambda-1)(\lambda+2)} \left[1 - \frac{3}{(2\lambda+1)^{2\lambda-1}}\right]^2.$$

The sums $\sum_{\lambda=2}^{\lambda=5} K_\lambda$ have been evaluated in Ref. [7]. The value of the sum amounts to 22.4.

$$P_{sc} = C - 0.25\, C^2 \left[\frac{1}{a_{s1} A_1^{2/3}} + \frac{1}{a_{s2} A_2^{2/3}}\right] = C - (D_1 + D_2) \tag{9}$$

with

$$D_i = +0.25 \frac{C^2}{a_{si} A_i^{2/3}}. \tag{10}$$

Equation (9) gives the potential energy of two deformed fragments in contact.

The mutual Coulomb energy C as well as the deformability parameter a_{si} both depend on Δ.

Equation (9) with $D_{Zi} = D_{Zio} + \Delta_i (dD_i/dZ)_{Zio} + F(\Delta^2)$ and $P_0 = C_0 - (D_{10} + D_{20})$ gives:

$$P_{sc} = P_0 + \left[\frac{5}{3} a_c \rho \frac{A_2 - A_1}{A_1^{1/3} + A_2^{1/3}} \left(1 - \frac{2(D_{10}+D_{20})}{C_0}\right) - \left(\frac{dD_1}{dZ}\right) + \left(\frac{dD_2}{dZ}\right)\right] \Delta$$

$$- \frac{5}{3} a_c \frac{1}{A_1^{1/3} + A_2^{1/3}} \left(1 - \frac{2(D_{10}+D_{20})}{C_0}\right) \Delta^2 . \qquad (11)$$

Calculation of the maximum energy release between saddle point and scission point

Equations (5) and (11) introduced into Eq. (3) give the value of Δ for maximum energy release.

$$\Delta_0 = \frac{2\rho (A_2^{2/3} - A_1^{2/3}) a_c - \frac{5}{3} \rho \gamma \frac{A_2 - A_1}{A_1^{1/3} + A_2^{1/3}} a_c + \left(\frac{dD_1}{dZ}\right) - \left(\frac{dD_2}{dZ}\right)}{2\left[\frac{4A}{A_1 A_2} a_a - \frac{5}{3} \gamma (A_1^{1/3} + A_2^{1/3})^{-1} a_c + (A_1^{-1/3} + A_2^{-1/3}) a_c\right]} \qquad (12)$$

with

$$\gamma = 1 - \frac{2(D_{10}+D_{20})}{C_0} = \frac{C_{12}}{C_0} . \qquad (13)$$

The maximum energy release E_{max} amounts to

$$E_{max} = E_0 + E_c \Delta_0^2 \qquad (14)$$

with

$$E_c = \frac{4A}{A_1 A_2} a_a - \frac{5}{3} \gamma \frac{a_c}{A_1^{1/3} + A_2^{1/3}} + a_c \left(\frac{1}{A_1^{1/3}} + \frac{1}{A_2^{1/3}}\right) \qquad (15)$$

and $E_0 = Q_0 - P_0$.

The charge dependence of the energy release E may be expressed in terms of Δ_0 and E_c.

$$E - E_0 = + Q_p + Q_s - E_c (\Delta - \Delta_0)^2 + E_c \Delta_0^2 \qquad (16)$$

The maximum energy release E_{max} is only slightly different from the energy release for constant charge density E_0. As will be shown later E_c amounts to ~ 1.8 MeV, and $\Delta_0 < 1$. The energy gain $(E_{max} - E_0)$ is of the same order of magnitude as the pairing energy and closed shell energies. All these energies are small compared to E_0, which is an order of magnitude larger than the different terms of Eq. (16). The charge effects range energetically among fine structure effects and pairing effects [8]. The energies involved are small compared to the deformation energies of the fragments and the mutual Coulomb energies.

RELATION BETWEEN EXCITATION AND KINETIC ENERGY OF THE FRAGMENTS AND THEIR NUCLEAR CHARGE

A numerical calculation of the primary charge Δ_0 from Eq. (12) does not seem to be feasible without a detailed theory of nuclear structure. The quantities γ and (dD_i/dZ) of Eq. (12) both depend on the deformation energies D_i, which on the other hand are related, according to Eq. (10), to the deformability parameter a_{si}. The deformability parameter depends on the nuclear structure of the fragments. Its absolute values differ for neutron-rich fission fragments and stable nuclei [1]. The unknown absolute value of the deformability parameter enters the absolute values of γ and (dD_i/dZ). Even if the absolute value of a_{si} were known, the deformation energies calculated from Eq. (10) cannot be expected to give any quantitative agreement, as this equation is derived neglecting all higher order and unlinearized terms of the potential energy

The quantities γ and (dD_i/dZ) are related to quantities measured in fission and nuclear structure experiments. These experimental data allow a replacement of γ and (dD_i/dZ) by measured quantities. The charge values Δ_0 will be calculated from two constants, the asymmetry constant a_a and the Coulomb constant a_c, and the experimentally determined mass dependence of the kinetic energy and the excitation energy of the fragments.

The mutual Coulomb energy is transferred into kinetic energy. The distribution of the energy E, released in the transition from saddle point to scission point, between kinetic energy of the fragments and excitation energy of the fragments, depends on the time scale of the fission process. E is transferred either predominantly into excitation energy, if statistical equilibrium between all degrees of freedom is established, or into kinetic energy of the fragments, if the time scale is long enough to apply an adiabatic or quasistatic approximation.

The total kinetic energy and the total excitation energy of the fragments are related to the Coulomb energy and the energy release E by Eq. (17).

$$\begin{aligned} E_k &= C_{12} + (1-\mu)E \\ E_x &= E_{x1} + E_{x2} = D + \mu E \end{aligned} \tag{17}$$

The factor μ equals ~ 1 if statistical theory is valid, it equals ~ 0 if the adiabatic or the quasistatic approximation is valid. In the following the time scale of the statistical theory is assumed. Arguments in favour of a time scale faster than the time scale necessary for the adiabatic approximation are summarized in Ref. [5]. With $\mu = 1$ Eq. (17) gives

$$\begin{aligned} E_k &= C_{12} \\ E_x &= E + D. \end{aligned} \tag{17a}$$

The distribution of the total kinetic energy between the two fragments is determined by momentum conservation.

The single fragment excitation energy E_{xi} is formed from its deformation energy D_i and from excitation energy E_i originating from the energy release between saddle point and scission point.

$$E_{xi} = D_i + E_i \tag{18a}$$

As there are only two measurable quantities, the two excitation energies E_{xi}, to determine the four quantities D_1, D_2, E_1 and E_2 it is necessary to make two more assumptions on the distribution of the energy available between E_i and D_i. The variables D_1, D_2, E_1, E_2 and E_{x1}, E_{x2} are replaced by

$$\frac{D_1 - D_2}{D_1 + D_2} = \delta \qquad D_1 + D_2 = D$$

$$\frac{E_1 - E_2}{E_1 + E_2} = \epsilon \qquad E_1 + E_2 = E$$

$$\frac{E_{x1} - E_{x2}}{E_{x1} + E_{x2}} = \alpha \qquad E_{x1} + E_{x2} = E_x .$$

The two Eqs. (17a) and (18a) allow the variables δ and D to be eliminated.

$$D = E_x - E \tag{17b}$$

$$\delta \times D = \alpha E_x - \epsilon E \tag{18b}$$

E and ϵE are assumed to be negligible compared to E_x and αE_x.

Most of the excitation energy originates from deformation energy [10, 11]. The assumption $E \ll D$ has been made implicitly by VANDENBOSCH [1] in the determination of the deformability from E_{x1} and E_{x2}. The further assumption $\epsilon \ll 1$ has been made explicitly. The energy E would divide into equal parts between the two fragments if the nuclear temperature and the level density parameters of the fragments were equal [12, 13]. As the latter show a strong shell effect, the assumption $\epsilon \ll 1$ will not be valid for fragment masses in the closed shell region. The quantity ϵE will be small compared to αE_x in any case as long as ϵ is restricted to small values and $E \ll D$.

The quantity γ of Eq. (13) equals the ratio of the mutual Coulomb energy C_{12} of the two deformed fragments to the mutual Coulomb energy C_0 of the two spherical fragments in contact. With Eq. (17a) and (17b) γ may be reduced to the measurable quantities E_k and E_x.

$$\gamma = \frac{E_k}{E_k + 2E_x} \tag{13a}$$

The deformation energy is related to the deformability by Eq. (10). It depends on the nuclear charge, as the deformability parameter a_{si} depends on the nuclear structure. A strong nuclear structure effect of the deformability parameter a_{si} may be directly confirmed from the energy of the first vi-

brational state for nuclei of different masses or indirectly from the interpretation of fission excitation energy data [1].

The series expansion of the deformation energy introduced into Eq. (11) takes into account the Z-dependence of the deformation energy. The energy $\hbar\omega$ of the lowest collective vibration is proportional to $a_{si}^{1/2}$.

$$\frac{dD_i}{dZ} = -2D_i \frac{d\ln(\hbar\omega)}{dZ} \tag{19}$$

The term $(dD_1/dZ)-(dD_2/dZ)$ of Eq. (12) is written with Eq. (19) and Eq. (18b)

$$\frac{dD_1}{dZ} - \frac{dD_2}{dZ} = 2\alpha E_x \frac{d\ln(\hbar\omega)}{dZ} \tag{20}$$

α and E_x are experimentally determined quantities.

The quantity $d\ln(\hbar\omega)/dZ$ may be taken from the experimentally determined values of the first 2^+-vibrational state of even-even stable nuclei [13]. In the mass regions $\begin{matrix} Z < 50 \\ N > 50 \end{matrix}$ and $\begin{matrix} N > 82 \\ N < 90 \end{matrix}$ the average value of $d\ln(\hbar\omega)/dZ$ is definitely positive. If the 2^+-state energies of two even-even nuclei of equal mass are compared, the 2^+-state energy of the nucleus with the smaller Z-value is found to be smaller than that of the nucleus with the higher Z-value. The average value of $d\ln(\hbar\omega)/dZ$ in the mentioned mass regions amounts to (0.17 ± 0.03). The mass dependence of $d\ln(\hbar\omega)/dZ$ is neglected. A tendency towards higher values seems to be indicated in the regions of closed shells. In these regions on the other hand the deformation energy D_i tends to very small values [9, 10]. Thus the product $D_i\, d\ln(\hbar\omega)/dZ$ will be small compared to its value for the highly deformed complementary fragment, as long as $d\ln(\hbar\omega)/dZ$ varies slowly near closed shells.

Replacing A_1 by $(1-\beta)A/2$ and A_2 by $(1+\beta)A/2$, and neglecting squares of β, Eq. (12) may be written using Eq. (13a) and (20)

$$\Delta_0 = \frac{\frac{8-5\gamma}{12} \times Z \times \left(\frac{A}{2}\right)^{-1/3} \times a_c \times \beta - \alpha E_x \frac{d\ln(\hbar\omega)}{dZ}}{16 \times A^{-1} \times a_a + \left(2 - \frac{5}{6}\gamma\right)\left(\frac{A}{2}\right)^{-1/3} a_c} \tag{21}$$

The energy E_c of Eq. (15) is written

$$E_c = 16 \times A^{-1} \times a_a + \left(2 - \frac{5}{6}\gamma\right)\left(\frac{A}{2}\right)^{-1/3} a_c \tag{22}$$

Eq. (21) gives the mass dependence of the primary charge in a semi-empirical representation. The mass dependence of α, γ and E_x may be taken from fission data. Figure 2 gives a plot of these quantities versus the mass of the fragments for U^{235} thermal fission. The mass dependence of γ is negligible in the region of high fission yields. With $\gamma \sim 0.80$ and the values of a_a and a_c introduced into Eq. (22) a value of $E_c = 1.78$ MeV is obtained for U^{235}.

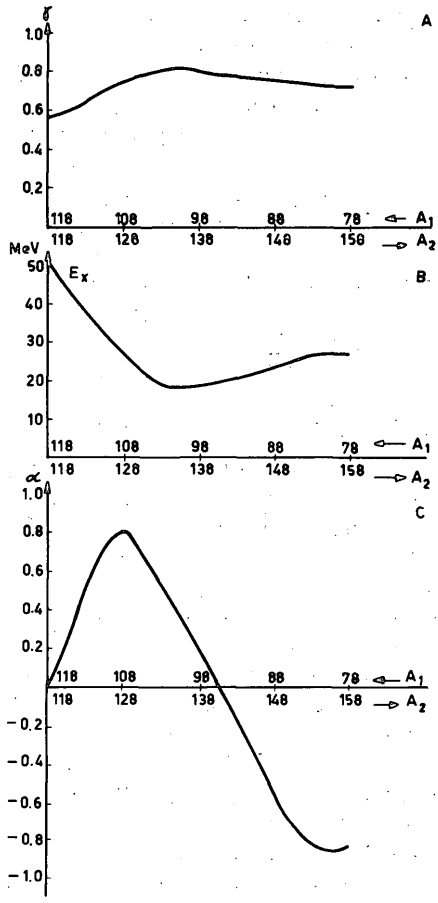

Fig. 2

Data used for a semi-empirical calculation of U^{235} charge distribution.

(a) The quantity γ versus fragment mass for U^{235}
(b) The total excitation energy and its mass dependence averaged between data from Refs. [9], [10] and [19]
(c) The quantity $\alpha = (E_{x1} - E_{x2})/E_x$ and its mass dependence according to Ref. [10]

The value of $d\ln(\hbar\omega)/dZ$ in the region of primary fission fragments may be expected to differ from the value derived from nuclei in the stable valley. The measured charge values for U^{235} fission fragments allow $d\ln(\hbar\omega)/dZ$ to be determined similarly from fission data, as the excitation energy has been used to derive the mass dependence of a_{si} [1]. From the value of $d\ln\hbar\omega/dZ$ obtained for U^{235} the mass dependence of the nuclear charge for other fissioning nuclei may be predicted in the calculation of Δ.

COMPARISON WITH EXPERIMENTAL RESULTS

Z_p-values of fission fragments have been measured with adequate accuracy only for U^{235}. The radiochemical results have been compiled by

WAHL et al. [14]. Z_p-values determined by physical methods have been published by ARMBRUSTER et al. [15]. THOMAS and VANDENBOSCH [8] correlated the fission-fragment kinetic energy fine structure with a semi-empirical mass surface. The mass of fission products before neutron emission has been determined by the two surface-barrier-detector technique. The maxima of the yield curves versus kinetic energy of one fragment with constant energy of the second fragment are correlated to the mass surface of even-even nuclei. Nuclear charges have been determined for the mass values in the maximum of the yield curves. All the maxima are correlated to even-even nuclei. From the charge values Δ-values of primary fission fragments have been calculated.

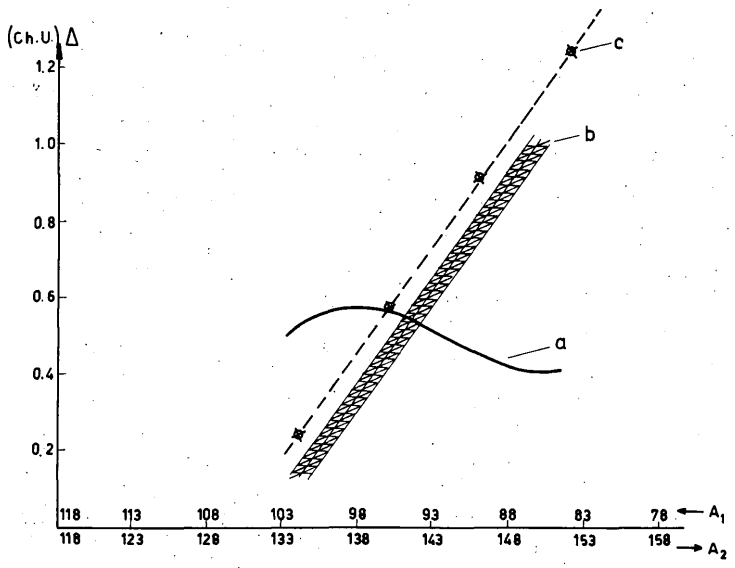

Fig. 3

Experimental values of the charge distribution of U^{235}

Curve (a) radiochemical data from Ref. [14]
(b) direct measurement from Ref. [15]
(c) even-even-nuclei, which yield a fine structure in the kinetic energy distribution [8].

Figure 3 gives the experimental Z_p-functions from [14] and [15], and the Z_p-values taken from the kinetic energy data [8]. The latter agree fairly well with the measurements of [15]. The agreement between the radiochemical results is as poor as the agreement between the radiochemical and the direct measurements of [15]. The slope $d\Delta/dA$ defined by the measurements [15] and [18] agrees within the accuracy of the measurements. The difference of 0.1 charge units in the absolute values of Δ may not be taken seriously, as the mean charge values measured in [15] are not necessarily identical with the yield maxima of primary even-even nuclei.

The experimentally determined values of Δ are fitted to Eq. (21). The first term of Eq. (21) gives a linear increase of Δ with the distance from the symmetry point. The slope of this line is negative (Fig. 4, curve a). With

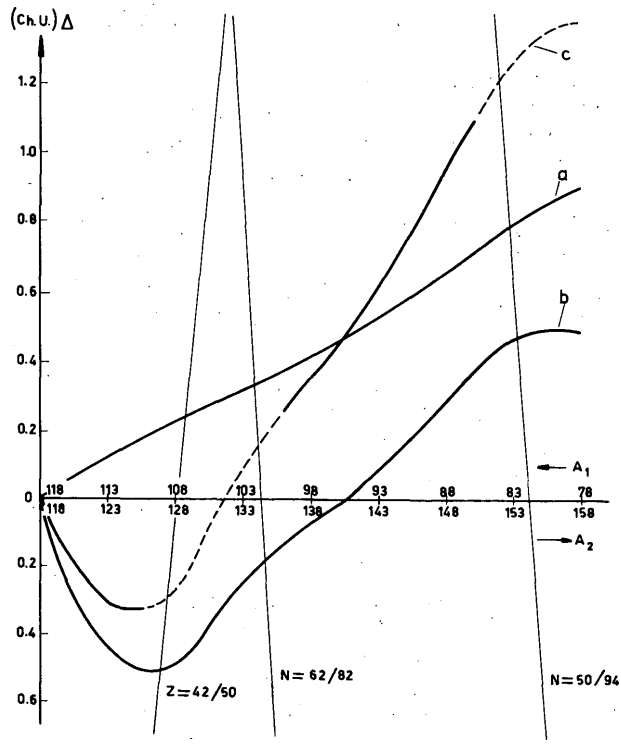

Fig. 4

Charge distribution calculated for U^{235} (curve c).
Curve (a) Contributions of Coulomb- and asymmetry terms to charge distribution
(b) Contribution of the deformation energy term fitted to the experimental data of [15] by a value of $d\ln(\hbar\omega)/dZ = 3.9 \times 10^{-2}$.

$\gamma = 0.80$ the slope determined by the first term amounts to $d\Delta/dA = -2.1 \times 10^{-2}$ charge units/mass units.

The second term is determined by the excitation energies. It is governed by the mass dependence of the quantity α (Fig. 2c). For symmetric fission and the most probable asymmetric fission the contribution of the second term is zero. The second term is plotted in Fig. 4, curve b. The average value of Δ over all fragment yields is only dependent on the first term of Eq. (18). The second term changes the slope $d\Delta/dA$. It is increased, as $d\ln(\hbar\omega)/dZ$ is positive.

The value of $d\ln(\hbar\omega)/dZ$ obtained from a fit to the measured value of Ref. [15] amounts to $d\ln(\hbar\omega)/dZ = 3.9 \times 10^{-2}$. This value is smaller than the value for stable nuclei $0.17 + 0.03$. The deformabilities of neutron-rich nuclei seem to decrease more slowly than the deformabilities in the region of the stable nuclei. A fit to the radiochemical data makes $d\ln(\hbar\omega)/dZ$ negative. This is not compatible with the nuclear data on $\hbar\omega$ for stable nuclei.

Figure 4, curve c, gives the mass dependence of Δ for the total mass range of the fission fragments in U^{235} fission with the value of $d\ln(\hbar\omega)/dZ$ fitted to the data of Ref. [15]. In the region of symmetric fission the values

of Δ are small. In the region of asymmetric fission the mass dependence of Δ is linear with a negative slope of $d\Delta/dA = -5.6 \times 10^{-2}$.

Z_p will be determined by Eq.(21), if the pairing energy Q_p and the shell energy Q_s may be neglected. The energy $E_c \sim 1.8$ MeV is of the same order of magnitude as Q_p and Q_s.

Figure 5 gives the energy $E = Q_p + Q_s - E_c(\Delta - \Delta_0)^2$, calculated from Eqs.(16) and (21), for all the fragment pairs in the fission of the compound nucleus U^{236}. The values used for Q_p and Q_s are the values taken from stable nuclei, $\delta = 1.2$ MeV, $Q_{N=50} = 2.3$ MeV, $Q_{N=82} = 1.9$ MeV, $Q_{Z=50} = 2.0$ MeV. The shell effects of the deformed fragments in the scission configuration may be much smaller than the values for stable nuclei. The conclusions concerning the influence of closed shells are not valid, if the shell effects are considerably smaller than assumed in the following.

Deviations from Eq.(21) are to be expected near closed shells, that is in the mass ranges $82 < A_p < 86$ and $124 < A_p < 136$, and in the complementary regions. In these regions Fig.4c is dotted. Energetically the average shell effect is equivalent to a shift of 1.1 charge units from the value given by Eq.(21). The shell effect of the double magic nucleus Sn^{132} would be compensated energetically by a shift of 1.5 charge units from Δ_0. In the region of closed shells the Z_p-function is expected to follow the lines $N = 50$, $N = 82$ and $Z = 50$. This gives rise to increased primary yields for Ge^{82}, Kr^{86} and the tin isotopes Sn^{124}, Sn^{126}, Sn^{130} and Sn^{132}. A rather high yield of the double magic nucleus Sn^{132} should be found, an experimental indication of which is given by the measurements of KONECNY et al. [6]. Tin and molybdenum isotopes are energetically favoured [14] for U^{235} fission.

The pairing energy Q_p may cause increased primary yields for even-even nuclei. Deviations from the values given by Eq.(21) might be found for the fragment pairs 100/136, 98/138, 94/142, 92/144 and 88/148.

A combined effect Q_p and Q_s should increase the width of the charge distribution in the chains $A_p = 82$, 86, 124 and 136.

The deviations caused by the pairing energy approximately cancel in pairs for neighbouring masses. They are not to be observed in [15], as the measurement averages over several masses. All deviations caused by Q_s are in mass regions of low mass yields, where [15] gives no values of Z_p. The fitting of Eq.(21) to the measurement [15] should be independent from local changes of the Z_p-function caused by Q_p and Q_s. Z_p-determinations for single decay chains of even A_p-values may give values of Z_p differing from the values of Fig.4c by as much as 0.4 charge units. For a comparison of the direct measurements [15] with other results only Z_p-values for odd A_p-values in the mass region $136 < A_p < 150$ should be used.

THE PRIMARY CHARGE DISTRIBUTION OF Cf^{252}

Nearly all quantities that have been measured for U^{235} are known for Cf^{252} also. The quantities α, γ and E_x of Eq.(21) may be derived from the measurements of BOWMAN et al. [11] and FRASER et al. [12]. The quantity $d\ln(\hbar\omega)dZ$ of Eq.(21) is taken to be independent of the fissioning nucleus. The value obtained from the fit to the U^{235} data will be used for all fissioning

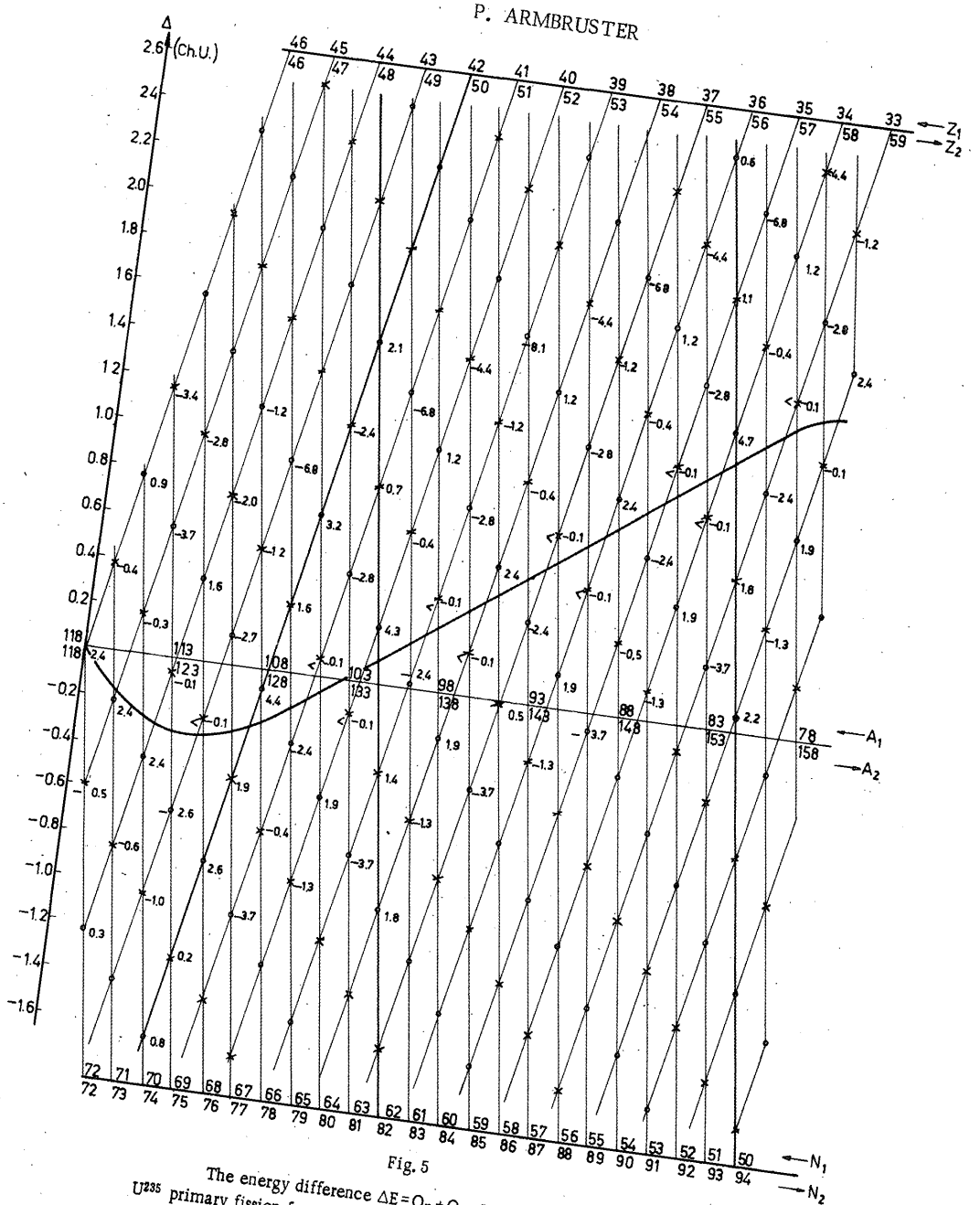

Fig. 5

The energy difference $\Delta E = Q_p + Q_s - E_C(\Delta - \Delta_0)^2$ of U^{235} primary fission fragments calculated from the charge distribution of Eq. (21), $Q_p = \pm 2.4$ MeV, $Q_s = (2.3\ \text{MeV} \rightarrow N = 50)$, $(1.9\ \text{MeV} \rightarrow N = 82)$ and $(2.0\ \text{MeV} \rightarrow Z = 50)$, $E_C = 1.8$ MeV.

● even-even nuclei
x even-odd nuclei
o odd-odd nuclei

nuclei. Equation (21) with α, γ and E_x taken from [11] and [12] gives for Cf^{252} the mass dependence of Δ plotted as curve b in Fig. 6. For comparison the U^{235}-charge distribution is given as curve a. There are some characteristic differences compared with U^{235}. (a) The Z-values of a certain mass value for Cf^{252} that is compared with U^{235} in the light fragment group is

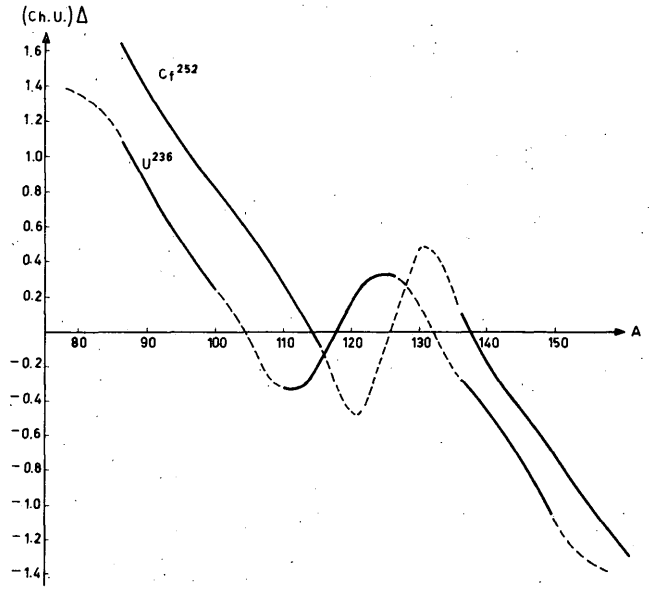

Fig. 6

Charge distribution of U^{235} and Cf^{252}

higher by about 0.5 charge units, in the heavy group it is higher by about 0.3 charge units. (b) In Fig. 7 the chain-length and its mass dependence is given for U^{235} and Cf^{252}. From this figure the deviation of the chain-lengths from the empirical rule of equal charge displacement of complementary fragments may be seen [17].

For U^{235} differences between chain-lengths of complementary fragments of up to 1.4 charge units have been found in the mass region $A_1/A_2 \sim 84/150$ and $A_1/A_2 \sim 106/128$, whereas differences smaller than 0.5 charge units have been found only in the mass range $A_1/A_2 \sim 94/142$. An average deviation from the equal charge displacement rule of 0.7 charge units is taken from the measurement [15]. In the region of high-mass yields the chain-length increases with increasing mass in both groups [18].

For Cf^{252} the differences between complementary fragments are much smaller. The average deviation from the equal charge displacement rule amounts to 0.2 charge units. Differences of more than 0.5 charge units will be found only in the mass region between A = 109 and A = 115, with a highest value of ~ 0.7 charge units. The equal charge displacement rule is fulfilled much better for Cf^{252} than for U^{235}.

A maximum of the chain-length will be expected in the mass range of highest yields for Cf^{252}.

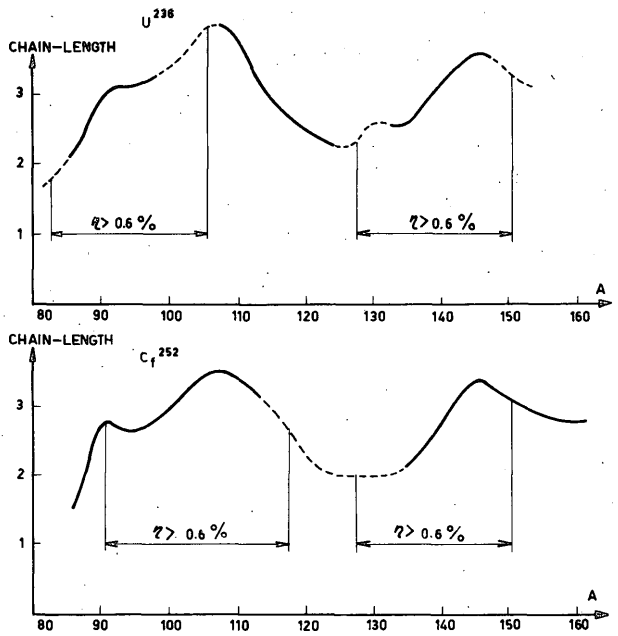

Fig. 7

The length of β-decay chains for U^{235} and Cf^{252}.
The regions of high mass yields are indicated by arrows.

A calculation of the charge distribution for other fissioning nuclei is possible if data on α and E_x are available. As this is not available, further calculations have not yet been done.

ACKNOWLEDGEMENTS

I am indebted to Dr. H. Schmitt, and to Professors R. Vandenbosch, W. Brenig, and W. Wild for stimulating discussions.

REFERENCES

[1] VANDENBOSCH, R., Nucl. Phys. 46 (1963) 129.
[2] PRESENT, R.D., Phys. Rev. 72 (1947) 7.
[3] FRANKEL, S. and METROPOLIS, N., Phys. Rev. 72 (1947) 914.
[4] SWIATECKI, W.J., Ann. Phys. 22 (1963) 406.
[5] FONG, P., Phys. Rev. 135 (1964) B 1338.
[6] FONG, P., Phys. Rev. 102 (1956) 434.
[7] WILETS, L., Theories of nuclear fission, Clarendon Press, Oxford (1964).
[8] THOMAS, T.D. and VANDENBOSCH, R., Phys. Rev. 133 (1964) B 976.
[9] MAIER-LEIBNITZ, H., SCHMITT, H. and ARMBRUSTER, P., "Average number and energy of gamma-rays emitted as a function of fragment mass in U^{235} thermal-neutron-induced fussion", these Proceedings II.

[10] APALIN, V.F., GRITSYUK, Yu.N., KUTIKOV, I.E., LEBEDEV, V.I. and MIKAELYAN, L.A., Nucl. Phys. 55 (1964) 249.
[11] BOWMAN, H.R., MILTON, J.C.D., THOMPSON, S.G. and SWIATECKI, W.J., Phys. Rev. 129 (1963) 2133.
[12] FRASER, J.S., MILTON, J.C.D., BOWMAN, H.R. and THOMPSON, S.G., Canad. J. Phys. 41 (1963) 2080.
[13] TEMMER, G.M. and HEYDENBURG, N.P., Phys. Rev. 104 (1956) 967.
[14] WAHL, A.C., FERGUSON, R.L., NETHAWAY, D.R., TROUTNER, D.E. and WOLFSBERG, K., Phys. Rev. 126 (1962) 1112.
[15] ARMBRUSTER, P., HOVESTADT, D., MEISTER, H. and SPECHT, H.J., Nucl. Phys. 54 (1964) 586.
[16] KONECNY, E., OPOWER, H., GUNTHER, H. and GÖBEL, H., "Primary distributions of nuclear charge for fission fragment masses 132, 134, 136 and 137 from thermal fission of U^{235}", these Proceedings I.
[17] GLENDENIN, L.E., CORYELL, C.D. and EDWARDS, R.R., Paper 52 in Natl. Nuclear Energy Series, Div. IV, (1951) 9.
[18] ARMBRUSTER, P. and MEISTER, H., Z. Phys. 170, (1962) 274.
[19] MILTON, J.C.D. and FRASER, J.S., Canad. J. Phys. 40 (1962) 1626.

DISCUSSION

S.S. KAPOOR: How does the physical reasoning on which Dr. Armbruster's calculations are based differ from the earlier approach, e.g. minimizing the potential energy or maximizing the excitation energy of the two touching fragments at scission?

P. ARMBRUSTER: The calculations were simplified to the maximum possible extent; they do not differ, in principle, from earlier calculations. The small energy shifts causing the charge distribution are described accurately enough by the leading terms of the mass formulas.

ОБ ОБОЛОЧЕЧНЫХ ЭФФЕКТАХ ПРИ ДЕЛЕНИИ ЯДЕР*

Б.Т. ГЕЙЛИКМАН
ГОСУДАРСТВЕННЫЙ КОМИТЕТ ПО ИСПОЛЬЗОВАНИЮ АТОМНОЙ ЭНЕРГИИ СССР, ИНСТИТУТ АТОМНОЙ ЭНЕРГИИ им. И.В. КУРЧАТОВА, МОСКВА
СССР

Abstract — Résumé — Аннотация — Resumen

SHELL EFFECTS IN NUCLEAR FISSION. The important part played by shell effects in nuclear fission has been reliably established experimentally and forms the basis of the theory of asymmetry of fission and other properties of fission fragments. However, from the theoretical point of view there are certain difficulties in understanding these effects, since at the moment of scission the fragments are considerably deformed. When the shell effects are calculated in succession, the energy of the fissioning nucleus before scission may be presented in the form of the sum of the energies of the spherical fragments taking shell effects into account, the Coulomb interaction energy of the fragments and their deformation energy. The deformation energy of the fragments should be calculated not using the elasticity values of the fragments according to the drop model, but, for very low deformations, the single particle elasticity values taking into account the magic effects, with a gradual transition to the drop values for deformations at which the levels of neighbouring shells intersect. The single-particle elasticity values can be obtained from the experimental data on the Coulomb excitation of the nuclei. In Vandenbosch's calculations of fragment deformation, the elasticity of the fragments was based on the condition of coincidence between the deformation energy of the fragments and the experimental values for their excitation energy. However, in this case the elasticity was assumed to be constant at all deformations, and for this reason, although the elasticity values found in Vandenbosch do show magic effects, they differ considerably in magnitude from the experimental elasticity values (see above). The calculations of Vandenbosch also failed to take into account the magic effects for non-deformed fragments that lead to a reduction in the energy of the magic nucleus. Therefore, according to these calculations fission should be symmetrical, since the elasticity and consequently also the deformation energy (at the same deformation) are greater for magic than for non-magic nuclei. In fact, since the energy gain for magic spherical fragments is greater than the loss resulting from the increase in elasticity, the formation of magic and near-magic fragments, i.e. asymmetrical fission, is energetically advantageous. This energy gain is essentially connected with the fact that because of the high elasticity value at low deformations the magic fragments are so little deformed that the deformation energy does not compensate for the difference in mass of magic and non-magic fragments. Apart from the deformation energy, the kinetic energy of the separating degrees of freedom at the moment of scission should be taken into account when calculating the excitation energy of fragments.

For the shell effects of the fragments to play an important part in fission, the process of deformation of the nucleus on descending from the saddle point (in the case of threshold fission) must be, as in fact it is, fairly slow with respect to the nucleonic degrees of freedom, i.e. $\tau_{def} \gg \tau_{nucleon}$ (τ_{def} is the descent time, $\tau_{nucleon} \sim \hbar/\Delta E_{nucleon}$, and $\Delta E_{nucleon}$ is the distance between the nucleon levels). In this case nucleonic shells are formed before scission. At the same time $\tau_{def} \ll \tau_{rot}$, i.e. the process of descent is fast with respect to the rotational degrees of freedom ($\tau_{rot} \hbar/\Delta E_{rot}$). In the case of fission of an excited nucleus with fairly high excitation energy at the saddle point, $\Delta E_{nucleon}$ may be so low that not only $\tau_{def} \ll \tau_{rot}$ but also $\tau_{def} \ll \tau_{nucleon}$, i.e. the process of descent is accelerated with respect to all the degrees of freedom. In this case the density matrix of the nucleus does not change on moving from the saddle point. This would seem to explain the fact that the theoretical angular distribution of fragments at fission of an excited nucleus agrees with the experimental value only when the parameters determining the rotational state of the nucleus (moment of inertia) at the saddle point and not at the scission point are used.

EFFETS DE COUCHES DANS LA FISSION NUCLÉAIRE. Le rôle essentiel joué par les effets de couches dans la fission nucléaire a été mis en évidence par voie expérimentale; il se trouve à la base de la théorie

* На симпозиуме зачитано только название доклада.

de l'asymétrie de la fission et d'autres propriétés des fragments de fission. Cependant, la compréhension des effets de couches suscite, du point de vue théorique, certaines difficultés du fait qu'au moment de la rupture du col, les fragments accusent une déformation marquée. Si l'on tient systématiquement compte des effets de couches, l'énergie du noyau qui subit la fission peut être exprimée par la somme des énergies des fragments sphériques compte tenu de ces effets, de l'énergie d'interaction coulombienne des fragments et de leur énergie de déformation. Pour calculer cette dernière énergie, il convient d'utiliser non pas les valeurs de l'élasticité des fragments conformément au modèle de la goutte, mais les valeurs de l'élasticité relatives à une seule particule, en tenant compte des effets magiques lorsque les déformations sont très petites, et en passant progressivement aux valeurs de l'élasticité conformes au modèle de la goutte lorsque les déformations sont telles qu'il y a intersection des niveaux des couches voisines. Les valeurs de l'élasticité relatives à une seule particule peuvent être obtenues à partir de données expérimentales sur l'excitation coulombienne des noyaux. Dans les calculs de Vandenbosch sur la déformation des fragments, on a choisi l'élasticité des fragments en admettant que leur énergie de déformation et les valeurs expérimentales de leur énergie d'excitation coïncident. On a supposé toutefois que l'élasticité reste alors constante pour toutes les déformations; c'est pourquoi, si les valeurs de l'élasticité déterminées dans les calculs de Vandenbosch accusent des effets magiques, elles diffèrent sensiblement, quant à leur ordre de grandeur, des valeurs expérimentales. Dans les calculs de Vandenbosch, on n'a pas non plus tenu compte, en ce qui concerne les fragments non déformés, des effets magiques qui entraînent une diminution de l'énergie du noyau magique. Il s'ensuit que, conformément à ces calculs, la fission devrait être symétrique, étant donné que l'élasticité et, partant, l'énergie de déformation (pour une même déformation) sont plus grandes pour les noyaux magiques que pour les noyaux non magiques. En réalité, le gain en énergie pour les fragments sphériques magiques étant plus grand que la perte en énergie due à l'accroissement de l'élasticité, la formation de fragments magiques et quasi magiques, c'est-à-dire la fission asymétrique, sera avantageuse du point de vue de l'énergie. Ce gain en énergie s'explique essentiellement par le fait que, vu la valeur élevée de l'énergie d'élasticité relative aux faibles déformations, les fragments magiques sont si peu déformés que l'énergie de déformation ne suffit pas pour compenser la différence entre les masses des fragments magiques et non magiques. En calculant l'énergie d'excitation des fragments, il faut tenir compte non seulement de leur énergie de déformation, mais aussi de l'énergie cinétique correspondant aux degrés de liberté de la fission au moment de la rupture du col.

Pour que les effets de couches des fragments puissent jouer un rôle important dans la fission, il est indispensable (comme le confirment d'ailleurs les phénomènes réels) que dans la période qui suit l'etranglement (dans le cas d'une fission à seuil) le noyau subisse une déformation relativement lente si l'on considère les degrés de liberté nucléoniques, c'est-à-dire que $\tau_{déf} \gg \tau_{nucl}$ ($\tau_{déf}$ étant la durée de cette période, $\tau_{nucl} \sim \hbar/\Delta E_{nucl}$ et ΔE_{nucl} la distance entre les niveaux nucléoniques). Dans ce cas, les couches de nucléons ont le temps de se former avant la scission. Simultanément $\tau_{déf} \ll \tau_{rot}$; **autrement dit, l'évolution pendant** cette période est relativement rapide, si l'on considère les degrés de liberté de rotation ($\tau_{rot} \sim \hbar/\Delta E_{rot}$). Lors de la fission d'un noyau excité sous l'effet d'une énergie suffisamment élevée au point d'étranglement, ΔE_{nucl} peut avoir une valeur si petite que, non seulement $\tau_{déf} \ll \tau_{rot}$, mais aussi $\tau_{déf} \ll \tau_{nucl}$; en d'autres termes, l'évolution pendant cette période est relativement rapide, si l'on considère tous les degrés de liberté. Dans ce cas, la matrice de densité du noyau n'a pas le temps de se modifier pendant la période qui suit l'étranglement. Ce phénomène semble expliquer le fait que, lors de la fission d'un noyau excité, la distribution angulaire théorique des fragments ne concorde avec la valeur expérimentale que si l'on utilise les valeurs des paramètres qui déterminent l'état de rotation du noyau (moment d'inertie) au point d'étranglement et non au point de scission.

ОБ ОБОЛОЧЕЧНЫХ ЭФФЕКТАХ ПРИ ДЕЛЕНИИ ЯДЕР. Существенная роль оболочечных эффектов при делении ядер надежно установлена экспериментальным путем и является основой теории асимметрии деления и других свойств осколков деления. Однако с теоретической точки зрения понимание оболочечных эффектов связано с известными трудностями, поскольку осколки в момент разрыва шейки обладают заметной деформацией. При последовательном учете оболочечных эффектов энергия делящегося ядра перед разрывом шейки может быть представлена в виде суммы энергий сферических осколков с учетом оболочечных эффектов, энергии кулоновского взаимодействия осколков и энергии деформации осколков. При вычислении энергии деформации осколков следует пользоваться значениями упругости осколков не по капельной модели, как в работе [4], а одночастичными значениями упругости с учетом магических эффектов — при очень малых деформациях с постепенным переходом к капельным значениям упругости при деформациях, при которых происходит пересечение уровней соседних оболочек. Одночастичные значения упругости могут быть получены из экспе-

риментальных данных по кулоновскому возбуждению ядер. В расчетах деформации осколков Ванденбоша [3] упругость осколков подбиралась до условия совпадения энергии деформации осколков с экспериментальными значениями их энергии возбуждения. При этом, однако, упругость предполагалась постоянной при всех деформациях; поэтому хотя найденные в [3] значения упругости и обнаруживают магические эффекты, но по величине заметно отличаются от экспериментальных значений упругости (см. выше). В [3] не учитывались также магические эффекты для недеформированных осколков, приводящие к уменьшению энергии магического ядра. Поэтому согласно [3] деление должно было бы быть симметричным т.к. упругость, а следовательно и энергия деформации (при той же деформации) для магических ядер больше, чем для немагических. В действительности, т.к. выигрыш в энергии для магических сферических осколков больше, чем проигрыш, связанный с увеличением упругости, образование магических и околомагических осколков, т.е. асимметричное деление будет энергетически выгодным. Этот выигрыш в энергии связан существенным образом с тем, что из-за большего значения упругости при малых деформациях магические осколки оказываются очень мало деформированными и при такой малой деформации энергия деформации еще не компенсирует различие в массах магических осколков. При вычислении энергии возбуждения осколков помимо их энергии деформации следует учитывать также кинетическую энергию делительных степеней свободы в момент разрыва шейки.

Для того, чтобы оболочечные эффекты осколков при делении играли существенную роль, необходимо (как это и оказывается в действительности), чтобы процесс деформации ядра при спуске с седловой точки (в случае порогового деления) был бы достаточно медленным по отношению к нуклонным степеням свободы, т.е. $\tau_{деф} \gg \tau_{нукл}$ ($\tau_{деф}$ – время спуска, $\tau_{нукл} \sim \frac{\hbar}{\Delta E_{нукл}}$; $\Delta E_{нукл}$ – расстояние между нуклонными уровнями). В этом случае нуклонные оболочки успевают образовываться перед разрывом шейки. В то же время $\tau_{деф} \ll \tau_{вращ}$, т.е. процесс спуска является быстрым по отношению к вращательным степеням свободы ($\tau_{вращ} \sim \hbar/\Delta E_{вращ}$). В случае деления возбужденного ядра при достаточно большой энергии возбуждения в седловой точке $\Delta E_{нукл}$ может оказаться настолько малым, что не только $\tau_{деф} \ll \tau_{вращ}$, но и $\tau_{деф} \ll \tau_{нукл}$, т.е. процесс спуска является быстрым по отношению ко всем степеням свободы. В этом случае матрица плотности ядра не успевает измениться при спуске с седловой точки. Этим, по-видимому, объясняется то обстоятельство, что теоретическое угловое распределение осколков при делении возбужденного ядра согласуется с экспериментальным лишь в том случае, если пользоваться значениями параметров, определяющих вращательное состояние ядра (момент инерции), в седловой точке, а не в точке разрыва шейки.

EL EFECTO DE CAPAS EN LA FISION NUCLEAR. Se ha determinado experimentalmente el importante papel que desempeña el efecto de capas en la fisión nuclear y que forma la base de la teoría relativa al carácter asimétrico de la fisión y de otras propiedades de los fragmentos de fisión. Sin embargo, al conocimiento teórico del efecto de capas se oponen ciertas dificultades debido a que en el momento de la escisión los fragmentos acusan una marcada deformación. Si se tiene en cuenta sistemáticamente el efecto de capas, la energía de fisión del núcleo antes de la escisión puede expresarse por la suma de las energías de los fragmentos esféricos tomando en consideración esos efectos, la energía de la interacción coulombiana de los fragmentos y su energía de deformación. Para calcular esa última energía, no conviene utilizar los valores relativos a la elasticidad de los mismos, según el modelo de la gota, sino los valores de elasticidad correspondientes a una sola partícula tomando en consideración los efectos mágicos cuando las deformaciones son muy pequeñas, y pasar gradualmente a los valores de elasticidad conformes al modelo de la gota para deformaciones en las que tiene lugar una intersección de las capas vecinas. Los valores de elasticidad para una sola partícula pueden deducirse de los datos experimentales sobre la excitación coulombiana de los núcleos. En los cálculos de Vandenbosch acerca de la deformación de los fragmentos, la elasticidad de éstos se eligió suponiendo que su energía de deformación coincide con los valores experimentales de su energía de excitación. Se había supuesto, sin embargo, que la elasticidad permanece constante para todas las deformaciones; por ello, los efectos mágicos observados en los valores calculados por Vandenbosch se distinguen marcadamente por su magnitud de los valores experimentales de elasticidad (véase supra). En los cálculos de Vandenbosch tampoco se tuvieron en cuenta los efectos mágicos correspondientes a los fragmentos no deformados, que provocan una reducción de la energía del núcleo mágico. Por ello, la fisión debería ser simétrica, dado que la elasticidad, y, en consecuencia, la energía de deformación (para la misma deformación) deben ser más importantes para los núcleos mágicos que para los que no tienen este carácter. En realidad, como la ganancia energética para los fragmentos esféricos mágicos es mayor que la pérdida relacionada con el aumento de elasticidad, podrá considerarse positivo el balance energético correspondiente a la formación de fragmentos

mágicos y cuasimágicos, es decir, la fisión asimétrica. Esta ganancia energética se explica esencialmente debido a que para pequeñas deformaciones los valores de elasticidad son elevados y los fragmentos mágicos sufren una deformación muy pequeña; en este caso, la energía de deformación no basta para compensar la diferencia entre las masas de los fragmentos mágicos y no mágicos. Al calcular la energía de excitación de los fragmentos, además de la energía de deformación, conviene tener en cuenta también la energía cinética correspondiente a los grados de libertad de fisión en el momento de la escisión.

Para que los efectos de capas de los fragmentos puedan desempeñar un papel importante en la fisión, es indispensable (como ocurre en realidad) que durante el descenso del punto de estrangulación (cuando se trata de una fisión umbral) el núcleo sufra una deformación suficientemente lenta con respecto a los grados de libertad nucleónicos, es decir, $\tau_{def} \gg \tau_{nucl}$.

(Siendo τ_{def} el tiempo de descenso, $\tau_{nucl} \sim \hbar/\Delta E_{nucl}$ y ΔE_{nucl} la distancia entre los niveles nucleónicos.) En este caso, las capas nucleónicas consiguen formarse antes de la escisión. Al mismo tiempo $\tau_{def} \ll \tau_{rot}$, es decir, el proceso de descenso es rápido con respecto a los grados de libertad de rotación ($\tau_{rot} \sim \hbar/\Delta E_{rot}$). En el caso de la fisión de un núcleo excitado, con una energía de excitación suficientemente grande en el punto de estrangulación, ΔE_{nucl} puede ser tan pequeño que no sólo $\tau_{def} \ll \tau_{rot}$, sino también $\tau_{def} \ll \tau_{nucl}$, es decir, el proceso de descenso es rápido respecto de todos los grados de libertad. En este caso, la matriz de densidad del núcleo no se modifica durante el descenso del punto de estrangulación. Este fenómeno explica al parecer, el hecho de que la distribución angular teórica de los fragmentos en la fisión de un núcleo excitado sólo concuerda con la establecida experimentalmente cuando se utilizan parámetros que determinan el estado de rotación del núcleo (momento de inercia) en el punto de estrangulación, pero no en el punto de escisión.

В настоящее время можно считать установленным, что одна капельная модель без учета оболочечных эффектов не в состоянии объяснить ряда важных особенностей процесса деления: асимметрию деления, распределение зарядов осколков деления, зависимость энергии возбуждения осколков и их кинетической энергии от отношения масс осколков (в особенности, в области симметричного деления) и т.д. В то же время все эти явления легко объясняются качественно, а иногда и количественно, если учесть оболочечные эффекты осколков при формировании осколков перед разрывом шейки делящегося ядра. Существование оболочечных эффектов доказано непосредственно экспериментами по массовому распределению осколков при увеличении энергии возбуждения делящегося ядра (исчезновение тонкой структуры массовой кривой при делении нейтронами с энергией 14 Мэв). Однако концепция, основывающаяся на существенной роли оболочечных эффектов, наталкивается на серьезные возражения чисто теоретического характера [1]: согласно оценкам, основанным на капельной модели, параметр симметричной деформации осколков в момент их образования $\alpha_2^{\text{ос к}} \sim 0{,}2-0{,}25$; при такой большой деформации, согласно модели Нильсона для деформированных ядер, должны были бы уже исчезнуть все оболочечные эффекты. Ниже показано, что при правильном рассмотрении учет оболочечных эффектов позволяет вполне удовлетворительно истолковать все основные особенности процесса деления.

Энергию делящегося ядра перед разрывом его шейки можно представить в виде суммы: 1) кулоновской энергии взаимодействия будущих осколков, 2) энергии сферических осколков, вычисляемой по формуле типа Вайцзекера с учетом оболочечных эффектов, и 3) энергии деформации осколков. Такие расчеты были проведены в работе [2], и при этом было показано, что минимум энергии, отличающийся на ~6 Мэв от энергии ядра при симметричном делении, соответствует асимметричному делению. Однако в работе [2], ввиду отсутствия в то время достаточно полных данных об упру-

гости ядер при малых деформациях, при вычислении энергии деформации осколков использовалась упругость по капельной модели. В действительности, при очень малых деформациях, при которых еще не происходит пересечения уровней соседних оболочек, упругость значительно больше капельной и имеет максимальное значение для магических ядер и минимальное—в середине оболочки. При увеличении деформации упругость понижается и при деформации, заметно превышающей то значение, при котором происходит пересечение уровней соседних оболочек, переходит в капельную упругость. Недавно Ванденбош вычислил деформацию осколков в момент их образования, сводя к минимуму энергию двух соприкасающихся осколков (их деформация описывалась лишь параметром α_2); значения упругости для каждого осколка подбирались таким образом, чтобы энергия возбуждения пары осколков, которая предполагалась равной их энергии деформации, совпадала с величиной, полученной из эксперимента [3]. При этом оказалось, что найденные таким образом значения упругости осколков имеют максимальное значение для магических осколков и минимальное—в середине оболочки (хотя абсолютные значения упругости заметно меньше, чем экспериментальные значения при малых деформациях) и что деформации магических осколков меньше, чем немагических. К сожалению, в работе [3] упругость осколка предполагалась одинаковой при всех деформациях и не учитывалось уменьшение энергии сферического осколка в области около магических ядер. Это привело бы, как легко видеть, к тому, что симметричное деление соответствовало бы меньшей энергии, чем асимметричное, т.к. энергия деформации при одинаковой деформации для магического осколка больше, чем для немагического.

В настоящей работе энергия делящегося ядра, как и в работе [2], вычисляется в виде суммы указанных выше трех слогаемых. Но для упругости осколков используются не капельные значения, а одночастичные с учетом оболочечных эффектов—при малых деформациях—с постепенным переходом к капельным значениям при больших деформациях. Одночастичные значения упругости были получены на основе экспериментальных значений упругости, вычисленных из данных по кулоновскому возбуждению ядер. Оценки показывают, что благодаря тому, что одночастичная жесткость магических осколков заметно больше, чем средняя жесткость в работе [3], магические и околомагические осколки оказываются еще менее деформированными, чем в работе [3] (а являющийся их партнером немагический осколок—еще более деформированным). При такой малой деформации магического осколка его упругость заметно больше капельной, т.е. еще не произошло полного перемешивания уровней разных оболочек. Поэтому проигрыш в энергии, связанный с большим значением упругости, не уничтожает полностью для магического осколка выигрыш, связанный с меньшим значением энергии сферического ядра. Таким образом, оболочечные эффекты в энергии сферического ядра, благоприятствующие асимметрии деления, перевешивают оболочечные эффекты для коэффициента упругости, действующие в противоположном направлении (из-за малой деформации магического осколка, вызванной оболочечными эффектами в коэффициенте упругости). Но разность энергии ядра при асимметричном и симметричном делении оказывается заметно меньше, чем в работе [2]. При вычислении энергии возбуждения осколков учитывается, помимо энер-

гии деформации осколков в момент их образования, также начальная кинетическая энергия делительных степеней свободы осколков [4]. Более подробные численные расчеты энергии делящегося ядра на основе изложенной выше схемы приводятся в докладе Г.И.Хлебникова и автора.

Для того, чтобы оболочечные эффекты при делении играли существенную роль, необходимо, чтобы процесс деформации делящегося ядра после прохождения через седловую точку являлся квазистатическим по отношению к нуклонным степеням свободы ядра. Только в этом случае оболочки осколков будут успевать складываться при деформации ядра перед разрывом шейки. Квазистатичность процесса деформации может быть показана с помощью простых оценок [4]. Однако этот вывод на первый взгляд противоречит данным, вытекающим из углового распределения осколков. Как известно, угловое распределение осколков при достаточно больших энергиях возбуждения описывается статистической теорией [5]. Величина входящего в распределение Больцмана эффективного момента инерции различна в седловой точке и в точке разрыва шейки. Анализ экспериментальных данных показывает, что для согласия теории с опытом следует подставить в распределение Больцмана значение эффективного момента инерции в седловой точке, это, казалось бы, свидетельствует о том, что процесс спуска ядра с седловой точки является очень быстрым [5]. Нетрудно, однако, видеть, что процесс деформации ядра может быть квазистатичным по отношению к нуклонным степеням свободы и неквазистатичным по отношению к вращательным степеням свободы. Действительно, при пороговом делении характерное нуклонное время

$$\tau_{\text{нукл}} \approx \frac{\hbar}{\Delta E_{\text{нукл}}} \sim 10^{-21}\ \text{сек}\ (\Delta E_{\text{нукл}} \sim 1\ \text{Мэв}),$$

а время деформации $\tau_{\text{деф}} \sim 3 \cdot 10^{-20}$ и $\tau_{\text{деф}} \gg \tau_{\text{нукл}}$. Но $\tau_{\text{вращ}} \sim \frac{\hbar}{\Delta E_{\text{вращ}}} \sim 10^{-19}$ сек (в седловой точке $\Delta E_{\text{вращ}} \approx \frac{\hbar^2}{\mathcal{J}} \sim 10$ кэв) и, следовательно, $\tau_{\text{деф}} \lesssim \tau_{\text{вращ}}$. При делении сильно возбужденного ядра, когда в седловой точке $\Delta E_{\text{нукл}}$ достаточно мало ($\Delta E_{\text{нукл}} < 10$ кэв), процесс деформации ядра может оказаться быстрым и по отношению к нуклонным степеням свободы [4]. Таким образом, квазистатичность процесса деформации ядра при пороговом делении по отношению к нуклонным степеням свободы не противоречит неквазистатичности процесса деформации по отношению к вращательным степеням свободы (с которыми связано угловое распределение осколков) и притом при делении возбужденного ядра.

ЛИТЕРАТУРА

[1] ГЕЙЛИКМАН Б.Т. Сборник докладов на Международной конференции по структуре ядра в Кингстоне. 1960.
[2] ГЕЙЛИКМАН Б.Т. "Атомная энергия", 6, 290, (1959).
[3] VANDENBOSCH R. Nucl. Phys., 46 (1963) 129.
[4] ГЕЙЛИКМАН Б.Т. "Атомная энергия", 6, 298 (1959).
[5] СТРУТИНСКИЙ В.М. "Атомная энергия", 2 (1957) 508; ЖЭТФ, 39, 781, 1960; доклад в этом томе.

ОБ ЭФФЕКТАХ СПАРИВАНИЯ ПРИ ДЕЛЕНИИ ЧЕТНО-ЧЕТНОГО СОСТАВНОГО ЯДРА ВБЛИЗИ ПОРОГА*

В.М. СТРУТИНСКИЙ и В.А. ПАВЛИНЧУК
ИНСТИТУТ АТОМНОЙ ЭНЕРГИИ им.И.В. КУРЧАТОВА, МОСКВА
ФИЗИКО-ЭНЕРГЕТИЧЕСКИЙ ИНСТИТУТ, ОБНИНСК
СССР

Abstract — Résumé — Аннотация — Resumen

PAIRING EFFECTS IN FISSION OF EVEN-EVEN COMPOUND NUCLEI NEAR THE THRESHOLD. The effects connected with discreteness of the number of excited quasi-particles at the saddle point, which are caused by nucleon pairing, are analysed. The weak dependence of density of the internal states in the range $(2\text{-}4)\Delta$ in comparison with the exponential dependence characteristic of high energies is shown to lead to a marked reduction in $d\bar{\nu}/dE$ in this energy range. At lower energies it would be reasonable to expect a sharp reduction in the $\bar{\nu}$ by ~ 0.2, corresponding to a reduction in internal excitation energy by $2\Delta = \sim 1.5$ MeV. However, as a result of the presence in the gap of the so-called β- and γ-vibration levels, which contribute to the internal excitation of the fissionable nucleus, there is a jump $\Delta\bar{\nu} = \sim 0.1$ at an energy of 0.6 - 0.7 MeV above the threshold, which corresponds to the position of these states. The dependence of $\bar{\nu}(E)$ calculated on the basis of these considerations is compared with the experimental figure for U^{235}.

It follows from an analysis of these and other effects that an applicable value for Δ_0 is ~ 0.7 MeV, i.e. approximately the same as for nuclei in the ground state.

EFFETS DE FORMATION DE PAIRES DANS LA FISSION D'UN NOYAU COMPOSÉ PAIR-PAIR AU VOISINAGE DU SEUIL. Les auteurs analysent les effets qui sont liés au caractère discontinu du nombre des quasi-particules excitées au point d'étranglement et sont dus à l'association des nucléons par paires. Ils montrent notamment que la faible dépendance de la densité des états internes dans l'intervalle $(2 \div 4)\ \Delta$ par rapport à la dépendance exponentielle caractéristique des grandes énergies entraîne une diminution sensible de $d\bar{\nu}/dE$ dans ce domaine d'énergie. Pour une énergie plus faible on pourrait s'attendre à une diminution brusque de $\bar{\nu}$ d'un ordre de grandeur de 0,2, qui correspond à une réduction de l'énergie d'excitation interne de $2\Delta \approx 1,5$ MeV. Cependant, comme on trouve, à l'intérieur de l'intervalle, des niveaux de vibration dits β et γ qui contribuent à l'excitation interne du noyau qui subit la fission, il se produit un saut de $\Delta\bar{\nu} \approx 0,1$ pour une énergie dépassant l'énergie de seuil de 0,6 à 0,7 MeV et correspondant à la position de ces états. La valeur de $\bar{\nu}$ (E) calculée sur la base de ces considérations est comparée à la valeur expérimentale pour ^{235}U.

L'analyse de ce phénomène et d'autres effets permet de conclure que Δ_0 peut être considéré comme égal à $\approx 0,7$ MeV, c'est-à-dire comme ayant à peu près la même valeur que pour les noyaux à l'état fondamental.

ОБ ЭФФЕКТАХ СПАРИВАНИЯ ПРИ ДЕЛЕНИИ ЧЕТНО-ЧЕТНОГО СОСТАВНОГО ЯДРА ВБЛИЗИ ПОРОГА. Анализируются эффекты, связанные с дискретностью чисел возбужденных квазичастиц в седловой точке, которые обусловлены спариванием нуклонов. В частности показано, что слабая зависимость плотности внутренних состояний в интервале $(2 \div 4)\Delta$ по сравнению с характерной для больших энергий экспоненциальной зависимостью приводит к заметному уменьшению $d\bar{\nu}/dE$ в этой области энергии. При меньшей энергии можно было бы ожидать резкого уменьшения $\bar{\nu}$ на величину $\sim 0,2$, соответствующую уменьшению энергии внутреннего возбуждения на $2\Delta \approx 1,5$ Мэв. Однако из-за присутствия внутри щели т.наз. β- и γ-вибрационных уровней, которые дают вклад во внутреннее возбуждение делящегося ядра, возникает скачок $\Delta\bar{\nu} \approx 0,1$ при энергии 0,6–0,7 Мэв выше порога, соответствующей положению этих состояний. Рассчитанная на основе этих соображений зависимость $\bar{\nu}(E)$ сравнивается с экспериментальной для U^{235}.

Из анализа этого и других эффектов следует, что приемлемой величиной для Δ_0 является значение $\sim 0,7$ Мэв, то есть примерно такое же, как и для ядер в основном состоянии.

* На симпозиуме зачитано только название доклада.

EFECTO DEL APAREAMIENTO DURANTE LA FISION DE NUCLEOS COMPUESTOS PAR-PAR CERCA DEL UMBRAL. Los autores analizan los efectos asociados al número discreto de las cuasipartículas excitadas en el punto de estrangulación, que están condicionados por el apareamiento de los nucleones. Demuestran en particular que la escasa influencia de la densidad sobre los estados internos en el intervalo (2 a 4) Δ, en comparación con la dependencia exponencial característica para las altas energías, conduce a una disminución notable de $d\bar{\nu}/dE$ en este intervalo. A energías más bajas, sería de esperar una disminución brusca de $\bar{\nu}$ de un orden de magnitud $\sim 0,2$, correspondiente a un decrecimiento de la energía de excitación interna de $2\Delta \approx 1,5$ MeV. Sin embargo, debido a la presencia dentro de ese intervalo de los niveles de vibración denominados β y γ, que contribuyen a la excitación interna del núcleo en fisión, se produce un salto $\Delta\bar{\nu} \approx 0,1$ para una energía superior a la energía umbral en 0,6 - 0,7 MeV, correspondiente a la posición de estos estados. La variación de $\bar{\nu}/(E)$ calculada sobre la base de estas consideraciones se compara con la determinada experimentalmente para el ^{235}U.

Del análisis de estos y otros efectos se desprende que el valor más probable de Δ_0 es $\sim 0,7$ MeV, esto es, un valor comparable al asignado al núcleo en el estado fundamental.

1. Данные о делимости четно-четных составных ядер вблизи порога деления свидетельствуют о том, что в спектре внутренних возбуждений переходного ядра в седловой точке имеется энергетическая щель $2\Delta_0 \sim 1,5$ Мэв. Недавно было экспериментально доказано [1,2] существование ряда важных эффектов, которые можно объяснить [3] скачкообразным изменением числа возбужденных квазичастиц при изменении энергии возбуждения в интервале нескольких Δ: среднее число возбужденных квазичастиц $\bar{n} = 0$, когда энергия переходного ядра $E^* < 2\Delta_0$, $\bar{n} = 2$, когда $2\Delta_0 < E^* < (4 \div 5)\Delta$. При дальнейшем увеличении энергии $\bar{n}$ практически монотонно возрастает в соответствии со статистической моделью: $\bar{n} \sim E/T \sim T$.

2. Связанное с этим неравномерное увеличение плотности внутренних уровней переходного ядра может привести к неравномерному увеличению внутренней энергии возбуждения такого ядра и к соответствующему эффекту в зависимости от энергии среднего числа нейтронов $\bar{\nu}$, испускаемых осколками деления. Согласно статистической модели распределение энергии полного возбуждения происходит пропорционально статистическому весу

$$\rho(U)dU, \tag{1}$$

где $\rho(U)$ — плотность состояний при энергии внутреннего возбуждения, $U = E^* - E_f - K$ (E_f - порог деления, K — кинетическая энергия).
Средняя энергия внутреннего возбуждения равна:

$$\langle U(E) \rangle = \frac{\int_{2\Delta_0}^{E} U\rho(U)\,dU}{N(E) + \int_{2\Delta_0}^{E}\rho(U)dU}, \tag{2}$$

где $N(E)$ — число коллективных состояний переходного ядра в седловой точке до энергии $E = E^* - E_f$.

3. В [4] было показано, что в четно-четном ядре полную плотность уровней внутреннего возбуждения можно приближенно описать при помощи формулы:

$$\rho(U) = g_0 \sum_{n=2,4,\ldots}^{n_{макс}} \frac{[g_0(U - n\Delta_0)]^{n-1}}{\left[\left(\frac{n}{2}\right)!\right]^2 (n-1)!}, \tag{3}$$

где g_0 – плотность одночастичных уровней вблизи границы Ферми. Таким образом, в существенном интервале энергий $2\Delta_0 < U < 4\Delta_0$:

$$\rho(U) = (U-2\Delta_0)\, g_0^2 . \qquad (4)$$

Если полная энергия возбуждения переходного ядра E* попадает в этот интервал, то отношение

$$\frac{N(E)}{N_{\text{внутр}}(E)} \approx \frac{1}{\frac{j^2}{2\ell_F^2}(g_0\Delta_0)^2} = \frac{1}{10} \div \frac{1}{20} . \qquad (5)$$

При этом было принято, что большая часть уровней ниже $2\Delta_0$ имеет коллективную природу, $\Delta_0 g_0 \sim 5 \div 6$, средний орбитальный момент нуклона $\ell_F = 3 \div 4$, а j – спин ядра – также порядка нескольких единиц. Очевидно, что членом N(E) в знаменателе (2) можно пренебречь. Из (2) с учетом (4) получается, что если полная энергия возбуждения ядра находится в интервале $(2 \div 4)\Delta_0$, то

$$\langle U(E) \rangle = \frac{2}{3}(\Delta_0 + E). \qquad (6)$$

При большей энергии

$$\langle U(E) \rangle \sim E - T , \qquad (7)$$

причем переход от (6) к (7) происходит весьма резко при $U \sim (4 \div 5)\Delta_0$ [4].

4. Этот эффект, по-видимому, наблюдается из опыта в виде изменения наклона кривой $\bar{\nu}$ (E)-энергетической зависимости среднего числа нейтронов, испускаемых осколками деления, которое было обнаружено экспериментально в ряде работ [5], [6], [7], [8] (см. рис. 1). Принято считать, что при большей энергии

$$\nu = \frac{U_{\text{оск}}}{B_n + 2T} \approx 1/7\, U_{\text{оск}}(\text{Мэв}) .$$

Энергия $U_{\text{оск}}$ состоит из энергии деформации и тепловой энергии осколков в момент разделения. Можно предположить, что тепловое возбуждение осколков в момент разделения складывается из тепловой энергии переходного ядра и той внутренней энергии, которая приобретается ядром в процессе деформации от седловой точки до точки разделения за счет возможного обмена энергией между внутренними и другими степенями свободы. Из экспериментальных данных известно, что $d\bar{\nu}/dE$ очень слабо меняется при больших энергиях возбуждения. Поэтому, можно считать, что вклад в $\bar{\nu}$ энергии деформации осколков и приобретаемой в процессе деформации тепловой энергии почти постоянен, по крайней мере в интервале интересующих нас энергий возбуждения порядка нескольких Мэв. Тогда наблюдаемое изменение $d\bar{\nu}/dE$ при энергии нейтронов в интервале $E_n = 0 \div 2$ Мэв можно

непосредственно сопоставить с ожидаемым изменением зависимости $<U(E)>$ от E, обусловленным описанными выше эффектами спаривания. В случае U^{235} указанная энергия нейтронов соответствует возбуждению переходного ядра $0 \div 2{,}5$ Мэв над порогом деления ($E_f = -0{,}4$ Мэв).
Из (6) и (7) найдем, что

$$\frac{\left(\frac{d\bar{\nu}}{dE}\right)_1}{\left(\frac{d\nu}{dE}\right)_2} \approx \frac{\left(\frac{d<U(E)>}{dE}\right)_1}{\left(\frac{d<U(E)>}{dE}\right)_2} = \frac{2}{3}, \tag{8}$$

что согласуется с экспериментом (индексы 1 и 2 относятся к области энергий $(2 \div 4)\Delta_0$ и выше 4Δ соответственно).

5. Формула (3) была получена при некоторых упрощающих предположениях: предполагалось, что при малом возбуждении ввиду относительной малости числа возбужденных квазичастиц, обусловленной щелью, можно пренебречь принципом Паули; для энергии возбуждения квазичастицы использовалось упрощенное выражение

$$E = \Delta_0 + \epsilon, \tag{9}$$

вместо более точного

$$E = \sqrt{\Delta_0^2 + \epsilon^2}, \tag{10}$$

не учитывалась зависимость Δ от энергии возбуждения. Все эти предположения оправданы при $E \sim$ нескольких Δ_0. Недавно были опубликованы более строгие численные расчеты [9] полной плотности состояний при малом возбуждении. Полученные результаты практически не отличаются от формулы (3). Сгущение одноквазичастичных состояний при $\epsilon \to 0$, которое получается в случае (10), приводит к тому, что скачки в плотности уровней становятся более резкими, причем в интервале $2\Delta_0 < U < 4\Delta$ $\rho(U)$ зависит несколько слабее, чем в случае (9). Приняв, что плотность уровней в этой области вообще является постоянной, получаем, что $\left(\frac{d\bar{\nu}}{dE}\right)_1 \Big/ \left(\frac{d\bar{\nu}}{dE}\right)_2$ $\sim 0{,}5$ вместо величины 0,67, найденной выше. Эффект уменьшения Δ при большом нагревании несущественен в интервале $(2 \div 4)\Delta$. При большей энергии нерегулярности в поведении будут исчезать быстрее.

6. На рис.1 приведены теоретические кривые согласно формулам (6) и (7). При этом принималось, что $\Delta_0 \sim 0{,}7$ Мэв, порог расположен в области отрицательных энергий при $E_n = -0{,}4$ Мэв. Абсолютные значения $\bar{\nu}$ нормированы по точке $E_n = 2$ Мэв. Пунктиром отмечена ожидаемая величина $\bar{\nu}$ в предположении, что при делении с $E_n < 2\Delta_0$ не происходит возбуждения внутренних состояний. Это, по-видимому, не совсем соответствует действительности, так как при энергии 0,6–0,7 Мэв имеется группа так называемых "вибрационных" β- γ- уровней положительной четности, так что деление через эти уровни может быть связано с передачей соответствующей энергии возбуждения составного ядра в тепловую энергию

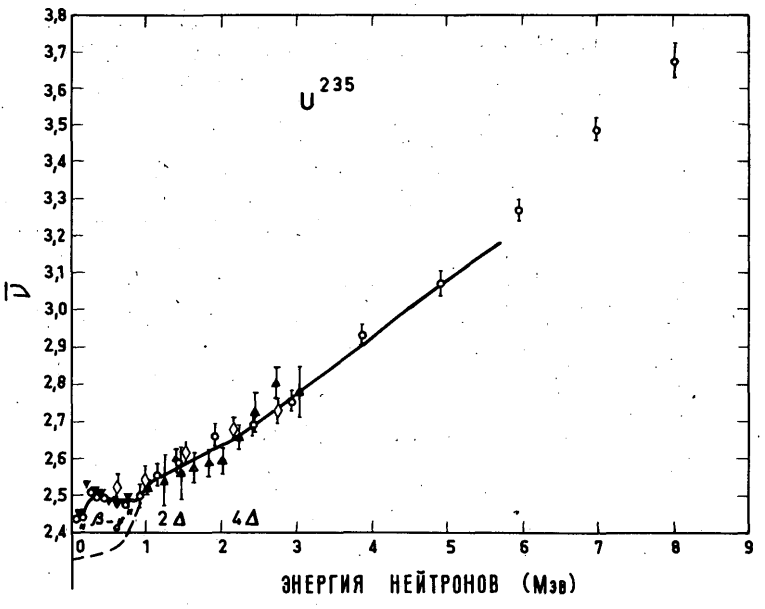

Рис.1

Зависимость $\bar{\nu}$ – среднего числа нейтронов деления – от энергии падающих нейтронов. Сплошной линией отмечены рассчитанные значения $\bar{\nu}$ (нормированные в точке $E_n = 2$ Мэв), пунктиром – ожидаемая величина $\bar{\nu}$ в предположении, что при делении с $E_n < 2\Delta_0$ не происходит возбуждения внутренних состояний. Значения ▼ ▲ взяты из [8], ◇ ◇ – из [5].

осколков. Вклад этих уровней может быть особенно существенен при делении урана-235 нейтронами, так как четность ядра урана-235 отрицательна, а при энергии нейтронов 0,3 – 1,5 Мэв вклад дают, в основном, p- и f-волны отрицательной четности. По-видимому, дополнительное изучение $\bar{\nu}$ при малых энергиях и в отрицательной области энергий могло бы дать существенно новую информацию, в особенности, если анализ этих экспериментов будет проводиться параллельно с изучением анизотропии осколков и вероятности деления.

7. Указанное значение Δ_0 может объяснить также наблюдаемые нерегулярности в зависимости среднего квадрата проекции момента ядра K_0^2 на ось деления [1].

Интересно, что даже небольшой вклад делений через коллективные состояния при большой энергии может привести к заметному уменьшению наблюдаемого значения K_0^2. Происходит это потому, что анизотропия с $K = 0$ велика как $\ell \sim 3 \div 5$, тогда как для двух квазичастичных состояний анизотропии деления $\sim \frac{\ell^2_{\text{макс}}}{8K_0^2} \sim (15 \div 20)\%$ при указанном значении орбитального момента. Поэтому дополнительный 5% вклад состояний с $K = 0$ может объяснить отклонение наблюдаемой величины K_0^2 в 1,5 – 2 раза от ожидаемого значения ~16 для одночастичных состояний (в интервале $(2 \div 4)\Delta$).

8. В работах [1], [10] предполагалось, что в седловой точке $\Delta_0 = 1{,}5$ Мэв, т.е. вдвое больше чем в исходном ядре. Хотя в принципе зависимость Δ_0 от формы ядра и возможна [11], но едва ли можно ожидать, что изменение Δ_0 будет столь большим, так как изменение поверхности у ядра на вершине барьера составляет около 15–20% по сравнению со сферическим ядром.

Другим аргументом [10], [12], [13] в пользу большого Δ_0 является малая величина эффективного момента инерции ядра в интервале энергий возбуждения до 5 Мэв по сравнению с твердотельным значением. В этих работах используют предположение о том, что в момент инерции, и одночастичная плотность уровней однозначно выражаются через величину r_0 или, соответственно, энергию ферми. Для плотности уровней берется выражение $g_0 = \left(\frac{16}{3\pi^2}\right)^{\frac{1}{3}} \frac{mr_0^2}{\hbar^2}$, которое основано на предположении о том, что все нуклоны ядра можно рассматривать как идеальный ферми-газ. Однако во всех приложениях модели Ферми-газа газовость требуется лишь для группы верхних состояний, и поэтому естественно рассматривать эту константу как свободный параметр, подлежащий определению из сравнения с опытом. Так, при сравнении с моделью Нильссона получается значение g_0, которое соответствовало бы величине $r_0 = 1{,}6$ Ферми согласно вышеприведенной формуле.

С другой стороны, для r_0, входящего в выражение для момента инерции, естественно взять значение $r_0 = (1{,}1 \div 1{,}2)$ Ферми. При этих величинах из сравнения с экспериментальным значением $J_{эфф}$ получается $\Delta_0 \sim 0{,}8$ Мэв, как в этом можно убедиться непосредственно с помощью простых формул, приведенных в работе [13]. (Рассматриваемое в [12] приближение $e^{\Delta_0/T} \gg 1$ фактически также означает пренебрежение принципом Паули для возбужденных квазичастиц при малых возбуждениях). Заметим, что такие значения r_0 и g_0 очень хорошо согласуются с плотностью нейтронных резонансов, рассчитанной по статистической модели с учетом спаривания нуклонов при экспериментальных значениях Δ_0 [13]. Наконец, величина Δ_0 может определяться из данных о делимости четно-четных составных ядер. Известно, что вероятность деления резко увеличивается при $E_n = 0{,}8$ Мэв и 1,5 Мэв, причем первый скачок может быть обусловлен группой так называемых β- и γ-"вибрационных" уровней, а второй – включением делений через внутренние состояния при $U > 2\Delta_0$. Такая картина согласуется со значением $\Delta_0 \approx 0{,}8$ Мэв.

9. Таким образом, нет оснований для того, чтобы предполагать большое значение Δ_0 для переходного ядра. Важные дополнительные данные могли бы быть получены из опытов по определению делимости четно-четных ядер при $E_n > 1{,}5$ Мэв и по измерению $\bar{\nu}$ при $E < \Delta_0$ (напрмер при фотоделении). В последнем случае можно ожидать значительного уменьшения $d\bar{\nu}/dE$ на величину, соответствующую уменьшению $< U(E) >$ на $2\Delta_0 \sim 1{,}5$ Мэв. Доказательство этого утверждения имело бы большое значение для понимания связи между коллективными и внутренними возбуждениями в делящемся ядре.

ЛИТЕРАТУРА

[1] BRITT H.C., STOCKES R.H., GIBBS W.R., GRIFFIN J.J. Phys.Rev.Lett., 11 (1963) 343.
[2] HUIZENGA J., UNIK J. Preprint (1964).
WILKINS B.D., UNIK J.P., HUIZENGA J.P. Phys.Lett., 12, (1964) 243.
[3] СТРУТИНСКИЙ В.М. Доклад С3596 на Международном Конгрессе по ядерной физике. Париж, 1964.
[4] STRUTINSKI V.M. Proc.of the Internat.Conf. on Nuclear Structure. Paris, 1958, p.617.
[5] MATHER D.S., FIELDHOUSE P., MOAT A. Phys.Rev., 133B (1964) 1463.
[6] DIVEN J.C., HOPKINS B.O. Nucl.Phys., 48 (1963) 433.
[7] MEADOUS J.W., WHALEN J.F. Phys.Rev., 126 (1962) 197.
[8] BLJUMKINA Ju.A., BONDARENKO I.I. et al. Nucl.Phys., 52 (1964) 648;
БОНДАРЕНКО И.И., КУЗНЕЦОВ В.Ф. и др. Доклад С336 на Международном Конгрессе по ядерной физике. Париж, 1964.
[9] KLUGE G. Nucl.Phys., 51 (1964) 41.
[10] GRIFFIN J.J. Phys.Rev., 132 (1963) 2204.
[11] HENLEY E.M., WILETS L. Phys.Rev., 133B, (1964) 1119.
[12] GRIN Ju.Y. Phys.Lett., 9 (1964) 248.
[13] ГРИНЬ Ю.Т., СТРУТИНСКИЙ В.М. "Ядерная физика" (в печати).

ФОТОДЕЛЕНИЕ ЧЕТНО-ЧЕТНЫХ ЯДЕР ВБЛИЗИ ПОРОГА

Н.С. РАБОТНОВ, Г.Н. СМИРЕНКИН
А.С. СОЛДАТОВ и Л.Н. УСАЧЕВ*
ФИЗИКО-ЭНЕРГЕТИЧЕСКИЙ ИНСТИТУТ, ОБНИНСК
С.П. КАПИЦА и Ю.М. ЦИПЕНЮК
ИНСТИТУТ ФИЗИЧЕСКИХ ПРОБЛЕМ, МОСКВА
СССР

Abstract — Résumé — Аннотация — Resumen

PHOTOFISSION OF EVEN-EVEN NUCLEI NEAR THE THRESHOLD. The results of measurements of the angular distributions of the fragments from photofission of U^{238}, Th^{232}, Pu^{240}, Pu^{239} in a beam of bremsstrahlung gamma-quanta are given. The gamma radiation source used was the 12-MeV microtron of the USSR Academy of Sciences, Institute of Physical Problems. The use of a microtron as a powerful source of gamma rays made it possible to measure angular distributions in the very interesting and hitherto uninvestigated gamma-quanta energy range $E_m < 6$ MeV.

For U^{238} the investigations were carried out in the energy range 5.2 MeV to 9.2 MeV, for Th^{232}, 5.4 MeV to 6.9 MeV, for Pu^{240}, 5.4 MeV to 7.9 MeV, and for Pu^{239}, 5.4 MeV to 7.9 MeV. Results of the measurements of angular distributions for photofission of U^{238} and Th^{232} by gamma-rays or the F^{19} $(p, \alpha\gamma)O^{16}$ reaction are also given. The gamma-radiation source used was a thick CaF_2 target irradiated with 1.45-MeV protons.

These measurements made it possible to establish, in agreement with most of the earlier experiments but in contradiction to the data of Lazareva et al. and Forkman and Johansson, that the contribution of fissions connected with the quadrupole absorption of photons to the total fission cross-section is low in the energy range $E \lesssim 6$ MeV. It is shown for the first time that, in agreement with the theoretical predictions based on A. Bohr's fission channel model, the relative weight of the quadrupole component becomes considerable only at excitation energies lower than the "dipole" fission threshold corresponding to the channel 1^- $(K = 0)$. For example, in the angular distributions of the photofission fragments of U^{238} at energies of the bremsstrahlung spectrum $E_m = 5.4$ MeV and 5.2 MeV the contributions of the quadrupole component to the total photofission cross-section is 10% and 43% respectively, while in the range $E_m < 6$ MeV this contribution does not exceed 3 to 3.5%. Of the even-even fissionable nuclei investigated, Pu^{240} shows the effect of "quadrupole" fission most clearly and Th^{232} least. The results of the measurements may be used to assess the relationship of the partial cross-sections of photoabsorption in heavy nuclei.

The question of the parity of the ground state of Pu^{239} is discussed in the context of the results of measurements of the angular distributions of Pu^{239} photofission fragments exhibiting a change in the anisotropy sign in accordance with the predictions of the theory for channels with $K = \frac{1}{2}$ and $\frac{3}{2}$.

PHOTOFISSION DES NOYAUX PAIR-PAIR AU VOISINAGE DU SEUIL. Les auteurs indiquent les résultats qu'ils ont obtenus en mesurant la distribution angulaire des fragments formés dans la photofission de ^{238}U, ^{232}Th, ^{240}Pu et ^{239}Pu; les mesures ont été faites à l'aide d'un faisceau gamma de rayonnement de freinage. Comme source de rayons gamma ils ont utilisé le microtron de 12 MeV de l'Institut de physique de l'Académie des sciences de l'URSS. Grâce à l'intensité du rayonnement émis, il a été possible de mesurer les distributions angulaires dans la région des énergies gamma à $E_{max} < 6$ MeV, qui revêt un intérêt particulier et n'a pas encore été étudiée.

Les recherches ont porté sur les gammes d'énergies ci-après: 5,2 à 9,2 MeV pour ^{238}U; 5,4 à 6,9 MeV pour ^{232}Th; 5,4 à 7,9 MeV pour ^{240}Pu; 5,4 à 7,9 MeV pour ^{239}Pu. Le mémoire indique les résultats de la mesure des distributions angulaires dans la photofission de ^{238}U et ^{232}Th par rayons gamma provenant de la réaction $^{19}F(p, \alpha\gamma)^{16}O$. Comme source de rayons gamma on a employé une cible épaisse en CaF_2 exposée à des protons de 1,45 MeV.

Ces mesures ont permis d'établir, conformément à la plupart des expériences antérieures, mais contrairement aux données obtenues par Lazaréva et al. ainsi que par Forkman et Johansson, que dans le domaine

* Доклад представил Б.Д. Кузьминов.

d'énergie $E \gtrsim 6$ MeV, les fissions liées à l'absorption quadripolaire des photons contribuent faiblement à la section efficace totale de fission. On montre pour la première fois que conformément aux prévisions théoriques fondées sur le modèle des voies de fission élaboré par A. Bohr, le poids relatif de la composante quadripolaire ne joue un rôle important que lorsque les énergies d'excitation sont inférieures au seuil de fission «bipolaire» correspondant à la voie $1\bar{v}(K=0)$. Ainsi, dans la distribution angulaire des fragments de photofission de ^{238}U, lorsque le spectre du rayonnement de freinage présente une énergie maximum $E_{max} = 5,4$ MeV et 5,2 MeV, la contribution de la composante quadripolaire à la section efficace totale de photofission s'élève respectivement à 10 et 43%, alors que pour $E_{max} > 6$ MeV, elle ne dépasse pas 3 à 3,5%. Parmi les noyaux fissiles selon le mode pair-pair, l'effet de fission «quadripolaire» apparaît le plus nettement pour ^{240}Pu et moins nettement pour ^{232}Th. Grâce aux résultats de ces mesures on peut évaluer le rapport entre les sections efficaces partielles de photoabsorption dans les noyaux lourds.

Les auteurs examinent la question de la parité de l'état fondamental de ^{239}Pu en tenant compte des résultats obtenus par les mesures de la distribution angulaire des fragments de photofission de ^{239}Pu, qui révèle une modification du signe de l'anisotropie conformément aux prévisions théoriques relatives aux voies à $K = \frac{1}{2}$ et $\frac{3}{2}$.

ФОТОДЕЛЕНИЕ ЧЕТНО-ЧЕТНЫХ ЯДЕР ВБЛИЗИ ПОРОГА. Сообщаются результаты измерений угловых распределений осколков при фотоделении U^{238}, Th^{232}, Pu^{240} и Pu^{239}, выполненных на пучке гамма-квантов тормозного излучения. Источником гамма-излучения служил микротрон Института физических проблем АН СССР с мощностью пучка 12 Мэв. Использование микротрона в качестве мощного источника гамма-лучей позволило произвести измерения угловых распределений в наиболее интересной и до сих пор не изученной области энергий гамма-квантов с $E_{макс} < 6$ Мэв.

Для U^{238} исследования были произведены в диапазоне энергий от 5,2 Мэв до 9,2 Мэв, для Th^{232} — от 5,4 Мэв до 6,9 Мэв, для Pu^{240} — от 5,4 Мэв до 7,9 Мэв и для Pu^{239} — от 5,4 Мэв до 7,9 Мэв. Приводятся также результаты измерений угловых распределений при фотоделении U^{238} и Th^{232} гамма-лучами реакции $F^{19}(p, \alpha\gamma)O^{16}$. Источником гамма-излучения являлась толстая мишень из CaF_2, облучавшаяся протонами с энергией 1,45 Мэв.

В результате этих измерений удалось установить, в соответствии с большинством выполненных ранее экспериментов, но в противоположность данным Лазаревой и др. и Форкмана и Юхансона, что вклад делений, связанных с квадрупольным поглощением фотонов в полное сечение деления мал в области энергий $E \gtrsim 6$ Мэв. Впервые показано, что в согласии с теоретическими предпосылками, основанными на модели каналов деления О. Бора, относительный вес квадрупольной компоненты становится существенным только при энергиях возбуждения ниже порога "дипольного" деления, соответствующего каналу 1^- ($K = 0$). Так, например, в угловых распределениях осколков фотоделения U^{238} при максимальных энергиях тормозного спектра $E_{макс} = 5,4$ Мэв и 5,2 Мэв вклад квадрупольной компоненты в полное сечение фотоделения составляет соответственно 10% и 43%, в то время как в области $E_{макс} > 6$ Мэв этот вклад не превышает 3 ÷ 3,5%. Из исследованных четно-четных делящихся ядер эффект "квадрупольного" деления более отчетливо проявляется у Pu^{240} и менее — у Th^{232}. По результатам измерений можно оценить отношение парциальных сечений фотопоглощения на тяжелых ядрах.

В связи с результатами измерений угловых распределений осколков фотоделения Pu^{239}, обнаруживающих изменение знака анизотропии в соответствии с предсказаниями теории для каналов с $K = 1/2$ и $3/2$, обсуждается вопрос о четности основного состояния Pu^{239}.

FOTOFISION DE LOS NUCLEOS PAR-PAR CERCA DEL UMBRAL. En la memoria se presentan los resultados de la medición de las distribuciones angulares de los fragmentos formados en la fotofisión del ^{238}U, ^{232}Th, ^{240}Pu y ^{239}Pu, en un haz de rayos gamma de frenado. Como fuente se utilizó el microtrón de 12 MeV del Instituto de Problemas Físicos de la Academia de Ciencias de la Unión Soviética. El empleo de esta fuente permitió medir la distribución angular en el intervalo de energías gamma, importante pero aún inexplorado, que abarca hasta $E_{máx} < 6$ MeV.

Para el ^{238}U las investigaciones se efectuaron en el intervalo energético 5,2 MeV - 9,2 MeV, para el ^{232}Th de 5,4 MeV a 6,9 MeV, para el ^{240}Pu de 5,4 MeV a 7,9 MeV y para el ^{239}Pu de 5,4 MeV a 7,9 MeV. En la memoria se presentan también los resultados de la medición de las distribuciones angulares en la fotofisión del ^{238}U y del ^{232}Th por rayos gamma procedentes de la reacción $^{19}F(p, \alpha\gamma)^{16}O$. Como fuente gamma se utilizó un blanco espeso de CaF_2 irradiado por protones de 1,45 MeV de energía.

Basándose en estas mediciones se consiguió establecer, de conformidad con muchos experimentos efectuados anteriormente, pero en oposición a los resultados logrados por Lazarev y colaboradores, Forkman y

Johannsen que la contribución de las fisiones, relacionadas con la absorción cuadrupolar de los fotones a la sección total de fisión, es pequeña en la región $E \gtrsim 6$ MeV. Por primera vez se ha demostrado que de conformidad con las suposiciones teóricas, basadas en el modelo de los canales de fisión de A. Bohr, el peso relativo del componente cuadrupolar sólo es esencial cuando las energías de excitación son inferiores al umbral de fisión "bipolar", correspondiente al canal $1^{-}(K=0)$. Así, por ejemplo, en la distribución angular de los fragmentos procedentes de la fotofisión del ^{238}U, siendo la energía del espectro de frenado $E_{máx} = 5,4$ MeV y 5,2 MeV, la contribución del componente cuadrupolar a la sección total de fotofisión es 10 y 43% respectivamente, mientras que para $E_{máx} > 6$ MeV, esta contribución no es superior a 3 - 3, 5%. En los núcleos par-par investigados, el efecto de fisión "cuadrupolar" se observa más claramente en el ^{240}Pu y con menos nitidez en el ^{232}Th. Los resultados de las mediciones permiten evaluar la razón de las secciones parciales de fotofisión para núcleos pesados.

Por último se estudia la cuestión de la paridad del estado fundamental del ^{239}Pu en relación con los resultados de las mediciones de la distribución angular de los fragmentos procedentes de la fotofisión del ^{239}Pu, donde se ha observado un cambio del signo de anisotropía, de conformidad con las previsiones teóricas para los canales $K = \frac{1}{2}$ y $\frac{3}{2}$.

1. ВВЕДЕНИЕ

Весьма привлекательной с точки зрения изучения физики деления является реакция (γ, f) при энергиях гамма-квантов, близких к порогу деления. Это объясняется двумя обстоятельствами. Во-первых, гамма-кванты с энергией 5—7 Мэв испытывают на тяжелых ядрах лишь электрическое дипольное и электрическое квадрупольное поглощение. Для четно-четных ядер-мишеней это приводит к образованию составных ядер лишь в двух возможных состояниях $2+$ и $1-$, причем из-за того, что длина волны гамма-квантов в рассматриваемой области энергий значительно превышает размеры ядра, сечение дипольного поглощения должно быть значительно больше сечения квадрупольного поглощения. Во-вторых, моменты составных ядер после поглощения гамма-кванта оказываются выстроенными вдоль направления пучка фотонов. В случае дипольного поглощения выстраивание является полным (для четно-четных мишеней), поскольку проекция полного момента фотона, равного единице, на направление пучка может принимать лишь значения ± 1 (но не 0).

О. Бор высказал предположение [1], что барьер деления сильно зависит от квантового числа K — проекции полного момента ядра на ось деления, и ядро проходит через седловую точку по одному из достаточно далеко отстоящих друг от друга по энергии "каналов". Ниже всего лежат барьеры для $K = 0$, поэтому при фотоделении имеется направление преимущественного вылета осколков и угловое распределение имеет вид $b \sin^2\vartheta + c \sin^2 2\vartheta$, где коэффициенты b и c связаны с сечениями "дипольного" и "квадрупольного" фотоделения. Если вклад дают каналы с $K = 0$, то в угловом распределении появляется изотропная компонента, обозначение ее a.

В экспериментальных исследованиях к гамма-лучам в качестве средства возбуждения деления прибегают гораздо реже, чем к нейтронам, поскольку сечение реакции (γ, f) в интересующей нас области энергий мало и измеряется обычно миллибарнами. Впервые экспериментальные указания на существование компоненты, пропорциональной $\sin^2 2\vartheta$ в угловом распределении осколков были получены при фотоделении U^{238} гамма-квантами тормозного излучения с максимальной энергией $E_{макс} = 9,4$ Мэв группой Лазаревой [2]. Большая величина наблюденного на опыте отношения c/b

~0,6 истолковывалась авторами как результат подавления дипольной компоненты в сечении нейтронной конкуренцией. Однако, аналогичные измерения группы Каца [3,4] для большого числа четно-четных мишеней, в том числе и для U^{238}, не показали сколько-нибудь существенного вклада квадрупольного фотопоглощения в процесс. Форкман и Юханссон [5] использовали γ-лучи реакции $F^{19}(p,\alpha\gamma)O^{16}$ и обнаружили на U^{238} при E = 6,1 Мэв значительную вероятность квадрупольного деления (c/b = 0,37). При исследовании углового распределения осколков при делении другого ядра U^{236} γ-квантами реакции $F^{19}(p,\alpha\gamma)O^{16}$, выполненном Коннером, Хенкелем и Симмонсом [6], не обнаружено заметной примеси компоненты

$$\sigma_{\gamma f}^{(2+,0)} \sim \sin^2 2\vartheta.$$

Угловые распределения осколков при делении U^{238} и Th^{232} γ-лучами, сопровождающими радиационный захват медленных нейтронов титаном, $E = 6{,}61^{+0{,}14}_{-0{,}20}$ были измерены группой итальянских и немецких физиков [7]. Эти измерения также показали, что вклад квадрупольной компоненты в угловое распределение незначителен. В работе Солдатова и др. [8] были повторены те измерения Лазаревой и др. [2] и Форкмана и Юханссона [5], которые обнаружили существенный вклад $\sigma_{\gamma f}^{(2+,0)}$. Повторные опыты не подтвердили результатов работ [5, 9]. Таким образом, большинство выполненных исследований фотоделения при квадрупольном поглощении γ-квантов показывает, что эффект, связанный с присутствием квадрупольной компоненты в угловом распределении осколков, в диапазоне энергий γ-квантов от 6 до 20 Мэв если и имеет место, то не выходит за пределы экспериментальных ошибок порядка нескольких процентов.

В работе Гриффина [9] было отмечено, что если порог деления для состояний 2^+ существенно ниже, чем для состояний 1^-, то при подпороговом делении большая проницаемость барьера для квадрупольного деления может существенно увеличить отношение $\sigma_{\gamma f}^{(2+)}/\sigma_{\gamma f}^{(1-)}$ по сравнению с отношением сечений фотопоглощения $\sigma_{\gamma}^{(2+)}/\sigma_{\gamma}^{(1-)}$.

В работе [10] было показано, что в пользу предположения о большой — порядка 0,5 Мэв — разнице в порогах между состояниями 1^- и 2^+ указывают некоторые экспериментальные данные по реакциям (α, pf), (n, f) и (γ, f). Если это справедливо, то заметный вклад квадрупольной компоненты следовало искать, углубляясь под порог "дипольного" деления — в область энергий возбуждения ниже 6 Мэв. Анализ угловых распределений в этом случае мог бы дать прямую информацию об относительном расположении порогов деления для различных каналов и позволил бы оценить отношение парциальных сечений дипольного и квадрупольного фотопоглощения, которое представляет самостоятельный физический интерес.

Поэтому мы предприняли подробное измерение угловых распределений осколков фотоделения при энергиях возбуждения порядка и меньше 6 Мэв на Th^{232}, U^{238} и Pu^{240}. Краткое сообщение о результатах для U^{238} было опубликовано в работе [25].

2. ЭКСПЕРИМЕНТАЛЬНАЯ ЧАСТЬ

2.1. Методика эксперимента

В настоящей работе использовалась простая, но весьма надежная методика регистрации осколков по следам, которые они оставляют при прохождении через стекло.

Путем травления поверхности стекла в 2,5%-ном растворе плавиковой кислоты при соответствующих условиях следы осколков доводятся до размеров, удобных для просмотра в обычный биологический микроскоп с увеличением в 150 раз.

Устройство, применявшееся для измерений угловых распределений осколков (рис.1), представляло собой кассету, в центре которой закреплялись слои из исследовавшихся делящихся веществ, а по окружности вокруг них через 15° между направлениями 0° (180°) и 90° по отношению к пучку γ-квантов располагались два набора пластинок из фотостекла. Некоторые количественные характеристики геометрии опыта в измерениях с γ-квантами реакции $F^{19}(p,\alpha\gamma)O^{16}$ и тормозного излучения показаны на рис.1.

Использовавшиеся слои естественного урана и Th^{232} были толщиной 1,0–1,5 мг/см^2, а изотопов плутония 0,1–0,2 мг/см^2.

При измерении угловых распределений осколков фотоделения [U^{238}] и [Th^{232}] в обе половины экспериментального устройства помещались практически одинаковые слои одного и того же вещества. При измерении угловых распределений осколков фотоделения Pu^{240} и Pu^{239} использовался двойной слой, на одну сторону которого наносился плутоний с содержанием 92% (Pu^{240}) и 8% (Pu^{239}), а на другую плутоний с содержанием 97% (Pu^{239}) и 3% (Pu^{240}). Из измерений числа делений в одинаковом потоке γ-квантов исключался вклад делений, который был связан с примесью изотопа Pu^{239} в Pu^{240} и определялся по отношению чисел делений в потоке нейтронов из тепловой колонны реактора, а также Pu^{240} в Pu^{239}, определяемый по скорости спонтанных делений. Результаты, полученные для фотоделения Pu^{239} приводятся и обсуждаются в работе [12].

Экспериментальные данные описывались выражением

$$W(\vartheta) = a + b\sin^2\vartheta + c\sin^2 2\vartheta\,, \qquad (1)$$

в самом общем виде представляющим угловое распределение осколков фотоделения четно-четных ядер дипольными и квадрупольными γ-квантами. Коэффициенты в выражении (1) определялись по способу наименьших квадратов с учетом конечного углового разрешения опыта и небольших вариаций эффективности регистрации осколков от пластинки к пластинке в пределах 2%. Ошибки измерений вычислялись как алгебраическая сумма статистической ошибки и неопределенности, связанной с расхождением результатов просмотра пластинок двумя наблюдателями (0,5%–2%).

Все представленные в работе угловые распределения осколков нормировались из условия $W(90°) = a + b = 1$.

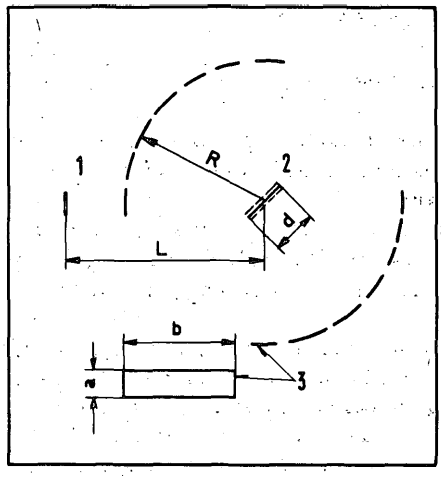

Рис.1

Экспериментальное устройство и схема опыта:

1 – источник γ-лучей; 2 – слой; 3 – стекло.

Источник γ-лучей	a	b	R	L	d
	см	см	см	см	см
$F^{19}(p,\alpha\gamma)$	1,0	3,6	5,0	7,0	1,5
Тормозное излучение	0,8	2,0	4,0	6,5	1,0

2.2. Измерения на γ-лучах реакции $F^{19}(p,\alpha\gamma)O^{16}$

В данном разделе сообщаются результаты измерения угловых распределений осколков при фотоделении U^{238} и Th^{232} γ-квантами реакции $F^{19}(p,\alpha\gamma)O^{16}$. Спектр γ-квантов, реализующихся в этой реакции, состоит из трех моноэнергетических линий 6,1; 6,9; 7,1 Мэв. При выполнении эксперимента были предприняты все меры для выполнений условий опыта поставленного Форкманом и Юханссоном [5]. Источником γ-квантов служила толстая мишень из кристалла CaF_2, облучавшаяся протонами с энергией 1,45 Мэв. При токе протонов ~30 мка мишень выгорала достаточно медленно, обеспечивая постоянный выход γ-квантов в течение 10 часов. Суммарная экспозиция при облучении U и Th составила 320 и 260 часов, соответственно. Кассета с пластинками в данном эксперименте помещалась внутрь герметической тонкостенной камеры, вакуумировавшейся на время облучения. Более подробно эти измерения описаны в работе [8].

На рис.2 и 3 приведены результаты измерений угловых распределений осколков для U^{238} и Th^{232}. Предварительные результаты этого опыта были представлены в работе [13]. Сплошные кривые представляют результаты обработки экспериментальных данных по методу наименьших квадратов:

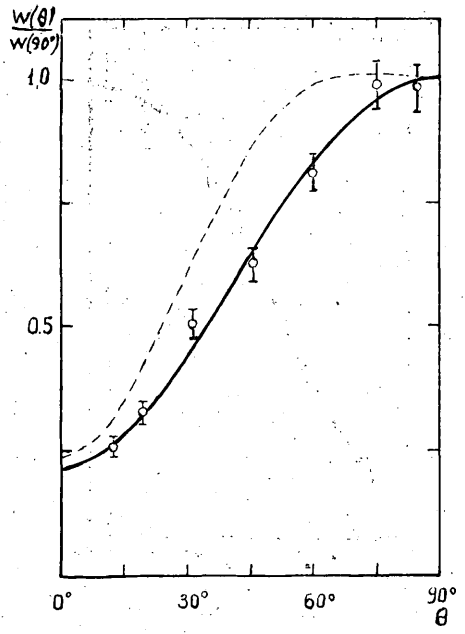

Рис.2

Угловое распределение осколков при делении U^{238} γ-квантами реакции $F^{19}(p,\alpha\gamma)O^{16}$. Сплошная кривая получена обработкой с помощью наименьших квадратов, пунктирная кривая описывает данные из работы [5].

для U^{238} $W(\vartheta) = 0,22 \pm 0,02 + (0,78 \pm 0,03)\sin^2\vartheta + (0,04 \pm 0,04)\sin^2 2\vartheta$;

для Th^{232} $W(\vartheta) = 0,07 \pm 0,01 + (0,93 \pm 0,03)\sin^2\vartheta + (0,12 \pm 0,04)\sin^2 2\vartheta$.

Полученные в настоящем эксперименте данные относятся к совокупности трех линий γ-квантов, отдельные интенсивности которых для толстой мишени из

$$I(6,1) : I(6,9) : I(7,1) = 1,00 : 0,15 : 0,17$$

измерены в работе [5]. Пунктиром на рис.2 показано угловое распределение осколков при фотоделении U^{238}:

$$W(\vartheta) = 0,24 + 0,76\sin^2\vartheta + 0,24\sin^2 2\vartheta,$$

соответствующее результатам опыта Форкмана и Юханссона для всего спектра γ-лучей при облучении толстой мишени из CaF_2 протонами $E = 1,45$ Мэв. Непосредственно это выражение в работе [5] не приводится. Численные значения коэффициентов в нем были рассчитаны на основе представленной в работе [5] экспериментальной информации для отдельных γ-линий.

На рис.2 отчетливо видно значительное расхождение результатов наших измерений и данных Форкмана и Юханссона. Тем не менее, значения угловой анизотропии $W(90°)/W(0°)$, как следует из соотношений (1) и (3), в обоих экспериментах оказались совпадающими в пределах ошибок опыта.

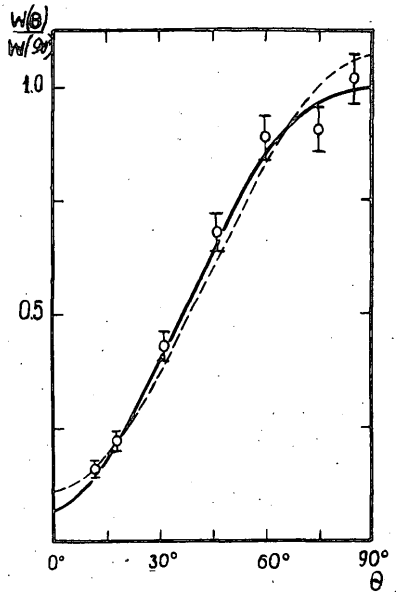

Рис.3

Угловое распределение осколков при делении Th^{232} γ-квантами реакции $F^{19}(p,\alpha\gamma)O^{16}$. Сплошная и пунктирная кривые описывают результаты обработки экспериментальных данных в предположении $c \neq 0$ и $c = 0$, соответственно.

Полученные экспериментальные данные для углового распределения осколков при фотоделении U^{238}, как следует из результатов обработки по методу наименьших квадратов, могут быть удовлетворительно описаны соотношением, не содержащим квадрупольной компоненты. Для Th^{232} угловое распределение осколков, представленное зависимостью без квадрупольной компоненты.

$$W(\vartheta) = 0{,}11 \pm 0{,}02 + (0{,}96 \pm 0{,}05) \sin^2\vartheta$$

(пунктирная кривая на рис.3) по критерию χ^2, не может быть отвергнуто с достаточно большой вероятностью $P = 0{,}1$ ($\chi^2_5 = 9{,}5$).

2.3. Измерения на пучке тормозного излучения микротрона

Опыты с пучком γ-квантов тормозного излучения были выполнены на микротроне Института Физических проблем АН СССР (мощностью пучка 12 Мэв) [14, 15]. Большое расстояние между электронными орбитами в микротроне (около 35 мм) позволило производить облучение непосредственно в вакуумной камере ускорителя. Мишенью служил вольфрамовый диск толщиной 1 мм, за которым помещалась кассета со слоем и стеклами. Заданное значение энергии $E_{макс}$ устанавливалось как переходом на разные орбиты, так и вариацией магнитного поля. Точность определения энергии с учетом нестабильности не хуже 0,1 Мэв. Средний ток электронов достигал 50 мка. В данном эксперименте был получен значительный выигрыш в интенсивности делений в сравнении с условиями опыта в аналогичных

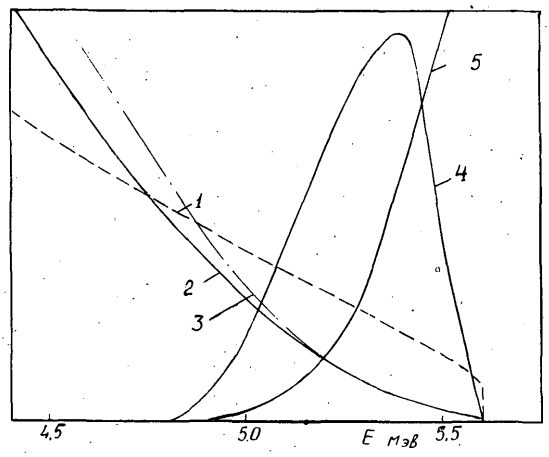

Рис.4

Энергетические распределения γ-квантов при $E_{макс} = 5{,}6$ Мэв:

1 – интегральный спектр тормозного излучения, рассчитанный Шиффом [16] $\varphi(E_{макс}, E)$ для тонкой мишени;

2 – распределение $f(E_{макс}, E) = \int_{E}^{E_{макс}} \varphi(E', E)dE'$ для толстой мишени,

вычисленное в предположении равномерной потери энергии электроном по толщине мишени.

3 – кривая $k(E_{макс} - E)^2$, которой спектр $f(E_{макс}, E)$ аппроксимировался при анализе экспериментальных данных (см. ниже).

4 – величина $\sigma_f(E) \cdot f(E_{макс}, E)$ – "эффективный спектр" гамма-лучей, вызывающих деление.

5 – сечение фотоделения $\sigma_f(E)$.

выполнениях ранее измеренных. Это преимущество дало возможность осуществить измерения в наиболее интересной и до сих пор неизученной области энергий γ-квантов с $E_{макс} < 6$ Мэв, где процесс дипольного деления становится существенно подбарьерным. В этой области $E_{макс}$ несмотря на то, что в спектре тормозного излучения присутствуют γ-кванты с энергией от 0 до $E_{макс}$ вследствие резкого уменьшения вероятности вблизи порога (см. рис.4), реальный спектр γ-квантов, производящих деление, имеет форму достаточно узкой линии с шириной ~0,4 Мэв. Измерения угловых распределений осколков были выполнены в интервале $E_{макс}$ от 5,2 до 9,25 Мэв.

Чтобы предотвратить нежелательный нагрев стеклянных пластинок под действием прямого пучка электронов, прошедших через мишень, за мишенью помещался алюминиевый поглотитель толщиной 1 см, достаточной для полного торможения электронов с энергией 10 Мэв. Контрольные опыты показали, что введение поглотителя не приводит к существенному изменению той части спектра γ-лучей, которая производит деление. Также было установлено, что фон делений, связанных с фотонейтронами и рассеянными γ-квантами, составляет менее 0,1% эффекта, наблюдаемого в прямом пучке.

Результаты, полученные путем обработки экспериментальных данных с помощью метода наименьших квадратов, представлены на рис.5–9. На

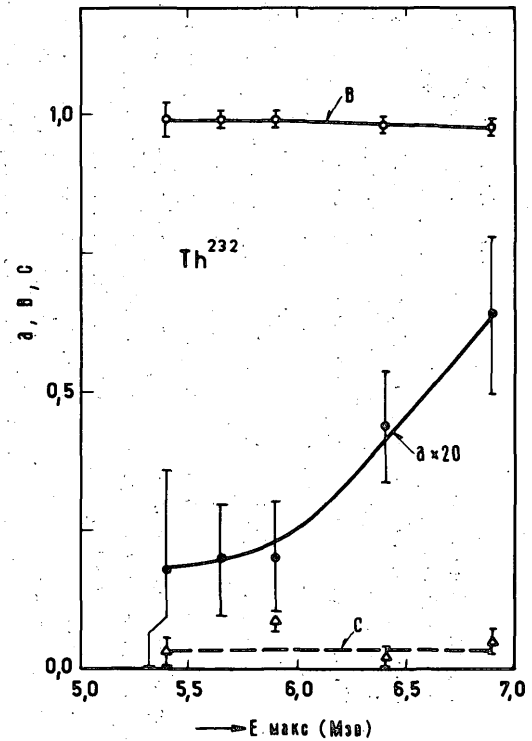

Рис. 5

Зависимость от $E_{макс}$ коэффициентов a, b, c для фотоделения Th^{232}.

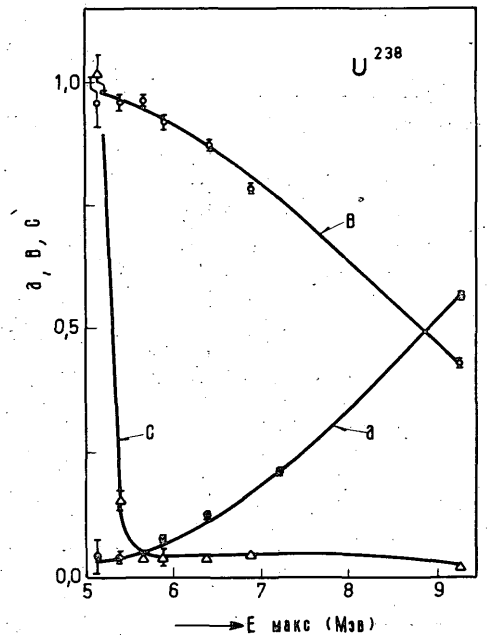

Рис. 6

Зависимость от $E_{макс}$ коэффициентов a, b, c для фотоделения U^{238}

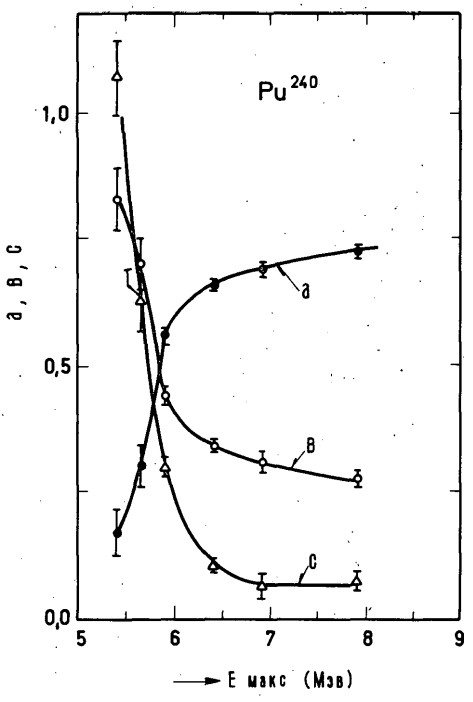

Рис.7

Зависимость от $E_{макс}$ коэффициентов a, b, c для фотоделения Pu^{240}.

рис.5—7 изображены энергетические зависимости коэффициентов a, b, c для Th^{232}, U^{238} и Pu^{240}. Значения анизотропии фотоделения

$$\frac{W(90°)}{W(0°)} - 1 = \frac{b}{a},$$

полученные в настоящей работе, на рис.8 сравниваются с данными Берга и др. [4]. Экспериментальные точки микротронных измерений лежат систематически выше. Контрольный опыт при $E_{макс} = 9{,}25$ Мэв с мишенями толщиной 1 и 0,05 мм убедил нас в том, что этот эффект обусловлен разницей в толщине мишени, а следовательно, и в спектрах тормозного излучения. На рис.9 приводятся результаты опыта и последующей математической обработки, полученные для трех исследовавшихся ядер при $E_{макс} = 5{,}4$ Мэв. Из представленных данных видно, что относительный вклад различных компонент зависит не только от энергии γ-квантов, но и заметно изменяется от ядра к ядру. Более детальный анализ результатов эксперимента проводится в следующем разделе.

3. АНАЛИЗ И ОБСУЖДЕНИЕ РЕЗУЛЬТАТОВ

Характерными чертами полученных угловых распределений осколков фотоделения являются почти полное исчезновение изотропного члена и рез-

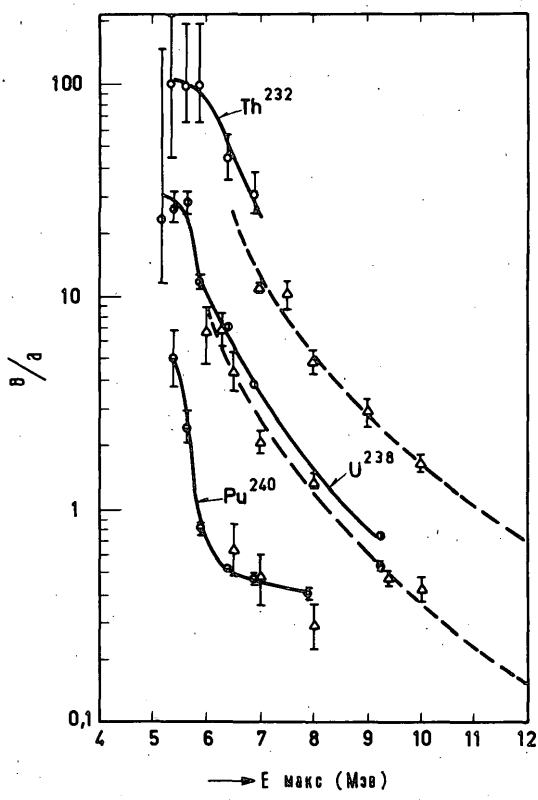

Рис.8

Зависимость угловой анизотропии фотоделения b/a от $E_{макс}$. Кружками (○ – Th^{232}, ◑ – U^{238}, ● – Pu^{240}) изображены результаты измерений с мишенью толщиной 1 мм. Полностью зачерненным кружком показана величина анизотропии фотоделения U^{238} при $E_{макс} = 9{,}25$ Мэв, наблюдаемая в опыте с мишенью толщиной 0,05 мм. Треугольниками изображены данные работы [4].

кое возрастание квадрупольной компоненты при уменьшении энергии гамма-квантов, вызывающих деление. Для изложения современных взглядов на природу этой анизотропии приведем цитату из основополагающей по этому вопросу работы О. Бора [1]: "При энергиях возбуждения, не сильно превышающих порог деления, ядро, проходящее через седловую точку, является по существу "холодным", так как большая часть его энергии представляет потенциальную энергию деформации. Квантовые состояния, в которых ядро может находиться в критической точке "каналов деления", сильно разделены и представляют относительно простой тип движения ядра, Можно ожидать, что спектр этих каналов будет похож на спектр, наблюдаемых при малых возбуждениях основного состояния ядра... Таким образом, можно ожидать, что вблизи седловой точки четно-четные ядра имеют самое низкое состояние I = 0+ и близко расположенные уровни коллективного возбуждения типа 2+, 4+, ..., так же как и состояние типа 1^-, 3^-, ..., хотя и с несколько более высокими энергиями".

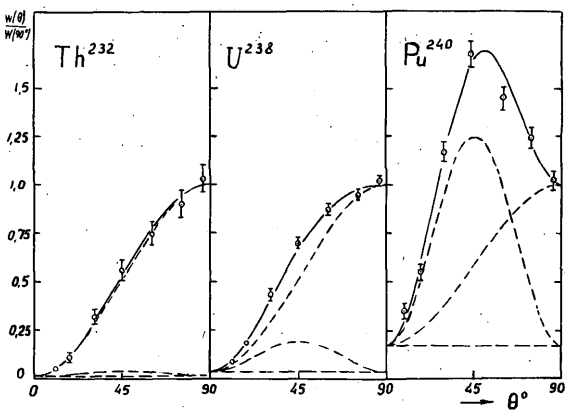

Рис.9

Угловые распределения осколков фотоделения Th^{232}, U^{238}, Pu^{240} при $E_{макс} = 5{,}4$ Мэв. Кривые рассчитаны методом наименьших квадратов. Пунктиром показаны отдельно дипольная квадрупольная и изотропная компоненты.

В обоих указанных ротационных полосах проекция полного момента на ось симметрии ядра, которая совпадает с направлением разлета осколков, $K = 0$, что и дает наблюдаемые угловые распределения

$$W(\vartheta) \sim \sin^2\vartheta \quad \text{при} \quad I^\pi = 1- \quad \text{и} \quad W(\vartheta) \sim \sin^2 2\vartheta \quad \text{при} \quad I^\pi = 2+.$$

Основная трудность, связанная с такой интерпретацией, неоднократно отмечалась. В работе Гриффина [9], например, говорится: "Предполагаемый спектр в седловой точке в лучшем случае является квазистационарным, и фактически понятие о таком спектре корректно только в том случае, если ядро находится в седловой точке значительно более продолжительное время, чем период возбуждения". Период, связанный, например, с вращением имеет порядок 10^{-19} сек. Оценки времени прохождения через барьер дают обычно заметно меньшие значения (см. напр. [17]). Причин, по которым это соотношение характерных времен изменилось бы до сих пор не указано. Поэтому мы предлагаем несколько другую точку зрения. Составное ядро живет 10^{-14} сек. Если в процессе эволюции составного ядра K сохраняется в течение отрезков времени больших времени деления, то в течение таких периодов сохраняется соответствующее этому значению распределение вероятности для ориентации оси ядра в пространстве и за время деления направление оси ядра не успеет измениться. Изложенные выше качественные соображения мы и использовали при анализе результатов эксперимента. Для получения количественных соотношений необходимо ввести некоторые дополнительные предположения.

Составное ядро образуется в рассматриваемой области энергий гамма-квантов лишь за счет электрического дипольного и квадрупольного поглощения. Анизотропные члены в угловом распределении соответствуют низшим каналам с $K = 0$. Изотропная компонента создается каналами с более высокими порогами, у которых все значения K равновероятны. Диффе-

ренциальное сечение фотоделения монохроматическими γ-квантами (с учетом нормировки угловых распределений) можно записать в виде:

$$\sigma(\theta, E) = \sigma_\gamma^{(1^-)} \left(\frac{\Gamma_f^{(1^-,0)}}{\Gamma_f + \Gamma_\gamma} \frac{3}{4} \sin^2\vartheta + \frac{1}{2} \frac{\Gamma_f^{(1^-,k)}}{\Gamma_f + \Gamma_\gamma} \right) +$$

$$+ \sigma_\gamma^{(2^+)} \left(\frac{\Gamma_f^{(2^+,0)}}{\Gamma_f + \Gamma_\gamma} \frac{15}{16} \sin^2 2\vartheta + \frac{1}{2} \frac{\Gamma_f^{(2^+,k)}}{\Gamma_f + \Gamma_\gamma} \right), \qquad (2)$$

где $\sigma_\gamma^{(1^-)}$ и $\sigma_\gamma^{(2^+)}$ – парциальные сечения дипольного и квадрупольного фотопоглощения соответственно;

$\Gamma_f^{(I^\pi,0)}$ – делительная ширина низшего канала с $K = 0$ для состояния со спином I и четностью π, а $\Gamma_f^{(I^\pi,k)} = \Gamma_f - \Gamma_f^{(I^\pi,0)}$, Γ_f – полная делительная, а Γ_γ – радиационная ширина.

Энергетическая зависимость средней делительной ширины уровней с заданным спином I и четностью π определяется формулой Бора-Уилера [18]:

$$\overline{\Gamma}^{I,\pi}(E) = \frac{\overline{D}^{I,\pi}}{2\pi} \sum_{i=1}^{\nu} P(E, E_f^{(i)}, E_{\text{крив}}^{(i)}), \qquad (3)$$

где $\overline{D}^{I,\pi}$ – среднее расстояние между уровнями, индекс i нумерует каналы деления, ν – полное число каналов, а P – проницаемость барьера для i-го канала.

Для проницаемости параболического барьера Хилл и Уилер [19] нашли

$$P(E, E_f^{(i)}, E_{\text{крив}}^{(i)}) = \left[1 + \exp \frac{2\pi (E_f^{(i)} - E)}{E_{\text{крив}}^{(i)}} \right]^{-1} \qquad (4)$$

В этом выражении E_f – высота барьера деления, а $E_{\text{крив}}$ – параметр, характеризующий кривизну вершины параболы, которая аппроксимирует форму барьера вблизи порога.

В формуле (3) множитель $\overline{D}^{I,\pi}$ слабо зависит от энергии, убывая, как $E^2 e^{-\sqrt{aE}}$, и в наших расчетах на протяжении энергетических интервалов порядка 0,5–1 Мэв его можно с той же, примерно, точностью, что и $\sigma_\gamma^{(2^+)} / \sigma_\gamma^{(1^-)}$, считать постоянным.

Однако наблюдаемые характеристики процесса – угловые распределения, сечения и т.д., определяются не только энергетической зависимостью предэкспоненциального множителя в выражении (3), но и его абсолютной величиной. Как показано в работе [10], при заданных E_f и $E_{\text{крив}}$ положение "наблюдаемого" порога T, то есть точки энергетической оси, где сечение деления достигает половины своего значения на плато, а также наклон кри-

вой сечения в этой точке сильно зависят от относительной величины множителя $D/2\pi$ и радиационной ширины Γ_γ.

В работе [10] показано, что формула (3) вполне удовлетворительно описывает обширную совокупность экспериментальных данных за единственным, но очень резким исключением — делительная ширина резонансов 0+ в реакции Pu^{239} (n, f) примерно в 70 раз меньше величины, предсказываемой выражением (3). Как относительно общего согласия, так и относительно указанного резкого исключения, одинаково трудно предположить, что они являются случайными. В книге Уилтеса [20] это положение объясняется следующим образом. "Возможным объяснением является то, что примесь самого нижнего адиабатического уровня (0+) в компаунд-состоянии невелика. Этот уровень изолирован от плотного спектра энергетической щелью в 1 или 2 Мэв... и переходы на него и с него сильно запрещены".

Все эти соображения относятся, конечно, и ко всей нижней полосе каналов с $K = 0$, построенной на состоянии 0^+. Если они справедливы, то при расчете делительной ширины для этих каналов правую часть в (3) надо поделить на величину A больше единицы. Как указывалось выше, сравнение с экспериментом для резонансов реакции $Pu^{239} + n$ дает $A \sim 70$. Помимо аномально малой делительной ширины состояний 0^+ у Pu^{240} такое предположение качественно объясняет обнаруженное в работе [21] преимущественное испускание осколков под углом 90° к пучку в реакции $U^{235} + n$ при энергии $E_n \sim 100$ кэв, и некоторые особенности энергетической зависимости угловых распределений осколков фотоделения (как будет показано ниже).

Измерения производились на сплошном спектре тормозного излучения. Поэтому анализ энергетических зависимостей угловых распределений осложняется, и получаемые оценки физических характеристик — таких, как высота и форма барьера деления, отношение парциальных сечений — становятся менее определенными. С учетом "размазывания" в толстой мишени близкий к верхней границе участок тормозного спектра может быть удовлетворительно представлен (рис. 4) функцией

$$f(E_{макс}, E)dE = k(E_{макс} - E)^2\, dE, \qquad (5)$$

где k практически не зависит от $E_{макс}$.

Радиационная ширина $\Gamma_\gamma \sim 30$ мв в рассматриваемой области энергий $E \sim 5{,}5 - 6$ Мэв. Оценка величины $\frac{D}{2\pi}$ по формулам для плотности уровней [22] дает значение порядка нескольких сот мв. Это означает, что для оценок можно считать, что $\frac{\bar{D}}{2\pi} \gg \Gamma_\gamma$, а $\frac{\bar{D}}{2\pi A} \ll \Gamma_\gamma$. Поэтому для $K = 0$ мы в в знаменателе дроби $\frac{\Gamma_f}{\Gamma_f + \Gamma_\gamma}$ можем пренебрегать величиной Γ_f по сравнению с Γ_γ.

Для каналов с $K \neq 0$ при подбарьерном делении это тоже, очевидно, возможно до тех пор, пока $\Gamma_\gamma > \Gamma_f^{(I^\pi, 0)} > \Gamma_f^{(I^\pi, k)}$, то есть при $b \gtrsim a$, но уже по другой причине — из-за большой величины $\exp \frac{2\pi(E_f - E)}{E_{крив}}$ по сравнению с единицей.

Интегрируя выражение (2) по спектру (5). учитывая все выше сказанное и выполняя несложные преобразования, легко показать, что

$$\frac{a}{b}(E_{макс}) = \frac{2A}{3}\frac{\Phi(E_{макс}, E_f^{(1^-,k)}, E_{крив}^{(1^-,k)})}{\Phi(E_{макс}, E_f^{(1^-,0)}, E_{крив}^{(1^-,0)})}; \tag{6}$$

$$\frac{c}{b}(E_{макс}) = \frac{3}{4}\frac{\sigma_\gamma^{(2^+)}}{\sigma_\gamma^{(1^-)}}\frac{\Phi(E_{макс}, E_f^{(2^+,0)}, E_{крив}^{(2^+,0)})}{\Phi(E_{макс}, E_f^{(1^-,0)}, E_{крив}^{(1^-,0)})}, \tag{7}$$

где

$$\Phi(E_{макс}, E_f, E_{крив}) = \int_0^\infty \frac{\epsilon^2 d\epsilon}{1+\exp\frac{2\pi}{E_{крив}}(\epsilon - E_{макс} + E_f)} \tag{8}$$

Интеграл (8) вычисляется точно лишь при $E_{макс} = E_f$, когда его значение равно

$$\Phi(E_{макс}, E_f, E_{крив}) = 1{,}8\left(\frac{E_{крив}}{2\pi}\right)^3 \tag{9}$$

но как только $E_{макс}$ отличается от E_f в ту или другую сторону на величину, большую, чем $E_{крив}/2\pi$, можно, сохраняя вполне достаточную точность, использовать асимптотические выражения:

$$\Phi(E_{макс}, E_f, E_{крив}) = \begin{cases} 1{,}8\left(\frac{E_{крив}}{2\pi}\right)^3 + \frac{(E_{макс}-E_f)^3}{3} & \text{при } E_{макс}-E_f > \frac{E_{крив}}{2\pi} \quad (10) \\ 2\left(\frac{E_{крив}}{2\pi}\right)^3 \cdot e^{-\frac{2\pi}{E_{крив}}(E_f - E_{макс})} & \text{при } E_f - E_{макс} > \frac{E_{крив}}{2\pi} \quad (11) \end{cases}$$

С помощью выражений (6 – 11) можно сделать следующие оценки:

1. Отношение a/b согласно (6) при $E_{крив}^{(1^-,0)} < E_{крив}^{(1^-,k)}$ должно с уменьшением $E_{макс}$ достигать минимума при $E_{макс} = E_f^{(1^-,0)}$. (После этого минимума начнется плавный подъем. Он соответствует тому факту, что отношение проницаемостей двух барьеров, отличающихся лишь вблизи вершины, с углублением в подбарьерную область должно стремиться к единице. Однако для четно-четных ядер это соответствует таким низким энергиям, возбуждения, где наблюдать деление уже трудно). Значение порога канала (1^-, к = 0) тогда, согласно табл.1 и рис.10, равны для U^{238} и Th^{232} 5,7 и 5,9 Мэв, соответственно. Эти значения совпадают с величинами, которые можно получить по кривым энергетической зависимости сечения фотоделе-

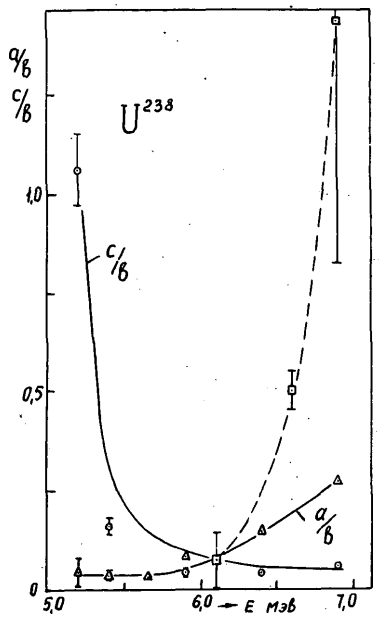

Рис.10

Сравнение экспериментальных и расчетных значений a/b и c/b в случае фотоделения U^{238}:
Δ, o – данные настоящей работы; □ – данные, полученные на моноэнергетических γ-квантах [5, 7]. Сплошные кривые рассчитаны по формулам (6) и (7), пунктирная кривая проведена по экспериментальным точкам.

ния для этих ядер, приведенным в работе [10]. На Pu^{240} до энергии $E_{макс}$ = 5,4 Мэв a/b монотонно падает, и таким образом, для этого ядра получается $E_f^{(1^-, 0)} \leq 5{,}4$ Мэв (см. рис.11).

2. Аналогично, отношение c/b с уменьшением энергии достигает максимума в точке $E_f^{(2^+, 0)}$. На эксперименте это отношение для U^{238} и Pu^{240} монотонно возрастает вплоть до самых низких исследованных значений $E_{макс}$ – 5,2 и 5,4 Мэв соответственно. Эти величины и являются верхними границами для $E_f^{(2^+, 0)}$ соответствующих ядер. Для Pu^{240} нижний порог известен из реакции (d, pf) и равен 4,8 Мэв [23], поэтому полученный нами результат лишь увеличивает вероятность того, что порог 4,8 Мэв соответствует полосе каналов с K = 0 и положительной четностью. Случай с U^{238} убедительно показывает, что разница по энергии между полосами 0^+, 2^+... и 1^-, 3^- составляет для этого ядра не менее 0,5 Мэв.

3. Точка, в которой достигается минимальное отношение a/b (или, что то же самое, максимальное значение анизотропии) для каналов 1^-, K = 1 является глубоко подбарьерной, а делительная ширина и сечение деления через канал (1^-, K = 1) в ней как раз выходят на насыщение. Измерения на монохроматических γ-лучах и тормозном спектре при этой энергии должны давать примерно одинаковую анизотропию. С повышением энергии изотропная компонента a/b на монохроматических γ-квантах должна возрастать экспоненциально.

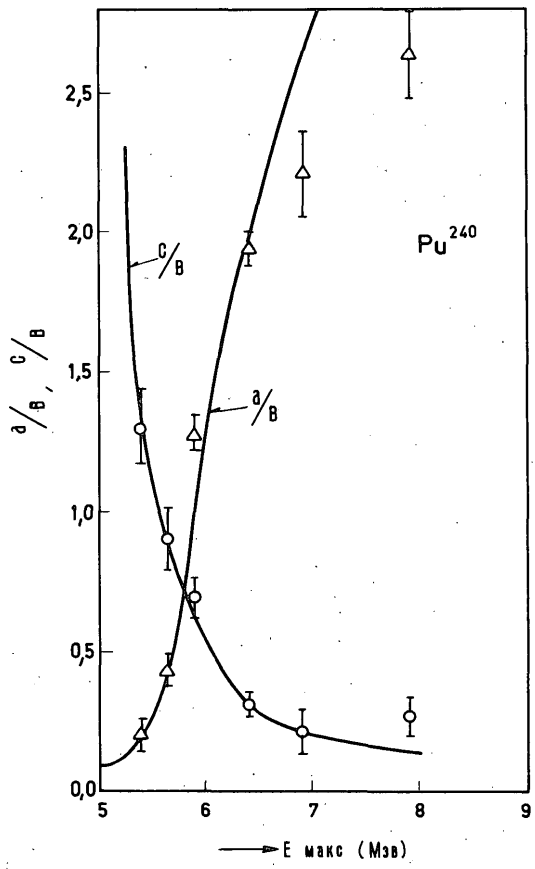

Рис.11

Сравнение экспериментальных и расчетных значений a/b и c/b в случае фотоделения Pu^{240} (обозначения те же, что и на рис.10).

$$\frac{a}{b} \sim \exp \frac{2\pi \left(E_f^{(1^-,k)} - E_{макс}\right)}{E_{крив}^{(1^-,k)}}, \tag{12}$$

а на тормозном спектре медленнее, по закону

$$\frac{a}{b} \sim \frac{\exp \frac{2\pi \left(E_f^{(1^-,k)} - E_{макс}\right)}{E_{крив}^{(1^-,k)}}}{\left(E_{макс} - E_f^{(1^-,0)}\right)^3}. \tag{13}$$

На эксперименте все это наблюдается (см. рис.10), и можно оценить значения параметров $E_f^{(1^-,k)}$ и $E_{крив}^{(1^-,k)}$, выбирая их так, чтобы кривая (6) про-

Таблица 1

ПАРАМЕТРЫ УГЛОВОГО РАСПРЕДЕЛЕНИЯ ОСКОЛКОВ

$E_{макс}$ Мэв	a	b	c
		Th^{232}	
5,4	0,009 ± 0,009	0,991 ± 0,027	0,030 ± 0,025
5,65	0,010 ± 0,005	0,990 ± 0,016	0*
5,9	0,010 ± 0,005	0,990 ± 0,016	0,084 ± 0,014
6,4	0,022 ± 0,005	0,978 ± 0,015	0,022 ± 0,014
6,9	0,032 ± 0,007	0,968 ± 0,024	0,020 ± 0,022
		U^{238}	
5,2	0,042 ± 0,035	0,958 ± 0,050	1,018 ± 0,068
5,4	0,038 ± 0,009	0,962 ± 0,017	0,155 ± 0,021
5,65	0,034 ± 0,005	0,966 ± 0,011	0,040 ± 0,010
5,9	0,078 ± 0,005	0,922 ± 0,014	0,039 ± 0,014
6,4	0,127 ± 0,004	0,873 ± 0,009	0,034 ± 0,008
6,9	0,213 ± 0,004	0,787 ± 0,008	0,047 ± 0,008
9,25	0,570 ± 0,006	0,430 ± 0,007	0,013 ± 0,007
		Pu^{240}	
5,4	0,171 ± 0,044	0,829 ± 0,061	1,072 ± 0,077
5,65	0,301 ± 0,038	0,699 ± 0,050	0,628 ± 0,064
5,9	0,561 ± 0,013	0,439 ± 0,017	0,302 ± 0,021
6,4	0,660 ± 0,008	0,340 ± 0,011	0,106 ± 0,012
6,9	0,689 ± 0,016	0,311 ± 0,021	0,067 ± 0,024
7,9	0,725 ± 0,012	0,275 ± 0,016	0,074 ± 0,018

* Обработка данных при $E_{макс} = 5{,}65$ Мэв для Th^{232} выполнена в предположении $C = 0$, поскольку в противном случае для C получается небольшое отрицательное значение.

ходила через экспериментальные точки. Это было проделано как для зависимостей $a/b(E_{макс})$, так и для $c/b(E_{макс})$. Для некоторых порогов значения параметров E_f и $E_{крив}$ получены в работах [3] и [23], в расчетах мы на них опирались. Расчетные кривые приведены на рис. 10 и 11, а результирующие значения параметров E_f и $E_{крив}$ собраны в табл. 2.

4. При значениях $E_{макс}$, заметно превышающих пороги $E_f^{(2^+,0)}$ и $E_f^{(1^-,0)}$, формула (10) дает асимптотическое значение

$$\frac{c}{b}(E_{макс}) \simeq \frac{3}{4}\frac{\sigma_\gamma^{(2^+)}}{\sigma_\gamma^{(1^-)}}\frac{(E_{макс} - E_f^{(2^+,0)})^3}{(E_{макс} - E_f^{(1^-,0)})^3}. \qquad (14)$$

Это соотношение позволяет оценить значения $\sigma_\gamma^{(2+)}/\sigma_\gamma^{(1-)}$ для Th^{232}, U^{238}, Pu^{240} в рассматриваемой области энергий. Они также приводятся в табл. 2.

Таблица 2

ЗНАЧЕНИЕ ПАРАМЕТРОВ E_f И $E_{крив}$, А ТАКЖЕ ОТНОШЕНИЯ $\sigma_\gamma^{(2+)}/\sigma_\gamma^{(1^-)}$, ПОЛУЧЕННЫЕ ИЗ АНАЛИЗА ЭКСПЕРИМЕНТАЛЬНЫХ РЕЗУЛЬТАТОВ

	Th^{232}	U^{238}	Pu^{240}
$E_f^{2^+,0}$	-	$\leq 5{,}2$	$<5{,}4$ (4,8)[а]
$E_{крив}^{2^+,0}$	-	0,7[б]	-
$E_f^{1^-,0}$	5,9	5,7	5,2
$E_{крив}^{1^-,0}$	0,7[б]	0,7[б]	0,4[а]
$E_f^{1^-,k}$	7,2	7,0	5,7
$E_{крив}^{1^-,k}$	1,0	1,1	0,5
$\sigma_\gamma^{(2+)}/\sigma_\gamma^{(1^-)}$	0,01 <	0,015	0,14

[а] Значение взято из работы [23].
[б] Значение получено по результатам работы [3].

Результаты, приведенные в табл.2, показывают, что для всех исследованных четно-четных ядер каналовая структура является достаточно четкой, т.е. пороги для разных каналов, как правило, отделены друг от друга значительными энергетическими интервалами. Расстояние между порогами $\Delta_1 E_f = E_f^{(2+,0)} - E_f^{(1^-,0)}$ для Pu^{240} и U^{238} составляет 0,4–0,5 Мэв. Для Th^{232} эту величину определить не удается, поскольку для этого ядра примесь квадрупольной компоненты в исследованном интервале энергий всюду находится на уровне экспериментальных ошибок. Расстояния между $E_f^{(1^-,0)}$ и $E_f^{(1^-,k)}$ находятся в качественном согласии с результатами работы [4] — возрастают от Pu^{240} к Th^{232} от 0,5 до 1,3 Мэв. Однако у нас во всех случаях получаются существенно — примерно вдвое — большие значения. Во-первых, пороги $E_f^{(1^-,0)}$ и $E_f^{(1^-,k)}$ несколько "раздвинулись" из-за введения множителя $\frac{1}{A} \sim \frac{1}{70}$ в правую часть формулы (3) для каналов с $k = 0$. Во-вторых, при обработке экспериментальных данных мы учитывали форму тормозного спектра (в работе [4] при вычислении величин $\Delta_2 E_f = E_f^{(1^-,k)} - E_f^{(1^-,0)}$ спектр γ-квантов приближенно заменялся монохроматической линией с $E = E_{макс}$). Это также приводит к увеличению $\Delta_2 E_f$. Величина $\Delta_1 E_f + \Delta_2 E_f = E_f^{(1^-,k)} - E_f^{(2^+,0)}$, связанная с "шириной энергетической щели в седловой точке" в предположении одночастичной природы каналов $(1^-, k)$, близка к 1 Мэв у Pu^{240} и к 2 Мэв у U^{238}.

Кривизна вершины более высокого порога должна быть больше [13]. Из таблицы 2 видно, что значения $E_{крив}$, действительно, увеличиваются с повышением порога.

Приведенные в таблице отношения сечений поглощения квадрупольных γ-квантов меняются от ядра к ядру, но по порядку величины согласуются с электродинамической оценкой $\left(\frac{R}{\lambda}\right)^2 \sim 5 \cdot 10^{-2}$ [24].

Изменение отношений сечений от ядра к ядру, по-видимому, указывает на существование зависимости этих сечений и от энергии для каждого из

ядер. Отсюда следует необходимость более детального изучения этого вопроса.

4. ЗАКЛЮЧЕНИЕ

В работе показано, что прежние публикации об обнаружении квадрупольной компоненты в угловом распределении осколков фотоделения U^{238} при энергиях 6—10 Мэв не подтверждаются. Квадрупольная компонента обнаружена в не изученной до сих пор области энергий γ-квантов 5—6 Мэв ниже порога дипольного деления в согласии с теоретическими представлениями, следующими из модели каналов деления. Анализ относительного вклада квадрупольной, дипольной и изотропной компонент углового распределения осколков показывает структуру каналов деления, находящуюся почти в буквальном соответствии с предсказаниями О. Бора.

Авторы выражают глубокую признательность академику П.Л. Капице за поддержку исследований, В.М. Струтинскому за полезное обсуждение, И.Е. Бочаровой и В.Г. Золотухину за проведение математической обработки экспериментальных результатов на электронно-вычислительной машине, М.К. Голубевой, Н.Е. Федоровой, Л.Д. Гордеевой и З.А. Александровой за участие в эксперименте.

ЛИТЕРАТУРА

[1] BOHR A., Proc. UN Int. Conf. PUAE (2)(1956) 99.
[2] БАЗ А.И., КУЛИКОВА Н.М., ЛАЗАРЕВА Л.Е., НИКИТИНА Н.В., СЕМЕНОВ В.А., Труды Второй Международной конференции по мирному использованию атомной энергии. Доклады советских ученых т.1, М., Атомиздат, 1959, стр.362.
[3] KATZ L., BAERG A.P., BROWN F., Sec. UN Int. Conf. on the Peaceful Uses of Atomic Energy (U.N., Geneva, 1958) v.15, p.188, 1958.
[4] BAERG A.P., BARTHOLMEV R.M., BROWN F., KATZ L., KOWALSKI S.B., Can. J. Phys. 37 (1959) 148.
[5] FORKMAN B., JOHANSSON S.A.E., Nucl. Phys. 20 (1960) 136.
[6] CONNER J.P., HENKEL R.L., SIMMONS J.E., Bull. Amer. Phys. Soc. II 4 (1959) 234.
[7] CARVALHO H.G. MANFREDINI A., MUCHNIK M., SEVERI M., BÖSCH H., WÖLFLE W., Nuovo Cimento 29 (1963) 464.
[8] СОЛДАТОВ А.С., АЛЕКСАНДРОВА З.А., ГОРДЕЕВА Л.Д., СМРЕНКИН Г.Н., Ядерная физика (в печати, 1965).
[9] GRIFFIN J.J., Phys. Rev. 116 (1959) 107.
[10] УСАЧЕВ Л.Н., ПАВЛИЧУК В.А., РАБОТНОВ Н.С. "Атомная энергия" 17 (1964) 479.
[11] ПЕРЕЛЫГИН В.П., ТРЕТЬЯКОВА С.П., ЗВАРА И., ПТЭ №4 (1964) 78.
[12] РАБОТНОВ Н.С., СМИРЕНКИН Г.Н., СОЛДАТОВ А.С., УСАЧЕВ Л.Н., КАПИЦА С.П., ЦИПЕНЮК Ю.М., Угловая анизотропия фотоделения и четность основного состояния Pu . "Ядерная физика" (в печати).
[13] РАБОТНОВ Н.С., СМИРЕНКИН Г.Н., СОЛДАТОВ А.С., УСАЧЕВ Л.Н., "Структура каналов деления четно-четных компаунд-ядер". Доклад на конгрессе по физике ядра №4е/с337, Париж, 1964.
[14] КАПИЦА С.П., БЫКОВ В.П., МЕЛЕХИН В.Н., ЖЭТФ 41 (1961) 368.
[15] ЗЫКИН Л.М., КАПИЦА С.П., МЕЛЕХИН В.Н., НЕДЕЛЯЕВ А.Г., Труды Международной конференции по ускорителям (Дубна, 1963). Атомиздат, М., 1964, стр.1049.
[16] SCHIFF L.I., Phys. Rev. 83 (1951) 252.
[17] ГЕЙЛИКМАН Б.Т., Материалы Первой Международной конференции по мирному использованию атомной энергии. (Объединенные нации, Женева, 1955); т.2, Физматгиз, М., 1956, стр.230.
[18] BOHR N., WHEELER J.A., Phys. Rev. 56 (1939) 426.

[19] HILL D.L., WHEELER J.A., Phys. Rev. 89 (1953) 1102.
[20] WILETS L., "Theories of Fission", Oxford Press, 1964.
[21] НЕСТЕРОВ В.Г., БЛЮМКИНА Ю.А., КАМАЕВА Л.А., СМИРЕНКИН Г.Н., "Атомная энергия" 16 (1964) 519.
[22] МАЛЫШЕВ А.В., ЖЭТФ 45 (1963) 316.
[23] NORTHROP J.A., STOKES R.H., BOYER K., Phys. Rev. 115 (1959) 1227.
[24] ДАВЫДОВ А.С., "Теория атомного ядра". Физматгиз, М., 1958, стр.422.
[25] SOLDATOV A.S., SMIRENKIN G.N., KAPITZA S.P., TSIPENIUK Yu.M., Phys.Let. 14 (1965) 217.

УГЛОВЫЕ РАСПРЕДЕЛЕНИЯ ОСКОЛКОВ ДЕЛЕНИЯ Th^{230}, Pu^{238} и Am^{241} НЕЙТРОНАМИ*

П.Е. ВОРОТНИКОВ, С.М. ДУБРОВИНА
В.А. ШИГИН и Г.А. ОТРОЩЕНКО
ГОСУДАРСТВЕННЫЙ КОМИТЕТ ПО ИСПОЛЬЗОВАНИЮ
АТОМНОЙ ЭНЕРГИИ СССР, ИНСТИТУТ АТОМНОЙ ЭНЕРГИИ
им. И.В. КУРЧАТОВА, МОСКВА
СССР

Abstract — Résumé — Аннотация — Resumen

FISSION DISTRIBUTION IN NEUTRON-INDUCED FISSION OF Th^{230}, Pu^{238} AND Am^{241}. The angular distribution of fragments in the neutron-induced fission of Th^{230}, Pu^{238} and Am^{241} was measured in the neutron energy range 100 - 1200 keV. Measurements were also made for Am^{241} at neutron energies of 4 and 5 MeV, and the dependence of the fission cross-section of Pu^{238} on neutron energy in the 50 - 1400 keV range was likewise determined.

The partial fission cross-sections for the different K-bands were derived for Th^{230} on the basis of the angular distributions obtained, using fission cross-sections taken from another paper, and also the neutron capture cross-sections of the neutron permeabilities calculated by the optical coefficients of adhesion. The following band sequence was established: $\frac{1}{2}^-$, $\frac{3}{2}^-$, $\frac{3}{2}^+$; the energy interval between the bands is ~100 keV.

The pattern of the cross-section for band $\frac{1}{2}^-$ shows in the sub-barrier region (at a neutron energy of 860 keV) the same dip as the total fission cross-section. This pattern in the sub-barrier region cannot be explained by the normal change in neutron width, as it can be in the case of fission above the barrier, and gives grounds for assuming the presence of some other mechanism powerfully affecting the fission cross-section. The angular distributions of the fragments can be explained satisfactorily only on the assumption that there is an energy shift between the individual states within the bands. This indicates that the widths of the levels at the saddle are probably less than the distances between the levels themselves. Assuming that the levels are rotatory, a value of about 4 keV is obtained for $\hbar^2/2J$.

From analysing the anisotropy of Pu^{238} fission, we may assume the band sequence $\frac{1}{2}^+$, $\frac{3}{2}^-$, $\frac{1}{2}^-$.

In the case of Am^{241} fission, the angular distributions show a weak energy dependence and little anisotropy; this is explained by the large number of participating states. The measurements at 4 and 5 MeV made it possible to determine the value of K_0^2, and to compare it with the data for Np^{237}. This comparison shows that the energy dependence of K_0^2 for odd-odd compound nuclei is apparently identical with that for even-odd nuclei.

DISTRIBUTION ANGULAIRE DES FRAGMENTS PROVENANT DE LA FISSION DE ^{230}Th, ^{238}Pu et ^{241}Am PAR DES NEUTRONS. Les auteurs ont mesuré les distributions angulaires des fragments formés lors de la fission de ^{230}Th, ^{238}Pu et ^{241}Am par des neutrons de 100 à 1200 keV. Pour ^{241}Am, les mesures ont également porté sur des énergies de 4 et 5 MeV. En outre, ils ont établi la relation de dépendance entre la section efficace de fission de ^{238}Pu et l'énergie des neutrons dans la gamme de 50 à 1400 keV.

En ce qui concerne ^{230}Th, les auteurs ont déterminé les sections efficaces partielles de fission pour les différentes bandes K, en se fondant sur les distributions angulaires obtenues et un utilisant les sections efficaces de fission indiquées dans une autre étude, ainsi que les sections efficaces de capture des neutrons et les degrés de perméabilité aux neutrons calculés d'après les coefficients optiques d'adhérence. Ils ont établi que les bandes se suivaient dans l'ordre ci-après: $\frac{1}{2}^-$, $\frac{3}{2}^-$, $\frac{3}{2}^+$, l'intervalle d'énergie entre les bandes étant d'environ 100 keV.

La courbe de la section efficace de fission relative à la bande $\frac{1}{2}^-$ accuse, dans la région située au-dessous de la barrière (pour une énergie des neutrons de 860 keV), la même inflexion que la section efficace totale de fission. Cette forme de la courbe dans la région mentionnée ne saurait s'expliquer par une modification normale de la largeur neutronique, comme dans le cas d'une fission au-dessus de la barrière; cela laisse supposer qu'il existe un autre mécanisme exerçant une forte influence sur l'évolution de la section efficace de fission. Les distributions angulaires des fragments ne peuvent être expliquées de façon satisfaisante que si l'on admet un

* На симпозиуме зачитано только название доклада.

déplacement d'énergie entre les différents états à l'intérieur des bandes. On peut en conclure qu'au point d'étranglement les largeurs des niveaux sont inférieures à la distance entre ces niveaux. En admettant que les niveaux aient un caractère de rotation, on a obtenu pour un $\hbar^2/2J$ une valeur d'environ 4 keV.

Après avoir analysé l'anisotropie de la fission de ^{238}Pu, les auteurs supposent que les bandes se suivent dans l'ordre suivant: $\frac{1}{2}^+$, $\frac{3}{2}^-$, $\frac{1}{2}^-$.

Dans le cas de la fission de ^{241}Am, les distributions angulaires accusent une faible dépendance par rapport à l'énergie et une anisotropie peu prononcée, ce qui s'explique par le grand nombre d'états qui participent à la réaction. Des mesures effectuées pour 4 et 5 MeV ont permis de déterminer la valeur de K_0^2 et de comparer celle-ci aux données obtenues par d'autres auteurs pour ^{237}Np. Cette comparaison indique que l'évolution de K_0^2 en fonction de l'énergie pour les noyaux impair-impair est probablement identique à celle de K_0^2 pour les noyaux pair-impair.

УГЛОВЫЕ РАСПРЕДЕЛЕНИЯ ОСКОЛКОВ ДЕЛЕНИЯ Th^{230}, Pu^{238} И Am^{241} НЕЙТРОНАМИ. Измерялись угловые распределения осколков деления Th^{230}, Pu^{238} и Am^{241} нейтронами в интервале энергий нейтронов от 100 до 1200 кэв. Для Am^{241} измерения были проведены также при энергиях нейтронов 4 и 5 Мэв. Была также определена зависимость сечения деления Pu^{238} от энергии нейтронов в интервале от 50 до 1400 кэв.

Для Th^{230} на основе полученных угловых распределений, используя сечения деления, взятые из работы [12], а также сечения захвата нейтронов и нейтронные проницаемости, вычисленные по оптическим коэффициентам прилипания [13, 15] были выделены парциальные сечения деления для отдельных K-полос. Установлена следующая последовательность полос: $\frac{1}{2}^-$, $\frac{3}{2}^-$, $\frac{3}{2}^+$; энергетический интервал между полосами ~100 кэв.

Ход сечения деления для полосы $\frac{1}{2}^-$ обнаруживает в подбарьерной области (при энергии нейтронов 860 кэв) такой же провал, как и полное сечение деления. Такой ход сечения деления в подбарьерной области не объясняется обычным изменением нейтронной ширины, как это может быть в случае деления выше барьера [11], и позволяет предположить наличие какого-то другого механизма, сильно влияющего на ход сечения деления. Угловые распределения осколков можно удовлетворительно объяснить лишь предположив энергетический сдвиг между отдельными состояниями внутри полос. Это говорит о том, что ширины уровней на седле, вроятно, меньше расстояния между уровнями. В предположении, что уровни имеют вращательный характер, для $\frac{\hbar^2}{2\mathcal{J}}$ получено значение около 4 кэв.

Из анализа анизотропии деления Pu^{238} можно предположить последовательность полос $\frac{1}{2}^+$, $\frac{3}{2}^-$, $\frac{1}{2}^-$.

В случае деления Am^{241} угловые распределения обнаруживают слабую зависимость от энергии и небольшую величину анизотропии, что объясняется большим количеством участвующих состояний. Измерения при 4 и 5 Мэв позволили определить величину K_0^2 и сравнить ее с данными по Np^{237} [18]. Сопоставление показывает, что энергетический ход K_0^2 для нечетно-нечетных составных ядер, по-видимому, одинаков с ходом K_0^2 для четно-нечетных ядер.

DISTRIBUCION ANGULAR DE LOS FRAGMENTOS DE LA FISION NEUTRONICA DEL ^{230}Th, ^{238}Pu Y ^{241}Am. Los autores han medido la distribución angular de los fragmentos de fisión del ^{230}Th, ^{238}Pu y ^{241}Am inducida por neutrones de 100 a 1200 keV. En el caso del ^{241}Am, las mediciones se efectuaron también para energías neutrónicas de 4 y 5 MeV. Por otra parte, determinaron la variación de la sección eficaz del ^{238}Pu en función de la energía de los neutrones entre 50 y 1400 keV.

Sobre la base de las distribuciones angulares obtenidas, utilizando las secciones eficaces de captura neutrónica y la permeabilidad a los neutrones, calculadas con ayuda del coeficiente de absorción óptica, separaron para el ^{230}Th las secciones eficaces parciales de fisión para las distintas bandas K. Establecieron que el orden de las bandas es el siguiente: $\frac{1}{2}^-$, $\frac{3}{2}^-$, $\frac{3}{2}^+$, siendo el intervalo energético entre bandas de ~100 keV.

La curva de la sección eficaz de fisión para la banda $\frac{1}{2}^-$ presenta en la región situada debajo de la barrera (para una energía neutrónica de 860 keV) el mismo valle que la sección eficaz total de fisión. Esta característica no puede explicarse por los cambios normales de la anchura neutrónica, a diferencia de la fisión por encima de la barrera; ello permite suponer la existencia de otro mecanismo que ejerce fuerte influencia sobre la sección eficaz de fisión. Las distribuciones angulares de los fragmentos sólo pueden explicarse satisfactoriamente suponiendo un desplazamiento energético entre los diversos estados en el interior de las bandas. Ello parece indicar que la anchura de los nivales en la estrangulación es probablemente menor que la distancia entre estos niveles. Admitiendo que los niveles poseen un carácter rotatorio, se ha obtenido un valor del orden de 4 keV para $\hbar^2/2J$.

Del análisis de la anisotropía de la fisión del ^{238}Pu puede deducirse el siguiente orden para las bandas: $\frac{1}{2}^+$, $\frac{3}{2}^-$, $\frac{1}{2}^-$.

En el caso de la fisión del ^{241}Am, las distribuciones angulares apenas varían en función de la energía y la anisotropía posee un valor bajo, lo que puede aclararse por el gran número de estados que intervienen. Las mediciones efectuadas a 4 y 5 MeV permitieron determinar la magnitud K_0^2 y compararla con los datos obtenidos para el ^{237}Np. Su comparación demuestra que la forma de la curva energética para K_0^2 en el caso de núcleos compuestos impar-impar, es al parecer idéntica con la correspondiente a K_0^2 en el caso de núcleos par-impar.

ВВЕДЕНИЕ

Обнаруженная более 10 лет назад связь углового распределения осколков деления тяжелых ядер с направлением движения вызвавших деление частиц [1] получила довольно полное объяснение в рамках обобщенной модели ядра [2]. Было показано [3], [4], что этот эффект может являться следствием сохранения момента количества движения I и его проекции K на ось симметрии ядра в процессе деления. Если предположить, что деформация ядра перед делением является аксиально-симметричной, а разлет осколков происходит преимущественно вдоль оси симметрии, то очевидно, что угловое распределение осколков определяется моментом I, зависящим от вносимого частицей момента ℓ, и взаимной ориентацией I и оси симметрии делящегося ядра или, что то же, величинами I и K. Благодаря этому изучение угловых распределений осколков может дать полезную информацию о степени деформации и квантовых характеристиках делящегося ядра вблизи седловой точки [5], [6]. В этой связи нами изучались угловые распределения осколков деления Th^{230}, Pu^{238} и Am^{241} нейтронами с энергией в интервале от 50 до 1400 кэв.

АППАРАТУРА

Измерения проводились на электростатическом ускорителе [7]. Источниками нейтронов служили бомбардируемые протонами твердые Ti+T и LiF мишени, диаметр которых составлял 5 мм. Охлаждение мишени водой [8] позволяло доводить ток на мишень до 60 мка. Разброс энергий нейтронов составлял ± 30 кэв. Поток нейтронов измерялся двумя длинными счетчиками [9], проградуированными по эталонному источнику нейтронов.

Слои делящихся веществ толщиной около 1 мг/см^2 и диаметром 12 мм наносились электролизом на платиновые подложки толщиной 0,1 мм. Расстояние от мишени ускорителя до слоя составляло 25 мм. Осколки деления регистрировались одновременно четырьмя круглыми стеклянными детекторами [10], диаметром 20 мм каждый, располагавшимися на расстоянии 50 мм от слоя, под углами 0, 30, 60 и 90° к направлению нейтронного потока. Слой делящегося вещества и детекторы находились в общем тонкостенном эвакуированном баллоне.

Каждое измерение состояло из двух серий, проводившихся в разных квадрантах, что позволяло получать непосредственно $\sigma(0°)/\sigma(90°)$ и $\sigma(30°)/\sigma(60°)$. Для определения относительной эффективности средних детекторов к крайним производились специальные измерения.

В результаты измерений вводились поправки на энергетическое и угловое (~12°) разрешения и на спонтанное деление (для Pu^{238}). Влияние нейтронов, рассеянных стенами помещения, определялось путем изменения расстояния от мишени ускорителя до слоя делящегося вещества (по отклонению от закона I/R^2). Оно не превышало 2%. Эта поправка, а также расчетная поправка на рассеяние нейтронов измерительной камерой, составлявшая от 5 до 9%, учитывались при измерении абсолютного сечения деления и не учитывались при измерениях угловых распределений.

При изучении Pu^{238} измерительная камера окружалась кадмиевым чехлом с толщиной стенки 0,5 мм.

Торий-230

Интерес к изучению ядра Th^{230} был вызван тем обстоятельством, что в подбарьерной области деления ход сечения не соответствовал тому, что можно было ожидать для четно-четного ядра.

Заметные максимумы в сечении деления тяжелых ядер нейтронами наблюдаются обычно только при небольших энергиях нейтронов E_n.

Деление четно-четных ядер является пороговым процессом и становится возможным при энергиях нейтронов, как правило, заметно больших, чем те, при которых наблюдаются отдельные максимумы. В связи с этим сечение деления в районе порога имеет монотонный, близкий к экспоненциальному рост, обусловленный увеличением проницаемости барьера с ростом энергии возбуждения делящегося ядра. Мы не касаемся здесь наблюдающихся в ряде случаев небольших (~10%) немонотонностей сечения деления выше порога деления, объясняющихся [11] вступлением в процесс деления отдельных каналов, разделенных интервалами в несколько сотен кэв.

В 1959 году было сообщено [12], что в сечении деления Th^{230} нейтронами при E_n ~750 кэв, т.е. заметно ниже порога деления (~1000 кэв), существует отчетливый максимум. При увеличении энергии нейтронов до 850 кэв сечение падает примерно в 2,5 раза, а затем вновь возрастает. Измерения показали, что в районе максимума отношение $\sigma(0°)/\sigma(90°)$ достигает значения 2,2, что является максимальным в этой области энергий нейтронов для изученных ядер.

В целях проведения анализа сечения деления Th^{230} нами были произведены более подробные измерения угловых распределений осколков деления в этой области энергий.

Общая схема расчета подобна использованной в [14]. Th^{230} является четно-четным ядром. При захвате нейтрона с орбитальным моментом ℓ образуется составное ядро Th^{231} с полным моментом $I = \ell \pm 1/2$ и четностью $\pi = (-)^{\ell}$. Используя оптические коэффициенты проницаемости для нейтронов $T_{I\pi}$ (за неимением данных по $T_{I\pi}$ для деформированных ядер мы использовали коэффициенты проницаемости из [13] для сферических ядер и нелокального потенциала), можно вычислить сечение образования составного ядра в состоянии $I\pi$:

$$\sigma^c_{I\pi} = \pi \lambda^2 (2I+1) T_{I\pi} . \qquad (1)$$

Конкурирующий процесс испускания нейтронов возбужденным составным ядром приводит к тому, что сечение деления составляет часть $\sigma^c_{I\pi}$. Мы предполагали, что эмиссия нейтронов зависит лишь от проницаемости центробежного барьера для переходов на те уровни ядра Th^{230}, которые доступны по энергии и допустимы условием сохранения I и π, т.е. не делали различия между вращательными и колебательными состояниями Th^{230}. Тогда для сечения деления мы можем написать ($\Gamma_f \ll \Gamma_n$):

$$\sigma^f_{I\pi} = \sigma^c_{I\pi} \frac{\Gamma_f}{\Gamma_f + \Gamma_n} \sim \frac{\sigma^c_{I\pi}}{P_{I\pi}} \Gamma_f , \qquad (2)$$

где $P_{I\pi}$ – сумма нейтронных проницаемостей для переходов на разрешенные состояния Th^{230}, вычисленная согласно [15]. Сведения об уровнях возбуждения Th^{230} взяты нами из данных по α-распаду U^{234} [16]. Предполагалось далее, что Γ_f не зависит от I, но вводилась поправка, учитывающая уменьшение энергии возбуждения делительных степеней свободы для вращающегося ядра, т.е. принималось,что

$$\Gamma^I_f(E_n) = \Gamma_f(E_n - E^I_{\text{вращ}}). \qquad (3)$$

Таким образом, дифференциальное сечение деления в случае, если деление идет через одну полосу с определенными значениями K и π, может быть представлено в виде:

$$\sigma^f_{K\pi}(\theta) = \frac{\lambda^2}{2} S \sum_I \frac{\sigma^c_{I\pi}(E_n)}{P_{I\pi}(E_n)} \Gamma_f(E_n - E^I_{\text{вращ}}) W(KI) , \qquad (4)$$

где S-нормирующий множитель, а W(KI) – парциальные угловые распределения для заданных K и I (приведены в [14]).

Если деление идет через две полосы с разной четностью, то дифференциальное сечение деления является просто суммой сечений для этих полос. Сложнее обстоит дело, если деление идет через полосы одинаковой четности. В этом случае $\sigma^c_{I\pi}/P_{I\pi}$ представляет сумму соответствующих количеств для состояний делящегося ядра, относящихся к разным полосам. Для каждой из этих полос коэффициенты $\sigma^c_{I\pi}/P_{I\pi}$, принадлежащие одинаковой паре $I\pi$, должны быть взяты с некоторым весом $\alpha^K_{I\pi}$, причем $\sum_K \alpha^K_{I\pi} = 1$.

На рисунке 1 приведены результаты измерений угловых распределений осколков деления Th^{230} нейтронами. Сплошные линии проведены через экспериментальные точки методом наименьших квадратов. Эти данные, а также полное сечение деления нейтронами Th^{230} [12], были использованы для вычисления парциальных сечений деления для отдельных K-полос. Результаты расчета показаны на рис.2.

Расчет показал, что угловые распределения осколков можно удовлетворительно объяснить, лишь учитывая энергетический сдвиг между отдель-

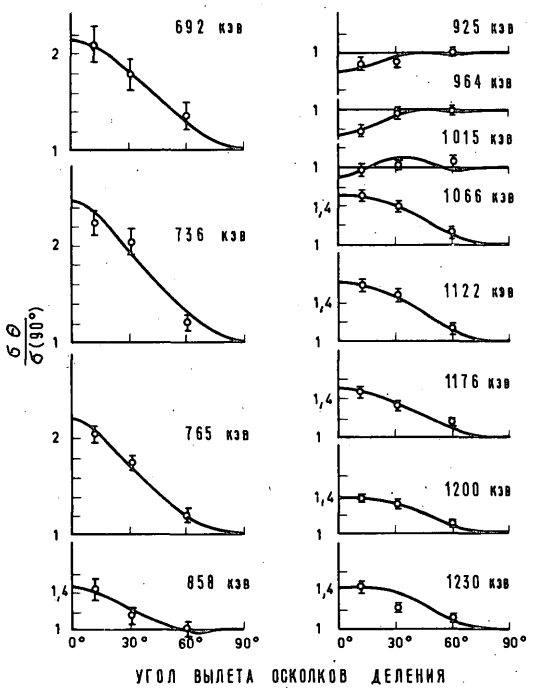

Рис.1

Результаты измерений угловых распределений осколков деления Th^{230} нейтронами.

ными состояниями внутри полосы. Это говорит о том, что ширины уровней в седловой точке, вероятно, меньше расстояний между уровнями. В предположении, что уровни имеют вращательный характер, для $\hbar^2/2\mathcal{J}$ получено значение 4 кэв. Анализ угловых распределений осколков при E_n = 692 кэв и E_n = 736 кэв позволил также оценить параметр развязывания [17] — его величина составляет около − 0,5.

Как видно из рис.2, пик сечения деления при E_n = 750 кэв принадлежит полосе с $K = 1/2^-$. При дельнейшем увеличении E_n сечение деления через полосу с $K = 1/2^-$ обнаруживает такой же провал, как и полное сечение деления. Уменьшение анизотропии в этой области E_n связано с быстрым ростом сечения деления через полосу с $K = 3/2^-$. Выше 900 кэв вновь возрастает роль полосы с K = 1/2. В связи с наличием нескольких полос анализ при этих значениях E_n затруднен, однако, если предположить, что

$$\alpha^{1/2}_{3/2}/\alpha^{3/2}_{3/2} = \alpha^{1/2}_{5/2}/\alpha^{3/2}_{5/2} = \alpha^{1/2}_{7/2}/\alpha^{3/2}_{7/2},$$

то расчет указывает, что это вновь полоса с $K = 1/2^-$. Последующее падение анизотропии, согласующееся с данными [18], вызвано делением через полосу с $K = 3/2^+$. Насколько мы знаем, это первый случай, когда после-

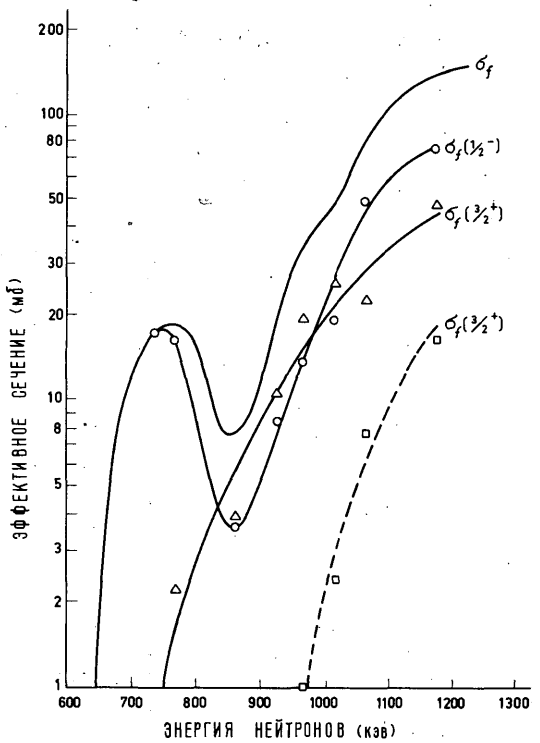

Рис.2

Парциальные сечения делений для отдельных К-полос.

довательность полос для четно-нечетного делящегося ядра отличается от $1/2^+, 3/2^-, 1/2^-$.

Максимум сечения при $E_n = 750$ кэв представляет определенный интерес. Обычное в таких случаях объяснение состоит в том, что предполагается открывание нового уровня для неупругого рассеяния нейтронов, т.е. резкое увеличение Γ_n [19]. Если наш анализ правильно отображает поведение сечения деления через полосу с $K = 1/2^-$, то необходимо предположить, что открывающийся уровень (или ряд уровней) имеет ширину по меньшей мере в 100 раз большую, чем сумма ширин всех открытых к этому моменту уровней, т.е. на три порядка превосходящую среднее значение Γ_n. Возможно, что этот результат связан с некорректностью использования в анализе коэффициентов $T_{I\pi}$ для недеформированных ядер.

Если выбрать другой потенциал для вычисления $T_{I\pi}$, например, учесть несферичность ядра Th^{230}, то результаты расчета как-то изменятся. Возможно, что второй подъем анизотропии окажется связанным с вступлением полосы $K = 1/2^+$. В этом случае, предполагая, что при $E_n = 850$ кэв Γ_f для первой полосы достигает насыщения, а последующий подъем сечения вызван другими полосами, необходимо объяснить увеличение Γ_n лишь примерно в 8 раз. Наиболее просто это можно сделать, если предположить, что первая полоса имеет $K = 1/2^-$. Тогда падение сечения деления через эту полосу можно связать с неупругим рассеянием нейтронов на известные виб-

рационные уровни Th^{230} при 634 и 676 кэв, причем необходимо предположить, что Γ_n для переходов на эти состояния примерно на порядок выше, чем на лежащие ниже вращательные уровни.

Современное состояние наших знаний о процессе деления не дает основания для объяснения такого хода сечения деления соответствующими изменениями σ^c или Γ_f. Представляются также менее вероятными объяснения связанные с наличием уровней Th^{230}, незамеченных при изучении α-распада U^{234}, или с несохранением K в процессе деления.

В заключение необходимо заметить, что в последнее время появились сообщения об обнаружении в подбарьерной области максимумов сечения деления нейтронами некоторых других ядер, соседних с Th^{230}. Так, отчетливый пик в сечении деления нейтронами Pa^{231} наблюдался при E_n = 330 кэв [20], небольшой максимум заметен и у U^{234} [14].

Плутоний-238

Общими отличительными особенностями деления нейтронами всех изученных до настоящего времени четно-четных ядер являются четко выраженный пороговый характер этого процесса и быстрые изменения около порога углового распределения осколков деления в зависимости от энергии нейтронов.

Особое место среди таких ядер занимает Pu^{238} – он обладает наибольшим среди изученных ядер значением параметра делимости Z^2/A и в отличие от остальных четно-четных ядер большим сечением деления тепловыми нейтронами – 18 барн [21]. Измеренная пороговая энергия деления Pu^{239} γ-лучами – 5,4 Мэв [22] и данные по энергии связи нейтрона – 5,6 Мэв [23] также позволяли предполагать, что деление Pu^{238} нейтронами не будет иметь порогового характера и связанных с порогом особенностей углового распределения осколков. Однако прямые экспериментальные данные о делении Pu^{238} нейтронами с энергией, отличной от тепловой, отсутствовали.

Нами были проведены измерения угловых распределений осколков и поперечного сечения деления Pu^{238} нейтронами с энергией от 50 до 1400 кэв.

Pu^{238} был получен путем α-распада Cm^{242}. Проведенный α-спектрометрический анализ слоя показал, что примеси составляют по весу не более

Cm^{242} – 10^{-9}	Am^{241} – $5\cdot10^{-5}$	Pu^{239} – $7\cdot10^{-4}$
Cm^{244} – 10^{-3}	Am^{242} – $1{,}5\cdot10^{-5}$	Pu^{240} – $2\cdot10^{-4}$
	Am^{243} – $7\cdot10^{-4}$	

В отличие от остальных измерений при изучении угловых распределений осколков деления Pu^{238} нейтронами осколки регистрировались четырьмя тонкими ионизационными камерами. Слой и камеры находились в общем тонкостенном баллоне, наполненном смесью A + 20% CH_4 до давления 180 мм рт.ст. Импульсы, создаваемые осколками, имели амплитуду около 160 мкв и длительность $5\cdot10^{-8}$ сек. Фон случайных совпадений α-частиц (около 10^6 α/сек камеру) не превышал 10^{-4} $сек^{-1}$.

Измерения показали, что дифференциальное сечение деления Pu^{238} нейтронами хорошо описывается выражением:

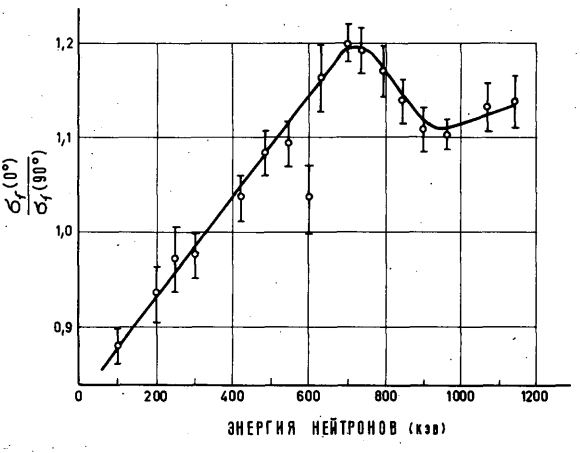

Рис.3

Результаты измерения угловых распределений осколков и поперечного сечения деления Pu^{238} нейтронами с энергией от 50 до 1400 кэв.

$$\sigma(\theta) = \sigma(90°)(1 + a\cos^2\theta) \qquad (5)$$

и не требует при нашей точности измерений более высоких степеней косинуса. Результаты измерений приведены на рис.3.

Те же ионизационные камеры были применены для измерения зависимости сечения деления от энергии нейтронов. Использовался счет всех четырех камер и в результаты вводилась поправка на анизотропию.

Абсолютизация сечения проводилась при энергии нейтронов 720 кэв. Количество вещества в слое определялось подсчетом актов спонтанного деления Pu^{238}. Так как темп счета этих актов составлял $\sim 10^{-3}$ сек, что приближается к скорости счета совпадений α-частиц, эти измерения проводились с использованием стеклянных детекторов, нечувствительных к α-частицам. Период спонтанного деления Pu^{238} принимался равным $5 \cdot 10^{10}$ лет [24].

Величина полного поперечного сечения деления подсчитывалась по формуле:

$$\sigma_f = \frac{4\left(1+\frac{a}{3}\right)}{4 + a\sum_{1}^{4}\cos^2\theta_i} \frac{N_f}{N} \frac{\lambda_{спонт} T_{изм}}{N_{спонт}}, \qquad (6)$$

где $a = \dfrac{\sigma(0°)}{\sigma(90°)} - 1$,

θ_i – угол между направлением нейтронного потока и направлением от слоя на i-й детектор,

N_f – полное число осколков деления, вызванных нейтронами,

N – полный поток нейтронов на $см^2$,

$N_{спонт}$ – число осколков спонтанного деления, зарегистрированных за время $T_{изм}$.

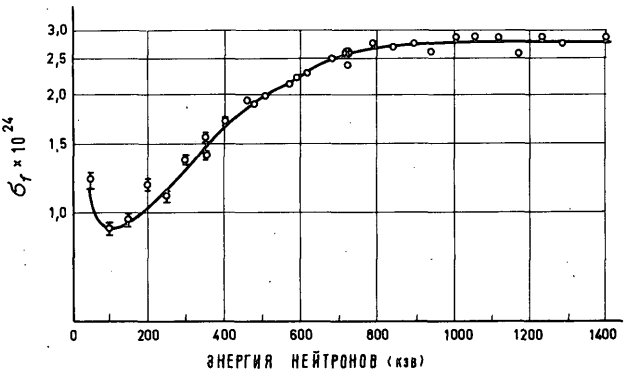

Рис.4

Сечение деления Pu^{238} нейтронами.

Полученное таким образом сечение деления Pu^{238} нейтронами изображено на рис.4. В приведенные на рисунке ошибки измерения не включена ошибка абсолютизации, составляющая 12%.

Полученные данные были использованы для К-полосного анализа сечения деления Pu^{238}. Деление тепловыми нейтронами указывает на то, что полоса с $K = 1/2^+$ присутствует уже при самых малых энергиях нейтронов. Наш расчет показал, что при энергии нейтронов 100 кэв деление через полосу $1/2^+$ вносит в общее сечение деления не более 10%. При более высоких энергиях нейтронов деление практически целиком идет через полосы с $K = 3/2^-$ и $K = 1/2^-$. Вычисленные на основании формулы (4) $\Gamma_f^{3/2-}$ и $\Gamma_f^{1/2-}$ имеют в области энергий нейтронов от 100 до 700 кэв практически одинаковый ход, увеличиваясь в e раз на интервале в 100 кэв.

Из-за небольшой величины анизотропии и присутствия нескольких полос при энергии нейтронов выше 700 кэв анализ затруднен, однако можно предполагать, что последующее падение анизотропии вызвано полосой с $K = 3/2^+$.

При энергии нейтронов выше 800 кэв полное сечение деления Pu^{238} остается постоянным и равным $2{,}8 \pm 0{,}3$ барна. Если для сечения захвата нейтронов использовать данные [13], то это приводит к отношению делительной и нейтронной ширин $\sim 2{,}6$ для ядра Pu^{239} при энергии возбуждения ~ 1 Мэв над порогом деления.

Америций-241

Среди нечетно-нечетных делящихся ядер угловые распределения осколков были измерены лишь для деления нейтронами Np^{237}. Было показано [12], что в районе порога деления анизотропия сравнительно невелика и мало меняется при изменении энергии нейтронов. Этот результат согласуется с предположением, что деление нечетно-нечетных компаунд-ядер идет через большое количество близко расположенных промежуточных состояний с различными K и наблюдаемое угловое распределение является суперпозицией многих парциальных распределений.

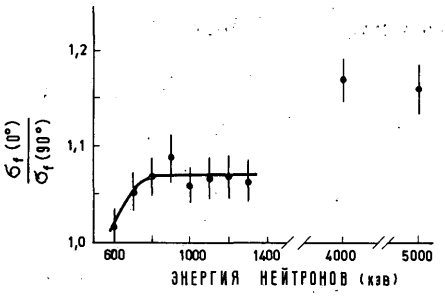

Рис.5

Результаты измерения угловых распределений осколков деления нейтронами Am^{241}.

В этом случае справедливо статистическое рассмотрение процесса. Если предположить [6], что распределение промежуточных состояний по K имеет гауссов характер:

$$F(K) \sim \exp(-K^2/2K_0^2), \tag{7}$$

то наблюдающаяся анизотропия

$$\frac{\sigma(0°)}{\sigma(90°)} = 1 + \frac{\mathcal{J}^2_{макс}}{8K_0^2}, \tag{8}$$

где $\mathcal{J}_{макс}$ – максимальный угловой момент, вносимый в ядро падающим нейтроном.

Измерения [18], проведенные для ядер различных типов четности в широкой области энергий нейтронов, позволили определить зависимость K_0 от энергии возбуждения делящегося ядра. Эти измерения показали, что при небольших энергиях возбуждения наименьшее значение K_0 имеют четно-четные ядра, а наибольшее – нечетно-нечетные, что, видимо, объясняется разными возможностями образования парных нуклонных конфигураций (и, следовательно, уменьшения K_0) для ядер разной четности. Обращал, однако на себя внимание тот факт, что с ростом энергии возбуждения величина K_0 для нечетно-нечетного компаунд-ядра Np^{238} не приближалась к значениям K_0 для ядер других типов четности.

Нами были произведены измерения угловых распределений осколков деления нейтронами Am^{241} – ядра того же типа четности, что и Np^{237}, имеющего тот же собственный спин 5/2. Небольшая величина анизотропии и ограниченная точность измерений позволили выделить лишь два члена в разложении угловых распределений по степеням косинуса:

$$\sigma(\theta) = \sigma(90°)(1 + a\cos^2\theta). \tag{9}$$

Результаты измерений приведены на рис.5. Как видно из рисунка, анизотропия деления в районе порога весьма невелика и слабо зависит от энергии нейтронов.

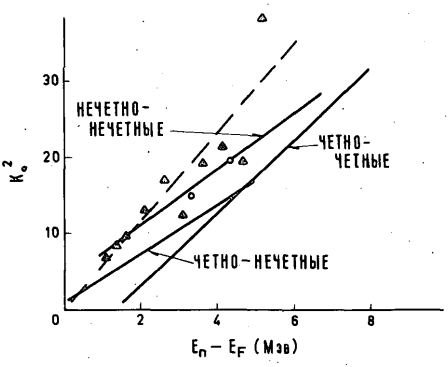

Рис. 6

Результаты измерения угловых распределений и значения K_0 при соответствующих возбуждениях компаунд-ядро Am^{242}: ▲ Np^{238} [18]; ⊙ Am^{242}.

Измерения угловых распределений при энергии нейтронов 4,0 и 5,0 Мэв позволили определить значения K_0 при соответствующих возбуждениях компаунд-ядра Am^{242}. Результаты изображены на рис. 6, совместно с данными по Np^{238} [18]. Так же, как и в работе [18] мы принимали в данном случае в качестве пороговой энергии энергию нейтронов, при которой сечение деления достигало 10% от сечения деления на плато, и полагали, что $\mathcal{J}_{макс} \simeq \sqrt{5E_n}$ Мэв. Видно, что согласие вполне удовлетворительное, кроме точки для Np^{238}, измеренной при энергии нейтронов 5,5 Мэв. Однако корректность этой точки в связи с близостью порога (n, n'f) процесса вызывает сомнения. Если же ее исключить, то зависимость K_0 от энергии возбуждения для нечетно-нечетных делящихся ядер обнаруживает заметную тенденцию к сближению с аналогичными зависимостями для ядер других типов четности.

ЛИТЕРАТУРА

[1] WINHOLD E.J., DEMOS P., HALPERN I. Phys. Rev., 87 (1952) 1139.
DICKINSON W.C., BROLLEY J.E. Phys. Rev., 90 (1953) 388.
[2] HILL D.L., WHEELER J.A. Phys. Rev., 89 (1953) 1102.
[3] BOHR A. Proc. Internat. Conf. Peaceful Uses At. Energy, Geneva, 1956, v.2, p.191.
[4] СТРУТИНСКИЙ В.М. ЖЭТФ, 30 (1956) 606.
[5] WILLETS L., CHASE D. Phys. Rev., 103, (1956) 1296.
[6] HALPERN I., STRUTINSKI V.M. Proc. Soc. U. N. Conf. Peaceful Uses At. Energy, Geneva, 1958, v.15, p.408.
[7] БАЕВ Б.В., ВОРОТНИКОВ П.Е., ГОХБЕРГ Б.М., СИДОРОВ Н.И., ШУФ А.В., ЯНЬКОВ Г.Б. ДАН, 101 (1955) 637.
[8] КОЛТЫПИН Е.А. ПТЭ, 4 (1960) 130.
[9] АЛЛЕН В. "Физика быстрых нейтронов", т.1, Атомиздат. М., 1963.
[10] КАПУСЦИК А., ПЕРЕЛЫГИН В.П., ТРЕТЬЯКОВА С.П. ПТЭ, 5 (1964) 72.
[11] НОСОВ В.Г. "Физика деления атомных ядер", Атомиздат, 1957.
[12] ГОХБЕРГ Б.М., ОТРОЩЕНКО Г.А., ШИГИН В.А. ДАН, 128,(1959) 1157.
[13] AUERBACH E.H., PEREY F. Opt. Model Neutron Transm. Coeff. BNL-765 (T-286).
[14] LAMPHERE R.W. Nucl. Phys., 38 (1962) 561.
[15] HAUSER W., FESHBACH H. Phys. Rev., 87 (1952) 366.
[16] LANDOLT-BÖRNSTEIN. Neue serie, v.1 (1961).
[17] ПРЕСТОН М. Физика ядра, М., 1964.

[18] SIMMONS J.E., HENKEL R.L. Phys. Rev., 120 (1960) 198.
[19] WHEELER J.A. Physica, 22 (1956) 1103.
[20] ДУБРОВИНА С.М., ШИГИН В.А. ДАН, 157 (1964) 561.
[21] HULET E.K., HOFF R.W., BOWMAN H.R., MICHEL M.C. Phys. Rev., 107 (1957)1294.
[22] HUGHES D.J. Neutron Cross Section BNL-325.
[23] EVERLING F., KONIG L.A., MATTAUCH J., WAPSTRA A.H. Nucl. Phys., 18 (1960)529.
[24] ДРУИН В.А., ФЛЕРОВ Г.Н. "Физйка деления атомных ядер", Атомиздат, М., 1962.

О ДЕЛЕНИИ ДЕФОРМИРОВАННЫХ ЯДЕР*

В.М. СТРУТИНСКИЙ
ГОСУДАРСТВЕННЫЙ КОМИТЕТ ПО ИСПОЛЬЗОВАНИЮ АТОМНОЙ ЭНЕРГИИ СССР.
ИНСТИТУТ АТОМНОЙ ЭНЕРГИИ им. И.В. КУРЧАТОВА
МОСКВА, СССР

Abstract — Résumé — Аннотация — Resumen

ANGULAR ANISOTROPY OF FISSION AND THE LIQUID DROP MODEL. The results of calculations of the moments of inertia of the nucleus at the saddle point are given for the liquid drop model of potential energy, which takes into account the effect of blurring of the edge of the nucleus in the form of a correction to surface tension depending on the curvature of the effective surface (the GN-correction).

If the GN-correction is applied when $\Gamma < 0$, the form of the nucleus at the saddle point is closely dependent on the basic fissionability parameter Z^2/A.

Unlike the normal liquid drop model, the value J_{eff} obtained in this way is in good agreement with the experimental figure found by Huizenga et al. from the angular anisotropy of fission, and at the same values $\Gamma \approx -0.1$ and $(Z^2/A)_{crit} \approx 45$, which agree best of all with other data. The data on the magnitude of J_{eff} make it possible to determine direct from the experiment and independently of the model the parameter $(Z^2/A)_{crit}$ for the excited nuclear model.

ANISOTROPIE DE LA DISTRIBUTION ANGULAIRE DES FRAGMENTS DE FISSION ET MODÈLE DE LA GOUTTE. L'auteur indique les résultats des calculs qu'il a faits pour déterminer les moments d'inertie des noyaux par rapport à l'étranglement pour le modèle de la goutte de l'énergie potentielle, qui tient compte de l'effet «d'évanouissement» du bord du noyau sous la forme d'une correction de la tension superficielle; cette correction dépend de la courbure de la surface réelle (correction GN).

Si l'on applique cette correction pour $G < 0$, la forme du noyau au point d'étranglement dépend étroitement du paramètre fondamental de fissibilité Z^2/A.

Contrairement au modèle de la goutte ordinaire, la valeur de J_{eff} ainsi obtenue est en bon accord avec celle que Huizenga et al. ont déterminée par voie expérimentale, en partant de l'anisotropie de la distribution angulaire des produits de fission, pour les même valeurs $G \approx -0,1$ et $(Z^2/A)_{crit} \approx 45$ qui concordent le mieux avec les autres données. Les données relatives à la grandeur de J_{eff} permettent de déterminer directement, sur la base de l'expérience et indépendamment du modèle, le paramètre $(Z^2/A)_{crit}$ pour le modèle du noyau excité.

УГЛОВАЯ АНИЗОТРОПИЯ ДЕЛЕНИЯ И КАПЕЛЬНАЯ МОДЕЛЬ. Представлены результаты расчетов моментов инерции ядра для седловой точки для капельной модели потенциальной энергии, в которой учитывается эффект размытости края ядра в виде зависящей от кривизны эффективной поверхности поправки к поверхностному натяжению (ГН-поправка).

При наличии ГН-поправки при $\Gamma < 0$, форма ядра в седловой точке резко зависит от основного параметра делимости Z^2/A.

В отличие от обычной капельной модели, полученная таким образом величина $Z_{эфф}$ хорошо согласуется с экспериментально найденной Хайзенгой и др. из угловой анизотропии деления, причем при тех же значениях $\Gamma \approx -0,1$ и $(Z^2/A)_{крит} \approx 45$, которые лучше всего согласуются с другими данными. Данные о величине $Z_{эфф}$ позволяют непосредственно из опыта и независимо от модели определить параметр $(Z^2/A)_{крит}$ для возбужденной ядерной модели.

ANISOTROPIA ANGULAR DE LA FISION Y MODELO DE LA GOTA. El autor presenta los resultados del cálculo de los momentos de inercia de un núcleo en el punto de estrangulación, basándose en el modelo de la gota para la energía potencial, en el que se ha tomado en consideración el efecto de la deformación de los bordes del núcleo; a tal fin, introduce en la tensión superficial una corrección que depende de la curvatura de la superficie efectiva.

En los casos en que esta corrección se aplica cuando $\Gamma < 0$, la forma del núcleo en el punto de estrangulación depende marcadamente del parámetro fundamental de fisibilidad Z^2/A.

* На симпозиуме зачитано только название доклада.

A diferencia del modelo corriente de la gota, el valor J_{ef} obtenido de esta forma concuerda satisfactoriamente con el hallado experimentalmente por Huizenga y col. a partir de la anisotropía angular de la fisión, para los mismos valores $\Gamma \approx 0{,}1$ y $(Z^2/A) \approx 45$, que son los que mejor concuerdan con otros datos. Los valores J_{ef} permiten determinar experimentalmente y sea cual fuere el modelo, el parámetro $(Z^2/A)_{crit}$ para un modelo de núcleo excitado.

О ДЕЛЕНИИ ДЕФОРМИРОВАННЫХ ЯДЕР

Феноменологическая модель

Капельная модель, которая используется для определения потенциальной энергии ядра в теории деления ядер, количественно точна только при условии достаточного "перемешивания" состояний отдельных частиц. Если частицы могут свободно переходить из одного состояния в другое, то зависимость энергии ядра от макроскопических переменных, описывающих деформацию, дается капельной моделью, в которой энергия ядра в весьма общем виде выражается через среднюю плотность частиц и ее градиенты [1]. При относительно малых энергиях в той или иной мере сказывается квантовое вырождение состояний. Для деления важнейшим из таких эффектов является возникающий в незаполненной оболочке квадрупольный момент, приводящий к возникновению стабильной деформации ядер. (О.Бор, Б.Мотельсон [2]). С ним связано важное для задачи определения порогов деления ядер уменьшение энергии ядра в основном состоянии (деформированном) по сравнению со сферически симметричным "капельным".

При малой деформации незаполненной сферической оболочки вследствие снятия вырождения по проекциям углового момента возникает индуцированный не зависящий от деформации квадрупольный момент, а в энергии ядра возникает член, линейно зависящий от величины деформации

$$W_1 \approx - K\alpha \qquad (1)$$

вследствие чего и происходит смещение положения равновесия к некоторой конечной деформации $\alpha_0 \neq 0$.

Можно показать, что квадрупольное взаимодействие вырожденных в сферическом ядре состояний (т.е. внутри оболочки) дает поправку (1) к энергии сферического ядра, тогда как взаимодействие разных оболочек дает обычную для классики квадратичную зависимость энергии от параметра квадрупольной деформации самосогласованного поля

$$W_2 = C\alpha^2 . \qquad (2)$$

В точке, соответствующей равновесной деформации, обе поправки (1) и (2) сравниваются. Здесь теория возмущений становится неприменимой. Таким образом, в нильссоновской модели деформированного самосогласованного поля равновесная деформация приближенно соответствует пересечению уровней разных j-оболочек. Из схем уровней Нильссона (см., например [4]) непосредственно видно, что это действительно так для ядер, далеких от магических ($\alpha \sim 0{,}15$). Деформирующие силы (1) — существенно квантового происхождения. При деформации большей, чем та, при кото-

рой пересекаются подоболочки (α^*), связанная с оболочками неравномерность распределения массы (внутренний квадрупольный момент) исчезает и зависимость энергии от деформации описывается капельной моделью. Другими словами, коэффициент К в формуле (1) при $\alpha \sim \alpha^*$ обращается в нуль. Так как энергия (1) отрицательная, в переходной к классике области возникают дополнительные силы, препятствующие деформации, возникает дополнительная устойчивость деформированного квантового состояния.

Нельзя исключить, что конкретная величина равновесной деформации ядер далеких от магических определяется именно этим переходом к нормальному классическому состоянию. Тогда стало бы понятным, почему стабильная деформация ядер так хорошо рассчитывается практически в любой теоретической модели, тогда как по мере приближения к магическим ядрам точность расчетов заметно ухудшается (см., напр., [5, 6], где имеются подробные ссылки на другие работы). Этим можно объяснить также, почему в области трансурановых ядер величина стабильной деформации изменяется очень мало, несмотря на резкое уменьшение квадрупольной жесткости, которое должно происходить из-за возрастания кулоновской энергии.

Энергию W_1 нужно рассматривать именно как поправку к капельной модели. Оценка жесткости формы ядра в любой модели независимых частиц со слабым остаточным взаимодействием едва ли законна, поскольку такое взаимодействие имеет мало общего с тем сильным взаимодействием, которым определяются объемная сжимаемость, поверхностное натяжение и параметры среднего поля ядра. В простой модели независимых частиц всегда получается очень большая жесткость ("одночастичная" жесткость). Если допускается возможность перехода нуклонов с орбиты на орбиту при пересечении уровней, "жесткость" значительно уменьшается, оставаясь все же весьма большой[1]. Из-за остаточных взаимодействий (т.е. столкновений нуклонов) требующиеся для перехода к классической жесткости переходы нуклонов с орбиты на орбиту начинаются раньше, чем происходит пересечение одночастичных уровней. Конкретные расчеты Шиманского [6] показали, что жесткость сильно уменьшается, если учитывается остаточное взаимодействие спаривания (рис. 1). После учета спаривания жесткость формы ядра при деформации порядка стационарной или большей очень мала, либо вообще отрицательна [5], [6]. Этот эффект не является неожиданным, так как при перемешивании нуклонных состояний должна наблюдаться квазиклассическая картина, когда энергия газа в потенциальной яме не зависит от формы последней, если "объем" ямы не изменяется.

Беляев показал [2], что на величину индуцированного в незаполненной оболочке квадрупольного момента существенно влияет спаривательное остаточное взаимодействие, при учете которого он оказывается пропорциональным деформации при очень малой деформации. Эти эффекты для нас не являются существенными, поскольку рассматриваются ядра далекие от магических и относительно большие деформации ($\alpha > 1/A^{2/3}$). В

[1] Предположение о том, что увеличение стабильности очень тяжелых ядер может быть связано с большой "частичной" жесткостью при малых деформациях, было высказано Д.Ф. Зарецким.

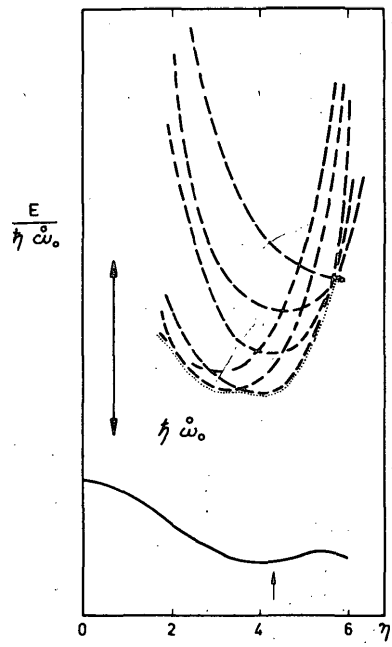

Рис.1

(Взято из [6]). Полная энергия ядра как функция деформации для ядра U^{230}. Параметр $\alpha = 0{,}033\,\eta$, единица энергии $\hbar w_0^0 = 41/A^{1/3} \approx 6$ Мэв. Пунктирные кривые – потенциальная энергия в модели Нильссона для разных нуклонных состояний, точки – огибающая, соответствующая основному состоянию в модели независимых частиц (учитываются переходы при пересечении уровней). Сплошная линия – потенциальная энергия с учетом парного взаимодействия нуклонов. Стрелкой отмечена равновесная деформация α_0. В этих расчетах не удается определить форму кривой потенциальной энергии при деформации порядка стационарной или большей. В то же время величина $w(\alpha_0)$ определяется достаточно однозначно.

этом случае формула (1) справедлива. По-видимому, подобный эффект могут вызывать также и другие остаточные взаимодействия, препятствующие возникновению квадрупольного момента в сферическом ядре, в особенности, противодействующие флуктуациям плотности нуклонов. Эти силы представляют особенный интерес, поскольку в капельной модели ядерная материя обычно предполагается несжимаемой или мало сжимаемой.

Таким образом, едва ли следует ожидать значительного отклонения ядерного поверхностного натяжения от капельного значения, хотя, конечно, нельзя исключить, что при малых деформациях поверхностное натяжение все же будет несколько отличаться от такового для больших деформаций. Эти эффекты не очень существенны для дальнейшего, хотя они могут несколько повлиять на численные результаты.

Основным эффектом, который рассматривается здесь, являются квантовые силы, деформирующие ядра в основном состоянии и исчезающие при деформации $\alpha \sim \alpha^*$. Учесть их можно, добавив к обычной капельной энергии

$$W_{\text{км}} \approx 0{,}4\,(1-x)\,\alpha^2 - 0{,}114\,\alpha^3 \qquad (3)$$

($|1-x|\ll 1$, $\alpha \equiv \alpha_2$ — параметр квадрупольной деформации) член вида[1]

$$W_1 = -k\alpha e^{-(\alpha/\alpha^*)^2}, \tag{4}$$

где K — коэффициент, так что потенциальная энергия при всех деформациях имеет вид:

$$W(\alpha) = W_{км}(\alpha) + W_1(\alpha). \tag{5}$$

Как обычно

$$x = \frac{E_c}{2E_s} \approx (Z^2/A)/(Z^2/A)_{крит}, \tag{6}$$

а энергия выражается в единицах капельной поверхностной энергии сферического ядра. Здесь рассматривается самый простой вариант капельной модели, точность которого для наших целей вполне достаточна.

Для всех x меньших некоторого $x_{крит}$, вообще говоря, отличного от единицы, потенциальная энергия (5) имеет два экстремума, минимум при $\alpha = \alpha_0$, соответствующий равновесной при данном x деформации (основному состоянию ядра) и максимум, соответствующий вершине барьера деления (α_f). Порог деления определяется как

$$E_f(x) = W(\alpha_f) - W(\alpha_0) \tag{7}$$

(см. рис. 2,3).

Если

$$\alpha_f > \alpha^*,$$

то α_f и $W(\alpha_f)$ такие же, как в капельной модели, т.е.

$$W(\alpha_f) \approx W_{км}(\alpha_f) \approx 0{,}72(1-x)^3.$$

Поэтому роль начальной деформации состоит в основном в увеличении E_f на $|W(\alpha_0)| \approx 2-3$ Мэв. Такая величина соответствует масштабу энергии квадрупольного взаимодействия в основном состоянии деформированного ядра [6]. Этот результат мало зависит от места перехода к капельной модели, если только α^* меньше, чем α_f для $x = 0{,}7-0{,}8$ (т.е. $\alpha^* \lesssim 0{,}3$). Основным следствием этого является более слабая зависимость E_f от x для ядер не очень близких к капельному пределу устойчивости к делению и соответственно более слабая зависимость от x проницаемости барьера для спонтанного деления из основного состояния.

По мере приближения x к единице капельное α_f должно было бы стремиться к нулю, так как в капельной модели

$$\alpha_f^{(км)} \approx 2{,}3(1-x).$$

[1] Гауссовский вид переходной функции выбран исключительно из соображений простоты.

Действительная ситуация зависит от того, насколько равновесная деформация (α_0) отличается от α^*. Если $\alpha_0 \ll \alpha^*$, то при достаточно большом x, когда $\alpha_f^{(KM)} < \alpha^*, \alpha_0$ и α_f быстро стремятся друг к другу из-за присутствия в (5) растягивающего ядро линейного члена, причем α_f и E_f по мере увеличения x уменьшаются быстрее, чем в капельной модели, а α_0 — возрастает. В результате величина $x_{крит}$, при котором $E_f = 0$, оказывается меньше единицы (т.е. (Z^2/A) кр. меньше "капельного" значения).

Иначе обстоит дело, если внутренний квадрупольный момент исчезает при деформации, близкой к стационарной (т.е., $\alpha^* - \alpha_0 \lesssim \alpha_0$). Как отмечалось выше, сама величина α_0 в этом случае определяется практически только этим эффектом. Для гауссовского перехода (4) к классике тогда получается, что

$$\alpha_0 \approx 0{,}7\,\alpha^*$$

и весьма слабо зависит от остальных параметров задачи, таких как K или x. В этом случае величина $x_{крит}$, вообще говоря, больше единицы.

Некоторые результаты расчетов приведены на рис.2 и 3. Величина K выбиралась так, чтобы при данном α^* получалось $\alpha_0 \approx 0{,}15 - 0{,}16$, что приближенно соответствует деформации урана и трансурановых ядер (см., напр., [4—6]). Для наименьшего α^* ($\approx 0{,}25$), когда α_0 слабо зависит от K, величина K подбиралась так, чтобы величина $W(\alpha_0)$ соответствовала 3 Мэв.

Некоторые следствия

Рассмотренная простая модель приводит к ряду важных для описания деления трансурановых элементов выводов. Для сравнения с конкретными ядрами нужно определить величину $(Z^2/A)_{крит}$. Примем, что

$$(Z^2/A)_{крит} = 45. \qquad (8)$$

Как было показано в [7], это значение практически независимо от теоретических моделей следует из известных экспериментальных данных [8] об угловой анизотропии деления. Формула (6) позволяет тогда определить величину капельной поверхности энергии сферического ядра. При $r_0 = 1{,}2 \cdot 10^{-13}$ см. для $A \approx 240$ получается $E_s \approx 600$ Мэв, что является единицей энергии при пересчете энергии в Мэв. Изменения этого масштаба энергии на 10—20% не имеют значения, поскольку в данном виде теория едва ли может претендовать на лучшую точность для абсолютных значений.

Пороги деления ядер из основного состояния

На рис.2 изображены некоторые рассчитанные кривые потенциальной энергии для разных α^*, на рис.3 — соответствующие рассчитанные пороги деления в зависимости от x. Основной особенностью этих кривых является слабая зависимость E_f от x по сравнению с капельной моделью, что, в основном, является следствием того факта, что к капельному порогу добавляется некоторое почти постоянное слагаемое, $+|W(\alpha_0)|$, которое для

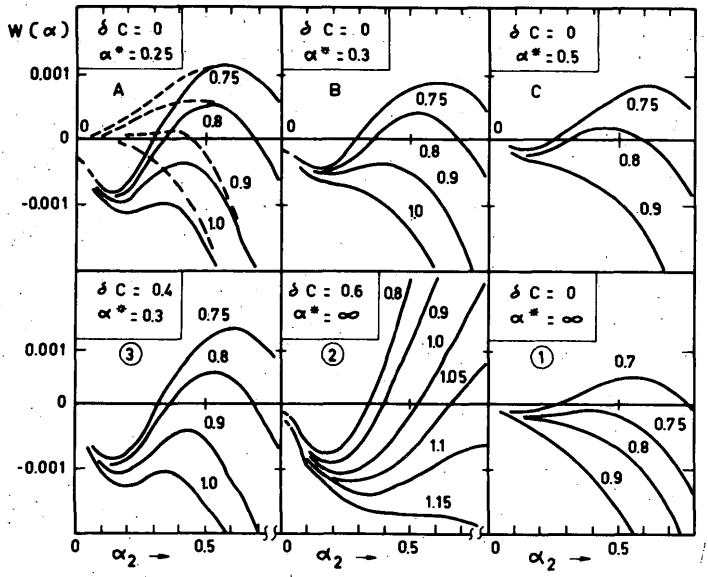

Рис.2

Потенциальная энергия (5) в зависимости от параметра деформации. Варианты A, B, C и "1" соответствуют капельному поверхностному натяжению ($\delta C = 0$) и указанным на рисунке значениям критической деформации α^*. Варианты с $\alpha^* = \infty$ соответствуют модели Хилла-Уиллера [11], причем в случае "2" поверхностное натяжение выбрано так, чтобы при $\alpha \leqslant \alpha_0$ получалась такая же потенциальная энергия, как и для варианта A, согласующаяся с расчетами Шиманского [6]. Вариант $\delta C = 0{,}4$ соответствует формуле (15). Пунктирные кривые для обычной капельной модели. Во всех случаях $\alpha_0 = 0{,}15-0{,}16$.

урана ($x \approx 0{,}79$) составляет около половины E_f. Величина $x_{крит}$ получается равной $1{,}1-1{,}2$ при меньших α^* и меньше единицы при $\alpha^* > 0{,}3$.

Известно, что резкая зависимость E_f от Z^2/A для самых тяжелых ядер, предсказываемая капельной моделью, не согласуется с опытом, хотя и обнаруживается некоторая тенденция к уменьшению порогов при увеличении Z^2/A [9]. Согласовать простую капельную модель с опытом особенно трудно при указанном выше относительно малом $(Z^2/A)_{крит}$. В рассматриваемой модели эта трудность практически отсутствует (рис.4), если только величина $\alpha^* \lesssim 0{,}3$, а α^* и K выбраны, как описано выше, таким образом, чтобы получались разумные значения для $W(\alpha_0)$ и α_0).

Периоды спонтанного деления ядер из основного состояния

На рис.3 изображены рассчитанные интегралы действия,

$$S(x) = \int_{\alpha_0}^{\alpha_{вых}} d\alpha \sqrt{|W(\alpha) - W(\alpha_0)|}\,, \qquad (9)$$

которыми определяется проницаемость барьера деления из основного состояния. Здесь также характерна более слабая зависимость от x, чем в

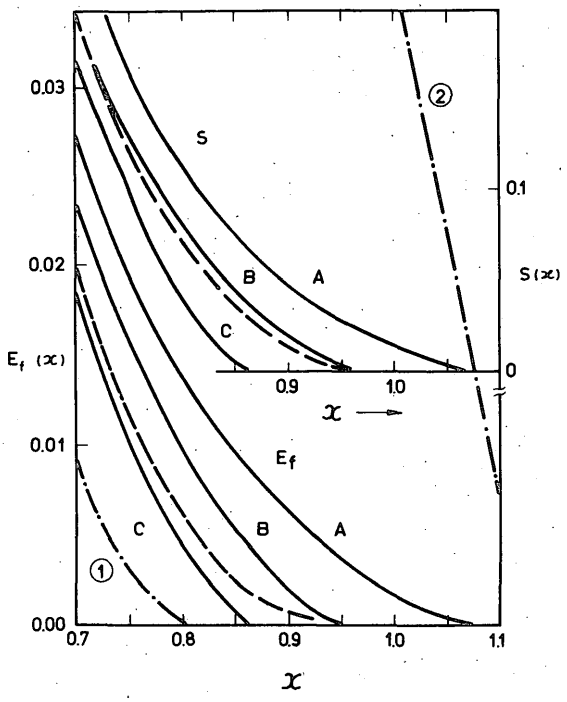

Рис.3

Пороги деления E_f (x) и интегралы действия S(x), соответствующие изображенным на рис.2 кривым потенциальной энергии. Пунктир – то же для обычной капельной модели (см. также подпись к рис.2).

простой капельной модели, причем этот эффект возникает в основном как следствие слабой зависимости от x величины E_f. Хотя расчет функции действия содержит весьма значительную неопределенность, существенное отличие от "капельной" кривой не вызывает сомнений: в случае обычной капельной модели зависимость S(x) от x очень сильная: S(x) пропорционально $(1-x)^n$, где $n = 5/2$ или 3 в зависимости от предположений о форме кривой потенциальной энергии.

Известно, что логарифмы среднего для данного элемента времени спонтанного деления четно-четных ядер приближенно согласуются со следующей линейной зависимостью от (Z^2/A) [9]:

$$\ln(\tau_{\text{спонт}}/\tau_0) \approx \text{конст}\,(46 - Z^2/A). \qquad (10)$$

Согласовать такую наблюдаемую зависимость от Z^2/A с сильной зависимостью, предсказываемой капельной моделью, можно только если выбрать $(Z^2/A)_{\text{крит}} > 55$, но это значение трудно согласовать с полуэмпирической формулой для масс ядер и другими известными данными о делении (величина порога деления, угловая анизотропия и т.п.).

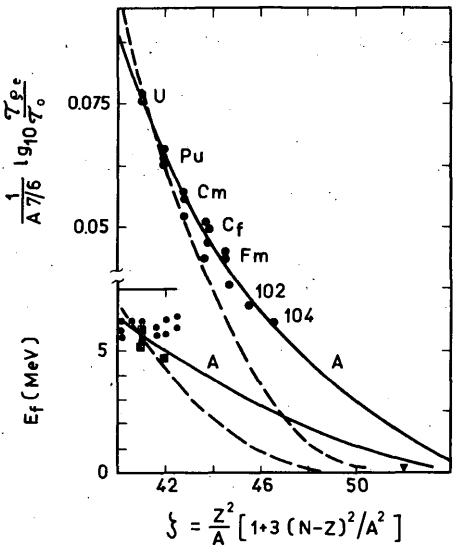

Рис.4

Сравнение с экспериментальными данными о временах спонтанного деления четно-четных ядер и порогах деления. Сплошные линии соответствуют варианту А на рис.2 и 3. Рассчитанные кривые нормированы по экспериментальным точкам для урана. Этим, в частности, исключается неопределенность в величине "массового коэффициента". Величина $(Z^2/A)_{крит} = 45$, что соответствует $\xi_{крит} = 52$. Пунктир – простая капельная модель при таком $(Z^2/A)_{крит}$; $\tau_0 = 3 \cdot 10^{-21}$ сек.

На рис.4 изображены экспериментальные значения величины $\ln(\tau_{спонт}/\tau_0)$ ($\tau_0 = 3 \cdot 10^{-21}$ сек) в зависимости от параметра

$$\xi = (Z^2/A)\,[1+3\,(N-Z)^2/A^2\,]. \qquad (11)$$

По оси ординат отложено

$$\frac{1}{A^{7/6}} \lg(\tau_{спонт}/\tau_0),$$

поскольку в капельной модели именно эта величина является функцией параметра делимости $E_c/2E_s$. Это следует из определения функции действия и размерности входящих туда величин. Для сравнения приведена нормированная по изотопам рассчитанная кривая, соответствующая кривой S(x) на рис.3 для $\alpha^* = 0{,}25$, а также "капельная кривая" для $(Z^2/A)_{крит} = 45$. Видно, что в отличие от простой капельной модели имеется достаточно хорошее согласие. В области ядер U–F_m средняя делимость приближенно согласуется с эмпирической формулой (10).

Деление нагретого ядра

Квантовые эффекты, приводящие к начальной деформации, исчезают не только при больших деформациях, но и при достаточном возбуждении ядра. В этом случае ядро делится из начального нагретого состояния, а вероятность деления определяется величиной "капельного" порога, т.е. $E_f \approx W_{км}(\alpha_f)$ формула (6). Для урана эта величина приблизительно вдвое меньше, чем порог деления из основного состояния, а для элементов с $Z>100$ E_f равняется нулю. Именно такой уменьшенный порог деления должен учитываться в определении относительной делимости ядер, равной [10]:

$$\frac{\Gamma_n}{\Gamma_f} \approx 4A^{2/3}\,\frac{mr_0^2\,T}{\hbar^2}\exp\left[\tfrac{1}{T}(E_f - B_n)\right] \qquad (12)$$

где B_n – энергия связи нейтрона. На первый взгляд может показаться, что обращение в нуль порога деления приведет к чрезмерному увеличению делимости. Этого не происходит, так как даже при $E_f = 0$ величина Γ_n/Γ_f остается конечной, причем

$$\left(\frac{\Gamma_n}{\Gamma_f}\right)_{min} \approx 5{,}5\; T_{Мэв} e^{-\frac{1}{T}B_n}.$$

Заметим, что по тем же причинам, что и для порога деления (разрушение квантовой структуры основного состояния при нагревании) при вычислении Γ_n в формулу (12) нужно подставлять одно и то же значение энергии связи нейтронов β_n независимо от четности числа нуклонов в ядре.

Из-за исчезновения квантовых эффектов в нагретом ядре величина $(Z^2/A)_{крит}$ определяется одними только "капельными" свойствами ядра, поэтому ее можно определить, изучая деление нагретых ядер. Именно это обстоятельство было использовано выше, когда $(Z^2/A)_{крит}$ определялось из данных об угловой анизотропии осколков деления при возбуждении порядка нескольких десятков Мэв.

Деление из возбужденного состояния

Из изложенного видно, что так наз. "потенциальная энергия" деления может сильно зависеть от конкретного квантового состояния ядра. При этом важным фактором является величина квадрупольного взаимодействия нуклонов незаполненной оболочки. Величина α^* также может быть разной для деления из разных квантовых состояний. В зависимости, в частности, от этого величина потенциальной энергии при деформации, соответствующей барьеру деления, может быть больше или меньше, чем для основного состояния.

В некотором смысле этот эффект обусловлен "внутренним запретом", связанным с оболочками. При наличии таких запретов обычное определение потенциальной энергии деформации, как "наименьшей энергии ядра при данной деформации", неполно, поскольку оно предполагает, что любое увеличение энергии по сравнению с этой минимальной величиной можно с точки

зрения деления рассматривать как дополнительную "кинетическую энергию" деления. Между тем, при наличии структурных запретов следует скорее говорить об изменении потенциальной энергии. Предположенная Уиллером [11] и Юханссоном [12] модель для объяснения известной проблемы времени спонтанного деления четно-четных и четно-нечетных ядер является, в сущности, примером такого более сложного понимания потенциальной энергии деления.

Нечто подобное может иметь место также и в случае спонтанного деления ядер из некоторых состояний, соответствующих сложному возбуждению частиц. Если в возбужденном состоянии потенциальная энергия при больших деформациях относительно больше, чем в основном состоянии, то вероятность спонтанного деления может даже уменьшаться при возбуждении ядра.

Нам кажется, что в эффектах такого рода может заключаться разгадка проблемы спонтанного деления из изомерных состояний. С.М. Поликановым и др. [14], [15] было обнаружено ускорение в $10^{15}-10^{20}$ раз спонтанного деления из некоторого изомерного состояния ядра при энергии 1,5–3,0 Мэв, тогда как Ванденбош и др. [6] обнаружили, что время спонтанного деления Cm^{244} мало отличается от такового для основного состояния, несмотря на то, что энергия возбуждения на 1,1 Мэв больше. Если даже большое ускорение деления в случае изомеров Поликанова и можно объяснить увеличением энергии, то ситуация с изомером Ванденбоша выглядит совершенно парадоксальной, если не учитывать изменение эффективной потенциальной энергии деления.

Квантовые флуктуации энергии основного состояния

Выше предполагалось, что перемешивание части частиц внутри оболочки приводит к исчезновению специфически квантовых "флуктуаций" энергии, обусловленных определенными квантовыми состояниями частиц. В действительности, это лишь приближенно верно, т.к. могут происходить относительно небольшие изменения потенциальной энергии, возникающие, например, из-за флуктуации плотности одночастичных состояний вблизи границы Ферми. Так, уменьшение на единицу числа одночастичных состояний в существенном для спаривания интервале Δ приводит к уменьшению энергии спаривания на величину

$$\delta\,(\rho\Delta^2/4)\sim\tfrac{1}{4}\Delta$$

порядка нескольких сот кэв ($\rho\Delta - 5-7$ есть среднее число состояний в интервале Δ). Такие "флуктуации" энергии спаривания могут быть особенно велики вблизи так называемой "оболочки N=152", возникающей при относительно большой деформации, порядка стабильной (см., напр., [4]), и исчезающей, при большей деформации. Эти флуктуации должны неизбежно приводить к колебаниям величины порогов деления и времени спонтанного деления, особенно заметным вблизи N = 152 и для ядер с относительно ма-

лым порогом деления. Корреляция времени спонтанного деления и порогов и масс ядер отмечалась Святецким в 1956 году [17].

Сравнение с другими расчетами

Описанная выше модель фактически соответствует т.наз. обобщенной модели ядер, развитой О. Бором и Б. Моттельсоном, дополненной замечанием об исчезновении деформирующих сил при достаточно большой деформации и в нагретых ядрах.

Эффект начальной деформации в делении рассматривался Хиллом и Уиллером [11]. Там предполагалось, что деформирующие ядро квадрупольные силы действуют при любой деформации (это соответствует $\alpha^* = \infty$). При этом получается, что величина порогов деления уменьшается по сравнению с простой капельной моделью, и, в частности, $x_{крит} > 1$.

Недавно Светецкий [13] предложил модель, в которой начальная деформация ядра учитывается добавлением к капельной энергии члена вида

$$S(A,Z)\, e^{-(\alpha/\bar{\alpha})^2}\ , \qquad (13)$$

так что при $S<0$ получается понижение энергии основного (сферического) состояния для замкнутых оболочек, а при $S>0$ ядро в основном состоянии деформировано. Физические основания такой модели совершенно отличны от рассматриваемой здесь, в которой получаются противоположные результаты: в модели Святецкого, как и в [11], порог деления получался бы меньше капельного[1]. Так, в модели Святецкого равновесная деформация

$$\alpha_0 \approx \bar{\alpha} \ln \frac{S}{0{,}4\,(1-x)\bar{\alpha}}\ ,$$

откуда видно, что величина $x_{крит} < 1$.

В заключение заметим, что некоторые расчеты были проведены с более сложными аппроксимациями потенциальной энергии деформированного ядра при $\alpha < \alpha^*$, например вместо линейной функции в (4) было взято

$$-|c|\alpha^2 + |D|\alpha^3\ . \qquad (14)$$

или

$$-\kappa\alpha + (\delta c)\alpha^2 \qquad (15)$$

[1] В работе [13] приложения к делению детально не рассматриваются. Заметим, что обычно предполагается, что энергия основного состояния деформированного ядра больше чем "капельного" сферического, на том основании, что так получается из сравнения масс ядер с полуэмпирической "гладкой формулой Грина". Этот довод несостоятелен, т.к. константы ф-лы Грина выбираются таким образом, чтобы она наилучшим образом воспроизводила в среднем массы всех ядер, в том числе магических. Рассчитанная таким образом "капельная" масса всегда будет меньше массы деформированных немагических ядер и больше массы ядер магических.

(в последнем случае как бы учитывается возможное отличие поверхностного натяжения от капельного при меньших деформациях). При этом получаются практически такие же результаты, что и описанные выше, если только параметры таковы, что они соответствуют такой же качественной картине. В частности, основную роль играет переход к классике в смысле исчезновения деформирующих сил при некоторой деформации. В этих более сложных вариантах приходится вводить большее число параметров. Однако даже для качественного согласия с опытом необходимо вводить переход к классике, причем α^* должно быть меньше 0,3—0,5, и этот эффект оказывается самым важным. Возникающая при этом в переходной области "жесткость" всегда по крайней мере столь же велика, как и другие возможные отклонения от "капельной" жесткости.

О возможных изотопических поправках в капельной модели порогов деления

Обычно в капельной модели предполагается, что поверхностное натяжение не зависит от изотопического состава ядра. В капельной модели потенциальной энергии могут возникать поправки, зависящие как от формы ядра, так и от изотопического состава, соответствующие члену $\sigma_{AS}(N-Z)^2/A^2$ в массовой формуле (см., напр., [18,19][1]. Эти поправки можно учесть, изменив величину поверхностного натяжения. Для этого нужно взять

$$E_s = \sigma_0\left[1 - \frac{\sigma_{AS}}{\sigma_0}\left(\frac{N-Z}{A}\right)^2\right]A^{2/3}, \qquad (16)$$

причем оказывается, что $(\sigma_{AS}/\sigma_0) \approx 3$. Вместо этого можно изменить определение параметра делимости, взяв вместо (Z^2/A)

$$\xi = \frac{Z^2}{A}\left[1 + 3\left(\frac{N-Z}{A}\right)^2\right] \qquad (17)$$

и увеличив величину $\xi_{крит}$ по сравнению с $(Z^2/A)_{кр}$ приблизительно на 14% в соответствии с масштабом поправки в квадратных скобках в (16). Таким образом получается, что $\xi_{крит} \approx 52$ при $(Z^2/A)_{крит} = 45$. Такая замена "параметра делимости" не устраняет полностью разброс экспериментальных значений на графиках, связанных, по-видимому, с другими причинами, в том числе, рассмотренными выше. Однако при этом расположении экспериментальных точек все же несколько упорядочивается. Это связано с тем, что величина ξ, определенная согласно (16), изменяется примерно так же, как и Z^2/A в зависимости от Z, но практически не меняется для разных изотопов одного и того же элемента (т.е. вблизи линии β-стабильности).

К сожалению, данные о делении слабо возбужденных ядер еще не позволяют утверждать, что такой изотопический эффект в поверхностном натяжении действительно существует. Данные же для большой энергии согласуются с предположением, что величиной, определяющей основные

[1] См. также частное сообщение А.С. Тяпина. Автор выражает признательность А.С. Тяпину за обсуждение этих вопросов.

свойства деления, является именно Z^2/A, а не ξ (см., напр., [8–10]). Это означало бы, что изотопический эффект в поверхностном натяжении исчезает при нагревании, как и другие квантовые эффекты.

Микроскопическая модель

Существенные отклонения от капельной модели при малых деформациях связаны с неоднородностями распределения плотности нуклонов, вызванными оболочками. Этот эффект учитывается, как поправка к классической капельной модели. Микроскопическое рассмотрение приводит к выражению для поправки такого же вида, как (4), однако в предэкспоненте имеется постоянное слагаемое:

$$W_1 = -(V_0 + \kappa\alpha)\, e^{-(\alpha/\alpha^*)^2}$$

При условии, что $V_0 > 0$, остаются в силе все основные результаты, описанные выше.

ЛИТЕРАТУРА

[1] СТРУТИНСКИЙ В.М., ТЯПИН А.С., ЖЭТФ 45 (1963) 960.
[2] BOHR Aa., MOTTELSOHN B., Mat. Fys. Medd. Dan. Vid. Selsk, 27, n. 16 (1953).
[3] BELYAEV S.T. Mat. Fys. Medd. Dan. Vid. Selsk, 31, n. 11, 1959.
[4] ПРЕСТОН М.А. Физика ядра, изд. Мир, 1964.
[5] BES D.R., SZYMANSKI Z. Nucl. Phys., 28, 42 (1961).
[6] SZYMANSKI Z. Nucl. Phys., 28, 63 (1961).
[7] СТРУТИНСКИИ В.М. Доклад "Угловая анизотропия деления и форма ядра в седловой точке" на Международной конференции по физике деления ядер в г. Зальцбурге, 1965.
[8] HUIZENGA J. et al. Preprint 1964.
[9] ХАЛПЕРН И., Деление ядер, Физматгиз, 1962.
[10] HUIZENGA J.R., VANDENBOSCH R. Nucl. Reacts, v. II, Amsterdam, 1962.
[11] HILL D., WHEELER J., Phys. Rev., 89 (1953) 1102.
[12] JOHANSSOHN S. Nucl. Phys., 12 (1959) 449.
[13] SWIATECKI W, Proc. of the UN Symposium on Nucl. Masses, Vienna, 1963.
[14] ПОЛИКАНОВ С.М. и др. ЖЭТФ 42 (1962) 1464.
[15] ДРУИН А.В. и др., препринт ОИЯИ Д-1693 (1964).
[16] VANDENBOSCH R., FIELDS P.R., VANDENBOSCH S.E., METHA D. J. Inorg. Nucl. Chem., 26 (1964) 219.
[17] SWIATECKI W. Phys. Rev., 101, 651, 104 (1956) 993.
(см. также в сб. Физика деления ядер. Госатомиздат, 1963).
[18] СТАВИНСКИЙ В., ЖЭТФ 42 (1962) 1614.
[19] WILETS L. Theories of Nucl. Fission, Oxford, 1964.

FISSION CROSS-SECTIONS, THRESHOLDS, RESONANCES

(Sessions II and III)

Review Paper

CROSS-SECTIONS FOR LOW-ENERGY NEUTRON-INDUCED FISSION

E. R. RAE
ATOMIC ENERGY RESEARCH ESTABLISHMENT,
HARWELL, DIDCOT, BERKS., UNITED KINGDOM

Abstract — Résumé — Аннотация — Resumen

CROSS-SECTIONS FOR LOW-ENERGY NEUTRON-INDUCED FISSION. The cross-sections of the heavy nuclei for neutron-induced fission are of fundamental importance to the technology of nuclear energy production. The manner in which these cross-sections vary with the neutron energy and with the mass and charge of the target nuclei also provides much information on the structure of heavy nuclei. In the case of a thermally fissile target nucleus, as the neutron energy is increased from thermal the cross-section first exhibits an inverse velocity dependence, followed by a region in which sharp resonance peaks appear, and finally a continuum region where the cross-section exhibits relatively smooth steps and breaks. All these phenomena can be explained in principle, but certain features of the data have proved very difficult to explain quantitatively.

Recent cross-section measurements, stimulated by the needs of reactor technology, have concentrated on improving the energy resolution and accuracy of the data on fuel materials, and this has led to a more detailed study of the resonance region, which is of considerable interest for reactor Doppler effect calculations. More accurate measurements at rather higher energies have established the existence of appreciable fission cross-sections below the so-called fission threshold in certain cases. Careful measurements of this nature have in turn stimulated interest in the interpretation of the cross-sections in terms of nuclear models on a firm quantitative basis.

This paper outlines the main features of neutron-induced-fission cross-sections and their interpretation. Some emphasis is placed on recent improvements in the quality of the measurements and in attempts at quantitative interpretation of certain aspects of the data.

SECTIONS EFFICACES DE FISSION POUR DES NEUTRONS DE FAIBLE ÉNERGIE. Les sections efficaces de fission des noyaux lourds ont une importance essentielle pour la technologie de la production d'énergie d'origine nucléaire. La manière dont ces sections efficaces varient selon l'énergie des neutrons et selon la masse et la charge des noyaux cibles fournit également de nombreux renseignements sur la structure des noyaux lourds. Dans le cas d'un noyau cible susceptible de fission thermique, lorsque l'énergie des neutrons augmente, la section efficace présente d'abord des variations inversement proportionnelles à la vitesse, puis une région où des pics de résonance aigus apparaissent, et en dernier lieu une région de continu caractérisée par des variations relativement régulières. Tous ces phénomènes peuvent recevoir une explication théorique, mais il semble très difficile d'expliquer quantitativement certaines caractéristiques des données.

Lors de mesures récentes de sections efficaces destinées à répondre aux besoins de la technologie des réacteurs, les chercheurs se sont surtout efforcés d'améliorer la résolution en énergie ainsi que la précision des données relatives aux combustibles; ils ont été ainsi amenés à étudier plus en détail la région de résonance qui a un grand intérêt pour les calculs de l'effet Doppler dans les réacteurs. Des mesures plus précises à des niveaux d'énergie assez élevés ont fait apparaître dans certains cas l'existence de sections efficaces de fission assez importantes en dessous du seuil d'énergie de fission. Ces mesures ont ensuite appelé l'attention des chercheurs sur l'interprétation des sections efficaces en fonction de modèles nucléaires qui reposent sur des données quantitatives sûres.

Le mémoire expose les principales caractéristiques des sections efficaces de fission par neutrons et en donne une interprétation. Il met l'accent sur les améliorations qui ont récemment été apportées à la qualité des mesures et aux essais d'interprétation quantitative de certains aspects des données recueillies.

СЕЧЕНИЯ ДЕЛЕНИЯ, ВЫЗВАННОГО НЕЙТРОНАМИ НИЗКОЙ ЭНЕРГИИ. Изучение сечений деления тяжелых ядер, вызванного нейтронами, имеет решающее значение для технологии производства ядерной энергии. Характер изменения величины сечений в зависимости от энергий нейтронов, массы и заряда ядер мишени также дает значительную информацию от-

носительно структуры тяжелых ядер. В случае термически делящегося ядра мишени, по мере увеличения энергии нейтронов, величина сечения проявляет вначале обратную зависимость от скорости, сменяемую областью, в которой появляются острые пики резонансов и, наконец, сплошной областью, в которой величина сечений сравнительно плавно то увеличивается, то уменьшается. Все эти явления можно в принципе объяснить, однако, некоторые характеристики данных оказались очень трудными для количественной интерпретации.

Во время последних измерений сечений, вызванных потребностями реакторной техники, внимание было сосредоточено на улучшении разрешения энергии и точности получаемых данных относительно топливных материалов. Это привело к более подробному изучению резонансной области, которая представляет значительный интерес при расчетах эффекта Доплера для реакторов. В результате более точных измерений при довольно повышенных энергиях выявлено наличие в некоторых случаях значительных величин сечений деления ниже так называемого порога деления. Тщательные измерения такого характера, в свою очередь, породили интерес к интерпретации сечений с точки зрения ядерных моделей на твердой количественной основе.

Намечаются основные черты сечений деления, вызванного нейтронами, и их интерпретации. Некоторый упор делается на последние усовершенствования в качестве измерений и на попытки количественной интерпретации некоторых аспектов данных.

SECCIONES EFICACES EN LA FISION INDUCIDA POR NEUTRONES DE BAJA ENERGIA. Las secciones eficaces de fisión, inducida por neutrones, de los núcleos pesados son de fundamental importancia para la tecnología de la producción de energía nuclear. Asimismo, la manera en que estas secciones eficaces varían según la energía neutrónica y la masa y carga de los núcleos tomados como blanco, proporciona abundante información sobre la estructura de los núcleos pesados. En el caso de un blanco constituído por un núcleo susceptible de fisión por bombardeo con neutrones térmicos, a medida que la energía aumenta y pasa de la zona térmica a niveles superiores, se observa que la sección eficaz varía primero en forma inversamente proporcional a la velocidad, abarcando después una región en la que aparecen picos de resonancia pronunciados, para llegar finalmente a una zona en que se presentan escalones de escasa pendiente y algunas discontinuidades. En principio, es posible explicar todos estos fenómenos, pero ciertos aspectos de los datos resultan sumamente difíciles de interpretar en sus aspectos cuantitativos.

En los últimos tiempos, los trabajos de medición de secciones eficaces, estimulados por los imperativos de la tecnología de reactores, tienden sobre todo a mejorar el poder resolutivo en energía y la precisión de los datos sobre materiales combustibles, lo que ha tenido como resultado un estudio más a fondo de la región de resonancia, que es de gran interés para el cálculo del efecto Doppler en los reactores. Una serie de mediciones más precisas, efectuadas a energías bastante elevadas, han puesto de manifiesto la existencia en ciertos casos, de apreciables secciones eficaces de fisión por debajo del denominado umbral de fisión. A su vez, las mediciones meticulosas de esta índole han estimulado el interés por la interpretación de las secciones eficaces en función de modelos nucleares sobre una base cuantitativa bien asentada.

En la memoria se exponen las principales características de las secciones eficaces con cierto detenimiento los recientes perfeccionamientos de las técnicas de medición y las tentativas de interpretar cuantitativamente ciertos aspectos de los datos.

MAIN FEATURES OF NEUTRON-INDUCED FISSION

Introduction

Neutron-induced fission is a phenomenon of special importance in any study of the nuclear properties of the heavy elements. The first fission events to be observed were caused by the bombardment of uranium with neutrons, and the whole of nuclear reactor technology is based on this reaction. This technological interest in the fission cross-sections of the heavy nuclei has led to very careful studies; the data available must be among the

best in the field of nuclear cross-sections, and these data are being continually improved as more intense neutron sources and better detectors and electronics are developed.

Apart from the purely technological interest in the cross-sections of the heavy nuclei, the neutron interaction provides a tool of unique power in the study of the fission process over a considerable range of excitation energies. In particular, because of the absence of an electrostatic barrier and the precision with which the energy of slow neutrons can be measured, it is possible to study with this reaction the fission of heavy nuclei from individual excited states whose spin and parity can, at least in principle, be determined.

The question of the discrete resonances seen in slow neutron-induced fission will be discussed later, but firstly a broad survey will be made of the general features of the neutron cross-sections and their significance.

Thresholds and channels

Since the ideas of the fission threshold and fission channels are fundamental to a description of the cross-section curves, a digression will be made to consider what is meant by these terms. Basically a nucleus is at the threshold of fission when it has been sufficiently excited for fission to become energetically possible. This is illustrated graphically in Fig. 1

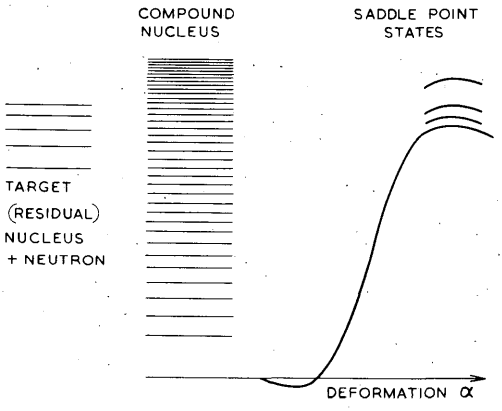

Fig. 1

Energy diagram for fission

where the potential energy of the ground state of a heavy nucleus is shown as a function of a deformation parameter α. (Any general description of the deformation of a spherical nucleus would require many parameters. For simplicity a single parameter is assumed that describes a route to the critical deformation with the potential energy always minimized.) As the nucleus is progressively deformed, energy must be added to it until a critical stage is reached beyond which an increase in deformation leads to a decrease in potential energy and a spontaneous separation into two fragments. On the liquid drop model the initial rise in the potential curve is due to work being

done against the surface tension forces, the electrostatic repulsion of the charge helping with the process. Beyond the summit of the potential energy curve the surface tension forces have been weakened by the constriction of the drop at its centre, and the electrostatic forces are now strong enough to drive the two ends of the distorted nucleus apart and finally to break them into two fragments. On this model, a spherical nucleus will undergo fission spontaneously if the ratio of its electrostatic energy to its surface energy exceeds a critical value, i.e. if Z^2/A exceeds a critical value.

Returning to Fig. 1, it is clear that if the nucleus under discussion is somehow excited to an energy that exceeds the height of the potential barrier, then this energy will have a finite probability of being concentrated into deforming the nucleus, and fission can occur. The energy may be added by any suitable interaction including the absorption of a neutron by an adjacent lighter isotope, in which case, provided the barrier height is greater than the binding energy of the neutron, the fission threshold will show as a sharp rise from zero in the fission cross-section. Potential barriers in quantum mechanical systems do not, of course, give rise to infinitely sharp changes in the probability that a process will occur, and the fission barrier can be penetrated even when the excitation energy is less than the barrier height. HILL and WHEELER [1] have related the probability of fission, expressed as a mean fission width $\langle \Gamma_F \rangle$, to the difference between the excitation energy and the barrier height, and have shown that

$$\frac{2\pi \langle \Gamma_F \rangle}{D} = \frac{1}{1 + \exp\{2\pi(E_F - E)/\hbar w\}} \tag{1}$$

where D is the level density in the compound nucleus, E_F is the height of the barrier, E is the excitation energy and w is measure of the barrier thickness. (w is the circular frequency associated with collective vibrations of the compound nucleus about the transition point with the sign of the deformation potential reversed.) $\hbar w$ is characteristically $\lesssim 1$ MeV.

This barrier penetration effect leads to a rather smooth step in $\langle \Gamma_F \rangle$ as the barrier is passed, $\langle \Gamma_F \rangle \to D/2\pi$ well above the barrier. Since the fission cross-section is related to the total cross-section for compound nucleus formation by the ratio,

$$\frac{\sigma_F}{\sigma_T} \approx \left\langle \frac{\Gamma_F}{\Gamma_F + \Gamma_n + \Gamma_\gamma} \right\rangle \tag{2}$$

it can be seen that in an energy region where the total cross-section is nearly constant, this leads to a similar smooth step in the fission cross-section, provided Γ_n and Γ_γ do not change appreciably over the region. All the discussion so far has ignored the fact that nuclear states have certain constants associated with them, in particular spin and parity. When these are taken into account, the concept of a fission channel (BOHR [2], WHEELER [3]) emerges, and the separate excited states of the fissioning nucleus as giving rise to separate and distinct potential barriers must be considered. This can be shown diagrammatically (Fig. 1) by drawing a series of excited states,

at the barrier, each state having definite spin and parity. If now the nucleus is excited so that fission can occur, in order to estimate $<\Gamma_F>$ the question must be asked what is the spin and parity of the state formed, since only the appropriate fission channels (states of corresponding spin and parity at the barrier) will contribute to the fission process in this case. The expression for $<\Gamma_F>$ now becomes

$$\frac{2\pi<\Gamma_F^{J,\pi}>}{D} = \sum_{\lambda} \frac{1}{1+\exp\{2\pi(E_{F,\lambda}^{J,\pi} - E)/\hbar w\}} \qquad (3)$$

the sum being over all states of appropriate spin and parity, at the barrier. The fission width would thus be expected to increase in a series of smooth steps with increasing excitation energy as successive channels become accessible. This complication in the picture destroys the simple concept of a threshold for the fission process, since there are clearly a series of "thresholds" corresponding to the opening of successive channels, and these may be closely spaced so that the individual steps are not observed. The term threshold is however frequently used to describe the steps actually observed in the fission cross-section curves, the threshold being taken as half-way up the rise, even although the observed rise may well be due to the opening of several fission channels. Before returning to the main subject of the discussion, it should be noted that as the excitation energy of the nucleus is increased, not only do fission channels open, but also neutron channels, as more and more levels in the residual nucleus become accessible to neutron emission (Fig. 1). The increases in the neutron width $<\Gamma_n>$ corresponding to the opening of these channels give rise to downward steps in the fission cross-section curves (Eq. 2). The radiation width changes only slowly with energy, and so the behaviour of the fission cross-section curve with increasing excitation energy is dominated by the competition between neutron emission and fission, and finally by the ratio of the level densities in the residual nucleus and the compound nucleus at the saddle point (fission barrier).

Fission cross-sections

Some real fission cross-section curves will now be examined in the light of the above discussion. Figure 2, taken from HENKEL [4], shows the curves for a number of heavy nuclei having $Z > 90$. The first obvious feature is that while most of the curves show a threshold type of behaviour, three of them, corresponding to U^{233}, U^{235} and Pu^{239}, do not, and their cross-sections actually rise at low neutron energies where the cross-section for compound nucleus formation increases as the neutron wavelength begins to exceed the nuclear dimensions. A closer inspection shows that all the nuclei showing threshold behaviour possess an even number of neutrons, and all those fissionable by slow neutrons an odd number. This then is a manifestation of the pairing effect on the binding energy of the added neutron, odd targets receiving ~ 1 MeV more excitation energy than even ones. The question of whether or not a nucleus is fissionable by slow neutrons depends on whether or not the binding energy of the last neutron exceeds the height

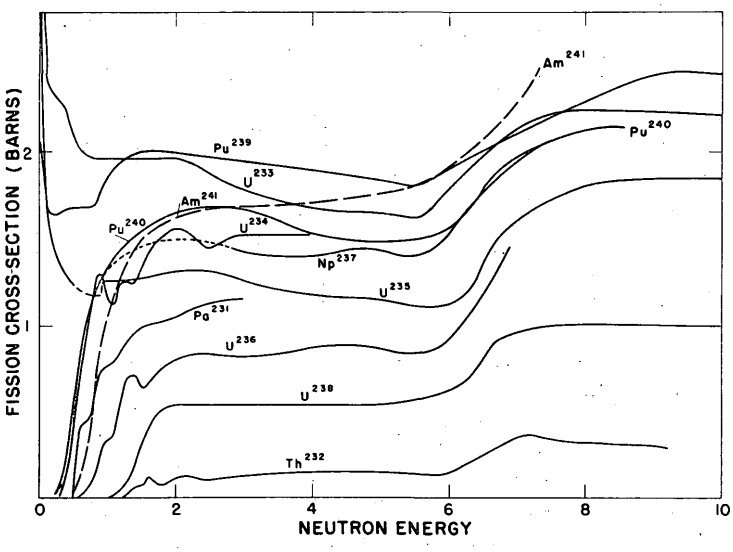

Fig.2

Compilation of fission cross-section curves for 11 nuclei [4]

of the fission barrier, and since for the nuclides shown in Fig.2 these two quantities are of the same order, the pairing effects are in those cases critical in determining the sign of the difference. The effect of pairing energy on the barrier height itself also contributes to this process, and accentuates the odd-even difference (HYDE [5]). This rule about the fissionability of nuclei of even and odd N is of course only valid over a restricted range of Z and N. No fission by slow neutrons has been observed for nuclei having $Z < 90$ since the fission barrier is here significantly greater than the neutron binding energy for both odd and even N. Likewise there are a few neutron-light isotopes of elements having $Z > 90$ where the barrier is low enough (high Z^2/A) and the neutron binding energy high enough to give fission by slow neutrons of isotopes of even N. A case in point is U^{232} that has a high binding energy (5.8 MeV) for an extra neutron, and where JAMES [6] has measured the resonance fission cross-section and reports a value of $2\pi \langle \Gamma_F \rangle / D \approx 0.3$ indicating that the fission threshold, if not actually at negative neutron energy, certainly lies below about 100 keV.

The second most obvious feature of the curves is the second step (first step for the nuclides that are fissionable with slow neutrons) that occurs in each case at a bombarding energy of about 6 MeV. This is, of course, the threshold for "second chance fission" where the compound nucleus can emit a neutron and the residual nucleus still possesses sufficient excitation to undergo fission. If the neutron energy is further increased, a third step is observed at about 12 or 13 MeV, corresponding to the emission of two neutrons followed by fission, and so on. In the case of U^{238}, three such steps are clearly seen with the suggestion of a fourth (n, 3 nF) near 19 MeV.

Several of the cross-section curves show fine structure close to the first threshold, which is surely due to the interplay between successive fission

channels, and neutron emission to levels in the residual (target) nucleus as discussed earlier. Even the apparently smooth rise in the U^{238} cross-section between 1 and 2 MeV, when looked at with high resolution, shows a step-like behaviour, and several of these steps appear to be associated with known levels in U^{238}.

Finally there is the relatively flat region of cross-section for each of the curves between the first and second thresholds. This flatness implies a nearly constant value for $<\Gamma_F>/<\Gamma_n>$ which requires that the level densities in the target nucleus and in the compound nucleus at the saddle point increase with energy in a similar manner. This in turn is because of the near equality of the neutron-binding energy and the excitation energy of the fission barrier. The actual level of these plateaus depends on the difference between these two energies, the level in general decreasing as the threshold energy for fission increases. The ratio $<\Gamma_F>/<\Gamma_n>$ for an excitation energy of about 3 MeV (mid-point of first plateau) in general increases with Z^2/A as one might expect, but the correlation is not simple. BARSCHALL [7] has pointed out that if the fission cross-section at 3 MeV is plotted against $Z^{4/3}/A$, a much better correlation is obtained, as shown in Fig. 3.

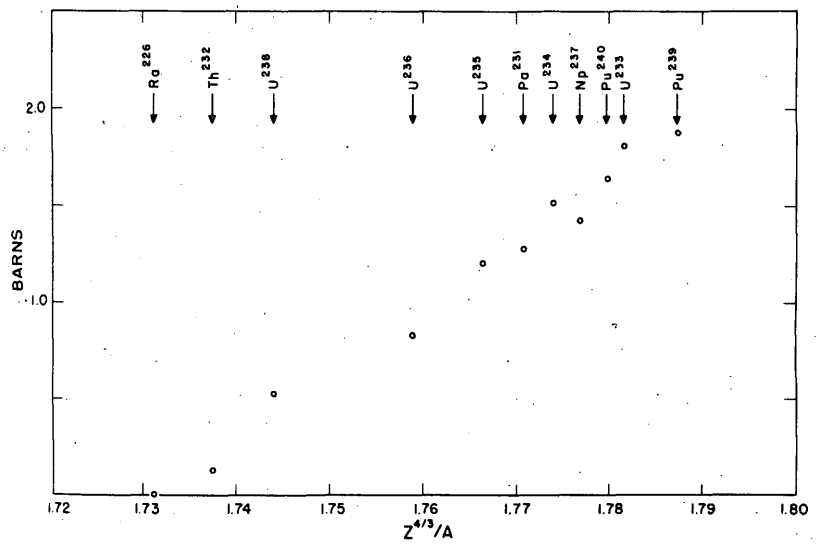

Fig. 3

Fission cross-sections at 3 MeV neutron energy as function of $Z^{4/3}$ A [7]

SUB-THRESHOLD FISSION

Recent careful measurements of fission cross-sections [8] have revealed the existence of small nearly constant cross-sections below the obvious threshold for a number of nuclides, and these observations at first glance appear to contradict the expected exponential increase in $<\Gamma_F>$ with excitation energy well below the threshold. The explanation, of course, lies in the fact that the cross-section for neutron-induced fission is

not simply proportional to $<\Gamma_F>$, but depends on competition with neutron emission and radiation, and what is more important, is also proportional to the total cross-section for compound nucleus formation that increases with decreasing neutron energy in the region below a few hundred keV. This increase in the compound nucleus cross-section tends to offset the decrease in $<\Gamma_F>$ with decreasing neutron energy, and indeed the surprising thing about the observed sub-threshold fission is not so much its existence, as its absence at thermal neutron energies for most nuclides with thresholds below

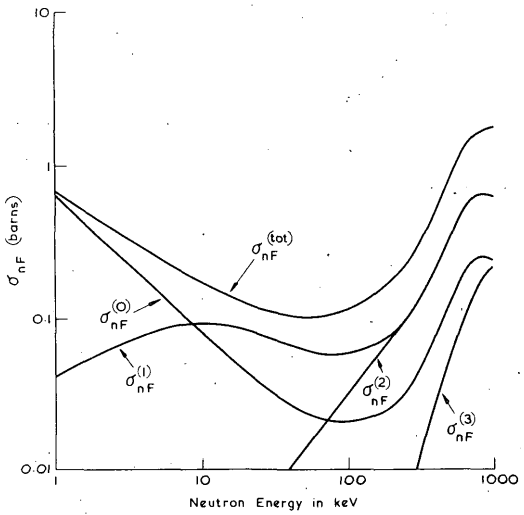

Fig. 4

Sub-threshold fission cross-section for even-even target nucleus, calculated from

$$\sigma_{nF} = \pi\lambda^2 \sum_{1} \frac{(21+1)\, T_n\, {}^{1}T_F}{T_n^1 + T_F + T_\gamma}$$

where $T = 2\pi\Gamma/D$, $T_F = \dfrac{1}{1 + \exp\{2\pi(E_F - E)/\hbar w\}}$

$E_F = 700$ keV, $\hbar w = 650$ keV

Inelastic scattering is ignored

about 1 MeV. Figure 4 shows the result of a simple calculation of the expected fission cross-section for an even-even target nucleus having a threshold at 700 keV corresponding to one channel for each value of J and π of the compound nucleus states formed, and a value of $\hbar w$ (Eq. (1)) of 650 keV. The radiation width $<\Gamma_\gamma>$ is taken to be 20 MeV and the level spacing 20 eV, and inelastic scattering, which would not affect the cross-section below about 50 keV, is ignored in the interest of simplicity. It will be seen that one would not only expect to observe sub-threshold fission, but would expect the cross-section to rise rapidly below 10 keV corresponding to a mean fission width at low energies of ≈ 4 MeV, which would mean that a considerable fraction of the thermal cross-section might be expected to be due to

fission. This anomaly was pointed out by WHEELER [9] in 1956 for the case of Pu^{240}, long before the sub-threshold fission had been observed, and he noted that either the fission width of the level at 1 eV (mainly responsible for thermal fission) that had been measured by LEONARD [10] to be $\approx 10^{-2}$ MeV was exceptionally small, or else s-wave fission that is responsible for the large cross-sections below 10 keV was forbidden. Later measurements by BROOKS and JOLLY [11] showed that the mean fission width for the resonances up to 120 eV was $\lesssim$ 0.6 MeV, which tended to favour Wheeler's second explanation, and the possibility that s-wave-induced fission is forbidden must be taken seriously. In this case, a glance at the partial wave cross-sections in Fig. 4 shows that the sub-threshold fission of $\approx$ 100 mb observed for Pu^{240} is almost certainly due to the p-wave interaction, and corresponds to a negative

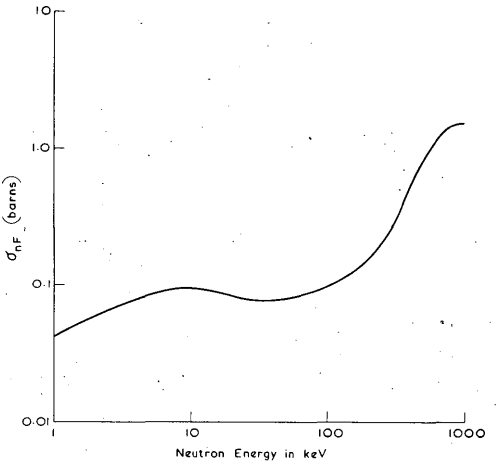

Fig. 5

Calculated sub-threshold fission cross-section for an even-even target nucleus with s-wave-induced fission inhibited

parity barrier state. Figure 5 shows the type of cross-section curve one would expect on omitting the s-wave interaction, and this is very similar to the type of curve actually observed in sub-threshold fission. The elimination of the s-wave component implies that the first barrier state of $\frac{1}{2}+$ character must lie at least 500 keV above the negative parity state. A detailed fit to the Pu^{240} data, including the effect of inelastic scattering, is given in a contribution to this Symposium by de Vroey, Ferguson and Starfelt[1].

If we attempt to calculate a thermal fission cross-section for a number of nuclides with thresholds below 1 MeV, we are led to the surprising result that in nearly all cases the observed cross-section is much smaller than one would expect. Table I contains observed thermal fission cross-sections of six nuclides with thresholds below 1 MeV, together with a calculated cross-section based on the simple relation

[1] DE VROEY, M., FERGUSON, A.T. and STARFELT, N., "The fission cross-section of Pu^{240} for 0.03-2.0 MeV neutrons", these Proceedings I.

$$\sigma_{nF}\ (\text{thermal}) \approx \frac{\langle \Gamma_F \rangle}{\langle \Gamma_F \rangle + \langle \Gamma_\gamma \rangle}\ \sigma_{Abs}\ (\text{thermal})$$

where

$$\langle \Gamma_F \rangle = \frac{D}{2\pi}\ \exp\left(\frac{-2\pi E_F}{\hbar w}\right)$$

E_F being the threshold energy.

$\hbar w$ was taken as 650 keV, Γ_γ as 20 MeV for the even isotopes, 40 MeV for the odd ones, and D was taken from BNL 325 except for Pa^{231} and Np^{237}, where

TABLE I

CALCULATED AND OBSERVED THERMAL FISSION CROSS-SECTIONS

Nucleus	E_F	σ_{nF} (thermal)	
		Calculated	Observed
Pa^{231}	650	2.5	0.010
U^{234}	550	25	$\leq$ 0.65
U^{236}	1000	0.2	-
Np^{237}	650	1.3	0.019
Pu^{240}	700	50	~0.05
Am^{241}	900	0.5	3.13

a value of 1 eV was assumed. The observed thermal cross-sections were taken from the compilation of HYDE [5]. It will be noted that only Am^{241} has a thermal cross-section consistent with allowed s-wave fission and a value of $\hbar w$ of 650 keV. The others show thermal cross-sections on the average a factor of 100 too low implying either forbidden s-wave fission or else a barrier corresponding to $\hbar w \lesssim 400$ keV. Such a thick barrier is inconsistent with observed p-wave fission and with most observations of the shape of the cross-section curves near threshold. It is, of course, close to the value obtained from spontaneous fission half-lives, but this is expected to yield a low value of $\hbar w$ because of the departure from a parabolic barrier shape at low excitation energies [12].

Calculations by JOHANSSON [13] of the position of shell model states in a potential well distorted to an extent corresponding to the fission barrier predict the order of the threshold states for the even-even heavy target nuclei (even-odd compounds) (Fig. 6). Johansson's calculations for U^{234}, U^{236} and Pu^{240} targets appear to predict that in each case the first state accessible to s-wave fission ($\frac{1}{2}$+) lies $\gtrsim$ 500 keV above the first threshold. We would there-

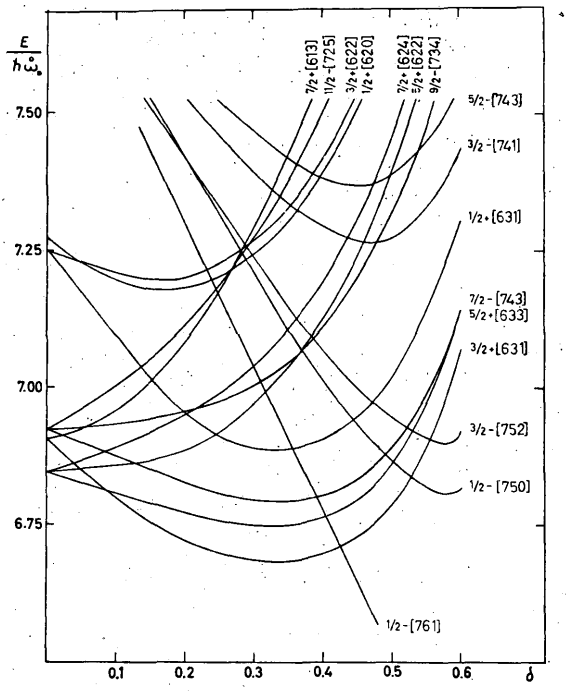

Fig. 6

Neutron levels for neutron numbers from 139 to 160. Spin, parity, and the asymptotic quantum numbers N, n_z and Λ are written beside each level.

fore expect s-wave fission to be inhibited for each of the three even-even nuclides studied, while the existence of low-lying $\frac{1}{2}$- and 3/2- states allows measurable sub-threshold fission. For the three odd-even target nuclides no prediction can be made, but it would seem reasonable to assume that even and odd parity lowest threshold states would be equally likely, in which case one might expect some inhibition of the s-wave fission in at least 50% of these cases. Recent measurements of the resonance fission cross-sections of U^{232} and Pu^{238}, which are discussed in a paper by James[2], indicate that these two nuclides also follow the shell model predictions of Johansson, s-wave fission being inhibited by a factor ~ 60 in Pu^{238} and appearing strongly in U^{232} only because of the high binding energy of the added neutron and the low fission barrier that presumably is located several hundred keV below the neutron binding energy. This means that the $\frac{1}{2}$+ state has moved down to a low positive neutron energy, and the observed value of $N_{effective} = 2\pi \langle \Gamma_F \rangle / D$ suggests that it lies below about 100 keV. It will be interesting to see whether the fission cross-section of this nuclide when measured shows any sign of such a threshold.

[2] JAMES, G. D., "Fission cross-section measurements on Pu^{239}, Pu^{241}, U^{232}, and a search for fission components in Pu^{238} resonances", these Proceedings I.

It would seem, therefore, that the observed behaviour of the fission cross-sections below threshold can be understood on the basis of the channel theory of fission and the nuclear shell model, suitably modified for a highly distorted potential well. It would be foolish to pretend that no problems remain. An alternative arrangement has been suggested [14] to explain the

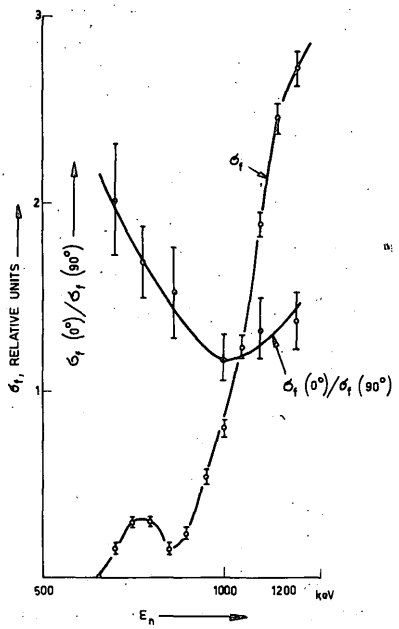

Fig. 7

Fission cross-section for Th^{230} [15]

variation with energy of the angular distributions of the fragments from neutron-induced fission of even-even targets, and one has only to look at the odd shape of the sub-threshold fission curve for Th^{230}, for example, which shows a peak in the cross-section at about 750 keV (Fig. 7[15]), to realize that further careful study is needed.

RESONANCE CROSS-SECTIONS

It is in the study of the resonance cross-sections that neutron-induced fission provides information of a detailed type that cannot be obtained in any other way. The growth of the power of neutron velocity selectors has led to the situation where a study can be made of so-called individual "resonances" in the cross-sections of Pu^{239} + n for example, up to a neutron energy of several hundreds of electron volts that represents over 100 resonances. A part of the fission cross-section as measured by DE SAUSSURE et al. at Saclay [16] is shown in Fig. 8, and measurements of even higher resolution are in progress in other laboratories. The angular momenta of a number

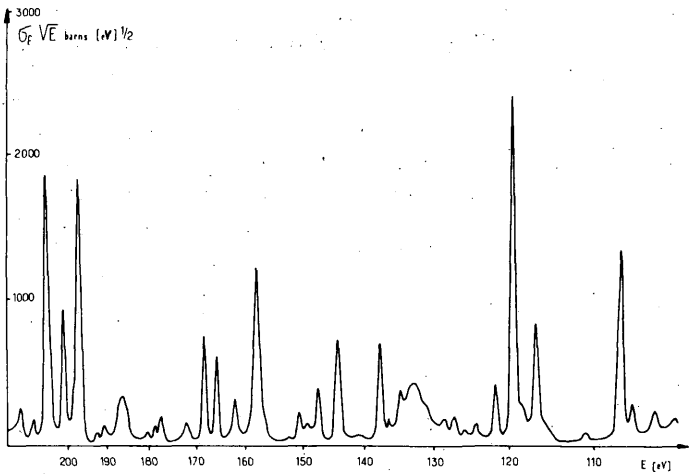

Fig. 8

Fission cross-section for Pu^{239} from 100 - 210 eV [16]

of resonances in Pu^{239} have been determined by neutron scattering measurements[17], and detailed fits have been made to the low-energy cross-sections of several fissile nuclides using many level formalisms that take into account interference effects between the broad fission levels [18]. Despite the steady improvement in the data, however, certain features of the results have been difficult to reconcile with theoretical ideas that are extremely successful in explaining the results of closely related experiments.

Perhaps the most important difficulty concerns the mean fission widths. Deuteron stripping experiments by NORTHROP, STOKES and BOYER [19], which effectively insert neutrons of negative energy into the target nucleus, indicate that the fission thresholds for U^{233}, U^{235} and Pu^{239} lie between 1 and 2 MeV below the neutron binding energy. Since these nuclei all form even-even compounds, the lowest threshold state would be expected to be of 0+ character with a closely spaced rotational band built on this state, and with vibrational states with their rotational bands also appearing within the first MeV of excitation. One would therefore expect several fission channels to be open for s-wave neutrons giving values of N_{eff} of at least 1 or 2. Measurements of the distribution of the fission widths observed in the resonances of these three nuclides suggest that these curves are best fitted by members of the χ^2 family having up to four degrees of freedom corresponding to the existence of up to four fission channels. The experimental values of N_{eff}, however, range from 0.18 to 0.65, and appear to be surprisingly low.

A second difficulty, especially in the case of U^{233}, is the existence of a rather large slowly varying cross-section underlying the resonance structure, which is difficult to explain in terms of normal distributions of parameters.

The third difficulty is that Γ_γ apparently fluctuates from resonance to resonance by up to a factor of 3 [20], in contrast to the rather small fluctuations $\lesssim$ 10% to be expected from heavy nuclei with close level spacing. (Such small fluctuations are indeed observed for those heavy nuclei like Th^{232} and U^{238} that are not fissionable by slow neutrons).

The final difficulty is the shape of the distribution curve for the level spacings, which shows strong level repulsion and seems to correspond to that expected for a single population (even-even target) instead of the two population distribution (with a finite probability of zero spacing) expected for these even-odd nuclei [21] that form levels of spins $I \pm \frac{1}{2}$ with s-wave neutrons, where I is the spin of the target nucleus.

Recently, however, LYNN appears to have thrown some light on this situation [22]. He was working on a multi-level fitting programme, and studying the behaviour of two interfering levels, when he generated the example shown in Fig. 9a. This example arose in a first selection of random level

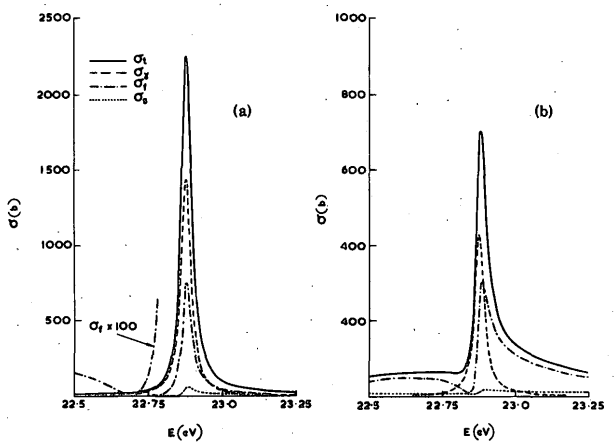

Fig. 9

Parameters for (a) are: $E_1 = 22.81$ eV, $(\Gamma_{1n}^0)^{1/2} = 0.159$ (MeV)$^{1/2}$, $(\Gamma_{1f})^{1/2} = -0.728$ (eV)$^{1/2}$, $\Gamma_\gamma = 0.025$ eV, $E_2 = 22.92$ eV, $(\Gamma_{2n}^0)^{1/2} = 0.384$ (MeV)$^{1/2}$, $(\Gamma_{2f})^{1/2} = 0.574$ (eV)$^{1/2}$. In (b) there is a change of sign of one reduced width amplitude [22].

parameters for 20 levels, generated from the usual distributions of spacings and widths assuming $N_{eff} = 1$. The curves in the figure may not appear to be remarkable until one realizes that the single sharp peak seen is in fact due to two levels 110 MeV apart having fission widths of 552 MeV and 332 MeV, radiation width of 25 MeV, and neutron widths of 0.12 and 0.71 MeV respectively. One fission channel is assumed, and constructive interference takes place between the levels. The result is a single narrow peak whose neutron width is very nearly the sum of the neutron widths of the component levels, i.e. most of the cross-section is in the peak, but whose total width corresponds to a fission width of only 14 MeV. Thus two levels of very large fission width have disappeared and a single "resonance" of small fission width has replaced them. The obvious question is whether reversing the sign of one reduced fission width amplitude and producing destructive interference between the levels would perhaps create the opposite effect. This is partly true, as shown in Fig. 9b, since now a part of the cross-section appears as a background that might be interpreted as a very wide level. The remainder of the cross-section, however, still appears as a sharp narrow peak, as before. Thus in both cases narrow "resonances" have been generated from the interference between two broad levels.

This result prompted Lynn to postulate that perhaps the disparity between the experimental fission widths and the Bohr theory arose out of a false interpretation of the cross-section curves. Some of these interpretations were frankly single level in nature, as was his interpretation of the single peak in Fig. 9. Others, such as the analyses of MOORE and REICH, and VOGT [18], were of multilevel nature, and allowed interference, but nevertheless associated levels with the experimentally observed peaks, except where extreme fitting difficulty occurred. Lynn's suggestion is that if the Bohr theory is correct, then the interference effects are much stronger than was supposed (with $N_{eff} = 1$ the probability of the sum of two fission widths being larger than the level spacing is 12%) so that the peaks observed in the experimental cross-section curves may show little correspondence with the true levels.

To test his hypothesis, Lynn did a calculation involving two spin states. In this case the probability of overlap of levels is even higher owing to the absence of level repulsion. He chose neutron widths from a Porter-Thomas distribution ($\nu = 1$) corresponding to a strength function $\langle \Gamma_n^0 \rangle / D$ of 10^{-4}. The fission width amplitudes were similarly generated for each fission channel, and three channels were assumed for one spin state and two for the other. Mean fission widths were made equivalent to $N_{eff} = 3 \times 1$ and $N_{eff} = 1 + 2 \times 0.1$ respectively. This gives an average N_{eff} of 2.1. Such values could be expected from the channel theory. The radiation widths were set equal to 25 MeV (constant).

The results of a section of this calculation are shown in Fig. 10, and it will be seen that some levels are undetectable and several pairs of levels appear as single "resonances".

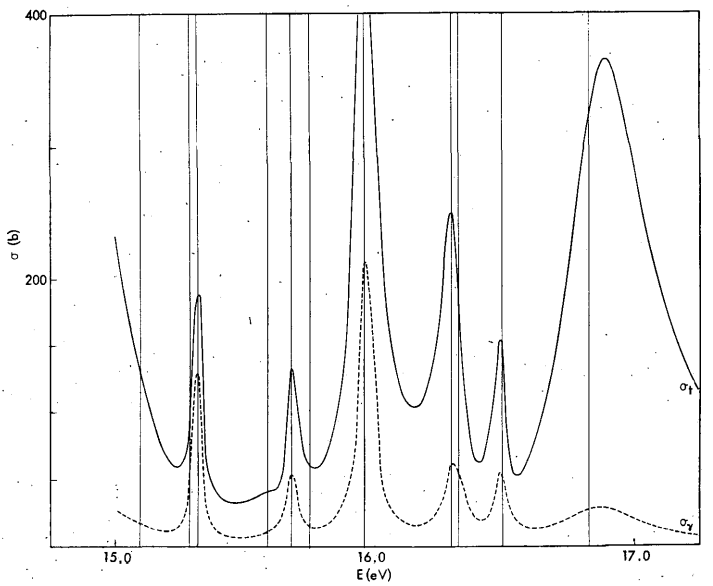

Fig. 10

Section of a computer-generated cross-section; solid lines are σ_t, dashed lines are σ_γ. The vertical lines on the abscissa are the actual positions of levels.

A single level analysis of the cross-section generated gives a value of $N_{eff} = 0.8 \pm 0.14$ ($\Gamma_F = 137$ MeV, $D = 1.06$ eV for each spin state) close to the U^{233} value. The histogram of the "fission widths" of the simulated cross-section can be fitted with a χ^2 distribution with approximately four degrees of freedom, again close to the U^{233} value. The "radiation widths" of the "resonances" fluctuate from 17 to 88 MeV, and many small level spacings are lost: for 34 levels entered in the programme, only 22 "resonances" are observed. Finally, the simulated total cross-section never falls to much less than 20 b in the minima.

Thus this example, starting from parameters close to those expected on the channel theory for U^{233}, has actually reproduced most of the features found in the experimental cross-section curves. It seems extremely plausible that the U^{233} and U^{235} cross-sections, and possibly also those of Pu^{239}, are fully consistent with the expectations of the channel theory of fission, and that it has been the assumptions made in analysing the data that have been at fault in the past.

SUMMARY

In this paper no attempt has been made to survey all the latest data on neutron-induced fission cross-sections. The problems involved in the accurate measurement of absolute fission cross-sections, so important to reactor physics, have not been mentioned, nor the annoying discrepancies still existing between different measurements, all apparently of high accuracy, and in the interests of brevity the topic of the ternary fission cross-sections has been ignored.

A general discussion has been presented of the main features of the fission cross-sections, with a more detailed treatment of the topics of sub-threshold fission and the resonance cross-sections. These discussions would appear to indicate that the energy variation of the neutron-induced fission cross-sections are now fairly well understood in terms of the channel theory of fission and the nuclear shell model.

ACKNOWLEDGEMENTS

The author wishes to acknowledge with pleasure his indebtedness to J. E. Lynn for many fruitful discussions.

REFERENCES

[1] HILL, D. L. and WHEELER, J. A., Phys. Rev. 89 (1953) 1102.
[2] BOHR, A., Proc. UN Int. Conf. PUAE 2 (1956) 220.
[3] WHEELER, J. A., Fast Neutron Physics 2 (MARION and FOWLER, Eds.) Interscience, New York (1963) 2051.
[4] HENKEL, R. L., Fast Neutron Physics 2 (MARION and FOWLER, Eds.) Interscience, New York (1963) 2001.
[5] HYDE, E. K., UCRL 9036 (1960).
[6] JAMES, G. D., Nucl. Phys. 55 (1964) 517.

[7] BARSCHALL, H.H., private communication (1954); quoted by HENKEL, R.L. [4].
[8] GOKHBERG, B.M., OTROSCHENKO, G.A. and SHIGIN, V.A., Dokl. Akad. Nauk. SSSR 128 (1959) 1157;
NESTEROV, V.G. and SMIRENKIN, G.N., J. nucl. Energy 16 (1962) 51;
RUDDICK, P. and WHITE, P.H., to be published in J. nucl. Energy.
[9] WHEELER, J.A. Physica XXII (1956) 1103.
[10] LEONARD, B.R., SEPPI, E.J., FRIESEN, W.J. and KINDERMAN, E.M., Bull. Amer. phys. Soc. II I (1956) 248.
[11] BROOKS, F.D. and JOLLY, J.E. AERE PR/NP 6 (1963) 13.
[12] HALPERN, I., Annu. Rev. nucl. Sci. 9 (1959) 245.
[13] JOHANSSON, S.A.E., Nucl. Phys. 12 (1959) 449.
[14] LAMPHERE, R.W., Nucl. Phys. 38 (1962) 561.
[15] GOKHBERG, B.M., OTROSCHENKO, G.A. and SHIGIN, V.A., Dokl. Akad. Nauk SSSR 128 (1959) 1157.
[16] DE SAUSSURE, G., BLONS, J., JOUSSEAUME, C., MICHAUDON, A. and PRANAL, Y., C.R. Acad. Sci., Paris 259 (1964) 3498.
[17] FRASER, J.S. and SCHWARTZ, R.B., Nucl. Phys. 30 (1962) 269.
[18] MOORE, M.S. and REICH, C.W., Phys. Rev. 118 (1960) 718;
VOGT, E., Phys. Rev. 118 (1960) 724.
[19] NORTHROP, J.A., STOKES, R.H. and BOYER, K., Phys. Rev. 115 (1959) 1277.
[20] MICHAUDON, A., J. Phys. Radium 220 (1961) 712.
[21] MICHAUDON, A., Phys. Lett. 7 (1963) 211.
[22] LYNN, J.E., Phys. Rev. Lett. 13 (1964) 412.

MESURE ET ANALYSE DE LA SECTION EFFICACE DE FISSION DU PLUTONIUM-239 DE 0 A 5 keV

G. de SAUSSURE*, J. BLONS, C. JOUSSEAUME,
A. MICHAUDON ET Y. PRANAL
CENTRE D'ÉTUDES NUCLÉAIRES DE SACLAY, FRANCE

Abstract — Résumé — Аннотация — Resumen

MEASUREMENT AND ANALYSIS OF THE FISSION CROSS-SECTION OF Pu^{239} FROM 0 TO 5 keV. The cross-section of Pu^{239} for low-energy neutrons was measured between 0.16 eV and 5 keV by the time-of-flight method, with a gas scintillator containing 310 mg of Pu^{239}. Under the best conditions and at high energy, the resolving power of the measurement was 3 ns/m.

We used the Saclay linear accelerator as a pulsed neutron source. The measurement consisted in the successive determination of the fission rate (by means of a gas scintillator) and the incident neutron energy spectrum (by means of a BF_3 counter whose efficiency was proportional to $E^{-\frac{1}{2}}$). The background was determined by interposing black resonance screens in the neutron beam. The quantity $\sigma_F\sqrt{E}$ is proportional to the ratio of the fission rate to the counting-rate of the BF_3 detector. It was calibrated by reference to the resonance at 7.8 eV, the parameters of which are known.

The gas scintillator consists of six independent cells, a 56 UVP photo-multiplier being coupled with each cell.

At the discrimination threshold, adjusted to an alpha-ray build-up rate of 1 counts/s, we obtained an efficiency of 65% for the detection of fissions.

The fission cross-section was measured in several sequences to observe the various energy ranges with sufficient resolving power.

A detailed description is given of the experimental apparatus, the tests with the scintillator and the experimental conditions in which the various measurement sequences were carried out. The paper presents a curve showing the fission cross-section as a function of energy; it also reports the results of an analysis of the resonance parameters.

MESURE ET ANALYSE DE LA SECTION EFFICACE DE FISSION DU ^{239}Pu DE 0 A 5 keV. La section efficace de ^{239}Pu pour des neutrons de basse énergie a été mesurée entre 0,16 eV et 5 keV par la méthode du temps de vol, avec un scintillateur gazeux contenant 310 mg de ^{239}Pu. Dans les meilleures conditions et à haute énergie, la résolution de la mesure est de 3 ns/m.

Les auteurs ont utilisé l'accélérateur linéaire de Saclay comme source de neutrons pulsée. La mesure consiste à déterminer successivement le taux de fission, avec un scintillateur gazeux, et le spectre d'énergie des neutrons incidents, avec un compteur à BF_3 dont l'efficacité est proportionnelle à $E^{-\frac{1}{2}}$. Les bruits de fond sont obtenus en interposant des écrans à résonances noires dans le faisceau de neutrons. La quantité $\sigma_F\sqrt{E}$ est proportionnelle au rapport du taux de fission au taux de comptage du détecteur à BF_3. Elle a été étalonnée par rapport à la résonance à 7,8 eV dont les paramètres sont connus.

Le scintillateur gazeux se compose de six cellules indépendantes, un photomultiplicateur 56 UVP étant associé à chaque cellule.

Au seuil de discrimination, réglé à un taux d'empilement des rayons α de 1 cps, l'efficacité pour la détection des fissions est de 65%.

La section efficace de fission a été mesurée en plusieurs séquences pour observer les différentes gammes d'énergie avec une résolution adéquate.

Les auteurs décrivent en détail l'appareil expérimental, les essais avec le scintillateur et les conditions expérimentales des différentes séquences de mesure. Ils présentent une courbe de la section efficace de fission en fonction de l'énergie, ainsi que les résultats d'une analyse des paramètres de résonances.

---

* Détaché au CEN de Saclay par l'Oak Ridge National Laboratory, USA

ИЗМЕРЕНИЕ И АНАЛИЗ ЭФФЕКТИВНОГО СЕЧЕНИЯ ДЕЛЕНИЯ ПЛУТОНИЯ-239 В ПРЕДЕЛАХ 0—5 кэв. Получаемое с помощью нейтронов низкой энергии эффективное сечение плутония-239 было измерено между 0,16 эв и 5 кэв по методу времени пролета. При этом использовался газовый сцинтиллятор, содержащий 310 мг плутония-239. В лучших условиях и при высокой энергии результат измерения составляет 3 н·сек/м.

В качестве источника импульсных нейтронов был использован линейный ускоритель в Сакле. Измерение заключалось в определении последовательно плотности делений при наличии газового сцинтиллятора и энергетического спектра бомбардирующих нейтронов, счетчика с трехфтористым бором, эффективность которого пропорциональна $E^{-\frac{1}{2}}$. Фоновые шумы возникали при помещении черных резонансных экранов в пучок нейтронов. Количество $\sigma_F\sqrt{E}$ пропорционально отношению плотности делений к скорости счета счетчика с трехфтористым бором. Это количество было установлено относительно резонанса в 7,8 эв, параметры которого известны.

Газовый сцинтиллятор состоит из шести независимых ячеек, фотоумножителя 56 UVP, связанного с каждой ячейкой.

На пороге дискриминации, регулируемом при коэффициенте наложения альфа-лучей при одном импульсе в секунду, в отношении обнаружения делений выявляется эффективность порядка 65%.

Эффективное сечение деления измерялось неоднократно, чтобы выявить различные области энергии с надлежащим разрешением.

Дается подробное описание экспериментальной установки, опытов с сцинтиллятором и экспериментальных условий, в которых проводились различные измерения. Приводится кривая эффективного сечения деления в зависимости от энергии, а также результаты анализа параметров резонансов.

MEDICIONES Y ANALISIS DE LA SECCION EFICAZ DE FISION DEL ^{239}Pu DE 0 A 5 keV. Se ha medido la sección eficaz de fisión del ^{239}Pu por neutrones de baja energía en el intervalo 0,16 eV - 5 keV por el método del tiempo de vuelo, con un centelleador gaseoso que contiene 310 mg de ^{239}Pu. En condiciones óptimas y a elevada energía, el poder resolutivo de la medición asciende a 3 ns/m.

Los autores han utilizado el acelerador lineal de Saclay como fuente pulsada de neutrones. La medición consiste en determinar sucesivamente el índice de fisiones, con un centelleador gaseoso, y el espectro de energía de los neutrones incidentes, con un contador de BF_3 cuya eficacia es proporcional a $E^{-\frac{1}{2}}$. Los ruidos de fondo se determinan interponiendo pantallas de resonancias negras en el haz de neutrones. El valor del producto $\sigma_F\sqrt{E}$ es proporcional a la razón índice de fisiones/índice de recuento del detector de BF_3. Dicha cantidad se ha contrastado con la resonancia a 7,8 eV, cuyos parámetros son conocidos.

El centelleador gaseoso se compone de 6 células independientes con un fotomultiplicador 56 UVP asociado a cada una de ellas.

En el umbral de discriminación, fijado para la acumulación de un impulso α por segundo, la eficacia de detección de fisiones es del 65%.

La sección eficaz de fisión se ha medido en varias series para poder observar los diferentes intervalos energéticos con un poder de resolución adecuado.

Los autores describen detalladamente el aparato experimental, los ensayos con el centelleador y las condiciones experimentales de las diferentes series de medición. Presentan una curva de la sección eficaz de fisión en función de la energía, así como los resultados de un análisis de los parámetros de resonancia.

I. INTRODUCTION

L'étude de l'interaction des neutrons lents ($E<10$ keV) avec les noyaux fissiles est d'un grand intérêt tant pour le calcul des piles atomiques que par l'information qu'elle apporte sur les niveaux excités des noyaux lourds et sur le processus de fission. Le noyau de plutonium-239 est particulièrement intéressant grâce à la faible valeur de son spin $I=\frac{1}{2}$. Les résonances sont ainsi plus espacées et plus grandes que pour les autres noyaux fissiles, ce qui facilite leur analyse. De plus la détermination de leur état de spin $J=I\pm\frac{1}{2}$ est plus aisée [1].

Malgré leur intérêt les sections efficaces du plutonium-239 ont été peu étudiées et jusqu'à présent, les paramètres des résonances ne sont connus que jusqu'à 50 eV [2]. Il nous a donc paru utile de reprendre la mesure de la section efficace de fission du plutonium-239 par la méthode du temps de vol [3] en bénéficiant des améliorations apportées ces dernières années aux spectromètres de neutrons tant du point de vue de la résolution que de l'intensité.

II. DESCRIPTION DE L'EXPÉRIENCE

a) Base de vol

Une première série de mesures à basses énergies (0,16 eV-100 eV) a été effectuée à 10,80 m sur une base de vol inclinée de 18° par rapport à la perpendiculaire à la cible d'uranium source de neutrons rapides et au modérateur en polyéthylène (20X20X3 cm).

Une deuxième série de mesures à hautes énergies (11 eV-5 keV) a été faite à 19 m sur une base de vol perpendiculaire au modérateur [4].

b) Détecteur

Le scintillateur gazeux était semblable à celui décrit par NIFENECKER et al. [5], il comprenait 6 cellules identiques vues chacune par un photomultiplicateur 56 UVP (fig. 1). L'étanchéité était assurée par des joints

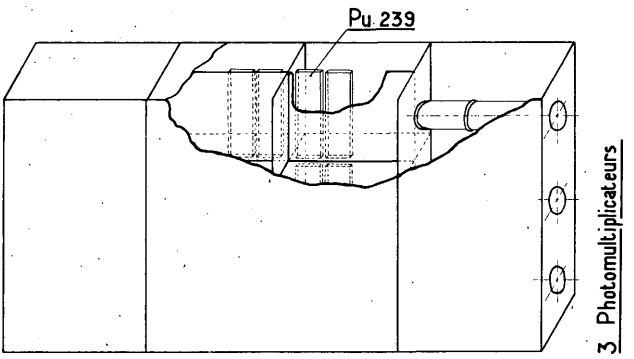

Figure 1

Scintillateur gazeux.

d'indium; avant le remplissage de xénon on faisait pendant une semaine un vide de quelque 10^{-6} mm Hg dans le scintillateur.

Le fort taux de désintégration α du plutonium-239 ($2{,}27 \cdot 10^9$ α/g/s) oblige à limiter la quantité de matière fissile mais il était intéressant d'en mettre la plus grande quantité possible pour avoir le taux de comptage maximum. Différents essais avec une source de californium-252 d'une intensité

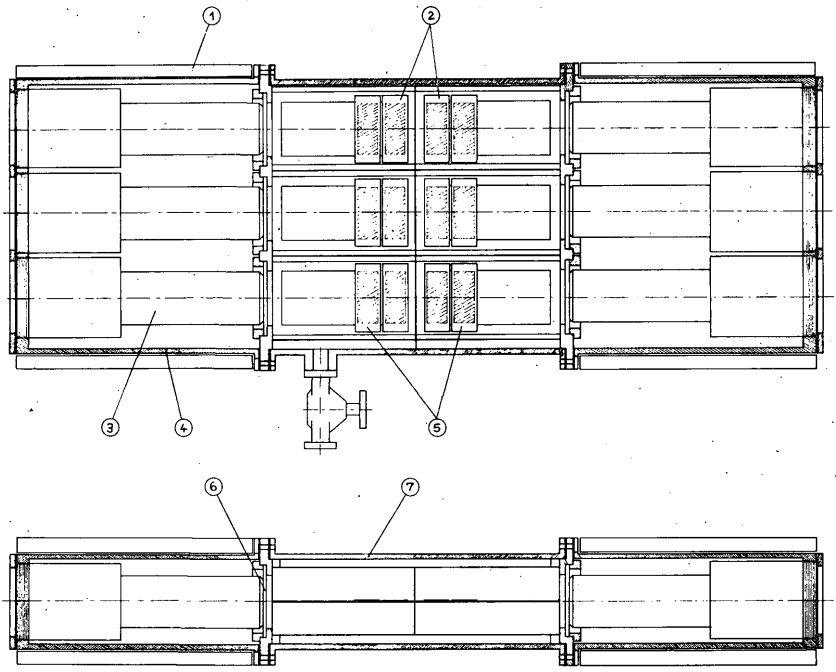

Figure 1 bis

Plan du scintillateur.

1 Chemise de refroidissement des photomultiplicateurs
2 Dépôts de Pu de 1,5 mg/cm²
3 Photomultiplicateurs 56 UVP
4 Boîtier support des photomultiplicateurs
5 Dépôts de Pu de 1,2 mg/cm²
6 Fenêtres de quartz
7 Enceinte à vide.

de 10^5 fissions/min* ont permis d'étudier l'amplitude des impulsions dues aux fissions et le taux d'empilement dû au rayonnement α en fonction de la position des dépôts de plutonium, de la pression et de la composition du gaz scintillant. La courbe de la figure 2 montre un essai de discrimination α/fission; on a mis dans une cellule 60 mg de plutonium-239 à la place indiquée sur la figure 1 et dans une autre cellule la source de californium. Le taux d'α du californium ($0{,}05 \cdot 10^6$ α/s) était négligeable en regard de celui du plutonium ($136 \cdot 10^6$ α/s). On a compté à différents seuils du discriminateur par le même photomultiplicateur et dans les mêmes conditions (HT = 2500 V) d'une part le taux des α, d'autre part les fissions du californium. La figure 2 montre que pour un taux d'empilement α de 60 coups/min le détecteur garde une efficacité d'environ 65% des fissions.

D'autre part, les meilleurs résultats ont été obtenus avec du xénon pur à la pression de 200 g/cm^2. Différents essais avec un mélange xénon-hélium ou avec de l'argon ont été moins concluants.

Le plutonium était fixé sous forme d'oxyde, en plusieurs couches, sur des plaquettes d'aluminium (6,5×2,5 cm). Nous avons mis au fond de la

* Cette source a été obligeamment prêtée par Monsieur Chesnay (Centre d'études nucléaires de Fontenay-aux-Roses).

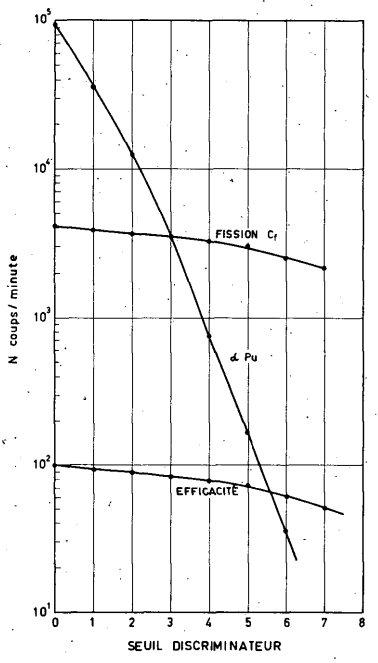

Figure 2

Discrimination α/ fission.

cellule la plaquette de plus forte densité (1,5 mg/cm²) puis celle dont la densité est de (1,2 mg/cm²)**.

Au total 310 mg de plutonium se répartissent sur 12 plaquettes d'aluminium, ces plaquettes sont aluminisées sous vide tant pour améliorer la réflexion que pour empêcher la contamination intérieure du scintillateur. La couche d'aluminium (50 μg/cm²) est déterminée par pesées.

La composition isotopique du plutonium est la suivante:

^{239}Pu	98,6%	±0,02%
^{240}Pu	1,37%	±0,02%
^{241}Pu	0,025%	±0,005%.

c) Chaînes d'enregistrement

Les six cellules du scintillateur sont vues par six photomultiplicateurs 56 UVP (refroidis à l'air comprimé) attaquant chacun un discriminateur rapide, les signaux étant mélangés à la sortie des discriminateurs. On règle le seuil de chaque discriminateur un à un à distance; le taux du bruit de fond α est relevé en cours des mesures sur un enregistreur MECI.

** Les dépôts de plutonium-239 ont été faits par Mademoiselle Valentin (Centre d'études nucléaires de Fontenay-aux-Roses).

Un moniteur composé d'un compteur à BF_3 permet à chaque instant de connaître d'éventuelles déformations du spectre de neutrons.

Le spectre de neutrons est mesuré par un ensemble de trois compteurs à BF_3 dont l'efficacité est proportionnelle à $E^{-\frac{1}{2}}$. Dans ce cas le discriminateur rapide est remplacé par un amplificateur 2 Mc/s.

Le taux de comptage du détecteur commande un dispositif automatique de sécurité qui arrête l'accumulation des données lors d'une diminution ou d'une augmentation de ce taux.

Le sélecteur à temps de vol utilisé est un 4096 canaux Intertechnique à largeur de canal variable de 50 ns à 3,2 μs [6].

III. CONDITIONS EXPÉRIMENTALES

	Mesure à basse énergie (0,16 à 100 eV)(a)	Mesure à haute énergie (11 eV à 5 keV) (b)
Accélérateur	500 impulsions à 100 ns/s	
Sélecteur à temps de vol à largeur de canal variable	Réglée entre 50 et 1600 ns	Réglée entre 50 et 400 ns
Longueur de vol	10,80 m	19 m base de vol perpendiculaire au ralentisseur
Durée d'accumulation	34 h	140 h
Résolution expérimentale	1,2 s/m à 0,16 eV 46 ns/m à 100 eV	35 ns/m à 12 eV, 11 ns/m à 100 eV, 6 ns/m à 5 keV
Filtre	Boral	Boral
Ecran de bruit de fond	Cobalt-Tantale	Tantale

a) Une mesure de 20 h a été faite dans les mêmes conditions mais avec comme écrans de bruit de fond du manganèse et du tantale.

b) Une mesure de 50 h a été faite dans les mêmes conditions sauf une largeur d'impulsion accélérateur de 20 ns: la résolution à 5 keV est alors 3 ns/m.

IV. ANALYSE DES RÉSULTATS

La mesure consiste à déterminer successivement le taux des fissions et le spectre d'énergie des neutrons incidents. Les bruits de fond sont obtenus en interposant des écrans à résonances noires dans le faisceau de neutrons.

On détermine une loi de bruit de fond par une séquence spéciale et on normalise ensuite cette séquence sur la surface de quelques résonances.

Nous avons obtenu 22 000 coups par canal de 0,400 μs au sommet de la résonance à 11 eV dans la mesure à basse énergie, et 6500 coups par canal de 0,050 μs au sommet de la résonance à 75 eV dans la mesure à haute énergie.

Les figures 3, 4 et 5 représentent pour la mesure à 19 m la courbe $\sigma_f\sqrt{E}$ en fonction de l'énergie après normalisation sur la surface de la résonance à 7,83 eV dont les paramètres sont connus [2]. Une mesure de nor-

malisation sur la valeur de σ_f aux énergies thermiques est en cours d'analyse.

L'analyse des résultats s'est faite par une méthode de moindres carrés en utilisant le calculateur IBM 7094 en supposant que toutes les résonances

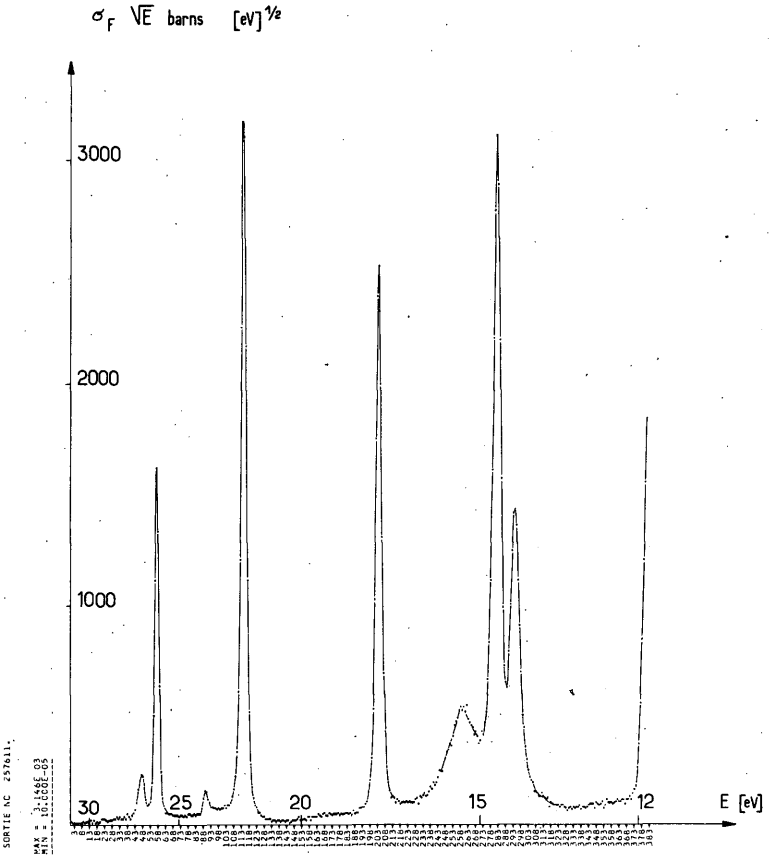

Figure 3

Section efficace de fission du ^{239}Pu.
Distance de vol: 19 m; sélecteur: 400 ns; accélérateur: 100 ns.

sont du type Breit-Wigner à un niveau [7]. Le programme d'analyse de forme ne comportait pas de terme d'interférences entre résonances.

Dans la fonction de résolution on a tenu compte:

de l'effet Doppler $\Delta_D = 2\left(\frac{kT}{A}\right)^{\frac{1}{2}} E^{\frac{1}{2}} = 0{,}0208E^{\frac{1}{2}}$;

du modérateur $\Delta_M = \left(\frac{2}{3}\right)^{\frac{1}{2}} \frac{6\lambda}{L} E = \frac{2\sqrt{3}\cdot 0{,}3}{72{,}3L} E$;

de l'inclinaison de la base $\Delta_I = \left(\frac{2}{3}\right)^{\frac{1}{2}} \frac{6{,}18}{L}\cdot 10^{-2} E$;

de l'électronique $\Delta_E = \left(\frac{2}{3}\right)^{\frac{1}{2}} \frac{(0{,}01+\tau^2)^{\frac{1}{2}}}{72{,}3L} E^{\frac{3}{2}}$.

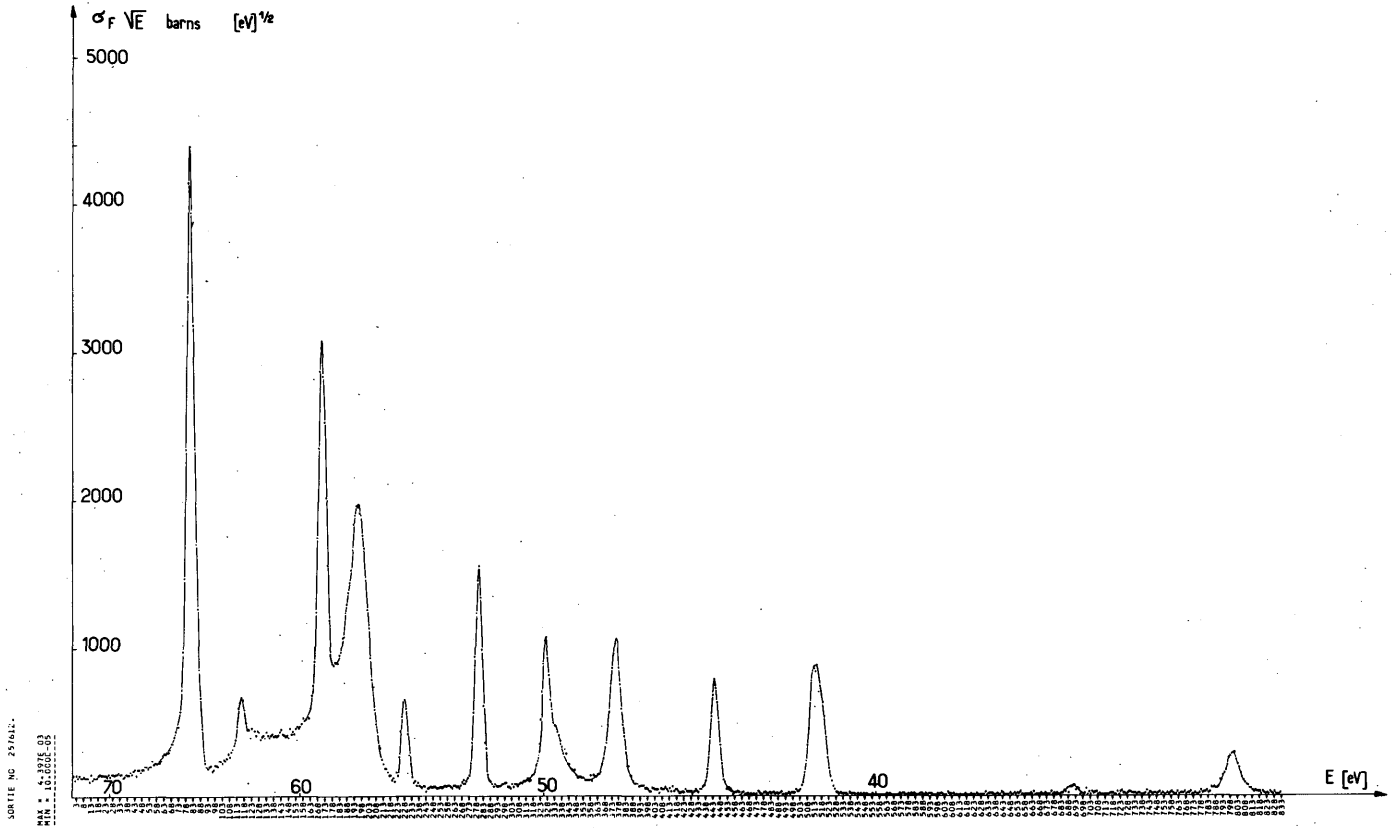

Figure 4

Section efficace de fission du ^{239}Pu.
Distance de vol: 19 m; sélecteur: 100 ns; accélérateur: 100 ns.

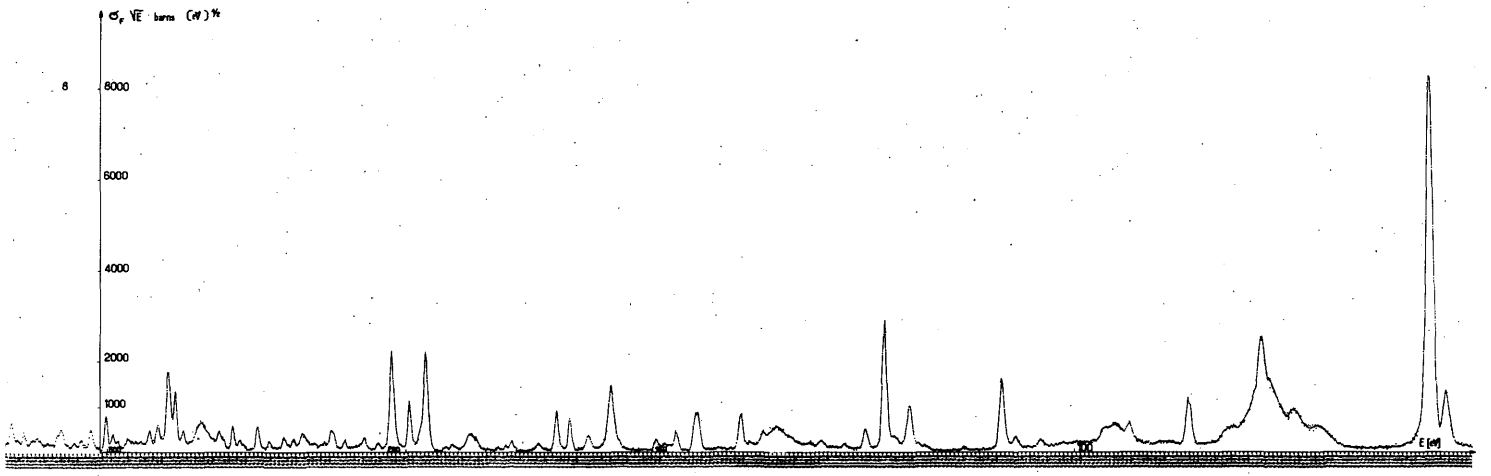

Figure 5

Section efficace de fission du ^{239}Pu.
Distance de vol: 19 m; sélecteur: 50 ns; accélérateur: 100 ns.

TABLEAU I

PLUTONIUM-239
ANALYSE DES RÉSONANCES (7,83 à 203,4 eV)

E_0 (eV)	Γ(Saclay) (meV)	$\sigma_0\Gamma_f$(Saclay) (b. eV)	Γ(Bollinger) (meV)	$\sigma_0\Gamma_f$ (Bollinger) (b. eV)	E_0 (eV)	Γ(Saclay) (meV)	$\sigma_0\Gamma_f$(Saclay) (b. eV)	E_0 (eV)	Γ(Saclay) (meV)	$\sigma_0\Gamma_f$(Saclay) (b. eV)	E_0 (eV)	Γ(Saclay) (meV)	$\sigma_0\Gamma_f$(Saclay)
7,83	84 ± 3	108,2 ± 0,5	83 ± 5	108,2 ± 3	57,4	593 ± 60	142 ± 8	103,1	400 ± 150	10,3 ± 1,8	146,3	200	17,7 ± 1
9,59	245 ± 65	6,1 ± 1	non observée		58,0	850 ± 120	102 ± 8	105,5	250	11 ± 1	147,3		4,4
10,93	185 ± 5	256 ± 3	180 ± 12	264,4 ± 6	59,1	239 ± 35	127,9 ± 5	106,8	150 ± 40	61,3 ± 1,3	148,1		5,3
11,48	480 ± 170	37,9 ± 15	non observée		61,1		240 ± 40	110,4	170	1,2 ± 0,4	149,4		7,7
11,90	68 ± 5	62,8 ± 1,5	64 ± 7	60,4 ± 3	62,9	147 ± 80	15 ± 1.5	114,5		1,9 ± 0,9	155,8		6,5 ± 2
14,28	145 ± 6	64,5 ± 1	(100.8 ± 11)		65,5	250 ± 25	208,4 ± 6	115,2		3,4 ± 1,1	157,0	720	109,9 ± 4
14,68	82 ± 3	115,4 ± 2	79.6 ± 8)		66,4		49,6 ± 5.3	116,2	300	50,4 ± 5	160,9	550	22,9 ± 2,5
15,5	895 ± 70	105,4 ± 8	800 ± 100		74,1	108 ± 25	35,4 ± 1.4	117,9		22,2 ± 2,8	164,4	250	36,5 ± 1,5
17,6	84 ± 4	93,8 ± 2	87 ± 6	94,1 ± 3	75,1	173 ± 8	337,8 ± 5	118,9	180 ± 40	112,3 ± 2,8	166,9	320	50,2 ± 2,2
22,2	101 ± 7	133,7 ± 3	113 ± 4	131,3 ± 4	81,7		50 ± 3	121,1	220	20,6 ± 0,8	170,5	880 ± 300	11,6 ± 1,3
23,9	692 ± 72	13,1 ± 1	(82 ± 10)		83,3		78,7 ± 6.9	123,5	100	5,1 ± 0,5	175,9		12,6 ± 1,1
26,2	89 ± 6	59,4 ± 2	80 ± 6	61,9 ± 3	84,9		144,9 ± 12.5	125,0		4,2 ± 0,7	177,1		4,1 ± 0,5
27,3	330 ± 30	15,5 ± 1	(43 ± 5)		85,6	260 ± 50	60,5 ± 7.7	126,3		10,6 ± 1	178,8		3,7 ± 0,5
32,3	176 ± 15	12,9 ± 0,5	230 ± 50	19 ± 3	86,0		141 ± 9.9	127,6		7,6 ± 1	181,7		0,3 ± 0,8
35,3	140 ± 70	1,9 ± 0,3	(44 ± 5)		87,9		41,3 ± 3.8	130,3		40,5 ± 2,4	184,0		38,9 ± 1,6
41,4	182 ± 8	44,6 ± 1	76 ± 10	40,8 ± 3	90,9	157 ± 25	40,1 ± 2.5	132,1		80 ± 2,9	185,2		19 ± 1,2
44,6	101 ± 8	25,9 ± 0,8	51 ± 10	23,2 ± 2	92,6		17,2 ± 2.6	133,8		19,2 ± 1,8	188,6		8,1 ± 0,9
47,6	310 ± 9	58,9 ± 1	350 ± 50	63,3 ± 5	95,5	270 ± 120	16,3 ± 1.5	135,5		4,5 ± 0,7	190,2		2,5 ± 0,8
49,7	881 ± 30	53,4 ± 2	non observée		96,7		73 ± 2.4	136,8	200	37,0 ± 1,3	195,1	760 ± 200	160,9 ± 12,9
50,0	50 ± 20	23,2 ± 2	80 ± 6	68,9 ± 5	97,6	400 ± 250	10,9 ± 1.4	140,0		2,4 ± 0,4	196,3		25,5 ± 5
52,5	92 ± 5	51,5 ± 1	57 ± 7	50,7 ± 4	100,0		16,5 ± 1.5	142,9		24,9 ± 3	199,1		65,7 ± 3,2
55,6	83 ± 26	21,6 ± 1	non observée		101,2	350	3,2 ± 0.6	143,4		27,3 ± 3.1	203,4		177,3 ± 6,2

Entre parenthèses: valeurs obtenues indirectement de η en prenant $\Gamma_\gamma = 40$ meV.

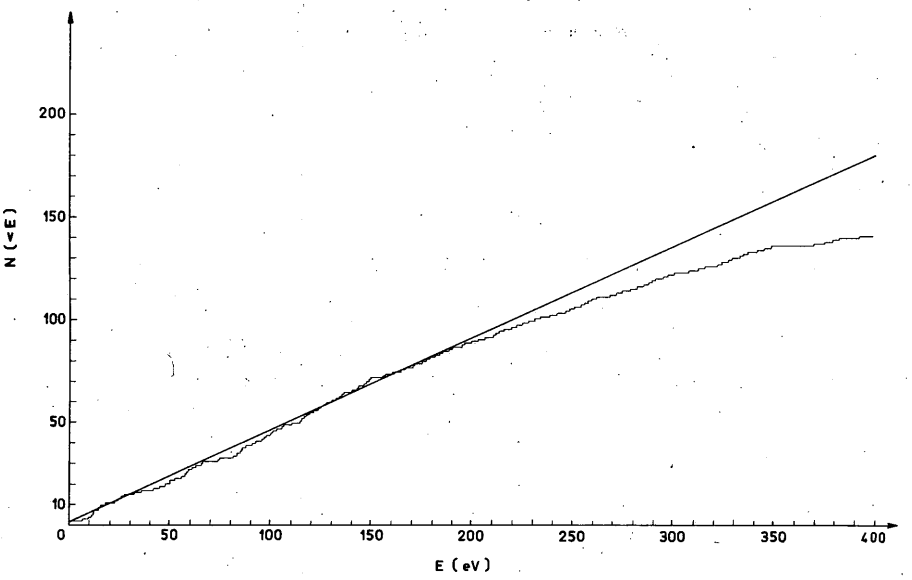

Figure 6

Nombre de niveaux en fonction de E
(D = 2,2 eV).

On s'est attaché à ce que la courbe théorique calculée suive d'aussi près que possible les résultats expérimentaux. Aux énergies suivantes, 11,48 eV, 49,7 eV, 58,0 eV, 61,1 eV, 66,4 eV, 84,9 eV, 86,0 eV, 143,4 eV, 157 eV, 196,3 eV, on a rendu compte de la dissymétrie des résonances en ajoutant un niveau supplémentaire.

La figure 6 montre le nombre de résonances observées jusqu'à 400 eV en fonction de l'énergie; jusqu'à 200 eV il y a peu de niveaux perdus. On en déduit l'espacement moyen des niveaux D = 2,2 eV.

Une distribution des espacements jusqu'à 100 eV est bien décrite par une loi de Wigner à deux populations.

Les valeurs de $\sigma_0\Gamma_f$ et de Γ (tableau I) sont en bon accord avec celles publiées par BOLLINGER et al. [2] sauf pour les valeurs de Γ qu'ils ont obtenues indirectement de η en prenant $\Gamma_\gamma = 40$ MeV.

Pour l'analyse complète des résonances, notamment pour la détermination de certaines valeurs de Γ que nous avons trouvées particulièrement grandes (> 1 eV) aux énergies suivantes: 81,7 eV, 83,3 eV, 84,9 eV, 86 eV, 87,9 eV, 92,0 eV, 132,1 eV et 196,3 eV, nous devons attendre une mesure de la section efficace totale en cours actuellement.

Nous somme heureux de remercier ici Mademoiselle Sanche, Messieurs P. Ribon et H. Derrien de leurs nombreuses suggestions lors du dépouillement des résultats, et Monsieur J. Cartier de son aide considérable lors de l'accumulation des données avec le sélecteur de temps de vol Intertechnique.

RÉFERENCES

[1] FRASER, J. S. and SCHWARTZ, R., Nucl. Phys. 30 (1962) 269.

[2] BNL 325, Suppl. n° 1 à la deuxième édition;
BOLLINGER, L. M. et al., "The Slow Neutron Cross-Sections of Plutonium-239", Actes 2e Conf. Genève 15 (1958) 127;
IGNATEV, K. G. et al., Akad. Nauk SSSR (traduction AEC-tr n° 5917, juillet 1963).

[3] CENTRE D'ÉTUDES NUCLÉAIRES DE SACLAY, Proc. of the Symposium on Neutron time-of-flight methods, Saclay (1962).

[4] RIBON, P. et al., Proc. of the Symposium on Neutron time-of-flight methods, Saclay (1962) 97;
BERGÈRE, R., Proc. of the Symposium on Neutron time-of-flight methods, Saclay (1962) 329.

[5] NIFENECKER, H. et al., Proc. of the Symposium on Neutron time-of-flight methods, Saclay (1962) 413.

[6] THÉNARD, J. et al., Nucl. Instrum. Meth. 26 (1964) 45-50.

[7] MICHAUDON, A., Contribution à l'étude par la méthode du temps de vol de l'interaction des neutrons lents avec l'uranium-235, Rapport CEA R. 2552.

DISCUSSION
(on the foregoing two papers)

M. NÈVE de MEVERGNIES: The analysis carried out by Lynn applies to phenomena that show interference like fission. Does this imply that for other interfering phenomena, such as neutron scattering, the cross-section curve would show "peaks" at energies different from those in the case of the fission cross-section curve? Would it also mean that the capture cross-section would have "peaks" at the true resonance energies?

E. R. RAE: Lynn's observations on fission interference would also apply to scattering interference although it would be difficult to find examples of scattering levels sufficiently wide to show such strong interference. I would agree that the peaks in the capture cross-section might be expected to follow the single-level curve, but Lynn's analysis appears to show that the capture cross-section too is distorted in the case of strong interference and also exhibits sharp pseudo-resonances coincident with the fission peaks. In this connection I should like to draw attention to Fig. 9 in my paper.

U. V. RYABOV: With regard to the paper presented by Dr. Blons, I should like to know whether wide levels (with large Γ_f values) were found at neutron energies between 50 eV and 200 eV. If so, I should also like to know how many there were, what were the Γ_f/Γ ratios involved, and the accuracy with which they were determined. Dr. Rae's paper refers to those data and he obviously had in mind level widths of the same order as the level width at an energy of $E_0 = 15.5$ eV.

J. BLONS: We have not yet got the measurement data on the total cross-section for plutonium, which we are at present investigating with a view to studying the resonances between 100 eV and 200 eV and gammas. At this stage all I can say is that we found quite wide gammas for certain resonances. This might be due to insufficient resolution and to one resonance group rather than to separate resonances.

G. D. JAMES: I should like to point out that Dr. C. A. Uttley at Harwell has measured the total cross-section of Pu^{239} at a resolution of 2 ns/m. He has analysed the resonances between 100 eV and 300 eV on the basis of the single-level Breit-Wigner formula and found several large values of the full-width Γ. Some examples are 3800 meV at 131.7 eV, 1300 meV at 170.0 eV, 1800 meV at 185.1 eV, and 6400 meV at 261.8 eV.

U. V. RYABOV: May I make a comment that relates not only to the papers under discussion but also to the paper presented by Dr. Griffin[1]? The analysis of the neutron resonance parameters in the case of U^{233}, U^{235} and Pu^{239} indicates an arbitrary separation of levels into two groups to which specific spin values are assigned. The calculations of the mean fission widths $\langle \Gamma_f \rangle$ for these groups, based on the formulas of Bohr and Wheeler, and making allowance for the fission barrier penetration determined by Hill and Wheeler, show that the spin $J = I - 1/2$ is assigned to the group with large $\langle \Gamma_f \rangle$ values and $J = (I + 1/2)$ to the group with smaller $\langle \Gamma_f \rangle$ values, as, for example, in the calculations of Gordeev and Bazyazyants. This was confirmed experimentally for U^{233} and U^{235}. This is not so, however, in the case of Pu^{239}, although the spins for some levels are known. In order to

[1] GRIFFIN, J. J., "Transition states at the fission barrier", these Proceedings I.

explain this inconsistency the Soviet scientists, Usachev, Rabotnov and Pavlinchuk, put forward the hypothesis that Pu^{239} in its basic state had negative parity. An attempt was made, using the pulsed reactor at Dubna, to verify this hypothesis by measuring the gamma-ray spectra of the $Pu^{239}(n, \gamma)Pu^{240}$ reaction in resonances with different spins. The spectra were found to be identical, and thus no conclusion could be drawn regarding the negative parity of Pu^{239} in its basic state. One of the papers[2] presented by Dr. Kuzminov at the present session shows that the parity is positive, and the question of $\langle \Gamma_f \rangle$ for groups of levels with $J = I \pm 1/2$ therefore remains open.

Dr. Rae, when referring to the large fluctuations in the total radiation width, obviously had in mind the Saclay data on U^{235}. Our measurements show that the Γ_γ fluctuations are not as great as would appear from the Saclay data, and there is no correlation between Γ_γ and Γ_f.

E. R. RAE: In reply to Dr. Ryabov's comment on the fluctuations in the radiation width of the U^{235} resonances, I would point out that I was indeed quoting the results obtained by Michaudon at Saclay, which suggested fluctuations of up to a factor of about three. I would also like to suggest that the data cited by Dr. Ryabov on the U^{235} radiation widths, while consistent with a constant value, would be equally consistent with fluctuations of the type suggested by Michaudon.

H. NIFENECKER: The value of the number of channels for U^{235} capture has been determined by Michaudon to be about 30, which is not an improbable result. The number of families of Pu^{239} has been found to be two on the basis of the new data obtained at Saclay and also the BNL data, using a maximum probability method. Our last analysis indicates that there is no slowly varying fission background in the case of the fission cross-section of U^{233}. Monte Carlo calculations of the same sort as those made by Lynn, but using single-level Breit-Wigner formulas, gave similar results to his.

J.J. GRIFFIN: May I ask Dr. Ryabov what factor has been established between the two average values of Γ_f in U^{233} and U^{235}?

U. V. RYABOV: As between the mean level widths ($\langle \Gamma_f \rangle$) for groups with spins $J = 3^-$ and $J = 4^-$ I assumed a factor of about three for U^{235}, for example.

J.J. GRIFFIN: Then I should like to refer to Fig. 1 in the paper[3] I presented in Session I, and point out that in that case a distinction is made that corresponds to penetration through a barrier of 1 MeV for slow-neutron fission through a 1+ state. Thus 1+ fission widths would be expected to be perhaps 10^5 or 10^8 times narrower than 0+ widths. The point is just that smaller factors from 3 to 10 are not enough to satisfy the stringent requirements that the large gap imposes on fission through two quasi-particle states. Then the fact that any fission at all is seen for a 1+ resonance requires a 1+ barrier state well below the lowest two quasi-particle transition state.

---

[2] Работнов, Н.С., Смиренкин, Г.Н., Солдатов, А.С., Усачев, Л.Н., Капица, С.П. и Ципенюк, Ю.М., "Фотоделение четно-четных ядер вблизи порога", these Proceedings I.

[3] GRIFFIN, J.J., "Transition states at the fission barrier", these Proceedings I.

MEASUREMENT OF FISSION CROSS-SECTIONS FOR NEUTRONS OF ENERGIES IN THE RANGE 40-500 keV

P. H. WHITE, J. G. HODGKINSON AND G. J. WALL
ATOMIC WEAPONS RESEARCH ESTABLISHMENT,
ALDERMASTON, BERKS., UNITED KINGDOM

Abstract — Résumé — Аннотация — Resumen

MEASUREMENT OF FISSION CROSS-SECTIONS FOR NEUTRONS OF ENERGIES IN THE RANGE 40-500 keV. Measurements have been made of the fission cross-section of U^{233}, U^{234}, U^{236}, Np^{237}, Pu^{239} and Pu^{241} at several neutron energies between 40 keV and 500 keV. Measurements in this energy range are of importance in reactor calculations especially in fast dilute systems where the neutron flux is high in the 10-100-keV energy range.

Recent measurements at this laboratory of the U^{235} fission cross-section gave absolute values slightly lower than previous data. The present series of measurements are made relative to the new values of the U^{235} fission cross-section using back-to-back ionization chambers. The fissile foils were assayed by α-assay, direct weighing and coulometry. Good agreement was obtained between these assays. The fission measurements have an estimated accuracy of between 1% and 2% and, combined with the error on the U^{235} fission cross-section, give a final error of about 3% in the fission cross-sections.

The present results together with those of previous measurements are given, and the corrections for fission-fragment absorption, backgrounds and scattering are discussed.

MESURE DES SECTIONS EFFICACES DE FISSION POUR DES NEUTRONS DONT L'ÉNERGIE EST COMPRISE ENTRE 40 ET 500 keV. L'auteur a mesuré les sections efficaces de fission de ^{233}U, ^{234}U, ^{236}U, ^{237}Np, ^{239}Pu et ^{241}Pu pour des neutrons de différents niveaux d'énergie, compris entre 40 keV et 500 keV. Les mesures effectuées dans ce domaine d'énergie sont intéressantes pour les calculs de réacteurs, en particulier dans le cas de systèmes dilués à neutrons rapides où le flux de neutrons est intense dans la gamme des énergies comprises entre 10 et 100 keV.

Des mesures encore inédites de la section efficace de fission de ^{235}U avaient fourni à l'auteur des valeurs absolues légèrement inférieures aux données antérieures. Il a établi la série de mesures décrite dans le mémoire en fonction des nouvelles valeurs de la section efficace de fission de ^{235}U, en utilisant des chambres d'ionisation montées dos à dos. Les feuilles fissiles ont été étudiées par dosage du rayonnement alpha, pesée directe et coulombmétrie. Les résultats de ces mesures ont concordé de manière satisfaisante. D'après les estimations, la précision des mesures est de l'ordre de 1 à 2%; et, combinée avec l'erreur sur la section efficace de fission de ^{235}U, il en résulte une erreur finale d'environ 3% dans les sections efficaces de fission.

Le mémoire rapproche les résultats de ces mesures de ceux de mesures antérieures et discute les corrections à apporter pour l'absorption des fragments de fission, les mouvements propres et la diffusion.

ИЗМЕРЕНИЯ СЕЧЕНИЙ ДЕЛЕНИЯ ДЛЯ НЕЙТРОНОВ С ЭНЕРГИЕЙ В ДИАПАЗОНЕ 40—500 кэв. Проведены измерения сечений деления U^{233}, U^{234}, U^{236}, Np^{237}, Pu^{239} и Pu^{241} при нескольких значениях энергии нейтронов между 40 и 500 кэв. Измерения в этом диапазоне энергии играют важную роль при расчетах реакторов, особенно при расчете систем быстрого разбавления, где поток нейтронов является плотным в диапазоне энергии 10—100 кэв.

Последние измерения в лаборатории сечения деления U^{235} дали абсолютные значения несколько ниже полученных ранее. На этот раз серия измерений проводилась в связи с новыми значениями сечения деления для U^{235} с использованием сдвоенных ионизационных камер. Фольги из расщепляющегося материала оценивались путем анализа по альфа-излучению, непосредственным взвешиванием и методами кулонметрии. Результаты оценки хорошо согласовались между собой. Измерения деления проводились с расчетной точностью порядка 1—2% и в сочетании с ошибкой в определении сечения деления для U^{235} привели к конечной ошибке при определении сечений деления равной приблизительно 3%.

Данные результаты приводятся совместно с результатами предыдущих измерений, и обсуждаются поправки относительно поглощения осколков деления, фонов и рассеяния.

MEDICION DE SECCIONES EFICACES DE FISION PARA NEUTRONES DE ENERGIA COMPRENDIDA ENTRE 40 Y 500 keV. Se han medido las secciones eficaces correspondientes a la fisión del ^{233}U, ^{234}U, ^{236}U, ^{237}Np, ^{239}Pu y ^{241}Pu por neutrones de energía comprendida entre 40 y 500 keV. Las mediciones en este intervalo de energía son importantes para el cálculo de reactores, sobre todo en el caso de los sistemas rápidos diluidos, en los que el flujo de neutrones de 10 a 100 keV es intenso.

Las mediciones de la sección eficaz de fisión del ^{235}U recientemente efectuadas en este laboratorio por el autor de la presente memoria (resultados próximos a publicarse) dieron valores absolutos ligeramente inferiores a los datos que se poseían. Las mediciones de la serie actual se efectúan con relación a los nuevos valores de la sección eficaz de fisión del ^{235}U, utilizando cámaras de ionización adosadas. Las láminas de material fisionable se analizaron por medición de la actividad, gravimetría directa y coulombimetría. Los resultados de estos análisis concuerdan satisfactoriamente. El error calculado de las mediciones de fisión oscila entre 1 y 2%, lo que junto con el error correspondiente a la sección eficaz de fisión del ^{235}U da un error final del 3%, aproximadamente, en la medición de las secciones eficaces de fisión.

Se exponen los resultados de esta serie de mediciones, así como los de mediciones anteriores y se estudian las correcciones que se han de introducir para tener en cuenta la absorción de fragmentos de fisión, la actividad de fondo y la dispersión.

INTRODUCTION

Accurate fission cross-section measurements of interest for neutrons in the kilovolt energy region are of special importance in neutronics calculations for fast critical assemblies. Previous measurements in this energy range, especially below 100 keV, are not in good agreement (see Figs. 3 to 8). Only three sets of measurements are quoted with accuracies better than 5%; LAMPHERE [2, 3], who measured U^{233}, U^{234} and U^{236} fission cross-sections relative to U^{235}, ALLEN and FERGUSON [4], who measured fission cross-sections of U^{233}, U^{238} and Pu^{239} absolutely by using a recoil proton counter to measure the neutron flux, and PERKIN et al. [5], who measured fission cross-sections of U^{233}, U^{234}, U^{236}, Np^{237}, Pu^{239} and Pu^{241} at 24-keV neutron energy using a calibrated antimony-beryllium neutron source. The largest source of error in these measurements is in the measurement of the neutron flux. Fission cross-section ratios have been quoted by many authors to an accuracy of better than ± 2%.

The present measurements in the energy range 40 keV - 500 keV were made relative to some recently measured absolute values of the U^{235} fission cross-section [1]. The fission rates of one of the isotopes of interest and of a foil of U^{235} were measured in two fission counters placed back to back in the same neutron flux. However, the present work differs from previous ratio measurements in that the U^{235} fission counter used for the ratio determination was the same as that used for the measurement of the absolute U^{235} fission cross-section. This reduced some of the errors that occur when ratio and absolute determinations are completely separate.

In addition to their technical importance, more accurate measurements of fission cross-sections in the threshold regions of some isotopes are of theoretical interest, and may help to establish whether the fission threshold can be explained on a single channel interpretation.

NEUTRON SOURCE

The $Li^7(p,n)$ reaction was used as a neutron source, using a target assembly similar to that described by BARRY et al. [6]. Lithium nitride targets 50-100 $\mu g/cm^2$ thick were evaporated onto silver backings and bombarded with 60-70 μA of protons from the 3-MV Van de Graaff accelerator at the Atomic Weapons Research Establishment, Aldermaston. The energy of the proton beam was measured to be stable to ± 3 keV by frequent reference to the threshold of the $Li^7(p,n)$ reaction. The spread in neutron energy introduced by the target thickness was between 7 and 15 keV.

MEASUREMENT OF THE FISSION-FRAGMENT COUNTING-RATE

The general details of the fission counters used and the preparation of the fission foils were similar to those described by WHITE [1] for the measurement of the U^{235} fission cross-section. Some chemical purification of the isotopes was made using an ion exchange technique, and the foils were painted on to platinum backings 0.013-cm thick from an acetone solution of the nitrate. Low geometry α-assay was used to determine the amount of fissile material on the foils using the half-lives given by HYDE [7] for U^{233}; FLEMING et al. [8] for U^{234} and U^{236}; BRAUER et al. [9] for Np^{237}; WALLMAN [10] for Pu^{239}; BROWN et al. [11] for Pu^{241}; and HALL and MARKIN [12] for Am^{241}. Pu^{241} was assayed by the growth of the daughter Am^{241}. In the cases of U^{234} and U^{236} some foils were sacrificed for coulometric assay [13]. The results of these assays agreed to within 0.5% with the low geometry α-particle assays. The chemical purification was found not to be very successful for the small samples of the various isotopes, and direct weighing was used to determine the impurity level of a sample. The physical properties of the foils are given in Table I.

Analysis of the fission fragment spectra followed in general the procedure described by WHITE [1] for U^{235}. Some of the isotopes in the present measurements were much more α-active than U^{235}, and to achieve satisfactory fission-fragment spectra with good discrimination against α-pulse pile-up the fission counter operating conditions were altered in two respects. Firstly, the counter was filled with krypton + 10% CO_2 mixture for which the pulse-rise time was measured to be 150 ns, and secondly, lower filling pressures (200-400 torr) were used that increased the fission-fragment pulse height relative to the α pulse height. Spectra obtained under these conditions are shown in Fig.1. For all the isotopes it was possible to obtain part of the fission-fragment spectrum undistorted by the finite counter geometry. The extrapolation of the spectrum to zero pulse height is indicated in Fig.1, and was made in a similar manner to that described by WHITE [1] for U^{235}. The fraction of fissions below the bias level can also be determined empirically to within 0.5% from the foil thickness, the bias level and the mean pulse height produced by the fission fragments. This relation enabled the total fission-rate to be determined to $\sim 0.5\%$ for U^{233} where, because of a combination of high α-decay-rate and foil thickness, only a very small part of the fission-fragment spectrum was undistorted by the counter geometry. Frag-

TABLE I

PHYSICAL PROPERTIES OF THE FISSILE FOILS

Main isotope	Isotopic composition mass number						Foil thickness (mg cm^{-2})	Assay error (%)	Impurity (%)
	233	234	235	236	237	238			
U^{233}	99.67	0.15				0.18	0.5	0.8	2
U^{234}		97.52	1.67	0.03		0.78	0.25 0.50	0.8	6
U^{235} (a)		0.11	99.33	0.25		0.31	0.5	1.0	2.4
(b)		1.19	92.95	0.18		5.68	0.5	0.7	0.7
U^{236}		0.01	1.1	98.46		0.42	0.4	1.0	3
Np^{237}					100[+]		0.5	0.75	5
	239	240	241	242					
Pu^{239}	99.985	0.012	0.003				0.5 0.1	0.5	14
Pu^{241}	5.12	5.53	88.95	0.40			0.25	2.0	16

[+] includes 0.05% Pu^{239}

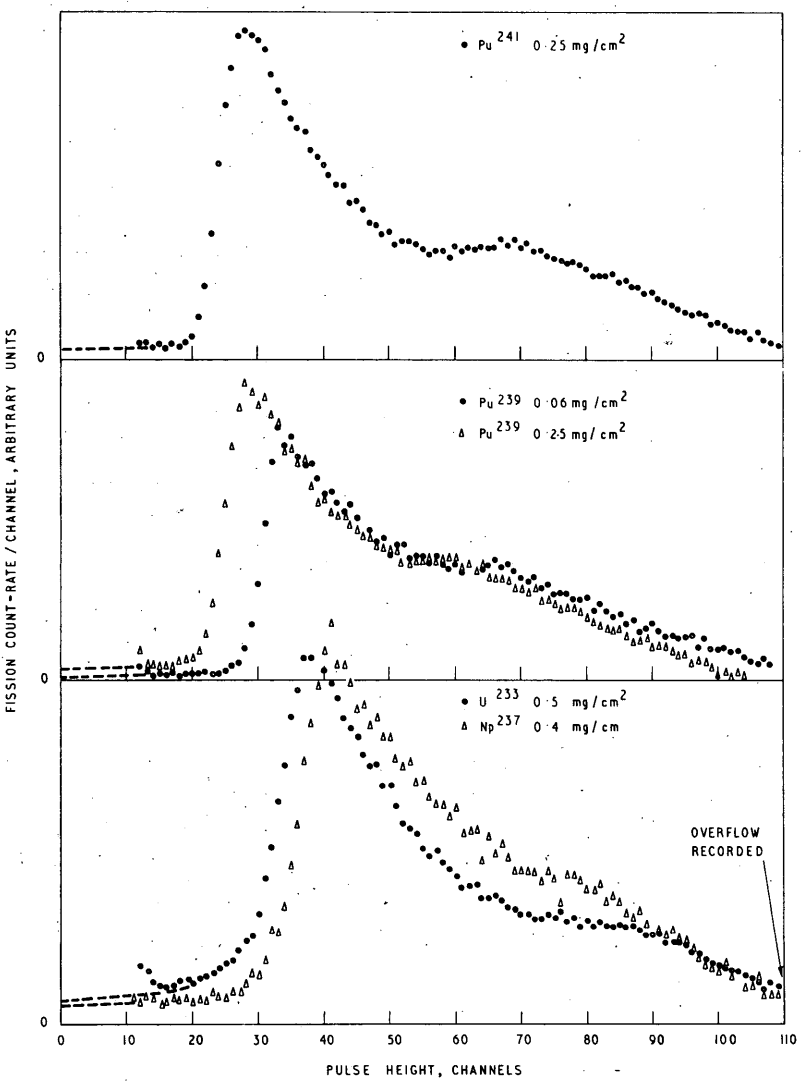

Fig. 1

Fission-fragment pulse-height spectra for the isotopes U^{233}, Np^{237}, Pu^{239} and Pu^{241}

ment spectra for U^{234} and U^{236} are not shown because of the poor counting statistics. Extrapolations of the spectra to zero pulse height for these foils were made in a manner similar to that used for U^{233}.

EXPERIMENTAL PROCEDURE

A fission counter containing a foil of one isotope was placed back to back with an identical counter containing a foil of U^{235} at approximately 14 cm

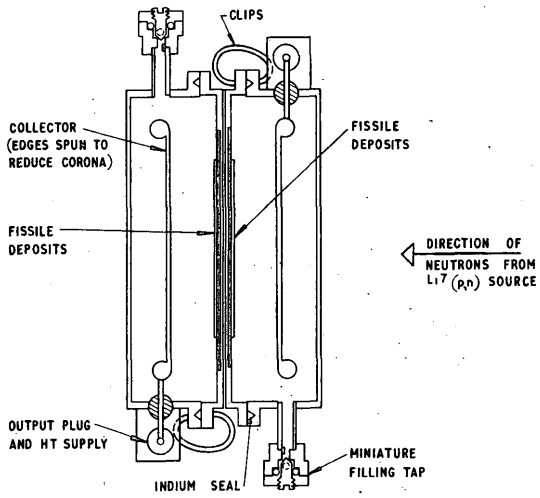

Fig. 2

Experimental arrangement of fission counters

from the neutron source and at 15° to the direction of the proton beam (Fig.2). The average fission count in each counter was measured for each orientation of the two counters, namely U^{235} counter nearer to the source and U^{235} counter further from the source, thereby averaging the distances of the two foils from the source and averaging the attenuation of the neutrons through the metal between the two fissile deposits. To make proper allowance for the background of neutrons scattered by the laboratory walls the above procedure was repeated at a further distance (~ 40 cm) from the source. The neutron background has previously been shown [1] to be uniform within ~ 0.5% up to at least 50 cm from the neutron source.

To check the corrections made for foil thickness the measurements on U^{234} and Pu^{239} were repeated using foils of different thicknesses. For the measurements at 67-keV and 40-keV neutron energy the angles between the neutron and proton directions were 40° and 60° respectively.

CORRECTIONS AND ERRORS

The mean kinetic energies of the fission fragments for U^{233} and Pu^{239} have been measured by LEACHMAN [14]. The corrections for loss of fission fragments due to the foil thickness were calculated from the ranges of these energy fragments in the oxides of uranium or plutonium, allowing for the impurity present. A non-uniformity of foil thickness of 0.8 measured by WHITE [1] for painted U^{235} foils was taken for the painted foils in the present experiment. The corrections calculated for U^{233} and Pu^{239} were within 0.1% of those calculated for U^{235}.

For the remaining isotopes of interest where the fragment energies are not known the foil thickness correction was calculated from the ranges of

U^{235} fission fragments in the oxide of the particular isotope, and a 0.1% error was added to the final cross-section error to include possible variations of fragment energy.

Corrections for neutron flux and energy variation across the fissile foil were calculated using the angular distributions for the $Li^7(p, n)$ reaction measured by TASCHEK and HEMMENDINGER [15]. These were negligible (< 0.2%) except for the threshold isotopes at 40-keV and 67-keV neutron energy where they were ≤ 2%.

The effects of neutron scattering in the fission counters and in the neutron source were calculated in a manner similar to that described by WHITE [1]. Because of the symmetry in these experiments between the two fission counters under comparison these corrections were all very much less than the error caused by counting statistics and have been ignored.

The cross-section errors for the thermally fissile isotopes are made up typically of a statistical counting error of 0.7%, a similar error for the U^{235} counter and systematic errors due to the variation of energy and neutron flux across the foil (0.1%), scattering corrections (0.1%), foil thickness correction (0.5 - 1.0%), extrapolation of the fission-fragment spectrum to zero bias (0.2 - 0.5%) assay of the foil (0.8%) and an error on the U^{235} fission cross-section of 3.0%. Typical errors are 2% on fission cross-section ratios and 3.5% on the fission cross-section. The errors on the cross-sections for the threshold isotopes were usually much larger due mainly to poor counting statistics.

The U^{235} foil used for the ratio measurements was the same foil as used in the measurement of the absolute U^{235} fission cross-section, therefore the error due to foil assay, foil thickness correction and extrapolation of the fission-fragment spectrum in the ratio measurement is correlated with the same error in the absolute measurement of the U^{235} fission cross-section by WHITE [1], and allowance has been made for this in the calculation of the cross-section and ratio errors.

RESULTS AND DISCUSSION

The values obtained for the fission cross-sections of U^{233}, U^{234}, U^{236}, Np^{237}, Pu^{239} and Pu^{241} are given in Table II, and are shown together with previous measurements in Figs. 3-8. The fission cross-section ratios relative to the U^{235} fission cross-section are given in Table III, and are also shown on some of the figures since many previous measurements have been made by this method, although in most cases different values for the U^{235} fission cross-section have been used for normalization.

U^{233}, Pu^{239}, Pu^{241}

The present measurements of cross-section ratios at energies greater than about 100 keV agree well with ALLEN and FERGUSON [4] for U^{233} and Pu^{239}, and with BUTLER and SJOBLOM [16] and SMITH et al. [17] for Pu^{241}. The different values of cross-section obtained are due entirely to the different values of the U^{235} fission cross-section used for normalization. This difference has been discussed by WHITE [1].

TABLE II

MEASURED FISSION CROSS-SECTIONS IN BARNS OF U^{238}, U^{234}, U^{236}, Np^{237}, Pu^{239} AND Pu^{241}, AND ALSO OF U^{235} USED FOR CALIBRATION

Neutron energy (keV)	Energy spread (± keV)	Isotope						
		U^{235}	U^{233}	U^{234}	U^{236}	Np^{237}	Pu^{239}	Pu^{241}
40	10	2.10 ± 0.06	2.74 ± 0.10	0.012 ± 0.002		0.013 ± 0.001	1.45 ± 0.05	2.76 ± 0.10
67	10	1.79 ± 0.05	2.37 ± 0.09	0.018 ± 0.002		0.012 ± 0.001	1.46 ± 0.05	2.38 ± 0.09
127	7	1.54 ± 0.04	2.22 ± 0.07	0.021 ± 0.002	0.0018 ± 0.0009	0.024 ± 0.002	1.51 ± 0.05	2.09 ± 0.07
312	7	1.30 ± 0.03	2.15 ± 0.07	0.186 ± 0.015	0.0037 ± 0.0014	0.069 ± 0.005	1.52 ± 0.05	1.68 ± 0.06
415	7	1.22 ± 0.03	1.97 ± 0.06					
505	10	1.17 ± 0.03	1.85 ± 0.06	0.56 ± 0.03	0.0069 ± 0.0006	0.47 ± 0.02	1.56 ± 0.05	1.47 ± 0.06

Below 100 keV the present ratio measurements for all three isotopes lie consistently below the previous results but do extrapolate smoothly to the results of PERKIN et al. [5] at 24-keV neutron energy. This latter experiment was performed relatively close to an antimony-beryllium neutron source where the effects of the low-energy neutrons produced by scattering in the walls of the laboratory were small. Both U^{233} and Pu^{239} have a higher epithermal-to-fast fission cross-section ratio than that for U^{235} and are therefore more affected by a background of low-energy neutrons. This is a possible cause for the higher values of fission cross-section ratio found in previous work.

The present measurements and those of PERKIN et al. [5] show no indication of structure in the fission cross-section of Pu^{239} as suggested by the compilation of Douglas [18], and the broad minimum in the fission cross-section in the energy range 50-100 keV indicated by these measurements is possibly due to competition from inelastic neutron scattering to the excited states in the ground state rotational band at 57-keV and 76-keV excitation [19]. From the results for U^{233} and Pu^{241} it can be seen that the effect of any similar such competition is not so pronounced.

U^{234}, U^{236}, Np^{237}

At 127 keV and 505 keV the present measurements agree well with the results of LAMPHERE [2] for U^{234} and U^{236}, and with KLEMA [20] for Np^{237}.

The errors on these cross-sections are in general much larger than for the thermally fissile isotopes, and the different values of U^{235} fission cross-section taken for normalization are not so important. Because of this, fission cross-section ratios have not been included in the figures.

In all three isotopes the fission cross-section does not fall exponentially with decreasing energy as would be expected from the single-level barrier penetration formula of HILL and WHEELER [21], although for U^{236} the measurement at 127 keV is only just significantly different from zero. The cross-sections for "sub-threshold" fission in U^{234}, U^{236} and Np^{237} are 15 ± 2, 2 ± 1 and 11 ± 1 mb respectively.

LAMPHERE [2] has interpreted the fission-fragment angular distribution for U^{234} in the energy range 0.4-1.0 MeV in terms of a 1/2+, 3/2-, 1/2- K-band structure at the saddle point of the fissioning nucleus. The present measurements suggest that in order to account for the observed fission below the main threshold, the 3/2- and/or the 1/2- bands lie in energy below that of the 1/2+ band by 300-400 keV. A similar explanation has been suggested by DE VROEY et al. [22] for the sub-threshold fission in Pu^{240} [22, 23].

In U^{238} [2] and possibly in U^{236} no such sub-threshold plateau has been found, and probably for these nuclei the 1/2+ band lies lower in energy than the negative parity bands.

Fission in Np^{237} is complicated by being through an odd-odd compound nucleus. The fission cross-section of 11 mb observed at energies below the main threshold is then, like U^{234} and Pu^{240}, probably induced by p-wave neutrons.

TABLE III

MEASURED FISSION CROSS-SECTION RATIOS OF U^{233}, U^{234}, U^{236} Np^{237}, Pu^{239} AND Pu^{241} RELATIVE TO U^{235}

Neutron energy (keV)	Energy spread (± keV)	Isotope					
		U^{233}	U^{234}	U^{236}	Np^{237}	Pu^{239}	Pu^{241}
40	10	1.30	0.006 ± 0.001		0.0060 ± 0.0005	0.690	1.31
67	10	1.33	0.010 ± 0.001		0.0064 ± 0.0003	0.816	1.33
127	7	1.44	0.014 ± 0.002	0.0012 ± 0.0006	0.0155 ± 0.0008	0.980	1.36
312	7	1.66	0.143 ± 0.007	0.0028 ± 0.0011	0.053 ± 0.004	1.17	1.30
415	7	1.62					
505	10	1.58	0.47 ± 0.02	0.0059 ± 0.0006	0.400 ± 0.009	1.34	1.26
Error[+] (%)		2.2				2.2	2.5

[+] unless otherwise specified

ACKNOWLEDGEMENTS

We wish to thank Dr. J.L. Perkin for many helpful discussions during this work.

REFERENCES

[1] WHITE, P.H., to be published in J. nucl. Energy.
[2] LAMPHERE, R.W., Nucl. Phys. 38 (1962) 561.
[3] LAMPHERE, R.W., Phys. Rev. 104 (1956) 1654.
[4] ALLEN, W.D. and FERGUSON, A.T.G., Proc. phys. Soc. A70 (1957) 573.
[5] PERKIN, J.L., WHITE, P.H., FIELDHOUSE, P., AXTON, E.J., CROSS, P. and ROBERTSON, J.C., private communication; to be published in J. nucl. Energy.
[6] BARRY, J.F., BUNCE, J. and WHITE, P.H., J. nucl. Energy A/B 18 (1964) 481.
[7] HYDE, E.K., National Nuclear Energy series PPR 17B P916, McGraw Hill (1959).
[8] FLEMING, E.H., GHIORSO, A. and CUNNINGHAM, B.B., Phys. Rev. 88 (1952) 642.
[9] BRAUER, F.P., STROMATT, R.W., LUDWICK, J.D., ROBERTS, F.P. and LYON, W.L., J. inorg. nucl. Chem. 12 (1960) 234.
[10] WALLMAN, J.C., University of California report UCRL 1255 (1951).
[11] BROWN, F., GEORGE, G.G., GREEN, D.E. and WALT, D.E., J. inorg. nucl. Chem. 13 (1960) 192.
[12] HALL, G.R. and MARKIN, T.L., J. inorg. nucl. Chem. 2 (1956) 202.
[13] SCHULTZ, W.D. and THOMASON, P.F., Analyt. Chem. 31 (1951) 492.
[14] LEACHMAN, R.B., Phys. Rev. 101 (1956) 1005.
[15] TASCHEK, R. and HEMMENDINGER, A., Phys. Rev. 74 (1948) 373.
[16] BUTLER, D.K. and SJOBLOM, R.K., Phys. Rev. 124 (1961) 1129.
[17] SMITH, H.L., SMITH, R.K. and HENKEL, R.L., Phys. Rev. 125 (1962) 1329.
[18] DOUGLAS, A.C. and BARRY, J.F., AWRE Rpt. 0-79/64 (1965).
[19] LANDOLT-BÖRNSTEIN, Zahlenwerte und Funktionen aus Naturwissenschaften und Technik. Neue Serie, Gp. 1. I Energie-Niveaus der Kerne. Springer Verlag, Berlin (1961).
[20] KLEMA, E.D., Phys. Rev. 72 (1947) 88.
[21] HILL, D.L. and WHEELER, J.A., Phys. Rev. 89 (1953) 1102.
[22] DE VROEY, M., FERGUSON, A.T.G., and STARFELT, N., private communication and to be published.
[23] RUDDICK, P. and WHITE, P.H., J. nucl. Energy A/B 18 (1964) 561.
[24] COTÉ, R.E., BOLLINGER, L.M., LE BLANC, J.M. and THOMAS, G.E., Bull. Am. phys. Soc. II. 1 (1956) 187.
[25] CRANBERG, G.L., DAY, R.G., HAWKINS, W., HENKEL, R.L., JARVIS, G.A., LAZAR, N., NOBLES, R., BARRY, J.E., SMITH, R. and WALT, M. (1952) Los Alamos Rpt. LA 1495.
[26] DOROFEEV, G.A, and DOBRYNIN, Y.P., Atomnaja energija 2 (1957) 10.
[27] DUBROVINA, S.M. and SHIGIN, V.A., Dokl. Akad. Nauk. SSSR 157 (1964) 561.
[28] GORLOV, G.V., GOKHBERG, B.M., MOROZOV, V.M., OTROSCHCHENKO, G.A. and SHIGIN, V.A., Atomnaja energija 6 (1959) 453.
[29] HENKEL, R.L., Los Alamos Rpt. LA 2114
[30] HUGHES, D.J. and SCHWARTZ, R.B., United States Atomic Energy Commission Rpt. BNL 325, 2nd Ed. (1958).
[31] JAMES, G.D., Atomic Energy Research Establishment Rpt. AERE-R4597 (1964).
[32] LAMPHERE, R.W. and GREENE, R.E., Phys. Rev. 100 (1955) 763.
[33] NETTER, F., Commissariat à l'energie atomique Rpt. CEA 1913.
[34] Oak Ridge annual progress Rpt. ORNL 1879 (1955).
[35] Oak Ridge semi-annual progress Rpt. ORNL 1975 (1955).
[36] SMIRENKIN, G.N., NESTEROV, V.G. and BONDARENKO, I.I., Atomnaja energija 13 (1962) 974.

Keys to Symbols used in Figs. 3-8

- ⊙ Present measurements
- ▽ -·- } ALLEN and FERGUSON [4]
- ▲ BUTLER and SJOBLOM [16]
- ⊖ COTÉ et al. [24]
- ⊠ CRANBERG et al. [25]
- ▽ DOROFEEV and DOBRYNIN [26]
- ····· DOUGLAS [18]
- ◭ DUBROVINA and SHIGIN [27]
- △ GORLOV et al. [28]
- ◬ HENKEL [29]
- —— HUGHES and SCHWARTZ [30]
- × JAMES [31]
- ⊕ KLEMA [20]
- ◇ LAMPHERE [2]
- ⊖ LAMPHERE [3]
- ◈ LAMPHERE and GREENE [32]
- \+ -+- } NETTER [33]
- ⊟ Oak Ridge progress report ORNL 1879 [34]
- ○ Oak Ridge progress report ORNL 1975 [35]
- ⊙ PERKIN et al. [5]
- -·-·- SMIRENKIN et al. [36]
- □ SMITH et al. [17]

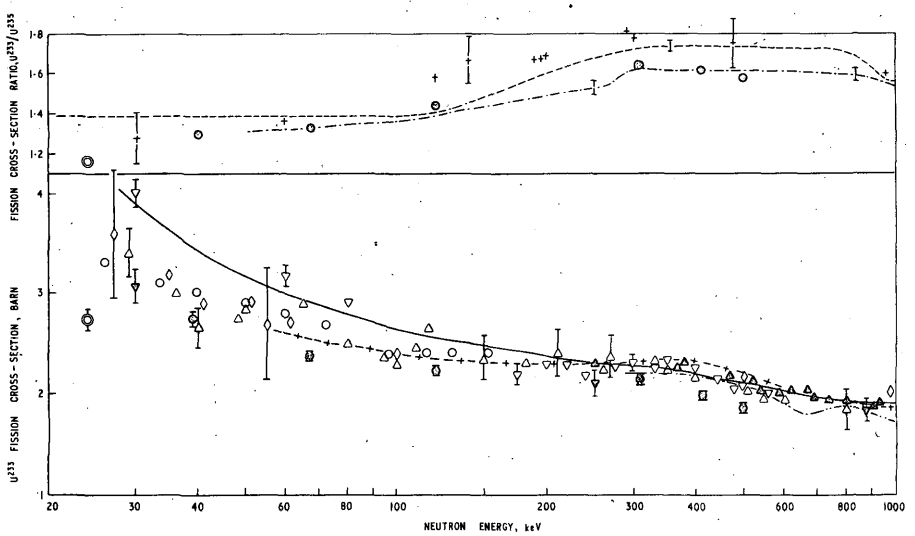

Fig. 3

Present and other measurements of the U^{233} fission cross-section and the fission cross-section ratio (U^{233}/U^{235})

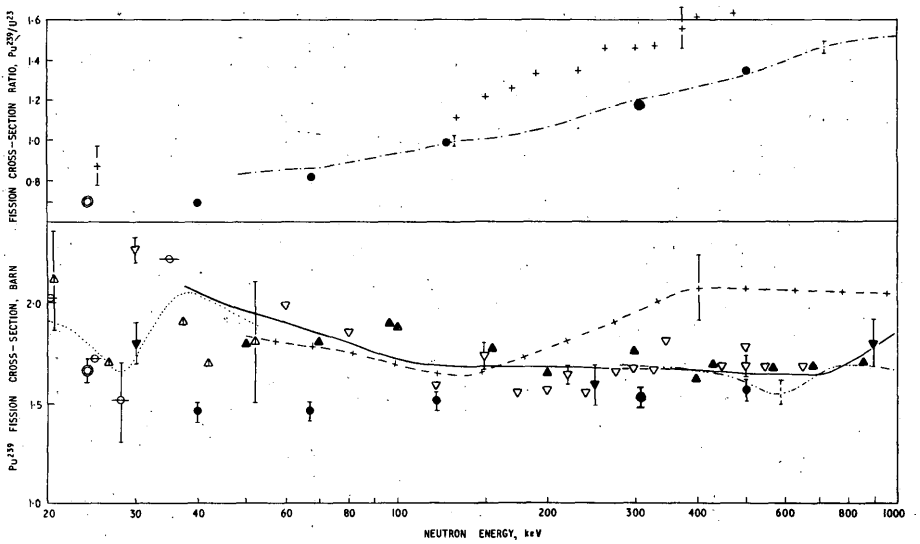

Fig. 4

Present and other measurements of the Pu^{239} fission cross-section and the fission cross-section ratio (Pu^{239}/U^{235})

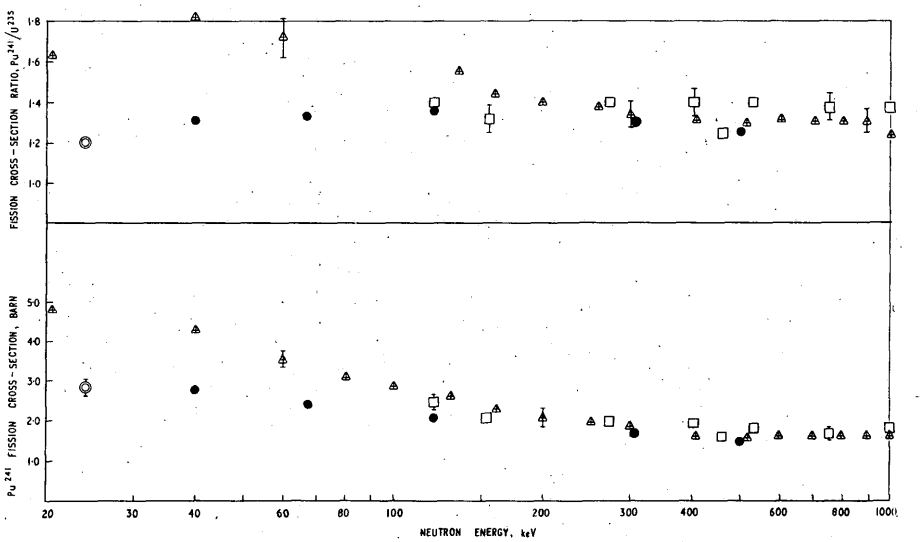

Fig. 5

Present and other measurements of the Pu^{241} fission cross-section and the fission cross-section ratio (Pu^{241}/U^{235})

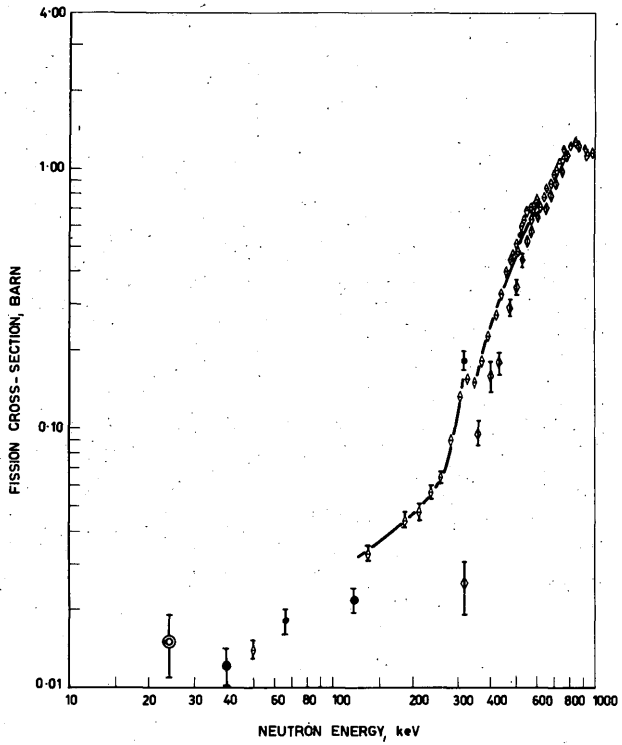

Fig. 6

Present and other measurements of the fission cross-section of U^{234}

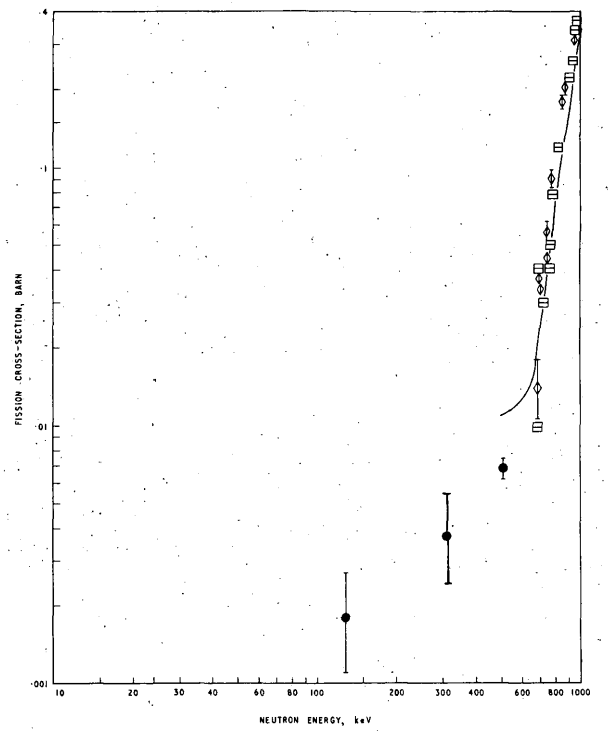

Fig. 7

Present and other measurements of the fission cross-section of U^{236}

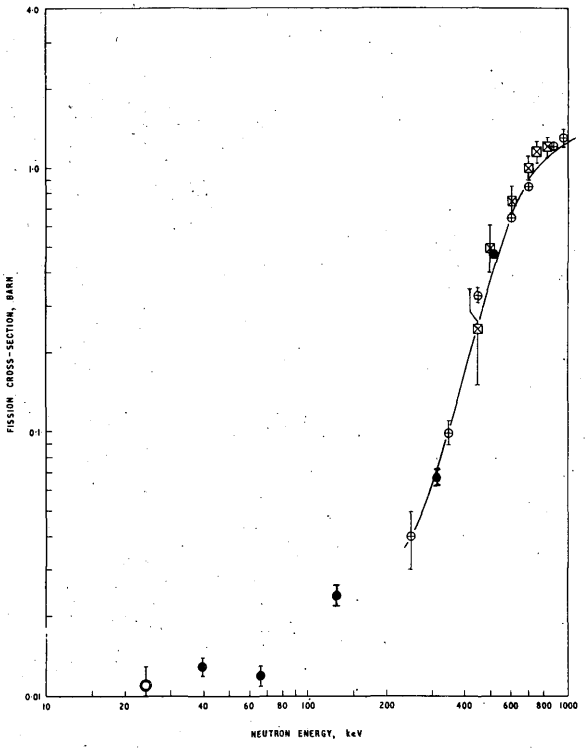

Fig. 8

Present and other measurements of the fission cross-section of Np^{237}

FISSION CROSS-SECTION MEASUREMENTS ON Pu^{239}, Pu^{241}, U^{232}, AND A SEARCH FOR FISSION COMPONENTS IN Pu^{238} RESONANCES

G. D. JAMES
ATOMIC ENERGY RESEARCH ESTABLISHMENT,
HARWELL, DIDCOT, BERKS., UNITED KINGDOM

Abstract — Résumé — Аннотация — Resumen

FISSION CROSS-SECTION MEASUREMENTS ON Pu^{239}, Pu^{241}, U^{232}, AND A SEARCH FOR FISSION COMPONENTS IN Pu^{238} RESONANCES. Fission cross-section measurements on Pu^{239} and Pu^{241} have been carried out from sub-thermal-neutron energy to the keV region; resonance parameters are given and errors in the average values of the cross-section are discussed. The discovery of large fission components in the U^{232} neutron resonances stimulated a search for fission components in Pu^{238}. The results of these experiments are given. All the measurements were performed on the Harwell time-of-flight spectrometer.

MESURE DES SECTIONS EFFICACES DE FISSION DE ^{239}Pu, ^{241}Pu, ^{232}U ET RECHERCHES DES COMPOSANTS DE FISSION DANS LES RÉSONANCES DE ^{238}Pu. L'auteur a fait des mesures des sections efficaces de fission de ^{239}Pu et ^{241}Pu, pour des neutrons des catégories allant des neutrons froids à ceux dont l'énergie est de l'ordre du keV; il donne les paramètres de résonance et discute les erreurs sur les valeurs moyennes de la section efficace. A la suite de la découverte d'importants composants de fission dans les résonances de ^{232}U, il a été amené à rechercher les composants de fission dans les résonances de ^{238}Pu. Il donne les résultats des expériences. Toutes les mesures ont été effectuées à l'aide du spectromètre à temps de vol de Harwell.

ИЗМЕРЕНИЯ СЕЧЕНИЙ ДЕЛЕНИЯ ДЛЯ ПЛУТОНИЯ-239, ПЛУТОНИЯ-241, УРАНА-232 И ИЗУЧЕНИЕ КОМПОНЕНТОВ ДЕЛЕНИЯ В РЕЗОНАНСАХ ДЛЯ ПЛУТОНИЯ-238. Измерения сечения деления для плутония-239 и плутония-241 проводились в диапазоне от энергии подтепловых нейтронов до значений кэв. Приводятся параметры резонансов и обсуждаются ошибки в средних значениях сечений. Открытие крупных компонентов деления в нейтронном резонансе урана-232 стимулировало проведение исследования компонентов деления в плутонии-238. Приводятся результаты этих экспериментов. Все измерения выполнялись на спектрометре по времени пролета в Харуэлле.

MEDICION DE LAS SECCIONES EFICACES DE FISION DEL ^{239}Pu, ^{241}Pu Y ^{232}U E INVESTIGACION DE COMPONENTES DE FISION EN LAS RESONANCIAS DEL ^{238}Pu. Se han medido las secciones eficaces de fisión del ^{239}Pu y del ^{241}Pu en el intervalo de energía neutrónica que va de la región subtérmica a la región del kiloelectrón voltio; se indican los parámetros de resonancia y se analizan los errores de los valores medios de las secciones eficaces. El descubrimiento de considerables componentes de fisión en la resonancia neutrónica del ^{232}U indujo a investigar los componentes de fisión en la resonancia del ^{238}Pu. Se indican los resultados de estos experimentos. Todas las mediciones se efectuaron con el espectrómetro de tiempo de vuelo de Harwell.

INTRODUCTION

The fission cross-sections of the nuclei Pu^{239} and Pu^{241} are required for the determination of the reactivity and Doppler coefficient of nuclear reactors. Reactivity calculations require data that provide accurate average values of the cross-section over wide neutron energy bands whereas a de-

termination of the Doppler coefficient requires a knowledge of the resonance parameters to as high a neutron energy as possible. These cross-sections are also interesting because they add to our knowledge of the relatively few nuclei that undergo fission by neutrons of thermal energy.

The even-even nuclei U^{232} and Pu^{238} are two of the few even mass nuclei that undergo fission by thermal neutrons. The discovery of large fission components in the neutron resonances of U^{232} [1], which has a thermal fission cross-section of 83b [2], has stimulated interest in the fission components of neutron resonances in the nucleus Pu^{238}, which, by comparison, has a thermal fission cross-section of 17b [3, 4].

Fission cross-section measurements on the four nuclei Pu^{239}, Pu^{241}, U^{232} and Pu^{238} have been carried out on a Harwell Neutron Project time-of-flight spectrometer. Basically the same experimental method was used to measure all the cross-sections, and a description of the method is given with reference to the Pu^{241} experiments. For this nucleus the data covered the range 0.01 eV to 3 keV. Below 11 eV the data are well described by the multilevel parameters of MOORE et al. [5]. A multilevel analysis of the present data from 11 eV to 17 eV has been carried out. The results of this analysis are given and the accuracy of the average fission cross-section is discussed. In a measurement of the Pu^{239} fission cross-section [6], average values of the cross-section in the energy range 1 keV to 160 keV were found to agree within experimental error with the data of ALLEN and FERGUSON [7] above 55 keV. These measurements have been repeated with better energy resolution in an attempt to deduce resonance parameters to as high an energy as possible. The results obtained from 55 eV to 90 eV are given. In a search for fission components in the Pu^{238} neutron resonances below 100 eV no fission yield greater than background noise was observed, and an upper limit to the fission width Γ_f for the three resonances below 20 eV has been set. The implication of these results in explaining the thermal fission cross-section and the fission cross-section near threshold is discussed.

FISSION CROSS-SECTION OF Pu^{241} FROM 0.01 eV TO 3 keV

Experimental method

The fission cross-section of Pu^{241} was measured using silicon-gold surface-barrier semiconductor detectors made from 300-Ωcm N-type silicon discs, as described by DEARNALEY and WHITEHEAD [8]. Two experiments were carried out: one using a 5-m flight path covered the neutron energy range 0.0087 eV to 20 eV, the other covered the range 3 eV to 3 keV and used a 15-m flight path. The experimental details are given in Table I. Signals from the surface barrier detectors were amplified and sent through a discriminator (which rejected pulses from alpha particles) to a magnetic tape time-of-flight analyser [9]. In both experiments the neutron spectrum was measured by using a BF_3 counter. The background for both fission and spectrum measurements was determined by placing resonant scatterers in the neutron beam, each sample being sufficiently thick to remove all neutrons

TABLE I

EXPERIMENTAL DETAILS

Material	Pu^{241}	Pu^{241}	Pu^{239}	Pu^{238}
Path length	5m	15 m	15 m	5 m
Weight of material	5 mg	10 mg	40 mg	0.338 mg
Type of detector	Si-Au solid state	Gas scintillator	Gas scintillator	Gas scintillator
Isotopic composition Pu^{238} Pu^{239} Pu^{240} Pu^{241} Pu^{242}	- 0.52% 1.44% 97.33% 0.71%	- 2.5% 2.48% 94.8% 0.28%	- 99.92% 0.072% 0.003% <0.003%	99.98% 0.02% - - -
Neutron filter	None	0.27 g cm^{-2} B_4C	0.27 g cm^{-2} B_4C & 0.22 g cm^{-2} ~~Cd~~ Cd	None
Materials used to determine background	W 18.8 eV Ta 4.28 eV In 1.457 eV Cd 0.178 eV	Na 2.3 keV Mn 335 eV Ta 4.28 eV In 1.457 eV	Al 35 keV Na 2.3 keV Mn 335 eV Ta 4.28 eV In 1.457 eV	W 18.8 eV Ta 4.28 eV In 1.457 eV Cd 0.178 eV
Electron pulse width	0.2 μs	1 μs	0.1 μs	0.1 μs
Timing channel width	1 μs	1 μs	1/16 μs	0.25 μs
Pulse repetition frequency	110 pps	200 pps	186 pps	186 pps
Number of timing channels	4096	4096	16 384	4096

at the resonant energy. The decrease in background caused by the presence of the scatterer was measured by introducing a second layer of scatterer and allowed for. For both detectors it was found that the background could be represented by the equation

$$B = B_0 + B_1 \exp(B_2 \ln E) \quad (1)$$

where B is the background counts per channel, E is the neutron energy and B_0, B_1 and B_2 are constants. In the 5-m experiment no background measurement was available below 0.178 eV, and the data have been evaluated on the basis of two possible assumptions about the background. Firstly, that the background below 0.178 eV is constant and equal to its value at 0.178 eV; and secondly, that a lower limit to the background below 0.01 eV is given by the count-rate observed with a single layer of cadmium in the beam. These extreme assumptions lead to an error due to background uncertainty of not more than 2% in the thermal value of the cross-section at which the data are normalized.

The fission cross-section was calculated on an IBM-7030 computer from an equation that assumes that the cross-section for the $B^{10}(n\alpha)Li^7$ reaction used to measure the spectrum is proportional to $E^{-\frac{1}{2}}$. A correction of up to 2% is made for the effect of self-shielding on the BF_3 counter efficiency. The data were normalized by equating the value of the cross-section at 0.0253 eV to 1010 b [10]. Because of the low statistical accuracy of the data near thermal-neutron energy all the data from 0.02 eV were used in the normalization by assuming that $\sigma_f\sqrt{E}$ is a linear function of E over this energy range. This gives a normalization error of ±1%. The 15-m data were normalized to the 5-m data by equating the areas under the fission cross-section curves from 4 eV to 32 eV, resulting in an additional normalization error for the 15-m data of ±2%.

The Pu^{241} fission cross-section

Figure 1 shows the Pu^{241} fission cross-section from 0.01 eV to 3 keV. It is found that the average value of the cross-section over energy ranges E to 2E is given to better than ±5% below 250 eV, except for the region of low cross-section near 1 eV, and to ±11% above 250 eV. Above 32 eV the major contribution to the uncertainty in the cross-section comes from the error in the energy range due to the finite timing channel width. Below 0.5 eV the data agree to ±5% with those of LEONARD and FRIESENHAHN [11]. Below 11 eV the data are in fair agreement with the curve given by the multilevel parameters of MOORE et al. [5]. A multilevel analysis of the data from 11 eV to 17 eV has been carried out using the computer programme of PATTENDEN and HARVEY [12], which is based on the formulae of VOGT [13]. As in the analysis of MOORE et al. [5] below 11 eV, it was found that the cross-section could be fitted by assuming one spin state and two fission channels with the width of each level assumed to lie entirely in one of the two channels. Figure 2 shows the multilevel curve obtained from the parameters given in Table II. In Table II E_λ is the resonance energy, g the spin weighting factor, Γ_n^0 the reduced neutron width, Γ_{f1} and Γ_{f2} the fission widths for the two fission

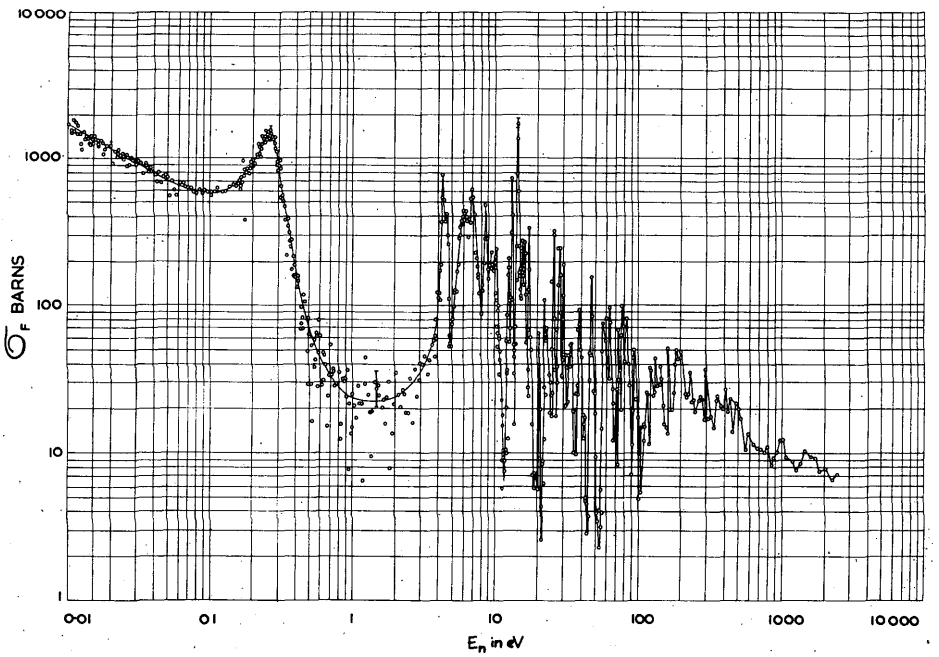

Fig. 1

Pu^{241} fission cross-section from 0.01 eV to 3 keV

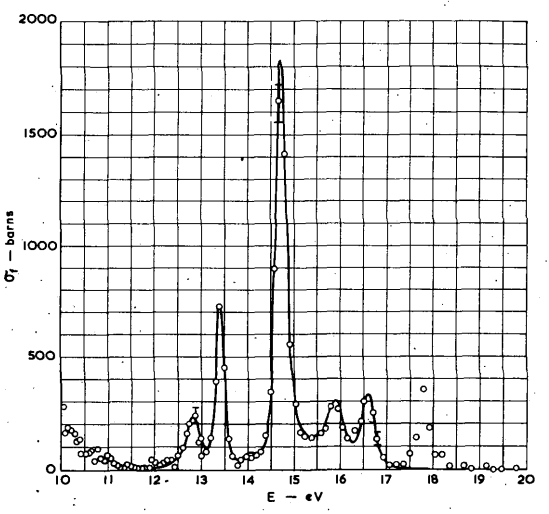

Fig. 2

Multilevel fit to Pu^{241} fission cross-section from 12 to 17 eV

channels, and Γ_γ the radiation width. Over this energy range MOORE et al. [5] made the same choice of fission channels and obtained parameters that agree to between 0% and 50% with the parameters of Table II. Unlike the resonances below 11 eV, the resonances from 11 eV to 17 eV do not fall into

TABLE II

MULTILEVEL PARAMETERS FOR Pu^{241} BETWEEN 12 eV and 17 eV

E_λ (eV)	$2g\Gamma_n^0$ (10^{-3} eV)	Γ_{f1} (10^{-3} eV)	Γ_{f2} (10^{-3} eV)	Γ_γ (10^{-3} eV)	Sign of $(\Gamma_{fi}/2)^{\frac{1}{2}}$
12.84	0.220	266		40	+
13.45	0.596		42	40	-
14.04	0.048	214		40	-
14.78	1.513	105		40	+
16.06	0.344	360		40	-
16.70	0.323		180	40	+

distinctly "broad" and "narrow" groups. Below about 20 eV, where resonances begin to be missed, the mean-level spacing D is 1.3 ± 0.2 eV. The data of Table II combined with the data of MOORE et al. [5] below 11 eV gives a strength function, $g\overline{\Gamma n^0}/D$ of $(1.4 \pm 0.6) \times 10^{-4}$. The distribution of $\Gamma_f / \overline{\Gamma}_f$ fits a χ squared distribution with $\nu = 2 \pm 0.2$ degrees of freedom. It is known that the resonances belong to two spin states that may have widely different values of $\overline{\Gamma}_f$; the value of ν for the combined distribution is not therefore meaningful.

FISSION CROSS-SECTION MEASUREMENTS ON Pu^{239}

Experimental method

The Pu^{239} fission cross-section has been measured from 4 eV to 35 keV in a 15-m flight path experiment similar to that described for Pu^{241}. The experimental details are set out in Table I. A continuous flow gas scintillator containing 40 mg of fissile material was used. Pulses from the 5 b AVP photomultipliers attached to the gas scintillators were passed through a fast tunnel diode discriminator set at 150 mV to remove unwanted alpha particles. A mixture of helium with 0.3% nitrogen, which acts as a wavelength shifter, was used as the scintillating medium. The data were normalized to those of BOLLINGER et al. [14] by equating the areas under the fission cross-sections between 4 eV and 16 eV.

The Pu^{239} fission cross-section from 50 eV to 100 eV

Figure 3 shows the Pu^{239} cross-section from 50 eV to 100 eV. All the resonances observed in this energy range by UTTLEY [15] in a measurement of the Pu^{239} total cross-section with superior energy resolution (2 ns/m) are seen in Fig. 3 showing that no resonances are missed below 100 eV. Table III

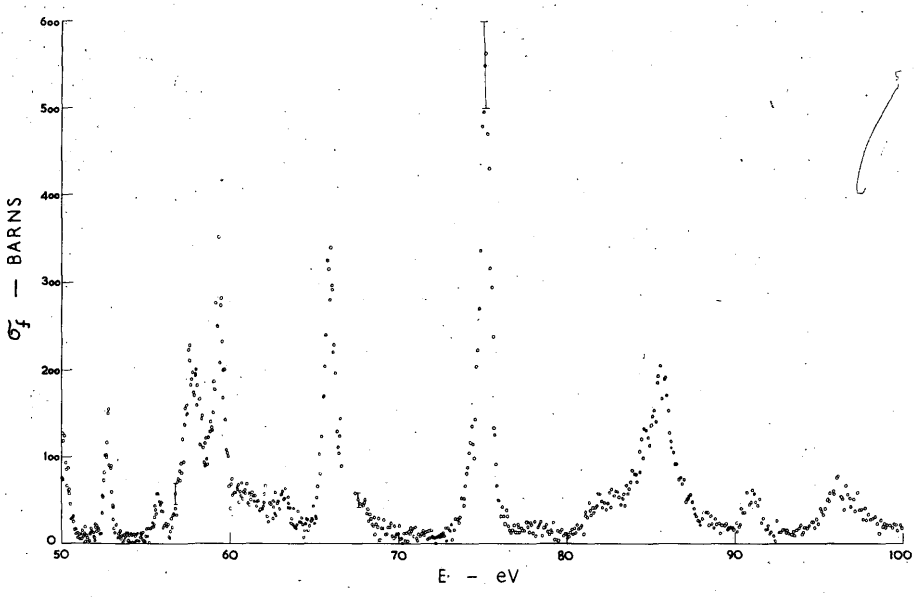

Fig. 3

Pu^{239} fission cross-section from 50 eV to 100 eV

TABLE III

VALUES OF $\sigma_{of}\Gamma$ FOR THE RESONANCES IN Pu^{239} FROM 55 eV TO 85 eV

E_λ (eV)	55.8	57.8	59.35	60.9	63.2	65.9	74.35	75.1	82.0	85.6
$\sigma_{of}\Gamma$(b-eV)	30	272	209	41	27	206	55	266	75	357

gives the values of $\sigma_{of}\Gamma$ (the product of the peak fission cross-section σ_{of} and the total width Γ) deduced from the areas under the resonances. "Wing corrections" were made using values of Γ estimated from "shape" analysis of the resonances by the method described by LYNN and RAE [16]. Some levels, notably those at 60.9 eV and 63.2 eV, are superimposed on a fission background caused either by a hidden broad resonance or by interference. For such levels an arbitrary constant background has been subtracted.

A SEARCH FOR FISSION COMPONENTS IN Pu^{238} RESONANCES

Experimental method

The fission yield from 0.338 mg of Pu^{238} has been measured, by the gas scintillator technique described for Pu^{239} and the time-of-flight method

described for Pu^{241}, on a 5-m flight path. The fission cross-section was determined relative to the U^{235} fission cross-section by measuring the yields of fission fragments from known quantities of these two materials using the same discriminator and photomultiplier under identical voltage conditions, and the same gas mixture and chamber geometry for both experiments. The amount of Pu^{238} and U^{235} on the foils was determined from the alpha source strength and the isotopic composition of the materials. The experimental details are again given in Table I.

The fission components of Pu^{238} neutron resonances

No positive indication of a fission component for any of the six known neutron resonances below 100 eV was observed. Upper limits to Γ_f for the three resonances below 20 eV have been found using the values of E_λ, Γ and Γ_n^0 given by YOUNG et al. [17]. The fission width for the negative level was deduced from the thermal fission cross-section [1] and the parameters of Young et al. after verifying that there was negligible contribution to the thermal-fission cross-section from the positive energy resonances. These values of Γ_f are given in Table IV. The fission width of the negative energy

TABLE IV

FISSION WIDTHS FOR NEUTRON RESONANCES IN Pu^{238}

E_λ(eV)	-0.5	2.89	9.98	18.57
Γ_f (MeV)	1.24	<0.083	<0.196	<0.202

level is at least three times the average fission width for the resonance below 20 eV. The probability of finding such a resonance is less than 10% if the fission widths follow a Porter-Thomas [18] distribution.

From the average fission width, $\overline{\Gamma}_f < 0.43$ MeV, and the level spacing, $D \sim 6$ eV, we can calculate the effective number of fission channels N from the formula $N = 2\pi\overline{\Gamma}_f/D$ given by WHEELER [19]. This value of N can then be used to estimate the ratio $E_f/\hbar w$ from the Wheeler penetration formula and gives $E_f/\hbar w > 1.22$. Here E_f is the fission threshold and w is the circular frequency of an inverted harmonic oscillator representing the fission barrier at the saddle point. The slope of the fission cross-section near threshold calculated from the penetration formula using this ratio, and the plateau fission cross-section given by BUTLER [20], is much steeper than the slope measured by BUTLER [20]. This discrepancy may be explained by the presence of a sub-threshold fission cross-section as found by NESTROV and SMIRENKIN [21] for Pu^{240}. These considerations call for a measurement of the Pu^{238} fission cross-section in the keV region below 150 keV.

ACKNOWLEDGEMENTS

The author is grateful to Dr. M.J. Poole and Dr. E.R. Rae for their advice and encouragement, to Mrs. K.M. Glover for preparing the Pu^{238} foil and Dr. P. White for measuring its alpha source strength, to Mr. D. Boreham for preparing the Pu^{241} foils and Mr. D.A.J. Endacott for help with the experiments.

REFERENCES

[1] JAMES, G.D., Nucl. Phys. 55 (1964) 517.
[2] ELSON, R., BENTLEY, W., GHIORSO, A. and Van WINKLE, Q., Phys. Rev. 89 (1953) 320.
[3] HULET, E.K., HOFF, R.W., BOWMANN, H.R. and MICHEL, M.C., Phys. Rev. 107 (1957) 1294.
[4] EASTWOOD, T.A., BAERG, A.P., BINGHAM, C.B., BROWN, F., CABELL, M.J., GRUMMIT, W.E., ROY, J.C., ROY, L.P. and SCHUMAN, R.P., Proc. 2nd UN Int. Conf. PUAE 16 (1958) 54.
[5] MOORE, M.S., SIMPSON, O.D., WATANABE, T., RUSSELL, J.E. and HOCKENBURY, R.W., Phys. Rev. 135 (1964) B945.
[6] JAMES, G.D., Symposium on the Absolute Determination of Neutron Flux in the Energy Range 1-100 keV, EANDC-33 "U" (1963) 14.
[7] ALLEN, W.D. and FERGUSON, A.T.G., Report AERE NP/GEN/3 (unpublished).
[8] DEARNALEY, G. and WHITEHEAD, A.B., Nucl. Instrum. Meth. 12 (1961) 205.
[9] WATERS, J.R. and BIRD, J.R., Nucleonics 19 (1961) 70.
[10] HUGHES, D.J., MAGURNO, B.A. and BRUSSEL, M.K., Supplement 1 to BNL 325 (2nd Ed.).
[11] LEONARD, B.R. and FRIESENHAHN, S.J., HW-62727 (unpublished).
[12] PATTENDEN, N.J. and HARVEY, J.A., Proc. Int. Conf. on Nuclear Structure, (North-Holland Publ. Co., Amsterdam) (1960) 882.
[13] VOGT, E., Phys. Rev. 112 (1958) 203.
[14] BOLLINGER, L.M., COTE, R.E. and THOMAS, G.E., Proc. 2nd UN Int. Conf. PUAE 15 (1958) 127.
[15] UTTLEY, C.A., private communication.
[16] LYNN, J.E. and RAE, E.R., J. nucl. Energy 4 (1957) 418.
[17] YOUNG, T.E., SIMPSON, F.B. and COOPS, M.S., Bull. Amer. phys. Soc. 7 (1962) 305, and Rep. IDO-16805.
[18] PORTER, C.E. and THOMAS, R.G., Phys. Rev. 104 (1956) 483.
[19] WHEELER, J.A., Rep. ORNL-2309 (unpublished).
[20] BUTLER, D.K., Rep. WASH-1044 (unpublished).
[21] NESTROV, V.G. and SMIRENKIN, G.N., Atomnaja energija 9 (1960) 16.

ANALYSE DE LA SECTION EFFICACE DE FISSION DE L'URANIUM-233 POUR DES NEUTRONS D'ÉNERGIE COMPRISE ENTRE 1, 7 eV ET 30 eV

H. NIFENECKER ET G. PERRIN
CENTRE D'ÉTUDES NUCLÉAIRES DE SACLAY, FRANCE

Abstract — Résumé — Аннотация — Resumen

ANALYSIS OF THE FISSION CROSS-SECTION OF U^{233} FOR NEUTRONS OF ENERGIES BETWEEN 1.7 AND 30 eV. The cross-section of U^{233} for resonance neutrons was analysed by the least-squares method. The paper discusses the need for using a multilevel formalism, and considers the statistical distributions of level spacing and partial widths. By the use of a study of level spacing as a starting point, particular attention is paid to the possibility of obtaining information on the relationship of populations of resonances of different spin.

ANALYSE DE LA SECTION EFFICACE DE FISSION DE ^{233}U POUR DES NEUTRONS D'ÉNERGIE COMPRISE ENTRE 1, 7 eV ET 30 eV. La section efficace de fission de l'uranium-233, pour des neutrons de résonance, a été analysée par la méthode des moindres carrés. La nécessité de l'utilisation d'un formalisme à plusieurs niveaux est discutée. Les distributions statistiques des espacements de niveaux et des largeurs partielles sont étudiées. En particulier, la possibilité de tirer des enseignements concernant le rapport des populations de résonances de spin différent, à partir de l'étude de l'espacement des niveaux, est examinée.

АНАЛИЗ ЭФФЕКТИВНОГО СЕЧЕНИЯ ДЕЛЕНИЯ УРАНА-233 ДЛЯ НЕЙТРОНОВ С ЭНЕРГИЕЙ МЕЖДУ 1,7 И 30 эв. Эффективное сечение деления урана-233 для резонансных нейтронов было проанализировано по методу наименьших квадратов. Обсуждается необходимость использования формализма разных уровней. Исследуются статистические распределения расстояний между уровнями и парциальных ширин. В частности, исследуется, с момента излучения расстояния между уровнями, возможность получения данных относительно правил плотностей резонансов отдельного спина.

ANALISIS DE LA SECCION EFICAZ DE FISION DEL ^{233}U PARA NEUTRONES DE ENERGIA COMPRENDIDA ENTRE 1, 7 Y 30 eV. Se ha analizado la sección eficaz de fisión del uranio-233 por neutrones de resonancia empleando el método de los cuadrados mínimos. La memoria discute la necesidad de emplear un formalismo de niveles múltiples. Estudia las distribuciones estadísticas de los espaciamientos de los niveles y de las anchuras parciales. En particular, examina en qué medida el estudio del espaciamiento de los niveles permite obtener datos sobre la relación de las poblaciones de resonancias de spin diferente.

1. INTRODUCTION

Nous avons effectué une analyse de forme de la section efficace de fission de l'uranium-233. Les résultats bruts de la mesure et la liste des paramètres approchés ont été précédemment publiés [1, 2]. L'analyse a été menée sur un calculateur IBM 7094 à l'aide d'un programme de moindres carrés mis au point par le service de Calcul électronique du CEA. Ce programme tend à rendre compte de la section efficace observée par une formule de la forme

$$\sigma_F(E) = \int_{-\infty} R(E - E')\Sigma_F(E')dE' + a\sqrt{E} + b$$

où

$$\Sigma_F(E') = \sum_r g\pi \lambda_r^2 \frac{\Gamma_n^r \Gamma_F^r}{(E - E_r)^2 + \Gamma_r^2/4}$$

et où la fonction R est une gaussienne dont la largeur rend compte de l'effet Doppler et de l'élargissement dû à la résolution. La sommation sur r peut être étendue à vingt résonances et le nombre de paramètres variables simultanément peut atteindre trente.

La largeur Doppler a été considérée comme fixe dans les calculs, et égale à

$$\Delta_{eV} = 2\left(\frac{kTEn}{A}\right)^{\frac{1}{2}} = 2,12 \cdot 10^{-2} \sqrt{E_{eV}}.$$

La résolution de l'expérience était limitée d'une part par la largeur de la bouffée de neutrons rapides, d'autre part par l'incertitude sur le temps de ralentissement. La largeur du canal d'analyse étant prise égale à la largeur de la bouffée de neutrons rapides, la fonction de résolution correspondant à la première de ces causes est un triangle de largeur à la base $2\Delta t$ où Δt est la largeur du canal d'analyse. La fonction de résolution due à l'incertitude sur le temps de ralentissement est de la forme $\frac{1}{2}\frac{t^2}{\tau^2}\exp\left(-\frac{t}{\tau}\right)$. Les fonctions de résolution intervenant dans le programme utilisé sont des gaussiennes. Nous avons égalé les moments d'ordre deux de ces gaussiennes et des fonctions de résolution vraies. Ceci donne pour l'incertitude due à la résolution d'analyse

$$\sigma_{eV_1}\sqrt{2} = \frac{10^{-3}}{\sqrt{3}} E_{eV}^{3/2} \Delta t_{\mu s}$$

où $\Delta t = 1\mu s$ à basse énergie et $\Delta t = 0,5\ \mu s$ à haute énergie et

$$\sigma_{eV_2}\sqrt{2} = 0,78 \cdot 10^{-3} E_{eV}$$

pour l'influence du temps de ralentissement.

2. RÉSULTATS DE L'ANALYSE

Nous avons divisé l'intervalle que nous désirons étudier en dix zones. Dans chacune des zones nous avons fait varier tout ou partie des paramètres des résonances en tenant compte dans les calculs de l'influence des résonances voisines encadrant la zone. Les paramètres approchés nécessaires comme données de départ pour l'utilisation de la méthode des moindres carrés ont été choisis égaux à ceux qui ont été déterminés dans un précédent article [2]. Nous avons cherché d'une part à assurer une concordance qualitative suffisante entre l'histogramme expérimental et la courbe théorique,

d'autre part à obtenir une valeur de X^2 aussi proche que possible du nombre de points de l'intervalle. Si l'analyse statistique est correcte on doit en effet avoir

$$N - \sqrt{2N} < X^2 < N + \sqrt{2N}$$

où N est le nombre de points de la zone diminué du nombre de paramètres variables. Nous avons rapidement constaté que dans toute la gamme d'analyse les constantes a et b étaient petites et pouvaient sans inconvénient être considérées comme égales à zéro. D'autre part l'accord entre les courbes théoriques et l'histogramme expérimental s'est révélé excellent à condition toutefois qu'on ajoute un petit nombre de résonances non détectées auparavant.

TABLEAU I

ZONES D'ANALYSE DE LA SECTION EFFICACE DE L'URANIUM-233

Numéro de la zone	Energies limites (eV)	Nombre de canaux - N	Valeurs de X^2	Nombre de résonances	Résonances nouvelles (eV)
I	1.75 - 2.70	300 288	361	3	2.19
II	2.70 - 4.18	240 234	221	2	3.45
III	4.18 - 9.09	318 300	318	8	6.72
IV	9.10 - 11.89	172 163	149	3	
V	11.45 - 14.79	144 135	124	3	
VI	14.84 - 17.66	88 76	91	4	15.69
VII	17.69 - 20.10	60 51	96	3	
VIII	20.14 - 24.80	90 72	106	6	22.03
IX	25.24 - 27.88	40 28	21	4	
X	27.95 - 33.02	62 47	79	5	

Le tableau I donne pour chaque zone le nombre de points expérimentaux, la valeur de X^2 obtenue, le domaine d'analyse en énergie, le nombre de résonances intéressées et l'énergie des nouvelles résonances introduites qui n'avaient pas été signalées dans la référence [2].

La méthode des moindres carrés décrite ci-dessus permet d'obtenir les trois quantités suivantes:

- l'énergie de la résonance
- la largeur Γ
- et la quantité $\frac{2g\Gamma_F\Gamma_n}{\Gamma}$ où l'on prendra $2g = 1$.

En attendant d'effectuer une analyse de forme sur les résultats obtenus par HARVEY [3] sur la transmission de l'uranium-233, nous supposerons ici que $\Gamma_\gamma = 45$ mV.

TABLEAU II

VALEUR DES PARAMÈTRES DES RÉSONANCES DE L'URANIUM-233

NOUVELLES VALEURS					ANCIENNES VALEURS		
Energie (eV)	Largeur totale (mV)	Largeur de fission (mV)	Largeur neutronique (mV)	Largeur neutronique réduite (mV)	Energie (eV)	Largeur de fission (mV)	$2g\Gamma_n^0$
1,823	309	264	0,484	0,354	1,799	277	0,330
2,191	160	115	0,072	0,048			
2,321	70,9	66,4	0,141	0,092	2,318	40,5	0,139
3,418	312	267	0,047	0,025			
3,678	182	137	0,110	0,058	3,69	185	0,074
4,819	857	809	0,298	0,135	4,83	720	0,108
5,995	421	376	0,156	0,064	6,02	431	0,086
6,723	750	705	0,398	0,153			
6,912	146	101	0,775	0,293	6,90	112	0,34
7,66	322	277	0,049	0,018	7,65	212	0,019
8,71	399	354	0,076	0,025	8,75	329	0,012
9,48	559	514	0,204	0,066	9,455	241	0,038
10,54	347	302	1,625	0,500	10,55	278	0,436
11,41	594	549	0,312	0,092	11,53	502	0,081
12,29	1102	1057	0,284	0,080	12,16	361	0,048
12,98	318	273	1,33	0,370	13,00	274	0,38
13,94	429	384	0,456	0,122	13,93	331	0,112
15,56	64	19	0,641	0,163			
15,69	230	185	0,500	0,126	15,64	148	0,186
16,48	672	627	1,300	0,320	16,56	675	0,337
16,81	182	137	0,492	0,120	16,82	60	0,070
18,27	158	113	0,250	0,0508	18,27	165	0,060
18,72	155	110	0,153	0,036	18,75	124	0,040
19,26	350	305	1,705	0,390	19,31	295	0,380
20,92	481	436	0,872	0,191	20,95	373	0,194
22,00	482	437	0,312	0,066			
22,23	205	160	0,791	0,168	22,24	354	0,153
22,69	445	400	3,023	0,635	22,69	357	0,714
23,17	1910	1865	1,812	0,376			
24,15	332	287	0,364	0,074	24,15	374	0,135
24,63	574	529	0,293	0,059	24,78	604	0,080
25,68	410	365	0,896	0,177	25,69	367	0,164
26,31	812	767	0,479	0,095	26,17	30	0,048
					26,50	235	0,037
27,00	542	497	0,571	0,112	27	433	0,104
28,14	503	458	0,017	0,003			
28,64	1390	1345	0,996	0,186	28,48	788	0,106
29,54	580	535	1,56	0,286	29,51	465	0,260

En faisant cette hypothèse on obtient le tableau II où les valeurs de E, de Γ_F et de Γ_n sont données ainsi que le rappel des valeurs données dans la référence [2]. Les figures 1 et 2 donnent des exemples de l'accord entre la courbe expérimentale et la courbe théorique.

La figure 3 représente le nombre de résonances détectées en fonction de l'énergie. On voit que l'histogramme reste sensiblement linéaire jusqu'à une énergie supérieure à 30 eV. C'est donc dans la région de 1,7 à 30 eV que nous pourrons faire une étude statistique valable des quantités caractéristiques des résonances.

De même les figures 4 et 5 représentent la somme des $g\Gamma_n^0$ et des Γ_F pour les résonances d'énergie inférieure à E. Là aussi la linéarité reste bonne jusque vers 30 eV. La pente des trois droites nous donne respectivement:

$$\langle D \rangle = 0,790 \text{ eV},$$

$$\frac{\langle 2g\Gamma_n^0 \rangle}{\langle D \rangle} = 0,209 \cdot 10^{-3} \text{ eV},$$

$$\frac{\langle \Gamma_F \rangle}{\langle D \rangle} = 0,435;$$

un calcul direct donne d'autre part $\langle 2g\Gamma_n^0 \rangle = 0,169$ mV et $\langle \Gamma_F \rangle = 0,389$ eV.

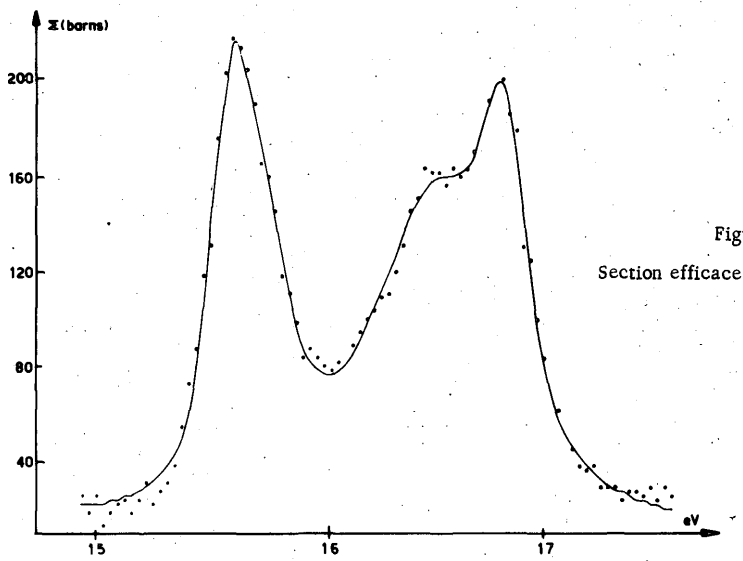

Figure 1

Section efficace de fission de ^{233}U.

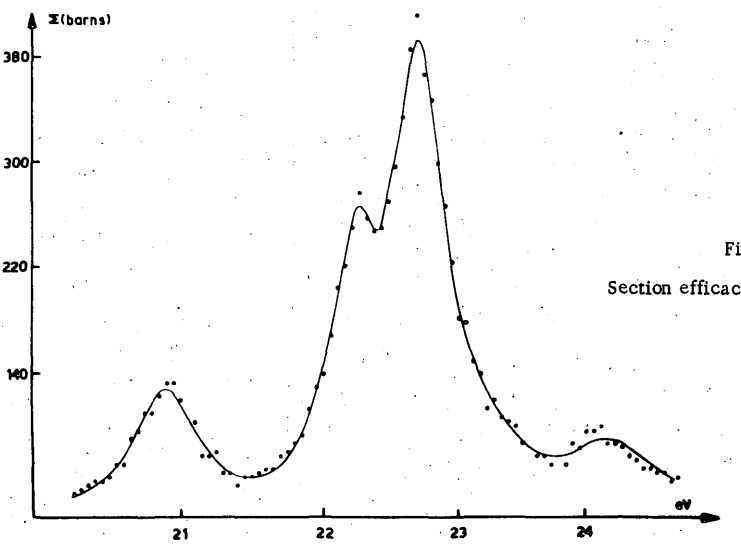

Figure 2

Section efficace de fission de ^{233}U.

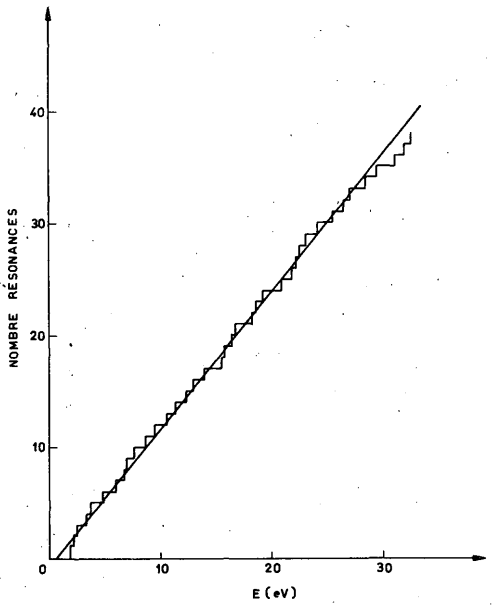

Figure 3

Courbe de linéarité de ^{233}U.

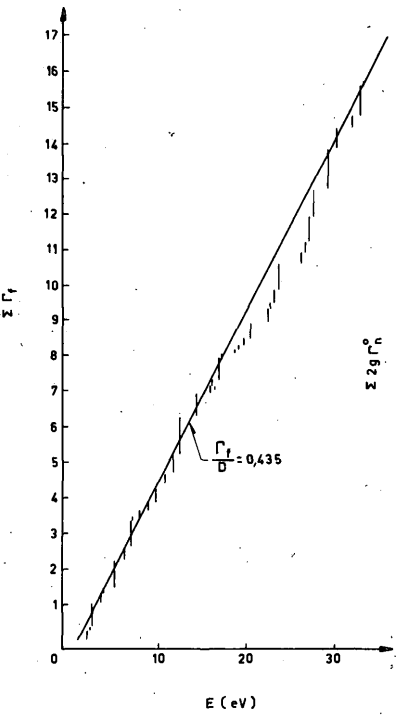

Figure 4

Détermination des fonctions densités de ^{233}U (somme des Γ_F).

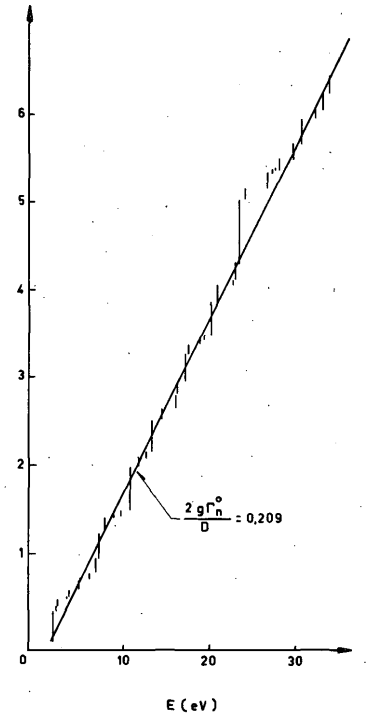

Figure 5

Détermination des fonctions densités de ^{233}U (somme des $g\Gamma_n^0$).

3. FLUCTUATIONS STATISTIQUES

Comparée à l'analyse statistique que nous avons faite sur les paramètres approchés, celle que l'on peut faire à l'aide des paramètres obtenus par la méthode des moindres carrés n'introduit une différence substantielle que dans la loi de distribution des espacements. La figure 6 représente

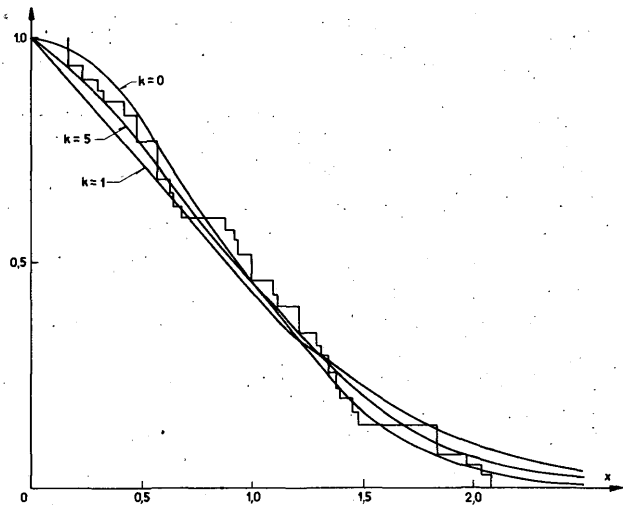

Figure 6

Distribution des espacements de niveaux.

le nouvel histogramme obtenu et l'on voit qu'il est beaucoup plus compatible avec la présence de deux populations indépendantes de résonances que celui présenté dans la référence [2]. Ce résultat à lui seul justifie partiellement la procédure consistant à ajouter un certain nombre de résonances. Par contre les distributions statistiques des largeurs neutroniques et des largeurs de fission n'ont pas été sensiblement modifiées. L'anomalie qui avait été signalée à propos de la distribution des largeurs neutroniques subsiste, ce qui signifie qu'un grand nombre de résonances de faible largeur neutronique n'ont toujours pas été détectées.

En appliquant la formule [4]

$$\nu_{eff} = \frac{2\langle \Gamma_F \rangle^2}{\langle \Gamma_F^2 \rangle - \langle \Gamma_F \rangle^2}$$

on trouve

$$\nu_{\Gamma_F} = 3,90 \quad \text{et} \quad \nu_{\Gamma_n} = 2,6.$$

On avait trouvé précédemment

$$\nu_{\Gamma_F} = 3,53 \quad \text{et} \quad \nu_{\Gamma_n} = 2,44.$$

4. CONCLUSION

Nous avons donc pu rendre compte d'une façon correcte de la section efficace de fission de l'uranium-233 entre 1,7 et 30 eV sans utiliser de formalisme à plusieurs niveaux. Il a suffit pour cela d'ajouter un petit nombre de résonances. Ce faisant nous avons aussi amélioré la distribution statistique des espacements.

Par ailleurs, la méthode de Monte-Carlo nous a permis de simuler des sections efficaces expérimentales et a montré qu'effectivement toutes les résonances injectées n'étaient pas détectées. Il nous paraît donc probable que les effets d'interférence sont faibles dans le cas de l'uranium-233 et que pour les mettre en évidence avec certitude il faudrait que les données expérimentales soient beaucoup plus précises. Il sera même difficile actuellement de tirer des conclusions de la comparaison entre section efficace totale et section efficace de fission car les résonances de forme asymétrique que nous avons rencontrées s'expliquent par la présence d'une résonance large dans le flanc d'une résonance étroite. Cette conjonction doit donner une section efficace de capture beaucoup plus symétrique que la section efficace de fission. Il faudrait évidemment expliquer la raison du peu d'importance des effets d'interférence. On peut pour cela raisonner sur la formule à plusieurs niveaux, dans sa forme simplifiée.

Celle-ci peut s'écrire:

$$\sigma_{n,F} = K \left[\sum_j \frac{\Gamma_n^j \Gamma_F^j}{(E - E_j)^2 + (\Gamma^j/2)^2} + \sum_{j \neq K} (\Gamma_n^j \Gamma_n^k \Gamma_F^j \Gamma_F^k)^{\frac{1}{2}} \cos(j,k) \right.$$

$$\left. \times \frac{(E - E_j)(E - E_K) + \Gamma_j \Gamma_K/4}{(E - E_j)^2 (E - E_k)^2 + 1/4 \left[\Gamma_j^2 (E - E_k)^2 + \Gamma_k^2 (E - E_j)^2 + (\Gamma_j \Gamma_k/4)^2\right]} \right].$$

D'après VOGT [5] pour $\nu = 4$, la valeur moyenne de cos (j, k) est de l'ordre de $\pm$ 0,4.

Les effets d'interférence devraient être surtout sensibles loin des résonances; ils sont alors de l'ordre de:

$$\left[\sum_{j \neq k} (\Gamma_n^j \Gamma_n^k \Gamma_F^j \Gamma_F^k)^{\frac{1}{2}} \cos(j,k) \right] 1/(E - E_j)(E - E_k).$$

Le facteur cos(j, k) implique qu'ils sont de l'ordre de 0,4 fois la section efficace due aux deux résonances les plus proches si l'on ne tient compte que de celles-ci.

En fait la contribution des résonances plus éloignées n'est nulle part négligeable dans l'uranium-233. Or cette contribution est nulle en moyenne en ce qui concerne les effets d'interférence. On peut donc penser que les effets d'interférence sont noyés dans la contribution des résonances lointaines.

Un autre aspect intéressant de la section efficace de fission de l'uranium-233 n'a pu être éclairci: il ne paraît pas évident d'après l'histogramme des largeurs de fission qu'on puisse ranger celles-ci en deux familles distinctes. Pour vérifier cette possibilité une analyse statistique plus précise est en cours.

Enfin, la faible valeur de la section efficace de fission résiduelle exclut l'existence d'une famille de résonances trop larges pour être isolées. Ceci signifie que les deux familles de résonances de spins 2 et 3 doivent être présentes dans notre analyse.

RÉFÉRENCES

[1] NIFENECKER, H., PAYA, D. et FAGOT, J., J. Phys. Radium 24 (1963) 254.
[2] NIFENECKER, H., J. Phys. Radium 25 (1964) 877.
[3] PATTENDEN, N.J. and HARVEY, J.A., WASH 1029-UC 34, 53.
[4] WILLETS, L., Phys. Rev. Lett. 9 (1962) 430.
[5] VOGT, E., Phys. Rev. 112 1 (1958) 203.

DISCUSSION

U. V. RYABOV: If I understood you correctly, the interference between the U^{233} levels was small and it is possible to use the single-level Breit-Wigner formula. I am wondering whether you added levels with large Γ_f values. If so, this might explain the large value for the inter-resonance cross-section, the so-called contribution of the non-resonance component in the U^{233} fission cross-section.

H. NIFENECKER: The interference effect seems to be weak if compared with the cross-section between resonances. We did not add very wide resonances although the mean width of the U^{233} resonances is rather large. The large cross-section between resonances is due to the contribution of far-away resonances and this is why it was found necessary to take account of at least 10 resonances simultaneously.

FISSION CROSS-SECTION MEASUREMENT OF U^{235} AND Pu^{239} FOR LOW-ENERGY NEUTRONS

G. FRAYSSE
EURATOM, CCR, ISPRA, ITALY
AND
A. PROSDOCIMI
EURATOM, CEN, CADARACHE, ITALY

Abstract — Résumé — Аннотация — Resumen

FISSION CROSS-SECTION MEASUREMENT OF U^{235} AND Pu^{239} FOR LOW-ENERGY NEUTRONS. Fast detection with a double gaseous scintillator and low geometry counting with a solid-state ion chamber were applied to determine the fission cross-section of U^{235} and Pu^{239}.

Monochromatic neutron beams of 0.0322 eV, 0.0626 eV and 0.275 eV were supplied by two crystal spectrometers at the EL3 reactor in CEN - Saclay. The monitoring of the neutron flux was been done by reference to the counting of a grid ion chamber mounted with a boron layer.

Both alpha and fission rates were measured, and the results at the reference energy of 0.0253 eV were calculated:

$$(\sigma_F)_0\, U^{235} = 582 \pm 10 \text{ b}$$

$$(\sigma_F)_0\, Pu^{239} = 738 \pm 7 \text{ b}.$$

MESURE DES SECTIONS EFFICACES DE FISSION DE ^{235}U ET ^{239}Pu POUR DES NEUTRONS DE FAIBLE ÉNERGIE. Par détection rapide au moyen d'un scintillateur gazeux double et comptage à basse géométrie au moyen d'une chambre d'ionisation à semi-conducteurs, les auteurs ont déterminé la section efficace de fission de l'uranium-235 et du plutonium-239.

Des faisceaux de neutrons monochromatiques d'une énergie de 0,0322 eV, 0,0626 eV et 0,275 eV ont été fournis par deux spectromètres à cristal installés auprès du réacteur EL3 du CEN à Saclay.

Le flux de neutrons a été déterminé par référence au taux de comptage d'une chambre d'ionisation à grille contenant une couche de bore.

Les auteurs ont procédé au comptage des particules alpha ainsi qu'à celui des fissions.

Les résultats du calcul pour une énergie de référence de 0,0253 eV sont les suivants:

$$(\sigma_F)_0\ ^{235}U = 582 \pm 10 \text{ b},$$

$$(\sigma_F)_0\ ^{239}Pu = 738 \pm 7 \text{ b}.$$

ИЗМЕРЕНИЕ СЕЧЕНИЯ ДЕЛЕНИЯ УРАНА-235 И ПЛУТОНИЯ-239 ДЛЯ НЕЙТРОНОВ НИЗКОЙ ЭНЕРГИИ. Применялось быстрое детектирование с использованием двойного газового сцинтиллятора и счета "плохой" геометрии с помощью твердой ионизационной камеры для определения сечения деления урана-235 и плутония-239.

Монохроматические нейтронные пучки с энергиями 0,0322; 0,0626 и 0,275 эв были получены с помощью двух кристаллических спектрометров на реакторе EL-3 в исследовательском ядерном центре в Сакле. Регулирование потока нейтронов осуществлялось с использованием в качестве эталона скорости счета ионизационной камеры с сеткой, содержащей калиброванный слой бора.

Измерялись как альфа, так и скорости деления. Были получены следующие результаты при энергии 0,0253 эв, взятой за эталон:

$$(\sigma_F)_0\ U^{235} = 588 \pm 10 \text{ барн},$$

$$(\sigma_F)_0\, Pu^{239} = 738 \pm 7 \text{ барн}.$$

MEDICION DE LAS SECCIONES EFICACES DE FISION, POR-NEUTRONES DE BAJA ENERGIA, DEL ^{235}U Y DEL ^{239}Pu. Se ha determinado la sección eficaz de fisión del uranio-235 y del plutonio-239 por detección rápida con un centelleador gaseoso doble y recuento mediante cámara de ionización de pequeño ángulo sólido, provista de detectores de semiconductores.

Se han utilizado baces neutrónicos monocromáticos de 0,0322 eV, 0,0626 eV y 0,275 eV, emitidos por dos espectrómetros de cristal instalados en el reactor EL3 de Saclay (CEN). La intensidad del flujo neutrónico se ha evaluado con referencia al índice de recuento de una cámara de ionización de rejilla provista de una capa de boro.

Se determinó el número de heliones y el de fisiones por unidad de tiempo y se calcularon los resultados para la energía de referencia de 0,0253 eV:

$$(\sigma_F)_0{}^{235}U = 582 \pm 10 \text{ b},$$

$$(\sigma_F)_0{}^{239}Pu = 738 \pm 7 \text{ b}.$$

PURPOSE OF THE MEASUREMENTS AND GENERAL ASPECTS

Since important discrepancies still remain in the thermal cross-section of U^{235} and of Pu^{239} in particular [1-21] (Fig. 1), redetermination of these data has been carried out.

To avoid difficulties in the direct measurements of the fissile quantities, the determination of the weight has been done by alpha counting in the same detector as the determination of the fission rate. This has enabled in some cases the influence of geometry to be eliminated, and in other cases has reduced its influence to a small value.

In the alpha counting of Pu^{239} there is the difficulty of a considerable pile-up contribution. To reduce this contribution to a proportion not exceeding a few per cent for an accurate correction of the alpha counting-rate and negligible perturbation of the fission spectrum, the ideal conditions for an experiment are the availability of a high flux reactor, and a detector with good discrimination qualities for alphas and fissions.

The determination of the total neutron current irradiating the fissile target was made by reference to the most accurate cross-section σ_a(B) of boron [22].

Mechanical limitations in the monochromators did not permit measurements at the reference energy of 0.0253 eV, therefore several experiments were performed at three different energies by means of two different detectors having an efficiency adapted to the variation in the energy of the beam intensities.

The conditions that must be fulfilled by the detectors are short resolution time, good energy resolution and high efficiency (according to the beam intensity). The best compromise was considered to be (i) a solid-state ionization detector having an energy resolution of about 2%, but a time resolution limiting the geometry to about 0.01 of 2π, with the fissile foils and the available beam intensities obtained at 0.0322 eV and 0.062 eV, and (ii) a 4π gaseous scintillation detector 50 times faster than the solid-state one (with the associated circuits), but having an energy resolution 10 times worse and much more difficult to utilize. For this reason, its use was limited to the neighbourhood of the Pu^{239} resonance (0.275 eV) where the low-beam intensity implied a high efficiency detector.

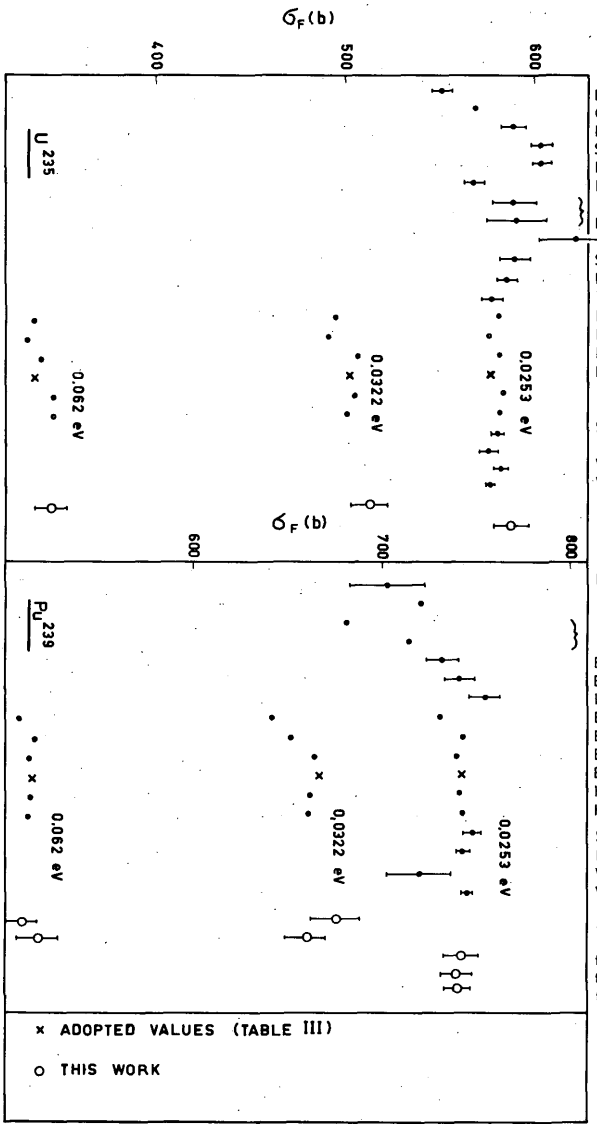

Leonard 1956	[11]
Gerasimov 1956	[20]
Egelstaff 1957	[4]
Saplakoglu 1958	[17,19,20]
Bollinger 1958	[4,13]
Bigham 1958	[17]
Raffle 1959	[4,17,19,20]
Safford 1959	[6,14,15]
Deruytter 1960	[17]
Leonard 1961	[4]
BNL 325 σ_F (E) 1961	[1]
BNL 325 σ_F (E) corr.	[1]
BNL 325 $\sigma_F \cdot \sqrt{E}$	[1]
BNL 325 $\sigma_F \cdot \sqrt{E}$ corr.	[1]
KFK 120 curves	[2]
KFK 120 tables	[2]
Sher 1962	[3]
BNL 325 rev. (w.c.s.)	[1]
Westcott, mean val.	[4]
Westcott, (w.c.s.) 1964	[4]
this work (Table IX)	
this work (Table XI)	
Raffle 1955	[7,19]
Gerasimov 1956	[20]
Leonard 1956	[11]
Egelstaff 1957	[3]
Bigham 1958	[20]
Leonard 1961	[4,18]
BNL 325 σ_F(E) 1961	[1]
BNL 325 σ_F(E) corr.	[1]
BNL 325 $\sigma_F \cdot \sqrt{E}$	[1]
BNL 325 $\sigma_F \cdot \sqrt{E}$ corr.	[1]
KFK 120 curves	[2]
KFK 120 tables	[2]
Sher 1962	[3]
BNL 325 rev.(w.c.s.)	[1]
Westcott. mean val.	[4]
Westcott. (w.c.s.) 1964	[4]
this work (Table IX)	
this work (Table X)	
this work (Table XII)	
this work (Table XII)	
this work (Table XII)	

Fig. 1

Present status of U^{235} and Pu^{239} fission cross-sections

From the values at the stated energies a renormalization of the $\sigma_F(E)$ curve was calculated to allow a direct comparison of these results with those previously published.

PRINCIPLE OF THE MEASUREMENTS

An absolute determination of the fission cross-section implies an accurate measurement of the following fundamental quantities: neutron energy, integration over time of the neutron current irradiating the area of the fissile target during all the measurements; the number of atoms of the fissile nuclide laid on the target; and detection efficiency in fission counting.

Each of these quantities will be analysed since they affect directly the reliability and the accuracy of the final results.

The neutron flux is supplied by a beam emerging from a crystal spectrometer. Its energy is then well defined, nevertheless besides the fundamental flux φ_1 that fulfils Bragg's condition

$$n\lambda = 2d \sin(\theta/2), \quad n = 1, 2, \ldots \tag{1}$$

for $n = 1$, there is also an harmonic contamination due to the **flux** φ_2 that satisfies Eq.(1) for $n = 2$.

If σ_1 and σ_2 are the reaction cross-sections for the fundamental (λ_1) and the harmonic (λ_2) wavelengths, being $\lambda_2 = \lambda_1/2$, the correction to be applied to the counting-rate in order to reject the harmonic contribution is

$$K_h = 1/\left(1 + \frac{\sigma_2}{\sigma_1}\frac{\varphi_2}{\varphi_1}\right). \tag{2}$$

The time integration of the neutron current is carried out by means of the absolute counting of a neutron reaction having a well-known cross-section. The $B^{10}(n,\alpha)Li^7$ reaction was chosen. A counter containing a uniform layer of boron with an atom density N_B (B at./cm^2) was introduced in the neutron beam before it reached the fissile target.

J_B is the total neutron current at the place of the boron layer, and if σ_B is the reaction cross-section and n_B the corresponding counting-rate, the reaction rate n_B^0 is derived after multiplication by an efficiency factor K_B

$$n_B^0 = K_B \times n_B = J_B \times N_B \times \sigma_B . \tag{3}$$

The fissile target is a uniform layer of an enriched isotope having an atom density for the main fissile nuclide N_F (at./cm^2). Since the fissile nuclides we are considering, U^{235} and Pu^{239}, are also α-emitters, this feature is then used to determine the atom density by measuring their α-activity, but not necessarily in an absolute way, as will be shown later.

The α-activity n_α^0 comes from the α-counting-rate n_α by means of an efficiency factor K_α, and after the introduction of the decay constant λ_α for the specific nuclide and the area A_α of the emitting layer

$$n_\alpha^0 = K_\alpha \times n_\alpha = \lambda_\alpha \times N_F \times A_\alpha . \tag{4}$$

In this way knowledge of N_F depends only on measurable quantities, and essentially on the α-counting efficiency factor K_α.

Finally, the fission rate n_F^0 is obtained in a similar way by a relationship containing the fission counting n_F, its efficiency coefficient K_F, the total neutron current J_F at the position of the fissile layer and the fission cross-section σ_F,

$$n_F^0 = K_F \times n_F = J_F \times N_F \times \sigma_F . \tag{5}$$

It must be observed that the boron layer and the fission counter are aligned along the neutron beam but are separated by some distance and by the detector walls. However, a suitable neutron diaphragm limits the beam cross-section making the same neutrons cross simultaneously the two counter targets. If the beam transmission through the detector walls is t, then

$$J_F = t \times J_B . \tag{6}$$

Comparison of Eqs.(3), (4), (5) and (6) leads to the elimination of the quantities N_F, J_B and J_F, and the following fundamental relationship can be written

$$\sigma_F = \sigma_B \times \frac{n_F}{n_B n_\alpha} \times \frac{K_F}{K_B K_\alpha} \times \frac{N_B A_\alpha \lambda_\alpha}{t} . \tag{7}$$

The interpretation of all these quantities is straightforward except perhaps for the efficiency coefficients, which will be analysed in detail.

We resolve K_B into several factors having a more direct and physical meaning,

$$K_B = K_t \times K_n \times K_{hB} \times K_{gB} \times K_d \times K_b \tag{8}$$

where

K_t = dead time correction
K_n = background noise correction
K_{hB} = harmonic correction
K_{gB} = geometrical efficiency correction
K_d = discrimination and self-absorption correction
K_b = back-scattering correction.

Furthermore it can be written

$$K_\alpha = K_{g\alpha} \times K_i \times K_e \tag{9}$$

where

$K_{g\alpha}$ = geometrical efficiency correction
K_i = isotopic correction, due to the presence of several α-emitters on the target
K_p = alpha pile-up and self-absorption correction.

Eventually also for fission counting it is

$$K_F = K_{gF} \times K_{hF} \tag{10}$$

with

K_{gF} = geometrical efficiency correction

K_{hF} = harmonic correction.

Corrections such as dead time and back-scattering for alphas and fission fragments, and self-absorption for fission fragments, will be treated directly in the measurement of n_α and n_F.

At this point a more useful form of the expression in Eq.(7) will be introduced

$$\sigma_F = \sigma_B \times \frac{(n_F^0/K_{gF})}{n_B^0 (n_\alpha^0/K_{g\alpha})} \times \frac{K_{gF}}{K_{g\alpha}} \times \frac{N_B A_\alpha \lambda_\alpha}{t} \qquad (11)$$

where some important parameters are better related to the measurable quantities.

In the new formulation in Eq.(11) the ratio of the geometrical efficiencies $K_{gF}/K_{g\alpha}$ has been particularly pointed out because of its special behaviour. In an ideal case of the uniform α-emitting layer irradiated by a neutron current of uniform density it should be $K_{gF}/K_{g\alpha} = \frac{1}{2}$, owing to the double multiplicity of the fission fragments.

In actual fact the neutron beam emerging from the reactor and the crystal spectrometer has a strong disuniformity. Its intensity profile (Fig. 2) is like

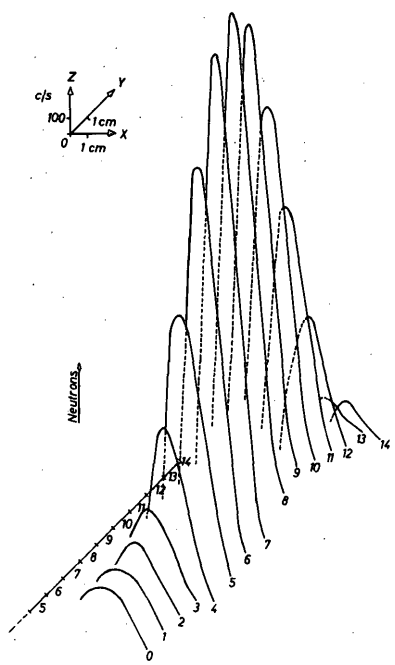

Fig. 2

Flux mapping at the beam H-2

X axis - horizontal direction

Y axis - vertical direction

Z axis - neutron beam intensity

a Gaussian, therefore the higher density along its axis produces more fissions in the central part of the fissile layer. Some of our detectors, i.e. the solid state ones (see below), have a higher efficiency for this region of the emitter than for its outer part, especially in the case of broad targets. For this reason one has to assume that in general it should be

$$K_{gF} / K_{g\alpha} \leq \tfrac{1}{2}. \tag{12}$$

This ratio will be evaluated below; the other quantities of Eq. (11) are otherwise measurable or assumed from the current references.

It has already been stated that a boron target is taken as reference because its reaction cross-section is one of the most accurate. However, U^{235} is also sometimes adopted as reference in fission cross-section measurements, the lower precision of its cross-section being compensated by the fact that a fission reaction occurs just like the one that is to be measured for the unknown sample. Furthermore in such a case knowledge of some parameters is not required because fission cross-section ratios may be obtained from the raw results, as for Pu^{239} and U^{235}. For instance, an absolute boron counting is not required in such a case because this counter has only the function of a relative flux monitor; moreover when the U^{235} and Pu^{239} fissions are counted under identical conditions all the efficiency factors are eliminated. It can be written

$$\frac{(\sigma_F)_{Pu}}{(\sigma_F)_U} = \frac{n^0_{FPu}}{n^0_{FU}} \times \frac{n^0_{\alpha U}}{n^0_{\alpha Pu}} \times \frac{\lambda_{\alpha Pu}}{\lambda_{\alpha U}} \times \frac{n_{BU}}{n_{BPu}}. \tag{13}$$

This result constitutes a valuable cross-check of the whole set of measurements.

Some physical considerations influenced the choice of the type of detectors in order to obtain the highest reliability in the absolute counting-rate. The following type was used: gridded pulse ion chamber for boron counting, chosen for well-known geometry and good energy resolution; a solid-state ion chamber with low geometry for the fissile targets when the neutron flux intensity was high enough to allow a suitable fission rate. This type of detector has been useful for Pu^{239} samples. In fact the α-pile-up was kept low enough so that only two-pulse pile-up occurred. Thus any interference of the α-pulse spectrum with the lower tail of the fission-fragment spectrum was avoided. The low sample window geometry produces some collimation effect that was able to minimize the self-absorption degradation of the spectrum both for alpha and for fission fragments. At 0.275 eV the low intensity of the neutron beam required a detector having a high efficiency and a xenon-filled scintillator was employed. In this case the interference of the high α-activity of Pu^{239} with fission detection was reduced to an acceptable degree by coincidence technique.

A 4π fissile target was counted by a double scintillator, and advantage was taken of the rapidity of the xenon scintillation to reduce the alpha pile-up to two pulses only.

Moreover the coincidence scheme was used to reject random α-pulses and to retain fission-fragment pulses.

DETECTORS AND COUNTING TECHNIQUES

Grid ionization chamber

This type of detector, shown in Fig. 3, was chosen for its interesting properties, i.e. 2π geometry, time stability, good energy resolution and solid basis for estimating its absolute efficiency.

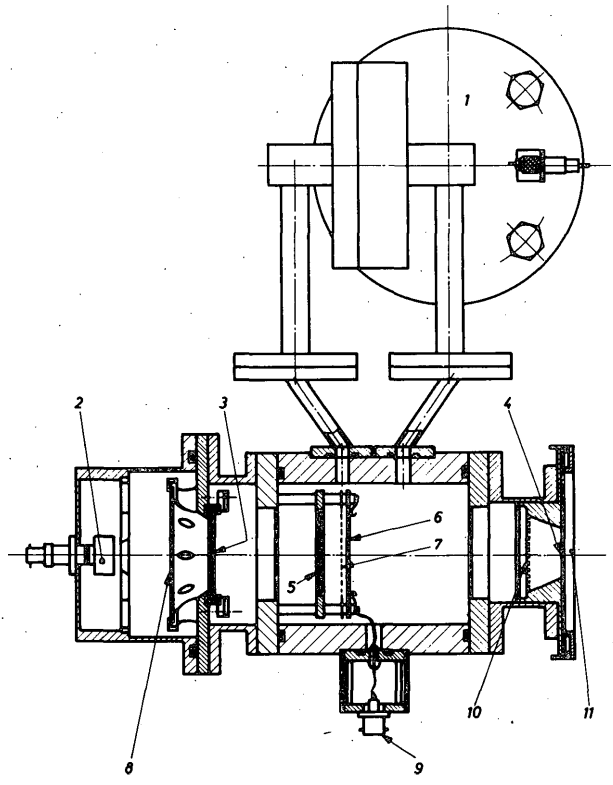

Fig. 3

Detector setup: gridded ion chamber and semi-conductor fission chamber

1. Calcium purifier
2. Surface barrier diode
3. Quartz window
4. Cadmium diaphragm
5. Boron layer
6. Collector
7. Gridded electrode
8. Fissile layer
9. Pulse output
10. Samarium filter
11. Boral shield

The negative electrode at -500 V supports the boron deposit, the collector at zero voltage is insulated and surrounded with a guard ring connected to the ground, and the grid at -225 V is situated at 4 mm from the collector. The distance between the electrodes is such that the range of the alpha particles at 1.48 and 1.78 MeV is totally absorbed when the filling is done with a mixture of 95% argon + 5% CO_2 at a pressure of 580 mm Hg. From time to time a calcium purifier connected with the chamber was heated up to 400°C in order to eliminate any gas impurity.

Boron samples

The thin high-purity boron layers were deposited by electron bombardment under vacuum on aluminium backings, and their weight was accurately determined before removing them from the vacuum system, so that spurious phenomena like oxidation or adsorption would not introduce errors [23].

The starting material was elemental boron, of so-called natural composition. The isotopic composition was checked by mass spectrometry against the standard boric acid of which a stock is available at CBNM-Geel. Boric acid from this stock was used for the B-10(n, α) cross-section determination [22]. No difference in isotopic composition between the starting material and the standard boric acid was detected. However, a fractionation effect has been observed with boron layers prepared in the same way as those used in the measurements, resulting in an enrichment in B^{10} to about 20.3 at.% compared with 19.8% for the starting material [37].

Impurities are inhomogeneously distributed over the grains of the starting material. Those grains contain silicon up to 0.25, carbon between 0.5 and 2, and other impurities up to 0.25 wt.% [38]. It is not known to what extent impurities were deposited in the evaporated layers. However, it has been assumed in the calculations that the boron layers were pure and contained 19.81 at.% of B^{10}. Two samples have been successively used, having a mean density of 3.329×10^{18} at.B/cm^2 and 4.183×10^{18} at.B/cm^2. The uncertainty concerning these values is of course important as long as no analysis has been performed directly on the layers actually used in the measurements.

Solid-state ion chamber

The collimation effect that reduces the geometry is produced by the distance between the fissile deposit and the semi-conductor detector, but a diaphragm eliminates most of the alpha particles scattered by the wall of the chamber. The surface barrier diode had a sensitive area of 1 cm^2. With silicon having a resistance of 450 Ω cm, a bias of 30 V produced a sensitive zone absorbing the whole energy of alphas and fission fragments. The system was maintained under vacuum.

Gas scintillation chamber

This chamber, shown in Fig. 4, consists of two scintillators on each side of the thin fissile foil, and is filled with xenon at a pressure of 1.5 atm.

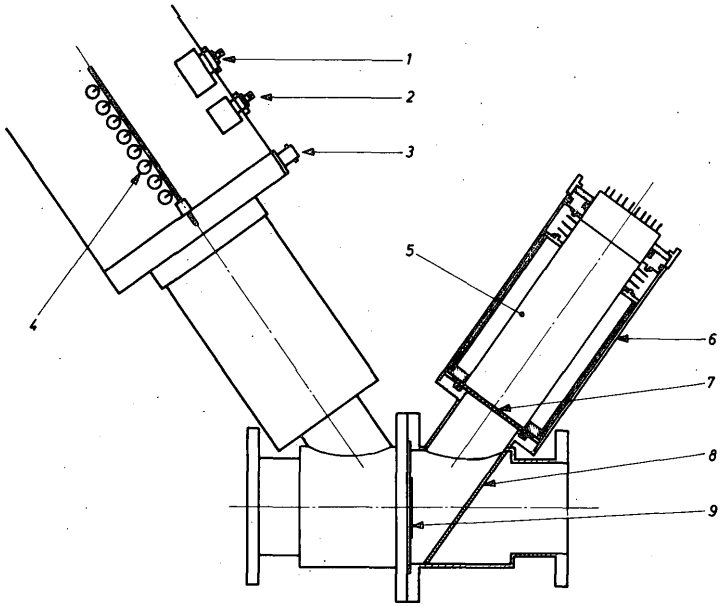

Fig. 4

Gas scintillation chamber

1. Focalizing electrode
2. Dynode voltage regulation
3. Pulse output
4. P. M. voltage divider
5. "56-UVP" photomultiplier
6. Magnetic shield
7. Quartz window
8. Magnesia light reflector
9. 4 π fissile layer

Xenon was chosen for its high scintillation efficiency and its short scintillation decay time. The whole energy of alphas and fission fragments is absorbed in the gas. Purification of the gas was carried out by circulating it over a calcium purifier heated at 400°C and stabilized by a temperature regulator. Stable operation was obtained less than 2 h after start-up. The walls of the chamber are coated with magnesium oxide used as a reflector. The external windows are inclined on the axis so that the volume is minimal and spurious light reflection in corners reduced. Two quartz windows allow the 56-UVP Radiotechnique fast photomultiplier to receive the light emitted in the gas, mostly in the ultra-violet range of wavelengths, without any shifter.

Fissile targets

The technique adopted for the preparation of fissile targets is described in Ref. [24]. Plastic foils of about 25 $\mu g/cm^2$ and 50 mm diam. were metallized with an evaporated aluminium layer to reduce strongly the light

transmission from one side to the other, as verified by a spectrophotometer, in the ultra-violet range of wavelengths corresponding to xenon scintillation. The fissile layers were then deposited by electro-spraying of an acetate uranium or plutonium solution; in the layer, composed of a mixture of $UO_2 \cdot (CH_3 \cdot COO)_2$ and $UO_2 \cdot (CH_3 \cdot COO)_3$, 2/3 of the total weight was fissile material.

Table I gives the characteristics of the different measured targets. It should be noted that the accuracy of the isotopic composition of the plutonium foils is not known.

The electronic chain associated with the Frisch grid ionization chamber is of a low noise conventional type. Due to the importance of the discrimination threshold, its calibration and stability were particularly checked during the different measurements. The dead time was also carefully measured with a double pulse generator and found equal to 2.0 μs.

Apart from the charge sensitive preamplifier, the chain associated with the surface barrier semi-conductor is also conventional, the scaler being replaced by a multi-channel analyser operated in live time.

The fast electronics are described in Ref. [25]. The shape of alpha and fission pulses was recorded with a 2000-MHz travelling wave oscilloscope of EGG-707 type. Alpha pulses were measured with a full-width-half-maximum of 4.5 ns and fission with 7.5 ns. In fission counting. the thresholds of the tunnel diode discriminators were adjusted to 7 MeV in order to eliminate the fundamental α-counting. A coincidence circuit with a resolution time of ± 3.35 ns operated when two fission fragments were simultaneously detected, one in each chamber. In this way the correction of fission counting loss due to threshold and self-absorption in the foil was easier. The need to determine several corrections in the differential α and fission spectra made it essential for them to be recorded on a pulse-height analyser. The fast pulses were sent to a special lengthener circuit operating in the sampling mode, so as to reduce their number with a known dead time of 186 μs and render their shape acceptable by the analyser. In the case of fissions, the coincidence signal opened the input gate of the analyser. Because of the importance of the α-spectra, all linearities (photomultipliers, tunnel diode discriminators, pulse lengthener, pulse-height analyser) were carefully checked with the help of pulse generators and simulation circuits, and dead times were measured with the help of a calibrated sampling oscilloscope.

THE EXPERIMENTAL SETUP

The main features of the experimental device were imposed by the particular neutron source available for the experiment. Two crystal spectrometers installed at the EL-3 reactor in CEN-Saclay (18 MW power) were employed at three different orientations of the crystal axis. This device was able to supply a monokinetic and gamma-free neutron source. The characteristics of the neutron beams are presented in Table II; the maximum neutron flux is merely indicative and it does not enter into the results. The ratio between the fundamental flux φ_1 and its first harmonic φ_2, has been

TABLE I

CHARACTERISTICS OF THE FISSILE TARGETS

Run No.	Isotope	Backing	Diameter (mm)	Total fissile weight*	Isotopic composition
U I	U^{235}	vynil	20 mm	1.238 mg	U^{234} 0.0108 U^{235} 0.9327 U^{236} 0.00205 U^{238} 0.0544
U II	U^{235}	alu-minium	40 mm	1.805 mg	U^{234} 0.0077 U^{235} 0.9010 U^{236} 0.0033 U^{238} 0.0880
U III	U^{235}	vynil	40 mm	0.750 mg	U^{234} 0.00165 ±0.00003 U^{235} 0.99216 ±0.00003 U^{236} 0.000264 ±0.000012 U^{238} 0.00594 ±0.00001
U IV	U^{235}	vynil	40 mm	1.372 mg	(identical with U III above)
P II	Pu^{239}	alu-minium	20 mm	0.269 mg	Pu^{239} 0.993 Pu^{240} 0.007
P III	Pu^{239}	vynil	40 mm	0.215 mg	(identical with P II above)
P IV	Pu^{239}	vynil	40 mm	0.128 mg	(identical with P II above)

* Indicative values deduced from alpha assay.

measured for the beam H-2 by means of the selective absorption of a samarium filter (Table III), and by measuring its neutron transmission. For the beam H-12-45° the diffraction of a nickel sample analysed this ratio

TABLE II

NEUTRON BEAM CHARACTERISTICS

Neutron beam	Neutron energy (eV)	Max. flux ($n/cm^2 \cdot s$)	Harmonic ratio φ_2/φ_1	L_H (cm)	L_V (cm)
H-12-45°	0.03216 ± 0.00004	1.9×10^4	0.142 ± 0.001	3.0	6.7
H-2	0.0626 ± 0.0001	1×10^6	0.025 ± 0.001	3.5	8.2
H-12-15°	0.275 ± 0.002	5.3×10^3	≃ 0	2.7	5.9

[26]: The harmonic ratio is assumed eventually to be negligible for the beam H-12-15° owing to the low intensity at that energy of the thermal neutron spectrum supplied by the reactor, and taking into account also the low luminosity of a crystal spectrometer at such an angle.

The shape of the neutron flux density has been measured for each beam along the main symmetry axis, i.e. the horizontal and the vertical, then the respective widths at half maximum were deduced and called L_H and L_V in Table II. It is necessary to know these quantities because of the need to evaluate the ratio $K_{gF}/K_{g\alpha}$, as explained above. In fact a numerical integration of the theoretical geometry efficiency [27], weighted by the local flux intensity over the whole target area according to its measured distribution, was carried out individually for each sample mounted in semiconductor fission chambers. Particular attention, of course, had to be given to centring and aligning the detector system on the axis of the neutron beam by means of a special optical device [28].

To obtain more detail, the neutron beam profiles were mapped by a detector having a high efficiency for thermal neutrons, namely a Li^7 glass scintillator. In order to obtain a fine resolution in space, a narrow neutron beam was allowed to enter the scintillator through a collimator of 1 or 5

TABLE III

FUNDAMENTAL NEUTRON CROSS-SECTIONS
(most important data is underlined)

eV / barns	0.0253	0.0322	0.1286	0.0626	0.250	0.275	1.100	Ref.
$\sigma_A(B_{nat})$	761 ± 2	674	443	483	242	231	115	[22]
$\sigma_F(U^{235})$	577 ± 5	503	212	336	183	188	96	[1]
$\sigma_F(Pu^{239})$	742 ± 4	666	504	514	1890	2815	31	[1]
σ_T(Sm)	-	-	-	9100	475	-	-	[1]

mm diam., according to the neutron intensity. The shape of the mapped flux looks like a Gaussian with different widths in the horizontal and in the vertical plane (Fig. 1).

The reference boron detector and the fission detector were fixed with respect to each other on the same axis and with their target layers perpendicular to the beam direction. Following the neutron path the boron layer in the ion chamber is first encountered (Fig. 2) and the fissile target further on. In order to make the fission-fragment emitting area coincide with the α-emitting one to minimize any difference in geometry efficiencies, the neutron beam was diaphragmed by a suitable cadmium screen placed in front of the complete detector set.

Some detector walls and target support were interposed between boron and fissile layer. To obtain the neutron transmission t, the contribution due to the aluminium walls was calculated on the basis of a constant $\sigma_T(Al) = 1.55$ b. The transmission of a quartz transparent window, used with the solid-state chamber, was actually measured and found

$$t(3 \text{ mm quartz}) = 0.933 \pm 0.001, \text{ at } 0.03216 \text{ eV}$$
$$t(3 \text{ mm quartz}) = 0.940 \pm 0.001, \text{ at } 0.0626 \text{ eV}.$$

MEASUREMENTS AND RESULTS

Firstly an account must be given of all the fundamental data derived from the current references, and utilized either to evaluate some correction parameters or to handle the measured cross-sections for calculating more conventional values.

Some data can affect more directly than others the results presented in this and in the following section; they are underlined in Table III in order to point out their importance; other data define minor corrections and less precision can be allowed for their values.

Fundamental neutron cross-sections at the conventional energy $E_0 = 0.0253$ eV, at the energy E_1 of the monochromatic neutron beams and their harmonics $E_2 = 4 E_1$ (in place of $\lambda_2 = \lambda_1/2$, see above), are reported in Table III. The absorption cross-section of natural boron is taken from Ref. [22]. For U^{235} and Pu^{239} the fission cross-sections have been calculated from the graphs ($\sigma_F \times \sqrt{E}$) versus E displayed by Ref. [1], after renormalization to the 2200 m/s values of the "world consistent set" recommended by the same reference.

Another set of fundamental data deals with the half-lives of the alpha decay (the corresponding disintegration constants) for all nuclides composing the fissile target. The data are presented in Table IV with the corresponding references. The decay constants appear in the Eqs. (7), (11) and (13) and contribute to build up the correction factor K_i of Eq. (9) together with the isotopic ratios of the fissile nuclides.

Where more determinations were available in the literature, their average has been adopted; nevertheless for U^{235} and Pu^{239} only a single recent determination has been retained because of its particular reliability due to improved experimental techniques.

TABLE IV

DISINTEGRATION CONSTANTS OF ALPHA EMITTERS

Nuclide	Half-life $T_{\frac{1}{2}}$ (yr)	Decay constant λ_α (α/s at.)	Ref.
U^{234}	2.505×10^5	$0.876 \times 10^{-13} \pm 0.6\%$	[29, 30]
U^{235}	$6.92 \pm 0.09 \times 10^8$	$0.316 \times 10^{-16} \pm 1.3\%$	[31]
U^{236}	2.39×10^7	0.905×10^{-15}	[29, 30]
U^{238}	4.52×10^9	0.485×10^{-17}	[29, 30]
Pu^{239}	24413 ± 30	$0.8996 \times 10^{-12} \pm 0.12\%$	[32]
Pu^{240}	6430	3.415×10^{-12}	[29, 30]

The classification described earlier for the measuring runs continued to be followed, and some complementary quantities required according to Eqs.(7), (11) and (13) are reported in Table V. This set of values are either measurable or calculable.

TABLE V

COMPLEMENTARY MEASUREMENTS

Run No.	α-emitter area A_α (cm^2)	Boron atom density N_B (B at./cm^2)	Geometry ratio $K_{gF}/K_{g\alpha}$
U I	3.142	4.183×10^{18}	0.500
U II	12.566	3.329×10^{18}	0.489
U III	12.566	3.329×10^{18}	0.490
U IV	12.566	3.329×10^{18}	0.490
P II	3.142	4.183×10^{18}	0.500
P III	12.566	3.329×10^{18}	0.489
P IV	12.566	4.183×10^{18}	0.500

The accuracy on the foil areas can be deduced from the following consideration. The uranium and plutonium foils have been prepared by electrospraying using diaphragms (diam.20 and 40 mm respectively) known to ±0.02 mm. Because of the edge effect during spraying the layers are not uniform in a border zone of about 1 mm. Furthermore they are not precisely circular. All this makes a precise measurement of the mean area A_α very difficult.

In the calculations A_α has been taken equal to the area of the spraying diaphragms, although the real mean area may be different up to 3% (for the 20-mm foils) or up to 1.5% (for the 40-mm foils).

$K_{gF}/K_{g\alpha}$ has been calculated and t has been calculated or determined as explained earlier. The boron atom density N_B has been discussed earlier.

Each fissile target has been submitted to an α-assay in the same detector employed later for fission counting. Typical α-pulse spectra are shown in Figs. 5 and 7. The former is produced by a xenon-filled gaseous

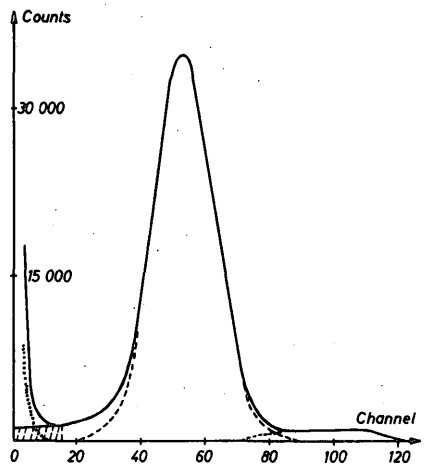

Fig. 5

Alpha-amplitude spectrum of gaseous scintillator (Run P IV)

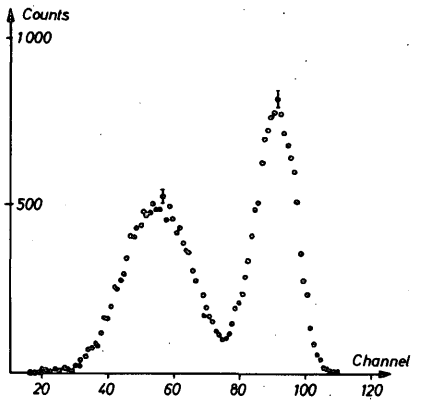

Fig. 6

Fission-fragment amplitude spectrum of gaseous scintillator (Run P IV)

scintillator, the pile-up tail (Fig. 5) is interpreted according to the theory developed in Ref. [25], the low energy tail is formed both by dispersion in light pulse collection and by self-absorption, and its treatment is done ac-

TABLE VI

ALPHA ASSAY RESULTS

Run No.	Counting-rate n_α (Hz)	Stat. S. D. (%)	Pile-up coeff. K_p	Isotopic coeff. K_i	Correct. counting-rate $n_\alpha^0/K_{g\alpha}$ (Hz)
U I	10.663	0.45	1.0000	0.0301	0.3209
U II	18.314	0.52	1.0000	0.0403	0.7380
U III	1.429	1.7	1.0000	0.1779	0.2541
U IV	2.6180	0.32	1.0000	0.1779	0.4656
P II	3531.1	0.14	1.0000	0.9739	3438.9
P III	2822	0.38	1.0000	0.9739	2748
P IV	151,106	0.10	1.0597	0.9739	155, 950

cording to the self-absorption theory (Ref. [33]) after a spectrum extrapolation towards zero amplitude. The latter two spectra were obtained by a solid-state chamber, the α-peaks show negligible pile-up and self-absorption tails, the corrections being correspondingly low. Table VI presents the results of the α-assay as far as $n_\alpha^0/K_{g\alpha}$, geometrical efficiency excluded. The isotopic correction necessary to resolve the α-activity of the main fissile nuclide by that of the whole target is

$$K_i = \lambda_0 \times a_0 / \sum_m \lambda_m a_m \qquad (14)$$

a_m being the isotopic ratio of the nuclide m and the sum extended to all the α-emitters.

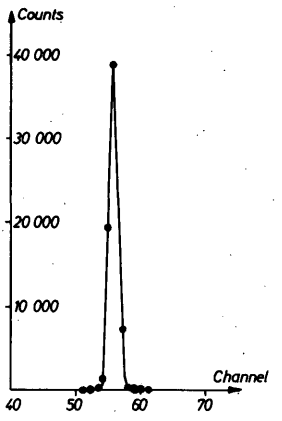

Fig. 7

Alpha-amplitude spectrum of solid-state detector (Run P III)

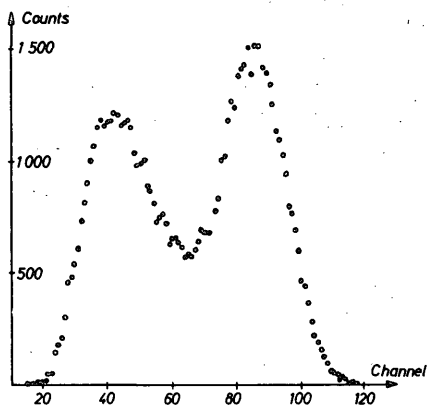

Fig. 8

Fission-fragment amplitude spectrum of solid-state detector (Run P III)

The fission counting was always carried out under good pulse amplitude conditions, as shown in Figs. 6 and 8.

The amplitude distribution of the fission pulses was satisfactory, so that the fission counting does not need any special treatment. Table VII shows the results for the fission rates corrected less the geometry efficiency that is to be eliminated by a comparison with α-counting.

The reference boron detector monitored the neutron flux that induces the fission counting; its counting-rate together with several corrections already explained earlier is presented in Table VIII. The correction factors

TABLE VII

FISSION COUNTING RESULTS

Run No.	Fission counting n_F (Hz)	Stat. S. D. (%)	Harmonic coeff. K_{hF}	Corr. counting-rate n_F^0/K_{gF} (Hz)
U I	1.4580	0.52	0.9426	1.3743
U II	1.9016	0.49	0.9865	1.8759
U III	0.9154	0.71	0.9865	0.9030
U IV	1.4368	0.54	0.9865	1.4174
P II	0.7883	0.50	0.9010	0.7102
P III	0.5044	0.63	0.9161	0.462
P IV	4.068	0.37	1.0000	4.068

TABLE VIII

BORON DETECTOR COUNTING RESULTS

Run No.	Counting-rate n_B(Hz)	St. S. D. (%)	Dead time K_t	B. noise K_n	Harmonic coeff. K_{hB}	Geometry K_{gB}	Discrimination selfab. K_d	Backscattering K_b	Reaction rate n_B^0(Hz)
U I	686.41	0.02	1.0013	0.9997	0.9146	2	1.040	0.991	1295
U II	1335.69	0.02	1.0026	0.9940	0.9876	2	1.042	0.991	2714
U III	1859.70	0.02	1.0037	0.9940	0.9876	2	1.042	0.991	3785
U IV	1624.25	0.02	1.0032	0.9940	0.9876	2	1.042	0.991	3302
P II	720.10	0.02	1.0014	0.9997	0.9146	2	1.040	0.991	1358
P III	1647.74	0.01	1.0033	0.9942	0.9876	2	1.042	0.991	3352
P IV	40.89	0.52	1.0000	0.548	1.0000	2	1.040	0.991	46.15

for K_d and K_b will be discussed in more detail. An absolute counting is achieved only by dealing with the pulse amplitude spectrum of the $B^{10}(n,\alpha)Li^7$ reaction. The amplitude distribution as given by the gridded ion chamber is that of Fig. 9. However, only the α-peak was taken into account. It must be borne in mind that the B^{10} reaction has two outlet channels having a branching ratio measurable under better energy resolution [34].

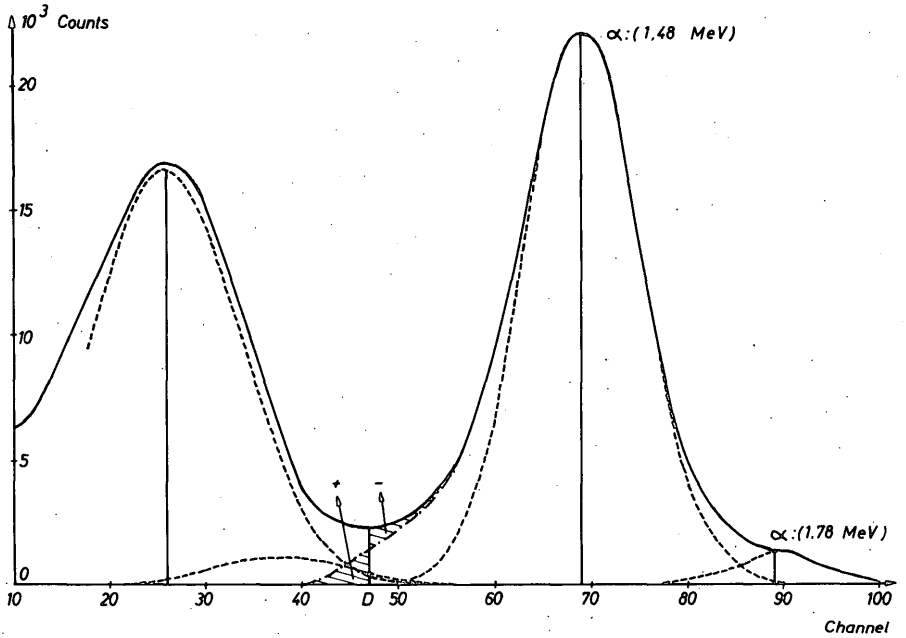

Fig. 9

Determination of the counting efficiency of the boron gridded ion chamber

——— experimental
- - - - - - - - fitted Gaussian
—·—·—·—·— self-absorption tail
boron layer density 59.64 μg/cm²

The two alpha- and the two Li^7 peaks have been localized on the amplitude axis relying on the energy linearity of the Frisch ion chamber [33, p. 123]. The Gaussian component has been separated from each peak by means of the standard deviation of the distribution obtained by an interpolation of those observed on the main peaks of the spectrum and of the measured branching ratio. The remaining part of the spectrum is caused by the self-absorption tail on the lower half of each peak, and by the background noise for the far lower amplitudes. In this way it was possible to evaluate the counting loss, or gain, due to the choice of a given discrimination threshold D, Fig. 9. It should be pointed out that a full application of the self-absorption theory [33, p. 228], has not been considered advisable because of the lack of agreement with the experimental results, due perhaps to the inadequacy of current absorption data for the 1.48 MeV alphas of this reaction, and to pos-

sible disuniformities of the boron coating. Nevertheless the theoretical correction for self-absorption efficiency

$$\epsilon = 1 - \frac{t_B}{2[R_0 - R(D)]} \qquad (15)$$

has been applied in a limited manner to the threshold $R(0) = 0$.

The correction factor K_d consists therefore of two parts: a correction for the alphas that are completely lost in the foil (equal to about 4% for a 60 $\mu g/cm^2$ boron foil); a correction, obtained graphically, for the difference between the alphas that come from the foil but are lost below the discrimination level D (Fig. 9) and the Li^7 particles, counted above the same level (this difference can be either negative or positive). The uncertainty concerning K_d may be quite high. One reason is that the Rossi and Staub formula is used for the first part of the correction only, for $R(E) = 0$. For the second part the formula was not used since the results from Fig. 9 do not in any way fit a distribution of the α-particles calculated from the formula.

The backscattering correction has been evaluated according to the theory of Ref. [35] after the suitable reduction to the actual alpha-energy and nature of the layer support.

The numerical calculation of Eq. (11) by means of the data and results given in Tables III-VIII leads to a set of fission cross-sections having as reference the absorption cross-section of boron (Table IX). When more determinations of the same quantity are obtained their weighted mean is also presented.

TABLE IX

RESULTS OF THE FISSION CROSS-SECTION MEASUREMENTS RELATIVE TO THE BORON CROSS-SECTION

Isotope	Run No.	Fissile layer (mm)	Neutron energy (eV)	Fission cross-section (b)	Average σ_F	Detector type
U^{235}	U I	4 π φ20	$0.03216 \pm 4\ 10^{-5}$	512 ± 11	512 ± 11	solid state
	U II	2 π φ40		357 ± 8		solid state
	U III	4 π φ40	0.0626 ± 10^{-4}	337 ± 10	343 ± 9	solid state
	U IV	4 π φ40		331 ± 8		solid state
Pu^{239}		2 πφ20	$0.03216 \pm 4\ 10^{-5}$	673 ± 13	673 ± 13	solid state
	P III	4 π φ40	0.0626 ± 10^{-4}	507 ± 9	507 ± 9	solid state
	P IV	4 π φ40	$0.275 \pm 2\ 10^{-3}$	3275 ± 30	3275± 30	gaseous scintillator

TABLE X

RESULTS OF THE Pu^{239} FISSION CROSS-SECTION MEASUREMENTS RELATIVE TO THE U^{235} CROSS-SECTION

Neutron energy (eV)	Run No.	$\frac{\sigma_F(Pu^{239})}{\sigma_F(U^{235})}$	Average ratio	Assumed $\sigma_F(U^{235})$ (b)	$\sigma_F(Pu^{239})$ (b)
0.03216 ± 0.00004	P II /U I	1.309 ± 0.023	1.309 ± 0.023	503	658 ± 12
0.0626 ± 0.0001	P III/U II	1.526 ± 0.035	1.533 ± 0.037	336	515 ± 12
	P III/U III	1.520 ± 0.042			
	P III/U IV	1.554 ± 0.34			

From the same results, but after the application of the relationship in Eq.(13), fission cross-sections of Pu^{239} relative to those of U^{235} at the same neutron energy have been calculated for two runs (Table X). The agreement between the two sets of results looks quite satisfactory, and can be taken as a positive check of the whole set of measurements.

Some comments are needed on the errors together with the measurements and the results at the different stages of handling. The errors given in Tables VI-VIII in fractional form only for a more direct appreciation are the standard deviations due to counting statistics only. Nevertheless the errors that affect the cross-sections in Tables XI and XII take into account also most of the errors in Eqs.(11) and (13), but not all. In particular the error on N_B pertains only to the weighting error, and it does not include the uncertainties on isotopic composition and chemical purity of the boron layers (see above). The error of 0.2% on K_d includes only an estimate of the uncertainty of the graphical treatment, but not of the uncertainty on the self-absorption correction for alpha particles completely absorbed in the boron layer. For A_α an error of 1% for 20-mm diameter foils, or 0.5% for 40-mm diameter foils, has been included. Indeed, if an edge effect also were to be taken into account it must be borne in mind that the fissile atom density N_F in this shadowed region could be much lower than its mean value as uniform layer, as assumed by Eq.(4).

TABLE XI

FISSION CROSS-SECTION OF U^{235} AT 0.0253 eV

Reference cross-section	Normalization factor ν	$(\sigma_F)_0$ (b)
$\sigma_a(B_{nat}) = 761$ b	1.008 ± 0.012	582 ± 10

TABLE XII

FISSION CROSS-SECTION OF Pu^{239} AT 0.0253 eV

Reference cross-section	Normalization factor ν	$(\sigma_F)_0$ (b)
σ_a (B_{nat}) = 761 b	0.9974 ± 0.0016	740 ± 10
$\sigma_F(U^{235})$ = 577 b	0.9932 ± 0.0069	737 ± 9
mean value	-	738 ± 7

For a more detailed error analysis see Ref. [28]. Here it will only be mentioned that an important source of error for the U^{235} runs comes from the ratio λ_α/K_i, more precisely from the U^{234} isotopic ratio and from the decay constant of U^{235}.

For the Pu^{239} runs, except P IV, the harmonic correction K_{hF} is rather substantial owing to the resonant behaviour of $\sigma_F(Pu^{239})$; for U^{235} also it is not negligible.

A weak counting statistics affects the reference counter in the P IV run whenever errors due to counting statistics on n_F become appreciable. Concerning Table XI, the errors on the normalization factor ν and of the renormalized cross-sections take into account the errors of the single measurements together with their deviations from the renormalized curve $\sigma_F(E)$.

DERIVATION OF THE 0.0253-eV FISSION CROSS-SECTIONS

The derivation of the fundamental cross-sections at the energy of 0.0253 eV can be made by normalization with a factor ν of the $\sigma_F(E)$ curve [1], which has a shape perfectly known between 0.0253 eV and 0.0626 eV, according to the weighted least-squares method [36]. The function

$$F(\nu) = \sum_{i=1}^{n} w_i [\nu \times \sigma(E_i) - \sigma_i]^2 \qquad (16)$$

must be minimized, being

$w_i = 1/(\Delta\sigma_i)^2$ the statistical weight of the value σ_i;

n = number of the measurements.

This gives

$$\nu = \frac{\Sigma_i [w_i \times \sigma_i \times \sigma(E_i)]}{\Sigma_i [w_i \times \sigma^2(E_i)]} . \qquad (17)$$

A comparison of the values of ν (Tables XI and XII) with the errors $\Delta\sigma_i$ of the observed fission cross-sections show that it is possible to renormalize

the $\sigma(E)$ curve without going over the error limits of the two measurements, the error brought in the calculation by ν being smaller than the error of the σ_i measurements.

The 0.0253-eV cross-section is then given by $\sigma_0 = \nu \times \sigma(E_0)$ and the error is obtained from the errors of σ_i and the residual values of σ_i from the $\nu \times \sigma(E)$ normalized curve. Table XI shows the result of this derivation for U^{235} and Table XII gives the result for Pu^{239}.

For Pu^{239}, the final value is then obtained by the combination of the values referred to boron and uranium-235. These values are included in Fig. 1 to make comparisons easier.

ACKNOWLEDGEMENTS

It is pleasure to acknowledge the part played by F. Netter in choosing the methods used for the measurements, the collaboration of C. Samour, and the help of J. Julien, L. Roussel and A. Bloch.

We are indebted to E. Cotton for welcoming us in the "Service de Physique Nucléaire à Basse Energie" at Saclay, and to P. Meriel to putting at our disposal his crystal spectrometers at the EL-3 reactor.

We also thank K. Lauer, H. Moret and their collaborators, who prepared the deposits, J. Winter, who developed most of the fast electronics; G. Gonano, M. Mailly, G. Weidenbach, who built the instrumentation, and K.H. Boeckhoff, who supported the measurements.

Finally, we are particularly grateful to W. Kley and J. Rousseaux for their help in the calculation of the errors.

REFERENCES

[1] HUGHES, D.J. and SCHWARTZ, R.B., Rpt. BNL 325, 2nd. ed. and Suppl. (1961).
[2] SCHMIDT, J.J., Rpt. KFK 120 (1962).
[3] SHER, R. and FELBERBAUM, J., Rpt. BNL 722 (1962).
[4] WESTCOTT, C.H., EKBERG, K., HANNA, G.C., PATTENDEN, N.J. and SANATANI, S., Proc. 3rd UN Int. Conf. PUAE (1964) (in press);
HANNA, G.C., AECL 873.
[5] HUGHES, D.J., Nucleonics 17 11 (1959) 132.
[6] SAFFORD, G.J. and HAVENS, W.W., Nucleonics 17 11 (1959) 134.
[7] RAFFLE, J.F. and PRICE, B.T., Proc. UN Int. Conf. PUAE 4 (1956) 422.
[8] AUCLAIR, J.M., GALULA, M., HUBERT, P., JACROT, B., JOLY, R., NETTER, F. and VENDRYES, G., Proc. UN Int. Conf. PUAE 4 (1956) 354.
[9] LYNN, J.E. and PATTENDEN, N.J., Proc. UN Int. Conf. PUAE 4 (1956) 423.
[10] ADAMCHUK, I.V., GERASIMOV, V.F., YEFIMOV, B.F., ZENKEVICH, V.S., MOSTOVOI, V.I., PEVZNER, M.L., CHERNYCHOV, A.A. and TSITOVICH, A.P., Proc. UN Int. Conf. PUAE 4 (1956) 645.
[11] LEONARD, B.R., Proc. UN Int. Conf. PUAE 4 (1956) 589.
[12] SAILOR, V.L., Proc. UN Int. Conf. PUAE 4 (1956) 586.
[13] BOLLINGER, L.M., COTE, R.E. and THOMAS, G.E., Proc. 2nd UN Int. Conf. PUAE 15 (1958) 127.
[14] SAFFORD, G.J., RUSTAD, B.M. and HAVENS, W.W., Jr., Pile Neutron Research in Physics, IAEA, Vienna (1962) 203.
[15] SAFFORD, G.J. and MELKONIAN, E., Phys. Rev. 113 (1959) 1285.
[16] MASLIN, E.E., Neutron Time-of-Flight Methods, EANDC - EURATOM, Brussels (1961) 127.

[17] DERUYTTER, A.J., Reactor Sci. Technol. 15 (1961) 165.
[18] LEONARD, B.R., Neutron Physics, New York & London (1962).
[19] SJÖSTRAND, N.G. and STORY, J.S., Rpt. AE-11 (1960).
[20] SJÖSTRAND, N.G. and STORY, J.S., Rpt. AEEW - M 125 (1961).
[21] FRAYSSE, G. and PROSDOCIMI, A., J. Phys. Radium 24 (1963) 899.
[22] PROSDOCIMI, A. and DERUYTTER, A.J., Reactor Sci. Technol. 17 (1963) 83.
[23] VAN AUDENHOVE, J., ESCHBACH, H.L. and MORET, H., Nucl. Instrum. Meth. 24 (1963) 465.
[24] LAUER, K.F. and VERDINGH, V., Nucl. Instrum. Meth. 21 (1963) 161.
[25] FRAYSSE, G., PROSDOCIMI, A. and WINTER, J., Electronique Nucléaire, OECD, Paris (1963).
[26] MERIEL, M., private communication.
[27] JAFFEY, A., Rev. sci. Instrum. 25 (1954) 349.
[28] FRAYSSE, G., PROSDOCIMI, A., NETTER, F. and SAMOUR, C., Rpt. CEA 2775 (1965).
[29] STROMINGER, D., HOLLANDER, J.M. and SEABORG, G.T., Rev. mod. Phys. 30 (1958) 585.
[30] DZHELEPOV, B. and PEKER, L.K., Decay Schemes of Radioactive Nuclei, O.U.P., London (1961).
[31] DERUYTTER, A.J., Nucl. Sci. Engng 21 (1965) 325.
[32] MARKIN, T.L., J. inorg. nucl. Chem. 9 (1958) 320.
[33] ROSSI, B. and STAUB, H.H., Ionization Chambers and Counters, NNES V-2, New York (1949).
[34] FRAYSSE, G. and PROSDOCIMI, A., Rpt. EUR 222f (1963).
[35] CRAWFORD, J.A., The Transuranium Elements, NNES IV-14 B, New York (1949).
[36] PARRAT, L.G., Probability and Experimental Errors in Science, New York (1961).
[37] DEBUS, G.H., private communication.
[38] LAUER, K.F., private communication.

DISCUSSION

C. WESTCOTT: The errors quoted in Table VI of your paper do not include uncertainties arising in connection with the composition and assay of the boron layer. Do you plan to investigate or reduce the possible inaccuracies? I would have thought that a magnitude of several per cent might be involved.

A. PROSDOCIMI: The boron target was prepared by electron vacuum evaporation of high-purity "spectro-grade" elemental boron, supplied by Merck. Some impurities were, I think, checked by Dr. Lauer, of the Central Bureau for Nuclear Measurements at Geel, who investigated boron grains from the same stock. However, no error of this kind can be taken into account until a certified, reliable chemical analysis has been made of the boron coating actually used.

M. PETRASCU: Could you please indicate the isotopic purity of the plutonium target?

A. PROSDOCIMI: The plutonium was supplied by the Atomic Energy Research Establishment, Harwell, and its isotopic content was given as 99.3% Pu^{239} and 0.7% Pu^{240}.

M. PETRASCU: In obtaining the pulse-height spectra of alpha particles and fission fragments, was any use made of collimation in the gaseous scintillation counter?

A. PROSDOCIMI: No collimation of any sort was used in the gaseous scintillator, which was a complete 2π-geometry detector.

M.S. MOORE: Can you tell me what corrections were made for non-uniformity of the foils and for beam composition? How did you determine the uniformity of the boron layer?

A. PROSDOCIMI: Satisfactory uniformity of the fissile coating was achieved by the method of electro-spraying. No macroscopic non-uniformity of the layer was observed; the neutron beam flux had a much higher degree of non-uniformity.

G. FRAYSSE: In addition to microscopic observations, we used a semi-conductor detector with a collimator of 2 mm to check the uniformity of the fissile layers. The non-uniformity observed did not play any part in our calculation of errors, except for the border zones, which were taken into account.

THE FISSION CROSS-SECTION OF Pu^{240} FOR 0.03-2.0 MeV NEUTRONS

M. De VROEY*, A. T. G. FERGUSON AND N. STARFELT**
NUCLEAR PHYSICS DIVISION,
ATOMIC ENERGY RESEARCH ESTABLISHMENT,
HARWELL, DIDCOT, BERKS., UNITED KINGDOM

Abstract — Résumé — Аннотация — Resumen

THE FISSION CROSS-SECTION OF Pu^{240} FOR 0.03-2.0 MeV NEUTRONS. The fission cross-section of Pu^{240} has been measured for neutrons having energies between 0.030 MeV and 2.0 MeV. The substantial values of this cross-section below the "threshold" at 200 keV are confirmed. The cross-section can be fitted on the assumption that at low energies only p-wave neutrons can induce fission using values of average resonance parameters derived from adjacent nuclei.

SECTION EFFICACE DE FISSION DE ^{240}Pu POUR DES NEUTRONS DE 0,03 A 2,0 MeV. Les auteurs ont mesuré la section efficace de fission de ^{240}Pu pour des neutrons de 0,03 à 2,0 MeV. Ces mesures ont confirmé les valeurs de cette section efficace au-dessous du «seuil» à 0,2 MeV. Si l'on suppose qu'aux basses énergies, seuls les neutrons d'onde-p peuvent provoquer la fission, on peut ajuster la section efficace en utilisant des valeurs de paramètres de résonance obtenues à partir des noyaux adjacents.

СЕЧЕНИЕ ДЕЛЕНИЯ ДЛЯ ПЛУТОНИЯ-240 В ДИАПАЗОНЕ ЭНЕРГИИ НЕЙТРОНОВ 0,03—2,0 мэв. Сечение деления для плутония-240 измерялось для энергии нейтронов в диапазоне 0,030—2,0 мэв. Подтверждаются сравнительно большие значения сечения деления ниже "порога" при энергии 200 кэв. Сечение можно определить в предположении, что при низких энергиях только p-волновые нейтроны могут вызывать деление с использованием средних параметров резонанса, выведенных из соседних ядер.

SECCION EFICAZ DEL ^{240}Pu PARA NEUTRONES DE 0,03-2,0 MeV. Los autores han medido la sección eficaz de fisión del ^{240}Pu por neutrones de energía comprendida entre 0.030 y 2,0 MeV. Los resultados obtenidos confirman los valores substanciosos de esa sección eficaz por debajo de la energía umbral, correspondiente a 200 keV. Empleando valores de los parámetros de resonancia media derivados de los núclidos contiguos, esa sección eficaz puede ajustarse a los valores teóricos admitiendo que, a bajas energías, sólo los neutrones de onda p pueden inducir la fisión.

INTRODUCTION

NESTEROV and SMIRENKIN [1] have reported that below the normally accepted fission threshold of Pu^{240}, at about 720 keV, the fission cross-section did not fall off rapidly but rather maintained a somewhat constant value of about 65 mb down to the lowest energies investigated (0.04 MeV). A cross-section of similar magnitude has also been observed by RUDDICK and WHITE [2]. A cross-section of this magnitude would make a significant contribution to the reactivity of a dilute fast reactor system fuelled with plutonium obtained from high burn-up thermal systems. Another effect would arise in the interpretation of spectral index measurements of the spectrum

* Present address: C.P.N.L., Avenue Cardinal Mercier, Heverle, Belgium.
** Present address: AB Atomenergi, Studsvik, Nyköping, Sweden.

in reactor systems using Pu^{240}, especially in systems with spectra having maxima in the keV region.

BROOKS and JOLLY [3] searched for fission components in 8 resonances in Pu^{240}. Their results show that the average fission width below 120 eV is smaller than 0.57 MeV. Using this fission width they calculated an upper limit for s-wave fission in the region around 100 keV that was one order of magnitude below the measured fission cross-section. To explain the observed fission cross-section it seems to be necessary [4, 5] to assume that fission below a few hundred kilo-electron-volts proceeds through a saddle point level of negative parity that can be reached only by p-wave neutrons. This may explain a strong increase in the cross-section between 120 eV and 30 keV. Calculations by JOHANSSON [6] indicate that the threshold for p-wave fission may well occur considerably below the s-wave threshold. A comparison between a calculated p-wave fission cross-section and the measured cross-section would then be interesting.

EXPERIMENT

The results of Smirenkin and Nesterov were obtained using a foil containing 7% Pu^{239} that gives a correction of the same magnitude as the Pu^{240} sub-threshold cross-section measured. Nesterov and Smirenkin determined the Pu^{239} content in an auxiliary experiment using thermal neutrons. Ruddick and White made two sets of measurements, one using a foil containing 7% Pu^{239}, another with 0.3% Pu^{239}. For both foils, the Pu^{239} content was derived from mass analysis.

For the present experiment a fission foil of Pu^{240} on a platinium backing was prepared from a stock whose mass analysis was Pu^{239} 0.26%, Pu^{240} 99.3%, Pu^{241} 0.3%, Pu^{242} 0.10%. The foil had a coating of Pu^{240} of 0.5 mg/cm^2 over an area of 5 cm. The foil was mounted on the central earthed electrode of a back-to-back fission chamber. The other foil in the chamber was of uranium whose mass analysis was U^{235} 80%, U^{234} 1% and U^{238} 19%. The quantity of thermally fissile material in the plutonium foil was determined by measurements of the fission counting-rates from the plutonium and uranium foils when the back-to-back fission chamber was placed in the neutron flux from the thermal column of the GLEEP reactor. Measurements were made with and without a cadmium sheath, the measurement with cadmium giving the background caused by epithermal neutrons and spontaneous fission. The quantity of thermally fissile material determined in this way was somewhat greater than that given by the mass analysis. This was assumed to be due to contamination of the foil with Pu^{239} in the course of manufacture. The value of the Pu^{239} content obtained by the thermal-neutron measurement was used in correcting the Pu^{240} fission cross-section at higher energies.

Using monoenergetic neutrons from the Harwell 5-MeV Van de Graaf, the variation of ratio of the fission cross-section of Pu^{240} to that of U^{235} was measured over the energy range 0.030-2.0 MeV. The fission chamber in its cadmium sheath was placed in the 0° position, i.e. with the fission foils on and normal to the beam axis, and 6 cm from the neutron-producing target. For energies up to 550 keV, neutrons from the $Li^7(p,n)Be^7$ reaction were used, the target being a lithium metal layer on a tantalum backing. The

target thickness was 8 keV as determined by threshold measurements. At the higher energies the T(p, n)He^3 reaction was used, the tritium being absorbed in a layer of titanium, 0.56 mg/cm^2 thick. Throughout the course of the experiment, measurements were made for alternate periods of 10 min with and without beam, in order to measure the number of spontaneous fissions. An analysis of all the "beam-off" runs gave no indication of any systematic drift in the number of spontaneous events observed. A check was made of the possible effect of epithermal neutrons by a run with the distance from target to foil increased by a factor of 10. In a standard 10-min run with "beam on", no significant counts were observed from the uranium foil and the count-rate from the plutonium foil was, within errors, identical with that in a "beam-off" run. It was concluded that there was no significant count-rate due to epithermal neutrons.

No attempt has been made to obtain absolute values of the Pu^{240} cross-section. The results were normalized to the ratios of the U^{235} and Pu^{240} cross-sections given by HUGHES and SCHWARTZ [7] at 2.0-MeV neutron energy, correcting respectively for the effects of the Pu^{239} and U^{238} components of the plutonium and uranium foils. The Pu^{240} cross-section at other energies was obtained relative to the cross-sections for U^{235} from the same compilation, correcting for the effects of the Pu^{239} and Pu^{241} content of the plutonium foil and the U^{238} content of the uranium foil. In the sub-threshold region, the correction to the Pu^{240} cross-section for the effect of the other plutonium isotopes was 20%. The background due to spontaneous fission was much larger than this, being as high as 80% of the total count at some energies.

RESULTS AND DISCUSSION

The cross-sections obtained are shown in Fig. 1. Statistical errors are shown in the figure, which also gives the results of NESTEROV and SMIRENKIN [1] and RUDDICK and WHITE [2]. In general all three sets of results are in good agreement within the experimental errors.

The cross-section of p-wave fission for a $\frac{1}{2}$-saddle-point state and the $\frac{3}{2}$-rotational level based on this was calculated from the expression

$$\sigma_f = (2e+1)\,2\pi^2\pi^2\,\overline{\Gamma}_f \times \frac{\overline{\Gamma}_f}{D} \times \frac{1}{\overline{\Gamma}} .$$

The fission width was derived from the barrier penetration formula of Hill and Wheeler.

$$\overline{\Gamma}_f = \frac{D}{2\pi} \frac{1}{1+e^{2\pi(E_f - E)/h\omega}} .$$

The values of D = 5.5 eV for the average level spacing and $\overline{\Gamma}_\gamma$ = 0.032 eV for the average radiation width were used [7]. The p-wave strength function $\overline{\Gamma}_{n/D}$ was given the value 2×10^{-4} as deduced from measurements on adjacent

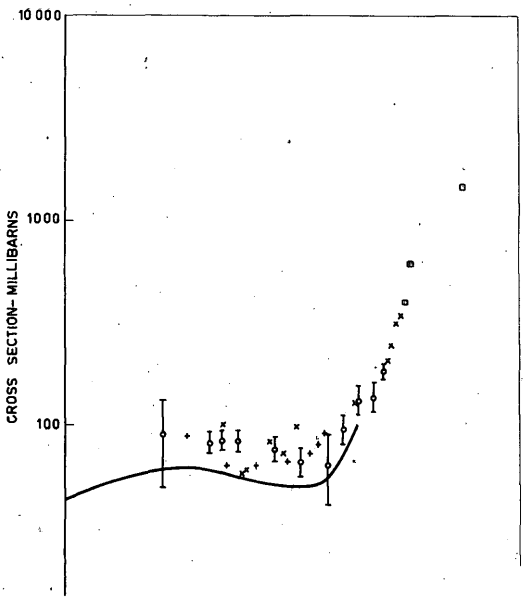

Fig. 1

Fission cross-section for Pu^{240}.

○ present experiment
× experiments of RUDDICK and WHITE [2]
+ experiment of NESTEROV and SMIRENKIN [1]
The solid curve is the calculated p-wave fission cross-section

heavy elements [8]. The contribution to the total width Γ from inelastic neutron scattering was calculated using the observed inelastic cross-section for the lowest excited state in U^{238} [9], which has the same energy, spin and parity as the corresponding state in Pu^{240}. Figure 1 shows the cross-section calculated using values of E_f and $\hbar\omega$, the fission barrier position and thickness, of 710 and 650 keV respectively [10].

Clearly a small adjustment of $\hbar\omega$ would further improve the agreement.

CONCLUSIONS

The experimental work described above, together with that of Smirenkin and Nesterov, and Ruddick and White, establishes that the "sub-threshold" fission cross-section of Pu^{240} exists, and has a magnitude of about 100 mb, while Brooks has shown that the cross-section in the eV region is vanishingly small. The discussion above indicates that these observations are consistent with the assumption that below about 400 keV, neutron-induced fission in Pu^{240} proceeds through a $\frac{1}{2}$-saddle-point state. The almost constant fission cross-section from 30 keV to 300 keV is due to the fact that the increase in fission barrier penetrability in this region is balanced by the decrease in p-wave compound nuclear cross-section.

ACKNOWLEDGEMENTS

The authors wish to express their gratitude to Dr. E. R. Rae for fruitful discussions. One of us, M. de Vroey, acknowledges the award of a bursary from the Belgian Institut Interuniversitaire des Sciences Nucléaires.

REFERENCES

[1] NESTEROV, V. G. and SMIRENKIN, G. N., J. nucl. Energy 16 (1962) 51.
[2] RUDDICK, P. and WHITE, P. H., to be published in J. nucl. Energy
[3] BROOKS, F. D. and JOLLY, J. E., AERE Rpt. PR/NP6 (1963) 13.
[4] WHEELER, J. A., Physica XXII (1956) 1103.
[5] RAE, E. R., private communication.
[6] JOHANSSON, S. A. E., Nucl. Phys. 12 (1959) 449.
[7] HUGHES, D. and SCHWARTZ, R., Neutron Cross Sections, BNL 325 (1958).
[8] UTTLEY, C. A., AERE Rpt. PR/NP 6 (1963) 2.
[9] BARNARD, E., FERGUSON, A. T. G., McMURRAY, R. and VAN HEERDEN, I. J., private communication.
[10] HALPERN, I., Annu. Rev. nucl. Sci. 9 (1959) 245.

ВЗАИМОДЕЙСТВИЕ НЕЙТРОНОВ С ЯДРАМИ УРАНА-235 В ОБЛАСТИ ЭНЕРГИЙ 0,002÷30 кэв

ВАН ШИ-ДИ, ВАН ЮН-ЧАН, Е. ДЕРМЕНДЖИЕВ и Ю.В. РЯБОВ
ОБЪЕДИНЕННЫЙ ИНСТИТУТ ЯДЕРНЫХ ИССЛЕДОВАНИЙ, ДУБНА СССР

Abstract — Résumé — Аннотация — Resumen

INTERACTION OF NEUTRONS WITH U^{235} NUCLEI IN THE ENERGY RANGE 2 eV - 30 keV. The fast pulsed reactor of the Joint Institute for Nuclear Research was used to measure the total cross-section, the fission cross-section and the radiative-capture cross-section of U^{235} by the time-of-flight method with a resolution of ~ 0.04 μs/m. The flight length was 1000 m. The time spectra were recorded by 2048-channel time analysers.

To measure the total cross-sections by the transmission method, a resonance-neutron scintillation counter with lithium glass was used. The fission, radiative-capture and total cross-sections were measured by the auto-indication method using a large liquid scintillation detector with cadmium added to the solution. The sample to be investigated was placed in the axis of a cylindrical opening in the vessel, in a geometry close to 4π. The volume of the detector was scanned by 32 FEU-24 photomultipliers. The fissions were identified by the delayed coincidences between the scintillations corresponding to the recording of the prompt gamma rays and the moderated prompt fission neutrons. Radiative capture is not accompanied by a delayed pulse. The efficiency of recording fissions and radiative capture was ~50% and ~25% respectively, while the background (expressed as a percentage of the strong resonances) was ~1% and ~15% respectively. The area method was used to obtain the parameters $g\Gamma_n$, Γ, Γ_f and Γ_γ for a number of low-lying levels. The average widths of $\bar{\Gamma}_\gamma$ and $\bar{\Gamma}_f$ over all the levels were (42±3) mV and (51±6) mV respectively. The levels were divided into two systems with $\alpha_1 < 1$ ($\bar{\alpha}_1 \sim 0.5$) and $\alpha_2 > 1$ ($\bar{\alpha}_2 \sim 1.5$) and $\bar{\Gamma}_f^1 \approx 72$ mV and $\bar{\Gamma}_f^2 \approx 25$ mV respectively, which may be connected with the two spin values 3^- and 4^- of the compound nucleus.

The energy dependence of the ratio of radiative-capture to fission cross-sections was obtained in the neutron-energy range from 2 eV to 30 keV.

Measurements using a sample of U^{238} instead of U^{235} made it possible to take into account experimentally the contribution of the radiative capture of U^{238} to α.

INTERACTION ENTRE NEUTRONS ET NOYAUX DE ^{235}U DANS LA REGION DES ÉNERGIES DE 2 eV A 30 keV. A l'aide du réacteur pulsé à neutrons rapides de l'Institut unifié de recherches nucléaires, les auteurs ont mesuré, par la méthode du temps de vol, avec un pouvoir de résolution de ≈ 0,04 μs/m, la section efficace totale, la section efficace de fission et la section efficace de capture radiative pour ^{235}U. Le parcours avait une longueur de 1 000 m. En vue d'enregistrer les spectres en fonction du temps, on a employé des analyseurs à 2 048 canaux.

Les sections efficaces totales ont été mesurées par la méthode de la transmission à l'aide d'un détecteur à scintillation (verre au lithium) pour les neutrons de résonance. Pour déterminer la section efficace de fission, celle de capture radiative et les sections efficaces totales par la méthode de l'autoindication, on a employé un grand détecteur à scintillateur liquide en ajoutant du cadmium à la solution. L'échantillon était placé dans l'axe de l'orifice cylindrique de la cuve dans une géométrie proche de 4π. Le volume du détecteur était examiné à l'aide de 32 photomultiplicateurs FEU-24. On identifiait les fissions par les coïncidences retardées entre les scintillations dues à l'enregistrement des rayons gamma instantanés et à celui des neutrons de fission instantanés ralentis. La capture radiative ne s'accompagne pas d'une bouffée retardée. L'efficacité d'enregistrement des fissions était d'environ 50% et celle de la capture radiative de 25%, le mouvement propre s'élevait respectivement à ≈ 1% et ≈ 15% du comptage dans les fortes résonances. Grâce à la «méthode des plages», on a obtenu les paramètres $g\Gamma_n$, $\bar{\Gamma}$, Γ_f et $\Gamma\gamma$ pour plusieurs niveaux peu élevés. Les largeurs moyennes de $\bar{\Gamma}\gamma$ et $\bar{\Gamma}_f$ s'élèvent, pour tous les niveaux, respectivement à (42±3) et (51±6) mV. On a partagé les niveaux en deux catégories telles que $\alpha_1 < 1$ ($\bar{\alpha}_1 \approx 0,5$) et $\alpha_2 > 1$ ($\bar{\alpha}_2 \approx 1,5$), $\Gamma^1_f \approx 72$ mV et $\bar{\Gamma}^2_f \approx 25$ mV, ce qui peut s'expliquer par le fait que le spin du noyau composé présente deux valeurs: 3^- et 4^-.

Dans la région des énergies des neutrons de 2 eV à 30 keV, on a déterminé la variation selon l'énergie du rapport entre la section efficace de capture radiative et la section efficace de fission.

Des mesures sur un échantillon de ^{238}U substitué à ^{235}U ont permis de prendre expérimentalement en considération la contribution de la capture radiative de ^{238}U à la valeur de α.

ВЗАИМОДЕЙСТВИЕ НЕЙТРОНОВ С ЯДРАМИ УРАНА-235 В ОБЛАСТИ ЭНЕРГИЙ 2 эв ÷ 30 кэв. На импульсном быстром реакторе Объединенного института ядерных исследований методом времени пролета с разрешением ~0,04 мксек/м проведены измерения полного сечения, сечений деления и радиационного захвата урана-235. Пролетное расстояние составляло 1000 м. Временные спектры регистрировались 2048-канальными временными анализаторами.

При измерениях полных сечений по методу пропускания использовался сцинтилляционный детектор резонансных нейтронов на литиевых стеклах. Измерения сечений деления, радиационного захвата и полных сечений методом самоиндикации проводились с помощью большого жидкостного сцинтилляционного детектора с введенным в раствор кадмием. Исследуемый образец помещался на оси цилиндрического отверстия бака в геометрии близкой к 4π. Объем детектора просматривался 32 фотоумножителями ФЭУ-24. Деления идентифицировались по задержанным совпадениям между сцинтилляционными вспышками, соответствующими регистрации мгновенных γ-лучей и замедлившихся мгновенных нейтронов деления. Радиационный захват не сопровождается задержанным импульсом. Эффективности регистрации делений и радиационного захвата составляли ~50% и ~25%, а фоны ~1% и ~15% от счета в сильных резонансах соответственно. "Методом площадей" получены для ряда низколежащих уровней параметры $g\Gamma_n$, Γ, Γ_f и Γ_γ. Средние ширины Γ_γ и Γ_f по всем уровням равняются (42 ± 3) мв и (51 ± 6) мв, соответственно. Проведено разделение уровней на две системы с $\alpha_1 < 1$ ($\bar{\alpha}_1 \sim 0{,}5$) и $\alpha_2 > 1$ ($\bar{\alpha}_2 \sim 1{,}5$) и $\overline{\Gamma_f^1} \approx 72$ мв и $\overline{\Gamma_f^2} \approx 25$ мв, соответственно, что, возможно, связано с двумя значениями спина 3^- и 4^- составного ядра.

В области энергий нейтронов от 2 эв до 30 кэв получена энергетическая зависимость отношения сечений радиационного захвата и деления.

Измерения с образцом урана-238, помещенного на место образца урана-235, позволили экспериментально учесть вклад радиационного захвата урана-238 в α.

INTERACCION DE LOS NEUTRONES CON LOS NUCLEOS DEL ^{235}U EN EL INTERVALO ENERGETICO 2 eV - 30 keV. En el reactor pulsado de neutrones rápidos del Instituto Central de Investigaciones Nucleares, los autores midieron por el método del tiempo de vuelo con un poder de resolución de ~ 0, 04 μs/m la sección eficaz total y las secciones eficaces de fisión y de captura radiativa del ^{235}U. La trayectoria del vuelo era de 1000 m. Los espectros en función del tiempo se registraron con un analizador de 2048 canales.

Para medir las secciones eficaces totales por el método de transmisión, se utilizó un detector de centelleo para neutrones de resonancia, con vidrio de litio. La sección eficaz de fisión, la de captura radiativa y las secciones eficaces totales se midieron por el método de autoindicación mediante un gran detector de centelleo líquido, con cadmio en solución. La muestra que se quería estudiar se colocó en el eje del orificio cilíndrico del recipiente, de geometría próxima a 4π. El volumen del detector fue abarcado por 32 fotomultiplicadores FEU-24. Las fisiones se identificaron por coincidencias retardadas entre impulsos de centelleo que corresponden al registro de los rayos gamma instantáneos y al de los neutrones instantáneos de fisión moderados. La captura radiativa no va acompañada de impulsos retardados. El rendimiento de registro de las fisiones y de la captura radiativa fue de ~ 1% y ~15% del recuento en la región de las resonancias fuertes. "Por el método de áreas" se obtuvieron para toda una serie de niveles inferiores los parámetros $g\Gamma_n$, Γ, Γ_f y Γ_γ. La anchura media de $\overline{\Gamma_\gamma}$ y $\overline{\Gamma_f}$ en todos los niveles es igual a (42 ± 3) mV y (51 ± 6) mV, respectivamente. Se efectuó una distribución de los niveles en dos sistemas con $\alpha_1 < 1$ ($\bar{\alpha}_1 \sim 0, 5$) y $\alpha_2 > 1$ ($\bar{\alpha}_2 \sim 1, 5$) y $\overline{\Gamma_f^1} \approx 72$ meV y $\overline{\Gamma_f^2} \approx 25$ MeV y $\Gamma_f \approx 25$ meV respectivamente, lo que puede explicarse por el hecho de que el spin del núcleo compuesto presenta dos valores, a saber 3^- y 4^-.

Para neutrones de energía comprendida entre 2 eV y 30 keV se determinó la influencia de la energía sobre la razón entre sección eficaz de captura radiativa y la sección eficaz de fisión.

Efectuando las mediciones con una muestra de ^{238}U, en lugar de ^{235}U, se pudo tener en cuenta experimentalmente la contribución de la captura radiativa del ^{238}U al valor α.

Исследованию взаимодействия нейтронов с ядрами урана-235 в широкой области энергий посвящено значительное число работ [1—7].

Для энергий $E_n < 50$ эв были определены параметры сильных уровней, однако точность определения $g\Gamma_n$, Γ, особенно Γ_f, оставалась невысокой.

Полная радиационная ширина Γ_γ, мало меняющаяся для первых низколежащих уровней, считалась постоянной и равной (33 ± 10) мэв.

В последние годы были измерены для урана-235 средние сечения деления в области энергий нейтронов до 20 кэв [5], средние полные сечения — в области энергий до 10 кэв [6] и средние сечения деления и радиационного захвата — в области энергий нейтронов выше 30 кэв [7].

В настоящей работе использована новая экспериментальная методика для исследования взаимодействия с ядрами урана-235 в области 0,002 ÷30 кэв с целью получения уровней и определения средних сечений деления и радиационного захвата.

МЕТОДИКА ИЗМЕРЕНИЙ

Измерения производились методом времени пролета с импульсным быстрым реактором Объединенного института ядерных исследований [8] в качестве источника резонансных нейтронов. Пролетное расстояние составляло 1000 м. Временные спектры регистрировались 2048-канальными анализаторами с ширинами каналов 32, 16 и 8 мксек при измерениях в энергетических интервалах 0,002 ÷0,005; 0,005 ÷1,5 и 1,5 ÷30 кэв, соответственно. Это обеспечивало $\Delta t/L \approx 0{,}04$ мксек/м.

Акты деления и радиационного захвата регистрировались с помощью детектора — цилиндрического бака с жидким сцинтиллятором, содержащим кадмий [9]. Исследуемый образец (D-образец) помещался на оси цилиндрического отверстия бака в геометрии близкой к 4π. Для уменьшения рассеяния нейтронов на воздухе этот объем откачивался. Схема детектора и блок-схема электронной аппаратуры показаны на рис.1.

Принцип регистрации основан на том факте, что деление сопровождается испусканием мгновенных γ-лучей и нейтронов, а радиационный захват — только γ-лучей. γ-лучи деления и радиационного захвата регистрировались по световой вспышке в сцинтилляторе. Нейтроны деления, замедляясь в водородосодержащей среде сцинтиллятора, захватывались ядрами кадмия и давали каскад γ-квантов с полной энергией $\approx 9{,}2$ Мэв, который также регистрировался по световой вспышке в сцинтилляторе. Среднее время жизни в детекторе ≈ 8 мксек.

Задержанное совпадение соответствовало акту деления, и эта информация накапливалась временным анализатором. Акты без сопровождающего импульса регистрировались другим временным анализатором. Последняя информация включала события, относившиеся к радиационному захвату нейтронов, делению, не зарегистрированному в делительном канале, и, наконец, фону.

Фон, создаваемый радиоактивностью помещения, космическим излучением и естественной γ-активностью образца, не зависит от времени и достаточно точно учитывается.

Для надежного исключения фона при работающем реакторе использовались помещенные в нейтронный пучок достаточно толстые фильтры из серебра, кобальта и марганца. Счет в резонансах при $E_n = 5{,}2$ эв (Ag), $E_n = 132$ эв (Co) и $E_n = 0{,}337$ и $2{,}36$ кэв (Mn) из-за полного поглощения фильтрами нейтронов этих энергий равен фону.

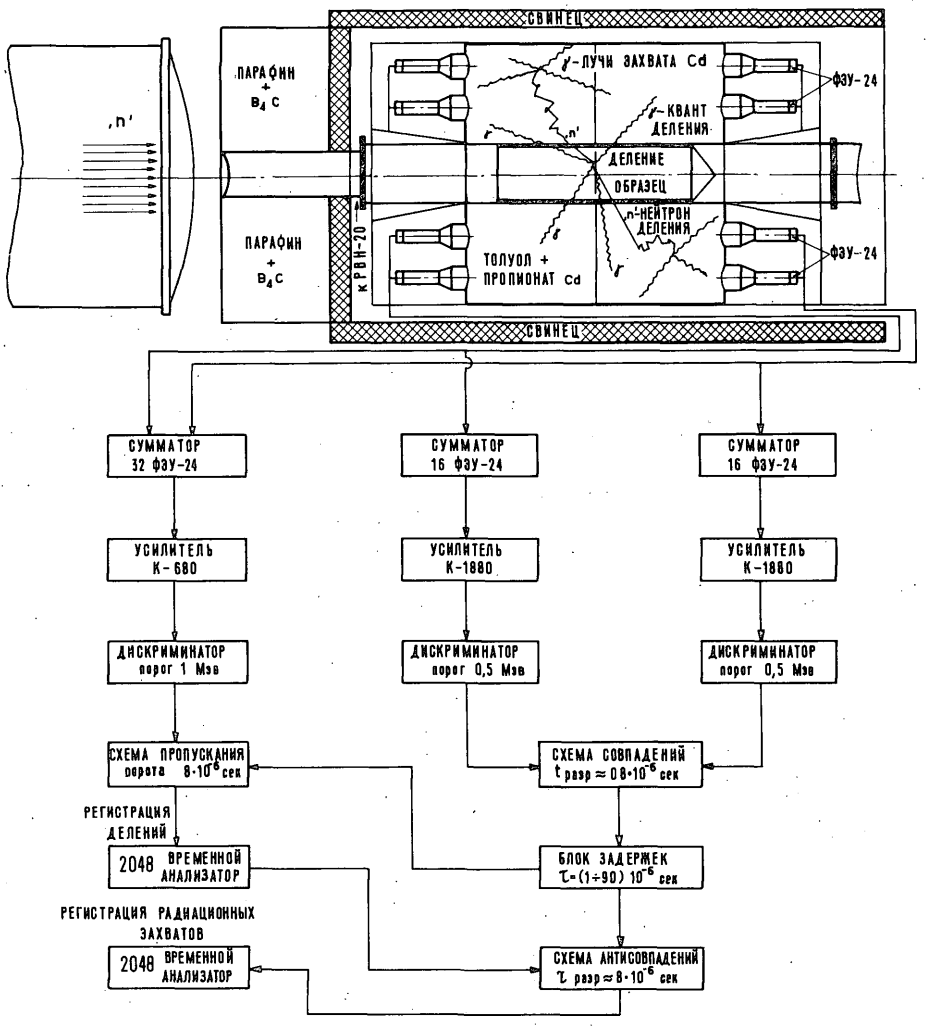

Рис.1

Продольный разрез детектора и его положение на нейтронном пучке. Блок-схема регистрирующей аппаратуры. (Обозначения указаны на рисунке).

Между чувствительным объемом детектора и образцом помещался фильтр из смеси парафина с Li_2CO_3 для снижения фона рассеянных образцом нейтронов. Фон, обусловленный потенциальным рассеянием нейтронов образцом урана-235, определялся из отдельных измерений с ураном-238 (низкоэнергетическая область) и свинцом в качестве образцов.

Таким образом, после учета фона счет в канале, регистрирующем радиационный захват, определялся только актами радиационного захвата и делениями, не зарегистрированными в делительном канале. Этот счет для одного канала временного анализатора можно представить в следующем виде:

$$\Delta N_0^i = \Delta N_\gamma^i + \frac{K}{\epsilon_f} \Delta N_f^i, \qquad (1)$$

где ΔN_γ^i – число зарегистрированных актов деления в i-том канале первого временного анализатора;

ΔN_f^i – число зарегистрированных актов радиационного захвата в i-том канале второго временного анализатора за одинаковое время измерений;

K – эффективность, с которой в канале радиационного захвата регистрируются акты, относящиеся к делению;

ϵ_f – эффективность регистрации актов деления в делительном канале.

Величина $K \approx 0{,}2$ и известна с точностью не хуже (2–3)%. Подробнее вопрос об определении поправки K обсуждается в работе [10].

Для учета фона в канале, регистрирующем деления, использовались задержанные совпадения с временем задержки, в ≈ 10 раз превышающем среднее время жизни нейтрона в детекторе. Это позволило учесть фон случайных совпадений в пределах отдельного резонанса.

При измерениях с образцами урана-235 фон в канале делений составлял не более (1 ÷ 2)%, а в канале регистрирующем радиационный захват, – не более 20% от счета в сильных резонансах (например, резонансы с E_0 = 8,77 эв и E_0 = 12,39 эв).

Эффективности регистрации актов деления и радиационного захвата в различных сериях измерений составляли $\epsilon_f \approx (40-60)\%$ и $\epsilon_\gamma \approx (20-30)\%$, соответственно.

Помимо описанного измерения, были проведены измерения полных сечений урана-235 методом самоиндикации и пропускания. В первом случае использовался делительный канал детектора, имеющий низкий уровень фона. Во втором случае использовался сцинтилляционный детектор на литиевых стеклах.

В длительных сериях измерения эффекта и фона чередовались, и полученная на временных анализаторах информация периодически передавалась в память электронной вычислительной машины, на которой производилась предварительная обработка экспериментальных данных. В измерениях использовались образцы урана-235 в виде металлических пластин и окиси, нанесенной на алюминиевую фольгу площадью до 250 см^2 и обогащением исследуемым изотопом до 90%.

Толщины образцов составляли:

при измерениях сечений деления и радиационного захвата –

$8 \cdot 10^{-5}$; $4 \cdot 10^{-4}$; $1 \cdot 10^{-3}$ и $2 \cdot 10^{-3}$ ядер/барн;

при измерениях самоиндикации –

D – образец $2 \cdot 10^{-3}$ ядер/барн,

T – образцы $4 \cdot 10^{-4}$ и $2 \cdot 10^{-3}$ ядер/барн;

при измерениях пропускания –

T – образцы $2 \cdot 10^{-3}$ и $2 \cdot 10^{-2}$ ядер/барн.

РЕЗУЛЬТАТЫ ИЗМЕРЕНИЙ И ОБРАБОТКА

Суммарное число отсчетов детектора по всему резонансу, приведенное к единичным потоку и эффективности, не зависит от разрешения и может быть записано в виде [12]:

$$\frac{\Sigma N(D)}{\Pi(E_0)\epsilon_j} = \frac{\Gamma_j}{\Gamma} A_D, \tag{2}$$

где $\Pi(E_0)$ – число нейтронов в единичном энергетическом интервале, падающих на всю площадь образца за время измерений;

Γ, Γ_j – полная и делительная или радиационная ширины рассматриваемого уровня;

ϵ_j – эффективность регистрации актов деления или радиационного захвата;

A_D – площадь провала на кривой пропускания;

n_D – число ядер/см^2 детекторного образца.

При вычислении площади резонанса производилось обрезание крыльев при энергиях $E_0 - \eta_1$ и $E_0 + \eta_2$. Соответствующая поправка вводилась в виде $\frac{n\sigma_0\Gamma^2}{4}\left(\frac{1}{\eta_1} + \frac{1}{\eta_2}\right)$. Вклад в площадь рассматриваемого резонанса крыльев соседних резонансов учитывался аналогичным образом. Группы резонансов, для которых эту процедуру невозможно было надежно выполнить из-за недостаточно высокого разрешения, обрабатывались с использованием геометрического разложения площадей. Это относится, главным образом, к области 40–50 эв.

Для того, чтобы избежать больших ошибок при определении величины $\Pi(E_0)\epsilon_f$, осуществлялась калибровка на тепловое сечение урана-235, принятое равным $\sigma_f(\text{th}) = (582 \pm 6)$ барн, и значение

$$\alpha(\text{th}) = \sigma_{n\gamma}(\text{th})/\sigma_f(\text{th}) = 0{,}176 \pm 0{,}002. \tag{3}$$

Ошибка калибровки – около 5%.

При измерениях методом самоиндикации из отношения суммарных скоростей счета по исследуемому резонансу с Т-образцом и без него получается выражение

$$S(D, T) = \frac{\sum_i N_i(D, T)}{\sum_i N_i(D)} \exp(n_T\sigma_p) = \frac{A_{D+T} - A_T}{A_D}, \tag{4}$$

где σ_p – сечение потенциального рассеяния. Это выражение не содержит значений потока и эффективности детектора и является функцией параметров, определяющих А, отношения n_D/n_T и σ_p.

Таблицы значений $S(D, T)$ были рассчитаны на электронной вычислительной машине. Находя экспериментальную величину $S(D, T)$, можно из выражения (4) получить зависимость $g\Gamma_n$ от Γ.

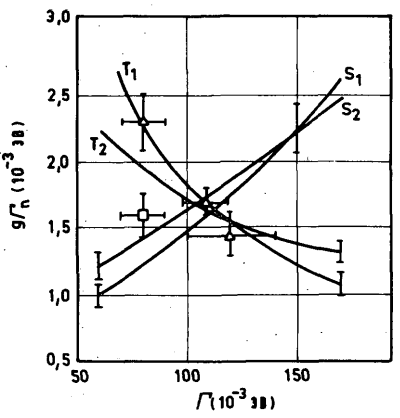

Рис.2

Определение параметров $g\Gamma_n$ и Γ из кривых самоиндикации ($S_1 S_2$) и пропускания ($T_1 T_2$) для уровня 19,3 эв.

▲ – данные работы [3],
△ – данные работы [2],
□ – данные работы [4],
● – данные настоящей работы.

Обработка кривых пропускания известным методом площадей, подробно описанном в работе [13], также позволяла получать зависимость $g\Gamma_n$ от Γ.

Кривые $g\Gamma_n = f(\Gamma)$, полученные методом самоиндикации и пропускания, пересекаются под большими углами (близкими к $\pi/2$), чем кривые, полученные только в экспериментах по пропусканию. Это позволяет с большей надежностью определять параметры уровней $g\Gamma_n$ и Γ. Эта процедура иллюстрируется рис.2 и 3 для уровней 19,3 и 10,2 эв. В табл.1 приведены параметры уровней урана-235 в области энергий 2–50 эв.

Из выражения (2) для случая $n\sigma_0 \ll 1$ были получены средние по нескольким образцам значения $\sigma_0\Gamma_\gamma$ и $\sigma_0\Gamma_f$ для данного резонанса, а величина α определялась как их отношение. В некоторых случаях величина α определялась непосредственно из отношения приведенных к одной эффективности и одному времени измерения аппаратурных спектров, соответствующих захватному и делительному каналам. В этом случае величина $\sigma_0\Gamma_\gamma$ определялась как $\alpha(\sigma_0\Gamma_f)$. Делительную ширину получали из выражения $\Gamma_f = \Gamma/1+\alpha$, полную радиационную – из $\Gamma_\gamma = \Gamma - \Gamma_f$. Для уровней с неизвестной полной шириной Γ радиационная ширина Γ_γ принималась постоянной и равной 40 мэв ($\Gamma_\gamma = 40$ мэв – среднее значение, полученное по 25 уровням, приведенным в таблице 1), а $\Gamma_f = \Gamma_\gamma/\alpha$.

Полное сечение $\sigma_0\Gamma$ для всех известных уровней урана-235 можно считать равным $\sigma_0\Gamma_\gamma + \sigma_0\Gamma_f$, так как величина $\sigma_0\Gamma_n$ пренебрежимо мала ($\Gamma_n \ll \Gamma_\gamma + \Gamma_f$). Отсюда можно определить $g\Gamma_n = (\sigma\Gamma_\gamma + \sigma_0\Gamma_f)/4\pi\lambda\!\!\!^{-}_0$, где $2\pi\lambda\!\!\!^{-}_0$ – длина волны нейтрона при энергии E_0. Эти значения $g\Gamma_n$ в пределах экспериментальных ошибок согласуются с величинами $g\Gamma_n$, полученными для тех же уровней из измерений пропускания и самоиндикации. В табл.1 приведены средние значения $g\Gamma_n$ для таких уровней.

В табл.2 приведены значения усредненных по выбранным энергетическим интервалам сечений деления и радиационного захвата, а также $\alpha = \langle\sigma_{n\gamma}(E)\rangle / \langle\sigma_f(E)\rangle$ в области энергий от 0,1 до 30 кэв. Как уже отме-

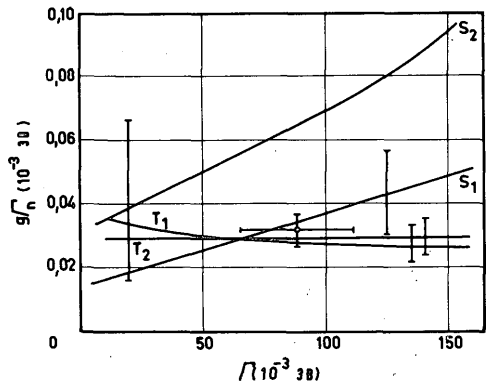

Рис.3

Определение параметров $g\Gamma_n$ и Γ из кривых самоиндикации ($S_1 S_2$) и пропускания ($T_1 T_2$) для уровня 10,2 эв.

чалось выше, возможная систематическая ошибка калибровки сечений деления и радиационного захвата по тепловым сечениям составляет ≈ 5%. Однако при определении сечения радиационного захвата в области нескольких кэв и выше возникают трудности, связанные с учетом возрастающего фона потенциально и резонансно рассеянных нейтронов. Для того, чтобы исключить значительные ошибки, связанные с учетом этого фона, осуществлялась нормировка значения α на значение $\alpha = 0{,}376 \pm 0{,}036$ при $E_n = 30$ кэв полученное в работе [7]. Эта нормировка приводит к появлению возможной систематической ошибки в сечении радиационного захвата ≈ 15% в этой области энергий.

Дополнительные измерения с образцом урана-238, помещенным на место исследуемого образца урана-235, позволили экспериментально учесть вклад радиационного захвата, обусловленного ураном-238.

ОБСУЖДЕНИЯ

При интерпретации экспериментальных данных для урана-235 в резонансной области существуют известные трудности, связанные с пропуском заметного числа уровней, недостаточно высокой точностью определения параметров уровней и, наконец, невозможностью до сих пор прямого экспериментального определения значений спинов уровней.

Из известной формулы Брейта-Вигнера для изолированного уровня следует, что величина сечения в резонансе пропорциональна Γ_n/Γ. Этот факт при достаточно широких распределениях Γ_n и Γ_f может привести к существованию заметного числа уровней с нейтронными ширинами, намного меньшими средних, и полными ширинами, значительную часть которых в большинстве случаев составляет делительная ширина, сравнимыми с расстояниями между уровнями. Такие резонансы экспериментально трудно обнаружить. На рис.4 показано экспериментально полученное распределение приведенных нейтронных ширин урана-235 для 78 уровней, которое удовлетворительно описывается χ^2 – распределением с числом степеней

Таблица 1

ПАРАМЕТРЫ УРОВНЕЙ УРАНА-235 В ОБЛАСТИ ЭНЕРГИЙ 2—50 эв

E, эв	α	$\sigma_0\Gamma_\gamma$	$\sigma_0\Gamma_\gamma$	$\sigma_0(\Gamma_\gamma+\Gamma_f)$	$\sigma_0\Gamma$	$2g\Gamma_n$	$2g\Gamma_n^0$	Γ	Γ_f	Γ_γ
		барн. эв				мэв				
0,282*±0,003	0,39±0,05	9,3 ±0,9	3,6 ±0,7	-	12,9± 1,3	0,0027±0,0003	0,0052±0,0005	114± 8	82± 8	32 ± 3
1,138*±0,010	0,40±0,05	12,1 ±1,2	4,9 ±0,9	-	17,0± 1,7	0,0149±0,0015	0,014 ±0,001	148±12	106±11	42 ± 4
2,026 ±0,004	2,8 ±0,3	1,47±0,05	4,1 ±0,6	5,6±0,6	-	0,0087±0,0009	0,0061±0,0006	54± 7	14± 2	40
2,84 ±0,02	0,3 ±0,1	1,15±0,25	0,35±0,14	1,5±0,3	-	0,0033±0,0007	0,0020±0,0004	173±53	133±40	40
3,136 ±0,006	0,33±0,08	7,9 ±0,6	2,6 ±0,4	10,5±0,8	11,6± 2,5	0,027 ±0,003	0,015 ±0,002	123±15	92±12	31 ± 6
3,584 ±0,006	0,62±0,09	10,3 ±0,5	6,4 ±0,7	16,7±0,9	17,2± 2,8	0,047 ±0,004	0,025 ±0,002	81± 7	50± 5	31 ± 4
4,81 ±0,01	6,5 ±0,9	2,6 ±0,2	16,8 ±0,9	19,4±0,9	16,2± 2,5	0,066 ±0,005	0,030 ±0,002	34±20	4,5± 3	29,5±19
5,45	1,9 ±0,4	2,1 ±0,3	4,0 ±1,3	6,1±1,4	4,8± 0,9	0,023 ±0,003	0,0099±0,0013	70±20	24± 7	46 ±11
5,82	0,64±0,30	1,6 ±0,5	1,0 ±0,7	2,6±0,9	-	0,012 ±0,004	0,005 ±0,002	103±49	63±30	40
6,20 ±0,01	0,55±0,15	4 ±1	2,2 ±0,8	6,2±1,3	6,7± 2,0	0,031 ±0,006	0,013 ±0,002	106±31	68±23	38 ±17
6,40 ±0,01	4,6 ±0,6	11,5 ±0,4	53 ±5	65 ±6	55 ± 4	0,30 ±0,02	0,118 ±0,008	63±15	11± 3	52 ±13
7,095 ±0,015	1,4 ±0,2	9,1 ±0,4	13 ±1	22 ±1	20 ± 2	0,115 ±0,006	0,043 ±0,002	52± 9	21± 4	31 ± 5
8,77 ±0,02	0,55±0,07	106 ±4	58 ±5	164 ±6	178 ±14	1,15 ±0,05	0,39 ±0,02	113±17	73±12	40 ± 7
9,30 ±0,03	0,50±0,09	13,1 ±0,5	6,8 ±0,9	20 ±1	21 ± 4	0,147 ±0,014	0,048 ±0,005	109±43	72±30	37 ±15
9,73 ±0,06	0,46±0,27	4,3 ±1,0	2 ±1	6,3±1,4	-	0,047 ±0,015	0,015 ±0,005	127±74	87±51	40
10,20 ±0,03	0,87±0,13	4,6 ±0,6	4,0 ±0,8	8,6±1,0	8,1± 1,2	0,066 ±0,006	0,021 ±0,002	88±23	47±13	41 ±14
10,65 ±0,06	~0,5	~2	~1	~3	-	~0,025	~0,007	120	80	40
11,05 ±0,03	~2,0	~1	~2	~3	-	~0,026	~0,008	60	20	40
11,66 ±0,04	6,20±0,06	10,3 ±0,3	63 ±5	73 ±5	66 ± 5	0,62 ±0,03	0,182 ±0,009	68±13	9± 2	59 ±11
12,39 ±0,04	1,8 ±0,2	47 ±2	85 ±5	132 ±5	137 ±10	1,29 ±0,05	0,367 ±0,014	65± 9	23± 4	42 ± 6

Таблица 1 (продолжение)

E, эв	α	$\sigma_0\Gamma_\gamma$	$\sigma_0\Gamma_\gamma$	$\sigma_0(\Gamma_\gamma+\Gamma_f)$	$\sigma_0\Gamma$	$2g\Gamma_n$	$2g\Gamma_n^0$	Γ	Γ_f	Γ_γ
		барн. эв				мэв				
12,82 ±0,04	0,63 ±0,16	3,1 ±0,4	1,9 ±0,6	5,0 ±0,8	4,3 ± 1,0	0,046 ±0,006	0,013 ±0,002	100 ±40	61 ±24	39 ±18
13,28 ±0,05	0,87 ±0,22	3,0 ±0,5	2,6 ±0,8	5,6 ±0,9	5,8 ± 1,4	0,057 ±0,009	0,016 ±0,002	90 ±30	51 ±16	45 ±17
13,67 ±0,10	0,42 ±0,15	3,7 ±1,5	1,5 ±0,8	5,2 ±2,1	-	0,055 ±0,023	0,015 ±0,006	135 ±48	95 ±34	40
13,98 ±0,05	0,23 ±0,11	30 ±7	7 ±3	37 ±8	-	0,40 ±0,09	0,11 ±0,03	214 ±102	174 ±83	40
14,50 ±0,06	1,2 ±0,2	7,3 ±1,9	8,7 ±2,7	16, ±3	-	0,18 ±0,04	0,047 ±0,009	73 ±12	33 ± 5	40
15,42 ±0,05	1,1 ±0,1	10,4 ±0,4	12 ±1	22 ±1	19 ± 2	0,24 ±0,01	0,061 ±0,003	93 ±27	44 ±13	49 ±14
16,08 ±0,05	2,1 ±0,2	9,6 ±0,3	20 ±2	30 ±2	26 ± 3	0,35 ±0,02	0,087 ±0,006	41 ±10	10 ± 3	31 ± 7
16,66 ±0,06	0,7 ±0,1	13,7 ±0,6	9 ±1	23 ±1	23 ± 2	0,30 ±0,01	0,074 ±0,003	74 ±19	44 ±12	30 ± 8
16,90 ±0,10	~3	~1	~3	~4	-	~0,05	~0,013	53	13	40
18,05 ±0,06	0,5 ±0,1	17,3 ±0,7	9 ±2	26 ±2	26 ± 3	0,36 ±0,03	0,085 ±0,006	108 ±26	72 ±18	36 ±10
18,6 ±0,1	~0,6	~3	~2	~5	-	~0,07	~0,02	107	67	40
19,30 ±0,05	0,8 ±0,1	112 ±4	90 ±10	202 ±11	229 ±14	3,2 ±0,13	0,73 ±0,03	108 ±10	60 ± 7	48 ± 6
20,10 ±0,08	0,7 ±0,3	3,5 ±1,3	2,5 ±1,4	6 ±1,9	-	0,09 ±0,03	0,020 ±0,006	97 ±41	57 ±24	40
20,62 ±0,06	1,8 ±0,3	5,8 ±0,8	10,4 ±2,2	16 ±2,3	-	0,25 ±0,04	0,055 ±0,008	62 ±10	22 ± 4	40
21,13 ±0,05	1,6 ±0,3	33 ±1	53 ±10	86 ±10	65 ±11	1,22 ±0,12	0,26 ±0,03	60 ±15	23 ± 6	37 ±11
21,8 ±0,1	~0,3	-	-	~1	-	~0,02	~0,0051	170	130	40
22,4 ±0,1	~0,3	-	-	~1	-	~0,02	~0,0055	170	130	40
22,99 ±0,06	1,2 ±0,2	13,0 ±0,3	16 ±3	29 ±3	23 ± 3	0,46 ±0,04	0,096 ±0,008	77 ±17	35 ± 7	42 ±11
23,43 ±0,15	5,8 ±1,4	4,5 ±0,9	26 ±8	31,0 ±8	-	0,55 ±0,14	0,11 ±0,03	47 ±13	7 ± 2	40
23,68 ±0,07	0,63 ±0,11	30 ±7	19 ±5	49 ±9	-	0,89 ±0,16	0,18 ±0,03	140 ±30	86 ±31	54 ±15
24,25 ±0,07	1,33 ±0,45	7,5 ±3,0	10 ±5	17,5 ±5,8	-	0,33 ±0,11	0,067 ±0,022	70 ±23	30 ±10	40
24,41 ±0,15	1,0 ±0,3	3,9 ±1,5	3,9 ±1,9	7,8 ±2,4	-	0,14 ±0,04	0,028 ±0,009	80 ±24	40 ±12	40

Таблица 1 (продолжение)

E, эв	α	$\sigma_0\Gamma_\gamma$	$\sigma_0\Gamma_\gamma$	$\sigma_0(\Gamma_\gamma+\Gamma_f)$	$\sigma_0\Gamma$	$2g\Gamma_n$	$2g\Gamma_n^0$	Γ	Γ_f	Γ
		барн. эв				мэв				
25,16 ±0,16	0,55 ±0,15	7,4 ±2,5	4,1 ±1,8	11,5 ±3,1	-	0,22 ±0,06	0,044 ±0,012	113 ±31	73 ±20	40
25,56 ±0,10	1,8 ±0,5	11 ±4	20 ±9	31 ±10	-	0,61 ±0,19	0,12 ±0,04	62 ±17	22 ± 6	40
25,84 ±0,15	0,8 ±0,3	3,0 ±1,5	2,4 ±1,5	5,4 ±2,1	-	0,11 ±0,04	0,022 ±0,009	90 ±33	50 ±19	40
26,55 ±0,07	0,4 ±0,1	15 ±3	6,2 ±2,0	21,2 ±3,6	-	0,43 ±0,07	0,08 ±0,01	138 ±34	98 ±24	40
27,16 ±0,07	1,2 ±0,3	3,9 ±1,6	4,6 ±2,1	8,5 ±2,6	-	0,18 ±0,06	0,035 ±0,011	74 ±18	34 ± 8	40
27,86 ±0,07	0,45 ±0,10	18 ±2	8 ±2	26 ±3	-	0,56 ±0,06	0,11 ±0,01	131 ±29	91 ±20	40
28,45 ±0,09	0,7 ±0,2	4,6 ±1,0	3,2 ±1,2	7,8 ±1,5	-	0,17 ±0,03	0,032 ±0,006	97 ±27	57 ±16	40
28,85 ±0,09	1,4 ±0,5	2,0 ±0,7	2,7 ±1,3	4,7 ±1,5	-	0,10 ±0,03	0,019 ±0,006	69 ±25	29 ±10	40
29,69 ±0,09	1,8 ±0,3	3,0 ±0,6	5,3 ±1,4	8,3 ±1,5	-	0,19 ±0,03	0,035 ±0,006	62 ±10	22 ± 4	40
30,55 ±0,20	1,3 ±0,4	4,1 ±0,9	5,4 ±2,0	9,5 ±2,2	-	0,22 ±0,05	0,040 ±0,009	70 ±21	30 ± 9	40
30,86 ±0,10	1,4 ±0,4	6,8 ±1,5	9,6 ±3,4	16,4 ±3,7	-	0,40 ±0,09	0,072 ±0,016	68 ±19	28 ± 8	40
32,10 ±0,09	1,10 ±0,15	38 ±5	42 ±6	80 ±8	-	1,97 ±0,20	0,35 ±0,04	96 ±10	46 ± 6	50 ± 7
33,58 ±0,09	1,6 ±0,3	26 ±5	41 ±6	67 ±8	-	1,7 ±0,2	0,29 ±0,03	65 ±12	25 ± 5	40
34,45 ±0,14	1,5 ±0,3	32 ±5	48 ±12	80 ±13	-	2,12 ±0,34	0,36 ±0,06	69 ±14	29 ± 6	40
34,90 ±0,20	1,6 ±0,5	13 ±4	21 ±9	34 ±10	-	0,9 ±0,3	0,15 ±0,05	65 ±20	25 ± 8	40
35,27 ±0,10	0,54 ±0,10	107 ±20	58 ±17	165 ±26	-	4,5 ±0,7	0,76 ±0,12	114 ±21	74 ±14	40
38,40 ±0,11	0,7 ±0,2	13 ±4	9 ±4	22 ±6	-	0,66 ±0,18	0,11 ±0,03	95 ±27	55 ±16	40
39,47 ±0,11	1,2 ±0,2	39 ±6	47 ±11	86 ±13	-	2,6 ±0,4	0,42 ±0,06	73 ±13	33 ± 6	40
39,9 ±0,2	0,6 ±0,2	8 ±3	5 ±2,5	13 ±4	-	0,40 ±0,12	0,063 ±0,019	105 ±31	65 ±20	40
40,50 ±0,15	0,40 ±0,15	12 ±4	5 ±3	17 ±5	-	0,53 ±0,16	0,083 ±0,024	140 ±52	100 ±37	40
41,3 ±0,2	1,32 ±0,35	7 ±3	9 ±4	16 ±5	-	0,51 ±0,16	0,079 ±0,025	70 ±19	30 ± 8	40
41,5 ±0,2	0,66 ±0,26	4 ±1,5	3 ±1,7	7 ±2,3	-	0,22 ±0,07	0,034 ±0,011	100 ±39	60 ±23	40
41,8 ±0,2	1,3 ±0,3	17 ±5	22 ±8	39 ±10	-	1,3 ±0,3	0,20 ±0,05	71 ±16	31 ± 7	40

Таблица 1 (продолжение)

E, эв	α	$\sigma_0\Gamma$	$\sigma_0\Gamma_\gamma$	$\sigma_0(\Gamma_\gamma+\Gamma_f)$	$\sigma_0\Gamma$	$2g\Gamma_n$	$2g\Gamma_n^0$	Γ	Γ_f	Γ_γ
		барн. эв				мэв				
42,2 ±0,3	0,75±0,30	4 ±1,7	3 ±1,7	7 ±2,4	-	0,23 ±0,08	0,035 ±0,012	93±37	53±21	40
42,7 ±0,3	1,4 ±0,4	2 ±0,8	2,8 ±1,4	4,8±1,6	-	0,15 ±0,05	0,023 ±0,008	69±20	29± 8	40
43,4 ±0,2	1,5 ±0,4	6 ±2	6,6 ±2,5	12,6±3,3	-	0,42 ±0,11	0,064 ±0,017	66±20	26±10	40
43,9 ±0,2	1,2 ±0,3	9 ±3	7 ±3	16 ±4	-	0,54 ±0,13	0,081 ±0,020	73±18	33± 8	40
44,6 ±0,2	0,54±0,25	12 ±5	4 ±2	16 ±6	-	0,55 ±0,21	0,082 ±0,031	114±52	74±34	40
45,0 ±0,3	0,40±0,2	6 ±2,5	2,2 ±1,5	8,2±3,0	-	0,30 ±0,11	0,045 ±0,016	140±70	100±50	40
45,8 ±0,2	1,7 ±0,5	5 ±2	8,5 ±4,2	13,5±4,5	-	0,48 ±0,16	0,071 ±0,023	63±18	23± 7	40
47,06 ±0,14	1,2 ±0,2	23 ±5	27 ±7	50 ±8	-	1,8 ±0,3	0,26 ±0,04	72±12	32± 5	40
48,0 ±0,15	1,6 ±0,4	10 ±3	16 ±6	26 ±7	-	1,0 ±0,3	0,14 ±0,04	65±16	25± 6	40
48,3 ±0,2	0,8 ±0,3	12 ±5	10 ±6	22 ±8	-	0,8 ±0,3	0,12 ±0,04	90±34	50±19	40
48,6 ±0,2	0,5 ±0,2	6,0 ±2,5	3 ±1,7	9 ±3	-	0,3 ±0,1	0,05 ±0,02	120±48	80±32	40
49,3 ±0,3	1,8 ±0,4	7 ±2	13 ±5	20 ±6	-	0,8 ±0,2	0,12 ±0,03	62±14	22± 5	40
50,2 ±0,3	1,6 ±0,4	4 ±1,5	6 ±3	10 ±3	-	0,4 ±0,1	0,06 ±0,015	65±16	25± 6	40

* Звездочкой отмечены уровни, параметры которых взяты из работы [2].

Таблица 2

ЗНАЧЕНИЯ УСРЕДНЕННЫХ ПО ВЫБРАННЫМ ЭНЕРГЕТИЧЕСКИМ ИНТЕРВАЛАМ СЕЧЕНИЙ ДЕЛЕНИЯ И РАДИАЦИОННОГО ЗАХВАТА, А ТАКЖЕ $\alpha = \langle \sigma_{n\gamma}(E) \rangle / \langle \sigma_f(E) \rangle$ В ОБЛАСТИ ЭНЕРГИЙ ОТ 0,1 ДО 30 кэв

E, кэв	σ_f, барн	$\sigma_{n\gamma}$, барн	$(\sigma_{n\gamma} + \sigma_f)$, барн	α
0,1 ÷ 0,2	20,60 ±0,10	19,1 ±0,5	39,70 ±0,50	0,91 ±0,02
0,2 ÷ 0,3	19,80 ±0,10	12,1 ±0,4	31,90 ±0,40	0,61 ±0,02
0,3 ÷ 0,4	12,7 ±0,14	6,1 ±0,3	18,80 ±0,33	0,48 ±0,02
0,4 ÷ 0,5	13,8 ±0,14	5,1 ±0,3	18,90 ±0,33	0,37 ±0,02
0,5 ÷ 0,6	14,8 ±0,15	3,6 ±0,2	18,40 ±0,25	0,24 ±0,01
0,6 ÷ 0,7	11,3 ±0,14	4,86 ±0,3	16,16 ±0,33	0,43 ±0,03
0,7 ÷ 0,8	10,7 ±0,14	4,2 ±0,2	14,90 ±0,25	0,39 ±0,02
0,8 ÷ 0,9	8,45 ±0,12	4,1 ±0,3	12,55 ±0,32	0,48 ±0,03
0,9 ÷ 1,0	8,00 ±0,12	3,28 ±0,3	11,28 ±0,32	0,41 ±0,04
1,0 ÷ 1,1	8,37 ±0,14	1,42 ±0,2	9,79 ±0,25	0,17 ±0,02
1,1 ÷ 1,2	9,68 ±0,18	2,9 ±0,3	12,58 ±0,34	0,30 ±0,03
1,2 ÷ 1,3	7,99 ±0,16	1,52 ±0,2	9,51 ±0,25	0,19 ±0,02
1,3 ÷ 1,4	8,43 ±0,16	2,45 ±0,3	10,88 ±0,34	0,29 ±0,03
1,4 ÷ 1,5	7,13 ±0,15	2,92 ±0,3	10,05 ±0,34	0,41 ±0,04
1,5 ÷ 1,6	6,59 ±0,14	3,62 ±0,4	10,21 ±0,42	0,55 ±0,05
1,6 ÷ 1,7	7,09 ±0,15	3,26 ±0,3	10,35 ±0,34	0,46 ±0,05
1,7 ÷ 1,8	7,07 ±0,15	3,25 ±0,3	10,32 ±0,34	0,46 ±0,05
1,8 ÷ 1,9	6,41 ±0,13	3,40 ±0,3	9,81 ±0,33	0,53 ±0,05
1,9 ÷ 2,0	6,70 ±0,14	3,69 ±0,4	10,39 ±0,42	0,55 ±0,05
2,0 ÷ 3,0	5,56 ±0,10	2,2 ±0,2	7,76 ±0,22	0,40 ±0,03
3,0 ÷ 4,0	4,88 ±0,10	2,9 ±0,2	7,78 ±0,22	0,59 ±0,04
4,0 ÷ 5,0	4,47 ±0,08	1,8 ±0,2	6,27 ±0,22	0,40 ±0,03
5,0 ÷ 6,0	3,97 ±0,08	1,2 ±0,1	5,17 ±0,13	0,31 ±0,03
6,0 ÷ 7,0	3,49 ±0,07	1,2 ±0,1	4,69 ±0,12	0,35 ±0,03
7,0 ÷ 8,0	3,40 ±0,09	0,9 ±0,1	4,30 ±0,13	0,26 ±0,03
8,0 ÷ 9,0	3,23 ±0,10	1,03 ±0,1	4,26 ±0,15	0,32 ±0,03
9,0 ÷10,0	3,37 ±0,11	1,1 ±0,1	4,47 ±0,15	0,32 ±0,03
10,0 ÷12,5	3,23 ±0,11	1,20 ±0,1	4,43 ±0,15	0,42 ±0,04
12,5 ÷15,0	3,36 ±0,11	0,74 ±0,1	4,10 ±0,15	0,22 ±0,02
15,0 ÷20,0	3,23 ±0,10	1,2 ±0,11	4,43 ±0,14	0,37 ±0,04
20,0 ÷25,0	3,29 ±0,11	1,18 ±0,1	4,47 ±0,15	0,36 ±0,04
25,0 ÷30,0	2,94 ±0,12	1,09 ±0,1	4,03 ±0,16	0,37 ±0,04

свободы $\nu = 1$. Однако видно, что χ^2 — распределение для 78 + 20% уровней (кривая б) лучше согласуется с экспериментальным. Это говорит о том, что в области до 50 эв возможен пропуск 10 — 15 уровней с $\Gamma_n \ll \bar{\Gamma}_n$.

Пропуск некоторого числа слабых уровней существенно не влияет на значение силовой функции, получаемой из гистограммы $\sum_0 2g\Gamma_n^0(E)$. Опре-

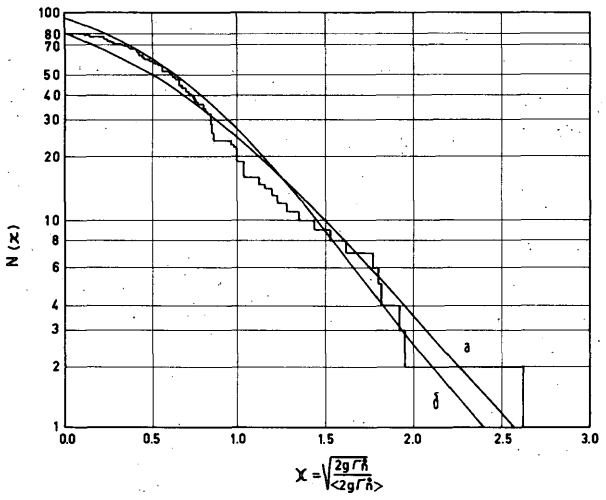

Рис.4

Распределение приведенных нейтронных ширин для 78 уровней U-235.

а – кривая Портера-Томаса для 78 уровней $\nu = 1$,
б – кривая Портера-Томаса для 78 + 20% уровней $\nu = 1$.

деленное таким образом значение силовой функции $S_0 = (0{,}92 \pm 0{,}17) \cdot 10^{-4}$. (Ошибка определялась как $S_0(2{,}5/m)^{\frac{1}{2}}$, где m – число рассматриваемых уровней [14].

Если включить в рассмотрение приведенную нейтронную ширину отрицательного уровня, взятую из работы [3], то это несколько изменит значение силовой функции, которое будет равным $S_0 = (1{,}07 \pm 0{,}19) \cdot 10^{-4}$.

Полученные значения силовой функции хорошо согласуются с рассчитанными в работе [5] для нейтронов с $\ell = 0$.

На рис.5 представлены экспериментально полученные распределения делительных ширин для 78 уровней (до $E_n = 50$ эв) и первых 32 уровней (до $E_n = 20$ эв). Средние делительные ширины равняются 52 и 58 мэв, соответственно. Хорошо видно, что оба распределения похожи и удовлетворительно описываются χ^2 – распределением с $\nu = 4$.

Это позволяет сделать заключение о том, что число степеней свободы $\nu = 4$ является реальным и не связано с появлением при ухудшении разрешения, систематически экспериментальных ошибок, искажающих распределение. Как уже отмечалось выше, возможный пропуск уровней с малыми Γ_n и большими Γ_f может привести к увеличению в основном числа уровней с $\Gamma_f > \overline{\Gamma_f}$ и мало изменит приведенное распределение.

Для урана-235 не были до сих пор проведены прямые измерения спинов уровней составного ядра. Поэтому пока были предприняты только попытки косвенного разделения на две системы уровней с $J = 3^-$ и $J = 4^-$ (спин ядра-мишени урана-235 $I = 7/2^-$).

В частности, в работе [6] отмечается наличие значительных флюктуаций полных радиационных ширин Γ_γ от уровня к уровню, которые связываются со значениями спинов этих уровней. В настоящей работе не обнаружены сколько-нибудь значительные флюктуации Γ_γ, выходящие за пределы ошибок измерений.

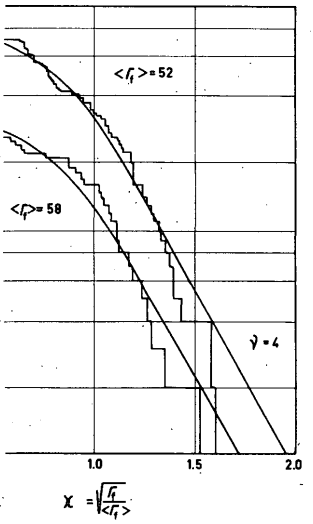

Рис.5

Распределение делительных ширин для энергетических участков 0 ÷ 20 эв (32 уровня) и 0 ÷ 50 эв (78 уровней). Кривые Портера-Томаса с $\nu = 4$.

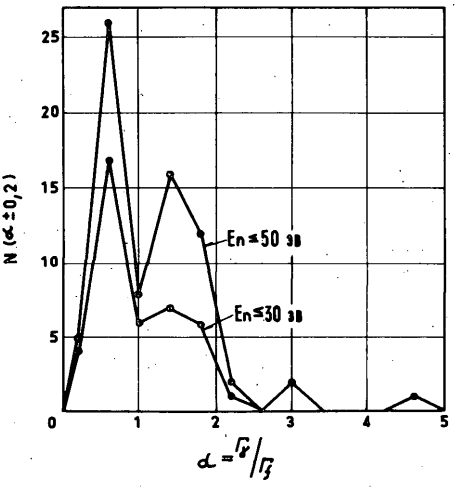

Рис.6

Распределение величин α для указанных на рисунке энергетических участков.

На рис.6 представлено распределение величин $\alpha = \Gamma_\gamma / \Gamma_f$ для энергетических интервалов до 30 и 50 эв. Так как Γ_γ – величина мало флюктуирующая от уровня к уровню, то практически изменения в α определяются флюктуациями в Γ_f. Характер распределения не изменяется в указанных энергетических интервалах, и это дает возможность считать, что два пика не являются следствием экспериментальных ошибок при определении α, связанных с изменением энергетического разрешения. Это распределение можно рассматривать как наложение двух перекрывающихся распределений,

Таблица 3

ДВЕ ГРУППЫ УРОВНЕЙ С ХАРАКТЕРИСТИКАМИ ОТНОШЕНИЯ СИММЕТРИЧНОГО ДЕЛЕНИЯ К АСИММЕТРИЧНОМУ

Энергия уровня, эв		Относительный выход осколков деления симметричной массы	
группа I	группа II	Больше	Меньше
0,28		+	
1,14		+	
	2,03	+	
2,84		+	
3,14		+	
3,58		+	
	4,81	+	
	5,45	+	
5,82		+	
6,20		+	
	6,40	+	
	7,10		+
8,77			(+)
9,30		+	
(10,2)*			+
	11,66	+	
	12,39		+
13,98		+	
	14,5		+
	(15,4)		+
	16,1		+
16,7			+
18,1			+
19,3			+
20,1		+	
	20,6		+
	21,1		+
	22,99		+
	23,43		+
	24,25		+
25,16		+	
	25,56		+
26,55		+	
	27,16		+
27,86			(+)
28,45		+	

Таблица 3 (продолжение)

Энергия уровня, эв		Относительный выход осколков деления симметричной массы	
группа I	группа II	Больше	Меньше
	29,69	+	
	(30,86)	+	
	(32,1)		(+)
	33,58		+
	34,45		+
35,27		+	
38,4			+
39,9		+	
	41,8		+
	43,9		+
44,6		+	
	(47,1)	+	
48,6			+

* В скобках отмечены уровни, которые нельзя однозначно отнести к той или иной группе. Это же относится и к характеристике выхода осколков симметричной массы.

связанных, возможно, с двумя значениями спина составного ядра. Для грубой оценки средних параметров этих групп уровней можно рассмотреть уровни с $\alpha>1$ и $\alpha<1$. Число уровней в каждой группе примерно одинаково, и это удовлетворительно согласуется с оценкой числа уровней одного спина $\approx (2J+1)$. Средние значения делительных ширин для группы с $\alpha>1$ 22 и 25 мэв, а для группы с $\alpha<1$ 77 и 79 мэв, в энергетических интервалах до 30 и до 50 эв, соответственно. В работе [17] были проведены расчеты средних делительных ширин для уровней урана-235 с различными спинами (по формуле Бора и Уиллера для делительных ширин с учетом проницаемости барьера деления по Хиллу и Уиллеру) и получены следующие результаты:

$$\overline{\Gamma}_f(J=3^-)\approx 81 \text{ мэв} \quad \text{и} \quad \overline{\Gamma}_f(J=4^-)\approx 32 \text{ мэв}.$$

Полученные в настоящей работе средние делительные ширины для двух групп уровней находятся в удовлетворительном согласии с расчетными, что позволяет условно приписать группе с $\alpha>1$ спин $J=4^-$, а группе с $\alpha<1$ — $J=3^-$.

В табл.3 приведены две группы уровней, и для каждого уровня указана характеристика отношения симметричного деления к асимметричному по результатам работ [18, 19], которое, согласно теории О. Бора [20], связано со спином уровня составного ядра. Видно, что для ряда сильных и хорошо разрешенных уровней наблюдается удовлетворительное согласие в разделении уровней на две группы. Однако окончательное заключение о

правильности такого заключения можно сделать после прямого измерения спинов уровней урана-235.

Авторами вместе с Ю. Фениным были проведены предварительные расчеты на электронной вычислительной машине силовых функций урана-235 для нейтронов $\ell = 0$ и 1, анализируя усредненное сечение реакции $\overline{\sigma}_r = \overline{\sigma}_{n\gamma} + \overline{\sigma}_f$ для области энергий 0,3–30 кэв [21]. Полученное значение $S_0 = (0{,}91 \pm 0{,}03) \cdot 10^{-4}$ хорошо согласуется с величиной, приведенной выше, а $S_1 = (2{,}8 \pm 0{,}4) \cdot 10^{-4}$ близко к величине S_1 для урана-238, полученной Линном [22] из анализа экспериментальных данных по пропусканию нейтронов.

В заключение авторы считают своим приятным долгом поблагодарить профессора Ф.Л. Шапиро и Л.Б. Пикельнера за обсуждения и ценные советы, И.И. Шелонцева и Н.Ю. Ширикову — за помощь при обработке данных на электронной вычислительной машине.

ЛИТЕРАТУРА

[1] HAVENS W.W., MELKONIAN E., Jr., RAINWATER L.I., ROSEN I.L., Phys.Rev., 116, No.6, 1538 (1959).
[2] HUGHES D.J., Second United Nations Inter. Conf. on the Peaceful Uses of Atomic Energy P/2438, Geneva.
[3] SHORE J., SAILOR V., Second United Nations Inter. Conf. on the Peaceful Uses of Atomic Energy, P/648, Geneva.
[4] ИГНАТЬЕВ К.П., КИРПИЧНИКОВ И.В., СУХОРОЧКИН С.И., "Атомная энергия", 16 (1964) 110.
[5] MICHAUDON A., BERGERE R., COIN A., JOLY R., Journal de Physique et Radium, 21 (1960) 429.
[6] RAE E.R., BATCHELOR R., EGELSTAFF P.A., FERGUSON A.T.G., Third United Nations Inter. Conf. on Peaceful Uses of Atomic Energy, P/167, Geneva, 1964.
[7] HOPKINS J.C., DIVEN B.C., Nucl. Science and Engineering, 12 (1962) 169.
[8] БЛОХИН Г.Е., БЛОХИНЦЕВ Д.И. и др. "Атомная энергия", 10, вып.5 (1961) 437.
[9] REINES F., COWAN C.L., HARRISON F.B., Jr., CARTER D.S., Rev. Sci. Instr., 25, No.11, 10 (1954) 1061.
[10] ВАН ШИ-ДИ, РЯБОВ Ю.В., Препринт ОИЯИ, 1685, Дубна, 1964.
[11] ROSEN I.L., DESJARDINS J.S., RAINWATER J., HAVENS W.W., Phys. Rev., 118 (1960) 687.
[12] ЗЕЛИГЕР Д., ИЛИЕСКУ Н., КИМ ХИ САН и др., ЖЭТФ, 45 (1963) 1295.
[13] HUGHES J., Journ Nucl. Energy, 1 (1955) 237.
[14] BILPUCH E.G., SETH K.K., BOWMAN C.D. et all, Annals of Physics, 14 (1961) 387.
[15] CHASE D.M., Proc. Inter. Conf. on Neutron Interactions with Nucleus, Columbia University, 1957.
[16] MICHAUDON A., DERRIEN H., RIBON P., SANCHE M., Доклад на Парижской конференции по ядерной физике, июль 1964.
[17] БАЗАЗЯНЦ Н.О., ГОРДЕЕВ И.В., "Атомная энергия", 13, вып.4 (1962) 321.
[18] COWAN G.A., TURKEVICH A., BROWNE C., Phys. Rev. 122, nN=4 (1961) 1286.
[19] COWAN G.A., BAYHURST B.P., PRESTWOOD P.J., Phys. Rev., 130, N=6 (1963) 2380.
[20] BOHR A., Proceedings of the Intern. Conf., Geneva, 1955.
[21] РЯБОВ Ю.В., ФЕНИН Ю.И., Препринт ОИЯИ, №Р-2068 Дубна, 1965.
[22] LYNN J.E., Proc. Phys. Soc., 82, N=530, 903 (1963).

DISCUSSION

M. S. MOORE: Did you interpret the two-group fission distributions as being due to s- or p-wave fission or to two spin states of s-wave fission?

U. V. RYABOV: They were interpreted as being due to two spin states of s-wave fission.

E. R. RAE: Could Dr. Ryabov please explain how the effect of scattered neutrons was allowed for in these experiments? Since the energy range extended up to 30 keV, it was presumably not practicable to screen out such neutrons, so that they would be recorded when captured in the cadmium in the scintillator tanks as though they represented capture events in the sample.

U. V. RYABOV: In the fission-recording channel, the scattered-neutron background is reduced to random coincidences and can be allowed for quite well by introducing a delay five-to-six times longer than the mean neutron lifetime in the detector. In the channel that registers radiation captures, the neutrons produced by resonance and potential scattering are recorded less effectively than radiative captures in the specimen. The background due to potential-scattering neutrons was determined by means of individual measurements using a lead or carbon scatterer. In order to calculate the contribution of resonance scattering at high energies, the $\sigma_{n\gamma}$ cross-section was calibrated with reference to Diven's data at E = 30 keV. This represented only a small correction.

G. COWAN: What is the number of neutrons per pulse and what is the repetition rate?

U. V. RYABOV: The mean number of neutrons is about 10^{14} n/s and the repetition rate is 1-100 pulses/s. The average power of the installation is approximately 1 kW.

G. COWAN: Has this apparatus been described in the literature?

U. V. RYABOV: There is a detailed description of the installation (Pulsed Fast Reactor of the Joint Institute for Nuclear Research) in Atomnaja Energija 10 (1961) 437, and information on the latest improvements made to the equipment was given at the 3rd UN Int. Conf. PUAE in 1964.

P. RIBON: Have you studied the distribution of the total radiation widths?

U. V. RYABOV: According to our data, the distribution of the total radiation widths is narrow, and is described by a Porter-Thomas distribution with V ~(40-50).

THE EXCITATION FUNCTION AND THE ISOMERIC YIELD RATIO FOR THE 14-ms FISSIONING ISOMER FROM DEUTERON IRRADIATION OF PLUTONIUM*

G. N. FLEROV, A. A. PLEVE AND S. M. POLIKANOV
JOINT INSTITUTE FOR NUCLEAR RESEARCH, DUBNA, USSR,
AND
E. IVANOV, N. MARTALOGU, D. POENARU AND N. VÎLCOV
INSTITUTE FOR ATOMIC PHYSICS, BUCHAREST, ROMANIA

Abstract — Résumé — Аннотация — Resumen

THE EXCITATION FUNCTION AND THE ISOMERIC YIELD RATIO FOR THE 14-ms FISSIONING ISOMER FROM DEUTERON IRRADIATION OF PLUTONIUM. In the past two years several workers have reported the existence of a spontaneous fission phenomena, with an anomalous short lifetime, explained as a fission from an excited state. In the present work some further studies are made on the excitation of the isomeric state by the deuteron bombardment of a plutonium target enriched in the 242-isotope. The cross-section of the excitation, as well as the isomeric yield ratio, was measured at different bombarding energies.

The deuteron beam energy was variated between 7 MeV and 12 MeV by both the cyclotron regime and the aluminium absorbers. The experimental technique used was based on the recoil method. The nuclei, knocked out from the target by the deuterons, are caught on a rotating disk and carried in front of several glass detectors for counting the fission fragments.

The cross-section of the 14-ms isomer, at a deuteron energy of 12 MeV, was determined to be about 4×10^{-30} cm^2. This value is a hundred times greater than that obtained with heavy ions. The excitation function shape verifies the assumption that the isomer is produced via the (d, 2n) process proving that Am^{242} is the spontaneously fissioning nucleus.

For measuring the ground state (d, 2n) cross-section the activation method was used, catching the knocked-out nuclei on an aluminium foil (the reaction Pu^{242} (d, 2n) leads to an alpha transition of 6.1 MeV energy). The (d, 2n) cross-section rises rapidly with the bombarding energy, attaining a value of $\sigma_n \sim 7.5$ mb for 12 MeV.

The small value of the isomeric yield ratio ($\sim 5 \times 10^{-4}$) thus obtained leads one to conclude that the total angular momentum of the excited state responsible for fission is high.

FONCTION D'EXCITATION ET RAPPORT DE RENDEMENT ISOMÉRIQUE DE L'ISOMÈRE DE FISSION DE 14 ms DÛ A L'IRRADIATION DU PLUTONIUM PAR DES DEUTÉRONS. Au cours des deux dernières années, plusieurs chercheurs ont fait état de l'existence de phénomènes de fission spontanée, d'une durée anormalement courte, qui est expliquée comme étant une fission due à un état d'excitation. Au cours des recherches qui font l'objet du mémoire, les auteurs se sont livrés à des études plus approfondies de l'excitation de l'état isomérique dû au bombardement par des deutérons d'une cible de plutonium enrichi en isotope 242. Ils ont mesuré, pour plusieurs énergies de bombardement, la section efficace de l'excitation de l'état isomérique ainsi que le rapport de rendement isomérique.

Les auteurs ont fait varier l'énergie du faisceau de deutérons entre 7 MeV et 12 MeV en utilisant à la fois le régime du cyclotron et des absorbeurs en aluminium. Le procédé expérimental utilisé est fondé sur la méthode du recul. Les noyaux, arrachés à la cible par les deutérons, sont captés par un disque tournant et transportés devant plusieurs détecteurs au verre pour le comptage des fragments de fission.

La section efficace de l'isomère de 14 ms, pour une énergie des deutérons de 12 MeV, a été évaluée à environ $4 \cdot 10^{-30}$ cm^2. Cette valeur est cent fois supérieure à celle qui a été obtenue avec des ions lourds. La forme de la fonction d'excitation vérifie l'hypothèse que l'isomère résulte du processus (d, 2n), ce qui prouve que ^{242}Am est le noyau qui subit la fission spontanée.

Pour mesurer la section efficace du processus état fondamental (d, 2n), les auteurs ont utilisé la méthode d'activation, les noyaux arrachés étant captés sur une feuille d'aluminium (la réaction ^{242}Pu (d, 2n) conduit

* Paper read by title only at the Symposium

à une transition alpha d'une énergie de 6,1 MeV). La section efficace du processus (d, 2n) augmente rapidement avec l'énergie du bombardement, et elle atteint une valeur de $\sigma_n \sim 7,5$ mb pour 12 MeV.

La valeur faible du rapport de rendement isomérique ($\sim 5 \cdot 10^{-4}$) ainsi obtenue donne à penser que le moment cinétique total de l'état d'excitation auquel la fission est due a une valeur élevée.

ФУНКЦИЯ ВОЗБУЖДЕНИЯ 14-МИЛЛИСЕКУНДНОГО ИЗОМЕРА, ОБРАЗУЮЩЕГОСЯ ПРИ БОМБАРДИРОВКЕ ПЛУТОНИЯ ДЕЙТРОНАМИ. В последние два года в некоторых работах сообщалось о наличии явлений спонтанного деления с очень коротким периодом полураспада, что объясняется процессом деления в состоянии возбуждения. В данной работе проводятся дальнейшие исследования относительно возбуждения изомерного состояния путем бомбардировки дейтронами плутониевой мишени, обогащенной изотопом плутоний-242. Таким образом, измерялись при различной энергии бомбардирующих частиц поперечное сечение возбуждения изомерного состояния, а также величина изомерного выхода.

Энергия пучка дейтронов изменялась в диапазоне 7—12 Мэв как в результате изменения режима работы циклотрона, так и с помощью алюминиевых поглотителей. Применяемый экспериментальный метод основан на методе отдачи. Ядра, выбиваемые из мишени дейтронами, захватываются вращающимся диском и переносятся перед несколькими стеклянными детекторами для проведения счета осколков деления.

Было определено, что поперечное сечение 14-миллисекундного изомера при энергии дейтронов 12 Мэв составляет приблизительно $4 \cdot 10^{-30}$ см^2. Эта величина в сто раз больше величины, полученной при использовании тяжелых ионов. Форма функции возбуждения подтверждает предположение, что изомер образуется в процессе реакции (d, 2n), при условии, что америций-242 представляет собой спонтанно делящееся ядро.

Для измерения поперечного сечения при реакции (d, 2n) в основном состоянии применялся метод активации с захватом выбитых ядер алюминиевой фольгой (реакция плутоний-242 (d, 2n) приводит к альфа-переходу с энергией 6,1 Мэв). Поперечное сечение реакции (d, 2n) быстро увеличивается с увеличением энергии бомбардирующих частиц, достигая величины $\delta_n \sim 7,5$ миллибарн при энергии 12 Мэв.

На основании факта, что до сих пор были получены небольшие значения величины изомерного выхода ($\sim 5 \cdot 10^{-4}$) делается вывод, что величина общего углового момента количества движения возбужденного состояния, определяющего процесс деления, является значительной.

FUNCION DE EXCITACION DEL ISOMERO DE 14 ms RESULTANTE DEL BOMBARDEO DEL PLUTONIO CON DEUTERONES. En los dos últimos años varios autores han dado cuenta de la existencia de un fenómeno de fisión espontánea, de duración anormalmente breve, que se explica como fisión consecutiva a un estado excitado. La memoria expone algunos nuevos estudios sobre la excitación del estado isomérico por bombardeo con deuterones de un blanco de plutonio enriquecido en el isótopo 242. En particular se ha medido, para diferéntes energías de bombardeo, la sección eficaz de excitación del estado isomérico y la razón de rendimiento isomérico.

La energía del haz de deuterones se modificó entre 7 MeV y 12 MeV alterando el régimen de funcionamiento del ciclotrón y empleando absorbentes de aluminio. La técnica experimental aplicada se basa en el método de retroceso. Los núcleos expulsados del blanco por los deuterones se captan en un disco rotativo y se hacen pasar delante de detectores de vidrio para contar los fragmentos de fisión.

La sección eficaz del isómero de 14 ms, determinada para una energía de los deuterones de 12 MeV, es del orden de $4 \cdot 10^{-30}$ cm^2. Este valor es cien veces mayor que el obtenido con iones pesados. La forma de la función de excitación confirma la hipótesis de que el isómero es producido en virtud de la reacción (d, 2n), lo cual demuestra que el núcleo que experimenta la fisión espontánea es el de ^{242}Am.

Para medir la sección eficaz correspondiente a la reacción (d, 2n) en el estado fundamental se ha aplicado el método de activación captando los núcleos expulsados en una lámina de aluminio (la reacción ^{242}Pu (d, 2n) origina una transición alfa de 6,1 MeV de energía). La sección eficaz (d, 2n) aumenta rápidamente con la energía de bombardeo y alcanza un valor de $\sigma_n \sim 7,5$ mb para 12 MeV.

El reducido valor de la razón de rendimiento isomérico ($\sim 5 \cdot 10^{-4}$) así obtenido permite llegar a la conclusión de que el momento angular total del estado excitado determinante de la fisión es elevado.

INTRODUCTION

Investigation of the spontaneous fission of nuclei in their excited states started in 1962, when an "anomalous fission" process, with a 13.5 ± 1.2-ms half-life, resulting from heavy ion bombardment of U^{238} and U^{235}, was observed [1]. Since then the 13-ms fission fragments have been produced in different transuranic targets by heavy ions, alpha-particles, deuterons [2] and fast neutrons [3]. They were assigned to a 13-ms isomeric state of Am^{242} decaying, at least partially, by fission. Recently, new fissioning isomeric states were discovered. Thus the 0.85-ms and 3.5-s isomeric states were excited by heavy ion bombardments [4]. The search for a spontaneous fission branch in an isomeric state of Cm^{244} excited by thermal-neutron activation led to an upper limit of 8×10^{-12} for the branching ratio of spontaneous fission to gamma-ray transition [5].

In the present work further studies are made concerning the excitation of the spontaneously fissioning isomeric state by deuteron bombardment of plutonium. To obtain more information about the isomeric state (spin and excitation energy), we measured its absolute cross-section, as well as the isomeric yield ratio, at different incident energies[1].

EXPERIMENTAL METHOD

The experimental technique was based on the recoil method [1]. The deuteron beam, accelerated in the IAP-U120 cyclotron, struck a 16-$\mu g/cm^2$ Pu^{242} target (T) (Fig. 1). The recoiling americium nuclei were extracted from the target and stuck to a rotating disk (D), which displayed them in front of a set of glass detectors (S) mounted on a circular arc. In this way the fission fragments were registered on different glass detectors, according to the lifetime of the fissioning nuclei. The rotating disk had a speed of

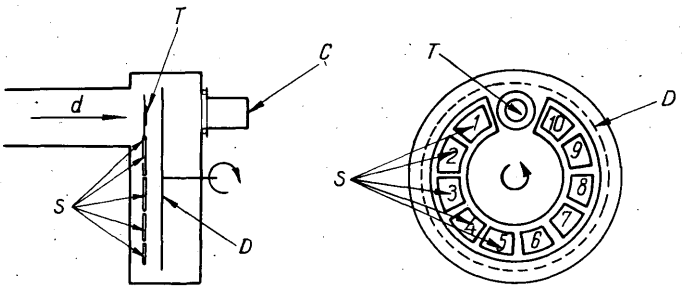

Fig. 1

Experimental arrangement

d deuteron beam
T plutonium target
D rotating disk
S glass detectors
C Faraday cup

[1] While this experiment was in progress we were informed about a similar study under way at the University of California, led by Professor A. Ghiorso.

670 rev/min, and the glass detectors recorded the fragments emitted by the nuclei, decaying between 7 and 83 ms.

After passing through the target and the rotating disk, the deteron beam was collected in a Faraday cup (C) and its charge measured by a current integrator. The primary energy (7-12 MeV) was variated by both aluminium absorbers (fine steps) and by changing the cyclotron regime (gross steps).

The cross-section of the Pu^{242}(d, 2n) Am^{242} reaction, leading to the ground state of Am^{242}, was measured by the activation method. The Am^{242} recoil nuclei were collected on a 5-μm aluminium foil and the alpha-activity of Cm^{242} was measured without any chemical treatment. As is known [6], the Am^{242} nuclei have a 16-h half-life and decay 84% by beta activity, leading to Cm^{242}. The 162.5-d alpha-activity of Cm^{242} was measured from the intensity of the 6.1-MeV peak (6.11-MeV + 6.06-MeV alpha lines), which contains 99.3% of the whole activity of Cm^{242}. The alpha-particles were detected by a silicon surface-barrier detector, 20 mm in diameter. The total resolution of the alpha spectrometer was 1.3% at E_α = 5.47 MeV. A typical alpha spectrum obtained at 10.5-MeV deuteron energy is given in Fig. 2. The 6.1-MeV alpha-peak is the most intensive and its growth curve corresponds to the 16-h half-life of the Am^{242} beta activity.

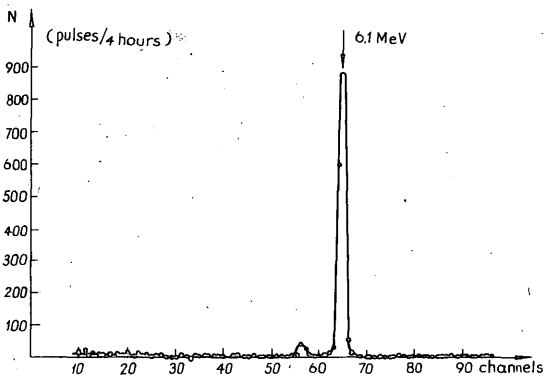

Fig. 2

Typical alpha spectrum used for measuring (d, 2n) cross-sections

In calculating the cross-section, one has to take into account the dependence of the "effective" thickness of the target on the primary energy [7]. For deuteron energies between 7 MeV and 12 MeV the thickness of this effective layer ranged from 6 to 10 $\mu g/cm^2$.

RESULTS

The decay curve of the fissioning isomeric state of Am^{242} is shown in Fig. 3. The measured half-life, $T_{1/2}$ = 14.0 ± 0.4 ms, agrees fairly well with the earlier experimental values [1-3]. In calculating the cross-section of the isomeric state, a value of 0.42 was used for the efficiency of the glass detectors [8].

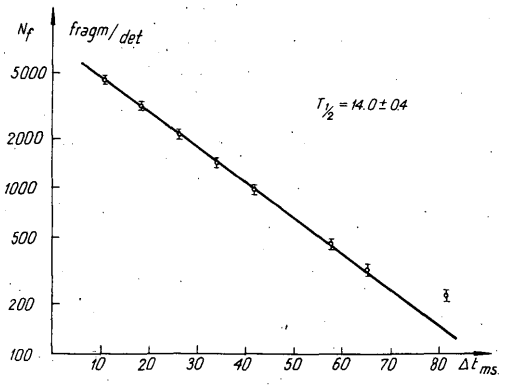

Fig. 3

Decay curve of the fissioning isomeric state of Am^{242}

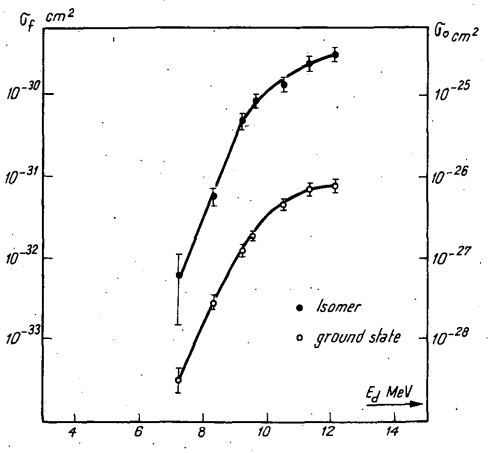

Fig. 4

Excitation functions of the isomeric and ground states of Am^{242}

The experimental results concerning the cross-section of both the 14-ms isomeric state as well as the Pu^{242}(d, 2n) reaction leading to the ground state of Am^{242}, for different bombarding energies, are given in Table I and in Fig. 4. The isomeric yield ratio resulted from the two excitation functions is plotted in Fig. 5.

DISCUSSION

The experimental measurements were affected by the following errors:

(a) The statistical error in counting N events;
(b) The error of the glass detector efficiency (10%);
(c) The error on the beam integrator (10%);

TABLE I

CROSS-SECTION OF THE (d, 2n) REACTION LEADING TO THE ISOMER (σ_f) AND THE GROUND-STATE (σ_0) OF Am^{242}

E_d MeV	7.2	8.3	9.2	9.6	10.4	11.3	12.1
$\sigma_f \times 10^{30}$ cm^2	0.0058 ± 0.0044	0.056 ± 0.013	0.47 ± 0.07	0.83 ± 0.13	1.34 ± 0.20	2.43 ± 0.40	3 ± 0.44
$\sigma_0 \times 10^{27}$ cm^2	0.031 ± 0.010	0.29 ± 0.04	1.20 ± 0.13	2 ± 0.22	4.6 ± 0.5	7 ± 0.75	75 ± 0.8

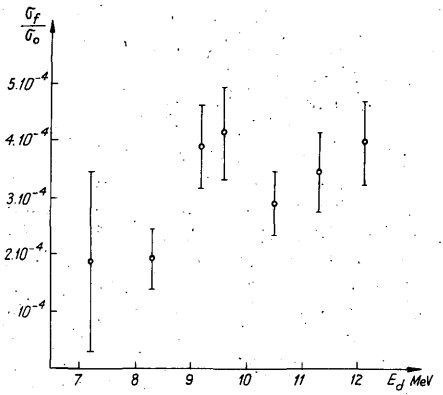

Fig. 5

Energy dependence of the isomeric yield ratio

(d) The error on the incident energy (3%);

(e) The discrepancy between theory and experiment for the recoil nuclei range-energy relation (20% [7]).

Item(e) is irrelevant in calculating the isomeric yield ratio.

The similar shape of the two excitation functions in Fig. 4 supports the assertion that the 14-ms fissioning isomeric state is obtained via a (d, 2n) process, i.e. it is an isomeric state of Am^{242}.

Taking the value of 8 MeV as the minimum deuteron energy at which the isomeric state is significantly excited, one may estimate its excitation energy. The (d, 2n) threshold for Pu^{242} is 3.7 MeV. The nuclear temperature in this range of mass number is about 1 MeV. Considering that each of the evaporated neutrons carries away a kinetic energy of 1 MeV (half the mean value of the statistical distribution), one obtains a maximum value of ~ 2 MeV for the excitation energy of the isomeric state.

The theoretical calculations for the competing (d, xn) processes, as well as for the isomeric yield ratios corresponding to different angular momenta of the isomeric state, are at present in progress.

ACKNOWLEDGEMENTS

These experiments were carried out at the Institute for Atomic Physics, Bucharest. We wish to thank the Director of the Institute, Professor Horia Hulubei, and also the cyclotron staff for operating the cyclotron, M. Macovei for beam energy measurements, K. Gavrilov for preparing the target layers, E. Ryndina and V. Kushniruk for preparing the silicon detectors, M. Sezon for her valuable help in the glass detector scanning, L. Kumpf and A. Pilkov for constructing the alpha spectrometer, and the technical group of the Cyclotron Laboratory for valuable help during the experiment.

REFERENCES

[1] POLIKANOV, S.M. et al., Ž. eksp. teor. Fiz. 42 (1962) 1464;
POLIKANOV, S.M. et al., Ž. eksp. teor. Fiz. 44 (1963) 804;
PERELYGIN, V.P. et al., Ž. eksp. teor. Fiz. 45 (1963) 863.
[2] FLEROV, G.N. et al., Ž. eksp. teor. Fiz. 45 (1963) 1396.
[3] LINEV, A.F. et al., Preprint D.1963, Joint Institute for Nuclear Research, Dubna (1964).
[4] LOBANOV, Yu. V. et al., Preprint P.1801, Joint Institute for Nuclear Research, Dubna (1964).
[5] VANDENBOSCH, R. et al., J. inorg. nucl. Chem. 26 (1964) 219.
[6] DZELEPOW, B.S. et al., Decay Schemes of Radioactive Nuclei, Moscow (1963).
[7] WINSBERG, J. et al., Phys. Rev. 121 (1961) 518.
[8] KAPUSTYK, A. et al., Prib. Teh. Eksp. 5 (1964) 72.

DISCUSSION

D. BRENNER: Have you studied the spontaneous fissile isomers of Am^{240} and Am^{244} and, if so, can you give us any information about the cross-sections?

N. MARTALOGU: No studies have been made of these isomers.

M. NÈVE DE MEVERGNIES: Are you certain that the 14-m/s product that you excite in you experiment is Am^{242m}?

E. IVANOV: Yes, we are sure about this. The same isomer was excited in the following reactions: $Pu^{239} + \alpha$; $Am^{242} + n$; and other reactions with heavy ions (Refs. [1-3]).

N. MARTALOGU: Our measured half-life $T_{\frac{1}{2}} = 14.0 \pm 0.4$ m/s agrees fairly well with the earlier experimental values of 13.5 ± 1.2 m/s (Refs. [1-3]).

DISTRIBUTION OF MASS AND CHARGE IN FISSION

(Sessions III and IV)

Review Paper

MASS AND CHARGE DISTRIBUTION IN LOW-ENERGY FISSION*

A.C. WAHL
WASHINGTON UNIVERSITY, ST. LOUIS, MO.,
UNITED STATES OF AMERICA

Abstract — Résumé — Аннотация — Resumen

MASS AND CHARGE DISTRIBUTION IN LOW-ENERGY FISSION. The mass and charge distributions for thermal-neutron fission of U^{235} are discussed in considerable detail and compared with the corresponding distributions in other low-energy fission processes. Points discussed in connection with the mass distributions for binary fission include the positions of the peaks, valley and fine structure in a mass yield curve with respect to filled nuclear shells and the changes in the positions that occur with changing fissioning nucleus and excitation energy. The mass distribution from ternary fission is discussed also. For both binary and ternary fission comments are made concerning the mass distributions of primary fragments (before neutron evaporation) and of fission products (after neutron evaporation).

Charge distribution is discussed in terms of charge dispersion among fission products with the same mass number and the variation with mass number of Zp, the "most probable charge" (non-integral) for a given mass number. Although direct information about charge distribution is limited to fission products, estimates are presented of charge distribution for primary fission fragments.

Knowledge and estimates of mass and charge distribution for a fission process allow estimation of primary yields of all fission products or fragments. Although many estimated primary yields are quite uncertain mainly because of lack of knowledge of charge distribution, especially for fission products formed in low yield, some estimates of primary yields are presented to illustrate the need for and possible practicality of further experimentation.

Fission processes other than thermal-neutron fission of U^{235} that are discussed include thermal-neutron fission of U^{233} and Pu^{239}, spontaneous fission of Pu^{240} and Cf^{252}, 14-MeV neutron fission of U^{235} and U^{238}, 11-MeV proton fission of Ra^{226} and 22-MeV deuteron fission of Bi^{209}.

RÉPARTITION DES MASSES ET DES CHARGES DANS LA FISSION A BASSE ÉNERGIE. L'auteur étudie de façon très détaillée la répartition des masses et des charges dans la fission de ^{235}U par neutrons thermiques et la compare ensuite à la répartition correspondante dans les autres processus de fission à basse énergie. Les questions à examiner en ce qui concerne la répartition des masses dans la fission comprennent les positions des sommets et de la vallée et la structure fine de la distribution des produits de fission selon la masse pour des couches fermées, ainsi que les changements de position qui se produisent lorsque le noyau subissant la fission et l'énergie d'excitation ne sont pas les mêmes. L'auteur examine également la répartition des masses dans le cas de la fission ternaire. Au sujet de la fission binaire et de la fission ternaire, il fait des observations touchant la répartition des masses entre les fragments primaires (avant «évaporation» des neutrons) et les produits de fission (après «évaporation» des neutrons).

L'auteur étudie la répartition des charges d'après la dispersion des charges entre les produits de fission ayant le même nombre de masse, et la variation de Z_p selon la masse, la «charge la plus probable» (non entière) pour une masse donnée. Bien que des renseignements directs sur la répartition des charges soient limités aux produits de fission, l'auteur présente des estimations de la répartition des charges pour les fragments de fission primaires.

D'après des données et des estimations relatives à la répartition des masses et des charges pour un procédé de fission, on peut déterminer les rendements primaires en tous produits ou fragments de fission. Bien que l'estimation de nombreux rendements primaires soit tout à fait approximative en raison surtout de l'absence de données sur la répartition des charges, notamment pour les produits de fission dont le rendement est faible, l'auteur présente des estimations des rendements primaires pour illustrer la nécessité d'une nouvelle expérimentation et ses possibilités pratiques de réalisation.

* Work supported by the United States Atomic Energy Commission

Les processus de fission - autres que la fission de ^{235}U par neutrons thermiques - qui sont étudiés comprennent la fission de ^{233}U et de ^{239}Pu par neutrons thermiques, la fission spontanée de ^{240}Pu et de ^{252}Cf, la fission de ^{235}U et de ^{238}U par des neutrons de 14 MeV, la fission de ^{226}Ra par des protons de 1 MeV, et la fission de ^{209}Bi par des deutérons de 22 MeV.

РАСПРЕДЕЛЕНИЕ МАССЫ И ЗАРЯДА ПРИ ДЕЛЕНИИ, ВЫЗВАННОМ ЧАСТИЦАМИ МАЛОЙ ЭНЕРГИИ. Распределения массы и заряда при делении урана-235, вызванном тепловыми нейтронами достаточно подробно обсуждаются и сравниваются затем с соответствующими распределениями при других процессах деления, вызванного частицами низкой энергии. В состав вопросов, подлежащих обсуждению в связи с распределениями масс при делении на две части, включаются вопросы относительно расположения пиков, впадины и тонкой структуры кривой выхода массы в отношении заполненных ядерных оболочек и изменений в расположении, что случается при изменении делящегося ядра и энергии возбуждения. Обсуждается также распределение масс при делении ядра на три части. Как при двойном, так и при тройном делении сделаны замечания относительно распределения масс первичных осколков (до нейтронной эмиссии) и продуктов деления (после нейтронной эмиссии).

Распределение заряда обсуждается в рамках дисперсии заряда среди продуктов деления с тем же массовым числом и изменением в массовом числе Z_p, "наиболее вероятный заряд" (неинтегральный), для данного массового числа. Хотя непосредственная информация относительно распределения заряда ограничена продуктами деления, представлены предположения относительно распределения заряда для первичных осколков деления.

Знания и предположения относительно распределения массы и заряда для процесса деления дают возможность оценить первичные выходы всех продуктов или осколков деления. Хотя многие расчетные данные относительно первичных выходов довольно неопределенны ввиду, главным образом, недостатка знаний относительно распределения зарядов, особенно для продуктов деления, образующихся при низком выходе, представлены некоторые оценки первичных выходов с целью иллюстрации необходимости проведения дальнейших экспериментов и их практической возможности.

В число процессов деления, кроме деления урана-235, вызванного тепловыми нейтронами, которые необходимо обсудить, включается деление урана-233 и плутония-239, вызванное тепловыми нейтронами, спонтанное деление плутония-240 и калифорния-252, деление урана-235 и урана-238 нейтронами с энергией 14 Мэв, деление радия-226 протонами с энергией 11 Мэв и деление висмута-209 дейтронами с энергией 22 Мэв.

DISTRIBUCION DE MASAS Y DE CARGAS EN LA FISION A BAJAS ENERGIAS. El autor examina con bastante detalle la distribución de las masas y de las cargas en la fisión del ^{235}U inducida por neutrones térmicos, comparándola seguidamente con las distribuciones observadas en otros procesos de fisión a bajas energías. Entre las cuestiones que estudia en relación con la distribución de las masas en la fisión binaria, figura la posición de los picos y del valle, así como la estructura fina en una curva de rendimiento másico respecto de las capas nucleares completas y los desplazamientos que se producen al cambiar el núcleo que se fisiona y la energía de excitación. También estudia la distribución de las masas en la fisión ternaria. Tanto en el caso de la fisión binaria como en el de la fisión ternaria, formula observaciones acerca de la distribución másica de los fragmentos primarios emitidos (antes de la evaporación de neutrones) y de los productos de fisión (emitidos después de esa evaporación).

Examina la distribución de las cargas atendiendo a la dispersión de éstas entre los productos de fisión de igual número de masa, y a la variación, en función de este número de masa, de Z_p, esto es, la "carga más probable" (valor no entero) para un número de masa dado. Aunque la información directa acerca de la distribución de las cargas se limita a los productos de fisión, el autor evalúa también la distribución de las cargas para los fragmentos de fisión primarios.

Los datos conocidos y los calculados, relativos a la distribución de las masas y de las cargas en un proceso de fisión, permiten calcular el rendimiento de todos los productos o fragmentos de fisión. Aunque muchos de los rendimientos calculados para los fragmentos primarios encierran considerables incertidumbres, debido principalmente a la falta de conocimientos sobre la distribución de las cargas, en particular en el caso de productos de fisión formados con un bajo rendimiento, el autor presenta algunos cálculos de los rendimientos primarios para destacar la necesidad de proseguir la labor de experimentación y la posibilidad de hacerlo.

Entre los procesos de fisión que examina, además de la fisión del ^{235}U inducida por neutrones térmicos, figuran los siguientes: fisión del ^{233}U y del ^{239}Pu inducida por neutrones térmicos, fisión espontánea del ^{240}Pu y del ^{252}Cf, fisión del ^{235}U y del ^{238}U inducida por neutrones de 14 MeV, fisión del ^{226}Ra inducida por protones de 11 MeV, y fisión del ^{209}Bi por deuterones de 22 MeV.

INTRODUCTION

Nuclear fission results in many hundreds of fission products; nearly 400 have been identified, and several hundred more are probably formed in appreciable yield but remain undiscovered. The relative probability of formation, or fission yield, of each product nuclide both before and after neutron evaporation would constitute a complete description of mass and charge distribution for a given fission process. This complete description does not exist. The partial descriptions that do exist for various fission processes include total cumulative yields for many mass numbers (the mass distribution) and independent yields and average or "most probable" atomic numbers for some of the primary products (the charge distribution).

This paper summarizes the current knowledge of mass and charge distribution for thermal-neutron fission of U^{235}, the fission process about which most is known, and then compares it with several other fission processes to illustrate the effects of nuclear composition and excitation energy on the mass and charge distributions. Only excitation energies less than about 20 MeV are considered.

Much of the information presented has been obtained from earlier reviews and compilations [1 - 5]. HERRMANN [1] has been especially useful. More recent information known to the author has been included, but an exhaustive literature search has not been made.

Throughout the rest of this paper the term fission fragment refers to fragments before prompt neutron emission, and the term fission product refers to products after prompt neutron emission.

MASS DISTRIBUTION

In low-energy fission the primary products are neutron rich and undergo negative beta decay, those of a given mass number forming a beta-decay

TABLE I

BETA DECAY CHAIN FOR MASS NUMBER 93

Yields are for thermal-neutron fission of U^{235}: ~ values are estimated from the curve in Fig. 7; Rb^{93} and Sr^{93} yields [6]; Y^{93} yield [7]; other yields [1, 5].

Fractional independent yields						
$\sim 8 \times 10^{-4}$	0.074	0.59	0.32	0.016	$\sim 6 \times 10^{-5}$	$\sim 1 \times 10^{-7}$
Br^{93}	Kr^{93}	Rb^{93}	Sr^{93}	Y^{93}	Zr^{93}	Nb^{93}
(?)	(1.2 s)	(5.1 s)	(7.5 min)	(10.2 h)	(1×10^6 yr)	(stable)
Cumulative yields: Zr^{93}, 6.45 ± 0.32% Y^{93}, 6.1 ± 0.6%					6.4 ± 0.3% = total chain yield	

chain. Since for a given mass number the charge dispersion is narrow and is centred several charge units below a stable isobar, the cumulative yield of the stable isobar, or of a radioactive isobar near the end of the chain, is to a very good approximation the sum of primary or independent yields of all products with that mass number, i.e. the total chain yield. Cumulative yields are measured radiochemically or mass-spectrometrically after the early, short-lived chain members have decayed. Table I shows a typical beta-decay chain.

Yields of primary fragments may be determined by physical methods. Velocities determined by time-of-flight measurements or kinetic energies determined with ionization chambers or solid-state detectors are related to mass through momentum conservation. The mass resolution is not perfect, as it is for the product yields, and corrections must be made for dispersion.

Figure 1 shows the yields of both products and fragments as a function of mass number for thermal-neutron fission of U^{235}. The approximate positions of nuclear shell edges[1] are shown as shaded areas. The difference

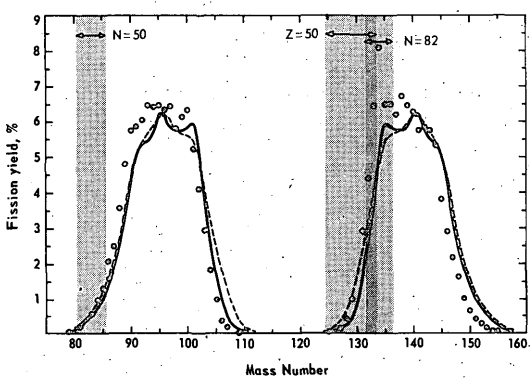

Fig.1

Yield versus mass number for thermal-neutron fission of U^{235}. Continuous line represents yields of fragments from time-of-flight measurements [8]; broken line represents fragment yields from kinetic-energy measurements with solid-state detectors [9]. Filled circles represent measured product yields: Se^{81} and Se^{83} [10]; Sb^{125} [11]; Sb^{127} and Sb^{129} [12]; other products [1,2]; Shaded areas indicate approximate positions of nuclear shell edges (see text).

between the product and fragment yields is the result of neutron emission and of mass dispersion in the fragment yield measurements. TERRELL has used the yields to calculate the number ν_f of neutrons emitted per fragment as a function of mass number, and obtained functions in good agreement with those derived from direct measurements [13]. Since mass dis-

[1] In a yield versus mass number plot nuclear shell edges cannot be located precisely because their effect, if any, is on the yields of individual primary products and fragments, and these yields can be estimated only approximately. The shaded regions in Figs. 1, 2 and 4 cover mass numbers for which it is estimated (see section Estimation of Primary yields) that > 10% of a cumulative yield is from primary products or fragments having a closed-shell structure. Of course, yields of complementary fragments would also be affected; these regions are not indicated but may be visualized approximately from the symmetry involved.

persion has prevented accurate measurement of fragment yields that are very small, Terrell was not able to determine values of ν_f for mass numbers in the valley of the mass-yield curve or on the wings of the two peaks.

A semi-logarithmic plot of the product yield data in Fig. 2 shows what is known for mass numbers formed in small yields in the valley and on the

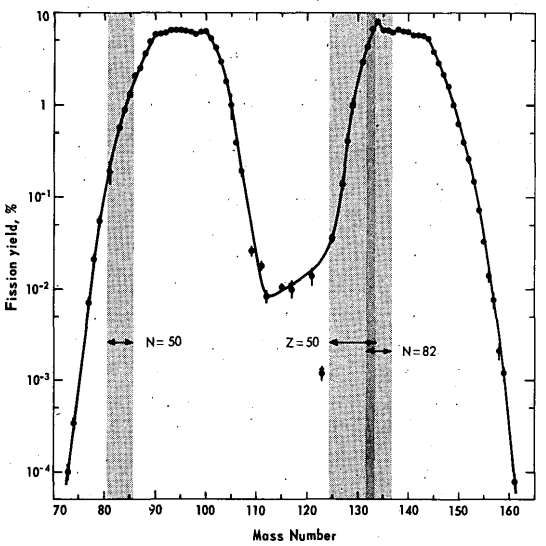

Fig. 2

Product yield versus mass number for thermal-neutron fission of U^{235}. Sources of data are the same as for Fig. 1. An arrow indicates that the yield of only one isomer has been determined.

wings of the peaks in the mass yield curve. As can be seen there are many mass numbers in the valley and a few on the wings for which there are no yield values. The shape of the valley is obviously poorly defined, and additional yield measurements are needed. The positions of the sharply drooping wings, on the other hand, are quite well defined, and may be used to estimate the total number of neutrons ν_t emitted in forming "complementary" products by noting the mass numbers that have equal yields or equal yield summations [13]. The estimates show that as asymmetry increases ($A_l < \sim 90$, $A_h > \sim 144$) the value of ν_t drops from ~ 2.6 to ~ 2.0, rather than increasing to ~ 3.8 as deduced from the direct measurements of the neutron number ν_f [14].

The sharp peak at A = 134 in the product-yield curve (Fig. 1) has been attributed to two causes: (a) a pile-up of products formed by neutron emission of heavier fragments, a result of the sharp increases in ν_f with mass number above 134 [13, 14], and possibly associated with changing neutron binding energies near the 82-neutron shell edge; (b) a preference in the fission process itself for fragments that lead to products with A = 134, again possibly associated with closed-shell structures. Support for (a) is given by the lower yields of products with mass numbers (~100) complementary to 134 and by the occurrence of peaks near A = 134 in product yield

curves for other fission processes. (The peaks are small except for thermal-neutron fission of U^{235}, Pu^{239} and Pu^{241} [15].) Support for (b) is given by the fragment yield curve shown in Fig. 1 from MILTON and FRASER's time-of-flight data [8] (solid line). The broad peak at A = 135 could be due to a sharp fragment peak that was broadened by the mass dispersion associated with the measurements. The fragment yield curve from the kinetic energy data of GIBSON, THOMAS and MILLER [9] (broken line) does not show this peak, however. Also there are no apparent peaks near A = 135 in the fragment yield curves for other fission processes [8, 16].

Ternary fission in which one of the three fragments is very light (He^4 or H^3) is well established. The yields of the other two fragments formed with an alpha particle vary with mass number similar to the yields in binary fission, but with a small shift to lower mass numbers, the shift being largest on the heavy side of each peak [17, 18].

Ternary fission in which the three fragments are of similar mass has been reported by MUGA [19]. He measured energies of coincident fragments using three solid-state detectors in a plane and separated by 120°. The observed yield for thermal-neutron fission of U^{235} was 1.2 ternary fissions per 10^6 binary fissions and was considered a lower limit because of the angular restrictions imposed by the experimental set-up. The yield as a function of mass number is shown in Fig. 3. As can be seen the reported minimal fragment yields are greater than the fission yields of some radio-

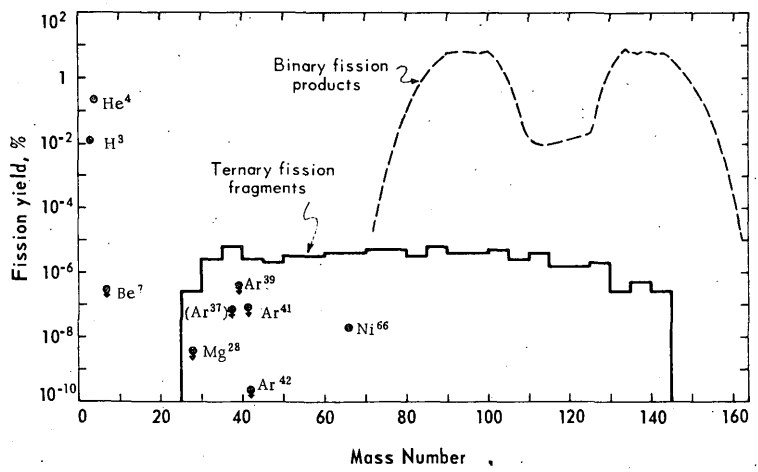

Fig. 3

Yields versus mass number for ternary fission of U^{235} by thermal neutrons. Solid line represents minimum yields of fragments [19]. Points represent yields of products: Be^7, Mg^{28}, Ni^{66} [20]; Ar^{41}, Ar^{42} [21]; He^4 [22]; H^3 [23].

active nuclides in the mass region of interest [20, 21]. Because of the large fragment excitation energy (estimated to be as high as ~55 MeV), Muga points out that neutron emission could result in some beta stable products. However, this cannot be true for all three complementary fragments, since emission of about 20 neutrons would be required; and it should be noted that

discrepancies in yield of several orders of magnitude exist in different mass regions.

Returning to binary fission, a striking feature of the mass distribution for a number of different fissioning nuclei is the constancy in position on the A axis of the heavy mass peak, especially the light side of the peak. The position of the light peak changes with changing mass of the fissioning nucleus; the position of the heavy peak is essentially constant as is shown in Fig. 4.

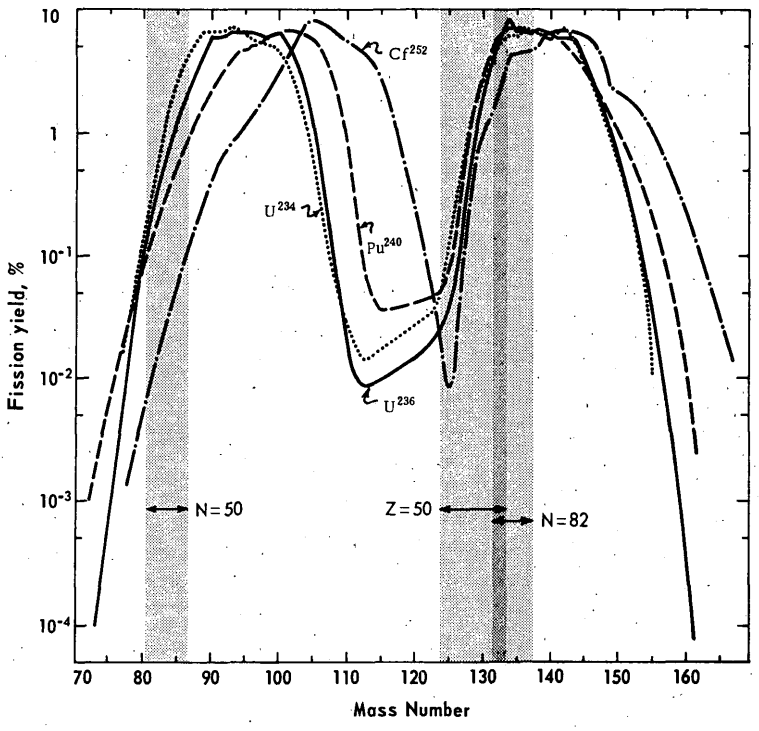

Fig. 4

Product yield curves for thermal-neutron fission of U^{233}, U^{235} and Pu^{239} and spontaneous fission of Cf^{252} [1]. Shaded areas indicate approximate positions of nuclear shell edges (see text). Curves are denoted by the symbol of the fissioning nucleus.

The 50-proton and 82-neutron shell edges are near the light side of the heavy mass peaks, and are often associated with the constancy of position. The different shapes of the peaks in the various product yield curves have been attributed to different contributions of various cluster pairs (A_l = 84, 90, 96, or 100 with A_h = 132) [24].

The effect of the excitation energy of U^{236} on the mass distribution of its fission products is shown in Fig. 5. The yields of products from near symmetric fission increase sharply with energy, the fine structure peak at A = 134 disappears, and the peaks are broadened somewhat. The rapid decrease in yields of products in the valley of the curve with decreasing excitation energy suggests that symmetric fission requires more excitation energy than asymmetric fission and raises the interesting question of the

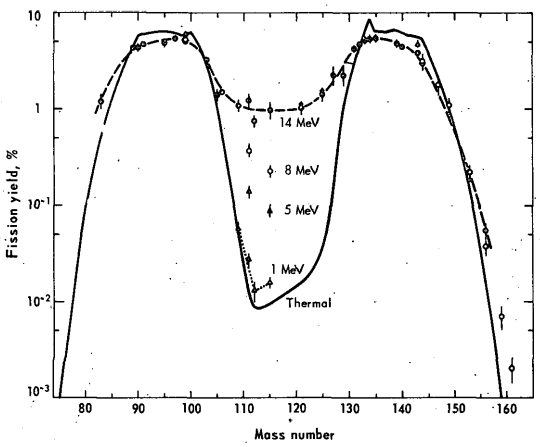

Fig. 5

Variation of product yields from neutron-induced fission of U^{235} as the neutron energy is varied [1]. Neutron energies are indicated.

probability of symmetric fission at zero excitation energy. Extrapolation of valley yields for neutron-induced fission of U^{235} indicates that the probability could be very small or zero. Unfortunately, low intensities of spontaneous fission sources have made measurement of yields less than ~0.01% impractical. (For Cf^{252} intensity is not a problem, but the valley is too narrow.)

Small variation of neutron energy in the resonance region just above thermal energies causes small variations, both up (22% maximum) and down (50% maximum), in yields of products in the valley of the mass yield curve for neutron-induced fission of U^{235} [25]. The variations are also small for neutron-induced fission of U^{233} and Pu^{241} [26, 27]; however, for Pu^{239} there are decreases in yields by factors of 2 and 3 for some energy regions [27].

As the mass and atomic numbers of fissioning nuclei decrease below those of the uranium isotopes, the probability of fission at small excitation energies decreases sharply, and, at the higher excitation energies necessary for fission, nearly symmetric mass division becomes more probable than asymmetric division. This change is illustrated in Fig. 6. It is noteworthy that as long as asymmetric division occurs the position of the heavy mass peak remains nearly constant.

CHARGE DISTRIBUTION

Charge distribution is usually discussed in terms of charge dispersion among fission products with the same mass number and variation with mass number of Z_P, the "most probable charge" (not necessarily integral), for a given mass number. Both types of information may be deduced from radiochemically determined yields of individual primary fission products, for which both mass and atomic numbers are known precisely. However, each yield determination involves a major research effort requiring careful and

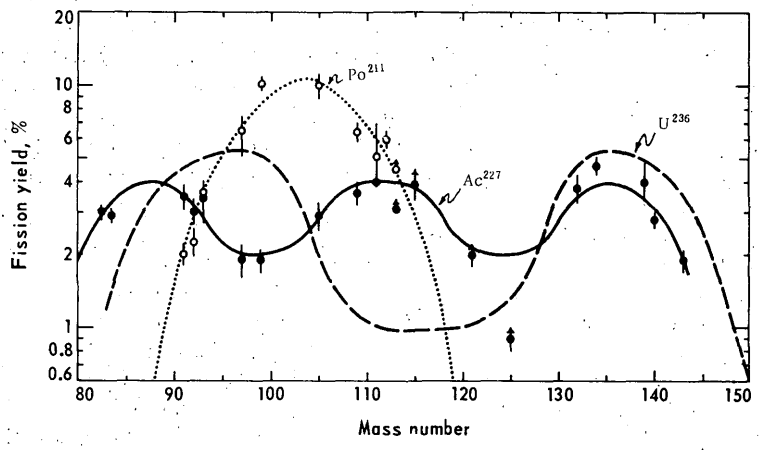

Fig. 6

Variation of product yield curves with nuclear composition:
– – 14-MeV neutron-induced fission of U^{235} [1] ($\sigma = \sim 2 \times 10^{-24}$ cm²; U^{236} excitation energy ~20 MeV);
–●– 11-MeV proton-induced fission of Ra^{226} ($\sigma = \sim 2 \times 10^{-27}$ cm², Ac^{227} excitation energy ~16 MeV) [28];
...○... 20-MeV deuteron-induced fission of Bi^{209} ($\sigma = \sim 1 \times 10^{-29}$ cm², Po^{211} excitation energy ~27 MeV, yields not shown: $Sb^{127} < 0.13\%$; $Ba^{139} < 0.08\%$) [29].

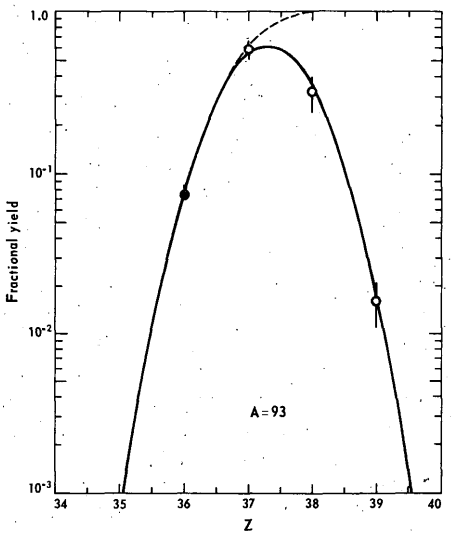

Fig. 7

Charge dispersion for products with A = 93 from thermal-neutron fission of U^{235} [5,6,7]:
○ independent yield, ● cumulative yield. Solid line represents Eq. (1) with c = 0.82 and Z_p = 37.30; broken line is for cumulative yields, ΣP(Z).

often rapid chemical separations and radioactivity measurements, so data accumulate slowly, and at present primary yields are available for only a small fraction of the fission products.

There are also two physical methods under investigation that give information about the average charge of primary products as a function of mass number. In one method, fission products are separated in a gas-filled mass spectrometer, and the number of beta disintegrations per fission is determined for each interval of mass [30]. Unfortunately, the mass resolution is poor so that the atomic number values obtained are averaged over many mass numbers.

The other physical method involves simultaneous measurement of K-X-rays in coincidence with fragments whose kinetic energies are determined with solid-state detectors [31, 32]. The X-ray energies define the atomic numbers, and kinetic energies define the masses of the fragments. Although there are abundant K-X-rays (~0.6 per fission), their origin appears to be vacancies produced by internal conversion of gamma rays emitted after fission. Therefore, X-ray intensities are determined not only by the fission yields of isotopes of an element but also by the gamma-ray intensities and conversion coefficients for each isotope, all unknown quantities.

The charge dispersion among products with A = 93 from thermal-neutron fission of U^{235} is shown in Table I and Fig. 7. As can be seen in Fig. 7 the fractional independent yield or relative probability P(Z) of formation of a product with atomic number Z is well represented by a Gaussian curve[2],

$$P(Z) = \frac{1}{\sqrt{c\pi}} e^{-(Z-Z_P)^2/c} . \qquad (1)$$

Also for three other mass numbers (92, 140, 141) there are three independently determined fractional yields, and the dispersion of charge for each mass number is well represented by a Gaussian curve with c = 0.84, 1.09 and 0.86, respectively [5, 6, 7]. In addition to the above evidence that charge dispersion is Gaussian and approximately constant in width, there are six mass numbers (91, 94, 95, 139, 142, and 143) for which two fractional yields have been determined; these establish the widths of the dispersion curves if the Gaussian shape is assumed. The average value of the constant c for the 10 mass numbers is 0.86 ± 0.04 [7].

The Z_P values for the ten mass numbers discussed above are determined directly from the dispersion curve for each mass number. Z_P values for other mass numbers, for which only one fractional yield has been measured, can be estimated on the assumption that a Gaussian isobaric dispersion curve with c = 0.86 ± 0.15 applies. A plot of the empirical Z_P values thus determined is shown in Fig. 8. The plot shows clearly that light products have more and heavy products less than the average density of charge. The average deviation from uniform charge density is about one-half charge unit. If fission fragments rather than products are considered by adding ν_f to A as an estimate of fragment mass number, similar conclusions can be drawn [5, 7].

Also shown in Fig. 8 are the bands of average charge Z_{AV} determined by ARMBRUSTER, HOVESTADT, MEISTER and SPECHT [30]. The bands,

[2] In the actual practice of fitting a Gaussian curve to fractional yield data it is convenient to use the cumulative form of the Gaussian representation [5].

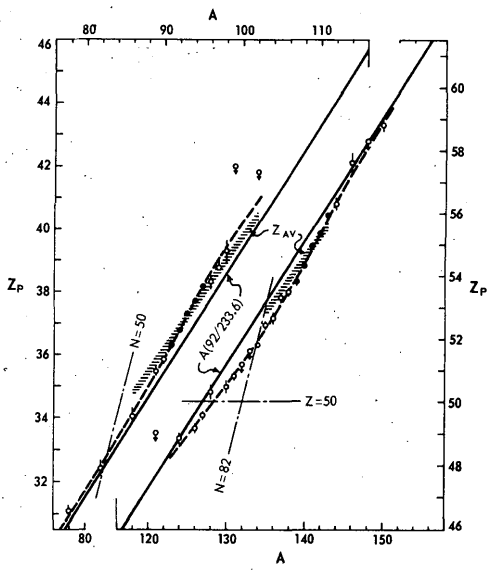

Fig. 8

Empirical Z_P values and average charge bands (Z_{AV}) [30] for products from thermal-neutron fission of U^{235}. • Z_P values obtained from Gaussian charge dispersion curves determined by two or more fractional yields [5,6,7]. ○ Z_P values estimated from the Gaussian isobaric charge dispersion curve with c = 0.86 ± 0.15 fitted to a single fractional yield value: Nb^{99} [33], Sn^{121} [34], Sb^{124} and Sb^{126} [11], Sb^{127} [35], Pm^{146} [36], others [5]. Continous lines are for average charge density, A(92/233.6). Broken lines represent an empirical Z_P function derived from the points.

0.3 charge unit in width, cover the area in which most of the data fall. As stated earlier, a measured average isobaric charge value is averaged, because of the poor mass resolution, over many mass numbers so no abrupt changes with mass number could have been observed [30]. Although the slopes of the Z_P and Z_{AV} functions are different, the magnitudes of the two functions are similar and agree in value where each is best known. The differences may well be due to the uncertainties in the Z_P function caused by lack of knowledge of charge dispersion for many mass numbers and to the uncertainties in the Z_{AV} function caused by poor mass resolution and uncertainties in the mass calibration. (The difference between Z_P and Z_{AV} for Gaussian dispersion is small.)

Charge distribution for other low-energy fission processes appears to be similar to that for thermal-neutron fission of U^{235} [37]. For several mass numbers and different fission processes two fractional yields have been independently determined and are represented well by a Gaussian curve with c = 0.86 ± 0.15, as is shown in Fig. 9. The empirical Z_P values for thermal neutron fission of U^{233} and Pu^{239}, for 14-MeV neutron fission of U^{235} and U^{238} [37], and for spontaneous fission of Cf^{252} [5] show trends with mass number similar to those observed for thermal-neutron fission of U^{235}, namely, that light products have more and heavy products less charge than that needed for the average charge density by about one-half charge unit. This generalization is restricted for all of the fission processes to those mass numbers

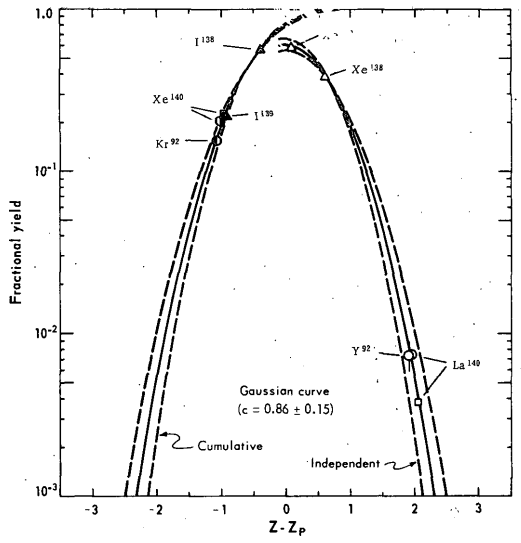

Fig. 9

Isobaric charge dispersion. Thermal-neutron fission of U^{233}: □ (Xe^{140} [37], La^{140} [5]). 14-MeV neutron-fission of U^{235}: ○ (Kr^{92} and Xe^{140} [37], Y^{92} [38], La^{140} [39]; and 14-MeV neutron fission of U^{238} : △ (I^{138} and Xe^{138} [37,40], I^{139} and Xe^{139} [37,41]). Filled symbols represent cumulative yields, and open symbols represent independent yields.

formed in high yield; little information is available for mass numbers formed in low yield.

ESTIMATION OF PRIMARY YIELDS

Since yields are known for relatively few primary products, methods of estimating primary yields are often needed. The methods generally involve estimation of Z_p for the mass number of interest and then calculation of the fractional yield from the appropriate charge dispersion curve. For mass numbers for which dispersion curves have been determined from two or more measured yields, the method is straightforward and probably quite reliable. For other mass numbers an isobaric charge dispersion curve must be assumed, and at present the best assumption is a Gaussian curve (Eq. (1)) with $c = 0.86 \pm 0.15$. It should be noted that the curve has not been tested for mass numbers for which a principal primary product has a closed-shell structure or for mass numbers resulting from nearly symmetric or very asymmetric fission.

The possible influence of closed-shell structures on charge dispersion is illustrated by the following examples. (1) If 136 is the correct mass assignment for the 86-s iodine fission product, its low cumulative fission yield [3] leads to a large independent yield for $_{54}Xe^{136}_{82}$ and, with the small independent yield of Cs^{136}, indicates that the charge dispersion is narrow (if Gaussian, $c = \sim 0.4$ for thermal-neutron fission of U^{233}, U^{235}, and Pu^{239}). (2) A large cumulative fission yield for $_{50}Sn^{131}_{81}$ [42] from thermal-neutron

fission of U^{235} indicates, with the independent yields of Te^{131} [5, 43] and I^{131} [5], that the charge dispersion is broad (if Gaussian, c = ~2.7).

For estimation of Z_P values, probably the best that can be done at present is to use either empirical values derived from a single fractional yield or an empirical Z_P function, such as is shown in Fig. 8, fitted to the empirical values [5, 7]. If too few data are available for this treatment, still other prescriptions are necessary.

WOLFSBERG [37] has investigated various prescriptions for estimating Z_P by comparing predicted values with empirical values for thermal-neutron fission of U^{233} and Pu^{239}, and for 14-MeV neutron fission of U^{235} and U^{238}. He found the most satisfactory prescription to be one that uses as reference empirical Z_P values for thermal-neutron fission of U^{235} [44]. However, neither this method nor the equal charge displacement postulate was satisfactory for charged-particle induced fission at moderate energies. Conversely, the unchanged-charge-distribution postulate, which has been used for charged-particle-induced fission [45], is not applicable to fission induced by neutrons of < 14-MeV energy.

The combination of a Z_P function, a general isobaric charge dispersion curve, and the mass yield curve for a fission process allows estimation of yields of individual primary fission products. Such estimates are probably not very reliable, in general, but may be helpful in correlating existing data in new and informative ways and in suggesting new experiments. For example, the estimates make possible the location of the mass numbers whose yields may be affected by nuclear shell edges (Figs. 1, 2 and 4)[3]. Also the estimates make possible the presentation of mass and charge distribution data as isotopic and isotonic yield plots [46]. The derived isotopic yield values serve as a useful check on the primary yield estimates because of the requirement that elements with complementary atomic numbers must have primary yields that are equal, or only slightly different because of small contributions from ternary fission. Estimates that have been made to date do not meet this requirement very well.

New experiments suggested by primary yield estimates include searches for new fission products for which yields are predicted to be moderately large [1, 46], and measurements of primary fractional yields predicted to be reasonably large for fission products with filled nucleon shells or formed in symmetric or very asymmetric fission. Such experiments could add greatly to our knowledge of charge and mass distribution in low-energy fission.

---

[3] The fractional yields of products from thermal-neutron fission of U^{235} were calculated from the Gaussian isobaric charge dispersion curve (Eq. 1) with c = 0.86 and the empirical Z_P function shown in Fig. 8 (dashed line). Mass numbers having an isobar with a closed-shell structure and formed with a fractional independent yield of > 0.1 were chosen. The largest mass number associated with a particular shell was increased by one so as to include fragments as well as products in each mass-number range.

For other fission processes estimates were made in a similar way except that the Z_P values were estimated by the method of CORYELL et al. [44]; the empirical Z_P function shown in Fig. 8 was used as reference.

ACKNOWLEDGEMENTS

It is a pleasure to thank B.R. Erdal and J.C. Williams for their help in analysing data and in preparing figures. The author is indebted to the following investigators who made their unpublished results available: N.E. Ballou, J.S. Fraser, L.E. Glendenin, M. Hillman, D.R. Nethaway, D.G. Sarantites, T.D. Thomas and K. Wolfsberg.

REFERENCES

[1] HERRMANN, G., Habilitationsschrift, Mainz (1961), unpublished.
[2] FARRAR, H. and TOMLINSON, R.H., Nucl. Phys. 34 (1962) 367.
[3] KATCOFF, S., Nucleonics 18, No.11 (1960) 201.
[4] WALKER, W.H., Chalk River Report CRRP-913 (1960), unpublished.
[5] WAHL, A.C., FERGUSON, R.L., NETHAWAY, D.R., TROUTNER, D.E., and WOLFSBERG, K., Phys. Rev. 126 (1962) 1112.
[6] NORRIS, A.E., FERGUSON, R.L. and WAHL, A.C., unpublished results (1964), Washington University and Oak Ridge National Laboratory.
[7] NORRIS, A.E. and WAHL, A.C., unpublished results (1964), Washington University; and NORRIS, A.E. Ph.D. thesis, Washington University (1963), unpublished.
[8] MILTON, J.C.D. and FRASER, J.S., Canad. J. Phys. 40 (1962) 1626; and private communication (1964).
[9] GIBSON, W.M., THOMAS, T.D. and MILLER, G.L., Phys. Rev. Lett. 7 (1961) 65; and private communication (1964).
[10] CROALL, I.F. and WILLIS, H.H., J. inorg. nucl. Chem. 24 (1962) 221.
[11] GLENDENIN, L.E., private communication (1964).
[12] HAGEBØ, E., J. inorg. nucl. Chem. 25 (1963) 615.
[13] TERRELL, J., Phys. Rev. 127 (1962) 880.
[14] APALIN, V.F., GRITSYUK, Yu.N., KUTIKOV, I.E., LEBEDEV, V.I. and MIKAELYAN, L.A., Nucl. Phys. 55 (1964) 249.
[15] FARRAR, H., CLARKE, W.B., THODE, H.G. and TOMLINSON, R.H., Canad. J. Phys. 42 (1964) 2063.
[16] FRASER, J.S., MILTON, J.C.D., BOWMAN, H.R. and THOMPSON, S.G., Canad. J. Phys. 41 (1963) 2080.
[17] SCHMIDT, H.W., NEILER, J.H., WALTER, F.J. and CHETHAM-STRODE, A., Phys. Rev. Lett 9 (1962) 427.
[18] SCHMIDT, H.S. and FEATHER, N., Phys. Rev. 134 (1964) B565.
[19] MUGA, M.L., Phys. Rev. Lett. 11 (1963) 129.
[20] ROY, J.C., Canad. J. Phys. 39 (1961) 315.
[21] HILLMAN, M. and STOENNER, R.W., private communication (1964).
[22] NOBLES, R.A., Phys. Rev. 126 (1962) 1508.
[23] SLOTH, E.N., HORROCKS, D.L., BOYCE, E.J. and STUDIER, M.H., J. inorg. nucl. Chem. 24 (1962) 337.
[24] FAISSNER, H. and WILDERMUTH, K., Nucl. Phys. 58 (1964) 177.
[25] COWAN, G.A., BAYHURST, B.P. and PRESTWOOD, R.J., Phys. Rev. 130 (1963) 2380.
[26] REGIER, R.B., BURGUS, W.H. and TROMP, R.L., Phys. Rev. 113 (1959) 1589.
[27] REGIER, R.B., BURGUS, W.H., TROMP, R.L. and SORENSEN, B.H., Phys. Rev. 119 (1960) 2017.
[28] JENSEN, R.C. and FAIRHALL, A.W., Phys. Rev. 109 (1958) 942.
[29] FAIRHALL, A.W., Phys. Rev. 102 (1956) 1335.
[30] ARMBRUSTER, P., HOVESTADT, D., MEISTER, H. and SPECHT, H.J., Nucl. Phys. 54 (1964) 586.
[31] THOMAS, T.D., ATNEOSEN, R.A., GIBSON, W.M. and PERLMAN, M.L., Abstract submitted for this Symposium; private communication (see Paper SM-60/57) (1964).
[32] GLENDENIN, L.E., GRIFFIN, H.C. and UNIK, J.P., Abstract submitted for this Symposium, private communication (see Paper SM-60/31) (1964).

[33] TROUTNER, D.E., FERGUSON, R.L. and O'KELLEY, G.D., Phys. Rev. 130 (1963) 1466.
[34] WAHL, A.C. and NETHAWAY, D.R., Phys. Rev. 131 (1963) 830.
[35] TROUTNER, D.E., WAHL, A.C. and FERGUSON, R.L., Phys. Rev. 134 (1964) B1027.
[36] ROBERTS, F.P., WHEELWRITE, E.J. and Van TOYL, H.H., J. inorg. nucl. Chem. 25 (1963) 1293.
[37] WOLFSBERG, K., submitted to Phys. Rev.; and private communication (1964).
[38] NETHAWAY, D.R., private communication (1964).
[39] NETHAWAY, D.R. and LEVY, H., private communication (1964).
[40] APOLLONOVA, A.M., KRISYUK, I.T. and USHATSKII, W.M., Radiohimija 4 (1964) 711.
[41] APOLLONOVA, A.M., KRISYUK, I.T. and USHATSKII, W.M., Radiohimija 4 (1962) 587. English translation: Soviet Radiochem. 4 (1962) 515.
[42] LOVE, D.L., STROM, P.O., GREENDALE, A.E., SAM, D., DELUCCHI, A. and BALLOU, N.E., private communication (1964).
[43] SARANTITES, D.G., GORDON, G.E. and CORYELL, C.D., submitted to Phys. Rev.; and private communication (1964).
[44] CORYELL, C.D., KAPLAN, M. and FINK, R.D., Canad. J. Chem. 39 (1961) 646.
[45] COLBY, L.J. and COBBLE, J.W., Phys. Rev. 121 (1961) 1410.
[46] TALÂT-ERBEN, M. and GÜREN, B., Phys. Rev. 129 (1963) 1762.

FISSION MASS YIELD STUDIES*

G. P. FORD AND R. B. LEACHMAN
LOS ALAMOS SCIENTIFIC LABORATORY, UNIVERSITY OF CALIFORNIA,
LOS ALAMOS, N. MEX., UNITED STATES OF AMERICA

Abstract — Résumé — Аннотация — Resumen

FISSION MASS YIELD STUDIES. Mass yields from fission induced by a span of neutron energies up to 18 MeV have been measured for Th^{232}, U^{235} and U^{238} target nuclei. Particular attention has been given to the dependence of symmetric fission yields on energy. To study the effect of angular momentum, fission yields from the U^{236} compound nucleus formed by alpha-particle irradiations of Th^{232} were also studied over the same span of excitation energies. A standard set of Pd^{109}, Ag^{111}, Pd^{112} and Ag^{113} symmetric fission yields was generally measured for all irradiations. In addition, yields of Eu^{156}, Cs^{136} and 2.3-d Cd^{115} were measured for some selected combinations of projectile, energy and target nucleus. Assays for Zr^{97} and sometimes also Ba^{139} served as fission monitors. Altogether 150 fission yields were measured for these combinations of target nucleus, projectile and incident energy. About one-third of these were checked by replicated irradiations.

At highest energies for the U^{236} compound nucleus the symmetric fission yield from alpha-particle-induced fission is about 13% higher than for neutron-induced fission. Dips in symmetric fission yield were observed at the energy onset of third-chance fission for each target and projectile. Some indication of a small central peak in the mass distribution was observed in the yields from U^{236} compound nucleus fission, but not from the Th^{233} compound nucleus fission.

Detailed mathematical methods have been developed to separate the effects of fissions preceding and following neutron emission. These methods were used to remove the effects of second- and third-chance fissions from the measured symmetric fission yields. These calculated yields for first-chance fission show no dips with energy. The calculations also show that perhaps half the difference between symmetric yields for alpha-particle-induced fission of Th^{232} and neutron-induced fission of U^{235} is attributable to angular momentum effects.

Both calculated first-chance yields and measured yields (resulting from first-, second- and third-chance fissions) for the U^{236} compound nucleus are compared with the two-mode-of-fission hypothesis. Similar analyses are made for yields from neutron-induced fission of Th^{232} and U^{238}.

ÉTUDES SUR LES RENDEMENTS DE FISSION SELON LA MASSE. Les auteurs ont mesuré la distribution, selon la masse, des produits de la fission de ^{232}Th, ^{235}U et ^{238}U par des neutrons d'une énergie allant jusqu'à 18 MeV. Ils ont accordé une attention particulière à la variation des rendements de la fission symétrique selon l'énergie. Pour étudier l'effet du moment cinétique, ils ont également étudié, pour la même gamme d'énergies d'excitation, les rendements de la fission du noyau composé ^{236}U formé avec une particule alpha comme projectile et ^{232}Th comme cible. Ils ont mesuré un ensemble normalisé de rendements de la fission symétrique de ^{109}Pd, ^{111}Ag, ^{112}Pd et ^{113}Ag, pour toutes les irradiations. En outre, ils ont mesuré les rendements en ^{156}Eu de ^{136}Cs et de ^{115}Cd (2, 3 j) pour certaines combinaisons projectile-énergie-noyau cible. Les dosages de ^{97}Zr et parfois de ^{139}Ba ont servi à vérifier les processus de fission. Les auteurs ont mesuré en tout 150 rendements de fission pour ces combinaisons noyau cible-projectile-énergie incidente. Environ un tiers de ces rendements ont été contrôlés par répétition.

Aux énergies les plus élevées pour le noyau composé ^{236}U, le rendement de la fission symétrique par particules alpha est plus élevé d'environ 13% que celui de la fission par neutrons. Les auteurs ont observé des dépressions dans le rendement de fission symétrique pour chaque combinaison cible-projectile lorsque l'énergie augmente et qu'apparaît le phénomène de la fission précédée de l'émission de deux neutrons. Ils ont observé des indications d'un petit pic central dans la distribution, selon la masse, des produits de la fission de noyau composé ^{236}U, mais non dans celle des produits de la fission du noyau composé ^{233}Th.

Les auteurs ont mis au point des méthodes mathématiques détaillées pour séparer les effets des fissions précédées ou suivies de l'émission de neutrons. Ils ont eu recours à ces méthodes pour éliminer, des rendements mesurés de la fission symétrique, les effets des fissions précédées de l'émission d'un ou de deux neutrons.

* Work done under the auspices of the United States Atomic Energy Commission.

La courbe des rendements ainsi calculés de la fission précédée de l'émission d'un neutron en fonction de l'énergie n'accuse aucune dépression. Les calculs indiquent également que peut-être la moitié de la différence entre les rendements symétriques pour la fission du ^{232}Th par particules alpha et la fission de ^{235}U par neutrons peut être attribuée aux effets du moment cinétique.

Les auteurs comparent à la fois les rendements calculés de la fission non précédée de l'émission de neutrons et les rendements mesurés (de la fission précédée ou non de l'émission d'un ou de deux neutrons) pour le noyau composé de ^{236}U avec l'hypothèse des deux modes de fission. Ils ont procédé à des analyses similaires pour les rendements de la fission de ^{232}Th et de ^{238}U par des neutrons.

ИЗУЧЕНИЕ ВЫХОДА МАССЫ ПРИ ДЕЛЕНИИ. Выходы массы при делении, вызванном нейтронами в интервале энергий до 18 Мэв, были измерены для ядер мишеней из тория-232, урана-235 и урана-238. Особое внимание уделялось зависимости образующихся при делении симметричных выходов от энергий. Для изучения влияния углового момента были исследованы также в том же интервале энергий возбуждения, выходы при делении сложных ядер урана-236, образующиеся при облучении тория-232 альфа-частицами. Для всех облучений обычно измерялась одинаковая серия образующихся при делении симметричных выходов палладия-109, серебра-111, палладия-112 и серебра-113. Кроме того, для некоторых избранных комбинаций налетающих частиц, энергий и ядер мишени были измерены также выходы европия-156, цезия-136 и кадмия-115 (с полупериодом жизни в 2,3 дня). В качестве регистраторов делений служили анализы по цирконию-97, а иногда также и по барию-139. Для этих комбинаций ядра мишени, налетающей частицы и энергии бомбардирующих частиц было измерено в общем итоге 150 полученных при делении выходов. Около одной трети этих выходов были проверены путем повторных облучений.

При наиболее высоких энергиях для сложного ядра урана-236 симметричный выход при делении, вызванном альфа-частицами, приблизительно на 13% выше, чем выход при делении, вызванном нейтронами. Спады в симметричном выходе при делении наблюдались в момент установления энергии, дающей для каждой мишени и для каждой налетающей частицы третий шанс деления. В выходах при делении сложного ядра урана-236 наблюдалось указание на наличие малого центрального пика в распределении массы, чего, однако, не наблюдалось при делении сложного ядра тория-233.

Были разработаны подробные математические методы для отделения влияний делений, происходящих до и после эмиссии нейтронов. Эти методы были использованы для исключения из измеренных симметричных выходов воздействия делений, которые происходят при втором и третьем шансах соударений. Для полученных по расчету выходов, образующихся при первом шансе деления, спадов в зависимости от энергии не наблюдалось. Расчеты показывают также, что, может быть, половина разницы между симметричными выходами при делении тория-232 под действием альфа-частиц и при делении урана-235 под действием нейтронов может быть приписана воздействию углового момента.

Как подсчитанные для сложного ядра урана-236 выходы при первом шансе деления, так и измеренные суммарные выходы (в результате делений при первом, втором и третьем шансах соударений) сопоставляются с гипотезой двойственного вида делений. Аналогичные анализы производятся для выходов при вызванном нейтронами делении тория-232 и урана-238.

ESTUDIOS SOBRE RENDIMIENTOS MASICOS EN LA FISION. Los autores han medido los rendimientos másicos en la fisión inducida por neutrones en el intervalo energético de hasta 18 MeV, respecto de núcleos-blanco de ^{232}Th, ^{235}U y ^{238}U. Han prestado particular atención a la variación de los rendimientos de fisión simétrica en función de la energía. Para estudiar el efecto del momento angular, han determinado también los rendimientos de fisión del núcleo compuesto de ^{236}U, formado por irradiación del ^{232}Th con heliones, para el mismo intervalo de energías de excitación. También han medido en general, para todas las irradiaciones, un conjunto normalizado de rendimientos de fisión simétrica del ^{109}Pd, ^{111}Ag, ^{112}Pd y ^{113}Ag. Además, han determinado los rendimientos del ^{156}Eu y del ^{136}Cs, así como del ^{115}Cd (período: 2, 3 d) para diversas combinaciones seleccionadas de proyectil, energía y núcleo-blanco. Las determinaciones del ^{97}Zr y, en ocasiones, también del ^{139}Ba, se emplearon como indicadores de la fisión. En conjunto, se midieron 150 rendimientos de fisión para estas combinaciones de núcleo-blanco, proyectil y energía incidente. Una tercera parte de ese total se comprobó mediante irradiaciones por duplicado.

Para las energías más altas del núcleo compuesto de ^{236}U, el rendimiento de la fisión simétrica inducida por heliones es aproximadamente un 13% mayor que en el caso de la fisión inducida por neutrones. Han podido observarse depresiones en la curva representativa del rendimiento de fisión simétrica correspondiente al umbral energético de la tercera probabilidad de fisión para cada blanco y proyectil. También se han observado indicios

de la existencia de un pequeño pico central en la curva de distribución másica para los rendimientos de fisión del núcleo de ^{236}U compuesto, pero no de la fisión del núcleo de ^{233}Th compuesto.

Los autores han perfeccionado métodos matemáticos detallados para separar los efectos de las fisiones que preceden y siguen a la emisión neutrónica, y han empleado esos procedimientos para eliminar de los rendimientos de fisión simétrica medidos los efectos de la segunda y tercera probabilidad de fisión. Estos rendimientos calculados para la primera probabilidad de fisión no presentan depresiones al variar la energía. Los cálculos realizados ponen también de manifiesto que tal vez la mitad de la diferencia entre los rendimientos de fisión simétrica correspondientes a la fisión del ^{232}Th inducida por heliones y los correspondientes a la fisión del ^{235}U inducida por neutrones, se deban a efectos del momento angular.

Los autores comparan con los resultados de la hipótesis de la fisión binaria tanto los rendimientos calculados de la primera probabilidad de fisión como los rendimientos medidos (resultantes de la primera, segunda y tercera probabilidad de fisión) del núcleo compuesto de ^{236}U. De manera análoga, analizan los rendimientos de la fisión del ^{232}Th y del ^{238}U inducida por neutrones.

INTRODUCTION

Fission yields from proton-induced fission of Th^{232}, photon-induced fission of U^{238}, alpha particle-induced fission of U^{238}, and deuteron-induced fission of natural uranium have previously been tested [1] for consistency with the two-mode-of-fission hypothesis [2]. Deviations were not statistically significant except for the yields of a few mass numbers at the highest excitation energies for photon-induced fission of U^{238}. SCHMITT and SUGARMAN [3] have proposed that one mode of fission is predominantly symmetric and the other predominantly asymmetric with the symmetric mode being more prevalent at higher excitation energies. FORD [1] found no compelling reason in the data then available to restrict the mode dominant at high energies to a single-hump yield curve. However, more recently BRITT et al. [4], from considerations of fission-fragment kinetic energies and velocities, have found support for the two-mode-of-fission hypothesis and have derived mass yield curves that are the single- and double-hump curves envisioned by Schmitt and Sugarman.

Recent mass yield data obtained by LEVY et al. [5] for the U^{236} compound nucleus generally agreed with the two-mode-of-fission hypothesis. However, it was disturbing that the yields from thermal-neutron-induced fission of U^{235} did not conform with these data within the framework of the two-mode-of-fission hypothesis. Continuation of this work [6] showed deviations at higher excitation energies for some mass numbers. These deviations gave rise to a second concern about mass yield tests of the two-mode-of-fission hypothesis, namely, that fissions following neutron emission perturb the results; the fission yield curves for the two hypothetical modes of fission cannot be expected to be exactly the same for fission of different compound nuclei. However, yields from the original compound nucleus, uncontaminated by fissions of the others, may still be expected to conform to the hypothesis.

The present study concerns recent data and an analysis method obtained by FORD and LEACHMAN [7] that are relevant to these two significant deviations from the two-mode-of-fission hypothesis.

For an initial U^{236} compound nucleus the emission of one or two neutrons followed by fission is possible at excitation energies of approximately

13.5 MeV and higher, or 20.5 MeV and higher, respectively. Fission before the emission of a neutron is called first-chance fission, fission after the emission of one neutron is called second-chance fission, etc. The competition between neutron emission and various fission chances is called the fission-chance split. Our data are better adapted to consider the effect of the fission-chance split than the data of HICKS et al. [6] in that the excitation energy of the original U^{236} compound nucleus is better known.

Our data analysis method is discussed in the following section; it consists of removing the effect of the fission-chance split to obtain first-chance yields from measured yields. Also averages and standard deviations of excitation energy for second- and third-chance fission and probabilities for first-, second- and third-chance fission, which are byproducts of the method, are given in the following section. The test of the two-mode-of-fission hypothesis for the U^{236} initial compound nucleus is then considered for both observed and first-chance fission yields. The test of the two-mode-of-fission hypothesis for observed mass yields from neutron-induced fission of Th^{232} and U^{238} is also considered. Finally, the results of the test are discussed.

MASS YIELDS FOR FIRST-CHANCE FISSION

In the following, Y terms are fission mass yields and σ terms are fission cross-sections. Superscripts 1, 2 and 3 refer to first-, second- and third-chance fission of U^{236}, U^{235} and U^{234}, respectively. The absence of a superscript denotes a combination of available stages. First-chance yields were estimated from observed yields as follows: (1) In the region below 13.5-MeV excitation energy of exclusively first-chance fission of the U^{236} compound nucleus, Y^1 is the observed yield Y; (2) In the region below 20.5-MeV initial excitation energy of first- and second-chance fission, the first chance yield is given by

$$Y^1 = (Y\sigma - \langle Y^2\rangle_{av.}\ \sigma^2)/\sigma^1. \tag{1}$$

(3) Above 20.5-MeV initial excitation energy where first-, second- and third-chance fission are possible, the first-chance yield is given by

$$Y^1 = (Y\sigma - \langle Y^2\rangle_{av.}\ \sigma^2 - \langle Y^3\rangle_{av.}\ \sigma^3)/\sigma^1. \tag{2}$$

In Eqs. (1) and (2) the averages are over excitation energies populated below 13.5 MeV and 20.5 MeV, respectively. It was necessary to approximate $\langle Y^2\rangle_{av.}$ and $\langle Y^3\rangle_{av.}$ by $\langle Y^1\rangle_{av.}$ since Y^1 is the only mass yield known in adequate detail. No attempt was made to correct for yields from direct-interaction fissions.

The probabilities of the various possible histories resulting from the U^{236} initial compound nucleus used in averaging Y^1 over the energies of second- and third-chance fission were obtained from Markov chain [8] theory which is applicable since the partial fission widths and partial neutron widths at any state of de-excitation are independent of the previous decay history. In our calculations the populations of 101 states of the system are given by

a 101-dimensional vector. States 1 to 99 are nuclei in one of 99 equal excitation-energy intervals. The system is in state 100 if a nucleus in a previous stage has fissioned, and the system is in state 101 if both neutron emission and fission were energetically impossible for a nucleus in a previous stage. For the initial compound nucleus U^{236} at our fixed irradiation energies, this population vector $\vec{q}^1 = (q_1^1, \ldots, q_{101}^1)$ is simply $\vec{q}^1 = (1, 0, \ldots, 0)$ but the corresponding population vectors $\vec{q}^2$ for U^{235}, $\vec{q}^3$ for U^{234} and $\vec{q}^4$ for U^{233} are to be calculated. The probability of a nucleus being in state j after the first neutron emission is q_j^2 and the conditioned probability $p_{jk}^{2\to3}$ is the probability of such a nucleus in state j contributing to the probability $\vec{q}_k^3$ of state k by means of neutron emission (or fission, or neither). The conditional probabilities are matrix elements of transition matrices $P^{(1\to2)}$, $P^{(2\to3)}$, etc. In terms of these matrices

$$\vec{q}^2 = \vec{q}^1 \; P^{1\to2}$$

$$\vec{q}^3 = \vec{q}^2 \; P^{2\to3} = \vec{q}^1 \; P^{1\to2} \; P^{2\to3}$$

$$\vec{q}^4 = \vec{q}^3 \; P^{3\to4} = \vec{q}^1 \; P^{1\to2} \; P^{2\to3} \; P^{3\to4} \; .$$

The last equations result from the Chapman-Kolmogorov equation $P^{(u\to w)} = P^{(u\to v)} P^{(v\to w)}$ for $u < v < w$. (Only the fission state 100 was needed in $\vec{q}^4$.) This detailed calculation of the decay chain was made at about 1-MeV intervals of initial U^{236} excitation energies over the span of energies under consideration. For each incident energy of the calculations the numbers $\vec{q}_i^2 \, p_{i,100}^{2\to3}$ give the probability of second-chance fission for nuclei in the energy interval i. There are similar expressions for third- and fourth-chance fission. The population vectors $\vec{q}^{(u)}$ are illustrated in Fig. 1 where probabilities have been converted to probability densities by dividing by the span energy of the state. Some of the transitions and conditional probabilities are also illustrated in Fig. 1. States 100 and 101 are not shown.

The conditional probabilities used in the transition matrices depend on the statistical formulation (N = 1 or 3 space co-ordinates for the phase spaces of the transition state, or saddle-point configuration, for fission) and on the level density formula and its parameter. The Fermi-gas level-density formula $\rho(E) = C_a \exp[2(aE)^{\frac{1}{2}}]$ and the constant-temperature level-density formula $\rho(E) = C_T \exp(E/T)$ with the parameters $a_n = 23.4$ MeV^{-1} and $T_n = 0.827$ MeV, respectively, for neutron emission were used with both N = 1 and N = 3. The corresponding parameters a_f and T_f for fission, the fission threshold for the U^{235} compound nucleus and the ratio K of C_a or C_T for neutron emission to C_a or C_T for fission were determined by fits to measured fission cross-sections for 1- to 6-MeV neutron-induced fission of U^{233} [9], U^{234} [9] and U^{235} [10]. Further discussion of the parameters used is given in [7]. Capture cross-sections calculated from an optical model were used [11]. The combinations with the Fermi-gas level-density formula for fission and the constant-temperature level-density formula for neutron emission were not considered; the effect of pairing on the density of fission channels favours the constant-temperature rather than the Fermi-gas level-density formula for fission [12]. The combinations with the constant-temperature level-density formula for fission and the Fermi-gas level-density formula

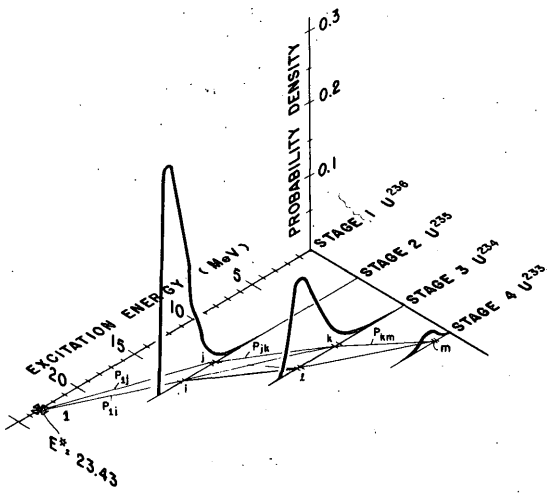

Fig. 1

Population vectors $\vec{q}^2$, $\vec{q}^3$, and $\vec{q}^4$ for an initial U^{236} compound nucleus excitation energy of 23.43 MeV.
Probabilities have been converted to probability densities
by dividing by the common length of the 99 energy intervals.
States 100 (fission) and 101 (neither fission nor neutron emission) are not shown.

for neutron emission resulted in extremely poor agreement between measured and calculated fission cross-sections in the 1- to 6-MeV neutron-energy range, and so were not used for further calculations.

First-chance yields for Ag^{113}, Pd^{112}, Ag^{111} and Pd^{109} for our favoured combination of the number N of space co-ordinates, level-density formula and parameter set are given as an example in Fig. 2. In this example (A), $a_n = 23.4\ MeV^{-1}$ and $a_f = 22.6\ MeV^{-1}$ in the Fermi-gas level-density formula, N = 3, the fission threshold for the U^{235} compound nucleus is $B_f^2 = 6.05$ MeV, and K = 10.5. This and the other combinations of parameter sets that were used are given in Table I.

Although our primary concern is to calculate average yields to use in Eqs. (1) and (2), energies were also averaged over the various possible histories resulting from the U^{236} initial compound nucleus for various initial excitation energies (at nearly 1-MeV intervals from 13.44 to 26.41 MeV) to give average energies for second-chance (U^{235}) and third-chance (U^{234}) fission. Similarly, standard deviations were derived by averaging the square of energies over these probabilities. All the combinations of the number N of space co-ordinates, level-density formulae and parameter sets listed above gave nearly the same average energies plotted in Fig. 3. The largest difference in average energy was 0.3 MeV for second-chance fission with an initial U^{236} excitation energy of 18.45 MeV. The standard deviations are also shown in Fig. 3. Extremes of the standard deviations (high for combination (C) and low for combination (B) are shown for third-chance fission; for lower energies they are nearly all the same for all the combinations (A) to (D) listed above.

The major difference in results for the different combinations of the number N of the space co-ordinates, level-density formula and parameter

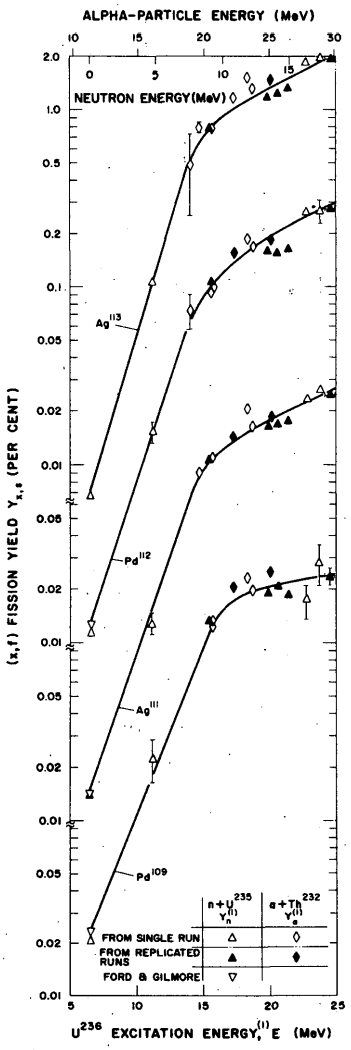

Fig. 2

First-chance fission yields from fission of the U^{236} compound nucleus. These yields were derived from observed yields by the method described in the text with the combination (A) of statistical formulation and parameter sets (see Ref. [7] for further information).

sets is in the fission chance split. The probabilities for second- and third-chance fission for the various combinations are shown in Fig. 4. Further numerical details are available from the authors.

TABLE I

PARAMETER SETS USED

The parameters from fits were derived in Ref. [7] by fits of calculated-to-observed fission cross-sections for neutron-induced fission of U^{233}, U^{234} and U^{235} in the 1- to 6-MeV neutron-energy region of exclusively first-chance fission

Combination letter and plotting symbol	Space co-ordinates assumed N	Level parameter assumed*	Parameters from fits		
			Level parameter*	U^{235} fission threshold (MeV)	Level-density coefficient K
A ———	3	$a_n = 23.4$	$a_f = 22.6$	6.05	10.5
B — — —	1	$a_n = 23.4$	$a_f = 27.0$	6.10	0.747
C — — — —	1	$T_n = 0.827$	$T_f = 0.80$	6.25	5.33
D - - - - - -	3	$T_n = 0.827$	$T_f = 0.80$	6.05	6.93

* Parameters a_n and a_f are in units of MeV^{-1}; T_n and T_f are in MeV.

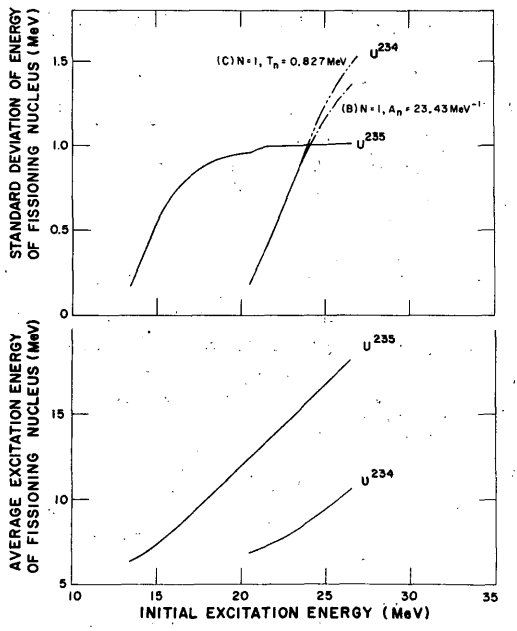

Fig.3

Average energies and standard deviations.
The abscissa is the excitation energy of the original U^{236} compound nucleus.
All the combinations of statistical formulation and parameter sets
of Table I gave nearly the same average energy.
The standard deviations were nearly all the same
except where the extremes are shown for third-chance fission.

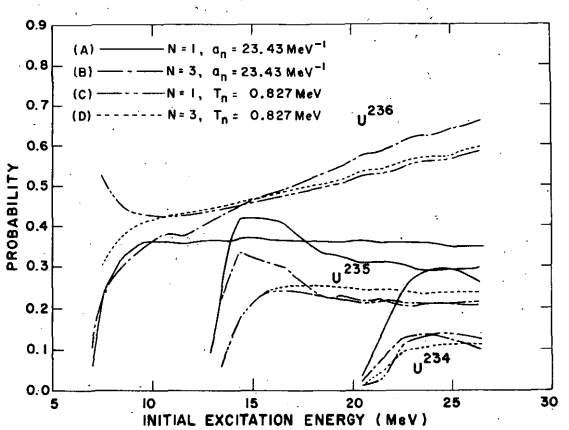

Fig. 4

Probabilities of first-, second- and third-chance fission.

TEST OF THE TWO-MODE-OF-FISSION HYPOTHESIS

It has been shown [1] that the two-mode-of-fission hypothesis implies that fission mass-yield curves (n-tuples of mass yields) lie in a two dimensional subspace of the vector space of n-tuples. This subspace inclusion is also valid for multiples of n-tuples of yields (i.e. necessarily normalized so that their sum is 200%). A linear relation

$$x_{ji} = u_j a_i + w_j b_i, \tag{3}$$

where x_{ji} is the yield of mass number A_i in fission yield curve j (or n-tuple of yields) and u_j and w_j are two other yields from fission yield curve j, was

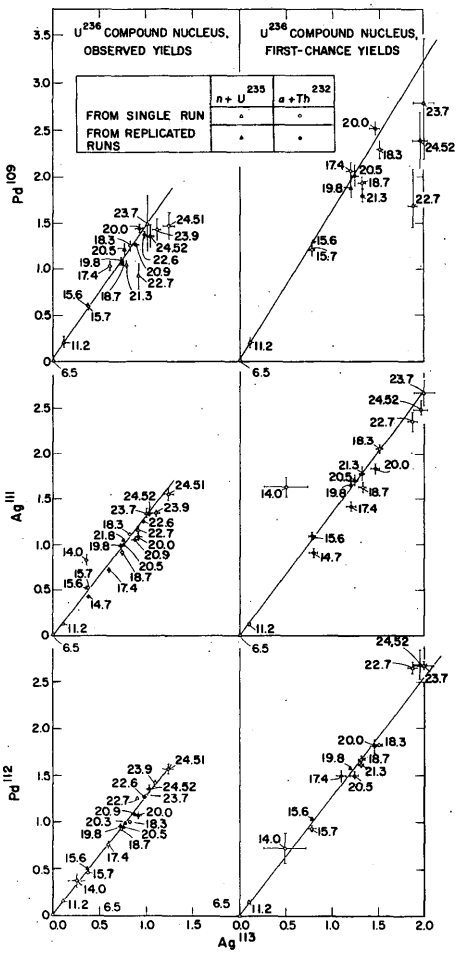

Fig. 5

Plot, based on Eq. (4), to test the two-mode-of-fission hypothesis for the initial U^{236} compound nucleus for both observed and first-chance yields. The numbers are excitation energies in MeV of the initial U^{236} compound nucleus. Thermal-neutron-induced fission of U^{236} has an initial excitation energy of 6.5 MeV.

derived from the subspace inclusion. (The subscript j denotes an irradiation condition.) With the added requirement that the fission mass-yield curves be normalized so that the sum of yields is 200% LEVY et al. [5] showed that the two-mode-of-fission hypothesis implies a linear relation

$$x_{ji} = c_i u_j + d_i \tag{4}$$

between two yields. By then relaxing the normalization requirement they arrive at an equation equivalent to Eq. (3), which they use [5, 6] to test the two-mode-of-fission hypothesis. Our yields are purported to be normalized so we are able to use Eq. (4) in a graphical test of the two-mode-of-fission hypothesis. The graphs, which should be straight lines if the two-mode-of-fission hypothesis holds, are shown in Figs. 5 and 6. The points are

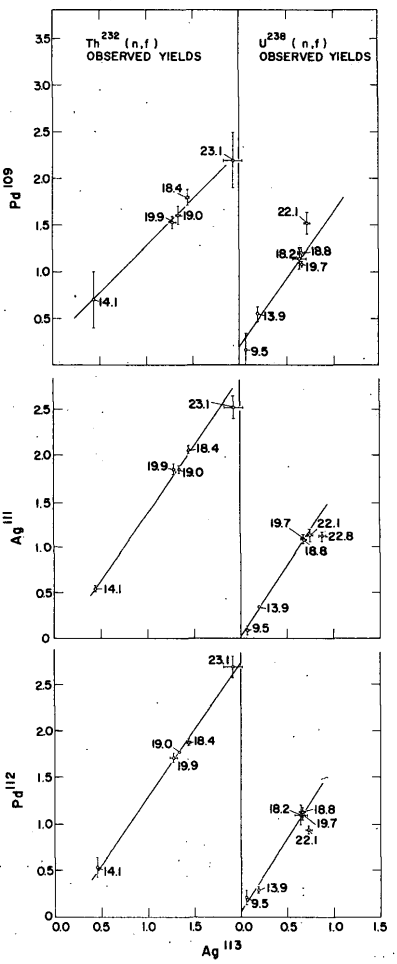

Fig. 6

Plots, based on Eq. (4) to test the two-mode-of-fission hypothesis for neutron-induced fission of Th^{232} and U^{238} for observed yields.

labelled with the excitation energy to provide ready identification with entries in Table I of Ref. [7]. In every case the abscissa u_j is the yield of Ag^{113}. Both observed and first-chance yields are shown for the U^{236} initial compound nucleus. First-chance yields for neutron-induced fission of U^{235} are sufficient to illustrate the situation above 19-MeV excitation energy; only neutron-induced first-chance yields were calculated above 19-MeV excitation energy. First-chance yields above 13-MeV initial excitation energy where second- and third-chance fission are possible were not calculated for neutron-induced fission of Th^{232} and U^{238}.

DISCUSSION

None of the plots show any systematic or significant deviations from linearity except the plots of yields of Pd^{109} for the U^{236} initial compound nucleus[1]. For neutron-induced fission of U^{238} the data for Ag^{111} and Pd^{112} exist in two clusters that may be connected by a line and thus do not provide an adequate test of the two-mode-of-fission hypothesis. For neutron-induced fission of Th^{232} and U^{238} the Pd^{109} data are better distributed and show no trend deviating from linearity such as is shown by Pd^{109} data for the U^{236} initial compound nucleus.

Our points for thermal-neutron-induced fission of U^{235} agree well with the two-mode-of-fission hypothesis in contrast with the results of LEVY et al. [5][2]. The lines in Fig. 5 are the result of least squares calculations based on Eq. (4).

For the U^{236} initial compound nucleus HICKS et al. [6] found significant deviations from linearity for Zn^{72}, Pd^{112}, Cd^{115m}, Cs^{136}, Sm^{153} and Tb^{161}. Of these we have no data for Zn^{72}, Sm^{153} and Tb^{161}. Our data for Cs^{136} and Cd^{115m} are rather sparse, and first-chance yields in the energy region where second- and third-chance fission are possible were not calculated. Our data for Pd^{112} show no significant deviations from linearity; our highest energies are less than those of HICKS et al. [6]. Our first-chance yields for Pd^{109} do not so clearly deviate from linearity as the observed yields; this can partly be attributed to the larger spreads and errors induced by substracting the effect of second- and third-chance yields. All the errors shown are the result of propagation of error from the errors in the observed yields on the assumption that the lower energy first-chance yields occurring in Eqs. (1) and (2) are accurately known. The effect of the replacement of Y^2 and Y^3 in the averages by Y^1 was not included in the error calculation. The remaining possible deviation of Pd^{109} first-chance yields from linearity for the U^{236} initial compound nucleus may possibly be attributed to this, or to errors in normalization. Normalization errors would be expected to affect the other

---

[1] Pd^{109} occurs on the BRITT et al. [4] curve for the symmetric mode at a point down from the maximum by approximately 0.75.

[2] A plot, using Eq. (3), of the data for neutron-induced fission of Pu^{239} in the near-thermal region presented in a paper in Session 3 of this Symposium (COWAN, G., BAYHURST, B.P., PRESTWOOD, R.J., GILMORE, J. S. and KNOBELOCH, G. W., "Symmetry of neutron-induced Pu^{239} fission in resonance region", these Proceedings I), shows no significant deviation from the two-mode-of-fission hypothesis for thermal neutrons.

plots too. HICKS et al.[6] use the three-yield Eq.(3) that does not require normalization. Correction for second- and third-chance fission is feasible with our computer codes only when the yields are normalized.

First-chance yields for combinations (B), (C) and (D) in Table I were in slightly better agreement with the two-mode-of-fission hypothesis than for combination (A) but not sufficiently better to warrant any one of them being chosen over combination (A).

REFERENCES

[1] FORD, G. P., Phys. Rev. 118 (1960) 1261.

[2] TURKEVICH, A. and NIDAY, J. B., Phys. Rev. 84 (1951) 52.

[3] SCHMITT, R. A. and SUGARMAN, N., Phys. Rev. 95 (1954) 1260.

[4] BRITT, H. C. and WHETSTONE, S. L., Jr., Phys. Rev. 133 (1964) B603;
BRITT, H. C., WEGNER, H. E. and GURSKY, J. C., Phys. Rev. 129 (1963) 2239.

[5] LEVY, H. B., HICKS, H. G., NERVIK, W. E., STEVENSON, P. C., NIDAY, J. B. and ARMSTRONG, J. C. Jr., Phys. Rev. 124 (1961) 544.

[6] HICKS, H. G., LEVY, H. B., NERVIK, W. E., STEVENSON, P. C., NIDAY, J. B. and ARMSTRONG, J. C. Jr., Phys. Rev. 128 (1962) 700.

[7] FORD, G. P. and LEACHMAN, R. B., Phys. Rev. 137 (1965) B826.

[8] ROSENBLATT, M., Random Processes, Oxford University Press, New York (1962) 36.

[9] ALLEN, W. D. and HENKEL, R. L., Progr. nucl. Energy 2 (1958) 1.

[10] SMITH, H. L., SMITH, R. K. and HENKEL, R. L., Phys. Rev. 125 (1962) 1329;
PANKRATROV, V. M., VLASOV, N. A. and RYBAKOV, B. V., Atomnaja energija 9 (1960) 399. (Translation: Soviet J. atomic Energy 9 (1960) 939.

[11] BEYSTER, J. R., SCHRANDT, R. G. and WALT, M., Los Alamos Scientific Laboratory Report, LA-2099 (1956) (unpublished). Unpublished calculations with extrapolations of these optical model parameters have been made by BLUMBERG, L. and MATTHEWS, J.

[12] GRIFFIN, J. J., Phys. Rev. 132 (1963) 2204; and private communication (1963).

SYMMETRY OF NEUTRON-INDUCED Pu^{239} FISSION IN RESONANCE REGION

G. COWAN, B.P. BAYHURST, R.S. PRESTWOOD, J.S. GILMORE AND G.W. KNOBELOCH
LOS ALAMOS SCIENTIFIC LABORATORY, UNIVERSITY OF CALIFORNIA, LOS ALAMOS, N. MEX., UNITED STATES OF AMERICA

Abstract — Résumé — Аннотация — Resumen

SYMMETRY OF NEUTRON-INDUCED Pu^{239} FISSION IN RESONANCE REGION. Symmetry of fission produced in Pu^{239} by time-of-flight energy-resolved neutrons has been radiochemically measured in the resonance region by a neutron time-of-flight method, called the "wheel" method, which has been described previously.

Data were obtained from 200 eV to 600 eV in energy intervals ranging from 10 eV to 25 eV in width, containing 3 to 12 resonances per sample. Both increases and decreases in symmetry of fission were observed as compared with thermal-neutron fission of Pu^{239}. Measured by the ratio of Cd^{115}, a "valley" fission product, to Mo^{99}, a "peak" fission product, the symmetric yield decreased by 18% at 250±4 eV, 29% at 307±5 eV and 33% at 395±6 eV. The symmetric yield increased by 16% at 206 eV. The average symmetry of fission over the energy region 196 eV to 585 eV showed a decrease of 8% from the thermal value. Changes in the ratio Ag^{111}/Mo^{99} appeared to be about one-third as great as changes in the Cd^{115}/Mo^{99} ratio from level to level.

The ratio Ba^{140}/Mo^{99} showed no systematic changes from the thermal value within analytical error and the average is within 1% of the thermal ratio, which permits the assumption that Mo^{99} and Ba^{140} yields are not variable for resonance fission and are the same as in thermal fission.

SYMÉTRIE DE LA FISSION DE ^{239}Pu INDUITE PAR DES NEUTRONS DANS LA REGION DE RÉSONANCE. Les auteurs ont procédé à la mesure radiochimique de la symétrie de la fission de ^{239}Pu produite par des neutrons dans la région de résonance, à l'aide d'une méthode du temps de vol des neutrons, déjà décrite par les auteurs dans un article de revue.

Les données ont été obtenues dans la gamme de 200 eV à 600 eV pour des intervalles d'énergies de 10 à 25 eV en largeur, contenant de 3 à 12 résonances par échantillon. Les auteurs ont observé à la fois les augmentations et les diminutions dans la symétrie de la fission par rapport à la fission de ^{239}Pu par neutrons thermiques. Le rendement symétrique, mesuré par le rapport entre ^{115}Cd (produit de fission de la «vallée») et ^{99}Mo (produit de fission du «sommet»), a diminué de 18% à 250±4 eV, de 29% à 307 ± 5 eV et de 33% à 395±6 eV. Le rendement symétrique a augmenté de 16% à 206 eV. La symétrie de fission moyenne pour la région des énergies allant de 196 eV à 585 eV a accusé une diminution de 8% par rapport à la valeur correspondante pour la fission par neutrons thermiques. Les variations du rapport ^{111}Ag/^{99}Mo semblent être d'un tiers plus grandes que le rapport ^{115}Cd/^{99}Mo d'un niveau à l'autre.

Le rapport ^{140}Ba/^{99}Mo n'a accusé aucune variation systématique par rapport à la valeur correspondante pour la fission par neutrons thermiques, dans la limite de l'erreur analytique, et la moyenne est égale, à 1% près, au rapport de fission par neutrons thermiques, ce qui autorise l'hypothèse selon laquelle les rendements de ^{99}Mo et de ^{140}Ba ne sont pas variables pour la fission par neutrons de résonance et sont les mêmes que dans la fission par neutrons thermiques.

СИММЕТРИЯ ВЫЗВАННОГО НЕЙТРОНАМИ ДЕЛЕНИЯ ПЛУТОНИЯ-239 В ОБЛАСТИ РЕЗОНАНСА. Симметрия деления, произведенная в плутонии-239 нейтронами, разрешенными энергией по времени пролета, измерена радиохимическими методами и способами в области резонанса методом по времени пролета нейтронов в качестве дублирования метода "колеса", описанного ранее.

Были получены данные от 200 до 600 эв в интервалах энергии от 10 до 25 эв по ширине, причем в каждом из интервалов содержалось от 3 до 12 резонансов для каждого образца. Наблюдались как увеличение, так и уменьшение симметрии деления по сравнению с делением плутония-239 под действием тепловых нейтронов. Симметричный выход, измеренный на основании соотношения между кадмием-115, являющимся продуктом деления у "минимума", и молибденом-99, являющимся продуктом деления у "максимума", уменьшался на 18% при

250 ± 4 эв, на 29% при 307 ± 5 эв и на 33% при 395 ± 6 эв. При энергии 206 эв симметричный выход увеличивался на 16%. При средней симметрии деления в диапазоне энергии 196–585 эв имело место уменьшение на 8% по сравнению с величиной, полученной под действием тепловых нейтронов. Изменения в соотношении серебро-111/молибден-99, по-видимому, в три раза меньше, чем изменения в соотношении кадмий-115/молибден-99 при переходе от одного уровня к другому.

Соотношение барий-140/молибден-99 не указывает на систематические изменения по сравнению с величиной, полученной под действием тепловых нейтронов, в пределах аналитической погрешности, и среднее значение его лежит в пределах 1% отклонений от соотношения, полученного под действием тепловых нейтронов, что дает возможность предположить, что выходы молибдена-99 и бария-140 не изменяются при резонансном делении и остаются такими же, как и при делении под действием тепловых нейтронов.

SIMETRIA DE LA FISION DE ^{239}Pu INDUCIDA POR NEUTRONES EN LA REGION DE RESONANCIA. Los autores midieron por vía radioquímica, en la región de resonancia, la simetría de la fisión inducida en el ^{239}Pu por neutrones cuyo espectro energético se resolvía por el método del tiempo de vuelo; para ello utilizaron el procedimiento denominado de la "rueda", ya descrito con anterioridad.

Se obtuvieron datos entre 200 eV y 600 eV, en intervalos de energía del orden de 10 a 25 eV de amplitud, que corresponden a un número de resonancias por muestra comprendido entre 3 y 12. En comparación con la fisión del ^{239}Pu inducida por neutrones térmicos, se observaron tanto aumentos como disminuciones de la simetría de fisión. Tomando como referencia la razón entre ^{115}Cd, producto de fisión correspondiente al "valle", y ^{99}Mo, producto de fisión correspondiente a la "cresta", el rendimiento simétrico disminuyó en 18% a 250 ± 4 eV, en 29% a 307 ± 5 eV y en 33% a 395 ± 6 eV. El rendimiento simétrico aumentó en 16% a 206 eV. La simetría media de fisión en el intervalo de energía comprendido entre 196 y 585 eV, mostró una disminución de 8% respecto al valor térmico. Las variaciones de la razón ^{111}Ag/^{99}Mo fueron aproximadamente un tercio de las experimentadas por la razón ^{115}Cd/^{99}Mo entre un nivel y otro.

Dentro de los límites del error analítico, la razón ^{140}/^{99}Mo no presentó variaciones sistemáticas respecto al valor térmico y el valor medio no difirió más de 1% de la razón térmica, lo que permite suponer que los rendimientos de ^{99}Mo y ^{140}Ba son invariables para la fisión por resonancia, e iguales a los encontrados en la fisión térmica.

Neutrons from a small nuclear device exploded on 29 April, 1964, have been used to examine the symmetry of Pu^{239} fission in the resonance region. The principles of the experimental technique used have been described in detail elsewhere [1, 2]. Briefly, fissile material is revolved rapidly past a collimating slit that defines a beam of neutrons resolved in energy by flight through a long, evacuated pipe. Fissions in various parts of the wheel are caused by neutrons in a known energy group and can be examined by radiochemical means for changes in symmetry.

The isotope Pu^{239} has a ground state spin $\frac{1}{2}+$. For s-wave neutron absorption, the compound nuclear states leading to fission are 0+ and 1+. It has been reported [3] that fission at the 0.297-eV resonance in Pu^{239} produces five times less symmetric fission than is observed in thermal fission. If this effect on symmetry is due to spin, it may be expected that resonances of the other possible spin, if they are large enough and sharp enough to be characterized as resonances, will have some other characteristic symmetry. At low excitations fission may occur through a predominantly 0+ channel with a symmetric α_3-vibrational wave function that permits a symmetric mode of fission. It may be possible to build a 1+ state at low excitation energy, not involving a single particle state, for which symmetric fission should be forbidden [4]. The present investigation was undertaken principally

to investigate further the applicability of channel analysis of fission in predicting symmetry of fission at individual resonances [5, 6, 7]. Other measurements with U^{235} [1, 2] and U^{233} [8] have indicated, in general, that differences exist in the frequency of symmetric fission at various resonances. The hypothesis that such differences are related to spin and might fall into two more or less well-defined groups, according to the spin of the nuclear state, has not yet been adequately tested.

EXPERIMENTAL PROCEDURE

A 60-cm diam. wheel with 0.038-cm-thick Pu^{239} metal fastened to the outer third of the wheel face was revolved past a tapered steel collimating slit 10-cm long and 0.2-cm wide at a distance of 2.630×10^4 cm from the source. The velocity of the wheel at the outer edge of the beam was 8909 cm/s. Under the conditions of this experiment the distance at which neutrons of a given energy fall measured along the rim of the plutonium metal is given by the equation

$$S = 169.3/E^{\frac{1}{2}}$$

where S is in centimetres and E is in electron-volts.

The collimating slit width defined an exposure time or channel width of 22.4 μs. The pulse width at the source was almost negligible compared with this interval. Thus the energy resolution corresponded to 0.09 μs/m. At 100 eV and 200 eV, for example, the time interval defined by the slit corresponds to resolutions of 2.4 eV and 6.7 eV respectively. The level spacing in Pu^{239} is approximately 2 eV. A composite lead, iron and polyethylene moderator was placed near the source. It was designed to produce $> 10^9 n/cm^2$-eV below 100 eV at the wheel, adequate for the resolution of single levels.

The wheel was recovered immediately after the event and the location of the resonance band was established by contact autoradiography on X-ray film. The autoradiograph of the relevant portion of the wheel was fastened to the metal and the regions of maximum and minimum contrast were sheared in strips of ~0.2-cm maximum width, corresponding to the collimating slit width. The metal was cleaned, dissolved and analysed for Mo^{99} and Ba^{140}, "peak" fission productions, and Ag^{111} and Cd^{115}, "valley" fission products.

EXPERIMENTAL RESULTS

Experimental data

The sample schedule and results are summarized in Table I. Background corrections are shown in Fig. 1 and discussed below. The ratios "r" indicate the ratio of Cd^{115} or Ag^{111} activity to Mo^{99} activity at a given neutron energy. The Pu^{239} thermal ratios, r_{th}, are 2.175×10^{-2} for

TABLE I

EXPERIMENTAL DATA

Sample Number	Mo^{99} obs c/m/g	S From middle of t_0 line (cm)		E n (ev)	Mo^{99} bkgd c/m/g Res	Mo^{99} bkgd c/m/g Fast	Mo^{99} corr c/m/g	Ag^{111} obs c/m/g	Ag^{111} bkgd c/m/g Res	Ag^{111} bkgd c/m/g Fast	Ag^{111} corr c/m/g	$r_{Ag^{111}/Mo^{99}}$ (units of 10^{-2})	Cd^{115} obs c/m/g	Cd^{115} bkgd c/m/g Res	Cd^{115} bkgd c/m/g Fast	Cd^{115} corr c/m/g	$r_{Cd^{115}/Mo^{99}}$ (units of 10^{-2})	$(r_{corr}/r_{th})_{Ag/Mo}$	$(r_{corr}/r_{th})_{Cd/Mo}$
1	20600	12.10	11.88	199	3350	360	16890	406	66	11	329	1.95	428	58	13	357	2.11	0.90	1.10
2	23360	---	11.73	206	3380	390	19590	448	66	12	370	1.89	508	58	15	435	2.22	0.87	1.16
3	23070	---	11.53	212	3410	450	19210	490	67	14	409	2.14	453	59	17	377	1.96	0.98	1.03
4	27870	---	11.33	219	3440	540	23890	545	67	17	461	1.93	509	59	20	430	1.800	0.89	0.94
5	32200	---	11.18	226	3470	650	28080	624	68	20	536	1.916	636	60	24	552	1.966	0.88	1.03
6	40390	---	11.01	233	3490	810	36000	785	68	25	692	1.922	769	60	30	679	1.886	0.88	0.99
7	46520	---	10.82	241	3530	950	42040	947	69	30	848	2.017	826	61	35	730	1.736	0.93	0.91
8	55740	---	10.65	249	3550	1120	51070	1100	70	35	995	1.948	905	61	42	802	1.570	0.90	0.82
9	77280	---	10.51	256	3580	1470	72230	1569	70	46	1453	2.012	1267	62	55	1150	1.592	0.93	0.83
10	103210	---	10.35	264	3600	1890	97720	2233	71	59	2103	2.152	1821	62	70	1689	1.728	0.99	0.90
11	134390	---	10.16	273	3630	2330	128430	2796	71	73	2652	2.065	2502	62	87	2353	1.837	0.95	0.96
12	116870	---	10.04	281	3650	2090	111100	2466	72	65	2329	2.096	2353	63	78	2212	1.991	0.96	1.04
13	75460	---	9.91	288	3680	1470	70310	1580	72	46	1462	2.079	1520	63	55	1402	1.994	0.96	1.04
14	72330	---	9.75	297	3700	1370	67260	1372	72	43	1257	1.869	1159	64	51	1044	1.552	0.86	0.81
15	65570	---	9.59	307	3730	1250	60590	1286	73	39	1174	1.938	939	64	47	828	1.366	0.89	0.71
16	49710	---	9.42	317	3760	990	44960	921	74	31	816	1.815	782	65	37	680	1.512	0.83	0.79
17	41350	---	9.28	328	3780	830	36740	838	74	26	758	2.008	682	65	31	586	1.594	0.92	0.83
18	35690	---	9.06	341	3820	710	31160	704	75	22	607	1.949	593	66	26	501	1.608	0.90	0.84
19	39570	---	8.90	356	3840	790	34940	740	75	25	640	1.832	691	66	29	596	1.706	0.84	0.89
20	42140	---	8.74	369	3870	840	37430	805	76	26	703	1.878	823	67	31	725	1.937	0.86	1.01
21	43330	---	8.61	381	3890	870	38570	823	76	27	720	1.867	815	67	32	716	1.856	0.86	0.97
22	47380	---	8.44	395	3920	940	42520	819	77	29	713	1.677	648	67	35	546	1.284	0.77	0.67
23	52230	---	8.25	412	3950	950	47330	970	77	30	863	1.823	751	68	35	648	1.369	0.84	0.72
24	38320	---	8.01	434	3990	730	33600	767	78	23	666	1.983	695	69	27	599	1.783	0.91	0.93
25	37980	---	7.89	454	4010	720	33250	818	79	22	717	2.156	648	69	27	552	1.660	0.99	0.87
26	37700	---	7.75	469	4030	720	32950	771	79	22	670	2.033	721	69	27	625	1.897	0.93	0.99
27	32800	7.68	7.52	496	4070	650	28080	641	80	20	541	1.927	596	70	24	502	1.788	0.89	0.94
28	28270	---	7.31	522	4110	560	23600	563	81	17	465	1.970	509	71	21	417	1.767	0.91	0.92
29	33970	---	7.14	549	4130	610	29230	734	81	19	634	2.169	661	72	23	566	1.936	1.00	1.00
30	29490	---	7.00	574	4160	590	24740	646	82	18	546	2.207	608	73	22	513	2.073	1.01	1.08
31	7870	3.27	3.10	2800	4800	160	2910	171	96	5	70	2.405	162	94	6	62	2.130	1.11	1.11
32	8530	1.50	1.34	14400	5500	170	2860	192	110	5	77	2.693	207	110	6	91	3.182	1.24	1.66
33	9370	1.06	0.92	29700	6300	190	2880	222	120	6	96	3.333	237	130	7	100	3.472	1.53	1.82
34	14260	0.63	0.42	---	---	---	---	322	---	---	---	---	366	---	---	---	---	---	---
35	122900	0.09	- 0.09	---	---	---	---	---	---	---	---	---	---	---	---	---	---	---	---
36	7790	- 0.4	- 0.6	---	---	---	---	204	---	---	---	2.618	265	---	---	---	3.402	1.56	1.78
37	3580	- 10.5	- 10.7	---	---	---	---	67.8	---	---	---	1.893	54.5	---	---	---	1.522	0.87	0.80
38	2210	+ 18.8	+ 19	---	---	---	---	39.3	---	---	---	1.778	37.9	---	---	---	1.715	0.82	0.90
39	800	180^0 from t_0		---	---	---	---	[11.2]	---	---	---	[1.40]	[< 12]	---	---	---	[< 1.5]	[0.64]	[< 0.8]

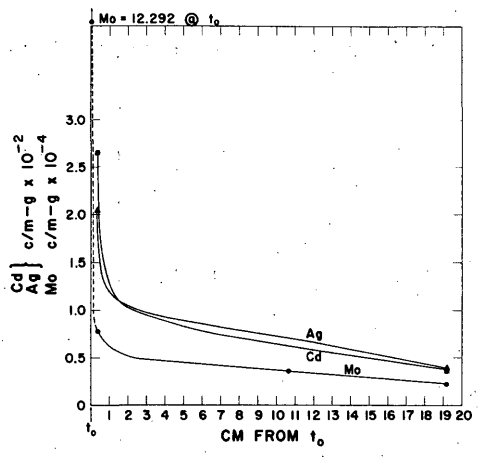

Fig. 1

"General" background correction curve

Ag^{111}/Mo^{99} and 1.911×10^{-2} for Cd^{115}/Mo^{99}. No data were obtained at energies below 200 eV due to an unexpectedly high acceleration of the moderator by nuclear shock, leading to a neutron spectrum in the laboratory frame-of-reference that peaked at about 300 eV, and was cut off absolutely at 200 eV. Therefore single levels were not resolved in this experiment. The probable number of levels included in each sample varied from 3-4 at 200 eV to 10-12 at 600 eV.

The fraction of Pu^{239} converted by fission versus neutron energy in the resonance region is presented in Fig. 2 together with the Pu^{239} fission cross-section taken from the Karlsruhe compilation [9]. The corrected activity ratios for Cd^{115} to Mo^{99} normalized to the same ratio measured for thermal fission in Pu^{239}, i.e. $(r_{corr}/r_{th})_{Cd/Mo}$, versus neutron energy in the resonance regions, are presented in Fig. 3.

Background corrections

The background fissions in each sample were caused by neutrons that can be characterized in three groups:

(1) Scattered neutrons from the transmitted beam striking surrounding materials;

(2) Fast neutrons from fission induced in the Pu^{239} by resonance neutrons;

(3) "Bad" neutrons from pipe walls, etc.

The effect of scattered neutrons that produce a general "fog" is responsible for the principal source of unwanted fissions. These neutrons appear to be in the resonance region. From measurements made on the portions of the wheel that were not exposed directly to any part of the neutron beam, a curve of "general" background versus position on the wheel was constructed (Fig. 1), and a correction was made for scattered neutrons originating chiefly in the steel wheel and adjacent hardware. The correction

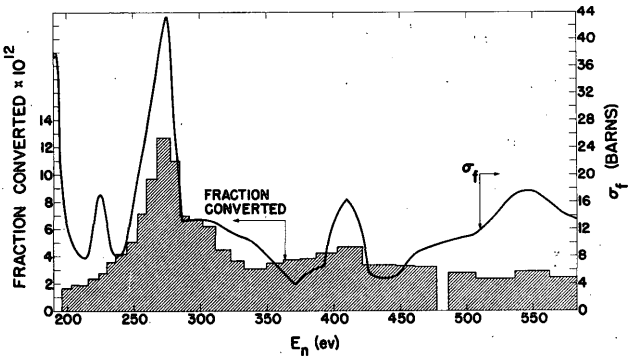

Fig. 2

Plot of fraction of Pu^{239} converted by fission in each sample versus neutron energy.
The fission excitation function is shown for comparison.
Width of individual sample cut is shown by width of horizontal bars in the bar graph.

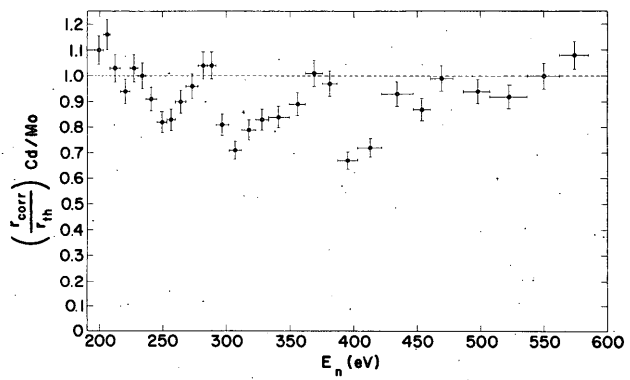

Fig. 3

The ratio of Cd^{115} activity to Mo^{99} activity, normalized to the same ratio for thermal fission in Pu^{239}, is plotted versus neutron energy. The horizontal bar indicates width of sample cut and the vertical bar indicates the estimated standard error in the measurement of the activity ratio.

was made iteratively since it was necessary to estimate average yields for Ag^{111} and Cd^{115} for fission in the resonance energy region, and to assume that resonance neutrons scattered back to the wheel would still be in the resonance region. Since the correction is no more than 10% of total activity observed in regions of greatest interest and a corresponding correction is made to observed Mo^{99} activity, the Ag^{111}/Mo^{99} and Cd^{115}/Mo^{99} corrected ratios are not very sensitive to the exact Ag^{111} and Cd^{115} yields chosen for background fission. The relative yields in the resonance region used for the correction were 0.9 of the Pu^{239} thermal fission values. The yield values used in the keV region were somewhat higher and are indicated in Fig. 2.

The effect of fast neutrons (for which the appropriate $(r_{fast}/r_{th})_{Ag/Mo}$ is taken as 1.43 and the appropriate $(r_{fast}/r_{th})_{Cd/Mo}$ is taken as 1.95) has been

estimated by means of a Monte Carlo calculation. The calculation indicated that the following correction applies:

$$F_{sec} = 1.52 \times 10^{-2} F_{P1} + 8.2 \times 10^{-4} (F_{P2L} + F_{P2R}) + 4.6 \times 10^{-4} (F_{P3L} + F_{P3R})$$

$$+ 3.2 \times 10^{-4} (F_{P4L} + F_{P4R}) + 2 \times 10^{-4} (F_{P5L} + F_{P5R})$$

where F_{P1} indicates resonance fissions in the sample itself; F_{P2L} and F_{P2R} indicate resonance fission on the immediately adjoining sample on the left and right respectively; F_{P3L} and F_{P3R} indicate the next adjoining samples, etc.

The effect of non-collimated neutrons scattered from the walls of the pipe was minimized by baffles along the walls and no correction has been applied.

Ba^{140} data

In addition to the tabulated data, Ba^{140} analyses on all samples showed an average activity ratio to Mo^{99} of 0.365 in the resonance region compared to a thermal ratio of 0.373, with a spread no greater than the analytical error. Based on this observation, the assumption is made that Mo^{99} and Ba^{140} yields are the same as in thermal fission; if their yields varied, it would be necessary to assume that they varied the same way and by the same amount, which seems unlikely.

DISCUSSION

Measured by the changes in the Cd^{115}/Mo^{99} activity ratio, the symmetric yield decreased by 18% at 250± 4 eV, 29% at 307 ± 5 eV, and 33% at 395 ± 6 eV. In the energy region 200-600 eV the symmetric yield is significantly greater than the thermal yield only at 206 eV (16%).

The Ag^{111} yield over the resonance region is more nearly constant than is the Cd^{115} yield. In the region of minimum Cd^{115} yield the yield of Ag^{111} is also lower than its average resonance value by an amount that is about one-third of the effect on Cd^{115}.

The Cd^{115}/Mo^{99} activity ratio, averaged over all samples in the resonance region, is 0.92 of the Pu^{239} thermal fission ratio. The Ag^{111}/Mo^{99} activity ratio, similarly averaged, is 0.91 of the thermal fission ratio.

If it is assumed that variations in the Cd^{115} yield are due to variations in the proportions in each sample of fission produced at two different kinds of resonances, attempts can be made to estimate the relative proportions of each of the two kinds of levels. One must further assume that each of the two kinds of levels has a characteristic value for $r_{Cd/Mo}$ that will be designated r_{min} and r_{max} respectively. The value of r_{min}/r_{th} may be as low as 0.2 at levels for which symmetric fission is forbidden [3] and, based on an extrapolation of the highest observed values, perhaps as high as 1.6 of the thermal value for levels at which symmetric fission is allowed. The

fraction of fission, X, that occurs in the less symmetric mode in any sample will be given by

$$X = \frac{1-(r_{obs}/r_{max})}{1-(r_{min}/r_{max})} .$$

If r_{max} and r_{min} are as assumed, X will have a maximum value of 0.67 at 395 eV in a cut containing about eight levels, and a minimum value of 0.32 at 206 eV in a cut containing about three levels. The value of X averaged over the entire region from 200 to 600 eV is 0.5. Assumptions on r_{max} and r_{min} that result in values of X as large as 0.6 or as small as 0.3 are somewhat less consistent with observations of the average yield values in each cut. Therefore it is reasonable to assume that these measurements indicate that the contribution from levels with the less symmetric mode of fission is about the same as the contribution from the more symmetric mode.

REFERENCES

[1] COWAN, G.A., TURKEVICH, A., BROWNE, C.I. and Los Alamos Radiochemistry Group, Phys. Rev. 122 (1961) 1286.
[2] COWAN, G.A., BAYHURST, B.P. and PRESTWOOD, R.J., Phys. Rev. 130 (1963) 2380.
[3] REGIER, R.B., BURGUS, W.H., TROMP, R.L. and SORENSEN, B.H., Phys. Rev. 119 (1960) 2017.
[4] GRIFFIN, J., private communication.
[5] BOHR, A., Proc. Int. Conf. PUAE 2 (1956) 151.
[6] WHEELER, J.A., Physica 22 (1956) 1103.
[7] WILETS, L., Fission Proceedings of the Rehovoth Conference on Nuclear Structure, North Holland Publishing Company, Amsterdam (1958) 122.
[8] REGIER, R.B., BURGUS, W.H. and TROMP, R.L., Phys. Rev. 113 (1959) 1589.
[9] SCHMIDT, J.J., Neutron Cross Sections for Fast Reactor Materials, Kernforschungszentrum, Karlsruhe (1962).

SOME YIELDS IN THE THERMAL-AND EPI-CADMIUM-NEUTRON FISSION OF Pu^{239}

I.F. CROALL AND H.H. WILLIS
CHEMISTRY DIVISION, ATOMIC ENERGY RESEARCH ESTABLISHMENT, HARWELL, DIDCOT, BERKS, UNITED KINGDOM

Abstract — Résumé — Аннотация — Resumen

SOME YIELDS IN THE THERMAL- AND EPI-CADMIUM-NEUTRON FISSION OF Pu^{239}. The yields of several nuclides in the thermal- and epi-cadmium-neutron fission of Pu^{239} have been measured and are reported. In epi-cadmium-neutron fission a decrease, relative to thermal fission, in the yields of Ag^{111} and Ag^{113}, i.e. an increased peak-to-valley ratio, was found. The yield of As^{77} and As^{78}, which represent highly unsymmetrical fission, were found to be greater in epi-cadmium-neutron fission than in thermal fission. This result is shown to be inconsistent with the simple two mode of fission hypothesis.

QUELQUES RENDEMENTS DE LA FISSION DE ^{239}Pu PAR DES NEUTRONS THERMIQUES ET ÉPI-CADMIQUES. Les auteurs indiquent les rendements en plusieurs nucléides de la fission de ^{239}Pu par des neutrons thermiques et épicadmiques. Ils ont observé une diminution des rendements en ^{111}Ag et ^{113}Ag dans la fission des neutrons épicadmiques par rapport à la fission par neutrons thermiques, c'est-à-dire une augmentation du rapport entre les valeurs «sommet» et «vallée». Ils ont établi que les rendements en ^{77}As et ^{78}As, qui résultent d'une fission fortement asymétrique, sont plus élevés dans la fission par neutrons épicadmiques que dans la fission par neutrons thermiques. Il est apparu que ce résultat ne concorde pas avec l'hypothèse simple des deux modes de fission.

НЕКОТОРЫЕ ВЫХОДЫ ДЕЛЕНИЯ ПЛУТОНИЯ-239 ПОД ДЕЙСТВИЕМ ТЕПЛОВЫХ И ЗАКАДМИЕВЫХ НЕЙТРОНОВ. Сообщается об измерениях выходов ряда нуклеидов при делении плутония-239 под действием тепловых и закадмиевых нейтронов. При делении под действием закадмиевых нейтронов было обнаружено уменьшение выходов серебра-111 и серебра-113 по сравнению с выходом под действием тепловых нейтронов; иными словами, было обнаружено увеличение соотношения между максимумом и минимумом. Было обнаружено, что выходы мышьяка-77 и мышьяка-78, являющихся примером чрезвычайно асимметричного деления под действием закадмиевых нейтронов, оказываются превышающими выходы, полученные при делении под действием тепловых нейтронов. Указывается, что этот результат несовместим с простой теорией двойственного вида деления.

RENDIMIENTO DE ALGUNOS NUCLIDOS EN LA FISION DEL ^{239}Pu POR NEUTRONES TERMICOS Y EPICADMICOS. Los autores han medido los rendimientos de varios núclidos en la fisión del ^{239}Pu por neutrones térmicos y epicádmicos. En este último tipo de fisión han observado, en comparación con la inducida por neutrones térmicos, una disminución del rendimiento de ^{111}Ag y de ^{113}Ag, esto es, un aumento de la razón cresta a valle. Los rendimientos de ^{77}As y de ^{78}As, que representan una fisión sumamente asimétrica, han resultado más elevados en la fisión provocada por neutrones epicádmicos que en la inducida por neutrones térmicos. Se demuestra que este resultado es incompatible con la hipótesis simple de fisión binaria.

INTRODUCTION

The yields of several nuclides from the fission of Pu^{239} by thermal and epi-cadmium neutrons are reported. These measurements were undertaken to fill some gaps in the mass yield curve of Pu^{239} thermal-neutron fission and to provide some information on the way these yields change with a small increase in the incident neutron energy. These experiments were

also intended to calibrate the counting system for work at present in progress on yields from the thermal-neutron fission of Pu^{241}.

EXPERIMENTAL

All irradiations were carried out in the pneumatic "rabbit" assembly in the graphite-moderated reactor BEPO. Samples of plutonium oxide wrapped in 0.01-in-thick aluminium foil, sealed in silica ampoules, were used for the total (thermal-neutron) yields. For the epi-cadmium neutrons the aluminium foil packet was placed inside a cadmium box of average wall thickness 1 mm, and the whole sealed in a silica ampoule for irradiation.

After irradiation and a suitable cooling period the aluminium foil and plutonium oxide were dissolved prior to radiochemical separation of the desired activities. The separation and purification schemes used in this work are described in Ref. [10]. In all experiments Mo^{99} was determined for use as a reference to which all other yields were referred. To eliminate as many as possible of the corrections usually required in radiochemical work all yields were measured in terms of an R-value defined by

$$R = \frac{(Yi/Y_{Mo})_1}{(Yi/Y_{Mo})_2},$$

where (Yi/Y_{Mo}) is the ratio of the yield of the nuclide i to the yield of Mo^{99} in a given type of fission process. For example, subscript 1 refers to epi-cadmium-neutron fission of Pu^{239} and subscript 2 to thermal-neutron fission of Pu^{239} for most of the nuclides considered in this work. Exceptions are the determinations of the yields of As^{77}, As^{78} and Br^{83}. Here subscript 2 refers to U^{235} thermal-neutron fission and subscript 1 to either thermal- or epi-cadmium-neutron fission of Pu^{239}.

To avoid confusion, R-values in which 2 refers to Pu^{239} thermal-neutron fission will be labelled R_p and those based on U^{235} thermal-neutron fission will be called R_u.

The only corrections necessary to obtain the R-values from the observed counting-rates are those for self-absorption and back-scattering in the counting samples, for chemical yield in the separation procedure, and for growth and decay during and after the irradiation. In particular, no corrections are necessary for the absolute efficiency of the counting system.

The radiochemically purified samples were counted on an end-window gas-flow proportional counter using pure methane gas. Decay curves were followed automatically, over several half-lives of the longest-lived component wherever possible. Counting data was recorded directly onto punched cards using the AERE 3016 Readout Scaler System [1], and the decay curves analysed on an IBM 7030 (Stretch) computer. The analysis programme, EVA 2, is a modified version of the programme CODA reported previously [2].

Self-absorption and back-scattering corrections were made using calibration curves prepared for the same counters as used in this work [3]. In all cases samples were corrected to the activity equivalent to 10 mg of precipitate on the counting tray.

TABLE I

R_u-VALUES FOR As^{77}, As^{78} AND Br^{83} IN Pu^{239} FISSION

	Thermal-neutron fission	Epi-cadmium-neutron fission
As^{77}	0.900 ± 0.042	1.655 ± 0.079
As^{78}	1.352 ± 0.073	1.80 ± 0.09
Br^{83}	0.587 ± 0.048	0.622 ± 0.046

TABLE II

R_p VALUES FOR YIELDS IN THE EPI-CADMIUM-NEUTRON FISSION OF Pu^{239}

Sr^{89}	1.026 ± 0.018
Zr^{95}	1.025 ± 0.052
Zr^{97}	1.052 ± 0.038
Ag^{111}	0.93 ± 0.04
Ag^{113}	0.720 ± 0.046
Ce^{141}	1.040 ± 0.024
Ce^{143}	1.011 ± 0.021

RESULTS

A minimum of three separate determinations of each of the parameters involved in any given R-value were made. The errors quoted on the R-values are estimated over-all standard deviations, i.e. they include possible errors in half-lives, and self-absorption and back-scattering corrections wherever possible.

Table I shows the R_u-values for the nuclides As^{77}, As^{78} and Br^{83}. R-values for all other nuclides were referred to the thermal-neutron fission of Pu^{239}, and these results are presented in Table II.

In order to convert these R-values to fission yields it is necessary to assume certain standard yields. The yield of Mo^{99} in the thermal-neutron fission of U^{235} was taken as 6.06% [4]. The yield of Mo^{99} in the thermal-neutron fission of Pu^{239} was taken as 0.966% of the yield in U^{235} thermal fission, i.e. 5.86% [5]. For the epi-cadmium-neutron fission of Pu^{239} the Mo^{99} yield was also taken as 5.86% [5].

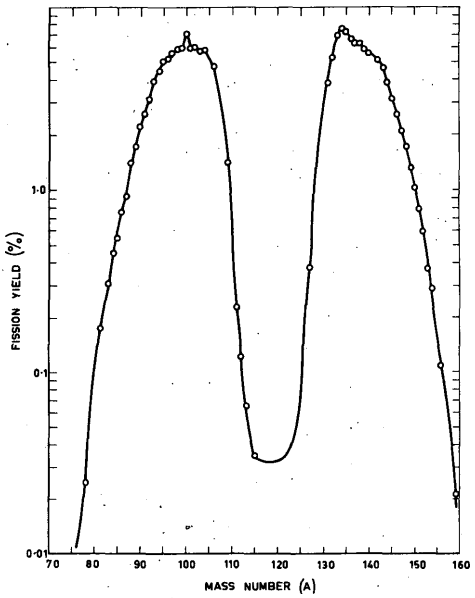

Fig. 1

Mass yield curve for thermal-neutron fission of Pu^{239}

To convert the arsenic and bromine R-values the following yields in the thermal-neutron fission of U^{235} were assumed: As^{77} 0.0083%, As^{78} 0.02% and Br^{83} 0.51% [4].

For the yields measured as R_p-values the thermal-neutron fission yields from Pu^{239} were taken from the literature, with the exception of that for Ag^{113}, which has not previously been determined. A tabulation of yields from the thermal-neutron fission is given in the Appendix, and a mass-yield curve in Fig. 1. The thermal-fission yield of Ag^{113} was calculated from the present results using the known Ag^{111} yield of 0.23% as a reference. Table III shows the yields determined in this work.

DISCUSSION

The thickness of cadmium used in these experiments is such that neutrons with energies less than 0.4 eV do not pass through. The effect of the cadmium is shown in Fig. 2, where the neutron energy spectra before and after passage through 1 mm of cadmium are given. Figure 3 shows the variation of the fission cross-section of Pu^{239} with neutron energy, with its prominent resonance at 0.297 eV. By combining these two graphs the variation in relative number of fissions with neutron energy can be plotted (Fig. 4) for the epi-cadmium-neutron spectrum. It will be seen that most fissions take place in the region 0.3 to 1.0 eV neutron energy.

The decrease observed in the yield of Ag^{111} and more especially Ag^{113} in the epi-cadmium fission is consistent with earlier work on the fission of Pu^{239} by mono-energetic neutrons. BURGUS [6] measured peak-to-valley

TABLE III

FISSION YIELDS FROM Pu^{239}

Nuclide	Thermal-neutron fission		Epi-cadmium-neutron fission
	(literature) (%)	(this work) (%)	(this work) (%)
As^{77}		0.0072	0.013
As^{78}		0.026	0.035
Br^{83}	0.30	0.29	0.31
Sr^{89}	1.71		1.75
Zr^{95}	5.00		5.08
Zr^{97}	5.25		5.51
Ag^{111}	0.23		0.214
Ag^{113}		0.065	0.047
Ce^{141}	4.54		4.72
Ce^{143}	4.48		4.53

ratios defined by the Mo^{99}/Cd^{115} yield ratio, and taking the ratio as 1.00 for the thermal-neutron fission of Pu^{239}, it was found that for neutrons of 0.297 eV, where 99% of the fissions take place through the resonance level, the R_p value, as defined earlier, was 0.33. For Ag^{113} the R_p value we obtained was 0.720 (Table II). The change in the Ag^{113} yield is not as great as for Cd^{115} due to the contribution of levels other than the 0.297 eV resonance to the total number of fissions.

With the exception of As^{77} and As^{78}, the yields of the other nuclides measured in this work do not change appreciably. This is to be expected as only small changes are observed even for fission with fission-spectrum neutrons (see the Appendix).

The observed changes in the arsenic yields are most unexpected. Although it is known that the yields of nuclides on the wings of the mass-yield curve increase in going from thermal-to 14-MeV-neutron fission (see e.g. Ref. [4]), no previous observations of this effect with neutrons of resonance energies have been made for Pu^{239} fission. ROELAND et al. [7] used an ionization chamber to obtain mass yield curves for the thermal- and 8.9-eV neutron fission of U^{235}. Only a small change in peak-to-valley ratio was observed, of about 20%, but there was an indication of some change in yield (< 10%) in the mass 75-85 region. In the case of the 0.297-eV resonance in Pu^{239} we

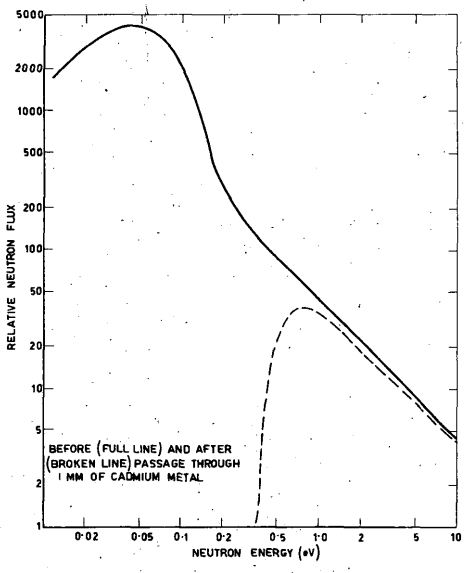

Fig. 2

Neutron energy spectra in a thermal reactor

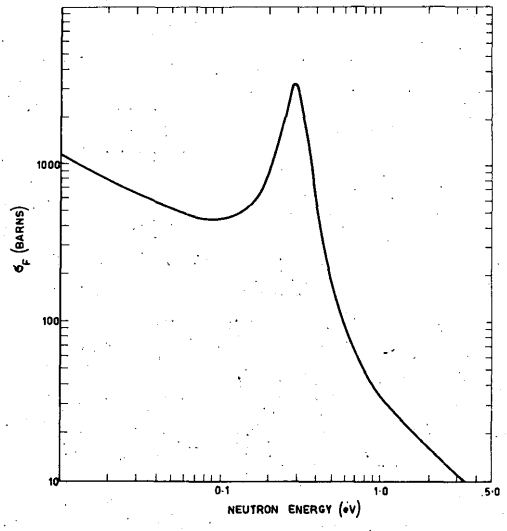

Fig. 3

Fission cross-section of Pu^{239}

have a very large change in peak-to-valley ratio, and if there is any effect in the 75–85 region it would also be expected to be more pronounced than for U^{235}, consistent with the observed changes in the As^{77} and As^{78} yields.

Results of peak-to-valley measurements for resonance fission have generally been interpreted [8, 9] in terms of changes in the ratio of a sym-

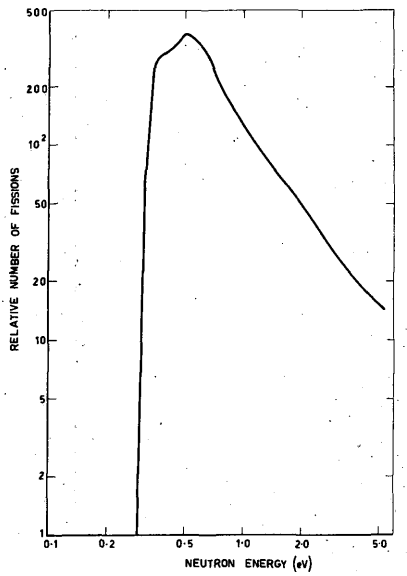

Fig. 4

Relative number of fissions in Pu^{239} for epi-cadmium neutrons

metric and an asymmetric mode of fission, the implication being that each mode has a distinct and constant shape for its mass-yield curve. The arsenic yields given here indicate that the shape of the asymmetric mass-yield curve also changes in resonance fission. These yields increase as the asymmetric yields decrease, and no combination of two modes can satisfy these results.

REFERENCES

[1] RICHARDS, J.M., BARNES, R.C.M., NAYLOR, L., DAVEY, C.N. and BEST, G.C., AERE - M 1332 (1964).
[2] CROALL, I.F., AERE - R 4227 (1963).
[3] CUNINGHAME, J.G., EDWARDS, M.P., GOODALL, J.A.B., KITT, G.P., WEBSTER, C.B. and WILLIS, H.H., AERE-R 4727 (1964).
[4] KATCOFF, S., Nucleonics 18 (1960) 201.
[5] COWAN, G.A., private communication (1963).
[6] BURGUS, W.H., IDO 16797 (1962).
[7] ROELAND, L.W., BOLLINGER, L.M. and THOMAS, G.E., Proc. 2nd UN Int. Conf. PUAE 15 (1958) 551.
[8] COWAN, G.A., BAYHURST, B.D. and PRESTWOOD, R.J., Phys. Rev. 130 (1963) 2380.
[9] FALER, K.T. and TROMP, R.L., Phys. Rev. 131 (1963) 1746.
[10] CROALL, I.F. and WILLIS, H.H., AERE-R 4723 (1964).

APPENDIX

SELECTED YIELDS IN THE THERMAL- AND FAST-NEUTRON FISSION OF Pu^{239}

Nuclide	Thermal	Fast	References [a]
Zn^{72}	0.00012		1
As^{77}	0.0073		9
As^{78}	0.025		9
Se^{81}	0.182		2 [b]
Se^{83}	0.16		2 [c]
Br^{83}	0.30		2
Kr^{83}	0.29		3, 4
Br^{84}	0.41		2 [d]
Kr^{84}	0.47		3, 4
Kr^{85}	0.54		4
Rb^{85}	0.54		3
Kr^{86}	0.75		4
Rb^{87}	0.912		3
Sr^{88}	1.42		3, 5
Sr^{89}	1.71	1.80	1, 3, 6, 23, 25
Sr^{90}	2.24	2.26	3, 5, 25
Sr^{91}	2.6		1, 6
Y^{91}	2.9		1
Zr^{91}	2.6		3
Zr^{92}	3.12		3
Zr^{93}	3.94		3
Zr^{94}	4.45		3
Zr^{95}	5.0	5.3	1, 3, 23
Mo^{95}	5.0		3
Zr^{96}	5.13		3

Notes: (a) These references refer to the list at the end of this Appendix
(b) Total for both isomers
(c) 25-min isomer only
(d) 32-min isomer only

APPENDIX (cont.)

Nuclide	Thermal	Fast	References
Zr^{97}	5.25	4.85	1, 19, 21, 25
Mo^{97}	5.61		3
Mo^{98}	5.84		3
Mo^{99}	5.86		1, 7, 21, 23, 24, 25
Mo^{100}	7.05		3
Ru^{101}	5.86		3
Ru^{102}	5.94		3
Ru^{103}	5.65	6.0	1, 3, 22, 24
Ru^{104}	5.88		3
Rh^{105}	3.90		1, 8
Ru^{106}	4.70	4.90	1, 3, 22, 24
Pd^{109}	1.40	1.65	1, 7, 8, 20, 21
Ag^{111}	0.23	0.43	1, 7, 8, 23, 24, 25
Pd^{112}	0.12	0.18	1, 7, 8, 20
Ag^{113}	0.065		9
Cd^{115}	0.035	0.075	1, 6, 20, 23, 25
Sb^{127}	0.0378		
I^{131}	3.75		1, 10
Xe^{131}	3.79		4
Xe^{132}	5.25		10
I^{133}	4.97		1
Xe^{133}	6.90		10
Cs^{133}	6.90		3, 4, 5
Xe^{134}	7.47		4, 10, 11
I^{135}	5.6		12, 13
Cs^{135}	7.17		3, 5, 14
Xe^{136}	6.65		4, 10, 14
Cs^{137}	6.30	6.06	3, 8, 14, 15, 16, 25
Ba^{138}	6.28		3, 5

APPENDIX (cont.)

Nuclide	Thermal	Fast	References
Ba^{139}	5.78		6
Ba^{140}	5.40	4.97	12, 13, 21, 23, 24, 25
Ce^{140}	5.56		3, 5, 14
La^{141}	5.47		6
Ce^{141}	4.54		1
Pr^{141}	5.30		5
Ce^{142}	4.97		3, 5, 14
Ce^{143}	4.48		1
Nd^{143}	4.57		3
Ce^{144}	3.7	3.76	1, 3, 17, 18, 25
Nd^{144}	3.84		3, 5, 14, 17
Nd^{145}	3.12		3, 5, 14, 17
Nd^{146}	2.57		3, 5, 14, 17
Nd^{147}	2.20	2.13	18, 25
Pm^{147}	1.94		5
Sm^{147}	2.07		3, 14, 17
Nd^{148}	1.70		3, 5, 14, 17
Pm^{149}	1.40		18
Sm^{149}	1.31		3, 5, 14, 17
Nd^{150}	1.01		3, 5, 14, 17
Sm^{151}	0.78		3, 5
Sm^{152}	0.59	0.48	3, 5, 14, 17, 21
Sm^{153}	0.37		1, 18
Sm^{154}	0.29		3, 5, 14, 17
Eu^{156}	0.11	0.15	1, 18, 25
Gd^{159}	0.021		18
Tb^{161}	0.0039		18
Dy^{166}	$6.8\ 10^{-5}$		18

REFERENCES TO APPENDIX

1 STEINBERG, E.P. and FREEDMAN, M.S., Radiochemical Studies: The Fission Products, Div.IV, 9, (CORYELL, C.D. and SUGARMAN, N., Eds.) McGraw-Hill, New York (1951).
2 CROALL, I.F., WILLIS, H.H., J.inorg. nucl. Chem. 25 (1963) 1213.
3 FICKEL, H.R. and TOMLINSON, R.H., Canad. J. Phys. 37 (1959) 216, 226.
4 FRITZE, K., McMULLEN, C.C. and THODE, H.G., Proc. 2nd UN Int. Conf. PUAE 15 (1958) 436.
5 ANIKHINA, M.P., Proc. 2nd UN Int. Conf. PUAE 15 (1958) 446.
6 BARTHOLOMEW, R.M., MARTIN, J.S. and BAERG, A.P., Canad. J. Chem. 37 (1959) 660.
7 FORD, G.P., LA 1997 (1956).
8 KIRBY, L.J., HW 77609 (1963).
9 This work.
10 FLEMING, W.H. and THODE, H.G., Canad. J. Chem. 34 (1956) 193.
11 BAYLY, J.G., DURET, M.F., POULSEN, N.B. and TOMLINSON, R.H., Canad. J. Phys. 39 (1961) 1391.
12 STEINBERG, E.P. and GLENDENIN, L.E., Proc. UN Int. Conf. PUAE 7 (1956) 3.
13 WALKER, W.H. and OKAZAKI, A., NDC 54 (1963).
14 WILES, D.M., PETRUSKA, J.A. and TOMLINSON, R.H., Canad. J. Chem. 34 (1956) 227.
15 COOK, G.B., Ph.D. Thesis (1951).
16 KAFALAS, P. and CROUTHAMEL, C.E., J. inorg. nucl. Chem. 4 (1957) 239.
17 KRIZHANSKII, L.M., Atomnaja Energija 2 (1957) 276.
18 BUNNEY, L.R., SCADDEN, E.M., ABRIAM, J.O. and BALLOU, N.E., Proc. 2nd UN Int. Conf. PUAE 15 (1958) 449.
19 CROALL, I.F. and WILLIS, H.H., unpublished (1963).

References 20–25 refer to fast-neutron fission of Pu^{239}

20 FORD, G.P. and GILMORE, J.S., LA 1997 (1956).
21 ENGELKEMEIR, D.W., FREEDMEN, M.S., SEILER, J.A., STEINBERG, E.P. and WINSBERG, L., N.N.E.S. Div. IV, 9 (McGraw-Hill, 1951) 1331.
22 BAK, M.A., Atomnaja Energija 6 (1959) 557.
23 PETRZHAK, K.A., AEC-tr-4696 (1960).
24 BONYUSHKIN, E.K., Atomnaja Energija 10 (1961) 13.
25 COWAN, G.A., Los Alamos, private communication (1963).

DISCUSSION
(on the foregoing four papers)

M. S. MOORE: Regarding Mr. Cowan's paper, I might mention that, in the work of Regier et al., the measured valley-to-peak ratio at the 0.29-eV resonance in Pu^{239} was ~0.3, compared to thermal. Calculations yield a ratio of 0.2 between two (assumed) spin states, or compared to thermal, limiting values of ~0.3 and ~1.5. This would be in agreement with the present paper.

G. COWAN: Yes, a value of 0.3 would be more consistent with the idea of a 50/50 distribution.

A. MOSSOP: I should like to comment on the direction of the change in symmetric to asymmetric yields, as measured by peak-to-valley ratio. According to Croall, this ratio increases with neutron energy for Pu^{239}, while in Wahl's paper the ratio is shown to decrease with energy. Admittedly Wahl's results refer to U^{235} and his first energy value above thermal is 1 MeV. In Cowan's paper the ratio both increases and decreases for Pu^{239} within the range 200-600 eV.

Are these various conclusions consistent with each other?

G. COWAN: I am not aware of any major inconsistencies but I agree it is confusing that these effects should go in both directions. My impression is that as soon as the energies are high enough, the effect always takes the form of an increase in the proportion of symmetry with increasing neutron energy. At low energies, which may amount to tens of keV, there are effects in both directions and these presumably have to do with spin at these lower energies and at somewhat higher energies where p-wave fission comes in, with the difference between s- and p-wave fission. Presumably d-wave fission is something else again. So it is only at an energy region where there is truly statistical sampling of all of these effects that consistency begins to appear.

M. MOSSOP: Have you considered using samarium instead of cadmium for these measurements? This would be advantageous inasmuch as the plutonium resonance peak, which is not really freed by cadmium, is freed to a very much greater extent by samarium, whose maximum cross-section is a lower value of neutron energy.

G. COWAN: We have considered the production of filtered spectra using all sorts of filters - boron, cadmium, samarium and other combinations of neutron-absorbing materials with good resonance peaks. The problem is really the one that was involved in your first question. After the thermal spectrum has been filtered out, there remains a slowing-down spectrum plus a fission unmoderated peak. The ratio of these two does not vary very much, and when the filtered spectrum has been produced there remains a mixed effect in which the weighting factor of the slowing-down spectrum and the weighting factor of the unmoderated fission spectrum peak tend to be in different directions and to give rise to an uninterpretable result. It is very difficult to produce a real slowing-down spectrum all by itself in a reactor. That is why we have been obliged to make use of a neutron explosion system in order to produce interpretable data. The time-of-flight method is the only method I know that will produce an unambiguous resonance-region neutron flux.

G. GORDON: In our investigations at the Massachusetts Institute of Technology we have looked for two-mode effects on fragment kinetic energies. In particular, Aras, Menon, and I measured differential range curves for near-symmetric fragments from the thermal-neutron fission of U^{235}. On the assumption that the two-mode hypothesis was valid, we thought that the two modes might have different total kinetic energy releases, thus yielding two different range groups for a given fragment having an appreciable yield from both the proposed modes. Our range curves show no such effect for products such as Ag^{111}, Cd^{115} and Sb^{127}.

D. S. Brenner and I have repeated the Russian studies (Komar et al.) on kinetic-energy distributions as a function of mass split for the photofission of Th^{232} and U^{238}. In our work, gold-silicon surface-barrier detectors were used to measure the fragment energies. We did not observe the effects found in Komar's work, carried out with ion chambers, which strongly suggested the existence of two different total kinetic energy groups, particularly for U^{238}. We conclude that, if there are two different fission modes in the systems studied, both modes have the same dependence of total kinetic energy release on the mass ratio of division. This is at variance with the work done at Los Alamos (Britt et al.) on charged-particle fission, which indicated lower total kinetic energy released for the presumed "symmetric mode".

GENERAL DISCUSSION

M. TÅLAT-ERBEN: Considerable interest attaches to the purely physical methods that are used in place of conventional radiochemical techniques for determining the most probable charge Z_p as a function of the mass number A.

By using the experimental mass-yield curve together with the charge dispersion curve and Professor Wahl's "empirical" Z_p function, it is possible to calculate a mass dispersion curve as well as the most probable fragment mass A_p for a given charge-number Z. We have performed this calculation and have observed that the A_p-versus-Z line is not identical with the Z_p-versus-A line. On the (A, Z) plane they intersect at the point $(\bar{A}, \bar{Z})$, where the coordinates are the mass and charge of the average (light or heavy) fragment. This result is in accordance with the bivariate normal distribution approach proposed by Levy and Nethaway [UCRL-6948 (1962)] to interpret Blann's experimental results [UCRL-9190 (1960)] on the fission of Au^{197} bombarded by 110-MeV C^{12} ions.

I should like to draw attention to the fact that the physical experiments (e.g. those based on measurement of the characteristic K-X-rays by the primary fragments) could probably be performed to obtain the relationship A_p-versus-Z in addition to Z_p-versus-A. If this were done, it would be extremely interesting to see whether the two lines do really differ and intersect at the mean point for either group of fission fragments. If the mass resolution of the apparatus is high enough, one would expect to obtain these so-called regression lines, since the closed-shell effects, although operative, would not alter the over-all statistical nature of the phenomenon of low-energy fission. [Cf. IAEA Technical Reports Series No. 17.]

DETERMINATION OF THE PRIMARY NUCLEAR CHARGE OF FISSION FRAGMENTS FROM THEIR CHARACTERISTIC K-X-RAY EMISSION IN SPONTANEOUS FISSION OF Cf^{252}*

L. E. GLENDENIN, J. P. UNIK AND H. C. GRIFFIN**
ARGONNE NATIONAL LABORATORY, ARGONNE, ILL.
UNITED STATES OF AMERICA

Abstract — Résumé — Аннотация — Resumen

DETERMINATION OF THE PRIMARY NUCLEAR CHARGE OF FISSION FRAGMENTS FROM THEIR CHARACTERISTIC K-X-RAY EMISSION IN SPONTANEOUS FISSION OF Cf^{252}. The distribution of nuclear charge in the spontaneous fission of Cf^{252} has been determined directly by simultaneous measurement of the masses and characteristic K-X-ray energies associated with the primary fission products. The X-rays were detected by a thin NaI (Tl) crystal (or by an argon-filled proportional counter) in coincidence with a pair of solid-state detectors for the complementary fission fragments. Preliminary to the three-parameter study of the charge-mass distribution the gross characteristics of the K-X-rays were examined in some detail. The average yield of K-X-rays is 0.55 ± 0.1 per fission (the heavy group accounting for 70% of the total). From delayed-coincidence and fragment time-of-flight experiments it was found that about 30% of the X-rays are emitted within 0.1 ns after fission, another 30% between 0.1 and 1 ns, 25% between 1 and 10 ns, the remainder appearing as two delayed components of equal intensity with half-lives of ~ 30 ns and ~ 100 ns. These characteristics indicate that the X-rays arise from internal conversion during de-excitation of the primary fission fragments, an interpretation supported by the observed yield (~ 1 per fission) of 50 - 300 - keV electrons emitted within 2 μs of fission. In the three-parameter experiments the yield and energy of K-X-rays emitted in the first centimeter (ns) of fragment flight were determined as a function of fragment mass. The yield of K-X-rays per fragment is a pronounced saw-tooth function of mass, rising from < 0.01 in the region below mass 92 ($N \sim 50$) to 0.1 in the light group, falling abruptly to near-zero in the mass region 128 - 132 ($Z \sim 50$), rising to 0.2 in the region of the heavy group mass-yield peak, and then increasing rapidly beyond mass 148 (region of deformed nuclei) to a maximum of 1 around mass 158. The observed correlation of K-X-ray energies with fragment mass leads to a smooth primary charge (Z_p) function in better agreement with the empirical rule of equal charge displacement (ECD) than with other postulates for charge division in nuclear fission.

DÉTERMINATION DE LA CHARGE NUCLÉAIRE PRIMAIRE DES FRAGMENTS DUS A LA FISSION SPONTANÉE DE ^{252}Cf, D'APRÈS L'ÉNERGIE CARACTÉRISTIQUE DES RAYONS X K QU'ILS ÉMETTENT. Les auteurs ont déterminé directement la distribution de la charge nucléaire, lors de la fission spontanée de ^{252}Cf, en mesurant simultanément les masses des produits de fission primaires et les énergies caractéristiques des rayons X K émis par ces produits. Pour déceler les rayons X, ils ont utilisé un cristal mince de NaI(Tl) (ou un compteur proportionnel rempli d'argon) monté en coïncidence avec deux détecteurs à semi-conducteurs pour les fragments de fission complémentaires. Avant de commencer l'étude à trois paramètres de la distribution charge-masse, ils ont examiné en détail les caractéristiques brutes des rayons X K. Le rendement moyen en rayons X K est de $0,55 \pm 0,1$ par fission (le groupe des éléments lourds représentant à lui seul 70% du total). Des expériences sur la coïncidence retardée et le temps de vol des fragments ont permis de déterminer que 30% environ des rayons X sont émis dans le dixième de nanoseconde (ns) qui suit la fission, 30% entre 0,1 et 1 ns, 25% entre 1 et 10 ns, le reste apparaissant sous la forme de deux composantes retardées d'intensité égale et de périodes voisines d'environ 30 ns et d'environ 100 ns respectivement. Ces caractéristiques montrent que les rayons X proviennent d'une conversion interne durant la désexcitation des fragments de fission primaires, cette interprétation étant étayée par le rendement observé en électrons de 50 à 300 keV (environ 1 par fission) émis dans les deux microsecondes qui suivent la fission. Lors des expériences à trois paramètres, le rendement

* Based on work performed under the auspices of the United States Atomic Energy Commission.
** Present address: Department of Chemistry, The University of Michigan, Ann Arbor, Michigan.

et l'énergie des rayons X K émis sur le premier centimètre (ns) du vol des fragments a été déterminé en fonction de la masse des fragments. Le rendement en rayons X K par fragment constitue une fonction en dents de scie de la masse; il passe d'une valeur inférieure à 0,01 dans la région des masses inférieures à 92 ($N \approx 50$) à 0,1 dans le groupe des masses faibles, pour tomber brusquement au voisinage de zéro dans la région des masses de 128 à 132 ($Z \approx 50$) et remonter à 0,2 dans la région du pic du rendement en fonction de la masse des éléments lourds, augmentant ensuite rapidement au-delà de la masse 148 (région des noyaux déformés) pour atteindre un maximum de 1 au voisinage de la masse 158. La corrélation observée entre l'énergie des rayons X K et la masse des fragments donne une courbe régulière pour la charge primaire (Z_p) qui est plus conforme à la règle empirique du déplacement égal des charges qu'à d'autres postulats relatifs au partage de la charge lors d'une fission nucléaire.

ОПРЕДЕЛЕНИЕ ПЕРВИЧНОГО ЯДЕРНОГО ЗАРЯДА ПРОДУКТОВ ДЕЛЕНИЯ НА ОСНОВАНИИ ХАРАКТЕРНОЙ ЭМИССИИ РЕНТГЕНОВСКИХ ЛУЧЕЙ "К" ПРИ САМОПРОИЗВОЛЬНОМ ДЕЛЕНИИ КАЛИФОРНИЯ-252. Распределение ядерного заряда при самопроизвольном делении калифорния-252 было определено непосредственно путем одновременного измерения масс и характерных энергий рентгеновского излучения, относящихся к первичным продуктам деления. Рентгеновские лучи обнаруживали при помощи тонкого кристалла NaJ(Tl) (или при помощи наполненного аргоном пропорционального счетчика) в совпадении с парой детекторов твердого состояния для регистрации дополнительных осколков деления. До трехпараметрового изучения распределения заряда в зависимости от массы предварительно были довольно подробно изучены общие характеристики рентгеновского К-излучения. Средний выход лучей рентгеновского К-излучения составляет $0{,}55 \pm 0{,}1$ на каждое деление (причем на долю тяжелой группы выпадает 70% общего количества). На основании экспериментов по запаздывающему совпадению и времени пролета осколков было найдено, что около 30% рентгеновских лучей испускается за первые 0,1 наносекунды после деления, следующая доля в 30% – за время от 0,1 до 1 наносекунды, еще 25% между 1 и 10 наносекундами, а остальная часть представляется в виде двух запаздывающих компонентов одинаковой интенсивности с полупериодами жизни приблизительно 30 и 100 наносекунд. Эти характеристики указывают на то, что рентгеновские лучи возникают из-за внутренней конверсии во время успокоения первичных осколков деления; это толкование подтверждается наблюдавшимся выходом (приблизительно 1 на каждое деление) электронов в интервале энергий от 50 до 300 кэв, испускаемых за 2 микросекунды с момента деления. При трехпараметровых экспериментах выход и энергия испускаемых лучей рентгеновского К-излучения на протяжении первого сантиметра (наносекунды) пролета осколка были определены в зависимости от массы осколка. Выход рентгеновских лучей К-излучения на каждый осколок носит явно выраженный зубчатый характер функции массы, и расчет от величины $< 0{,}01$ в области массы меньшей 92 ($N \sim 50$) до 0,1 для легкой группы затем круто падает почти до нуля в области масс 128–132 ($Z \sim 50$) и снова возрастает до 0,2 в области пика выхода массы тяжелой группы а затем быстро увеличивается для массы свыше 148 (область деформированных ядер) до максимума, равного единице вблизи массы 158. Наблюдавшаяся корреляция энергий лучей рентгеновского К-излучения с массой осколка ведет к получению плавной функции (Z_p) первичного заряда, что лучше согласуется с эмпирическим правилом равного вытеснения заряда (РВЗ), чем с другими постулатами относительно разделения заряда при ядерном делении.

DETERMINACION DE LA CARGA NUCLEAR PRIMARIA DE LOS FRAGMENTOS DE FISION, PARTIENDO DE LA EMISION DE RAYOS X CARACTERISTICOS DE LA SERIE K EN LA FISION ESPONTANEA DEL ^{252}Cf. Los autores han determinado directamente, por medición simultánea de las masas y de las energías de los rayos X característicos de la serie K asociadas a los productos de fisión primarios, la distribución de la carga nuclear en la fisión espontánea del ^{252}Cf. La detección de los rayos X se efectuó con ayuda de un cristal delgado de NaI(Tl) (o con un contador proporcional lleno de argón), en coincidencia con un par de detectores de estado sólido para el registro de los fragmentos de fisión complementarios. Antes de proceder al estudio con tres parámetros de la distribución de la cargas y de las masas, los autores examinaron con cierto detenimiento las características fundamentales de los rayos X característicos. El rendimiento medio de rayos X de la serie K es de $0{,}55 \pm 0{,}1$ por fisión (correspondiendo el 70% del total al grupo de los fragmentos pesados). Los experimentos realizados por los procedimientos de coincidencia retardada y de tiempo de vuelo de los fragmentos han revelado que un 30% aproximadamente de los rayos X se emite antes de transcurrir 0,1 ns a contar desde el momento de la fisión, un 30% entre 0,1 y 1 ns, y un 25% entre 1 y 10 ns, presentándose la emisión restante como dos componentes retardados de igual intensidad con períodos de ~ 30 ns y ~ 100 ns. Estas características revelan que los rayos X proceden de la conversión interna durante la desexcitación de los fragmentos primarios;

esta interpretación queda corroborada por el rendimiento observado (~1 por fisión) de electrones de 50 - 300 keV emitidos en los 2 μs que siguen a la fisión. En los experimentos realizados, haciendo intervenir tres parámetros, los autores han determinado el rendimiento y la energía de los rayos X característicos de la serie K en el primer centímetro (ns) del vuelo de los fragmentos como función de la masa de éstos. El rendimiento de rayos X característicos de la serie K por fragmento es una neta función en dientes de sierra de la masa, que aumenta desde <0, 01 en la región por debajo de la masa 92 (N~50) hasta 0, 1 en el grupo de fragmentos ligeros, descendiendo bruscamente hasta las proximidades de cero en las regiones de masa de 128 - 132 (Z ~ 50) para elevarse a 0, 2 en la región del pico de rendimiento de masas correspondiente al grupo de los fragmentos pesados y seguir ascendiendo luego rápidamente hasta rebasar la masa 148 (región de los núcleos deformados) y alcanzar un máximo de 1 en torno a la masa 158. La relación observada entre las energías de los rayos X característicos de la serie K y la masa de los fragmentos conduce a una función continua para la carga primaria (Z_p) que concuerda mejor con la regla empírica del equidesplazamiento de las cargas que con los demás postulados relativos a la división de las cargas en la fisión nuclear.

INTRODUCTION

Since the earliest studies [1] of the distribution of nuclear charge in fission by the indirect radiochemical method of fractional chain yield measurements the desirability of a more direct physical approach to the problem has been recognized. With the discovery of the emission of characteristic fission-fragment X-rays coincident with fission [2, 3, 4, 5] it became obvious that a direct physical determination of the average nuclear charge (Z_p) of a primary fission fragment as a function of its mass (A) is attainable from simultaneous measurements of the characteristic X-ray energies and complementary fragment masses associated with a fission event. The recent development of solid-state detectors with good mass resolution for fission fragments (full width at half maximum (FWHM) ≃ 4 amu for Cf^{252}) has made this method most attractive.

The results of another physical approach to the problem of charge division have been reported by ARMBRUSTER et al. [6]. Their method involves the measurement of the average β-decay-chain length as a function of mass by absolute counting of the β-particles emitted by mass-separated fission products. These results (for thermal-neutron-induced fission of U^{235}) are in disagreement with the charge division, or Z_p function (Z_p versus A), deduced from the large body of radiochemical data obtained over the past 20 years and recently summarized by WAHL et al. [7].

In this paper we report the results of an investigation of charge division in the spontaneous fission of Cf^{252}. Our procedure consists of a three-parameter measurement of the K-X-rays in coincidence with complementary fission fragments whose kinetic energies are determined with a pair of solid-state detectors. The measured K-X-ray energies define the primary nuclear charges or atomic numbers, and the observed ratio of kinetic energies gives the masses of the fragments. The availability of Cf^{252} for our first investigation by this method proved to be of great value since a spontaneously fissioning source permits convenient probing of the various aspects of the experimental method, and obviates the difficulties often associated with the use of a reactor or an accelerator. A further advantage, undoubtedly owing to this great convenience, is that a wealth of detailed information (obtained with high-resolution time-of-flight techniques) is now available on the characteristics of Cf^{252} fission such as mass distributions, neutron emission

and total kinetic energy as a function of mass, and other data required for accurate determination of primary fragment masses with solid-state detectors. The spontaneous fission of Cf^{252} will thus become the "calibration standard" for our future studies of induced fission.

ORIGIN AND CHARACTERISTICS OF K-X-RAYS IN FISSION

The occurrence of K-X-rays coincident with fission and characteristic of the fission fragments naturally raises the question of origin. An expected source of X-rays lies in internal conversion of the prompt γ-rays from the de-excitation of the primary fission fragments. The yield of K-X-rays by this process can be roughly estimated from conversion coefficients [8] and the known yield and energy spectrum [9] of the prompt γ-rays emitted in spontaneous fission of Cf^{252}. A calculation (based on the expected dominance of M1 and E2 transitions) predicts a total yield of about 0.6 K-X-rays per fission, with two-thirds of the total being emitted by the heavy group fragments [10]. Another possible source of X-rays lies in the disruption of the electron cloud during the process of nuclear fission and the subsequent rearrangement of electrons around the separated fragments. If K-electron vacancies are produced by this process, the K-X-rays will be emitted with lifetimes of the order of 10^{-16} s [11], whereas the lifetimes of K-X-rays resulting from internal conversion will be characteristic of transitions among the excited nuclear states of the fragment. For the expected transitions of low multipolarity (M1, E2 and E1) and of energies prodominantly in the range 100-300 keV, as indicated by the prompt γ-ray spectrum [9], the lifetimes of K-X-rays from internal conversion should fall in the range 10^{-10} to 10^{-7}s [12]. Conversion electrons coincident with fission would also be expected (mainly in the energy region of 50-300 keV) with a yield (K+L) of about 0.9 per fission. Measurements were therefore made [10] of the yield, energy spectrum and time distribution of the K X-rays coincident with fission; a cursory search for coincident conversion electrons was also made.

For these measurements the fission source consisted of Cf^{252} ($\sim$3000 fissions/s) deposited on a mica backing of sufficient thickness (5 mg/cm^2) to stop all fission fragments. Fission events were selected by a silicon-gold surface-barrier detector facing the source at close geometry (nearly 2π) in an aluminium vacuum chamber. This arrangement ensured the entrapment of all fragments in the small space ($\sim$2 mm) between source backing and fission detector, thus providing a reasonably constant geometric efficiency for the detection of the X-rays by a 25-mm diam. $\times$ 3-mm thick NaI(Tl) detector placed outside the chamber at a distance of $\sim$4 cm. Absolute detection efficiencies and energy response functions for X-rays in this arrangement were determined with standardized samples of Fe^{55}, Zn^{65}, Sr^{85}, Cd^{109}, Cs^{137} and Dy^{159}). A fast-slow coincidence and linear gate circuit (equipped with variable delay and resolving times) selected events in the X-ray channel coincident (2τ = 300 ns) with fission fragments entering the solid-state detector. The output of the linear gate was recorded in a multichannel analyser. An empirical correction for the "background" spectrum of pulse-heights in the X-ray region (10-50 keV) caused by the higher-energy

prompt γ-rays was obtained with a graded filter (0.5 g Cu/cm^2 + 0.1 g Al/cm^2), opaque to photons of energy $\lesssim$50 keV. Chance coincidences were determined by inserting a delay of 0.35 μs into the X-ray channel. The net K-X-ray spectrum (essentially identical with the curve labelled "all masses" in Fig.4) has light- and heavy-group maxima at about 18 and 32 keV, corresponding to atomic numbers of about 43 and 55 respectively. With corrections for detection efficiency, transmission through the mica source backing and through the beryllium windows of the vacuum chamber and NaI(Tl) detector, the escape peak in NaI for K-X-rays of $E > 33$ keV, and K-X-rays ($\sim$3%) delayed beyond 150 ns, the summation of the spectrum from 10 to 50 keV corresponds to a total yield of 0.57$\pm$0.06 K-X-rays per fission. Of the total yield the light and heavy groups account for 0.17$\pm$0.02 (30%) and 0.40$\pm$0.04 (70%) respectively. These results for Cf^{252} are comparable with the heavy-group K-X-ray yields of 0.45$\pm$0.15 and 0.42$\pm$0.12 reported by VOITOVETSKII et al. [2] and SKLIAREVSKII et al. [3] for thermal-neutron fission of U^{235}, but are much higher than HOHMANN's value of 0.2$\pm$0.06 for the total K-X-ray yield in U^{235} fission [13].

The time distribution for K-X-ray emission was studied by a combination of delayed-coincidence and time-of-flight methods. With the experimental arrangement and techniques just described and a coincidence resolving time (2τ) of 60 ns, delayed coincidence data were obtained over a range of 500 ns. The time delays were calibrated by comparison with standard delay lines and by measurement of the Am^{241} α-(L-X-ray) coincidences through the 63-ns state in Np^{237}. The delayed coincidence data for emission of K-X-rays in the energy region 10-45 keV (Fig. 1) is resolved into three components with half-lives (and intensities) of $\lesssim$10 ns (85%), $\sim$30 ns (7%), and $\sim$100 ns (8%) to illustrate the relative grouping of half-lives in what is probably a complex mixture. Additional data obtained separately for light-group K-X-rays (10-25 keV) and for heavy-group K-X-rays (25-45 keV) indicate that the $\sim$30-ns component is associated predominantly with the light group, whereas the $<$10-ns and the $\sim$100-ns components are associated with both groups. There is evidence from preliminary measurements of the Cf^{252} fission β-rays that the delayed states are associated with specific mass regions [14].

For shorter times a fragment time-of-flight technique was used in which the X-ray detector viewed a beam of fragments (at 90° to the flight path) during various portions of the total flight (2 cm or $\sim$2 ns) from source to fragment detector. Copper collimators restricted the field of view to various times after fission as short as 0.1 ns. By this method it was observed that (30$\pm$10)% of the K-X-rays are emitted in the interval 0 to 0.1 ns and (30$\pm$10)% in the interval 0.1 to 1 ns. These results in combination with the delayed coincidence data indicate an emission of (25$\pm$10)% from 1 to $\sim$10 ns and (15$\pm$5)% after $\sim$10 ns.

The occurrence of electrons coincident with fission as expected from internal conversion was verified experimentally with a weak Cf^{252} source ($\sim$100 fissions/s) in a 2π gas-flow proportional counter operated in coincidence ($2\tau = 4\mu$s) with a fission-fragment detector situated in the floor of the counter. Absorption curves in beryllium, aluminium and gold were obtained in order to distinguish electrons from low-energy photons and to establish approximate electron energies. These measurements indicate the average

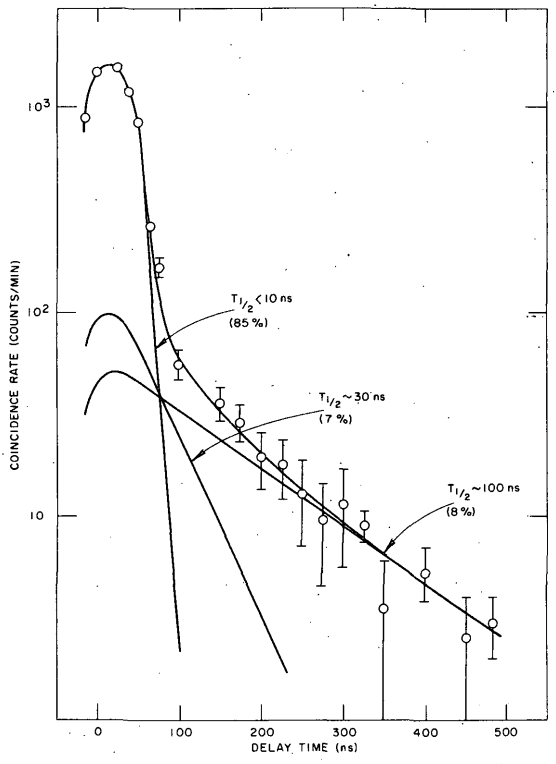

Fig. 1

Delayed coincidence data for emission of K-X-rays by Cf^{252} fission fragments

emission of 1.0±0.2 electrons per fission over an energy range of 50 to ~300 keV.

It is clearly evident from the observed characteristics of the K-X-ray emission in fission of Cf^{252} that internal conversion processes in de-excitation of the primary fragments play the dominant role in formation of K-vacancies. If any are formed by disruption of the electron cloud in the fission process, an upper limit of ~0.2 K-vacancies per fission is obtained from the observed fraction (30%) of K-X-rays emitted before 10^{-10} s. Further data limiting the possible role of this process is presented below in the section on the yield of K-X-rays as a function of fragment mass. In certain mass regions (near closed shells) the observed yield is as low as 0.05 K-vacancies per fragment. At any rate, the point of importance in the investigation of charge division is that the K-X-ray from either mode of formation is characteristic of the atomic number of the primary fission fragment.

VARIATION OF NUCLEAR CHARGE WITH FRAGMENT MASS

Experimental procedure and apparatus

Essentially weightless sources of Cf^{252} for this investigation were prepared by volatilization in vacuum from a hot filament onto a thin carbon

film ($\sim 30\ \mu g/cm^2$) that was then placed between two supporting films of VYNS plastic (each $\sim 15\ \mu g/cm^2$) on a source holder. The intensity of the source used with the NaI(Tl) X-ray detector (in fast coincidence, $2\tau = 100$ ns) was ~ 4000 fissions/s (f/s); a source of less intensity (~ 1600 f/s) was required with the gas-flow proportional X-ray detector (in slow coincidence, $2\tau = 2\mu s$) in order to achieve a reasonably low ratio ($\sim 10\%$) of chance-to-true coincidence rates.

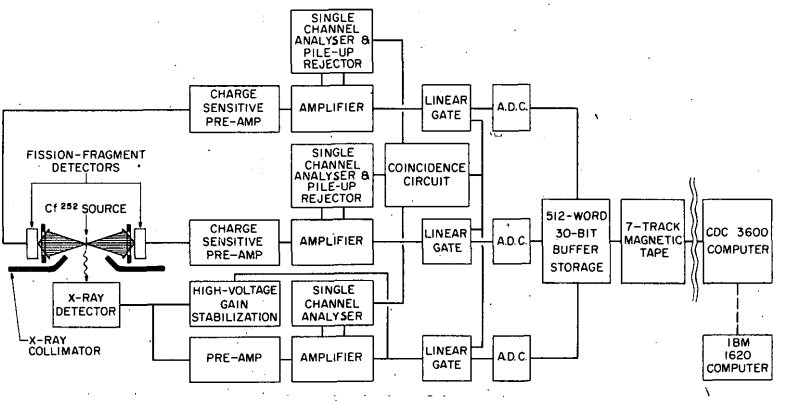

Fig. 2

Schematic diagram of source and detector arrangement and data recording system used in the three-parameter investigation of nuclear charge division in spontaneous fission of Cf^{252}

A schematic diagram of the arrangement of source and detectors, the electronic system, and the data recording and computing equipment is shown in Fig. 2. The Cf^{252} source was located between two fission-fragment detectors at a distance of 2 cm from each. The detectors (n-type surface-barrier) were operated at an optimum bias (60-70 V) for minimum change in response with the increasing leakage current due to damage by fission fragments. A circular aluminium collimator on each detector defined a detection area of 2.0 cm^2 (geometric efficiency $\sim 5\%$). A copper collimator (0.75 g/cm^2) was placed so as to restrict the "view" of the X-ray detector to fission fragments in the first centimetre (~ 1 ns) of flight, corresponding to about 60% of the total K-X-ray emission. This collimation served not only to maintain a reasonably well-defined geometric efficiency for X-ray detection but, more importantly, to avoid measurement of K-X-rays from delayed transitions (>1 ns) in the fragments that might emphasize a particular nuclear charge rather than the average for a given mass region. The fission source, detectors and X-ray collimator were enclosed in an aluminium vacuum chamber (maintained at a pressure of $\sim 10\ \mu m$) equipped with a beryllium window (285 mg/cm^2) for high X-ray transmission.

An X-ray detector (with a 95 mg/cm^2 Be window) was located outside the chamber at 90° to the flight path of the fragments (for minimum Doppler broadening) at a distance of ~ 4 cm from the Cf^{252} source (geometric efficiency $\sim 3\%$). Two types of X-ray detectors were used: a thin NaI(Tl) scintillator (described above), and a gas-flow (90% argon-10% methane) proportional counter (9-cm diam) operated at atmospheric pressure. A gain

stabilization circuit that senses the peak amplitude for an X-ray monitor (Fe^{55}) and controls the high-voltage supply to the proportional counter was used to counteract gain drift caused by variations in atmospheric pressure. The observed resolution (FWHM), determined with several K-X-ray sources (listed above), was equivalent to 5.5 nuclear charge units for the NaI detector and 2.0 for the proportional detector.

The preamplified signals from the X-ray and fission-fragment detectors were fed to the amplifiers of the three-parameter system (Fig. 2). Gain stability for all three channels was monitored continuously over the course of each experiment. The maximum gain drift was ±0.3% for the NaI channel (unstabilized) and ± 0.1% for the proportional counter channel. The fission detectors suffered an unavoidable pulse-height decrease of ~ 0.6% owing to damage by the fragments (a correction for this effect was made by the computer during data reduction). A single-channel analyser selected the pulse-height range of interest for each parameter, and pile-up rejectors were used in the fission channels to prevent spectral distortion by the alpha radiation from Cf^{252}. Pulses in triple coincidence were selected by the coincidence circuit, passed through linear gates, digitized in the A.D.C. circuits, stored temporarily in a 30-bit buffer, and finally stored in groups of 512 words (events) on a 7-track magnetic tape for subsequent computer analysis.

The main bulk of data sorting and reduction was accomplished off-line with a CDC 3600 computer programmed to obtain the primary fragment mass and total kinetic energy distributions, the total kinetic energy as a function of mass and the coincident K-X-ray spectra as a function of mass. Further calculations and data reduction of a less complicated nature, such as dispersion corrections and subtraction of prompt γ-ray background and chance coincidence effects (see above), were accomplished with an IBM 1620 computer.

Fragment mass distribution

The primary fragment masses (before neutron emission) were computed for each event in the following manner: (a) The final energies of the coincident fragments (after neutron emission) were calculated from the observed pulse heights using the final-fragment-mass dependent energy calibration described by SCHMITT et al. [15]. (b) These final energies were corrected for the average number of neutrons emitted as a function of the fragment mass, $\overline{\nu}_A$, using the data of BOWMAN et al. [16], to yield the kinetic energies of the light and heavy fragments, E_L and E_H, before neutron emission. (c) The primary masses of the fission fragments, A_L and A_H, were then calculated using the following equations:

$$A_L = A_F \frac{E_H}{E_L + E_H} \text{ and } A_H = A_F - A_L \qquad (1)$$

where A_F is the mass of the fissioning nucleus.

Since the calculations (a) and (b) depend on the primary and final fragment masses, these masses were first approximated. From the primary masses calculated after the first approximation and the neutron emission data [16], better estimates of the primary and final masses were obtained.

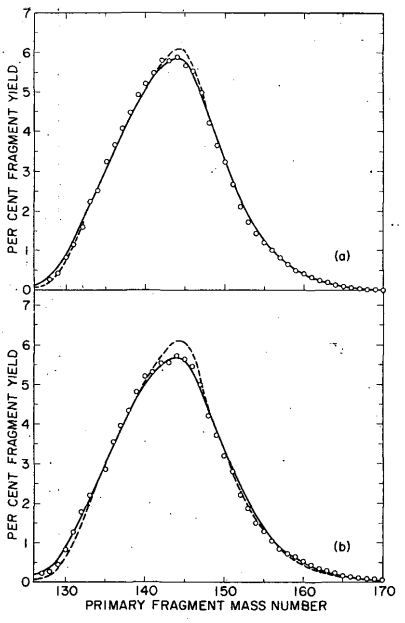

Fig. 3

Binary mass distributions for Cf^{252} obtained from double-fragment kinetic energy measurements. Open circles represent experimental data from this work.
Dashed curves show, for comparison, the mass distribution obtained using time-of-flight techniques [17] with an experimental mass resolution FWHM = 2.1 amu.

(a) Mass distribution obtained during proportional counter experiments. Solid curve shows the mass distribution calculated by dispersing the time-of-flight mass distribution (corrected for experimental resolution) using a Gaussian dispersing function with σ_T^2 given by Eq. 2 and B = 0; average FWHM = 4.2 amu.

(b) Mass distribution obtained during NaI experiments. Solid curve as in (a) except B = 2.5; average FWHM = 5.6 amu.

The calculations (a), (b) and (c) were then repeated until the computed primary masses for each event converged to within 0.1 amu.

The mass resolution for each experiment was determined by comparing the computed binary mass distribution with that determined by WHETSTONE [17] using time-of-flight techniques (dashed curves in Fig. 3). The mass resolution in Ref. [17] is relatively small and well-known (FWHM = 2.1 amu). The mass distribution from [17] was first corrected for the quoted mass resolution and then dispersed with a Gaussian function having a total variance, σ_T^2, given by Eq. (2)

$$\sigma_T^2(A_{L,H}) = \frac{4\bar{\nu}A_L A_H M_N \bar{E}_N}{3A_F \bar{E}_T} + \frac{1}{4}\sigma^2(\bar{\nu}) + \frac{0.41}{\bar{E}_T^2}[A_L^2 + A_H^2] + B. \qquad (2)$$

Here $\bar{\nu}$ represents the average total number of neutrons emitted from A_L and A_H; M_N and $\bar{E}_N$ are the mass and average centre-of-mass energy of the

neutrons, $\bar{E}_T$ is the average total fragment kinetic energy; and $\sigma^2(\bar{\nu})$ is the variance about the average number of emitted neutrons. The dominant first two terms of Eq. (2) approximate the broadening for a calculated mass due to varying directions, energies and numbers of emitted neutrons [18]; the third small term is due to an intrinsic energy resolution (FWHM = 1.5 MeV) for heavy-ion energies measured with solid-state detectors [15]; and the last term, B, is an empirically adjustable parameter to take into account any unexpected instrumental mass broadening. The solid curve of Fig. 3(a) shows the result of this computation, for B = 0, compared with the experimentally determined binary mass distribution (open circles) obtained during the experiments in which the proportional X-ray detector was used. The mass resolution established in this manner corresponds to an average FWHM = 4.2 amu. The binary mass distributions obtained during experiments with the NaI X-ray detector exhibited a broader mass resolution due to poorer quality fission-fragment detectors. By empirical adjustment of B a mass resolution with an average FWHM = 5.6 amu was determined for these experiments. With this resolution, the mass distribution calculated using Whetstone's unfolded mass distribution is shown as a solid curve in Fig. 3(b) to be compared with the experimental mass distribution (open circles). Within experimental error the agreement of our data with the theoretically dispersed time-of-flight data is very good, and lends confidence to the experimental mass resolution used in the determination of the average fragment mass for a given mass interval.

Energy and yield of K-X-rays as a function of mass

The K-X-ray pulse-height data for each coincident event were sorted by the computer according to the calculated primary fragment mass distribution into complementary mass intervals of 4 amu over the range A_L = 82 to 125 and A_H = 127 to 170. In Fig. 4 are shown some typical K-X-ray energy spectra for several intervals over this range in comparison with the spectrum for all masses. The plotted points and solid curves represent data obtained with the NaI detector. Typical spectra obtained with the proportional counter are shown (dashed curves with arbitrary ordinate) for two intervals in the light-group mass region. The use of this detector was required for the region below mass 100 where good K-X-ray spectra could not be obtained with the NaI scintillator due to serious intereference by the escape peak for K-X-rays (E > 33 keV) of the heavy group. The proportional counter was not useful, however, for K-X-ray measurements in the heavy group because of its poor efficiency at higher energies. The spectra in Fig. 4 illustrate clearly the expected trend of average K-X-ray energy with mass and also reveal the interesting fact that near symmetry (spectrum at left centre) the emission of K-X-rays by the light fragment is greater than that for the heavy, whereas the reverse is true for very asymmetric mass splits (spectrum at right centre).

The yields of K-X-rays per fission fragment obtained from the K-X-ray energy spectra are listed in Table I as observed (column 4) and corrected for mass resolution (column 5). The corrected yields are plotted in Fig. 5 as a function of the average primary fragment mass (column 2) correspond-

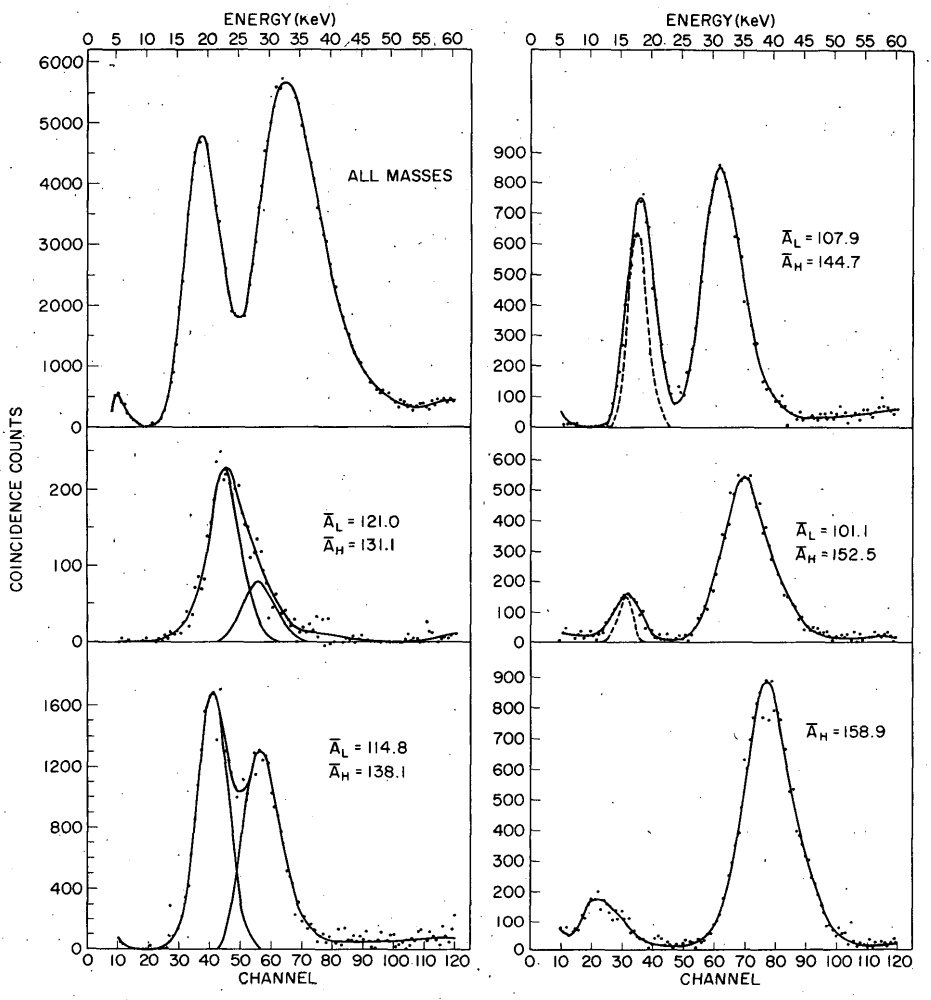

Fig. 4

Energy spectra of K-X-rays emitted by Cf^{252} fission fragments for various complementary mass intervals. $\bar{A}$ refers to average primary fragment mass. Spectra obtained with a NaI detector and a gas-flow proportional detector are shown as continuous and broken curves respectively.

ing to the selected mass interval (column 1). The emission of K-X-rays is seen to be a pronounced function of mass rather analogous to the saw-tooth neutron emission function [16] that reflects the excitation energy of the fragments. Since the K-X-rays arise predominantly from internal conversion of the prompt γ-rays, the yield of K-X-rays per fragment would be expected to depend not only on the fragment excitation energy but also on nuclear structure, i. e. the number, energy and multipolarity of the prompt γ-rays emitted from each fragment. The observed distribution of K-X-rays may then be interpreted in terms of fragment excitation energy and nuclear structure in the following way. In the lighter fragments of the light- and heavy-mass groups near the closed shells (N = 50) and (Z = 50, N = 82) where ex-

TABLE I

VALUES OF K-X-RAY YIELD PER FRAGMENT (X/f) AND AVERAGE PRIMARY NUCLEAR CHARGE (Z_p) AS A FUNCTION OF AVERAGE PRIMARY MASS ($\bar{A}$)

Selected mass interval	$\bar{A}$	Z_p	X/f (observed)	X/f (corrected)
(Light group)				
86-89[a]	89.0 ± 1.0[a]		0.05 ± 0.03[a]	0.05 ± 0.03[a]
90-93[a]	92.5 ± 1.0[a]	36.7 ± 0.3[a]	0.05 ± 0.02[a]	0.05 ± 0.02[a]
94-97[a]	96.5 ± 0.6[a]	38.4 ± 0.3[a]	0.04 ± 0.01[a]	0.05 ± 0.01[a]
98-101[a]	100.5 ± 0.3[a]	39.9 ± 0.2[a]	0.06 ± 0.01[a]	0.06 ± 0.01[a]
98-101	101.1 ± 0.3	40.0 ± 0.2	0.057 ± 0.005	0.056 ± 0.005
102-105[a]	104.4 ± 0.3[a]	41.0 ± 0.2[a]	0.10 ± 0.01[a]	0.10 ± 0.01[a]
102-105	104.8 ± 0.3	41.5 ± 0.2	0.094 ± 0.005	0.097 ± 0.005
106-109[a]	107.8 ± 0.3	42.1 ± 0.2[a]	0.12 ± 0.01[a]	0.12 ± 0.01[a]
106-109	107.9 ± 0.3	42.7 ± 0.2	0.115 ± 0.003	0.120 ± 0.003
110-113[a]	111.3 ± 0.3[a]	43.3 ± 0.2[a]	0.14 ± 0.02[a]	0.15 ± 0.02[a]
110-113	111.1 ± 0.3	44.0 ± 0.2	0.123 ± 0.006	0.130 ± 0.006
114-117[a]	115.1 ± 0.3[a]		0.11 ± 0.02[a]	0.10 ± 0.02[a]
114-117	114.8 ± 0.3	45.4 ± 0.2	0.106 ± 0.005	0.102 ± 0.005
118-121[a]	118.4 ± 0.4[a]		0.12 ± 0.03[a]	0.13 ± 0.03[a]
118-121	118.3 ± 0.3	47.0 ± 0.5	0.13 ± 0.01	0.13 ± 0.01
122-125	121.0 ± 0.5	47.1 ± 0.5	0.12 ± 0.01	0.13 ± 0.01
(Heavy group)				
127-130	131.1 ± 1.0	52.4 ± 1.0	0.05 ± 0.01	0.04 ± 0.01
131-134	134.7 ± 1.0	52.7 ± 1.0	0.05 ± 0.01	0.05 ± 0.01
135-138	138.1 ± 0.5	53.0 ± 0.2	0.096 ± 0.005	0.111 ± 0.006
139-142	141.2 ± 0.3	54.6 ± 0.2	0.137 ± 0.004	0.144 ± 0.004
143-146	144.7 ± 0.3	55.7 ± 0.2	0.168 ± 0.005	0.165 ± 0.005
147-150	148.6 ± 0.3	56.9 ± 0.2	0.258 ± 0.007	0.242 ± 0.007
151-154	152.5 ± 0.3	58.7 ± 0.2	0.49 ± 0.03	0.53 ± 0.03
155-158	155.7 ± 0.3	60.2 ± 0.2	0.84 ± 0.04	0.94 ± 0.05
159-162	158.9 ± 0.5	61.5 ± 0.2	0.87 ± 0.04	0.95 ± 0.05
163-166	162.5 ± 0.8	63.3 ± 0.3	0.67 ± 0.05	0.66 ± 0.04
167-170	166 ± 2	64.9 ± 0.5	0.60 ± 0.05	

[a] Data for experiments with proportional X-ray detector; all other data with NaI detector.

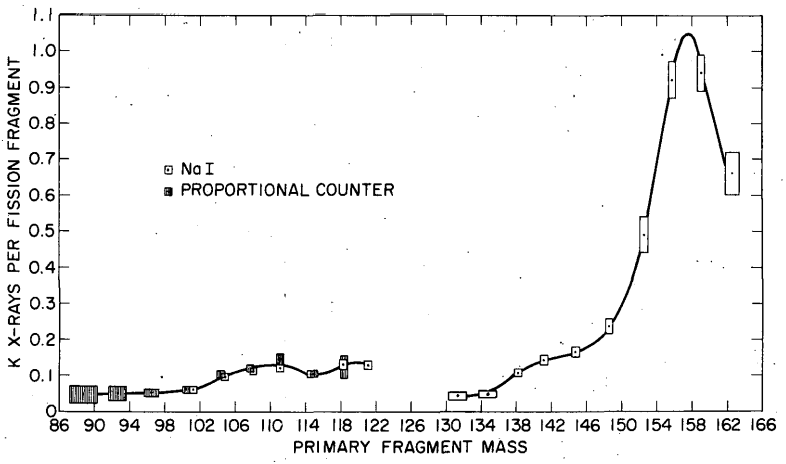

Fig. 5

Yield of K-X-rays emitted by Cf^{252} fission fragments as a function of mass. Size of data symbol represents estimated errors in determinations of yield and mass.

citation energy and level density are lower, fewer γ-rays (possibly of higher average energy) should be emitted resulting in a lower yield of K-X-rays. Conversely, in the heavier fragments of the two mass groups where excitation energy and level density are higher, one might expect enhanced emission of γ-rays (possibly of lower average energy) and hence an increased yield of K-X-rays. In addition, the sharp increase at about mass 150 ($N \sim 92$) occurs just at the beginning of the region of deformed nuclei [19] characterized by rotational states and an abundance of low-energy (highly converted) E2 transitions. The decrease in K-X-ray yield above mass 160 ($N > 98$), however, is not understood at this time, but one is tempted to infer that a change in the nuclear structure of the fragments occurs at this point.

Results and discussion

Values for the most probable primary nuclear charge (Z_p) of the fission fragment calculated from the observed average K-X-ray energy associated with each fragment mass interval (using X-ray energy data tables in Ref. [12]) are tabulated in Table I, column 3. Values of the average primary fragment mass for each mass interval, corrected for experimental mass resolution (see above) and the observed variation of K-X-ray yield with mass (Fig. 5), are listed in Table I, column 2. The Z_p values are plotted as a function of mass in Fig. 6. Estimated errors in Z and A are indicated by the size of the data symbol and are also given in Table I. Also shown in the figure for comparison with the experimental data are Z_p functions according to various postulates for the most probable charge division. The unchanged charge density (UCD) function is based on the simple assumption that the charge-to-mass ratio of the fragments is constant and equal to that of the fissioning nucleus ($Z_F/A_F = 0.3889$ for Cf^{252}). The MER function represents the charge division corresponding to the maximum release of energy in fission (calculated for Cf^{252} by MILTON [16]). The ECD function is given by the empirical

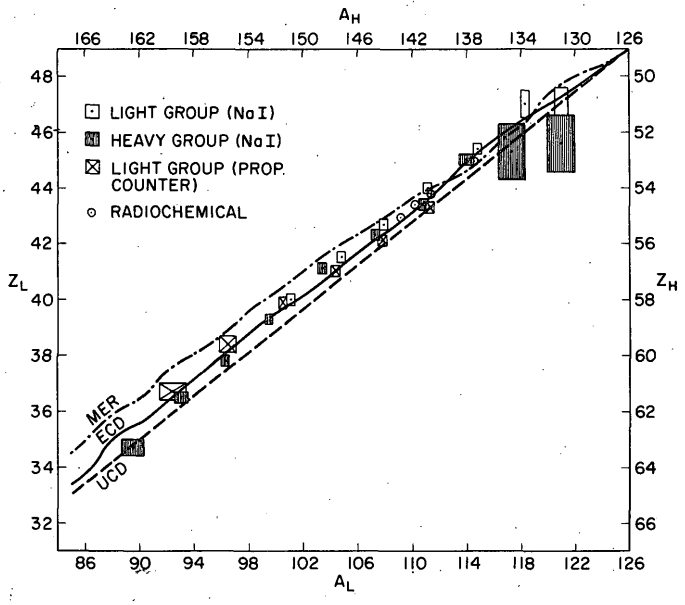

Fig. 6

Average primary nuclear charge as a function of primary fragment mass in spontaneous fission of Cf^{252}. Size of data symbol represents estimated errors in determinations of Z and A. Charge and mass of light-group (Z_L, A_L) and heavy-group (Z_H, A_H) fragments are folded around symmetric fission (Z = 49 and A = 126). Curves for various postulates of charge division are identified as MER (•••), maximum energy release; ECD (——), equal charge displacement; and UCD (--), unchanged charge density.

rule [1] that the most probable charges of complementary fragments are equally displaced from the stability line Z_A, i.e. $(Z_A - Z_P)_L = (Z_A - Z_P)_H$. For calculation of the ECD function Z_A values were taken from the recent analysis of beta-decay energies by DEWDNEY [20] and the modern mass tables by HILLMAN [21]. The Z_A values from these compilations are in good agreement and differ only slightly from those used in Ref. [1]. It is apparent even from the gross plot in Fig. 6 that only the ECD function is in reasonable agreement with our experimental data. The radiochemical data for Cf^{252} fission (open circles) based on fractional chain yield measurements for Cs^{136}, Xe^{139}, Xe^{140} and Xe^{141} [7] are also in good agreement with the physical data and with the ECD function.

A more sensitive test of the fit of the experimental data to the various Z_P functions is provided in Fig. 7 where the function $Z_P - A(Z_P/A_F)$, representing the difference of the most probable charge Z_P from that given by the charge density of the fissioning nucleus (UCD) is plotted against fragment mass A. The straight line EXPTL is the result of a weighted linear least-squares fit to the experimental data of Table I over the mass ranges 89-115 and 137-163 (with heavy-group data converted to light-group complements). The shaded area represents the error band (90% confidence level) for the least-squares analysis. The Z_P function β was calulated by ARMBRUSTER [22] and represents the charge division expected for Cf^{252} by analogy with his

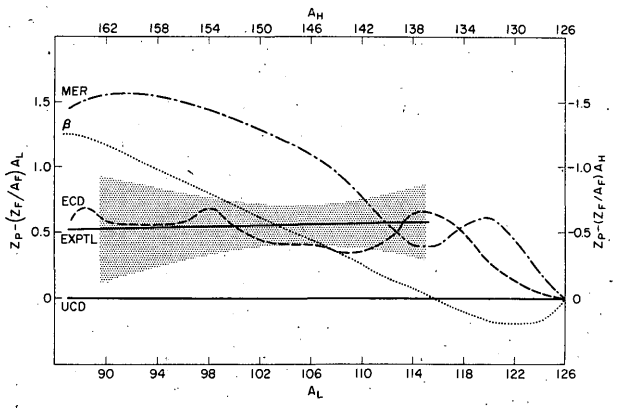

Fig. 7

Difference of the average primary nuclear charge, Z_P, from that given by the charge density of the fissioning nucleus, $(Z_F/A_F)A$, as a function of fragment mass, A. The functions MER (·-·), ECD(--) and UCD (——) are defined in the caption for Fig. 6. The function β(···) is due to ARMBRUSTER [22] and represents the charge division expected for Cf^{252} by analogy with the observed β-decay chain lengths in thermal-neutron-induced fission of U^{235} [6]. The straight line EXPTL is the result of a linear least-squares fit to the data of Table I over the mass ranges 89-115 and 137-163 (with heavy-group data converted to light-group complements). The shaded area represents the error band (90% confidence level) for the least-squares analysis.

measurements of the average β-decay chain lengths in thermal-neutron-induced fission of U^{235} [6]. It is clearly evident that among the various Z_P functions only ECD is consistent with the experimental data. In fact, a χ-squared test for goodness-of-fit shows that the ECD and EXPTL functions represent the data equally well.

A few concluding remarks should be made regarding the reliability of the K-X-ray method for determination of primary nuclear charge. Since the K-X-rays are produced by the process of internal conversion, there is the possibility that the process might be selective and give rise to K-X-rays not representative of the average atomic number for a given mass interval. In this case one would expect to find local deviations in the Z_P values (well outside of experimental error) from one mass interval to another, and also failure of charge conservation ($Z_L + Z_H = Z_F$) for the complementary Z_P values associated with a given mass split. By reference to Fig. 6 it is seen that these signs of selectivity do not occur even in the complementary mass regions 92-104 and 148-160 where there is a wide disparity in K-X-ray yield (Fig. 5). It is therefore concluded from this work with spontaneous fission of Cf^{252} that the K-X-ray method gives a reasonably accurate picture of charge division and will become a powerful tool in future investigations of charge distribution in nuclear fission.

ACKNOWLEDGEMENTS

The authors wish to express their gratitude to the Argonne heavy element chemistry group for making available sources of Cf^{252}, and to thank

Dr. A. H. Jaffey for helpful discussions concerning the statistical analysis of the experimental data.

REFERENCES

[1] GLENDENIN, L. E., CORYELL, C. D. and EDWARDS, R. R., in Radiochemical Studies: the Fission Products (CORYELL, C. D. and SUGARMAN, E., Eds.) National Nuclear Energy Series IV-9, McGraw-Hill, New York (1951) 489.
[2] VOITOVETSKII, V. K., LEVIN, B. A. and MARCHENKO, E. V., Soviet Physics-JETP 5 (1957) 184.
[3] SKLIAREVSKII, V. V., FOMENKO, D. E. and STEPANOV, E. P., Soviet Physics-JETP 5 (1957) 220.
[4] LEACHMAN, R. B., Proc. 2nd UN Int. Conf. PUAE 15 (1958) 331.
[5] SKLIAREVSKII, V. V., STEPANOV, E. P. and MEDVEDV, B. A., Soviet Physics-JETP 36 (1959) 225.
[6] ARMBRUSTER, P., HOVESTADT, D., MEISTER, H. and SPECHT, H. J., Nucl. Phys. 54 (1964) 586.
[7] WAHL, A. C., FERGUSON, R. L., NETHAWAY, D. R., TROUTNER, D. E. and WOLFSBERG, K., Phys. Rev. 126 (1962) 1112.
[8] ROSE, M. E., Internal Conversion Coefficients, North Holland Publishing Co., Amsterdam (1958).
[9] SMITH, A. B., FIELDS, P. R. and FRIEDMAN, A. M., Phys. Rev. 104 (1956) 699.
[10] GRIFFIN, H. C. and GLENDENIN, L. E., Bull. Amer. phys. Soc. II 9 (1964) 665; Phys. Lett. (1965, in press).
[11] COMPTON, A. H. and ALLISON, S. K., X-Rays in Theory and Experiment, Van Nostrand, New York (1935) 745.
[12] WAPSTRA, A. H., NIJGH, G. J. and VAN LIESHOUT, R., Nuclear Spectroscopy Tables, North Holland Publishing Co., Amsterdam (1959) 71.
[13] HOHMANN, H., Z. Phys. 172 (1963) 143.
[14] UNIK, J. P., unpublished work (1964).
[15] SCHMITT, H. W., KIKER, W. E. and WILLIAMS, C. W., to be published in Phys. Rev. (1965).
[16] BOWMAN, H. R., MILTON, J. C. D., THOMPSON, S. G. and SWIATECKI, W., Phys. Rev. 129 (1963) 2133.
[17] WHETSTONE, S. L., Phys. Rev. 131 (1963) 1232.
[18] TERRELL, J., Phys. Rev. 127 (1962) 880.
[19] BOHR, A. and MOTTELSON, B. R., Mat.-fys. Meddr. 27 No. 16 (1953).
[20] DEWDNEY, J. W., Nucl. Phys. 43 (1963) 303.
[21] HILLMAN, M., Brookhaven National Laboratory Report BNL 846 (T-333) (1964).
[22] ARMBRUSTER, P., private communication (1964).

X-RAYS EMITTED IN COINCIDENCE WITH THE FISSION OF Cf^{252} *

T.D. THOMAS AND R.A. ATNEOSEN
PRINCETON UNIVERSITY,
W.M. GIBSON
BELL TELEPHONE LABORATORIES,
AND
M.L. PERLMAN
BROOKHAVEN NATIONAL LABORATORY,
UNITED STATES OF AMERICA

Abstract — Résumé — Аннотация — Resumen

X-RAYS EMITTED IN COINCIDENCE WITH THE FISSION OF Cf^{252}. A possible technique for studying charge distribution in fission is the simultaneous measurement of the kinetic energies of both fragments and the energy of the K-X-rays emitted in coincidence with fission. The two kinetic energies define the masses of the fragments and the X-ray energy defines the atomic number of one fragment.

For such a measurement to yield information on charge distribution, it is necessary that the number of vacancies in the K-shell vary slowly with the mass and charge of the fragments. If the vacancies are produced in the fission act itself, it seems likely that this condition is satisfied. X-rays so produced would be emitted within $\sim 10^{-15}$ s after fission.

If, on the other hand, the vacancies are produced by internal conversion of gamma rays emitted after fission, it is quite possible that the yield of X-rays may vary markedly from one nucleus to the next. Such X-rays would be emitted with lifetimes characteristic of the converted gamma rays - probably at least as long as 10^{-12} s.

We have measured the lifetime of the X-rays emitted in coincidence with fission with a time resolution of ~1 ns. The spectrum of X-rays shows two peaks, one at the proper energy for light fission fragments, the other at the proper energy for heavy fragments. The number of K-X-rays per fission is approximately 0.6.

The two peaks fall off in approximately the same manner with increasing time after fission. The apparent mean lifetime is about 1 ns, but the decay curve is complex and does not contain any obvious single component. There is no evidence of an appreciable number of K-X-rays emitted with lifetimes less than about 0.4 ns. Our conclusions from these results are that most, if not all, of the K-vacancies are due to internal conversion, but that many different gamma-ray lifetimes appear in the decay curve.

Experiments are in progress to measure simultaneously the kinetic energies of the two fragments and the K-X-ray energy.

ÉMISSION DE RAYONS X EN COINCIDENCE AVEC LA FISSION DE ^{252}Cf. Une méthode possible pour étudier la distribution des charges lors d'une fission consiste à mesurer simultanément les énergies cinétiques des deux fragments et l'énergie des rayons X K émis en coïncidence avec la fission. Les énergies cinétiques définissent les masses de ces fragments et l'énergie des rayons X caractérise le numéro atomique de l'un d'entre eux.

Pour que cette mesure fournisse des renseignements sur la distribution des charges, il faut que le nombre de lacunes dans la couche K varie lentement avec la masse et la charge des fragments. Si les lacunes sont produites au cours du phénomène de fission proprement dit, cette condition sera probablement remplie. Les rayons X ainsi obtenus seraient émis dans l'espace de 10^{-15} s environ qui suit la fission.

Si en revanche les lacunes sont produites par conversion interne des rayons gamma émis après la fission, il est fort possible que le rendement en rayons X varie sensiblement d'un noyau à l'autre. Ces rayons X seraient émis avec des durées de vie caractéristiques pour des rayons gamma de conversion - probablement de 10^{-12} s au minimum.

* This work supported in part by the United States Atomic Energy Commission.

Les auteurs ont mesuré la durée de vie des rayons X émis en coïncidence avec la fission, avec une résolution dans le temps de l'ordre d'une nanoseconde. Le spectre des rayons X présente deux pics, l'un pour l'énergie propre aux fragments légers, l'autre pour celle qui est propre aux fragments lourds. Le nombre de rayons X K par fission est d'environ 0,6.

Les deux pics se tassent de façon à peu près identique avec le temps après la fission. La durée de vie moyenne apparente est de l'ordre d'une nanoseconde, mais la courbe de décroissance est complexe et ne comporte pas de composante unique évidente. Rien ne prouve que soient émis un nombre appréciable de rayons X K ayant une vie inférieure à environ 0,4 ns. Ces résultats permettent aux auteurs de conclure que les lacunes K sont dues pour la plupart, sinon en totalité, à une conversion interne, mais que de nombreuses durées de vie gamma différentes apparaissent dans la courbe de décroissance.

Des expériences sont en cours pour mesurer simultanément les énergies cinétiques des deux fragments et l'énergie des rayons X K.

РЕНТГЕНОВСКИЕ ЛУЧИ, ИСПУСКАЕМЫЕ В СОВПАДЕНИИ С ДЕЛЕНИЕМ КАЛИФОРНИЯ-252. Возможным способом изучения распределения заряда при делении является одновременное измерение кинетических энергий обоих осколков и энергии рентгеновского К-излучения, испускаемого в совпадении с делением. Обе кинетические энергии определяют массы осколков, а энергия рентгеновских лучей определяет атомный номер одного осколка.

Для того, чтобы такое измерение дало информацию о распределении заряда, необходимо, чтобы количество вакансий в оболочке К плавно изменялось в зависимости от массы и заряда осколков. Если вакансии образуются при самом акте деления, то вполне возможно, что это условие удовлетворяется. Рентгеновские лучи, полученные таким образом, испускались бы в течение $\sim 10^{-15}$ сек после деления.

С другой стороны, если вакансии образуются посредством внутреннего преобразования гамма-лучей, испускаемых после деления, то вполне возможно, что выход рентгеновских лучей может существенно меняться от одного ядра к последующему. Такие рентгеновские лучи испускались бы по характеристике времени жизни преобразованных гамма-лучей вероятно в течение по крайней мере 10^{-12} сек.

Мы замерили продолжительность жизни рентгеновских лучей, испускаемых в совпадении с делением при разрешающей способности по времени ~1 наносек. Спектр рентгеновских лучей показывает два пика, один при энергии, достаточной для легких осколков деления, а другой — при энергии, достаточной для тяжелых осколков. Количество рентгеновского К-излучения, приходящееся на одно деление, составляет приблизительно 0,6.

Спад обоих пиков происходит приблизительно одинаково с увеличением времени после деления. Кажущееся среднее время жизни составляет величину порядка 1 наносек, однако кривая распада сложна и не содержит какого-либо очевидного отдельного компонента. Не имеется никаких данных относительно значительного количества рентгеновского К-излучения с временем жизни менее 0,4 наносек. Наше заключение на основании этих результатов сводится к тому, что большинство, если не все К-вакансии образуются за счет внутреннего преобразования, но, что в кривой распада появляется много различных периодов жизни гамма-лучей.

Проводятся эксперименты с целью одновременного измерения кинетических энергий обоих осколков и энергии рентгеновского К-излучения.

RAYOS X EMITIDOS EN COINCIDENCIA CON LA FISION DEL ^{252}Cf. Para estudiar la distribución de las cargas en la fisión, puede utilizarse, entre otros, un método consistente en la medición simultánea de las energías cinéticas de los dos fragmentos de fisión y de la energía de los rayos X de la serie K emitidos en coincidencia con la fisión. Los dos valores de la energía cinética definen las masas de los fragmentos en tanto que la energía de los rayos X define el número atómico de uno de ellos.

Para que tales mediciones proporcionen información sobre la distribución de las cargas, es necesario que el número de huecos en la capa K varíe lentamente con la masa y la carga de los fragmentos. Si esos huecos se producen en el acto de fisión propiamente dicho, es probable que esa condición quede satisfecha. La emisión de los rayos X así formados tendría lugar en el intervalo de $\sim 10^{-15}$ s subsiguiente a la fisión.

Si, por el contrario, esos huecos se producen por conversión interna de los rayos gamma emitidos después de la fisión, cabe suponer que el rendimiento de rayos X varíe marcadamente de un núcleo al siguiente. El período de los rayos X que se emiten de esa forma sería el característico de los rayos gamma convertidos, es decir, probablemente hasta de 10^{-12} s como mínimo.

Los autores han medido el período de los rayos X emitidos en coincidencia con la fisión, con una resolución en tiempo de ~1 ns. El espectro de esos rayos X presenta dos picos, uno correspondiente a la energía

propia para los fragmentos de fisión ligeros, y el otro a la energía propia de los fragmentos pesados. El número de rayos X de la serie K por cada fisión es de 0,6 aproximadamente.

Los dos picos se atenúan de manera comparable al aumentar el tiempo transcurrido desde la fisión. El período medio aparente es del orden de 1 ns, pero la curva de desintegración es compleja y no comprende ninguna componente evidente. No hay pruebas de que la emisión incluya un número apreciable de rayos X de la serie K con períodos inferiores a unos 0,4 ns. Teniendo en cuenta estos resultados, los autores llegan a la conclusión de que la mayoría, si no todos los huecos en la capa K se deben a la conversión interna, aunque la curva de desintegración refleje la presencia de rayos gamma de períodos muy distintos.

Los autores están llevando actualmente a cabo experimentos para medir simultáneamente las energías cinéticas de los dos fragmentos de fisión y la energía de los rayos X de la serie K.

INTRODUCTION

The traditional method for measuring the mass and charge distributions of fission fragments has been the radiochemical isolation of specific fission products. This method has the disadvantage of requiring a great deal of work to determine one mass yield curve or one charge distribution curve. Because of uncertainties in half lives and other decay properties of the nuclides involved, results obtained in this way are often less accurate than might be desired.

In the last few years it has been demonstrated that a pair of semiconductor detectors can be used to give a rather accurate mass yield curve in a short time [1, 2]. Each detector determines the kinetic energy of one of the two coincident fission fragments. From conservation of momentum and mass it is possible to calculate the masses of the two fragments from their kinetic energies.

A possible method to determine the charge distribution is to measure the spectrum of K-X-rays emitted in coincidence with a fission event. Since the X-rays are characteristic of the atomic number of the fission fragment emitting the radiation, such a measurement should be equivalent to a measurement of the nuclear charge distribution of the fission fragments. Similarly, a simultaneous measurement of the K-X-ray energy and the kinetic energies of the two fission fragments gives both the mass and charge of the fragments, and hence the charge distribution for a given mass. The results of such measurements for the spontaneous fission of Cf^{252} have been reported by UNIK and GLENDENIN [3].

For this technique to be applicable, it is important that the probability of producing a K-electron vacancy on a given fragment as a function of mass and charge of the fragment either be known or vary slowly and smoothly as a function of these variables. If this probability varies erratically when the mass or charge of the fragment varies by only a few units, the measured charge distribution may be a bad representation of the true charge distribution.

If the K-electron vacancies are produced by a disruption of the electron cloud by the separating fragments, the yield of vacancies per fission should vary smoothly with the mass and charge of the fragments. However, the fission fragments move with velocities that are about a factor of 10 smaller than the velocities of the electrons that become K-electrons in the final fragments. It seems likely that the electron cloud is able to adjust adiabatically

to the changing nuclear environment and that no vacancies are produced by this mechanism.

The work of GRIFFIN and GLENDENIN [4] indicates that the K-shell vacancies are produced by internal conversion in the fragments after fission. In this case vacancy production is subject to the vagaries of the nuclear de-excitation process and of the conversion coefficients. However, if for each mass and charge there is a large variety of transitions being converted, it is possible that fluctuations in yield may be averaged out and there will be a smooth variation in yield from one mass or charge to the next.

Some information concerning the source of the K-shell vacancies can be obtained by measuring the apparent lifetime of the K-X-rays. If the vacancies are produced by a disruption of the electron cloud, the X-rays will be emitted with lifetime of about 10^{-16} s [5]. On the other hand, if the vacancies are produced by internal conversion the lifetimes will be those of the nuclear states undergoing conversion. The Weisskopf estimate for E1 transitions of low enough energy to be appreciably converted is 10^{-12}s [6]. Experimentally, low-energy E1 transitions are 10^3 to 10^7 times slower than predicted by the Weisskopf estimate [7]. These considerations and similar ones for E2 and M1 transitions indicate that the shortest lifetimes observed should be about 10^{-9} s.

Approximate measurements of the lifetime of low-energy photons emitted in coincidence with fission have been made by SKLIAREVSKII, FOMENKO and STEPANOV [8], using a time-of-flight method, and by DESI, LAJTAI and NAGY [9], using fast electronic methods. Griffin and Glendenin have made measurements of the X-ray lifetimes. All the results indicate lifetimes of the order of 10^{-9} s.

Another experiment that should shed light both on the source of the K-shell vacancies and on the suitability of using K-X-ray measurements to determine charge distribution is to determine the yield and spectrum of electrons in coincidence with fission for the various mass divisions. If the K-shell vacancies are produced by internal conversion, then it may be possible to detect peaks in the electron spectrum corresponding to the discrete energies of the converted transitions. If the electron spectrum for a given mass shows only a few peaks, then only a few transitions are being converted and it is likely that the X-ray distribution will depend as much on fluctuations in the number, energies and multipolarities of transitions being converted as on the actual nuclear charge distribution. On the other hand, if the electron spectrum indicates that a large number of transitions are undergoing internal conversion we may hope that the fluctuations will be averaged out and that the yield of vacancies per fission will be a slowly varying function of mass and charge.

In the first of the two following sections we present the results of measurements of the lifetimes of the K-X-rays emitted in coincidence with the fission of Cf^{252}. Also included is information on the spectrum of K-X-rays and the number of K-X-rays per fission. In the second of the two sections we give the results of measurements of the yield and spectrum of electrons emitted in coincidence with the fission of Cf^{252} as a function of the mass division.

K-X-RAY MEASUREMENTS

Experimental method

The experimental method is based on the fact that the fission fragments have velocities of about 10^9 cm/s. If an X-ray detector is so collimated that it can detect X-rays only from those fragments that have moved a distance between x and $x+\Delta x$ cm from the source it will thus detect only those X-rays that are emitted between x and $x+\Delta x$ ns after fission.

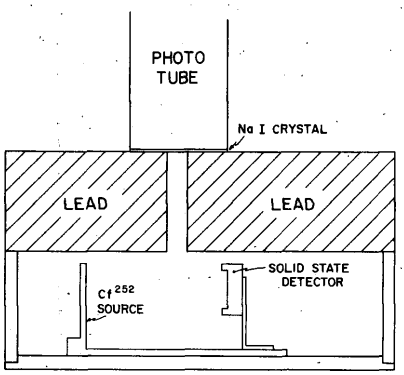

Fig. 1

Schematic drawing of apparatus used in the X-ray timing experiments

A schematic drawing of the apparatus is shown in Fig. 1. The californium source and a semiconductor fission-fragment detector were attached to a movable slide in an evacuated chamber. One wall of the chamber was a 2-in lead block with a slot 1-cm wide cut in it. Directly above this slot was placed a sodium iodide crystal attached to a photomultiplier tube. The scintillation crystal was 1-mm thick and 5 cm in diameter; this thickness was chosen to minimize the sensitivity of the detector to high-energy gamma rays and neutrons.

The source could be positioned anywhere from a point directly under the collimating slot to a point about 6.5 cm back from the slot. The dimensions of the slot and of the semiconductor detector were such that any fission fragment that struck the detector must have passed under the collimator. This arrangement guaranteed that, to first order, the geometrical detection efficiency of the system did not depend on the source-to-collimator distance. Only X-rays emitted when the fragment was directly opposite the slot could reach the scintillation detector.

The signals from the two detectors were amplified in conventional preamplifiers and linear amplifiers. The output pulses from the two amplifiers were fed to a coincidence circuit having a resolving time of about 130 ns. The pulses from the X-ray detection system were also sent to a multichannel pulse-height analyser, which was gated on when the coincidence conditions were satisfied.

Two measurements were made at each source-to-collimator distance. One was made with no absorber between the sodium iodide crystal and the

chamber other than the necessary thin aluminium windows. The other was made with a copper (0.4 g/cm^2) and aluminium (0.2 g/cm^2) absorber covering the entrance to the collimator. The transition of this absorber for 50-keV photons was calculated to be 31% [10]. The absorber was essentially opaque for X-rays of interest (20 to 40 keV) and practically transparent for higher energy photons. The spectra measured with the absorber in place represent the background due to high-energy photons (in coincidence with fission) that deposited a small fraction of their energy in the crystal. The difference between the two spectra was taken to be the true spectrum of low-energy photons in coincidence with fission.

For small distances the background represented about 40% of the counting-rate; for the largest distances the background was as much as 90% of the rate. The data collected at large distances will be strongly influenced by errors in the background. Experiments using twice as much absorber indicate that this method underestimates the background.

Results

A spectrum obtained with the source at zero distance from the collimator is shown in Fig. 2. The "zero" position is with the source directly

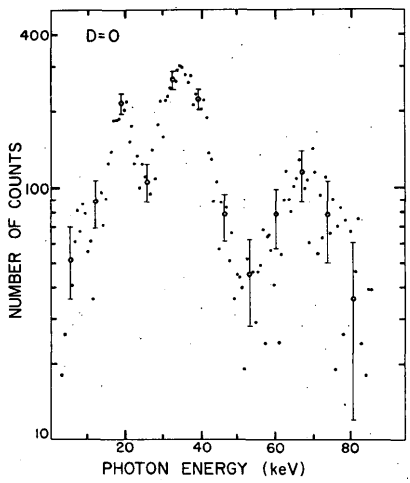

Fig. 2

Low-energy photons detected in coincidence with fission. Source-to-collimator distance is D = 0.

below one edge of the collimator, so Fig. 2 represents an integral of X-ray emissions occurring during the first centimetre of flight, or the first nanosecond. The two major peaks, at ~20 and ~35 keV, are due to K-X-rays from the light and heavy fission fragments respectively. The small peak at about 10 keV is an escape from the group at 35 keV. The peak at ~70 keV is at the energy of platinum K-X-rays; the fission source was mounted on platinum and there is presumably fluorescence of this backing material either by the fission fragments or by the post-fission gamma rays. This peak did

not appear when the source-to-collimator distance was such that the backing could not be seen by the scintillator.

If we integrate the intensity under the light- and heavy-fragment peaks separately, we obtain the total coincidence rate for each. In Fig. 3 we have plotted these rates as a function of the source-to-collimator distance. The

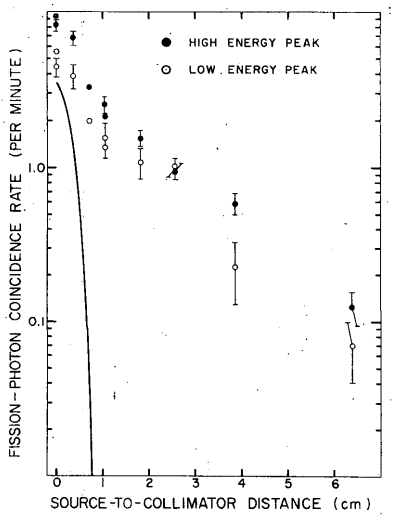

Fig. 3

Fission-photon coincidence rate as a function of source-to-collimator distance. The solid curve is the rate of coincidences between Cf^{252} alpha particles and curium L-X-rays.

solid line in Fig. 3 represents results of measurements of the rate of coincidences between the Cf^{252} alpha particles and curium L-X-rays produced in the alpha decay of Cf^{252}. This curve indicates the resolution of the system for prompt coincidences. These results are in agreement with those of GRIFFIN and GLENDENIN [4], who found that there are about twice as many K-X-rays from the heavy fragments as from the light and that about half of the X-rays are emitted in the first nanosecond. If we integrate the data of Fig. 3 over all distances and combine the result with an estimated geometry for the scintillation crystal, we calculate that there are about 0.6 K-X-ray per fission. This number is also in agreement with that obtained by Griffin and Glendenin.

Discussion

The obvious conclusion from the data presented in Fig. 3 is that the lifetime for X-ray emission is approximately 1 ns. This lifetime is not consistent with the K-shell vacancies being produced by a disruption of the electron cloud in the fission process. It is, however, about right if the vacancies are produced by internal conversion.

We can make a more quantitative estimate of the range of lifetimes represented in the data of Fig. 3. We assume that there is a large variety of transitions undergoing internal conversion and that these transitions have

lifetimes ranging from some minimum value τ_{min} to some maximum value τ_{max}. We make the approximation that there is no delay between the fission event and production of the state that undergoes conversion. We further assume that the probability of producing a nuclear state for which the logarithm of the lifetime is between y and y+Δy is constant between τ_{min} and τ_{max}. In other words, there are as many states formed with lifetimes between 1 and 2 ns as between 2 and 4 ns or between 4 and 8 ns. The probability of producing a nuclear state with lifetime between τ and $\tau+d\tau$ is then proportional to $1/\tau$.

The X-ray emission rate R is given by the expression

$$R = \text{const} \int_{\tau_{min}}^{\tau_{max}} \frac{\lambda e^{-\lambda t}}{\tau} \, d\tau ,$$

where λ is the decay constant for a state of lifetime $\tau(\lambda = 1/\tau)$ and t is the time since fission. Integrating this expression we obtain

$$R = \frac{\text{const}}{t} \left[\exp(-t/\tau_{max}) - \exp(-t/\tau_{min})\right] .$$

To obtain the experimentally observed rate, this expression must also be integrated over the 1 ns time interval in which the fragments are opposite the collimator.

By trial and error we have found the values of τ_{max} (5.0 ns) and τ_{min} (0.33 ns) that give the best fit to our data. The resulting curve is shown as a solid line in Fig. 4, where it is compared with the data from the high-energy X-ray peak. The vertical normalization is arbitrary; only the shape has been fitted. For comparison we show as a dashed line the result if we assume τ_{min} = 0.10 ns and as a dotted line the result if we assume τ_{max} = 10 ns. It is clear that values of the maximum and minimum lifetimes very far from those indicated will not give a satisfactory fit to the data, given the assumptions outlined above. However, since we did not make measurements for source-to-collimator distances greater than 6.5 cm, we obtained essentially no information on the existence of states having lifetimes longer than about 50 ns. The work of GRIFFIN and GLENDENIN [4] indicates that about 7% of the X-rays are emitted with a half-life of 30 ns and about 8% with a half-life of 100 ns. Our experimental results are not inconsistent with the existence of this much long-lived activity, and the inclusion of a contribution from this activity in the calculated curves of Fig. 4 does not appreciably distort their shape.

In view of the considerations mentioned in the introduction, it is not surprising that the shortest lifetimes are about 0.3 ns. Transitions having lifetimes shorter than this are high-energy transitions and are not highly converted. Because of the uncertainties of the background subtraction and because our measurements did not go beyond a source-to-collimator distance of 6.5 cm, the upper limit on the lifetimes is not well defined. However, except for the final stages of nuclear de-excitation, these low-energy

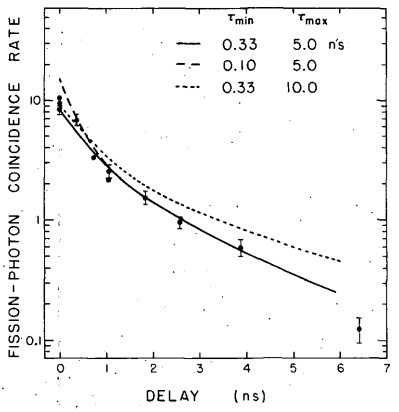

Fig. 4

Fission-photon coincidence rate for X-rays emitted by the heavy fission fragments. The curves have been calculated by the method indicated in the text.

converted transitions may have to compete with high-energy unconverted transitions. In this case only those having short lifetimes will compete effectively and we might expect the total range of lifetimes to be small.

Although these experiments tend to confirm the belief that the K-shell vacancies are produced by internal conversion, they do not shed much light on the question of the suitability of this method for determining charge distribution. The shape of the X-ray spectrum does not change much during the first few nanoseconds after fission, indicating that there is about the same range of lifetimes for all modes of fission. The lack of any pronounced variation in the decay curve as a function of X-ray energy suggests that for each mode of fission there are at least several transitions that lead to K-shell vacancies.

ELECTRON MEASUREMENTS

Experimental method

A schematic drawing of the apparatus used for the electron measurements is shown in Fig. 5. A source of Cf^{252} yielding about 5×10^5 fissions per minute was sandwiched between two nickel foils, 50 and 100 $\mu g/cm^2$ thick. Two diffused-junction semiconductor detectors subtending angles of 16° each were placed on either side of the source to detect the coincident fission fragments. A surface barrier detector with a depletion depth of about 1 mm was placed so as to detect electrons emitted at 90° to the direction of the fission fragments; this detector subtended an angle of 22°. The electron detector was cooled to dry-ice temperature.

Preamplifiers and amplifiers for the fission detectors were conventional. In order to minimize problems due to the overload pulses that occurred when a fission fragment or an alpha particle struck the electron detector we incorporated diode-limiting circuits in the preamplifier and

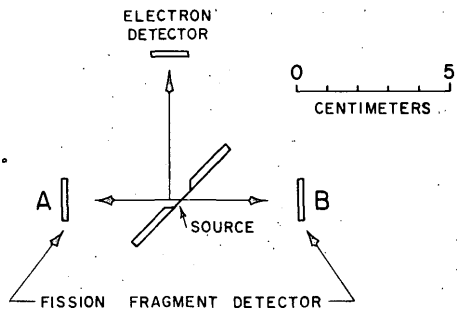

Fig. 5

Schematic drawing of the apparatus used to measure the spectra of electrons emitted in coincidence with fission

amplifier for the electron detector. A coincidence circuit produced a gating pulse for the pulse-height analyser if pulses from the three amplifiers arrived within 1 μs of each other. Even with the diode-limiting circuits the amplifier did not return to its quiescent state for about 60 μs after a fission pulse. We therefore used the fission and alpha-particle pulses to generate a signal that prevented the coincidence circuit from producing a gate for 60 μs after such an overload pulse.

Measurements with Cs^{137} and Hg^{203} indicated that the resolution of the electron detection system was about 14 keV full width at half maximum. Reliable information could be obtained from electrons with energies as low as 35 to 40 keV.

The two fission pulses were fed to an adder-divider circuit [11] that generated a pulse proportional to A/(A+B), where A and B are the two pulse heights. Since the pulse-height defect will cancel to first order in such a calculation, this ratio is proportional to the mass of fragment B.

The output of the divider circuit and the output from the amplifiers in the electron detector circuit were used as the two inputs of a two-parameter pulse-height analyser. The data stored in the analyser thus represented the electron spectrum as a function of the mass division.

Background measurements were taken with an aluminium absorber 1-mm thick over the electron detector. This absorber stops electrons up to about 700 keV but has a negligible effect on gamma rays. The difference between the spectra taken with and without the absorber represents the electron spectrum. The background accounted for about 32% of the total coincidence rate.

Results and discussion

In Fig. 6 are displayed the electron spectra for several different mass divisions. There are occasional peaks standing out above the average level of intensity, indicating that at least some of the electron vacancies are produced by conversion. However, the curves are, for the most part, rather featureless and we conclude either that the spectra contain a component that

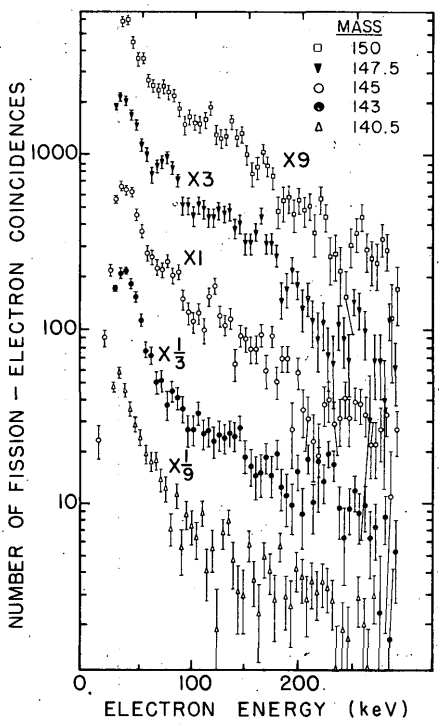

Fig. 6

Energy spectra of electrons detected in coincidence with the fission of Cf^{252} for various mass divisions. Squares correspond to a fragment of mass 150 into detector A; inverted triangles, mass 147.5; open circles, mass 145; closed circles, mass 143; open triangles, mass 140.5. The numbers above each curve give the factor by which those data have been multiplied before plotting.

varies smoothly with energy or that the various converted transitions are closely spaced on the average.

If all the spectra of the type shown in Fig. 6 are integrated over the electron energy, we obtain the curve shown in Fig. 7, the electron yield as a function of the mass of the fragment going into detector A (see Fig. 5). The curve is clearly asymmetric. However, inspection of Fig. 5 shows that the apparatus is also asymmetric; electrons emitted from certain fragments headed towards counter B cannot reach the electron detector because of the source mount. We therefore conclude that the high yield for asymmetric divisions of the mass arises largely from the heavy fragments. This conclusion is in agreement with the measurements of UNIK and GLENDENIN [3] who found that the K-X-ray yield was very high for the heaviest fragments.

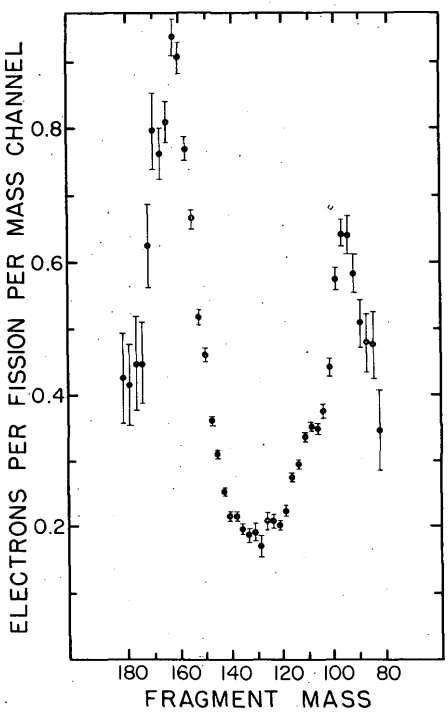

Fig. 7

The number of electrons between 35 and 260 keV per fission fragment as a function of the mass of the fragment incident on detector A

ACKNOWLEDGEMENTS

The Cf^{252} from which the sources were prepared was obtained from the Lawrence Radiation Laboratory, to whom we are grateful.

REFERENCES

[1] GIBSON, W.M., THOMAS, T.D. and MILLER, G.L., Phys. Rev. Lett. 7 (1961) 65.
[2] BRITT, H.C., WEGNER, H.E. and WHETSTONE, S.L., Nucl. Instrum. Meth. 24 (1963) 13.
[3] UNIK, J.P. and GLENDENIN, L.E., Bull. Amer. phys. Soc. II, 10 (1964) 13.
[4] GRIFFIN, H.C. and GLENDENIN, L.E., Bull. Amer. phys. Soc., II, 9 (1963) 665.
[5] COMPTON, A.H. and ALLISON, S.K., X-Rays in Theory and Experiment, D. Van Nostrand Co., Inc., New York (1935) 745.
[6] WAPSTRA, A.H., NIJGH, G.J. and VAN LIESHOUT, R., Nuclear Spectroscopy Tables, North Holland Publishing Co., Amsterdam (1959) 74.
[7] GOLDHABER, M. and SUNYAR, A.W., in Beta- and Gamma-Ray Spectroscopy (SIEGBAHN, K., Ed.) North Holland Publishing Co., Amsterdam (1955) 453.
[8] SKLIAREVSKII, V.V., FOMENKO, D.E. and STEPANOV, E.P., Ž. eksp. teor. Fiz. 32 (1957) 256; (Translation: Soviet Physics-JETP 5 (1957) 220).
[9] DESI, S., LAJTAI, A. and NAGY, L., Acta phys. Acad. Sci. hung. 15 (1962) 185.

[10] GRODSTEIN, G. W., X-ray Attenuation Coefficients from 10 keV to 100 MeV, National Bureau of Standards Circular 583, United States Government Printing Office, Washington (1957).
[11] MILLER, G. L. and GERE, E. A., Institute of Electronical and Electronics Engineers Trans. on Nucl. Sci. NS-11 (1964) 382.

DISCUSSION

(on the foregoing two papers)

R. VANDENBOSCH: I would like to offer an explanation for the decrease in K-X-ray yield for very heavy fragments. As Dr. Glendenin has mentioned, the increase in K-X-ray yield between A = 150 and A = 155 can be attributed to the onset of permanent nuclear deformation characterized by low-lying collective levels with large conversion coefficients. As one gets farther into the deformed region, the decrease in the energy of the first excited state and the increase in the K-electron binding energy will prevent K-conversion from occurring. The K-X-ray yield will actually start to decrease with decreasing transition energies somewhat before reaching the K-electron binding energy as the L/K ratio becomes appreciably greater than 1.0. An extrapolation of known first excited state energies into the neutron-rich primary fission-fragment region indicates this might occur at about the right mass region where Glendenin observes the decrease in K-X-ray intensity.

I agree with Dr. Thomas that such an explanation does not help in understanding the yield of high-energy electrons. It should be mentioned, however, that the K-conversion electrons of the first excited state of even-even nuclei will be below his experimental cut-off for masses heavier than about A = 150, and hence the effect I am discussing could not be observed in his experiment.

T.D. THOMAS: Your comment offers a satisfactory explanation for K-X-rays but the similar behaviour of the electrons still needs to be explained.

N. FEATHER: Would one not expect double K-vacancies in the case of fragments of mass greater than 150? The average number of such vacancies per fragment is already about 1.0 in this mass region.

T.D. THOMAS: A vacancy in the K-shell would be filled in approximately 10^{-16} s. The time for vacancy production by the conversion process is found to be about 10^{-9} s. Thus any vacancy produced would be filled in a time that is short compared with the time taken to produce a second vacancy.

PRIMARY DISTRIBUTIONS OF NUCLEAR CHARGE FOR FISSION-FRAGMENT MASSES 132, 134, 136 AND 137 FROM THERMAL FISSION OF U^{235}

E. KONECNY, H. OPOWER, H. GÜNTHER AND H. GÖBEL
PHYSIK-DEPARTMENT DER TECHNISCHEN HOCHSCHULE MÜNCHEN, MUNICH
AND II. PHYSIKALISCHES INSTITUT
DER JUSTUS LIEBIG-UNIVERSITÄT GIESSEN,
FEDERAL REPUBLIC OF GERMANY

Abstract — Résumé — Аннотация — Resumen

PRIMARY DISTRIBUTIONS OF NUCLEAR CHARGE FOR FISSION-FRAGMENT MASSES 132, 134, 136 AND 137 FROM THERMAL FISSION OF U^{235}. By a mass spectrometer fission fragments from thermal fission of U^{235} are exactly separated with respect to mass and kinetic energy within a time of 10^{-6} s after fission. The separated fragments are caught in a β-sensitive Ilford G 5 emulsion that is located in the focal plane of the spectrometer. Development of the irradiated emulsions is carried out, if possible, after a time long compared with the longest half-life of the regarded decay chain. Half-lives of days or longer are not taken into account, but corrections can be easily made for them. After development of the emulsions all beta tracks emerging from the end of every fission-fragment track can be seen under the microscope. The possibility of correlating every single β-track with a particular fission-fragment track allows the evaluation of the number n(x) of fission fragments possessing x β-tracks, thus giving not only the mean chain length but also the β-particle distribution. As the stable end product of each decay chain is known, this β-distribution is an exact image of the primary nuclear charge distribution. In the measurements done up to now only β-particles emitted into the half solid angle formed by the emulsion plate were registered, but a simple statistical calculation enables the desired 4π-distribution to be evaluated. By this method β-distributions at fixed kinetic energies near the mean kinetic energy of each fragment mass are given for the masses 132, 134, 136 and 137. For the lower masses 132 and 134 the neutron shell N = 82 is responsible for the most probable primary charges near 50 and 52 respectively. For M = 136 and 137 the primary charge is about 53 and 53.2. Additional approximative corrections in respect of conversion electrons (by omitting very short β-tracks corresponding to very low β-energies) and to delayed neutrons (for mass 137) were not very large. Similar measurements carried out directly in 4π-geometry to avoid the statistical error arising from the transformation from 2π- to 4π-distribution, and for various kinetic energies as parameters, are in preparation.

RÉPARTITION PRIMAIRE DE LA CHARGE NUCLÉAIRE POUR LES FRAGMENTS DE MASSE 132, 134, 136 ET 137, PROVENANT DE LA FISSION DE ^{235}U PAR NEUTRONS THERMIQUES. A l'aide d'un spectromètre de masse, on sépare avec précision les fragments de la fission thermique de ^{235}U d'après leur masse et leur énergie cinétique dans la microseconde qui suit la fission. Les fragments séparés sont retenus dans une émulsion Ilford G 5 sensible aux particules β, qui est placée dans le plan focal du spectromètre. Les émulsions irradiées sont développées, dans la mesure du possible, après un délai relativement long par rapport à la période la plus longue de la série radioactive considérée. Les périodes de l'ordre de plusieurs jours ou plus longues encore ne sont pas prises en considération, mais il est facile d'appliquer un facteur de correction approprié. Après avoir développé les émulsions, on peut observer au microscope toutes les traces β qui prolongent chacune des traces de fragments de fission. La possibilité d'établir une corrélation entre une trace β et une trace de fragment de fission permet d'évaluer le nombre n(x) de fragments de fission possédant un nombre x de traces β, ce qui indique non seulement la longueur moyenne de la série mais aussi la distribution des particules β. Le nucléide stable de chaque série étant connu, la distribution des particules β constitue une image exacte de la répartition primaire des charges nucléaires. Au cours des mesures effectuées jusqu'à présent, on n'a enregistré que les particules β émises dans le demi-angle solide formé par la plaque d'émulsion, mais un calcul statistique simple permet d'évaluer la distribution 4π voulue. Grâce à cette méthode, on obtient la distribution des particules β à des énergies cinétiques déterminées proches de l'énergie cinétique moyenne de chaque fragment pour les masses 132, 134, 136 et 137. Pour les masses 132 et 134, c'est à la couche de neutrons

N = 82 que sont dues les charges primaires les plus probables voisines de 50 et 52 respectivement. Lorsque M = 136 ou 137, la charge primaire est d'environ 53 et 53,2. Il s'est révélé que les corrections approximatives supplémentaires pour tenir compte des électrons de conversion (en négligeant les traces β très courtes correspondant à des énergies β très faibles) et des neutrons retardés (pour la masse 137) ne sont pas très importantes. On prépare actuellement des mesures analogues qui seront effectuées directement dans une géométrie 4π, de manière à éviter l'erreur statistique qu'entraîne la transformation de la distribution 2π en distribution 4π, et qui porteront sur différentes énergies cinétiques prises comme paramètres.

ПЕРВИЧНЫЕ РАСПРЕДЕЛЕНИЯ ЯДЕРНЫХ ЗАРЯДОВ ОСКОЛКОВ ДЕЛЕНИЯ С МАССАМИ 132, 134, 136 и 137 ПРИ ДЕЛЕНИИ УРАНА-235 ПОД ДЕЙСТВИЕМ ТЕПЛОВЫХ НЕЙТРОНОВ. При помощи масс-спектрометра осколки, образующиеся при делении урана-235 под действием тепловых нейтронов, точно отделяются по массе и кинетической энергии за промежуток времени в 10^{-6} сек после деления. Извлеченные осколки захватываются на эмульсию Ильфорда G5, чувствительную к бета-частицам и расположенную в плоскости фокуса спектрометра. Облученные эмульсии проявляются по мере возможности спустя достаточно долгое время после деления по сравнению с наиболее долгим полупериодом жизни рассматриваемой цепочки распада. Полупериоды жизни порядка нескольких дней или более не принимаются во внимание, но в отношении их легко внести соответствующие поправки. После проявления эмульсий все бета-следы, идущие от конца каждого следа осколков деления, ясно видны под микроскопом. Возможность корреляции каждого отдельного бета-следа с определенным следом осколка деления делает возможным установить число n (x) осколков деления, имеющих "x" бета-следы, что дает не только среднюю длину цепочки, но также распределение бета-частиц. Так как устойчивый конечный продукт каждого распада в цепочке известен, то это распределение бета-частиц является точным изображением распределения первичного ядерного заряда. При измерениях, проводившихся до настоящего времени, регистрировались только бета-частицы, излученные в половине пространственного угла, образованного эмульсионной пластинкой; однако простой статистический подсчет дает возможность установить желаемое распределение в геометрии 4π. На основании этого метода распределения бета-частиц при определенных кинетических энергиях, близких к средней кинетической энергии каждой массы осколков, даются для масс 132, 134, 136 и 137. Для более низких из этих масс, , а именно 132 и 134, нейтронная оболочка N = 82 определяет наиболее вероятные первичные заряды соответственно около 50 и 52. Для M = 136 и 137 первичный заряд составляет около 53 и 53,2. Дополнительные приблизительные поправки на электроны конверсии (не считая очень коротких бета-следов, соответствующих очень малым бета-энергиям) и на запаздывающие нейтроны (для массы 137) оказываются не очень значительными. В настоящее время подготавливаются аналогичные измерения непосредственно в геометрии 4π во избежание статистических погрешностей, возникающих от преобразования распределения 2π в распределение 4π, а также для различных кинетических энергий, принимаемых в качестве параметров.

DISTRIBUCIONES PRIMARIAS DE LAS CARGAS NUCLEARES DE LOS FRAGMENTOS DE MASA 132, 134, 136 Y 137, RESULTANTES DE LA FISION DEL ^{235}U POR NEUTRONES TERMICOS. Los fragmentos resultantes de la fisión del ^{235}U por neutrones térmicos se separan exactamente según su masa y energía cinética con ayuda de un espectrómetro de masas en el microsegundo que sigue a la fisión. Los fragmentos separados se recogen en una emulsión Ilford G-5 sensible a las particulas beta, colocada en el plano focal del espectrómetro. El revelado de las emulsiones irradiadas se efectúa, en lo posible, después de haber transcurrido un tiempo suficientemente largo en relación con el período más prolongado que aparece en la cadena de desintegración considerada. Los períodos del orden de días o más largos no se tienen en cuenta, pero pueden introducirse fácilmente las correcciones adecuadas. Después del revelado de la emulsión, pueden verse al microscopio todas las trazas de partículas beta que surgen del extremo de la traza de cada fragmento de fisión. La posibilidad de correlacionar cada traza de partícula beta con la traza de un fragmento de fisión determinado permite calcular el número n(x) de fragmentos de fisión a los que corresponden x trazas de partículas beta, lo que indica no sólo la longitud media de la cadena, sino también la distribución de las partículas beta. Como el producto final estable de cada cadena es conocido, esta distribución de las partículas beta refleja fielmente la distribución primaria de las cargas nucleares. En las mediciones realizadas hasta ahora, sólo se han registrado las partículas beta recogidas en el semiángulo sólido formado por la placa portadora de la emulsión, pero un simple cálculo estadístico permite determinar la distribución 4π apetecida. En la memoria se indican las distribuciones de partículas beta, obtenidas por este método, a energías cinéticas fijas, próximas a la energía cinética media de cada fragmento, para las masas 132, 134, 136 y 137. En lo que respecta a las masas 132

y 134, la capa neutrónica N = 82 determina las cargas primarias más probables en las proximidades de 50 y 52, respectivamente. Para M = 136 y 137, la carga primaria es de 53 y 53,2. No resultan muy considerables las correcciones aproximadas, de carácter complementario para tener en cuenta los electrones de conversión (omitiendo las trazas muy cortas de partículas beta correspondientes a energías muy bajas) y los neutrones retardados (en el caso de la masa 137). Se están preparando mediciones análogas que se efectuarán directamente en geometría 4π para evitar el error estadístico debido a la transformación de la distribución 2π en 4π, con varias energías cinéticas como parámetros.

INTRODUCTION

The most important method for the determination of primary charge of fission fragments is connected with the measurement of their β-decays. β-unstable nuclei decay in a time greater than 10^{-2} s after being formed. For shorter half-lives the decay energies would be so high that a more stable state is reached also by neutron emission, which occurs in a much shorter time. This state immediately after neutron evaporation is called "primary". Information about primary charge distribution, which is not only an average over all masses, requires previous separation of the fission fragments. The possibility of chemical separation involves the difficulty that the shortest half-lives cannot be included quantitatively due to the unavoidable time required by the chemical separation method. Therefore ARMBRUSTER et al. [1] used a mass separator of the Cohen-type [2], which separates the fission fragments in the time given by the time-of-flight of the fragments, with a resolution of about 5 amu full width at half maximum (FWHM). For our measurements we used a double-focusing mass spectrometer of the Mattauch-Herzog-type [3, 4] (resolution $M/\Delta M$ about 400 FWHM), which collects the fission fragments in the focal plane separated in respect to mass and kinetic energy in a time of approximately 10^{-6} s after the fission process. This time is short enough to include even the shortest β-decays and long enough to exclude prompt conversion electrons occurring in a time shorter than 10^{-8} s.

By measuring the number of betas from the collected fission fragments during collection time one obtains the build-up of β-activation that directly corresponds to the mean chain length [1]. Additional determination of β-distribution, i. e. the number of fission fragments n(x) of a certain mass that emit x β-particles requires a correlation of each β-particle to its parent fragment. This correlation could be achieved by using highly sensitive nuclear emulsions (Ilford G5). Under the microscope each β-track can be seen and correlated to the fission fragment from which it emerges. For example, Fig. 1 shows four betas emerging from the end of one fission fragment track. Enumerating the betas of a large number of fission fragment tracks allows the determination of n(x).

MASS SEPARATION

The fission fragments are separated in the successive electrostatic and magnetic fields of the spectrometer corresponding to Eqs. (1) and (2),

$$M m_0 (v^2/a_e) = e e_0 F \tag{1}$$

$$M m_0 (v^2/a_m) = e e_0 v B \tag{2}$$

where

M = mass number,
m_0 = atomic mass unit,
v = fragment velocity,
e = ionic charge number,
e_0 = elementary charge,
F = electrical field strength,
B = magnetic flux density,
a_e = mean deflection radius in the electrostatic field,
a_m = deflection radius in the magnetic field.

By eliminating v there follows

$$\frac{M}{e} = \frac{a_m^2}{a_e} \frac{B^2}{F} \frac{e_0}{m_0} . \tag{3}$$

$\frac{M}{e}$ is the magnitude respective to which the particles are deflected.

A separation of M alone due to slightly different M/e-values at some places of the M/e scale in general requires too high a resolution that cannot be achieved because of reasons of intensity. Therefore on principle a mixture of several masses with different ionic charge numbers at approximately equal M/e is focused on one place. Nevertheless, for the heavy fission-fragment group a mass separation is possible, based on two facts [4]: firstly, only a definite interval of E/e of about 1% is selected by the electrostatic field; secondly, due to the kinematics of the fission process itself the distribution of kinetic energy with which a fragment with a specific mass number occurs is nearly Gaussian with about 12% FWHM, and the mean value of kinetic energy in the heavy-fragment group drops heavily with mass ($dE/dM \simeq -1.2$ MeV/amu). In consequence of these two conditions within this group only one mass is focused with appreciable intensity on one place of the focal plane. Imagine the desired mass be M_1 having the ionic charge number e_1; the next mass number that can possibly contribute is M_2 with ionic charge number $e_1 + 1$, M_2 then is about 5% greater than M_1 ($e_1 \simeq 20$). With 5% higher ionic charge number a 5% higher kinetic energy is correlated according to Eq. (2). Conversely, a mean kinetic energy approximately 8 MeV lower than that of M_1 corresponds to a 5% higher mass. In consequence the selected energy is very far from the mean energy of the particle of mass M_2 and therefore particles with M_2 cannot contribute with appreciable intensity. An experimental proof of the purity of a mass spectral line is easily possible: according to Eq. (2) a contribution from another ionic charge has another kinetic energy that becomes visible in an energy spectrum of the mass line being considered. Such multichannel analyser spectra were taken by a solid-state detector for each of the mass lines for which the β-distribution curves were determined. They showed that the sum of all undesired contributions of other masses was less than 5% in every case. An absolute determination of mass was possible from the following:

Fig. 1

Microscopic photograph of 4 electrons leaving the end of one fission particle track. The length of this track is about 10 μm.

(1) Comparison of the measured intensity of the mass lines with radiochemical yield data. To the mass line with highest intensity in the region of low masses within the heavy group M = 134 was assigned.

(2) Calibration of the spectrograph by Po^{210}-α-particles, the M, E, and e of which are known. The ionic charge number e can be unequivocally determined by two independent methods [4, 5].

Together with the exact relative measurement of field strengths from Eq. (3), M is determinable.

EXPERIMENTAL ARRANGEMENT

The experimental arrangement is shown in Fig. 2. Fission fragments of a certain mass and kinetic energy pass a 3-mm wide slit in the focal plane of the spectrograph and are collected afterwards in a G5-emulsion. The angle between the direction of the particle beam and the emulsion surface is about 10°. Emulsions of 100 μm thickness are sufficient, because only the number of β-particles, not their energy, is to be evaluated. For unequivocal visibility of the β-tracks the emulsions must be almost free from background. Therefore the latent images of old tracks were erased just before exposure by exposing the emulsions for about 7 h to an atmosphere of saturated water vapour at a temperature of 60° C [6]. During the irradiation in the reactor hall the emulsions were shielded by the thick iron plates of the spectrometer magnet. Nevertheless, the irradiation time could not exceed about half an hour. To make certain that the sensitivity of the emulsions was not reduced by the erasing procedure they were tested by irradiating them with a known number of β-particles from the background of a magnetic conversion electron spectrometer at energies ranging from 100 keV to 5 MeV. The betas of the whole energy range were registered quantitatively.

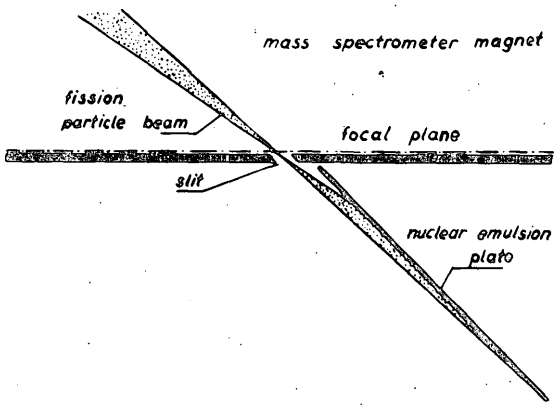

Fig. 2

Experimental arrangement

The intensity of the mass spectrometer was about 50 particles per min and mass line, and the irradiation time was 30 min. For each mass chain three emulsions were irradiated. Thus differences eventually occurring in the visibility of β-tracks between the three emulsions would very probably be detected. The total number of evaluated fission tracks was about 1000 for each mass.

The irradiated emulsions were developed after about 10 and 1.5 h for masses 134 and 136 respectively, which is about 10 times longer than the longest half-life of the respective mass chain. At these times nearly all betas have been emitted. The long half-lives of all the decay chains under examination were assumed to be well-known and were taken from Refs. [7, 8]. At M = 132 and M = 137 the half-lives 3.1 min and 3.9 min were assumed to be the longest effective half-lives, as the longer ones (77 h and 29.7 yr) are so large that they do not disturb the measurements of the precursory decays. The time interval between irradiation and development of the emulsions was chosen as 1 h in both cases. Corrections were made for the decays not included.

The evaluation of the emulsions was done under the microscope. In the nuclear emulsions only the β-particles going into the half solid angle are recorded. Obviously the β-tracks leading steeply downward (in a cone of about 10°) cannot be recognized, but on the other hand another contribution is added because the fission fragment tracks are not entirely parallel to the surface so that the ends of the tracks lie about 2 μm beneath the surface; both contributions result in an enlargement of the real solid angle of about 4% of 2π. From the measured number of fission fragments m (x') possessing x' β-tracks in the comprehended solid angle the interesting quantity in 4π, n (x), can be calculated by

$$n(x) = \left(\frac{1}{p}\right)^x (-1)^x \sum_{x'=0}^{\infty} (-1)^{x'} \binom{x'}{x} \left(\frac{1-p}{p}\right)^{x'-x} m(x') \,, \qquad (4)$$

where p is the comprehended part of the solid angle. In our case p = 0.52.

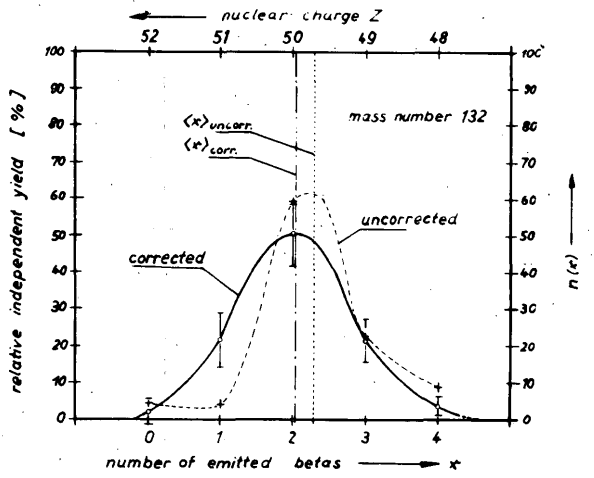

Fig. 3

Distribution of the number of fission fragments n(x) of M = 132 possessing x β-tracks (without including the two more decays with long half-lives).
The upper scale gives primary nuclear charge.
Full line and circles correspond to data corrected for conversion electrons by omitting β-tracks shorter than 30 μm, dashed line and crosses give the uncorrected data.
Statistical errors are plotted for the corrected data.

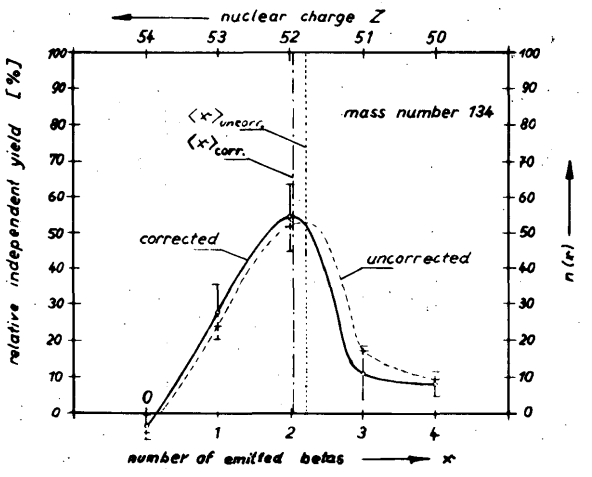

Fig. 4

Nuclear charge distribution of fission particles with M = 134.
Further explanation as in Fig. 3

The calculation to full solid angle increases the statistical error considerably, which is shown in Figs. 3 to 6. To avoid this increase in statistical error we are preparing a direct method of measurement in 4π by alternately irradiating and covering the emulsion plate by a second plate in a time ratio of 1: 10 [9].

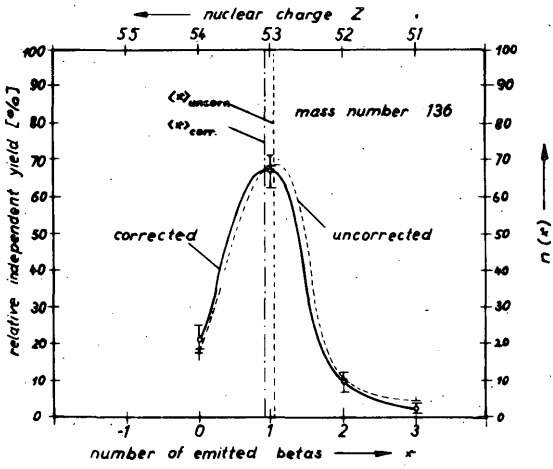

Fig. 5

Nuclear charge distribution of fission particles with M = 136.
Further explanation of the figure as in Fig. 3.

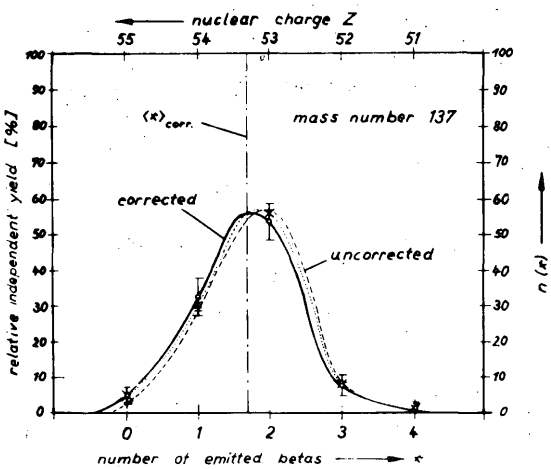

Fig. 6

Nuclear charge distribution of fission particles with M = 137.
In the number x of β-tracks (lower scale) the one more decay with long half-life is not included.
Full line and open circles correspond to data corrected for conversion electrons
by omitting β-tracks shorter than 30 μm, dashed line and crosses (+) give the uncorrected data.
Dotted line and crosses (x) refer to additional correction for emitted delayed neutrons.

RESULTS

In the method described all electrons are counted irrespective of whether they stem from β-decays or from γ-conversion processes. Inclusion of the latter electrons leads to an incorrect enlargement of the measured chain lengths. Because of the relatively poor intensity a direct measure-

ment of the contribution of conversion electrons has not so far been attempted. Therefore only a very rough correction could be made by omitting all electrons with energies < 75 keV corresponding to a track length of 30 μm in the emulsion [10]. The expected fraction of real betas in this energy region is about 4% under the assumption of allowed beta decays with a mean kinetic energy of 1.1 MeV [11]. On the other hand, the contribution of conversion electrons from the γ-data of FISHER and ENGLE [12] and of MAIENSCHEIN et al. [13] and conversion coefficients of ROSE [14] (assuming a mixture of E1, E2 and M1 transitions) equally amount to about 4%. Thus the correction applied should be relevant, at least on the average. Obviously, at single mass chains, where γ-emission with high multipole order occurs, a falsification of the distributions cannot be excluded. Therefore we intend to measure the mean chain length by counting the betas in a 4π-G-M-counter that does not count the conversion electrons as they coincide within time resolution of the counter with the precursory β-particles. By comparing this value with the mean chain length evaluated from the emulsion method we hope to check this latter method for each mass line.

In Figs. 3, 4, 5 and 6 the β-distributions identical to the nuclear charge distributions are given for M = 132, 134, 136 and 137 respectively. The solid curves correspond to corrected values (the β-tracks with ranges below 30 μm being omitted), the dashed curves show the uncorrected data. The difference is not very large and still inside the statistical error, which may be interpreted as showing that possible falsification by conversion electrons is not likely to be very heavy. Table I (column 4) moreover gives the total percentage of omitted betas for the respective mass numbers. For the corrected data the statistical errors, caused mainly by the calculation from 2π- to 4π-distribution, are plotted.

The mass chains 132 and 137 possess beta decays with long half-lives that could not be assessed in our measurements. At M = 132, accounting for the two additional decays with half-lives of 77.7 h and 2.28 h [8], there is only a displacement of the distribution curve of two units; this is justified, as in the respective distribution (Fig. 4) fission particles with zero decays do not occur, and thus this indicates that the independent yield of the nuclide with Z = 52 with 77.7 h half-life is approximately zero. It is therefore very probable that the nuclide Z = 53 cannot be formed independently also. This means that each fragment showing x beta tracks emits x+2 betas in infinite time.

At M = 137 one further decay has to be added (half-life 29.7 a). Moreover for this mass number emission of delayed neutrons is expected from the I^{137} precursor leading to stable Xe^{136} with a total yield of about 3×10^{-2} per fission event in which M = 137 is formed [7]. This value results from assuming that I^{137} yields about half the 22 s-delayed neutron period under examination and is very probably over-estimated. But even with this high value (corresponding to 11% of all delayed neutrons in thermal U^{235} fission) only an almost negligible change in the charge distribution curve is produced, as shown in Fig. 6 (dotted line). The exact influence of delayed neutrons can easily be accounted for when the branching ratio of the neutron emitter is known.

TABLE I

EMPIRICAL Z_p-VALUES

1	2	3	4	5	6	7
Mass number M	Number of enumerated fission tracks	Fragment kinetic energy (MeV)	Share of omitted low-energy electrons (%)	Mean chain length (to infinite time)		
				Uncorrected	Corrected by omitting electrons < 75 keV	Corrected also for delayed neutrons
132	1098	77.0	10.72	4.27	4.02	
134	1000	77.0	7.08	2.22	2.06	
136	1000	73.4	9.22	1.02	0.93	
137	1500	73.4	6.43	2.80	2.69	2.72

1	8	9	10	11	12
Mass number M	Most probable (mean) charge Z_p	rms deviation σ	Prompt mass number M'	$Z_p - M' \frac{92}{236}$	
				Normal	Neglecting prompt neutron emission
132	49.98	0.82	132.6	-1.71	-1.48
134	51.94	0.59	134.8	-0.61	-0.30
136	53.07	0.62	136.9	-0.30	
137	53.28	0.72	138.0	-0.52	

Errors in the mass separation of the spectrometer from contributions of other masses were not taken into account, because they amounted to less than 5%, as indicated in the energy spectra (section B). For M = 134 an example of such a spectrum is shown in Fig. 7.

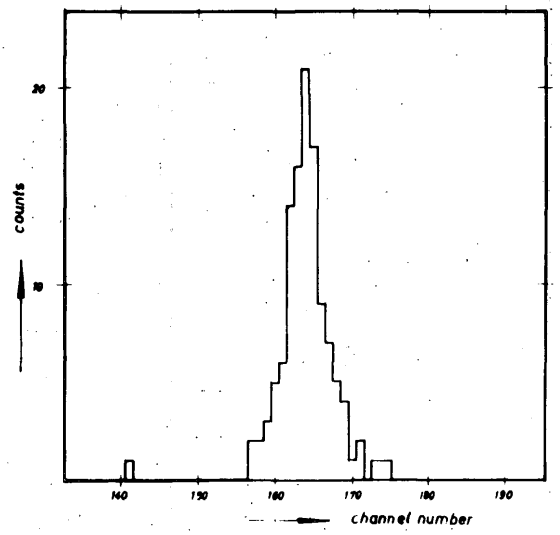

Fig. 7

Multichannel analyser energy spectrum of the investigated fission fragments of M = 134 shown by a solid-state detector.
Contributions of undesired masses should become visible in this spectrum at energies at least 5% different from the main peak shown (explanation in the text).
Such contributions are less than 5%.

DISCUSSION

In columns 8 and 9 of Table I the mean (most probable) values of nuclear charge, Z_p, and rms widths σ are given. In order to compare our results with data from radiochemical measurements the diagram of WAHL et al. [15] is reproduced in Fig. 8 and their curve that best fits the widely spread experimental data is plotted together with our points of Z_p (full circles) and the results observed by ARMBRUSTER et al. [1]. On the abscissa of this figure is plotted the primary mass M' (column 10 in Table I) before prompt neutron emission, calculated by correction of the measured masses M for emission of prompt neutrons with the data calculated by TERRELL [16] from mass yields before and after neutron evaporation; the ordinate gives the difference between the observed most probable primary charge and the expected one, if uniform charge distribution were valid. In the region of M = 136 and 137 our data agree sufficiently with the data of Armbruster. The agreement with Wahl's curve is poor, but it is very good with his experimental values of Z_p, given in Table V of Ref. [15] (53.53 and 52.58 for M' = 136; 53.26 for M = 137). In the case of M = 132 and 134, however, our values of $Z_p - M' \times (92/236)$ drop significantly, parallel to the straight line indicating the neutron shell N = 82. Apparently this shell is reponsible for

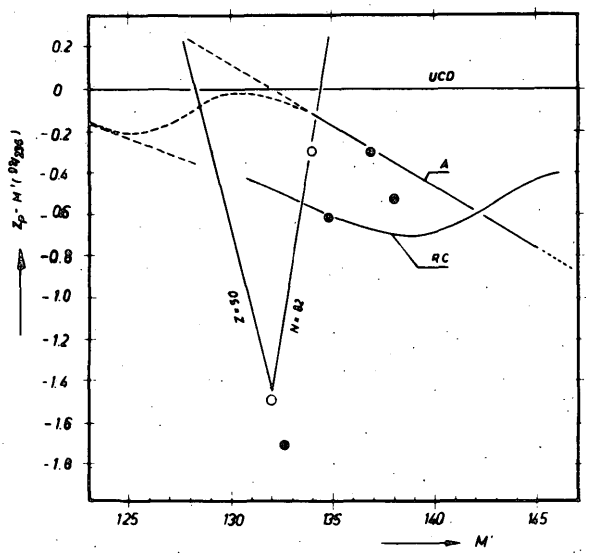

Fig. 8

Comparison of different experimental values of most probable nuclear charge, Z_p. R. C. = radiochemical empirical curve of Wahl et al., A = Armbruster's measurement, full circles = our measurement; open circles correspond to values of Z_p for M = 132 and 134 if emission of prompt neutrons is neglected.

the Z_p values of M = 132 and 134. This fact becomes still more visible if near this closed shell neutron emission is neglected. Then the measured values of Z_p exactly coincide with the N = 82 line (open circles in Fig. 8). An indication that this might be approximately correct is the observed dip of the measured neutron yield curve in this mass region as given by APALIN [17]. For M = 132 the maximum of the Z-distribution proves to be very close to the double magic nucleus $^{82}_{50}Sn^{132}$, as predicted by FAISSNER and WILDERMUTH [18].

The values of Z_p and σ given in Table I are the mean values and root mean square widths of the measured distributions plotted in Figs. 3-6. No attempt was made to fit the data by Gaussian distributions, since at least at high kinetic energies of the fragments (corresponding to low excitation energies) even-even odd-odd effects or the influence of closed shells should become relevant [19] and distort Gaussian distribution curves. In this connection it should be noted that there is some methodical difference between the radiochemical data and our data, as ours refer to only one distinct kinetic energy of the fission fragments for each mass. This energy is given in column 3 of Table I. In this measurement the kinetic energies were chosen close to (within about 1 MeV) the most probable energy of each mass [20]. Measurements with kinetic fragment energy as parameter are now being prepared.

ACKNOWLEDGEMENTS

The authors wish to thank Professor H. Ewald, Giessen, for suggesting this work, and Professor H. Maier-Leibnitz, Munich, for his continuous interest.

REFERENCES

[1] ARMBRUSTER, P., HOVESTADT, D., MEISTER, H. and SPECHT, H.J., Nucl. Phys. 54 (1964) 586.
[2] COHEN, B.L. and FULMER, C.B., Nucl. Phys. 6 (1958) 547.
[3] EWALD, H., KONECNY, E., OPOWER, H. and RÖSLER, H., Z. Naturforsch. 19a (1964) 194.
[4] KONECNY, E., OPOWER, H. and EWALD, H., Z. Naturf. 19a (1964) 200.
[5] OPOWER, H., KONECNY, E. and SIEGERT, G., Z. Naturf. 20a (1965) 131.
[6] BARKAS, W.H., Nuclear Research Emulsions I, Academic Press, New York and London (1963) 93.
[7] HYDE, E.K., UCRL-Rpt. 9036 (1960).
[8] HERRMANN, G., to be published in Radiochem. Acta.
[9] OPOWER, H., KONECNY, E. and GUNTHER, H., Proc. 5th Int. Conf. Nuclear Photography, Geneva (1964).
[10] BARKAS, W.H., Nuclear Research Emulsions I, Academic Press, New York and London (1963) 444.
[11] ARMBRUSTER, P. and MEISTER, H., Z. Phys. 170 (1962) 274.
[12] FISHER, P.C. and ENGLE, L.B., Phys. Rev. 134 (1964) B796.
[13] MAIENSCHEIN, F.C. PEELLE, R.W., ZOBEL, W. and LOVE, T.A., Proc. 2nd Int. UN Conf. PUAE 15 (1958) 366.
[14] ROSE, M.E., Internal Conversion Coefficients, Amsterdam, North Holland Publishing Company (1958).
[15] WAHL, A.C., FERGUSON, R.L., NETHAWAY, D.R., TROUTNER, D.E. and WOLFSBERG, K., Phys. Rev. 126 (1962) 1112.
[16] TERRELL, J., Phys. Rev. 127 (1962) 880.
[17] APALIN, V.F., DOBRYNIN, Y.P., ZAKHAROVA, V.P., KUTIKOV, L.E. and MIKAELYAN, L.A., Atomnaja Energija 8 (1960) 15.
[18] FAISSNER, H. and WILDERMUTH, K., Phys. Lett. 2 (1962) 212.
[19] THOMAS, T.D. and VANDENBOSCH, R., Phys. Rev. 133 (1964) B976.
[20] MILTON, J.C.D. and FRASER, J.S., Canad. J. Phys. 40 (1962) 1626.

FISSION YIELDS OF SOME ISOTOPES IN THE FISSION OF Th^{232} BY REACTOR NEUTRONS

A. WYTTENBACH AND H.R. VON GUNTEN
EIDG. INSTITUT FÜR REAKTORFORSCHUNG,
WÜRENLINGEN, SWITZERLAND

Abstract — Résumé — Аннотация — Resumen

FISSION YIELDS OF SOME ISOTOPES IN THE FISSION OF Th^{232} BY REACTOR NEUTRONS. The fission yields of the longer-lived isotopes produced in the fission of Th^{232} are not very well known; existing data show rather large discrepancies and/or uncertainties. Since we feel that at least some of these discrepancies arise from difficulties in measuring the absolute activities of the fission products, we measured the fission yield of 10 selected isotopes whose decay schemes are well understood.

The thorium foils were irradiated in a position at the edge of the core of the SAPHIR swimming pool reactor. Following irradiation, the thorium was dissolved after addition of appropriate carriers. The fission products of interest were determined by conventional radiochemical methods that had to be modified slightly to ensure good decontamination from the abundantly formed Pa^{233}. The chemical yields were determined by gravimetric methods.

Counting was done preferentially on a γ-spectrometer that had been calibrated at 11 different energies by standards either obtained from the IAEA or prepared by $4\pi\beta$-counting. In the case of Sr^{90}, Ru^{106} and Ce^{144} a β-proportional counter was used that had been calibrated for these isotopes.

In addition to the sought elements, Mo^{99} was isolated from each foil to serve as an internal monitor for the number of fissions taking place. The experiment thus gave the ratio of the yield of the sought element to the yield of Mo^{99}. This ratio "R" was obtained for Sr^{90}, Ru^{103}, Ru^{106}, Ag^{111}, Pd^{112}, I^{131}, Cs^{137}, Ba^{140}, Ba^{141}, Ce^{141} and Ce^{144}. Results indicate the existence of a third peak in the yield mass curve in the region of symmetric fission.

Yields of fission products relative to the Mo^{99} yields are given, and the absolute yields calculated by assuming $y_{Mo^{99}} = 2.78\%$. This number was derived from the work of Iyer et al., and was obtained by normalizing the area under the yield mass curve to 200%.

RENDEMENTS EN CERTAINS RADIOISOTOPES DE LA FISSION DE ^{232}Th PAR LES NEUTRONS D'UN RÉACTEUR. Les rendements de la fission de ^{232}Th en radioisotopes de longue période sont encore assez mal connus; les données disponibles comportent des marges d'erreur ou d'incertitude relativement importantes. Comme, de l'avis des auteurs, ces marges sont dues, au moins en partie, aux difficultés que suscite la mesure des activités absolues des produits de fission, ils ont mesuré le rendement en dix radioisotopes choisis dont les schémas de désintégration sont bien connus. Ils ont irradié des feuilles de thorium placées à la limite du coeur de la piscine SAPHIR. Après irradiation, le thorium a été dissous après addition d'entraîneurs appropriés. Les produits de fission considérés ont été déterminés par des méthodes radiochimiques classiques qu'il a fallu modifier légèrement pour éliminer ^{233}Pa qui se forme en abondance. Les rendements chimiques ont été déterminés par des procédés gravimétriques.

Pour le comptage, on a utilisé un spectromètre gamma qui avait été étalonné pour 11 énergies différentes à l'aide d'étalons fournis par l'AIEA ou préparés par comptage bêta 4π. Dans les cas de ^{90}Sr, ^{106}Ru et ^{144}Ce, on a fait appel à un compteur proportionnel β préalablement étalonné pour ces radioisotopes.

Outre les éléments recherchés, on a extrait de chaque feuille ^{99}Mo qui a servi de «contrôleur» interne du nombre des fissions. Ainsi, cette expérience a permis d'établir les rapports entre les rendements en éléments recherchés et le rendement en ^{99}Mo. Ce rapport (R) a été déterminé pour ^{90}Sr, ^{103}Ru, ^{106}Ru, ^{111}Ag, ^{112}Pd, ^{131}I, ^{137}Cs, ^{140}Ba, ^{141}Ba, ^{141}Ce et ^{144}Ce. Les résultats montrent que la courbe de la distribution des produits de fission selon la masse présente un troisième pic dans la région de la répartition symétrique.

Les valeurs de R sont indiquées, ainsi que les rendements absolus qui ont été calculés en admettant que le rendement en ^{99}Mo est égal à 2,78%. Cette valeur a été établie en partant des travaux d'autres chercheurs (Iyer et al.) et en normalisant la surface délimitée par la courbe à 200%.

ВЫХОДЫ НЕКОТОРЫХ ИЗОТОПОВ ПРИ ДЕЛЕНИИ ТОРИЯ-232 С ПОМОЩЬЮ НЕЙТРОНОВ РЕАКТОРА. Выходы более долгоживущих изотопов, образующихся при делении тория-232, мало известны; в существующих данных встречаются довольно значительные расхождения, неопределенности или и то и другое. Поскольку авторы считают, что по меньшей мере часть этих расхождений возникает в результате трудностей при измерении абсолютных активностей продуктов деления, они измерили выходы при делении десяти изотопов, схемы распада которых хорошо известны.

Фольга из тория облучалась в положении на краю активной зоны реактора бассейнового типа "Сапфир". После облучения и добавления надлежащих носителей торий растворялся. Изучаемые продукты деления определялись обычными радиохимическими методами, которые пришлось несколько видоизменить для обеспечения хорошей дезактивации от образующегося в больших количествах протактиния-233. Химические выходы определялись по гравиметрическому методу.

Счет производился предпочтительно при помощи гамма-спектрометра, который был калиброван для 11 различных энергий на основании стандартных образцов, либо полученных от МАГАТЭ, либо изготовленных на основании бета-счета в геометрии 4π. Для стронция-90, рутения-106 и церия-144 был использован пропорциональный бета-счетчик, калиброванный для этих радиоизотопов.

В дополнение к изучаемым элементам из каждой фольги был выделен молибден-99 с целью использования его в качестве внутреннего регистратора числа происходящих делений. Таким образом, эксперимент давал соотношение между выходом изучаемого элемента и выходом молибдена-99. Это соотношение "R" было получено для стронция-90, рутения-103, рутения-106, серебра-111, палладия-112, йода-131, цезия-137, бария-140, бария-141, церия-141 и церия-144. Результаты указывают на наличие третьего пика у кривой выхода в зависимости от массы в области симметричного деления.

Даются выходы продуктов деления по сравнению с выходами молибдена-99, а также абсолютные выходы, подсчитанные, исходя из предположения, что выход молибдена-99 равен 2,78% . Это последнее число было выведено на основании работы Айера и др. и было получено посредством нормализации до 200% площади, охваченной кривой выхода в зависимости от массы.

RENDIMIENTOS DE ALGUNOS ISOTOPOS EN LA FISION DEL ^{232}Th POR NEUTRONES GENERADOS EN REACTOR. Los rendimientos de fisión de los isótopos de período largo producidos en la fisión del ^{232}Th no se conocen con precisión. Los datos publicados presentan discrepancias e indeterminaciones bastante considerables. Los autores estiman que estas discrepancias se deben, al menos en parte, a la dificultad de determinar la actividad absoluta de los productos de fisión, por lo que han medido el rendimiento de fisión de diez isótopos cuyos esquemas de desintegración son bien conocidos.

Las láminas de torio se irradiaron en una posición al borde del núcleo del reactor SAPHIR (de tipo piscina). Seguidamente se disolvió el torio después de añadir los portadores adecuados. Los productos de fisión de interés se determinaron por métodos radioquímicos clásicos, que hubieron de modificarse ligeramente para eliminar de manera satisfactoria el ^{233}Pa formado en cantidades considerables. Los rendimientos químicos se determinaron por métodos gravimétricos.

El recuento se efectuó principalmente con un espectrómetro gamma calibrado para 11 energías diferentes mediante patrones proporcionados por el OIEA, o preparados con ayuda de un contador $\beta\,4\pi$. En el caso del ^{90}Sr, ^{106}Ru y ^{144}Ce, se utilizó un contador proporcional β calibrado para esos isótopos.

Además de los elementos buscados, se separó en cada lámina el ^{99}Mo contenido para utilizarlo como indicador interno del número de fisiones que se producían. Como resultado del experimento se obtuvo, pues, la razón del rendimiento del elemento analizado al rendimiento del ^{99}Mo. Esta razón "R" se determinó en el caso del ^{90}Sr, ^{103}Ru, ^{106}Ru, ^{111}Ag, ^{112}Pd, ^{131}I, ^{137}Cs, ^{140}Ba, ^{141}Ba, ^{141}Ce y ^{144}Ce. Los resultados indican la existencia de un tercer pico en la curva que representa el rendimiento en función de la masa, en la región de fisión simétrica.

Se indican los rendimientos de productos de fisión referidos al rendimiento del ^{99}Mo, así como los rendimientos absolutos que se han calculado suponiendo que el del ^{99}Mo es igual a 2, 78%. Este dato, deducido de los trabajos de Iyer y col., se ha determinado asignando el valor de 200% al área comprendida bajo la curva de rendimiento.

INTRODUCTION

The process of fission of thorium by neutrons was demonstrated at the beginning of 1939 [1, 2]. Afterwards most work on that subject was temporarily postponed because of the emphasis on U^{235} fission, but interest was later revived because of general curiosity and the possible use of thorium as a breading material. For this purpose, knowledge of the yields of the thorium fission products was needed to indicate such points as the required shielding and poisoning of the fission reaction.

The early radiochemical work on thorium fission by pile-neutron was done by TURKEVICH and NIDAY [3], and demonstrated successfully the main features of the mass distribution curve. However these first measurements were estimated to be accurate only to ± 30%. Moreover, later values [4, 5] for quite a few isotopes were out by even more than 30%. We therefore decided to try to resolve some of these discrepancies, and to concentrate on obtaining accurate values for a few isotopes.

Most radiochemical determinations of fission yields are done by comparing the absolute counting-rate of two chemically isolated fission products. One of these fission products serves as monitor for the number of fissions that have taken place and remains the same throughout the investigation. The other isotope is the fission product actually studied. Thus the method does not give absolute yields, but rather fission yields relative to the fission yield of the monitor isotope. Absolute fission yields can be obtained from these data by normalizing the area under the mass yield curve to 200%.

The need for absolute counting has sometimes been avoided by isolating and counting the same pairs of isotopes from irradiated U^{235} and from Th^{232}. When comparing these two pairs, the counter efficiencies drop out of the equation; however, the result will be dependent on the accuracy with which the fission yields from U^{235} are known, which will be generally ±10% [6]. Moreover, the genetic relationships must be the same in both U^{235} and Th^{232} fission.

We therefore decided that in order to get results better than ±10% it was necessary to count the isolated isotopes absolutely. Since we planned to rely for most of the absolute counting on γ-spectroscopy, we were restricted to isotopes whose decay schemes are well-known and not too complicated.

EXPERIMENTAL METHODS

Material

Foils, fabricated from reactor grade thorium, weighed 100–200 mg each and had a thickness of 100 mg/cm^2. Analysis showed the natural uranium contamination to be less than 10 ppm, which is insufficient to affect the results by fission of either U^{235} or U^{238}.

Irradiation

Normally four foils were stacked together, wrapped in 350 mg/cm^2 cadmium foil and irradiated in the "Saphir" swimming pool reactor in a central

position at the side of the core. The power of the reactor was kept constant within ± 5% during each irradiation. The flux of neutrons above 1 MeV varied for the different irradiations between 1.0 and 1.4×10^{12} n/cm^2 · s at the position of the sample and the irradiation time between 6 and 20 h.

Chemistry

The irradiated foils were dissolved separately in 6M HCl with the addition of a drop of concentrated HF and appropriate carriers in amounts of 10 or 20 mg. Chemical analysis was done by standard radiochemical procedures, using appropriate modifications to separate from the thorium daughter products and Pa^{233}, which is formed in quite large quantities.

The final precipitates were filtered through ash-free filter paper discs, the yields of the chemical separations determined by gravimetric methods, and the samples placed on aluminium counting cards and covered with mylar foils of about 1 mg/cm^2.

Counting

The isotopes Ru^{103}, Ag^{111}, Pd^{112}, I^{131}, Cs^{137}, Ba^{140} and Ce^{141} were counted by γ-spectrometry using a 3-in × 3-in crystal. The crystal was calibrated at 11 different energies by standards either obtained from the International Atomic Energy Agency or prepared in this laboratory by $4\pi\beta$-counting. Since none of these calibration points showed a deviation greater than 2% when compared with a theoretical detector efficiency curve [7], the calibration is believed to be accurate to ± 2%. The necessary data for the conversion of γ-counts to disintegration rates were taken from the Nuclear Data Sheets. Appropriate coincidence loss corrections have been applied where necessary.

The isotopes Ru^{106}, Sr^{90} and Ce^{144} were counted on a gas-flow proportional counter that had been calibrated for these isotopes by standards from the International Atomic Energy Agency. The decay of all samples was followed over a period not exceeding 3 months. The decay curves were analysed by a least square computer programme, and samples showing signs of a contamination were discarded.

RESULTS

In our experiments we chose Mo^{99} as the reference isotope. Our results are therefore expressed as the ratio of the sought fission yield to the fission yield of Mo^{99}. Since we waited long enough for all precursors to decay, the values relate to the cumulative yield of the decay chain in question down to and including the nuclide actually determined. No attempt has been made to correct for perturbations resulting from neutron capture by the fission products. Table I gives our results. In column 2 we have listed the yield relative to Mo^{99}, as determined by experiment. The given errors are one standard deviation[1]. Not included in this error are the systematic errors

[1] As calculated from $\sigma = \sqrt{\frac{(\bar{x} - x)^2}{n - 1}}$

TABLE I

FISSION YIELDS RELATIVE TO THE FISSION YIELD OF Mo^{99}
Experimental results

Measured isotope	Fission yield x / Fission yield Mo^{99}	Standard deviation	Number of determinations	Absolute yield (%) [a]
Sr^{90}	2.52	± 0.03	4	6.99
Ru^{103}	0.053	0.003	3	0.15
Ru^{106}	0.022	0.001	3	0.062
Ag^{111}	0.029	0.001	5	0.082
Pd^{112}	0.032	0.001	3	0.090
I^{131}	0.77	0.02	8	2.13
Cs^{137}	2.37	0.07	6	6.59
Ba^{140}	2.78	0.04	6	7.72
Ce^{141}	2.61	0.04	7	7.26
Ce^{144}	2.87	0.11	7	7.98

[a] based on yield of Mo^{99} = 2.78%

like calibration of the counters and errors in the decay schemes and half-lives; in general, these combined errors should not exceed 5%.

The absolute yields are listed in column 3; they were calculated on the basis of 2.78% for the fission yield of Mo^{99}. This value was taken from the work of IYER et al. [4], who obtained it from normalizing the area under their fission yield curve to 200%. It should be noted that an error in the absolute fission yield of Mo^{99} will introduce an additional systematic error in our results.

DISCUSSION

To our knowledge, apart from the original work of TURKEVICH and NIDAY [3], there exist three sets of data. All these experiments have been carried out with the fast flux of a reactor; since thorium has a fission threshold of approximately 1.1 MeV, the mean energy of the neutrons causing

TABLE II

FISSION YIELD RELATIVE TO THE FISSION YIELD OF Mo^{99}
Comparison of three sets of data: yield x/yield Mo^{99}

Isotope	This work	Iyer et al. [4]	Crook and Voigt [5]
Sr^{90}	2.52 ± 0.03	2.66 ± 0.10	2.70 ± 0.15
Ru^{103}	0.053 ± 0.003	0.054 ± 0.003	-
Ru^{106}	0.022 ± 0.001	0.014 ± 0.001	-
Ag^{111}	0.029 ± 0.001	0.024 ± 0.001	-
Pd^{112}	0.032 ± 0.001	0.023 ± 0.002	-
I^{131}	0.77 ± 0.02	0.62 ± 0.03	-
Cs^{137}	2.37 ± 0.07	1.60 ± 0.02	-
Ba^{140}	2.78 ± 0.04	3.06 ± 0.08	2.48 ± 0.14
Ce^{141}	2.61 ± 0.04	2.83 ± 0.13	2.36 ± 0.15
Ce^{144}	2.87 ± 0.11	2.85 ± 0.01	2.56 ± 0.15

fission[2] is for the most part only sensitive to the energy distribution of the fission neutrons, which is the same for all three experiments listed in Table II. It should therefore be possible to compare these experiments. The data of CROOK and VOIGT [5] and our data have been obtained by using calibrated counters, and the data of IYER et al. [4] were obtained by comparison with U^{235} fission.

Comparison of the results shows that the scattering is much worse than could be expected from the reproducibility given by the different authors. A large part of these discrepancies is probably due to incorrect counter calibration. The results on Sr^{90}, Ru^{103} and Ce^{144} can be considered good; there is fair agreement for Ag^{111}, I^{131}, Ba^{140} and Ce^{141}, whereas the discrepancies for Ru^{106}, Pd^{112} and Cs^{137} are exceedingly large.

From the evidence of earlier radiochemical work [3, 4] there have been hints regarding the existence of a third peak in the mass-yield curve, which would be attributed to symmetric fission. Due to some uncertainties in the results, however, neither author has given a very positive answer to that question. Nor can we give a better answer. The following, however, can

[2] As defined by $\bar{E} = \dfrac{\int_0^\infty \sigma_f(E)\,\Phi(E)\,E\,dE}{\int_0^\infty \sigma_f(E)\,\Phi(E)\,dE}$

$\bar{E}$ is close to 3 MeV for a fission neutron spectrum.

be said: although our values for the fission yields in the region of symmetric fission are only in qualitative agreement with the values of Iyer et al., they seem to confirm the general trend of the mass yield curve in the valley region found by other workers. Indeed our lowest value is Ru^{106}, while the values towards mass number 115 become higher again.

As was already said, the conversion of relative to absolute fission yields can be the source of an additional error. Indeed the three sets of data given in Table II have been converted to absolute yields by their authors on quite a different basis. While Crook and Voigt used the yield for Ba^{140} as given by Turkevich, Iyer et al. used a value for Mo^{99} derived from their own normalization. The difference between these two conversion modes amounts to 11%. We used the same value for Mo^{99} as Iyer et al, but we would like to stress the necessity for a more accurate conversion procedure. Possibly better values can be obtained by the use of a fission chamber with subsequent recovery of some fission product out of the chamber. We have begun such experiments for U^{235} and we hope we shall be able to carry them out with Th^{232} also.

REFERENCES

[1] ROBERTS, R.B. et al., Phys. Rev. 55 (1939) 416.
[2] FOWLER, R.D. and DODSON, R.W., Phys. Rev. 55 (1939) 417.
[3] TURKEVICH, A. and NIDAY, J.B., Phys. Rev. 84 (1951) 52.
[4] IYER, R.H. et al., J. inorg. nucl. Chem. 25 (1963) 465.
[5] CROOK, J.M. and VOIGT, A.F., TID-4500 (1963).
[6] KATCOFF, S., Nucleonics 18 (1960) 201.
[7] HEATH, R.L., IDO-16408 (1957).

MASS AND CUMULATIVE YIELDS IN NEAR-SYMMETRIC FISSION OF U^{235} WITH THERMAL NEUTRONS PART I. THE 121-MASS CHAIN

H.V. WEISS AND N.E. BALLOU
U.S. NAVAL RADIOLOGICAL DEFENSE LABORATORY, SAN FRANCISCO, CALIF., UNITED STATES OF AMERICA

Abstract — Résumé — Аннотация — Resumen

MASS AND CUMULATIVE YIELDS IN NEAR-SYMMETRIC FISSION OF U^{235} WITH THERMAL NEUTRONS. PART I. THE 121-MASS CHAIN. Determination of fission yield of mass 121 and of cumulative yields of members of that decay chain have been made as part of a study of symmetric and near-symmetric fission of uranium-235 with thermal neutrons. Fast chemical separation methods have been developed that permit isolation of selected fission product elements in 3-30 s. The methods have been applied to identification and characterization of new, short-lived radionuclides in addition to their use in studies of distribution of nuclear charge in fission.

The cumulative fission yield of Sn^{121} (27.5h) was measured to be $(1.1 \pm 0.1)\ 10^{-2}$ % as compared to the single literature value of 1.5×10^{-2} %. Taking the cumulative yield of Sn^{121m} (~25 yr) as 0.08×10^{-2} %, and making the reasonable assumption that the independent fission yield of Sb^{121} is negligible, we obtain a fission mass yield of $(1.2 \pm 0.1)\ 10^{-2}$ % for mass chain 121 in thermal-neutron fission of uranium-235.

Identification of Cd^{121} was made. Its half-life and cumulative fission yield were determined to be $12.8\ ^{+0.4}_{-0.3}$ s and $(6.4 \pm 0.5)\ 10^{-3}$ % respectively. If the nuclear charge distribution curve is Gaussian and if a width parameter σ of 0.62 as given by Wahl et al. is taken, the cumulative fission yield of Cd^{121} leads to a value of 48.35 for the most probable nuclear charge (Z_p) for mass chain 121. This value of Z_p, combined with published values for other mass chains more removed from symmetric fission, indicates in a preliminary way that the Z_p function proceeds towards the point of symmetric fission by a gentle rather than an abrupt approach.

Fast chemical separation techniques have been developed based on sublimation of metal chelates, precipitation and metal reduction reactions. Isolation of indium in about 30 s was accomplished by precipitation and sublimation of its acetylacetonate. With this procedure the cumulative fission yield of In^{121} (3.1 min) was determined to be 3.2×10^{-3} %. Cadmium as an ammine complex was separated in 3 s from hydroxide and oxalate precipitates of other chain members, indium and tin. Isolation of silver was accomplished in 3 s by reduction of ionic silver by finely divided copper powder. With this procedure no evidence for Ag was seen; thus its half-life is shorter than several seconds or its fission yield is inordinately low.

RENDEMENT SELON LA MASSE ET RENDEMENT CUMULATIF DE LA FISSION QUASI SYMÉTRIQUE DE ^{235}U PAR DES NEUTRONS THERMIQUES. PARTIE I. LA SÉRIE DE MASSE 121. Le rendement en produits de fission de masse 121 et les rendements cumulatifs en éléments de cette série radioactive ont été déterminés dans le cadre d'une étude de la fission symétrique et quasi symétrique de ^{235}U par des neutrons termiques. On a élaboré des méthodes de séparation chimique rapide qui permettent d'isoler les produits de fission voulus en un espace de temps de 3 à 30 s. On les a utilisées non seulement pour étudier la distribution de la charge nucléaire dans la fission, mais aussi pour identifier et caractériser de nouveaux radionucléides de courte période.

Les mesures ont montré que le rendement de fission cumulatif en ^{121}Sn (27,5 h) s'élève à $(1,1 \pm 0,1)\ 10^{-2}$ % alors que la seule valeur publiée jusqu'à présent était de $1,5 \cdot 10^{-2}$ %. En admettant que le rendement cumulatif en ^{121m}Sn (~25 a) soit de $0,08 \cdot 10^{-2}$ % et, ce qui semble légitime, que le rendement de fission indépendant en ^{121}Sb soit négligeable, on obtient pour la fission de ^{235}U par des neutrons thermiques un rendement, selon la masse, en produits de fission de $(1,2 \pm 0,1)\ 10^{-2}$ % pour la série radioactive de masse 121.

On a également identifié ^{121}Cd. On a établi que sa période et le rendement de fission cumulatif étaient de $12,8\ ^{+0,4}_{-0,3}$ s et de $(6,4 \pm 0,5)\ 10^{-3}$ % respectivement. Si la courbe de la distribution des charges nucléaires est gaussienne et le paramètre de largeur σ est de 0,62, comme indiqué par Wahl et al., le rendement

de fission cumulatif en ^{121}Cd donne une valeur de 48, 35 pour la charge nucléaire la plus probable (Z_p) dans la série radioactive de masse 121. De cette valeur de Z_p, combinée aux valeurs publiées pour d'autres séries radioactives plus éloignées de la fission symétrique, on peut conclure à titre préliminaire que la fonction Z_p tend vers le point de fission symétrique de façon régulière.

On a élaboré des méthodes de séparation chimique rapide qui sont fondées sur la sublimation de composés métalliques chélatés, la précipitation et des réactions de réduction à l'état de métal. L'indium a pu être isolé en 30 s environ, par précipitation et sublimation de son acétylacétonate. Ce procédé a permis de fixer le rendement de fission cumulatif en ^{121}In (3, 1 min) à $3,2 \cdot 10^{-3}$ %. Le cadmium, sous la forme d'un complexe aminé, a été séparé en trois secondes des précipités d'hydroxyde et d'oxalate d'autres éléments de la série, l'indium et l'étain. La séparation de l'argent a pu se faire en 3 s par réduction d'argent ionique à l'aide de cuivre en poudre très fine. Cette méthode n'a pas permis de constater la présence de ^{121}Ag; on peut en conclure que sa période est inférieure à quelques secondes ou que le rendement en ce produit de fission est excessivement faible.

ВЫХОДЫ МАССЫ И СОВОКУПНЫЕ ВЫХОДЫ ПРИ ПОЧТИ СИММЕТРИЧНОМ ДЕЛЕНИИ УРАНА-235 ПОД ДЕИСТВИЕМ ТЕПЛОВЫХ НЕИТРОНОВ. ЧАСТЬ I. ЦЕПОЧКА МАССЫ 121. Определение выхода массы 121 при делении и выходов элементов этой цепочки распада проводилось как часть изучения симметричного и почти симметричного деления урана-235 под действием тепловых нейтронов. Были разработаны методы быстрого отделения изотопов, которые позволяют извлекать отдельные продукты деления в течение 3–30 секунд. Эти методы применялись для выявления и определения характеристик новых короткоживущих радиоизотопов, помимо их использования при изучении распределения ядерного заряда при делении.

Измерения показали, что совокупный выход деления олова-121 (27,5 часов) составлял $(1,1 \pm 0,1)\,10^{-2}$ % по сравнению с единственной опубликованной в литературе величиной в $1,5 \cdot 10^{-2}$ %. Принимая совокупный выход олова-121^m (приблизительно 25 лет) равным $0,08 \cdot 10^{-2}$ % и, исходя из приемлемой гипотезы, что независимый выход деления сурьмы-121 незначителен, авторы определили, что для цепочки массы 121 выход массы при делении урана-235 под действием тепловых нейтронов составляет $(1,2 \pm 0,1)10^{-2}$ %.

Было выявлено наличие кадмия-121. Было определено, что период его полураспада и совокупный выход деления составляют соответственно $12,8\,^{+0,4}_{-0,3}$ сек и $(6,4 \pm 0,5)10^{-3}$%. Если кривая распределения ядерного заряда соответствует гауссиановому распределению и если принять в качестве параметра ширины $\sigma = 0,62$, согласно Валю и др., то совокупный выход кадмия-121 при делении дает величину наиболее вероятного ядерного заряда (Z_p), равную 48,35 для цепочки массы 121. Эта величина Z_p в сопоставлении с опубликованными величинами других цепочек масс, более значительно отступающих от симметричного деления, указывает в предварительном порядке на то, что функция Z_p приближается к точки симметричного деления не в виде крутой, а скорее плавной кривой.

Были выработаны методы быстрого химического отделения, основанные на сублимации внутрикомплексных металлических соединений, последующем осаждении и затем на реакциях восстановления металла. Извлечение индия приблизительно за 30 сек было достигнуто осаждением и сублимацией его ацетил-ацетонатов. На основании этого метода совокупный выход индия-121 (3,1 мин) при делении составил $3,2 \cdot 10^{-3}$%. Кадмий был выделен в качестве аминового комплекса за 3 сек из гидроокиси и оксалата других элементов цепочки, а именно индия и олова. Извлечение серебра было достигнуто за 3 сек с помощью восстановления ионного серебра при помощи тонко размельченного медного порошка. Этот метод не показал наличия серебра-121; таким образом, его период полураспада должен быть короче нескольких секунд, или же его выход при делении необычайно незначителен.

FISION CUASI SIMETRICA DEL ^{235}U INDUCIDA POR NEUTRONES TERMICOS: RENDIMIENTO MASICO Y ACUMULATIVO - PARTE I. LA CADENA DE MASA 121. En el marco de un estudio de la fisión simétrica y cuasi simétrica del uranio-235 inducida por neutrones térmicos, los autores han determinado los rendimientos de fisión del núclido de masa 121 y los rendimientos acumulativos de los eslabones de la correspondiente cadena de desintegración. Han perfeccionado métodos químicos de separación rápida que permiten aislar determinados productos de fisión en 3 a 30 s. Dichos métodos se han aplicado al estudio de la distribución de la carga nuclear en la fisión y, además, a la identificación y caracterización de nuevos radionúclidos de período corto.

Para el rendimiento de fisión acumulativo del ^{121}Sn (27, 5 h) se obtuvo un valor de $(1, 1 \pm 0, 1)\,10^{-2}$ %, mientras que el único valor que figura en la bibliografía es $1,5 \cdot 10^{-2}$ %. Si se supone que el rendimiento

acumulativo de ^{121m}Sn (~25 a) asciende a $0,08 \cdot 10^{-2}$ %, y, como es razonable, que el rendimiento independiente de fisión del ^{121}Sb es despreciable, se obtiene en el caso de la fisión de uranio-235 inducida por neutrones térmicos un rendimiento de $(1,2 \pm 0,1)\,10^{-2}$ % para la cadena de masa 121.

Entre los productos de fisión obtenidos, los autores identificaron el ^{121}Cd. Se estableció que su período y su rendimiento acumulativo de fisión son, respectivamente, $12,8^{+0,4}_{-0,3}$ s y $(6,4 \pm 0,5)\,10^{-3}$ %. Si la curva de distribución de la carga nuclear es gaussiana y se supone un parámetro de anchura de 0,62 como indican Wahl y col., el rendimiento acumulativo de fisión del ^{121}Cd conduce a un valor de 48,35 para la carga nuclear más probable (Z_p) de la cadena de masa 121. Este valor de Z_p, combinado con los datos que se han publicado para otras cadenas cuya fisión es menos simétrica, parece indicar que la función Z_p se desplaza de modo más bien lento hacia el punto de fisión simétrica.

Los autores han perfeccionado técnicas químicas de separación rápida que se basan en la sublimación de quelatos metálicos, en la precipitación y en la reducción a metal. El indio se separó en unos 30 s precipitando y sublimando su acetilacetonato. Por este procedimiento se determinó que el rendimiento acumulativo de fisión del ^{121}In (3,1 min.) es $3,2 \cdot 10^{-3}$ %. El cadmio se separó en forma de amminocomplejo de los precipitados de hidróxidos y oxalatos correspondientes a otros eslabones de la cadena (indio y estaño); la operación exigió 3 s. La separación de plata se logró también en 3 s por reducción de plata iónica con cobre finamente dividido. Esta operación no reveló la presencia de vestigios de ^{121}Ag, lo que indica que su período es inferior a pocos segundos o que su rendimiento de fisión es extraordinariamente bajo.

INTRODUCTION

The fission yield of mass 121 and the cumulative yield of a member of that decay chain were determined as part of a study of symmetric and near-symmetric fission of U^{235} with thermal neutrons. This study has received impetus from the observation of a pronounced decrease in kinetic energy [1] in the region of symmetric fission. This observation coupled with the paucity of data on nuclear charge dispersion curves and on most probable nuclear charge, Z_p, for mass numbers produced in near-symmetric fission has indicated the need for extended independent fission yield measurements in this mass region. The following is a report on some of these measurements.

The elements in the mass-121 chain studied were silver, cadmium, indium and tin. Sn^{121} was measured to give data on the total mass-121 chain yield in U^{235} thermal neutron fission. Previously only an unpublished value was reported for this yield [2]. To evaluate the yields of the other chain members rapid methods were developed to separate a specific chain element to the exclusion of other chain members. Separations were made at various times after fission and descendant Sn^{121} (half-life 27.5 h) was measured. The quantity of Sn^{121} in relation to the separation time constitutes a decay curve for the isolated precursor.

This report describes the separation procedures developed and gives (1) a value for the mass-121 chain yield, (2) the cumulative yields of an In^{121} isomer and of Cd^{121}, and (3) the results of a search for Ag^{121}. The most probable nuclear charge (Z_p) for mass 121 was computed from the cumulative yield of Cd^{121} and compared with an empirical Z_p function.

PROCEDURES

Irradiation procedure

A solution of enriched U^{235} (93.17%) was placed in a pneumatically driven sample carrier (rabbit). A gold foil taped to the bottom of the rabbit served as a monitor of fissions in the sample. (Au^{198} foil activity had been calibrated in terms of number of fission events through simultaneous irradiation of Au and U^{235}, and subsequent measurements of Au^{198} and of Mo^{99} and Ba^{140} activities; the latter two fission product radionuclides provide a measure of the number of fissions in the sample.) The rabbit was positioned in the Vallecitos Nuclear Test Reactor where the neutron flux was about 10^{12} n/s cm^2, irradiated for a predetermined interval, and then automatically returned to the working area with the NRDL pneumatic rabbit transport facility [3]. The irradiated solution was transferred into a reaction vessel through polyethylene tubing. This tubing extended from the hypodermic needle upon which the rabbit impinged, through a tightly fitting hole in a rubber stopper, to a reaction vessel. Transfer of the fission solution from the rabbit occurred upon applying vacuum to the reaction vessel and capping it with the rubber stopper (see Fig. 1).

Indium

The procedure developed for indium was based upon the volatility of indium acetylacetonate at moderate temperatures [4], and the separation was effected by sublimation.

Sublimation and filtration apparatus

The sublimation apparatus consisted of a heating block and a two-piece glass sublimation assembly (Fig. 1). The heating block was constructed from a solid aluminium rod, of 5-in diam. and 7-in long. The side of the block was wrapped with a layer of asbestos paper and then carefully wound with 25 ft of nichrome wire (0.725 Ω/ft), each turn being secured with asbestos cord. The side and bottom of the block were covered with several layers of thick asbestos cloth. The ends of the nichrome wire protruded through the covering and were connected to a temperature controller (Model 40, F & M Corporation). The thermocouple of the controller was inserted into a 3-in hole drilled from the top of the block and 3/4 in in from the side. A cavity centred in the top was machined to be complementary in shape with the lower half of the glass sublimation assembly.

The glass sublimation assembly was constructed from a 50/30 pyrex glass ball-and-socket joint. The bottom half of the assembly consisted of the socket section that was sealed to form a flat base at a distance 1.5 in from the socket. This section resided in the aluminium block and was filled to within 0.5 in of the joint with a low-melting alloy (Cerrolow 117, Lockheed Corporation). The upper ball joint section was fitted with a cold finger that entered the wall about 1 in from the joint and extended down through the centre of the piece to a point parallel with the edge of the joint. The upper

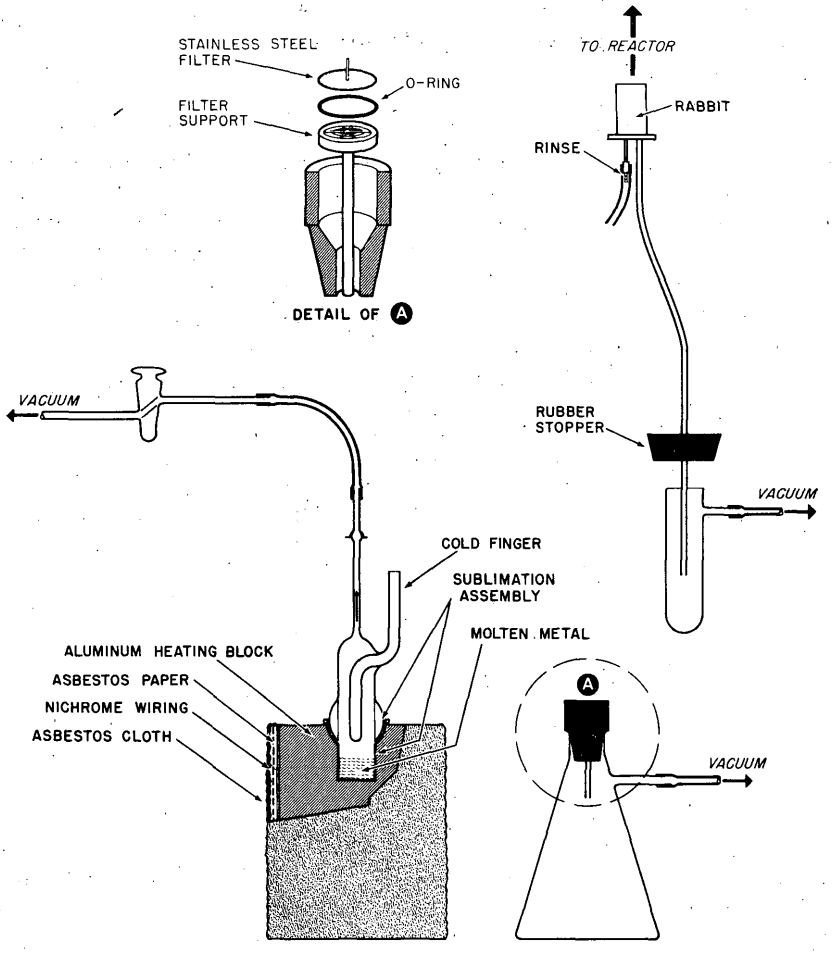

Fig. 1

Precipitation, filtration, and sublimation apparatus

part of this section was tapered and ended with a short length of tubing and a 12/5 ball joint. By clamping this smaller ball joint to a mate, connection with a stop-cock-controlled high-vacuum line was made.

The filtering apparatus consisted of a suction flask connected to a vacuum line. A 35-ml Walter crucible holder, with the glass funnel stem removed, was fitted into the neck of the flask. A base plate (E-8B, precipitation apparatus, Tracerlab Division, Laboratory for Electronics, Inc., Richmond, Calif.) was seated snugly into the taper of the holder. This plate served as support for the filter, which was made from stainless steel wire mesh, 10-μm pore size (Chas. Lowe Co., San Francisco, Calif.). The wire mesh was of 7/8 in diam, and in its centre was peened a 1/16-in-diam. stainless steel rod, 3/8-in long. (The rod facilitated the rapid transfer of the precipitate to the sublimation assembly.) An O-ring of 13/16-in I. D.

and 1/16-in wall thickness was interposed between the stainless steel mesh and the supporting plate to create an effective vacuum seal.

Separation procedure

The irradiation schedule for the indium separations is shown in Table I. The time of separation was the difference in time between the mid-point of the irradiation time and the mid-point of the sublimation time. The duration

TABLE I

IRRADIATION SCHEDULE

Time of separation[a] (s)	Duration of irradiation (s)	Starting time of precipitation[b] (s)
33	10	2 (approx.)
36	10	2 "
40	10	2 "
50	10	2 "
60	10	2 "
70	10	2 "
80	10	2 "
90	10	2 "
100	20	2 "
150	20	2 "
200	20	60
250	30	100
300	40	150
400	50	300
500	70	400
600	100	500

[a] The time of separation is the difference between the mid-point of the irradiation time and the mid-point of the sublimation time.

[b] The starting time of precipitation is the interval of time between the end of the irradiation and the addition of the precipitating reagent.

of sublimation time was maintained constant (10 s), while the irradiation time ranged from 10 to 100 s. Also included in the table is the time at which precipitation was initiated for each separation time.

U^{235} (100 mg) together with indium carrier (20 mg In^{+++}) were irradiated. The reaction vessel into which the irradiated solution was transferred consisted of a 50-ml round-bottom centrifuge tube, fitted with a side-arm for

connection to vacuum. This vessel contained 1 mg tin carrier, ethyl alcohol (0.3 ml) and acetylacetone (0.50 ml). After transfer, the rabbit was immediately washed by the action of suction with 0.5 ml of water (see Fig. 1), and then 25 ml, of 1.1 N NaOH were similarly introduced into the reaction vessel through the same wash channel.

The tube was vigorously agitated for 10 s, at which time the crystal size was sufficiently large for effective filtration. The mixture was rapidly filtered on the stainless steel wire mesh, and both filter and precipitate were immediately floated on the molten alloy maintained at 425°C. The upper section of the sublimation assembly, previously lubricated with Apiezon Grease H and charged with liquid nitrogen in the cold finger, was quickly mated to the lower section and was simultaneously evacuated. After 10 s the sublimation was terminated by separation of the ball joint from its socket.

The sublimate was dissolved from the cold finger and surrounding parts with 1 N HCl and diluted to a standard volume with the same acid. The indium yield was determined on 0.1 aliquot of this solution by extraction with 8-quinolinol in chloroform, after adjustment of the solution to pH 4.5 [5]. The remainder of the solution was consumed in the determination of Sn^{121} by the radiochemical procedure of COWAN [6]. The decay of beta-ray activity was measured on a gas-flow beta-ray proportional counter. After subtraction of a long-lived component, the decay curve for 27.5-h Sn^{121} was obtained. The extrapolated count was corrected for chemical yield, aliquot, self-absorption, and tin contamination, with an average co-sublimation factor of 0.0022, and the value for the fraction of Sn^{121} formed from In^{121} isomers by the time of sublimation (see Results below and Fig. 2).

With this procedure, the indium chemical yield was (25 ± 10)% and contamination of the sublimate by tin, cadmium and silver was 0.2%, 0.7% and 0.4% respectively.

Cadmium

The method developed for the separation of cadmium from its descendants was based upon the solubility of a cadmium-ammine complex and the insolubility of tin and indium in an ammoniacal oxalate solution. Further decontamination from interfering daughter elements was effected by filtration of the precipitated solution through an adsorbent.

Filtration apparatus

The filtration apparatus (Fig. 3) consisted of two 50/30 ball joints, between which a stainless steel plate (3/8-in thick, 3-in diam.) was interposed. This plate served as a support for a 3.75-in square of stainless steel filtering mesh of 2-μm pore size (Chas. Lowe Co., San Francisco, Calif.).

The stem of the lower ball joint was tapered and sealed to a 4-in length of 13-mm tubing to permit connection through a rubber stopper to a 250-ml suction flask.

A 1/4-in wide X 1/16-in deep cut from the outside of the bottom surface of the steel plate provided for a seat on the lower ball joint. A hole (3/4-in

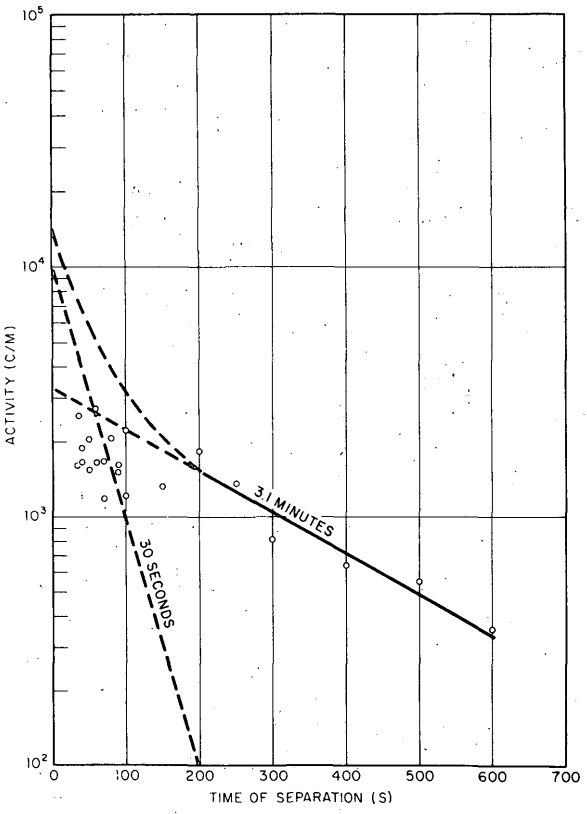

Fig. 2

The growth of Sn^{121} activity from In^{121} at various times of In separation.
(The time of separation is the difference between the mid-point of the irradiation time and the mid-point of the sublimation time.)

diam.) was drilled through the centre of the plate. Three concentric channels (1/4-in wide) and eight symmetrically radiating channels were machined into the top surface of the plate to expedite the filtration.

The rim of the upper ball joint was placed on top of the filtering screen and the assembly was rigidly maintained by securing both joints with a pinch clamp (Size 50). To direct the precipitated solution effectively and rapidly into the filtration apparatus, a powder funnel (100-mm top diam.) was inserted into the upper ball joint.

To prepare the filter bed, 0.5 g of Bentone 38 (primarily a hectorite clay, supplied by National Lead Company, New York, N. Y.) was transferred onto the stainless steel filter. The clay was repeatedly washed with warm 1N HNO_3 until it supported (without suction) 20 ml of water with only dropwise leakage.

Separation procedure

A solution of enriched U^{235} (100 or 200 mg), cadmium carrier (28 mg Cd^{++}) and indium carrier (20 mg In^{+++}) was irradiated for 10 s. The

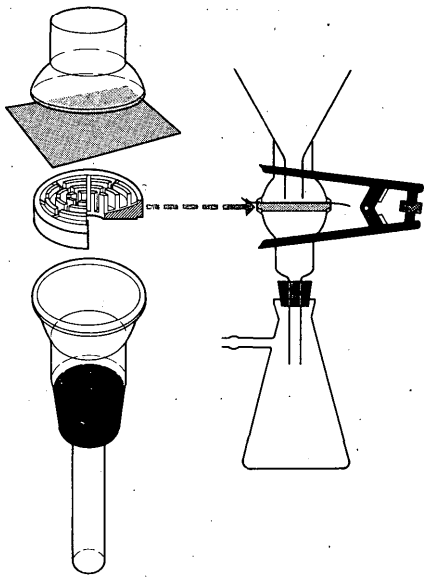

Fig. 3

Filtration apparatus for cadmium separations

irradiated solution was transferred to a reaction vessel constructed from a 100-ml round bottom centrifuge tube, fitted with a side-arm for connection to vacuum. This vessel contained 22 ml of the precipitating solution. (The precipitating solution consisted of NH_4OH (1.5N) and $(NH_4)_2C_2O_4$ (0.05 M).) The solution was heated to ebullition just before transfer of the fission solution. Following this transfer the precipitated fission solution was poured onto the prepared filter at a predetermined time. The filtration was complete in about 1 s. The suction flask that collected the filtrate contained a definite volume of standardized tin carrier.

The filtrate was acidified with concentrated HCl and was diluted to 25.0 ml. A colorimetric procedure [7] was applied to a 1-ml aliquot of this solution to determine the cadmium yield. Several hours after irradiation, the remainder of the diluted filtrate was treated, first with 10N NaOH until the appearance of permanent slight turbidity and then with 1.5 ml of concentrated HCl. After this pH adjustment Sn^{121} was determined as described above.

By this separation procedure 40-50% of the cadmium was recovered in the filtrate. Contamination by indium and tin in this solution was 0.06% and 0.3% respectively.

Silver

The separation of silver from the descendant chain elements was based upon the well-known reduction of ionic silver by metallic copper.

Filtration apparatus

The filtration apparatus was adapted from a commercially available filter tower (Tracerlab). A disc (7/8-in diam) of 10-μm pore size stainless steel mesh (Chas. Lowe Co., San Francisco) replaced the porous steel stem. The wire mesh supported 1 g of copper powder. The powder was washed several minutes before use with 10 ml 1.6N HNO_3. The tower was connected to a suction flask and the filtration rate was 30 ml/s.

Separation procedure

U^{235} (100 mg) in 0.6 ml 4N HNO_3 was irradiated 10 s and then transferred by suction to a tube containing 10 ml of 4N HNO_3. The rabbit was washed with 5 ml 4N HNO_3 and the combined solution was passed through the filtration apparatus at a definite time after the irradiation. The copper bed was washed immediately with 5 ml 1.6N HNO_3. Copper and supporting stainless steel mesh were transferred to a centrifuge tube containing a known volume of standardized tin carrier. Concentrated HNO_3 was added dropwise to dissolve the copper, and 10 ml saturated NH_4Cl were added to the solution. The solution was adjusted to pH 8 with NH_4OH, and the precipitate that formed was collected by centrifugation. To the precipitate were added 10 ml of concentrated NH_4OH and the mixture was stirred thoroughly to solubilize the residual copper precipitate. The mixture was centrifuged and, after decanting the excess supernatant liquid, 1 ml of concentrated HCl was added to the precipitate. The resultant solution was analysed for Sn^{121}.

By this procedure silver was essentially quantitatively recovered (98.3%) and the copper bed was contaminated with cadmium, indium and tin to the extent of 0.06%, 0.06% and 0.03% respectively.

Mass-121 chain yield

Two rabbits each with 100 mg of U^{235} solution were irradiated for 300 s. About 18 h after the irradiation, standardized tin carrier was added to the solution, and then the solution was diluted to 25.0 ml with water. Two 10-ml aliquots from each sample were radiochemically analysed for tin. Beta-decay measurements were made as before and the data were resolved into 27.5 h Sn^{121}, 9.4-d Sn^{125} and 125-d Sn^{123} by a computer programme method. Mo^{99} radiochemical analyses [8] were performed in duplicate on 2-ml aliquots from each sample to estimate the total number of fissions.

RESULTS

Indium

The numbers of Sn^{121} counts normalized to 10^{12} fissions and extending from separation times of 33 to 600 s appear as circles in Fig. 2. For comparative purposes the curve described by WAHL and NETHAWAY [9], together with the relative contribution of each of two indium isomers, are

shown by interrupted lines. Over the interval 200-600 s, a region in which the contribution of the 30-s In^{121} isomer is negligible, linear regression analysis yielded a half-life of $3.1^{+0.4}_{-0.3}$ min for the longer-lived isomer. This value coincides with the previously reported half-life [9, 10], and is represented by the solid line in Fig. 2. A cumulative fission yield of 3.2×10^{-3}% was calculated for this longer-lived isomer.

The experimental points obtained for shorter separation times deviate sharply from the previously described relationship of Wahl and Nethaway. These points are more or less randomly distributed within a cluster and lie considerably below the cumulative curve.

Cadmium

Figure 4 shows the count-rate of Sn^{121} normalized to 10^{12} fissions for 18 separations of cadmium extending in time from 3 to 42 s after fission. Separations beyond 42 s were precluded by low count-rate and relatively greater contribution of a component longer lived than Sn^{121}. The linear re-

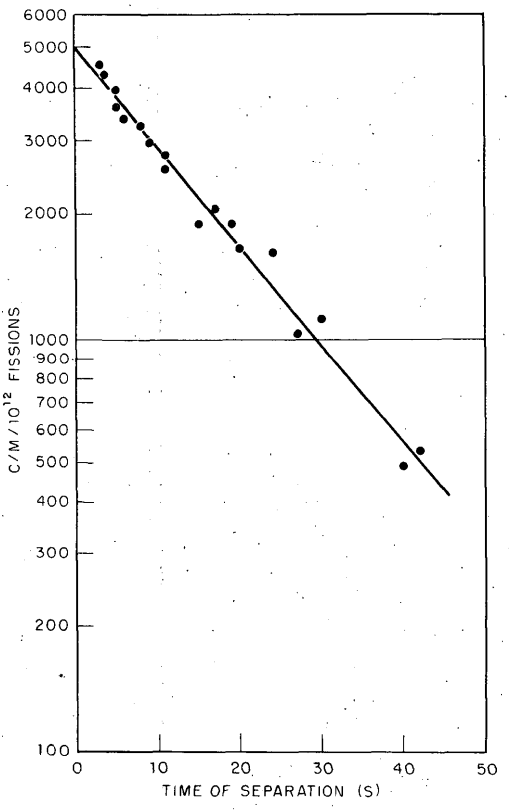

Fig. 4

The growth of Sn^{121} activity from Cd^{121} at various times of Cd separation. (The time of separation is the difference in time between the end of the irradiation and the end of filtration.)

lationship between the logarithm of the count-rate and separation time is apparent. The half-life of Cd^{121} derived from these data by the method of least squares is $12.8^{+0.4}_{-0.3}$ s. An empirically determined correction for the counting efficiency of a 0.38-MeV beta ray was applied to the counting rate of Sn^{121} to obtain the quantity of Cd^{121} present at the end of the irradiation. Cd^{121} was corrected for its decay during the course of the irradiation by the expression

$$Y = \frac{N'(\lambda)}{F(1 - e^{-\lambda\tau})(e^{-\lambda t})}$$

where Y is the cumulative Cd^{121} yield, N' the number of atoms at time t, t the time since the end of the irradiation, F the fission rate, τ the duration of the irradiation, and λ the decay constant for Cd^{121}. The cumulative fission yield of Cd^{121} thus was calculated as $(6.4 \pm 0.5) \times 10^{-3}$ %. Therefore, the cumulative fractional fission yield of Cd^{121} is 0.53 ± 0.09 (computed with the value for the total chain yield given below).

Silver

In the search for Ag^{121} 12 irradiations were performed and separations were made in the interval of 3.5 to 60 s after the end of fission. Daughter Sn^{121} was undetected even in the shortest time of separation.

Mass-121 chain yield

The mass-121 chain yield as measured by 27.5 h Sn^{121} was determined to be $(1.1 \pm 0.1) \times 10^{-2}$ %. This value together with the fission yield of Sn^{121m} (~25 yr) [11] gives a total chain yield of $(1.2 \pm 0.1) \times 10^{-2}$ %.

DISCUSSION

The deviation of experimental points obtained for short indium separations from the data of WAHL and NETHAWAY [9] is explained by the dependence of In^{121} upon fission precursors. By contrast with separations at 200 s and later, for shorter times (33-150 s) the acetylacetonate was precipitated very soon after the irradiation (Table I). In the precipitation phase of separation the indium precursors, silver and cadmium, may be expected to form an insoluble oxide and hydroxide respectively. Although the time between precipitation and sublimation is a period in which these precursors probably have fully decayed, the indium produced in this decay was presumably in a form different from the sublimable acetylacetonate; therefore its presence was undetected.

The results of the silver separations indicate either that the half-life of Ag^{121} is considerably less than several seconds or that its fission yield is inordinately low.

From the yields for Cd^{121}, and the assumptions that the distribution of nuclear charge is Gaussian and that the width parameter σ is 0.62 [12], a value of 48.45 was computed for Z_p.

Experimental information about charge distribution for mass numbers in the region of near symmetric fission was previously unavailable. It was therefore of interest to compare Z_p for A = 121 with the empirical Z_p function described by WAHL et al. [12]. This function is shown in Fig. 5, in which complementary light (l) and heavy (h) primary fragments were matched on the abscissa according to their mass number (A') before neutron evaporation. The fragment mass number A' was interpolated from data on the

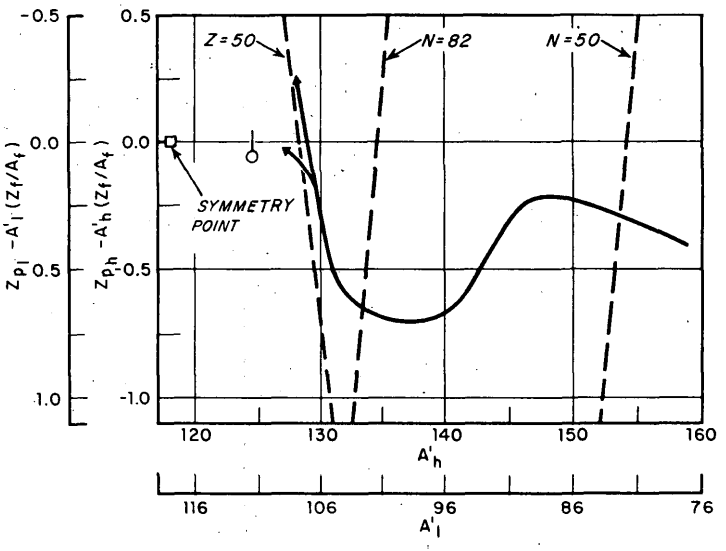

Fig. 5

Z_p value from this work and the empirical Z_p function of WAHL et al. [12]

number of neutrons emitted per fragment [1]. In the ordinate a multiple of the mass number is subtracted from Z_p. The multiple is (Z_f/A_f), the ratio of atomic to mass number for the fissioning nucleus, U^{236}. The smooth and continuous line represents the Z_p function that best fits the experimental data. The bifurcation shown by two arrows displays alternatives in the Z_p function. The sharp rise in Z_p near the 50-proton shell edge was based on the small independent yield of I^{128}. With recognition that evidence for this relationship rested heavily on only a single value, the less radical alternative was also drawn by WAHL et al. [12]. The experimental value for Z_p at A = 121 (A' = 124.4) favours the latter alternative (see Fig. 5).

The effect of possible isomerism in Cd^{121} on the Zp function was considered. The existence of two isomeric states for Cd^{121} is suggested by comparison of the nuclide with the characteristics of related neighbouring nuclides that contain an odd neutron or proton, e.g. Cd^{115}, Cd^{117}, Cd^{119}, Sn^{123}, Te^{125} and Xe^{127}. If one of the isomeric states were substantially shorter lived than the several seconds required for separation, it would

remain undetected. Such a circumstance would result in an apparent value of Z_P greater than the actual value.

Clearly further information is required to characterize the nature of Z_P in the region of symmetric fission.

The cumulative fission yield of Sn^{121} (27.5h) was measured to be $(1.1 \pm 0.1) \times 10^{-2}$ %, as compared to the single literature value of 1.5×10^{-2}%. Taking the cumulative yield of Sn^{121m} (25 yr) as 0.08×10^{-2} % and with the reasonable assumption that the independent fission yield of Sb^{121} is negligible, the fission mass yield for mass-chain 121 is $(1.2 \pm 0.1) \times 10^{-2}$ % in thermal-neutron fission of U^{235}.

The currently available information on the genetic relationships among the members of the mass-121 chain formed in the thermal-neutron fission of U^{235} are shown below, together with half-lives, cumulative fission yields and an upper limit for the independent yield of Sn^{121}. The value for the independent formation of Sn^{121}, and the fractional contribution of In isomers to Sn^{121} yield were given by WAHL and NETHAWAY [9] and the yield of Sn^{121m} was determined by ORTH [11].

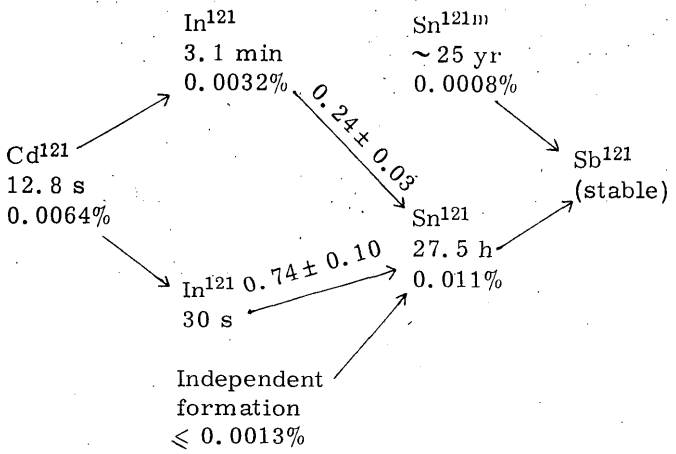

SUMMARY

Cd^{121} was identified, and its half-life and cumulative fission yield were determined to be $12.8^{+0.4}_{-0.3}$ s and $(6.4 \pm 0.5) \times 10^{-3}$ % respectively. If the nuclear charge distribution curve is Gaussian with a width parameter of 0.62 as given by Wahl et al., the cumulative fission yield of Cd^{121} leads to a value of 48.45 for the most probable nuclear charge (Z_P) for mass-chain 121. A 50-proton shell effect is not evident from this value of Z_P; alternatively, the value suggests a smooth approach of the Z_P function towards the point of symmetric fission.

The cumulative fission yield of In^{121} (3.1 m) was determined to be 3.2×10^{-3}%.

Evidence for existence of Ag^{121} was not observed; thus either its half-life is shorter than several seconds or its fission yield is inordinately low.

The fission yield for mass-chain 121 in thermal-neutron fission of U^{235} was determined to be $(1.2 \pm 0.1) \times 10^{-2}$ %.

Fast chemical separation techniques have been developed based on sublimation of a metal chelate, precipitation and metal reduction reactions. Isolation of indium in about 30 s was accomplished by precipitation and sublimation of its acetylacetonate. Cadmium as an ammine complex was separated 3 s after fission from hydroxide and oxalate precipitates of chain members, indium and tin. Isolation of silver was accomplished in 3 s by reduction of ionic silver by finely divided copper powder.

REFERENCES

[1] MILTON, J.C.D. and FRASER, J.S., Canad. J. Phys. 40 (1962) 1626.
[2] STEINBERG, E.P., Editors' Note in Radiochemical Studies: The Fission Products (CORYELL, C.D. and SUGARMAN, N., Eds.) National Nuclear Energy Series IV-9, McGraw-Hill Book Co., New York (1951) 913.
[3] GREENDALE, A.E. and LOVE, D.L., Nucl. Instrum. Meth. 23 (1963) 209.
[4] SIDGWICK, N.V., Chemical Elements and Their Compounds, Clarendon Press, Oxford (1950) 474.
[5] SNELL, F.D. and SNELL, C.T., Colorimetric Methods of Analysis, 3rd ed., II, D. Van Nostrand Co., New York (1949) 222.
[6] COWAN, G.A. in Collected Radiochemical Procedures, Los Alamos Scientific Laboratory Report LA-1721, 2nd ed. (1958).
[7] KNAPP, J.R., Van AMAN, R.E. and KANZELMAN, J.H., Analyt. Chem. 34 (1962) 1374.
[8] SCADDEN, E.M., Nucleonics 15 No.4 (1957) 102.
[9] WAHL, A.C. and NETHAWAY, D.R., Phys. Rev. 131 (1963) 830.
[10] YUTA, H. and MORINAGA, H., Nucl. Phys. 16 (1960) 119.
[11] ORTH, private communication to WAHL and NETHAWAY [9].
[12] WAHL, A.C., FERGUSON, R.L., NETHAWAY, D.R., TROUTNER, D.E. and WOLFSBERG, D., Phys. Rev. 126 (1962) 112.

NEUTRON-INDUCED FISSION OF ACTINIUM-227, PROTACTINIUM-231 AND NEPTUNIUM-237: MASS DISTRIBUTION

R.S. IYER, H.C. JAIN, M.N. NAMBOODIRI, M. RAJAGOPALAN RAJKISHORE, M.V. RAMANIAH, C.L. RAO, N. RAVINDRAN AND H.D. SHARMA
RADIOCHEMISTRY AND ISOTOPE DIVISION,
ATOMIC ENERGY ESTABLISHMENT TROMBAY, BOMBAY, INDIA

(Presented by S.S. Kapoor)

Abstract — Résumé — Аннотация — Resumen

NEUTRON-INDUCED FISSION OF ACTINIUM-227, PROTACTINIUM-231 AND NEPTUNIUM-237: MASS DISTRIBUTION. Results of radiochemical studies on the mass distribution in the neutron-induced fission of actinium-227, protactinium-231 and neptunium-237 have been presented. This work has been carried out as part of a programme to determine the mass distribution in the fission of heavy elements as a function of Z and A. All irradiations have been carried out in the core of the swimming-pool type reactor APSARA with cadmium shielding wherever necessary. Relative yields of several fission product nuclides have been obtained by a method involving a comparison of the fission product activities from the respective targets with those formed from uranium-235 simultaneously irradiated. Thermal-neutron fission yields of uranium-235 have been assumed. These results indicate a predominantly asymmetric mass distribution in all the three cases, and also a distinct though small symmetric peak in the case of actinium-227.

FISSION DE ^{227}Ac, ^{231}Pa ET ^{237}Np PAR DES NEUTRONS: DISTRIBUTION DES PRODUITS SELON LA MASSE. Les auteurs indiquent les résultats d'études radiochimiques sur la distribution, selon la masse, des produits de la fission de ^{227}Ac, ^{231}Pa et ^{237}Np par des neutrons. Ces travaux ont été exécutés dans le cadre d'un programme de détermination de cette distribution dans le cas d'éléments lourds. Toutes les opérations d'irradiation ont eu lieu dans le coeur de la pile piscine APSARA, en prévoyant une protection en cadmium lorsqu'il le fallait. Pour obtenir les rendements relatifs en plusieurs produits de fission, les auteurs ont utilisé une méthode comportant la comparaison entre l'activité des produits de la fission des diverses cibles et celle des produits de la fission de l'uranium-235 irradié simultanément. Pour les rendements de la fission de ^{235}U par neutrons thermiques, ils ont adopté les valeurs déjà établies. Les résultats révèlent pour tous les trois cas une distribution essentiellement asymétrique, ainsi que la présence d'un pic symétrique très net quoique faible dans le cas de l'actinium-227.

РАСПРЕДЕЛЕНИЕ МАСС ПРИ ДЕЛЕНИИ АКТИНИЯ-227, ПРОТАКТИНИЯ-221 И НЕПТУНИЯ-237, ВЫЗВАННОМ НЕЙТРОНАМИ. Сообщаются результаты радиохимического исследования распределения масс при делении актиния-227, протактиния-231 и нептуния-237 под действием нейтронов. Эта работа была проведена в качестве части программы по определению распределения масс при делении тяжелых элементов как функции Z и A. Все облучения были произведены в активной зоне реактора бассейнового типа "Апсара" с использованием кадмиевой защиты там, где это представлялось необходимым. Относительные выходы различных радиоизотопов, образующихся в качестве продуктов деления, были получены путем сравнения активностей продуктов деления, полученных от соответствующих мишеней, с активностями продуктов деления одновременно облученного урана-235. Было сделано предположение, что эти выходы продуктов деления урана-235 получены под действием тепловых нейтронов. Эти результаты указывают на то, что во всех трех случаях преобладает асимметричное распределение масс и что для актиния-227 наблюдается определенный, хотя и малый симметричный пик.

DISTRIBUCION DE MASAS EN LA FISION DEL ACTINIO-227, PROTACTINIO-231 Y NEPTUNIO-237 INDUCIDA POR NEUTRONES. La memoria presenta los resultados de estudios radioquímicos de la distribución de masas en la fisión del actinio-227, protactinio-231 y neptunio-237 inducida por neutrones. Estos trabajos

se llevaron a cabo como parte de un programa de determinaciones de la distribución másica en función de Z y A durante la fisión de elementos pesados. Todas las irradiaciones se efectuaron en el cuerpo del reactor "APSARA", de tipo piscina, empleando un blindaje de cadmio en caso de necesidad. Los rendimientos relativos de varios núclidos producidos por fisión se han determinado comparando sus actividades en los blancos respectivos con las halladas en el uranio-235 irradiado simultáneamente. Los cálculos se basaron en los rendimientos de fisión del uranio-235 por neutrones térmicos. Los resultados indican que en los tres casos se produce una distribución másica predominantemente asimétrica; para el actinio-227, se observa además un máximo simétrico, de poca altura pero bastante nítido.

INTRODUCTION

Fission of nuclei in the region of gold [1], bismuth [2] and lead [3] is symmetric while low-energy fission of uranium, plutonium and heavier elements is highly asymmetric [4]. In between these two mass regions, a transition from symmetric to predominantly asymmetric fission seems to exist [3]. Thus, fission of Ra^{226} induced by charged particles [5-8] and photons [9] results in triple-peaked mass distribution. Helium ion-induced fission of even a heavier nucleus like U^{233} has been found to give a triple-humped distribution while U^{235} and U^{238} gave only double-peaked curves [10, 11]. The neutron-induced fission of actinide elements has been undertaken to find the trend in mass distribution. Work on the fission of Th^{232} by fast neutrons from the swimming pool reactor APSARA has shown the presence of a small third peak in the trough region [12]. This observation suggested that a study of the neutron-induced fission of actinium may be more interesting, particularly as there is no reported data on the fission of any actinium isotope. This paper describes the relative yields in the fission of Ac^{227}, Pa^{231} and Np^{237} by reactor neutrons. The reported [4] thresholds for neutron-induced fission for these three nuclides are 1.3 MeV, 0.4 MeV and 0.3 MeV respectively. While the fission of Np^{237} was earlier studied by FORD and GILMORE [13] with fission spectrum neutrons and by COLEMAN et al. [14] with 14-MeV neutrons, Ac^{227} and Pa^{231} are reported here for the first time.

EXPERIMENTAL

The general experimental techniques used for the determination of mass yields are similar to those reported earlier [12]. Only essential points are mentioned here.

The comparison method was used for the determination of the relative fission yields [12]. Uranium was always irradiated simultaneously with the target nuclide under study, and the fission products under consideration were isolated from both. The reference nuclide (Sr^{91} in the case of Ac^{227} and Ba^{140} in the other two cases) was isolated in all irradiations and used as an internal standard. Mounting and counting of the corresponding samples was done in the same way so that geometry, absorption and scattering corrections were cancelled.

Defining "D" as the ratio of the total activity A_X of any fission product X formed to that of the total activity A_S of the reference nuclide S formed in

the same fission under the same conditions, and "R" as the ratio of D_N, the D-value in a particular fission (where N = Ac^{227}, Pa^{231} or Np^{237}) and D_U = the D-value in uranium fission, we have

$$D_N = (A_X)N/(A_S)N;\ D_U = (A_X)U/(A_S)U \text{ and } R_X = D_N/D_U .$$

The activity A_X is related to the fission yield as given by the expression

$$A_X = Y_X \lambda_X f E_X$$

where Y_X is the fission yield of the particular nuclide, λ_X its decay constant, f the total number of fission events taking place in the target and E_X the counting efficiency for the fission product. Then

$$R = \frac{(Y_X \lambda_X f E_X)_N}{(Y_S \lambda_S f E_S)_N} \Big/ \frac{(Y'_X \lambda_X f' E_X)_U}{(Y'_S \lambda_S f' E_S)_U} = \frac{(Y_X/Y_S)_N}{(Y'_X/Y'_S)_U}$$

$$Y_X = R\, Y'_X \frac{Y_S}{Y'_S}.$$

If Y_S/Y'_S is arbitrarily set equal to 1, then $Y_X = R\, Y'_X$. The product of R and (Y'_X) gives a relative value for the yield of X in the fission of the nuclide N. This comparison method obviates the necessity of absolute counting of the nuclides under consideration, but is comparable in accuracy to other methods.

Ac^{227} obtained from Amersham was used in this study. The Ra^{226} content of the sample was estimated and found to be less than 0.1%, and the fission contribution from this would be much less than 0.1%. The Ac^{227} was electroplated on platinum backing in 100-μg amounts following a procedure reported elsewhere [15] and used as a target. The target was covered with two thin aluminium foils, 0.2 mg/cm^2 each (to prevent direct contact between the recoil catcher, and actinium and its daughter products) and then with "superpure" aluminium foil, 0.001-in thick, as catcher for recoiling fission fragments. A few blank foils of "superpure" aluminium were also kept behind the target, and this target-recoil catcher assembly was then wrapped with cadmium foil (about 500 mg/cm^2) to reduce the fission of Th^{227} (daughter of Ac^{227}) and (n, γ) reactions in actinium and in any trace impurities in the recoil catcher. The entire assembly was enclosed in an aluminium container and irradiated.

The recoil technique allowed an actinium target to be re-used for irradiation, and also simplified chemical separations by avoiding the presence of actinium and its daughter products in the solution to be analysed.

Uranium content of Pa^{231} obtained from Harwell was checked by solvent extraction of uranium and fluorimetric estimation of the same and found to be less than 0.1%. Np^{237}, which was obtained from Oak Ridge National Laboratory and found to contain small quantities of Pu^{239}, was purified by solvent extraction with TTA, and the purified material contained no detect-

able amounts of plutonium. Suitable aliquots of Pa^{231} (about 1 mg) and Np^{237} (about 2 mg) were evaporated in quartz ampoules and wrapped in cadmium foils. In the case of protactinium, the cadmium wrapping was to reduce the (n, γ) reaction and fission of Th^{227} (daughter of Pa^{231}), Pa^{232} and also of U^{232}, which have a very high cross-section for thermal fission. Similarly with Np^{237}, thermal fission of Np^{238} and any Np^{236} was reduced by cadmium wrapping.

Natural uranium was irradiated with the above materials in the same container. Irradiations were carried out in a fixed position in the core of APSARA reactor so that the same neutron spectrum would cause fission with no major variations from one experiment to another. The duration of an irradiation varied from 8 to 48 h depending on the nuclides to be studied. After irradiation, the targets were treated as follows. For Ac^{227}, the catcher foil and the blank foils were separated from the target, dissolved in an appropriate acid and analysed radiochemically for fission products. Sr^{91} was isolated as a reference nuclide in all experiments. In some cases only one nuclide (and the reference) could be isolated per irradiation since the activity was low. Blank foils were also processed for the nuclide in question and no detectable activities were found. Quartz ampoules containing Pa^{231} and Np^{237} were crushed in an appropriate acid and the nuclides of interest were isolated radiochemically. Uranium targets were also treated similarly.

A known amount of inactive carrier of an element was added to an aliquot of the solution and allowed to interchange with the fission product nuclides of the same element. After interchange was completed, the element was separated and purified from target material (or aluminium) and other fission products, and finally obtained as a precipitate for mounting. Standard radiochemical procedures taken from literature [16-18] were used with appropriate modifications.

The precipitates were filtered through No. 42 filter using a perspex filter assembly, washed, dried and weighed along with the filter paper, centred on aluminium plates or circular discs with double-coated cellulose tape and covered with cellophane paper of thickness about 3 mg/cm^2.

Activities of separated fission products with Ac^{227} were very low (sometimes as low as 5 counts/min above background) since the amount of Ac^{227} used was small and the fission cross-section low. For this reason a low background counter consisting of a Sugarman type methane flow beta proportional counter and a plastic scintillator cosmic ray guard was used. The parameters of the coincidence circuit were so adjusted that the counting loss due to coincidence gammas of up to 2.7 MeV was eliminated. A background count of about 2.5 counts/min was obtained. Activities in the other two cases were higher by an order of magnitude and they were analysed using Sugarman type methane flow beta proportional counters.

RESULTS AND DISCUSSION

Relative fission yields of 12, 17 and 19 nuclides have been determined in the reactor neutron fission of Ac^{227}, Pa^{231} and Np^{237} respectively, and

TABLE I

RELATIVE FISSION YIELDS OF Ac^{227}, Pa^{231} AND Np^{237}

Nuclide	Relative yields in the fission of		
	Ac^{227}	Pa^{231}	Np^{237}
Br^{83}	7.01 (3)*	--	0.43 (1)
Sr^{89}	8.02 (4)	6.83 (4)	2.96 (2)
Sr^{91}	5.81	6.79 (2)	4.60 (2)
Zr^{97}	0.32 (2)	4.18 (1)	--
Mo^{99}	0.11 (1)	2.40 (3)	7.83 (2)
Ru^{103}	--	0.30 (3)	5.48 (2)
Ru^{105}	0.084 (2)	--	--
Ru^{105}	--	0.14 (4)	3.23 (3)
Ru^{106}	--	0.10 (2)	2.06 (2)
Pd^{109}	0.24 (3)	0.077 (3)	0.45 (2)
Ag^{111}	0.18 (6)	0.092 (3)	0.13 (2)
Ag^{112}	0.17 (5)	--	--
Pd^{112}	--	0.056 (3)	0.063 (2)
Ag^{113}	--	0.071 (3)	0.057 (1)
Cd^{115}	--	0.074 (2)	0.061 (2)
Sn^{121}	0.12 (1)	0.088 (2)	0.078 (2)
Sn^{125}	--	--	0.124 (2)
Sb^{127}	--	1.00 (2)	0.595 (1)
Te^{129}	--	1.16 (1)	3.18 (1)
Te^{132}	5.13 (1)	3.16 (3)	5.65 (1)
Ba^{140}	8.48 (3)	6.44	6.44
Ce^{141}	--	--	4.31 (1)
Ce^{143}	6.10 (2)	5.66 (2)	--
Ce^{144}	--	--	2.90 (1)

* The numbers in parentheses indicate the number of determinations of the yield of the nuclide

these are given in Table I. For Ac^{227} and Pa^{231}, most of the yields have been determined in more than one experiment, while 7 out of the 19 yields in the fission of Np^{237} reported here are the results of a single experiment. When more than one experiment was done, the reported value is the average of the determinations. The data are plotted in Figs. 1, 2 and 3. Smooth curves have been drawn through experimental points only for Pa^{231} and Np^{237}, while

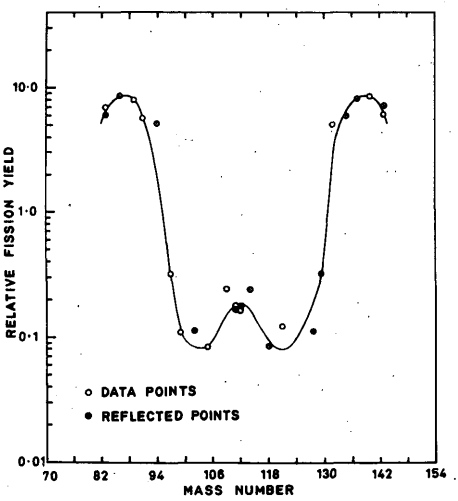

Fig.1

Relative fission yield of Ac^{227}

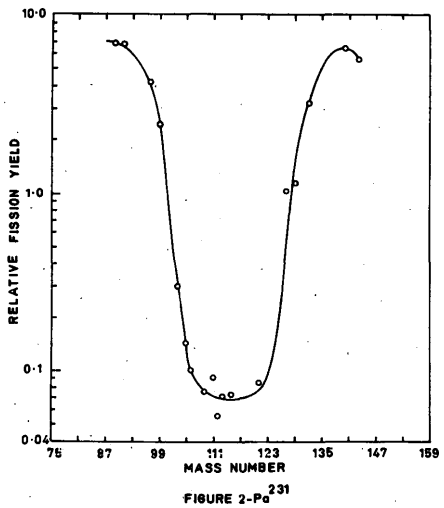

Fig.2

Relative fission yield of Pa^{231}

mirror points have also been used for Ac^{227} as the data in this case is limited. The mirror points were obtained by using the expression

$$A' = A_{F.N.} - (A + \nu) - \nu'$$

where $A_{F.N.}$ is the mass number of the fissioning nucleus, A is the mass number of the fragment for which relative yield is known, A' is the mirror

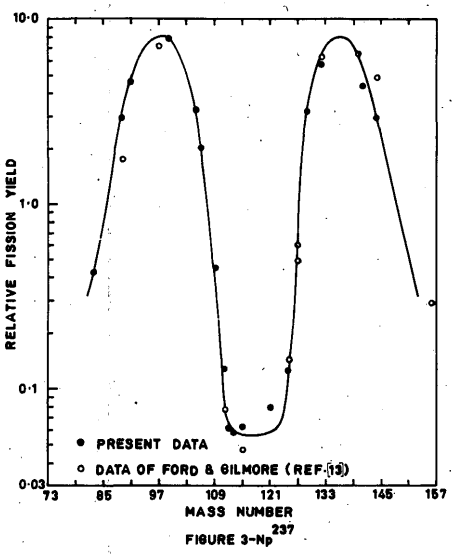

Fig.3

Relative fission yield of Np^{237}

point of A, and ν and ν' are the neutrons obtained from TERREL's curve [19]. This method of obtaining mirror points is considered somewhat better than using an average number of neutrons emitted per fission.

For Ac^{227}, corrections of up to 7% have been applied to the relative fission yields to account for the differences in the fraction of fission fragments stopped in the spacer foils (0.4 mg/cm^2).

The relative yields could not be converted into absolute yields as it was not possible to get data in all the mass regions. For Np^{237}, the results of FORD and GILMORE [13] are also plotted for comparison, and it can be seen that the agreement between the two sets of data is good.

The various factors that contribute to the errors in the reported values may be mentioned briefly. The errors in the U^{235} yields used for calculating the relative yields [4] will be reflected in the values reported here. The yields of mass numbers 103 to 125 also need upward revision due to the fast fission contribution of U^{238} (since natural uranium was used as targets), and it is estimated that the yields reported in Table I will be affected by 3 to 15% in the above mass range. In addition to these, the usual experimental errors associated with the sample mounting, counting, etc. are also to be considered. The counting errors are particularly important in actinium fission because of the low activities obtained. The error involved in the assumption that the genetic relationships and the charge distribution in the reactor neutron fission of actinium, protactinium and neptunium are the same as those in thermal fission of U^{235} is probably a minor one. While it is rather difficult to assess the individual errors and estimate the overall reliability of the values, the yield may be considered to be good to about 20%, although the internal consistency of the data is much better.

From the data obtained here, the fission cross-sections were estimated to be about 50 mb, 2 b and 1.5 b for Ac^{227}, Pa^{231} and Np^{237} respectively with

the reactor neutrons used here. The reported fission cross-section [20] for Np^{237} varied between 1.4 and 2 b with neutrons of energies between 1 and 7 MeV.

The yield data conform to the established trend [4] that the heavy peak in the mass yield curve remains rather fixed while the light peak moves to lower mass numbers with decreasing mass of the fissioning nucleus (F.N.). The separation between light and heavy peaks is about 50, 48 and 41 mass numbers respectively for Ac^{227}, Pa^{231} and Np^{237}, in good agreement with 47.8, 47 and 43.3 mass numbers calculated for the same nuclides using the equation of SWIATECKI [21].

A small third peak in the trough region was obtained with Ac^{227}, estimated to be caused by less than 1% of the total fissions, as with Th^{232}. The data on Pa^{231} and Np^{237} give the usual double-humped shape for the mass yield curves. The peak-to-trough ratios are approximately 100 and 140 for Pa^{231} and Np^{237} respectively. The asymmetric peak to symmetric peak ratio is about 42 for Ac^{227}.

Mass distribution in general in the fission of bismuth and heavier elements may be examined in terms of the two-mode fission hypothesis first suggested by TURKEVICH and NIDAY [22] and further supported by the results of SCHMITT and SUGARMAN [23], LEVY et al. [24] and BRITT et al. [7, 25]. According to this hypothesis, any measured mass distribution in fission is due to the superposition of two components, one characteristic of asymmetric fission and the other of symmetric fission. The asymmetric mode of fission produces a double-peaked curve, the heavy peak of which remains relatively fixed (and is insensitive to the mass A and the excitation energy, E*, of the fissioning nucleus (F.N.) due to the preferential formation in fission of 50-proton [26] or 82-neutron [27] fragments, while the light peak adjusts itself accordingly, resulting in a shift of the same towards higher mass numbers with increasing A of the F.N. (spontaneous fission of heavy elements provides an example for a nearly true asymmetric fission). Symmetric mode of fission yields a single peaked curve, the peak position being at about $(A - \nu)/2$. The probability of symmetric fission is dependent, at least to a large extent, on E* of the F.N. and increases rapidly with increasing E*. The width of the single peaked curve also increases with increasing E* due to the competition of particle emission with fission and the resulting contribution to fission of more than one nucleus.

As one passes from spontaneous fission through thermal fission to fission by particles of tens of MeV energy, the peak/trough ratio of the mass yield curve decreases gradually [4] until finally at high energies only a single-peaked distribution is observable when the symmetric fission becomes predominant.

In the low-energy region and up to about 30-40 MeV E*, in some cases triple-peaked distributions are observed [5, 6, 8, 12]. These may be explained as caused by the superposition of the two types of distributions. The relative prominence and observability of the symmetric peak and the asymmetric peaks then depend on the relative contributions of asymmetric and symmetric (which is dependent on the E*) modes and the relative position of the asymmetric peaks (dependent on A). A decrease in the separation

between the light peak and the heavy peak (resulting from increase in A) can lead to the masking of the central peak by the asymmetric peaks, particularly if the central peak happens to be rather broad and small in magnitude.

In addition to the above two factors, the variation in neutron emission with fragment mass may contribute to the appearance of a small maximum in the trough region of the final mass yield curve. If the universal neutron yield curve with its saw-tooth shape suggested by TERREL [19] is assumed to hold in all cases, it appears that starting from an assumed constant prompt-fission yield in the mass region of about 110-124 one could obtain a small third peak in this region of the final mass yield curve, similar in magnitude to that observed in the neutron fission of Th^{232} [12]. Here again, the observability of this small central peak will be strongly influenced by the position of the light peak. As the third peak in the trough region arising from the discontinuity in the neutron yield curve is expected to remain relatively fixed in the mass region of 112-113, a shift of the light peak towards higher masses might mask the third peak to a large extent. The above considerations seem to make it unnecessary to assume any sharp transition in the shape of mass distribution and its strong dependence on Z, as has been suggested earlier [3].

In the light of the above qualitative considerations regarding mass distribution, small third peaks observed in the fission of Ac^{227} and in Th^{232} [12] may be considered to be due to the superposition of the two types of distributions and/or neutron emission. It is difficult to estimate to what extent these two effects contribute. While the non-existence of a similar third peak in Np^{237} may be caused by its masking by the relative position of the asymmetric peaks on the basis of much larger A but the same E^*, it is difficult to explain the situation in Pa^{231} on the basis of A and E^*. The large magnitude of the central third peak in the proton- and deuteron-induced fission of Ra^{226} (where the central peak is as prominent as the asymmetric peaks) [5, 6] compared with that of Ac^{227} may be attributed to the high E^* in the proton and deuteron fission of radium.

Finally it may be stated that the two-mode fission hypothesis seems to explain qualitatively different kinds of mass distribution in the fission of elements, bismuth and above, including those obtained in Ac^{227} and Th^{232}. More work in this mass region will be interesting.

ACKNOWLEDGEMENT

The authors are grateful to Dr. Brahm Prakash, the Director of the Metallurgy Group, for his interest and for kindly examining the manuscript.

REFERENCES

[1] NEUZIL, E.F. and FAIRHALL, A.W., Phys. Rev. 129 (1963) 2705.
[2] FAIRHALL, A.W., Phys. Rev. 102 (1956) 1335.
[3] FAIRHALL, A.W., JENSEN, R.C. and NEUZIL, E.F., Proc. 2nd UN Int. Conf. PUAE 15 (1958) 452.
[4] HYDE, E.K., Rpts. UCRL-9036, UCRL-9065 (1960).

[5] JENSEN, R.C. and FAIRHALL, A.W., Phys. Rev. 109 (1958) 942.
[6] JENSEN, R.C. and FAIRHALL, A.W., Phys. Rev. 118 (1960) 771.
[7] BRITT, H.C., WEGNER, H.E. and GURSKY, J.C., Phys. Rev. 129 (1963) 2239.
[8] UNIK, J.P. and HUIZENGA, J.R., Phys. Rev. 134 (1964) B 90.
[9] DUFFIELD, R.B., SCHMITT, R.A. and SHARP, R.A., Proc. 2nd UN Int. Conf. PUAE 15 (1958) 202.
[10] GUNNIK, R. and COBBLE, J.W., Phys. Rev. 115 (1959) 1247.
[11] COLBY, L.J., SHOAF, M.L. and COBBLE, J.W., Phys. Rev. 121 (1961) 1415.
[12] IYER, R.H., MATHEWS, C.K., RAVINDRAN, N., RENGAN, K., SINGH, D.V., RAMANIAH, M.V. and SHARMA, H.D., J. inorg. nucl. Chem. 25 (1963) 465.
[13] FORD, G.P. and GILMORE, J.S., Rpt. LA-1997 (1956).
[14] COLEMAN, R.F., HAWKER, B.E. and PERKIN, J.L., J. inorg. nucl. Chem. 14 (1960) 8.
[15] IYER, R.H., JAIN, H.C., RAMANIAH, M.V. and RAO, C.L., Radiochim. Acta (in press)
[16] CORYELL, C.D. and SUGARMAN, N. (Eds.), Radiochemical Studies: Fission Products, N.N.E.S., Div. IV 19, McGraw Hill, New York (1951).
[17] KLEINBERG, J., Rpt. LA-1721 (1954).
[18] LINDNER, M., Rpt. UCRL-4377 (1954).
[19] TERREL, J., Phys. Rev. 127 (1962) 880.
[20] SCHMITT, H.W. and MURRAY, R.B., Phys. Rev. 116 (1959) 1575.
[21] SWIATECKI, W.J., Phys. Rev. 100 (1955) 936.
[22] TURKEVICH, A. and NIDAY, J.B., Phys. Rev. 84 (1951) 52.
[23] SCHMITT, R.A. and SUGARMAN, N., Phys. Rev. 95 (1954) 1260.
[24] LEVY, H.B., HICKS, H.G., NERVIK, W., STEVENSON, P.C., NIDAY, J.B. and ARMSTRONG, J.C., Phys. Rev. 124 (1961) 544.
[25] BRITT, H.C. and WHETSTONE, S.L., Jr., Phys. Rev. 133 (1964) B 603.
[26] ATEN, A.H.W., Jr., Physica 28 (1962) 262.
[27] VANDENBOSCH, R., Nucl. Phys. 46 (1963) 129.

DISTRIBUTION OF ENERGY IN FISSION

(Sessions IV and V)

Review Paper

THE ENERGY RELEASE IN LOW-ENERGY FISSION

J. S. FRASER
CHALK RIVER NUCLEAR LABORATORIES,
ATOMIC ENERGY OF CANADA LIMITED,
ONTARIO, CANADA

Abstract — Résumé — Аннотация — Resumen

THE ENERGY RELEASE IN LOW-ENERGY FISSION. Recent advances in semi-conductor detector and time-of-flight techniques have led to precise measurements of the fragment kinetic energies in thermal-neutron and spontaneous fission. The resolution obtainable is limited by the effects of the prompt neutron recoil. Detailed measurements of the variation of the kinetic energy release with neutron bombarding energy have been correlated with the number of prompt neutrons emitted. An interpretation of this correlation in terms of channel effects has been proposed. The fine structure observed in the kinetic energy measurements has been shown to be connected with the extra energy available from the pairing energy in even-even fragments.

LIBÉRATION D'ÉNERGIE DANS LA FISSION A BASSE ÉNERGIE. De récents perfectionnements des méthodes fondées sur l'emploi de détecteurs à semi-conducteurs et sur le temps de vol ont permis de mesurer avec précision l'énergie cinétique des fragments dans la fission spontanée et la fission par neutrons thermiques. Le pouvoir de résolution est limité par les effets du recul dû aux neutrons instantanés. Les mesures détaillées de la variation que subit l'énergie cinétique libérée, selon l'énergie des projectiles, ont été mises en corrélation avec le nombre des neutrons instantanés émis. On a proposé une interprétation de cette corrélation fondée sur les effets des voies de fission. L'auteur montre que la structure fine observée lors des mesures de l'énergie cinétique est liée à l'énergie supplémentaire provénant de l'énergie d'appariage dans les fragments pairs-pairs.

ВЫСВОБОЖДЕНИЕ ЭНЕРГИИ ПРИ ДЕЛЕНИИ В ОБЛАСТИ МАЛЫХ ЭНЕРГИЙ. Достигнутые за последнее время успехи в методах применения полупроводниковых детекторов и детекторов по времени пролета дали возможность проведения точных измерений кинетических энергий осколков при делении как под действием тепловых нейтронов, так и при самопроизвольном делении. Получаемое разрешение ограничивается действием отдачи мгновенных нейтронов. Подробные измерения высвобождения кинетической энергии в зависимости от энергии бомбардирующих нейтронов были коррелированы с числом испускаемых мгновенных нейтронов. Предлагается истолковать эту корреляцию как зависимость от воздействия канала. Показано, что при измерениях кинетической энергии тонкая структура связана с избыточной энергией, высвобождаемой из энергии спаривания четно-четных осколков.

LIBERACION DE ENERGIA EN LA FISION DE BAJA ENERGIA. Los adelantos de las técnicas de tiempo de vuelo y de detección con semiconductores han permitido medir con precisión las energías cinéticas de los fragmentos formados durante la fisión espontánea o inducida por neutrones térmicos. El grado de resolución queda limitado por los efectos de retroceso de los neutrones inmediatos. Las mediciones detalladas de la variación de la energía cinética liberada en función de la energía de los neutrones incidentes se han relacionado con el número de neutrones inmediatos emitidos. Se ha propuesto una interpretación de esta correlación basada en efectos de canal, demostrándose que la estructura fina observada en las mediciones de la energía cinética guarda cierta relación con el exceso de energía disponible debida al apareamiento en los fragmentos par-par.

INTRODUCTION

In the last few years advances in semi-conductor and time-of-flight techniques have led to improved precision in the measurements of fragment kinetic energies in thermal-neutron and spontaneous fission. In any method

the resolution is limited by the effects of the prompt neutron recoil but in the semi-conductors there appears to be an inherent limit to energy resolution of 1.5 MeV.

The new techniques have revealed a fine structure in the kinetic energy release and mass yields and have led to a re-examination of the so-called "energy deficit"; i.e. the decrease, near symmetric fission, of the total kinetic energy release below that expected from the smooth variation of the Coulomb potential energy of two fragments in contact.

Another topic of recent interest is the variation of the total kinetic energy with the energy of the fission-inducing neutrons and its connection with changes in the slope of the ν curve. A small effect has been observed at neutron energies below 1 MeV and interpreted in terms of channel effects. A more pronounced change in slope of the ν curve at a neutron energy of 3 MeV appears to require a different explanation.

PRECISE KINETIC ENERGY MEASUREMENTS

Apart from the intrinsic interest in fission kinetics, the usefulness of sources of Cf^{252} for the calibration of detectors has led to careful measurements of the energies and velocities of its fission fragments at three laboratories. Two of the measurements, by WHETSTONE [1] and by FRASER, MILTON, BOWMAN and THOMPSON [2], used the double velocity methods, and the third, by SCHMITT, KIKER and WILLIAMS [3], a combination of velocity and energy measurements on single fragments.

The recent double velocity measurements represent a refinement of an established method. Improved electronics have reduced the instrumental resolution so that the limitation is the neutron recoil dispersion - about 3% in the velocities for Cf^{252}. The precision of the measurements is based on velocity of propagation of signals in coaxial cables.

The new work by Schmitt et al. combines fragment energies as measured by a semi-conductor detector with velocities measured by the time-of-flight method. Both systems were calibrated with momentum-analysed bromine and iodine ions with energies of 30 to 120 MeV from a tandem accelerator. The correlated velocity and energy serves to identify the mass of the fragment after the emission of the prompt neutrons. The results are illustrated in Fig. 1. On the abscissa time increases from right to left; the ordinate is the pulse-height scale that does not turn out to be linear in the energy of the fragment but depends also on the mass. The curves are the constant mass loci and the straight lines show how the pulse height varies with mass for constant energy.

Table I is a compilation of the results from the three sets of measurements. Schmitt et al. do not measure the total kinetic energy. The remaining quantities in the second column are measured after neutron emission. The fragment energies in parentheses are estimated energies before neutron emission and may be compared with the data of Whetstone and Fraser et al. The agreement of the several measurements is, on the whole, quite satisfactory. The direct computation results of Fraser et al. are systematically lower than the other two. In later work this has been

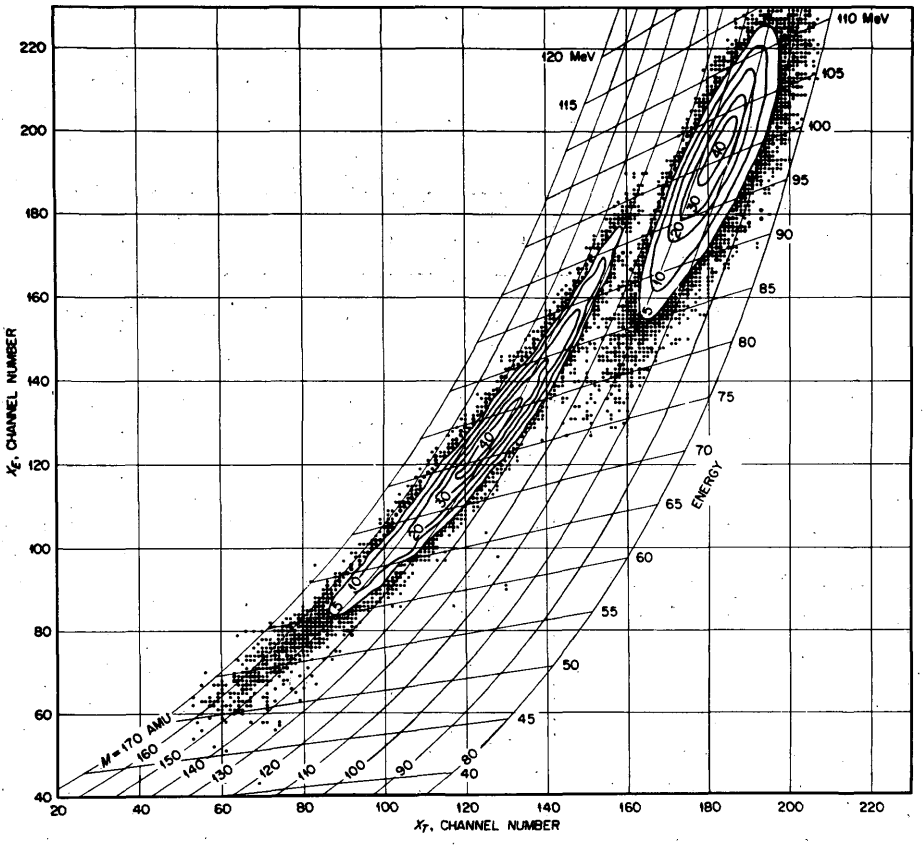

Fig. 1

Correlation of energy with time-of-flight for Cf^{252} spontaneous fission fragments (Ref. [13].)

shown to be due to the energy degradation of a small percentage of the fission fragments by scattering from the walls of the drift tubes. The experimental importance of scattering has recently been demonstrated by ENGELKEMEIER and WALTON [4] who showed that over 40% of fragments incident on platinum at a grazing angle are scattered in a manner approaching specular reflection (see Fig. 2). For aluminium and iron the fractions scattered are about 4 and 9% respectively. The effect, consequently, is particularly pernicious in time-of-flight apparatus. The use of anti-scattering diaphragms or very large diameter flight tubes is recommended.

A very useful technical bi-product of the work of SCHMITT, KIKER and WILLIAMS [3] is a scheme for the calibration of semi-conductor detectors for fission work. They have shown that the response of these detectors to heavy ions is dependent on the mass. Figure 3 shows their energy-pulse-height curves as well as a Cf^{252} fragment spectrum on the same pulse-height scale. The important feature of the upper curves is that the relation is linear for ions of a given mass in the energy range of fission fragments. The pulse-height defect is nearly the same for bromine and iodine so that it may

TABLE I

Cf^{252}

MEAN VALUES AND rms WIDTHS OF THE DISTRIBUTIONS

	Schmitt et al.[a]	Whetstone		Fraser et al.	
	Direct computation	Direct computation	Gaussian fit	Direct computation	Gaussian fit
E_K (MeV)		185.7	186.4	182.1 ± 1.7	184.9
σ_{EK} (MeV)		11.3	11.3	15.2	11.1
E_L (MeV)	103.77 (105.7)[b] ± 0.5	105.71 ± 1.06	106.16 ± 1.06	104.4 ± 1.0	105.7
σ_{EL} (MeV)	5.48	5.86	5.66	7.5	5.58
E_H (MeV)	79.37 (80.3)[b] ± 0.5	80.01 ± 0.80	80.55 ± 0.81	78.3 ± 0.7	79.6
σ_{EH} (MeV)	8.23	8.53	8.62	9.5	8.87
V_L (cm/ns)	1.383 ± 0.006	1.375 ± 0.007	1.372 ± 0.007	1.364	1.370
σ_{VL} (cm/ns)	0.0693	0.0665	0.063	0.084	0.065
V_H (cm/ns)	1.036 ± 0.005	1.036 ± 0.005	1.041 ± 0.005	1.023	1.034
σ_{VH} (cm/ns)	0.0831	0.0795	0.075	0.087	0.077
M_L (amu)	106.0	108.39		107.8	
M_H (amu)	141.9	143.61		144.2	
σ_{ML} (amu)	6.53	6.77		7.27	
σ_{MH} (amu)	6.55				

[a] Post-neutron emission quantities except where noted
[b] Pre-neutron emission quantities

be assumed to vary linearly with mass. Thus we have for the relation between energy E and pulse-height X

$$E = (a + a'M)X + b + b'M .$$

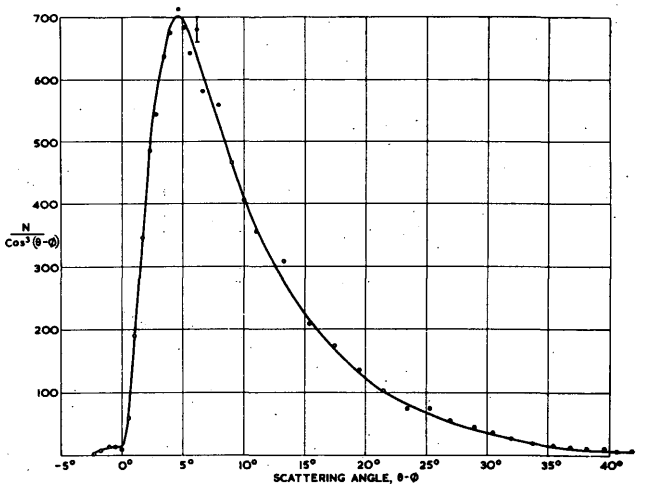

Fig. 2

Angular distribution of fission fragments scattered from platinum. Grazing angle is 5°. (Ref. [4].)

The four constants can be evaluated from the data of Fig. 3 in terms of P_H and P_L. The reader is referred to the original paper [3] for a complete discussion.

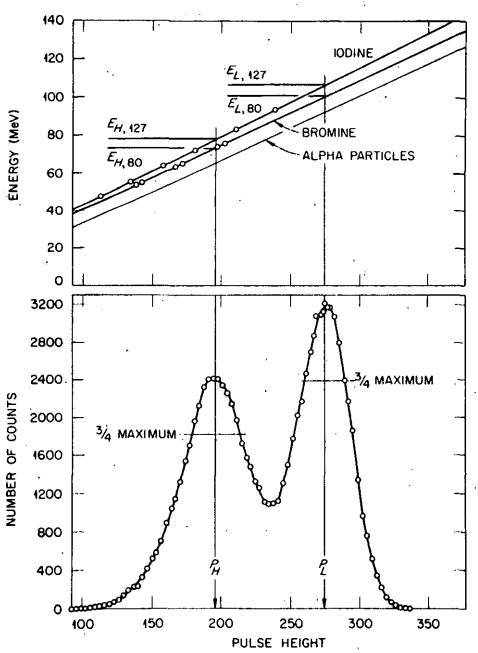

Fig. 3

Comparison of energy versus pulse-height curves for heavy ions and Cf^{252} spontaneous fission-fragment pulse-height spectrum. (Ref. [3].)

THE ENERGY DEFICIT

It has long been known that the large kinetic energy of the fission fragments arises almost entirely from the Coulombic repulsion of the fragments at the time of scission. Figure 4, taken from the work of TERRELL [5], shows the systematic variation of the average total kinetic energy with

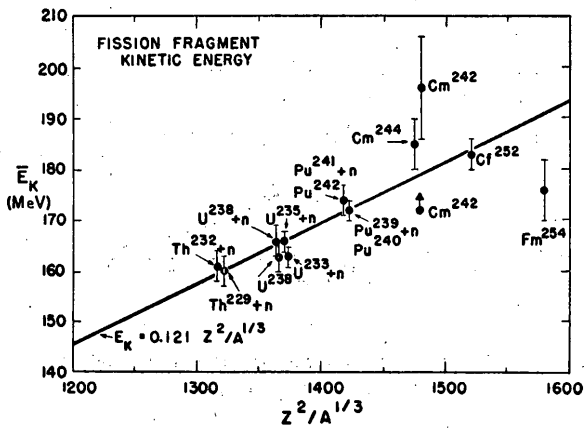

Fig. 4

Dependence of the average total kinetic energy E_K of fission fragments (before neutron emission) on $Z^2/A^{1/3}$. The straight line is a least-squares fit to the data. (Ref. [5].)

$Z^2/A^{1/3}$. If the fragments were assumed to be spherical the kinetic energy would be

$$E_K = Z_L Z_H e^2 / r_0 (A_L^{1/3} + A_H^{1/3}).$$

The fitted line in the figure leads to a value of $r_0 = 1.82 \times 10^{-13}$ for a mass ratio of 1.45. This value of r_0 is about 25% larger than those obtained by other methods. Clearly the difference must be due to distortion and, possibly, expansion of the highly excited fragments.

If the charge divides in nearly the same ratio as the mass, the kinetic energy would be expected to decrease monotonically from symmetric to asymmetric fissions. In fact, it is observed in the double velocity [1, 2], energy [3, 6] and range [7, 8, 9] measurements that the kinetic energy in symmetric fission of U^{236} is about 30 MeV lower than the value predicted on this simple model. The average total kinetic energy variation with fragment mass is shown in Fig. 5 for several nuclei. We interpret the dip now as a variation of the fragment distortion with mass number.

The solid curves are calculated Coulomb energies for tangent spheroids, the potential energy being minimized. This refinement gives the correct average value of E_K for acceptable values of r_0 but fails to predict the correct variation with fragment mass. A more realistic model incorporating the deformability of non-magic fragments has been used in the so-called

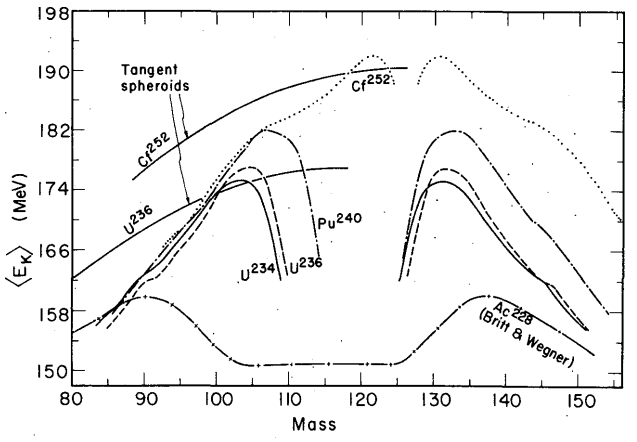

Fig. 5

Variation of the average total kinetic energy of fission fragments with the mass of the fragments. The solid curves at the upper left are calculated Coulomb potential energy curves for tangent spheroids. (Ref. MILTON, J.C.D. and FRASER, J.S., Canad. J. Phys. 40 (1962) 1626.)

fragment-shell theories discussed by TERRELL [10], VANDENBOSCH [11], and MILTON and SWIATECKI [12]. In this model the potential energy of the fragments at scission is given by the sum of the deformation energies and the Coulomb interaction energy between two spheroids,

$$P = D_1 + D_2 + C_{12}.$$

If this potential energy is minimized, the fragments that are soft are deformed at the expense of the Coulomb energy. The Coulomb energy will appear later as the kinetic energy of the fragments. The deformation energy will appear as the excitation energy that will finally give rise to neutron emission. The stiffness parameter found by VANDENBOSCH [11] from fitting the fragment kinetic energies and neutron yields is shown in Fig. 6a. The nuclear deformability (or more correctly the stiffness) parameter C_2 shown in Fig. 6b was obtained by Vandenbosch by the extrapolation of lifetime and Coulomb excitation results to the primary fission product region. The nuclei in the symmetric fission-fragment region, 110 to 120, are seen to be very soft towards deformation. In fission the large deformation of both nearly symmetric fragments is accompanied by a decrease in the Coulomb energy.

In 1961 MILTON and FRASER [13], on the basis of the available data showed that the energy deficit may be associated with enhanced neutron emission. This has been substantiated by the more detailed measurements on neutron yields from individual fragments by APALIN et al. [14] and by MILTON and FRASER at Chalk River [15]. In the latter work the correlated velocities of the two fragments and prompt neutrons are measured and hence the neutron energy is known in each event. Thus it is possible to ob-

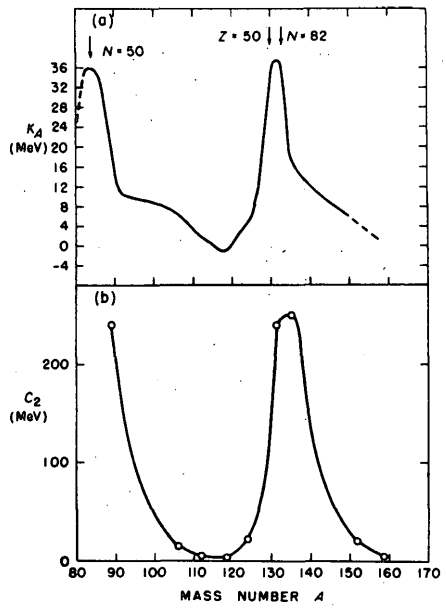

Fig. 6

(a) Nuclear stiffness parameter k_A determined by a fit to the U^{235} kinetic energy release and neutron yields.
(b) Nuclear stiffness parameter C_2 as obtained from extrapolation of lifetimes and Coulomb excitation results to the primary fission-fragment region. (Ref. [11].)

tain directly that part of the total excitation energy that gives rise to neutron emission. Assuming that the total gamma-ray energy has no anomalous variations, the result is that for U^{236} fission the total excitation energy is nearly constant except near symmetric fission where there is a rise of 25 to 30 MeV. Thus a consistent picture emerges. Although some argument may remain as to the exact amount of the energy deficit as measured experimentally, there is little doubt as to the origin of the phenomenon.

FINE STRUCTURE

A concise way of depicting certain characteristics of the fission process is the contour diagram. In Fig. 7 are shown the probability contours on the mass-light fragment energy plane for U^{235}+n fission taken from Ref. [2]. On the upper side of the diagram the periodic wavy structure indicates the existence of a fine structure. If one takes a cut along a horizontal line at $E_L = 107$ MeV the yield curve in the upper part of Fig. 8 is obtained. The peaks are at mass numbers 134-5, 140, 146 and 152. The curves in the lower part of the figure are the total available excitation energies for even-even fragments (open circles) and the maximum values for odd-A products (solid circles). THOMAS and VANDENBOSCH [16] have pointed out that the pairing energy depresses the energy surface for odd-mass fragments below

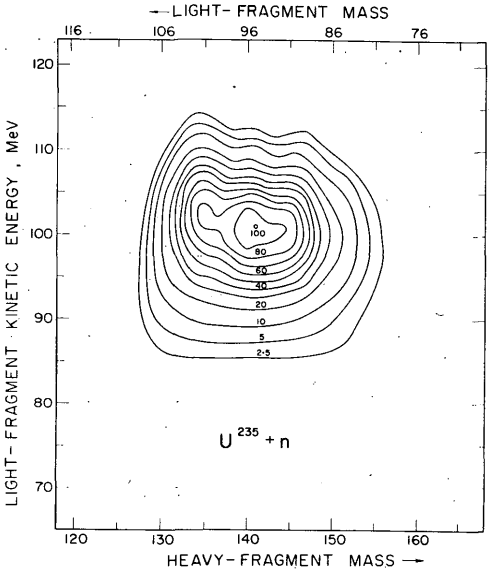

Fig. 7

Mass-energy contour diagram for U^{235} + n fission. (Ref. [2].)

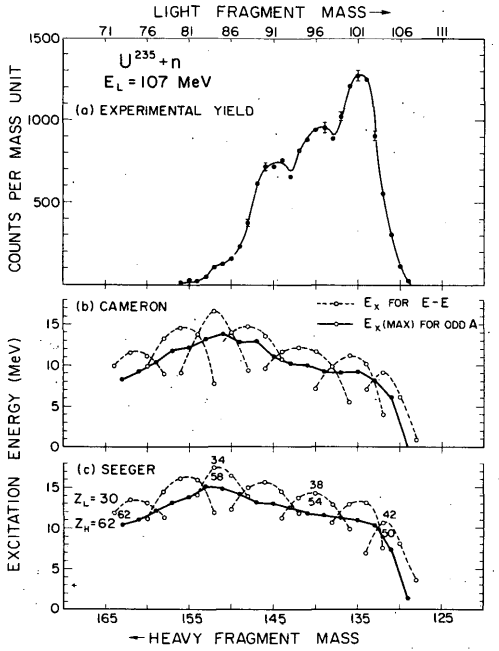

Fig. 8

(a) Conditional mass yield curve for U^{235} + n fission with E_L = 107 MeV. Total fragment excitation energy curves corresponding to (a) using Cameron's mass formula (b) and Seeger's mass formula (c). The open circles are the valves for even-even fragments and the solid circles are the maxima for odd A fragments.

that for even-even fragments so that the maxima should be separated by 2A/Z (approximately 5) mass units.

Similar results have been obtained by GIBSON et al. [6] for U^{233}+n and Pu^{239}+n in measurements with semi-conductor detectors (Fig.9). In the

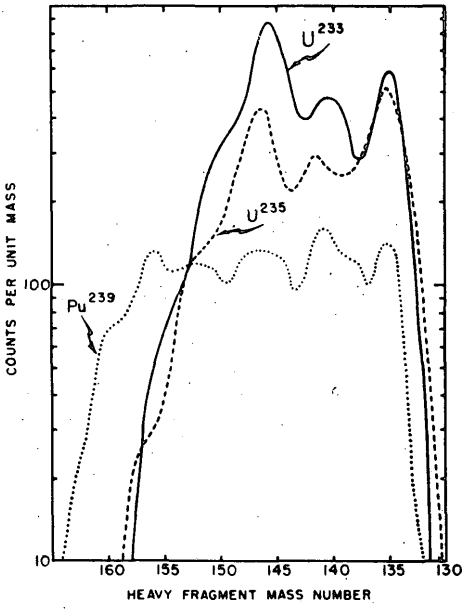

Fig.9

Experimentally observed fine structure for thermal-neutron-induced fission of U^{233} (solid curve), U^{235} (dashed curve), and Pu^{239} (dotted curve). (Ref. [16].)

spontaneous fission of Cf^{252} the contours are not conveniently parallel to the mass axis but the structure can be emphasized (Fig.10) by plotting the yield in an interval that follows the average position of the contours. Here again the peaks are at mass numbers 134, 140, 146, 152 and possibly 156-7 and 162. The structure is evidently associated with particular fragment masses and charges.

An interesting point to note is that the formation of even-even fragments is strongly favoured, particularly at low excitation or high kinetic energies. It follows then that the charge division curve must be markedly different than the usually assumed smooth form. Techniques are now being developed for examining the charge distribution (for example by observing the X-rays from fragments before β-decay occurs) in the low excitation energy region.

Another interesting point is the persistence of the structure (see Fig.7) to the peak of the probability distribution where the final excitation energy is larger. This is to be expected if at scission most of what appears later as final excitation energy is energy of deformation. The model of cold, but deformed, fragments at scission is just the one that emerges from the study of neutron yields from individual fragments.

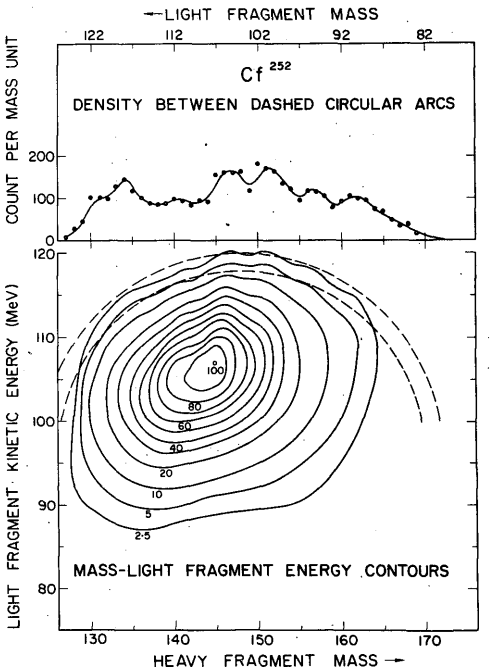

Fig. 10

The lower part of the figure shows the mass-light fragment energy contours observed for Cf^{252} spontaneous fission. The upper part shows the density of events between the dashed circular arcs drawn on the contour diagram. (Ref. [2].)

DEPENDENCE OF E_K ON E_n

In recent years measurements have been made at several laboratories [17, 18, 20] of the dependence of the number of prompt neutrons on the energy of the neutrons inducing the fission. A typical result for a U^{235} target is shown in Fig. 11, taken from Ref. [7]. At 8 MeV the slope is from 0.18 to 0.16 corresponding to 5.6 to 6.3 MeV per neutron emitted. This agrees well with the energy required to separate one neutron and give it the known average kinetic energy of prompt neutrons. Below 3 MeV the slope of 0.088 MeV corresponds to 11.4 MeV per neutron. In order to conserve energy it would appear that, on the one hand, the neutron binding energy and/or kinetic energy should vary or, on the other hand, that the fragment kinetic energy should vary. Until recently no attempt had been made to study the variation of the fragment kinetic energy with incident neutron energy in sufficient detail to show any significant correlation.

In 1963, BLYUMKINA et al. [19] at Obninsk reported such a measurement in which the incident neutron energy ranged from 80 keV to 5 MeV. Their ν data for $U^{235}+n$ are shown as the solid circles and triangles in Fig. 12. The other points are from Refs. [17, 18] and [20]. They looked for variations in the fragment kinetic energy in the neutron energy region where they found a discontinuity in the ν curve. The ratio of the average

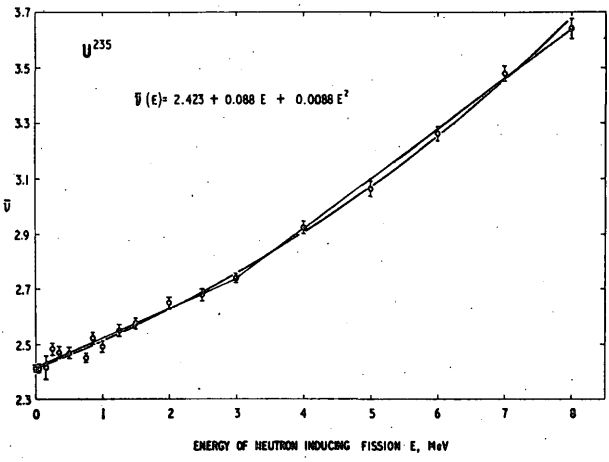

Fig. 11

The average number $\bar{\nu}$ of the prompt neutrons for $U^{235}+n$ fission as a function of incident neutron energy (Ref. [17])

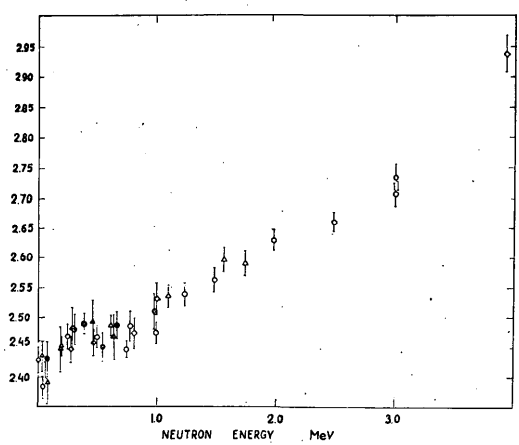

Fig.12

$\bar{\nu}$ versus the incident neutron energy E_n for $U^{235}+n$ (Ref. [19])

amplitudes of the fragments in the fission by fast and thermal neutrons was measured directly in an ionization chamber.

The differences in average kinetic energies for U^{233} and U^{235} between thermal- and fast-neutron fission are given in Fig. 13. For U^{235} they found a significant rise at a neutron energy of about 0.3 MeV and for U^{233} a drop at about 0.7 MeV.

These authors have interpreted their results in terms of the BOHR model [21] but with axial symmetry excluded. Bohr suggested that the nucleus at the saddle point is pear-shaped. The tunnelling frequency between the mirror-symmetric states determines the elevation of a rotational

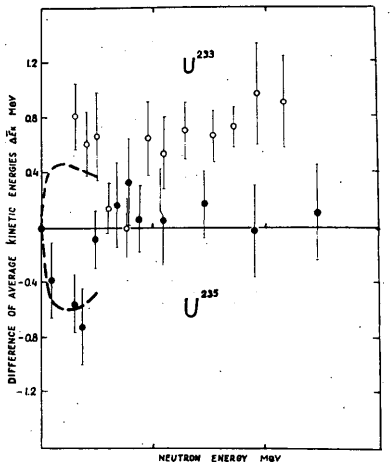

Fig. 13

Energy dependence of the deviation of the total kinetic energy from the average on the incident neutron energy. The dashed curves are given by the calculation. (Ref. [19].)

band of negative parity (1^-, 2^-, 3^-, 4^-...) above the ground state band of positive parity (0^+, 2^+, 3^+, 4^+...). In Fig. 14 this scheme is shown together with the thresholds for fission found in the d, pf reaction by NORTHROP, STOKES and BOYER [22]. The two rotational bands are identified with the first two fission channels. In the case of U^{235} with a ground state $J^\pi = 7/2^-$,

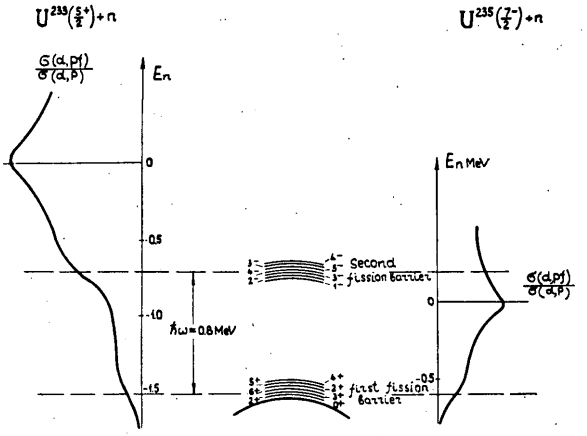

Fig. 14

The low-lying level scheme at the saddle point of a non-axially symmetric even mass nucleus. The rotational bands of levels of positive and negative parity separated by 0.8 MeV are identified with the first two fission barriers. The assumption is illustrated by the comparison of the position of the rotational levels with a schematically shown channel structure for U^{234} and U^{236} derived from the (d, pf) reaction.

s-wave neutrons cause fission through the second channel ($E_n = 0.2$ MeV) and p-wave neutrons through the first channel ($E_n = -0.6$ MeV). The interpretation for U^{233} ($J^\pi = 5/2^+$) is less definite, but they have assumed that s-wave neutrons cause fission through the first channel and p-wave neutrons through the second.

In order to explain the results it is necessary to make additional assumptions, namely that the rotational energy and the energy of the gap produced by the tunnelling at the barrier are weakly coupled to the inner degrees of freedom, unlike the deformation energy that is strongly coupled. As the nucleus proceeds from the saddle point to scission, the excitation energy of the second rotational band passes into the kinetic energy of the fragments.

The jump in E_K occurs at the transition from s-wave to p-wave fission and the magnitude of the change is

$$\Delta E_K = 0.8 \frac{\sigma_f^1}{\sigma_f^0 + \sigma_f^1 + \sigma_f^2} \text{ MeV}$$

where σ_f^ℓ is the partial fission cross-section for neutrons of angular momentum ℓ. The dashed curves in Fig. 13 are calculated from this expression. At neutron energies above 0.5 MeV the ΔE_K behaviour is presumed to be affected by higher lying channels.

Returning to the ν curve of Fig. 11, the change in slope of the curve over a broad energy range seems to require another explanation. It is interesting to speculate on the part that the so-called "scission neutron" may play in this connection. It has been found in the detailed studies of prompt neutron angular distributions [13, 23, 24] that from 10 to 15% of the prompt neutrons have an isotopic distribution in the laboratory system. These have been called "scission neutrons" because they may be produced at scission rather than by evaporation from moving fragments.

Now the ν curve of Fig. 11 can be equally well fitted by two straight lines, viz.:

$$\nu(E_n) = (2.418 \pm 0.008) + (0.109 \pm 0.006) E_n$$

from 0 to 3 MeV and

$$\nu(E_n) = (2.200 \pm 0.023) + (0.181 \pm 0.005) E_n$$

from 3 to 8 MeV.

If it is assumed that the second fit applies to fragment evaporation neutrons, the slope would be expected to remain constant to low neutron energies. If this component is subtracted from the first fit, the difference is

$$\nu_s(E_n) = 0.218 - 0.072 E_n.$$

For thermal-neutron fission ($E \cong 0$), the observed isotropic, or scission, component is about the same size as ν_s. The variation of ν_s with E_n remains to be explained but the constant slope of the evaporation component is readily understood.

REFERENCES

[1] WHETSTONE, S.L., Jr., Phys. Rev. 131 (1963) 1232.
[2] FRASER, J.S., MILTON, J.C.D., BOWMAN, H.R. and THOMPSON, S.G., Canad. J. Phys. 41 (1963) 2080.
[3] SCHMITT, H.W., KIKER, W.E. and WILLIAMS, C.W., to be published in Phys. Rev.
[4] ENGELKEMEIER, D. and WALTON, G.N., unpublished Harwell Rpt. AERE-R-4716 (1964).
[5] TERRELL, J., Phys. Rev. 113 (1959) 527.
[6] GIBSON, W.M., THOMAS, T.D. and MILLER, G.L., Phys. Rev. Lett. 7 (1961) 65.
[7] NIDAY, J.B., Phys. Rev. 121 (1961) 518.
[8] ALEXANDER, J.M., GAZDIK, M.F., TRIPS, A.R. and WASIF, S., Phys. Rev. 129 (1963) 2659.
[9] ARAS, N.K., MENON, M.P. and GORDON, G.E., to be published.
[10] TERRELL, J., Phys. Rev. 127 (1962) 880.
[11] VANDENBOSCH, R., Nucl. Phys. 46 (1963) 129.
[12] MILTON, J.C.D. and SWIATECKI, W.J., to be published; MILTON, J.C.D., unpublished Kjeller Rpt. KR-64.
[13] MILTON, J.C.D. and FRASER, J.S., Phys. Rev. Lett. 7 (1961) 67.
[14] APALIN, V.F., GRITZYUK, Yu.N., KUTIKOV, I.E., LEBEDEV, V.I. and MIKAELYAN, L.A., Soviet Phys.-JETP 16 (1963) 235.
[15] MILTON, J.C.D. and FRASER, J.S., "The energies, angular distribution and yields of the prompt neutrons from individual fragments in the thermal-neutron fission of U^{233} and U^{235}", these Proceedings II; Bull. Amer. phys. Soc. 8 (1963) 370.
[16] THOMAS, T.D. and VANDENBOSCH, R., Phys. Rev. 133 (1964) B976.
[17] MATHER, D.S., FIELDHOUSE, P. and MOAT, A., Phys. Rev. 133 (1964) B1403.
[18] HOPKINS, J.C. and DIVEN, B.C., Nucl. Phys. 48 (1963) 433.
[19] BLYUMKINA, Yu.A., BONDARENKO, I.I., KUZNETSOV, V.G., NESTEROV, V.G., OKOLOVITCH, V.N., SMIRENKIN, G.N. and USACHEV, L.N., Nucl. Phys. 52 (1964) 648.
[20] MEADOWS, J.W. and WHALEN, J.F., Phys. Rev. 126 (1962) 197.
[21] BOHR, A., Proc. UN Int. Conf. PUAE 2 (1956) 151.
[22] NORTHRUP, STOKES and BOYER, Phys. Rev. 115 (1959) 1277.
[23] BOWMAN, A.R., MILTON, J.C.D., THOMPSON, S.G. and SWIATECKI, W.J., Phys. Rev. 129 (1963) 2133.
[24] SKARSVAG, K. and BERGHEIM, K., Nucl. Phys. 45 (1963) 72.

DISCUSSION

A. MOSSOP: Power generation distributions in sub-critical and critical systems are often estimated from measurements of fission rate. In converting from fission rate to power it is necessary to allow for the difference in total kinetic energy released by Pu^{239} and U^{235} fissions. Does the work reported by Dr. Fraser suggest a new value for the Pu^{239}/U^{235} relative energy ratio that at the moment is in the region of 1.04?

J.C.D. MILTON: I gather you would like to know whether the subsequent discovery of the large effect of scattering on time-of-flight data affects

the ratio of the average kinetic energy of Pu^{239} to U^{235} thermal-neutron fission, as reported in a paper by Dr. Fraser and myself that was published in 1962[1]. The answer is no.

[1] MILTON, J. C. D. and FRASER, J. S., "Time-of-Flight Fission Studies on U^{233}, U^{235}, and Pu^{239}", Can. J. Phys. 40 (1962) 1626.

THERMAL-NEUTRON-INDUCED FISSION OF U^{235}, U^{233} AND Pu^{239}*

T. D. THOMAS
PRINCETON UNIVERSITY, PRINCETON, N.J.,
AND BROOKHAVEN NATIONAL LABORATORY,
W. M. GIBSON
BELL TELEPHONE LABORATORIES, MURRAY HILL, N.J.,
AND BROOKHAVEN NATIONAL LABORATORY
AND
G. J. SAFFORD**
COLUMBIA UNIVERSITY, NEW YORK, N.Y., AND
BROOKHAVEN NATIONAL LABORATORY

Abstract — Résumé — Аннотация — Resumen

THERMAL-NEUTRON-INDUCED FISSION OF U^{235}, U^{233} AND Pu^{239}. We have used solid-state detectors to measure the kinetic energies of the coincident fission fragments in the thermal-neutron-induced fission of U^{235}, U^{233} and Pu^{239}. Special care has been taken to eliminate spurious events near symmetry to give an accurate measure of such quantities as the average total kinetic energy at symmetry. For each fissioning system over 10^6 events were recorded. As a result the statistics are good enough to see definite evidence for fine structure over a wide range of masses and energies.

The data have been analysed to give mass yield curves, average kinetic energies as a function of mass, and other quantities of interest. For each fissioning system the average total kinetic energy goes through a maximum for a heavy fragment mass of about 132 and for the corresponding light fragment mass. There is a pronounced minimum at symmetry, although not as deep as that found in time-of-flight experiments. The difference between the maximum average kinetic energy and that at symmetry is about 32 MeV for U^{235}, 18 MeV for U^{233} and 20 MeV for Pu^{239}. The dispersion of kinetic energies at symmetry is also smaller than that found in time-of-flight experiments.

Fine structure is apparent in two different representations of the data. The energy spectrum of heavy fragments in coincidence with light fragment energies is greater than the most probable value. This structure becomes more pronounced as the light fragment energy increases. The mass yield curves for a given total kinetic energy show a structure suggesting a preference for fission fragments with masses ~134, ~140 and ~145 (and their light fragment partners).

Much of the structure observed can be understood by considering a semi-empirical mass surface and a simple model for the nuclear configuration at the saddle point.

FISSION DE ^{235}U, ^{233}U ET ^{239}Pu, PAR LES NEUTRONS THERMIQUES. Les auteurs ont utilisé des détecteurs à semi-conducteurs pour mesurer les énergies cinétiques des fragments coïncidents provenant de la fission de ^{235}U, ^{233}U et ^{239}Pu par neutrons thermiques. Ils se sont efforcés d'éliminer les événements fortuits au voisinage de la symétrie, de manière à parvenir à une mesure exacte de quantités telles que la moyenne de l'énergie cinétique totale au point de répartition symétrique. Pour chaque système subissant la fission, ils ont enregistré plus de 10^6 événements. Les données statistiques ainsi obtenues suffisent pour mettre clairement en évidence l'existence d'une structure fine pour une gamme étendue de masses et d'énergies.

Les données ont été analysées en vue d'obtenir les courbes de la distribution des produits de fission et des énergies cinétiques moyennes selon la masse ainsi que d'autres quantités intéressantes. Pour chaque système subissant la fission, la moyenne de l'énergie cinétique totale passe par un maximum pour les fragments lourds

* Work supported by the United States Atomic Energy Commission.

** Now at Union Carbide Corporation, Nuclear Division, Tuxedo, New York.

ayant une masse d'environ 132 et pour les fragments légers correspondants. Au point de répartition symétrique on constate un minimum très net qui, cependant, n'est pas aussi bas que le minimum obtenu dans les expériences de temps de vol. L'écart entre le maximum de l'énergie cinétique moyenne et le minimum au point de répartition symétrique est d'environ 32 MeV pour ^{235}U, 18 MeV pour ^{233}U et 20 MeV pour ^{239}Pu. La dispersion des énergies cinétiques au point de répartition symétrique est également plus faible que la dispersion obtenue dans les expériences de temps de vol.

La structure fine est mise en évidence par deux différentes représentations des données. Le spectre énergétique des fragments lourds en coincidence avec des fragments légers correspond à des énergies supérieures à la valeur la plus probable. Cette structure devient encore plus petite à mesure que l'énergie du fragment léger augmente. Les courbes de distribution selon la masse pour une énergie cinétique totale donnée accusent une structure qui semble révéler une tendance vers la formation de fragments de fission de masse ~134, ~140 et ~145 (et des fragments légers correspondants).

La structure observée peut être expliquée en grande partie à l'aide d'une surface de masse semi-empirique et d'un modèle simple décrivant la configuration nucléaire au point d'étranglement.

ДЕЛЕНИЕ УРАНА-235, УРАНА-233 И ПЛУТОНИЯ-239, ВЫЗВАННОЕ ТЕПЛОВЫМИ НЕЙТРОНАМИ. Для измерения кинетической энергии осколков совпадающих делений при делении урана-235, урана-233 и плутония-239, вызванном тепловыми нейтронами, были использованы кристаллические детекторы. Особое внимание было уделено устранению ложных явлений вблизи симметрии с тем, чтобы точно измерить такие величины, как средняя общая кинетическая энергия при симметрии. Для каждой делящейся системы зарегистрировано более 10^6 явлений. Полученные в результате этого статистические данные являются достаточно хорошим доказательством тонкой структуры для широкого диапазона масс и энергий.

Полученные данные были проанализированы с целью получения кривых выхода масс, средних кинетических энергий как функций массы и других интересующих величин. В каждой делящейся системе средняя общая кинетическая энергия проходит через максимум для масс тяжелых осколков, составляющих около 132, и для соответствующих масс легких осколков. При симметрии существует резко выраженный минимум, хотя и не такой глубокий, как был обнаружен при проведении измерений по времени пролета. Разница между максимальной средней кинетической энергией и энергией при симметрии составляет около 32 Мэв для урана-235, 18 Мэв для урана-233 и 20 Мэв для плутония-239. Дисперсия кинетических энергий при симметрии также меньше, чем симметрия, обнаруженная при проведении измерений по времени пролета.

Тонкая структура обнаруживается при двух различных представлениях этих данных. Энергетический спектр тяжелых осколков при совпадении с энергиями легких осколков превышает наиболее вероятное значение. Эта структура становится более выраженной при увеличении энергии легких осколков. Кривые выхода масс для данной общей кинетической энергии показывают структуру, позволяющую предположить преобладание осколков деления с массами ~134, ~140 и ~145 (и их легких партнеров).

Большая часть наблюдаемой структуры может быть понята, если принять во внимание полуэмпирическую поверхность масс и простую модель ядерной конфигурации в седловой точке.

FISIÓN DEL ^{235}U, ^{233}U Y ^{239}Pu INDUCIDA POR NEUTRONES TERMICOS. Los autores han utilizado detectores de estado sólido para medir las energías cinéticas de los fragmentos coincidentes en la fisión del ^{235}U, ^{233}U y ^{239}Pu, inducida por neutrones térmicos. Han procurado eliminar cuidadosamente los sucesos parásitos en las proximidades de la región de simetría, a fin de poder medir con precisión magnitudes tales como la energía cinética total media en dicha región. Para cada sistema de fisión, se registraron más de 10^6 sucesos. Los abundantes datos estadísticos obtenidos revelan claramente la existencia de una estructura fina en un amplio intervalo de masas y energías.

Se han analizado los datos para obtener las curvas de rendimiento másico, la energía cinética media en función de la masa y otras magnitudes de interés. En cada sistema de fisión, la energía cinética total media pasa por un máximo para el fragmento pesado de masa igual a 132, aproximadamente, así como para la masa correspondiente del fragmento ligero. La región de simetría presenta un mínimo acusado, aunque no tanto como el que se observa en experimentos de tiempo de vuelo. La diferencia entre el promédio de las energías cinéticas máximas y la correspondiente a la región de simetría es del orden de 32 MeV para el ^{235}U, de 18 MeV para el ^{233}U y de 20 MeV para el ^{239}Pu. La dispersión de la energía cinética en la región de simetría es también menor que la observada en experimentos de tiempo de vuelo.

La estructura fina se manifiesta en dos representaciones diferentes de los datos: el espectro energético de los fragmentos pesados en coincidencia con fragmentos ligeros corresponde a energías superiores al valor

más probable. Esta estructura se acentúa a medida que aumenta la energía de los fragmentos ligeros. Las curvas de rendimiento másico para una energía cinética total dada presentan una estructura que indica preferencia por los fragmentos de fisión de masa ~134, ~140 y ~145 (y por los fragmentos ligeros complementarios).

La estructura observada puede explicarse en gran parte considerando una superficie de masa semiempírica y un modelo simple de configuración nuclear en el punto de estrangulación.

INTRODUCTION

MILTON and FRASER [1] have used the time-of-flight method to study thermal-neutron-induced fission of U^{235}, U^{233} and Pu^{239}. Their results indicate considerable structure in the mass-yield curve and in other representations of their data. Their work also established beyond doubt that the average total kinetic energy of the fission fragments goes through a minimum for symmetric fission. However, there is some question as to the exact size of the difference between the maximum and minimum values of this average total kinetic energy.. Milton and Fraser's results indicate a dip of more than 35 MeV for U^{235}, whereas the range measurements of NIDAY [2] as interpreted by ALEXANDER, GAZDIK, TRIPS and WASIF [3] and those of ARAS, MENON and GORDON [4] indicate a dip of about 20 to 25 MeV.

GIBSON, THOMAS and MILLER [5] have shown that solid-state detectors give sufficiently good resolution for investigation of fine structure effects in fission. At the same time they found that it was possible to obtain peak-to-valley ratios in the mass-yield curves approaching the radiochemical values. These detectors can be used in higher geometry than is possible with the time-of-flight method. They thus provide a useful tool for studying the fission process in general and for studying fission phenomena for which high statistical accuracy in particular is important.

There are two principal disadvantages to the solid-state detector method. The first is that these detectors measure energies rather than velocities, and the results are more influenced by the effects of neutron emission than those obtained by the time-of-flight method. TERRELL [6] has pointed out that small variations in the number of neutrons emitted may make pronounced changes in quantities depending on the kinetic energies of the fragments. The second drawback is the existence of a mass-dependent pulse-height defect in the response of these detectors to fission fragments [7-9]. This effect leads to problems of absolute energy calibration and, if not properly handled, will give rise to erroneous results in some representations of the data.

We report here the results of a study of the thermal-neutron-induced fission of U^{235}, U^{233} and Pu^{239} in which solid-state detectors were used to measure the kinetic energies of both fission fragments. Especial care has been taken to eliminate spurious events from the symmetric region in order to provide as reliable data as possible. Particular attention has been paid to removal of the effects due to the mass-dependent pulse-height defect.

Since these three systems have been studied extensively by Milton and Fraser, there is no need to present all the results of our experiments. We shall show that, for the most part, there is very good agreement between the results obtained by the two methods. We shall concentrate on those parts of the data where the higher statistical accuracy of the solid-state detector method allows us to investigate phenomena not fully covered by the time-of-

flight experiments, and on those parts where there is disagreement between the results of the two methods.

EXPERIMENTAL METHOD

The experimental method was the same as that outlined by GIBSON, THOMAS and MILLER [5] and will not be discussed in detail here. The two energies of a pair of coincident fission fragments are converted to pulse heights by the semiconductor detectors and their associated electronics. These pulse heights are then fed to the two axes of a 64 × 64 two-parameter pulse-height analyser, where the number of events corresponding to each pair of pulse heights is stored.

TREATMENT OF DATA

Energy calibration

The energy calibration was based on the assumption that the energy corresponding to a given pulse height is a linear function of the pulse height and mass of the fragment. SCHMITT, KIKER and WILLIAMS [8] and SCHMITT, GIBSON, NEILER, WALTER and THOMAS [9] have shown that this assumption agrees with what is known about pulse-height defect in semiconductor detectors.

The various constants for the calibration were obtained by making a detailed comparison of the single-fragment pulse-height spectra for light and heavy fragments with the corresponding single-fragment kinetic-energy spectra determined by MILTON and FRASER [1] and adjusted for effects of neutron emission.

Transformations of the data

The data, as collected, are in a 64×64 grid, with each point of the grid corresponding to the number of events at a particular pair of pulse heights, one pulse height for each of the two fragments. Once the energy calibration was determined this grid was transformed to a new grid whose axes were the kinetic energies of each fragment. The method of subdivisions described by THOMAS and GIBSON [10] with 100 subdivisions per grid point was used for this transformation. The data were summed along lines of constant single-fragment energy to give single-fragment kinetic energy spectra.

This new grid was transformed to a grid whose axes were the total kinetic energy and the mass of one fragment. The masses were calculated from the approximate relationship

$$M_1 = ME_2/(E_1 + E_2),$$

where M_1 is the mass of one fragment, M the mass of the fissioning nucleus, and E_1 and E_2 the kinetic energies of the two fragments. An interpolation

method was used for this transformation. The data were summed and averaged along lines of constant mass to give the mass-yield curve and the average total kinetic energy as a function of mass.

RESULTS

Single-fragment spectra

Because of the nature of the energy calibration process, the single-fragment spectra, average energies for light and heavy fragments, and corresponding variances agree closely with those obtained by adjusting the data of Milton and Fraser for neutron emission. Use of an independent energy scale based on bromine and iodine ion measurements as outlined by SCHMITT, GIBSON, NEILER, WALTER and THOMAS [9] shifts the particle detector results to higher energy by about 2%. Such a shift does not appreciably affect the mass distributions, the relative shapes of the energy distributions or the conclusions of the present work.

It has been pointed out that a very striking presentation of fine structure in fission can be obtained by plotting the kinetic energy spectrum of the heavy fragment for a fixed kinetic energy of the light fragment [5]. Such curves are shown for the three fissioning systems in Fig. 1. Each curve corresponds to a particular kinetic energy of the light fragment. These curves differ somewhat from those shown by GIBSON, THOMAS and MILLER [5] and those used by THOMAS and VANDENBOSCH [11] because the mass de-

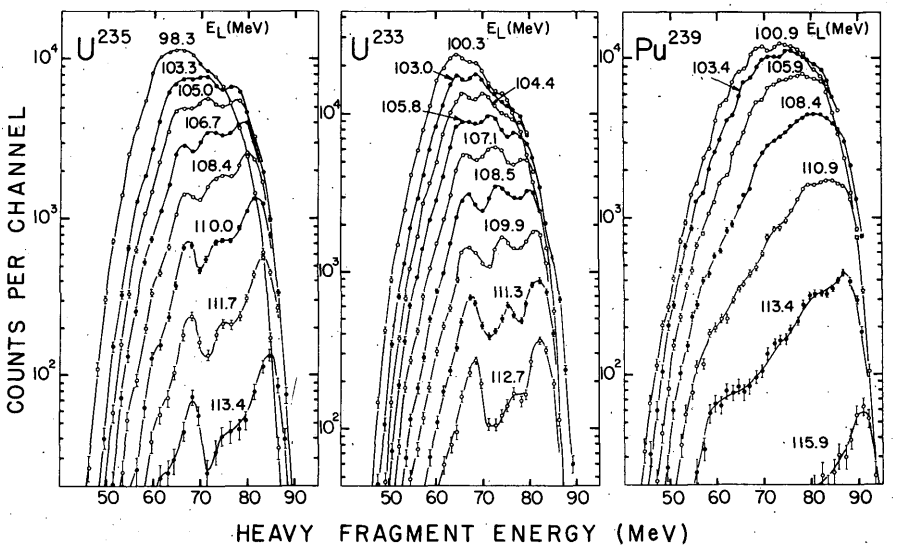

Fig. 1

Kinetic energy spectra of heavy fission fragments
in coincidence with light fragments of the indicated energy

pendence of the pulse-height defect was not properly taken into account in these earlier works.

The highest curve in each case corresponds to the most probable light-fragment kinetic energy. Essentially no structure is seen for light-fragment kinetic energies less than the most probable value. However, it is clear from these data, as it is from those of MILTON and FRASER [1], that, although the structure is most pronounced for the highest light-fragment energies, it persists down to the most probable energy.

FRASER, MILTON, BOWMAN and THOMPSON [12] have calculated from time-of-flight data the mass spectrum of fragments in coincidence with light fragments of 107-MeV kinetic energy produced in the thermal-neutron-induced fission of U^{235}. If the curve labelled 106.7 in Fig. 1 is transformed to the same co-ordinate system, the resulting curve agrees closely in shape and position with that determined by FRASER et al. [12]. Since the shape of such curves can be distorted by the mass-dependent pulse-height defect, this agreement is evidence that we have properly accounted for this phenomenon.

Mass-yield curves

Plotted in Fig. 2 are mass-yield curves for three values of the total kinetic energy for the system U^{235} plus thermal neutrons. The points are our data for 170 MeV (open circles), 148 MeV (closed circles) and 129 MeV (triangles). The curves are Milton and Fraser's data for 170, 150 and 130 MeV. The agreement between our data and theirs for the two higher energies is good. There is, however, strong disagreement at the lower energy. In particular their results indicate that the energy spectrum for symmetric fission peaks between 120 and 130 MeV, whereas our data show a monotonic decrease from a most probable value of about 148 MeV.

Similar comparisons between our data and theirs for the other two systems yield similar conclusions. There is very good agreement between our results and theirs at higher energies, but our yields are as much as a factor of 10 smaller than theirs at the lower energies.

GIBSON, MILLER and THOMAS [5] reported that the most probable value of the mass for a given total kinetic energy is constant over a range of energies. MILTON and FRASER [1] showed that this most probable value changes abruptly between one region of constant value and the next. For all three fissioning systems the most probable heavy mass is 134 at high energies. There is a preference for heavy fragments of mass about 140 at intermediate energies and about 145 at low energies.

The same effect appears in our results, as can be seen from Fig. 3, where we have plotted mass-yield curves for 18 different total kinetic energies for the system U^{233} plus thermal neutrons. We have indicated by a vertical line on each curve the position of the most probable value reported by Milton and Fraser. The most striking feature of these curves is seen in the transition region from one most probable value to another. The shape of the curves in these regions indicates that the shift in the most probable value is not due to a smooth change over the range of masses of interest, but rather to the disappearance of a peak centred at one mass and the ap-

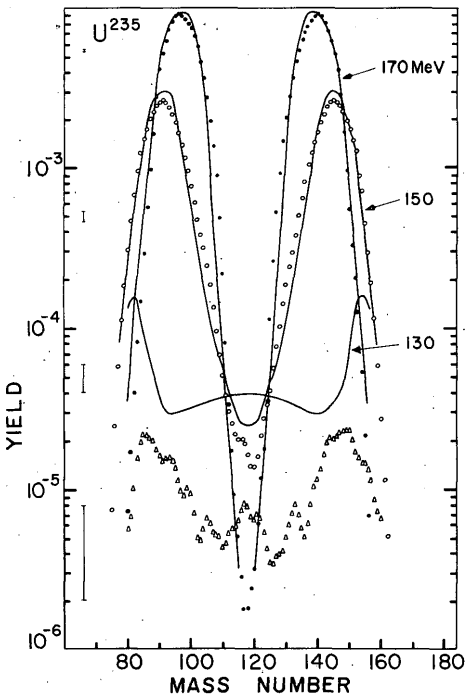

Fig. 2

Mass-yield curves for three values of the total kinetic energy for the system U^{235} plus thermal neutrons.
The points are from this work; solid lines are from MILTON and FRASER [1].
Closed circles: 170 MeV; open circles: 148 MeV; triangles: 129 MeV.

pearance of one centred about 6 mass units away. This phenomenon suggests that certain mass fragments may be formed preferentially, while other intermediate mass fragments are formed hardly at all.

There is no obvious structure in these curves for energies below the most probable energy, just as in Fig. 1 there is no structure for energies below the most probable value.

The average total kinetic energy

In Fig. 4a we have plotted the average total kinetic energy of fragments from thermal-neutron-induced fission of U^{235} as a function of fragment mass. Our data, shown as open circles, have been corrected for the loss in energy due to neutron emission and therefore represent energies of the prompt fragments. This correction has been made under the assumption that the number of neutrons emitted per fragment is given by TERRELL's "universal curve" [6].

The solid curve in Fig. 4a represents the measurements made by MILTON and FRASER [1]. The agreement is excellent over the light-fragment mass range 85 to 101 (heavy fragments 135 to 151). Disagreement

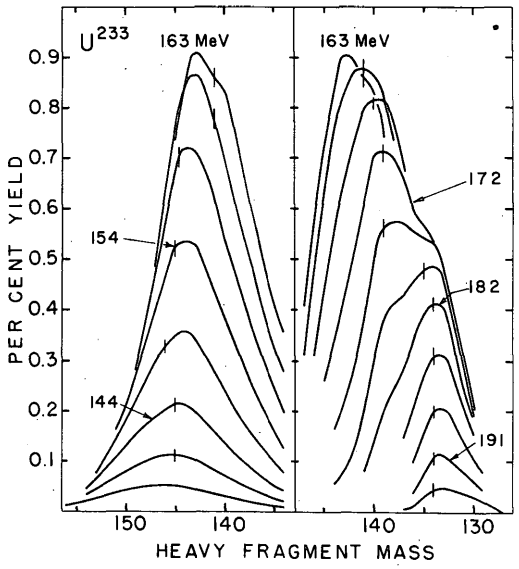

Fig. 3

Heavy fragment mass-yield curves for different values of the total kinetic energy for the system U^{233} plus thermal neutrons.
The vertical lines on each curve indicate the most probable value of the mass reported by MILTON and FRASER [1].

appears at the point where the mass-yield curve begins to fall towards its very low value at symmetry.

The region at symmetry is particularly susceptible to distortion by a relatively small number of spurious events. Milton and Fraser have estimated by comparison of their mass-yield curves with radiochemical data that between masses 112 and 124 approximately one third of the events are real. A similar comparison indicates that over the same range slightly more than half of the events are real in our data.

There are two likely sources of spurious events in this region. The dispersion in energy (or velocity) due to neutron emission will cause some asymmetric events (and, hence, high-energy events) to appear as symmetric events. The observed average energy will be higher than the true energy. Energy degradation of the high-energy fragments before they reach the detector may cause them to have approximately the same energy as their low-energy partners; such events will be recorded as low-energy symmetric events.

We estimate that the point at symmetry would be about 1 MeV lower if there were no effects from neutrons. It might be as much as 6 MeV higher if correction were made for low-energy tailing.

Range measurements of fragments from the thermal-neutron-induced fission of U^{235} have been made by NIDAY [2] and by ARAS, MENON and GORDON [4]. Average total energies have been calculated from these ranges; in Fig. 4b we compare the results of Aras et al. (triangles) with ours (solid

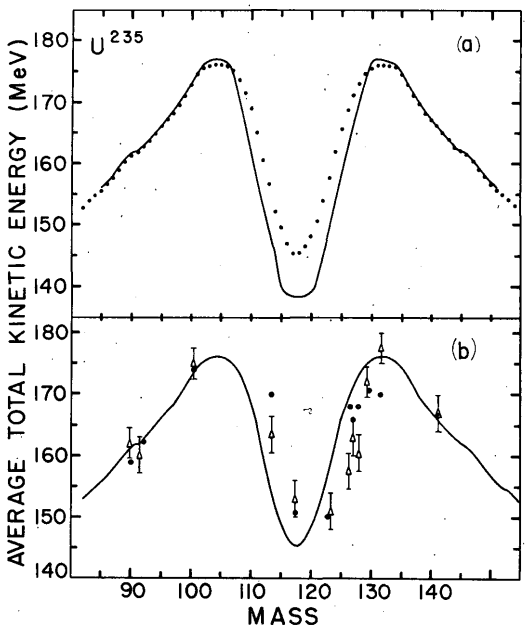

Fig. 4

(a) Average total kinetic energy for prompt fragments produced in the fission of U^{235} with thermal neutrons. Points are from this work; solid lines are from MILTON and FRASER [1].

(b) As for 4(a). Solid curve is from this work; triangles from ARAS, MENON and GORDON [4]. Solid points were calculated as described in the text.

curve). At symmetry their energy is about 7.5 MeV higher than ours. Furthermore, on the high-mass side of symmetry their numbers tend to be lower than ours, and on the low-mass side theirs tend to be higher.

It is important to recognize that these two experiments measure different quantities. To first approximation, the energies determined by the semiconductor detector measurements are characteristic of a single mass division. On the other hand, a radiochemical measurement at mass 115, for instance, represents contributions from fragments having masses from 115 to 120 emitting from 0 to 5 n. We can use our data as the basis for an estimate of the average total kinetic energies that would be determined by a radiochemical measurement of ranges. We make the following assumptions: (1) the mass-yield curve and average total energy as a function of mass for prompt fragments are as determined in our experiments; (2) the average number of neutrons emitted as a function of mass is given by the same curve that was used by ARAS, MENON and GORDON [4]; (3) the probability of emitting a particular number of neutrons is given by a Poisson distribution; and (4) if a fragment emits n more (or fewer) neutrons than the average number for its mass, it must have 6n MeV more (or less) excitation energy and therefore 6n MeV less (or more) kinetic energy.

The results of calculations based on these assumptions are shown as the solid points of Fig. 4b. With the exception of the one point at mass 132 the agreement with the data of Aras et al. is good. We conclude that the dis-

agreement between their results and ours is more apparent than real. If the calculated point at symmetry is raised by 6 MeV to correct for the possible effects of tailing, it is still almost within the error bar given by Aras et al.

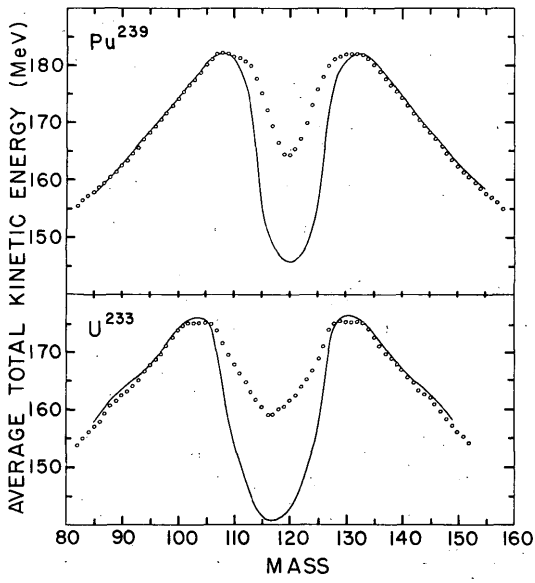

Fig. 5

Average total kinetic energy for prompt fragments produced in the fission of U^{233} and Pu^{239} with thermal neutrons.
Points are from this work; solid lines from MILTON and FRASER [1].

Figure 5 shows the average total kinetic energy as a function of fragment mass for U^{233} and Pu^{239}. As before, the open circles represent our data and the solid lines those of Milton and Fraser. The disagreement at symmetry between the two sets of data is very pronounced. A comparison of our mass yield curves with radiochemical results indicates that for both U^{233} and Pu^{239} about 80% of the symmetric events in our data are real. There should, therefore, be only a slight distortion of the average energies due to spurious events.

DISCUSSION

The data presented here and the results obtained by MILTON and FRASER [1] indicate that there is a preference for formation of heavy fragments with masses of about 134, 140 and 145 in the thermal-neutron-induced fission of U^{235}, U^{233} and Pu^{239}. The existence of this preference suggests that the properties of the final fragments or of the fragments existing at the scission point play an important role in determining the mass division in fission.

MILTON and FRASER [1] and THOMAS and VANDENBOSCH [13] have pointed out that for very high kinetic energies of the fragments there is a thermodynamic limitation on what fragments can be formed. Because of structure in the mass surface, it is energetically impossible to form certain mass fragments even though it is possible to form fragments of slightly higher and lower mass. It has been shown that there is a good correlation between the structure observed at high kinetic energies and the structure in the mass surface for thermal-neutron-induced fission of U^{235}, U^{233} and Pu^{239}. However, we can see from Figs. 1 and 3 that the structure persists at kinetic energies sufficiently low that the restrictions imposed by the variations in mass of the separated fragments should not be important.

VANDENBOSCH [13] has successfully accounted for the variation of the average total kinetic energy and of the average number of emitted neutrons with fragment mass by considering the properties of the fragments at the scission point. He has assumed that the scission point configuration is two tangent prolate spheroids having collinear major axes. The energy at scission is assumed to be composed of three parts: a potential energy of deformation, which eventually becomes excitation energy of the fragments; a Coulomb interaction energy between the two fragments, which eventually appears as kinetic energy; and excitation energy, which is the difference between the total available energy and the sum of the deformation and Coulomb interaction energies.

We can combine these two points of view to give some indication of why the structure in the yield surface should persist at kinetic energies that impose no thermodynamic restriction on what separated fragments can form. Let us consider, as an example, the formation of a pair of fragments, $_{38}Sr^{96}$ and $_{54}Xe^{140}$, by the thermal-neutron-induced fission of U^{235}. According to MILTON's [14] calculations, the total possible energy release is 192 MeV.

Using the method outlined by Vandenbosch, we have calculated the deformation energy E_D, the Coulomb interaction energy E_I and their sum as a function of deformation for this pair of fragments. The results are shown in Fig. 6. The scission point configuration is assumed to correspond to the minimum in the total potential energy curve. The horizontal line in Fig. 6 represents the total available energy; the difference between this line and the potential energy curve is the excitation energy of the fragments.

The symbol $\langle E_K \rangle$ designates a point on the interaction energy curve corresponding to the measured average total kinetic energy for this mass division. The position of this point agrees fairly well with the position of the minimum in the total potential energy curve. The two lines above and below the line labelled $\langle E_K \rangle$ represent the variance of the kinetic energy spectrum for this mass division. We notice that the total potential energy varies from the highest to the lowest of the three lines - about 18 MeV. Thus we might conclude that the entire range of kinetic energies and excitation energies of the separated fragments corresponds to a rather small variation in the total potential energy at scission.

The small excitation energy (about 5 MeV, in this case) will be sensitive to variations in the total available energy. Furthermore, the excitation energy varies only slightly over the whole range of observed kinetic energies. Thus, if fluctuations in the available energy produce fluctuations in

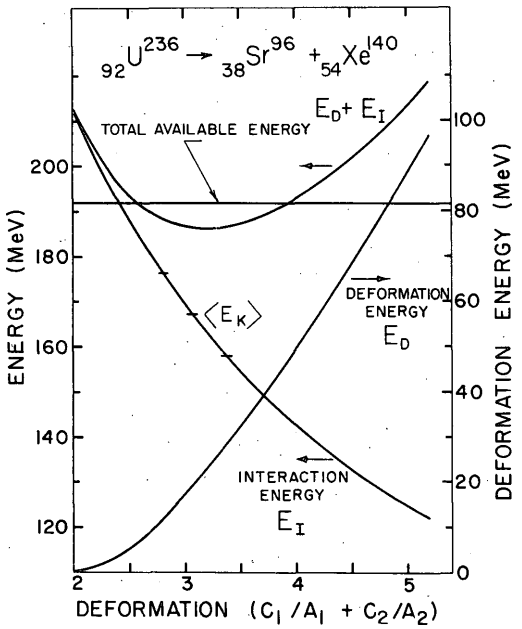

Fig. 6

Deformation energy, Coulomb interaction energy and total potential energy at the scission point as a function of deformation for the indicated pair of fragments

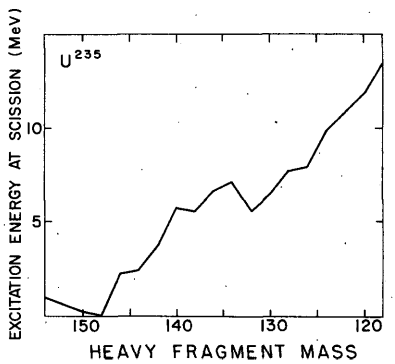

Fig. 7

Excitation energy of the fragments at scission as a function of fragment mass for fission of U^{235} by thermal neutrons

the yield at the highest kinetic energies, we can expect that they would also produce similar fluctuations at energies as low as the lowest observed. The failure to see structure for kinetic energies lower than the most probable value may be an experimental problem. The low kinetic energies correspond to high deformation energies and relatively large numbers of emitted neutrons. The increased dispersion in mass due to increased neutron emission may cause the structure to be obscured.

We have done similar calculations for a range of mass and charge divisions to give the excitation energy at scission for the system formed from U^{235} plus thermal neutrons. The method and parameters used were essentially those given by VANDENBOSCH [13], and there was reasonably good agreement between the calculated interaction energies and the observed average total kinetic energies. The results are shown in Fig. 7, where we have plotted as a function of mass the excitation energy at scission for that charge division giving the highest excitation energy.

We see in this graph maxima at heavy-fragment masses 134 and 140, and a shoulder at mass 146, corresponding rather well with the masses preferred in fission. The fact that the excitation energy increases steadily as we move towards symmetry suggests, however, that there are factors other than excitation energies that are determining the yield near symmetry.

ACKNOWLEDGEMENTS

We are indebted to G.L. Miller for the design of the special preamplifiers and for help in operating them, also for advice and help in the measurements, to T.C. Madden for fabricating the solid state detectors and to Dr. S.G. Thompson, of the Lawrence Radiation Laboratory, for making available Cf^{252} spontaneous-fission sources that were invaluable for the system calibration.

REFERENCES

[1] MILTON, J.C.D. and FRASER, J.S., Canad. J. Phys. 40 (1962) 1626.
[2] NIDAY, J.B., Phys. Rev. 121 (1961) 1471.
[3] ALEXANDER, J.M., GAZDIK, M.F., TRIPS, A.R. and WASIF, S., Phys. Rev. 129 (1963) 2659.
[4] ARAS, N.K., MENON, M.P. and GORDON, G.E., to be published.
[5] GIBSON, W.M., THOMAS, T.D. and MILLER, G.L., Phys. Rev. Lett. 7 (1961) 65.
[6] TERRELL, J., Phys. Rev. 127 (1962) 880.
[7] BRITT, H.C. and WEGNER, H.E., Rev. sci. Instrum. 34 (1963) 274.
[8] SCHMITT, H.W., KIKER, W.E. and WILLIAMS, C.W., to be published in Phys. Rev.
[9] SCHMITT, H.W., GIBSON, W.M., NEILER, J.H., WALTER, F.J. and THOMAS, T.D., "Absolute energy calibration of solid-state detectors for fission fragments and heavy ions", these Proceedings I.
[10] THOMAS, T.D. and GIBSON, W.M., Proc. Conf. on the Utilization of Multiparameter Analysers in Nuclear Physics, Columbia University, New York (1962) 132.
[11] THOMAS, T.D. and VANDENBOSCH, R., Phys. Rev. 133 (1964) B976.
[12] FRASER, J.R., MILTON, J.C.D., BOWMAN, H.R. and THOMPSON, S.G., Canad. J. Phys. 41 (1963) 2080.
[13] VANDENBOSCH, R., Nucl. Phys. 46 (1963) 129.
[14] MILTON, J.C.D., Univ. Calif. Radiation Lab. Rpt. UCRL-9883 Rev.

DISCUSSION

J.C.D. MILTON: I think Dr. Thomas's remarks on the energy deficit at symmetric fission are correct. I would like to point out that the number of events in this region is lower than the most probable by nearly three orders of magnitude. The data we used date from 1959 and at that time we

paid no particular attention to this point. In the paper I referred to in my earlier reply to Dr. Mossop[1] we devoted an entire paragraph to the reliability of the measurements in this region and I do not think it needs rewording at present. The point we were emphasizing in showing the results in the symmetric region was simply that there was a large decrease in the average kinetic energy.

D.M. NADKARNI: Recent measurements made at Trombay on the variation of total kinetic energy distribution of fission fragments in thermal-neutron fission of U^{235}, using solid-state detectors, indicated a similar discrepancy compared with the time-of-flight measurements. It is important, I think, to establish whether this discrepancy is caused by the large percentage of false symmetric events in the latter case or the incomplete understanding of the energy defect in solid-state detectors in the former case. This has a bearing on whether or not the so-called universal curve of neutron emission from individual fragments is really universal.

S.S. KAPOOR: I should like to ask Dr. Thomas whether the symmetric yields were corrected for the mass dispersion and how the mass dispersion was estimated. Were the energy balance calculations applied to see whether the kinetic energy measured in the symmetric region was consistent with the neutron yield as measured by Apalin recently?

T.D. THOMAS: The data as shown have not been corrected for mass dispersion. For the average total energies as a function of mass we have made an estimate of the correction at symmetry. The value of the energy at symmetry might be as much as 1 MeV lower than is indicated in the figures. The bases for estimating the dispersion are the figures given by Terrell (Ref. [6] in the paper) and the energy resolution of solid-state detectors measured by Schmitt et al.[2] I have not yet seen the recent work of Apalin, and have not done the energy balance calculations.

P. ARMBRUSTER: The fine structure observed in the kinetic energy distribution, which was mentioned by Dr. Thomas, has been explained by a preferential formation of even-even nuclei. If we accept this interpretation, it would seem to be possible to determine, for these preferentially formed nuclei, the primary charge Z_p. This would be a determination of the primary charge for nuclei before prompt neutron emission. Does Dr. Thomas think this method could be used as a further physical method of charge determination?

T.D. THOMAS: I think it might be presumptuous to extend the correlation Dr. Vandenbosch and I made between the energy surface and the yield surface to calculate charge distribution. It would be good if such a calculation showed that there was agreement between a measured charge distribution and what one had predicted, but I should not venture to predict charge distribution in this way.

---

[1] MILTON, J.C.D. and FRASER, J.S., Time-of-Flight Fission Studies on U^{233}, U^{235}, and Pu^{239}, Can. J. Phys. 40 (1962) 1626.

[2] SCHMITT, H.W., GIBSON, W.M., WEILER, J.H., WALTER, F.J. and THOMAS, T.D., "Absolute energy calibration of solid-state detectors for fission fragments and heavy ions", These Proceedings I.

SIMULTANEOUS MEASUREMENTS OF FLIGHT TIMES AND ENERGIES OF FISSION FRAGMENTS

G. ANDRITSOPOULOS*, T. CORNELL**AND A. L. RODGERS
UNITED KINGDOM ATOMIC ENERGY AUTHORITY,
ATOMIC WEAPONS RESEARCH ESTABLISHMENT,
ALDERMASTON, BERKS., UNITED KINGDOM

Abstract — Résumé — Аннотация — Resumen

SIMULTANEOUS MEASUREMENTS OF FLIGHT TIMES AND ENERGIES OF FISSION FRAGMENTS. In a companion paper the results of measuring the prompt neutron emission from individual fission fragments arising in thermal fission are reported. In that experiment a large volume liquid scintillation counter was used to record the fission neutrons, and fragment mass was identified by a gold silicon surface barrier counter arrangement.

An alternative way of measuring the prompt neutron emission is described here. Fragment time-of-flight apparatus is mounted in an evacuated tube that passes laterally through the thermal column of the 5-MW research reactor HERALD. A centrally positioned thin source produces 3×10^5 fissions s^{-1}. Fragments travel distances of 180 cm and 300 cm respectively to the terminal detectors, and in passing through a VYNS film, positioned 180 cm from the source along the longer flight path, eject electrons that are used to form a reference time-signal.

Essentially the times of flight of both fission fragments are measured simultaneously with the kinetic energy of one of the pair. This is achieved by using a surface barrier counter for the 300-cm detector. The difficulty of maintaining good timing and energy resolutions simultaneously is overcome by routing the pulse to the charge sensitive preamplifier through a delay line amplifier from which a fast timing pulse is derived.

The collected data enables the fragment mass to be determined both before and after prompt neutrons have been emitted. Hence the experiment provides a means for studying the behaviour of neutron emission from individual fragments.

The experimental uncertainties are those associated with the measurement of small differences, and an appraisal is made of the errors and calibrations that enter into the measurements. Of particular importance, the response of the surface barrier counter to fission fragments is obtained directly from the collected data from events in which the neutron emission is low. These calibrations are used in the measurements of post-neutron mass.

MESURE SIMULTANÉE DU TEMPS DE VOL ET DE L'ÉNERGIE DES PRODUITS DE FISSION. Les résultats des mesures de l'émission de neutrons instantanés par différents fragments de fission produits au cours de fissions thermiques sont indiqués dans un autre mémoire. Lors de cette expérience, on a utilisé un grand compteur à scintillateur liquide pour enregistrer les neutrons de fission et identifié la masse des fragments à l'aide d'un dispositif de comptage à barrière de surface Au-Si.

Les auteurs décrivent une autre méthode permettant de mesurer l'émission de neutrons instantanés. Un appareil de mesure du temps de vol des fragments est monté dans un tube à vide qui traverse latéralement la colonne thermique du réacteur de recherche HERALD, de 5 MW. Une source mince disposée au centre produit $3 \cdot 10^5$ fissions par seconde. Les fragments parcourent des distances de 180 et 300 cm respectivement en direction des détecteurs terminaux et en passant à travers un film VYNS placé à 180 cm de la source sur le plus long parcours, ils expulsent des électrons qui donnent un signal-temps de référence.

Le principe est le suivant: on mesure les temps de vol des deux fragments de fission simultanément avec l'énergie cinétique de l'un des deux. On le fait en associant un compteur à barrière de surface au détecteur à 300 cm. Pour surmonter la difficulté de maintenir une bonne résolution en temps et en énergie, on dirige

* University of Reading

** Now at Rolls Royce

l'impulsion vers le préamplificateur sensible à la charge par l'intermédiaire d'un amplificateur à ligne de retard qui fournit une impulsion rapide de synchronisation.

Les données recueillies permettent de déterminer la masse des fragments avant et après l'émission des neutrons instantanés. Ainsi, cette expérience fournit un moyen pour étudier l'allure de l'émission de neutrons par les différents fragments.

La marge d'incertitude expérimentale est celle que comporte la mesure de petites différences. Les auteurs procèdent à une évaluation des erreurs que ces mesures comportent et des opérations d'étalonnage qu'elles exigent. D'une importance particulière est le fait que la réponse du compteur à barrière de surface aux fragments de fission est obtenue directement à partir des données recueillies, à partir d'événements comportant une faible émission de neutrons. Ces opérations d'étalonnage sont faites pour mesurer la masse après émission de neutrons.

ОДНОВРЕМЕННЫЕ ИЗМЕРЕНИЯ ВРЕМЕНИ ПРОЛЕТА И ЭНЕРГИЙ ОСКОЛКОВ ДЕЛЕНИЯ. В представленном докладе сообщаются результаты измерения эмиссии мгновенных нейтронов отдельными осколками деления, возникающими при делении под действием тепловых нейтронов. В описываемом эксперименте был использован жидкий сцинтилляционный счетчик большого объема для регистрации нейтронов деления, тогда как масса осколков устанавливалась при помощи устройства из счетчика с поверхностным барьером из золота и кремния.

Описывается также альтернативный способ измерения эмиссии мгновенных нейтронов. Прибор для измерения времени пролета осколков смонтирован в вакуумной трубке, которая проходит поперек тепловой колонны исследовательского реактора "Геральд" мощностью 5 мгвт. Расположенный в центре тонкий источник производит $3 \cdot 10^5$ делений в 1 сек$^{-1}$. Осколки пробегают расстояния соответственно 180 и 300 см до расположенных в конце пути детекторов и, проходя через пленку VYNS, расположенную на расстоянии 180 см от источника в направлении более длинного пути пролета, выбивают электроны, которые используются в качестве исходного сигнала времени.

Основная доля времени пролета обоих осколков деления измеряется одновременно с кинетической энергией одной их пары. Это достигается путем использования счетчика с поверхностным барьером для детектора, расположенного на расстоянии 300 см. Затруднения в одновременном соблюдении как времени, так и разрешения по энергии преодолеваются благодаря направлению импульса в чувствительный к заряду предварительный усилитель, через усилитель линии замедления, из которого извлекается быстрый импульс отсчета времени.

Собранные данные дают возможность определять массу фрагментов до и после эмиссии мгновенных нейтронов. Тем самым этот эксперимент дает возможность изучать поведение эмиссии нейтронов от отдельных осколков.

Экспериментальные неопределенности связаны с необходимостью измерения небольшой по величине разницы, что ведет к необходимости определения входящих в результаты измерений погрешностей и калибровок. Особое значение имеет то обстоятельство, что реакция счетчика с поверхностным барьером на осколки деления получается непосредственно из собранных данных, т.е. из явлений, при которых эмиссия нейтронов незначительна. Эти калибровки используются при измерениях массы после эмиссии нейтронов.

MEDICION SIMULTANEA DE LOS TIEMPOS DE VUELO Y DE LAS ENERGIAS DE LOS FRAGMENTOS DE FISION. En la memoria SM-60/47 se exponen los resultados de mediciones de la emisión de neutrones inmediatos por distintos fragmentos de fisión, que tiene lugar en un proceso de fisión térmica. A tal efecto, se utilizó un contador de centelleador líquido de gran volumen para el registro de los neutrones de fisión, identificándose la masa del fragmento mediante una combinación de contadores de Au-Si de barrera superficial.

En la presente memoria, los autores describen otro método para medir la emisión de neutrones inmediatos. El aparato empleado en la determinación del tiempo de vuelo de los fragmentos va instalado en un tubo en cuyo interior se ha hecho el vacío, y que atraviesa lateralmente la columna térmica del reactor de investigación HERALD, de 5 MW. Una fuente de reducido espesor, situada en el centro del tubo, produce $3 \cdot 10^5$ fisiones/s. Los fragmentos de cada fisión recorren 180 y 300 cm, respectivamente, hasta los detectores terminales, y al atravesar una película de VYNS situada a 180 cm de la fuente en la misma línea de la trayectoria más larga, despiden electrones que se utilizan para dar origen a una señal sincronizadora de referencia.

En esencia, los tiempos de vuelo de los dos fragmentos formados en cada fisión se miden simultáneamente con la energía cinética de uno de los componentes del par. Esto se consigue con ayuda de un contador de

barrera superficial en calidad de detector colocado al final de la trayectoria de 300 cm. La dificultad que entraña el mantener simultáneamente buenas resoluciones de tiempos y energías se supera transmitiendo el impulso al preamplificador sensible a las cargas, a través de un amplificador de línea de retardo del cual se deriva un impulso sincronizador rápido.

Los datos así obtenidos permiten determinar la masa de los fragmentos antes y después de la emisión de los neutrones inmediatos. De esta forma, este experimento proporciona un medio para estudiar el comportamiento de los distintos fragmentos durante la emisión neutrónica.

Las incertidumbres experimentales son las propias de la medición de pequeñas diferencias, y los autores evalúan los errores y las calibraciones que intervienen en las mediciones. Particular importancia reviste el hecho de que la respuesta del contador de barrera superficial a los fragmentos de fisión se obtiene directamente de los datos acopiados, correspondientes a fisiones en las que la emisión neutrónica es poco intensa. Estas calibraciones se emplean en la medición de la masa de los fragmentos con posterioridad a la emisión neutrónica.

INTRODUCTION

Surface barrier counters are being used on the HERALD research reactor to measure, simultaneously, the times of flight and the kinetic energies of fission fragments that arise from the thermal-neutron-induced fission of U^{235}.

The interest in the work stems from the fact that the arrangement is capable of studying the average prompt-neutron emission from individual fragments. This is achieved by recording simultaneously the mass of a fragment both before and after the neutrons have been emitted, the two masses being respectively derived from the two flight times, and one flight time and the corresponding kinetic energy.

The kinetic energy is obtained from the output pulse of a surface barrier counter, and an essential calibration measurement is to establish its pulse-height response to fission fragments. Although a linear relationship has been commonly accepted and used in mass determinations from coincident energy experiments, it is vital in the present work to use the correct expression in deriving the post-neutron mass.

The pulse-height response of surface barrier counters to heavy particles has hitherto been determined by SCHMITT et al. [1] and measurements on actual fission fragments have been reported by CORNELL [2]. In the latter work the information was derived from separate experiments on similar counters. The present experiment allows a direct examination to be made, and the pulse-height response for fragments of a specified mass and kinetic energy are recorded with the information necessary to establish the neutron emission.

EXPERIMENTAL APPARATUS

A schematic diagram of the apparatus is shown in Fig. 1. A 50-μg cm^{-2} evaporated deposit of U^{235} on 70-μg cm^{-2} nickel is centrally placed within an evacuated flight tube that passes laterally through the thermal column of the reactor. In a region of 7×10^9 thermal neutrons cm^{-2} s^{-1} approximately 5×10^5 fissions s^{-1} are produced, and sister fragments travel distances of 170 cm and 367 cm respectively to terminal detectors. In transit

the fragment travelling to the 367-cm detector passes through a gold-covered VYNS film, positioned 180 cm from the source, and in so doing ejects electrons by the ionization process. The electrons are focused electrostatically on to a disc of NE-102 plastic scintillator of 13-μm thickness, and the transduced pulse fed to a Mullard type 56 AVP photomultiplier. This output pulse is used for a reference time signal.

Two further time signals are available, one from each of the terminal detectors. The detector at 367 cm from the source is a gold-silicon surface barrier counter of diam. 1.8 cm and 300 Ω cm resistivity. The amplitude of the integrated output pulse for this counter is also recorded, and defines the kinetic energy of the fragment once the calibration relationship is known.

The nature of the 170-cm terminal detector depends to some extent upon the experiment being undertaken. In experiments to measure prompt-neutron emission it is important to collect fragments over the largest possible angle to preserve high detection efficiency with neutron mode. This implies a large sensitive area for a specified flight distance. For example, with a detector at 170 cm, of maximum possible radius 10 cm, the efficiency for detection of a fission mode emitting six neutrons is better than 95%, and this improves as the number of neutrons is reduced.

Because of the development problems encountered in the placing of a large area detector in the present system, a series of measurements have been undertaken with a 3-cm-diam. surface barrier counter at the 170-cm terminal detector position. With this arrangement the over-all efficiency is considerably smaller than for a large area counter, and there is also a larger spread in efficiency with neutron number. This system has been used to provide information on the response of the 367-cm surface barrier counter to fission fragments. Although the essential requirement for the 170-cm detector is to provide a timing signal a separate energy pulse from this detector has also been recorded.

The timing signal pulses from each of the terminal detectors are amplified and then used to start the timing ramps of separate time-to-pulse-height convertors (time-sorters). The amplified pulse from the reference time detector (VYNS film) is passed through separate delay boxes and used to stop each time-sorter. This timing sequence was chosen to prevent the time-sorters from being overloaded by spurious start pulses from the high background level encountered in the reference time detection system. The level of spurious operation under these conditions is $\sim 0.1‰$.

The voltage output of each time-sorter is proportional to the flight time of one fragment and the timing difference between sister fragments respectively. A knowledge of the delay in the circuitry, the geometrical constants of the apparatus and the time-sorter calibration enables both times-of-flight to be calculated, and hence the pre-neutron mass and initial kinetic energy of either fragment to be derived.

Each of the time-sorter outputs are fed to a 400-channel amplitude to digital convertor and stored on paper tape. Pulses corresponding to the kinetic energies of sister fragments are derived separately from each terminal detector, and after amplification and digitalization are stored similarly on the paper tape.

The difficulty of obtaining good time-of-flight and energy resolution simultaneously was overcome by passing the signal from each surface

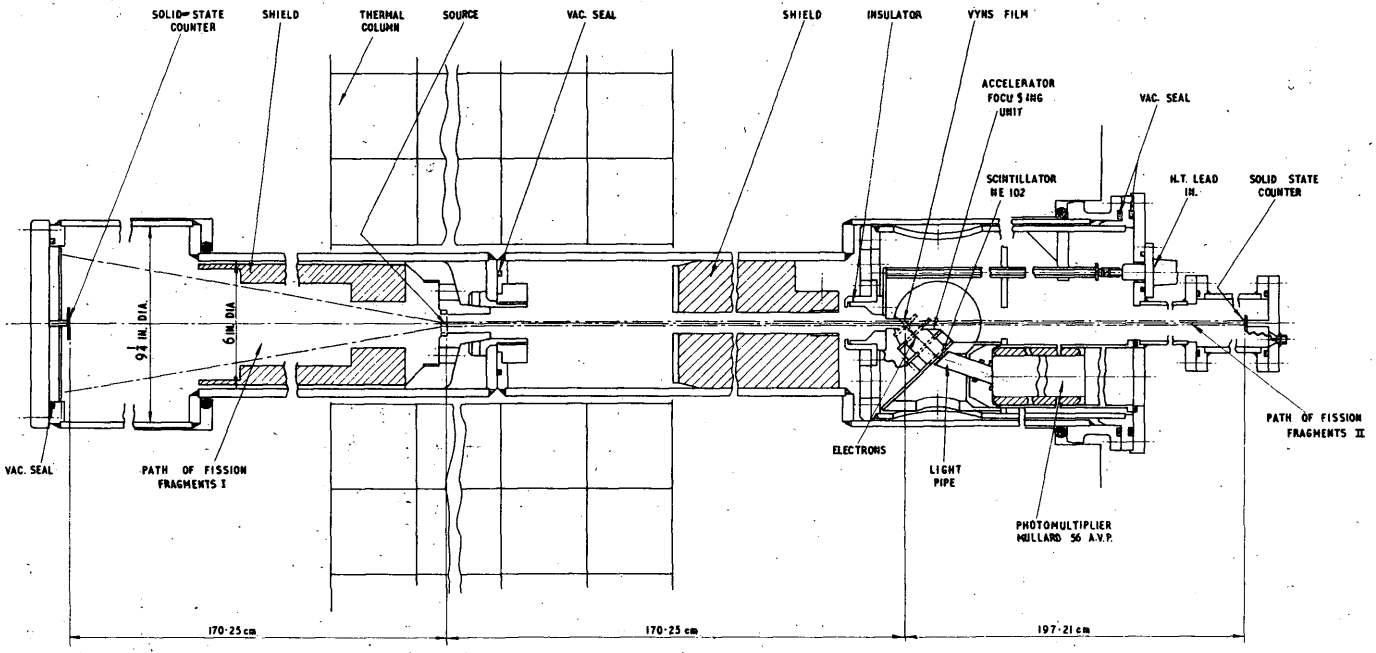

Fig. 1

Schematic diagram of the time-of-flight apparatus

barrier counter to a charge-sensitive preamplifier via a distributed line amplifier. This type of amplifier, in which the valve grids are connected at intervals down a delay line, has very short time response but does not have the linear charge response necessary for the energy measurement. However, the counter pulse emerges virtually unchanged from the end of the grid delay line and, instead of being terminated conventionally, i.e. a matching resistor, it is passed to the charge-sensitive preamplifier where the energy is measured. A separate fast pulse is available for timing at the input valve anodes. Earlier experiments using short (2-cm) flight paths in subsidiary equipment showed that there was no measurable degradation in the energy spectrum of the surface barrier counter from that obtained with the charge preamplifier connected directly to the surface barrier counter. Moreover it was possible to distinguish the light mass group from the heavy mass group over the 2-cm flight path, and this showed a timing resolution better than 1 ns for an individual fission event.

RESULTS AND DISCUSSION

Using the 1.8-cm and 3-cm-diam. surface barrier counters for the terminal detectors the four parameter ($E_1E_2T_1T_2$) coincidence rate is 1.5 min^{-1}. The singles rates are respectively 10 min^{-1} and 300 min^{-1} for the two terminal detectors. The electron fragment coincidence rate exceeded 95% for a bias level yielding a background count of 2×10^3 s^{-1} in the reference time detection system.

The four spectra of Fig. 2 are the raw data for the 7000 4-parameter events recorded. No attempt has been made at this stage to correct for electronic drifts, but it is concluded from the quality of the spectra, and from the computer print-outs, that the drifts are probably unimportant over the experimental running period.

Data analysis is accomplished entirely by a large off-line computer. Calculations are made to convert time-sorter outputs into time-of-flight for the sister fragments, from which are derived the pre-neutron mass and initial kinetic energy of the fragment that travels towards the 367-cm surface barrier counter. These are correlated with the pulse height appropriate to the same event and the result is presented, for six different mass groups, in the computer graphical display of Fig. 3.

Graphical read-outs of both time-of-flight spectra and the pre-neutron mass and kinetic energy distributions are also provided by the computer, and help in the appraisal of the data.

In making general observations from Fig. 3 it is observed that the average pulse-height response is not inconsistent with an approximately linear relationship with kinetic energy, but of slope that decreases with increasing mass. An extrapolation to zero pulse height indicates a much smaller "ionization defect" than is obtained by the conventional mass-independent linear relationship, and more in agreement with the empirical expressions of Schmitt and of Cornell. A computer programme now being written for the data will provide the numbers of events in the pulse-height-energy matrix for specified mass groups. This should enable the pulse-height response to be determined quantitatively.

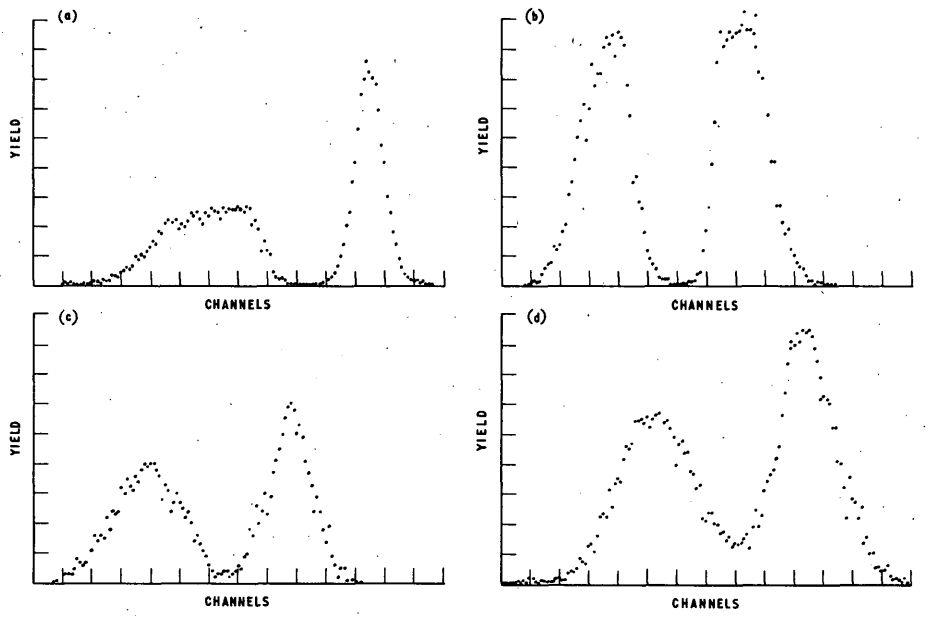

Fig. 2

Fission-fragment channel spectra

(a) Time-of-flight to 367-cm detector
(b) Difference in time-of-flight between sister fragments
(c) Pulse height for 367-cm detector
(d) Pulse height for 170-cm detector

The dispersion of the separate events for a specified mass group of Fig. 3 is due partly to the inherent resolution of the counter and partly to neutron emission. Strictly the pulse height should be compared with the appropriate post-neutron kinetic energy value, but it is the initial kinetic energy that is calculated from the flight times. It can be shown that a dispersion in the points is introduced by correlating with the initial energy values. The average response, however, is insignificantly affected.

Indeed the ideal situation can only be realized by recording only those modes where no neutrons are emitted. The practical implication is to have a 170-cm terminal detector of infinitesimally small radius, and this is ruled out by intensity considerations.

In view of the absence of any direct measurements on the energy resolution of this type of barrier counter to fission fragments it is worth noting that the method is capable of yielding this information. Although a quantitative picture should be revealed when the new computer programme comes into operation present results suggest that the resolution may be as high as ± 2.5 MeV for a typical median mass fragment.

Once the pulse-height response has been ascertained it is intended to use the apparatus for measuring average neutron emission behaviour from individual fragments and from fragment pairs of U^{235} thermal fission.

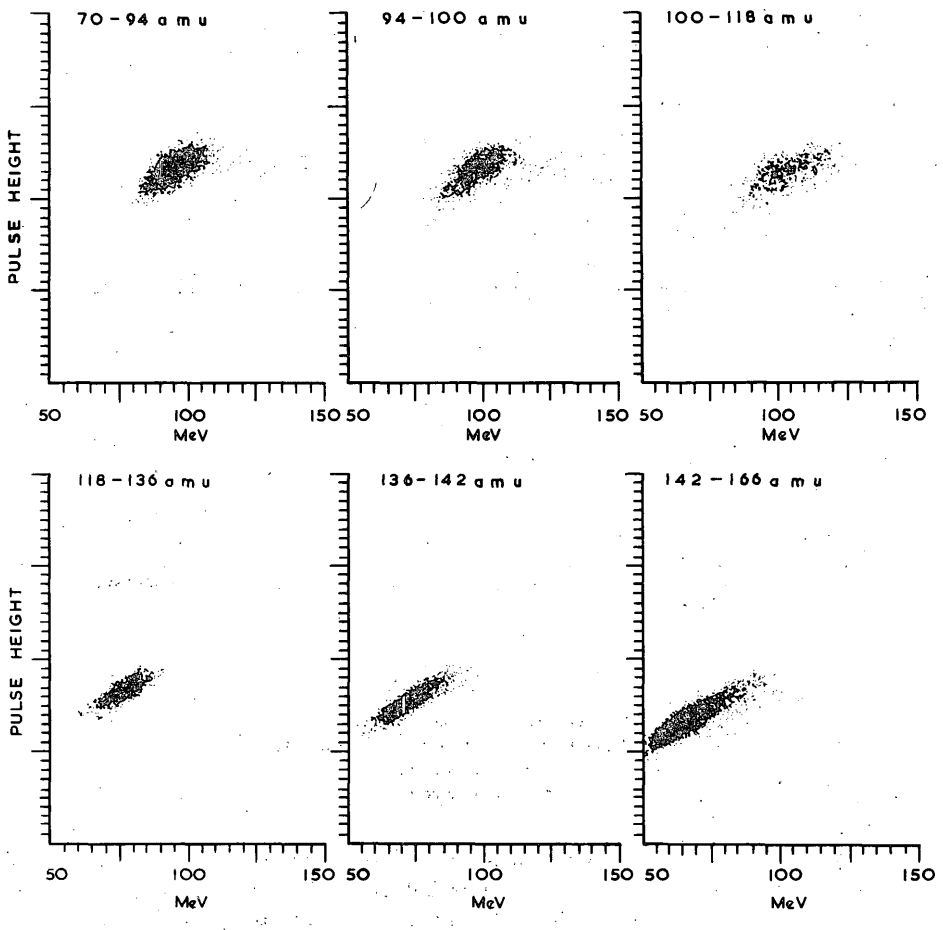

Fig. 3

Pulse-height response to fission fragments of a
300 Ω cm 1.8 diam. gold-silicon surface barrier counter

ACKNOWLEDGEMENTS

The authors wish to express their thanks to E.E. Maslin for his help in compiling the computer programme.

REFERENCES

[1] SCHMITT, A.W., WALTER, F.J., NEILER, J.H., MOAK, C.D., GIBSON, W.M. and THOMAS, T.D., ORNL 3425 (1963) 130.

[2] CORNELL, T. and RODGERS, A.L., Congrès International de Physique Nucléaire (1964) Paper 4e/C139.

DISCUSSION

E. KONECNY: With our fission-particle mass-spectrometer we had no difficulty in measuring quite accurately the dependence of surface barrier detectors on the mass and kinetic energy of fission particles. The results will be published. What we found agrees well with the work done at Oak Ridge. We did not find negative intercepts in the pulse-height versus energy plot for extrapolation to zero energy, as reported in the paper presented by Dr. Rodgers.

SIMULTANEOUS VELOCITY AND ENERGY MEASUREMENT OF FISSION FRAGMENTS*

W. E. STEIN
LOS ALAMOS SCIENTIFIC LABORATORY,
UNIVERSITY OF CALIFORNIA,
LOS ALAMOS, N. MEX., UNITED STATES OF AMERICA

Abstract — Résumé — Аннотация — Resumen

SIMULTANEOUS VELOCITY AND ENERGY MEASUREMENT OF FISSION FRAGMENTS. Semi-conductor detectors have been used in a double-velocity apparatus for a simultaneous measurement of fragment velocities and detector pulse heights. The purposes of this measurement were (1) to obtain the pulse-height-to-energy calibration of these detectors for fission fragments and (2) to evaluate a technique for the simultaneous determination of pre- and post neutron emission parameters of the fission process from a coincident measurement of fragment velocities and energies. Fast and slow output signals were obtained from the detectors for use in the time-of-flight and pulse-height measurements respectively. The recorded data were the flight times of both fragments and the pulse height from one of the detectors for a total of 46 000 Cf^{252} fission events. Fragment velocities, initial masses and initial energies were obtained in the usual manner from the time-of-flight data.

The detector calibration function was determined from the correlation between the recorded pulse heights and the final parameters of the corresponding fragments. The latter values were obtained from the initial mass, initial energy and the published values of $\bar{\nu}(m, E_K)$ for californium fragments. Finally, the calibration function was corrected for instrumental dispersions and the dependence of the average energy on fragment mass.

The post-neutron-emission parameters were obtained from the recorded data and available detector calibration procedures including the one given above. The average number of neutrons emitted as a function of fragment mass was obtained from the event-by-event differences of the initial and final masses. This result provided a sensitive test of the validity of this proposed technique and the various calibration procedures. Agreement with published data was found for the calibration procedure based on these data and one derived from the response of semi-conductor detectors to accelerated bromine and iodine ions. In each case the root mean square deviation from the published values of $\bar{\nu}$ was less than 0.7 of a neutron.

MESURES SIMULTANÉES DE LA VITESSE ET DE L'ÉNERGIE DES FRAGMENTS DE FISSION. L'auteur a utilisé des détecteurs à semi-conducteurs dans un appareil à deux vitesses pour mesurer simultanément la vitesse des fragments et l'amplitude des impulsions du détecteur. Ces mesures avaient pour but: 1. d'étalonner ces détecteurs pour les fragments de fission en déterminant l'amplitude d'impulsion correspondant à chaque niveau d'énergie; 2. d'évaluer une méthode de détermination simultanée des paramètres de fission avant et après émission de neutrons à partir d'une mesure en coïncidence de la vitesse et de l'énergie des fragments. L'auteur a obtenu des signaux rapides et lents à la sortie des détecteurs, qui servent respectivement pour des mesures de temps de vol et de l'amplitude d'impulsion. Les données enregistrées sont le temps de vol de chacun des deux fragments et l'amplitude d'impulsion fournie par l'un des détecteurs, ceci pour un nombre total de fissions dans ^{252}Cf égal à 46 000. L'auteur a déduit la vitesse des fragments, les masses initiales et les énergies initiales de la manière habituelle à partir des résultats de la méthode du temps de vol.

Il a déterminé la fonction d'étalonnage du détecteur d'après la corrélation entre les amplitudes d'impulsion enregistrées et les paramètres finals des fragments correspondants. Il a déduit ces paramètres de la masse initiale, de l'énergie initiale et des valeurs publiées de $\bar{\nu}(m, E_K)$ pour les fragments du californium. Enfin, il a corrigé la fonction d'étalonnage pour tenir compte des dispersions dues aux appareils et de la variation de l'énergie moyenne selon la masse du fragment.

Il a obtenu les paramètres après émission de neutrons à partir des données enregistrées, en utilisant les méthodes utilisables d'étalonnage des détecteurs, y compris celle indiquée plus haut. Il a calculé le nombre moyen de neutrons émis en fonction de la masse du fragment à partir de la différence, événement par événement, des masses initiale et finale. Ce résultat lui a fourni la preuve de la validité de la méthode

* Work performed under the auspices of the United States Atomic Energy Commission.

proposée et des divers procédés d'étalonnage. L'accord avec les données publiées était bon pour la méthode d'étalonnage fondée sur ces données et pour une méthode dérivée de la réponse des détecteurs à semiconducteurs sous l'action d'ions brome et iode accélérés. Dans chaque cas, l'écart moyen quadratique par rapport aux valeurs publiées de $\bar{\nu}$ était inférieur à 0,7 neutron.

ОДНОВРЕМЕННЫЕ ИЗМЕРЕНИЯ СКОРОСТИ И ЭНЕРГИИ ОСКОЛКОВ ДЕЛЕНИЯ. Полупроводниковые детекторы использовались в двускоростных приборах для одновременного измерения скоростей осколков деления и амплитуд импульсов детекторов. Задача этих измерений состояла в том, чтобы 1) прокалибровать эти детекторы по зависимости амплитуды импульсов от энергии осколков деления и 2) оценить метод одновременного измерения параметров процесса деления до и после испускания нейтронов путем совпадающего измерения скоростей и энергий осколков. Быстрые и медленные выходные сигналы из детекторов использовались для измерения соответственно времени пролета и высоте импульсов. Зарегистрированные данные представляют собой время пролета осколков и высоту импульса, полученные с помощью одного из детекторов для 46 000 актов деления калифорния-252. Скорости осколков, начальные массы и начальные энергии были получены обычным путем по данным о времени пролета.

Калибровочная функция детектора была определена в результате корреляции между зарегистрированными амплитудами импульсов и окончательными параметрами соответствующих осколков. Последние величины были получены по начальным массам, начальным энергиям и опубликованным величинам $\bar{\nu}(m, E_K)$ для осколков калифорния. И, наконец, в калибровочную функцию была внесена поправка на приборное рассеяние и зависимость средней энергии от масс осколков.

Параметры процессов деления после испускания нейтронов были получены на основании зарегистрированных данных и с помощью известных методов калибровки детекторов, включая описанный выше. Средние количества испускаемых нейтронов как функция масс осколков были получены по разницам начальных и окончательных масс следующих друг за другом явлений. Полученный результат является проверкой пригодности этого предлагаемого метода и различных методов калибровки. Было обнаружено, что опубликованные данные согласуются с методом калибровки, основанным на этих данных, и с методом, разработанным на основании реакции полупроводниковых детекторов на ускоренные ионы брома и иода. В каждом случае среднеквадратическое отклонение от опубликованных значений $\bar{\nu}$ было меньше 0,7 нейтрона.

MEDICION SIMULTANEA DE LA VELOCIDAD Y DE LA ENERGIA DE LOS FRAGMENTOS DE FISION. El autor ha utilizado detectores de semiconductores en un aparato de dos velocidades a fin de medir simultáneamente las velocidades de los fragmentos y las amplitudes de impulsos en los detectores. El objeto de estas mediciones era: a) determinar la razón amplitud de impulso/energía calibrada de estos detectores para los fragmentos de fisión, y b) evaluar las posibilidades técnicas de la determinación simultánea de los parámetros de la emisión de fragmentos anterior y subsiguiente a la emisión neutrónica, en el proceso de fisión, partiendo de una medición coincidente de las velocidades y energías de los fragmentos. El autor obtuvo de los detectores señales de salida lentas y rápidas que utilizó en las mediciones de tiempo de vuelo y de amplitud de impulso, respectivamente. Los datos registrados fueron los de los tiempos de vuelo de los dos fragmentos de fisión y la amplitud del impulso obtenida de uno de los detectores, para un total de 46 000 fisiones del ^{252}Cf. Las velocidades de los fragmentos, así como las masas y energías iniciales, se determinaron de la manera usual partiendo de los datos relativos a los tiempos de vuelo.

La función de calibración de los detectores se determinó tomando como base la relación existente entre las amplitudes registradas de los impulsos y los parámetros finales de los fragmentos correspondientes. Los valores de éstos se obtuvieron de la masa y de la energía iniciales y de los valores publicados de $\bar{\nu}(m, E_K)$ para los fragmentos de Cf. Por último el autor corrigió la función de calibración para tener en cuenta las dispersiones debidas a los instrumentos y la variación de la energía media en función de la masa de los fragmentos.

Los parámetros de la emisión de fragmentos posterior a la emisión neutrónica se obtuvieron de los datos registrados y de los procedimientos disponibles de calibración de los detectores, incluido el anteriormente descrito. El número medio de neutrones emitidos en función de la masa de los fragmentos se determinó partiendo de las diferencias entre las masas inicial y final correspondientes a cada fisión. Este resultado constituye una prueba sensible de la validez de la técnica propuesta y de los diversos procedimientos de calibración. El autor comprobó que los resultados obtenidos con el procedimiento de calibración basado en estos datos y el derivado de la respuesta de los detectors de semiconductores a iones acelerados de yodo y de bromo

concordaban con los datos publicados. En uno y otro caso, la desviación cuadrática media respecto de los valores publicados de $\bar{\nu}$ fue inferior a 0,7 neutrones.

INTRODUCTION

The development of semiconductor detectors has made possible the simultaneous determination of the salient pre- and post-neutron emission parameters of the fission process. These detectors provide good pulse-height resolution together with a fast response time, and therefore exhibit the two characteristics required for a coincident measurement of fission-fragment velocities and energies. Such measurements, however, are sensitive to the absolute pulse-height-to-energy calibration of these detectors. Previous measurements with accelerated bromine and iodine ions [1] have shown that the response of these detectors is dependent on the mass of the incident ion. Fortunately detailed information in regard to this detector calibration can be obtained from a coincident measurement of the velocities of the fragment pairs and the pulse-height response of the semiconductor detector to Cf^{252} fragments. In this case the dependence of $\bar{\nu}(M, E_K)$, the average number of neutrons emitted from each fragment as a function of fragment mass, M, and total kinetic energy, E_K, of the fission event is known [2]. For each fragment incident on the detector, the initial (before neutron emission) mass and energy of the fragment as well as the total kinetic energy of the event may be found from the velocities of the fragment pairs. The corresponding final (after neutron emission) mass and energy of the incident fragment then may be obtained from these initial values and the function $\bar{\nu}(M, E_K)$. Thus it appears possible with the same apparatus to obtain not only the proper pulse-height-to-energy calibration for a particular semiconductor detector for incident Cf^{252} fission fragments but also the initial and final parameters of other fissioning systems.

The purposes of this paper are to describe the apparatus developed for the simultaneous measurement of fragment velocities and detector pulse heights, and to present results obtained with a spontaneous fission source of Cf^{252}. These data have been analysed to obtain an approximate pulse-height-to-energy calibration for the particular detector used. In addition the same data have been analysed using the above calibration and the one derived from the response of semiconductor detectors to accelerate bromine and iodine ions [3]. Some of the interesting initial and final distributions are presented and, in particular, the dependence of $\bar{\nu}$ on fragment mass obtained from both calibration procedures is given. The degree of similarity between these results and published values [2, 4] is considered to be a sensitive test of the accuracy of this method.

APPARATUS

A block diagram of the apparatus used in this measurement is shown in Fig. 1, where the two surface barrier detectors (Oak Ridge Technical Enterprises Corp., Oak Ridge, Tenn.), with sensitive areas of 300 mm^2 masked to 200 mm^2 and 950 mm^2, are shown in the "remote" configuration. The

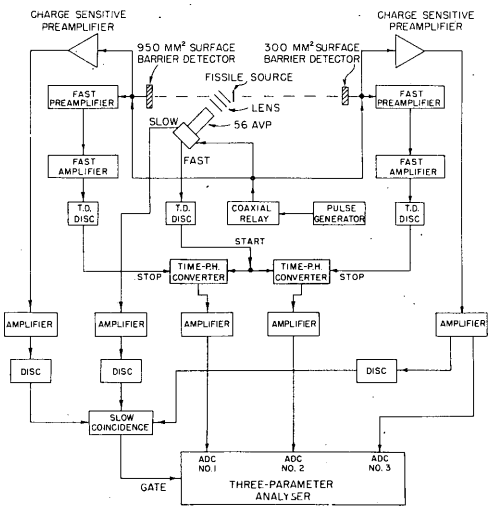

Fig. 1

Block diagram of the apparatus used in the simultaneous measurement of fission-fragment velocities and detector pulse height. Position and orientation of the surface barrier detectors were changed for the zero-time measurements.

Abbreviations are : T.D. Disc = tunnel diode discriminator; ADC = analogue-to-digital converter.

Cf^{252} source that was mounted on a thin (0.1 mg/cm^2) nickel backing was placed between the two detectors with the fissile deposit facing the smaller detector. The time-zero signal was obtained from an electron detector [5] consisting of an electron lens, a 0.002-in-thick plastic scintillator and a 56-AVP photomultiplier. One of the fragments from each of the detected pairs traversed the source backing and another thin nickel foil (0.1 mg/cm^2) mounted on the first element of the lens, and continued to the larger remote detector. Electrons ejected from the second nickel foil by the emerging fragments were accelerated and focused to the scintillator that was glued to the photomultiplier face. The distance between the source and the centre of this tilted foil was 3.3 cm. In addition to the fast, time-zero signal obtained from the anode, a slow signal was obtained from the ninth dynode of the photomultiplier for use in establishing a triple coincidence between the three fragment detectors.

Both a linear signal, related to the fragment energy, and a fast pulse were obtained from each of the surface barrier detectors by means of parallel capacitive coupling. To provide the fastest possible rise time, the detectors were mounted directly on the input of a fast, low impedance preamplifier which was placed inside the evacuated flight tube. This preamplifier consisted of the first stage of a nanosecond pulse amplifier designed by LUNSFORD [6]. After amplification by the remainder of this amplifier, which was located outside but adjacent to the evacuated system, the fast pulses were fed to a special tunnel diode discriminator that had an avalanche transistor output. This output pulse provided the stop signal for the time-to-pulse-height converter [7]. Start signals for both converters were obtained from the electron detector and a similar tunnel diode discrimi-

nator. Linear signals from the surface barrier detectors were fed first to conventional charge sensitive preamplifiers and then to Cosmic amplifiers, discriminators and a coincidence circuit (Cosmic Radiation Labs., Inc., Bellport, N.Y.). Time-of-flight and pulse-height data were recorded on paper tape by means of a 400-channel, three-parameter pulse-height analyser.

A precision pulser and time-controlled coaxial relay were also included in this system for stability tests and calibration purposes. Signals from this pulser were periodically introduced into the system by means of decoupling circuits at the output of each fragment detector. Both the amplitudes and time separation of these pulses were adjusted to provide a pulser peak in the upper portion of each of the recorded distributions. These fictitious events were easily identified and removed from the fission data in subsequent analysis.

A set of Styroflex (Phelphs Dodge Electronic Products Corp., North Haven, Conn.) delay cables was used to determine the absolute time-calibration of this system. Pulse delay times of these coaxial cables were measured to an accuracy of ± 0.1 ns by a technique similar to one previously described [8].

SYSTEM PERFORMANCE

Before the correlated data were accumulated, the energy and time resolution of this system were investigated. For the first of these measurements, the 300 mm^2, 950 Ωcm surface barrier detector was operated on the plateau of the pulse-height versus bias curve with ~290 pF capacitance. With the fast-timing system connected and operating, the measured energy resolution for U^{233} and Pu^{239} alpha particles was less than 200 keV full-width at half maximum (FWHM). Previous measurements [1] with accelerated bromine and iodine ions (artificial fission fragments) have shown that the resolution of these detectors is approximately 1-2 MeV (FWHM). Since the present width is negligible compared to the inherent energy resolution of these detectors for fission fragments, the energy data of this experiment are insignificantly affected by the addition of the fast timing circuit.

The time resolution of this system was obtained from a comparison of the measured and intrinsic time spectra for a flight path of ~8 cm. To obtain the intrinsic spectrum, the time scale of published data [9], taken with a 182.5-cm flight path and 3.5-ns time resolution, was corrected so as to correspond to this shorter distance. An example of this comparison for the 300-mm^2 detector mounted on the electron-detector side of the source is shown in Fig. 2. In this case the time resolution was estimated to have been 0.6 ± 0.1 ns (FWHM) and the "time walk" of the heavy fragment group was less than 0.2 ns.

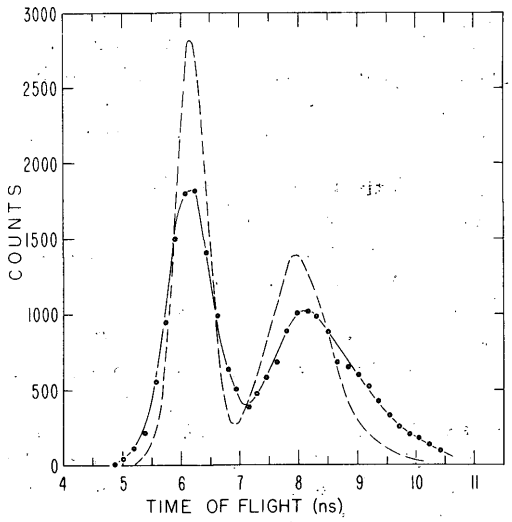

Fig. 2

Time spectrum obtained with a 300-mm², 950-Ωcm surface barrier detector located on the electron-detector side of the apparatus. Flight path was 8 cm. The intrinsic time spectrum (dashed curve) was from Ref. [9].

DATA ACQUISITION AND ANALYSIS

Zero-time measurements

The response of each timing system for a nearly zero fragment flight time was determined by positioning the surface barrier detectors a distance of 8 cm from the electron detector or source. The time spectrum for fragments incident on the smaller surface barrier detector located on the electron detector side of the source is shown in Fig. 3a. Figure 3b is the time distribution of the complementary fragments incident on the other detector. Similar measurements were made with the positions of the detectors interchanged. These results provided an estimate of the time resolution of the two timing systems as well as the required zero-time values. The latter were obtained from the average values of the peaks and an extrapolation to zero flight paths. Measured time resolutions were 0.6 ns and 1.5 ns for the timing system associated with the smaller and larger detectors respectively.

Correlated velocity and pulse-height measurement

The data recorded were the outputs of the two time-to-pulse-height converters and the pulse height from the smaller surface barrier detector for 46 000 Cf^{252} fission events. For these measurements the detector orientation shown in Fig. 1 was used. The smaller detector faced the Cf^{252} deposit with a flight path of 59.7 cm and the larger detector was positioned

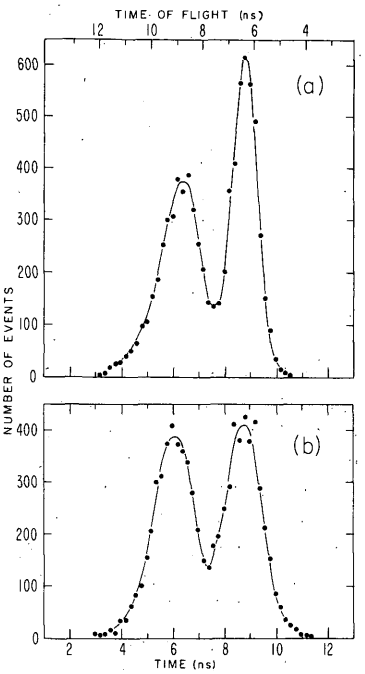

Fig. 3

Time spectra from one of the zero-time measurements. The smaller detector was on the electron-detector side with 8.4-cm flight path and the larger detector was 7.4 cm from the source. Parts (a) and (b) refer to time spectra obtained from timing circuits associated with the smaller and larger detectors respectively.

at a distance of 37.3 cm from the centre of the nickel foil mounted on the electron lens. Thus the flight times and pulse heights obtained from the smaller detector were those associated with unslowed fragments. Velocity loss corrections were however required for the complementary fragments that were incident on the other detector and slowed by the two nickel foils. These corrections were obtained from the data of WHETSTONE [10] and the assumption of a linear dependence of velocity loss on foil thickness; they were 5.5 and 6.2% for the light and heavy fragments respectively.

Velocities of the fragment pairs were obtained from the recorded data, zero-time values and the flight paths. Since the neutron-emission time of about 10^{-14} s [11] is small compared with the fragment flight times in this experiment of 30 to 50 ns, the measured quantities were the velocities after neutron emission. It has been shown [2], however, that the neutron angular distribution is approximately isotropic in the centre-of-mass system of the fragment. Therefore on the average fission fragment velocities are essentially unchanged by neutron emission. Thus the measured final velocities were considered to be the fragment velocities before neutron emission, with an increased velocity dispersion for each prompt neutron emitted in addition to the instrumental dispersion. Since the dispersions associated with these quantities are unequal, it will be useful to distinguish between all pre- and

post-neutron-emission parameters with capital and lower case symbols respectively. Conservation of momentum and mass number yield the relations between the initial masses and velocities of the two fragments: $M_1 V_1 = M_2 V_2$ and $M_1 + M_2 = M$, where M is the mass number of the fissioning nucleus. The initial mass and energy of each fragment incident on the smaller surface barrier detector are given by $M_1 = M/(1+V_1/V_2)$ and $E_1 = M_1 V_1^2/2$. Similar equations yield the energy of the complementary fragment, E_2, and the total kinetic energy of the event, E_K, is given by $E_K = E_1 + E_2$.

Detector calibration

To obtain the pulse-height-to-energy calibration of this detector for final fragments the published [2] dependence of $\bar{\nu}(M_1, E_K)$ on initial mass and total kinetic energy for Cf^{252} was used. For each fragment incident on the detector the final mass and energy were obtained from the relations $m_1 = M_1 - \bar{\nu}(M_1, E_K)M_n$, where M_n (neutron mass) is taken to be unity, and $\epsilon_1 = m_1 v_1^2/2$. These values together with the recorded pulse height, P_1, were used to obtain the average pulse height for various final masses and energies. These results, uncorrected for dispersions and the finite width of the mass and energy intervals (2.7 units), are shown in Fig. 4. The data indicate a linear dependence of pulse height on energy for fragments of constant mass, and are well represented by a family of nearly parallel straight lines in the pulse-height, energy plane. Slopes and intercepts of the lines shown were obtained by a least-squares fit of the observed data. In a manner previously described [12], these values were corrected for dispersions and the dependence of the average energy on fragment mass. The corrected slopes and energy intercepts when plotted versus fragment mass are consistent with a calibration function represented by a nearly constant slope and an intercept increasing linearly with mass of the form $\epsilon = (a_1 + a_2 m) P + (b_1 + b_2 m)$ proposed by SCHMITT et al. [3].

Corrected slopes and intercepts for the masses 99.1 and 147.7 were used to obtain the four constants in this expression. Energies corresponding to the average pulse heights of the light and heavy groups were then found for these two fragment masses. In this determination the average pulse heights were obtained from a least-squares fit of two Gaussian distributions to the observed pulse-height spectrum. The energies so determined were as follows:
$E_L(147.7) = 112.47$ MeV; $E_H(147.7) = 81.20$ MeV; $E_L(99.1) = 103.40$ MeV; $E_H(99.1) = 72.74$ MeV.

Post-neutron emission parameters

With a given detector calibration, the present data may be analysed to obtain the final masses and energies of the fragments incident on the smaller detector. These values were found for each fission event by a solution of the following equations: $\epsilon_1 = m_1 v_1^2/2$ and $\epsilon_1 = (a_1 + a_2 m_1) P_1 + b_1 + b_2 m_1$. In addition the mass differences were obtained for each event, $\nu_1 = (M_1 - m_1)/M_n$ and the average value of ν was found as a function of initial mass, $\bar{\nu}(M)$. For

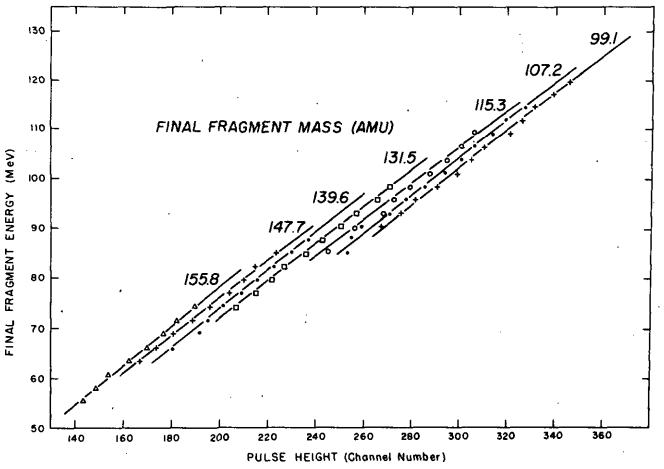

Fig. 4

Energy versus pulse-height relation of the smaller surface barrier detector for final fragments. Lines represent least-squares fits to a linear function for selected fragment masses.

this analysis the detector calibration described by SCHMITT et al.[3] and the one given in the previous section were used.

RESULTS AND DISCUSSION

A pulse-height-to-energy calibration based on the response of semiconductor detectors to accelerated bromine and iodine ions [3] was used to obtain the post-neutron-emission parameters. Initial and final energy distributions of the fragments incident on the smaller detector are shown in Fig. 5. The distortion of the energy spectrum by neutron emission is evident. Also shown is the increased energy shift of the light fragments, which is consistent with the larger energy per nucleon of these fragments. This feature has been discussed previously by TERRELL [4].

Shown in the lower part of Fig. 6 are the initial and final mass distributions of fragments incident on the smaller detector. As is evident from the relative areas of the two peaks in the initial distribution, the light and heavy fragments were recorded with slightly different efficiencies. This small difference, which is presumably caused by preferential scattering of the heavier fragments in the nickel foils, is of little consequence. Here these distributions represent the same fission data analysed by different procedures. The initial mass distribution exhibits most of the known deviations [10] from a smooth curve and a hint of another near mass pair 95-157. This discontinuity corresponds to the weak structure at mass 156 reported by FRASER et al. [13] for $U^{235}+n$ and Cf^{252} and also by THOMAS and VANDENBOSCH [14] for $U^{235}+n$, $U^{233}+n$, $Pu^{239}+n$. These investigators have shown that the perturbations of the mass yield curve are related to the even-odd structure of the mass surface, which results in a larger energy release for even-even products than for odd-odd fragments. Consequently

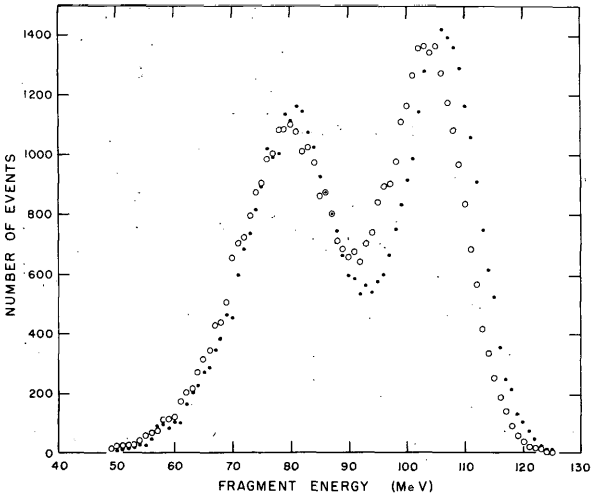

Fig. 5

The observed energy distribution. Solid circles represent the initial energy spectrum obtained from the time-of-flight data. Open circles are the final energy spectrum obtained from these data and the detector calibration of Ref. [3].

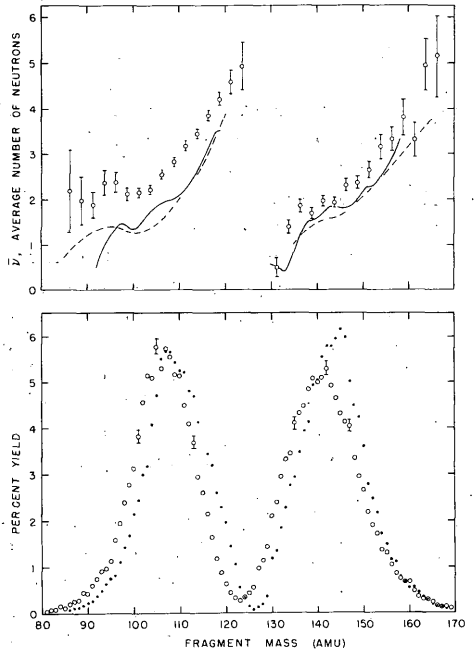

Fig. 6

Mass distributions and average number of neutrons $\bar{\nu}(M)$. Detector calibration was from Ref. [3].

the even-even fragments may share a larger excitation energy than the odd-odd products. Corresponding discontinuities are reflected in the displaced, final mass distribution in most instances.

The average number of neutrons emitted as a function of fragment mass, $\bar{\nu}(M)$, is shown in the upper part of Fig. 6. Included for comparison are the results of BOWMAN et al. [2] (dashed line) and TERRELL [4] (solid line) for Cf^{252}. The general saw-tooth dependence of $\bar{\nu}$ on mass is well reproduced in these results. Although the present values are high in the region of the light fragments, they indicate a possible peak of the neutron yield near mass 95, a levelling-off in the mass region 135 to 145 and a dip at mass 132 in general agreement with previous determinations. The root-mean-square deviation of these results from published values [4] is less than 0.7 of a neutron.

Calibration based on fission data

The detector calibration given above was also used with these data. A final energy distribution with characteristics similar to the one shown in Fig. 5 was obtained.

Shown in the lower part of Fig. 7 is the final mass distribution obtained with this calibration. For comparison the same initial mass distribution derived from the velocity measurements is repeated. Although they are less pronounced, discontinuities are observed in the final distribution that reflect the preferred yields in the initial mass distribution.

Values of $\bar{\nu}(M)$ in the upper part of Fig. 7 exhibit the same general trends as the previous results, but are in better agreement with the published data. This better agreement is undoubtedly caused by the additional constraints placed on the $\bar{\nu}$ values at the masses (99.1 and 147.7) selected for this calibration procedure. An enhanced neutron yield in the vicinity of mass 95, a levelling-off in the region of masses 135 to 145 and a dip at mass 133 are again evident in these results obtained with this different detector calibration.

CONCLUSIONS

The crucial item in the extension of the double-velocity technique to determine the post-neutron-emission parameters as well as the initial quantities appears to be the pulse-height-to-energy calibration of the surface barrier detectors. Further studies with a variety of fissioning nuclei will be required to obtain a sufficiently accurate universal calibration procedure that would allow the precise determination of the absolute values of $\bar{\nu}(M)$. The creditability of the calibration given above must still be established for fragments of widely different masses and energies from those encountered in this measurement.

In the absence of this universal function, however, it is possible by means of this technique to obtain useful and interesting information regarding the qualitative features of the post-neutron-emission parameters of the fission process. With the aid of constraints on $\bar{\nu}(M)$, obtained from measured or calculated values of the total number of neutrons emitted either

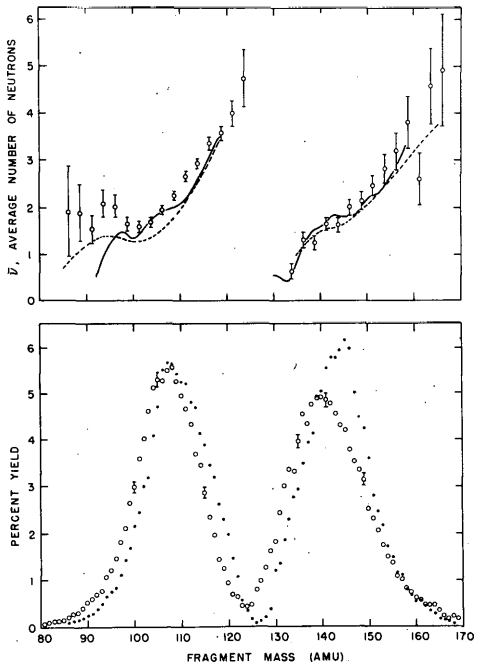

Fig. 7

Mass distributions and average number of neutrons $\bar{\nu}(M)$.
Detector calibration was as described in the text.

as a function of mass ratio or averaged over-all fission modes, it should be possible to obtain final parameters and $\bar{\nu}(M)$ values as accurate as those given in this work for fission at low, moderate or high excitation energies of the compound nucleus.

A possible correlation exists in these results between the enhanced neutron yield and the irregularities of the initial mass distribution. This may be an indication of the energetically favoured even-even fragments sharing a larger than normal excitation energy.

ACKNOWLEDGEMENTS

The author is especially grateful to S.G. Thompson and his co-workers for the Cf^{252} source, and to H.C. Britt for his help and interest during the initial stages of this work. It is a pleasure to acknowledge the contributions made by J.S. Lunsford and N.A. Lindsay in the development of the fast-timing techniques used in this experiment, by E.L. Cooperman in the preparation of computer programmes, by J. Terrell in many discussions and by K.H. Harper in the preparation of this manuscript.

REFERENCES

[1] SCHMITT, H.W., WALTER, F.J., NEILER, J.H., MOAK, C.D., GIBSON, W.M. and THOMAS, T.D., ORNL Physics Division Annual Rpt., ORNL-3425 (1963).
[2] BOWMAN, H.R., MILTON, J.C.D., THOMPSON, S.G. and SWIATECKI, W.J., Phys. Rev. 129 (1963) 2133.
[3] SCHMITT, H.W., KIKER, W.E. and WILLIAMS, C.W., Phys. Rev. (in press).
[4] TERRELL, J., Phys. Rev. 127 (1962) 880.
[5] STEIN, W.E. and LEACHMAN, R.B., Rev. sci. Instrum. 27 (1956) 1049.
[6] LUNSFORD, J.S., Rev. sci. Instrum. 35 (1964) 1483.
[7] WEBER, W., JOHNSTONE, C.W. and CRANBERG, L., Rev. sci. Instrum. 27 (1956) 166.
[8] McALEER, H.T., Electronics (13 Jan. 1961) 102.
[9] MILTON, J.C.D. and FRASER, J.S., Phys. Rev. 111 (1958) 877.
[10] WHETSTONE, S.L., Phys. Rev. 131 (1963) 1232.
[11] FRASER, J.S., Phys. Rev. 88 (1952) 536.
[12] STEIN, W.E. and WHETSTONE, S.L., Jr., Phys. Rev. 110 (1958) 476.
[13] FRASER, J.S., MILTON, J.C.D., BOWMAN, H.R. and THOMPSON, S.G., Canad. J. Phys. 41 (1963) 2080.
[14] THOMAS, T.D. and VANDENBOSCH, R., Phys. Rev. 133 (1964) B976.

EXPERIMENTS WITH MASS-SPECTROSCOPICALLY SEPARATED FISSION PRODUCT IONS

H. EWALD, E. KONECNY AND H. OPOWER
II. PHYSIKALISCHES INSTITUT DER JUSTUS LIEBIG-UNIVERSITÄT GIESSEN AND PHYSIK-DEPARTMENT DER TECHNISCHEN HOCHSCHULE MÜNCHEN, MUNICH, FEDERAL REPUBLIC OF GERMANY

Abstract — Résumé — Аннотация — Resumen

EXPERIMENTS WITH MASS-SPECTROSCOPICALLY SEPARATED FISSION PRODUCT IONS. After a short description of the fission product mass spectrograph installed at the reactor at Garching (Munich) a survey is given of the experiments done with it. Some of these concern the interaction of the swift separated fission product ions with matter. Exact distributions of ion charge numbers were obtained for particles having almost their initial kinetic energies and for those slowed down more or less in thin foils. Their multiple scattering in such foils was also measured. It is hoped that in addition their single scattering on gas atoms can be examined. The energy losses in foils will be studied exactly. The pulse-height defects observed in counting fission particles with surface barrier counters were measured extensively.

Other experiments are concerned with features of the fission process and decays of the fission products. In nuclear emulsions the number of β-particle tracks emerging from the ends of the tracks of fission particles of definite mass numbers were counted. From the distributions of these numbers conclusions can be drawn on the distributions of the initial nuclear charges in the decay chains. In addition to this the β-decays of the particles of definite mass numbers are examined directly with a 4π counter. The distributions of the initial kinetic energies of the particles of different mass numbers are also studied. The possibility is discussed of measuring in coincidence, with the help of two such spectrographs, both particles of the fission processes travelling in opposite directions. It might also be of advantage to use a mass spectrograph in connection with a large accelerator to study the products of spallation and fragmentation processes.

For experiments on the interaction of fission particles with matter the intensity of our spectrograph is sufficient in most cases. In studies of the fission process and the β decays often a much higher rate of separated particles would be desired. Therefore plans have been made for a new spectrograph, which when installed at a larger reactor will give us intensities larger by a factor of about 100 compared to the present one. This will probably be a second-order focusing parabola spectrograph.

EXPÉRIENCES AVEC DES IONS PRODUITS PAR FISSION ET SÉPARÉS PAR SPECTROMÉTRIE DE MASSE. Après une courte description du spectromètre de masse pour produits de fission installé près du réacteur de Garching (Munich), l'auteur relate les expériences effectuées avec cet appareil. Certaines d'entre elles concernent l'interaction des ions produits par fission et séparés immédiatement avec la matière. Il a obtenu la distribution exacte des nombres de charge pour les particules ayant une énergie cinétique proche de l'énergie initiale et pour celles qui sont plus ou moins ralenties par des feuilles minces. L'auteur a mesuré également leur diffusion multiple dans ces feuilles. Il espère qu'en plus il pourra examiner leur diffusion simple sur les atomes de gaz. Il étudie avec une grande exactitude les pertes d'énergie dans les feuilles. Il a mesuré avec soin les défauts d'amplitude qu'il a observés dans le comptage des particules de fission avec des compteurs à barrière de surface.

D'autres expériences portent sur les caractéristiques du processus de fission et la désintégration des produits de cette fission. Les nombres des traces β qui, dans une émulsion nucléaire, prennent naissance à l'extrémité des traces des particules de fission de nombre de masse donné ont été comptés. A partir de la distribution de ces nombres, l'auteur peut tirer des conclusions sur la distribution des charges nucléaires initiales dans les séries radioactives. En plus, il a observé directement la décroissance β des particules d'un nombre de masse donné, avec un compteur 4π. Il étudie aussi la distribution des énergies cinétiques initiales des particules ayant des nombres de masse différents. Il examine la possibilité de mesurer par coïncidence les deux particules, produites par une fission, qui se déplacent dans des directions opposées, en utilisant deux spectrographes. Il serait peut-être également avantageux d'utiliser un spectrographe de masse et un grand accélérateur, afin d'étudier les produits de spallation et de fragmentation.

Pour les expériences sur l'interaction des particules de fission avec la matière, l'intensité du spectrographe de Garching est suffisante dans la plupart des cas. Dans les études sur la fission et la décroissance β, il faudrait bien souvent une proportion beaucoup plus élevée de particules séparées. Aussi, l'auteur-a-t-il étudié un nouveau spectrographe qui, installé près d'un réacteur plus grand, permettrait d'obtenir des intensités environ 100 fois plus élevées que le spectrographe actuel. La meilleure solution serait probablement un spectrographe à parabole focalisante du second ordre.

ЭКСПЕРИМЕНТЫ С РАЗДЕЛЕННЫМИ МАСС-СПЕКТРОСКОПИЧЕСКИМ ПУТЕМ ИОНАМИ, ЯВЛЯЮЩИМИСЯ ПРОДУКТАМИ ДЕЛЕНИЯ. После краткого описания спектрографа для измерения масс продуктов деления, установленного на реакторе в Гарчинге (Мюнхен), дается описание экспериментов, выполненных с его помощью. Некоторые из этих экспериментов были проведены по взаимодействию быстро разделенных ионов, являющихся продуктами деления, с веществом. Были получены точные распределения зарядов ионов для частиц, имеющих почти начальные кинетические энергии, и для частиц, которые были более или менее замедлены в тонких фольгах. Было также измерено их многократное рассеяние на таких фольгах. Есть надежда, что, помимо этого, может быть также изучено их однократное рассеяние на атомах газа. Будут точно изучены потери энергии в фольгах. Были тщательно изучены дефекты амплитуд импульсов, которые были замечены при счете частиц деления с помощью счетчиков с поверхностными полупроводниковыми барьерами.

Другие эксперименты связаны с характеристиками процессов деления и с распадом продуктов деления. В ядерных эмульсиях было подсчитано количество следов β-частиц, выходящих из концов следов частиц деления с определенными массовыми числами. На основании распределения этих чисел можно сделать вывод о распределении начальных ядерных зарядов в цепочках распада. Кроме того, с помощью 4π-счетчика изучаются β-распады частиц с определенными массовыми числами. Исследуются также распределения начальных кинетических энергий частиц с различными массовыми числами. Рассматривается возможность проведения измерений при совпадении обеих частиц процесса деления, движущихся в противоположных направлениях, с помощью двух таких спектрографов. Возможно, будет полезно использовать масс-спектрограф на крупном ускорителе для изучения продуктов расщепления и взрывов ядер.

Для экспериментов по взаимодействию частиц деления с веществом в большинстве случаев достаточно интенсивности нашего спектрографа. При изучении процессов деления β-распадов часто может потребоваться значительно более высокая скорость разделенных частиц. Поэтому разрабатываются планы нового спектрографа, который, будучи установленным на более крупном реакторе, даст нам интенсивности, превышающие примерно в 100 раз интенсивности существующего спектрографа. Возможно, это будет спектрограф с фокусировкой по параболе второго порядка.

EXPERIMENTOS CON IONES DE PRODUCTOS DE FISION SEPARADOS POR ESPECTROSCOPIA DE MASAS. Después de una breve descripción del espectrógrafo de masas para separar productos de fisión instalado junto al reactor de Garching (Munich), la memoria describe panorámicamente los experimentos que se han realizado con ese aparato. Algunos están relacionados con la interacción con la materia de los iones de los productos de fisión separados rápidamente. Se han obtenido las distribuciones exactas de las cargas iónicas de las partículas que prácticamente conservan toda su energía cinética inicial y de otras frenadas en grado variable mediante láminas delgadas. También se midió su dispersión múltiple en esas láminas. Se espera poder examinar además su dispersión simple por átomos gaseosos. Las pérdidas de energía en las láminas se estudiarán con la mayor precisión posible. Se han medido los defectos de amplitud de impulso observados al contar partículas de fisión con contadores de barrera superficial.

Otros experimentos tratan de las características de los procesos de fisión y de la desintegración de los productos de ésta. Se contó el número de trazas de partículas beta que se observan en emulsiones nucleares en el extremo de las trazas de fragmentos de fisión de número másico definido. De la distribución del número de trazas beta puede deducirse la distribución de las cargas nucleareas iniciales en las cadenas de desintegración. Además, se examinan directamente con un contador 4π las desintegraciones beta de los fragmentos de determinados números másicos. Asimismo se estudian las distribuciones de las energías cinéticas iniciales de partículas de números másicos distintos. Se discute la posibilidad de medir con dos espectrógrafos de esta índole montados en coincidencia las dos partículas emitidas en sentidos opuestos durante el proceso de fisión. También podría ofrecer ventajas el empleo de un espectrógrafo de masas en relación con un acelerador grande para estudiar los productos formados por espalación y fragmentación.

En la mayoría de los casos, la intensidad observada en cada canal del espectrógrafo empleado basta para los experimentos sobre la interacción de las partículas de fisión con la materia, pero al estudiar los procesos de fisión y las desintegraciones beta sería con frecuencia deseable poder separar las partículas a un ritmo mucho más rápido. Por tanto, se está estudiando un espectrógrafo que, instalado en un reactor de mayor potencia, dará intensidades aproximadamente 100 veces más elevadas que el actual. Probablemente se tratará de un espectrógrafo de parábola de enfoque de segundo orden.

THE FISSION PARTICLE MASS SPECTROMETER AT GARCHING AND ITS SPECTRA

Details of the fission particle mass spectrometer (FPMS) [1, 2] at Garching may be seen from Fig. 1. This is a schematic drawing of the whole arrangement in which the transversal dimensions are enlarged to give a better understanding of the paths of the particles.

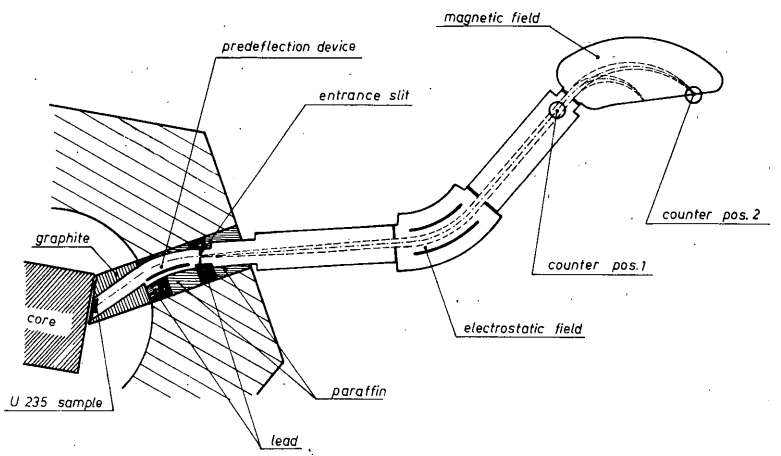

Fig. 1

Schematic view of the complete arrangement of the mass spectrograph

In an evacuated beam tube a thin sheet of U^{235} is located in the high neutron flux near the core of the reactor. The fission products come out of the sheet in all directions with high initial kinetic energies of about 50 to 110 MeV and a distribution of ionic charge numbers between about 18 to 25. Those fission products travelling approximately in the direction of the beam tube are sent through the electric and magnetic fields of the mass spectrograph and are separated there in a mass spectrum. The time-of-flight of the particles through the spectrograph, and therefore the separation time, is of the order of 10^{-6} s. The field combination used is of the Mattauch-Herzog type giving radial angle and energy focusing for all masses at the place of the straight exit boundary of the magnetic field. To obtain a higher particle density in the mass lines the cylinder condenser commonly used in such an apparatus is replaced by a toroidal one. In this manner an ad-

ditional, axial focusing is achieved in the direction of the magnetic field lines (stigmatic imaging).

The deflection angles of the particles in the electric and the magnetic fields are $\phi_e = 29.5°$ and $\phi_m = 90°$; the mean radii of curvature of the trajectories of the particles in the fields are $a_e = 234$ cm and $a_m = 92$ cm. The separation of the electrodes of the electric field is 8 cm, and the separation of the pole shoe faces of the magnetic field is 7 cm. Deflection voltages of 200 - 300 kV and magnetic field strengths up to 8000 Oe are used. The full lengths of the paths of the particles in the apparatus is about 17 m.

The deflection of particles of such high kinetic energies in fields of such dimensions and strengths is possible only because of the high ionic charges with which they leave the thin sheets. In reality the spectrograph separates the particles with respect to their ratios M/e (M = mass number, e = charge number). Because of the above-mentioned broad distribution of the charge numbers of the particles several mass spectra are correspondingly displaced and partly overlap each other. But by working with an entrance slit 6 mm in width and a resolution of about 400 we have been able to obtain many M/e-lines of the heavy fission particles group well separated from each other.

The fission particles coming from the thin uranium sheet undergo an electric predeflection of about 10° inside the reactor beam tube. This predeflection is necessary for reasons of radiation shielding. The fission particles are bent out of the neutron and γ-rays coming directly from the core. Just behind the predeflection electrode the entrance slit of the mass spectrograph is arranged. This predeflection device is so effective that almost no other shielding of the apparatus is necessary apart from the concrete shielding of the reactor.

To detect particles separated in the mass lines, nuclear emulsions, scintillation counters and solid-state surface barrier counters are used. Figure 2 shows a spectrum of fission particles of the heavy group recorded on Ilford KO nuclear plates with a total length of about 20 cm. The dots in the curve give the numbers N of fission particle tracks counted under the

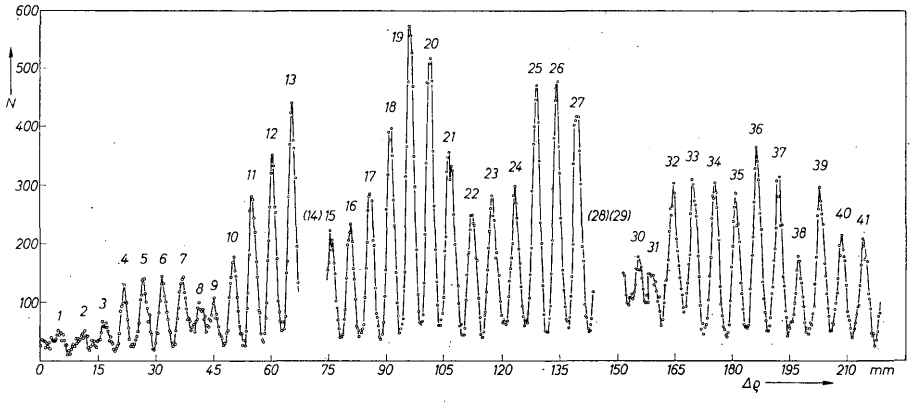

Fig. 2

Spectrum of separated fission particles of the heavy group recorded on nuclear plates. The field strength in the toroidal condenser used for this spectrum was 28.3 kV/cm.

microscope in strips on the plates that have a width of 0.1 mm, a length of 2 cm parallel to the direction of the mass lines, and which are 0.3 mm apart from each other. The exposure time of these plates was 90 min. The intensities of the lines show a characteristic periodicity.

The lines of this spectrum are provided with arbitrary numbers. The mass numbers M, effective mass numbers M/e and charge numbers e of these lines can be taken by comparison from Fig. 3, which is a calculated

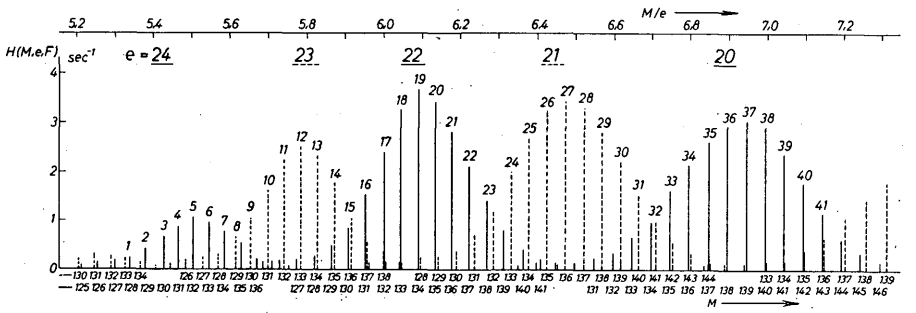

Fig. 3

Calculated spectrum of the heavy fission particle group.
H(M, e, F) is the expected intensity of the lines in particles per second,
F = 28.3 kV/cm the field strength in the toroidal condenser.

spectrum of the same lines denoted by the same numbers. The expected positions and relative intensities of the lines of Fig. 3 are derived for the same electric field strength as was used for the experimental spectrum of Fig. 2 from the known abundance distributions of ionic charge numbers, mass numbers and energies E of the fission particles. In this calculation it is taken into account that the electric field of the spectrograph acts as a E/e-selector letting through only particles of a narrow range of E/e-values of a relative width of 1.3%. The correlation between Figs. 2 and 3 was made very probable by an examination of the relative distances and intensities of the lines in both figures. In this examination use was made of the fact that the mass yield curve for fission products has a strong fine structure at mass number 134.

It is to be seen from Fig. 3 that in the case of particles of the heavy fission particle group the lines of definite charge numbers form humps that are only moderately overlapped by the lines of particles of neighbouring charge numbers. Consequently the most abundant lines in each hump are almost free from overlapping by lines of neighbouring ionic charge states. After calculations have been made of analogous spectra for the particles of the light fission particle group, in this case the relative shift of the humps of lines of neighbouring charge states is much smaller so that quite a heavier overlapping takes place. Thus for the lines of the light particle group a higher resolution would be needed in order to obtain many M/e-lines almost free from overlapping. This difference in behaviour of the light and heavy particle groups results from the fact that particles of neighbouring charge numbers e and e+1 passing the diaphragms between the electric and magnetic field have energies E and E_1 differing by about 5% (related by the

equation $E/e = E_1/e+1$, e being about 20), and from the fact that the mean total energy of the most abundant fission processes decreases for increasing ratio M_H/M_L of the masses of the simultaneously created heavy and light particles.

The intensities of the separated particles are such that about three particles per second reach the places where there are the most abundant lines. That means that about 10^4 particles are sampled per hour in such lines. This is in accordance with estimates taking into account the thickness of the U^{235} sheet, the neutron flux of the reactor, the neutron capture cross-section, the small solid angle defined by the entrance slit, the other diaphragms and the dimensions of the whole arrangement, and considering that the spectrograph selects only a small interval of E/e-values.

EXPERIMENTS WITH THE FPMS

Experiments carried out with the FPMS or that are in preparation or discussion will be described. Some of these experiments are concerned with features of the fission process and decays of the fission products, others with the interaction of the swift separated fission product ions with matter.

1. The calculated spectrum of Fig.3 is based on diagrams of the distributions of masses and energies of the fission products resulting from time-of-flight measurements. These diagrams correspond to the distributions of the primary fission products before evaporation of the prompt neutrons. For this and other reasons they do not exhibit fine structures in the fission product yields. Such fine structures, however, are shown up by radiochemical and mass spectroscopical measurements that are related to fission products that have already lost their prompt neutrons. The same applies to fission products separated in our spectrograph. Therefore by exactly comparing the relative intensities of the corresponding lines of the measured and calculated spectra of Figs. 2 and 3 one is able to examine the fine structures of the fission yields. The result of a preliminary trial is shown in Fig. 4, which shows relative fission yields derived from time-of-flight measurements, radiochemical and mass spectrometric measurements, and from our own data. The fine structure at mass number 134 is clearly demonstrated also from our measurements. Similar and more exact determinations of fine structures of the fission products will be undertaken.

2. Extended examinations of the relative yields and radioactive decays in the chains at different mass numbers can be made. For instance, we have sampled in some cases particles of definite mass lines and then measured their β-decays. The results are still preliminary, but they will be useful in confirming the given assignments of mass numbers to the observed lines. They will possibly give us also more information on the half-lives and the relative fission yields within the chains. But the success of such measurements will probably be limited because the number of particles per line that can be sampled in reasonable times is too small with the present spectrograph (of the order of 10^4 h). These experiments are being continued in a reciprocal manner measuring the building up of the β-activity of particles of definite mass numbers while they are sampled in a 4π-counter.

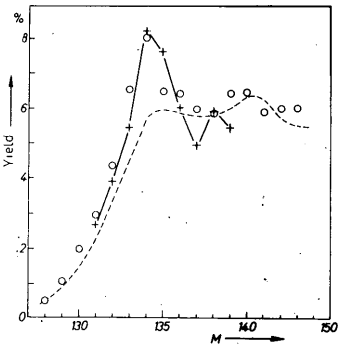

Fig. 4

Relative fission yields [2] derived from our measurements (+++) compared with results from radiochemical measurements (WALKER, ooo) and time-of-flight measurements (MILTON and FRASER, - - -)

A method of examining the distributions of the initial nuclear charges within the different decay chains, which is working quite well, has been presented in detail in this Symposium.[1] Fission products of definite mass numbers are sampled under a flat angle in Ilford G5 nuclear emulsions. These plates are developed ten or more hours after the exposures to give the fission particles time to undergo most of their β-decays. Then the number of β-particles coming from the ends of the different fission particle tracks are counted under the microscope. The distribution of the number of β-tracks per fission event taken over 1000 or more events can be transformed to 4π-geometry and corrected for lost β-particles of long half-lives. From these statistics a direct conclusion can be drawn on the relative abundances of the initial nuclear charges within the chain under examination. In all cases the atomic numbers Z of the stable end products of the chains are known. In the resulting corrected statistics the particles showing no β-tracks correspond to these end products. They have the initial charge Z after evaporation of the prompt neutrons. The particles whose tracks show one β-track are separated with initial nuclear charges Z-1, and so on. This seems to be a laborious but helpful way to study the lengths of the chains and their relative yields.

3. The intensities of the different lines can be measured for a number of values of the deflection voltage. From these we can obtain exact distributions of the kinetic energies of particles of the different decay chains and look for peculiarities between these distributions. By the use of a solid-state counter and a multichannel analyser discriminations of the results by overlapping lines of particles from other charge numbers can be eliminated. By using G5 emulsions and the method of counting the distributions of β-tracks emerging from the ends of the fission tracks explained above, the energy distributions will be obtained separately for each component of the decay chain.

---

[1] KONECNY, E., OPOWER, H., GUNTHER, H. and GÖBEL, H., "Primary distributions of nuclear charge for fission-fragment masses 132, 134, 136 and 137 from thermal fission of U^{235}", these Proceedings I.

4. Plans have been prepared to carry out coincidence experiments using two such spectrographs connected to both ends of a through-going reactor beam tube. In this manner both particles of single fission events could be measured in coincidence giving us an optimum of information about the fission process. Details of the fine structures of the energies and the evaporations of prompt neutrons from the fission products can be expected from such measurements. The uranium in this case will be deposited on a thin foil, and mounted in the beam tube in the neighbourhood of the core with its plane vertical to the axis of the tube. The coincidence rates will be fairly good because the angles between the two particles of the events resulting from the evaporation of the prompt neutrons and the multiple scattering in the foils are only about 1°. The radial and axial angles of divergence of the particles that can be used in the spectrographs are about the same size. Using spectrographs of the Garching type coincidence rates of a few per minute could be expected. These rates could be enlarged by the help of focusing parabola spectrographs (see below) because in these E/e-intervals in the particles of about 5 to 10% are usable. They may be further increased by putting detectors on the parabolas of all the different charge states of the mass numbers in question in one experiment.

5. A short discussion only will be given on the possibility that such a spectrograph may be used advantageously also for the analysis of the spectra of spallation and fragmentation particles emerging from thin foils struck by ions of high kinetic energy from an accelerator. The ion current to the effective areas of the foils in such experiments will be comparable to the current of slow neutrons to the uranium sheet in our present measurements. The smaller cross-sections of the spallation and fragmentation reactions compared to the neutron capture cross-section leading to the fission process will be counter-balanced more or less by the fact that the spallation and fragmentation particles will emerge predominantly in the forward direction.

6. Extended studies were undertaken of the distributions of the ionic charge states of the fission products coming from the thin uranium sheet [3]. For this purpose a surface barrier counter is placed in front of the magnetic field (position 1 in Fig. 1) and connected to a 1024 channel analyser. As the electric field is an E/e-analyser we obtain for each value of the field strength a series of discrete equidistant values for the energy of the particles that have passed through the condenser to the detector corresponding to their different charge numbers. Figure 5 shows such an energy spectrum. It is easy to assign charge numbers to the observed peaks by examining their displacements connected with the changes of the deflection voltage.

The results of a larger number of such measurements using different deflection voltages in the condenser allow us to obtain the distributions of the charge numbers of fission particles of definite kinetic energies. Examples of two such distributions are given in Fig. 6 for particles of 64 and 95 MeV. For each such curve we can calculate the mean charge number belonging to the particle energy in question. The dependence of these mean values on the energies of the particles is drawn in Fig. 7. The left straight part of the curve belongs to the heavy fission particle group, the right part to the light group. The charge numbers increase with the energies. The left and right straight parts of the curve are shifted against each other by about

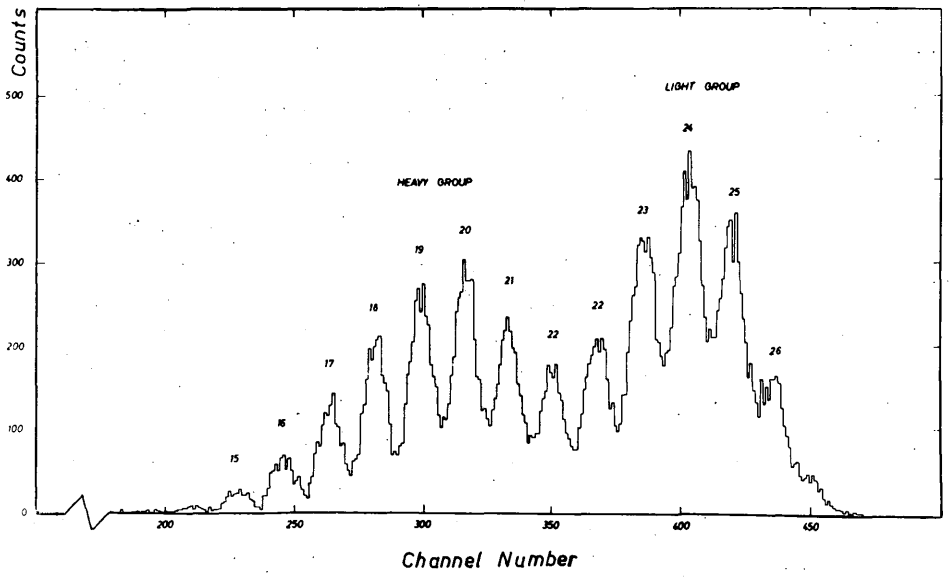

Fig. 5

Energy spectrum of fission particles that have passed the toroidal condenser measured by a solid-state counter. The field strength used had such a value that particles of the light and heavy group contributed to the spectrum.

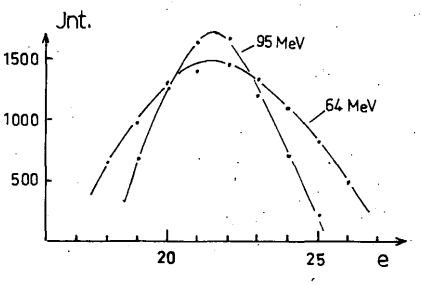

Fig. 6

The distributions of the charge numbers of the particles emerging with energies of 64 and 95 MeV from the thin uranium sheet

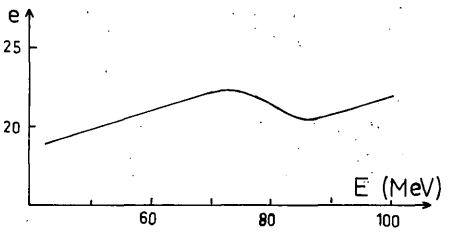

Fig. 7

The energy dependence of the mean values of the ionic charge of the fission particles emerging from the thin uranium sheet

4 charge units. Analogous curves have been obtained for particles that were more or less slowed down in Formvar foils of different thickness. They extend to smaller charge numbers, as is seen in Fig. 8. In this case the predeflection voltage was adjusted to two different values so that only either

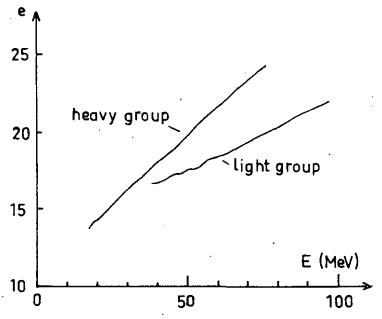

Fig. 8

The energy dependence of the mean values of the ionic charge of fission particles more or less slowed down in Formvar foils

particles of the light group or of the heavy group entered the entrance slit. The results of these measurements can be compared to theoretical considerations of N. Bohr and others on the equilibrium ionic charges of fission particles traversing thin sheets of solid material.

7. In the experiments described above the charge numbers of the particles of the different peaks (e.g. in Fig. 5) followed from the shifts of these peaks observed when the deflecting field strength in the condenser was charged by known relative amounts. The effective field strengths were calibrated by placing a thin polonium-α-source at the entrance slit and measuring the 5.3-MeV α-particles of this source with the electric field and the solid-state counter as is done with the fission particles. Assuming a fixed value of the radius of curvature of the mean path of the particles in the electric field, and knowing the exact values of the effective deflection field strengths in the fission particle measurements, one is able to calculate exactly the energies E of the particles belonging to the observed peaks of the different known charge numbers.

The surface barrier counter connected to the multiple channel analyser was calibrated also by the use of Po-α-rays assuming a linear response to the energy of the α-particles and the absence of any pulse-height defects. However, such pulse-height defects are effective as is shown when such a counter is used for fission particles. Thus from multiple channel spectra as given in Fig. 5 we can deduce energy values E^* of the peaks that are smaller by certain amounts than the real energies E, the evaluation of which is indicated above. The differences $E - E^*$ give us values for the pulse-height defects of the counter for the different fission particle energies E.

If the counter is placed to the rear of an exit slit behind the magnetic field (position 2 in Fig. 1) to measure particles of definite masses the results can be extended to give us also the mass dependence of the pulse-height defects [4]. The results of such measurements for two different counters

are shown in Fig. 9, revealing quite a steep increase in the defects in the mass range of the fission products.

8. The multiple scattering of fission particles of definite energies and mass numbers in thin foils have been studied using narrow axial diaphragms

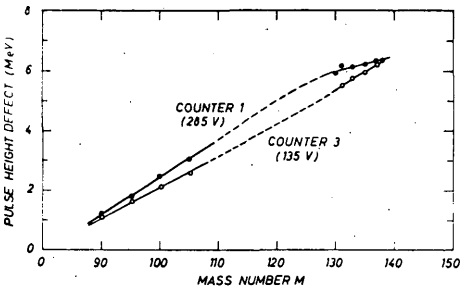

Fig. 9

The mass dependence of the pulse-height defects of two different solid-state counters for fission particles

between the fields and at the exit slit. The foils are located just behind the exit slit and the scattered particles are caught in nuclear plates 30 cm behind the foils. The plates have not yet been evaluated. The results will be compared to other experiments on the multiple scattering of heavy ions and to existing theories. In principle also the single scattering of fission particles on gas atoms could be measured in a similar manner.

9. The energy losses of fission particles of definite masses in traversing thin sheets of solid material will be examined thoroughly. For this purpose a time-of-flight device will be connected to the exit side of the spectrograph.

PLANS FOR THE CONSTRUCTION OF A SECOND FPMS

For the experiments on the interaction of fission particles with matter the intensity of our spectrograph is sufficient in most cases. But in the studies of the fission process and the β-decays often a much higher rate of separated particles would be desired. Therefore plans have been drawn up for a new spectrograph, which when installed at a larger reactor will give us intensities larger by a factor of about 100 compared to the present one. This new apparatus will be a focusing parabola spectrograph [5] consisting of a homogeneous magnetic sector field and an electric cylinder field. Both fields are arranged at a short distance behind each other, their mean planes of deflection being vertical to each other. The field combination focuses in both directions of deflection at the same distance behind it, there giving rise to sharp mass parabolas. Resolutions of 1000 and more are easy to obtain. The apparatus will be corrected for second order aberrations, fringing field effects included; such calculations have been performed during the past year [6, 7]. One advantage of such a parabola spectrograph is that the particles traverse first the magnetic and then the electric field. Thus

the necessity of the predeflection device probably can be avoided. Neutrons and γ-rays coming together with the fission particles from the core of the reactor can pass the magnetic field without touching the pole shoes and can be caught in a beam catcher behind this field while the fission particles are bent out of these rays in the magnetic field. Another advantage of the parabola spectrograph is that large parts of the energy distributions of the fission products can pass the fields and be focused in the parabolas.

ACKNOWLEDGEMENTS

The experiments have been performed together with H. Rösler, H. Gunther, G. Siegert, H. Göbel, K. Hetwer, Dr. H. Wollnik and others.

REFERENCES

[1] EWALD, H., KONECNY, E., OPOWER, H. and RÖSLER, H., Z. Naturf. 19a (1964) 194.
[2] KONECNY, E., OPOWER, H. and EWALD, H., Z. Naturf. 19a (1964) 200.
[3] OPOWER, H., KONECNY, E. and SIEGERT, G., Z. Naturf. 20a (1965) 131.
[4] KONECNY, E. and HETWER, K. (in preparation).
[5] NEUMANN, S. and EWALD, H., Z. Phys. 169 (1962) 224.
[6] WOLLNIK, H., Nucl. Instrum. Meth. (in press).
[7] WOLLNIK, H. and EWALD, H., Nucl. Instrum. Meth. (in press).

CORRELATED FRAGMENT ENERGY MEASUREMENTS AND MASS-VERSUS-ANGLE CORRELATIONS IN Ra^{226} + p FISSION*

H. W. SCHMITT, J. W. T. DABBS AND P. D. MILLER
OAK RIDGE NATIONAL LABORATORY, OAK RIDGE, TENN., UNITED STATES OF AMERICA

Abstract — Résumé — Аннотация — Resumen

CORRELATED FRAGMENT ENERGY MEASUREMENTS AND MASS-VERSUS-ANGLE CORRELATIONS IN Ra^{226} + p FISSION. Correlated energies of fragment pairs from the proton-induced fission of Ra^{226} were measured using protons obtained from the Oak Ridge tandem Van de Graaff accelerator at energies E_p = 11.0, 12.0 and 13.5 MeV. Corresponding excitation energies in Ac^{227} are 16.3, 17.3 and 18.8 MeV respectively. Detailed kinematic calculations from these data have provided mass distributions, kinetic energy distributions and mass versus energy correlations. At E_p = 13.5 MeV, such determinations were made at angles of 30°, 40°, 60° and 90° with respect to the incident proton beam; the resulting mass distributions and kinetics have been investigated in detail as a function of angle.

The mass distribution for Ra^{226} + p fission has long been known to be triple-peaked; in the present experiment, for θ = 90°, the ratio ρ of fragment abundance at the symmetric peak to that at the asymmetric peak was found to increase from 1.11 for 11.0-MeV protons to 1.27 for 12.0-MeV protons and to 1.54 for 13.5-MeV protons. For all three proton energies, the average total fragment kinetic energy as a function of mass, $E_K(M)$, remains constant at ~143 MeV through much of the symmetric peak. $E_K(M)$ then increases for increasing asymmetry and reaches a maximum of ~152 MeV at $M_H \cong 134$ amu (two mass units lower than the peak in the asymmetric mass yield). The maximum in $E_K(M)$ is attributed to the closure of the Z = 50 and N = 82 shells in this range of heavy-fragment masses, as in the case of spontaneous and thermal-neutron-induced fission. The results of detailed analyses are given.

Comparison of the ~50 000-event mass distributions obtained at the four fragment angles indicated above, for E_p = 13.5 MeV, shows that the mass distribution does vary with angle. The effect is not large: preliminary analyses indicate a monotonic increase in the ratio ρ from ~1.46 for θ = 30° to ~1.54 for θ = 90°, which is well outside statistical and experimental uncertainties. The direction of the observed effect is in agreement with that expected from arguments based on the reduced excitation energy for p,n-fission and p,2n-fission, and the consequent increase in the 0°/90° ratio for asymmetric fragments. A more complete analysis is in progress to determine the quantitative validity of such arguments.

MESURES DES ÉNERGIES DES FRAGMENTS EN CORRÉLATION, ET CORRÉLATIONS MASSE-ANGLE DANS LA FISSION DE ^{226}Ra PAR DES PROTONS. Les auteurs mesurent les énergies en corrélation de paires de fragments provenant de la fission de ^{226}Ra par des protons fournis par l'accélérateur Van de Graaff tandem d'Oak Ridge à des énergies E_p = 11,0, 12,0 et 13,5 MeV. Les énergies d'excitation correspondantes pour ^{227}Ac sont respectivement de 16,3, 17,3 et 18,8 MeV. Des calculs détaillés de cinématique fondés sur ces données permettent d'obtenir la distribution des masses, la distribution des énergies cinétiques et la corrélation masse-énergie. Pour E_p = 13,5 MeV, ces déterminations ont été faites à des angles de 30°, 40°, 60° et 90° par rapport au faisceau de protons incident; les distributions de masse et la cinétique qui en résultent sont étudiées en détail en fonction de l'angle.

On sait depuis longtemps que la distribution des masses pour la fission ^{226}Ra + p se caractérise par une courbe à trois pics; dans l'expérience actuelle, pour θ = 90°, le rapport ρ de l'abondance des fragments au pic symétrique à cette même abondance au pic asymétrique passe de 1,11 pour les protons de 11,0 MeV à 1,27 pour les protons de 12,0 MeV et à 1,54 pour les protons de 13,5 MeV. Pour ces trois énergies de protons, l'énergie cinétique totale moyenne des fragments en fonction de la masse, $E_K(M)$, reste constante à une valeur voisine de 143 MeV pour la plus grande partie du pic symétrique. $E_K(M)$ croît alors lorsque l'asymétrie

* Research sponsored by the United States Atomic Energy Commission under contract with the Union Carbide Corporation.

augmente et atteint un maximum d'environ 152 MeV lorsque $M_H \cong 134$ uma (deux unités de masse de moins que le pic du rendement asymétrique selon la masse). Le maximum de $E_K(M)$ est attribué à la saturation des couches pour Z = 50 et N = 82 dans cette gamme de masses de fragments lourds, comme dans le cas de la fission spontanée et de la fission par neutrons thermiques. Les auteurs donnent le résultat des analyses détaillées.

La comparaison des distributions de masses au voisinage de 50 000 événements obtenues pour les quatre angles indiqués plus haut dans le cas où l'énergie des protons est de 13,5 MeV montre que la distribution des masses ne varie pas avec l'angle. L'effet n'est pas important: les analyses préliminaires indiquent une augmentation monotone du rapport ρ qui passe d'environ 1,46 pour $\theta = 30°$ à environ 1,54 pour $\theta = 90°$, résultat nettement en dehors de la marge d'incertitude statistique et expérimentale. La direction de l'effet observé concorde avec celle à laquelle on s'attend d'après des arguments fondés sur l'énergie d'excitation réduite pour la fission (p,n) et la fission (p,2n) et l'augmentation correspondante du rapport 0°/90° pour les fragments asymétriques. Les auteurs ont entrepris une analyse plus complète pour déterminer la validité quantitative de ces arguments.

ИЗМЕРЕНИЯ КОРРЕЛЯЦИИ ЭНЕРГИИ ОСКОЛКОВ И КОРРЕЛЯЦИИ МАССЫ И УГЛА ПРИ ДЕЛЕНИИ Ra^{226} +p. Корреляций энергий пар осколков деления радия-226, вызванного протонами, были измерены с помощью протонов, полученных на Окриджском тандемном ускорителе Ван де Граафа при энергиях E_p = 11,0; 12,0 и 13,5 Мэв. Соответствующие энергии возбуждения в актинии-227 составляли соответственно 16,3; 17,3 и 18,8 Мэв. Подробные кинематические расчеты, основанные на этих данных, позволили получить распределения масс, распределения кинетических энергий и корреляции масс и энергий. При E_p = 13,5 Мэв такие расчеты падающего пучка протонов производились при углах 30, 40, 60 и 90°; полученные в результате этого распределения масс и кинетика были подробно исследованы как функция угла.

Давно известно, что распределение масс для деления радия-226+p имеет три пика; в данном эксперименте было обнаружено, что для $\theta = 90°$ отношение ρ распространенности осколков при симметричном пике к распространенности осколков при асимметричном пике возрастает с 1,11 для протонов с энергией 11,0 Мэв до 1,27 для протонов с энергией 12,0 Мэв и до 1,54 для протонов с энергией 13,5 Мэв. Для всех этих трех энергий средняя общая кинетическая энергия осколков как функция массы $E_K(M)$ остается постоянной при ~143 Мэв в большой части симметричного пика. Затем $E_K(M)$ увеличивается для возрастающей асимметрии и достигает максимума ~152 Мэв при $M_H \cong 134$ аем (на две единицы массы ниже, чем пик при асимметричном выходе масс). Максимум при $E_K(M)$ объясняется заполнением оболочек Z = 50 и N = 82 в этом диапазоне масс тяжелых осколков, как и в случае спонтанного деления и деления, вызванного тепловыми нейтронами. Приводятся результаты подробного анализа.

Сравнение распределения масс примерно для 50 000 явлений при четырех вышеуказанных углах движения осколков для E_p = 13,5 Мэв показывает, что распределение масс меняется в зависимости от угла. Этот эффект является небольшим: предварительный анализ показывает монотонное увеличение отношения ρ с ~1,46 для $\theta = 30°$ до ~1,54 для $\theta = 90°$, что находится далеко за пределами статистических и экспериментальных неопределенностей. Направление наблюдаемого эффекта согласуется с тем направлением, которое ожидалось, исходя из аргументов, основанных на пониженной энергии возбуждения для p, n-деления и p, 2n-деления и последующем увеличении отношения 0°/90° для асимметричных осколков. В настоящее время проводится более подробный анализ для определения количественной справедливости таких аргументов.

MEDICION DE ENERGIAS CORRELACIONADAS DE LOS FRAGMENTOS Y CORRELACIONES MASA-ANGULO EN LA FISION DEL ^{226}Ra INDUCIDA POR PROTONES. Se han medido las energías correlacionadas de pares de fragmentos resultantes de la fisión del ^{226}Ra, inducida por protones procedentes del acelerador Van de Graaff en tándem de Oak Ridge a energías E_p = 11,0, 12,0 y 13,5 MeV. Las correspondientes energías de excitación en el ^{227}Ac son 16,3, 17,3 y 18,8 MeV, respectivamente. Mediante cálculos cinemáticos detallados basados en esos datos, se han obtenido distribuciones de la masa y de la energía cinética, así como correlaciones masa-energía. Para E_p = 13,5 MeV, estas determinaciones se han efectuado a ángulos de 30°, 40°, 60° y 90° respecto del haz protónico incidente; las distribuciones de masa y la cinética resultante se han investigado detalladamente en función del ángulo.

Desde hace tiempo se sabe que en la fisión del ^{226}Ra inducida por protones, la curva de distribución másica presenta tres picos; en el presente experimento, para $\theta = 90°$, se comprobó que la razón ρ de la abun-

dancia de fragmentos en el pico simétrico a la abundancia de fragmentos en el pico asimétrico pasa de 1,11, para protones de 11,0 MeV, a 1,27 para protones de 12,0 MeV, y a 1,54, para protones de 13,5 MeV. Para estas tres energías protónicas, la energía cinética total media de los fragmentos, expresada en función de la masa $E_K(M)$, presenta un valor constante de ~143 MeV, en gran parte del pico simétrico. Seguidamente, $E_K(M)$ aumenta con la asimetría, hasta alcanzar un máximo de ~152 MeV para $M_H \cong 134$ uma (esto es, dos unidades de masa menos que el pico en el rendimiento asimétrico). El máximo en $E_K(M)$ se atribuye al cierre de las capas Z = 50 y N = 82 en este intervalo de masa de fragmentos pesados, como en el caso de la fisión espontánea y de la inducida por neutrones térmicos. Los autores indican los resultados de análisis detallados.

La comparación de las distribuciones de masa en unos 50 000 sucesos, obtenidas en los cuatro ángulos de fragmentación indicados anteriormente, para E_p = 13,5 MeV, muestra que la distribución de la masa varía realmente con el ángulo. El efecto no es muy acusado: los análisis iniciales indican un aumento monótono de la razón ρ de ~1,46 para $\theta = 30°$, a ~1,54 para $\theta = 90°$, valor que de todos modos rebasa el margen de indeterminación estadístico y experimental. La dirección del efecto observado coincide con la prevista fundándose en la disminución de la energía de excitación para la fisión p, n y la fisión p, 2n, y el consiguiente aumento de la razón 0°/90° para fragmentos asimétricos. Los autores proceden a un análisis más completo con miras a determinar en qué medida estos argumentos poseen valor cuantitativo.

INTRODUCTION

The charged-particle-induced fission of Ra^{226} exhibits unique and interesting features. In particular, the fragment mass distribution for proton-induced fission of Ra^{226} was found by JENSEN and FAIRHALL [1] to contain three distinct peaks. Since the discovery of this "anomalous" mass distribution, radiochemical measurements for Ra^{226} fission have been extended to include mass distribution studies of deuteron- and helium-ion-induced fission [2], angular distribution measurements [3] and yield measurements for a few nuclei over a wider range of incident proton energies [4]. More recently a number of kinetic experiments have been carried out for deuteron-induced [5] and helium-ion-induced [5, 6] fission of Ra^{226}; total fragment angular distribution measurements for proton-, deuteron-, and helium-ion-induced fission of Ra^{226} have also been reported [7].

It has seemed especially appropriate to us to study also in detail the kinetics of proton-induced fission of Ra^{226}; in this case the excitation energy of the compound nucleus (Ac^{227}) is sufficiently low so that the probability for second-chance (p, nf) fission is much reduced in comparison with that for first-chance (p, f) fission. Thus the kinetic energies, mass distributions, etc. should be characteristic of first-chance fission principally and, in addition, a search for any appreciable correlation between the mass distribution and angle of emission of the fragments might be meaningful.

In the present work, detailed fragment energy correlation measurements were carried out for fragments emitted at a centre-of-mass angle θ=90° with respect to the incident proton beam, for proton energies E_p = 11.0, 12.0 and 13.5 MeV. In our search for a mass-angle correlation, similar measurements were carried out for E_p = 13.5 MeV, at angles θ = 30°, 40°, 60° and 90°.

EXPERIMENTAL METHOD

A schematic diagram of the experimental arrangement is shown in Fig. 1 together with a block diagram of the electronic equipment. The target con-

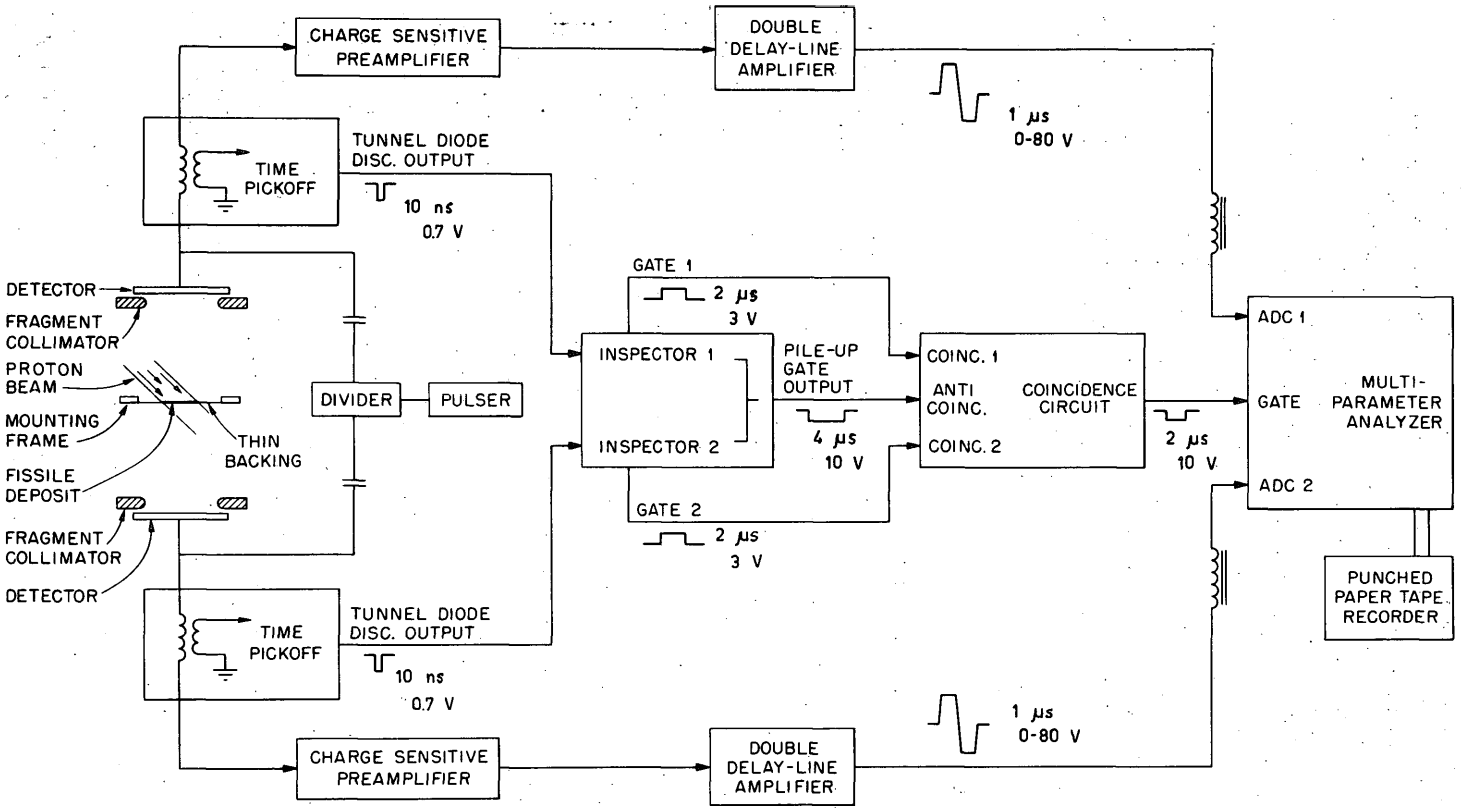

Fig. 1

Schematic diagram of source and detector arrangement, and block diagram of electronic equipment

sisted of a 1-cm diam. vacuum-evaporated deposit of radium bromide about 20 μg per cm^2 thick on a 2.5-cm diam. carbon backing film about 20 μg per cm^2 thick. The proton beam was focused and collimated to a diameter of less than ~5 mm.

Rounded collimators were used in front of the silicon detectors as shown in Fig. 1 to minimize low-energy tailing effects in the fragment pulse-height and energy spectra. The surface barrier detectors were operated in the saturation region of the pulse-height versus applied bias curve. The absolute energy calibration of the detectors was accomplished with reference to Cf^{252} spontaneous-fission-fragment spectra by the method previously developed and described in Refs. [8,9].

The linear circuitry indicated in Fig. 1 is self-explanatory. All units were connected into the system throughout the runs; periodic checks of stability and linearity of the system were made with the pulser. The function of the inspector circuit was to reject pile-up pulses, i.e. pulses resulting from the near superposition of a fission-fragment pulse with an accidental scattered-proton or natural alpha-particle pulse. Pairs of pulses in either detector whose time separations were in the range from 20 ns to 2 μs were detected by the inspector circuit, and the anti-coincidence signals generated in such cases served to reject these events. When no pile-up occurred, the two coincident fission-fragment pulse heights (channel numbers) were recorded event-by-event on punched paper tape; the data were sorted, summed and otherwise processed by means of a digital computer.

EXPERIMENTAL RESULTS

The two-parameter data array is given by $N(x_1, x_2)$, where N is the number of counts appearing in the combination of channel numbers x_1 and x_2 corresponding to detectors 1 and 2 respectively. This array was transformed to an array given by $N(\mu_1, E_K)$ where E_K is the measured total kinetic energy and μ_1 is a "mass" of the fragment detected in detector 1. For fragments emitted at centre-of-mass angle $\theta = 90°$ with respect to the beam, the quantity μ_1 is calculated from the data with the assumption of linear momentum conservation applied to the measured fragment energies E_1 and E_2 ; the relationships among the various quantities are then

$$\mu_1 E_1 = \mu_2 E_2 \tag{1}$$

$$\mu_1 + \mu_2 = A \tag{2}$$

$$E_1 + E_2 = E_K \tag{3}$$

where A is the mass of the fissioning nucleus (in the present case 227 amu). The average total kinetic energy $\langle E_K \rangle$ as a function of μ_1 and the "mass" distribution $N(\mu_1)$ were obtained directly from the array $N(\mu_1, E_K)$. For fragment angles other than 90° the data were processed in the same manner; then additional transformations of the final functions were carried out to correct for the centre-of-mass motion.

We have chosen to use the symbols μ_1 and μ_2 to distinguish these "masses" from the actual pre-neutron-emission masses m_1^* and m_2^* (*denotes highly

excited or neutron-rich nuclei) and post-neutron-emission masses m_1 and m_2. In practice the μ_i do not differ greatly ($\lesssim 2$ amu) from the m_i^*, inasmuch as both fragments emit neutrons and the error is to some extent cancelled by the use of the measured, post-neutron-emission energies in Eq. (1). We have not included neutron-emission corrections in the results reported here. Such corrections would change slightly the shape of the mass distributions; the total pre-neutron-emission kinetic energies E_K^* would be larger than the values of E_K reported here by an amount (up to a few percent) that takes into account the mass changes of the fragments in neutron emission.

A summary of the results for proton energy $E_p = 13.5$ MeV, for fragments emitted at a mean centre of mass angle $\theta = 90°$ with respect to the beam, is shown in Fig. 2. A similar summary of results for $E_p = 11.0$ MeV,

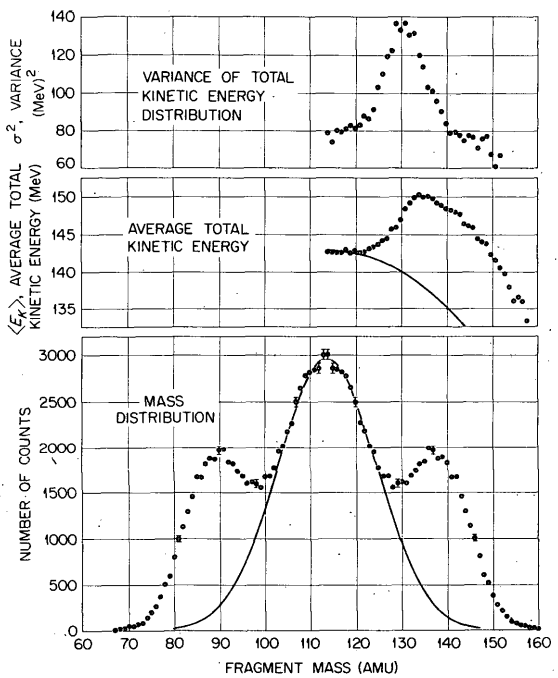

Fig. 2

Summary of results for proton-induced fission of Ra^{226}, $E_p = 13.5$ MeV, $\Theta = 90°$.
No corrections for neutron emission have been included.
The solid curves are calculated (see text for discussion).

$\theta = 90°$ is given in Fig. 3. In the lowest part of each figure the mass distribution $N(\mu)$ is shown; the average total fragment kinetic energy $\langle E_K \rangle$ as a function of μ is shown in the centre portion of each figure, and the variance σ^2 of the total kinetic energy distribution for a given μ is shown as a function of μ in the uppermost position of each figure. The mass distributions are triple-peaked, as expected from previous studies [1, 2, 5, 6] of proton-, deuteron-, and alpha-induced fission of Ra^{226}. The average total kinetic energy is seen to reach a maximum in the region where the heavy-fragment mass is ~134 amu, slightly above the masses where the $Z = 50$ and $N = 82$

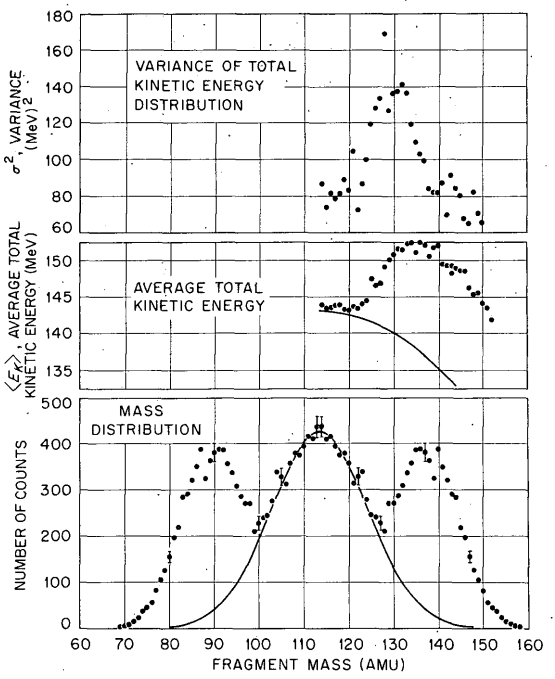

Fig. 3

Summary of results for proton-induced fission of Ra^{226}, $E_p = 11.0$ MeV. No corrections for neutron emission have been included. The solid curves are calculated (see text for discussion).

shells close. Maximum values of $\langle E_K \rangle$ in the region of Z = 50 or N = 82 nuclei have been observed for many cases of both intermediate and low excitation fission. The variance of the kinetic energy distribution as a function of mass appears to be nearly the same in the region of symmetric fission and very asymmetric fission, but peaks quite strongly in the region of $\mu \sim$ 130 amu. Various features of these and related curves will be discussed further in the following section.

In Fig. 4 we have plotted the mass distributions for the three different proton energies: 11.0, 12.0 and 13.5 MeV. All these distributions were obtained at $\theta = 90°$. For ease of comparison we have drawn only the smooth curves through the points and normalized the distributions at the asymmetric peak. The ratio ρ of fragment abundance at the symmetric peak to that at the asymmetric peak is seen to increase from 1.11 for 11.0 MeV protons to 1.27 for 12.0 MeV protons and to 1.54 for 13.5 MeV protons. The total increase in fragment yield at the symmetric peak relative to that at the asymmetric peak, i.e. the increase in ρ, is thus about 40% for the proton energy increase from 11.0 to 13.5 MeV.

In our search for a possible correlation between fragment mass and angular distribution, mass distributions were obtained at centre-of-mass angles $\theta = 30°, 40°, 60°$ and $90°$, for $E_p = 13.5$ MeV. The ratio ρ was determined for each of these angles and is plotted in Fig. 5 as a function of θ. An

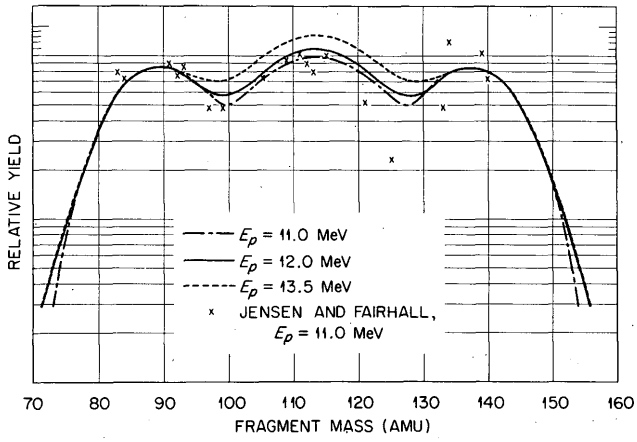

Fig. 4

Comparison of fragment mass distributions observed in proton-induced fission of Ra^{226} for $E_p = 11.0$, 12.0 and 13.5 MeV. Smooth curves were drawn through the data points and are shown normalized at the asymmetric peak.

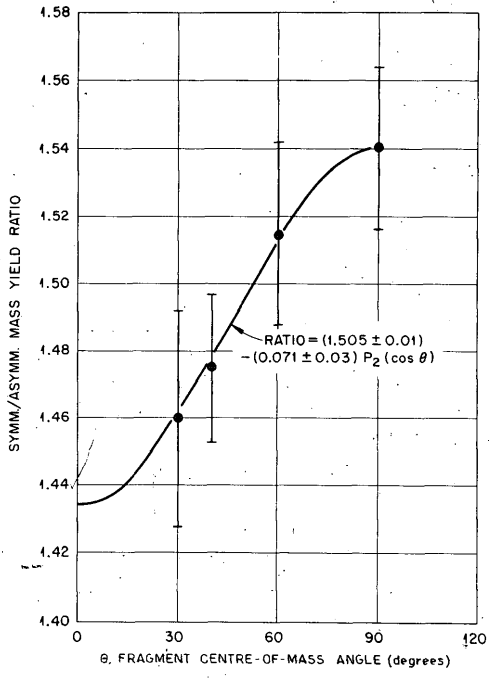

Fig. 5

Mass-angle correlations. $E_p = 13.5$ MeV. Symmetric/asymmetric peak yield ratios are plotted as a function of angle.

increase of ~5% in ρ is observed from $\theta = 30°$ to $\theta = 90°$, the statistical uncertainties are quite large, as shown, and the uncertainty in the coefficient of $P_2(\cos\theta)$ is ± 0.03.

ANALYSIS AND DISCUSSION

We shall divide our discussion of the results into two parts. Firstly, we shall consider the mass distributions obtained as a function of incident proton energy together with the total fragment kinetic energy as a function of mass, particularly as these functions relate to the two-mode hypothesis. Secondly, we shall consider the observed mass-angle correlation.

Kinetic energy and mass distributions

The suggestion that fission could be discussed meaningfully in terms of two modes, symmetric and asymmetric, was made by TURKEVICH and NIDAY in 1951 [10]. A number of authors [11], notably JENSEN and FAIRHALL [1, 2] with respect to radium, have employed the two-mode hypothesis and have further suggested its validity in discussions of the differences in fragment mass distributions observed as functions of the Z and A of the fissioning nucleus and as functions of the energy of the bombarding particle. More recently, a number of authors [5, 6, 12, 13] have discussed the results of various kinetic experiments in terms of two modes of fission. These include results for deuteron-induced [5] and helium-ion-induced [5, 6] fission of Ra^{226}. Principal evidence in favour of the two-mode hypothesis consists of (1) the analysis of the shapes of the fragment mass distributions in terms of symmetric and asymmetric components whose relative yields are functions of the fissioning nucleus and incident particle energy, and (2) the analysis of the average total kinetic energy as a function of fragment mass in terms of an effective separation $\overline{D}$ of charge centres, which appears to have different but approximately constant values for the two modes.

In the present experiment, the two-mode hypothesis suggests itself almost immediately in the results of Fig. 4. The principal difference in the mass distributions is seen in the increased yield of the entire symmetric peak relative to the asymmetric peak as the incident proton energy is increased. Because of this result, and particularly in view of the recent success of non-viscous liquid drop model calculations [14] as applied in the case of Bi^{209} [6] and other nuclei whose mass yields are symmetric and single-peaked, it is tempting to analyse the data of the present experiment in terms of two modes of fission with the symmetric mode described by the non-viscous liquid drop model. The region of masses around radium, $A \sim 226$, represents roughly the upper limit of validity of NIX's calculations [14], hence some minor departures may be expected. Nevertheless we have carried out a preliminary analysis from this basic assumption, as follows.

On the assumption that the contribution of the asymmetric mode is negligible near symmetry, we obtained least-squares fits of the mass distributions covering 18 mass units centred on symmetry, to the Gaussian function [14]:

$$N = N_0 \exp - \{[0.5 - (\mu/A)]^2 / C_m\} . \qquad (4)$$

For proton energies $E_p = 11.0$ and 13.5 MeV, the values of the constant C_m (Nix's notation) were found to be 0.00453 and 0.00456 respectively. These

values agree within their uncertainties and correspond to an equivalent standard deviation in mass of ~10.8 amu. Plots of the calculated distributions are given as solid curves in Figs. 2 and 3, along with the measured distributions.

The total translational kinetic energy at symmetry is given by Nix in terms of the surface energy $E_s^{(0)}$ at the saddle point and as a function of the fissionability parameter x, where $x = (Z^2/A)/(Z^2/A)_{crit}$, with $(Z^2/A)_{crit} = 50.13$. The surface energy is given as

$$E_s^{(0)} = a_s A^{2/3} \tag{5}$$

where a_s is a constant and is specified [14] as 17.80 MeV. The calculated total kinetic energy for symmetric fragments in the present case would then be $E^{(0)} \cong 158$ MeV, or ~15 MeV larger than the measured value and ~12 MeV larger than the approximate neutron-corrected value. This discrepancy can be accounted for by errors in the nuclear constants, e.g. ~10% error in a_s. Since such constants of the mass formula are not precisely known for nuclei in the region of fission fragments, perhaps it is justified to consider a_s as a somewhat free parameter adjusted (within 10%) so that for the present discussion $E^{(0)} = \langle E_K \rangle_{sym} = 143$ MeV, as measured. (A simple calculation based on Nix's equations then leads to an effective temperature t of ~0.95 MeV at the saddle point.) We have used Nix's formulation with the adjusted values of a_s to calculate the average total fragment kinetic energy characteristic of liquid-drop fission as a function of fragment mass. The results are shown as solid curves in the centre portions of Figs. 2 and 3 along with the measured values of $\langle E_K \rangle$ for $E_p = 13.5$ and 11.0 MeV respectively. We shall discuss these curves again below.

Note now, however, that the measured $\langle E_K \rangle$ is approximately the same at symmetry for the two proton energies (Figs. 2 and 3, centre portions), while in the region of the asymmetric mass yield peak $\langle E_K \rangle$ is somewhat lower for the higher proton energy. This observation may be accounted for as follows: if the total kinetic energy that is characteristic of liquid drop fission is lower than that characteristic of the asymmetric mode, then as the contribution in yield at the asymmetric peak from the symmetric mode increases, the average measured kinetic energy $\langle E_K \rangle$ for those masses must decrease. We may express this by means of an equation of the form

$$\langle E_K \rangle = f_{LD} E_{KLD} + (1 - f_{LK}) E_{KA} \tag{6}$$

where E_{KLD} and E_{KA} are the average total kinetic energies at mass μ characteristic of the "liquid drop" mode and "asymmetric" mode respectively. Thus, for example, in the mass region $\mu \sim 138$ amu, the liquid drop fission energy E_{KLD} is from Fig. 3 $\approx$ 136.4 MeV, the measured energy is $\langle E_K \rangle \cong$ 149.3 MeV for $E_p = 13.5$ MeV, and $f_{LD} \cong 0.12$; the calculated energy E_{KA} characteristic of the asymmetric mode is then 151 MeV, a value that is quite consistent with low-excitation fission systematics.

A complete analysis would give quantitative results on these points for all masses; however, neutron-emission and mass-resolution effects must be taken into account for detailed accuracy, and we have not included these

in the preliminary calculations reported here. Note that a straightforward calculation for the variance σ^2 based on the two-mode hypothesis can be carried out, since the yields, energy distributions and variances of the two modes can be estimated or deduced. These calculations have been postponed until the neutron-emission and mass-resolution corrections have been made. The peaks in the variance curves of Figs. 2 and 3 appear to be consistent with this hypothesis, however.

It is suggested, then, on the basis of analyses to date, that the two-mode hypothesis is valid for Ra^{226} (p, fission), and further that one of the two modes is describable in terms of the non-viscous liquid drop model [14] and is therefore indeed a symmetric mode. The so-called "asymmetric mode" may possibly have no fixed, general description or configuration, but may exhibit properties determined by the nuclear structure parameters of the fragments themselves, as occurs for the low-excitation fission of heavier elements [15].

Mass-angle correlation

The present form of the theory of angular distribution of fission fragments was advanced by BOHR [16]. For cases where the compound nucleus is oriented by virtue of the incoming angular momentum, the theory has been amplified and applied by many authors including HALPERN and STRUTINSKI [17], GRIFFIN [18] and HUIZENGA et al. [7, 19]. In the theory, the angular distribution is determined by the K distribution of the compound nucleus before scission, where K is the projection of the total angular momentum I on the nuclear symmetry axis. For moderately high excitation energies, for which statistical considerations may be applied, the K distribution is characterized by a parameter K_0^2 defined by

$$K_0^2 = t\mathcal{J}_{eff}/\hbar^2 \tag{7}$$

where t is the effective nuclear temperature and $\mathcal{J}_{eff}$ is the effective moment of inertia given by $\mathcal{J}_\perp \mathcal{J}_\parallel / (\mathcal{J}_\perp - \mathcal{J}_\parallel)$, where $\mathcal{J}_\perp$ and $\mathcal{J}_\parallel$ are the perpendicular and parallel components of the moment of inertia. For small values of K_0^2, the theory predicts anisotropic fragment distributions that peak towards 0° and 180°; for larger values of K_0^2 the theory predicts more nearly isotropic distributions.

The mass-angle effect observed (see Fig. 5) is not sufficiently large to indicate a difference in angular distributions for masses in the symmetric and asymmetric peaks for first-chance fission. The 5% effect which is observed may be interpreted on the basis of a small probability for second-chance fission; these arguments have been outlined by Halpern and Strutinski [17]. In essence, the excitation energy of the compound nucleus in second-chance fission will be lower than in the case of first-chance fission, hence K_0^2 for second-chance fission will be smaller and the angular distribution will be more anisotropic for those events. It has been shown above and in Fig. 4 that asymmetric fission is relatively more abundant for lower excitations; therefore if both first- and second-chance fission occur, the asymmetric fragments should exhibit a somewhat more anisotropic angular distribution, as indeed occurs (Fig. 5).

ACKNOWLEDGEMENTS

The authors gratefully acknowledge the preparation of the radium target by E.H. Kobisk. The assistance of C.W. Nestor and Mary F. Patterson in processing the data is gratefully acknowledged.

REFERENCES

[1] JENSEN, R.C. and FAIRHALL, A.W., Phys. Rev. 109 (1958) 942.
[2] JENSEN, R.C. and FAIRHALL, A.W., Phys. Rev. 118 (1960) 771.
[3] COFFIN, C.T. and HALPERN, I., Phys. Rev. 112 (1958) 536.
[4] WOLKE, R.L., Phys. Rev. 120 (1960) 543.
[5] BRITT, H.C., WEGNER, H.E. and GURSKY, J.C., Phys. Rev. 129 (1963) 2239.
[6] UNIK, J.P. and HUIZENGA, J.R., Phys. Rev. 134 (1964) B90.
[7] GINDLER, J.E., BATE, G.L. and HUIZENGA, J.R., Phys. Rev. 136 (1964) B1333.
[8] SCHMITT, H.W., KIKER, W.E. and WILLIAMS, C.W., Phys. Rev. 137 (1965) B837.
[9] SCHMITT, H.W., GIBSON, W.M., NEILER, J.H., WALTER, F.J., and THOMAS, T.D., "Absolute energy calibration of solid-state detectors for fission fragments and heavy ions", these Proceedings I.
[10] TURKEVICH, A. and NIDAY, J.B., Phys. Rev. 84 (1951) 52.
[11] HALPERN, I., Annu. Rev. nucl. Sci. 9 (1959) 245.
[12] BRITT, H.C. and WHETSTONE, S.L., Phys. Rev. 133 (1964) B603.
[13] WHETSTONE, S.L., Phys. Rev. 133 (1964) B613.
[14] NIX, J.R., University of California Rpt. UCRL-11338 (1964), unpublished.
[15] VANDENBOSCH, R., Nucl. Phys. 46 (1963) 129.
[16] BOHR, A. Proc. UN Int. Conf. PUAE 2 (1956) 151.
[17] HALPERN, I. and STRUTINSKI, V.M., Proc. 2nd UN Int. Conf. PUAE 15 (1958) 408.
[18] GRIFFIN, J., Phys. Rev. 116 (1959) 107; ibid. 127 (1962) 1248.
[19] HUIZENGA, J.R. and VANDENBOSCH, R., in Nuclear Reactions 2 (ENDT, P.M. and SMITH, P.B., Eds.) North Holland Publishing Company, Amsterdam (1962).

DISCUSSION

G. GORDON: Have you analysed your data in terms of total-kinetic-energy (TKE) distributions at various mass ratios of division? It seems to me that this would be a good test for the proposed two-mode hypothesis. If the hypothesis is valid, one would expect a second peak in the TKE spectrum to "grow in" at low energy when symmetric division is approached. At symmetric fission this should be the predominant peak, the high-energy peak being very small or zero. I would find the two-mode hypothesis much more convincing if the data were presented in that way and if one observed the trends mentioned above instead of a continuous variation in position of the most probable TKE with mass ratio.

J. DABBS: We have not made this analysis. Thank you for the suggestion, which has also been made by Dr. Nix.

G. GORDON: Are your statistics good enough to permit this kind of analysis of the data?

J. DABBS: In the case of 13.5-MeV proton-induced fission of Ra^{226}, we have ~80 000 events, which is probably sufficient.

F. NETTER: Do you plan to make time-of-flight measurements of the neutron rate associated with each fragment? This should provide a very specific test of the basic symmetric mode in fission induced by protons in Ra^{226}.

J. DABBS: We are limited in the number of events at higher proton energies by the speed of the paper-tape punch (10 events/s) and at lower proton energies by the lower cross-section. It would probably be too difficult to carry out the neutron measurements you suggest.

J.R. HUIZENGA: What are your measured anisotropy values $\sigma_f(0°)/\sigma_f(90°)$ for 11.12- and 13.5-MeV proton-induced fission of Ra^{226}?

J. DABBS: We were unfortunately unable to determine the total fragment angular distribution because of failure of a monitoring scaler, which occurred at a critical moment.

S.S. KAPOOR: Have you made any quantitative calculations of the percentage of any second-chance fission that may occur? It is possible that the second-chance fission at the excitation energy at which you are working may be negligible, in which case the asymmetry-versus-anisotropy relation you observe may be inherently associated with the process at a single excitation energy.

J. DABBS: I have not made any detailed calculations, but I do not think that the possibility of a few per cent second-chance fission is necessarily ruled out at 13.5 MeV.

ABSOLUTE ENERGY CALIBRATION OF SOLID-STATE DETECTORS FOR FISSION FRAGMENTS AND HEAVY IONS*

H. W. SCHMITT, W. M. GIBSON**, J. H. NEILER+,
F. J. WALTER++ AND T. D. THOMAS+++
OAK RIDGE NATIONAL LABORATORY, OAK RIDGE, TENN.,
UNITED STATES OF AMERICA

Abstract — Résumé — Аннотация — Resumen

ABSOLUTE ENERGY CALIBRATION OF SOLID-STATE DETECTORS FOR FISSION FRAGMENTS AND HEAVY IONS. Detailed measurements of the pulse-height response of silicon solid-state detectors to energetic heavy ions and fission fragments have been made. These studies have now led to a reliable method of absolute energy calibration of solid-state detectors for fission fragments, as well as to a better understanding of the somewhat peculiar response characteristics of the detectors to fission fragments and heavy ions.

The use of silicon solid-state detectors in fragment kinetic energy measurements in recent years has been widespread; at the same time, questions have been raised about the detailed interpretation of such measurements because of the increasing evidence for anomalous behaviour in charge production, charge collection and charge multiplication in the case of densely ionizing particles. The present report discusses systematics and possible origins of these effects. Application of the absolute energy calibration method, which takes into account the mass and energy dependence of the response, is based simply on a Cf^{252} or U^{235} fragment pulse-height spectrum. Our studies were carried out with mono-energetic Br^{71}, Br^{81} and I^{127} ions of energies from 30 to 120 MeV, and with fission fragments from spontaneous fission of Cf^{252} and neutron-induced fission of U^{235} and Pu^{239}. It is shown that for a given fragment mass, over a wide energy range, the fragment energy versus pulse-height relationship is of the form $E = ax + b$, where E is the fragment energy and x is the measured pulse height. A dependence of pulse height on fragment mass has also been established, which leads to an energy versus pulse-height relationship, for the range of fission-fragment masses and energies, of the form $E = (a + a'm)x + b + b'M$, where M is the fragment mass. The effect of detector window and of detector type, resistivity and electric field have been studied. Guides to the selection of detectors and to their use with fission fragments are given. The effect of the more exact calibration procedure outlined above, relative to standard approximate calibration methods, is discussed quantitatively with the aid of appropriate comparisons of fission-fragment mass and energy distributions derived from correlated fragment energy measurements.

ÉTALONNAGE EN ÉNERGIE ABSOLUE DES DÉTECTEURS A SEMI-CONDUCTEURS POUR FRAGMENTS DE FISSION ET IONS LOURDS. On a procédé à des mesures détaillées de la réponse en amplitude d'impulsion de détecteurs au silicium pour des ions lourds et des fragments de fission de haute énergie. Ces études ont permis d'élaborer une méthode fidèle d'étalonnage en énergie absolue des détecteurs à semi-conducteurs pour fragments de fission et de mieux comprendre la réponse assez particulière des détecteurs pour des fragments de fission et des ions lourds.

L'emploi de détecteurs au silicium pour les mesures de l'énergie cinétique des fragments s'est répandu depuis quelques années. En même temps des questions se sont posées à propos de l'interprétation détaillée de ces mesures, parce que l'on constatait de plus en plus souvent un comportement anormal en ce qui concerne la production, la collection et la multiplication des charges dans le cas de particules fortement ionisantes. Le mémoire contient une étude théorique et pratique des origines de ces effets. L'application de la méthode

* Research sponsored by the United States Atomic Energy Commission under contract with the Union Carbide Corporation.

** Bell Telephone Laboratories, Inc., Murray Hill, N.J.

+ Present Address: Oak Ridge Technical Enterprises Corporation, Oak Ridge, Tenn.

++ Present Address: Radiation Instrument Development Laboratories, Oak Ridge, Tenn.

+++ Princeton University, Princeton, N.J.

d'étalonnage en énergie absolue, qui tient compte de la variation de la réponse selon la masse et l'énergie, repose tout simplement sur un spectre d'amplitudes d'impulsion des fragments de ^{252}Cf ou de ^{235}U. Ces expériences ont été effectuées avec des ions monoénergétiques ^{71}Br, ^{81}Br et ^{127}I ayant des énergies allant de 30 à 120 MeV et avec des fragments de fission provenant de la fission spontanée de ^{252}Cf et de la fission de ^{235}U et de ^{239}Pu par des neutrons. On montre que, pour une masse donnée du fragment, sur une large gamme d'énergie, la relation entre l'énergie du fragment et l'amplitude d'impulsion est une fonction de la forme $E = ax + b$, dans laquelle E est l'énergie du fragment et x l'amplitude d'impulsion mesurée. On a également mis en évidence une dépendance de l'amplitude d'impulsion et de la masse du fragment. Celle-ci conduit à une relation entre l'énergie et l'amplitude d'impulsion qui, dans la gamme des masses et des énergies des fragments de fission, est de la forme $E = (a + a'm)x + b + b'M$, M étant la masse du fragment. Les auteurs ont étudié également les effets de la fenêtre du détecteur, ainsi que ceux du type de détecteur, de la résistivité et du champ électrique. Ils donnent des conseils pour choisir les détecteurs et les utiliser pour les fragments de fission. Ils étudient quantitativement les résultats de la méthode d'étalonnage plus précise qui vient d'être décrite en la comparant avec les méthodes d'étalonnage approximatif habituelles. Ils font pour cela des comparaisons appropriées des distributions des fragments de fission selon la masse et l'énergie déduites des mesures des énergies des fragments en corrélation.

АБСОЛЮТНАЯ ЭНЕРГЕТИЧЕСКАЯ КАЛИБРОВКА ДЕТЕКТОРОВ ТВЕРДЫХ ТЕЛ ДЛЯ ОСКОЛКОВ ДЕЛЕНИЯ И ТЯЖЕЛЫХ ИОНОВ. Были проведены тщательные измерения реакции амплитуд импульсов кремниевых детекторов твердых тел на энергетические тяжелые ионы и осколки деления. Эти исследования привели к созданию надежного метода абсолютной энергетической калибровки детекторов твердых тел для осколков деления, а также к лучшему пониманию несколько необычных характеристик реакции этих детекторов на осколки деления и тяжелые ионы.

В последние годы для измерения кинетических энергий осколков стали широко применять кремниевые детекторы. В то же время возник вопрос о подробной интерпретации результатов таких измерений в связи с все большей очевидностью аномального поведения при образовании зарядов, сборе зарядов и усилении зарядов в случае плотно ионизированных частиц. В данном докладе рассматриваются систематика и возможные причины этих эффектов. Применение метода абсолютной энергетической калибровки, при котором учитывается зависимость реакции от массы и энергии, основано просто на использовании спектра амплитуд импульсов осколков калифорния-252 или урана-235. Наши исследования проводились с моноэнергетическими ионами брома-71, брома-81 и йода-127, имеющими энергии от 30 до 120 Мэв, и осколками спонтанного деления калифорния-252, а также деления урана-235 и плутония-239, вызванного нейтронами. Показано, что для данных масс осколков в широком диапазоне энергий отношение амплитуды импульсов к энергии осколков имеет вид $E = ax + b$, где E – энергия осколков, а x – измеренная амплитуда импульса. Была также установлена зависимость амплитуды импульса от массы осколка, что позволило получить отношение энергии к амплитуде импульса для данного диапазона масс и энергий осколков деления, которая имеет вид $E = (a + a'm)x + b + b'M$, где M-масса осколка. Были изучены эффект окошка и типа детектора, удельного сопротивления и электрического поля. Даются практические советы по выбору детекторов и их использованию для работ с осколками деления. Эффект вышеуказанного более точного метода калибровки по сравнению со стандартными методами приблизительной калибровки рассматривается количественно путем сравнения распределений масс и энергий осколков деления, полученных в результате коррелированных измерений энергий осколков.

CALIBRACION ENERGETICA ABSOLUTA DE DETECTORES DE ESTADO SOLIDO DESTINADOS A MEDICIONES DE FRAGMENTOS DE FISION E IONES PESADOS. Se han realizado mediciones detalladas de la respuesta en amplitud de impulsos de los detectores de silicio en estado sólido a los fragmentos de fisión y a los iones pesados energéticos. Estos estudios han conducido a la elaboración de un método fidedigno de calibración energética absoluta de los detectores de estado sólido para mediciones de los fragmentos de fisión así como a una mejor comprensión de las características un tanto peculiares de la respuesta de los detectores a los fragmentos de fisión y a los iones pesados.

En los últimos años se ha extendido considerablemente el empleo de detectores de silicio en estado sólido para medir la energía cinética de los fragmentos; al mismo tiempo, han surgido problemas en cuanto a la interpretación detallada de tales mediciones, como consecuencia de la creciente abundancia de pruebas de un comportamiento anómalo de esos detectores respecto de la producción, el acopio y la multiplicación

de las cargas en el caso de partículas densamente ionizantes. Los autores examinan la sistemática y el origen probable de estos efectos. Su empleo del método de calibración absoluta en términos de la energía, que tiene en cuenta la variación de la respuesta en función de la masa y de la energía, se basa simplemente en un espectro de amplitud de impulsos de fragmentos de ^{252}Cf o de ^{235}U. Han realizado sus estudios empleando iones monoenergéticos de ^{71}Br, ^{81}Br y ^{127}I, animados de energías comprendidas entre 30 y 120 MeV, así como fragmentos procedentes de la fisión espontánea del ^{252}Cf y de la fisión neutrónica del ^{235}U y del ^{239}Pu. Los autores señalan que, en un amplio intervalo de energías y para una masa dada del fragmento, la relación entre la energía de éste y la amplitud del impulso presenta la forma $E = ax + b$, siendo E la energía del fragmento y x la amplitud medida del impulso. También han determinado una variación de la amplitud del impulso en función de la masa del fragmento, que en la gama de energías y masas de los fragmentos de fisión, conduce a una relación entre la energía y la amplitud del impulso, del tipo $E = (a + a'm)x + b'M$, expresión en la que M representa la masa de los fragmentos. Asimismo han estudiado el efecto de la naturaleza del detector y de su ventana, de la resistividad y de la intensidad del campo eléctrico. En la memoria se facilitan orientaciones para la selección de detectores y para su empleo con fragmentos de fisión. Con ayuda de comparaciones adecuadas de las distribuciones másicas y energéticas de los fragmentos de fisión derivadas de mediciones correlacionadas de la energía de los fragmentos, los autores examinan, desde el punto de vista cuantitativo, el efecto del procedimiento más exacto de calibración anteriormente descrito, en relación con los métodos corrientes de calibración aproximada.

INTRODUCTION

The present study of the response of a wide variety of silicon semiconductor detectors to fission fragments and to mono-energetic "artificial fission fragments" was conducted with a two-fold objective: firstly, to obtain calibration information to allow precise particle energies to be obtained from pulse-height measurements; second, to obtain new information on the charge production process and on conduction processes in silicon diodes at very high ionization densities. Only the first of these will be discussed here.

From the earliest measurements it was observed that the amount of energy needed to produce an electron-hole pair (commonly denoted as ϵ) in silicon was apparently larger for fission fragments than for light particles such as protons or alpha particles [1]. The apparent deficiency of charge was called the "pulse-height defect" following the terminology used for the similar effect in ionization chambers [2, 3]. For several years the magnitude, indeed the very existence of the pulse-height defect, was in question as a result of conflicting reports from several laboratories, and as a result of discrepancies between the reported fragment velocity measurements that were necessary to obtain the fragment energy distribution. Systematic studies of fission-fragment pulse-height distributions [4, 5] and precise remeasurement of fragment velocities [6-8] have firmly established the existence of a fission-fragment pulse-height defect. However, questions concerning the origin of the effect, its dependence on fragment mass and energy, and on detector type, resistivity and operating conditions have not been answered in sufficient detail to assure precise determination of fragment energies from pulse-height measurements. The possibility of obtaining mono-energetic ions of bromine and iodine in the fission energy range [9] prompted a detailed reinvestigation of fission-fragment pulse-height defects in silicon semiconductor particle detectors. Measurements have been made for surface-barrier and diffused junction detectors of widely varying resistivities with different window thicknesses and diffusion depths for a broad range of operating conditions. To allow direct correlation of the heavy ion

and fission fragment results, measurements were also made with fragments from the spontaneous fission of Cf^{252} and thermal-neutron-induced fission of U^{235} and Pu^{239} under the conditions of the heavy ion measurements.

Since the energies of the mono-energetic bromine and iodine ions could be determined directly, they afford an absolute fragment energy calibration independent of fragment velocity measurements. Also, measurements were made of the energy resolution of the detectors for these ions in the energy range of fission fragments.

EXPERIMENTAL

A continuous spectrum of bromine and iodine ions of energy 20 to 120 MeV were produced in the Oak Ridge Tandem Van de Graaff accelerator using the techniques described previously [10]. Selection of various energy groups (one for each ion charge state emerging from the accelerator) was accomplished with a 90° analysing magnet, which passes all ions of constant mE/q^2, where m, E and q are the ion mass, energy and charge. The ions were then allowed to impinge on the detector as shown in Fig. 1. Typical pulse-height spectra obtained for bromine and iodine ions are shown in Fig. 2. The double peaks in Fig. 2a occur because both isotopes of natural bromine (Br^{79} and Br^{81}) are present in the beam although their relative intensities are dependent on the field of the 20° ion source magnet (see Fig. 1). Natural iodine consists only of I^{127} hence only single peaks are observed in the iodine spectrum.

By assuming that the ion energy and pulse-height are linearly related (see below), and by measuring the spectra at two different fields of the beam analysing magnet, we were able to determine the charge state corresponding to each of the peaks in the pulse-height distribution. The magnet was calibrated in the high-field range used in this work by measurements of the $D(O^{16}, n)F^{17}$ reaction threshold. These measurements combined with precise measurements of the magnet current versus field linearity and hystereses showed excellent agreement with lower field threshold measurements made previously. The ion energy corresponding to each peak in the pulse-height distribution was then computed.

A block diagram of the instrumentation is shown in Fig. 1. A mercury-relay pulser with highly stable reference voltage and precision attenuator network combined with a stable capacitor was used as a reference source throughout this work. All pulse-height measurements are reported in terms of the setting on the pulse generator that produced a charge pulse through the calibrating capacitor equivalent to that being measured. In this way all measurements could be directly and unambiguously related. As a check on the system, the value of ϵ, the charged particle energy loss per electron-hole pair, was determined for alpha particles. The value obtained, $\epsilon = 3.55 \pm 0.03$ eV, is in good agreement with the accepted value, $\epsilon = 3.55 \pm 0.1$ eV [11].

Pulse-height spectra for Cf^{252} spontaneous fission and U^{235} and Pu^{239} thermal-neutron-induced fission fragments were also measured. The electronic measurement system used in these cases was the same as that used for the heavy ion measurements and is shown in the block diagram of Fig. 1.

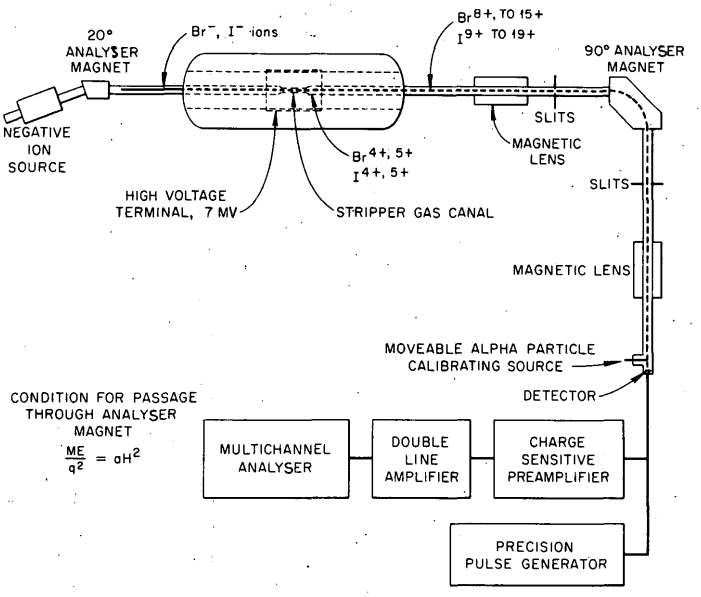

Fig. 1

Schematic diagram of experimental arrangement

The thin Cf^{252} source was prepared by self-transfer onto a platinum disc. The neutron irradiation of thin ($\sim 20\ \mu g/cm^2$) U^{235} and Pu^{239} samples was carried out at the Oak Ridge Research Reactor. The sources were vacuum evaporated onto very thin nickel; the source was oriented so that the measured fragments did not pass through the backing material. For the neutron irradiations the chamber and techniques described by WALTER, SCHMITT and NEILER [12] were used. The neutron beam was collimated so that the primary beam would not strike the detector or the mounting ring that held the thin target-supporting film. The pulse-height spectrum obtained in each fission measurement could be directly related to the heavy ion measurements via the reference pulse generator and capacitor.

DETECTOR RESPONSE

Heavy ions

The measured pulse height for mono-energetic iodine ions as a function of the maximum applied electrical field (given by $2V/w$, where V is the applied voltage and w is the depletion layer thickness) for a typical diffused junction detector and a typical surface barrier detector is shown in Fig. 3. Three regions of applied field are apparent in Fig. 3.

1. Region I is a low field region in which the measured pulse height rises as the field is increased. In this region, charge carriers are incompletely collected because of trapping or recombination along the track of the incident particle. As shown in Fig. 3, Region I usually extends to appreci-

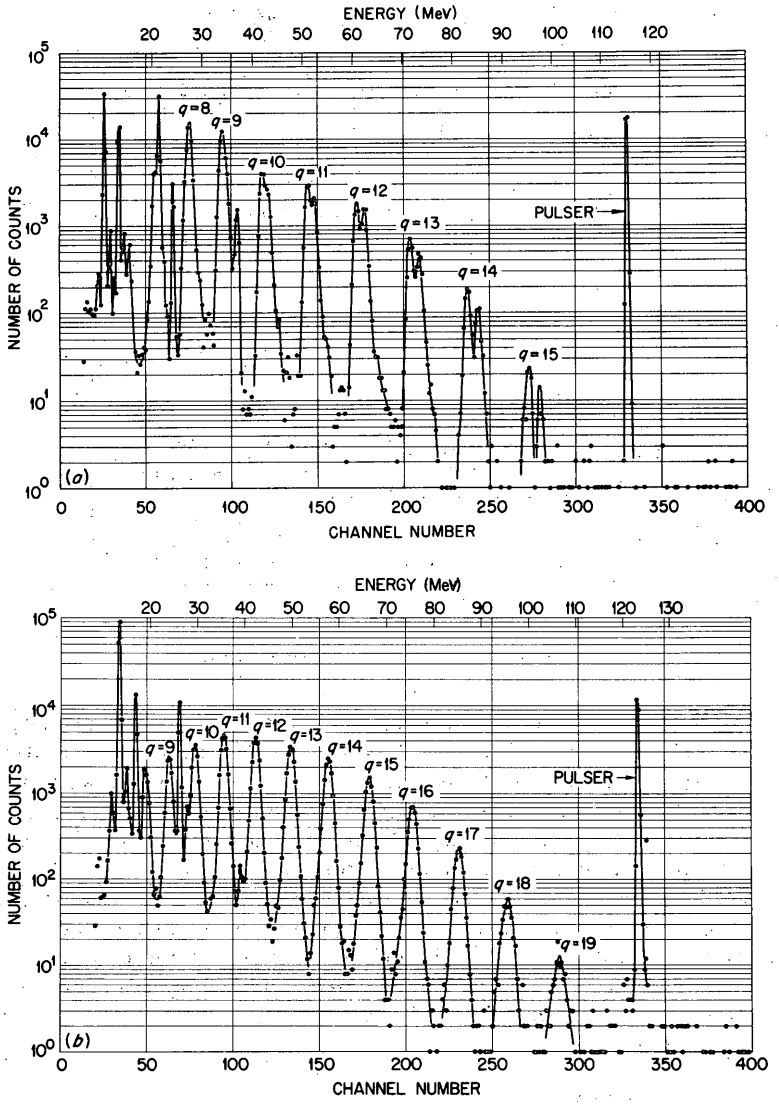

Fig. 2

Typical pulse-height spectra for (a) bromine ions and (b) iodine ions.
The double peaks in (a) occur because both isotopes, Br^{79} and Br^{81} are present in the beam.
Single peaks occur in (b) because natural iodine consists of I^{127} only.

ably higher fields for diffused junction detectors than for surface barrier detectors. This is probably caused by introduction of charge recombination centres by the high temperature diffusion process, and by the bias-voltage-dependent dead layer thickness in the case of diffused junctions. For similar reasons, Region I extends to higher applied bias voltages as either type of detector undergoes radiation damage.

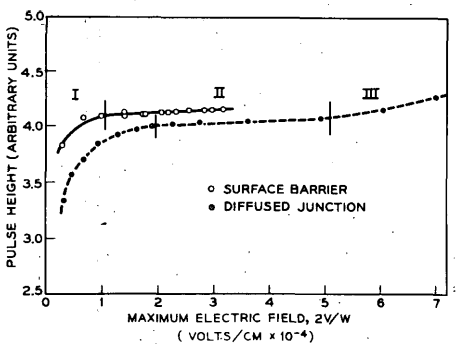

Fig. 3

Pulse height versus maximum electric field for I^{137} ions incident on a typical diffused junction detector and on a typical surface barrier detector.
The three regions I, II and III, are discussed in the text.

2. Region II is an intermediate field region sometimes called the "saturation region" in which charge collection is thought to be complete and in which the pulse height does not continue to increase with increasing field. Aside from dependence of the pulse height at which saturation occurs on the evaporated gold layer thickness or phosphorus diffusion depth, the detector operation in this region was found to be independent of detector type, resistivity or fabrication procedure. This is the region recommended for fission fragment measurements and for which the calibration procedure outlined below is applicable.

3. Region III is a high field region in which charge multiplication occurs. In this region, differences between surface-barrier and diffused detectors reappear. For diffused detectors charge multiplication has been observed only at field strengths approaching the bulk breakdown field of silicon ($\sim 10^5$ V/cm) and is discernable as a general shift of the spectra to higher pulse height. For surface barrier detectors charge multiplication often appears at fields considerably lower than for diffused junctions and has been observed at fields as low as $\sim 10^4$ V/cm [13, 14]. The field at which multiplication occurs is apparently determined at least in part by the surface treatment the detector has received [14] and may vary with time. In this case the multiplication does not usually appear as a spectral shift but as a distortion of the spectrum at high pulse heights. It is most easily seen in semi-logarithmic presentations.

The extent and separation of the three field regions depends on the mass, energy and angle of incidence of the particle, and on the resistivity, type, fabrication method and radiation history of the detector. The field region of primary interest for particle energy determinations is Region II, the saturation region. The position and extent of this region should be determined for each detector used for measurement of very heavy ions or fission fragments. In the present work the absence of a long and well-defined saturation plateau (Region II) was cause for rejection of any detector. Our experience has shown that use of silicon in the resistivity range ~ 100 to ~ 600 -cm is advisable for both diffused and gold surface barrier detectors for fission spectrometry.

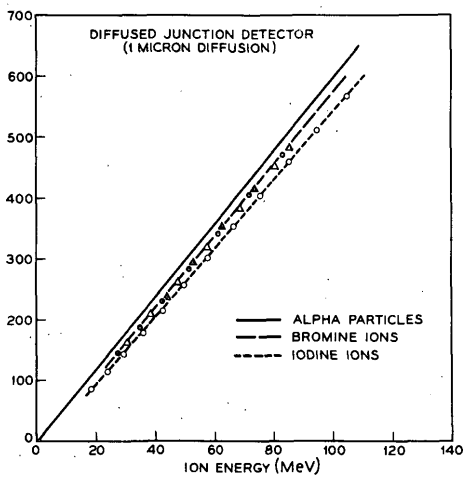

Fig. 4

Pulse-height response of a typical detector to iodine and bromine ions in the energy range 20 to 100 MeV. Shown also is a line corresponding to $\epsilon = 3.55$ eV/ion pair, obtained from alpha-particle and pulse generator measurements. Heavy-ion curve for detectors with shallow diffusions (~0.1 μm) or with thin evaporated gold films ($\lesssim 50$ μg/cm^2) are displaced less from the alpha-particle line than those shown.

As noted above, except for window thickness effects that should in any case be included in a practical calibration procedure, operation in Region II gave results independent of the detector used. The remaining discussion applies to the range of detectors studied (surface barrier detectors from 100 to 3500 Ω-cm n-type silicon and phosphorus diffused junctions from 300 - 5000 Ω-cm p-type silicon). Figure 4 shows the pulse-height response of a detector to iodine and bromine ions of energy from 20 to 100 MeV. The line obtained from alpha-particle measurements, corresponding to a value of ϵ of 3.55 eV, is also shown. The pulse heights for both bromine and iodine were less than that corresponding to collection of a charge pair for each 3.55 eV of energy lost. Furthermore the displacement in pulse-height is larger for the heavier iodine ions than for bromine. In each case the pulse height-versus-energy relation was linear from about 30 to over 100 MeV.

Measurements of the pulse-height produced by particles entering the detector at different angles of incidence showed a large part of the displacement to be due to a dead layer or window in the detector. From these measurements, together with the dE/dx measurements of MOAK et al. [15], we determined a residual pulse-height defect of 1.3 ± 0.5 MeV for bromine, and 5.5 ± 1 MeV for iodine. The significance and origin of this residual defect will not be discussed here.

All detectors exhibited an energy resolution between 0.8 and 1.6 MeV for iodine when operated in Region II. The resolution for bromine was difficult to determine because of the presence of two bromine isotopes, but appears to be slightly better than for iodine.

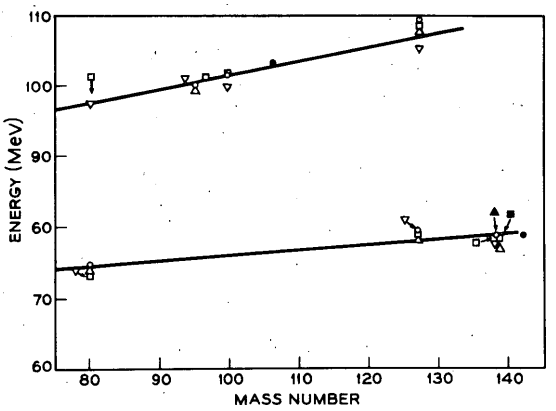

Fig. 5

Heavy-ion and fission-fragment energies as a function of mass. This graph serves as reasonable justification for the form of the mass-dependent energy calibration given in Eq. (1). See Experimental section of text.

Fission fragments

For the purpose of comparing the heavy-ion data with fission-fragment data, and for the purpose of determining initially the form of the mass dependence that is required in the energy calibration, it is desirable to consider selected points in the fission spectrum (say one point each in the light- and heavy-fragment peaks) together with the appropriate masses and energies derived from time-of-flight data. We have chosen the midpoint between the 3/4-maximum points in each peak; these points are easily obtained and are not strongly subject to resolution and tailing effects. Thus the energies appropriate to these pulse heights were obtained from the data of MILTON and FRASER [16] corrected for neutron emission, and the appropriate masses were taken to be the average post-neutron-emission masses [17].

For direct comparison of the pulse-height defect (taken as the displacement in energy from the expected line for $\epsilon = 3.55$) for fission fragments and heavy ions, it is convenient to consider data corresponding either to one energy or to one pulse height. We have therefore adjusted the light-fragment energies for U^{235} and Pu^{239} fission to the energies that the fragments of the appropriate masses would have if they produced the same pulse height as the Cf^{252} light fragment. Because the slopes of the pulse height versus energy curves are known from the heavy-ion data, this adjustment can be made with reasonable accuracy. Similarly, the heavy fragment energies for U^{235} and Pu^{239} were adjusted to the energies that these fragments would have if they produced the same pulse height as the Cf^{252} heavy fragments. We also determined the energies of bromine and iodine ions that would give pulse heights equal to those corresponding to the Cf^{252} light and heavy fragments. The energies obtained in this way are independent of dead-layer thickness and are plotted against the particle masses in Fig. 5 for a

number of detectors. Since Cf^{252} was taken as the reference point there is no scatter in the data corresponding to Cf^{252} fission fragments.

Within experimental uncertainties, the points of Fig. 5 lie on straight lines, suggesting that for a given pulse height there is a linear relationship between the kinetic energy and mass. The heavy ion experiments show a linear relationship between pulse height and kinetic energy for a given mass. Thus a fit to all our data is obtained with an expression of the form

$$E = (a + a'm)x + b + b'm \quad (1)$$

where E is the kinetic energy of the fragment, m is the mass, x the pulse height and a, a', b and b' are constants. We should note that there is no justification for using such an expression outside the range of masses and energies considered here or for detectors operated outside the saturation region of pulse height versus bias.

In the present study, the values of the constants of Eq. (1) may be obtained for each detector used directly from pulse height versus energy data such as that shown in Fig. 4. It would be impractical to carry out such measurements for every detector to be used for fission fragment energy determinations. Thus a method has been developed [8] for obtaining precise values of the constants from a pulse-height spectrum of Cf^{252} spontaneous fission or U^{235} thermal-neutron fission fragments.

The fragment energy spectrum is used to define two pulse heights that we will call P_L and P_H. The pulse height P_L corresponds to the mid-point between the 3/4 maximum points of the light fragment peak; the pulse-height P_H to the midpoint between the 3/4 maximum points in the heavy fragment peak. As discussed above, the bromine and iodine energies corresponding to each pulse height can be determined. These then become "universal" energies for the types of detectors used in this work, and can be used to set up four simultaneous equations for evaluation of the constants of Eq. (1). These evaluations have been carried out for Cf^{252} and U^{235} fragments, for each of several detectors. Best values of the constants of Eq. (1), expressed in terms of P_L and P_H, are given for each of the two fission cases in Table I.

From a determination of P_L and P_H for one of these two cases under the exact conditions of any experiment, the numerical values of the constants a, a', b and b' can then be determined for the detector, source and electronic measuring system being used. It is important that the calibrating fragments be exposed to the same effective absorber thickness (source plus backing) as the fragments being studied in the experiment.

EFFECTS OF NOT CORRECTING FOR THE MASS DEPENDENCE OF THE PULSE-HEIGHT DEFECT

The detector calibration method that has generally been used heretofore involved fitting the pulse-height spectrum to an energy spectrum obtained from time-of-flight velocity measurements. This calibration method fails to correct properly for the mass dependence of the pulse-height defect. It is of interest therefore to compare the results obtained from the usual approximate calibration procedure with that outlined here.

TABLE I

CONSTANTS IN THE ENERGY CALIBRATION EQUATION,
$E = (a + a'm)x + b + b'm$

The constants are expressed in terms of the observed pulse heights P_L and P_H that correspond to the mid-points between the 3/4-maximum points in the light (L) and heavy (H) groups respectively. Constants are given for both Cf^{252} spontaneous fission and U^{235} thermal-neutron-induced fission.

Cf^{252}	U^{235}
$a = \frac{24.0203}{P_L - P_h}$	$a = \frac{30.9734}{P_L - P_H}$
$a' = \frac{0.03574}{P_L - P_h}$	$a' = \frac{0.04596}{P_L - P_H}$
$b = 89.6083 - aP_L$	$b = 87.8626 - aP_L$
$b' = 0.1370 - a'P_L$	$b' = 0.1345 - a'P_L$

The dashed curve of Fig. 6a represents the post-neutron energy spectrum of fragments from the thermal-neutron-induced fission of U^{235}, derived from the time-of-flight data of Milton and Fraser. The solid curve is a similar spectrum measured with a semiconductor detector. For evaluation of the effect of mass dependence only, without regard to absolute energies, we have used as the calibration for this spectrum a single pulse-height-versus-energy line, which is defined by assigning the average light- and heavy-fragment energies to the average light- and heavy-fragment pulse heights respectively. The two sets of data are normalized to the same total number of counts. We see that the curves based on time-of-flight results are noticeably broader than those taken with solid-state detectors. Figure 6b shows the same comparison after a suitable mass dependent energy calibration had been applied to the solid-state detector results, but with the same absolute normalization to time-of-flight data.

A comparison of the average total kinetic energy as a function of mass number, calculated from the single line calibration and from the mass-dependent calibration, is given in Fig. 7a. We see that the effect of the mass dependent pulse-height defect is to cause an apparent increase in the lower energies and an apparent decrease in the higher energies. The magnitude of the kinetic energy dip at symmetry is apparently diminished and the slope of the wings of the curve decreased. Finally, Fig. 7b shows a comparison of the second central moments, σ, of the total energy distribution as a function of mass number, $(\sigma^2 = (E^2)_{avg} - (E_{avg})^2)$. Since the mass dependent pulse-height defect tends to reduce high energies and increase low energies it is not surprising that it also causes σ to appear smaller.

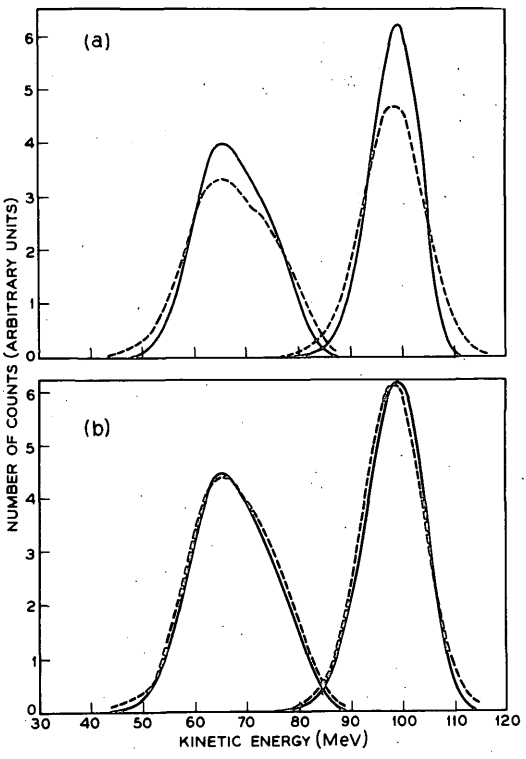

Fig. 6

Effect of mass-dependent energy calibration in single-fragment kinetic energies. Dashed curves show the single-fragment energy spectrum obtained from time-of-flight data [16]; solid curves show the same spectrum obtained from semiconductor detector data. For (a), a single line, mass-independent energy calibration was used for the semiconductor detector data; for (b), the mass dependent calibration was used. (To demonstrate this effect, the absolute energies were normalized to the time-of-flight values and are somewhat lower than the best values obtained from the heavy-ion calibrations.)

The comparisons of Figs. 6 and 7 show the importance of using a mass-dependent energy calibration. The constants of Table I that derived directly from heavy ion measurements give values for the absolute fragment energies that are slightly higher than those shown in Figs. 6 and 7. The apparent discrepancy between the absolute energies based on heavy-ion measurements and those based on the time-of-flight data of MILTON and FRASER [16] is shown in Fig. 8. For Cf^{252} the double energy measurements with solid-state detectors using the calibration method outlined above are in good agreement with energies derived from the time-of-flight fragment velocity measurements of WHETSTONE [18]. These differences are believed to arise from velocity tailing effects in the time-of-flight measurements.

Inclusion of the mass dependent energy calibration tends to have a very small effect in fragment mass distributions derived from correlated fragment kinetic energy measurements since the pulse-height defects for the two fragments tend to cancel one another in the calculation of the mass ratio. On

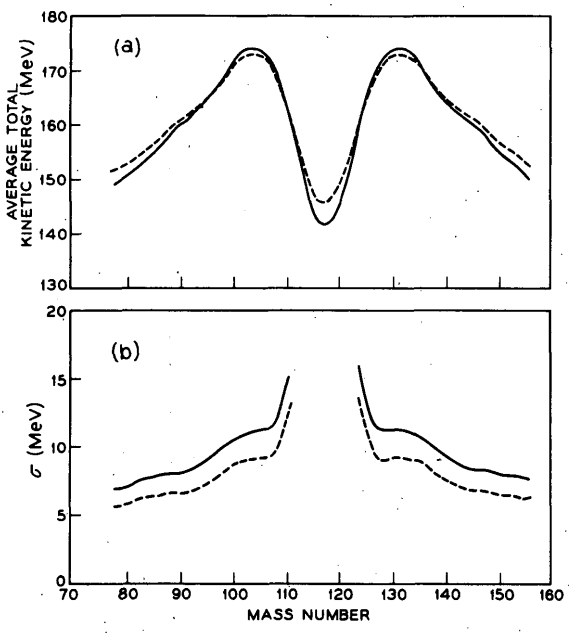

Fig. 7

Effect of mass-dependent energy calibration (a) in total kinetic energy and (b) in the variance of the total kinetic energy distributions, as functions of mass. Dashed curves give results based on a single-line, mass-independent calibration; solid curves give results based on the mass-dependent calibration. As in Fig. 6, absolute energies were normalized to time-of-flight values and are somewhat lower than the best values obtained from heavy-ion calibrations.

the other hand determination of mass ratios by simultaneous measurement of fragment mass and velocity is quite sensitive to the energy calibration [8]. It is important to note that representations of mass and energy other than those discussed here may be modified significantly by inclusion of a mass dependent energy calibration.

ACKNOWLEDGEMENTS

The authors are indebted to C.D. Moak for his assistance in the work on heavy ion. The fabrication of the Cf^{252} source by S.G. Thompson and the fabrication of the U^{235} and Pu^{239} targets by E.H. Kobisk are gratefully acknowledged.

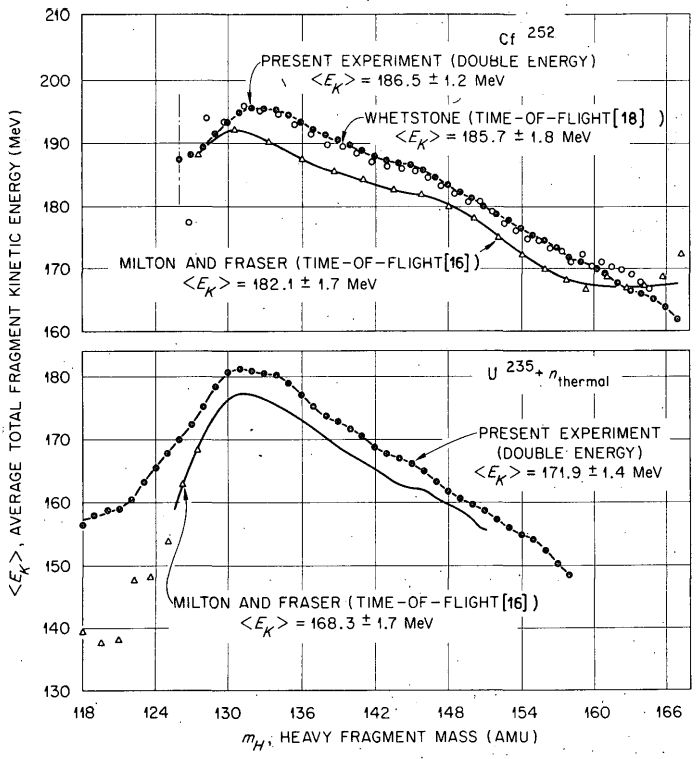

Fig. 8

Comparison of the average total fragment kinetic energy as a function of heavy fragment mass derived from time-of-flight fragment velocity measurements with those derived from direct kinetic energy measurements using the calibration procedure outlined in this paper. The double energy measurements shown are from work by H.W. Schmitt, J.H. Neiler and F.J. Walter to be published.

REFERENCES

[1] Semiconductor Nuclear Particle Detectors (DABBS, J.W.T. and WALTER, F.J., Eds.) National Academy of Sciences, National Research Council (1960) Publication 871.

[2] LEACHMAN, R.B., Phys. Rev. 87, (1962) 444.

[3] SCHMITT, H.W. and LEACHMAN, R.B., Phys. Rev. 102 (1956) 183.

[4] SCHMITT, H.W., NEILER, J.H., WALTER, F.J. and SILVA, R.J., Bull. Amer. phys. Soc. 6 (1961) 240.

[5] BRITT, H.C. and WEGNER, H.E., Rev. sci. Instrum. 34 (1963) 274.

[6] WHETSTONE, S.L., Phys. Rev. 131 (1963) 1232.

[7] FRASER, J.S. and MILTON, J.C.D., Canad. J. Phys. 41 (1963) 2080.

[8] SCHMITT, H.W., KIKER, W.E. and WILLIAMS, C.W., Phys. Rev. 137 (1965) B837.

[9] ALMQVIST, E., BROUDE, C., CLARK, M.A., KUCHNER, J.A. and LITHERLAND, A.E., Canad. J. Phys. 40 (1962) 954.

[10] MOAK, C.D., NEILER, J.H., SCHMITT, H.W., WALTER, F.J. and WELLS, G.F., Rev. sci. Instrum. 34 (1963) 853.

[11] GIBSON, W.L., MILLER, G.L. and DONOVAN, P.F., in Alpha, Beta and Gamma Spectroscopy (SIEGBAHN, K., Ed.) North-Holland Publishing Co., Amsterdam (1964).

[12] WALTER, F.J., SCHMITT, H.W. and NEILER, J.H., Proc. Int. Conf. on Nucl. Phys. with Reactor Neutrons, Rpt. ANL-6797, Argonne National Laboratory, Argonne, Ill. (1963) 441.
[13] BRITT, H.C. and WEGNER, H.E., Rev. sci. Instrum. 34 (1963) 627.
[14] WALTER, F.J., I.E.E.E. Trans. on Nucl. Sci., NS-11 (1964) 232.
[15] MOAK, C.D. and BROWN, M.D., Phys. Rev. Lett. 11 (1963) 284.
[16] MILTON, J.C.D. and FRASER, J.S., Canad. J. Phys. 40 (1962) 1626.
[17] TERRELL, J., Phys. Rev. 127 (1962) 880.
[18] WHETSTONE, S.L. Jr., Phys. Rev. 131 (1963) 1232.

DISCUSSION

N. FEATHER: The comparison of the mass distributions in binary and alpha-particle-accompanied fission was made by Schmitt et al. before the calibration of solid-state detectors was carried out. In your view, is it likely that the published results need significant correction?

W. GIBSON: The mass dependence of the pulse-height calibration should have only a very small effect on these mass distributions since mass ratios determined by double-energy measurements are obtained by taking ratios of energies. Thus, the pulse-height defect cancels to first order. The published results should not, therefore, need significant correction. It should be noted, however, that mass distributions determined from simultaneous measurement of fragment energy and velocity are extremely sensitive to the details of the calibration procedure. As implied by the results reported in the papers presented by Stein[1] and Signarbieux[2], the mass dependence of the pulse-height defect is important in cases of this type.

J. DABBS: Recently, at Oak Ridge, W.W. Walker, C.D. Moak and I measured the response of germanium surface-barrier detectors at 77°K in the same manner as that described by Dr. Gibson. The pulse-height defect was in general somewhat smaller and the observed resolution somewhat poorer than in silicon, although the latter effect may have been due to the particular surface conditions obtaining in the six detectors measured. The linearity of the pulse-height-versus-energy curves was excellent.

M. SOWINSKI: I should be interested to hear Dr. Gibson's views on the use of semi-conductor surface-barrier detectors for making precise measurements of the energy distribution of fission fragments. We have also made some measurements of this kind and our results indicate that the multiplication effects of the charges – appearing in the form of high-energy tails, peak broadening and spectrum shift – are much lower than 3×10^4 V/cm.

W. GIBSON: The differences between diffuse detectors and surface-barrier detectors appear in what I indicated as Region I. In the case of diffuse detectors a constant pulse-height-versus-field dependence is normally reached at higher fields than in the case of surface-barrier detectors. That is one difference. This is a somewhat variable factor as between different diffuse detectors and it is probably related to the lower lifetime at the front surface of the detector introduced during the diffusion. In addition, there

[1] STEIN, W.E., "Simultaneous velocity and energy measurement of fission fragments", these Proceedings I.

[2] SIGNARBIEUX, C. et RIBRAG, M., « Etude des spectres en masse des fragments de fission après émission neutronique prompte », these Proceedings I.

are considerable differences corresponding to the onset of multiplication. As was indicated, the type of multiplication is also very different. We have also seen multiplication in surface-barrier detectors in very low fields – as low as 1×10^4 V/cm – but by suitable surface conditioning this multiplication onset could usually be moved up to field strengths of the order of 3 or 4×10^4; in some cases it could be moved to field strengths comparable to the onset of multiplication for diffuse detectors. I fully agree that this introduces an additional complication and one that users of surface-barrier detectors should be aware of. I do not want to take sides in this question of whether one should use diffuse dectectors or surface-barrier detectors, but personally I use diffuse detectors.

M. SOWINSKI: At what fission-fragment doses did you observe deterioration effects in the spectrometric characteristics of your detectors?

W. GIBSON: The flux strength at which radiation damage appears is very sensitive to the field in the detector, i.e. to the field in which the charges are collected. By operating at higher collecting fields one can tolerate from a factor of 10 to as much as a factor of 100 more particles before distortion of the spectrum appears. This is perhaps another argument in favour of using diffuse detectors since they can be operated reliably at higher field strengths. On the question of the point at which the radiation damage appears, we have seen distortions in surface-barrier detectors at fluxes as low as 10^6 but normally they do not appear until there is an integrated number of particles of the order of 10^8 or $10^9/cm^2$ in the detector. We have used very-high-field diffuse detectors for integrated fission-fragment intensities up to about a few times 10^{10}.

FISSION-FRAGMENT ANGULAR, ENERGY, AND MASS DIVISION CORRELATIONS FOR THE $U^{234}(d, pf)$ REACTION*

R. VANDENBOSCH
UNIVERSITY OF WASHINGTON, SEATTLE, WASH.
AND
J.P. UNIK AND J.R. HUIZENGA
ARGONNE NATIONAL LABORATORY,
ARGONNE, ILL., UNITED STATES OF AMERICA

Abstract — Résumé — Аннотация — Resumen

FISSION-FRAGMENT ANGULAR, ENERGY, AND MASS DIVISION CORRELATIONS FOR THE $U^{234}(d,pf)$ REACTION. The fission of the compound nucleus U^{235} in the neighbourhood of its fission threshold has been studied by means of the $U^{234}(d,pf)$ reaction. A three-parameter analyser was used to record simultaneously the two fission-fragment kinetic energies and the proton energy for each coincident event. The excitation energy at which fission occurs is defined by the kinetic energy of the stripped proton. The variation of angular anisotropy with excitation energy shows considerably more structure than that obtained by Lamphere for the same nucleus resulting from fast-neutron bombardment of U^{234}. At least eight fission channels at the saddle point have been observed for the energy region between threshold and 2 MeV above threshold. Nilsson-type calculations of single particle energies for deformed nuclei have been made for the larger deformations more nearly describing the saddle-point configuration. The single particle states identified by Lamphere are consistent with those calculated to be close to the Fermi surface for reasonable saddle-point deformations.

The primary motivation for this experiment was to search for a possible correlation between mass asymmetry and angular anisotropy. Mass yields obtained from the correlated fragment energies show no variation of the anisotropy with mass ratio, in contrast with experiments where the excitation energy at which fission is occurring is not fixed and where a dependence of anisotropy on mass ratio has been observed. There is therefore no evidence from anisotropy measurements that the properties of the saddle point influence the final mass division. The average total kinetic energy release in fission varies by less than 0.5% for the different saddle-point channels observed. The variation of total kinetic energy with mass ratio has also been investigated.

CORRÉLATION DES ANGLES, DES ÉNERGIES ET DES MASSES POUR LES FRAGMENTS DE FISSION PRODUITS PAR LA RÉACTION $^{234}U(d,pf)$. Les auteurs ont étudié la fission du noyau composé ^{235}U au voisinage de son seuil de fission par la réaction $^{234}U(d,pf)$. A l'aide d'un analyseur à trois paramètres ils ont enregistré simultanément les énergies cinétiques des deux fragments de fission et l'énergie du proton pour chaque coïncidence. L'énergie d'excitation pour laquelle la fission se produit est définie par l'énergie cinétique du proton libéré. Les variations de l'anisotropie angulaire selon l'énergie d'excitation ont une structure beaucoup plus nette que celle que Lamphère a obtenue pour le même noyau, en bombardant ^{234}U par des neutrons rapides. Les auteurs ont observé au moins huit voies de fission au point d'étranglement dans la région des énergies comprises entre le seuil et 2 MeV au-dessus du seuil. Ils ont calculé (calculs de type Nilsson) des énergies de particules isolées pour des noyaux déformés dans le cas de déformations plus grandes qui donnent une description plus précise de la configuration au point d'étranglement. Les états d'une particule isolée identifiés par Lamphère sont en accord avec ceux dont on a trouvé par le calcul qu'ils sont voisins de la surface de Fermi pour des déformations raisonnables au point d'étranglement.

Ces expériences avaient primitivement pour but de rechercher s'il n'y avait pas une corrélation entre l'asymétrie de masse et l'anisotropie angulaire. Les rendements selon la masse obtenus à partir des énergies de fragments en corrélation ne font apparaître aucune variation de l'anisotropie selon le rapport des masses, contrairement à ce que se passe dans les expériences où l'on ne fixe pas l'énergie d'excitation à laquelle la fission a lieu (expériences où l'on observe effectivement une variation de l'anisotropie selon le rapport des

* Work supported in part by the United States Atomic Energy Commission.

masses). On ne saurait donc affirmer, d'après les mesures de l'anisotropie, que les propriétés du point d'étranglement influencent la répartition finale des masses. La moyenne de l'énergie cinétique totale libérée au cours de la fission varie dans une proportion inférieure à 0,5% pour les différentes voies à l'étranglement observées. Les auteurs ont aussi étudié la variation de l'énergie cinétique totale en fonction du rapport des masses.

КОРРЕЛЯЦИЯ МЕЖДУ РАСПРЕДЕЛЕНИЕМ ОСКОЛКОВ ДЕЛЕНИЯ ПО УГЛУ, ПО ЭНЕРГИИ И ПО МАССЕ В РЕЗУЛЬТАТЕ РЕАКЦИЙ (d, pf) УРАНА-234. Деление сложного ядра урана-235 при приближении к порогу его деления изучалось при помощи реакции (d, pf) урана-234. В целях одновременной регистрации для каждого совпадающего события двух кинетических энергий осколков деления и энергий протона был использован трехпараметровый анализатор. Энергия возбуждения, при которой происходит деление, определяется кинетической энергией срыва протона. Изменение угловой анизотропии в зависимости от энергии возбуждения указывает на значительно большую зависимость от структуры, чем это было получено Ламфиром для того же ядра в результате бомбардировки урана-234 быстрыми нейтронами. В седловине наблюдалось по меньшей мере восемь каналов деления для интервала энергии между порогом и 2 Мэв свыше порога. Для более значительных деформаций, более точно описывающих конфигурацию седловины, были проделаны расчеты типа Нилссона для энергии одиночной частицы для деформированного ядра. Состояния одиночной частицы, выявленные Ламфиром, совместимы с подсчитанными состояниями, приолижающимися к поверхности Ферми для ограниченных деформаций седловины.

Главной причиной для проведения этого эксперимента было стремление изыскать возможную корреляцию между асимметрией массы и угловой анизотропией. Выходы массы, полученные из коррелированных энергий осколков, не указывают на изменение анизотропии в зависимости от массового соотношения в противоположность экспериментам, в которых энергия возбуждения, при которой происходит деление, не является постоянной, и при которой наблюдалась зависимость анизотропии от массового соотношения. Поэтому измерения анизотропии не дают указаний на то, что свойства седловины влияют на окончательное распределение массы. Среднее общее высвобождение кинетической энергии в процессе деления изменяется в пределах менее чем 0,5% для различных наблюдавшихся в седловине каналов. Было обследовано также изменение общей кинетической энергии в зависимости от массового соотношения.

CORRELACIONES ENTRE LA DISTRIBUCION ANGULAR, LA ENERGIA Y LA DIVISION MASICA DE LOS FRAGMENTOS EN LA REACCION ^{234}U (d,pf). Los autores han estudiado la fisión del núcleo compuesto de ^{235}U en las proximidades del umbral de fisión, recurriendo a la reacción ^{234}U (d,pf). Emplearon un analizador de tres parámetros para registrar simultáneamente las energías cinéticas de los dos fragmentos de fisión y la energía protónica correspondientes a cada coincidencia. La energía de excitación a que se produce la fisión queda definida por la energía cinética del protón liberado. La variación de la anisotropía angular con la energía de excitación se caracteriza por una mayor estructuración que la obtenida por Lamphere para el mismo núcleo, resultante del bombardeo de ^{234}U con neutrones rápidos. Para el intervalo de energías comprendido entre la de umbral y 2 MeV por encima de ésta, se han observado por lo menos ocho canales de fisión en el punto de estrangulación. Se han calculado por el método de Nilsson las energías de las diversas partículas, correspondientes a los núcleos deformados, para las deformaciones más acusadas que describen con mayor aproximación la configuración del punto de estrangulación. Los estados de las partículas individuales identificados por Lamphere son compatibles con los que se consideran próximos a la superficie de Fermi en el caso de deformaciones razonables del punto de estrangulación.

Este experimento se llevó a cabo con el propósito principal de encontrar una posible relación entre la asimetría másica y la anisotropía angular. Los rendimientos másicos deducidos de las energías correspondientes de los fragmentos no revelan ninguna variación de la anisotropía en función de la razón másica, a diferencia de lo que ocurre en los experimentos en los que no queda fijada la energía de excitación a que se produce la fisión y en los que se ha observado una variación de la anisotropía en función de esa razón másica. Por tanto, las mediciones de la anisotropía no proporcionan pruebas de que las propiedades del punto de estrangulación influyen sobre la división final de las masas. El promedio de la energía cinética total liberada en la fisión varía en menos del 0,5% para los distintos canales observados en el punto de estrangulación. También se ha estudiado la variación de la energía cinética total en función de la razón másica.

INTRODUCTION

In the earliest investigations [1-3] of the angular distribution of fission fragments, a dependence of the angular anisotropy on the mass asymmetry was noted. At the time of the development of the theory of fission-fragment angular distributions it was recognized that this dependence of anisotropy on mass asymmetry might not be a direct dependence, but only reflect the fact that fission was occurring at a variety of excitation energies depending on the number of neutrons emitted before fission [4]. The observed trend [1-3] of larger anisotropies with increasing mass asymmetry was consistent with this explanation, as the anisotropy is larger for fission occurring at lower excitation energies and it is known that asymmetric fission predominates at low excitation energies. A test of this proposed explanation would however be highly desirable. A measurement of the mass-asymmetry dependence of fission-fragment anisotropy for a system where fission can only occur at a unique excitation energy would provide such a test, as has been suggested by HALPERN [5]. Apart from answering the question as to whether the observed effect is due to multichance fission (fission occurring at a variety of excitation energies), the presence or absence of a mass-ratio dependence of anisotropy at a unique excitation energy might have important implications concerning the stage of the fission process at which the mass distribution is determined. Since the fragment angular distribution is believed to be determined by nuclear properties at the saddle point [6], the presence of a dependence of anisotropy on mass ratio might imply that the factors that determine the final mass distribution are already becoming operative at this early stage of development of the fission process.

One experimental approach to the problem of studying fission at a unique excitation energy is to study fission induced by mono-energetic neutrons of less than about 5 MeV. Several such studies have been attempted [7-9].

The primary difficulty in these experiments was lack of fragment mass-ratio resolution and an insufficient number of events. The former problem can be largely solved by the use of semiconductor detectors, although at the expense of intensity compared to the emulsion technique. The second problem is more persistent, but considerable improvement is possible by exploiting the (d, pf) reaction. The (d, p) reaction is a mechanism for adding a neutron, either bound or unbound, to a target nucleus. This reaction has been used by NORTHROP et al. [10] to study fission in the excitation energy region corresponding to capture of a bound neutron. The capture of an unbound neutron by a target through a (d, p) reaction is in many respects similar to bombardment of the target by MeV-energy neutrons. By examining fission fragments in time coincidence with protons of a given energy, the excitation energy of the fissioning nucleus can be determined. By varying the proton energy accepted, the excitation energy dependence of fission-fragment angular distributions, mass distributions and kinetic energy distributions may be studied.

EXPERIMENTAL PROCEDURE

The fissioning nucleus U^{235} was produced by means of the U^{234}(d, p) reaction using 13 MeV deuterons from the Argonne tandem Van de Graaff ac-

celerator. The proton detector was placed at an angle of 90° with respect to the incident deuteron beam. This angle was chosen on the basis of an earlier exploratory experiment that showed that the maximum proton yield occurred at about this angle. The location of the fission-fragment detectors is governed by the location of the symmetry axis describing the distribution of angular momentum vectors in the U^{235} intermediate nucleus. The direction of the symmetry axis with respect to the proton direction depends on certain details of the nuclear interaction. We are indebted to GIBBS and GRIFFIN [11] for providing us with sample distorted wave calculations that give the symmetry axis as a function of proton angle. These calculations reveal that for proton angles (with respect to the incident deuteron beam direction) of less than approximately 90° the symmetry axis differs from the recoil axis depending on the orbital angular momentum transfer. At proton angles of 90° or more the symmetry axis nearly coincides with the recoil axis and is essentially independent of the angular momentum transfer. At a proton angle of 90° the recoil axis (and presumably the symmetry axis) is at approximately 330° with respect to the beam. The pair of fission detectors was placed either at 145° and 325°, representing a measurement very nearly parallel to the recoil direction, or at 55° and 235°, representing a measurement very nearly perpendicular to the recoil direction. The detector arrangement is illustrated schematically in Fig. 1. A block diagram for the electronics used is also shown in this figure. The details of the data collection system will be described elsewhere [12].

RESULTS

A total of 16 200 net coincident events corresponding to protons in the energy region of 6-11 MeV were recorded for the configuration with the fission counters parallel to the recoil axis. A total of 27 500 net coincident events were obtained with the fission counters perpendicular to the recoil axis. The spectra of protons in coincidence with fission fragments at the two angles are shown in Fig. 2. The fission cross-sections obtained by LAMPHERE [13] for fast-neutron-induced fission of U^{234} are also shown. The relationship between the proton energy and neutron energy is

$$E_n = E_d - 2.23 - E_p \qquad (1)$$

where all quantities are in the centre-of-mass system. The centre-of-mass corrections are approximately 0.15 MeV.

The anisotropy as a function of proton energy obtained in the present experiment is illustrated in Fig. 3. No correction has been made for the finite solid angle subtended by the detectors (14° for the proton detector and 28° for the fission detectors). The anisotropy obtained by LAMPHERE [13] is also illustrated for comparison.

The next step in the data analysis was extraction of mass yield curves at the two fission-fragment detector angles. This turned out to require considerable care, as the mass distributions were very steep with a deep valley

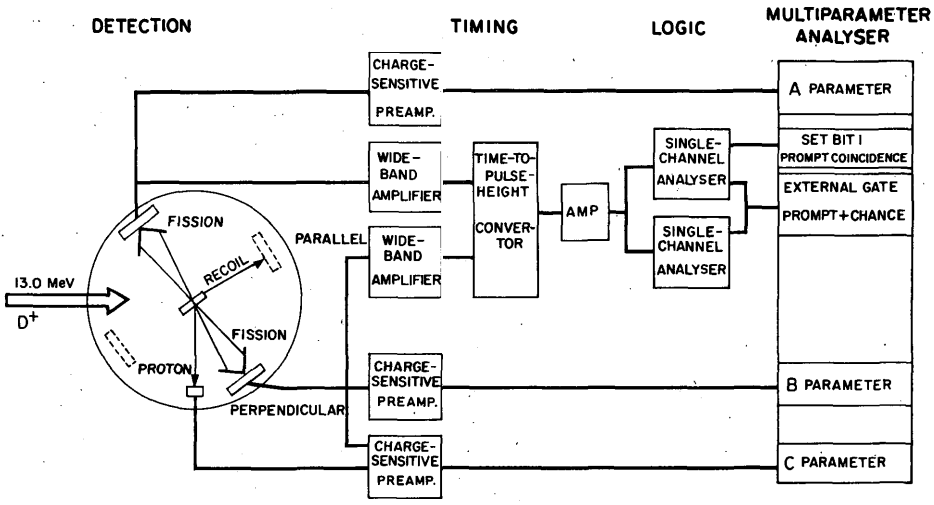

Fig. 1

Schematic diagram of the data recording system.
The location of the proton and fission detectors are shown on the left-hand side of the drawing.
The proton detector remains fixed at 90° with respect to the incident deuteron beam.
One set of measurements is taken with the fission counters as indicated by the full lines,
and a second set, corresponding to a different angle with respect to the recoil axis,
is taken with the fission detectors at the positions indicated by the dotted lines.
The right-hand side of the drawing shows the data recording system.
(Angles are measured clockwise from the beam direction.)

at symmetry. The mass number is obtained from conservation of linear momentum yielding the relation

$$M_A = M_T\left(\frac{E_B}{E_A+E_B}\right) \qquad (2)$$

where M_T is the mass of the fissioning nucleus and E_A and E_B are the two fission-fragment kinetic energies. Unfortunately the pulse height from the detector is not simply proportional to the fission-fragment energy. Corrections have to be made for the pulse-height defect [14, 15] of the counters, fragment-energy loss in the target and backing material and in the detector window, loss in kinetic energy due to neutron emission from the moving fragments, and centre-of-mass shifts. The correction for the pulse-height defect was made using an expression of the form

$$E = (a+a'M)X+b+b'M$$

where X is the pulse height, E and M are the fragment energy and mass, and a, a', b and b' are constants. The form of this equation has been shown [16] to describe the response of semiconductor detectors to a fairly wide range of heavy ions and fission fragments. The constants were determined by the method suggested by SCHMITT et al. [16] using calibrations per-

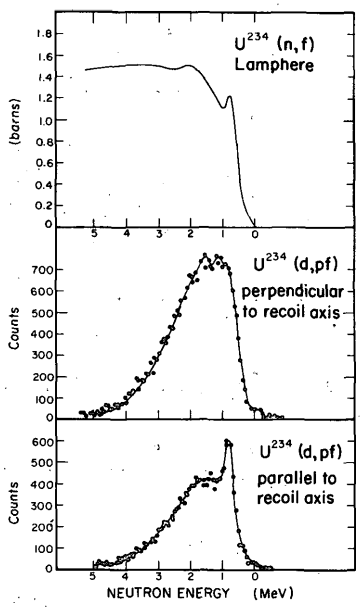

Fig. 2

The upper part of the figure shows the $U^{234}(n, f)$ excitation function reported by Lamphere. The lower parts of the figure show the $U^{234}(d, pf)$ fission yields at two angles with respect to the recoil axis. The abscissa is proportional to the proton energy, corresponding to decreasing neutron energy according to the relation $E_n = E_d - E_p - 2.23$.

formed during the course of the run using a Cf^{252} spontaneous fission source. Small renormalizations between different runs were required. The mass resolution of this experiment due to neutron emission from the fragments and the varying fragment energy loss in the target material was estimated to be 4.0 amu.

A mass yield curve for fission following deuteron capture (obtained from the "chance" events) is shown in Fig. 4. Mass yield curves for fission accompanying the (d, pf) reaction were extracted for two proton energy regions, one corresponding to neutron energies between 0.65 and 1.2 MeV (designated "most anisotropic" region) and the other corresponding to neutron energies between 1.2 and 3.5 MeV (designated "least anisotropic" region). The mass yield curves at the two angles and for a given proton energy region have been folded and summed to obtain the mass distributions given in Fig. 4. The mass distribution curves before folding exhibited good reflection symmetry.

An examination of the data for a possible dependence of angular anisotropy on mass ratio was performed by dividing the mass yield distribution obtained with the fission detectors parallel to the recoil axis by the mass distribution obtained with the fission detectors perpendicular to the recoil axis. Before division, the mass distributions were first folded, corrected for chance, and then averaged over 4 mass-unit intervals. The results are illustrated in Fig. 5. The error flags represent standard deviations due to

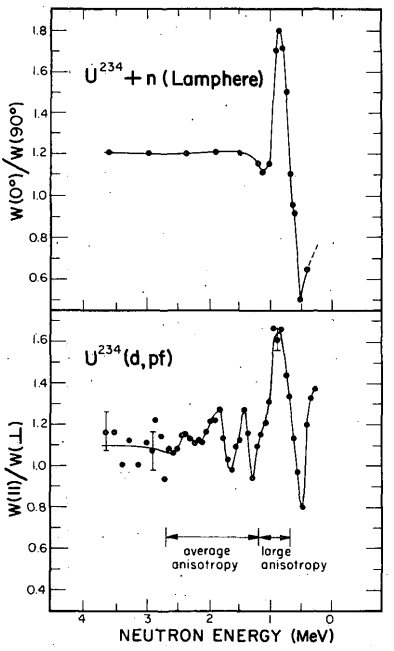

Fig. 3

The upper part of the figure shows the angular anisotropy as a function of neutron energy obtained by Lamphere. The lower part of the figure shows the anisotropy obtained in the $U^{234}(d,pf)$ reaction.

statistical uncertainties only. An additional source of error arises from small uncertainties in the parameters required to transform fission-fragment pulse-heights to fragment masses. Since the mass distributions have very steep slopes the measured anisotropy is rather sensitive to the transformation parameters near symmetry and for large mass ratios. This uncertainty may be comparable to the statistical uncertainties in these mass ratio regions.

The three-parameter pulse-height correlations were also examined for a possible dependence of the total kinetic energy release on excitation energy as defined by the proton kinetic energy. The proton energy spectrum was divided into several groups, each of which corresponds to a maxima or minima in the angular anisotropy due to the opening of a new saddle-point channel. The results are given in Fig. 6.

DISCUSSION

The principal motivation of this experiment was to search for a possible correlation between angular anisotropy and mass asymmetry. Within the accuracy of our experiment we conclude that there is no detectable dependence of the anisotropy on mass asymmetry. The data in Fig. 5a may represent fission occurring primarily through a single saddle-point channel,

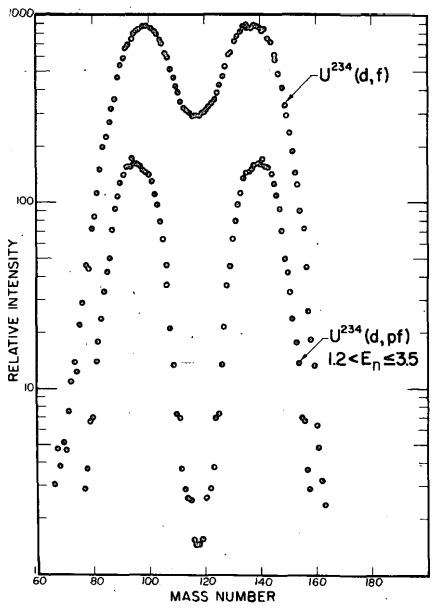

Fig. 4

Fission mass yield curves are shown for fission following deuteron capture (fission occurring at high excitation energies) and for fission occurring after the $U^{234}(d,p)$ reaction. The latter yield curve corresponds to fission occurring at excitation energies resulting from capture of neutrons with energies between 1.2 and 3.5 MeV.

and hence might not be expected to show any dependence of anisotropy on asymmetry. The data in Fig. 5b corresponding to fission induced by neutrons with energies between 1.2 and 3.5 MeV represent a region where at least eight fission channels are open. Failure to observe a dependence of anisotropy with mass ratio in this energy region implies that there is no evidence that the mass division has any direct connection with the saddle-point channels. The mass distribution and the angular anisotropy may each be determined at different, unrelated stages of the distortion that ultimately leads to fission. Theoretical speculations on possible connections between saddle-point symmetry properties and mass distributions for even-even fissioning nuclei have been offered [6, 17]. It is not clear at this point whether the small variations [18, 19] in mass symmetry observed for different capture resonances in low-energy (eV) fission can be attributed to the properties of saddle-point channels. An alternative explanation might be that they reflect some unknown dependence, at a later stage of distortion, of the mass division on the spin of the capturing state.

The angular anisotropy exhibited in Fig. 3 shows considerable structure. The first detailed interpretation of this type of structure was given by WILETS and CHASE [20]. They analysed the anisotropy for fast-neutron-induced fission of Th^{232} and concluded that the observed sidewise-peaking of the fission-fragment angular distribution near threshold was due to a fission channel at the saddle point with $K = 3/2$. As the neutron energy is increased other saddle-point channels are opened and the anisotropy is changed.

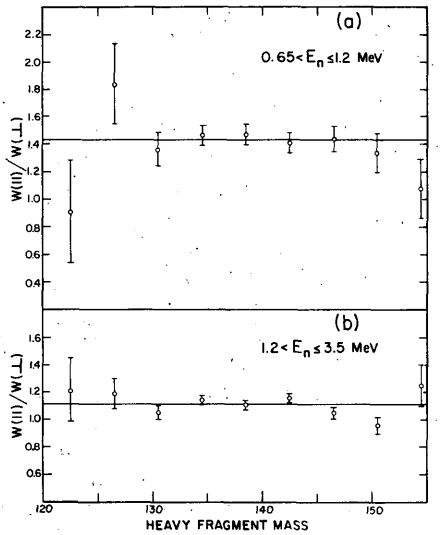

Fig. 5

The dependence of the angular anisotropy on mass asymmetry (as defined by the heavy fragment mass number) is shown for two neutron energy regions as defined by the proton kinetic energy.

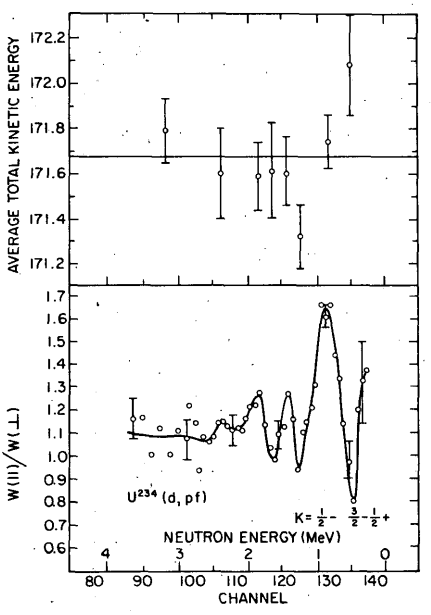

Fig. 6

The upper part of the figure shows the average total fission-fragment kinetic energy as a function of neutron energy. The error flags indicate the relative statistical uncertainty in the average kinetic energy. The absolute value of the total kinetic energy has an uncertainty of 2.0 MeV.

LAMPHERE [13] has performed a channel analysis of his data for neutron-induced fission of U^{234} and concluded that $K = 1/2+$, $K = 3/2-$, and $K = 1/2-$ bands are contributing near threshold.

Considerably more structure in the anisotropy as a function of excitation energy is seen in the (d, pf) experiment than was seen by Lamphere. This may be attributed to two factors. In the first place, Lamphere measured the anisotropy only at intervals of approximately 500 keV at neutron energies above the first large maximum and hence may have missed some structure. Secondly, larger angular momentum transfer is possible with the (d, p) reaction than with fast neutron capture. At the excitation energy corresponding to capture of 1.5 MeV neutrons, distorted-wave calculations indicate that the (d, p) reaction can occur with significant probability for angular momentum transfers as high as $\ell = 6$, whereas capture of 1.5 MeV neutrons gives significant contributions only for $\ell = 3$ and less. This means that there are high K-channels at the saddle-point not accessible in the (n, f) reaction. If one attributes each of the maxima or minima in the angular anisotropy to the opening of a new channel, the data illustrated in Fig.3 indicate that there are approximately 8 channels opened within the first 2 MeV above threshold. It is interesting to note that this average spacing of 250 keV for single-particle (or hole) states is very nearly identical to that observed near the ground states of odd-mass nuclei in the transuranic region [21]. The gradual damping of the amplitudes of the maxima and minima in the angular anisotropy may be attributed to the fact that once a channel is opened it is expected that it will remain open, and hence at high excitation energies many channels are open and the fluctuations will disappear. One might expect an increasingly rapid disappearance of the variations in anisotropy as the excitation energy exceeds the energy gap for three-particle excitations [22]. This might occur at an excitation energy of about 2 MeV. The statistical accuracy of our data in this region is insufficient to permit any conclusion to be drawn concerning a more rapid decrease in the fluctuations in this energy region.

WILETS and CHASE [20] and LAMPHERE [13] have analysed angular distributions for neutron-induced fission of Th^{232} and U^{234} and assigned K and π values to several states close to the Fermi level at the saddle-point of the odd-A nuclei Th^{233} and U^{235}. In principle it should be possible to calculate theoretically the single particle levels for a nucleus stretched to the saddle-point deformation. Such a calculation requires a knowledge of the shape of the nucleus at the saddle point, a property that is poorly defined both experimentally and theoretically. Despite this severe limitation we have attempted to calculate the energies of single particle states at very large deformations using the procedure of NILSSON [23]. We are indebted to R.R. Chasman for providing a computer code enabling us to diagonalize the Nilsson Hamiltonian. Slight modifications of the resulting energy level diagram were made in order to improve agreement with experiment for ground-state equilibrium deformations.

LAMPHERE [13] has assigned K and π values for three states, namely $3/2-$, $1/2+$ and $1/2-$. The first of these states had been previously assigned by WILETS and CHASE [20] as a saddle-point state for Th^{233}, which has 143 neutrons as does U^{235}. One can then ask, at what deformations does the Nilsson model predict these states to be close to the Fermi surface?

TABLE I

THE CALCULATED SINGLE PARTICLE LEVELS, OCCUPIED BY THE N-th NEUTRONS, AS A FUNCTION OF THE NUCLEAR DEFORMATION

U^{235} has 143 neutrons. The states that have been identified experimentally are: K = 1/2+, K = 3/2-, and K = 1/2-. Single particle states with these quantum numbers are underlined for those deformations where possible candidates for all three observed states are calculated to lie fairly close to the Fermi surface.

N/δ	0.3	0.35	0.4	0.45	0.5	0.55
138	5/2-	1/2-	7/2-	1/2+	1/2+	1/2+
140	5/2+	1/2+	1/2+	1/2-	11/2+	11/2+
142	7/2-	3/2-	1/2-	3/2-	7/2-	7/2-
144	1/2-	13/2+	3/2-	9/2-	9/2-	3/2-
146	1/2+	5/2-	3/2-	5/2+	3/2-	5/2-
148	1/2-	1/2-	5/2-	9/2-	5/2+	9/2-
150	5/2+	1/2-	13/2+	3/2-	9/2-	9/2-

(It would seem unrealistic to expect the model to give the exact ordering of the states.) The seven closest to the Fermi level for N = 143 are shown in Table I for several values of the deformation parameter δ. It is seen that the three experimentally-identified saddle-point states are not all found near the Fermi level when δ is 0.5 or larger. This might indicate that the saddle-point is characterized by a deformation of $\delta < 0.5$, which corresponds to a spheroid with a ratio of major to minor semi-axes of less than 1.71. Such a limit does not do violence to any well-established ideas about the saddle-point deformation. On the other hand one must recognize the limitations of the calculation. In the first place, the class of distortions examined was restricted to ellipsoidal shapes with axial symmetry. Liquid-drop model calculations as well as intuition suggest that more cylindrical shapes are quite likely, not to mention the possibility of lack of axial symmetry or reflection symmetry. In the second place, it is not clear that the modified harmonic oscillator potential yields reasonable nuclear densities at larger deformations, as volume conservation is not treated exactly. The qualitative succes of the comparison does suggest the exciting prospect that fission may be useful in studying the single particle level structure of nuclei exhibiting deformations much larger than those exhibited in their ground states.

REFERENCES

[1] COHEN, B.L., JONES, W.H., McCORMICK, G.H. and FERRELL, B.L., Phys. Rev. 94 (1954) 625.
[2] COHEN, B.L., FERRELL-BRYAN, B.L., COOMBE, D.J. and HULLINGS, M.K., Phys. Rev. 98 (1955) 685.
[3] FAIRHALL, A.W., HALPERN, I. and WINHOLD, E.J., Phys. Rev. 94 (1954) 733.
[4] HALPERN, I. and STRUTINSKI, V.M., Proc. 2nd UN Int. Conf. PUAE 15 (1958) 408.
[5] HALPERN, I., Annu. Rev. nucl. Sci. 9 (1959) 245.
[6] BOHR, A., Proc. UN Int. Conf. PUAE 2 (1959) 245.
[7] BARANOV, I.A., PROTOPOPOV, A.W. and EISMONT, V.P., Soviet Physics - JETP 14 (1962) 713.
[8] KUZ'MINOV, Soviet Physics - JETP 15 (1962) 75.
[9] MANLEY, J.H., Nucl. Phys. 33 (1962) 70.
[10] NORTHROP, J.A., STOKES, R.H. and BOYER, K., Phys. Rev. 115 (1959) 1277.
[11] GIBBS, W.R. and GRIFFIN, J.J., private communication.
[12] VANDENBOSCH, R., UNIK, J. and HUIZENGA, J.R., to be published.
[13] LAMPHERE, R.W., Nucl. Phys. 38 (1962) 561.
[14] BRITT, H.C. and WEGNER, H.E., Rev. sci. Instrum. 34 (1963) 274.
[15] WALTER, F.J., MOAK, C.D., NEILER, J.H., SCHMITT, H.W., GIBSON, W.M. and THOMAS, T.D., Bull. Amer. phys. Soc. II 8 (1963) 39.
[16] SCHMITT, H.W., GIBSON, W.M., NEILER, J.H., WALTER, F.J. and THOMAS, T.D., to be published.
[17] WHEELER, J., Physica XXII (1956) 1103.
[18] COWAN, G.A., BAYHURST, B.P. and PRESTWOOD, R.J., Phys. Rev. 130 (1963) 2380.
[19] REGIER, R.B., BURGUS, W.H., TROMP, R.L. and SORENSEN, B.H., Phys. Rev. 119 (1960) 2017.
[20] WILETS, L. and CHASE, D.M., Phys. Rev. 103 (1956) 1296.
[21] STEPHENS, F.S., ASARO, F. and PERLMAN, I., Phys. Rev. 113 (1959) 212.
[22] GRIFFIN, J.J., Phys. Rev. 132 (1963) 2204.
[23] NILSSON, S.G., Mat.-fys. Meddr. 29 (1955) No. 16.

DISCUSSION

R. RAMANNA: I should like to suggest that use of the (dpf) reaction is not the same as using neutrons directly. In this process a high spin of about six-seven units is introduced and this may have an effect on the already complicated process of fission, especially in the determination of K_0^2. In this connection, I would draw attention to our paper in the "Physical Review" for February 1965, which reports results that are indicative of a relation between anisotropy and asymmetry. In this work we used 4-MeV-neutron fission of U^{235} and we observed the same kinetic energy distributions with mass as have been reported by other investigators in the present Symposium. The anisotropy decreases near the shell regions. We believe that this is a more direct method of observing the phenomena and feel that the results reported in Dr. Vandenbosch's paper do not establish definitively that there is no correlation between anisotropy and asymmetry.

R. VANDENBOSCH: There does appear to be an experimental discrepancy between these results and ours. I find it a little difficult to believe, however, that the (dp) process should fail to observe such an effect. Any neutron process would. Comparison with Lamphere's data shows that we have a wider variety of saddle-point states contributing to the fission process rather than fewer; and if there is any difference associated with saddle-point states, then I would expect that by having a lot of different states available one would be able to see the effect.

S.S. KAPOOR: It is possible that the discrepancy between our results on mass asymmetry versus anisotropy and yours may be due to the different excitation energies involved in the two cases. Another point is that the dependence of mass distribution on the resonance channels is known, and this is indicative of a possible dependence of mass asymmetry on the saddle-point states.

R. VANDENBOSCH: I should like to comment on this question of a possible dependence of mass asymmetry on the resonance spin. There is some evidence that fluctuations occur in mass asymmetry as one goes from resonance to resonance. To my knowledge, however, the idea that this dependence is determined at the saddle point is pure speculation. I know of no experimental evidence that indicates that this dependence on spin is manifested in the fission process at a stage of distortion as early as the saddle point. It would certainly be interesting to hear any evidence based on mass asymmetry data for resonance events indicative of the fact that this is a spin effect that can be attributed to the saddle point.

B.D. KUZMINOV: The individual fission channels are fairly clearly separated in the work reported by Dr. Vandenbosch, and perhaps he could give us some information on the subject of fission-fragment yields with different masses in different channels.

R. VANDENBOSCH: One of the unfortunate consequences of our superior mass resolution was that it was not possible with our very deep valleys to obtain statistically significant data if we tried to sort them into too many individual channels. We were only able, therefore, to sort our data into the two different regions that have been mentioned. The argument that makes this relevant to the way we carried out our experiment is that if one looks at the mass distribution for a mixture of channels, and if one of these channels has a mass distribution different from that of another channel, it should be possible to see a dependence of the angular anisotropy upon mass asymmetry. It would have been useful to have sorted the data in smaller bands but we only had approximately 20 000 events and it was not possible to make a division into smaller regions.

M.S. MOORE: May I also offer some remarks on this question of evidence for a mass dependence of the channel structure at the saddle point, as shown in the low-energy resonances. The evidence we have is indirect. It is well established, however, that low-energy-resonance fission is a few-channel process. The fact that there are variations in the mass distribution from resonance to resonance is also well established. It thus seems reasonable to assume that the few channels of low-energy-resonance fission belong in fact to the same type of channel for which we have direct evidence in (dpf) reactions, for example.

R. VANDENBOSCH: I would agree that the channels we observe in (dpf) reactions are undoubtedly the same as those observed in the resonance region. I just know of no experimental evidence that would indicate that the characteristics of these channels, as far as the mass distribution is concerned, are those of the channel at the saddle point.

J. GRIFFIN: Could you comment on the statistical reliability of the points plotted in Fig. 6 of your paper, since error bars were not given for each point?

R. VANDENBOSCH: Representative error bars are given in Fig. 6. Reference to Fig. 2, where the number of counts observed as a function of energy is given, will enable you to obtain the errors for the other points by interpolation.

G. RIPKA: In connection with your identification of Nilsson orbits corresponding to various deformations, I would like to draw attention to the restricted Hartree-Fock methods that are available. These are restricted Hartree-Fock calculations because nucleons are placed on orbits of a harmonic oscillator of a given size, and deformations are described by mixing various angular-momenta states in the single-particle orbits; these orbitals are similar to Nilsson orbitals except that the Nilsson coefficients are determined in a self-consistent way by the nucleon-nucleon interaction.

These methods have been successfully used in light nuclei. The simplicity in such cases makes it reasonable to suppose that they can be applied to heavy nuclei to describe deformations from the ground state to the saddle point. One difference with the liquid-drop model is that the surface tension would be replaced by the nucleon-nucleon interaction. In addition, the energy of Nilsson orbits often differs a great deal from the Hartree-Fock orbits, usually in the direction of experimental evidence.

R. VANDENBOSCH: I realize that this comparison with the Nilsson model is very qualitative and is subject to many criticisms. I have outlined in my paper some of the doubts I feel on this score. One problem is that the Nilsson calculation is for a spheroidal nucleus whereas the saddle point may not be spheroidal; in fact it may be more nearly cylindrical, for example.

ÉTUDE DES SPECTRES EN MASSE DES FRAGMENTS DE FISSION APRÈS ÉMISSION NEUTRONIQUE PROMPTE

C. SIGNARBIEUX ET M. RIBRAG
CENTRE D'ÉTUDES NUCLÉAIRES DE SACLAY, FRANCE

Abstract — Résumé — Аннотация — Resumen

A STUDY OF THE MASS SPECTRA OF FISSION FRAGMENTS AFTER PROMPT NEUTRON EMISSION. The distribution of the masses of fission fragments, following neutron emission, was obtained by simultaneously measuring the velocity and energy of each particle. The special feature of this method is that it is essentially independent of the initial energy of the fragments, so that we were able to use relatively thick targets of fissionable material (0.1 mg/cm^2). The energy measurement is made by a gold-silicon surface barrier detector; the velocity measurement was made on a flight path of 130 cm, with a total resolving power of 1.5 ns. The "starting" detector consisted of a windowless photomultiplier that detected directly the secondary electrons emitted by a thin metallic sheet during the passage of the fission fragments. The "stop" signal is picked up directly, by means of a transformer, on the semi-conductor detector. The results given in the paper relate to the thermal fission of U^{235}, and are compared with the results obtained by the radiochemical method.

ETUDE DES SPECTRES EN MASSE DES FRAGMENTS DE FISSION APRÈS EMISSION NEUTRONIQUE PROMPTE. Nous avons obtenu la distribution des masses des fragments de fission après émission neutronique en mesurant simultanément, sur chaque particule, sa vitesse et son énergie. Cette méthode offre la particularité d'être essentiellement indépendante de l'énergie initiale des fragments: nous avons donc pu utiliser des cibles relativement épaisses de matériau fissile (0,1 mg/cm^2). La mesure d'énergie est effectuée par un détecteur à barrière de surface Au-Si; la mesure de vitesse était effectuée sur une base de vol de 130 cm avec une résolution globale de 1,5 ns. Le détecteur «start» est constitué par un photomultiplicateur sans fenêtre, détectant directement les électrons secondaires émis par une feuille métallique mince, au passage des fragments de fission. Le signal «stop» est prélevé directement, au moyen d'un transformateur, sur le détecteur à semi-conducteur.

Les résultats donnés ici concernent la fission thermique de ^{235}U et sont comparés aux résultats obtenus par la méthode radiochimique.

ИЗУЧЕНИЕ МАСС-СПЕКТРОВ ОСКОЛКОВ ДЕЛЕНИЯ ПОСЛЕ МГНОВЕННОГО НЕЙТРОННОГО ИЗЛУЧЕНИЯ. После нейтронного излучения и путем измерения одновременно скорости и энергии каждой частицы было получено распределение масс осколков деления. Этот метод дает возможность быть в значительной степени независимым от начальной энергии осколков: поэтому можно было использовать относительно толстые мишени делящегося материала (0,1 мг/см^2). Измерение энергии проводилось с помощью детектора с перегородкой, поверхность которой была покрыта золотом и кремнием; измерение скорости проводилось на основе пролета в 130 см с полной разрешающей способностью в 1,5 н/сек. Детектором "Пуск" является фотоумножитель без окна, который непосредственно обнаруживает вторичные электроны, излучаемые тонким металлическим листом, при прохождении осколков деления. Сигнал "Стоп" принимается полупроводниковым детектором непосредственно через трансформатор.

Приводимые здесь результаты относятся к делению на тепловых нейтронах урана-235 и сравниваются с результатами, полученными радиохимическим методом.

ESTUDIO DE LOS ESPECTROS MASICOS DE LOS FRAGMENTOS DE FISION DESPUES DE LA EMISION DE NEUTRONES INMEDIATOS. Los autores han determinado la distribución másica de los fragmentos de fisión después de la emisión neutrónica, midiendo simultáneamente la velocidad y la energía de cada partícula. Este método tiene la particularidad de ser esencialmente independiente de la energía inicial de los fragmentos, lo que ha permitido a los autores utilizar blancos de materiales fisionables relativamente gruesos (0,1 mg/cm^2). La medición de la energía se efectúa con un detector de Au-Si de barrera superficial, y la de la velocidad, sobre una base de vuelo de 130 cm con una resolución global de 1,5 ns. El detector inicial está constituido por un fotomultiplicador sin ventana, que detecta directamente los electrones secundarios emitidos por una

lámina metálica delgada al paso de los fragmentos de fisión. La señal terminal se toma directamente del detector de semiconductor por medio de un transformador.

Los resultados presentados en la memoria se refieren a la fisión térmica del ^{235}U y se comparan con los obtenidos por el método radioquímico.

Le développement des techniques de mesure précise de l'énergie de la vitesse des fragments de fission permet d'envisager la détermination de la distribution de probabilité $P(M_1, M_2, E_{ct}, n_1, n_2)$*, apportant ainsi une contribution importante à la connaissance de l'état de déformation du noyau au moment de la scission. L'expérience consiste à mesurer, pour chaque événement de fission, les vitesses et les énergies non dégradées des deux fragments.

Dans le cadre de ce projet, nous présentons ici une expérience de corrélation énergie-vitesse réalisée sur un seul fragment: cette mesure, par application de la relation $E = 1/2\ MV^2$, permet de déterminer directement la distribution des masses des fragments après émission des neutrons prompts; cette méthode de détermination des masses ne dépend pas de l'état cinétique de la particule, ce qui permet d'utiliser des cibles relativement épaisses de matériau fissile.

Dans notre expérience la vitesse des fragments est mesurée par la méthode du temps de vol sur une base de vol de 130, 6 cm; l'énergie est mesurée par un détecteur à barrière de surface Au-Si. La cible d'uranium-235 était placée dans un faisceau neutronique non filtré de la pile EL2 de Saclay ($\sim 10^7 n_{th}/cm^2\ s$). La cible de 100 $\mu g/cm^2$ d'uranium-235, enrichi à 99, 51%, était obtenue par déposition électrochimique. Le schéma général de l'appareillage est montré à la figure 1.

I. MESURE DES VITESSES DES FRAGMENTS

1. Détecteur de temps zéro

Ce détecteur est fondé sur le principe suivant [1] : lorsqu'une particule ionisante traverse une feuille métallique, elle éjecte en surface des électrons secondaires dont l'énergie moyenne est de quelques eV (les fragments de fission, au début du parcours, arrachent 120 électrons en moyenne [2]).

La figure 2 montre la coupe du détecteur que nous avons utilisé: un trou dans le cylindre de l'optique d'entrée d'une structure multiplicatrice d'électrons permet au faisceau des fragments de fission de frapper la cathode dont la partie centrale est constituée par une feuille mince d'acétate de cellulose (12 $\mu g/cm^2$) rendue conductrice par un voile d'Au (20 $\mu g/cm^2$). La structure multiplicatrice et son optique d'entrée sont du type 56 AVP, spécialement étudiés pour des mesures de temps (temps de montée de l'impulsion anodique: 3 ns, fluctuation du temps de transit: quelques dixièmes de ns, gain : 10^8).

La figure 3 montre la distribution des amplitudes des impulsions anodiques en coïncidence avec les particules α et les fragments de fission. L'ef-

* M_1, M_2 : masses primaires des deux fragments; E_{ct} énergie cinétique des deux fragments avant l'émission prompte des neutrons; n_1, n_2 nombres de neutrons prompts relatifs aux deux fragments.

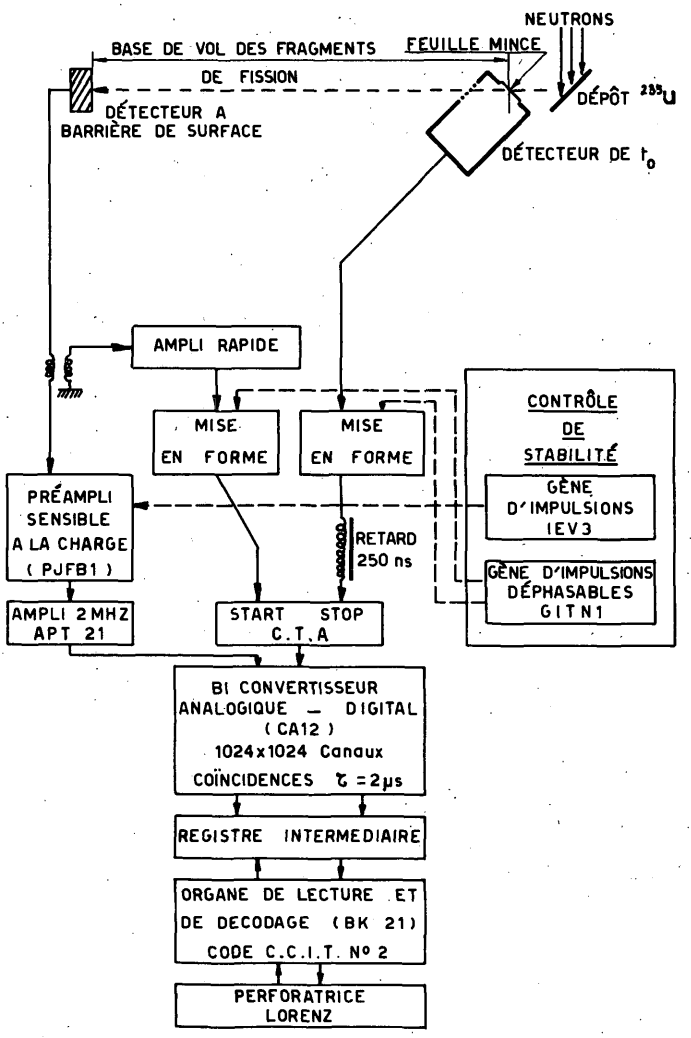

Figure 1

Schéma de l'installation.

ficacité pour les fragments de fission était strictement 100%, l'efficacité pour les particules α était 85%. Le spectre de la figure 1 appelle la remarque suivante: le pic fission présente bien la même forme que le pic obtenu par une autre méthode de détection [2]; par contre, la mauvaise séparation α-fission semble indiquer une mauvaise efficacité de collection des électrons secondaires, qui s'explique si le spectre des vitesses des électrons secondaires est très étalé.

Les avantages de ce mode de détection des électrons secondaires sont l'absence de bruit de fond thermoélectronique, la très faible efficacité à une ambiance γ et neutrons rapides (d'où facilité d'utilisation à proximité d'un faisceau de pile) et le faible encombrement.

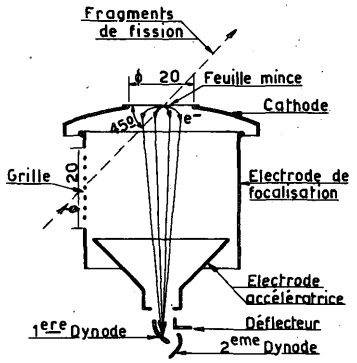

Figure 2

Coupe d'un détecteur de temps zéro.

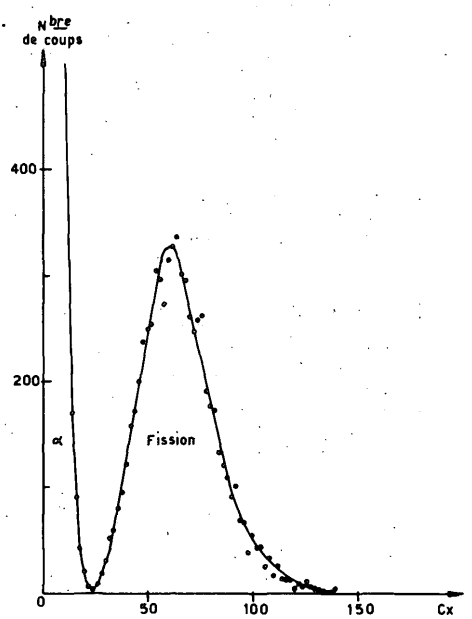

Figure 3

Spectre d'amplitude du détecteur de temps zéro.

2. *Signal « stop »*

Nous avons utilisé le principe indiqué par WILLIAMS et al. [3] : un signal rapide est prélevé au secondaire d'un transformateur dont le primaire est en série avec le détecteur à semi-conducteur. Ce signal rapide est amplifié dans un circuit de gain 60 et de 4 ns de temps de montée.

3. Conversion temps-amplitude:

Les signaux « start » et « stop » étaient mis en forme afin de conserver la fonction temps quelle que soit l'amplitude du signal. Le principe [4] consiste à superposer à l'impulsion originale une impulsion identique, retardée, amplifiée et en opposition de phase telle que la pente de l'impulsion résultante soit maximum au passage à zéro. Nous montrons à la figure 4 la façon dont la superposition est réalisée dans un transformateur de rapport 1.

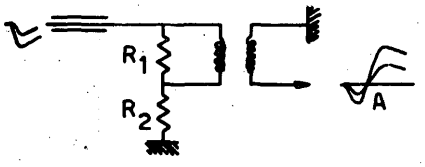

Figure 4

Superposition d'impulsions dans un transformateur de rapport 1.

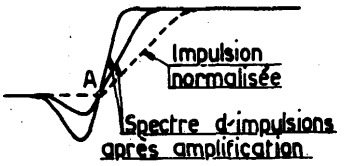

Figure 5

Spectre d'impulsions amplifié, écrêté et normalisé.

Compte tenu du temps de montée des impulsions origine, nous avons ajusté les paramètres $R_1/(R_1+R_2)$ et la longueur l des enroulements pour obtenir au point A une pente maximum. Le spectre d'impulsions résultant est amplifié, écrêté et finalement normalisé (fig. 5).

Sur la voie « start » un retard fixe, supérieur au temps de vol le plus long, permet d'inverser les fonctions des deux voies. Les signaux « stop » et « start » retardé sont alors mélangés pour attaquer une diode tunnel fonctionnant en bistable. Les créneaux engendrés, de largeur proportionnelle au temps de vol, sont convertis de façon classique en impulsions d'amplitude proportionnelle. La résolution intrinsèque du convertisseur temps-amplitude est de $7 \cdot 10^{-11}$ s. Dans la plage d'analyse utilisée dans la présente expérience, la linéarité était meilleure que 1%. Pendant tout le temps de l'expérience (environ 100 h) la stabilité de l'ensemble était meilleure que 0,5%.

4. Résolution obtenue sur les mesures de temps

Une expérience à longueur de vol nulle a été réalisée en substituant à la feuille mince placée sur la cathode du détecteur de temps zéro la surface d'un détecteur Au-Si. Nous avons ainsi mesuré une résolution en temps de 1,2 ns. Compte tenu des fluctuations sur la longueur des trajectoires de vol des fragments, nous obtenons une résolution en temps globale de 1,5 ns.

5. Calibration absolue des mesures de temps

Nous avons réalisé successivement deux expériences de temps de vol correspondant à deux bases de vol différentes: 90,6 cm et 130,6 cm. Dans les deux cas nous avons déterminé le temps de vol le plus probable T du groupe des fragments légers en lissant le pic expérimental par une fonction gaussienne. L'écart ($T_{130,6} - T_{90,6}$) a été étalonné avec un générateur d'impulsions déphasables dont la calibration a été soigneusement vérifiée. La connaissance précise des deux longueurs de la base de vol et la bonne linéarité dans la plage d'analyse permettent ainsi de calculer avec une précision meilleure que 1% les valeurs absolues des vitesses.

II. MESURE DE L'ÉNERGIE CINÉTIQUE DES FRAGMENTS

Nous avons utilisé un détecteur à barrière de surface Au-Si (ORTEC) de 2 cm^2 de surface active et un préamplificateur sensible à la charge et à faible bruit de fond (résolution de 45 keV pour des α de 5 MeV). Nous avons pris la précaution d'opérer dans la région de saturation du détecteur (amplitude du signal indépendante de la polarisation).

La calibration en énergie a été obtenue par la méthode proposée récemment par SCHMITT et al. [5]. La relation de correction fait intervenir la masse M du fragment; si X est l'amplitude de la réponse de la jonction, l'énergie est donnée par la relation.

$$E = (a + a' M) X + (b + b' M).$$

Les coefficients a, a', b, b' peuvent être calculés à partir de la distribution des énergies des fragments de fission du ^{252}Cf. Nous montrons sur la figure 6 notre spectre et le spectre de référence de SCHMITT [5]. La similitude des deux spectres est totalement satisfaisante.

III. ENREGISTREMENT ET TRAITEMENT DES DONNÉES

Les impulsions de la voie énergie et de la voie temps sont analysées en amplitude au moyen de deux convertisseurs analogiques digitaux de 1024 canaux, fonctionnant en coïncidence ($\tau = 0,5\ \mu s$) (figure 1). Chaque information (énergie-temps de vol) est stockée dans un registre binaire décimal et décodée sur bande perforée. Les informations sont ensuite transférées sur bande magnétique et dépouillées sur calculateur IBM 7092. L'ensemble des données expérimentales est présenté sous forme de tableau carré sur lequel ont été tracées des courbes de niveau (fig.7).

Le problème de la transformation d'une distribution expérimentale fonction de deux paramètres en distribution de deux variables différentes, fonctions des deux premières, a été discuté par plusieurs auteurs [6]. Nous avons adopté la solution suivante:

a) Utilisation d'une résolution d'analyse maximum pour chaque paramètre (950 canaux pour l'énergie, 600 canaux pour le temps).

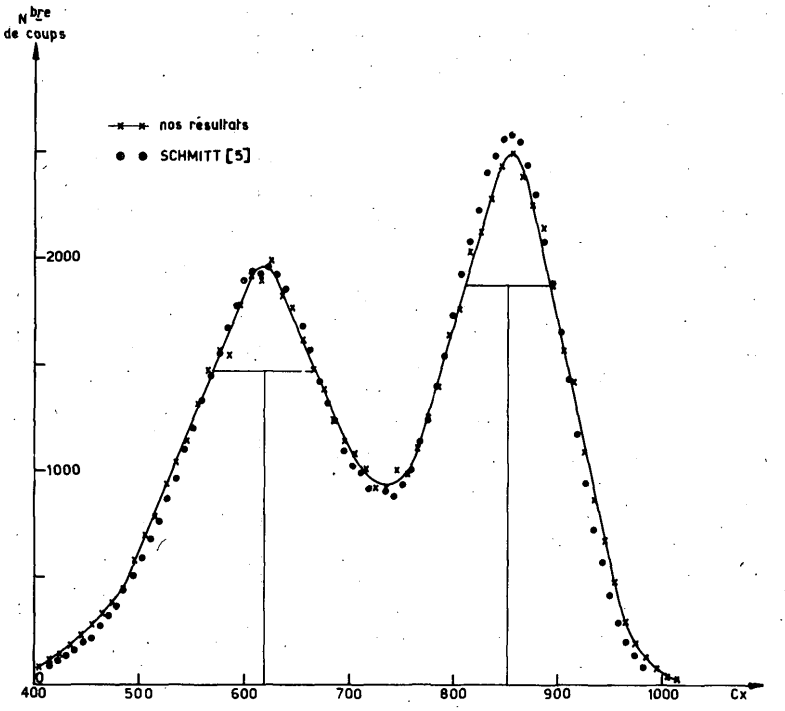

Figure 6

Spectre des énergies de ^{252}Cf utilisé pour la calibration du détecteur à semi-conducteur.

b) Calcul de la masse, événement par événement:
- en résolvant en M l'équation : $E = 1/2\ MV^2 = (a + a' M) X_E + (b + b' M)$;
- en ajoutant statistiquement à la masse ainsi calculée $\pm\ \Delta M$ (ΔM étant la variation de la masse dans la case (X_E, V) considérée);
- en prenant la partie entière du résultat.

IV. RÉSULTATS

Il a été montré [5] que dans un détecteur à semi-conducteur la résolution en énergie est indépendante de la masse et de l'énergie des fragments; de même, nous avons vérifié que notre résolution en temps était pratiquement indépendante de l'énergie; dans ces conditions, la résolution en masse varie peu en fonction de la masse : sa valeur moyenne était de 4 unités de masse (largeur à mi-hauteur).

La distribution des masses non corrigée de la résolution est montrée sur la figure 8; nous avons également porté les valeurs obtenues par les radiochimistes [7]. L'accord entre les deux distributions est bon. Pour tester de façon plus précise nos méthodes de calibration, nous avons lissé chacune de ces deux distributions par deux fonctions gaussiennes: nous présentons dans le tableau ci-après les masses lourde et légère les plus probables ainsi

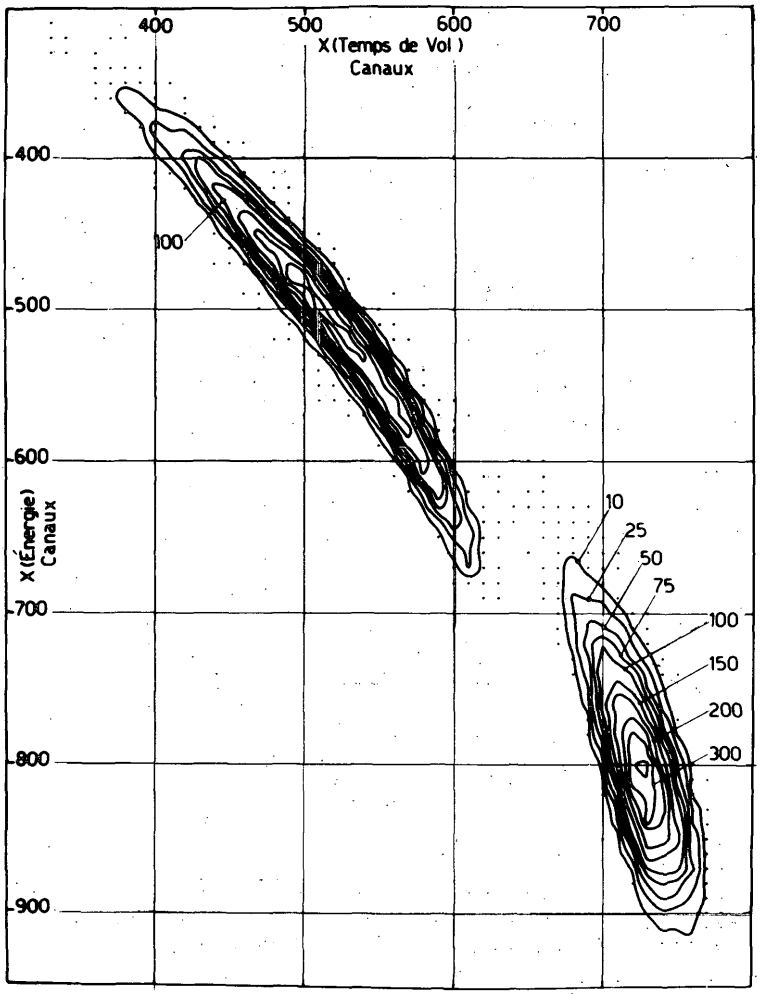

Figure 7

Fission thermique de ^{235}U (données correlées).
Énergie - temps de vol des fragments (25 100 informations).

que les largeurs Σ_M des pics lourd et léger (corrigées de la résolution dans notre cas).

	$M_{léger}$	M_{lourd}	$\sigma_{léger}$	σ_{lourd}
Radiochimie	95, 3	138, 0	6, 15	6, 28
Cette expérience	95, 2	138, 0	6, 25	6, 35

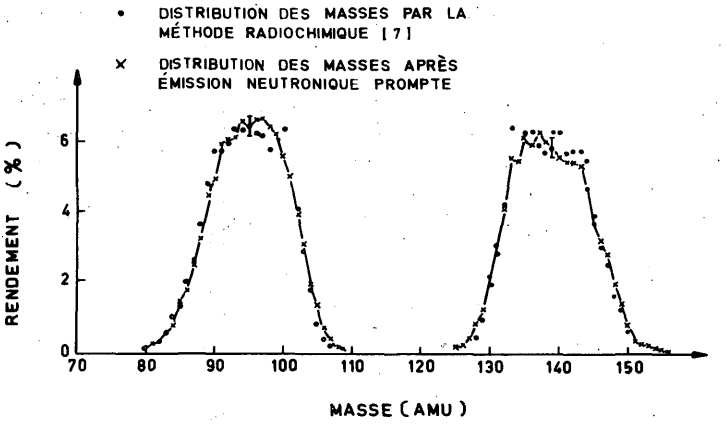

Figure 8

Fission thermique de ^{235}U.

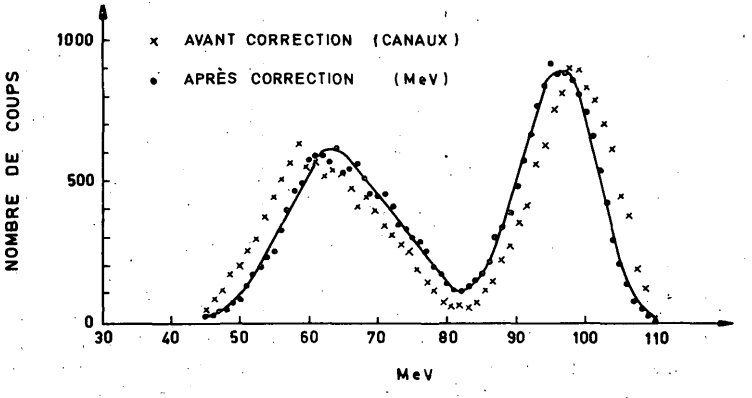

Figure 9

Spectre d'énergie de ^{235}U obtenu avec un détecteur à barrière de surface.

L'accord entre ces valeurs est excellent et parfaitement compatible avec la précision des mesures.

L'existence de structures fines sur la distribution des masses obtenue par les radiochimistes n'est pas retrouvée de façon significative dans nos mesures: il est clair que la faible statistique et la faible résolution en masse de notre expérience ne permettent pas de tirer des conclusions.

Sur la figure 9 est montrée la distribution des énergies des fragments après corrections, ainsi que la distribution des amplitudes du détecteur Au-Si. Arbitrairement nous avons fait coïncider les creux des spectres afin de mettre en évidence de façon frappante la distorsion introduite par le « défaut d'amplitude » de ce type de détecteur: si la forme des pics est assez bien conservée, leur séparation est très augmentée avec, corrélativement, une augmentation importante du rapport (pic léger/creux).

Sur la figure 10 nous présentons la variation de l'énergie cinétique moyenne en fonction de la masse des fragments: nous observons des caractéristiques identiques à celles obtenues dans des expériences de double temps de vol (mesures avant émission des neutrons prompts) [8] : variation pratiquement constante pour les masses légères, variation décroissante quand la masse croît pour les masses lourdes et un creux assez prononcé dans la région des masses moyennes. Ce dernier point, bien que signalé par plusieurs auteurs [8], reste sujet à caution, du fait que les modes de fission

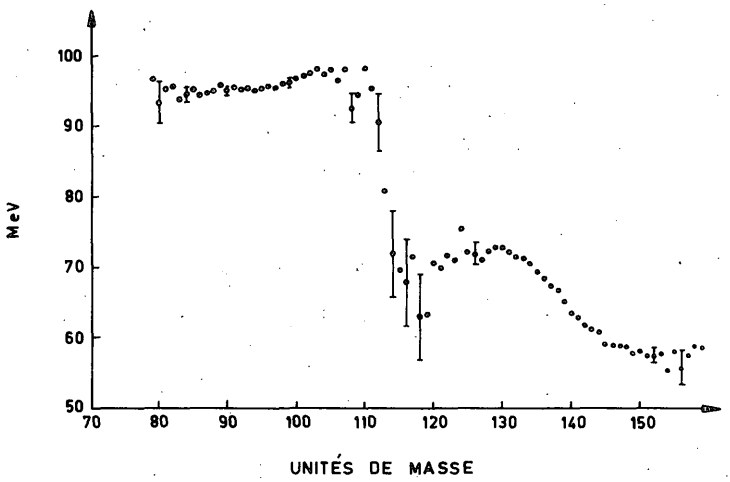

Figure 10

^{235}U-énergie cinétique moyenne en fonction de la masse des fragments.

près de la symétrie ont de très faibles probabilités et que les méthodes physiques introduisent des événements aberrants dus aux queues des fonctions de résolution (les radiochimistes trouvent 0, 12% des fragments pour les 16 unités de masse voisines de la symétrie; dans le même intervalle nous détectons 0, 4% des fragments). Ce problème sera complètement résolu dans les expériences à quatre dimensions (mesures simultanées des énergies et vitesses sur les deux fragments d'une même fission): des tests de concordance entre les quatre paramètres permettront d'éliminer sans ambiguité les informations aberrantes.

D'une façon générale l'excellent accord entre nos résultats et ceux de la radiochimie donne une confiance augmentée dans la valeur de la calibration des détecteurs à semi-conducteurs proposée par SCHMITT et al. [5].

RÉFÉRENCES

[1] STEIN, W.E., and LEACHMAN, R.B., Rev. sci. Instrum. 27 (1956) 1049.
[2] FRASER, J.S., and MILTON, J.C.D., Nucl. Instrum. Meth. 2 (1958) 275-80.
[3] WILLIAMS, C.W., KIKER, W.E. and SCHMITT, H.W., Rev. sci. Instrum. 35 (1964) 1116-23.
[4] BASIRE, A., DE COSNAC, B. et LABBÉ, J., Électronique Nucléaire 1963, OCDE-Agence européenne pour l'énergie nucléaire (1964) 325-32.

[5] SCHMITT, H.W., KIKER, W.E. and WILLIAMS, C.W., Phys. Rev. (à paraître).
[6] THOMAS, T.D. and GIBSON, W.M., CU (PN PL) - 227 (1963) 132-7.
[7] WALKER, W.H., AECL-1054 (1960) 16-7.
[8] MILTON, J.C.D. and FRASER, J.S., Canad. J. Phys. 40 (1962) 1626-63.

RANGE AND RANGE DISPERSION OF SOME FISSION PRODUCTS FORMED BY THE Pu^{239} (n_{th}, f) REACTION

H. MÜNZEL, M. HOLLSTEIN AND T. ISHIMORI
KERNFORSCHUNGSZENTRUM KARLSRUHE,
KARLSRUHE, FEDERAL REPUBLIC OF GERMANY

Abstract — Résumé — Аннотация — Resumen

RANGE AND RANGE DISPERSION OF SOME FISSION PRODUCTS FORMED BY THE Pu^{239} (n_{th}, f) REACTION. The range of some Pu^{239} fission products ($83 \leq A \leq 143$) in aluminium was determined by the thick-target/thick-catcher method and from this their kinetic energy was calculated. A Pu^{239}-aluminium-alloy was used as the target material. An analysis of the results based upon the Whetstone model indicates that both Pu^{239} and U^{235} undergo practically the same fission mechanism with thermal neutrons. In this analysis the ranges measured in air by Katcoff also were used after a transformation to ranges in aluminium.

Furthermore the differential distribution of the "cumulative" ranges of Ba^{140} and Sb^{127} were determined by means of the aluminium-stripping method. The half-widths of the distribution for the two masses are $(20.2 \pm 1.0)\%$ and $(23.1 \pm 1.7)\%$ respectively, and correspond to respective mean ranges of (3.00 ± 0.10) and (3.6 ± 0.2) mg Al/cm^2.

The former values are nearly a factor of two greater than those determined with gaseous stopping materials. A background found in the low-range side of the distribution could not be explained, but some possibilities concerning its origin have been eliminated experimentally. Another result of the experiments showed that the aluminium-stripping method gives broadened distribution curves for elements more electropositive than aluminium.

According to the experiments of Niday, as well as Brown and Oliver, the range of shielded nuclides is unexpectedly small. To examine this effect, the "fragment"-ranges of Ba^{139} and Cs^{139} in aluminium were determined by the thick target/thick catcher method. These ranges are also smaller than the mean range for the isobaric chain 139. This deficiency increases with increasing value of $Z - Z_p$. The influence of this range deficit on the calculated width of the kinetic energy distribution is discussed.

PARCOURS ET DISPERSION DU PARCOURS DE CERTAINS PRODUITS DE LA FISSION DE ^{239}Pu PAR DES NEUTRONS THERMIQUES. Les auteurs déterminent le parcours de certains produits de la fission de ^{239}Pu ($83 \leq A \leq 143$) dans l'aluminium par la «méthode du piège épais et de la cible épaisse» et calculent à partir de là leur énergie cinétique. L'analyse des résultats d'après le modèle de Whestone indique que ^{239}Pu et ^{235}U suivent pratiquement le même mécanisme de fission par les neutrons thermiques. Pour cette analyse, on a pris les parcours mesurés dans l'air par Katcoff et on les a transformés pour les adapter aux parcours dans l'aluminium.

De plus, on a déterminé la distribution différentielle des parcours «cumulatifs» de ^{140}Ba et de ^{127}Sb par la méthode du stripage dans l'aluminium. Les demi-largeurs de la distribution pour les deux masses sont respectivement $(20,2 \pm 1,0)\%$ et $(23,1 \pm 1,7)\%$ et correspondent aux parcours moyens respectifs de $(3,00 \pm 0,10)$ et $(3,6 \pm 0,2)$ mg Al/cm^2.

Les valeurs précédentes sont supérieures d'un facteur de presque 2 à celles qui sont déterminées avec des matières d'arrêt gazeuses. Les auteurs n'ont pas trouvé l'explication du bruit de fond constaté dans la partie à faible parcours de la distribution, mais ils ont pu éliminer expérimentalement certaines hypothèses concernant leur origine. Un autre résultat des expériences est que la méthode du stripage dans l'aluminium donne des courbes de distribution élargies pour les éléments plus électropositifs que l'aluminium.

D'après les expériences de Niday ainsi que celles de Brown et Oliver, le parcours des nucléides blindés est singulièrement faible. Pour examiner cet effet, les auteurs ont observé les parcours de ^{139}Ba et ^{139}Cs dans l'aluminium par la «méthode du piège épais et de la cible épaisse». Ces parcours sont également plus faibles que le parcours moyen de la série isobare de numéro 139. La différence croît lorsque la valeur de $Z - Z_p$ augmente. Les auteurs discutent l'influence de cette différence de parcours sur la largeur calculée de la distribution de l'énergie cinétique.

ПРОБЕГ И ПРБЕГ-ДИСПЕРСИЯ НЕКОТОРЫХ ПРОДУКТОВ ДЕЛЕНИЯ, ОБРАЗОВАВШИХСЯ ПРИ РЕАКЦИИ ($n_{тепл}$ f) ПЛУТОНИЯ-239. Пробег некоторых продуктов деления плутония-239 ($83 \leq A \leq 143$) в алюминии был определен с помощью метода толстой мишени – толстой ловушки, и по этим данным была рассчитана их кинетическая энергия. Сплав плутоний-239 – алюминий использовался в качестве материала мишени. Анализ результатов, основанный на модели Уетстоуна, показывает, что плутоний-239 и уран-235 имеют практически одинаковый механизм деления тепловыми нейтронами. В этом анализе использовались также пробеги, измеренные в воздухе Катковым, но перед этим производился их перерасчет в пробеги в алюминии.

Кроме того, дифференциальное распределение "совокупных" пробегов бария-140 и сурьмы-127 было определено с помощью метода стриппинга алюминия. Полуширина распределения для этих двух масс составляет соответственно $(20,2 \pm 1,0)\%$ и $(23,1 \pm 1,7)\%$ и отвечает соответствующим средним пробегам, составляющим $(3,00 \pm 0,10)$ и $(3,6 \pm 0,2)$ мг алюминия на 1 $см^2$.

Первые значения почти в 2 раза превышают значения, полученные с помощью газообразных тормозящих материалов. Фон, обнаруженный в части распределения с малым пробегом, объяснен быть не может, однако экспериментальным путем были устранены некоторые возможные причины его возникновения. Другой результат этих экспериментов показал, что метод стриппинга алюминия дает уширенные кривые распределения для более электропозитивных элементов, чем алюминий.

Согласно данным экспериментов Нидея, а также Брауна и Оливера, пробег экранированных изотопов является неожиданно небольшим. Для изучения этого эффекта пробеги "осколков" бария-139 и цезия-139 в алюминии были определены с помощью метода толстой мишени – толстой ловушки. Эти пробеги были также меньше, чем средний пробег для изобарической цепочки 139. Дефект увеличивается с увеличением значения $Z - Zp$. Рассматривается вопрос о влиянии этого недостатка пробега на вычисленную ширину распределения кинетической энергии.

ALCANCE Y DISPERSION DE ALCANCES DE ALGUNOS PRODUCTOS DE FISION RESULTANTES DE LA REACCION $^{239}Pu(n_t, f)$. Se calculó el alcance de algunos productos de fisión del ^{239}Pu ($83 \leq A \leq 143$) en aluminio, por el método del blanco y colector gruesos, y sobre esa base, se ha deducido la energía cinética de los mismos. Como blanco se utilizó una aleación de ^{239}Pu y Al. Un análisis de los resultados, con arreglo al modelo de Whetstone, indica que tanto el ^{239}Pu como el ^{235}U experimentan prácticamente el mismo mecanismo de fisión por neutrones térmicos. Para el análisis se emplearon los alcances medidos en aire por Katcoff, después de reducirlos a alcances en aluminio.

Asimismo, se ha determinado, por el método de absorción con aluminio, la distribución diferencial de los alcances "acumulativos" del ^{140}Ba y del ^{127}Sb. La semiamplitud de la distribución de las dos masas asciende a $(20,2 \pm 1,0)\%$ y $(23,1 \pm 1,7)\%$, respectivamente, y corresponde a alcances medios respectivos de $(3,00 \pm 0,10)$ y $(3,6 \pm 0,2)$ mg Al/cm^2.

Estos valores son casi el doble de los determinados con materiales de frenado gaseosos. No ha sido posible explicar una actividad de fondo observada al principio de la curva de distribución, pero se han descartado experimentalmente algunos orígenes que en un principio parecían plausibles. Otro resultado de los experimentos es que, con el método de absorción mediante Al, se obtienen curvas de distribución aplanadas para los elementos de carácter más electropositivo que el aluminio.

En comparación con los experimentos de Niday y de Brown y Oliver, el alcance de los núclidos blindados es sorprendentemente pequeño. Para estudiar este efecto, se ha determinado el alcance de los fragmentos de fisión del ^{139}Ba y ^{139}Cs en aluminio, por el método del blanco y colector gruesos. Estos alcances son también menores que el alcance medio correspondiente a la cadena isobárica 139. Esta diferencia aumenta al crecer los valores de $Z - Z_p$. Se examina la influencia de la cortedad del alcance en el cálculo de la amplitud de distribución de la energía cinética.

The sequence of a nuclear fission event can be described schematically as follows:

$$\underset{(A,Z)}{\text{fissile nucleus}} \rightarrow \underset{(A_B,Z_B)_L+(A_B,Z_B)_H}{\text{primary fragments}} \rightarrow \underset{(A_F,Z_F)_L+(A_F,Z_F)_H}{\text{primary fission products}} \xrightarrow{\beta^-} \underset{(A_S,Z_S)_L+(A_S,Z_S)_H}{\text{fission products}}$$

(A = mass number; Z = atomic number; L or H = light or heavy nucleus, respectively).

Only the properties of the primary and later fission products, but not those of the primary fragments, can be determined experimentally. The properties of primary fission products, designated by the index F, are in most cases hard to determine since their half-life is often too short to permit nuclear chemistry investigation. The majority of previous fission studies, therefore, have dealt with the determination of the properties of fission products, e.g. fission product yield, kinetic energy, etc. When evaluating these results one has to consider that they represent the sum or the average, as the case may be, of the properties of all fragments with $Z_F \leq Z_S$ within a particular isobaric chain A_S. In the following paragraphs we discuss the properties of isobaric chains (index IS) if $Z_S \geq Z_P + 2$ (Z_P = most probable charge). Elsewhere we shall use the term cumulative properties (index C).

The aim of the present investigations was to obtain more data on the energy conditions existing in the fission of Pu^{239} by thermal neutrons. We therefore determined the range (R_{IS}) and range dispersion of certain isobaric chains as well as the range (R_F) of particular primary fission products. The investigations are still under way and the following represents only a preliminary evaluation of the data.

RANGE OF AN ISOBARIC CHAIN

The ranges R_{IS} for some fission products were determined by the thick-target-thick-catcher method [1]. The target arrangement consisted of a thick target covered on both sides by an aluminium catcher (thickness about 12 mg/cm^2, purity = 99.99%). The target material used was a homogeneous Pu^{239}-Al alloy. The plutonium content of this alloy varied between 0.01 and 0.1%, depending upon the fission product to be investigated. The target thickness was 10 to 50 mg/cm^2. After irradiation, the target and catcher were dissolved separately. Desired fission products in the two solutions were chemically separated and their activity determined. The range R_{IS} was then calculated by Eq. (1) (W = target thickness in mg/cm^2; A_T = target activity; A_K = catcher activity)

$$R = 2W \frac{A_K}{A_K + A_T}. \tag{1}$$

This equation holds under the assumption that the fission is isotropic and that the range distribution is symmetrical around the average range. The use of a plutonium-aluminium alloy as target material gives the following advantages:

(i) For range determinations it is possible to use the thick-target-thick-catcher method, which supplies more exact results than the thin-target-thin-catcher method.

(ii) Target and catcher are of the same material and thus have the same scattering cross-sections. The necessary corrections for fission product scattering are therefore negligible.

TABLE I

ISOBARIC RANGES R_{IS}

Nuclide	R_{IS} (mg Al/cm^2)	Number of experiments
Sr^{89}	4.17 ± 0.05	12
Sr^{91}	4.16 ± 0.04	10
Zr^{97}	4.12 ± 0.10	10
Mo^{99}	4.00 ± 0.05	6
Ag^{112}	3.74	3
Cd^{118}	3.35	3
Ba^{140}	3.04 ± 0.03	12
Ce^{141}	2.95 ± 0.04	10
Ce^{143}	2.90 ± 0.06	10

The results of our investigations, corrected for the edge effect [1], are listed in Table I.

In determining the ranges of Ag^{112} and Cd^{118} electropolished targets were used. There is evidence from other experiments that these ranges may be too high by perhaps 1 to 2%. This increase may be attributed to a slight enrichment of plutonium on the surface of the target caused by the electropolishing process. As is explained below in connection with the stripping process, the electrolytic oxidation of aluminium alloys may cause a "migration" of the more electropositive constituents of the alloy. The influence of this "migration" on range is being investigated more closely.

A comparison of our results with those obtained by KATCOFF et al. [3] for the range of fission products in air (cf. Fig. 1) leads to the conversion equation

$$R\,(\text{cm air NTP})/R\,(\text{mg Al/cm}^2) = 0.549 + 0.00067\,A_S. \qquad (2)$$

The constants were calculated by a least squares fit. For the reason given above the values for Ag^{112} and Cd^{118} were not included in this calculation. For a preliminary evaluation of the results, the measured ranges were converted into kinetic energies of the fission products. The equation used for this conversion was obtained from the combination of the range-energy relationship given by SUGARMAN et al. [2] with the function

$$R\,(\text{mg U/cm}^2)/R\,(\text{mg Al/cm}^2) = \varphi\,(A_S)$$

determined by PANONTIN et al. [1].

The total kinetic energy $E_K{}^T$ released per fission was also calculated for certain mass splits from the kinetic energy of the fission products. Neutron evaporation was considered in this calculation. If this kinetic energy originates from the Coulomb energy only, one may calculate $E_K{}^T$ by means of Eq. (3), which results from the two-sphere model

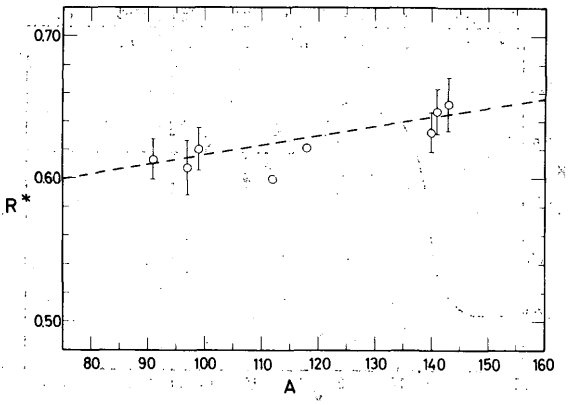

Fig. 1

Dependence of ratio R on mass number A of the fission products

$$R = \frac{\text{Range in cm air (NTP)}}{\text{Range in mg Al/cm}^2}$$

$$E_K^T = \frac{K(Z_B)_L \quad (Z_B)_H}{(A_B)_L^{1/3} + (A_B)_H^{1/3}} \quad \text{with } K = \frac{U\, e^2}{r_0\, D} = \frac{c}{D} \tag{3}$$

(e = electron charge; U = conversion factor erg - MeV; r_0 = nuclear radius parameter; c = constant).

D is the ratio of the actual distance between the two centres of the spheres at the instant of fission to the sum of the radii of the spheres. Thus this quantity is an approximate measure of the elongation of the nucleus at the saddle point. The larger the deformation of the nucleus at the saddle point, the smaller the quantity K should be. Figure 2 shows the values of K calculated for the different fission products versus the mass ratio $V = (A_B)_H/(A_B)_L$. For comparison, Fig. 2 shows also the K-values for the thermal-neutron fission of U^{235}.

Although the evaluation is not yet finished, one may conclude from Fig. 2 that the saddle-point shapes for U^{235} and Pu^{239} are very similar. The deviations outside the limits of error at $V \approx 1.25$ (iodine isotopes) may be due to experimental errors. The preliminary evaluation of some experiments that we have carried out gives a larger range of iodine-131 and thus a higher value for K compared with the results derived by KATCOFF et al. [3].

A possible interpretation of the K-dependence on V may be given as follows: The two plateaus of K indicate that a characteristic saddle-point shape can be attributed to symmetric fission and another to asymmetric fission. The characteristics of these shapes are only slightly influenced by the mass ratio V. The maximum of K in the region of asymmetric fission is probably caused by the formation of nuclei with magic numbers in the preformed fissioning nucleus. Thus, asymmetric fission is influenced by the magic numbers only within a small range of the mass ratio V.

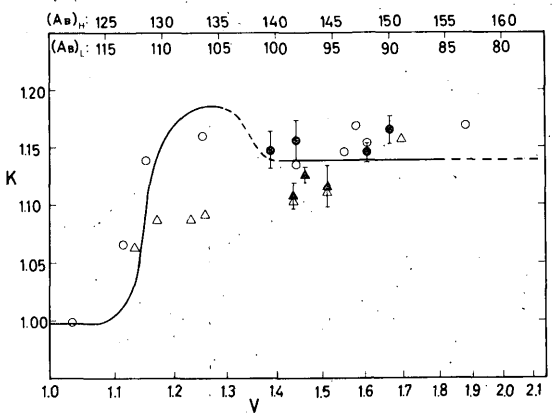

Fig. 2

K as function of the mass ratio V or of the mass number of the primary fragments $(A_B)_H$ and $(A_B)_L$

$$V = \frac{(A_B)H}{(A_B)_L} .$$

For explanations, see text.

RANGE DISTRIBUTION OF ISOBARIC CHAINS

More information on the conditions in nuclear fission may be obtained by an investigation of the distribution of the kinetic energy of fission products. The differential range distribution of 20 fission products has been determined by KATCOFF et al. [3]. If one plots the relative width S_{IS} of these distributions, $(FWHM/R_{IS})$ versus the mass number of the fission products, a curve results from which it is possible to draw contradictory conclusions:

(i) The range dispersion is independent of the mass number (the conclusion of Katcoff et al.);

(ii) The range dispersion decreases with increasing mass-yield of the fission products.

In order to choose between these two explanations we tried to determine the range dispersion for Ba^{140}, Sb^{127} and Ag^{111} by the method described by BROWN and OLIVER (7). The experimental setup (cf. Fig. 3) consisted of a thin target of $Pu^{239}O_2$, a collimator and a thick aluminium catcher.

The collimator used was an aluminium plate 5-mm high with 60 holes each of 1-mm diam. After irradiation the aluminium catcher was separated as thin layers by a stripping procedure [5]. In this procedure a thin layer of aluminium is first anodically oxidized and then dissolved without any attack of the residual aluminium. The surprising results of the experiment were that practically no Ag^{111} activity was found in the stripped fractions and the range of Sb^{127} was about 6% greater than expected (cf. Fig. 4). In order to explain these results, the stripping-procedure was investigated more closely. It became evident that elements more electropositive than aluminium are only partially stripped. With the simple assumption that a constant percent-

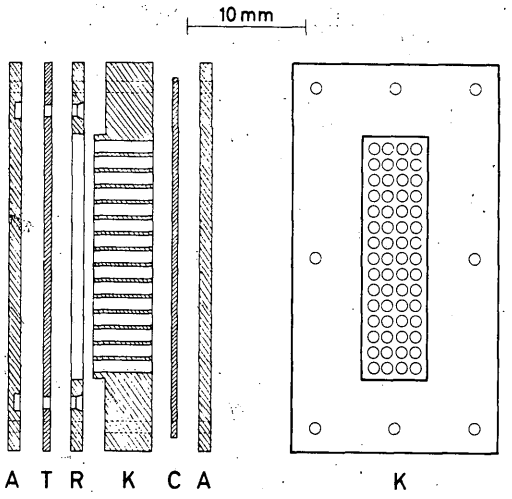

Fig. 3

Target arrangement of Experiment 1

K: Collimator
C: Catcher
T: Target
R: Spacer
A: Cover plates

age of a particular element contained in aluminium is always stripped, a "migration" factor may be defined as follows:

$$k = 1 - A_i' / A_i. \qquad (4)$$

A_i' represents the amount of a particular element determined in a layer of aluminium that has been stripped. A_i represents the amount of the same element present in this aluminium layer before the stripping procedure.

The "migration" factors k, independent of the amount of carrier present in the stripping solution, are shown in Table II.

The range distribution for Sb^{127} is shown in Fig. 4 after correction for "migration". The average range corresponding to the maximum of this curve agrees with the expected value. Thus, the aluminium stripping method is useful only to a limited extent in investigating the dependence of range distribution on mass number.

The experimental results were analysed by the method of logarithmic differentiation under the assumption that the shape of the range distribution is Gaussian. The values obtained from the analyses are listed in Table III. The value for S_{IS} determined for Ba^{140} corresponds roughly to the value of 17.5% given by BROWN and OLIVER (7). Whether the difference between the relative range dispersions of barium and antimony is real can hardly be decided on the basis of the available data. In this comparison it should be noted that because of the large stripping "migration" correction the S_{IS} - value for antimony is rather uncertain.

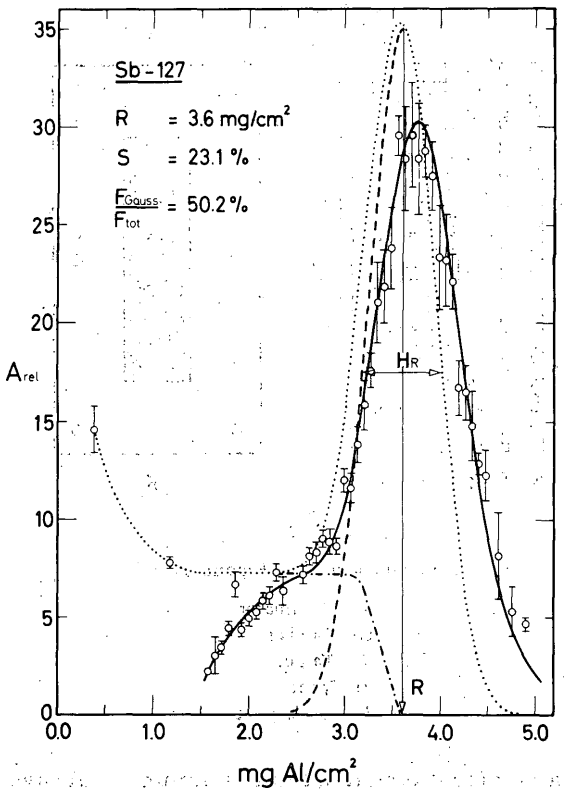

Fig. 4

Isobaric range distribution of Sb^{127}

0 : Experimental points with limits of error
——— : Experimental curve
. . . . . : Curve after correction for stripping "migration"
- - - - - - - : Calculated Gaussian distribution
-.-.-.-.- : Background

TABLE II

"MIGRATION" FACTORS k

Fission product	k
Ba^{140}	0.0 ± 0.01
Sb^{127}	0.80 ± 0.02
Ag^{111}	0.98 ± 0.01

The subtraction of the Gaussian range distribution from the experimentally determined distribution results in a background (Fig. 3). The origin of this background may be attributed to various effects:

TABLE III

ISOBARIC RANGES R_{IS} AND RELATIVE WIDTHS S_{IS} OF THE RANGE DISTRIBUTIONS FROM DIFFERENTIAL RANGE EXPERIMENTS

Fission product	R_{IS}(mg Al/cm^2)	S_{IS}(FWHM/R_{IS}) (%)
Ba^{140}	2.95 ± 0.10	(20.3 ± 1.0)
Sb^{127}	3.6 ± 0.2	(23.1 ± 1.7)

(i) Fission-product scattering on the collimator wall.
(ii) Contamination of the collimator wall and catcher by Pu^{239}.
(iii) Fission-product scattering in the target, in the gas between target and catcher, and in the catcher itself.

By using a "low-scattering" collimator in which the effective wall surface was reduced to 1% of the surface in the original collimator, the effect of wall scattering could be essentially eliminated (Experiment 2). The distance between the target and catcher was 3 cm in this collimator. After irradiation the gas pressure was about 10 mm Hg. In another experiment (Experiment 3) contamination of the collimator by plutonium was prevented by covering the target with a 100 μc/cm^2 foil of Al_2O_3. The results are given in Fig. 5.

Comparison between Experiments 2 and 3 shows that the background cannot be attributed to contamination of the collimator. Moreover, the agreement in shape between the righthand sides of the two background distributions in Experiments 1 and 2 indicates that the effect of wall-scattering may be demonstrated by the dashed line e in Fig. 4. Since the collimators used in Experiments 1 and 2 differ in their absolute, but not in their relative dimensions, the larger background in Experiment 2 may be attributed to scattering in the residual gas of the collimators. However, to explain this increase, a qualitative estimate indicates that a much larger scattering cross-section must be assumed than the one obtained from Coulomb scattering. Specially designed experiments are needed, therefore, to give a satisfactory explanation of this background. A comparison of the results of range distributions determined by both solid and gaseous absorbers, e.g. [7] and [3] respectively, shows the definite superiority of the latter. The widths of the distributions obtained with solid absorbers are about a factor of two greater than those expected on the basis of investigations with gaseous absorbers. For calculations of the kinetic energy distribution of fission products the range distributions measured in gaseous absorbers are therefore more suitable. From the values existing in Refs. [8], [9] and [4] a relative energy dispersion of approximately 11% is shown for light or heavy fission products.

RANGE OF FRAGMENTS

Previous analyses of fission product energy distributions have assumed the range of isobaric fragments to be equal. A similar premise was made

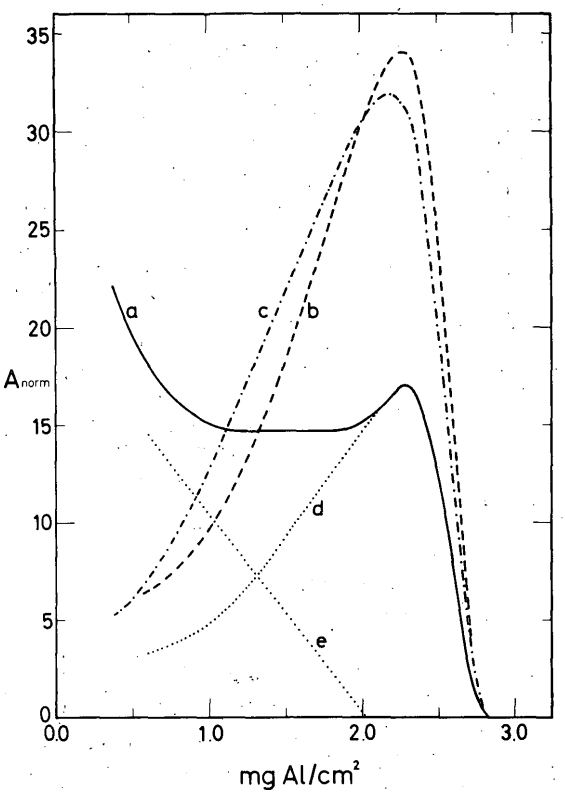

Fig. 5

Background of range distribution curves of Ba^{140} from Experiments 1, 2 and 3, normalized to the same area and range

(a) Experiment 1
(b) Experiment 2
(c) Experiment 3
(d) Distribution b standardized to the maximum of a
(e) Residual curve after subtraction of curve d from a

for the range dispersion. The first doubts concerning this assumption stemmed from the results of NIDAY [10] and of BROWN and OLIVER [7]. They showed that the shielded nuclei Rb^{86} and Cs^{137} have ranges smaller by about 10% than those that result from a smooth plot of R_{IS} versus A. In order to investigate this range deficit more closely, we determined the range R_F for the fragments Ba^{139} and Cs^{139}, and the cumulative ranges R_c for Ba^{139}, Cs^{139} and Xe^{139}. The results are listed in Table IV.

If one plots the ratio of fragment range to the average range of the isobaric chain ($U = R_F/R_{IS}$) versus the difference $Z_F - Z_P$, a straight line results (Fig. 6). The range deficit can then be calculated by the equation

$$R_F/R_{IS} = 1.0 - 0.037\,(Z_F - Z_P). \qquad (5)$$

TABLE IV

FRAGMENT RANGES R_F AND CUMULATIVE RANGES R_c

Nuclide	R_F (mg Al/cm²)	R_c (mg Al/cm²)
Ba^{139}	2.75 ± 0.06	2.96 ± 0.03
Cs^{139}	2.86 ± 0.20	2.98 ± 0.04
Xe^{139}	-	3.05 ± 0.09

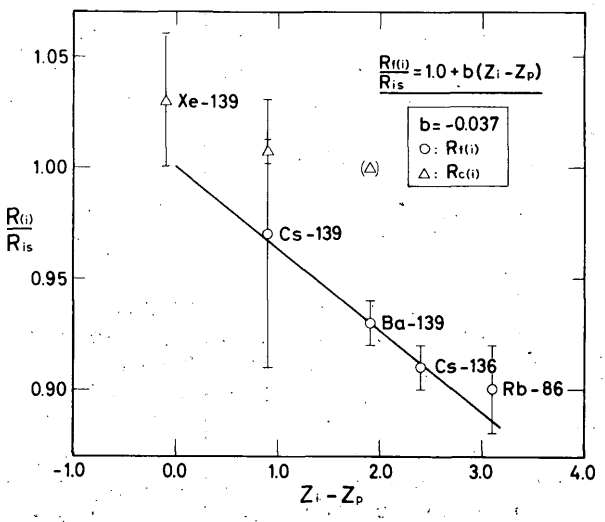

Fig. 6

Relative range of fragments R_F/R_{IS} and cumulative range R_C/R_{IS} of the fragment of fission product as a function of $Z_F - Z_B$.
Values for Cs^{136} and Rb^{86} are from Niday (10) and Brown and Oliver (7).

Figure 6 also shows the values of U for Cs^{136} and Rb^{86}. The straight line calculated for heavy fragments is also valid in good approximation for the light fragments.

The range distributions determined for fission products are thus composed of the distributions of the individual fragments. The centres of the latter do not necessarily coincide with the centre of the over-all distribution. As is evident from the data of BROWN and OLIVER [7] for Cs^{136}, the fragment ranges give a distribution that is approximately Gaussian in shape. The width σ_F of the range distributions for individual fragments may be calculated from the over-all distribution taking into consideration Eq. (5). The assumption is made that σ_F is identical for all fragments.

The ratio σ_F/σ_{IS} depends on the quantity σ_{IS} and is shown in Fig. 7 as a function of S_{IS}. Thus, for example, the relative width S_{IS} of 17.0% found by Brown and Oliver for Cs^{137} represents a σ_F/σ_{IS} ratio of 0.945. From this one calculates a full width at half maximum (FWHM) of 0.468 mg Al/cm² for

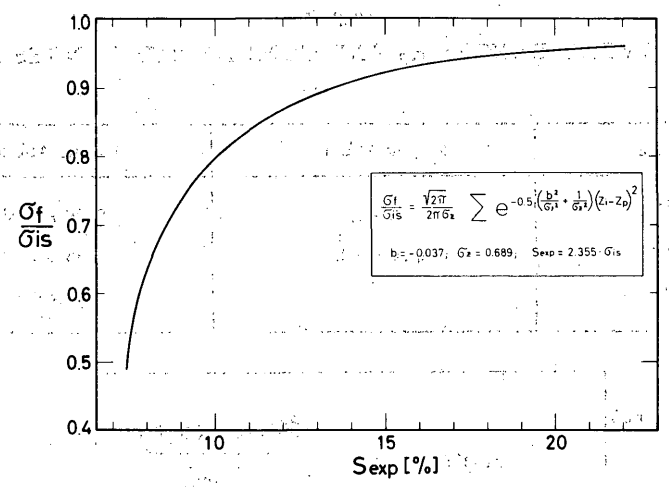

Fig. 7

$\frac{F}{I_S}$ as a function of S_{exp} (S_{exp} = experimentally determined S_{IS})

the individual fragment range distribution of Cs^{137}. This value is in very good agreement with the FWHM of the fragment range distribution for Cs^{136} found by the same authors. This seems to justify the above assumption of equal widths of range distribution for individual fragments.

Using the ratio of σ_F/σ_{IS} to calculate the dispersion in kinetic energy of fragments one obtains a value of about 5%. Accordingly, the energy dispersion is smaller by about a factor of two than formerly had been assumed on the basis of the experimental results. This is ample reason for once more checking the conclusions previously drawn from experimental data.

REFERENCES

[1] PANONTIN, J. A. and SUGARMAN, N., J. inorg. nucl. Chem. 25 (1963) 1321.
[2] SUGARMAN, N., MÜNZEL, H., PANONTIN, J. A., WIELGOZ, C., LANGE, G. and MENCHERO, E., to be published in Phys. Rev.
[3] KATCOFF, S., MISKEL, J. A. and STANLEY, C. W., Phys. Rev. 74 (1948) 631.
[4] GOOD, W. M. and WOLLAN, E. O., Phys. Rev. 101 (1956) 249.
[5] DAVIES, J. A., FRIESEN, J. and McINTYRE, J. D., Canad. J. Chem. 38 (1960) 1526.
[6] PREUSS, L. G. and ESCARFAIL J. P., Nucl. Instrum. Meth. 9 (1960) 212.
[7] BROWN, F. and OLIVER, B. H., Canad. J. Chem. 39 (1961) 616.
[8] PETRZHAK, K. A., PETROV, Y. U., SHLYAMIN, E. A., Soviet Phys. - JETP 11 (1960) 1244.
[9] COHEN, B. L., COHEN, A. F. and COLEY, C. D., Phys. Rev. 104 (1956) 1046.
[10] NIDAY, J. B., Phys. Rev. 121 (1961) 1471.

DISCUSSION

G. SIMONOFF: The thin target-thin catcher method is usually criticized on the grounds of the inhomogeneity of the thin aluminium catchers.

It would be interesting to know how you measure the homogeneity of the Pu^{239}-Al alloy target.

H. MÜNZEL: It is expected that these thick target-thick catcher experiments will yield more accurate results for average ranges than the thin target-thin catcher experiments. This is because it is rather difficult to obtain thin catcher foils of uniform thickness. On the other hand, the accuracy of the ranges determined by us depends on the homogeneity of the target alloy used. We checked this experimentally and were unable to detect any inhomogeneity.

НЕЙТРОНЫ И КИНЕТИЧЕСКАЯ ЭНЕРГИЯ ОСКОЛКОВ ПРИ ДЕЛЕНИИ ТЯЖЕЛЫХ ЯДЕР

В.Ф. АПАЛИН, Ю.Н. ГРИЦЮК, И.Е. КРУТИКОВ, В.И. ЛЕБЕДЕВ
и
Л.А. МИКАЭЛЯН
ГОСУДАРСТВЕННЫЙ КОМИТЕТ ПО ИСПОЛЬЗОВАНИЮ АТОМНОЙ ЭНЕРГИИ СССР, ИНСТИТУТ АТОМНОЙ ЭНЕРГИИ им. И.В. КУРЧАТОВА, МОСКВА
СССР

Abstract — Résumé — Аннотация — Resumen

NEUTRONS AND KINETIC ENERGY OF FRAGMENTS IN FISSION OF HEAVY NUCLEI. The distribution of excitation energy and kinetic energy depending on the mass of the fragment formed in heavy-isotope fission by thermal neutrons is experimentally investigated. The excitation energy is shown to have a low minimum in the region of the double-magic fragment (M ~132), to increase in the symmetrical fission area and to be at its maximum for fragments complementary to magic. The kinetic energy of the fragments measured for U^{235} correlates with the excitation energy. The total energy release according to the experimental data is in good agreement with calculations according to Milton's mass tables in every case except that of strongly asymmetric fission.

In the measurements conducted, the ratio of the maximum of the fragment yield curve to the minimum (after neutron escape) was 500 : 1.

ÉNERGIE CINÉTIQUE DES FRAGMENTS DANS LA FISSION DES NOYAUX LOURDS PAR DES NEUTRONS THERMIQUES. Les auteurs ont étudié par voie expérimentale la distribution de l'énergie d'excitation et de l'énergie cinétique en fonction de la masse des fragments qui se forment lors de la fission de radioéléments lourds par des neutrons thermiques. Ils montrent que la distribution de l'énergie d'excitation présente une vallée très profonde dans la région du fragment doublement magique (M ~132), augmente dans celle de la fission symétrique et atteint le sommet pour les fragments complémentaires des fragments magiques. L'énergie cinétique des fragments, mesurée pour ^{235}U, est en corrélation avec l'énergie d'excitation. La quantité totale d'énergie libérée, déterminée sur la base des données expérimentales, concorde bien avec les calculs effectués conformément au tableau des masses de Milton, sauf pour la fission fortement asymétrique.

Dans les mesures qui ont été faites, le rapport des rendements en fragments sommet/vallée (après la fuite des neutrons) était de 500 : 1.

НЕЙТРОНЫ И КИНЕТИЧЕСКАЯ ЭНЕРГИЯ ОСКОЛКОВ ПРИ ДЕЛЕНИИ ТЯЖЕЛЫХ ЯДЕР. Экспериментально исследовано распределение энергии возбуждения и кинетической энергии в зависимости от массы образовавшегося осколка при делении тяжелых изотопов тепловыми нейтронами. Показано, что энергия возбуждения имеет глубокий минимум в районе дважды магического осколка (M ~ 132), нарастает в области симметричного деления и максимальна для осколков, дополнительных к магическим. Кинетическая энергия осколков, измеренная для U^{235}, коррелирует с энергией возбуждения. Полное энерговыделение, найденное по экспериментальным данным, хорошо согласуется с вычислениями по таблицам масс Милтона всюду, кроме сильно асимметричного деления.

В проведенных измерениях отношение максимума к минимуму кривой выхода осколков (после вылета нейтронов) составляло 500:1.

NEUTRONES Y ENERGIA CINETICA DE LOS FRAGMENTOS EN LA FISION DE NUCLEOS PESADOS. Los autores han estudiado experimentalmente la distribución de la energía de excitación y de la energía cinética en función de la masa del fragmento que se forma en la fisión de isótopos pesados inducida por neutrones térmicos. Demuestran que la energía de excitación presenta un mínimo muy acusado en la región del fragmento doblemente mágico (M ~132), aumenta en la región de fisión simétrica y alcanza su valor máximo para los fragmentos complementarios de los fragmentos mágicos. Existe una correlación entre la energía

cinética de los fragmentos, medida para el ^{235}U, y la energía de excitación. El valor experimental de la energía desprendida concuerda satisfactoriamente con el que figura en los cuadros másicos de Milton, excepto para la fisión muy asimétrica.

En las mediciones efectuadas, la razón de cresta a valle de la curva de rendimiento de los fragmentos (después de la emisión neutrónica) fue de 500 : 1.

В последние годы изучение деления ядер пошло по пути исследования детальных характеристик этого процесса. Изучение энергетического распределения осколков для различных способов деления выявило интересные особенности. До недавнего времени считалось, что кинетическая энергия осколков должна быть максимальной в области, где осколки имеют близкие заряды, т.е. при симметричном делении. Однако исследования Фрезера и Милтона [1], проведенные с использованием техники времени пролета, а также появившаяся одновременно работа Гиббсона, Томаса и Миллера [2], выполненная на полупроводниковых детекторах, показали, что как раз наоборот — при приближении к симметричному делению кинетическая энергия осколков резко падает, а ее максимум находится при отношении масс 1,2. Это чрезвычайно интересное обстоятельство, подтвержденное в дальнейшем в целом ряде работ (Нидей [3], Александер и др. [4]), вызвало широкое обсуждение возможных последствий. Полная энергия деления, рассчитанная обычным образом на основании таблиц масс, слабо изменяется в этом районе отношений осколков. Если верить правильности этих расчетов, то возникшее различие между полной энергией деления и кинетической энергией осколков должно было приводить к увеличению энергии возбуждения осколков. Эта гипотеза была высказана сразу же в первой работе Фрезера, Милтона. Можно было предполагать также, что в районе симметричного деления заряд осколков сильно отличается от наиболее вероятного заряда. Не исключено, что могло быть и то и другое.

В связи с вышесказанным представлялось интересным непосредственно измерить число нейтронов, являющееся мерой энергии возбуждения осколков, для различных отношений масс. Подобные измерения проводились и раньше, начиная с 1953 г. (Фрезер, Милтон [5], Апалин и др. [6]), однако разрешение по массам в этих работах было недостаточным и не позволило сделать каких-либо суждений о симметричной области. Весьма ценные сведения о нейтронах спонтанного деления Cf^{252}, полученные Ветстоном [7] и в особенности Бовманом и др. [8], не решали вопроса, поскольку в поведении суммарной кинетической энергии этого изотопа вблизи симметричного деления не обнаружено заметных особенностей.

В 1961—1962 гг. мы провели измерения числа нейтронов в зависимости от отношения масс осколков для изотопов урана-233, 235 и плутония-239 при делении их тепловыми нейтронами [9]. Измерения четко показали, что для всех трех исследованных изотопов число нейтронов коррелирует со значениями суммарной кинетической энергии осколков: минимум выхода нейтронов соответствует максимуму кинетической энергии, а по мере приближения к симметричному делению число нейтронов резко возрастает. Подобное поведение зависимости $\nu(M_1/M_2)$ наблюдается для всех трех исследованных изотопов. В качестве примера на рис.1 показаны результаты для U^{235}.

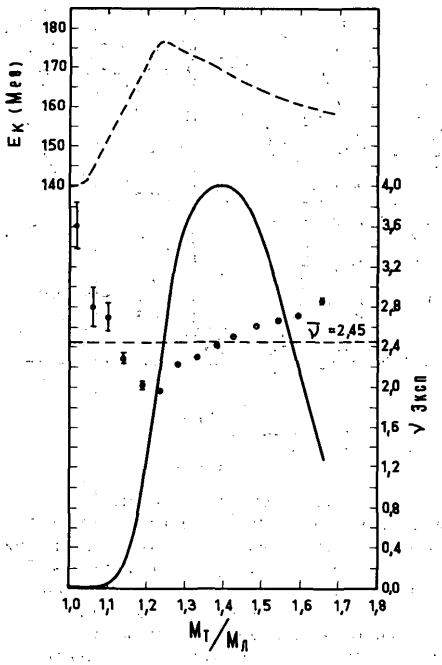

Рис.1

Зависимость числа нейтронов от отношения масс осколков для U^{235}.

Разрешающая способность применявшегося здесь детектора осколков уже была достаточна для убедительного доказательства возрастания энергии возбуждения осколков в симметричной области, однако для количественных измерений необходимо было улучшить фиксацию масс осколков. Кроме того, представлялось интересным исследовать распределение энергии возбуждения между легким и тяжелым осколками.

С этой целью были предприняты измерения числа нейтронов в зависимости от массы осколков при делении U^{233}, U^{235} и Pu^{239} тепловыми нейтронами. В этих измерениях нам удалось более надежно выделить случаи симметричного деления. Полученные результаты будут представлены ниже.

И,наконец, для получения более полной энергетической картины деления и с целью замкнуть цикл проведенных исследований, в тех же экспериментальных условиях была измерена зависимость кинетической энергии осколков от способа деления.

В измерениях в качестве детектора осколков применялся испытанный временем прибор – ионизационная камера с сетками. Для выделения направления движения осколков в экспериментах по определению числа нейтронов в зависимости от массы осколков применялась диафрагма. На диафрагму подавалось напряжение, которое позволяло вытягивать электроны, образованные между мишенью и диафрагмой в рабочий объем камеры. Установка диафрагмы, как показали контрольные опыты, не искажает энергию осколков больше, чем на 1 Мэв. Схематический вид камеры представлен на рис.2. Здесь видна коллимирующая диафрагма и кольца, корректирующие электрическое поле в камере. В отличие от других методов, в слу-

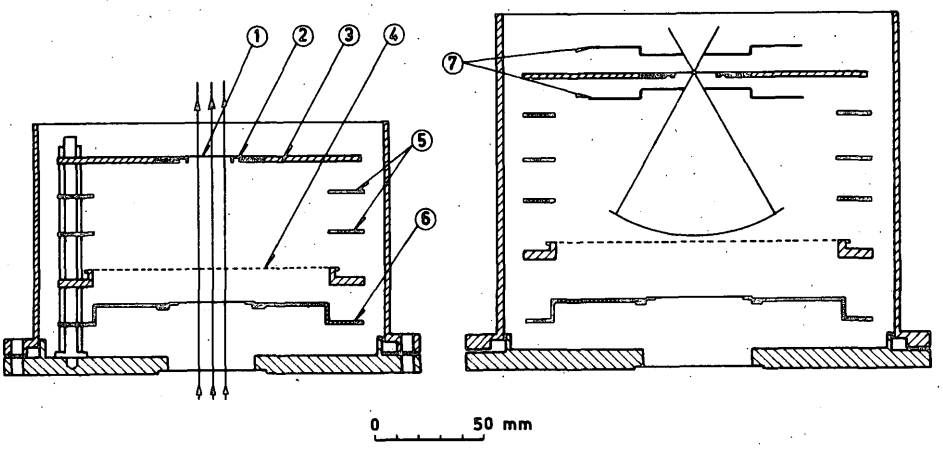

Рис.2

Ионизационные камеры.
Камера 1 для измерения суммарного числа нейтронов:
1 – слой; 2 – держатель слоя, виден бортик, ограничивающий углы вылета осколков; 3 – высоковольтный электрод; 4 – сетка; 5 – кольца, задающие потенциал на границе рабочего объема; 6 – собирающий электрод.
Камера 2 для измерения числа нейтронов, испущенных отделными осколками:
7 – диафрагмы для коллимации осколков.

чае ионизационной камеры, весьма трудно определить истинную разрешающую способность и поэтому, как впрочем это делают и в других случаях, о разрешающей способности метода можно судить по отношению пика к провалу получаемой экспериментально массовой кривой деления.

Для более детальной оценки количества ложных случаев деления, попавших в симметричную область из других областей за счет конечного разрешения ионизационной камеры, мы сравнили наши экспериментальные распределения масс с данными радиохимического анализа выходов осколков. Для этого в опытные значения были внесены поправки на ионизационный дефект и выход нейтронов. Ввиду того, что радиохимические кривые относятся к конечным массам, наши данные для этого сравнения были также выражены в конечных массах. В расчетах мы использовали полученные в этой же работе значения выходов нейтронов. Результаты сравнения для U^{235} приведены на рис.3, из которого видно, что массовое распределение, полученное в данной работе, близко совпадает с радиохимической кривой, а отличие в симметричной области составляет 10–20%. Следует, к сожалению, отметить, что даже последние наиболее полные данные по выходам осколков деления, приведенные в обзорной работе Каткова [10], в симметричной области имеют большие значения ошибок (~10–15%), и имеется целый ряд изотопов в этой области, выходы которых не определялись.

Нейтроны деления в наших экспериментах регистрировались с помощью жидкого сцинтиллятора, содержавшего кадмий.

Схематический вид установки по измерению числа нейтронов с отдельных масс представлен на рис.4.

Как известно, возможность измерения числа нейтронов, испущенных одним осколком, основана на том, что угловое распределение нейтронов

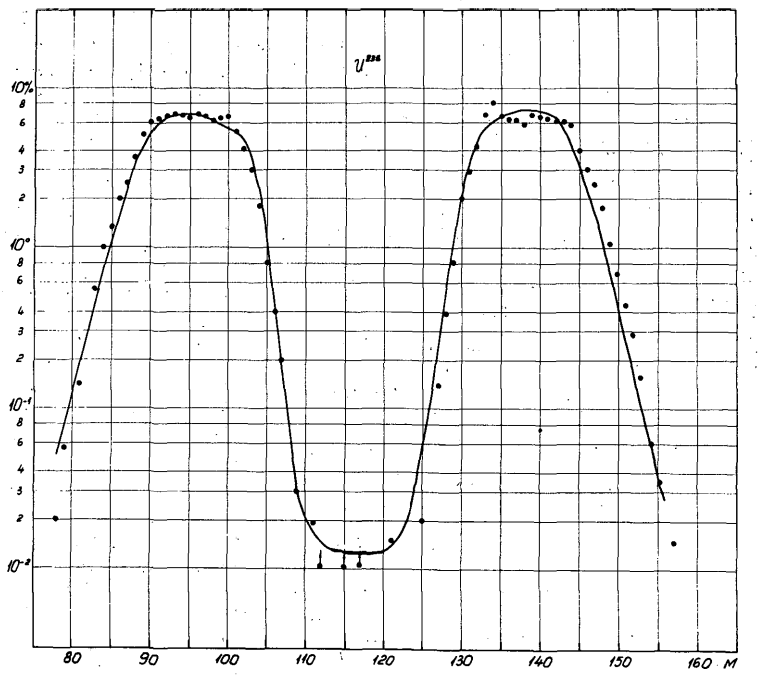

Рис.3

Распределение осколков деления U^{236}, по конечным массам. Сплошная кривая получена из измеренного распределения событий по отношению ионизаций. Точки – данные радиохимических и масс-спектрометрических исследований (Катков [10]).

в лабораторной системе координат сильно вытянуто в направлении полета осколка. Степень вытянутости при изотропном испарении нейтронов относительно осколка определяется скоростью осколка и спектром нейтронов в системе координат, в которой осколок покоится. Поэтому вероятность попадания нейтронов в детектор является неявной функцией массы осколка. Вопросы углового распределения нейтронов подробно обсуждались в недавней работе Террела [11], где приведено аналитическое выражение интеграла от углового распределения. Подынтегральное выражение зависит только от двух параметров: кинетической энергии, приходящейся на нуклон осколка, и средней энергии испаряющихся нейтронов. При проведении расчетов мы воспользовались формулами Террела. Расчеты проводились с учетом следующих обстоятельств и допущений:

1. Разброс кинетических энергий для определенной массы осколка не принимался во внимание.

2. Принималось, что нейтроны с приближающегося к детектору осколка регистрируются в конусе, охватывающем полярные углы от 0 до 30°, а удаляющегося – от 150 до 180°, причем угловой разброс направлений вылетов осколков не принимался во внимание.

3. Принималось, что эффективность регистрации нейтронов, попавших в детектор, не зависит от их энергии.

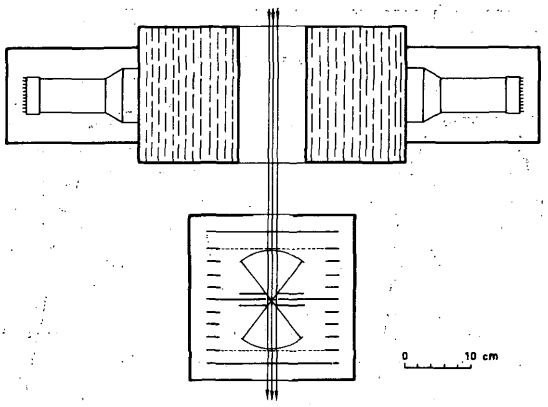

Рис.4

Схематический вид установки

4. Абсолютные значения ν были получены нормировкой на известные средние числа нейтронов на акт деления: $\nu(U^{233})=2{,}50$; $\nu(U^{235})=2{,}44$; $\nu(Pu^{239})=2{,}88$.

Для определения возможных ошибок, возникших при этих расчетах, было найдено суммарное значение $\nu_л+\nu_т$ для легкого и соответствующего тяжелого осколка и произведено сравнение с результатами нашей предыдущей работы, где величина $\nu_л+\nu_т$ находилась непосредственно в геометрии, близкой к 4π. Сравнение показало, что обсуждаемая погрешность в ходе кривой может составлять 5–7%.

На рис.5 приведены все известные нам результаты по числу нейтронов для U^{233}, U^{235} и Pu^{239}. Это работы Фрезера и Милтона 1954 г.[5], Апалина и др.1956–1960 гг.[6] и данные Террела 1962 г. [11], полученные им путем обработки массовых распределений по времени пролета и радиохимическим методом. Как уже говорилось, здесь отсутствует (ввиду известных трудностей) информация о симметричной области. Внизу приведены наши данные, полученные описанным выше способом. В эти данные не вносились никакие поправки, связанные с разрешающей способностью анализа масс осколков.

Видно, что самые легкие осколки почти не испускают нейтронов, затем ν растет и при массах 107–112 испускается уже около 4 нейтронов. Далее, в области симметричного деления ν падает почти линейно. В районе осколков с массой 128–132 имеется глубокий минимум – около 0,3–0,4 нейтрона, и далее, по мере увеличения массы, ν растет так, что наиболее тяжелые осколки испускают около 3,5 нейтрона. На этом же рисунке показано общее число нейтронов $\nu_л+\nu_т$ в функции массы тяжелого осколка. Виден заметный рост в симметричной области, который наблюдался уже в первых наших работах, о чем здесь говорилось выше. Но здесь, за счет лучшего разрешения, видно, что суммарное значение $\nu_л+\nu_т$ имеет некоторое плато в симметричной области и только потом довольно резко падает.

Вернемся снова к нейтронам из отдельных осколков (рис.6). В левом углу приведены в одних и тех же координатах наши результаты и данные, полученные Бовманом и др.[8] в их интересной работе по Cf^{252}. Видно,

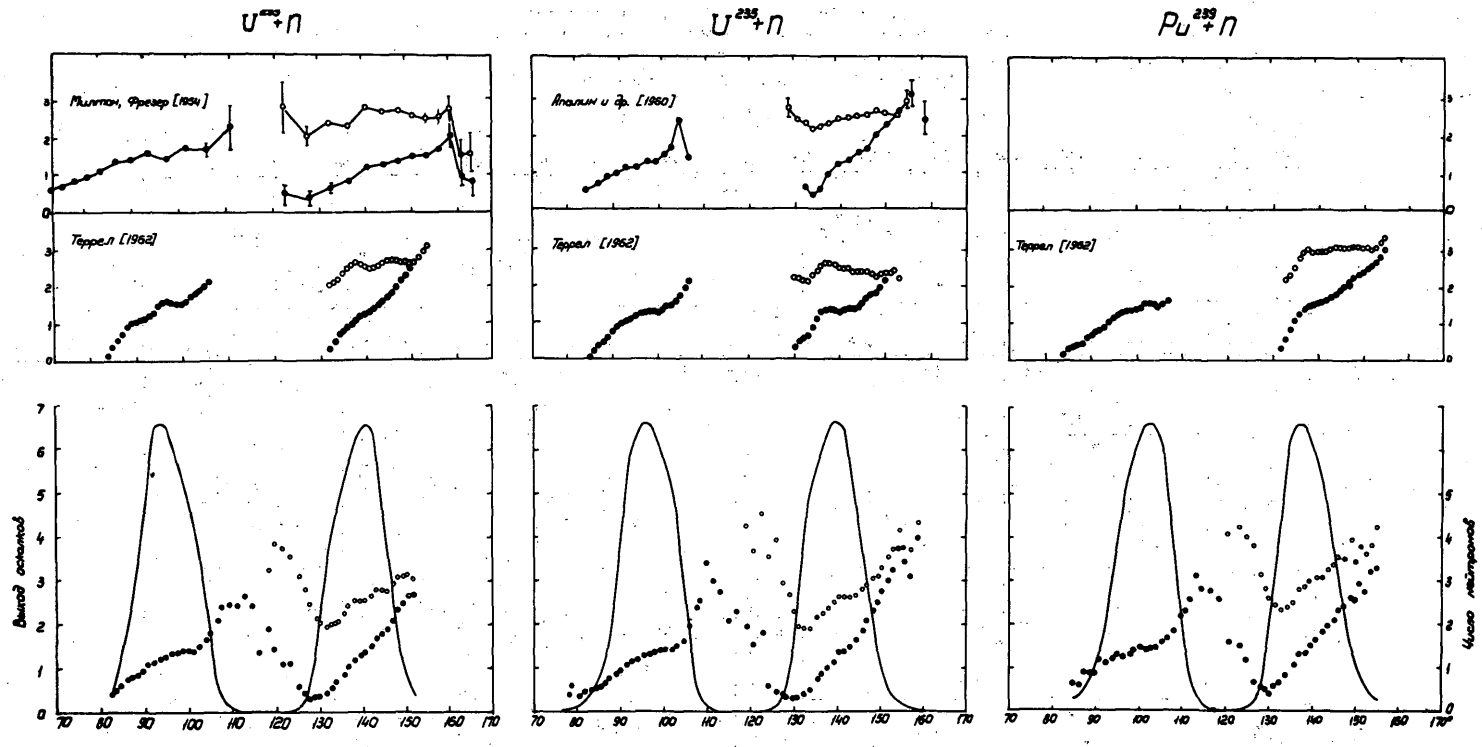

Рис.5

Все известные на 1964 год данные об эмиссии нейтронов для деления U^{236}, U^{234} и Pu^{239} тепловыми нейтронами:
●●● ν(М); ooo ν (М)+ν(Мо−М).
Верхний ряд − измерения Милтона и Фрезера (1954) и Апалина и др. (1960).
Средний ряд − результаты Террела, полученные из анализа массовых распределений (1960).
Нижний ряд − результаты авторов.

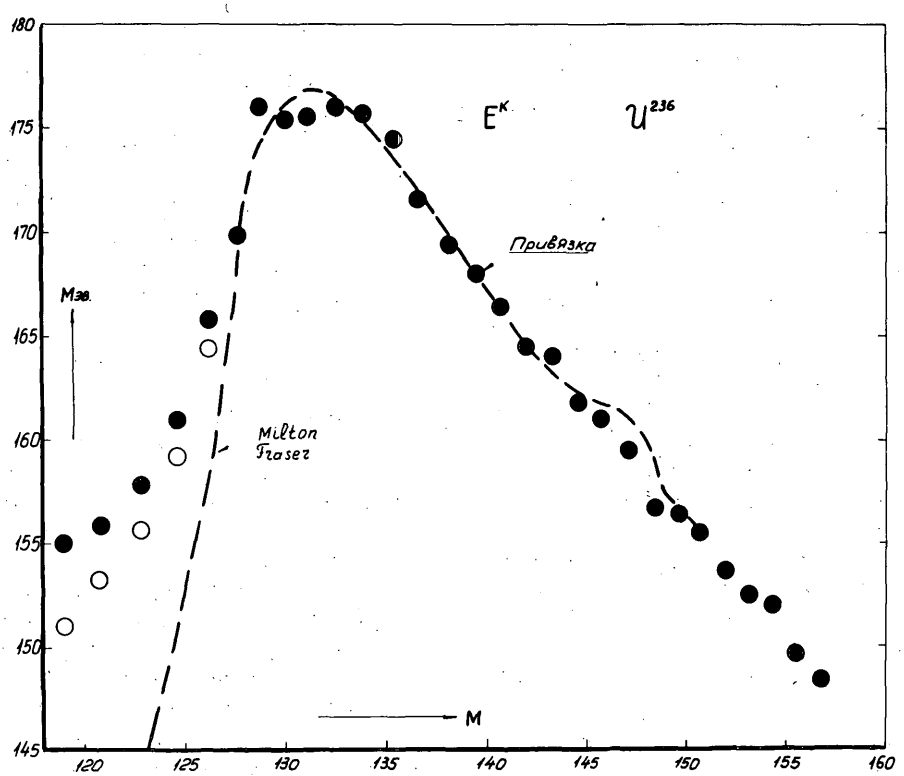

Рис.7

●●● среднее значение суммарной кинетической энергии осколков U^{236} в функции начальной массы тяжелого осколка,
ooo непоправленные на второй пик значения (см.рис.8),
--- данные Милтона и Фрезера [1].

в два раза хуже, чем для первой. Видно, что ложные случаи деления, которые попадают в этот интервал отношений масс, лежат в левом склоне основного распределения, приводят к уменьшению средней энергии (указано на рисунке стрелками) и тем самым углубляют минимум кривой $\overline{E_K\left(\frac{M_1}{M_2}\right)}$.

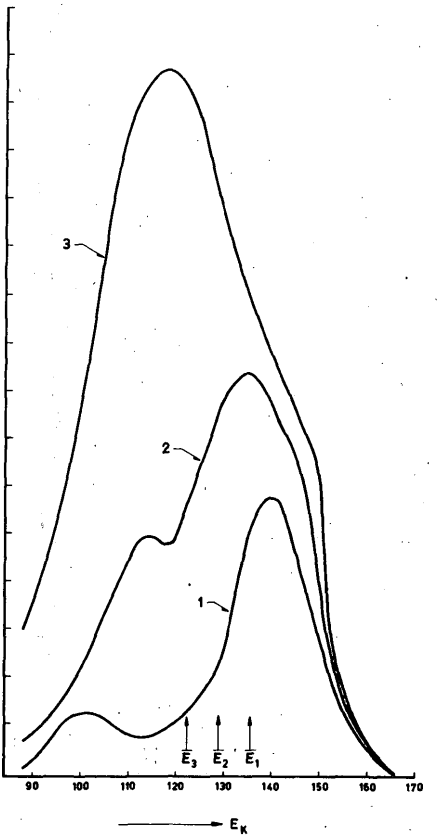

Рис.8

Спектры суммарной кинетической энергии осколков U^{236} в области симметричного деления для различных слоев (E_K – произвольные единицы):
1 – рабочий слой (~20% ложных событий),
2 – 55% ложных событий,
3 – 80% ложных событий.

ЛИТЕРАТУРА

[1] MILTON J.C.D., FRASER J.S. Phys.Rev.Letter., v.7, n.2, 67 (1961); Canad.J.Phys., v.40, n.11, 1926 (1962).
[2] GIBSON W.U., THOMAS T.D., MILLER G.L. Phys.Rev.Letter., v.7, n.2, 65. (1961).
[3] NIDAY J. Phys.Rev., 121 (1961) 1471.
[4] ALEXANDER J., GAZDIK M., TRIPS A., WASIF S. Phys.Rev., 129, 2691 (1963).
[5] MILTON J.C.D., FRASER J.S. Phys.Rev., 93 (1954) 818.
[6] АПАЛИН В.Ф., ДОБРЫНИН Ю.П., ЗАХАРОВА В.П., КУТИКОВ И.Е., МИКАЭЛЯН Л.А. "Атомная энергия", 8, в.1, 15 (1960).
[7] WHETSTONE S.L. Phys.Rev., 114 (1959) 581.
[8] BOWMAN H., MILTON J., THOMPSON S., SWIATECKI W. Phys.Rev., 129 (1963) 2133.
[9] АПАЛИН В.Ф., ГРИЦЮК Ю.Н., КУТИКОВ И.Е., ЛЕБЕДЕВ В.И., МИКАЭЛЯН Л.А., ЖЭТФ 43, 329.
[10] KATCOFF S. Nucleonics, 18 (1961) 163.

МНОГОПАРАМЕТРОВЫЕ ИССЛЕДОВАНИЯ ОСКОЛКОВ ПРИ ДЕЛЕНИИ ЯДЕР БЫСТРЫМИ НЕЙТРОНАМИ

П.П. ДЬЯЧЕНКО и Б.Д. КУЗЬМИНОВ
ФИЗИКО-ЭНЕРГЕТИЧЕСКИЙ ИНСТИТУТ, ОБНИНСК
СССР

Abstract — Résumé — Аннотация — Resumen

MULTI-PARAMETER INVESTIGATIONS OF FAST FISSION FRAGMENTS. A number of investigators have noted the peculiar dependence of kinetic energy on the mass of the fragments. This dependence differs considerably for the fission of nuclei by thermal neutrons, neutrons with an energy of 14 MeV and α-particles. It may be that this is a result of the difference not only in excitation energy, but also in the moment introduced by the particle causing fission. It is obviously difficult to deny the part played by nuclear shells in the formation of fragments according to mass, and in this connection the study of the kinetic energy of fragments as a function of their mass is of great interest, as are the corresponding investigations of the widths of distribution of the kinetic energy. Particular attention is given to the characteristics of symmetrical fission of U^{235}, and it is found that when tails appear in the apparatus spectra of the fission fragments, there occur in the symmetrical mass-region pulses with a most probable total energy of ~120 MeV. Actual symmetrical fission events correspond to a total mean energy of ~155 MeV.

The kinetic energy of paired fragments was measured using two surface-barrier silicon counters. The impulses are analysed for amplitude by a two-dimensional 128 x 128 channel analyser with a memory on ferrite.

The neutron source used was the BR-5 fast neutron reactor, the mean energy of the fast neutron spectrum being ~250 keV. Layers of fissile isotopes with a thickness of 20-30 μg/cm² were used. The fission of U^{235} by thermal neutrons gave an experimental curve for the mass yield with a 250 : 1 ratio between peak and valley. Comparison of the characteristics of the fragments (kinetic energy and mass distribution) showed no noticeable difference in the fission of U^{235} by thermal and fast neutrons. The total kinetic energy of the fragments in the symmetrical fission of U^{235} by thermal and fast neutrons proved to be identical, equalling ~155 MeV, which agrees, within the limits of experimental error, with the corresponding figures for fission of U^{235} by neutrons with an energy of 14 MeV and of Th^{232} by α-particles.

ÉTUDE DE PLUSIEURS PARAMÈTRES DES FRAGMENTS DE LA FISSION PAR NEUTRONS RAPIDES. Plusieurs chercheurs ont constaté qu'il existait une relation de dépendance d'un caractère particulier entre l'énergie cinétique et la masse des fragments. Cette dépendance varie sensiblement selon que la fission des noyaux est provoquée par des neutrons thermiques, des neutrons de 14 MeV ou des particules alpha. Il est possible que ce phénomène soit dû à une différence non seulement dans l'énergie d'excitation mais aussi dans le moment attribuable à la particule qui provoque la fission. Il semble difficile d'ignorer le rôle des couches nucléaires dans la formation des fragments d'après la masse; sous ce rapport l'étude de l'énergie cinétique des fragments en fonction de leur masse revêt une grande importance. Les recherches correspondantes sur les largeurs des sommets de la courbe de distribution de l'énergie cinétique sont également intéressantes. Les auteurs accordent une attention particulière aux caractéristiques de la fission symétrique de ^{235}U. Ils montrent que lorsque les spectres des fragments, fournis par les instruments, présentent des queues, on constate dans la région symétrique des masses l'apparition d'impulsions dont l'énergie totale la plus probable est d'environ 120 MeV. Aux événements de fission symétrique réels correspond une énergie moyenne totale d'environ 155 MeV.

L'énergie cinétique des fragments pairs a été mesurée à l'aide de deux compteurs à silicium à barrière de surface. Pour analyser les impulsions en fonction de leur amplitude, on a employé un analyseur bidimensionnel à 128 x 128 canaux, avec mémoire en ferrite.

La source de neutrons était constituée par le réacteur à neutrons rapides BR-5. Le spectre des neutrons rapides accusait une énergie moyenne d'environ 250 keV. On a employé des couches de radioéléments fissiles d'une épaisseur de 20 à 30 μg/cm². Lors de la fission de ^{235}U par des neutrons thermiques, on a obtenu une courbe expérimentale du rendement selon la masse présentant un rapport des rendements sommet-vallée de

Энергия нейтронов, Мэв	<0,04	0,04–0,1	1,1–0,2	0,2–0,8	0,8–1,4	1,4–3	>3
Относительное число делений	0,131	0,105	0,150	0,285	0,122	0,141	0,066

Поверхностно-барьерные счетчики изготавливались из кремния n-типа с удельным сопротивлением $\rho = 400$ ом.на 1 см. Напряжение обратного смещения – 40 вольт. Основным препятствием для получения надежной информации о симметричных и других маловероятных способах деления служило наличие "хвоста" в амплитудном распределении импульсов. В настоящей работе было проведено исследование природы этого явления. На рис.1 показаны распределения кинетической энергии осколков при делении урана-235 тепловыми нейтронами. Приведенные данные получены методом времени пролета [2] и двумя различными кремниевыми счетчиками. Видно, что распределения в основном совпадают. На этом же рисунке в увеличенном масштабе показаны "хвосты" энергетического распределения, наблюдавшиеся при работе с кремниевыми счетчиками. Распределение импульсов в "хвосте" свидетельствует о том, что осколки могут потерять любую долю своей энергии с равной (но малой) вероятностью. Такая маловероятная нерегистрируемая потеря энергии осколками деления, по-видимому, обусловлена локальными эффектами. Таковыми могут быть следующие явления:

а) наличие ловушек или центров рекомбинации в обедненном слое счетчика;

б) краевые эффекты на счетчике;

в) краевые эффекты на диафрагме, ограничивающей рабочую поверхность счетчика;

г) локальные неоднородности в слое делящегося вещества и подложке, на которую он нанесен;

д) наличие кратеров на поверхности счетчика.

Оценки показывают, что объяснить наличие "хвоста" первым явлением нельзя. Экспериментальные исследования краевых эффектов на счетчике и на диафрагме, выполненные в данной работе, показали, что их вклад незначителен.

Измерения односторонних спектров осколков при использовании нескольких мишеней из делящегося вещества, нанесенных на органические пленки и на металлические подложки, показали, что возможными локальными неоднородностями можно объяснить лишь небольшую часть импульсов в "хвосте".

Поскольку счетчики обладают "входным окошком" конечной толщины, наличие кратеров на их поверхности может служить одной из основных причин появления "хвоста" в амплитудном распределении. Толщина входного нечувствительного слоя, состоящего из слоя золота, окисной пленки кремния и слоя P-типа, определялась из измерений энергии осколков, падающих на поверхность счетчика под разными углами, и составляла для изготовленных нами счетчиков около 0,07 μ.

Исследование поверхности счетчиков под микроскопом показало наличие кратеров самых разнообразных форм и размеров, среди которых в частности встречаются и такие, размеры которых сравнимы с пробегом осколков в кремнии ($\sim$10 микрон). Ясно, что осколки, попадающие в стенки кратеров, могут терять в нерабочем слое любую долю своей энергии.

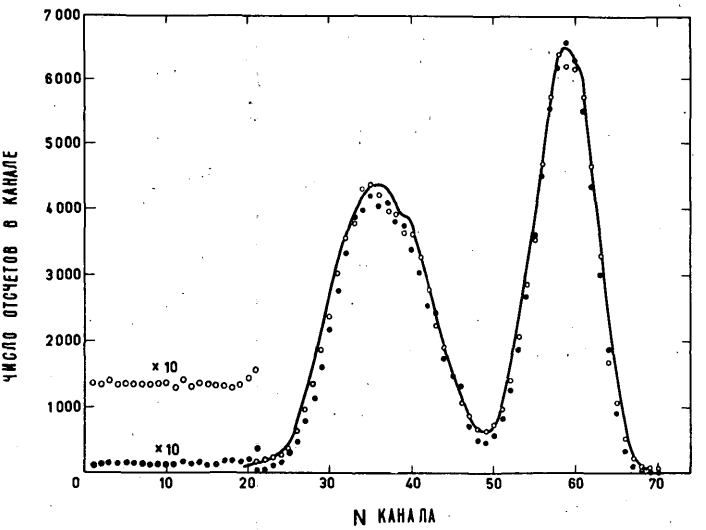

Рис. 1

Односторонние спектры кинетических энергий осколков при делении урана-235 тепловыми нейтронами:

—— время пролета [2],
о о о счетчик первой партии,
● ● ● счетчик второй партии.

Для исследования влияния этого эффекта нами были изготовлены две партии счетчиков с различным состоянием поверхности. На поверхности счетчиков второй партии количество кратеров было существенно уменьшено.

На рис.1 одна кривая соответствует счетчикам из первой партии, а другая — из второй. Число импульсов в хвосте распределения 2-й партии примерно в 10 раз меньше соответствующего распределения 1-й партии. Отношение выходов наиболее вероятных и симметричных осколков, полученное со счетчиками второй группы в 10 раз больше, чем полученное со счетчиками первой группы и составляет 300 : 1. Для проведения данной работы были использованы два счетчика из второй партии.

РЕЗУЛЬТАТЫ ИЗМЕРЕНИЙ

Одновременное измерение кинетической энергии каждого из двух образующихся при делении ядра осколков позволяет определить первичные массы этих осколков, если известно среднее число нейтронов, испускаемых каждым осколком. Для случая деления урана-235 быстрыми нейтронами такие данные отсутствуют.

Поскольку нас интересовало в основном различие результатов при делении урана-235 быстрыми и тепловыми нейтронами (при прочих равных условиях), мы ограничились рассмотрением аппаратурных распределений.

Для характеристики масс осколков использовался параметр $M = A(E_1/(E_1+E_2))$, где E_1 и E_2 — кинетические энергии осколков, заре-

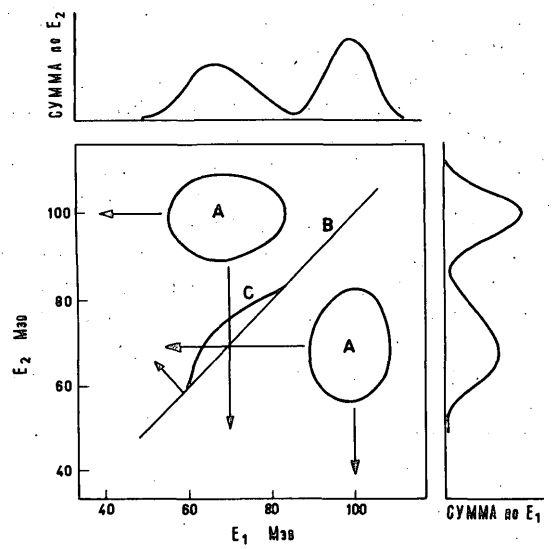

Рис. 4

Схема для определения спектра энергий ложных событий:

A – области, в которых сосредоточено основное число актов деления;
B – линия, соответствующая симметричным способам деления;
C – энергетический спектр ложных событий, зарегистрированных в области симметричных способов деления.

Стрелками показаны направления перемещения места записи акта деления, когда один из осколков случайно теряет часть своей энергии.

рого из первого. Второе распределение нормировалось на 50% от общего числа делений в интервале значений $M = 116 \div 118$. Среднее значение энергии для исправленного распределения составляет 156 Мэв. Дисперсия этого распределения равна 9 Мэв. Наблюдаемое на опыте увеличение дисперсии в области способов деления, близких к симметричному, несомненно связано с наложением ложных событий, тем более, что увеличение дисперсии начинается именно там, где мал истинный выход осколков. Следует отметить, что дисперсия распределений кинетической энергии в области наиболее вероятных способов деления в данной работе составляет 8 Мэв (в работе [2] дано значение $\sigma = 8{,}8$ Мэв); при этом не было введено поправок на аппаратурные эффекты и на эффекты, вносимые самим процессом деления. Проведенный анализ распределений кинетических энергий осколков в интервале $116 \leq M \leq 118$ позволяет заключить, что величина средней кинетической энергии равна 156 ± 2 Мэв и в пределах ошибок опыта одинакова при делении тепловыми и быстрыми нейтронами ($E_n = 720$ кэв), что приблизительно на 10 Мэв меньше, чем при делении нейтронами с энергией $E_n > 7$ Мэв.

Авторы признательны А. Екатову, В. Смирнову, В. Семенкову и В. Чернухину за помощь в проведении двухпараметровых измерений.

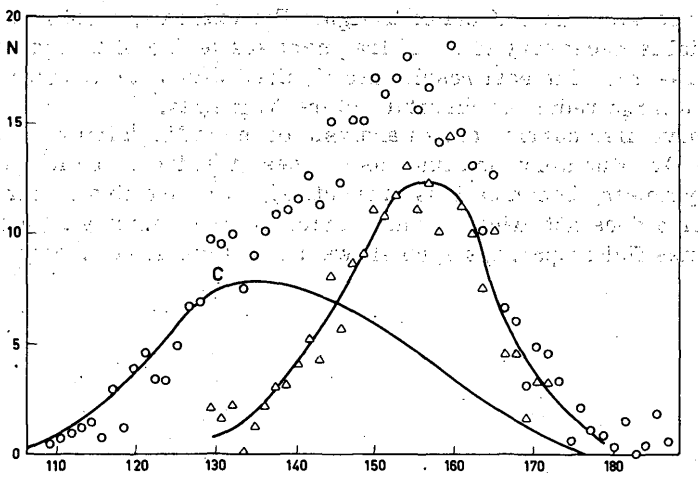

Рис.5

Распределение суммарных кинетических энергий при делении урана-235 тепловыми нейтронами, исправленное на примесь ложных событий:

О – экспериментальное распределение
Δ – исправленное распределение,
С – энергетический спектр ложных событий.

ЛИТЕРАТУРА

[1] АПАЛИН В., ГРИЦЮК Ю., КУТИКОВ В., ЛЕБЕДЕВ В., МИКАЭЛЯН Л. ЖЭТФ 46, (1964) 1197.
[2] MILTON J., FRASER J. Canad. Journ. Phys. 40, 1626 (1962).
[3] GIBSON W., THOWAS T., MILLER G. Phys. Rev. Letter 7, 65 (1961).
[4] ALEXANDER J., GAZDIK M., TRIPS A., WASIF S. Phys. Rev. 129, 2659 (1963).
[5] ДЬЯЧЕНКО П.П., КУЗЬМИНОВ Б.Д., КУЦАЕВА Л.С., ОКОЛОВИЧ В.Н., СМИРЕНКИН Г.Н., УТЮЖНИКОВ А.Н. ЖЭТФ, 45, 8 (1963).
[6] BRITT H.C. and WHETSTONE S.L., Ir. Phys. Rev. Vol. 133, No 38, 603–612 (1964).
[7] ЕКАТОВ А.Б., МАТАЛИН Л.А., СЕМЕНКОВ В.Ф., СМИРНОВ В.И., ЧУБАРОВ С.И., ШИМАНСКИЙ А.М. ПТЭ, №3, 72 (1963).
[8] CUNINGHAME J.G., KITT G.P., RAE E.R. Nucl. Phys. 27, (1961) 154.

DISCUSSION

T.D. THOMAS: In our investigations we have also seen tailing effects similar to those reported by Dr. Kuzminov and we have attributed them to fragments hitting the edges of the counters. We have managed to reduce these effects substantially – although we have not been able to eliminate them completely – by collimating the detectors in such a way that no fragments can hit the edges of the detectors.

W. GIBSON: It is, of course, important to collimate the fragments away from the detector edges but in addition it should be realized that tailing is

also very sensitive to collimator design. For example, a collimator of low Z-material is necessary to avoid fragment scattering of the type reported by Dr. Fraser [1]. The best results are obtained with a low Z-collimator that presents a large radius of curvature to the fragments.

We have also carried out an analysis of the tailing similar to that described by Dr. Kuzminov and find, as he does, that the so-called energy deficit at symmetry becomes less pronounced. We also find that the energy dispersion σ does not exhibit a sharp increase as symmetry is approached but becomes flat or perhaps even shows a slight dip at symmetry.

[1] FRASER, J.S., "The energy release in low-energy fission", these Proceedings 1.

УГЛОВАЯ АНИЗОТРОПИЯ И АСИММЕТРИЯ МАСС ОСКОЛКОВ ПРИ ДЕЛЕНИИ ТОРИЯ-232 НЕЙТРОНАМИ

Б.Д. КУЗЬМИНОВ и А.И. СЕРГАЧЕВ
ФИЗИКО-ЭНЕРГЕТИЧЕСКИЙ ИНСТИТУТ, ОБНИНСК
СССР

Abstract — Résumé — Аннотация — Resumen

ANGULAR ANISOTROPY AND MASS ASYMMETRY OF THORIUM-232 FISSION FRAGMENTS. A large number of experimental and theoretical papers on the angular distribution of the fission fragments of nuclei indicate that it is satisfactorily described by the parameters of the fissioning nucleus at the saddle point. The problem of the effect of these parameters on the distribution of the fragments according to mass has as yet found no generally accepted solution. It remains unclear to what extent the "good" quantum numbers characteristic of the nucleus at the saddle point remain equally "good" when the nucleus passes from the saddle point to the moment of breakdown. If at the saddle point the nucleus has a set of different configurations, this must be apparent in some way in the distribution of the fragments by mass and in their angular distribution (via the moment of inertia of the nucleus).

The paper investigates the angular anisotropy of fragments with different masses in the fission of thorium-232 by fast neutrons. The masses of the fragments were determined by simultaneous recording of the kinetic energy of paired fragments in a double ionization chamber with grids. The direction of flight of the fragments was determined using a mechanical collimator. The neutrons causing fission had an extended spectrum, but the contribution of fissions via the (n,n'f) reaction did not exceed a few per cent. The fragments were sorted out according to energy by a two-dimensional 128 x 128 channel analyser with a memory on ferrite.

The dependence of angular anisotropy on the mass of the fragments and on their kinetic energy with fixed mass is discussed.

The first dependence makes it possible to judge the degree to which the saddle point affects the distribution of the fragments according to mass, while the second gives information about the degree to which the configuration of the nucleus at the moment of breakdown affects the angular anisotropy of the fragments.

ANISOTROPIE DE LA DISTRIBUTION ANGULAIRE ET ASYMÉTRIE DE LA DISTRIBUTION SELON LA MASSE POUR LES FRAGMENTS DE FISSION DU THORIUM-232. Tout un ensemble d'études expérimentales et théoriques consacrées à la distribution angulaire des fragments de fission atteste que leur distribution angulaire peut être décrite de façon satisfaisante à l'aide des paramètres du noyau qui subit la fission au point d'étranglement. Le problème de l'effet que ces paramètres produisent sur la distribution des fragments selon la masse n'a pas encore trouvé de solution acceptable pour tous. Il n'est pas encore clair dans quelle mesure les « bons » nombres quantiques, qui caractérisent le noyau au point d'étranglement, gardent cette qualité pendant l'évolution du noyau entre l'étranglement et la rupture. Si au point d'étranglement le noyau peut présenter une série de configurations différentes, ce phénomène devrait exercer une influence sur la distribution des fragments selon la masse et sur leur distribution angulaire (par l'intermédiaire du moment d'inertie du noyau).

Les auteurs ont étudié l'anisotropie de la distribution angulaire des fragments de masse différente dans la fission de ^{232}Th par des neutrons rapides. Ils ont déterminé les masses des fragments par enregistrement simultané de l'énergie cinétique des fragments pairs dans une chambre d'ionisation double pourvue de grilles. Pour déterminer la direction du vol des fragments, ils ont utilisé un collimateur mécanique. Ils ont constaté que le spectre des neutrons qui provoquaient la fission était étendu, mais que la contribution des fissions résultant de la réaction (n,n'f) ne dépassait pas quelques unités pour cent. Le triage des fragments selon l'énergie s'est fait à l'aide d'un analyseur bidimensionnel à 128 x 128 canaux, avec mémoire en ferrite.

Les auteurs examinent les relations de dépendance entre l'anisotropie de la distribution angulaire et la masse des fragments ou, lorsque la masse est invariable, leur énergie cinétique.

Si la première relation permet de se faire une idée de la mesure dans laquelle le point d'étranglement affecte la distribution des fragments selon la masse, la deuxième fournit des renseignements sur l'influence que la configuration du noyau exerce, au moment de la rupture, sur l'anisotropie de leur distribution angulaire.

УГЛОВАЯ АНИЗОТРОПИЯ И АСИММЕТРИЯ МАСС ОСКОЛКОВ ПРИ ДЕЛЕНИИ ТОРИЯ-232 НЕЙТРОНАМИ. Целый комплекс экспериментальных и теоретических работ, посвященных угловому распределению осколков деления ядер, свидетельствует о том, что угловое распределение осколков можно удовлетворительно описать параметрами делящегося ядра в седловой точке. Вопрос о влиянии параметров ядра в седловой точке на распределение осколков по массам до сих пор не нашел единодушно воспринимаемого решения. Не ясен вопрос о том, насколько "хорошие" квантовые числа, характерные для ядра в седловой точке, остаются такими же "хорошими" при спуске ядра с седловой точки до момента разрыва. Если ядро в седловой точке может обладать набором различных конфигураций, то это должно как-то проявиться на распределении осколков по массам и на угловом распределении осколков (через момент инерции ядра).

Исследовалась угловая анизотропия осколков с различными массами при делении тория-232 быстрыми нейтронами. Массы осколков определялись путем одновременной регистрации кинетической энергии парных осколков в двойной ионизационной камере с сетками. Направление вылета осколков фиксировалось механическим коллиматором. Нейтроны, вызывавшие деления, обладали протяженным спектром, однако вклад делений через реакцию (n, n'f) не превышал нескольких процентов. Сортировка осколков по энергиям осуществлялась двухмерным 128×128 канальным анализатором с памятью на ферритах.

Рассматриваются зависимости угловой анизотропии от масс осколков и от кинетической энергии осколков при фиксированной массе.

Если первая зависимость позволяет судить о степени влияния седловой точки на распределение осколков по массам, то вторая зависимость дает сведения степени влияния конфигурации ядра в момент разрыва на угловую анизотропию осколков.

ANISOTROPIA ANGULAR Y ASIMETRIA MASICA DE LOS FRAGMENTOS DE LA FISION DEL TORIO-232. La gran cantidad de trabajos experimentales y teóricos consagrados a la distribución angular de los fragmentos de fisión es prueba de que dicha distribución puede describirse satisfactoriamente por los parámetros del núcleo en el punto de estrangulación. Hasta la fecha no se ha podido hallar una respuesta concluyente al problema de la influencia de esos parámetros sobre la distribución de los fragmentos según su masa. No se sabe con exactitud hasta qué punto los números cuánticos «correctos», característicos del núcleo en el punto de estrangulación, conservan su validez cuando el núcleo pasa por el punto de estrangulación. Si en ese punto el núcleo posee una serie de configuraciones, ello debe reflejarse en la distribución de los fragmentos según su masa, así como en la distribución angular de los fragmentos.

En la memoria se examina la anisotropía angular de los fragmentos de distinta masa procedentes de la fisión del torio-232 por neutrones rápidos. La masa de los fragmentos se determina mediante el registro simultáneo de la energía cinética de los pares de fragmentos en una cámara de ionización doble dotada de rejillas. La dirección en que se emiten los fragmentos se estableció por medio de un colimador mecánico. El espectro de los neutrones causantes de la fisión era amplio; sin embargo, la contribución de las fisiones en virtud de la reacción (n, n'f) sólo fue del orden de algunos por cientos. La selección de los fragmentos según su energía se efectuó por medio de un analizador bidimensional de 128 × 128 canales, con memoria de ferrita.

Los autores examinan la variación de la anisotropía angular en función de la masa de los fragmentos y de la energía cinética de los fragmentos para una masa fija.

Si la primera relación de dependencia permite evaluar la influencia del punto de estrangulación sobre la distribución de los fragmentos según su masa, la segunda aclara la influencia de la configuración del núcleo en el momento de la ruptura sobre la anisotropía angular de los fragmentos.

I. ВВЕДЕНИЕ

Вопрос о динамике процесса деления ядер до настоящего времени не нашел своего решения. Характер деформации ядра на его пути от седловой точки до момента развала и связь состояний осколков деления в момент их образования с состояниями и формой ядра в седловой точке по-прежнему остаются не понятыми. Некоторая информация об этом участке процесса деления может быть получена из исследований связи угловой анизотропии осколков деления с их массами. В настоящее время известно, что решающая роль в формировании углового распределения осколков принадлежит состояниям ядра в седловой точке, через которые протекает процесс де-

ления. Распределение же массы делящегося ядра между осколками заканчивается на самой последней стадии процесса деления — в момент развала ядра. Если спуск от седловой точки до точки разрыва в какой-то мере зависит от состояния ядра в седловой точке, через которое шел процесс деления, то это может отразиться на связи угловой анизотропии осколков с их массами. Этой проблеме был посвящен ряд экспериментальных работ [1—7]. К сожалению, все эти работы выполнены для различных делящихся ядер, при различных энергиях возбуждения и разнообразными методами, а их результаты довольно противоречивы. Результаты работ [1,2], в которых исследовался процесс деления ядер при больших энергиях возбуждения, интерпретировать трудно, поскольку из-за реакций типа (α, K_{nf}) деления ядер происходили при самых различных энергиях возбуждения. Именно этим обстоятельством можно объяснить наблюдавшуюся в отмеченных работах сильную зависимость угловой анизотропии от масс осколков.

В работе [6] исследовалась зависимость угловой анизотропии осколков от их масс при делении висмута-209 и свинца-206 α-частицами с энергией 42 Мэв. Для идентификации осколков авторы использовали радиохимический метод. Угловая анизотропия в пределах ошибок опыта одинакова для всех выделявшихся осколков, за исключением брома-83.

Другая часть работ [3—5,7], в которых исследовалось деление ядер при малых энергиях возбуждения, выполнена с использованием ионизационных методов определения масс осколков. В работах [3—5] связь анизотропии и асимметрии осколков в пределах ошибок опытов не обнаружена. Результаты работы [7] свидетельствуют о наличии связи между анизотропией и асимметрией осколков при делении урана—235 нейтронами с энергией 4 Мэв.

Таким образом, на основании рассмотренных работ трудно сделать заключение о том, существует ли связь между угловой анизотропией и массами осколков.

Публикуемая работа является продолжением более ранней работы [5] и отличается лучшим разрешением по массам и большей статистической точностью.

II. МЕТОД ИЗМЕРЕНИЙ

Для регистрации осколков деления использовалась двухсторонняя ионизационная камера с сетками, которая позволяла измерять кинетические энергии парных осколков. Применение обычного механического коллиматора для выделения направления движения осколков приводит к двум нежелательным эффектам. Во-первых, электрическое поле не полностью вытягивает электронный заряд, созданный в отверстиях коллиматора осколками. Во-вторых, у некоторой части осколков происходит частичная потеря кинетической энергии на краях стенок коллимирующих отверстий, что является основной причиной регистрации ложных событий, наиболее нежелательных в области осколков с малым выходом.

В данных исследованиях была применена камера, конструкция которой предложена в работе [8]. Она позволяла фиксировать угол разлета осколков, была лишена первого недостатка, а доля осколков, претерпевших

частичную потерю энергии, была существенно меньше, чем в камере с обычным механическим коллиматором. Диафрагмы, применявшиеся в камере, выделяли телесный угол 0,1 стерадиана. Делящееся вещество наносилось на органическую пленку толщиной 6 мкг/см^2, покрытую слоем золота (25 мкг/см^2). Толщина слоя нитрата тория составляла около 20 мкг/см^2. Два сигнала от камеры после соответствующего усиления поступали на вход двухмерного 128×128 канального амплитудного анализатора импульсов с памятью на ферритах [9]. Память анализатора была разбита на две части: в одну половину записывались данные для осколков, летящих под 0° к пучку нейтронов, в другую — под 90°. Для контроля за стабильностью аппаратуры в процессе измерений применялся генератор импульсов со стабильной амплитудой. Измерения велись короткими сериями попеременно под 0° и 90°. Деления ядер тория-232 вызывались нейтронами, выведенными из активной зоны реактора на быстрых нейтронах БР-5.

Ниже приведены цифры, характеризующие доли делений, вызванных нейтронами с различной энергией. Основное число делений (85%) вызвано нейтронами с энергией $1{,}5 \leqslant E_n \leqslant 5$ Мэв.

III. ОБСУЖДЕНИЕ РЕЗУЛЬТАТОВ ИЗМЕРЕНИЙ

Одновременное измерение энергий парных осколков позволяет получить информацию об исходных массах осколков только в том случае, если известно среднее число нейтронов, испускаемых каждым осколком. Для тория-232 такие данные отсутствуют. Поэтому для характеристики масс осколков был выбран параметр $M_т = 230(E_л/(E_n + E_т))$, который очень близок к истинному значению масс тяжелых осколков. Поскольку поправки на вылет нейтронов не вводились, то все характеристики, приписываемые актам деления с определенным значением параметра $M_т$, фактически являются усредненными по осколкам, отличающимся на $1 \div 2$ массовые единицы.

Результаты измерений, представленные в данной работе, являются итогом анализа $4 \cdot 10^4$ актов деления, при которых осколки летели под 0° к направлению пучка нейтронов, и такого же количества событий, при которых осколки летели под 90°.

На рис. 1 б представлены выходы осколков с различными массами при их движении под 0° и 90° к направлению полета нейтронов. Обе кривые почти совпадают. Они также хорошо согласуются с результатами радиохимических исследований [10].

На рис. 1 а представлена зависимость угловой анизотропии от масс осколков. Для интервала масс от 123 до 152 угловая анизотропия в пределах ошибок измерений не зависит от масс осколков деления. Эта область масс соответствует осколкам с наибольшим выходом. Форма кривой выходов этих осколков почти не меняется с увеличением энергии нейтронов, вызывающих деления, по крайней мере до 6 Мэв [10]. Благодаря этому обстоятельству, зависимость анизотропии от энергии нейтронов, вызывающих деления, не имела существенного значения в данной работе, хотя для исследований использовались нейтроны с широким спектром энергий (см. таблицу). Для указанного интервала масс осколков в рассматриваемых измерениях могла проявиться только связь состояний ядра в седловой точ-

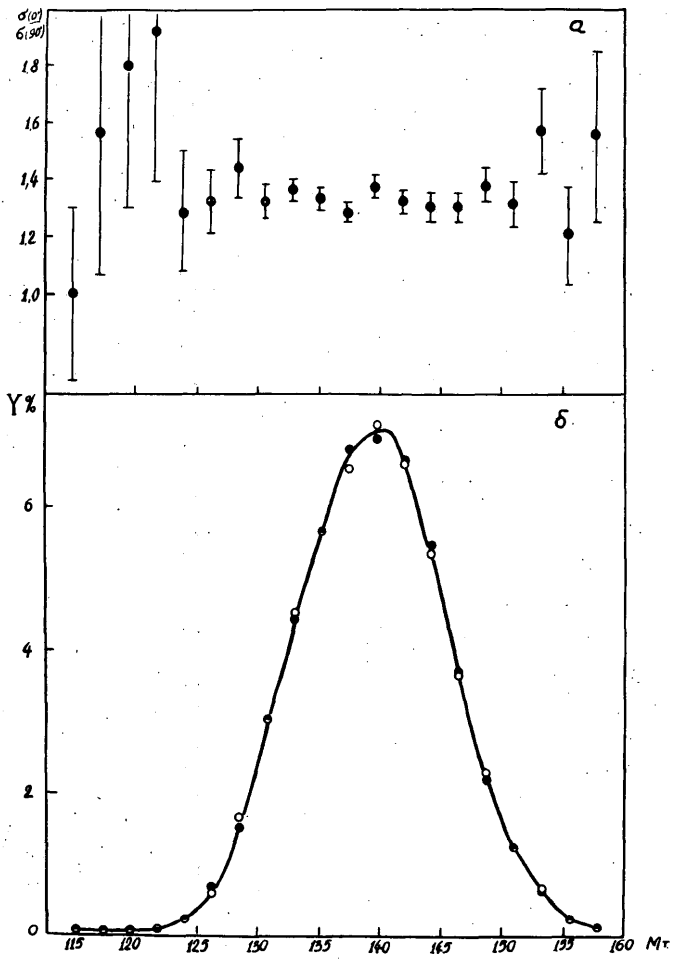

Рис.1

а) Зависимость угловой анизотропии от массы тяжелого осколка;

б) Выходы осколков с различными массами:

o – под 0° к направлению пучка нейтронов;

● – под 90° к направлению пучка нейтронов.

ДОЛИ ДЕЛЕНИЙ, ВЫЗВАННЫХ НЕЙТРОНАМИ С РАЗЛИЧНОЙ ЭНЕРГИЕЙ (Мэв)

E_n	$E_n \leqslant 3$	$3 \leqslant E_n \leqslant 5$	$5 \leqslant E_n \leqslant 7$	$E_n > 7$
α	0,51	0,34	0,10	0,05

ке со способами разрыва. Экспериментальные результаты свидетельствуют, что в пределах точности измерений $\sigma(0^\circ)/\sigma(90^\circ)(\sim 3\%)$ эта связь отсутствует.

Выход осколков с массами меньше 123 и больше 152 существенно зависит от энергии нейтронов, вызывающих деления. Поэтому здесь могла проявиться случайная связь между анизотропией и массами осколков. Это обстоятельство послужило основанием для исключения из обсуждения угловой анизотропии осколков с указанными массами. Кроме того, в этой области масс слишком мала статистическая точность.

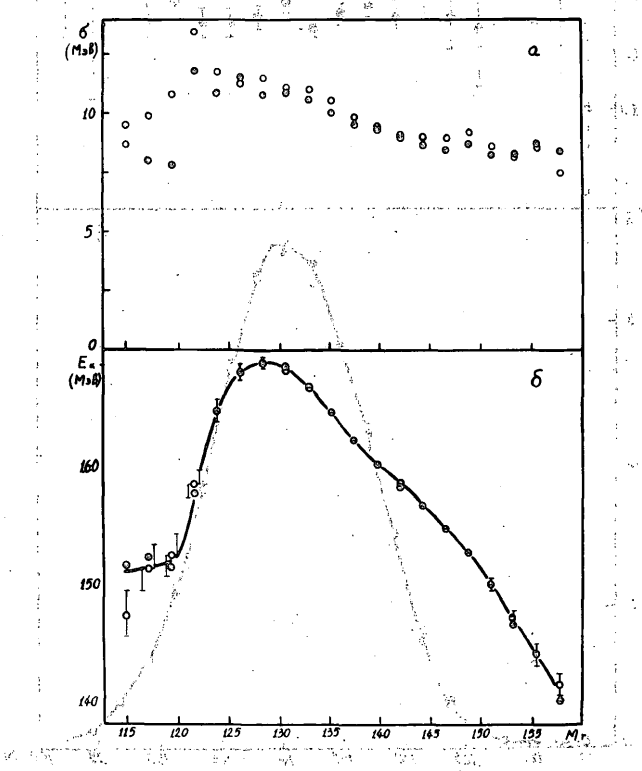

Рис.2

а) Зависимость дисперсий энергетических распределений от массы тяжелого осколка:
o – под 0° к направлению пучка нейтронов,
⊙ – под 90° к направлению пучка нейтронов.

б) Распределения суммарных кинетических энергий при делении тория-232 нейтронами спектра деления:
o – под 0° к направлению пучка нейтронов,
⊙ – под 90° к направлению пучка нейтронов.

На рис.2 показаны энергетические характеристики осколков, зарегистрированных под 0° и под 90° к направлению пучка нейтронов. Зависимости суммарных кинетических энергий осколков в обоих случаях совпадают. Максимальная кинетическая энергия составляет 169 Мэв и относится к осколкам, массы которых $M_т$ близки к 128. При делении на осколки с приблизительно равными массами величина кинетической энергии составляет около 150 Мэв. Таким образом, разница между максимальным значением кинетической энергии и ее значением в провале равна 19 Мэв.

Несмотря на малую статистику (80 событий) в области осколков с приблизительно равными массами, полученные значения кинетической энергии кажутся вполне достоверными, поскольку измеренные выходы осколков в этой области масс хорошо согласуются с радиохимическими данными [10], и следовательно трудно ожидать, чтобы в числе зарегистрированных событий заметную часть составляли бы ложные события. Об этом же свидетельствуют дисперсии (σ) распределений кинетических энергий, показанные на рис.2а.

Кривая зависимости дисперсий от масс осколков очень похожа на соответствующие кривые, приведенные в работе [11]. В этой работе выходы масс и энергетические характеристики осколков интерпретируются с точки зрения гипотезы о двух способах деления. Именно сравнимым выходом осколков в обоих способах деления объясняется зависимость дисперсий от масс осколков. В нашей работе энергия возбуждения не велика и выход симметричных осколков мал, однако форма обсуждаемой кривой такая же, как и в случае деления ядер при большой энергии возбуждения.

Авторы признательны А. Екатову, В. Смирнову, В. Семенкову и В. Чернухину за помощь в проведении двухпараметровых измерений.

ЛИТЕРАТУРА

[1] FAIRHALL A.W., HALPERN I. and WINHOLD E.J., Phys. Rev. 94 (1954) 733.
[2] COHEN B.L., JONES W.H., McCORMICK G.H. and FERELL B.L., Phys. Rev. 94(1954)625.
[3] БАРАНОВ И.А., ПРОТОПОПОВ А.Н. и ЭЙСМОНТ В.П., ЖЭТФ 14 (1962) 713.
[4] MANLEY J.H. Nuclear Phys. 33 (1962)70.
[5] КУЗЬМИНОВ Б.Д., КУЦАЕВА Л.С., БОНДАРЕНКО И.И., ЖЭТФ 42 (1962) 75.
[6] FLYNN K.F., GLENDENIN L.E. and HUIZENGA J.R., Nuclear Phys. 58 (1964) 321.
[7] KAPOOR S.S., NADKARNI D.M., RAMANNA R., RAMA RAO P.N., MURTHY S.R.S. and BALLAL R.R., Nuclear Phys. and Solid State Physics Symposium 1964. Part "A" – Nuclear Phys.
[8] АПАЛИН В.Ф., ГРИЦЮК Ю.Н., КУТИКОВ И.Е., ЛЕБЕДЕВ В.И, МИКАЭЛЯН Л.А. ЖЭТФ 46 (1964) 1197.
[9] ЕКАТОВ А.Б., МАТАЛИН Л.А., СЕМЕНКОВ В.Ф., СМИРНОВ В.И., ЧУБАРОВ С.И., ШИМАНСКИЙ А.М., ПТЭ 3, (1963) 72.
[10] ЗЫСИН Ю.А., ЛБОВ А.А., СЕЛЬЧЕНКОВ А.И. Выходы продуктов деления и их распределение по массам. Госатомиздат, 1963.
[11] BRITT H.C., WEGNER H.E., GURSKY J.C., Phys. Rev. 129,(1963)2239.

APPLICATIONS OF NEW FISSION DATA TO NUCLEAR TECHNOLOGY

(Session V)

Review Paper

FISSION DATA AND NUCLEAR TECHNOLOGY

G.C. HANNA
CHALK RIVER NUCLEAR LABORATORIES,
CHALK RIVER, ONT., CANADA

Abstract — Résumé — Аннотация — Resumen

FISSION DATA AND NUCLEAR TECHNOLOGY. Accurate nuclear data for fissile nuclei are required not only by reactor designers, but also by reactor physicists for the interpretation of integral experiments, e.g. studies of the change of reactivity with irradiation. Some of the requests that have been made for such fission data, and the reasons behind them, are discussed, along with the progress that has been made towards their fulfilment. An attempt is made to outline those areas where better data are required.

CONSTANTES DE FISSION ET TECHNOLOGIE NUCLÉAIRE. On a besoin de valeurs exactes des constantes nucléaires concernant les noyaux fissiles, non seulement pour les études de réacteurs, mais également pour la physique des réacteurs lorsqu'on veut interpréter les expériences intégrales, c'est-à-dire dans les études sur les modifications de la réactivité avec l'irradiation. L'auteur discute certaines des demandes de renseignements sur les constantes de fission, les raisons pour lesquelles elles ont été faites et la mesure dans laquelle elles ont pu être satisfaites. Il s'efforce également de délimiter les domaines dans lesquels on aurait besoin de valeurs plus précises.

ДАННЫЕ О ДЕЛЕНИИ И ЯДЕРНАЯ ТЕХНОЛОГИЯ. Точные ядерные данные о расщепляющихся ядрах необходимы не только конструкторам реакторов, но также и физикам-реакторщикам для интерпретации интегральных экспериментов, то есть для изучения изменения реактивности по мере облучения. Рассмотрены некоторые просьбы о предоставлении таких данных о делении и причины, вызвавшие эти просьбы, а также успехи, достигнутые в деле их удовлетворения. Сделана попытка наметить те области, где требуются более точные данные.

DATOS SOBRE LA FISION Y TECNOLOGIA NUCLEAR. No sólo quienes trabajan en el proyecto de reactores requieren datos nucleares exactos sobre los núcleos fisionables, sino que también los físicos de reactores los necesitan para interpretar los resultados de experimentos integrales, como por ejemplo, en los estudios sobre la variación de la reactividad en función de la irradiación. El autor describe algunas de las peticiones de datos de esa clase que se han formulado, así como los adelantos realizados con objeto de satisfacerlas. También indica, en líneas generales, aquellas esferas en las que se necesitan datos más amplios y exactos.

INTRODUCTION

The idea that reactor designers and reactor physicists need fundamental nuclear data for their work would seem at first sight to be a reasonable one, and certainly there is no shortage of requests for precise measurements of a very wide range of nuclear parameters. Nevertheless it is not altogether obvious that there really is a genuine need for very accurate fundamental data, especially in view of the large effort devoted to reactor physics experiments, and a comprehensive examination of the way in which these two approaches complement each other would make an interesting survey paper. This is a task for a reactor physicist; the present paper is given by a nuclear physicist, who is a part-time nuclear-data measurer, to an audience containing few reactor physicists. It will therefore start

with a relatively uncritical acceptance of the reactor people's requests and be mainly concerned with questions of the extent to which these requests have been met, and what is being done to improve the situation, with, inevitably, an uneven treatment biased by the author's own current interests. There will be some overlap with the survey paper on nuclear data presented by Dr. C.H. Westcott at the 3rd UN Int. Conf. PUAE in 1964 [1], of which the writer was a co-author, but the emphasis will be rather different in view of the different audience. A further difference will be the restriction to fissile nuclei; the whole body of reactor requests concerns, of course, fissile and fertile materials, and the poisons they produce, as well as the properties of moderators and structural and shielding materials.

BASIS OF REQUESTS FOR DATA

The reactor designer is concerned with predicting not just the reactivity of a proposed system but such details as the distribution of heat output through the reactor, the response to temperature changes and to voids in coolant channels and, of course, the change of these properties, especially reactivity, during prolonged operation. These features affect capital and operating costs, directly as with fuelling charges, or indirectly as with some aspects of control and safety. Of course they do not wholly determine these costs: the cost of processing plutonium can be as important as its fission cross-section, and is more subject to change. But, just because the value of a reactor concept does depend on outside circumstances, the reactor designer must be able to respond quickly and confidently to changes in the rules.

Until comparatively recently the available theory was inadequate, and simplified models had to be used in conjunction with empirical constants derived from lattice experiments. With the development of reliable methods of calculating neutron spectra, which are based on experimental studies of neutron scattering and checked by spectrum measurements, and with computers able to handle the calculations, a more fundamental approach using basic nuclear data is now possible [2]. Theoretical treatments of various degrees of sophistication are available for various problems.

This improved, or at least potentially improved, situation does not imply that reactor-physics studies of the integral-experiment type are becoming less important. The emphasis may change, of course, but it seems unlikely that any power reactor will actually be built without extensive measurements on mock-up lattices, and there will always be special problems, e.g. of local geometrical disturbances, that are more easily elucidated experimentally. Moreover the present situation is a transitional one in that experiments are still needed either to provide verification of still relatively new calculational methods, where basic nuclear data are reliable, or to fill in gaps due to poor basic data. In the context of the problem of initial behaviour the present situation appears to be that for thermal reactors the data are more reliable than the design methods, but for fast power reactors the present data are inadequate [3].

The problem of the change of reactivity with irradiation is more complicated, and even in thermal reactors requires data that are not well known,

e.g. on fission product poisoning. In natural uranium reactors there is a near cancellation of the effects of U^{235} destruction and Pu^{239} production, which is of great practical importance. The achievable burn-up is high (> 2n/kb) and an adequate set of reactivity-change measurements involves protracted irradiations. It is therefore appropriate to extend the scope of measurements on the irradiated fuel to provide as complete a picture as possible of the changes that occur (e.g. in isotopic composition), and to correlate them with calculations based on basic nuclear data, with the object of applying the results to reactor systems somewhat different from that used in the experiments [4].

As might well be expected from the very large and diverse programmes in the general field of reactor design and development, the requests for nuclear data cover a very wide field, and the lists of requests for measurements are very long. There are in fact formal "request lists", which will be mentioned again later in connection with problems of organization, but the immediate question is the justification of the accuracy requested for any given parameter. One could argue, quite correctly, that there is no point in providing nuclear data for calculations that are much more accurate than the calculational methods themselves. However, as has already been mentioned, these methods are continually improving, and the possibility of experimental checks will justify a continuing request for nuclear data that are more accurate than the theory. One must set a sensible limit to such escalation, but it is difficult to specify some ultimate accuracy that will be sufficient for all forseeable requirements.

For instance, to what accuracy is it desirable to predict the initial reactivity of a proposed reactor? This depends ultimately on the cost of the error, which may be either in initial over-design or in the measures that have to be taken to increase reactivity. What can be done to remedy a situation, or what could have been saved by building a smaller reactor, are questions that can be properly answered only for a particular reactor design. In spite of such difficulties, indeed with full appreciation of them, some groups have formulated general recommendations. For example, the accuracy requirements adopted by STORY, POPE and BARRINGTON [5] are designed to permit calculations to about ± 1/2% in reactivity for natural uranium reactors, ± 2% for enriched thermal reactors and ± 1% for fast reactors. Such criteria of course are subject to considerable debate, both by requesters and measurers of data; a particularly vexed question is that of priorities.

Thus comparisons of the available data with the requests can only lead to definite conclusions when it is clear either that the most exacting requirements have been met, or that the available accuracy falls far short of what has been requested. In the next section of the paper, where such an appraisal is attempted, many examples will be found of requests that are very far from being satisfied, and a few where recent measurements will allow some very welcome deletions to be made in the next editions of request lists.

STATUS OF NUCLEAR DATA

The requirements for nuclear data are most conveniently discussed according to the energy of the neutron inducing the reaction. For the necessarily short survey presented here only three distinct ranges will be considered, fast, intermediate and thermal, and the treatment of the first will be extremely brief.

Fast-neutron data

In the neutron energy range above ~ 100 keV requests for measurements on U^{233}, U^{235} and Pu^{239} typically specify accuracies of about 1% for fission cross-sections and ν values, and about 5% for radiative capture cross-sections. Accurate and extensive data on inelastic scattering are also required, but these will not be considered here.

In spite of a very large number of measurements in many different laboratories the fission cross-sections are not yet known to 1% accuracy. The best data are those for U^{235}; recent measurements by WHITE [6] achieve an accuracy of 2.5 - 3%. Above 1 MeV his results agree well with the older, somewhat less accurate data, but between 0.1 and 0.5 MeV they lie about 5% lower, a difference within the combined uncertainties of the new and old results. It seems very difficult to improve on this at present and efforts are being devoted to bringing measurements on the other fissile nuclei up to the standard of accuracy achieved for U^{235} rather than trying to improve this further[1].

The measurements of $\alpha = \sigma_\gamma/\sigma_f$ by HOPKINS and DIVEN [7], and WESTON et al. [8] are accurate to about 10% for U^{235} in the range 0.1-1 MeV. At lower energies the accuracy falls off somewhat, and at higher energies also, though this is less serious because of the smaller value of α. Again, the values for U^{233} and Pu^{239} are less accurately known.

The situation for ν is better. Several groups [9, 10, 11, 12, 13] have put considerable effort into measurements on the variation of ν with neutron energy, and the requested standards of accuracy have been met. The requesters have been lucky in that this variation turned out to be more complicated than had been expected, and a pure-physics-motivated desire to establish its departure from linearity and investigate how this depended on the fissioning nucleus has produced much accurate information. There are some discrepancies between different measurements but these are at energies higher than those of reactor interest, and there is the question of the absolute scale of ν values, but this is really a separate matter and will be taken up later.

Intermediate energy range

Although one can draw a useful distinction between the energy regions where the resonances of fissile nuclei are resolved and where they are not,

---

[1] Cf. WHITE, P.H., HODGKINSON, J.G. and WALL, G.J., "Measurement of fission cross-sections for neutrons of energies in the range 40-500 keV", these Proceedings I.

it will not be emphasized here. All reactor designs, even well-moderated thermal reactors, demand some knowledge of behaviour in this region, but it is most important for the so-called intermediate (i.e. very undermoderated) reactors and for fast power reactors, where the relatively large mass of structural and coolant materials seriously degrades the spectrum. The development of fast power reactors especially has stimulated a great demand for improved data in this region. The requests typically call for accuracies of a few percent for both fission and capture cross-sections, the assumption being, apparently, that ν is almost constant, increasing by about 1/2% over the range 0-100-keV neutron energy.

The observations by BLYUMKINA et al. [13], at neutron energies of a few hundred kilovolts, of rather abrupt changes in $\bar{\nu}$, anticorrelated with changes in fragment kinetic energy, do not imply that this assumption is seriously in error if, as the authors believe, the phenomenon is due to the rapidly increasing importance of p-wave fission. The evidence for the constancy of ν at lower energies is based, however, on a relatively small number of experiments. Several comparisons of ν in the thermal and 0.3 eV resonance regions of Pu^{239} [14, 15, 16] have shown that the difference is less than 1/2%, and a similar series of measurements has been made at very low energy in U^{235} [15]. BOLLINGER [16] extended these measurements to a dozen resonances below 100 eV in Pu^{239} and found that ν was constant to a statistical accuracy of 3 to 4%.

However, other investigations have shown significant changes in mass yield curve and fragment kinetic energy from one resonance to another [17, 18, 19, 20] so that small variations in ν would certainly be expected. There is no reason to believe that these will be important to reactor design, or that they are involved in any of the discrepancies that exist, but it will be well to keep this possibility in mind now that fission cross-section data are being requested with an accuracy of a few percent over this region.

Few reactors are so dilute that self-shielding in resonances can be ignored. For example, this self-shielding increases the reactivity of a typical dilute fast power reactor by 3%, according to SMITH et al. [21], and the effect of the Doppler broadening of these resonances is of prime importance in determining the temperature coefficient of reactivity, an important safety consideration in fast reactors. There is interest in reliable calculations of this effect for reactors that would operate at such high temperatures that experimental studies are not feasible. Thus information is required on resonance parameters, and also on their distribution for calculating behaviour in the region where the resonances cannot be resolved experimentally; the accuracy requested is typically ± 10%. This represents a very large undertaking and it is fortunate that such measurements have a considerable theoretical interest.

Information in the resonance region was originally obtainable only from measurements of total and fission cross-sections. Especially at higher energies this is unsatisfactory because of the relatively large correction for scattering. Often the only available total and fission data came from independent experiments with different instrumental resolution, and sometimes with transmission samples so thick that the apparent average total cross-section was seriously in error. The development of efficient direct

and gamma detection systems has now made possible direct measurements of η and σ_γ [16, 35, 36].

The difficulties of flux measurement at higher energies were discussed at a special symposium about 18 months ago [22]. Improved fission cross-section measurements have recently been reported, one by an extension of the proton recoil technique of flux measurement down to 40 keV [23], another by the use of a calibrated antimony-beryllium source to provide a known flux of 24 keV neutrons [24]. In each case the accuracy was about ± 2.5%.

It is not possible here to give an adequate survey of the intermediate energy region. Considerable progress is being made towards the fulfilment of requests, and many of the papers presented at this Symposium, especially those of Sessions II and III, illustrate this progress. However a particular problem, of considerable interest to the reactor people, suggests that we may still have some way to go.

This problem is the apparent discrepancy between the directly measured values of the capture resonance integral $\int \sigma_\gamma \, dE/E$ for U^{235} (or $\langle\alpha\rangle$ its ratio to the fission resonance integral) and the values of these quantities calculated from the neutron spectrometer data on the variation of the cross-sections with energy. The direct determinations of the fission resonance integral are in good agreement, and BIGHAM [25] has recommended a value of 277 ± 5 b above 0.45 eV. Accurate direct measurements of the capture resonance integral have only recently been made; DURHAM et al. [26] measured it as 144 ± 5 b, and CONWAY et al. [27] and ESCH et al. [28] obtained values of 0.55 ± 0.04 and 0.486 ± 0.025 respectively for $\langle\alpha\rangle$. The weighted mean is 0.512 ± 0.014, including DURHAM et al.'s result. Older data from filtered neutron experiments [29, 30] and under-moderated assemblies [31, 32] are more complicated to interpret, but they support a value of $\langle\alpha\rangle$ close to 0.5.

Values calculated from $\sigma(E)$ measurements are much higher, for example PERSIANI et al. [33] give $\langle\alpha\rangle = 0.72$. Although HANNA and WALKER [34] calculated a value of 0.53 ± 0.09, it is probably too low, since it involved unreliable data on the total cross-section in the region 50-100 eV obtained from measurements on insufficiently thin samples.

The work of BROOKS [35] on the variation of η with energy avoids the uncertainty associated with the subtraction of fission and scattering from the total cross-section, as does that of WESTON et al. [36] in which σ_γ is measured directly. Unfortunately both these measurements appear to give a high value of $\langle\alpha\rangle$. There seems to be little doubt about the region below ~20 eV or, as a result of UTTLEY'S measurements [37], above 100 eV. Thus the essential discrepancy appears to involve the high values of α obtained in the 20-100 eV region[2].

---

[2] Information from E.R. Rae and M.G. Sowerby, communicated just before this Symposium, shows that, following a renormalization of fission data, the results of Brooks are no longer in serious conflict with the integral measurements. The information in the following paper has not yet been examined: **Ван Ши-ди, Ван Юн-чан, Дерменджиев, Е. и Рябов, Ю.В., "Взаимодействие нейтронов с ядрами урана-235 в области энергий 0,002 ÷ 30 кэв"**, these Proceedings I.

Thermal-neutron data

Many of the fundamental investigations of the nature of the fission process have used thermal-neutron-induced fission, e.g. the time-of-flight studies on the details of kinetic energy release and neutron emission. The reactor designer however is not interested in such details but only in the average kinetic energy, and the over-all lab. energy spectrum of the neutrons. Conversely the practical need for precise values of fission and capture cross-sections excites no response from those interested in the physics of fission. This need arises partly as a direct result of thermal-reactor design requirements from such data, but also because of their utility as standards, especially for measurements of fission cross-sections and ν or η values at higher energies. The reactor requests typically specify accuracies of 1/2 - 1% for σ_f ν and η.

There exist several tabulations of best values of the 2200 m/s cross-sections, and ν and η values, for the three principal thermally fissile nuclei U^{233}, U^{235} and Pu^{239}. The most recent of these comes from WESTCOTT et al., a preliminary account of which was given at the Third United Nations International Conference on the Peaceful Uses of Atomic Energy [1], and which is to be published in greater detail shortly [38]. In common with other earlier attempts, e.g. [39], it adopts a least-squares fitting procedure. Specifically a weighted least-squares fit is performed for the three independent quantities σ_f, η and ν for each nucleus, i.e. for nine independent parameters, using as input data all available direct measurements of these quantities, all measurements of the derived quantities σ_a, σ_γ and α (= σ_γ/σ_f), and all measurements of ratios, such as σ_f (U^{233})/σ_f (U^{235}).

Since the accuracy assigned to a measurement determines its weight in the analysis, it is very important to be satisfied that the accuracies claimed are reasonable and consistent (i.e. denote standard deviations). Some experiments are written up in sufficient detail for this to raise no difficulty. Sometimes, especially with recent work, correspondence with experimenters provides the necessary clarification, but inevitably some measurements, especially the older ones, have to be treated in a somewhat arbitrary fashion. This particular fit is characterized by a ruthless downweighting of old and inadequately documented measurements.

For reasons that will be clear later, it is useful to examine first the results obtained up to November 1964; these are summarized in Tables I and II, which list the average input data and the results of the least squares fit ("output").

Although Table II does not show it, the measurements of an individual parameter were found to be consistent within their stated errors. Certain well-known anomalies, e.g. σ_f (U^{235}), lost much of their impact when the quoted errors were increased in accordance with estimates of uncertainties not fully taken into account by the original experimenters.

In contrast with this, it was found that the output values differed from the input values by rather more than would be expected. An increase of 10 or 20% in all errors would render this over-all trend non-significant (from the point of view of a χ^2 test) but certain differences would still look rather large, e.g. that for the (Pu^{239}/U^{235}) ratio. Certainly a precise

TABLE I

INPUT DATA FOR U^{233}, U^{235} AND Pu^{239}

Quantity	U^{233}			U^{235}			Pu^{239}		
	Value	Error	N	Value	Error	N	Value	Error	N
σ_a	575.1	2.8	(8)	680.4	2.6	(8)	1006.8	6.1	(5)
σ_f	517.0	4.5	(4)	583.7	4.0	(6)	719.9	16.6	(2)
σ_γ	52.7	3.0	(1)	No value			276.3	7.9	(2)
α	0.0941	29	(4)	0.1733	20	(6)	0.3590	68	(2)
ν	2.4950	210	(2)	2.4320	143	(5)	2.8979	276	(2)
η	2.2933	98	(2)	2.0759	104	(2)	2.1400	150	(1)
	U^{233}/U^{235}			U^{239}/U^{235}			Pu^{239}/Pu^{233}		
	Ratio	Error	N	Ratio	Error	N	Ratio	Error	N
σ_f	0.9110	26	(1)	1.3073	125	(1)	1.4325	125	(2)
ν	1.0191	51	(4)	1.1817	77	(3)	1.1602	215	(2)
η	1.1064	51	(4)	1.0320	120	(1)	No value		
$\eta\sigma_a$	0.9434	172	(1)	1.4857	270	(1)	1.5714	286	(1)
$(\eta-1)\sigma_a$	1.0127	179	(4)	1.4948	323	(4)	1.4737	391	(2)

N = number of measurements used to obtain the mean

Values and errors for cross-sections are in barns. All ratios are dimensionless and their errors are in units of 10^{-4}.

measurement of the Pu^{239} fission cross-section with monokinetic neutrons would be most welcome, but with several unhappy memories of fission cross-section measurements, such an experiment would attract much careful scrutiny[3]. However, even with the errors increased by 20% or so the accuracy of the output values, even for Pu^{239}, is very good. The very high accuracies of the σ_a values, which are essentially transmission measurements corrected for scattering, are still under review by N. J. Pattenden at the Atomic Energy Research Establishment, Harwell. That the fission cross-sections are of comparable accuracy is due to measurements of α and σ_γ for which high accuracy is claimed. However, these measurements were made in reactor spectra and although the claims seem to be justifiable the question of the accuracy of the conversion from a Maxwellian spectrum to 2200 m/s (by the Westcott g factor) is being investigated by Vogt at Chalk River.

[3] The measurements in the following paper have not been included because a final statement of errors is not yet available: FRAYSSE, G. and PROSDOCIMI, A., "Fission cross-section measurement of U^{235} and Pu^{239} for low-energy neutrons", these Proceedings I.

TABLE II

OUTPUT OF LEAST-SQUARES FIT OF 2200 m/s PARAMETERS FOR THE THREE FISSILE NUCLIDES

Quantity	U^{233}		U^{235}		Pu^{239}	
	Value	Error	Value	Error	Value	Error
σ_a	575.3	1.8	679.3	1.9	1008.9	4.5
σ_f	525.9	1.6	578.3	1.6	743.1	3.5
σ_γ	49.4	1.2	100.9	1.0	265.8	3.2
α	0.0939	23	0.1745	1.8	0.3577	48
ν	2.5075	81	2.4422	71	2.8807	123
η	2.2923	68	2.0793	60	2.1217	90
	U^{233}/U^{235}		Pu^{239}/U^{235}		Pu^{239}/U^{233}	
	Ratio	Error	Ratio	Error	Ratio	Error
σ_f	0.9094	22	1.2849	60	1.4130	67
ν	1.0267	30	1.1795	48	1.1488	52
η	1.1024	31	1.0204	43	0.9256	42
$\eta\sigma_a$	0.9337	33	1.5156	78	1.6233	88
$(\eta-1)\sigma_a$	1.0140	53	1.5436	120	1.5223	125

Values and errors for cross-sections are in barns. All ratios are dimensionless and their errors are in units of 10^{-4}.

Unfortunately this apparently satisfactory situation has been seriously disturbed by Colvin and Sowerby's revised value of ν for U^{235}, which is 2.4 ± 0.6% smaller than the output value of Table II. No doubt they will be discussing this in Session VI [40] but two points might be made here:

(i) The basic discrepancy is between their boron-pile measurements, and those made in liquid scintillation tanks, of ν for Cf^{252} and therefore has nothing to do with possible variations of ν at low-neutron energy.

(ii) If such a result were fed into a weighted least-squares fit the output ν and η values would change by only 1/2 % or so. However, the low value from the very careful boron-pile raises the question of the possible existence of serious systematic errors in the different determinations (involving also, via α, the ORNL η measurements [41,42]) so that the over-all situation cannot be regarded as satisfactory.

Certainly any suggestion that η for U^{235} is 2% lower, i.e. about 2.03, would raise considerable protest from those reactor physicists who claim to understand their lattice data. On the other hand, had it not been for this recent development, one would have said rather confidently that the accuracy

of the basic data is considerably better than that obtainable from any but the most basic type of integral experiments (such as GWIN and MAGNUSON'S measurements of η by experiments on homogeneous aqueous solutions [42].

Two recent experiments on the comparison of the reactivity of uranium and plutonium in lattices provide an example of checks of 2200 m/s data from integral experiments. TRETIAKOFF [43] has reported $\eta(Pu^{239})/\eta(U^{235}) = 1.007$ and ASKEW and SANDERS [44] 1.015 for the same ratio. The estimated accuracy was not stated explicitly but the context implies $\sim \pm 1/2\%$. The output value of Table II is $1.020 + 0.004$. It might also be mentioned in this connection that SPINRAD and MEIER suggested [45] that, because of the great sensitivity of reactivity change with burn-up to small errors in cross-section data, the observation of reactivity change could be a "sensitive indicator of the cross-section parameter involved", but they concluded that the principal uncertainty in the interpretation is the neutron spectrum.

INTERNATIONAL CO-OPERATION

In spite of the difficulty mentioned earlier of specifying the precise accuracy to which a particular parameter should be determined, and with what priority, there is a broad area of agreement among requesters that transcends national boundaries. Correspondingly, the results of measurements undertaken in one laboratory may be keenly awaited in another. Indeed the best way of fulfilling a request from one area might well involve measurements in another institution on sample material provided by a third.

During the past five years the European American Nuclear Data Committee, an organization of the OECD countries, has attempted, with some success, to foster co-operation of just this type. A necessary prerequisite is general agreement that the requests for data are well founded, also that the suggested measurements will give basic information of appropriate accuracy, rather than, for example, operating characteristics of a particular reactor. One of the most important tasks of this committee has therefore been the critical assessment of the status of nuclear data relative to the requests. Regarding the request lists themselves, these are painstakingly scrutinized and kept up-to-date. A system of priority definitions has been set up, and requesters are asked to provide documentation. The more recently formed European American Committee on Reactor Physics is expected to take an increasingly important part in recommending priorities.

A further step towards fully international co-operation in the nuclear data field was taken two years ago when the International Atomic Energy Agency formed its own nuclear data unit in Vienna under Dr. C. H. Westcott, and a compilation centre is to be set up.

A striking feature of the last few years is the gap that is opening between the readily available data compilations and the mass of data that actually exists. A prime difficulty is the degree of detail now available: the log-log format of BNL-325 just cannot handle it. In fact there is no longer much sense in trying to prepare compilations where all experimental measure-

ments are fully displayed. There is not room to put them on a graph with adequate accuracy, and the first thing the user has to do is to take them off again. He would prefer to pick up a phone and ask a "cross-section centre" to send him a magnetic tape, or a deck of cards, or perhaps a printout, and indeed this is now becoming possible.

Clearly such compilation centres need to be organized on a level of active international co-operation. A close relationship already exists between the Brookhaven Sigma Centre and the ENEA compilation centre at Saclay, and it is understood that arrangements are being made for co-operation between them and the IAEA centre in Vienna, and possibly other centres also.

A data compilation may be just a listing of the available data. Even this involves considerable effort, now fortunately reduced by the availability of the CINDA bibliographic index of nuclear data [46], which has recently begun to operate on an international level. The compilers may exercise some degree of selection, e.g. in omitting very old data (or just giving a reference), or of assessment, e.g. in the drawing of a line through a mass of points. A reactor designer will generally prefer a compilation that suppresses the raw data entirely and provides only a single recommended value, or curve. Such "evaluation" calls for a careful appraisal of the measured data, and a consideration, where appropriate, of the results of integral experiments as well as microscopic measurements. It may also involve the use of theory to bridge gaps in the measurements. Evidently it is a laborious and exacting task calling for close co-operation between the reactor physicists and designers, who are principally interested in the result, and the experimental measurers who are needed to advise on discrepancies. The amount of effort required argues strongly for the development of international co-operation, a need stressed by STORY et al. [47] in their recent paper on nuclear data evaluation.

REFERENCES

[1] WESTCOTT, C.H., EKBERG, K., HANNA, G.C., PATTENDEN, N.J. and SANATANI, S., Proc. 3rd UN Int. Conf. PUAE (1965) P/717.

[2] JOANU, G.D. and STEWART, H.B., Annu. Rev. Nucl. Sci. 14 (1964) 259.

[3] CAMPBELL, C.G., KINCHIN, G.H., SMITH, R.D., Exponential and Critical Experiments, IAEA, Vienna (1964) 29.

[4] DURET, M.F., DURHAM, R.W., LOUNSBURY, M., OKAZAKI, A., WALKER, W.H., WARD, A.G. and PEASE, L., Proc. 3rd UN Int. Conf. PUAE (1965) P/26.

[5] STORY, J.S., POPE, A.L. and BARRINGTON, E.P., INDSWG-42 (1962).

[6] WHITE, P.H., to be published in J. Nucl. Energy.

[7] HOPKINS, J.C. and DIVEN, B.C., Nucl. Sci. Engng. 12 (1962) 169.

[8] WESTON, L.W., de SAUSSURE, G. and GWIN, R., Nucl. Sci. Engng. 20 (1964) 80.

[9] MEADOWS, J.W. and WHALEN, J.F., Phys. Rev. 126 (1962) 197.

[10] HOPKINS, J.C. and DIVEN, B.C., Nucl. Phys. 48 (1963) 433.

[11] MATHER, D.S., FIELDHOUSE, P. and MOAT, A., Phys. Rev. 133 (1964) B1403.

[12] ASPLUND-NILSSON, I., CONDE, H. and STARFELT, N., Nucl. Sci. Engng. 20 (1964) 527.

[13] BLYUMKINA, Yu.A., BONDARENKO, I.I., KUZENTSOV, V.F., NESTEROV, V.G., OKOLOVITCH, V.N., SMIRENKIN, G.N. and USACHEV, L.N., Nucl. Phys. 52 (1964) 648.

[14] AUCLAIR, J.M., LANDON, H.H. and JACOB, M., C.R. Acad. Sci., Paris 241 (1955) 1935.

[15] LEONARD, B.R., Jr., Neutron Physics, Academic Press Inc., New York (1962) esp. p.23.

[16] BOLLINGER, L.M., ORNL-2309 (1957) 167.
[17] COWAN, G.A., BAYHURST, B.P. and PRESTWOOD, R.J., Phys. Rev. 130 (1963) 2380.
[18] FALER, K.T. and TROMP, R.L., Phys. Rev. 131 (1963) 1746.
[19] MEHTA, G.K., Thesis, Columbia University (1963).
[20] MILLER, L.G. and MOORE, M.S., Bull. Amer. phys. Soc. 9 (1964) 422.
[21] SMITH, R.D., BAKER, A.R., HICKS, E.P., MANN, J.E., ROWLANDS, J.L., SMITH, D.C. and WEAL, J., Proc. 3rd UN Int. Conf. PUAE (1965) P/166.
[22] Symposium on the Absolute Determination of Neutron Flux in the Energy Range 1-100 keV, EANDC-33.
[23] WHITE, P.H., HODGINKSON, J.G. and WALL, G.J., "Measurement of fission cross-sections for neutrons of energies in the range 40-500 keV", these Proceedings I.
[24] PERKIN, J.L., WHITE, P.H., FIELDHOUSE, P., AXTON, E.J., CROSS, P. and ROBERTSON, J.C., to be published.
[25] BIGHAM, C.B., AECL-1910 (1964).
[26] DURHAM, R.W., HART, R.G., LOUNSBURY, M. and HANNA, G.C., unpublished, quoted in Ref. [34].
[27] CONWAY, D.E., COOK, H.D. and GUNST, S.B., Trans. Amer. nucl. Soc. 7 (1964) 78.
[28] ESCH, L.J., FEINER, F., MEWHERTER, J.L., HEIKAMP, A.F. and EILAND, H.M., Trans. Amer. nucl. Soc. 7 (1964) 78, 272.
[29] KANNE, W.R., STEWART, H.B. and WHITE, F.A., Proc. UN Int. Conf. PUAE 4 (1956) 315.
[30] SPIVAK, P.E., EROZOLIMSKY, B.G., DOROFEEV, G.A., LAVRENCHIK, Y.N., KUTIKOV, I.G. and DOBRYNIN, Y.P., J. nucl. Energy II 4 (1957) 70.
[31] GOODJOHN, A.J. and WIKNER, N.F., GA-2151 (1961).
[32] DOYAS, R.J. and CANFIELD, E.H., UCRL-7827 (1964).
[33] PERSIANI, P.J., KAGANOVE, J.J. and McARTHY, A.E., ANL Reactor Physics Constants Centre, Newsletter No.10 (1963).
[34] HANNA, G.C. and WALKER, W.H., ENADC(Can)20 (1963).
[35] BROOKS, F.D., Proc. Saclay Symposium on Neutron time-of-flight Methods, Euratom, Brussels (1961) 131, and private communications from RAE, E.R.; see also Proc. 3rd UN Int. Conf. PUAE (1965) P/167.
[36] WESTON, L.W., de SAUSSURE, G., GWIN, R., RUSSELL, J.E. and HOCKENBURY, R.W., Trans. Amer. nucl. Soc. 7 (1964) 270.
[37] UTTLEY, C.A. private communication; see also Proc. 3rd UN Int. Conf. PUAE (1965) P/167.
[38] WESTCOTT, C.H. et al., Atomic Energy Rev. IAEA, Vienna III 2 (1965).
[39] SJOSTRAND, N.G. and STORY, J.S., AEEW-M 125 (INDSWG-14) (1961).
[40] COLVIN, D.W. and SOWERBY, M.G., "Boron-pile ν measurements", these Proceedings II.
[41] MACKLIN, R.L., de SAUSSURE, G., KINGTON, J.D. and LYON, W.S., Nucl. Sci. and Engng. 8 (1960) 210.
[42] GWIN, R. and MAGNUSON, D.W., Nucl. Sci. and Engng. 12 (1962) 364.
[43] TRETIAKOFF, O., Proc. 3rd UN Int. Conf. PUAE (1965) P/77.
[44] ASKEW, J.R. and SANDERS, J.E., Proc. 3rd UN Int. Conf. PUAE (1965) P/165.
[45] SPINRAD, B.I. and MEIER, R.W., Heavy Water Lattices, Technical Reports Series No.20, IAEA, Vienna (1963) 599.
[46] GOLDSTEIN, H. and KALOS, M.H., DASA-1535 (1964).
[47] STORY, J.S., JAMES, M.F., KERR, W.M.M., PARKER, K., PULL, I.C. and SCHOFIELD, P., Proc. 3rd UN Int. Conf. PUAE (1965) P/168.

DISCUSSION

M. PETRASCU: Can you indicate how you processed the individual errors in the final data, shown in Table 1 of your paper, that were used as input data for the least-squares calculation?

G. HANNA: The published accounts of the individual measurements were examined critically to see whether the accuracy claimed by the experimenters appeared to be justifiable. In some cases an additional error was folded in to take account of an uncertainty that had been ingnored; in

others, where the published account was very incomplete or unsatisfactory, an arbitrary down-weighting was applied. Each input value is the weighted mean value, with corresponding error, of all the individual measurements of each parameter, the individual errors determining the weights.

U.V. RYABOV: In the intermediate energy range the values of $\langle \alpha \rangle$ are liable to vary as a function of the experimental method used to obtain them, viz. $\langle \sigma_{n\gamma} \rangle / \langle \sigma_f \rangle$, $\langle \sigma_{n\gamma} / \sigma_f \rangle$, $\langle \Gamma_\gamma \rangle / \langle \Gamma_f \rangle$ or from $\langle \eta \rangle$ measurements. I imagine this would have to be allowed for.

G. HANNA: We did integrate the cross-section data separately over the energy ranges and α, as defined in that way, was the ratio of the integrated cross-section for capture divided by the integrated cross-section for fission. It is therefore directly comparable with the integral measurement.

G. FRAYSSE: In comparing the σ_f of Pu^{239} from input and output data of the least squares fit, I notice there is a difference that is much higher than the errors given (743.1 against 719.9). Do you think that this fact is liable to affect the validity of an error calculation carried out by a least-squares fit, since the result of the fit does not overlap the input data?

G. HANNA: No. The difference of input and output values is 23.2 b but the error (standard deviation) of the input value is 16.6 b.

G. FRAYSSE: Is it possible that the other parameters contribute much more to the build-up of the fitted 743 value than the input direct measurement of 719 b?

G. HANNA: Yes, of course.

A.T.G. FERGUSON: In discussing the fission cross-section of U^{235} in the fast region you pointed out a discrepancy of about 5% between the results obtained recently by Dr. White and earlier measurements. Below 100 keV, attention should also be drawn to a much greater discrepancy, of about 25%. This energy range is just at the peak of the fast reactor neutron spectrum and I feel it is a matter of the utmost urgency to verify this result independently.

G. HANNA: I fully agree with you. My paper is naturally influenced by my own personal preoccupations but you are absolutely right. This is the worst area facing us and I think it is very largely because of the difficulty of measuring the neutron flux in this region.

P. WHITE: I should like to add that the measurements on the fission cross-sections in the energy region above 40 keV, where the flux measurement is difficult, can be extrapolated smoothly to a measurement made by Perkin, White and Fieldhouse in conjunction with the National Physical Laboratory (United Kingdom) at 24 keV neutron energy. In this work use was made of an antimony-beryllium neutron source calibrated in an entirely different manner from the higher energy measurements.

SYMPOSIUM ON THE PHYSICS AND CHEMISTRY OF FISSION

HELD IN SALZBURG, 22-26 MARCH 1965

CHAIRMEN OF SESSIONS

Session I	R. JOLY	CEN de Saclay, Gif-sur-Yvette
Session II	N. FEATHER	University of Edinburgh
Session III	L.E. GLENDENIN	Argonne National Laboratory
Session IV	R. RAMANNA	Trombay Atomic Energy Establishment, Bombay
Session V	G. HANNA	Atomic Energy of Canada Ltd.
Session VI	N. STARFELT	AB Atomenergi, Studsvik, Nyköping
Session VII	G. RUDSTAM	CERN, Geneva
Session VIII	N.A. PERFILOV	Radium Institute W.G. Hlopin, Leningrad
Session IX	H. MAIER-LEIBNITZ	Technische Hochschule, Munich

SECRETARIAT OF THE SYMPOSIUM

Scientific Secretaries:	G.R. KEEPIN	Division of Research and Laboratories, IAEA
	G.B. COOK	Division of Research and Laboratories, IAEA
Administrative Secretary:	H.H. STORHAUG	Division of Scientific and Technical Information, IAEA
Editor:	S.M. FREEMAN	Division of Scientific and Technical Information, IAEA
Records Officer:	T.B. DUNNE	Division of Languages, IAEA

IAEA SALES AGENTS

Orders for Agency publications can be placed with your bookseller or any of our sales agents listed below:

ARGENTINA
Comisión Nacional de
Energía Atómica
Avenida del Libertador
General San Martin 8250
Buenos Aires - Suc. 29

AUSTRALIA
Hunter Publications,
23 McKillop Street
Melbourne, C.1

AUSTRIA
Georg Fromme & Co.
Spengergasse 39
Vienna V

BELGIUM
Office international de librairie
30, avenue Marnix
Brussels 5

BRAZIL
Livraria Kosmos Editora
Rua do Rosario, 135-137
Rio de Janeiro

Agencia Expoente Oscar M. Silva
Rua Xavier de Toledo, 140-1° Andar
(Caixa Postal No. 5.614)
São Paulo

BYELORUSSIAN SOVIET SOCIALIST REPUBLIC
See under USSR

CANADA
The Queen's Printer
Ottawa, Ontario

CHINA (Taiwan)
Books and Scientific Supplies
Service, Ltd.,
P.O. Box 83
Taipei

DENMARK
Ejnar Munjsgaard Ltd.
6 Nörregade
Copenhagen K

FINLAND
Akateeminen Kirjakauppa
Keskuskatu 2
Helsinki

FRANCE
Office international de
documentation et librairie
48, rue Gay-Lussac
Paris 5e

GERMANY, Federal Republic of
R. Oldenbourg
Rosenheimer Strasse 145
8 Munich 8

ISRAEL
Heiliger and Co.
3 Nathan Strauss Street
Jerusalem

ITALY
Agenzia Editoriale Internazionale
Organizzazioni Universali (A.E.I.O.U.)
Via Meravigli 16
Milan

JAPAN
Maruzen Company Ltd.
6, Tori Nichome
Nihonbashi
(P.O. Box 605)
Tokyo Central

MEXICO
Libraria Internacional
Av. Sonora 206
Mexico 11, D.F.

NETHERLANDS
N.V. Martinus Nijhoff
Lange Voorhout 9
The Hague

NEW ZEALAND
Whitcombe & Tombs, Ltd.
G.P.O. Box 1894
Wellington, C.1

NORWAY
Johan Grundt Tanum
Karl Johans gate 43
Oslo

PAKISTAN
Karachi Education Society
Haroon Chambers
South Napier Road
(P.O. Box No. 4866)
Karachi 2

POLAND
Ośrodek Rozpowszechniana
Wydawnictw Naukowych
Polska Akademia Nauk
Pałac Kultury i Nauki
Warsaw

SOUTH AFRICA
Van Schaik's Bookstore (Pty) Ltd.
Libri Building
Church Street
(P.O. Box 724)
Pretoria

SPAIN
Librería Bosch
Ronda de la Universidad 11
Barcelona

SWEDEN
C.E. Fritzes Kungl. Hovbokhandel
Fredsgatan 2
Stockholm 16

SWITZERLAND
Librairie Payot
Rue Grenus 6
1211 Geneva 11

TURKEY
Librairie Hachette
469, Istiklâl Caddesi
Beyoğlu, Istanbul

UKRAINIAN SOVIET SOCIALIST REPUBLIC
See under USSR

UNION OF SOVIET SOCIALIST REPUBLICS
Mezhdunarodnaya Kniga
Smolenskaya-Sennaya 32-34
Moscow G-200

UNITED KINGDOM OF GREAT BRITAIN AND NORTHERN IRELAND
Her Majesty's Stationery Office
P.O. Box 569
London, S.E.1

UNITED STATES OF AMERICA
National Agency for
International Publications, Inc.
317 East 34th Street
New York, N.Y. 10016

VENEZUELA
Sr. Braulio Gabriel Chacares
Gobernador a Candilito 37
Santa Rosalía
(Apartado Postal 8092)
Caracas D.F.

YUGOSLAVIA
Jugoslovenska Knjiga
Terazije 27
Belgrade

IAEA publications can also be purchased retail at the United Nations Bookshop at United Nations Headquarters, New York, at the news-stand at the Agency's Headquarters, Vienna, and at most conferences, symposia and seminars organized by the Agency.

In order to facilitate the distribution of its publications, the Agency is prepared to accept payment in UNESCO coupons or in local currencies.

Orders and inquiries from countries where sales agents have not yet been appointed may be sent to:

Distribution and Sales Unit, International Atomic Energy Agency,
Kärntner Ring 11, Vienna I, Austria

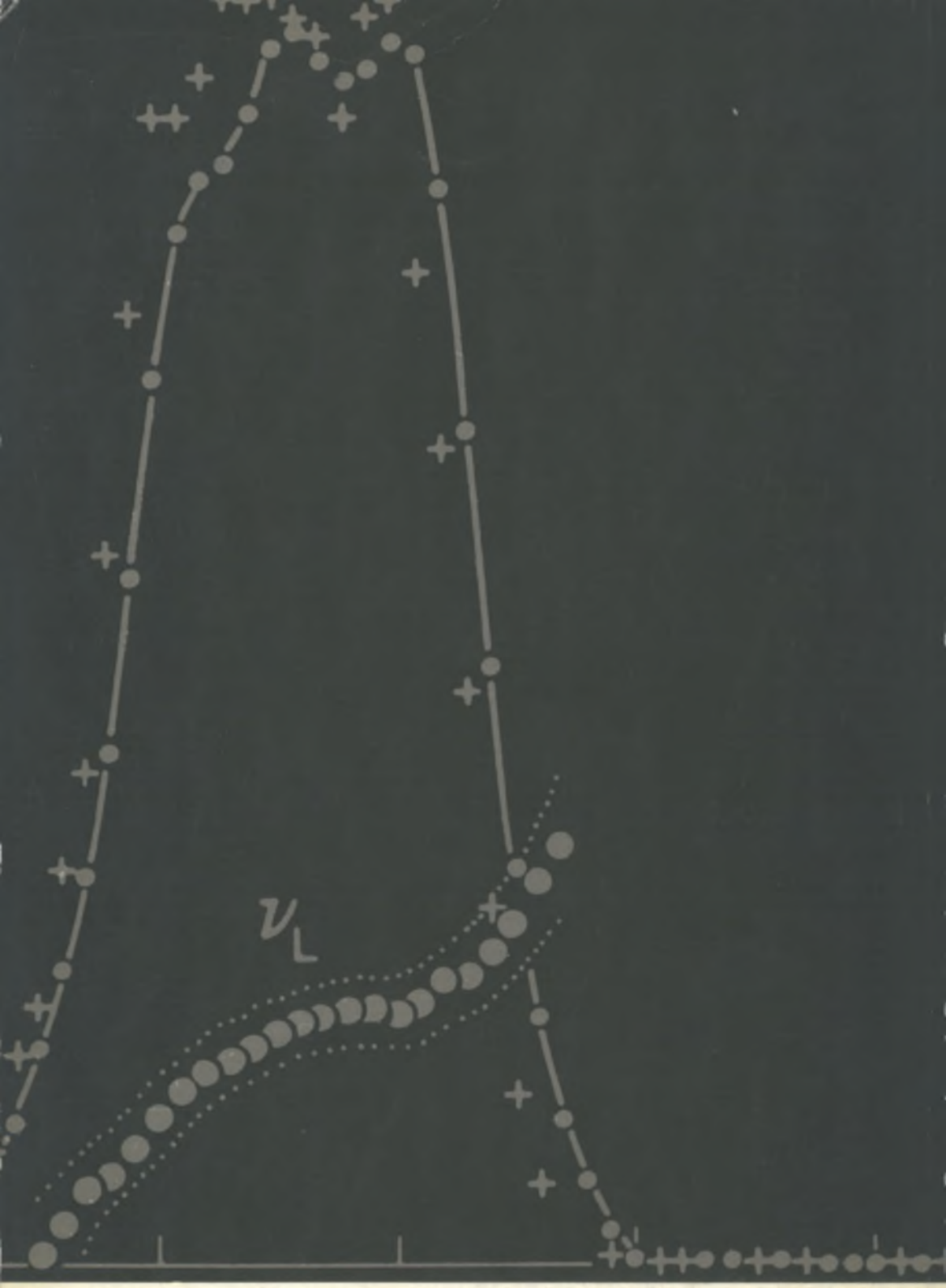

INTERNATIONAL
ATOMIC ENERGY AGENCY,
VIENNA, 1965

PRICE: USA and Canada: US $13.00
Austria and elsewhere: S 273,-
(£3.18.0; F.Fr.52,-; DM 45,50)